© 2000 ASM International. All Rights Reserved.
ASM Specialty Handbook: Nickel, Cobalt, and Their Alloys (#06178G)

Contents

Introduction to Nickel and Nickel Alloys 1

The Nickel Industry: Occurrence, Recovery, and Consumption 3
Uses of Nickel 7
Wrought Corrosion Resistant Nickels and Nickel Alloys 14
Cast Corrosion Resistant Nickel Alloys 55
Cast Heat Resistant Nickel-Chromium and Nickel-Chromium-Iron Alloys 62
Superalloys 68
Special-Purpose Nickel Alloys 92
Nickel Coatings 106

Corrosion Behavior of Nickel and Nickel Alloys 125

Corrosion Behavior of Nickel Alloys in Specific Environment 127
Stress-Corrosion Cracking and Hydrogen Embrittlement of Nickel Alloys 141
High-Temperature Corrosion Behavior of Nickel Alloys 167

Fabrication and Finishing of Nickel and Nickel Alloys 189

Forming of Nickel Alloys 191
Forging of Nickel Alloys 198
Powder Metallurgy Processing of Nickel Alloys 203
Heat Treating of Nickel Alloys 230
Machining of Nickel Alloys 235
Welding and Brazing of Nickel Alloys 245
Cleaning and Finishing of Nickel Alloys 273
High-Temperature Coatings for Superalloys 281

Metallography, Microstructures, and Phase Diagrams of Nickel and Nickel Alloys 291

Metallography and Microstructures of Nickel, Nickel-Copper, and Nickel-Iron Alloys 293
Metallography and Microstructures of Heat Resistant Alloys 298
Phase Diagrams of Binary and Ternary Nickel Systems 331

Introduction to Cobalt and Cobalt Alloys 343

The Cobalt Industry: Occurrence, Recovery, and Consumption 345
Uses of Cobalt 349
Phase Diagrams of Binary and Ternary Cobalt Systems 356
Cobalt-Base Alloys 362

Properties and Fabrication Characteristics of Cobalt and Cobalt Alloys 371

Properties of Cobalt Alloys 373
Wear Behavior of Cobalt Alloys 387
Corrosion Behavior of Cobalt Alloys 395
Fabrication and Metallography of Cobalt Alloys 401

Subject Index 407

Alloy Index 422

© 2000 ASM International. All Rights Reserved.
ASM Specialty Handbook: Nickel, Cobalt, and Their Alloys (#06178G)

ASM Specialty Handbook®

Nickel, Cobalt, and Their Alloys

Edited by
J. R. Davis
Davis & Associates

Prepared under the direction of the
ASM International Handbook Committee

ASM International Staff
Scott D. Henry, Assistant Director of Reference Publications
Bonnie R. Sanders, Manager of Production
Nancy Hrivnak, Copy Editor
Kathleen S. Dragolich, Production Supervisor
Jill A. Kinson and Candace K. Mullet, Production Coordinators
William W. Scott, Jr., Director of Technical Publications



ASM International
Materials Park, OH 44073
www.asminternational.org

© 2000 ASM International. All Rights Reserved.
ASM Specialty Handbook: Nickel, Cobalt, and Their Alloys (#06178G)
www.asminternational.org

Copyright © 2000
by
ASM International®
All rights reserved

No part of this book may be reproduced, stored in a retrieval system, or transmitted, in any form or by any means, electronic, mechanical, photocopying, recording, or otherwise, without the written permission of the copyright owner.

First printing, December 2000

Great care is taken in the compilation and production of this book, but it should be made clear that NO WARRANTIES, EXPRESS OR IMPLIED, INCLUDING, WITHOUT LIMITATION, WARRANTIES OF MERCHANTABILITY OR FITNESS FOR A PARTICULAR PURPOSE, ARE GIVEN IN CONNECTION WITH THIS PUBLICATION. Although this information is believed to be accurate by ASM, ASM cannot guarantee that favorable results will be obtained from the use of this publication alone. This publication is intended for use by persons having technical skill, at their sole discretion and risk. Since the conditions of product or material use are outside of ASM's control, ASM assumes no liability or obligation in connection with any use of this information. No claim of any kind, whether as to products or information in this publication, and whether or not based on negligence, shall be greater in amount than the purchase price of this product or publication in respect of which damages are claimed. THE REMEDY HEREBY PROVIDED SHALL BE THE EXCLUSIVE AND SOLE REMEDY OF BUYER, AND IN NO EVENT SHALL EITHER PARTY BE LIABLE FOR SPECIAL, INDIRECT OR CONSEQUENTIAL DAMAGES WHETHER OR NOT CAUSED BY OR RESULTING FROM THE NEGLIGENCE OF SUCH PARTY. As with any material, evaluation of the material under end-use conditions prior to specification is essential. Therefore, specific testing under actual conditions is recommended.

Nothing contained in this book shall be construed as a grant of any right of manufacture, sale, use, or reproduction, in connection with any method, process, apparatus, product, composition, or system, whether or not covered by letters patent, copyright, or trademark, and nothing contained in this book shall be construed as a defense against any alleged infringement of letters patent, copyright, or trademark, or as a defense against liability for such infringement.

Comments, criticisms, and suggestions are invited, and should be forwarded to ASM International.

Library of Congress Cataloging-in-Publication Data
ASM specialty handbook: nickel, cobalt, and their alloys / edited by J. R. Davis;
prepared under the direction of the ASM International Handbook Committee.
p. cm.
Includes bibliographical references and index.
1. Nickel—Handbooks, manuals, etc. 2. Nickel alloys—Handbooks, manuals, etc. 3. Cobalt—Handbooks, manuals, etc.
4. Cobalt alloys—Handbooks, manuals, etc. I. Davis, J.R. (Joseph R.) II. ASM International. Handbook Committee.
TA480.N6 A28 2000 620.1'88—dc21 00-059348

ISBN: 0-87170-685-7
SAN: 204-7586

ASM International®
Materials Park, OH 44073-0002
www.asminternational.org

Printed in the United States of America

© 2000 ASM International. All Rights Reserved.
ASM Specialty Handbook: Nickel, Cobalt, and Their Alloys (#06178G)

Contents

Preface . . . . . **v**

Introduction to Nickel and Nickel Alloys **1**

The Nickel Industry: Occurrence, Recovery, and Consumption 3
Elemental Nickel 3
Occurrence and Supply 4
Extraction and Refining 4
End Uses of Nickel 6
Uses of Nickel 7
Nickel in Ferrous Alloys 7
Nickel and Nickel-Base Alloys 9
Nickel Coatings 10
Nickel in Nonferrous Alloys 10
Nickel Powders 10
Wrought Corrosion Resistant Nickel and Nickel Alloys 14
Physical Metallurgy of Nickel and Nickel Alloys 14
Commercial Nickel and Nickel Alloys 15
Properties of Wrought Nickel and Nickel Alloys 19
Nickel 200 19
Nickel 201 20
Nickel 270 21
Duranickel 301 22
Monel 400 23
Monel R-405 25
Monel K-500 26
Inconel 600 27
Inconel 622 29
Inconel 625 30
Inconel 686 31
Inconel 690 32
Inconel 718 33
Inconel 725 36
Incoloy 800 37
Incoloy 801 39
Incoloy 825 39
Hastelloy B-2 41
Hastelloy B-3 42
Hastelloy C-4 43
Hastelloy C-22 44
Hastelloy C-276 45
Hastelloy C-2000 46
Hastelloy G 47
Hastelloy G-3 48
Hastelloy G-30 49
Hastelloy G-50 50
Hastelloy N 51
Hastelloy S 52
Hastelloy W 53
Hastelloy X 53
Cast Corrosion-Resistant Nickel Alloys 55
Standard Grades 55
Nickel-Base Proprietary Alloys 57
Cast Heat Resistant Nickel-Chromium, Nickel-Iron-Chromium, and Nickel-Chromium-Iron Alloys 62
Nickel-Chromium Alloys to Resist Fuel Oil Ash Corrosion . . . 62
Nickel-Iron-Chromium Alloys 63
Nickel-Chromium-Iron Alloys 66
Superalloys 68
General Background 68
Processing 73
Properties and Microstructure 79
Environmental Effects 85
Special-Purpose Nickel Alloys 92
Commercially Pure Nickel for Electronic Applications 92
Resistance Heating Alloys 92
Thermocouple Alloys 94
Nickel-Iron Soft Magnetic Alloys 94
Low-Expansion Alloys 96
Nickel-Titanium Shape Memory Alloys 101
Nickel-Beryllium Alloys 102
Ordered Intermetallic Alloys of Ni_3Al 104
Nickel Coatings 106
Nickel Plating 106
Electroforming 114
Electroless Nickel Plating 115
Thermal Spray Coatings 120
Weld-Overlay Coatings 120
Solid-State Nickel Cladding 122

Corrosion Behavior of Nickel and Nickel Alloys **125**

Corrosion Behavior of Nickel Alloys in Specific Environments 127
Alloy Characteristics 127
Effects of Major Alloying Elements 129
Corrosion in Specific Environments 130
Corrosion of Nickel and High-Nickel Alloy Weldments . . . 137
Stress-Corrosion Cracking and Hydrogen Embrittlement of Nickel Alloys 141
Physical Metallurgy of Nickel-Base Alloys 141
SCC in Halide Environments 143
SCC in Environments Containing Sulfur Species 147
SCC in High-Temperature Water and Dilute Aqueous Solutions 152
SCC in Caustic Environments 154
Cracking in Other Environments 157
Hydrogen Embrittlement 157
SCC Testing Methods 160
High-Temperature Corrosion Behavior of Nickel Alloys 167
Oxidation 167
Carburization 172
Nitridation 173
Sulfidation 176
Halogenation 177
Hot Corrosion 182
Ash/Salt Deposit Corrosion 183
Corrosion in Waste Incineration Environments 183
Molten Salt Corrosion 184
Molten Metal Corrosion 186

© 2000 ASM International. All Rights Reserved.

Fabrication and Finishing of Nickel and Nickel Alloys 189

Forming of Nickel Alloys 191
Factors Influencing Formability 191
Special Considerations for Heat-Resistant Alloys 191
Lubricants 192
Tools and Equipment 192
Shearing, Blanking, and Piercing 193
Deep Drawing 193
Spinning 194
Bending Tube and Pipe 195
Bending of Plate, Sheet, and Strip 196
Expanding 196
Forming of Rod and Bar 196
Cold Heading and Cold Extrusion 197
Straightening 197
Cold-Formed Parts for High-Temperature Service 197
Forging of Nickel Alloys 198
Die Materials and Lubrication 198
Heating for Forging 198
Cooling after Forging 199
Forging Practice for Specific Alloys 199
Thermal-Mechanical Processing (TMP) 201
Isothermal Forging 202
Powder Metallurgy Processing of Nickel Alloys 203
Production of Nickel Powders 203
Sintering of Nickel and Nickel Alloys 211
Roll Compacting of Nickel and Nickel Alloys 214
Conventional P/M Superalloy Processing 215
Specialized P/M Superalloy Processing 220
Heat Treating of Nickel Alloys 230
Types of Heat Treatment 230
Annealing 231
Process Control Factors in Annealing 232
Stress Relieving 233
Stress Equalizing 233
Age Hardening 233
Thermomechanical Processing 234
Machining of Nickel Alloys 235
Machinability Categories 235
Basic Principles Applicable to All Machining Operations . . 236
Recommendations for Machining 237
Welding and Brazing of Nickel Alloys 245
Welding Metallurgy of Corrosion Resistant Alloys 245
Welding Metallurgy of Corrosion Resistant Alloys Containing Molybdenum 251
Welding Metallurgy of Heat Resistant Alloys 255
Consumable Selection, Procedure Development, and Practice Considerations 257
Brazing of Heat Resistant Nickel-Base Alloys 267
Cleaning and Finishing of Nickel Alloys 273
Cleaning and Finishing of Corrosion Resistant Nickel Alloys 273
Cleaning and Finishing of Heat Resistant Nickel Alloys . . . 278
High-Temperature Coatings for Superalloys 281
Coating Requirements 281
Types of Coatings 281
Methods of Applying Diffusion Coatings 283
Properties of Diffusion Coatings 284
Practical Applications of Diffusion Coatings 286
Methods of Applying Overlay Coatings 287
Thermal Barrier Coatings 287
Coating Performance 288

Metallography, Microstructures, and Phase Diagrams of Nickel and Nickel Alloys 291

Metallography and Microstructures of Nickel, Nickel-Copper, and Nickel-Iron Alloys 293
Metallography and Microstructures of Nickel and Nickel-Copper Alloys 293
Metallography and Microstructures of Nickel-Iron Alloys . . 294
Metallography and Microstructures of Heat Resistant Alloys 298
Specimen Preparation 298
Microexamination 300
Microstructures of Wrought Heat Resistant Alloys 301
Phases in Wrought Heat Resistant Alloys 302
Phase Diagrams of Binary and Ternary Nickel Systems 331

Introduction to Cobalt and Cobalt Alloys 343

The Cobalt Industry: Occurrence, Recovery, and Consumption 345
Elemental Cobalt 345
Occurrence and Supply 345
Extraction and Refining 345
End Uses of Cobalt 347
Uses of Cobalt 349
Metallurgical Uses of Cobalt 349
Nonmetallurgical Uses of Cobalt 354
Phase Diagrams of Binary and Ternary Cobalt Systems 356
Cobalt-Base Alloys 362
Cobalt-Base Wear Resistant Alloys 363
Cobalt-Base Heat Resistant Alloys 365
Cobalt-Base Corrosion Resistant Alloys 367
Alloy Compositions and Product Forms 368

Properties and Fabrication Characteristics of Cobalt and Cobalt Alloys 371

Properties of Cobalt Alloys 373
AiResist 13 (AR-13) 373
AiResist 213 (AR-213) 373
AiResist 215 (AR-215) 373
Duratherm 600 374
Elgiloy 374
FSX-414 376
Haynes 25 (L-605) 376
Haynes 188 377
MAR-M 302 379
MAR-M 322 379
MAR-M 509 379
MP35N 380
MP159 382
Stellite 6B (Haynes 6B) 382
Stellite 6K 384
Ultimet 384
UMCo-50 (Haynes 150) 385
X-40/X-45 386
Wear Behavior of Cobalt Alloys 387
Types of Wear 387
Wrought Alloy Wear Data 388
Hot Hardness Values for Wrought Alloys 392
Wear-Related Applications for Wrought Alloys 393
Wear Behavior of Cobalt-Base Hardfacing Alloys 393
Corrosion Behavior of Cobalt Alloys 395
The Effect of Alloying Elements 395
Behavior of Cobalt Alloys in Corrosive Aqueous Environments 395
Environmental Embrittlement of Cobalt Alloys 398
High-Temperature Corrosion of Cobalt Alloys 399
Fabrication and Metallography of Cobalt Alloys 401
Heat Treatment 401
Workability 401
Joinability 402
Machinability 403
Metallography 404

Subject Index 407

Alloy Index 422

© 2000 ASM International. All Rights Reserved.

Preface

The history and development of nickel and cobalt, as well as their alloys, parallel one another in a number of ways. Nickel was first used by ancient man in swords and implements fashioned from iron-nickel meteorites. The first authenticated artifact from such a source is what is believed to be a portion of a dagger found at the Sumerian city of Ur (circa 3100 B.C.); analysis has shown it to contain 10.9% nickel. The earliest recorded use of nickel in modern times (i.e., the last few hundred years) was in coins made from "pai-thung," a white copper-nickel alloy first developed in China. Nickel was first identified as an element by Alex F. Cronstedt in 1751 and named nickel from the ore "kupfernickel," so-called by superstitious miners who believed that the ore was bedeviled. The modern nickel industry dates back from the opening of the New Caledonia mines in 1875 and those of Sudbury, Ontario, Canada, in 1886. The first nickel-base alloy developed was "Monell Metal" (now known as Monel alloy 400), a nickel-copper alloy containing nominally 67% nickel with the balance copper. The alloy's origin was derived from the ores of the Sudbury basin in Ontario that contain nickel and copper in approximately the same two-to-one ratio. The trademark for Monel was first registered in 1906. Today nickel is widely used as a key constituent in stainless steels, low-alloy steels, and cast irons, as the base element for many corrosion and heat resistant alloys, as wear or corrosion resistant coatings, and in special-purpose materials such as magnetic alloys and controlled-expansion alloys.

Although isolation of metallic cobalt was first effected by Swedish chemist G. Brandt in 1735, compounds derived from mineral ores containing cobalt had been used for more than 2000 years as coloring agents (blue and green) for glass and ceramics in Persia and Egypt. Cobalt was a major coloring agent used by Greek glassworkers about the beginning of the Christian era. Chinese pottery produced during the Tang and Ming dynasties (A.D. 600 to 900 and A.D. 1350 to 1650) used cobalt widely, and Venetian glass produced in the early 15th century also shows the use of cobalt. The term "kobold" was used applied by miners in Germany in the 16th century to an ore that did not yield the expected copper when reduced by the normal procedure and emitted dangerous arsenical fumes when roasted. The word means a goblin or "ill-natured fairy." The modern cobalt industry dates back to the opening of the New Caledonia mines in 1875 and the discovery of cobalt-bearing ores in Africa in the early 20th century. The first cobalt-base alloy was a cobalt-chromium alloy containing nominally 25% chromium called "Stellite," which was developed by Elwood Haynes and patented in 1907. Haynes took the name Stellite from the Latin word for star, *stella*, because of the alloy's permanent starlike luster. Today cobalt is used as a critical alloying element in superalloys, cemented carbides, and high-speed tool steels, as the base element for wear, heat, and corrosion resistant alloys, in magnetic alloys and controlled-expansion alloys, and in various electronic components and chemicals.

In recognition of the importance of these versatile and strategic metals, ASM decided that this Handbook, the eighth to be published in the *ASM Specialty Handbook* series, would cover the metallurgy, properties, fabrication characteristics, and applications associated with nickel, cobalt, and their alloys. It is intended to provide the most comprehensive and up-to-date information available on these metals that is suitable for engineers, designers, teachers, and students.

Much of the information and data included in this Handbook has been supplied by Haynes International, Special Metals Corporation, Carpenter Technology Corporation, Deloro Stellite Inc., Wall Colmonoy Corporation, Timken Latrobe Steel, SPS Technologies Aerospace Fasteners Group, Elgiloy Specialty Metals, the Cobalt Development Institute, and the Nickel Development Institute. Gratitude is extended to these organizations and to the ASM Editorial and Library staffs, since without these resources it would not have been possible to compile this Handbook.

Joseph R. Davis
Davis & Associates
Chagrin Falls, Ohio

ASM Specialty Handbook: Nickel, Cobalt, and Their Alloys
J.R. Davis, editor, p 3-6
DOI:10.1361/ncta2000p003

Copyright © 2000 ASM International®
All rights reserved.
www.asminternational.org

The Nickel Industry: Occurrence, Recovery, and Consumption

NICKEL is one of the most versatile and important of the major industrial metals. It is a vital alloying element in cast irons, steels (most notably austenitic stainless steels containing 8 to 35% Ni), and nonferrous alloys. Nickel-base alloys are used in demanding corrosion-resistant and heat-resistant applications. Nickel-iron alloys have been developed for applications requiring controlled thermal expansion or soft magnetic characteristics. Nickel coatings and nickel articles made by electroforming are also technologically important. Nickel and/or nickel compounds are also used in coinage, batteries, catalysts, ceramics, and magnetic superconductors.

Elemental Nickel

Although nickel can be produced commercially to a purity of 99.99%, most of the data reported in the literature concern nickel (plus cobalt) of 99.95% purity. This degree of purity is satisfactory for the determination of many properties, but certain properties, for example, electrical resistivity, are very sensitive to impurities in solid solution.

Most of the data given below are taken from Volume 2 of the *ASM Handbook* (see page 1143). More detailed information about the physical, mechanical, and chemical properties of pure nickel can be found in Ref 1 and 2.

Physical Properties

General. Nickel (symbol Ni) is number 28 in the periodic table of the elements. The three metals—iron, nickel, and cobalt—constitute the transition group in the fourth series in the periodic table. The atomic weight of nickel is 58.6934, representing a composite of five stable isotopes.

Crystal Structure. The normal structure of nickel throughout the entire range of temperatures up to the melting point is face-centered cubic (fcc). The lattice constant of the fcc form is 0.35167 nm at 20 °C (68 °F).

Density. The density of nickel at 25 °C (77 °F) is 8.902 g/cm^3. The density of liquid nickel at its melting point is 7.9 g/cm^3 and, with increasing temperature, falls approximately linearly to 7.0 g/cm^3 at 2500 K (~2227 °C, or 4040 °F).

Thermal Properties. The melting and boiling points of nickel are 1453 °C (2647 °F) and approximately 2730 °C (4946 °C), respectively. Other important thermal properties include the following:

- *Coefficient of linear thermal expansion:* 13.3 μm/m · K at 0 to 100 °C (32 to 212 °F)
- *Specific heat:* 0.471 kJ/kg · K at 100 °C (212 °F)
- *Recrystallization temperature:* 370 °C (698 °F)
- *Thermal conductivity:* 82.9 W/m · K at 100 °C (212 °F)

Electrical Properties. The electrical resistivity of pure nickel is negligible at extremely low temperatures but increases with increasing temperature and increasing amounts of impurities. The resistivity of nickel at 20 °C (68 °F) is 68.44 nΩ · m, and the electrical conductivity is 25.2% IACS.

Magnetic Properties. Nickel is one of the three elements (iron and cobalt being the others) that are strongly ferromagnetic at ambient temperature. Typical normal induction curves of annealed samples of the elements iron, nickel, and cobalt are shown in Fig. 1. Pure nickel is seldom used itself as a magnetic material except for certain special purposes, such as magnetostriction applications. Many types of nickel-containing alloys, however, exploit the ferromagnetic properties of nickel. Examples include materials ranging from high-permeability, soft magnetic alloys to high-coercivity, permanent magnet alloys. Although these alloys are generally iron-base, they frequently contain 10 to 20% Ni or more. Such alloys are described in the article "Special-Purpose Nickel Alloys" in this Handbook. Examples of magnetic properties of nickel are given below:

- *Magnetic permeability:* μ_{max} = 1240 at B = 1900 G
- *Coercive force:* 167 A · m^{-1} from H = 4 kA · m^{-1}
- *Saturation magnetization:* 0.616 T at 20 °C (68 °F)
- *Residual induction:* 0.300 T
- *Hysteresis loss:* 685 J/m^3 at B = 0.6 T
- *Curie temperature:* 358 °C (676 °F)

The Curie temperature, in the same manner as other structure-sensitive properties, is dependent on purity and on the prior history of the sample but in general lies between 350 and 360 °C (660 and 680 °F) for high-purity nickel (the 358 °C, or 676 °F, previously given value is from Volume 2 of the *ASM Handbook*).

Mechanical Properties

Tensile Properties. Tensile properties for annealed high-purity nickel have been reported as follows:

- *Tensile strength*: 317 MPa (46 ksi)
- *0.2% offset yield strength*: 59 MPa (8.6 ksi)
- *Elongation in 50 mm (2 in.):* 30%

Suitable choice of hot rolling, annealing, and cold drawing or cold rolling can yield tensile strengths ranging from 448 to 793 MPa (65 to 115 ksi) in rods and bars, as high as 896 MPa (130 ksi) in strip, and 1103 MPa (160 ksi) in wire.

Hardness. Values as low as 64 HV (35 HRB) have been reported for annealed high-purity nickel. Cold work and the presence of impurities increase the hardness.

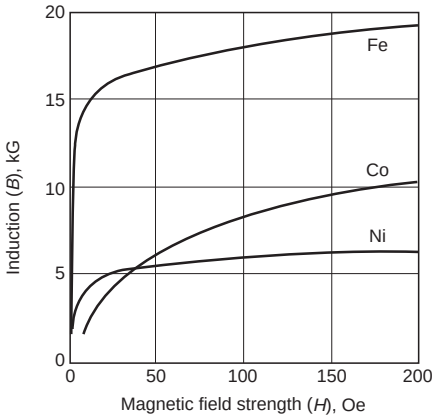


Fig. 1 Typical normal induction curves of annealed samples of iron, nickel, and cobalt. Source: Ref 1

Elastic Properties. Average values of Young's modulus of elasticity are 207 GPa (30×10^6 psi) for 99.95% Ni. The modulus of shear is 76 GPa (11×10^6 psi). Poisson's ratio, that is, the ratio of transverse contraction to longitudinal extension under tensile stress, is 0.31 for nickel.

Chemical Properties

Nickel is not an active element chemically and does not readily evolve hydrogen from acid solutions; the presence of an oxidizing agent is usually required for significant corrosion to occur. Generally, reducing conditions retard corrosion, whereas oxidizing conditions accelerate corrosion of nickel in chemical solutions. However, nickel may also form a protective corrosion-resistant, or passive, oxide film on exposure to some oxidizing conditions. Additional information is available in the article "Corrosion Behavior of Nickel Alloys in Specific Environments" in this Handbook.

Occurrence and Supply

A large number of nickel-bearing minerals have been identified, but relatively few are abundant enough to be industrially significant. Nickel materials that are or have been important are classified as sulfides, laterites (which include oxides and silicates), and arsenides. Of these, the most important present-day ores are sulfides and laterites.

Sulfide Ores. In the sulfide ores, nickel occurs chiefly as the mineral pentlandite, $(Ni,Fe)_9S_8$, in association with large amounts of pyrrhotite, Fe_7S_8, and usually with a significant amount of chalcopyrite, $CuFeS_2$. In addition to nickel, iron, and copper, these ores contain varying amounts of cobalt and precious metals: the platinum group metals, gold, and silver. Their chemical composition falls in the general range of 0.4 to 3% Ni, 0.2 to 3% Cu, 10 to 35% Fe, and 5 to 25% S, with the balance being substantially SiO_2, Al_2O_3, MgO, and CaO.

Sulfide ores are generally found in areas where glacial action has removed much of the overburden of weathered rock. Important known deposits are in Sudbury, Ontario, Canada; in the Voisey's Bay deposit in northeastern Labrador, Canada; in the Thompson-Moak Lake area of northern Manitoba, Canada; in Russia at Norilsk in Siberia; in the Kola Peninsula bordering Finland; in western Australia; and in South Africa.

Laterites. The oxide resources of nickel (commonly known as laterite ores) are generally found in tropical regions, with the largest deposits being in Cuba, New Caledonia, Indonesia, the Philippines, and Central and South America. These ores formed through weathering processes that resulted in nickel being leached from surface rock layers and precipitated at lower levels.

Two general types of oxide ore can be distinguished: silicate-type ore, in which nickel is contained in the lattice of hydrated magnesium-iron-silicates, of which garnierite $(Ni,Mg)_6Si_4O_{10}(OH)_8$ is the most common; and limonitic-type ore, predominantly the hydrated mineral goethite, $(Ni,Fe)_2,O_3{\cdot}H_2O$, in which nickel is dispersed. The chemical composition of oxide ores varies widely and, in addition to 1 to 3% Ni, may comprise significant amounts of cobalt and chromium. Silicate-type ore in New Caledonia analyzes about 2 to 3% Ni, 0.1% Co, 2% Cr_2O_3, and 10 to 25% MgO. Cuban ore, primarily of the limonitic type, analyzes in the range of about 1.2 to 1.4% Ni, 0.1 to 0.2% Co, 3% Cr_2O_3, and 35 to 50% Fe.

Extraction and Refining (Ref 3)

Recovery from Sulfide Ores. Figure 2 illustrates the major processes for the extraction and recovery of nickel from sulfide ores. These ores are first crushed and ground to liberate the mineral values and then subjected to froth flotation to concentrate the valuable constituents and reject the gangue or rock fraction. Depending on the copper and pyrrhotite (iron) contents of the ore, it is sometimes appropriate to produce a separate copper concentrate and a separate pyrrhotite concentrate.

Selective flotation and magnetic separation may be employed to divide the bulk concentrate into nickel, copper, and iron-rich fractions for separate treatment (see process A in Fig. 2). A high-grade iron ore, nickel oxide, and sulfuric acid are recovered from the iron concentrate. The nickel concentrate is treated by pyrometallurgical processes. The major portion undergoes partial roasting in multihearth or fluidized-bed furnaces to eliminate about half of the sulfur and to oxidize the associated iron. The hot calcine, plus flux, is smelted in natural gas or coal-fired reverberatory furnaces operating at about 1200 °C (2200 °F) to produce a furnace matte that is enriched in nickel and a slag for discard. The furnace matte is transferred to Pierce-Smith converters and blown with air in the presence of more flux to oxidize the remaining iron and associated sulfur, yielding Bessemer matte containing nickel, copper, cobalt, small amounts of precious metals, and approximately 22% sulfur. The slag that is generated in the converting operation is returned to the smelting furnace to recover its metal values.

The molten Bessemer matte is cast into 25 ton molds in which it undergoes controlled slow cooling to promote formation of relatively large, discrete crystals of copper sulfide, nickel sulfide, and a small quantity of a metallic phase, a nickel-copper alloy that collects most of the precious metals. After crushing and grinding, the metallics are removed magnetically and treated in a refining complex for recovery of metal values, and the main sulfide fraction is separated into copper sulfide and nickel sulfide concentrates by froth flotation.

The nickel sulfide is converted to granular nickel oxide sinter in fluidized-bed reactors. A portion of this product is marketed directly for alloy steel production. Another part of the granular oxide is treated by chlorination at high temperature (1200 °C, or 2200 °F) to lower its copper content to approximately 0.5%, and then reduced by hydrogen at about 500 °C (930 °F) to yield a highly metallized product (95% Ni) for market.

Two processes are employed to convert the remaining oxide to pure metal for market. One involves reduction smelting to metal anodes and is followed by electrolytic refining, using a sulfate-chloride electrolyte with divided cells and continuous electrolyte purification. The product of this operation is electrolytic nickel cathodes, and the by-products are cobalt and precious metals.

The other process is the atmospheric-pressure carbonyl process, which is used in Clydach, Wales, United Kingdom, and in Copper Cliff, a subdivision of Sudbury, Ontario, Canada. The nickel oxide sinter is reduced with hydrogen and treated with carbon monoxide at approximately 50 °C (120 °F) to volatilize nickel as gaseous nickel carbonyl. This compound is decomposed at approximately 200 °C (390 °F) to yield high-purity nickel in pellet form. Copper and cobalt salts and precious metals are recovered from the residue. Nickel powder is also produced at this plant in a pressure carbonyl system.

The nickel-copper alloy from the matte separation step, containing significant platinum-group metal values, is melted in a top-blown rotary converter, and its sulfur content is adjusted by blowing with oxygen at temperatures up to 1600 °C (2900 °F). The metal product is granulated with water, and the dried metal granules are treated in high-pressure (6.7 MPa, or 970 psi) reactors with carbon monoxide at 150 °C (300 °F) to form nickel carbonyl and some iron carbonyl. The mixed carbonyls are separated by fractionation, and the pure nickel carbonyl is decomposed at approximately 200 °C (390 °F) to yield high-purity nickel pellets and nickel powder for market.

There is a simpler procedure that can be used to process nickel sulfide ores with lower copper contents. As shown by process B in Fig. 2, selective flotation is employed to produce a nickel concentrate low in copper and a small amount of copper concentrate for treatment elsewhere. The dewatered nickel concentrate is fluid-bed-roasted for partial elimination of sulfur, and the calcine plus flux is smelted in arc-type electric furnaces. Waste furnace slag is granulated for disposal while the molten matte is transferred to Pierce-Smith converters for further upgrading to Bessemer matte. The conventional procedure of flux addition and blowing with air removes all but traces of iron from the matte, and the slag produced is returned to the electric furnace for recovery of metal values. The converter matte, essentially nickel sulfide (Ni_3S_2), is cast into anodes and electro-

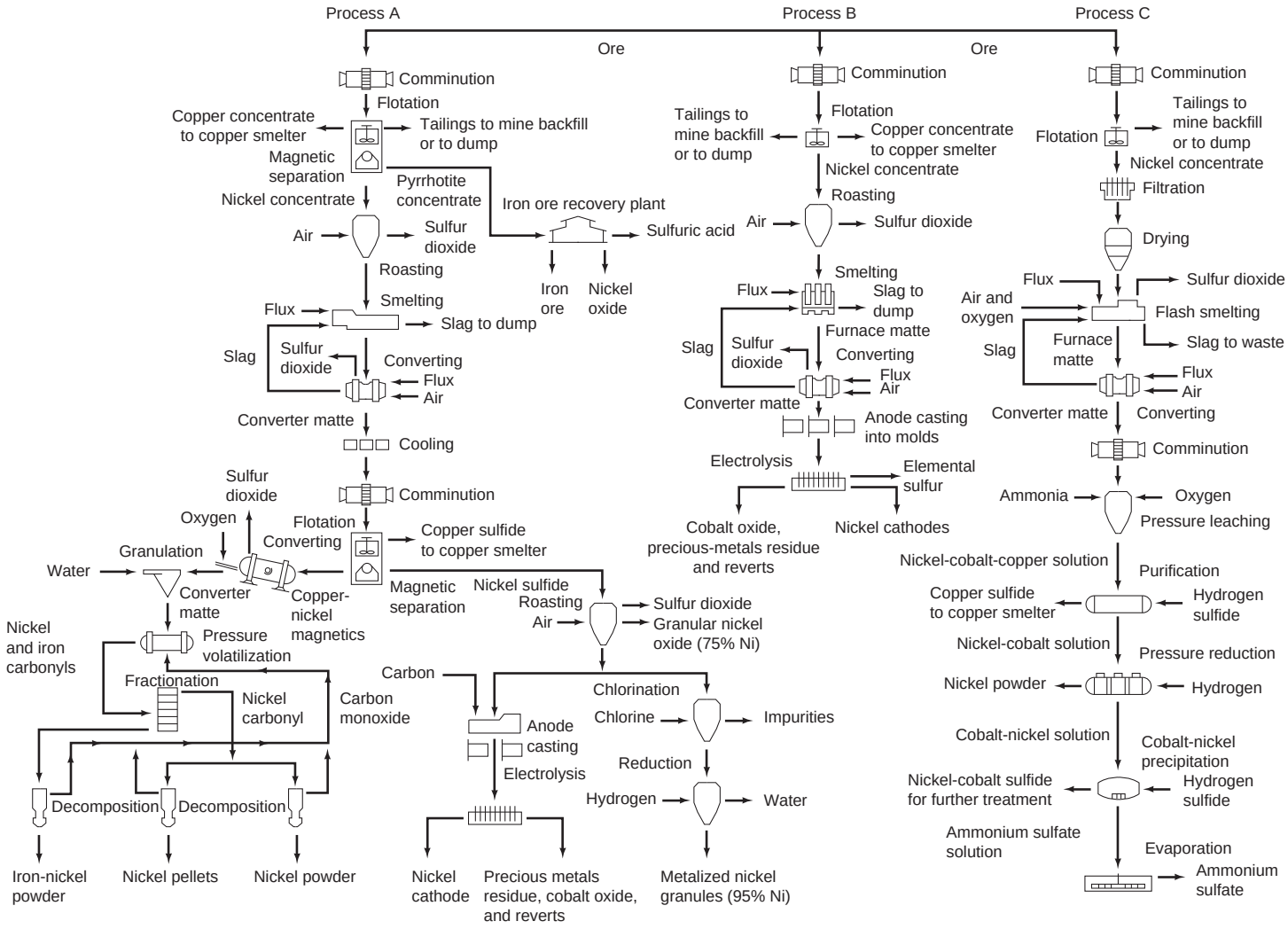


Fig. 2 Flow sheets for three methods of nickel recovery from sulfide ores. See text for processing details. Source: Ref 3

lyzed to yield elemental sulfur at the anode and pure nickel at the cathode. The refining operation also produces cobalt oxide and precious-metal residues.

In the all-hydrometallurgical Sherritt process (see process C in Fig. 2), the nickel ore is concentrated by conventional froth flotation, and the dried nickel concentrate is flash-smelted with oxygen-enriched air and flux to produce furnace matte and waste slag. The furnace matte is cooled, crushed, and finely ground as feed for the hydrometallurgical plant, where it is leached under pressure with a strong ammonia solution and air to solubilize the base metal values, with the simultaneous production of ammonium sulfate. The pregnant leach liquor is treated to remove impurities and then reduced with hydrogen at elevated pressure (3 MPa, or 435 psi) and temperature (190 °C, or 375 °F) to yield a granular nickel powder product. The tail liquor from this operation is treated further to recover ammonium sulfate crystals and a mixed nickel-cobalt sulfide.

Recovery from Laterite Ores. The bulk of the nickel originating from lateritic ores is marketed as ferronickel. The process employed is basically simple and involves drying and preheating the ore, usually under reduction conditions. The hot charge is then further reduced and melted in an electric arc furnace, and the crude metal is refined and cast into ferronickel pigs. A typical operation is shown in Fig. 3 (process A).

A substantial amount of nickel is produced from lateritic ores by the nickel-sulfide matte technique. In this process the ore is mixed with gypsum or other sulfur-containing material such as high-sulfur fuel oil, followed by a reduction and smelting operation to form matte. As in the treatment of sulfide concentrates, the molten furnace matte is upgraded in either conventional or top-blown rotary converters to a high-grade matte, which can be further refined by roasting and reduction to a metallized product. An example of this procedure is shown in Fig. 3 (process B).

Other large-scale operations are based on selective reduction of the ore followed by ammoniacal leaching at atmospheric pressure to dissolve the nickel values. The pregnant liquor is treated to remove impurities and then heated in suitable vessels to drive off ammonia and carbon dioxide and to precipitate a basic nickel carbonate. This material may be sintered under reducing conditions to yield a metallized nickel oxide sinter, or the carbonate may be redissolved in ammoniacal solution and then treated with hydrogen under pressure to yield nickel powder for briquetting. This process is depicted by process C in Fig. 3. Process D in Fig. 3 depicts a process wherein limonitic-type ores are leached with sulfuric acid at elevated temperature and pressure to solubilize nickel and cobalt. The pregnant solution is then treated with hydrogen sulfide to precipitate mixed nickel-cobalt sulfides. This precipitate may be treated by the Sherritt pressure, ammonia-leach process to yield separate nickel and cobalt powders.

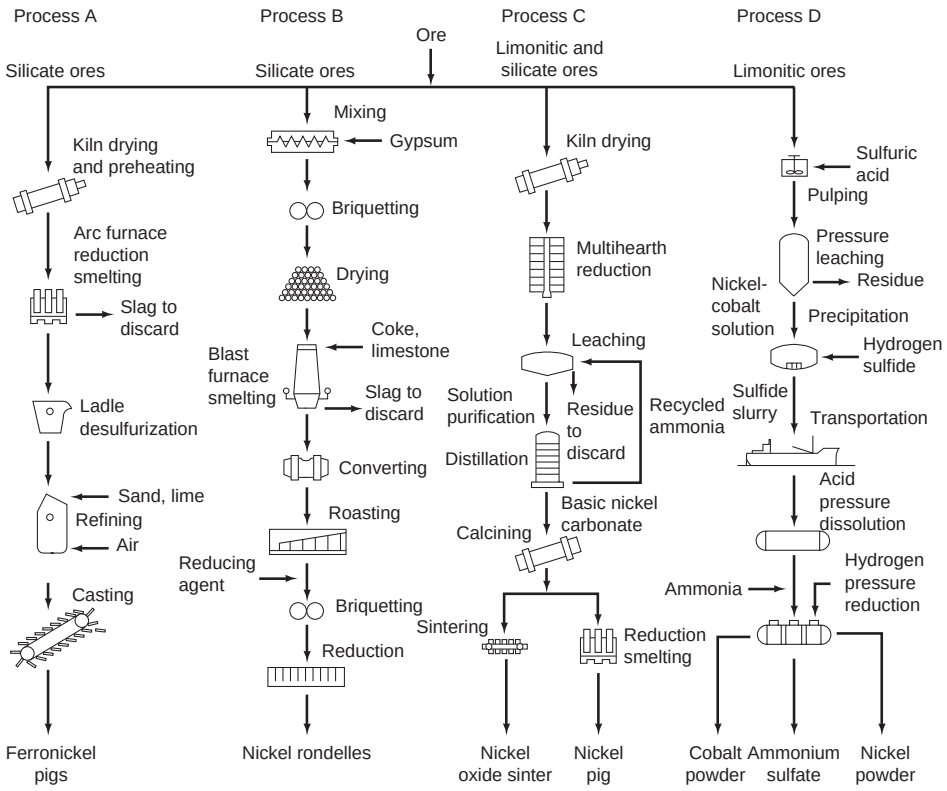


Fig. 3 Flow sheets for four methods of nickel recovery from laterite ores. See text for processing details. Source: Ref 3

End Uses of Nickel

According to the Nickel Development Institute, worldwide consumption of nickel can be broken into the following market segments:

Use	Nickel consumption, %
Stainless steel	62.7
Nickel-base alloys	11.9
Plating	9.7
Alloy steels	9.0
Foundry products	3.5
Copper-base alloys	1.4
Other	1.8

Consumption statistics in the United States follow similar trends (Table 1), with stainless steels making up about 55% of all nickel consumed. According to the American Iron and Steel Institute, nickel-bearing grades accounted for 63% of the total stainless steel production for 1997. Demand for austenitic stainless steels is expected to continue to drive the world nickel market for at least another 20 years. Demand for nickel-bearing superalloys is also expected to grow. In 1997, U.S. consumption of primary nickel in superalloys increased almost 20% because of growing orders in the aerospace industry (Table 1).

The use of primary nickel by battery manufacturers is another potential growth market for nickel. Rechargeable nickel-cadmium and nickel-metal hydride batteries are used in handheld power tools, cellular telephones, laptop computers, and camcorders. Nickel base batteries, including the more recently developed sodium metal-nickel battery called the ZEBRA (Zero Emission Batterie Research Activity), are also being used in electric vehicles and the rapidly growing electric scooter/bicycle market. Nickel consumption patterns could change significantly due to tightening oil supplies combined with increased oil and gasoline prices. The market for large energy-storage devices for nationwide communications systems and for emergency power supplies would also grow, further encouraging the scale-up of both nickel-metal hydride and sodium metal-nickel batteries.

Table 1 Consumption of nickel in the United States by end use

	Form/tonnes of contained nickel(a)(b)(c)								
								Grand total	
Use	Metal	Ferronickel	Oxide and oxide sinter	Chemicals	Other forms	Total primary	Secondary (scrap)	1997	1996
Cast irons	168	W	…	1	45	214	428	642	563
Chemicals and chemical uses	W	…	W	2,730	…	2,730	…	2,730	5,350
Electric, magnet, expansion alloys	W	W	…	(d)	…	(d)	W	W	W
Electroplating (sales to platers)	15,800	…	W	61	1	15,800	…	15,800	16,300
Nickel-copper and copper-nickel alloys	2,650	W	W	…	W	2,650	3,390	6,040	7,280
Other nickel and nickel alloys	17,000	W	W	…	W	17,000	2,040	19,100	19,300
Steel									
Stainless and heat resistant	26,100	21,000	1,760	…	57	48,900	56,900	106,000	94,100
Alloys (excludes stainless)	5,180	1,090	1,060	(d)	W	7,320	1,330	8,650	6,970
Superalloys	18,200	…	(d)	1	465	18,700	W	18,700	15,600
Other(e)	6,000	410	79	645	1,070	8,210	4,790	13,000	13,300
Total reported	**91,000**	**22,500**	**2,890**	**3,440**	**1,640**	**122,000**	**68,800**	**190,000**	**179,000**
Total all companies, apparent	**NA**	**NA**	**NA**	**NA**	**NA**	**154,000**	**38,100**	**192,000**	**181,000**

(a) Data are rounded to three significant digits and may not add to totals shown. (b) W, withheld to avoid disclosing company proprietary data; included with "Other.". (c) NA, not applicable. (d) Less than ½ unit. (e) Includes batteries, catalysts, ceramics, coinage, other alloys containing nickel, and data indicated by symbol "W." Source: U.S. Geological Survey

REFERENCES

1. S.J. Rosenberg, *Nickel and Its Alloys*, National Bureau of Standards Monograph 106, U.S. Department of Commerce, May 1968
2. W. Betteridge, *Nickel and Its Alloys*, Ellis Horwood Ltd., 1984
3. A. Illis, Nickel Metallurgy, *McGraw-Hill Encyclopedia of Science and Technology*, Vol 11 (MET-NIC), 7th ed., 1992, p 711–714

ASM Specialty Handbook: Nickel, Cobalt, and Their Alloys
J.R. Davis, editor, p 7-13
DOI:10.1361/ncta2000p013

Copyright © 2000 ASM International®
All rights reserved.
www.asminternational.org

Uses of Nickel

THE MOST IMPORTANT INDUSTRIAL USE of nickel is that of an alloying element in ferrous alloys, including stainless steels, low-alloy steels, cast irons, and some specialty steels. Nickel is also used as an alloying element in nonferrous alloys, most notably copper alloys. Other important end uses for nickel include nickel-base alloys used for corrosion resistant and heat resistant applications, nickel coatings (primarily electroplated nickel), and nickel powders in powder metallurgy (P/M) alloys, coinage, battery electrodes, and filters. The role of nickel as a catalyst in chemical processes is perhaps the least known of its uses. Finely divided nickel-base catalysts are key to several important reactions, including the hydrogenation of vegetable oils, reforming of hydrocarbons, and the production of fertilizers, pesticides, and fungicides.

Nickel is also an important component in various battery systems. Nickel-cadmium rechargeable batteries containing nickel electrodes and nickel hydroxide have been in use for a number of years. Nickel metal-hydride batteries have been introduced more recently, employing some nickel-rare earth alloys to absorb large amounts of hydrogen. These higher performance rechargeable batteries have, in turn, led to improved performance from cordless power tools, portable computers, and other mobile electronic devices. The hydrogen storage alloys may find wider application if greater use is made of hydrogen as a fuel in the future.

Nickel in Ferrous Alloys

Stainless steels, principally the austenitic 300-series, account by far for the largest consumption of nickel. More than 50% of the nickel consumed in the United States is used in stainless steels. Table 1 lists the chemical compositions of commonly used nickel-bearing austenitic stainless steels.

Nickel, in sufficient quantities, will stabilize the austenitic structure; this greatly enhances mechanical properties and fabrication characteristics. Nickel is effective in promoting repassivation, especially in reducing environments. Nickel is particularly useful in resisting corrosion in mineral acids. Increasing nickel content in an 18% chromium steel to approximately 8 to 10% decreases resistance to stress-corrosion cracking (SCC), but further increases begin to restore SCC resistance. Resistance in most service environments is achieved at approximately 30% Ni. Figure 1 shows the effect of increasing nickel content on the resistance to chloride SCC of stainless steel test specimens. Nickel is also beneficial when resistance to cyclic oxidation is a requirement.

In the more recently developed ferritic grades, in which the nickel addition is less than that required to destabilize the ferritic phase (≤2 wt% Ni), there are still substantial effects. In this range, nickel increases yield strength, toughness, and resistance to reducing acids, but it makes the ferritic stainless steels susceptible

Table 1 Chemical compositions of nickel-bearing standard (SAE-AISI) austenitic stainless steels

Some nonstandard grades have nickel contents of up to approximately 35%.

UNS No.	Type/ designation	Composition(a), %							
		C	Mn	Si	Cr	Ni	P	S	Other
S20100	201	0.15	5.5–7.5	1.00	16.0–18.0	3.5–5.5	0.06	0.03	0.25 N
S20200	202	0.15	7.5–10.0	1.00	17.0–19.0	4.0–6.0	0.06	0.03	0.25 N
S20500	205	0.12–0.25	14.0–15.5	1.00	16.5–18.0	1.0–1.75	0.06	0.03	0.32–0.40 N
S30100	301	0.15	2.0	1.00	16.0–18.0	6.0–8.0	0.045	0.03	…
S30200	302	0.15	2.0	1.00	17.0–19.0	8.0–10.0	0.045	0.03	…
S30215	302B	0.15	2.0	2.0–3.0	17.0–19.0	8.0–10.0	0.045	0.03	…
S30300	303	0.15	2.0	1.00	17.0–19.0	8.0–10.0	0.20	0.15 min	0.6 Mo(b)
S30323	303Se	0.15	2.0	1.00	17.0–19.0	8.0–10.0	0.20	0.06	0.15 min Se
S30400	304	0.08	2.0	1.00	18.0–20.0	8.0–10.5	0.045	0.03	…
S30403	304L	0.03	2.0	1.00	18.0–20.0	8.0–12.0	0.045	0.03	…
S30451	304N	0.08	2.0	1.00	18.0–20.0	8.0–10.5	0.045	0.03	0.10–0.16 N
S30500	305	0.12	2.0	1.00	17.0–19.0	10.5–13.0	0.045	0.03	…
S30800	308	0.08	2.0	1.00	19.0–21.0	10.0–12.0	0.045	0.03	…
S30900	309	0.20	2.0	1.00	22.0–24.0	12.0–15.0	0.045	0.03	…
S30908	309S	0.08	2.0	1.00	22.0–24.0	12.0–15.0	0.045	0.03	…
S31000	310	0.25	2.0	1.50	24.0–26.0	19.0–22.0	0.045	0.03	…
S31008	310S	0.08	2.0	1.50	24.0–26.0	19.0–22.0	0.045	0.03	…
S31400	314	0.25	2.0	1.5–3.0	23.0–26.0	19.0–22.0	0.045	0.03	…
S31600	316	0.08	2.0	1.00	16.0–18.0	10.0–14.0	0.045	0.03	2.0–3.0 Mo
S31620	316F	0.08	2.0	1.00	16.0–18.0	10.0–14.0	0.20	0.10 min	1.75–2.5 Mo
S31603	316L	0.03	2.0	1.00	16.0–18.0	10.0–14.0	0.045	0.03	2.0–3.0 Mo
S31651	316N	0.08	2.0	1.00	16.0–18.0	10.0–14.0	0.045	0.03	2.0–3.0 Mo; 0.10–0.16 N
S31700	317	0.08	2.0	1.00	18.0–20.0	11.0–15.0	0.045	0.03	3.0–4.0 Mo
S31703	317L	0.03	2.0	1.00	18.0–20.0	11.0–15.0	0.045	0.03	3.0–4.0 Mo
S32100	321	0.08	2.0	1.00	17.0–19.0	9.0–12.0	0.045	0.03	5 × %C min Ti
S34700	347	0.08	2.0	1.00	17.0–19.0	9.0–13.0	0.045	0.03	10 × %C min Nb
S34800	348	0.08	2.0	1.00	17.0–19.0	9.0–13.0	0.045	0.03	0.2 Co; 10 × %C min Nb; 0.10 Ta
S38400	384	0.08	2.0	1.00	15.0–17.0	17.0–19.0	0.045	0.03	…

(a) Single values are maximum values unless otherwise indicated. (b) Nominal compositions

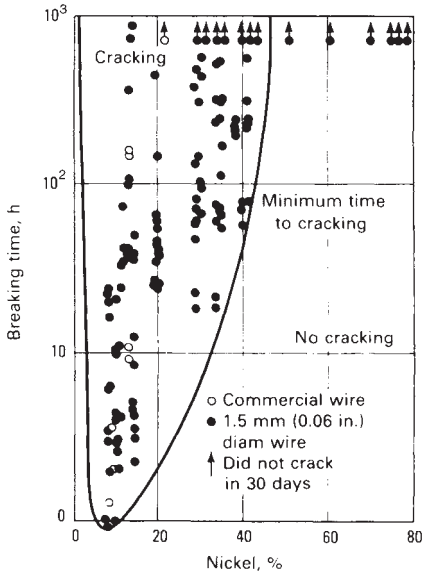


Fig. 1 Effect of nickel additions to a 17 to 24% Cr steel on resistance to SCC in boiling 42% magnesium chloride. 1.5 mm (0.06 in.) diam wire specimens deadweight loaded to 228 or 310 MPa (33 or 45 ksi). Source: Ref 1

to SCC in concentrated magnesium chloride solutions. More detailed information on the effect of nickel on the properties of stainless steels can be found in Ref 2.

Low-Alloy Steels. Nickel, when used as an alloying element in low-alloy structural steels, is a ferrite strengthener. Because nickel does not form any carbide compounds in steel, it remains in solution in the ferrite, thus strengthening and toughening the ferrite phase. Nickel steels are easily heat treated because nickel lowers the critical cooling rate. In combination with chromium, nickel produces alloy steels with greater hardenability, higher impact strength, and greater fatigue resistance. Nickel alloy steels have superior low-temperature strength and toughness (Fig. 2). Reference 4 describes the effects of nickel additions on the properties and characteristics of low-alloy steels.

As indicated in Table 2, the nickel content in nickel-bearing low-alloy steels generally ranges from 0.30 to 5.00%, although some nickel steels for cryogenic service contain higher nickel contents. For example, 8% nickel steels are specified for equipment operating at temperatures as low as –170 °C (–275 °F) and are covered by ASTM standard A 553. The 9% nickel steels, which can be used at temperatures as low as –195 °C (–320 °F), are covered by both ASTM A 353 and ASTM A 553.

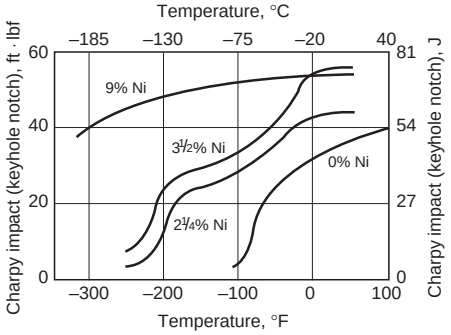


Fig. 2 Effect of nickel on toughness of normalized and tempered 13 mm (½ in.) plates of carbon steel. Source: Ref 3

Maraging steels develop high strength and hardness by quite different mechanisms than steels dependent on carbon content for strength. Despite the low carbon content (carbon is actually considered an impurity), the high nickel content (18% Ni) of the maraging steels ensures that martensite forms on air cooling (the physical metallurgy of maraging steels is detailed in Ref 5). The low-carbon, low-strength martensite is then hardened by fine-scale precipitation of intermetallic compounds, such as Ni_3Mo, by aging around 480 °C (895 °F). The maraging steels are used for many structural applications that require ultrahigh strength and high fracture toughness. Nominal compositions, heat treatments, and properties of maraging steels are listed in Table 3.

Austenitic manganese steels are wear-resistant steels containing nominally about 1.2% C and 12.5% Mn. Special grades contain small additions of nickel, chromium, or molybdenum. Nickel, in amounts up to 4%, stabilizes the austenite because it remains in solid solution. It is particularly effective for suppressing precipitates of carbide platelets, which can form between approximately 300 and 550 °C (570 and 1020 °F). Therefore, the presence of nickel helps retain nonmagnetic qualities in the steel, especially in the decarburized surface layers. Nickel additions increase ductility, decrease yield strength slightly, and lower the abrasion resistance of manganese steel. Nickel is used primarily in the lower-carbon or weldable grades of cast manganese steel and in wrought manganese steel products (including welding electrodes). In wrought products, nickel is sometimes used in conjunction with molybdenum. Table 4 contains compositional and tensile data for nickel manganese steels used in naval applications.

Other Nickel-Containing Steels. Nickel is added to some tool steels and iron-nickel-cobalt steels to improve toughness. Examples include the following:

- Air-hardening cold-work tool steels such as A9 (1.5% Ni) and A10 (1.75% Ni)
- Low-carbon mold steels such as P3 (1.25% Ni), P6 (3.5% Ni), and P21 (4% Ni)
- Ultrahigh strength steels capable of yield strengths reaching 1380 MPa (200 ksi) and fracture toughness (K_{Ic}) values of ≥100 MPa $\sqrt{m}$ (91 ksi$\sqrt{in.}$). Examples include HP-9-4-30 (7.5% Ni), AF1410 (10% Ni), and AerMet 100 (11.5% Ni).

Cast Irons. Nickel is used to enhance the strength, toughness, hardenability, and corrosion resistance of cast irons. Small additions of nickel up to 5% have been made to low-alloy gray cast iron for many years when improved properties and a more uniform graphite structure are required. In low-alloy ductile irons,

Table 2 Nickel-bearing alloy steels covered by SAE/AISI designations

Numerals and digits	Type of steel and nominal alloy content, %
Nickel steels	
23*xx*	Ni 3.50
25*xx*	Ni 5.00
Nickel-chromium steels	
31*xx*	Ni 1.25; Cr 0.65 and 0.80
32*xx*	Ni 1.75; Cr 1.07
33*xx*	Ni 3.50; Cr 1.50 and 1.57
34*xx*	Ni 3.00; Cr 0.77
Nickel-chromium-molybdenum steels	
43*xx*	Ni 1.82; Cr 0.50 and 0.80; Mo 0.25
43BV*xx*	Ni 1.82; Cr 0.50; Mo 0.12 and 0.25; V 0.03 min
47*xx*	Ni 1.05; Cr 0.45; Mo 0.20 and 0.35
81*xx*	Ni 0.30; Cr 0.40; Mo 0.12
86*xx*	Ni 0.55; Cr 0.50; Mo 0.20
87*xx*	Ni 0.55; Cr 0.50; Mo 0.25
88*xx*	Ni 0.55; Cr 0.50;p Mo 0.35
93*xx*	Ni 3.25; Cr 1.20; Mo 0.12
94*xx*	Ni 0.45; Cr 0.40; Mo 0.12
97*xx*	Ni 0.55; Cr 0.20; Mo 0.20
98*xx*	Ni 1.00; Cr 0.80; Mo 0.25
Nickel-molybdenum steels	
46*xx*	Ni 0.85 and 1.82; Mo 0.20 and 0.25
48*xx*	Ni 3.50; Mo 0.25

Table 3 Compositions, heat treatments, and typical mechanical properties of standard 18Ni maraging steels

Grade	Nominal composition, wt%	Heat treatment(a)	Tensile strength MPa	Tensile strength ksi	Yield strength MPa	Yield strength ksi	Elongation in 50 mm (2 in.), %	Reduction in area, %	Fracture toughness MPa$\sqrt{m}$	Fracture toughness ksi$\sqrt{in.}$
18Ni(200)	Fe-18Ni-3.3Mo-8.5Co-0.2Ti-0.1Al	A	1500	218	1400	203	10	60	155–240	140–220
18Ni(250)	Fe-18Ni-5.0Mo-8.5Co-0.4Ti-0.1Al	A	1800	260	1700	247	8	55	120	110
18Ni(300)	Fe-18Ni-5.0Mo-9.0Co-0.7Ti-0.1Al	A	2050	297	2000	290	7	40	80	73
18Ni(350)	Fe-18Ni-4.2Mo-12.5Co-1.6Ti-0.1Al	B	2450	355	2400	348	6	25	35–50	32–45
18Ni(Cast)	Fe-17Ni-4.6Mo-10.0Co-0.3Ti-0.1Al	C	1750	255	1650	240	8	35	105	95

(a) Treatment A: solution treat 1 h at 820 °C (1500 °F), then age 3 h at 480 °C (900 °F). Treatment B: solution treat 1 h at 820 °C (1500 °F), then age 12 h at 480 °C (900 °F). Treatment C: anneal 1 h at 1150 °C (2100 °F), age 1 h at 595 °C (1100 °F), solution treat 1 h at 820 °C (1500 °F) and age 3 h at 480 °C (900 °F)

Table 4 Compositions and tensile properties of 14Mn-Ni steels meeting MIL-S-17758 (Ships)

Element or property	Alloy(a) Type 1	Alloy(a) Type 2
Composition limits		
Carbon	0.70–0.90	0.70–0.90
Manganese	13–15	13–15
Silicon	0.50–1.00	0.50–1.00
Nickel	3.0–3.5	1.75–2.25
Chromium	0.50 max	0.50 max
Molybdenum	···	0.35–0.55
Phosphorus	0.07 max	0.07 max
Sulfur	0.05 max	0.05 max
Minimum tensile properties		
Tensile strength, MPa (ksi)	690 (100)	690 (100)
Yield strength(b), MPa (ksi)	345 (50)	345 (50)
Elongation in 50 mm (2 in.),%	18	18
Elongation plus reduction in area, %	56	56

(a) These grades are intended primarily for nonmagnetic applications and have maximum surface permeability of 1.2, measured with a go/no go low permeability, μ, indicator, as described in MIL-I-17214 and MIL-N-17387. The comparable casting specification, MIL-S-17249 (Ships), includes only the standard 1.00 to 2.35% C grade. (b) 0.2% offset

nickel, in concert with molybdenum, manganese, and/or copper, is added to improve hardenability. Nickel contents generally range from 0.5 to 3.75%. In austempered ductile irons, up to 2% Ni may be used to improve hardenability. For austempering temperatures below 350 °C (675 °F), nickel reduces tensile strength slightly but increases ductility and fracture toughness.

Nickel is also added to high-alloy white, gray, and ductile cast irons. The oldest group of high-alloy irons of industrial importance, the nickel-chromium white irons (Ni-Hard irons), have been produced for more than 50 years and are cost-effective materials for crushing and grinding. In these martensitic white irons, nickel is the primary alloying element, because 3 to 5% Ni is effective in suppressing the transformation of the austenite matrix to pearlite, thus ensuring that a hard, martensitic structure (usually containing significant amounts of retained austenite) will develop on cooling in the mold. Chromium is included in these alloys, at levels from 1.4 to 4% (one alloy modification contains 7 to 11% Cr), to ensure that the irons solidify carbidic (i.e., to counteract the graphitizing effect of nickel). Compositions of Ni-Hard irons are listed in Table 5.

The nickel-alloyed austenitic irons (Ni-Resists) are produced in both gray and ductile cast iron versions for elevated-temperature service. Austenitic gray irons date back to the 1930s, when they were specialized materials of minor importance. After the invention of ductile iron, austenitic grades of ductile iron were also developed. These nickel-alloyed austenitic irons have been used in applications requiring corrosion resistance, wear resistance, and elevated-temperature stability and strength. Additional advantages include low thermal expansion coefficients, nonmagnetic properties, and good toughness at low temperatures. As listed in Tables 6 and 7, nickel contents in Ni-Resist irons range from approximately 15 to 35%.

Nickel and Nickel-Base Alloys

Characteristics. The second most important end use for nickel is as the base metal for a wide variety of alloy systems. Nickel and nickel-base alloys are vitally important to modern industry because of their ability to withstand a wide variety of severe operating conditions involving corrosive environments, high temperatures, high stresses, and combinations of these factors. There are several reasons for these capabilities. Pure nickel is ductile and tough because it possesses a face-centered cubic (fcc) structure up to its melting point (1453 °C, or 2647 °F). Therefore, nickel and nickel alloys are readily fabricated by conventional methods—wrought, cast, and powder metallurgy (P/M) products are available—and they offer freedom from the ductile-to-brittle transition behavior of other metals and alloys, including steels. Nickel has good resistance to corrosion in the normal atmosphere, in natural freshwaters, and in deaerated nonoxidizing acids, and it has excellent resistance to corrosion by caustic alkalies. Therefore, nickel offers very useful corrosion resistance, and it is an excellent base on which to develop specialized alloys that can capitalize on the unique properties of specific alloying elements.

Because nickel has an extensive solid solubility for many alloying elements, the microstructure of nickel alloys consists of the fcc solid-solution austenite (γ) in which dispersoid and precipitate particles can form. Nickel forms a complete solid solution with copper and has nearly complete solubility with iron. It can dissolve ~35% Cr, 20% each of molybdenum and tungsten, and 5 to 10% each of aluminum, titanium, manganese, and vanadium. Thus, the tough, ductile fcc matrix can dissolve extensive amounts of elements in various combinations to provide solution hardening, as well as improved corrosion and oxidation resistance.

The degree of solution hardening has been related to the atomic size difference between nickel and the alloying element, and, therefore, the ability of the solute to interfere with dislocation motion. Tungsten, molybdenum, niobium, tantalum, and aluminum, when aluminum is left in solution, are strong solution hardeners, with tungsten, niobium, tantalum, and molybdenum also being effective at temperatures above 0.6 T_m (T_m is melting temperature), where diffusion-controlled creep strength is important. Iron, cobalt, titanium, chromium, and vanadium are weaker solution-hardening elements.

Finally, unique intermetallic phases can form between nickel and some nickel alloying elements. For example, aluminum and titanium are usually added together for the age-hardening γ′ precipitate $Ni_3(Al, Ti)$. This enables the formation of alloys with very high strengths for high-temperature services.

Applications. Nickel and nickel-base alloys are used for a wide variety of applications, the majority of which involve corrosion resistance and/or heat resistance. Some of these include the following:

- *Chemical and petrochemical industries:* bolts, fans, valves, reaction vessels, tubing, transfer piping, pumps
- *Pulp and paper mills:* tubing, doctor blades, bleaching circuit equipment, scrubbers

Table 5 Composition of abrasion-resistant Ni-Hard white irons per ASTM A 532

			Composition, wt%								
Class	Type	Designation	C	Mn	Si	Ni	Cr	Mo	Cu	P	S
I	A	Ni-Cr-HiC	2.8–3.6	2.0 max	0.8 max	3.3–5.0	1.4–4.0	1.0 max	…	0.3 max	0.15 max
I	B	Ni-Cr-LoC	2.4–3.0	2.0 max	0.8 max	3.3–5.0	1.4–4.0	1.0 max	…	0.3 max	0.15 max
I	C	Ni-Cr-GB	2.5–3.7	2.0 max	0.8 max	4.0 max	1.0–2.5	1.0 max	…	0.3 max	0.15 max
I	D	Ni-HiCr	2.5–3.6	2.0 max	2.0 max	4.5–7.0	7.0–11.0	1.5 max	…	0.10 max	0.15 max

Table 6 Compositions of flake-graphite (gray) austenitic cast irons per ASTM A 436

		Composition, %					
Type	UNS No.	TC(a)	Si	Mn	Ni	Cu	Cr
1(b)	F41000	3.00 max	1.00–2.80	0.50–1.50	13.50–17.50	5.50–7.50	1.50–2.50
1b	F41001	3.00 max	1.00–2.80	0.50–1.50	13.50–17.50	5.50–7.50	2.50–3.50
2(c)	F41002	3.00 max	1.00–2.80	0.50–1.50	18.00–22.00	0.50 max	1.50–2.50
2b	F41003	3.00 max	1.00–2.80	0.50–1.50	18.00–22.00	0.50 max	3.00–6.00(d)
3	F41004	2.60 max	1.00–2.00	0.50–1.50	28.00–32.00	0.50 max	2.50–3.50
4	F41005	2.60 max	5.00–6.00	0.50–1.50	29.00–32.00	0.50 max	4.50–5.50
5	F41006	2.40 max	1.00–2.00	0.50–1.50	34.00–36.00	0.50 max	0.10 max(e)
6(f)	F41007	3.00 max	1.50–2.50	0.50–1.50	18.00–22.00	3.50–5.50	1.00–2.00

(a) TC, total carbon. (b) Type 1 is recommended for applications in which the presence of copper offers corrosion resistance advantages. (c) Type 2 is recommended for applications in which copper contamination cannot be tolerated, such as handling of foods or caustics. (d) Where some machining is required, 3.0 to 4.0 Cr is recommended. (e) Where increased hardness, strength, and heat resistance are desired and where increased expansivity can be tolerated, Cr may be increased to 2.5 to 3.0%. (f) Type 6 also contains 1.0% Mo.

Table 7 Compositions of nodular-graphite (ductile) austenitic cast irons per ASTM A 439

		Composition, %					
Type	UNS No.	TC(a)	Si	Mn	P	Ni	Cr
D-2	F43000	3.00 max	1.50–3.00	0.70–1.25	0.08 max	18.0–22.0	1.75–2.75
D-2b	F43001	3.00 max	1.50–3.00	0.70–1.25	0.08 max	18.0–22.0	2.75–4.00
D-2c	F43002	2.90 max	1.00–3.00	1.80–2.40	0.08 max	21.0–24.0	0.50 max
D-3	F43003	2.60 max	1.00–2.80	1.00 max	0.08 max	28.0–32.0	2.50–3.50
D-3a	F43004	2.60 max	1.00–2.80	1.00 max	0.08 max	28.0–32.0	1.00–1.50
D-4	F43005	2.60 max	5.00–6.00	1.00 max	0.08 max	28.0–32.0	4.50–5.50
D-5	F43006	2.60 max	1.00–2.80	1.00 max	0.08 max	34.0–36.0	0.10 max
D-5b	F43007	2.40 max	1.00–2.80	1.00 max	0.08 max	34.0–36.0	2.00–3.00
D-5S	…	2.30 max	4.9–5.5	1.00 max	0.08 max	34.0–37.0	1.75–2.25

(a) TC, total carbon

- *Aircraft gas turbines:* disks, combustion chambers, bolts, casings, shafts, exhaust systems, blades, vanes, burner cans, afterburners, thrust reversers
- *Steam turbine power plants:* bolts, blades, stack gas reheaters
- *Reciprocating engines:* turbochargers, exhaust valves, hot plugs, valve seat inserts
- *Metal processing:* hot-work tools and dies
- *Medical applications:* dentistry uses, prosthetic devices
- *Space vehicles:* aerodynamically heated skins, rocket engine parts
- *Heat-treating equipment:* trays, fixtures, conveyor belts, baskets, fans, furnace mufflers
- *Nuclear power systems:* control rod drive mechanisms, valve stems, springs, ducting
- *Pollution control equipment*: scrubbers, flue gas desulfurization equipment (liners, fans, stack gas reheaters, ducting)
- *Metals processing mills:* ovens, afterburners, exhaust fans
- *Coal gasification and liquefaction systems:* heat exchangers, repeaters, piping
- *Automotive industry:* spark plugs, glow plugs (in diesel engines), catalytic converters

Table 8 provides guidelines for the selection of various nickel alloys for specific applications. Compositions and properties of these alloys are presented in the four articles that immediately follow in this Handbook.

A number of other applications exploit the unique physical properties of nickel-base or high-nickel alloys. These include the following:

- Nickel-iron low-expansion alloys
- Nickel-chromium or nickel-chromium-iron electrical resistance alloys
- Nickel-iron soft magnetic alloys
- Nickel-titanium shape memory alloys

These alloys are described in the article "Special-Purpose Nickel Alloys" in this Handbook.

Nickel Coatings

A brief summary of some of the important processes for depositing nickel and nickel alloy coatings is given below. More detailed information can be found in the article "Nickel Coatings" in this Handbook.

The nickel plating process is used extensively for decorative, engineering, and electroforming purposes because the appearance and other properties of electrodeposited nickel can be varied over wide ranges by controlling the composition and operating parameters of the plating solution. Decorative applications account for approximately 80% of the nickel consumed in plating; 20% is consumed in engineering and electroforming purposes.

Electroless nickel coatings are produced by the autocatalytic chemical reduction of nickel ions from an aqueous solution. They do not require electrical current to be produced. Three types of electroless coatings are produced: nickel-phosphorus (6 to 12% P), nickel-boron (~5% B), and composite coatings (combination of nickel-phosphorus and silicon carbide, fluorocarbons, or diamond particles). These coatings are used for applications requiring a combination of corrosion and wear resistance.

Thermal Spray Coatings. Atomized nickel alloy powders deposited by various thermal spray techniques are used for wear-resistant applications. Alloys include nickel-chromium boride, nickel-chromium carbide, and nickel-tungsten carbide.

Weld-overlay coatings are applied for either wear-resistant applications (hardfacing alloys) or corrosion resistant applications (weld claddings). Hardfacing alloys include nickel-base/boride alloys and nickel-base/Laves phase alloys. Corrosion-resistant weld claddings that are generally applied on carbon steels include pure nickel, nickel-copper, nickel-chromium-iron, nickel-molybdenum, and nickel-chromium-molybdenum alloys.

Nickel in Nonferrous Alloys

Copper-nickel alloys, also commonly referred to as cupronickels, have desirable physical and mechanical properties and are resistant to corrosion in many media. Consequently, almost every possible composition from 1 to 50% Ni has been marketed under one or more trade names. Currently the most widely used alloys are 70Cu-30Ni (UNS C71500), 80Cu-20Ni (C71000), and the 90Cu-10Ni (C70600) copper-nickel groups. Properties of these and other cupronickels are given in Table 9.

Cupronickels containing 10 to 30% Ni have long been noted for their resistance to seawater, which led to many marine applications, particularly in the field of heat exchanger tubes, condensers, saltwater piping, and so forth. The 70Cu-30Ni alloy has the best general resistance to aqueous corrosion of all the commercially important copper alloys, but 90Cu-10Ni is often selected because it offers good resistance at lower cost. All three cupronickels are superior to coppers and to other copper alloys in resisting acid solutions and are highly resistant to SCC and impingement corrosion.

Nickel silvers are a family of copper-nickel-zinc alloys (nickel brasses) valued for their strength, formability, and corrosion and tarnish resistance, and, for some applications, metallic white color (the addition of nickel to brass gradually changes the normally yellow color to white so that at approximately 12% nickel, the typically brass appearance is gone). The two most common nickel silvers are 65Cu-18Ni-17Zn (C75200) and 55Cu-18Ni-27Zn (C77000). They have good resistance to corrosion in both fresh and salt waters. Primarily because of their high nickel content, these alloys are much more resistant to corrosion in saline solutions than are brasses of similar copper content. Properties of common nickel silvers are given in Table 9.

Coinage Alloys. The oldest use for copper-nickel alloys is coinage. In both the United States and Canada, 5-cent coins are composed of a 75Cu-25Ni (C71300) alloy. The U.S. 10-cent piece and 25-cent piece coins have a core of pure copper (C11000) that is clad with the 75Cu-25Ni alloy. The total nickel content of the coins is 8.33%. In Canada, dimes and quarters are made entirely from pure nickel. Canada has had coins composed of 100% Ni since at least 1922.

The European Monetary Union is planning to have its new euro coinage in circulation by January 1, 2002. For the most part these coins will be nickel free in order to minimize the potential risk of hypersensitive members of the public contracting nickel dermatitis.

Thermocouple and Electrical Resistance Alloys. Constantan, having an approximate composition of 55Cu-45Ni, has about the highest electrical resistivity, the lowest temperature coefficient of resistance, and the highest thermal emf against platinum of any of the copper-nickel alloys. Because of the first two of these properties, Constantan is used for electrical resistors, and, because of the latter property, for thermocouples.

Other nickel-containing resistance alloys include the copper-nickel "radio alloys" containing 78 to 98% Cu and 22 to 2% Ni and copper-manganese-nickel alloys, generally referred to as Manganins, which contain 4% Ni.

Permanent Magnet Alloys. Alnico alloys (aluminum-nickel-cobalt-iron) constitute a group of industrial permanent magnet materials developed in the 1940s and 1950s that are still widely used. Both cast (with equiaxed or columnar grain structures) and sintered forms of Alnico magnets are available. Nickel contents in the most commercially important grades range from 14 to 19%. Compositions and properties of Alnico alloys are given in the article "Uses of Cobalt" in this Handbook.

Nickel in Cobalt Alloys. Cobalt-base alloys are often designed with significant levels of nickel. The addition of nickel (frequently in the range of 10 to 35%) stabilizes the desired fcc matrix, contributes to solid-solution strengthening, and improves SCC resistance. More detailed information, including composition and property data, can be found in the articles "Cobalt-Base Alloys" and "Corrosion Behavior of Cobalt Alloys" in this Handbook.

Nickel Powders

Powder Metallurgy Steels. As with other forms of primary nickel, a major outlet for nickel powder is as an alloying element in P/M steels. The nickel-bearing low-alloy P/M steels generally contain from 0.45 to 6% Ni. Nickel strengthens ferrous P/M alloys by solid-solution strengthening and increases their hardenability.

Table 8 General properties and applications of nickel and nickel alloys

UNS No.	Common name	General properties	Applications
N02200	Nickel 200	Resistant to reducing acids, strong bases, high electrical conductivity	Chemical processing, electronics
N02201	Nickel 201	Same as Nickel 200 but also resists embrittlement at elevated temperature	Chemical processing, electronics
N02211	Nickel 211	Electrical	Electronics
N04400	Alloy 400	Resistant to a wide range of moderately aggressive environments, higher strength than nickel	Chemical processing, power, marine
N05500	Alloy K-500	High strength, age hardenable, corrosion similar to alloy 400	Pump shafts, impellers, springs, bolting, valve trim
N06002	Alloy HX	Oxidation resistance, high-temperature strength	Thermal processing, aerospace and LBGT
N06003	Alloy 80-20	Cyclic oxidation resistance	Resistance heating
N06004	Alloy 65-15	Oxidation resistance	Resistance heating braking resistors
N06022	Alloy C-22 Alloy 622	Resists highly aggressive oxidizing and reducing aqueous environments, resists localized corrosion	Chemical process, pollution control, pulp and paper
N06025	Alloy 602CA	Resistance to oxidizing atmospheres, high-temperature strength, and creep properties	Thermal processing, automotive
N06030	Alloy G-30	Resists highly oxidizing environments, phosphoric acid	Chemical process, phosphoric acid plants, pickling operations, nuclear waste processing
N06045	Alloy 45 TM	Sulfidation, oxidation resistance	Thermal processing
N06059	Alloy 59	Resists highly aggressive oxidizing and reducing aqueous environments, optimum resistance to localized corrosion	Chemical process, pollution control
N06075	Alloy 75	Oxidation resistance	Aerospace thermal processing, LBGT
N06200	Alloy C-2000	Resists highly aggressive oxidizing and reducing aqueous environments, advanced general corrosion	Chemical process
N06230	Alloy 230	High-temperature strength, oxidation, and nitridation resistance	Thermal processing
N06455	Alloy C-4	Resists highly aggressive aqueous environments, resists weld heat affected zone attack	Chemical process
N06600	Alloy 600	Resistant to reducing environments, high-temperature strength, and oxidation resistance	Chemical process, heat treating, power, electronic
N06601	Alloy 601	Resistance to oxidizing atmospheres, high-temperature strength, and creep properties	Thermal processing, automotive, chemical
N06601	Alloy 601GC	As above plus high temperature stability	Thermal processing
N06617	Alloy 617	High-temperature strength and creep properties. Oxidation resistance	Thermal processing, aerospace
N06625	Alloy 625	Resistant to many aqueous environments, high-temperature strength	Aerospace, chemical process, marine, automotive
N06626	Alloy 625 LCF	Resistant to low-cycle fatigue and many aqueous environments, high-temperature strength	Bellows, aerospace, automotive, chemical process
N06686	Alloy 686	Resists highly aggressive oxidizing and reducing aqueous environments, optimum resistance to localized corrosion	Chemical process, pollution control
N06950	Alloy G-50	Hydrogen sulfide SCC resistance	Oil and gas production
N06985	Alloy G-3	Aqueous corrosion resistance in a variety of environments	Chemical process and deep sour gas wells
N07001	Waspaloy	Age hardened, high-temperature strength, and oxidation resistance	Aerospace
N07031	Pyromet 31	Age hardened, high-temperature strength, sulfidation and oxidation resistance	Automotive
N07080	Alloy 80A	Age hardened, high-temperature strength, sulfidation and oxidation resistance	Automotive, aerospace, LBGT
N07090	Alloy 90	Age hardened, high-temperature strength	Automotive, springs, aerospace
N07214	Alloy 214	Oxidation resistance	Thermal processing
N07716	Alloy 625Plus	Resistant to many aqueous environments, high low-temperature strength, age hardened	Oil and gas production, marine
N07718	Alloy 718	Age hardened, high-temperature corrosion resistance	Aerospace and based gas turbines, oilfield, springs
N07725	Alloy 725	Resistant to many aqueous environments, high low-temperature strength, age hardened	Oil and gas production, marine
N07750	Alloy X-750	Age hardened	Automotive, spring
N07751	Alloy 751	Age hardened, oxidation resistance	Automotive
N07754	Alloy MA754	Mechanically alloyed, high-temperature strength	Aerospace
N08800	Alloy 800	Resists oxidation, moderately corrosive conditions	Heat exchanger tubing, power, heat treating, domestic appliances, petrochemical
N08810	Alloy 800H	High-temperature strength	Thermal processing petrochemical
N08811	Alloy 800HT	High -temperature strength, creep and oxidation resistance	Thermal processing petrochemical
N08825	Alloy 825	Resists wide range of corrosive environments and intergranular sensitization	Chemical process, oil and gas recovery, acid production, radioactive waste handling
N09925	Alloy 925	Resists wide range of corrosive environments, high low-temperature strength, age hardened	Oil and gas production, marine
N10276	Alloy C-276	Resists highly aggressive aqueous environments, resists localized corrosion	Chemical process, pollution control, oil and gas recovery
N10665 N10675 N10629	Alloy B-2 Alloy B-3 Alloy B-4	Resists highly reducing environments such as high temperature, concentrated hydrochloric acid	Chemical process
N12160	Alloy HR-160	Nitridation resistance	Thermal processing
R30556	Alloy 556	Sulfidation, carburization, and oxidation resistance	Thermal processing chemical
S35135	Alloy 684	Resists hot salt corrosion, fatigue, oxidation and aqueous corrosion	Automotive exhaust and other high-temperature applications
	Nickel 212	Electrical	Electronics
	Nickel 240	Electrical	Automotive spark plugs
	Alloy 671	Resistance to high sulfur coals and vanadium fuel oils	Superheater tubing
	Alloy DS	Resistance to oxidizing/reducing atmospheres	Thermal processing, resistance heating, braking resistors
	Alloy 803	Oxidation, sulfidation resistant	Thermal processing, petrochemical
	Alloy 70	Age hardened	Automotive
	Alloy 101	Age hardened	Automotive, aerospace
	Nimonic 86	High-temperature oxidation resistance	Aerospace, thermal processing
	INCOCLAD 671	Fuel ash corrosion resistance	Thermal processing
	Nimonic 105	Age hardened, high-temperature strength, and corrosion resistance	Aerospace
	Alloy PE16	Controlled thermal expansion	Nuclear fuel rods

LBGT, land-based gas turbines. Source: Ref 6

Table 9 Nominal compositions, product forms, and tensile properties of wrought cupronickels and nickel silvers

UNS No.	Nominal composition, %	Commercial forms(a)	Mechanical properties(b)				Elongation in 50 mm (2 in.)(b), %
			Tensile strength		Yield strength		
			MPa	ksi	MPa	ksi	
Cupronickels							
C70600 (copper-nickel, 10%)	88.7Cu, 1.3Fe, 10.0Ni	F, T	303–414	44–60	110–393	16–57	42–10
C71000 (copper-nickel, 20%)	79.0Cu, 21.0Ni	F, W, T	338–655	49–95	90–586	13–85	40–3
C71300	75Cu, 25Ni	F	338–655	49–95	90–586	13–85	40–3
C71500 (copper-nickel, 30%)	70.0Cu, 30.0Ni	F, R, T	372–517	54-75	138–483	20–70	45–15
C71700	67.8Cu, 0.7Fe, 31.0Ni, 0.5Be	F, R, W	483–1379	70–200	207–1241	30–180	40–4
Nickel silvers							
C73500	72.0Cu, 10.0Zn, 18.0Ni	F, R, W, T	345–758	50–110	103–579	15–84	37–1
C74500 (nickel silver, 65–10)	65.0Cu, 25.0Zn, 10.0Ni	F, W	338–896	49–130	124–524	18–76	50–1
C75200 (nickel silver, 65–18)	65.0Cu, 17.0Zn, 18.0Ni	F, R, W	386–710	56–103	172–621	25–90	45–3
C75400 (nickel silver, 65–15)	65.0Cu, 20.0Zn, 15.0Ni	F	365–634	53–92	124–545	18–79	43–2
C75700 (nickel silver, 65–12)	65.0Cu, 23.0Zn, 12.0Ni	F, W	359–641	52–93	124–545	18–79	48–2
C76200	59.0Cu, 29.0Zn, 12.0Ni	F, T	393–841	57–122	145–758	21–110	50–1
C77000 (nickel silver, 55–18)	55.0Cu, 27.0Zn, 18.0Ni	F, R, W	4 14–1000	60–145	186–621	27–90	40–2
C72200	82.0Cu, 16.0Ni, 0.5Cr, 0.8Fe, 0.5Mn	F, T	317–483	46–70	124–455	18–66	46–6
C78200 (leaded nickel silver, 65–8–2)	65.0Cu, 2.0Pb, 25.0Zn, 8.0Ni	F	365–627	53–91	159–524	23–76	40–3

(a) F, flat products; T, tube; W, wire; R, rod. (b) Ranges are from softest to hardest commercial forms. The strength of the standard copper alloys depends on the temper (annealed grain size or degree of cold work) and the section thickness of the mill product. Ranges cover standard tempers for each alloy.

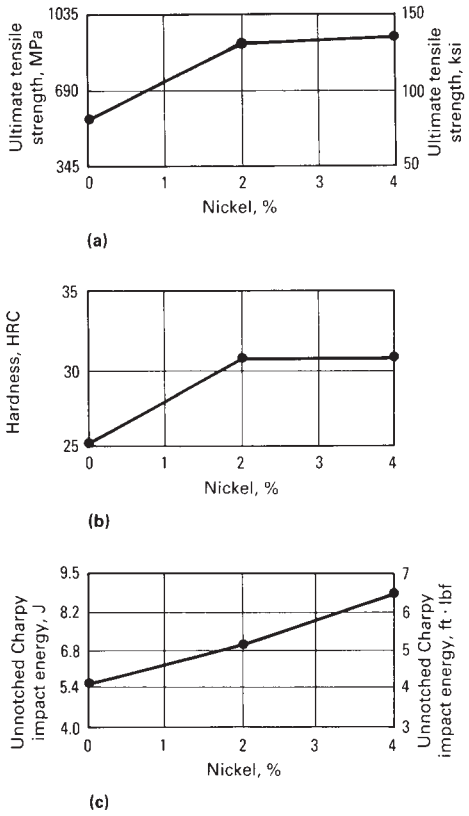


Fig. 3 Effect of nickel on the mechanical properties of heat treated P/M steels (7.0 g/cm^3). (a) Ultimate tensile strength. (b) Hardness. (c) Impact toughness

The effect of nickel content on the properties of P/M nickel steels is shown in Fig. 3.

Nickel is also an alloying element in P/M stainless steels. Its role is the same as that described earlier for wrought stainless steels.

Powder Metallurgy Nickel-Base Superalloys. The development of superalloys has been driven by the need for increasingly higher strength at higher temperatures for advanced aircraft engines. As the strength of these materials increased, hot workability decreased. Additional problems were encountered as the result of increased segregation associated with more complex alloying and the need for larger ingots for larger turbine disks. A solution to these problems was to minimize segregation through rapid solidification of the metal by atomization to powder and consolidation by methods that do not melt the powder particles but still attain full density. A further benefit of the P/M process is that the consolidated products were superplastic and amenable to isothermal forging. Thus, force requirements were greatly reduced and near-net forgings could be made. Near-net shapes are also made by hot isostatic pressing (HIP). Whereas P/M alloys cost more than conventional wrought alloys, they have allowed designers to design to higher creep strength and tensile capability while maintaining the expected cyclic life of components. The value added to the system in terms of the performance benefit gained by the system operating temperature and weight reduction more than balances the increased cost of P/M application.

Most nickel-base P/M superalloys are used for rotating aircraft turbine components. A typical aircraft engine will utilize anywhere from 680 to 2040 kg (1500 to 4500 lb) of nickel-base superalloy powder isothermal forgings. Processing and properties of these alloys are described in the article "Powder Metallurgy Processing of Nickel Alloys" in this Handbook.

Nickel in Cemented Carbides. The addition of nickel (or alloyed nickel) to the usual cobalt binder for tungsten carbide (WC), or the substitution of nickel entirely for cobalt, always improves the corrosion and oxidation resistance of cemented carbides. Nickel, however, does not wet the WC particles as effectively as cobalt, and nickel also results in a sacrifice in strength, hardness, and wear resistance. Corrosion-resistant WC-Ni grades, which usually contain 6 to 10% Ni, are used in corrosive fluid-handling components, for example, valves and nozzles, and rotary seals and bearings. Alloyed WC grades containing 3 to 9% NiCoCr have also been used in harsh chemical environments.

Nickel is a superior binder for cemented titanium carbide (TiC) and, therefore, is used in all cemented TiC materials, regardless of the need for corrosion resistance. For corrosion resistant applications, unalloyed nickel (6 to 10%) is used. For oxidation-resistant applications, TiC-NiMo_2C alloys containing 12.5 to 22.5% Ni are used.

Figure 4 compares the corrosion resistance versus pH for three different types of cemented carbides: straight WC-Co, alloyed WC-Ni, and alloyed TiC-Ni. Both of the nickel-bearing materials exhibit superior corrosion resistance.

Nickel in Electrical Contact Materials. Silver-nickel P/M composites are widely used for motor-starting contacts and as a general-purpose contact for various types of relays and switches. The dispersed nickel phase functions as a hardener and improves the mechanical properties of the silver matrix.

The combinations most widely used are 60Ag-40Ni (the hardest material in the silver-nickel series) and 85Ag-15Ni (the most widely used material in the silver-nickel series). These materials are very ductile and can be formed in all of the shapes in which silver contacts are used, including very thin sheets for facing large contact areas. This material is ideal for use under heavy sliding pressures. It does not gall like fine silver and coin silver, but instead takes on a smooth polish. It is therefore suitable for sliding contact purposes, as well as for make-break contacts. Silver nickel can handle much higher currents than fine silver before it begins to weld. It has a tendency to weld when operated against itself.

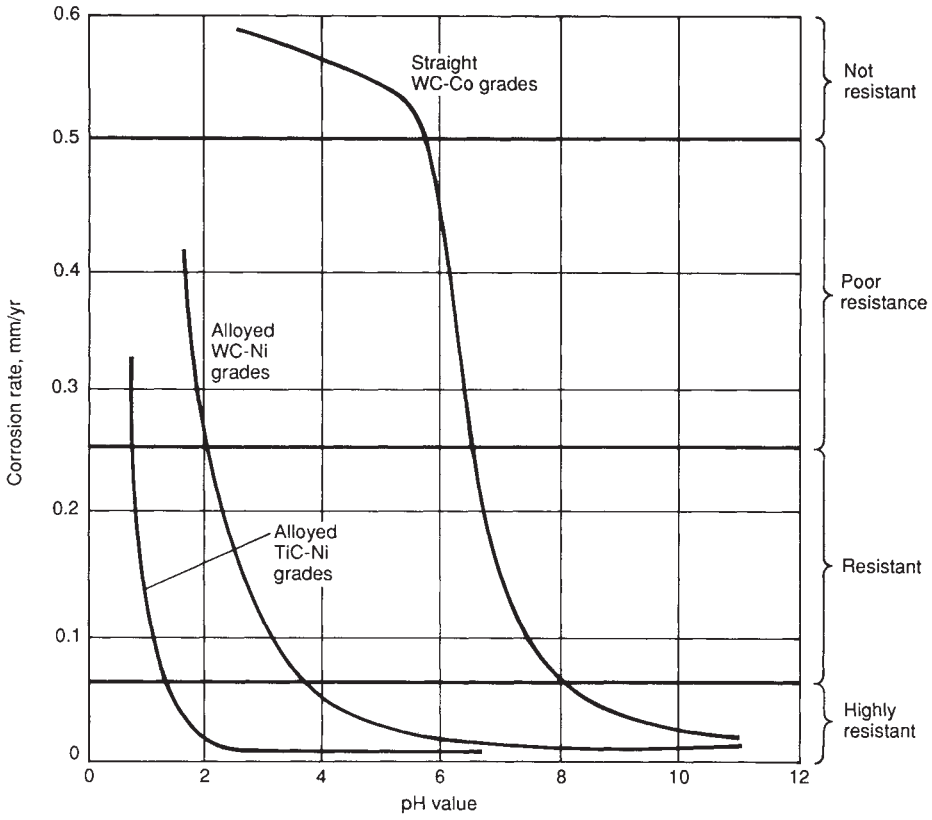


Fig. 4 Effect of nickel on the corrosion resistance of cemented carbides. Source: Ref 7

Therefore, it is frequently used against silver graphite.

Other applications for nickel powders include porous battery electrodes and filtering devices, and roll-compacted strip used for electrical, electronic, and magnetic applications. Processing of these materials is described in the article "Powder Metallurgy Processing of Nickel Alloys" in this Handbook.

REFERENCES

1. H.R. Copson, Effect of Composition on Stress Corrosion Cracking of Some Alloys Containing Nickel, *Physical Metallurgy of Stress Corrosion Fracture*, T.N. Rhodin, Ed., Interscience, New York, 1959, p 247–272
2. E. Snape, Effect of Nickel on the Structure and Properties of Wrought and Cast Stainless Steels, *Handbook of Stainless Steels*, D. Peckner and I.M. Bernstein, Ed., McGraw-Hill Book Company, 1977, p 12–1 to 12–40
3. Low-Temperature Properties of Steels, *ASM Specialty Handbook: Carbon and Alloy Steels*, J.R. Davis, Ed., ASM International, 1996, p 230–244
4. S.J. Rosenberg, *Nickel and Nickel and Its Alloys*, National Bureau of Standards Monograph 106, U.S. Department of Commerce, May 1968
5. K. Rohrbach and M. Schmidt, Maraging Steels, *Properties and Selection: Irons, Steels, and High- Performance Alloys*, Vol 1, *ASM Handbook*, ASM International, 1990, p 793–800
6. J.R. Crum, E. Hibner, N.C. Farr, and D.R. Munasinghe, Nickel-Based Alloys, *Practical Handbook of Stainless Steels & Nickel Alloys*, S. Lamb, Ed., Casti Publishing and ASM International, 1999, p 259–324
7. H.S. Kalish, Corrosion of Cemented Carbides, *Corrosion*, Vol 13, *ASM Handbook*, ASM International, 1987, p 846–858

ASM Specialty Handbook: Nickel, Cobalt, and Their Alloys
J.R. Davis, editor, p 14-54
DOI:10.1361/ncta2000p014

Copyright © 2000 ASM International®
All rights reserved.
www.asminternational.org

Wrought Corrosion Resistant Nickel and Nickel Alloys

WROUGHT NICKEL AND NICKEL ALLOYS are often classified as either corrosion resistant or heat resistant alloys. This somewhat arbitrary distinction centers on whether the alloy composition and microstructure is optimized for aqueous corrosion resistance or elevated-temperature service. Heat resistant alloys can be further subdivided according to whether they are designed primarily for corrosion resistance to hot aggressive environments or for optimal strength and metallurgical stability. In practice, there is considerable overlap, and some versatile alloys are capable of serving effectively in multiple capacities. For example, alloy 718 (UNS N07718) resists corrosion in organic acids, alkalies and salts, and seawater; it is resistant to high-temperature oxidation, carburization, and nitridation; and it exhibits high strength at temperatures up to 700 °C (1300 °F). As a result, alloy 718 can be considered a corrosion resistant alloy, a heat resistant alloy, and/or a high-performance superalloy. The wrought alloys described in this article are resistant to aqueous corrosion, high-temperature corrosion, or both.

Physical Metallurgy of Nickel and Nickel Alloys

Because nickel is a versatile element and has solubility for a number of other metals, many different commercial alloys are available. Nickel and copper have complete solid solubility. Iron and cobalt are soluble in nickel to a very high degree. The limit of solubility of chromium in nickel is 35 to 40% and is about 20% for molybdenum. The face-centered cubic (fcc) structure of the nickel matrix (γ) can be strengthened by solid-solution strengthening, carbide precipitation, and precipitation (age) hardening. An overview of each of these strengthening mechanisms as they apply to wrought alloys follows. Figure 1 shows the many alloying combinations that make up the nickel alloy family. More detailed information on the metallurgy of nickel alloys can be found in the articles "Superalloys" and "Metallography and Microstructures of Heat Resistant Alloys."

Solid-Solution Strengthening. Cobalt, iron, chromium, molybdenum, tungsten, vanadium, titanium, and aluminum are all solid-solution strengtheners in nickel. The elements differ with nickel in atomic diameter from 1 to 13%. Lattice expansion related to atomic diameter oversize can be related to the hardening observed (Ref 1 and 2). Above 0.6 T_m (melting temperature), which is the range of high-temperature creep, strengthening is diffusion

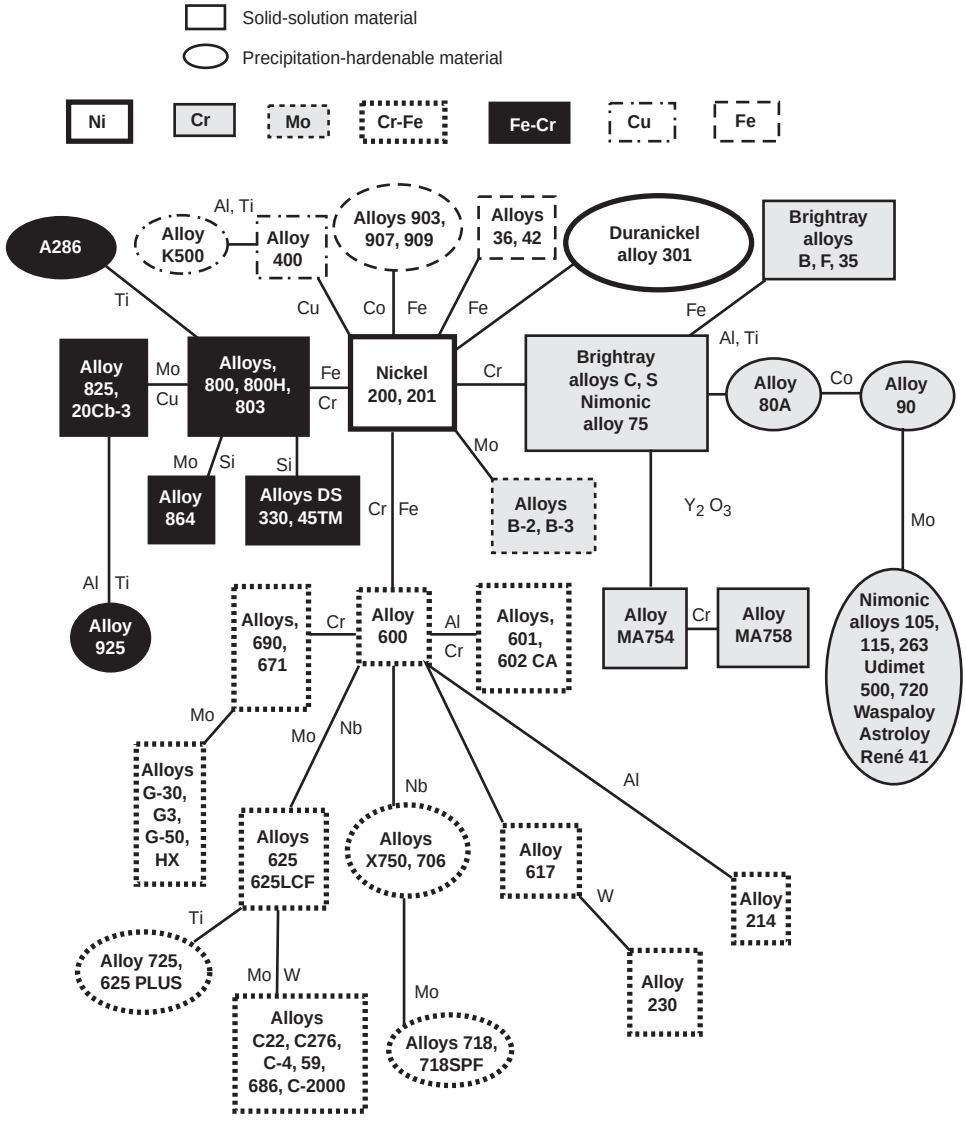


Fig. 1 Development of wrought nickel alloys

dependent and large slow diffusing elements, such as molybdenum and tungsten, are the most effective hardeners (Ref 3).

Carbide Strengthening. Nickel is not a carbide former. Carbon reacts with other elements alloyed with nickel to form carbides that can be either a bane or a blessing to the designer of alloys. An understanding of the carbide class and its morphology is beneficial to the alloy designer.

The carbides most frequently found in nickel-base alloys are MC, M_6C, M_7C_3, and $M_{23}C_6$ (where M is the metallic carbide-forming element or elements). MC is usually a large blocky carbide, random in distribution, and generally not desired. M_6C carbides are also blocky. Formed in grain boundaries, they can be used to control grain size; precipitated in a Widmanstätten pattern throughout the grain, these carbides can impair ductility and rupture life. M_7C_3 carbides (predominately Cr_7C_3) form intergranularly and are beneficial if precipitated as discrete particles. They can cause embrittlement if they agglomerate, forming continuous grain-boundary films. This condition will occur over an extended period of time at high temperatures. $M_{23}C_6$ carbides show a propensity for grain-boundary precipitation. The $M_{23}C_6$ carbides are influential in determining the mechanical properties of nickel-base alloys. Discrete grain-boundary particles enhance rupture properties. Long time exposure at 760 to 980 °C (1400–1800 °F) will cause precipitation of angular intragranular carbides as well as particles along twin bands and twin ends.

Heat treatment provides the alloy designer with a means of creating desired carbide structures and morphologies before placing the material in service. The alloy chemistry, its prior processing history, and the heat treatment given to the material influence carbide precipitation and, ultimately, performance of the alloy. Each new alloy must be thoroughly examined to determine its response to heat treatment or high temperature.

Precipitation Hardening. The precipitation of γ', $Ni_3(Al,Ti)$, in a high-nickel matrix provides significant strengthening to the material. This unique intermetallic phase has an fcc structure similar to that of the matrix and a lattice constant having 1% or less mismatch in the lattice constant with the γ matrix (Ref 3). This close matching allows low surface energy and long time stability.

Precipitation of the γ' from the supersaturated matrix yields an increase in strength with increasing precipitation temperature, up to the overaging or coarsening temperature. Strengthening of alloys by γ' precipitation is a function of γ' particle size. The hardness of the alloy increases with particle-size growth, which is a function of temperature and time. Several factors contribute to the magnitude of the hardening, but a discussion of the individual factors is beyond the scope of this paper.

The volume percent of γ' precipitated is also important because high-temperature strength increases with amount of the phase present. The amount of gamma prime formed is a function of the hardener content of the alloy. Aluminum, titanium, niobium, and tantalum are strong γ' formers. Effective strengthening by γ' decreases above about 0.6 T_m as the particles coarsen. To retard coarsening, the alloy designer can add elements to increase the volume percent of γ' or add high-partitioning, slow-diffusing elements, such as niobium or tantalum, to form the desired precipitate.

The γ' phase can transform to other (Ni_3X) precipitates if the alloy is supersaturated in titanium, niobium, or tantalum. Titanium-rich metastable γ' can transform to (Ni_3Ti), or eta phase (η), a hexagonal close-packed (hcp) phase. Formation of η-phase can alter mechanical properties, and effects of the phase must be determined on an individual alloy basis. Excess niobium results in metastable η transforming to γ'' (body-centered tetragonal phase) and ultimately to the equilibrium phase Ni_3Nb (orthorhombic phase). Both γ' and γ'' can be present at peak hardness, whereas transformation to the coarse, elongated Ni_3Nb (orthorhombic) results in a decrease in hardness. The phases precipitated are functions of alloy chemistry and the heat treatment given the material prior to service or the temperature/time exposure of in-service application.

Commercial Nickel and Nickel Alloys

Table 1 lists the compositions of commonly used wrought corrosion resistant alloys. As this table indicates, nickel-base alloys range in composition from commercially pure nickel to complex alloys containing as many as 12 or more alloying elements. A summary of alloying additions and their effects on high-temperature and aqueous corrosion is provided in Table 2. More detailed information can be found in the articles "Corrosion Behavior of Nickel Alloys in Specific Environments," "Stress-Corrosion Cracking and Hydrogen Embrittlement of Nickel Alloys," and "High-Temperature Corrosion Behavior of Nickel Alloys" in this Handbook.

Representative mechanical property data of selected nickel and nickel-base alloys are presented in Table 3. More extensive property information can be found in the data compilations of individual alloys presented later in this article.

The commercially pure nickel grades, Nickel 200 to 205, are highly resistant to many corrosive media, especially in reducing envi-

Table 1 Compositions of commonly used wrought corrosion-resistant nickel and nickel alloys

Alloy	UNS No.	Composition(a), wt%							
		Ni	Cu	Fe	Mn	C	Si	S	Other
Commercially pure nickels									
Nickel 200	N02200	99.0 min	0.25	0.40	0.35	0.15	0.35	0.01	…
Nickel 201	N02201	99.0 min	0.25	0.40	0.35	0.02	0.35	0.01	…
Nickel 205	N02205	99.0 min(b)	0.15	0.20	0.35	0.15	0.15	0.008	0.01–0.08 Mg, 0.01–0.05 Ti
Nickel 212	…	97.0 min	0.20	0.25	1.5–2.5	0.10	0.20	…	0.20 Mg
Nickel 220	N02220	99.0 min	0.10	0.10	0.20	0.15	0.01–0.05	0.008	0.01–0.08 Mg
Nickel 225	N02225	99.0 min	0.10	0.10	0.20	0.15	0.15–0.25	0.008	0.01–0.08 Mg, 0.01–0.05 Ti
Nickel 230	N02230	99.0 min	0.10	0.10	0.15	0.15	0.01–0.035	0.008	0.04 –0.08 Mg, 0.005 Ti
Nickel 270	N02270	99.97 min	0.001	0.005	0.02	0.02	0.001	0.001	0.001 Co, 0.001 Cr, 0.001 Ti
Low-alloy nickels									
Nickel 211	N02211	93.7 min	0.25	0.75	4.25–5.25	0.20	0.15	0.015	…
Duranickel 301	N03301	93.00 min	0.25	0.60	0.50	0.30	1.00	0.01	4.00–4.75 Al, 0.25–1.00 Ti
Alloy 360	N03360	bal	…	…	…	…	…	…	1.85–2.05 Be, 0.4–0.6 Ti
Nickel-copper alloys									
Alloy 400	N04400	63.0 min(b)	28.0–34.0	2.5	0.20	0.3	0.5	0.024	…
Alloy 401	N04401	40.0–45.0(b)	bal	0.75	2.25	0.10	0.25	0.015	…
Alloy 404	N04404	52.0–57.0	bal	0.50	0.10	0.15	0.10	0.024	0.05 Al
Alloy R-405	N04405	63.0 min(b)	28.0–34.0	2.5	2.0	0.3	0.5	0.25–0.060	…
Alloy K-500	N05500	63.0 min(b)	27.0–33.0	2.0	1.5	0.25	0.5	0.01	2.30–3.15 Al, 0.35–0.85 Ti

(continued)

(a) Single values are maximum unless otherwise indicated. (b) Nickel plus cobalt content

Table 1 (continued)

Alloy	UNS No.	Composition(a), wt%													
		Ni	Cr	Fe	Co	Mo	W	Nb	Ti	Al	C	Mn	Si	B	Other
Nickel-molybdenum alloys															
Hastelloy B	N10001	bal	1.0	6.0	2.5	26.0–33.0	…	…	…	…	0.12	1.0	1.0	…	0.60 V
Hastelloy B-2	N10665	bal	1.0	2.0	1.0	26.0–30.0	…	…	…	…	0.02	1.0	0.10	…	…
Hastelloy B-3	N10675	65.0	1.0–3.0	1.0–3.0	3.0	27.0–32.0	3.0	0.20	0.20	0.50	0.01	3.0	0.10	…	0.20 Ta
Nicrofer 6629 (B-4)	N10629	bal	0.5–1.5	1.0–6.0	2.5	26.0–30.0	…	…	…	0.1–0.5	0.01	1.5	0.05	…	…
Nickel-chromium-iron alloys															
Inconel 600	N06600	72.0 min(b)	14.0–17.0	6.0–10.0	…	…	…	…	…	…	0.15	1.0	0.5	…	0.5 Cu
Inconel 601	N06601	58.0–63.0	21.0–25.0	bal	…	…	…	…	…	1.0–1.7	0.10	1.0	0.50	…	1.0 Cu
Inconel 690	N06690	58.0 min	27.0–31.0	7.0–11.0	…	…	…	…	…	…	0.05	0.50	0.50	…	0.50 Cu
Haynes 214	N07214	bal	15.0–17.0	2.0– 4.0	2.0	0.5	0.5	…	0.5	4.0–5.0	0.05	0.5	0.2	0.006	0.05 Zr, 0.002–0.040Y
Iron-nickel-chromium alloys															
Incoloy 800	N08800	30.0–35.0	19.0–23.0	39.5 min	…	…	…	…	0.15–0.60	0.15–0.60	0.10	1.5	1.0	…	…
Incoloy 800HT	N08811	30.0–35.0	19.0–23.0	39.5 min	…	…	…	…	0.15–0.60	0.15–0.60	0.06– 0.10	1.5	1.0	…	0.895–1.20 Al + Ti
Incoloy 801	N08801	30.0–34.0	19.0–22.0	bal	…	…	…	…	0.75–1.5	…	0.10	1.5	1.0	…	0.5 Cu
Incoloy 803	S35045	32.0–37.0	25.0–29.0	37.0 min	…	…	…	…	0.15–0.60	0.15–0.60	0.06 –0.10	1.5	1.0	…	0.75 Cu
Nickel-chromium-molybdenum alloys															
Hastelloy C	N10002	bal	14.5–16.50	4.0–7.0	2.5	15.0–17.0	3.0–4.5	…	…	…	0.08	1.0	1.0	…	0.35 V
Hastelloy C-4	N06455	bal	14.0–18.0	3.0	2.0	14.0–17.0	…	…	0.70	…	0.015	1.0	0.08	…	…
Hastelloy C-22	N06022	bal	20.0–22.5	2.0–6.0	2.5	12.5–14.5	2.5–3.5	…	…	…	0.015	0.5	0.08	…	0.35 V
Hastelloy C-276	N10276	bal	14.5–16.50	4.0–7.0	2.5	15.0–17.0	3.0–4.5	…	…	…	0.02	1.0	0.08	…	0.35 V
Hastelloy C-2000	N06200	bal	22.0–24.0	3.0	2.0	15.0–17.0	…	…	…	0.5	0.010	0.5	0.08	…	1.3–1.9 Cu
Nicrofer 5923 (Alloy 59)	N06059	bal	22.0–24.0	1.5	0.3	15.0–16.5	…	…	…	0.1–0.4	0.010	0.5	0.10	…	…
Inconel 617	N06617	44.5 min	20.0–24.0	3.0	10.0–15.0	8.0–10.0	…	…	0.6	0.8–1.5	0.05–0.15	1.0	1.0	0.006	0.5 Cu
Inconel 625	N06625	58.0 min	20.0–23.0	5.0	1.0	8.0–10.0	…	3.15–4.15	0.40	0.40	0.10	0.50	0.50	…	…
Inconel 686	N06686	bal	19.0–23.0	5.0	…	15.0–17.0	3.0–4.4	…	0.02–0.25	…	0.010	0.75	0.08	…	…
Hastelloy S	N06635	bal	14.5–17.0	3.0	2.0	14.0–16.5	1.0	…	…	0.1–0.50	0.02	0.3–1.0	0.20–0.75	0.015	0.35 Cu, 0.01–0.10 La
Allcorr	N06110	bal	27.0–33.0	…	12.0	8.0–12.0	4.0	2.0	1.50	1.50	0.15	…	…	…	…
Nickel-chromium-iron-molybdenum alloys															
Incoloy 825	N08825	38.0–46.0	19.5–23.5	bal	…	2.5–3.5	…	…	0.6–1.2	0.2	0.05	1.0	0.5	…	…
Hastelloy G	N06007	bal	21.0–23.5	18.0–21.0	2.5	5.5–7.5	1.0	1.75–2.5	…	…	0.05	1.0–2.0	1.0	…	…
Hastelloy G-2	N06975	47.0–52.0	23.0–26.0	bal	…	5.0–7.0	…	…	0.70–1.5	…	0.03	1.0	1.0	…	0.7–1.20 Cu
Hastelloy G-3	N06985	bal	21.0–23.5	18.0–21.0	5.0	6.0–8.0	1.5	…	…	…	0.015	1.0	1.0	…	1.5–2.5 Cu, 0.50 Nb + Ta
Hastelloy G-30	N06030	bal	28.0–31.5	13.0–17.0	5.0	4.0–6.0	1.5–4.0	0.3–1.5	…	…	0.03	1.5	0.8	…	1.0–2.4 Cu
Hastelloy G-50	N06950	50.0 min	19.0–21.0	15.0–20.0	2.5	8.0–10.0	1.0	0.5	…	…	0.015	1.0	1.0	…	0.5 Cu
Hastelloy D-205	…	65.0	20.0	6.0	…	2.5	…	…	…	…	0.03	…	5.0	…	2.0 Cu
Hastelloy N	N10003	bal	6.0–8.0	5.0	0.2	15.0–18.0	0.5	…	…	…	0.010	1.0	1.0	0.010	0.50 V, 0.35 Cu
Hastelloy X	N06002	bal	20.5–23.0	17.0–20.0	0.5–2.5	8.0–10.0	0.20–1.0	…	…	…	0.05–0.15	1.0	1.0	…	…
Nicrofer 3033 (Alloy 33)	R20033	30.0–33.0	31.0–35.0	bal	…	0.5–2.0	…	…	…	…	0.015	2.0	0.5	…	0.3–1.2 Cu
Nickel-chromium-tungsten, nickel-iron-chromium, and nickel-cobalt-chromium-silicon alloys															
Haynes 230	N06230	bal	20.0–24.0	3.0	…	1.0–3.0	13.0–15.0	…	…	0.20–0.50	0.05–0.15	0.3–1.0	0.25–0.75	0.015	0.005–0.05 La
Haynes HR-120	N08120	35.0–39.0	23.0–27.0	bal	3.0	2.5	2.5	0.4–0.9	0.20	0.40	0.02–0.1	1.5	1.0	0.010	0.5 Cu
Haynes HR-160	N12160	bal	26.0–30.0	3.5	27.0–33.0	1.0	1.0	…	0.20–0.80	…	0.15	1.5	2.4–3.0	…	…
Precipitation-hardening alloys															
Alloy 625 Plus	N07716	57.0–63.0	19.0–22.0	bal	…	7.0–9.50	…	2.75–4.0	1.0–1.60	0.35	0.03	0.20	0.20	…	…
Inconel 718	N07718	50.0–55.0	17.0–21.0	bal	1.0	2.80–3.30	…	4.75–5.50	0.35	0.20–0.80	0.08	0.35	0.35	0.06	0.3 Cu
Inconel 725	N07725	55.0–59.0	19.0–22.5	bal	…	7.0–9.50	…	2.75–4.0	1.0–1.70	0.35	0.03	0.35	0.50	…	…
Inconel 925	N09925	38.0–46.0	19.5–23.5	22.0 min	…	2.50–3.50	…	0.50	1.9–2.40	0.10–0.50	0.03	1.0	0.50	…	1.5–3.0 Cu

(a) Single values are maximum unless otherwise indicated. (b) Nickel plus cobalt content

ronments, but also in oxidizing environments where they can maintain the passive nickel oxide surface film. They are used in the chemical processing and electronics industries. They are hot worked at 650 to 1230 °C (1200–2250 °F), annealed at 700 to 925 °C (1300–1700 °F), and are hardened by cold working. For processed sheet, for example, the tensile properties in the annealed condition (460 MPa, or 67 ksi, tensile strength; 148 MPa, or 22 ksi, yield strength; and 47% elongation) can be increased by cold rolling up to 760 MPa (110 ksi) tensile strength, 635 MPa (92 ksi) yield strength, and 8% elongation. Because of nominal 0.08% C content (0.15% max), Nickel 200 (N02200) should not be used above 315 °C (600 °F) because embrittlement results from the precipitation of graphite in the temperature range 425 to 650 °C (800–1200 °F). The more widely used low-carbon alloy Nickel 201 (N02201), with 0.02% max C, can be used at temperatures above 290 °C (550 °F).

Higher-purity nickel is commercially available for various electrical and electronic applications. For example, Nickel 270 (N02270) contains a minimum of 99.9% Ni. Additional information on high-purity alloys used in electrical, electronic, and other specialized applications can be found in the article “Special-Purpose Nickel Alloys” in this Handbook.

Low-alloy nickels contain 94% min Ni. The 5% Mn solid-solution addition in Nickel 211 (N02211) protects against sulfur in service en-

vironments. As little as 0.005% S can cause liquid embrittlement at unalloyed nickel grain boundaries in the range between 640 and 740 °C (1185 and 1365 °F).

Duranickel alloy 301 (N03301), which contains 4.5% Al and 0.6% Ti, offers the corrosion resistance of commercially pure nickel with the strengthening provided by the precipitation of γ′. There are sufficient alloying additions in alloy 301 to lower the Curie temperature, making the alloy weakly ferromagnetic at room temperature.

Another low-alloy nickel of commercial importance is the nickel-beryllium alloy 360 (N03360). Containing about 2 wt% Be and 0.5% Ti, this precipitation-hardening alloy is used primarily as mechanical and electrical/electronic components that must exhibit good spring properties at elevated temperatures. Both wrought and cast nickel-beryllium alloys are discussed in the article "Special-Purpose Nickel Alloys" in this Handbook.

Nickel-Copper Alloys. The first useful corrosion resistant nickel-base alloy was the nickel-copper alloy Monel 400 (N04400), which was developed in 1905. Strong and tough, it was found to be resistant to corrosion in various environments, including brine, sulfuric acid, and other acids, and was immune to stress-corrosion cracking (SCC). Alloy 400 and other nickel-copper alloys are used in chemical processing and pollution equipment.

Capable of precipitating γ′, $Ni_3(Al,Ti)$ with 2.7Al-0.6Ti alloy addition, alloy K-500 (N05500) adds an age-hardening component to the good solution-strengthening and work-hardening characteristics already available with the nominal 30% Cu in alloy 400. The composition of these alloys can be adjusted to decrease the Curie temperature to below room temperature.

Nickel-Molybdenum Alloys. The original nickel-molybdenum alloy, Hastelloy B (N10001), was introduced in 1923. It displays excellent resistance to hydrochloric acid and other reducing environments. A minimum molybdenum content of 26% is needed for very low corrosion rates in boiling hydrochloric acid even when dilute. In 1974 an improved version of alloy B with low-iron and low-carbon contents was introduced. Called Hastelloy B-2 (N10665), it contains nominal 28% Mo, 0.8% Fe, and 0.002% C. Twenty years later, Hastelloy B-3 (N10675) (with nominal 28.5% Mo, 1.5% Cr, 1.5% Fe, and 0.003% C) and Nicrofer 6628 or B-4 (N10629) (with nominal 28% Mo, 1.3% Cr, 3% Fe, and 0.005% C) were introduced. These alloys provide a level of thermal stability superior to alloy B-2.

Slightly lowering the molybdenum content to a nominal 24% Mo and adding 6% Fe, 5% Cr, and 2.5% Co produces Hastelloy W (N10004). This alloy is widely used as a weld filler metal used to join dissimilar high-temperature alloys. It is used extensively in aircraft engine repair and maintenance.

The Ni-Cr-Fe alloys might simply be thought of as nickel-base analogs of the iron-base austenitic stainless steel alloys, with an interchange of the iron and nickel contents. In these commercially important alloys, the chromium content in general ranges from 15 to 30%, and iron ranges from 3 to 20%. With a well-maintained Cr_2O_3 surface film, these alloys offer excellent corrosion resistance in many severe environments, showing immunity to chloride-ion SCC. They also offer good oxidation and sulfidation resistance with good strength at elevated temperatures. These nickel-rich Ni-Cr-Fe alloys have maximum operating temperatures of approximately 1200 °C (2200 °F). Alloy 600 (N06600), which was developed in 1931 and contains a nominal 15% Cr and 8% Fe, is a single-phase alloy that can

Table 2 Effects of alloying elements on the corrosion resistance of nickel alloys

Element	Effect
Nickel	Improves high-temperature strength
	Improves resistance to oxidation, nitridation, carburization, and halogenation
	Detrimental to sulfidation
	Improves metallurgical stability
	Improves resistance to reducing acids and caustic
	Improves resistance to stress-corrosion cracking
Aluminum	Improves oxidation and sulfidation resistance
	Age-hardening component
Iron	Improves economy of alloy
	Controlled thermal expansion addition
Rare earth elements lanthanum and yttrium	Improves adherence of oxide layer
Copper	Improves resistance to reducing acids and salts (Ni-Cu alloys)
	Improves resistance to sulfuric acid
Niobium	Improves high-temperature strength
	Improves resistance to pitting
	Carbide stabilization component
	Age-hardening component
Sulfur	Improves machinability
Chromium	Improves oxidation and sulfidation resistance
	Below 18% can improve resistance to halogens or high-temperature halides
	Improves aqueous corrosion resistance
Carbon	High-temperature strength
Silicon	Improves oxidation and carburization resistance, especially under alternating oxidizing and reducing conditions
Cobalt	Improves high-temperature strength and oxidation resistance
	Controlled thermal expansion addition
Molybdenum	Improves high-temperature strength
	May reduce oxidation resistance
	Improves resistance to pitting and crevice corrosion
	Improves resistance to reducing acids
Nitrogen	Can improve high-temperature strength by precipitation of stable nitrides
	Improves pitting and crevice corrosion resistance
	Improves metallurgical stability by acting as an austenitizer
Titanium	Detrimental to oxidation due to titanium oxides disrupting primary oxide scale
	Age-hardening component
	Carbide stabilization component
Tungsten	Improves resistance to pitting and crevice corrosion
	Improves high-temperature strength
Yttrium oxide	Improves high-temperature strength
	Improves grain size control
	Improves resistance to oxidation

Table 3 Room-temperature mechanical properties of selected nickel-base alloys

	Ultimate tensile strength		Yield strength (0.2% offset)		Elongation in 50 mm	Elastic modulus (tension)		
Alloy	MPa	ksi	MPa	ksi	(2 in), %	GPa	10^6 psi	Hardness
Nickel 200	462	67	148	21.5	47	204	29.6	109 HB
Nickel 201	403	58.5	103	15	50	207	30	129 HB
Nickel 205	345	50	90	13	45	…	…	…
Nickel 211	530	77	240	35	40	…	…	…
Nickel 212	483	70	…	…	…	…	…	…
Nickel 222	380	55	…	…	…	…	…	…
Nickel 270	345	50	110	16	50	…	…	30 HRB
Duranickel 301 (precipitation hardened)	1170	170	862	125	25	207	30	30–40 HRC
Alloy 400	550	80	240	35	40	180	26	110–150 HB
Alloy 401	440	64	134	19.5	51	…	…	…
Alloy R-405	550	80	240	35	40	180	26	110–140 HB
Alloy K-500 (precipitation hardened)	1100	160	790	115	20	180	26	300 HB
Alloy 600	655	95	310	45	40	207	30	75 HRB
Alloy 601	620	90	275	40	45	207	30	65–80 HRB
Alloy 617 (solution annealed)	755	110	350	51	58	211	30.6	173 HB
Alloy 625	930	135	517	75	42.5	207	30	190 HB
Alloy 690	725	105	348	50.5	41	211	30.6	88 HRB
Alloy 718 (precipitation hardened)	1240	180	1036	150	12	211	30.6	36 HRC
Alloy C-22	785	114	372	54	62	…	…	209 HB
Alloy C-276	790	115	355	52	61	205	29.8	90 HRB
Alloy G3	690	100	320	47	50	199	28.9	79 HRB
Alloy 800	600	87	295	43	44	193	28	138 HB
Alloy 825	690	100	310	45	45	206	29.8	…
Alloy 925 (a)	1210	176	815	118	24	…	…	36.5 HRC

Properties are for annealed sheet unless otherwise indicated. (a) Annealed at 980 °C (1800 °F) for 30 min, air cooled, and aged at 760 °C (1400 °F) for 8 h, furnace cooled at a rate of 55 °C (100 °F)/h, heated to 620 °C (1150 °F) for 8 h, air cooled

be used at temperatures from cryogenic to 1093 °C (2000 °F). The modest yield strength of strip in the annealed condition (207–310 MPa, or 30–45 ksi) can be readily work hardened by cold rolling to reach yield strengths of 827 to 1100 MPa (120–160 ksi) and can retain most of this strength up to approximately 540 °C (1000 °F).

Other alloys in this family include the higher-chromium-content (29% Cr) alloy 690 (N06690) developed for improved performance in nuclear steam generators, aluminum-containing (1.4% Al) alloy 601 (N06601) developed for improved oxidation resistance, and the Ni-Cr-Al-Fe alloy 214 (N07214) that contains 4.5% Al and has the highest oxidation resistance of any wrought alloy at temperatures of 955 °C (1750 °F) and above.

The Fe-Ni-Cr alloys are also an extension of stainless steel technology. Incoloy alloy 800 (N08810) was designed as a leaner nickel version of the Ni-Cr-Fe series of materials described previously. It offers good oxidation resistance and was introduced as a sheathing material for electric stove elements. The 800 alloy series has also found extensive use in high-temperature petrochemical environments, where sulfur-containing feedstocks (naptha and heavy oils) are cracked into component distillate parts. Not only are they resistant to chloride-ion SCC, but they also offer resistance to polythionic acid cracking. (Alloy 801 offers optimum resistance.) The Fe-Ni-Cr alloys also offer excellent strength at elevated temperature (creep and stress rupture).

The Ni-Cr-Mo alloys consist of a large family of alloys that are used in the chemical processing, pollution control, and waste treatment industries due to their excellent heat and corrosion resistance. As indicated in Table 1, these alloys contain a nominal 52 to 60% Ni, 15 to 31% Cr, 9 to 16% Mo, and smaller additions of other elements, such as iron and tungsten.

The Hastelloy C series of alloys was introduced in the 1930s. The original alloy C (N30002) served the chemical processing industry for approximately 30 years. However, it had several serious limitations. In many applications, vessels fabricated from alloy C had to be solution heat treated to remove detrimental weld heat-affected zone (HAZ) precipitates. When used in the as-welded condition, alloy C was often susceptible to serious intergranular corrosion attack in many oxidizing and chloride-containing environments. The first modification of alloy C was an alloy that had carbon and silicon contents reduced more than tenfold, typically 0.005% C and 0.04% Si. This alloy came to be known as C-276 (N10276).

Several variants of C-276 have also been introduced, including:

- *Alloy C-4 (N06455),* which has improved thermal stability. In this alloy, the tungsten was totally omitted and the iron content was reduced to approximately 1%. The alloy also contains approximately 0.3% Ti.
- *Alloy C-22 (N06022),* which has better resistance to chloride-induced localized corrosion and SCC. In this alloy, the chromium content was raised to approximately 21% and molybdenum content reduced to approximately 13%. It also contains approximately 0.2% V and 1.7% Co.
- *Alloy 59 (N06059),* with a chromium content of approximately 23%, iron less than 1%, and approximately 0.2% Al for very severe corrosive applications
- *Alloy C-2000 (N06200),* with approximately 1.6% Cu added for improved corrosion resistance in sulfuric acid and reducing media

Alloys 625 and 617, which were introduced in the 1960s, were developed for aircraft engines but have found wide use in other applications requiring high-temperature strength and corrosion resistance. Alloy 625 (N06625) contains a nominal 20% Cr, 9% Mo, and 2.5% Fe, and is stabilized with approximately 3.5% Nb. In alloy 617 (N06617), some of the nickel has been replaced with cobalt (~12.5% Co). Other 600-series Ni-Cr-Mo alloys include alloys 622 (N06022) and 686 (N06686), both of which contain tungsten additions.

Hastelloy S (N06635) contains a nominal 67% Ni, 16% Cr, and 15% Mo, as well as other alloying elements that improve its thermal stability, fatigue life, oxidation resistance, and low-expansion characteristics. It is used in low-stress gas turbine parts and is an excellent dissimilar filler metal.

The Ni-Cr-Fe-Mo alloys constitute another large family of nickel alloys. Alloy 825 (N08825) was developed in the 1950s for sulfuric acid service. It contains a nominal 42% Ni, 22% Cr, 32% Fe, 2.5% Mo, and 2% Cu, and is stabilized with 0.8% Ti. The Hastelloy G series of alloys was developed for use in wet-process phosphoric acid service. They contain a nominal 22 to 30% Cr, 15 to 20% Fe, 5 to 7% Mo, and smaller additions of cobalt and niobium. The lower carbon variants of the predecessor alloy G (N06007), which include G-3 (N06985) and G-30 (N06039), have improved resistance to HAZ carbide precipitation, improved resistance to hot cracking, and improved weld metal bend ductility. Alloy G-50 was developed for use in sour gas environments.

Other alloys in the Ni-Cr-Fe-Mo family include:

- *Hastelloy X (N06002),* which contains a nominal 47% Ni, 22% Cr, 18% Fe, and 9% Mo and is widely used for aircraft, marine, and industrial gas turbine combustors and fabricated parts
- *Hastelloy N (N10003),* which contains a nominal 71% Ni, 7% Cr, 5% Fe, and 16% Mo and is highly resistant to molten fluoride salts
- *Hastelloy D-205 (UNS No. pending),* which contains a nominal 65% Ni, 20% Cr, 6% Fe, and 2.5% Mo, plus additions of 5% Si and 2% Cu, and is highly resistant to hot concentrated sulfuric acid
- *Nicrofer 3033,* also referred to as alloy 33 (R20033), which contains a nominal 31% Ni, 33% Cr, 32% Fe, and 1.6% Mo, plus an addition of 0.4% N, and is highly resistant to sulfuric acid

Miscellaneous Solid-Solution Alloys. Some of the more recently developed alloys that exhibit excellent resistance to high-temperature corrosion do not fit into the alloy families described above. Three examples are:

- *Alloy 230 (N06230),* which is a Ni-Cr-W alloy (see Table 1 for the composition). It has an excellent balance of strength, thermal stability, oxidation resistance, thermal cycling resistance, and fabricability. It is used in gas turbine combustors and other key stationary components. It is also used for heat treating and industrial heating applications, and in the chemical/petrochemical process industry and in fossil fuel energy plants.
- *HR-120 (N08120),* which is a Ni-Fe-Cr alloy containing a wide variety of alloying elements (see Table 1). Because of its high iron content (33% Fe), this is an economical alloy that exhibits high strength and excellent resistance to carburization and sulfidation. It is used in heat-treating fixtures and industrial heating applications.
- *HR-160 (N12160),* which is a Ni-Co-Cr-Si-Fe alloy (see Table 1). It has outstanding resistance to sulfidation and chloride attack and is used in a variety of fabricated components that are used in municipal, industrial, and nuclear waste incinerators.

Precipitation-Hardening Alloys. The increasing use of nickel alloys in natural gas production led to the development of high-strength, corrosion resistant, age-hardenable alloy 925 (N09925) and age-hardening variations of alloy 625, including alloy 725 (N07725) and 626 PLUS (N07716). Alloy 925 offers corrosion resistance comparable with that of alloy 825, but with higher strength obtained by age hardening (see Table 3). A similar relationship exists between alloys 725 and 625 PLUS and solid-solution strengthened alloy 625.

As stated in the introductory paragraph of this article, alloy 718 (N07718) is another age-hardenable alloy that is highly corrosion resistant. Its high strength, corrosion resistance, and ease of weld fabrication have made alloy 718 the most popular superalloy used in industry.

REFERENCES

1. R.M.N. Pelloux and N.J. Grant, *Trans. AIME,* Vol 218, 1960, p 232
2. E.R. Parker and T.H. Hazlett, Principles of Solution Hardening, *Relation of Properties to Microstructures*¸ American Society for Metals, 1954, p 30
3. R.F. Decker, "Strengthening Mechanisms in Nickel-Base Superalloys," paper presented at the Climax Molybdenum Co. Symposium (Zurich), May 1969

SELECTED REFERENCES

- J.R. Crum, E. Hibner, N.C. Farr, and D.R. Munasinghe, Nickel-Based Alloys, *Practical Handbook of Stainless Steels & Nickel Alloys*, S. Lamb and J.E. Bringas, Ed., Casti Publishing Inc. and ASM International, 1999, p 259–324
- W.L. Mankins and S. Lamb, Nickel and Nickel Alloys, *Properties and Selection: Nonferrous Alloys and Special-Purpose Materials*, Vol 2, *ASM Handbook*, ASM International, 1990, p 428–445

Properties of Wrought Nickel and Nickel Alloys

Nickel 200

Specifications

ASTM. B 160 (rod and bar), B 161 (seamless pipe and tube), B 162 (plate, sheet, and strip), B 163 (condenser and heat exchanger tube), B 366 (welding fittings), B 564 (forgings), B 725 (welded pipe), B 730 (welded tube), B 751 (welded tube, general requirements), B 775 (welded pipe, general requirements), B 829 (seamless pipe and tube, general requirements)
ASME. SB-160, SB-161, SB-162, SB-163, SB-366, SB-564, SB-751, SB-775, SB-829
UNS number. N02200

Chemical Composition

Composition limits. 99.0 min Ni + Co; 0.15 max C; 0.25 max Cu; 0.40 max Fe; 0.35 max Mn; 0.35 max Si; 0.01 max S

Applications

Typical uses. Chemical and food processing, electronic parts, aerospace equipment
Precaution in use. Should not be used at service temperatures above 315 °C (600 °F)

Mechanical Properties

Tensile properties. See Tables 1 and 2.
Compressive properties. See Table 3.
Hardness. See Table 3.
Poisson's ratio. 0.264 at 20 °C (68 °F)
Elastic modulus. Tension, 204 GPa (29.6 × 10^6 psi) at 20 °C (68 °F); torsion, 81 GPa (11.7 × 10^6 psi) at 20 °C (68 °F)
Impact strength. See Table 4.
Fatigue strength. See Table 5.

Physical Properties

Density. 8.89 g/cm^3 (0.321 lb/in.^{3}) at 20 °C (68 °F)
Liquidus temperature. 1466 °C (2635 °F)
Solidus temperature. 1435 °C (2615 °F)
Coefficient of thermal expansion. See Table 6.
Specific heat. 456 J/kg · K (0.106 Btu/lb · °F) at 21 °C (70 °F)
Thermal conductivity. See Table 6.
Electrical conductivity. Volumetric, 18.2% IACS at 21 °C (70 °F)
Electrical resistivity. See Table 6.
Magnetic permeability. Ferromagnetic
Curie temperature. 360 °C (680 °F)

Chemical Properties

General corrosion behavior. Nickel 200 is highly resistant to many corrosive media. Although most useful in reducing environments, it can be used also under oxidizing conditions that cause the formation of a passive oxide film. The alloy has excellent resistance to caustics, high-temperature halogens and hydrogen

Table 1 Tensile properties of Nickel 200

Form and condition	Tensile strength		Yield strength (0.2% offset)		Elongation, %
	MPa	ksi	MPa	ksi	
Rod and bar					
Hot finished	414–586	60–85	103–310	15–45	55–35
Cold drawn	448–758	65–110	276–690	40–100	35–10
Annealed	379–517	55–75	103–207	15–30	55–40
Plate					
Hot rolled	379–690	55–100	138–552	20–80	55–35
Annealed	379–552	55–80	103–276	15–40	60–40
Sheet					
Hard	621–793	90–115	483–724	70–105	15–2
Annealed	379–517	55–75	103–207	15–30	55–40
Strip					
Spring temper	621–896	90–130	483–793	70–115	15–2
Annealed	379–517	55–75	103–207	15–30	55–40
Tubing					
Stress relieved	448–758	65–110	276–621	40–90	35–15
Annealed	379–517	55–75	83–207	12–30	60–40
Wire					
Annealed	379–586	55–85	103–345	15–50	50–30
Spring temper	862–1000	125–145	724–931	105–135	15–2

Values shown represent usual ranges for common section sizes. In general, values in the higher portions of the ranges are not obtainable with large section sizes, and exceptionally small or large sections can have properties outside the ranges.

Table 2 Typical tensile properties of annealed Nickel 200 as a function of temperature

Temperature		Tensile strength		Yield strength (0.2% offset)		Elongation,
°C	°F	MPa	ksi	MPa	ksi	%
20	68	462	67.0	148	21.5	47.0
93	200	458	66.5	154	22.3	46.0
149	300	460	66.7	150	21.7	44.5
204	400	458	66.5	139	20.2	44.0
260	500	465	67.5	135	19.6	45.0
316	600	456	66.2	139	20.2	47.0
371	700	362	52.5	117	17.0	61.5

Table 3 Typical compressive strength and hardness of Nickel 200

Material condition	Compressive yield strength (0.2% offset)		Hardness, HB
	MPa	ksi	
Hot rolled	159	23.0	107
Cold drawn 24%	400	58.0	177
Annealed	179	26.0	109

Table 4 Typical impact strength of Nickel 200

Material condition	Impact strength			
	Izod		Charpy V-notch	
	J	ft · lb	J	ft · lb
Hot rolled	163	120	271	200
Cold drawn, stress relieved	163	120	277	204
Cold drawn, annealed	163	120	309	228

Table 5 Typical fatigue strength of Nickel 200

	Fatigue strength			
	Cold drawn rod		Annealed rod	
Cycles	MPa	ksi	MPa	ksi
10^4	751	109	…	…
10^5	579	84	358	52
10^6	434	63	276	40
10^7	358	52	234	34
10^8	345	50	228	33

Table 6 Thermal and electrical properties of annealed Nickel 200

Temperature		Mean linear expansion(a)		Thermal conductivity		Electrical
°C	°F	μm/m · K	μin./in. · °F	W/m · K	Btu/ft · h · °F	resistivity, nΩm
–253	–423	8.5	4.7	…	…	…
–184	–300	10.4	5.8	…	…	27
–200	–129	11.2	6.2	77.2	44.6	43
–100	–73	11.3	6.3	…	…	58
–18	0	…	…	72.1	41.7	80
21	70	…	…	…	…	95
93	200	13.3	7.4	67.1	38.8	126
204	400	13.9	7.7	61.3	35.4	188
316	600	14.4	8.0	56.3	36.5	273

(a) From 21 °C (70 °F) to temperature shown

Table 7 Corrosion of Nickel 200 in caustic soda solutions

	Temperature		Corrosion rate	
Environment	°C	°F	μm/yr	mils/yr
Laboratory tests in 4% solution	20	68		
Quiet immersion			1	0.05
Air-agitated immersion			1	0.05
Continuous alternate immersion			13	0.50
Intermittent alternate immersion			15	0.60
Spray test			1	0.05
Plant tests in 14% solution in first effect of multiple-effect evaporator	88	190	0.5	0.02
Plant tests in 23% solution in tank receiving liquor from evaporator	104	220	4.1	0.16
Plant tests in single-effect evaporator concentrating solution from 30 –50%	82	179	2.5	0.10
Plant tests in evaporator concentrating to 50% solution			3	0.1
Laboratory tests during concentration from 32–52% (vacuum, 640–685 mm Hg)	85–91	185–196	33	1.3
Tests in storage tank containing 49–51% solution	55–75	131–167	0.5	0.02
	121	250	25	1.0
Laboratory tests in 75% solution	204	400	20	0.8
Plant tests in 70% electrolytic solution in receiving tank	90–115	194–239	3	0.1

halides, and salts other than oxidizing halides. It is also well suited to food processing, in which product purity must be maintained. Nickel 201 (low-carbon nickel) should be used for applications involving temperatures above 315 °C (600 °F).

Resistance to specific corroding agents. An outstanding characteristic of Nickel 200 is its resistance to caustic soda and other alkalies except ammonium hydroxide. Table 7 gives corrosion rates in caustic soda.

Nickel 201

Specifications

ASTM. B 160 (rod and bar), B 161 (seamless pipe and tube), B 162 (plate, sheet, and strip), B 163 (condenser and heat exchanger tube), B 366 (welding fittings), B 725 (welded pipe), B 730 (welded tube), B 751 (welded tube, general requirements), B 775 (welded pipe, general requirements), B 829 (seamless pipe and tube, general requirements)

ASME. SB-160, SB-161, SB-162, SB-163, SB-366, SB-564, SB-751, SB-775, SB-829

AMS. 5553 (sheet and strip)

UNS number. N02201

Chemical Composition

Composition limits. 99.0 min Ni + Co; 0.02 max C; 0.25 max Cu; 0.40 max Fe; 0.35 max Mn; 0.35 max Si; 0.010 max S

Table 8 Typical tensile properties of annealed Nickel 201 as a function of temperature

Temperature		Tensile strength		Yield strength (0.2% offset)		Elongation,
°C	°F	MPa	ksi	MPa	ksi	%
20	68	403	58.5	103	15.0	50
93	200	387	56.1	106	15.4	45
149	300	372	54.0	99	14.4	46
204	400	372	54.0	102	14.8	44
260	500	372	54.0	101	14.6	41
316	600	362	52.5	105	15.3	42
371	700	325	47.2	97	14.1	53
427	800	284	41.2	93	13.5	58
482	900	259	37.5	89	12.9	58
538	1000	228	33.1	83	12.1	60
593	1100	186	27.0	77	11.2	72
649	1200	153	22.2	70	10.2	74

Applications

Typical uses. Caustic evaporators, combustion boats, plater bars, electronic parts

Mechanical Properties

Tensile properties. See Table 8.

Elastic modulus. Tension, 207 GPa (30×10^6 psi)

Creep and stress-rupture characteristics. See Fig. 1 and 2.

Physical Properties

Density. 8.88 g/cm^3 (0.321 lb/in.^{3}) at 20 °C (68 °F)

Liquidus temperature. 1446 °C (2635 °F)

Solidus temperature. 1435 °C (2615 °F)

Coefficient of thermal expansion. 13.3 μm/m · K (7.4 μin./in. · °F) at 21 to 93 °C) (70–200 °F)

Specific heat. 456 J/kg · K (0.106 Btu/lb · °F) at 21 °C (70 °F)

Thermal conductivity. See Table 9.

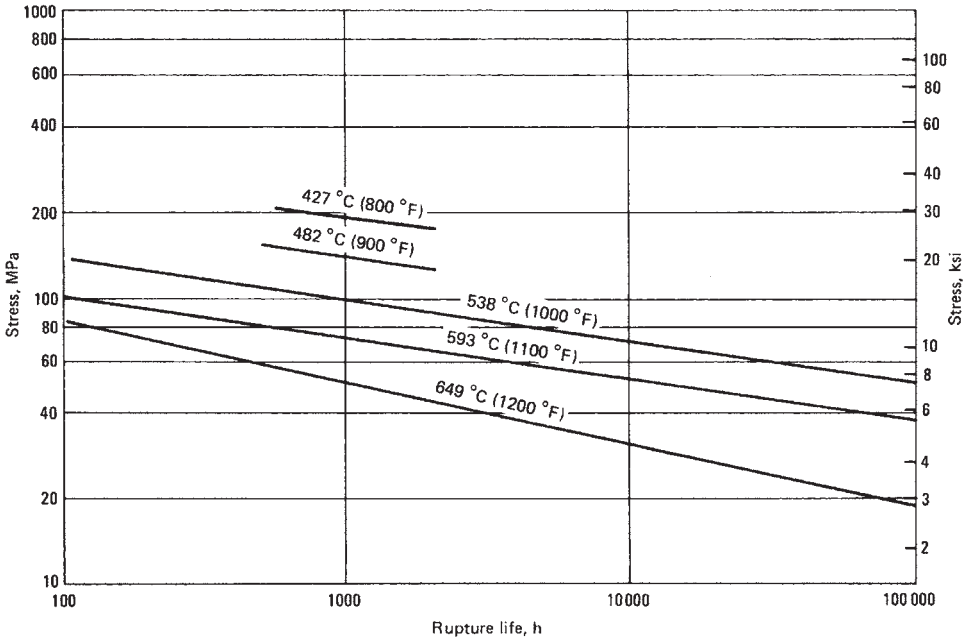


Fig. 1 Typical stress-rupture strength of annealed Nickel 201

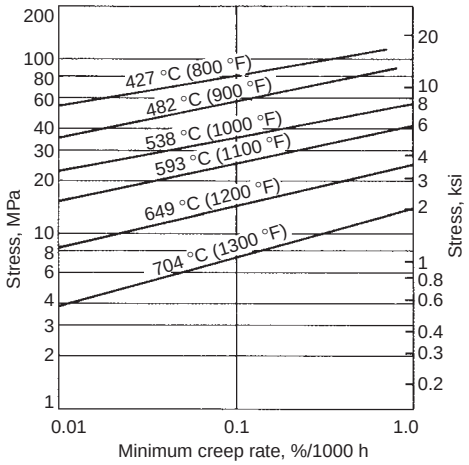


Fig. 2 Typical creep strength of annealed Nickel 201

Electrical conductivity. Volumetric, 20.5% IACS at 27 °C (80 °F)
Electrical resistivity. See Table 9
Magnetic permeability. Ferromagnetic
Curie temperature. 360 °C (680 °F)

Chemical Properties

General corrosion behavior. Nickel 201 has the same corrosion resistance as Nickel 200. Nickel 201, however, has a low carbon content and is not subject to embrittlement by precipitated carbon or graphite at high temperatures. It is therefore preferred to Nickel 200 for use at temperatures above 315 °C (600 °F).

Table 9 Thermal and electrical properties of Nickel 201

Temperature		Thermal conductivity		Electrical resistivity,
°C	°F	W/m · K	Btu/ft · h · °F	nΩ · m
–196	–320	…	…	16.6
–184	–300	95.5	55.2	…
–73	–100	…	…	48.2
–18	0	90.9	52.5	71.5
27	80	…	…	84.8
38	100	…	…	91.4
93	200	73.8	42.6	118.0
204	400	66.4	38.4	182.9
316	600	58.8	33.9	266.0
427	800	56.5	32.6	347.4
538	1000	59.1	34.1	385.7
649	1200	61.7	35.6	420.6
760	1400	64.2	37.1	455.5
871	1600	66.8	38.6	483.8
982	1800	69.2	40.0	512.0
1093	2000	…	…	523.7

Nickel 270

Specifications

ASTM. F 3 (strip)
UNS number. N02270

Chemical Composition

Composition limits. 99.97 min Ni; 0.02 max C; 0.005 max Fe; 0.001 max Cu; 0.001 max Mn; 0.001 max Si; 0.001 max S; 0.001 max Co; 0.001 max Cr; 0.001 max Mg; 0.001 max Ti

Applications

Typical uses. Cathode shanks, fluorescent lamps, hydrogen thyratrons, anodes and passive cathodes, heat exchangers, heat shields

Mechanical Properties

Tensile properties. See Table 10.
Hardness. See Table 10.
Elastic modulus. Tension, 207 GPa (30×10^6 psi)

Table 10 Typical room-temperature tensile properties and hardness of Nickel 270

Form and condition	Tensile strength		Yield strength (0.2% offset)		Elongation,	Hardness,
	MPa	ksi	MPa	ksi	%	HRB
Rod and bar, hot finished	345	50	110	16	50	40
Strip						
Cold rolled	655	95	621	90	4	95
Annealed	345	50	110	16	50	35
Sheet, annealed	345	50	110	16	45	30

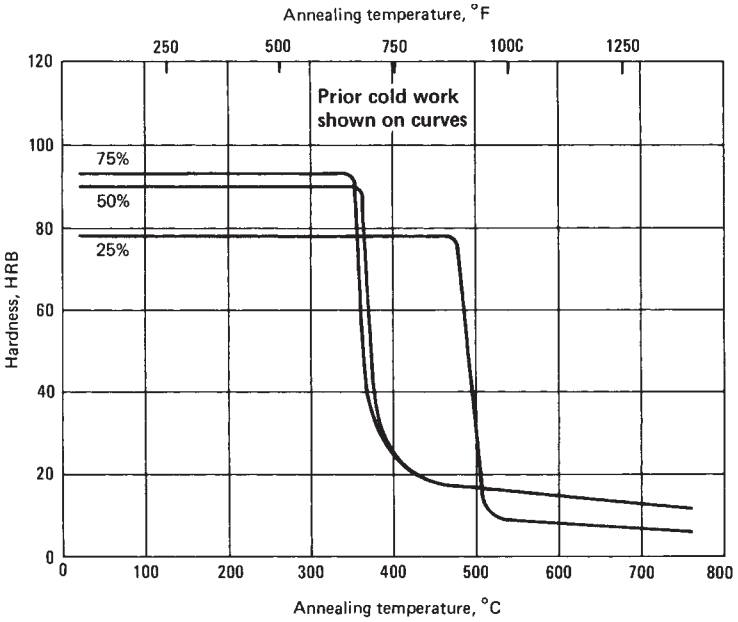


Fig. 3 Recrystallization behavior of Nickel 270 (annealing time, 30 min)

Table 11 Thermal and electrical properties of Nickel 270

Temperature		Mean linear expansion(a)		Thermal conductivity		Electrical resistivity,
°C	°F	μm/m · K	μin./in. · °F	W/m · K	Btu/ft · h · °F	nΩ · m
–196	–320	…	…	…	…	6.6
–129	–200	…	…	108	62.4	23.
–18	0	…	…	91	52.6	59.8
27	80	…	…	…	…	74.8
93	200	13.3	7.4	79	45.6	106.4
204	400	13.7	7.6	70	40.4	169.6
316	600	14.4	8.0	62	35.8	254.3
427	800	15.1	8.4	59	34.1	329.2
538	1000	15.5	8.6	62	35.8	364.1
649	1200	15.8	8.8	65	37.6	395.6
760	1400	16.2	9.0	67	38.7	425.6
871	1600	16.6	9.2	70	40.4	448.8
982	1800	…	…	73	42.2	480.4
1093	2000	…	…	…	…	510.4

(a) From 21 °C (70 °F) to temperature shown

Physical Properties

Density. 8.88 g/cm^3 (0.321 lb/in.^{3}) at 20 °C (68 °F)
Melting point. 1454 °C (2650 °F)
Recrystallization temperature. See Fig. 3.
Coefficient of thermal expansion. See Table 11.
Specific heat. 460 J/kg · K (0.107 Btu/lb · °F) at 20 °C (68 °F)
Thermal conductivity. See Table 11.
Electrical conductivity. Volumetric, 23.0% IACS at 27 °C (80 °F)
Electrical resistivity. See Table 11.
Magnetic permeability. Ferromagnetic
Curie temperature. 358 °C (676 °F)

Chemical Properties

General corrosion behavior. Nickel 270 has essentially the same corrosion resistance as Nickel 200 and Nickel 201. Nickel 270 is a high-purity product and therefore can be more susceptible to sulfur embrittlement under certain conditions.

Duranickel 301

Specifications

UNS number. N03301

Chemical Composition

Composition limits. 93.0 min Ni + Co; 0.25 max Cu; 0.60 max Fe; 0.50 max Mn; 0.30 max C; 1.0 max Si; 0.01 max S; 4.0 to 4.75 Al; 0.25 to 1.0 Ti

Applications

Typical uses. Duranickel 301 is used for applications that require the corrosion resistance of commercially pure nickel but the greater strength or spring properties. Examples are diaphragms, springs, clips, press components for extrusion of plastics, and molds for production of glass articles.

Mechanical Properties

Tensile properties. See Table 12.
Compressive properties. Compressive yield strength, hot-rolled and aged material: 948 MPa (137.5 ksi) at 0.2% offset
Poisson's ratio. 0.31
Elastic modulus. Tension, 207 GPa (30 × 10^6 psi) at 27 °C (80 °F)
Fatigue strength. Hot-rolled and aged material, rotating beam: 352 MPa (51 ksi) at 10^8 cycles

Physical Properties

Density. 8.25 g/cm^3 (0.298 lb/in.^{3}) at 20 °C (68 °F)
Liquidus temperature. 1438 °C (2620 °F)
Solidus temperature. 1399 °C (2550 °F)
Coefficient of thermal expansion. See Table 13.
Specific heat. Mean, 435 J/kg · K (0.101 Btu/lb · °F) at 21 to 100 °C (70–212 °F)
Thermal conductivity. See Table 13.
Electrical conductivity. Volumetric, 4.1% IACS at 21 °C (70 °F)
Electrical resistivity. See Table 13.
Magnetic properties versus treatment. In the annealed condition, the alloy is slightly magnetic at room temperature and nonmagnetic above approximately 49 °C (120 °F). Age hardening increases the magnetic properties

Table 12 Typical tensile properties of age-hardened Duranickel 301

Temperature		Tensile strength		Yield strength (0.2% offset)		Elongation,
°C	°F	MPa	ksi	MPa	ksi	%
21	70	1276	185	910	132	28
316	600	1158	168	827	120	29
371	700	1124	163	807	117	27
427	800	1069	155	786	114	24
482	900	972	141	752	109	11
538	1000	814	118	683	99	7
593	1100	648	94	517	75	5
649	1200	476	69	372	54	4
704	1300	290	42	234	34	8
760	1400	172	25	97	14	60
816	1500	117	17	62	9	98

slightly and raises the Curie temperature to approximately 93 °C (200 °F).
Curie temperature. Annealed, 16 to 49 °C (60–120 °F); aged, 93 °C (200 °F)

Chemical Properties

General corrosion behavior. The corrosion resistance of alloy 301 is essentially the same as that of Nickel 200. Alloy 301 has exceptional resistance to fluoride glasses and is used for glass molds.

Table 13 Thermal and electrical properties of age-hardened Duranickel 301

Temperature		Mean linear expansion(a)		Thermal conductivity		Electrical resistivity,
°C	°F	μm/m · K	μin./in. · °F	W/m · K	Btu/ft · h · °F	nΩ · m
21	70	…	…	23.8	13.8	424
93	200	13.0	7.2	25.4	14.7	465
204	400	13.7	7.6	28.6	15.9	500
316	600	14.0	7.8	32.2	18.6	530
427	800	14.4	8.0	35.0	19.4	560
538	1000	14.8	8.2	38.2	22.1	580
649	1200	15.3	8.5	41.2	23.8	595
760	1400	15.8	8.8	44.1	25.4	610
871	1600	16.4	9.1	47.0	27.2	630
982	1800	…	…	49.3	28.5	650
1093	2000	…	…	51.6	29.8	670

(a) From 21 °C (70 °F) to temperature shown

Monel 400

Specifications

ASTM. B 127 (plate, sheet, and strip), B 163 (condenser and heat exchanger tube), B 164 (rod, bar, and wire), B 165 (seamless pipe and tube), B 366 (welding fittings), B 564 (forgings), B 725 (welded pipe), B 730 (welded tube), B 751 (welded tube, general requirements), B 775 (welded pipe, general requirements), B 829 (seamless pipe and tube, general requirements)
ASME. SB-127, SB-163, SB-164, SB-165, SB-366, SB-564, SB-751, SB-775, SB-829
AMS. 4544 (sheet, strip, and plate), 4574 (seamless tubing), 4575 (brazed tubing), 4730 (wire), 4731 (wire and ribbon), 7233 (rivets)
UNS number. N04400

Chemical Composition

Composition limits. 63.0 to 70.0 Ni + Co; 0.30 max C; 2.0 max Mn; 2.5 max Fe; 0.24 max S; 0.50 max Si; bal Cu

Applications

Typical uses. Valve and pump parts, propeller shafts, marine fixtures and fasteners, electronic components, chemical processing equipment, gasoline and freshwater tanks, petroleum processing equipment, boiler feedwater heaters and other heat exchangers

Mechanical Properties

Tensile properties. See Tables 14 and 15 and Fig. 4.
Compressive properties. See Table 15.
Hardness. Annealed bar, 110 to 150 HB
Poisson's ratio. 0.32
Elastic modulus. Tension and compression, 179 GPa (26×10^6 psi); torsion, 66 GPa (9.5×10^6 psi)
Impact strength. See Table 16.

Table 14 Tensile properties of Monel 400

Form and condition	Tensile strength		Yield strength (0.2% offset)		Elongation,
	MPa	ksi	MPa	ksi	%
Rod and bar					
Annealed	517–621	75–90	172–345	25–50	60–35
Hot finished	552–758	80–110	276–690	40–100	60–30
Cold drawn, stress relieved	579–827	84–120	379–690	55–100	40–22
Plate					
Hot rolled	517–655	75–95	276–517	40–75	45–30
Annealed	483–586	70–85	193–345	28–50	50–35
Sheet					
Annealed	483–586	70–85	172–310	25–45	50–35
Hard	690–827	100–120	621–758	90–110	15–2
Strip					
Annealed	483–586	70–85	172–310	25–45	55–35
Spring temper	690–965	100–140	621–896	90–130	15–2
Tubing, cold drawn					
Annealed	483–586	70–85	172–310	25–45	50–35
Stress relieved	586–827	85–120	379–690	55–100	35–15
Wire					
Annealed	483–655	70–95	207–379	30–55	45–25
Spring temper	1000–1241	145–180	862–1172	125–170	5–2

Values shown represent usual ranges for common section sizes. In general, values in the higher portions of the ranges are not obtainable with large section sizes, and exceptionally small or large sections may have properties outside the ranges.

Table 15 Typical tensile and compressive properties of Monel 400

	Tension							Compression			
	Tensile strength		Yield strength (0.01% offset)		Yield strength (0.2% offset)		Elongation,	Yield strength (0.01% offset)		Yield strength (0.2% offset)	
Material condition	MPa	ksi	MPa	ksi	MPa	ksi	%	MPa	ksi	MPa	ksi
Hot rolled	579	84	255	37	283	41	39.5	228	33	262	38
Cold drawn, stress equalized	669	97	517	75	600	87	27.0	400	58	558	81
Cold drawn, annealed	538	78	193	28	228	33	44.0	131	19	193	28

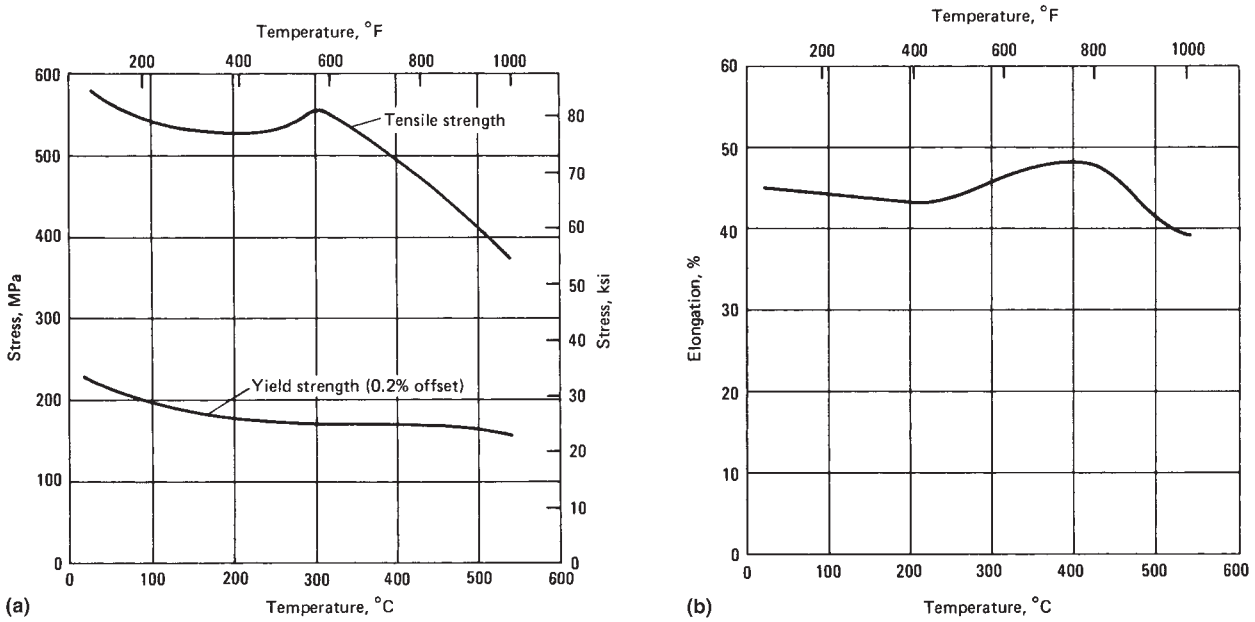


Fig. 4 High-temperature tensile properties of annealed Monel 400. (a) Tensile and yield strength. (b) Elongation

Table 16 Impact strength of Monel 400

Material condition	Impact strength			
	Izod		Charpy V-notch	
	J	ft · lbf	J	ft · lbf
Hot rolled	136–163+	100–120	298	220
Forged	102–156	75–115	…	…
Cold drawn	102–156	75–115	203	150
Annealed	122–163+	90–120	291	215

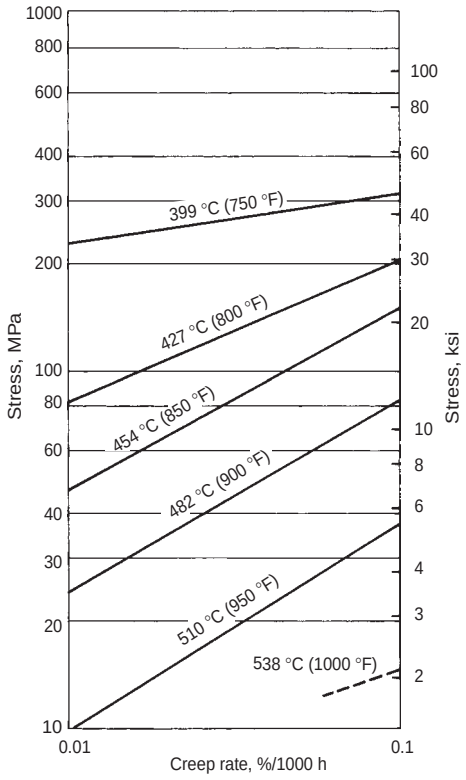


Fig. 5 Creep properties of 20% cold-drawn stress-relieved (538 °C/8 h) Monel 400

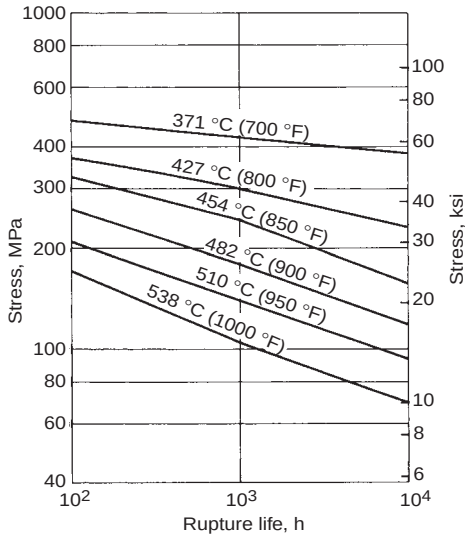


Fig. 6 Rupture properties of cold-drawn stress-relieved (538 °C/8 h) Monel 400

Fatigue strength. Rod, rotating beam: hot rolled, 290 MPa (42.0 ksi); cold drawn, 279 MPa (40.5 ksi); annealed, 231 MPa (33.5 ksi). All values at 10^8 cycles

Creep and stress-rupture properties. See Fig. 5 and 6.

Physical Properties

Density. 8.83 g/cm^3 (0.319 lb/in.^{3}) at 20 °C (68 °F)

Liquidus temperature. 1349 °C (2460 °F)

Solidus temperature. 1299 °C (2370 °F)

Coefficient of thermal expansion. See Table 17.

Specific heat. 427 J/kg · K (0.099 Btu/lb · °F) at 21 °C (70 °F)

Thermal conductivity. See Table 17.

Electrical conductivity. Volumetric, 3.4% IACS at 21 °C (70 °F)

Electrical resistivity. See Table 17.

Table 17 Thermal and electrical properties of Monel 400

Temperature		Mean linear expansion(a)		Thermal conductivity		Electrical resistivity, nΩ · m
°C	°F	μm/m · K	μin./in. · °F	W/m · K	Btu/ft · h · °F	
–196	–320	…	…	…	…	341
–184	–300	11.0	6.1	16.3	9.4	…
–129	–200	11.5	6.4	18.8	10.9	…
–73	–100	12.1	6.7	20.0	11.6	…
21	70	…	…	21.8	12.6	510
93	200	13.9	7.7	24.1	14.0	535
204	400	15.5	8.6	27.8	16.1	560
316	600	15.8	8.8	31.0	18.9	575
427	800	16.0	8.9	34.3	19.8	590
538	1000	16.4	9.1	38.1	22.0	610
649	1200	16.7	9.3	41.4	23.9	630
760	1400	17.3	9.6	44.9	25.9	650
871	1600	17.6	9.8	48.3	27.9	670
982	1800	18.0	10.0	51.9	30.0	690
1093	2000	18.5	10.3	…	…	710

(a) From 21 °C (70 °F) to temperature shown

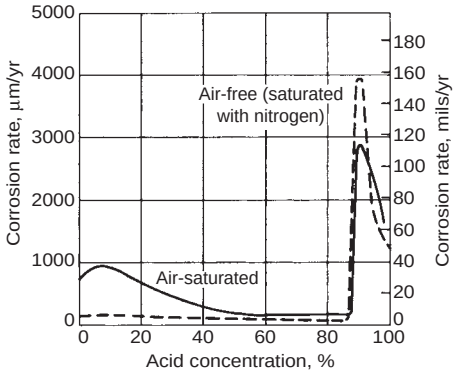


Fig. 7 Corrosion of Monel 400 in sulfuric acid (temperature 66 °C, or 151 °F, velocity, 8.6 mm/s, or 17 ft/min)

Magnetic properties versus treatment. The Curie temperature of Monel 400 is near room temperature and is affected by normal variations in chemical composition. Therefore some lots of material may be magnetic at room temperature and others may not.
Curie temperature. –7 to +10 °C (20–50 °F)

Chemical Properties

General corrosion behavior. Monel 400, a nickel-copper alloy, is more resistant than nickel to corrosion under reducing conditions and more resistant than copper under oxidizing conditions. An important characteristic of the alloy is its general freedom from stress-corrosion cracking. It is highly resistant to seawater or brackish water, chlorinated solvents, glass-etching agents, many acids including sulfuric and hydrochloric, and nearly all alkalies.

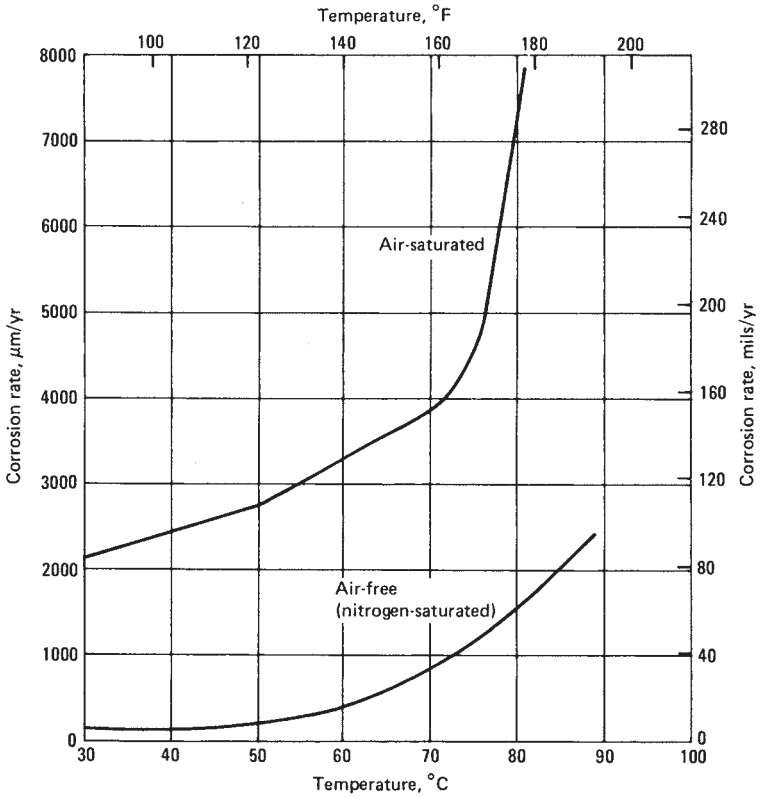


Fig. 8 Effect of temperature on corrosion of Monel 400 in 5% hydrochloric acid

Resistance to specific corroding agents. Corrosion rates in strongly agitated and aerated seawater usually do not exceed 25.4 µm (1 mil) per year. Figure 7 shows corrosion rates in sul-

---

Monel R-405

Specifications

ASTM. B 164 (rod, bar, and wire)
ASME. SB-164
AMS. 4674 (bars and forgings), 7234 (rivets)
UNS number. N04405

Chemical Composition

Composition limits. 63.0 min Ni + Co; 0.3 max C; 2.0 max Mn; 2.5 max Fe; 0.025 to 0.060 S; 0.5 max Si; 28.0 to 34.0 Cu

Applications

Typical uses. Monel R-405 is a free-machining version of Monel 400 designed for parts to be produced by automatic machining. Applications include screw-machine products, water meter parts, valve-seat inserts, and fasteners for nuclear equipment.

Mechanical Properties

Tensile properties. See Table 18.
Compressive properties. See Table 18.
Poisson's ratio. 0.32
Elastic modulus. See Monel 400.
Impact strength. Charpy V-notch: hot rolled, 254 J (187 ft · lbf); cold drawn, 190 J (140 ft · lbf); annealed, 266 J (196 ft · lbf)
Fatigue strength. Rod, rotating beam: hot rolled, 248 MPa (36 ksi); cold drawn, 252 MPa (36.5 ksi); annealed, 207 MPa (30 ksi). All values at 10^8 cycles

Physical Properties

Density. 8.83 g/cm^3 (0.319 lb/in.^{3}) at 20 °C (68 °F)
Liquidus temperature. 1350 °C (2460 °F)
Solidus temperature. 1300 °C (2370 °F)
Coefficient of thermal expansion. Linear: 13.9 µm/m · K (7.7 µin./in. · °F) from 21 to 93 °C (70–200 °F); 15.7 µm/m · K (8.7 µin./in. · °F) from 21 to 260 °C (70–500 °F); 16.4 µm/m · K (9.1 µin./in. · °F) from 21 to 538 °C (70–1000 °F)

Table 18 Typical tensile and compressive properties of Monel R-405

	Tension							Compression			
	Tensile strength		Yield strength (0.01% offset)		Yield strength (0.2% offset)		Elongation,	Yield strength (0.01% offset)		Yield strength (0.2% offset)	
Material condition	MPa	ksi	MPa	ksi	MPa	ksi	%	MPa	ksi	MPa	ksi
Hot rolled	524	76	228	33	248	36	39.5	179	26	234	34
Cold drawn, stress equalized	572	83	427	62	510	74	28.0	352	51	455	66
Cold drawn, annealed	503	73	172	25	193	28	44.5	159	23	179	26

Specific heat. 427 J/kg · K (0.009 Btu/lb · °F) at 20 °C (68 °F)
Thermal conductivity. See Monel 400.
Electrical conductivity. Volumetric, 3.4% IACS at 20 °C (68 °F)
Electrical resistivity. See Monel 400.
Magnetic properties versus treatment. See Monel 400.
Curie temperature. –7 to +10 °C (19–50 °F)

Chemical Properties

General corrosion behavior. See Monel 400.

Monel K-500

Specifications

AMS. 4676 (bars and forgings)
UNS number. N05500

Chemical Composition

Composition limits. 63.0 min Ni + Co; 0.25 max C; 1.5 max Mn; 2.0 max Fe; 0.01 max S; 0.5 max Si; 2.30 to 3.15 Al; 0.35 to 0.85 Ti; 27.0 to 33.0 Cu

Applications

Typical uses. Monel K-500 is an age-hardenable Ni-Cu alloy used for applications that require the corrosion resistance of Monel 400 but greater strength. Examples are pump shafts and impellers, doctor blades, oil well drill collars, springs, and valve trim.

Mechanical Properties

Tensile properties. See Table 19 and Fig. 9.
Compressive properties. See Table 19.
Hardness. See Table 19.
Poisson's ratio. 0.32
Elastic modulus. Tension, 179 GPa (26×10^6 psi); torsion, 66 GPa (9.5×10^6 psi)
Impact strength. Aged bar, Charpy V-notch: 50 J (36.9 ft · lbf) at 20 °C (68 °F); 42 J (30 ft · lbf) at –196 °C (–320 °F)
Fatigue strength. Rod, rotating beam: annealed, 262 MPa (38 ksi); hot rolled, 296 MPa (43 ksi); hot rolled and aged, 352 MPa (52 ksi). All values at 10^8 cycles
Creep and stress-rupture characteristics. See Fig. 10 and 11.

Table 19 Typical tensile properties, compressive properties, and hardness of Monel K-500

Property	Hot rolled	Age hardened
Tension		
Tensile strength, MPa (ksi)	690 (100)	1041 (151)
Yield strength (0.2% offset), MPa (ksi)	324 (47)	765 (111)
Elongation, %	42.5	30.0
Compression		
Yield strength (0.2% offset), MPa (ksi)	276 (40)	834 (121)
Yield strength (0.1% offset), MPa (ksi)	234 (34)	662 (96)
Hardness, HB	165	300

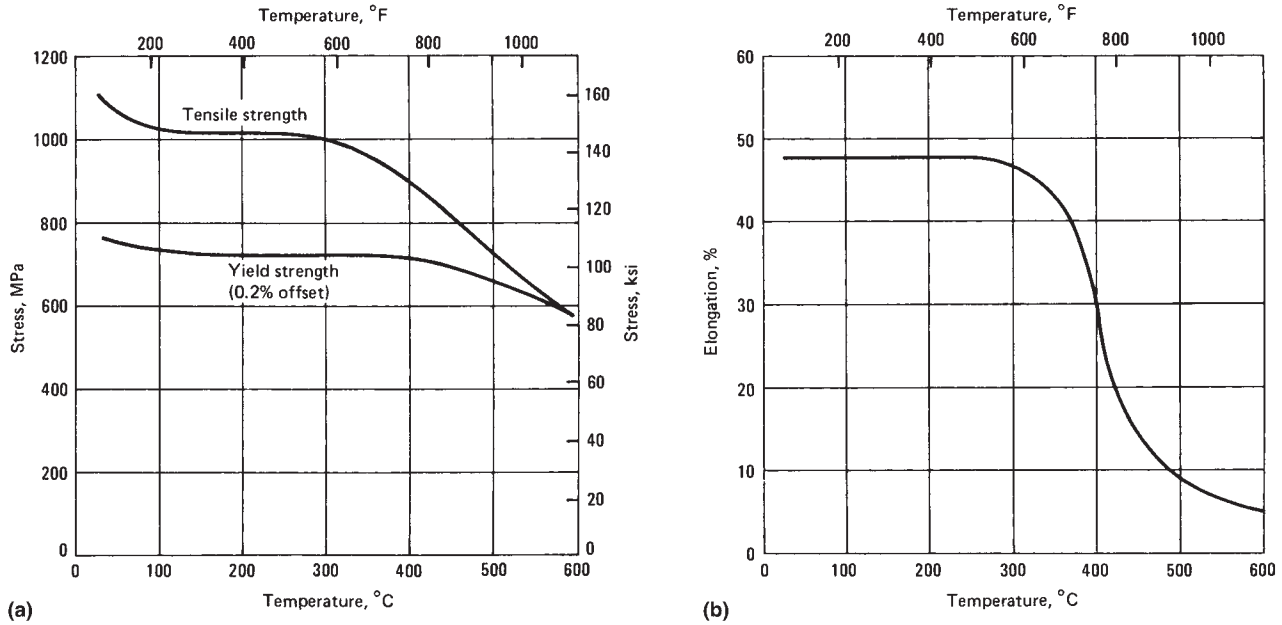


Fig. 9 High-temperature tensile properties of hot-finished, age-hardened Monel K-500. (a) Tensile and yield strengths. (b) Elongation

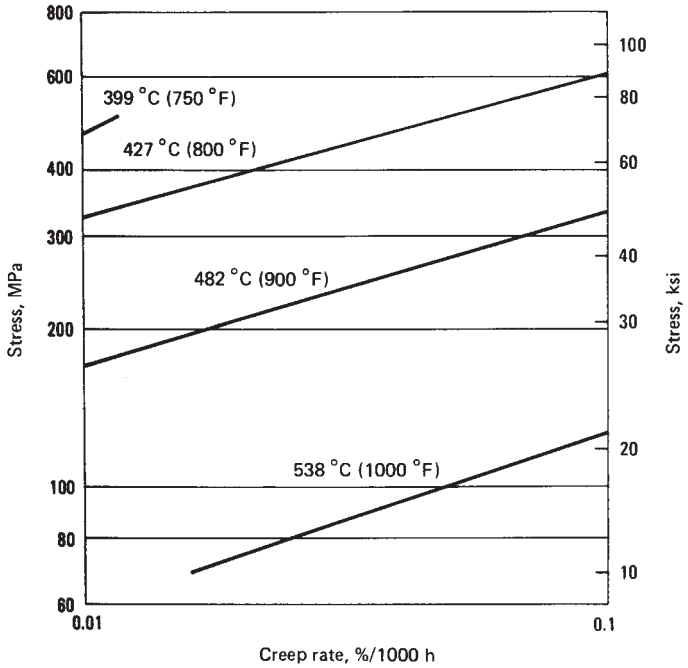


Fig. 10 Creep properties of Monel K-500 (cold drawn and aged)

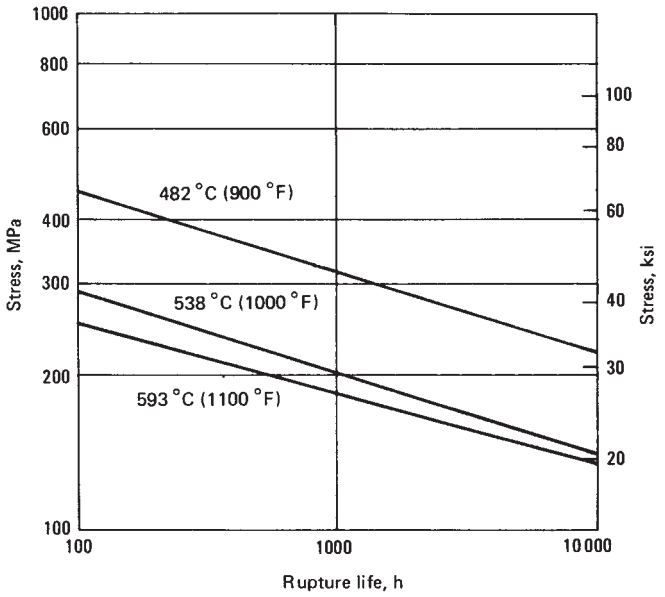


Fig. 11 Stress-rupture life of hot-finished and aged Monel K-500

Physical Properties

Density. 8.47 g/cm^3 (0.305 lb/in.^{3}) at 20 °C (68 °F)
Liquidus temperature. 1350 °C (2460 °F)
Solidus temperature. 1315 °C (2400 °F)
Coefficient of thermal expansion. See Table 20.
Specific heat. 419 J/kg · K (0.097 Btu/lb · °F) at 21 °C (70 °F)
Thermal conductivity. See Table 20.
Electrical conductivity. Volumetric, 2.8% IACS at 21 °C (70 °F)
Electrical resistivity. See Table 20.
Magnetic permeability. Annealed and age-hardened material, 1.0018 at a field strength of 15.9 kA/m
Curie temperature. –134 °C (–210 °F)

Table 20 Thermal and electrical properties of Monel K-500 as a function of temperature

Temperature		Mean linear expansion(a)		Thermal conductivity		Electrical
°C	°F	μm · K	μin./in. · °F	W/m · K	Btu/ft · h · °F	resistivity, nΩ · m
–196	–320	11.2	6.2	…	…	550
–157	–250	11.7	6.5	12.4	7.2	…
–129	–200	12.2	6.8	13.3	7.7	…
–73	–100	13.0	7.2	14.9	8.6	…
21	70	…	…	17.4	10.0	615
93	200	13.7	7.6	19.6	11.3	618
204	400	14.6	8.1	22.5	13.0	628
316	600	14.9	8.3	25.7	14.8	640
427	800	15.3	8.5	28.6	16.5	648
538	1000	15.7	8.7	31.7	18.3	653
649	1200	16.4	9.1	34.6	20.0	658
760	1400	16.7	9.3	37.8	21.8	665
871	1600	17.3	9.6	40.7	23.5	678

(a) From 21 °C (70 °F) to temperature shown

Chemical Properties

General corrosion behavior. The corrosion resistance of Monel K-500 is essentially the same as that of Monel 400 except that, in the age-hardened condition, Monel K-500 is more susceptible to stress-corrosion cracking in some environments.

Inconel 600

Specifications

ASTM. B 163 (condenser and heat exchanger tube), B 166 (rod, bar, and wire), B 167 (seamless pipe and tube), B 168 (plate, sheet, and strip), B 366 (welding fittings, permissible raw materials), B 516 (welded tube), B 517 (welded pipe), B 564 (rod), B 751 (welded tube, general requirements), B 775 (welded pipe, general requirements), B 829 (seamless pipe and tube, general requirements)
ASME. SB-163, SB-166, SB-167, SB-168, SB-366, SB-516, SB-517, SB-564, SB-751, SB-775, SB-829
AMS. 5540 (sheet, strip, and plate), 5580 (seamless tubing), 5665 (bars, forgings, and rings), 5687 (wire), 7232 (rivets)

UNS number. N06600

Chemical Composition

Composition limits. 72.0 min Ni + Co; 14.0 to 17.0 Cr; 6.0 to 10.0 Fe; 0.15 max C; 1.0 max Mn; 0.015 max S; 0.50 max Si; 0.50 max Cu

Applications

Typical uses. Inconel 600 is used in a variety of applications involving temperatures from cryogenic to 1093 °C (2000 °F). Examples are chemical processing vessels and piping, heat treating equipment, aircraft engine and airframe components, electronic parts, and nuclear reactors.

Mechanical Properties

Tensile properties. See Tables 21, 22, and 23.
Compressive properties. See Table 22.
Hardness. See Table 23.
Tensile properties versus temperature. See Table 24.
Poisson's ratio. 0.29
Elastic modulus. Tension, 207 GPa (30×10^6 psi); torsion, 76 GPa (11×10^6 psi)
Impact strength. Plate, Charpy keyhole: 86.1 J (63.5 ft · lbf) at 21 °C (70 °F); 88.8 J (65.5 ft · lbf) at –79 °C (–110 °F); 82.4 J (60.8 ft · lbf) at –196 °C (–320 °F)
Fatigue strength. Rotating beam: annealed, 269 MPa (39.0 ksi); hot rolled, 279 MPa (40.5 ksi); cold drawn, 310 MPa (45.0 ksi). All values at 10^8 cycles and 21 °C (70 °F)
Stress-rupture characteristics. See Table 25.

Physical Properties

Density. 8.42 g/cm^3 (0.304 lb/in.^{3}) at 20 °C (68 °F)
Liquidus temperature. 1415 °C (2575 °F)
Solidus temperature. 1355 °C (2470 °F)
Coefficient of thermal expansion. 15.1 µm/m · K (8.4 µin./in. · °F) at 538 °C (1000 °F); 16.4 µm/m · K (9.1 µin./in. · °F) at 871 °C (1600 °F)
Specific heat. 444 J/kg · K (0.103 Btu/lb · °F) at 21 °C (70 °F)
Thermal conductivity. 14.8 W/m · K (103 Btu/ft^2 · in. · h · °F) at 21 °C (70 °F); 22.8 W/m · K (158 Btu/ft^2 · in. · h · °F) at 538 °C (1000 °F); 28.8 W/m · K (200 Btu/ft^2 · in. · h · °F) at 871 °C (1600 °F)
Electrical conductivity. Volumetric, 1.7% IACS at 21 °C (70 ° F)
Electrical resistivity. 1030 nΩ · m at 21 °C (70 °F)
Magnetic permeability. 1.010 at a field strength of 15.9 kA/m
Curie temperature. –124 °C (–192 °F)

Chemical Properties

General corrosion behavior. The high nickel content of Inconel 600 provides good resistance to corrosion under reducing conditions, and its chromium content, resistance under oxidizing conditions. The alloy is virtually immune to chloride stress-corrosion cracking.
Resistance to specific corroding agents. Inconel 600 has useful resistance to many acid solutions, both oxidizing and reducing. For corrosion rates in sulfuric acid and hydrofluoric acid, see Table 26 and Fig. 12, respectively. This alloy resists dilute hydrochloric acid but not concentrated or hot solutions. It is resistant to all concentrations of phosphoric acid at room temperature. It has poor resistance to nitric acid. Inconel 600 has excellent resistance to alkalies; Fig. 13 shows corrosion rates in boiling sodium hydroxide. Inconel 600 is unaffected by most neutral and alkaline salt solutions and resists many acid salts. It is one of the few materials suitable for use in hot, strong solutions of magnesium chloride, usually having a corrosion rate of about 25 µm (1 mil) per year.

Table 21 Tensile properties for Inconel 600

Form and condition	Tensile strength MPa	Tensile strength ksi	Yield strength (0.2% offset) MPa	Yield strength (0.2% offset) ksi	Elongation, %
Rod and bar					
Annealed	552–690	80–100	172–345	25–50	55–35
Cold drawn	724–1034	105–150	552–862	80–125	30–10
Hot finished	586–827	85–120	241–621	35–90	50–30
Plate					
Hot rolled	586–758	85–110	241–448	35–65	50–30
Annealed	552–724	80–105	207–345	30–50	55–35
Sheet					
Annealed	552–690	80–100	207–310	30–45	55–35
Hard	586–1034	120–150	621–862	90–125	15–2
Strip					
Annealed	552–690	80–100	207–310	30–45	55–35
Spring temper	1000–1172	145–170	827–1103	120–160	10–2
Tubing					
Hot finished	517–690	75–100	172–345	25–50	55–35
Cold drawn and annealed	552–690	80–100	172–345	25–50	55–35
Wire					
Annealed	552–827	80–120	241–517	35–75	45–20
Spring temper	1172–1517	107–220	1034–1448	150–210	5–2

Values shown represent usual ranges for common section sizes. In general, values in the higher portions of the ranges are not obtainable with large section sizes, and exceptionally small or large sections can have properties outside the ranges.

Table 22 Typical tensile and compressive yield strengths of Inconel 600

	Tension				Compression			
	0.02% offset		0.2% offset		0.02% offset		0.2% offset	
Material condition	MPa	ksi	MPa	ksi	MPa	ksi	MPa	ksi
Hot rolled and annealed	268	38.9	303	43.9	276	40.0	309	44.8
Cold drawn and stress relieved	552	80.0	619	89.8	513	74.4	605	87.7
As extruded (tubing)	174	25.2	212	30.8	192	27.9	224	32.5

Table 23 Typical tensile properties and hardness of Inconel 600

Form and condition	Tensile strength MPa	Tensile strength ksi	Yield strength (0.2% offset) MPa	Yield strength (0.2% offset) ksi	Elongation, %	Hardness
Rod						
As rolled	672	97.5	307	44.5	46	86 HRB
Annealed	624	90.5	210	30.4	49	75 HRB
Plate						
As rolled	682	99.0	346	50.2	42	87 HRB
Annealed	639	92.7	199	28.9	49	75 HRB
Tubing						
As drawn	993	144.0	916	132.8	8	34 HRC
Annealed	693	100.5	279	40.5	43	83 HRB

Table 24 Typical elevated-temperature tensile properties of Inconel 600 bar

Temperature °C	Temperature °F	Tensile strength MPa	Tensile strength ksi	Yield strength MPa	Yield strength ksi	Elongation, %
21	70	620	90	250	36	47
540	1000	580	84	195	28	47
650	1200	450	65	180	26	39
760	1400	185	27	115	17	46
870	1600	105	15	62	9	80

Table 25 Typical stress-rupture strengths of Inconel 600

Temperature °C	Temperature °F	For stress rupture at: 100 h MPa	100 h ksi	1000 h MPa	1000 h ksi
815	1500	55	8	39	5.6
870	1600	37	5.3	24	3.5

Table 26 Corrosion rates for Inconel 600 in various concentrations of sulfuric acid at room temperature and at boiling temperature

Acid concentration, %	Corrosion rate at: Room temperature mm/yr	Room temperature mils/yr	Boiling temperature mm/yr	Boiling temperature mils/yr
10	0.081	3.2	3.43	135
20	0.051	2.0	4.72	186
30	0.064	2.5	5.49	216
40	0.046	1.8	17.8	700
50	0.041	1.6	…	…
60	0.048	1.9	…	…
70	0.058	2.3	…	…
80	0.566	22.3	…	…
90	0.013	0.5	…	…
98	0.188	7.4	…	…

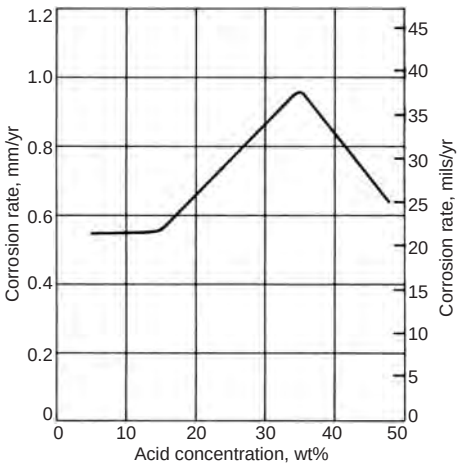


Fig. 12 Corrosion rates for Inconel 600 in hydrofluoric acid at 75 °C (167 °F)

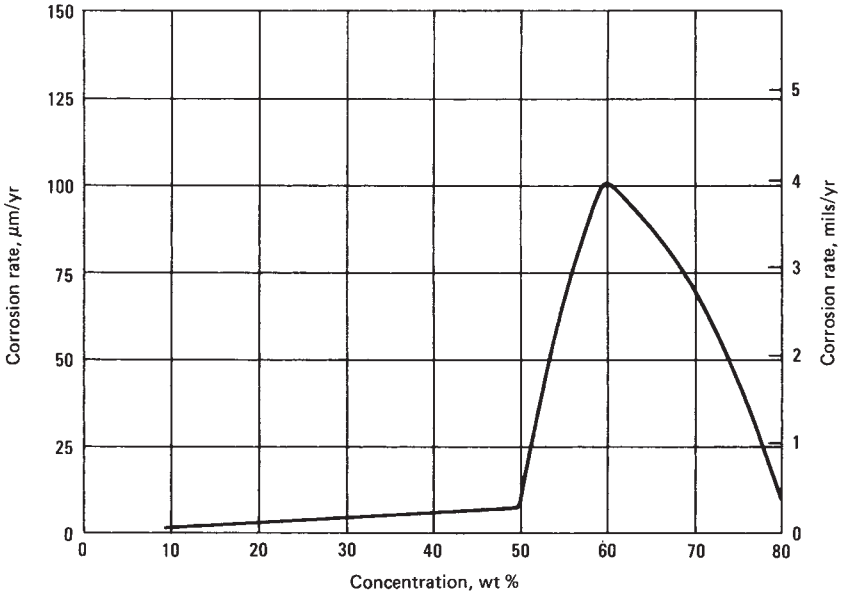


Fig. 13 Corrosion rates for Inconel 600 in boiling sodium hydroxide

Inconel 622

Specifications

ASTM. B 366 (welding fittings, permissible raw materials), B 564 (forgings), B 574 (rod), B 575 (plate, sheet, and strip), B 619 (welded pipe), B 622 (seamless pipe and tube), B 626 (welded tube), B 751 (welded tube, general requirements), B 775 (welded pipe, general requirements), B 829 (seamless pipe and tube, general requirements)
ASME. SB-366, SB-564, SB-574, SB-575, SB-619, SB-622, SB-626, SB-751, SB-775, SB-829
UNS number. N06022

Chemical Composition

Nominal composition. 20.5 Cr; 14.2 Mo; 2.3 Fe; 3.2 W; 2.5 max Co; 0.35 max V; 0.015 max C; 0.50 max Mn; 0.02 max S; 0.08 max Si; 0.02 max P; bal Ni

Applications

Typical uses. Equipment for chemical processing, flue gas desulfurization, hazardous waste incineration, and pulp and paper processing

Mechanical Properties

Tensile properties. See Table 27.
Hardness. See Table 27.

Elastic modulus (dynamic). 209 GPa (30.3×10^6 psi)

Physical Properties

Density. 8.61 g/cm^3 (0.311 lb/in.^{3}) at room temperature
Melting range. 1351 to 1387 °C (2464–2529 °F)
Coefficient of thermal expansion. 12.44 µm/m · K at 25 to 94 °C (6.91 µin./in. · °F at 77 to 200 °F)

Table 27 Typical room-temperature mechanical properties of Inconel 622

Form	Material thickness or diameter mm	Material thickness or diameter in.	Tensile strength MPa	Tensile strength ksi	Yield strength (0.2% offset) MPa	Yield strength (0.2% offset) ksi	Elongation, %	Hardness, HRB
Plate	12.7	0.500	733	106.3	330	47.9	69	85
	6.4	0.250	700	101.5	311	45.1	69	85
Sheet	1.5	0.060	783	113.5	380	55.1	54	90
Round	38.1	1.500	786	114.0	365	52.9	57	92

Specific heat. 381 J/kg · K (0.091 Btu/lb · °F) at room temperature
Electrical resistivity. 1.215 μΩ · m (730.7 Ω circular-mil/ft) at room temperature

Chemical Properties

General corrosion behavior. Alloy 622 resists oxidizing as well as reducing acids, such as sulfuric and hydrochloric acids. Other corrosive media to which the alloy has high resistance are oxidizing acid chlorides, wet chlorine, formic and acetic acids, ferric and cupric chlorides, seawater, brines, and many mixed or contaminated chemical solutions, both organic and inorganic. Alloy 622 also resists localized forms of attack (pitting and crevice corrosion) in these environments.
Resistance to specific corroding agents. See Table 28.

Table 28 Comparative corrosion rates for Inconel 622 and Hastelloy C-22 in various corrosive media

Test solution	Alloy	Corrosion rate	
		mm/yr	mils/yr
10% H_2SO_4 (boiling)	Inconel 622	0.56	22
	Hastelloy C-22	0.56	22
2% HCl (boiling)	Inconel 622	1.32	52
	Hastelloy C-22	1.63	64
80% H_2SO_4 (80 °C, or 175 °F)	Inconel 622	1.32	52
	Hastelloy C-22	1.30	51
10% H_2SO_4 + 2% HCl (boiling)	Inconel 622	7.09	279
	Hastelloy C-22	9.40	370
40% H_2SO_4 + 10% HCl (80 °C, or 175 °F)	Inconel 622	0.81	32
	Hastelloy C-22	0.97	38
10% H_2SO_4 + 5% HCl (boiling)	Inconel 622	11.6	456
	Hastelloy C-22	12.3	484
10% H_2SO_4 + 5% HCl (80 °C, or 175 °F)	Inconel 622	2.08	82
	Hastelloy C-22	2.77	109
20% H_2SO_4 + 2% HCl (boiling)	Inconel 622	11.4	448
	Hastelloy C-22	13.7	539
85% H_3PO_4 (boiling)	Inconel 622	0.58	23
	Hastelloy C-22	0.61	24
10% HNO_3 + 3% HF (boiling)	Inconel 622	0.61	24
	Hastelloy C-22	0.58	23

Inconel 625

Specifications

ASTM. B 366 (welding fittings, permissible raw materials), B 443 (plate, sheet, and strip), B 444 (seamless pipe and tube), B 446 (rod and bar), B 564 (forgings), B 704 (welded tube), B 705 (welded pipe), B 751 (welded tube, general requirements), B 775 (welded pipe, general requirements), B 829 (seamless pipe and tube, general requirements)
ASME. SB-336, SB-443, SB-444, SB-446, SB-564, SB-704, SB-705, SB-751, SB-775, SB-829
AMS. 5581 (seamless and welded tubing), 5599 (sheet, strip, and plate), 5666 (bars, forgings, and rings), 5837 (wire), 5869 (sheet, strip, and plate)
UNS number. N06625

Chemical Composition

Composition limits. 20.0 to 23.0 Cr; 5.0 max Fe; 8.0 to 10.0 Mo; 3.15 to 4.15 Cb + Ta; 0.10 max C; 0.50 max Mn; 0.50 max Si; 0.015 max P; 0.015 max S; 0.40 max Al; 0.40 max Ti; 1.0 max Co; 58.0 min Ni

Table 29 Typical elevated-temperature tensile properties of Inconel 625 bar

Temperature		Tensile strength		Yield strength		Elongation,
°C	°F	MPa	ksi	MPa	ksi	%
21	70	855	124	490	71	50
540	1000	745	108	405	59	50
650	1200	710	103	420	61	35
760	1400	505	73	420	61	42
870	1600	285	41	475	40	125

Applications

Typical uses. Chemical processing equipment, aircraft engine and airframe components, ship and submarine parts, nuclear reactors

Mechanical Properties

Tensile properties. See Table 29.
Poisson's ratio. Annealed material, 0.278 at 21 °C (70 °F)
Elastic modulus. Annealed material: tension, 208 GPa (30 × 10^6 psi) at 21 °C (70 °F); torsion, 81 GPa (11.8 × 10^6 psi) at 21 °C (70 °F)
Impact strength. As-rolled plate, Charpy keyhole: 66 J (48.7 ft · lbf) at 29 °C (85 °F); 60 J (44.2 ft · lbf) at –79 °C (–110 °F); 47 J (34.7 ft · lbf) at –196 °C (–320 °F)
Fatigue strength. See Fig. 14.
Stress-rupture characteristics. See Table 30.

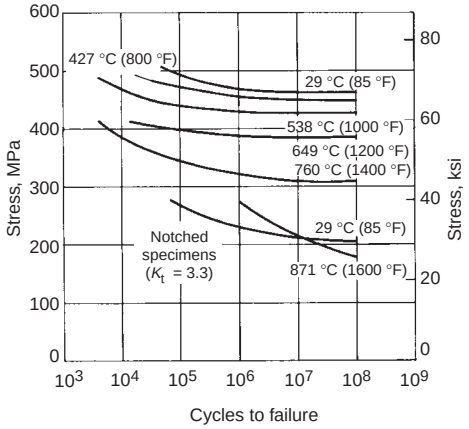


Fig. 14 Rotating-beam fatigue strength of hot-rolled solution-treated Inconel 625 bar (15.9 mm, or 0.625 in., diam) at elevated temperature. Average grain size, 0.10 mm (0.004 in.)

Physical Properties

Density. 8.44 g/cm^3 (0.305 lb/in.^{3}) at 20 °C (68 °F)
Liquidus temperature. 1350 °C (2460 °F)
Solidus temperature. 1290 °C (2350 °F)
Coefficient of thermal expansion. 14.0 μm/m · K (7.8 μin./in. · °F) at 538 °C (1000 °F); 15.8 μm/m · K (8.8 μin./in. · °F) at 871 °C (1600 °F)
Specific heat. 410 J/kg · K (0.095 Btu/lb · °F) at 21 °C (70 °F)
Thermal conductivity. 9.8 W/m · K (68 Btu/ft^2 · in. · h · °F) at 21 °C (70 °F); 17.5 W/m · K (121 Btu/ft^2 · in. · h · °F) at 538 °C (1000 °F); 22.8 W/m · K (158 Btu/ft^2 · in. · h · °F) at 871 °C (1600 °F)
Electrical conductivity. Volumetric, 1.3% IACS at 21 °C (70 °F)
Electrical resistivity. 1290 nΩ · m at 21 °C (70 °F)
Magnetic permeability. 1.006 at a field strength of 15.9 kA/m
Curie temperature. <–196 °C (<– 320 °F)

Table 30 Typical stress-rupture strengths of solution treated (1150 °C, or 2100 °F) Inconel 625

Temperature		For stress rupture at:			
		100 h		1000 h	
°C	°F	MPa	ksi	MPa	ksi
650	1200	440	64	370	54
815	1500	130	19	93	13.5
870	1600	72	10.5	48	7

Chemical Properties

General corrosion behavior. The high alloy content of Inconel 625 enables it to withstand a wide variety of corrosive environments. The alloy is almost completely resistant to mild environments such as the atmosphere, fresh water and seawater, neutral salts, and alkaline media. In more severe environments, the combination of nickel and chromium provides resistance to oxidizing chemicals, and the combination of nickel and molybdenum provides resistance to reducing conditions. The molybdenum content also makes Inconel 625 highly resistant to pitting and crevice corrosion. The columbium stabilizes the alloy against sensitization and prevents intergranular corrosion. The high nickel content provides freedom from chloride stress-corrosion cracking.

Resistance to specific corroding agents. Table 31 gives corrosion rates in sulfuric and hydrochloric acides; Fig. 15 shows resistance to phosphoric acid. In boiling 65% nitric acid, Inconel 625 typically corrodes at a rate of 0.76 mm (30 mils) per year. In boiling 50% sodium hydroxide, the corrosion rate is 0.13 mm (5.0 mils) per year. Additional data comparing alloy 625 with other corrosion resistant alloys can be found in Tables 48, 65, 69, and 70.

Table 31 Corrosion rates for Inconel 625 in sulfuric and hydrochloric acids at various concentrations

	Corrosion rate	
Concentration, %	mm/yr	mils/yr
Sulfuric acid(a)		
15	0.188	7.40
50	0.432	17.0
60	0.711	28.0
70	1.626	64.0
80	2.286	90.0
Hydrochloric acid(b)		
5	1.803	71.0
10	2.057	81.0
15	1.651	65.0
20	1.270	50.0
25	0.965	38.0
30	0.864	34.0
Conc(c)	0.381	15.0

(a) At 80 °C (176 °F). (b) At 66 °C (151 °F). (c) Conc, concentrated, approximately 37.1%

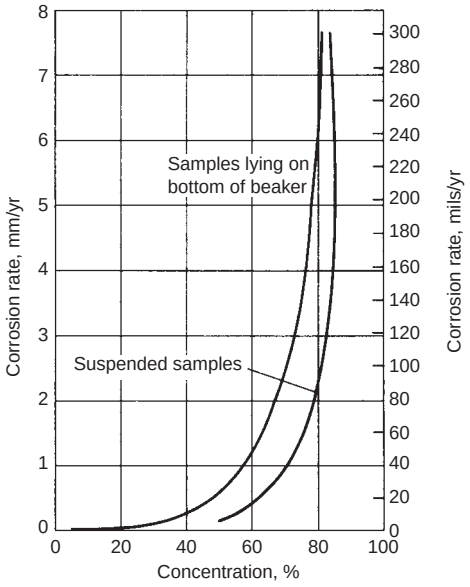


Fig. 15 Corrosion of Inconel 625 in boiling phosphoric acid solutions

Inconel 686

Specifications

ASTM. B 564 (forgings), B 574 (wire), B 575 (plate, sheet, and strip), B 619 (welded pipe), B 622 (seamless tube and pipe), B 626 (welded tube), B 751 (welded tube, general requirements), B 775 (welded pipe, general requirements), B 829 (seamless tube and pipe, general requirements)

ASME. SB-564, SB-574, SB-575, SB-619, SB-622, SB-626, SB-751, SB-775, SB-829

UNS number. N06686

Chemical Composition

Composition limits. 19.0 to 23.0 Cr; 15.0 to 17.0 Mo; 3.0 to 4.4 W; 0.02 to 0.25 Ti; 1.0 max Fe; 0.01 max C; 0.75 max Mn; 0.02 max S; 0.08 max Si; 0.04 max P; bal Ni

Applications

Typical uses. Used for resistance to aggressive media in chemical processing, pollution control, pulp and paper manufacture, and waste management applications

Mechanical Properties

Tensile properties. See Tables 32 (room-temperature data) and 33 (elevated-temperature data).

Elastic modulus. See Table 34.

Shear modulus. See Table 34.

Poisson's ratio. See Table 34.

Impact strength. See Table 35.

Table 32 Typical room-temperature tensile properties of Inconel 686

	Thickness or diameter		Tensile strength		Yield strength (0.2% offset)		Elongation,
Product form	mm	in.	MPa	ksi	MPa	ksi	%
Plate	12.7	0.500	722	104.7	364	52.8	71
	6.35	0.250	733	106.3	399	57.9	68
Sheet	3.18	0.125	803	116.5	421	61.1	59
	1.57	0.062	848	123.0	408	59.2	59
Rod	38.1	1.50	810	117.5	359	52.1	56

Table 33 Typical elevated-temperature tensile properties of Inconel 686

Temperature		Yield strength		Tensile strength		
°C	°F	MPa	ksi	MPa	ksi	Elongation, %
24	75	396	57.5	740	107.3	60
93	200	323	46.8	691	100.2	69
204	400	290	42.1	635	92.1	67
316	600	288	41.7	602	87.3	60
427	800	224	32.5	570	82.6	69
538	1000	261	37.9	545	79.1	61

Physical Properties

Density. 8.73 g/cm^3 (0.315 lb/in.^{3})

Melting range. 1338 to 1380 °C (2440–2516 °F)

Coefficient of thermal expansion. See Table 36.

Specific heat. See Table 36.

Electrical resistivity. See Table 36.

Magnetic permeability. 1.0001 at a field strength of 15.9 kA/m

Chemical Properties

General corrosion behavior. The high nickel and molybdenum contents of alloy 686 provide good resistance in reducing conditions, whereas the high chromium content offers resistance to oxidizing media. Molybdenum and

Table 34 Moduli of elasticity and Poisson's ratio of Inconel 686

Temperature, °F	Elastic modulus, 10^6 psi	Shear modulus, 10^6 psi	Poisson's ratio	Temperature, °C	Elastic modulus, GPa	Shear modulus, GPa	Poisson's ratio
70	30.0	11.1	0.35	20	207	77	0.34
200	29.7	10.9	0.36	100	205	75	0.37
400	28.5	10.5	0.36	200	197	72	0.37
600	28.0	10.2	0.37	300	193	70	0.38
800	26.9	9.9	0.36	400	185	69	0.34
1000	26.0	9.5	0.37	500	183	67	0.37
1200	24.6	9.1	0.35	600	173	65	0.33
				700	165	61	0.35

Table 35 Effect of 100 h high-temperature exposure on room-temperature Charpy V-notch impact strength of Inconel 686

Exposure temperature		Impact strength	
°C	°F	J	ft · lbf
Test temperature 20 °C (70 °F)			
As annealed		405	299
540	1000	400	295
650	1200	401	296
760	1400	25.1	18.5
870	1600	8.1	6.0
980	1800	2.7	2.0
Test temperature –196 °C (–320 °F)			
As annealed		404	298
540	1000	405	299
650	1200	403	297
760	1400	12.2	9.0
870	1600	3.4	2.5
980	1800	2.7	2.0

tungsten aid resistance to localized corrosion, such as pitting. Low carbon helps minimize grain-boundary precipitation to maintain corrosion resistance in the heat-affected zones of welded joints. Alloy 686 is especially suited to handling mixed acids containing high concentrations of halides. It has shown good resistance to mixed acid media with pH levels of 1 or less, and chloride levels of more than 100,000 ppm.

Resistance to specific corroding agents. See Tables 37 and 38.

Table 36 Thermal and electrical properties of Inconel 686

Temperature, °F	Specific heat, Btu/lb · °F	Coefficient of expansion(a), μin./in. · °F	Electrical resistivity, Ω · circular-mil/ft	Temperature, °C	Specific heat, J/kg · °C	Coefficient of expansion(a), μm/m · K	Electrical Resistivity, μΩ · cm
0	0.087	…	…	–15	364	…	…
70	0.089	…	744.4	20	373	…	123.7
200	0.092	6.67	749.2	100	389	11.97	124.6
400	0.098	6.81	756.7	200	410	12.22	125.7
600	0.104	7.00	760.9	300	431	12.56	126.3
800	0.110	7.17	765.6	400	456	12.87	127.2
1000	0.116	7.25	779.8	500	477	13.01	128.9
1200	0.122	7.49	776.1	600	498	13.18	129.5
				700	519	…	127.9

(a) Mean coefficient of linear expansion between room temperature and temperature shown

Table 37 Corrosion rates of Inconel 686 and other nickel alloys in various acid solutions (one week test duration)

	Corrosion rate, mm/yr (mils/yr)			
Alloy	80% H_2SO_4 80 °C (176 °F)	2% HCl boiling	10% H_2SO_4 + 2% HCl boiling	10% H_2SO_4 + 5% HCl 80 °C (176 °F)
Inconel 686(a)	0.10 (4)	0.15 (6)	3.35 (132)	0.86 (34)
Alloy C-276	0.58 (23)	1.09 (43)	3.51 (138)	…
Inconel 622	1.32 (52)	1.32 (52)	7.09 (279)	2.08 (82)
Alloy C-22	1.30 (51)	1.40 (55)	9.40 (370)	2.77 (109)

(a) Average of two tests

Table 38 Corrosion rates of Inconel 686 and other nickel alloys in hydrochloric and phosphoric acids (192 h tests)

	Temperature		Corrosion rate, mm/yr (mils/yr)			
Solution	°C	°F	Alloy C-276	Alloy 25-6MO	Inconel 622	Inconel 686
0.2% HCl	Boiling	Boiling	<0.025 (<1)	<0.025 (<1)	<0.025 (<1)	<0.025 (<1)
1% HCl	Boiling	Boiling	0.33 (13)	3.02 (119)	0.08 (3)	0.05 (2)
5% HCl	70	158	0.33 (13)	3.61 (142)	0.48 (19)	0.25 (10)
	50	122	0.10 (4)	1.09 (43)	0.13 (5)	0.05 (2)
85% H_3PO_4	Boiling	Boiling	0.25 (10)	2.90 (114)	0.33 (13)	0.41 (16)
	90	194	<0.025 (<1)	0.30 (11)	<0.025 (<1)	<0.025 (<1)

Inconel 690

Specifications

ASTM. B 163 (condenser and heat exchanger tube), B 166 (rod, bar, and wire), B 167 (seamless pipe and tube), B 168 (plate, sheet, and strip), B 564 (forgings), B 829 (seamless pipe and tube, general requirements)

ASME. SB-163, SB-166, SB-167, SB-168, SB-564, SB-751, SB-775, SB-829

UNS number. N06690

Chemical Composition

Composition limits. 27.0 to 31.0 Cr; 7.0 to 11.0 Fe; 0.05 max C; 0.50 max Cu; 0.50 max Mn; 0.0015 max S; 0.50 max Si; 58.0 min Ni

Applications

Typical uses. Applications involving nitric acid or nitric-plus-hydrochloric acid. Examples are tail-gas reheaters used in production of nitric acid and steam-heating coils in nitric-plus-hydrochloric acid solutions used for pickling stainless steels and reprocessing nuclear fuels. Inconel 690 is also useful for high-temperature service in gases containing sulfur.

Table 39 Typical tensile properties and hardness of Inconel 690

Material condition	Tensile strength		Yield strength (0.2% offset)		Elongation, %	Hardness, HRB
	MPa	ksi	MPa	ksi		
Tube, annealed	731	106	365	53	41	97
Strip, annealed	758	110	372	54	40	88
Rod, as rolled	765	111	434	63	40	90
Rod, annealed	710	103	317	46	49	90
Plate, as rolled	765	111	483	70	36	95

Table 40 Thermal and electrical properties of Inconel 690 as a function of temperature

Temperature		Mean linear expansion(a)		Thermal conductivity		Electrical resistivity,
°C	°F	μm/m · K	μin./in. · °F	W/m · K	Btu/ft · h · °F	nΩ · m
26	78	…	…	13.9	8.0	148
93	200	13.5	7.5	15.0	8.7	161
204	400	…	…	17.0	9.8	181
316	600	15.3	8.5	18.8	10.9	202
427	800	…	…	20.5	11.8	224
538	1000	…	…	22.8	13.1	238
649	1200	16.2	9.0	24.2	14.0	238
760	1400	…	…	26.0	15.0	245
871	1600	…	….	27.8	16.1	252
982	1800	17.6	9.8	29.5	17.0	263
1093	2000	…	…	31.2	18.0	277
1204	2200	…	…	32.8	18.9	292

(a) From 21 °C (70 °F) to temperature shown

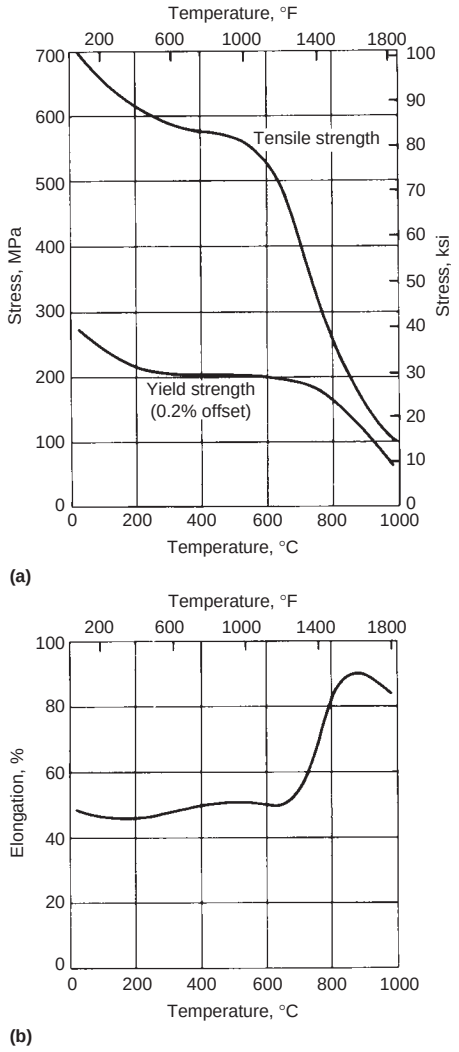


Fig. 16 High-temperature tensile properties of Inconel 690 annealed at 1095 °C (2000 °F) for 1 h and water quenched. (a) Tensile and yield strengths. (b) Elongation

Mechanical Properties

Tensile properties. See Table 39 and Fig. 16.
Hardness. See Table 39.
Poisson's ratio. 0.289
Elastic modulus. Tension, 210 GPa (30.5×10^6 psi)

Physical Properties

Density. 8.14 g/cm^3 (0.29 lb/in.^{3}) at 20 °C (68 °F)
Liquidus temperature. 1375 °C (2510 °F)
Solidus temperature. 1345 °C (2450 °F)
Coefficient of thermal expansion. See Table 40.
Thermal conductivity. See Table 40.
Electrical conductivity. Volumetric, 1.5% IACS at 26 °C (78 °F)
Electrical resistivity. See Table 40.

Chemical Properties

General corrosion behavior. A high chromium content gives Inconel 690 good resistance to oxidizing chemicals, such as nitric acid, and to sulfur-containing gases at high temperature.
Resistance to specific corroding agents. Corrosion rates in nitric-plus-hydrofluoric acid solutions at 60 °C (140 °F) are:

Solution	Corrosion rate	
	mm/yr	mils/yr
10% HNO_3, 3% HF	0.15	6.0
15% HNO_3, 3% HF	0.25	10.0
20% HNO_3, 3% HF	0.15	6.0

Inconel 718

Specifications

ASTM. B 637 (rod, bar, forgings, and forging stock), B 670 (plate, sheet, and strip)
ASME. SB-637
AMS. 5589 (seamless tubing), 5590 (seamless tubing), 5596 (sheet, strip, and plate), 5597 (sheet, strip, and plate), 5662 (bars, forgings, and rings), 5663 (bars, forgings, and rings), 5664 (bars, forgings, and rings), 5832 (welding wire)
UNS number. N07718

Chemical Composition

Composition limits. 50.0 to 55.0 min Ni + Co; 17.0 to 21.0 Cr; 4.75 to 5.50 Nb; 2.80 to 3.30 Mo; 0.65 to 1.15 Ti; 0.20 to 0.80 Al; 1.00 max Co; 0.08 max C; 0.35 max Mn; 0.35 max Si; 0.015 P; 0.015 S; 0.006 max B; 0.30 max Cu; bal Fe

Table 41 Room-temperature tensile properties of hot-rolled Inconel 718 bar

Diameter(a)			Tensile strength		Yield strength (0.2% offset)		Elongation,	Reduction of area,	
mm	in.	Heat treatment(b)	MPa	psi	MPa	psi	%	%	Hardness
16	5/8	As-rolled	965	140,000	591	85,700	46	58	23 HRC
		955 °C (1750 °F)/1 h	965	140,000	572	83,000	45	49	99 HRB
		1065 °C (1950 °F)/1 h	810	117,500	334	48,500	58	64	85 HRB
		955 °C (1750 °F)/1 h, age	1,434	208,000	1,241	180,000	21	39	46 HRC
		1065 °C (1950 °F)/1 h, age	1,338	194,000	1,083	157,000	23	34	45 HRC
16	5/8	As-rolled	958	139,000	541	78,500	46	62	20 HRC
		955 °C (1750 °F)/1 h	952	138,000	521	75,500	54	49	97 HRB
		1065 °C (1950 °F)/1 h	796	115,500	331	48,000	64	67	85 HRB
		955 °C (1750 °F)/1 h, age	1,438	208,500	1,238	179,500	20	39	45 HRC
		1065 °C (1950 °F)/1 h, age	1,341	194,500	1,089	158,000	20	26	44 HRC
25	1	As-rolled	896	130,000	448	65,000	54	67	16 HRC
		955 °C (1750 °F)/1 h	889	129,000	445	64,500	55	61	94 HRB
		1065 °C (1950 °F)/1 h	776	112,500	359	52,000	64	68	87 HRB
		955 °C (1750 °F)/1 h, age	1,389	201,500	1,207	175,000	20	36	46 HRC
		1065 °C (1950 °F)/1 h, age	1,296	188,000	1,048	152,000	21	34	45 HRC
38	1 1/2	As-rolled	1,014	147,000	727	105,500	40	52	32 HRC
		955 °C (1750 °F)/1 h	976	141,500	500	72,500	46	45	97 HRB
		1065 °C (1950 °F)/1 h	827	120,000	379	55,000	58	60	89 HRB
		955 °C (1750 °F)/1 h, age	1,413	205,000	1,155	167,500	20	28	46 HRC
		1065 °C (1950 °F)/1 h, age	1,317	191,000	1,055	153,000	24	36	43 HRC
100	4	955 °C (1750 °F)/1 h	810	117,500	379	55,000	53	52	90 HRB
		1065 °C (1950 °F)/1 h	776	112,500	331	48,000	60	63	87 HRB
		955 °C (1750 °F)/1 h, age	1,324	192,000	1,138	165,000	17	24	46 HRC
		1065 °C (1950 °F)/1 h, age	1,348	195,500	1,138	165,000	21	34	43 HRC

(a) Five separate heats represented. All tests are longitudinal. (b) When annealing is at 955 °C (1750 °F), aging is 720 °C (1325 °F) for 8 h, furnace cool to 625 °C (1150 °F) hold at 625 °C (1150 °F) for total aging time of 18 h. When annealing is at 1065 °C (1950 °F), aging is 760 °C (1400 °F) for 10 h, furnace cool to 650 °C (1200 °F), hold at 650 °C (1200 °F) for total aging time of 20 h

Applications

Typical uses. Age-hardenable alloy 718 combines high-temperature strength up to 700 °C (1300 °F) with corrosion resistance and excellent fabricability. Its welding characteristics, especially its resistance to postweld cracking, are outstanding. Because of these attributes, alloy 718 is used for parts for aircraft turbine engines; high-speed airframe parts, such as wheels, buckets, and spacers; high-temperature bolts and fasteners, cryogenic tankage, and components for oil and gas extraction and nuclear engineering.

Mechanical Properties

Effect of heat treatment on properties. For most applications, alloy 718 receives one of two heat treatments:

- Anneal at 925 to 1010 °C (1700–1850 °F), age at 720 °C (1325 °F) for 8 h, furnace cool to 620 °C (1150 °F), hold at 620 °C (1150 °F) for 18 h, air cool
- Anneal at 1035 to 1065 °C (1900–1950 °F), age at 760 °C (1400 °F) for 10 h, furnace cool to 650 °C (1200 °F), hold at 650 °C (1200 °F) for 20 h, air cool

The 925 to 1010 °C (1700–1850 °F) anneal and age is the optimum heat treatment where a combination of stress-rupture life, notch-rupture life, and rupture ductility is of greatest concern. The highest room-temperature tensile and yield strengths are also associated with this treatment. The 1035 to 1065 °C (1900–1950 °F) anneal and aging treatment is preferred in tensile-limited applications because it promotes the best transverse ductility in heavy sections, impact strength, and low-temperature notch tensile strength. However, this treatment has a tendency to produce notch brittleness in stress rupture.

Table 42 Room-temperature tensile properties of Inconel 718 cold-rolled sheet, annealed and aged in accordance with AMS 5597A

Thickness		Tensile strength		Yield strength		Elongation,
mm	in.	MPa	psi	MPa	psi	%
0.25	0.010	1,327	192,500	1,189	172,500	17
0.30	0.012	1,407	204,000	1,169	169,500	19
0.38	0.015	1,365	198,000	1,117	162,000	19
0.41	0.016	1,351	196,000	1,127	163,500	19
0.46	0.018	1,355	196,500	1,072	155,500	21
0.53	0.021	1,396	202,500	1,165	169,000	20
0.64	0.025	1,372	199,000	1,120	162,500	20
0.79	0.031	1,358	197,000	1,103	160,000	21
1.02	0.040	1,434	208,000	1,186	172,000	16
1.19	0.047	1,372	199,000	1,148	166,500	20
1.27	0.050	1,455	211,000	1,220	177,000	16
1.57	0.062	1,403	203,500	1,179	171,000	18
1.98	0.078	1,324	192,000	1,093	158,500	17
2.03	0.080	1,379	200,000	1,127	163,500	20
2.36	0.093	1,372	199,000	1,151	167,000	19
2.54	0.100	1,434	208,000	1,214	176,000	18
2.77	0.109	1,407	204,000	1,179	171,000	19
3.18	0.125	1,403	203,500	1,186	172,000	16
3.96	0.156	1,355	196,500	1,110	161,000	21
4.75	0.187	1,431	207,500	1,255	182,000	18
5.33	0.210	1,341	194,500	1,103	160,000	22
6.35	0.250	1,413	205,000	1,176	170,500	19

Tensile properties. Room-temperature tensile properties for hot-rolled bar and cold-rolled sheet are listed in Tables 41 and 42, respectively. High-temperature tensile properties for annealed and aged bar are given in Fig. 17.

Hardness. See Table 41.

Elastic modulus. See Table 43.

Creep and stress-rupture characteristics. See Fig. 18 and 19.

Impact strength. Room-temperature Charpy V-notch values for annealed and aged (per AMS 5596) 25 mm (1 in.) thick plate range from 26.4 to 30.5 J (19.5–22.5 ft · lbf); at –160 °C (–320 °F), Charpy V-notch values range from 25.1 to 26.4 J (18.5–19.5 ft · lbf)

Fatigue strength. See Table 44.

Physical Properties

Density. 8.19 g/cm^3 (0.296 lb/in.^{3})

Melting range. 1260 to 1336 °C (2300–2437 °F)

Coefficient of thermal expansion (linear):

Temperature		Average coefficient(a)(b)	
°C	°F	μm/m · K	μin./in. · °F
–195	–320	10.6	5.9
95	200	13.2	7.31
205	400	13.6	7.53
315	600	13.9	7.74
425	800	14.3	7.97
540	1000	14.6	8.09
650	1200	15.1	8.39
760	1400	16.0	8.91

(a) From 20 °C (70 °F) to temperature shown. (b) Values for annealed and aged material

Specific heat. 435 J/kg · K (0.104 Btu/lb · °F)
Thermal conductivity. For annealed and aged bar: 11.4 W/m · K (79 Btu/ft^2 · in. · h · °F) at 21 °C (70 °F)
Electrical resistivity. For annealed and aged bar: 1218 nΩ · m (733 Ω circular-mil/ft)
Magnetic permeability. For annealed and aged material: 1.0011 at room temperature
Curie temperature. For annealed and aged material: –112 °C (–170 °F)

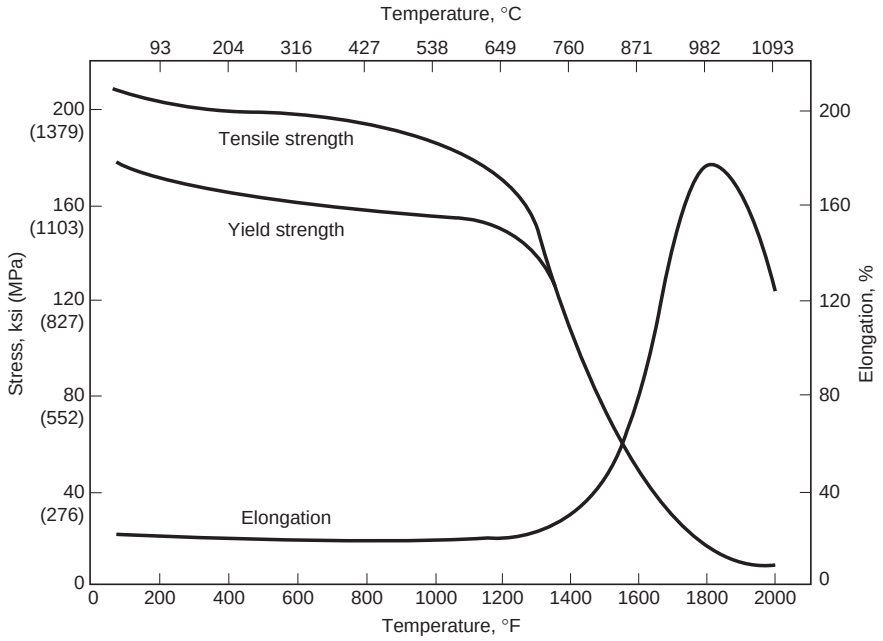


Fig. 17 Elevated-temperature tensile properties of hot-rolled, annealed, and aged 13 mm (½ in.) diam Inconel 718 bar

Table 43 Modulus of elasticity of hot-rolled, annealed, and aged Inconel 718 flat product

Temperature		Elastic modulus		Torsional modulus		
°C	°F	GPa	psi × 10^6	GPa	psi × 10^6	Poisson's ratio
20	70	200	29.0	77	11.2	0.294
40	100	199	28.8	77	11.2	0.291
95	200	196	28.4	76	11.0	0.288
150	300	193	28.0	75	10.9	0.280
205	400	190	27.6	74	10.8	0.280
260	500	187	27.1	73	10.6	0.275
315	600	184	26.7	72	10.5	0.272
370	700	181	26.2	71	10.3	0.273
425	800	178	25.8	70	10.1	0.271
480	900	174	25.3	68	9.9	0.272
540	1000	171	24.8	67	9.7	0.271
595	1100	167	24.2	65	9.5	0.276
650	1200	163	23.7	63	9.2	0.283
705	1300	159	23.0	61	8.9	0.292
760	1400	154	22.3	59	8.5	0.306
815	1500	147	21.3	56	8.1	0.321
870	1600	139	20.2	52	7.6	0.331
925	1700	130	18.8	49	7.1	0.334
980	1800	120	17.4	45	6.5	0.341
1040	1900	110	15.9	40	5.8	0.366
1095	2000	98.6	14.3	35	5.1	0.402

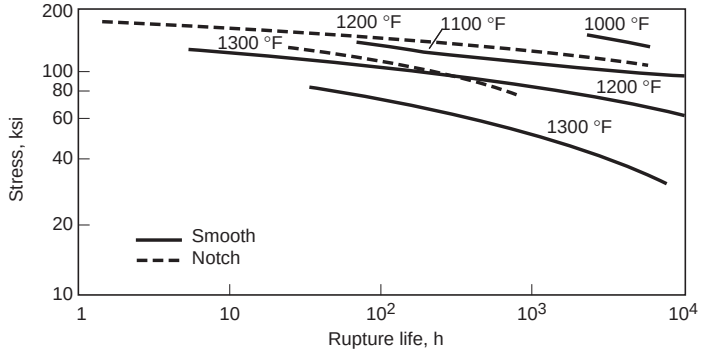


Fig. 18 Smooth and notch stress-rupture life of hot-rolled Inconel 718 bar, 16 mm (⅝ in.) diam, that was annealed at 980 °C (1800 °F) for 1 h, water quenched and aged at 720 °C (1325 °F) for 8 h, furnace cooled to 620 °C (1150 °F), and held at 620 °C (1150 °F) for a total aging time of 18 h. Stress-concentration factor, K_t = 4

Table 44 Effect of temperature on the rotating-beam fatigue strength of hot-rolled, annealed, and aged Inconel 718 bar

Test temperature		Fatigue strength, MPa (ksi)			
°C	°F	10^5 cycles	10^6 cycles	10^7 cycles	10^8 cycles
Room temperature		910 (132)	696 (101)	634 (92)	621 (90)
315	600	793 (115)	758 (110)	758 (110)	758 (110)
540	1000	765 (111)	703 (102)	655 (95)	621 (90)
650	1200	690 (100)	648 (94)	607 (88)	496 (72)

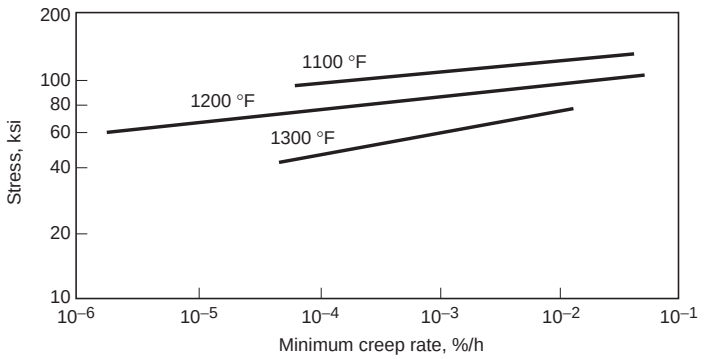


Fig. 19 Creep strength of hot-rolled Inconel 718 bar, 16 mm (⅝ in.) diam, that was heat treated the same manner as in Fig. 18

Chemical Properties

General corrosion behavior. Good to excellent resistance to organic acids, alkalies and salts, and seawater. Fair resistance to sulfuric, hydrochloric, hydrofluoric, phosphoric, and nitric acids. Good to excellent resistance to oxidation, carburization, nitridation, and molten salts. Fair resistance to sulfidation

Inconel 725

Specifications

ASTM. B 805 (bar and wire)
NACE International. MR-01-75 (materials for use in sour gas wells)
UNS number. N07725

Chemical Composition

Composition limits. 55.0 to 59.0 Ni; 19.0 to 22.5 Cr; 7.0 to 9.5 Mo; 2.75 to 4.0 Nb; 1.0 to 1.7 Ti; 0.35 max Al; 0.03 max C; 0.35 max Mn; 0.20 max Si; 0.015 max P; 0.010 max S; bal Fe

Applications

Typical uses. Age-hardenable alloy 725 is used for hangers, landing nipples, side pocket mandrels, and polished bore receptacles in sour gas service. Also used for high-strength fasteners in marine applications. Its combined high strength and hardness make alloy 725 a suitable choice for polymer extrusion dies.

Mechanical Properties

Tensile properties. See Table 45 (room-temperature data) and Fig. 20 (elevated-temperature data).
Hardness. See Table 45.
Elastic modulus. 204 GPa (29.6×10^6 psi) at 20 °C (70 °F)
Shear modulus. 78 GPa (11.3×10^6 psi) at 20 °C (70 °F)
Poisson's ratio. 0.31 at 20 °C (70 °F)
Impact strength. See Table 45.

Physical Properties

Density. 8.31 g/cm^3 (0.300 lb/in.^{3})
Melting range. 1271 to 1343 °C (2320–2449 °F)
Coefficient of thermal expansion. See Table 46.
Electrical resistivity. See Table 46.
Magnetic permeability. <1.001 at a field strength of 15.9 kA/m

Chemical Properties

General corrosion behavior. Alloy 725 is especially resistant to media containing carbon dioxide, chlorides, and hydrogen sulfide, such as those encountered in deep sour gas wells. In such environments, it resists general corrosion, pitting, sulfide stress cracking (hydrogen embrittlement), and stress-corrosion cracking. Alloy 725 also displays resistance to corrosion in brines and seawater.
Resistance to specific corroding agents. Table 47 compares the resistance of alloys 725, 625, and 718 in a simulated sour well environment. Corrosion rates for alloys 725, 625, and C-276 in mineral acids are compared in Table 48.

Table 45 Typical room-temperature tensile, hardness, and impact properties of Inconel 725

Form	Condition	Yield strength (0.2% offset)		Tensile strength		Elongation,	Hardness,	Charpy impact	
		MPa	ksi	MPa	ksi	%	HRC	J	ft · lbf
Round(a)	Annealed	427	62.0	855	124.0	57	5	…	…
	Age hardened	917	133.0	1241	180.0	30	36	92	68
Round(b)	Age hardened	903	131.0	1241	180.0	31	36	132	97
Tube	Annealed	334	48.4	783	113.6	60	5	…	…
	Age hardened	921	133.6	1268	183.9	27	39	…	…

(a) Transverse specimens from hot-finished rounds of 102 to 190 mm (4.0–7.5 in.) diameter. (b) Longitudinal specimens from hot-finished rounds of 13 to 190 mm (0.5–7.5 in.) diameter

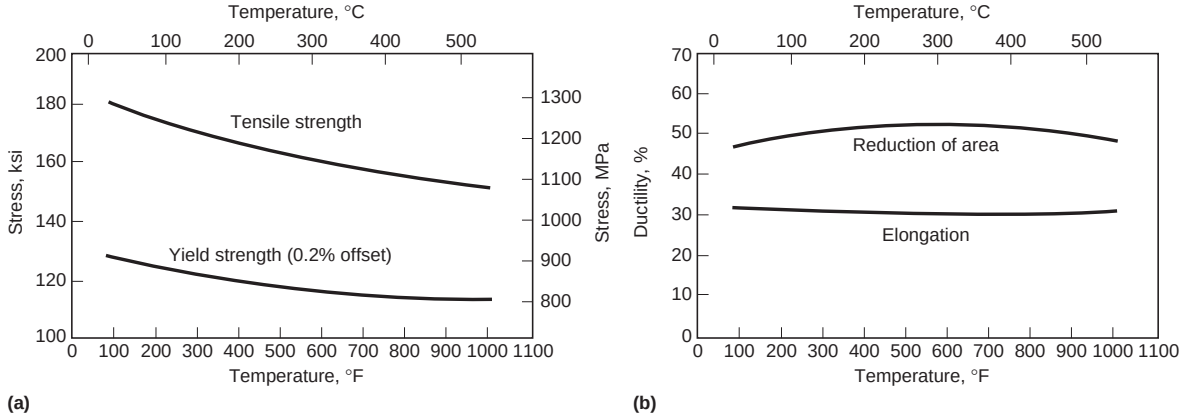


Fig. 20 Elevated-temperature tensile properties of annealed and aged Inconel 725. (a) Tensile and yield strengths. (b) Elongation and reduction of area

Table 46 Thermal and electrical properties of Inconel 725

Temperature		Coefficient of thermal expansion(a)		Electrical resistivity	
°C	°F	μm/m · K	μin./in. · °F	μΩ · m	Ω · circular-mil/ft
20	70	…	…	1.144	688.3
100	200	13.0	7.22	1.158	696.2
200	400	13.1	7.21	1.179	710.4
300	600	13.4	7.44	1.206	727.1
400	800	13.7	7.68	1.226	741.3
500	1000	14.1	7.79	1.251	758.6
600	1200	14.4	8.05	1.265	761.7
700	1400	…	…	1.273	776.1
800	1600	…	…	1.302	784.6

(a) Mean coefficient of linear expansion between 20 °C (70 °F) and the temperature shown

Table 47 Stress-corrosion cracking tests of Inconel alloys 725, 625, and 718 in a simulated sour gas well environment(a)

		Yield strength (0.2% offset)		Stress-corrosion cracking at:						
Alloy	Material condition	MPa	ksi	177 °C (350 °F)	191 °C (375 °F)	204 °C (400 °F)	218 °C (425 °F)	232 °C (450 °F)	246 °C (475 °F)	260 °C (500 °F)
Inconel 725	Age hardened	811	117.6	No	No	No	No	No	Yes(a)	No
	Age hardened	887	128.6	No	No	No	No	Yes	…	…
	Age hardened	916	132.9	No	No	No	No	No	No	No
	Age hardened	917	133.0	No	No	No	No	No	Yes(a)	No
Inconel 625	Cold worked	993	144.0	No	Yes	…	…	…	…	…
	Cold worked	1103	160.0	No	Yes	…	…	…	…	…
Inconel 718	Age hardened	898	130.3	Yes(b)	…	…	…	…	…	…

C-ring autoclave tests of 14 day duration at 100% of yield strength in 25% NaCl plus 0.5% acetic acid plus 1 g/L sulfur plus 827 kPa (120 psi) H_2S. (a) One of two specimens cracked. (b) At 135 °C (275 °F)

Table 48 Average corrosion rates for Inconel 725, Inconel 625, and alloy C-276 in various mineral acids (2 week test duration)

	3% HCl 66 °C (150 °F)		5% HCl 66 °C (150 °F)		10% HCl 66 °C (150 °F)		Boiling 10% H_2SO_4		Boiling 10% HNO_3		Boiling 30% H_3PO_4		Boiling 85% H_3PO_4	
Alloy	mm/yr	mils/yr	mm/yr	mils/yr	mm/yr	mils/yr	mm/yr	mils/yr	mm/yr	mils/yr	mm/yr	mils/yr	mm/yr	mils/yr
Inconel 725 (a)	<0.03	<1	<0.03	<1	2.67	105	0.64	25	<0.03	<1	0.08	3	1.85	73
Inconel 725 (b)	<0.03	<1	<0.03	<1	6.81	268	0.64	25	<0.03	<1	0.13	5	1.57	62
Inconel 725 (c)	<0.03	<1	<0.03	<1	6.35	250	0.64	25	<0.03	<1	0.08	3	1.14	45
Inconel 725 (d)	<0.03	<1	<0.03	<1	5.54	218	0.71	28	<0.03	<1	0.05	2	0.89	35
Inconel 625	<0.03	<1	1.75	69	2.36	93	0.45	18	<0.03	<1	<0.25	<10	0.63	25
Alloy C-276	<0.03	<5	0.13–0.51	5–20	0.51	20	0.51	20	0.41	16	<0.13	<5	0.13–0.64	5–25

(a) 1038 °C (1900 °F) anneal. (b) 1038 °C (1900 °F) anneal + 760 °C (1400 °F)/6 h/air cool. (c) 1038 °C (1900 °F) anneal + 746 °C (1375 °F)/8 h, furnace cool at 56 °C (100 °F)/h to 620 °C (1150 °F)/8 h/air cool. (d) 1038 °C (1900 °F) anneal + 732 °C (1350 °F)/8 h, furnace cool at 56 °C (100 °F)/h to 620 °C (1150 °F)/8 h/air cool

Incoloy 800

Specifications

ASTM. B 163 (condenser and heat exchanger tube), B 366 (welding fittings, permissible raw materials), B 407 (seamless pipe and tube), B 408 (rod and bar), B 409 (plate, sheet, and strip), B 514 (welded pipe), B 515 (welded tube), B 564 (forgings), B 751 (welded tube, general requirements), B 775 (welded pipe, general requirements), B 829 (seamless pipe and tube, general requirements)
ASME. SB-163, SB-366, SB-407, SB-408, SB-409, SB-514, SB-515, SB-564, SB-751, SB-775, SB-829
UNS number. N08800

Chemical Composition

Composition limits. 30.0 to 35.0 Ni; 19.0 to 23.0 Cr; 0.10 max C; 1.50 max Mn; 0.015 max S; 1.0 max Si; 0.75 max Cu; 0.15 to 0.60 Al; 0.15 to 0.60 Ti; 39.5 min Fe

Applications

Typical uses. Heat treating equipment, petrochemical pyrolysis tubing and piping systems, sheathing for electrical heating elements, food processing equipment

Mechanical Properties

Tensile properties. See Tables 49 and 50.
Compressive properties. See Table 50.
Poisson's ratio. Annealed material, 0.339 at 24 °C (75 °F)
Elastic modulus. Annealed material: tension, 195 GPa (28.35 × 10^6 psi) at 24 °C (75 °F); torsion, 73 GPa (10.64 × 10^6 psi) at 24 °C (75 °F)
Stress-rupture characteristics. See Table 51.
Impact strength. Annealed plate, Charpy keyhole: 122 J at 21 °C (70 °F); 122 J at –79 °C (–110 °F); 106 J at –196 °C (–320 °F); 99 J at –253 °C (–423 °F)
Fatigue strength. Rotating beam: hot rolled, 352 MPa (51 ksi); cold drawn, 228 MPa (33 ksi); annealed, 214 MPa (31 ksi). All values at 10^8 cycles

Table 49 Tensile properties of Incoloy 800

Form and condition	Tensile strength MPa	Tensile strength ksi	Yield strength (0.2% offset) MPa	Yield strength (0.2% offset) ksi	Elongation, %
Rod and bar					
Annealed	517–690	75–100	207–414	30–60	60–30
Hot finished	552–827	80–120	241–621	35–90	50–25
Cold drawn	690–1034	100–150	517–862	75–125	30–10
Plate					
Hot rolled	552–758	80–110	207–448	30–65	50–25
Annealed	517–724	75–105	207– 414	30– 60	50–30
Sheet, annealed	517–724	75–105	207–379	30–55	50–30
Strip, annealed	517–690	75–100	207–379	30–55	50–30
Tubing					
Hot finished	517–724	75–105	172–414	25–60	50–30
Cold drawn, annealed	517–690	75–100	207–414	30– 60	50– 30
Wire					
Annealed	552–758	80–110	241–448	35–65	45–25
Spring temper	965–1207	140–175	896–1172	130–170	5–2

Values shown represent usual ranges for common section sizes. In general, values in the higher portions of the ranges are not obtainable with large section sizes, and exceptionally small or large sections can have properties outside the ranges.

Table 50 Typical tensile and compressive properties of Incoloy 800

Material condition	Tensile strength MPa	Tensile strength ksi	Tension: Yield strength (0.02% offset) MPa	Tension: Yield strength (0.02% offset) ksi	Tension: Yield strength (0.2% offset) MPa	Tension: Yield strength (0.2% offset) ksi	Compression: Yield strength (0.02% offset) MPa	Compression: Yield strength (0.02% offset) ksi	Compression: Yield strength (0.2% offset) MPa	Compression: Yield strength (0.2% offset) ksi
Annealed bar	616	89.3	268	38.8	283	41.1	269	39.0	287	41.6
As-extruded tube	479	69.5	145	21.0	190	27.5	145	21.0	175	25.4

Physical Properties

Density. 7.94 g/cm^3 (0.287 lb/in.^{3}) at 20 °C (68 °F)
Liquidus temperature. 1385 °C (2525 °F)
Solidus temperature. 1355 °C (2475 °F)
Specific heat. 502 J/kg · K (0.117 Btu/lb · °F) at 20 °C (68 °F)
Electrical conductivity. Volumetric, 1.7% IACS at 21 °C (70 °F)
Electrical resistivity. 989 nΩ · m at 21 °C (70 °F)
Magnetic permeability. Annealed material, 1.0092 at a field strength of 15.9 kA/m
Curie temperature. –115 °C (–175 °F)

Chemical Properties

General corrosion behavior. A high chromium content gives Incoloy 800 good resistance to oxidation. It also resists many aqueous media and is relatively free from stress-corrosion cracking.
Resistance to specific corroding agents. Incoloy 800 has excellent resistance to nitric acid at concentrations up to approximately 70% and at temperatures up to the boiling point. It also has good resistance to organic acids, such as formic, acetic, and propionic. It resists a variety of oxidizing and nonoxidizing salts, but not halide salts. Corrosion rates in various media are given in Table 52.

Table 51 Typical stress-rupture strengths of Incoloy alloys 800 and 801

Temperature °C	Temperature °F	For stress rupture at: 100 h MPa	100 h ksi	1000 h MPa	1000 h ksi
Incoloy 800					
650	1200	220	32	145	21
760	1400	115	17	69	10
870	1600	45	6.5	33	4.8
Incoloy 801					
650	1200	250	36	…	…
730	1350	145	21	…	…
815	1500	62	9	…	…

Table 52 Corrosion rates for Incoloy 800 in various media (laboratory tests at 80 °C, or 176 °F)

Environment	Test duration, days	Corrosion rate mm/yr	Corrosion rate mils/yr	Pitting resistance
Acetic acid (10%)	7	0.0003	0.01	No pitting
Acetic acid (10%) + sulfuric acid (0.5%)	7	0.0006	0.02	No pitting
Acetic acid (10%) + sodium chloride (0.5%)	42	0.0008	0.03	Incipient pits visible at 30× after 42 days
Aluminum sulfate (5%)	7	0.0003	0.01	No pitting
Ammonium chloride (5%)	42	0.0006	0.02	Pitting after 42 days
Ammonium hydroxide (5%)	7	0.0003	0.01	No pitting
Ammonium hydroxide (10%)	7	0.0003	0.01	No pitting
Ammonium sulfate (5%)	7	0.00	0.00	No pitting
Barium chloride (10%)	42	0.0008	0.03	Pitting after 42 days
Bromine water (saturated)	42	0.19	7.6	Pitting after 7 days
Calcium chloride (5%)	42	0.0003	0.01	Pitting after 42 days
Chromic acid (5%)	7	0.041	1.6	No pitting
Citric acid (10%)	7	0.00	0.00	No pitting
Copper sulfate (10%)	7	0.00	0.00	No pitting
Ferric chloride (5%)	42	11	420	Pitting after 7 days
Ferrous ammonium sulfate (5%)	7	0.002	0.08	No pitting
Lactic acid (10%)	7	0.001	0.04	No pitting
Methanol (absolute)	7	0.00	0.00	No pitting
Oxalic acid (5%)	7	0.003	0.12	No pitting
Oxalic acid (10%)	7	0.28	11.0	No pitting
Potassium ferricyanide (5%)	7	0.001	0.04	No pitting
Sodium bisulfite (5%)	7	0.0008	0.03	No pitting
Sodium carbonate	7	0.00	0.00	No pitting
Sodium chloride (10%)	42	0.0003	0.01	Incipient pits visible at 30× after 42 days
Sodium chloride (20%)	42	0.0086	0.34	Pitting after 7 days
Sodium hypochlorite (1%)	42	0.127	5.0	Pitting after 7 days
Sodium hypochlorite (5%)	42	0.2	8.0	Pitting after 7 days
Sodium sulfate (5%)	7	0.00	0.00	No pitting
Sodium sulfate (10%)	7	0.0006	0.02	No pitting
Sulfurous acid (5%)	7	1.09	43.0	No pitting
Tartaric acid (10%)	7	0.0006	0.02	No pitting
Zinc chloride (10%)	42	0.0003	0.01	Pitting after 42 days

Incoloy 801

Specifications

ASTM. B 163 (condenser and heat exchanger tube), B 407 (seamless pipe and tube), B 829 (seamless pipe and tube, general requirements)
ASME. SB-163, SB-407, SB-829
AMS. 5552 (sheet, strip, and plate)
UNS number. N08801

Chemical Composition

Composition limits. 30.0 to 34.0 Ni; 19.0 to 22.0 Cr; 0.10 max C; 1.5 max Mn; 0.015 max S; 1.0 max Si; 0.5 max Cu; 0.75 to 1.5 Ti; bal Fe

Applications

Typical uses. Incoloy 801 is a modification of Incoloy 800 that is higher in titanium; it is used for hydrodesulfurizers in petrochemical processing and for other applications involving polythionic acid.

Mechanical Properties

Tensile properties. Annealed extruded tubing: tensile strength, 514 MPa (74.6 ksi); yield strength, 197 MPa (28.6 ksi) at 0.2% offset; elongation, 53%
Poisson's ratio. 0.413 at 26 °C (78 °F)
Elastic modulus. Tension, 207 GPa (30.07×10^6 psi) at 26 °C (78 °F); torsion, 73 GPa (10.64×10^6 psi) at 26 °C (78 °F)
Impact strength. Charpy V-notch: annealed, 324 J (239 ft · lbf); aged, 127 J (93.7 ft · lbf)
Fatigue strength. Annealed material, rotating beam: 255 MPa (37 ksi) at 27 °C (80 °F); 179 MPa (26 ksi) at 732 °C (1350 °F); 76 MPa (11 ksi) at 816 °C (1500 °F)
Stress-rupture characteristics. See Table 51.

Physical Properties

Density. 7.94 g/cm^3 (0.287 lb/in.^{3}) at 20 °C (68 °F)
Liquidus temperature. 1385 °C (2525 °F)
Solidus temperature. 1355 °C (2475 °F)
Coefficient of thermal expansion. 17.3 μm/m · K (9.6 μin./in. · °F) at 538 °C (1000 °F); 18.7 μm/m · K (10.4 μin./in. · °F at 871 °C (1600 °F)
Specific heat. 452 J/kg · K (0.105 Btu/lb · °F) at 26 ° (78 °F)
Thermal conductivity. 12.4 W/m · K (86 Btu/ft^2 · in. · h · °F) at 21 °C (70 °F); 20.7 W/m · K (143 Btu/ft^2 · in. · h · °F) at 538 °C (1000 °F); 25.6 W/m · K (177 Btu/ft^2 · in. · h · °F) at 871 °C (1600 °F)
Electrical conductivity. Volumetric, 1.7% IACS at 26 °C (78 °F)
Electrical resistivity. 1012 nΩ · m at 26 °C (78 °F)

Chemical Properties

General corrosion behavior. In most environments, the corrosion resistance of Incoloy 801 is similar to that of Incoloy 800. However, Incoloy 801 has greater resistance to intergranular corrosion because its higher titanium content stabilizes the alloy against sensitization.
Resistance to specific corroding agents. Incoloy 801 is especially resistant to stress-corrosion cracking in solutions of polythionic acid.

Incoloy 825

Specifications

ASTM. B 163 (condenser and heat exchanger tube), B 366 (welding fittings, permissible raw materials), B 423 (seamless pipe and tube), B 424 (plate, sheet, and strip), B 425 (rod and bar), B 564 (forgings), B 704 (welded tube), B 705 (welded pipe), B 751 (welded tube, general requirements), B 775 (welded pipe, general requirements), B 829 (seamless pipe and tube, general requirements)
ASME. SB-163, SB-366, SB-423, SB-424, SB-425, SB-564, SB-704, SB-705, SB-751, SB-775, SB-829
UNS number. N08825

Chemical Composition

Composition limits. 38.0 to 46.0 Ni; 19.5 to 23.5 Cr; 2.5 to 3.5 Mo; 1.5 to 3.0 Cu; 0.6 to 1.2 Ti; 0.05 max C; 1.0 max Mn; 0.03 max S; 0.5 max Si; 0.2 max Al; bal Fe

Applications

Typical uses. Phosphoric acid evaporators, pickling equipment, chemical processing vessels and piping, equipment for recovery of spent nuclear fuel, propeller shafts, tank trucks

Mechanical Properties

Tensile properties. See Table 53.
Compressive properties. Annealed bar with tensile yield strength of 396 MPa (57.5 ksi): compressive yield strength, 423 MPa (61.4 ksi) at 0.2% offset
Elastic modulus. Tension, 195 GPa ($28.3 \cdot 10^6$ psi) at 27 °C (80 °F)
Impact strength. Plate, Charpy keyhole: 107 J (78.9 ft · lbf) at 20 °C (68 °F); 106 J (78.2 ft · lbf) at –79 °C (–110 °F); 91 J (67.1 ft · lbf) at –196 °C (–320 °F); 92 J (67.8 ft · lbf) at –253 °C (–420 °F)

Physical Properties

Density. 8.14 g/cm^3 (0.294 lb/in.^{3}) at 20 °C (68 °F)
Liquidus temperature. 1400 °C (2550 °F)
Solidus temperature. 1370 °C (2500 °F)
Coefficient of thermal expansion. See Table 54.
Thermal conductivity. See Table 54.
Electrical conductivity. Volumetric, 1.5% IACS at 26 °C (78 °F)
Electrical resistivity. See Table 54.
Magnetic permeability. 1.005 at 21 °C (70 °F) and a field strength of 15.9 kA/m
Curie temperature. <–196 °C (<–320 °F)

Chemical Properties

General corrosion behavior. Incoloy 825 has exceptional resistance to seawater and to reducing chemicals, such as sulfuric and phosphoric acids. Because it is stabilized against sensitization, Incoloy 825 resists intergranular corrosion. This alloy contains sufficient nickel to make it resistant to chloride stress-corrosion cracking. Its molybdenum content provides resistance to pitting. Its chromium content provides resistance to oxidizing media, such as nitric acid, nitrates, and oxidizing salts.

Table 53 Tensile properties of annealed Incoloy 825 as a function of temperature

Temperature		Tensile strength		Yield strength (0.2% offset)		Elongation,
°C	°F	MPa	ksi	MPa	ksi	%
29	85	693	100.5	301	43.7	43
93	200	655	95.0	279	40.4	44
204	400	637	92.4	245	35.6	43
316	600	632	91.7	232	33.6	46
371	700	621	90.0	234	34.0	46
427	800	610	88.5	228	33.0	44
482	900	608	88.2	221	32.0	42
538	1000	592	85.9	229	33.2	43
593	1100	541	78.5	222	32.2	38
649	1200	465	67.5	213	30.9	62
760	1400	274	39.7	183	26.5	87
871	1600	135	19.6	117	17.0	102
982	1800	75	10.9	47	6.8	173
1093	2000	42	6.1	23	3.3	106

Resistance to specific corroding agents. Corrosion rates in sulfuric acid are shown in Fig. 21. Results of plant corrosion tests in phosphoric and nitric acid solutions are given in Tables 55 and 56. Table 57 gives corrosion rates in hydrochloric acid, and Table 58 gives rates in various organic acids.

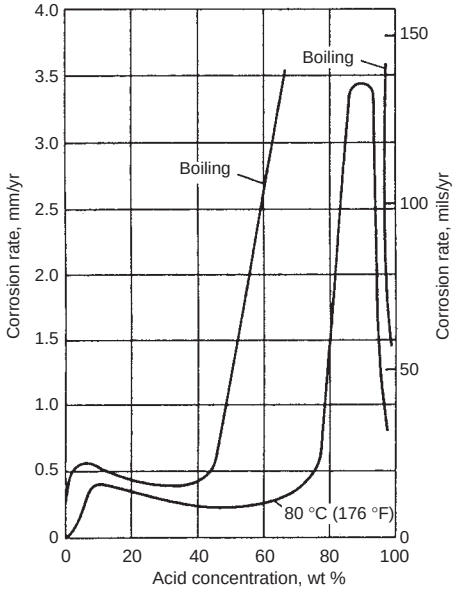


Fig. 21 Laboratory corrosion rates of Incoloy 825 in chemically pure sulfuric acid solutions

Table 54 Thermal and electrical properties of Incoloy 825 as a function of temperature

Temperature		Mean linear expansion(a)		Thermal conductivity		Electrical resistivity,
°C	°F	μm/m · K	μin./in. · °F	W/m · K	Btu/ft · h · °F	nΩ · m
26	78	…	…	11.1	6.4	1127
38	100	…	…	11.3	6.5	1130
93	200	14.0	7.7	12.3	7.1	1142
204	400	14.9	8.3	14.1	8.1	1180
316	600	15.3	8.5	15.8	9.1	1210
427	800	15.7	8.7	17.3	10.0	1248
538	1000	15.8	8.8	18.9	10.9	1265
649	1200	16.4	9.1	20.5	11.8	1267
760	1400	17.1	9.5	22.3	12.9	1272
871	1600	17.5	9.7	24.8	14.3	1288
982	1800	…	…	27.7	16.0	1300
1093	2000	…	…	…	…	1318

(a) From 27 °C (80 °F) to temperature shown

Table 55 Plant corrosion tests of Incoloy 825 immersed in wet-process phosphoric acid solutions

Test solution	Temperature		Duration of test, days	Corrosion rate	
	°C	°F		mm/yr	mils/yr
Recycle liquor from evaporator fume scrubber containing 15% H_3PO_4, 20% H_2SiF_6, 1% H_2SO_4	75–85	165–185	16	0.025	1.0
Solution containing 20% H_3PO_4 and 20% HF in tank	20–30	70–85	13	0.036	1.4
Slurry in digester tank. Mixture contains 20% H_3PO_4, 2% H_2SO_4, 1% HF, 40% H_2O, plus $CaSO_4$	75–95	170–200	117	0.02	0.7
Slurry containing 37% H_3PO_4 (27% P_2O_5) in acid transfer tank. Velocity 1 m/s (3 ft/s)	65–90	150–190	46	0.02	0.7
Slurry containing 31.4% H_3PO_4, 1.6% H_2SO_4, 1.5% H_2SiF_6, 0.12% HF, plus $CaSO_4$ in filter tank	45–60	115–140	8.3	<0.003	<0.1
Thickener in evaporated acid containing 54% H_3PO_4, 1.7% HF, 2% H_2SO_4, 2% $CaSO_4$	50–65	125–150	51	0.01	0.5
Evaporator heated with hot gases in acid containing 53% H_3PO_4, 1–2% H_2SO_4, 1.5% HF plus Na_2SiF_6	120	250	42	0.15	6.0
In wet separator on top of concentrating drum in vapors from concentration of crude acid to 50–55% H_3PO_4 containing HF	105–150	225–300	21	0.79	31.0
Defluorinator in acid containing 75–80% H_3PO_4, 1% H_2SO_4, with some HF. Violent agitation	120–155	250–315	8	3.048	120.0

Table 56 Plant corrosion tests of Incoloy 825 in nitric acid mixtures

Test conditions(a)	Temperature		Duration of test, days	Corrosion rate	
	°C	°F		mm/yr	mils/yr
In evaporator during concentration of nitric acid solution saturated with potassium nitrate and containing chlorides					
Liquid: 40–70% HNO_3, 0.2–0.02% Cl	105–115	220–240	4.2	0.10	4.0
Vapor: 50–10% HNO_3, 0.05–1.5% Cl	105–115	220–240	4.2	0.279	11.0
In evaporator during concentration of nitric acid solution from 35–45% nitric acid, saturated with zirconyl nitrate and containing 10–35% $ZrO(NO_3)_2$ crystals					
Liquid	115–125	235–255	29	0.533	21.0
Vapor	115–125	235–255	29	0.660	26.0
In 40% nitric acid solution containing some nitrogen tetroxide and nitrous acid. Location in N_2O_2 absorption tower immediately below distributor	30–40	85–105	15	<0.003	<0.1
In evaporator during concentration of 20% nitric acid solution containing 6% metal nitrates (iron, magnesium, lead and aluminum), 2% sulfate as metal sulfates	70–90	160–190	52	0.01	0.4
Laboratory test in 53% nitric acid containing 1% hydrofluoric acid					
Liquid	80	176	7	5.080	200.0
Vapor	80	176	7	2.18	86.0
In vapor during concentration of nitric acid solution containing 35–45% nitric acid, 3–20% chlorine as chlorides, and 10–20% metal nitrates (mainly zirconium)					
Liquid	115–125	240–260	21	0.330	13.0
Vapor	115–125	240–260	21	0.15	5.8
In evaporator during concentration of 36% nitric acid solution containing 30% potassium nitrate, some sodium, iron, calcium and magnesium nitrates, and 0.05–0.10% chlorine as chloride. Intermittently exposed to liquid and vapor	65–80	150–180	8	0.01	0.5
In evaporator during concentration of nitric acid solution containing metal nitrates (mostly zirconium) and small amount of chlorides					
Liquid at bottom of column (58% nitric acid, 5 ppm chlorides, 11–13% metal nitrates)	115–130	240–265	10	0.660	26.0
Liquid on 10th tray of column (2.21% nitric acid, 3–13 ppm chlorides, 0–25% metal nitrates)	105–130	225–265	10	0.12	4.6
In evaporator during concentration of raffinate solution containing 30–40% nitric acid and variable chlorides up to 2000 ppm Cl					
Liquid	80(b)	175(b)	92	0.02	0.7
Vapor	80(b)	175(b)	92	0.028	1.1

(a) Specimens were immersed in solution unless otherwise stated. (b) Average

Table 57 Corrosion rates for Incoloy 825 in hydrochloric acid at three temperatures

Acid concentration, %	Temperature °C	Temperature °F	Corrosion rate mm/yr	Corrosion rate mils/yr
5	20	68	0.12	4.9
	40	104	0.45	17.8
	66	150	2.00	79
10	20	68	0.18	7.2
	40	104	0.47	18.6
	66	150	2.60	102
20	20	68	0.18(a)	7.3(a)
	40	104	0.44	17.2
	66	150	1.52	60

(a) 15% acid concentration

Table 58 Plant corrosion tests of Incoloy 825 in organic acids

Test conditions	Temperature °C	Temperature °F	Duration of test, days	Corrosion rate mm/yr	Corrosion rate mils/yr
In vapors of 85% acetic acid, 10% acetic anhydride, 5% water, plus some acetone, acetonitrile, in vapor line just before condenser	115–135	240–275	875	0.008	0.3
In 99.9% acetic acid, less than 0.1% water in still	105	225	40	0.006	0.2
In mixture of 94% acetic acid, 1% formic acid, 5% high boiling esters	125	260	465	0.02	0.7
In mixture of 96.5–98% acetic acid, 1.5% formic acid, 1–1.5% water	125	255	262	0.15	6.0
In mixture of 91.5% acetic acid, 2.5% formic acid, 6.0% water	110–125	230–260	55	0.079	3.1
In mixture of 95% acetic acid, 1.5–3.0% formic acid, 0.5% potassium permanganate, balance water	110–145	230–290	55	0.038	1.5
In mixture of 40% acetic acid, 6% propionic acid, 20% butane, 5% pentane, 8% ethyl acetate, 5% methyl ethyl ketone, plus other esters and ketones	175	345	217	0.051	2.0
In liquid phthalic anhydride containing phthalic acid, some water, and small amounts of maleic acid, maleic anhydride, benzoic acid, and napthaquinones. On reflux plate of crude phthalic anhydride still	165–260	330–500	70	0.20	8.0

Hastelloy B-2

Specifications

ASTM. B 333 (plate, sheet, and strip), B 335 (rod), B 366 (welding fittings), B 619 (welded pipe), B 622 (seamless pipe and tube), B 626 (welded tubes)
ASME. SB-333, SB-335, SB-366, SB-619, SB-622, SB-626
UNS number. N10665

Chemical Composition

Composition limits. 26 to 30 Mo; 2.00 max Fe; 1.00 max Co; 1.00 max Cr; 1.00 max Mn; 0.10 max Si; 0.040 max P; 0.030 max S; 0.02 max C; bal Ni

Applications

Typical uses. Suitable for most chemical process applications in the as-welded condition. Well suited for equipment handling hydrochloric acid in all concentrations and temperatures. Resistant to hydrogen chloride gas and sulfuric, acetic, and phosphoric acids. Principal high-temperature uses are those in which a low coefficient of thermal expansion is required.
Precautions in use. Exposure to temperatures of 540 to 815 °C (1000–1500 °F) should be avoided because of a reduction in the ductility of the alloy. In oxidizing gases such as air, B-2 can be used at temperatures up to 540 °C (1000 °F). In reducing gases or in vacuum, the alloy can be used from 815 °C (1500 °F) to substantially higher temperatures. Ferric or cupric salts might develop when hydrochloric acid comes in contact with iron or copper, so Hastelloy B-2 should not be used with copper or iron piping in a system containing hydrochloric acid.

Mechanical Properties

Tensile properties. See Table 59.
Hardness. See Table 59.
Elastic modulus. See Table 60.

Physical Properties

Density. 9.22 g/cm^3 (0.333 lb/in.^{3}) at 22 °C (72 °F)
Coefficient of thermal expansion (linear):

Temperature °C	Temperature °F	Coefficient μm/m · K	Coefficient μin./in. · °F
20–93	68–200	10.3	5.7
20–204	68–400	10.8	6.0
20–316	68–600	11.2	6.2
20–427	68–800	11.5	6.4
20–538	68–1000	11.7	6.5

Specific heat:

Temperature °C	Temperature °F	Specific heat J/kg · K	Specific heat Btu/lb · °F
0	32	373	0.089
200	390	406	0.097
400	750	431	0.103
600	1100	456	0.109

Thermal conductivity:

Temperature °C	Temperature °F	Conductivity W/m · K	Conductivity Btu/ft · h · °F
0	32	11.1	6.4
100	232	12.2	7.1
200	390	13.4	7.75
300	570	14.6	8.5
400	750	16.0	9.25
500	930	17.3	10.0
600	1100	18.7	10.8

Table 59 Average tensile properties for Hastelloy B-2

Temperature °C	Temperature °F	Tensile strength MPa	Tensile strength ksi	0.2% yield strength MPa	0.2% yield strength ksi	Elongation in 50 mm (2 in.), %	Rockwell hardness
Sheet, 1.3 to 3 mm (0.05–0.12 in.) thick(a)							
RT	RT	965	140	525	76	53	22 HRC
204	400	885	128	450	65	50	…
316	600	860	125	425	62	49	…
427	800	860	125	415	60	51	…
Sheet and plate, 2.5 to 9 mm (0.10–0.35 in.) thick(a)							
RT	RT	895	130	415	60	61	95 HRB
204	400	850	123	350	51	59	…
316	600	820	119	325	47	60	…
427	800	805	117	310	45	60	…
Plate, 9 to 50 mm (0.36–2 in.) thick(a)							
RT	RT	905	131	405	59	61	94 HRB
204	400	870	126	360	52	60	…
316	600	840	122	340	49	60	…
427	800	820	119	315	46	61	…

RT, room temperature. (a) Solution treated at 1065 °C (1950 °F) and rapidly quenched

Table 60 Average dynamic modulus of elasticity of Hastelloy B-2

Form	Condition	Test temperature °C	Test temperature °F	Dynamic modulus of elasticity GPa	Dynamic modulus of elasticity 10^6 psi
Plate, 13 mm (½ in.) thick	Heat treated at: 1065 °C (1950 °F), rapid quenched	RT	RT	217	31.4
		315	600	202	29.3
		425	800	196	28.4
		540	1000	189	27.4

Thermal diffusivity:

Temperature °C	Temperature °F	Diffusion coefficient, $10^{-6}m^2/s$
0	32	3.2
100	212	3.4
200	390	3.6
300	570	3.8
400	750	4.0
500	930	4.2
600	1100	4.5

Electrical resistivity:

Temperature °C	Temperature °F	Resistivity, μΩ · m
0	32	1.37
100	212	1.38
200	390	1.38
300	570	1.39
400	750	1.39
500	930	1.41
600	1100	1.46

Chemical Properties

General corrosion behavior. Superior resistance to hydrochloric acid, aluminum chloride catalysts, and other strongly reducing chemicals. Alloy B-2 has excellent resistance to pitting, stress-corrosion cracking, and to knife-line and heat-affected zone attack. It resists the formation of grain-boundary carbide precipitates in the weld heat-affected zone, thus making it suitable for most chemical process applications in the as-welded condition. Limited tests indicate that the corrosion resistance of alloy B-2 in boiling 20% hydrochloric acid is not affected by cold reductions up to 50%. As stated earlier, contact with ferric or cupric salts can cause rapid and premature corrosion failure.

Resistance to specific corroding agents. See Table 61.

Table 61 Average corrosion rates of Hastelloy B-2 in boiling acids(a)

Media	Concentration, wt%	Average corrosion rate mm/yr	Average corrosion rate mils/yr
Acetic acid	10	<0.02	0.5
	30	0.01	0.4
	50	0.01	0.4
	70	<0.01	0.3
	99 (glacial)	<0.01	0.3
Formic acid	10	<0.01	0.3
	20	<0.02	0.6
	30	<0.02	0.7
	40	<0.02	0.7
	60	<0.02	0.5
	89	<0.02	0.5
Hydrochloric acid	1	0.02	0.8
	2	0.08	3
	5	0.13	5
	10	0.18	7
	15	0.28	11
	20	0.38	15
	20	0.51(a)	20(a)
Phosphoric acid (chemically pure)	10	0.05	2
	30	0.08	3
	50	0.15	6
	85	0.63	25
Sulfuric acid	2	<0.02	0.5
	5	0.08	3
	10	0.05	2
	20	<0.02	0.7
	30	<0.02	0.7
	40	<0.03	0.9
	50	0.03	1
	50	0.05(a)	2(a)
	50	0.03(b)	1(b)
	60	0.05(b)	2(b)
	70	0.23(b)	9(b)

Determined in laboratory tests of 120 h duration. It is recommended that samples be tested under actual plant conditions. All test specimens were heat treated at 1065 °C (1950 °F), water quenched unless otherwise noted. (b) As gas-tungsten arc welded. (b) Aged 48 h at 540 °C (1000 °F)

Hastelloy B-3

Specifications

ASTM. B 333 (plate, sheet, and strip), B 335 (rod), B 366 (welding fittings), B 564 (forgings), B 619 (welded pipe), B 622 (seamless pipe and tube), B 626 (welded tube)
ASME. SB-333, SB-335, SB-366, SB-564, SB-619, SB-622, SB-626
UNS number. N10675

Chemical Composition

Nominal composition. 65 min Ni; 28.5 Mo; 1.5 Cr; 1.5 Fe; 3 max Co; 3 max Mn; 0.5 max Al; 0.2 max Ti; 0.1 max Si; 0.01 max C

Applications

Typical uses. Hastelloy B-3 is suitable for use in all applications previously requiring the use of Hastelloy B-2.

Precautions in use. Like alloy B-2, Hastelloy B-3 is not recommended for use in the presence of ferric or cupric salts because these salts can cause premature failure.

Mechanical Properties

Tensile properties. See Table 62.
Elastic modulus. 216 GPa (31.4×10^6 psi) at room temperature

Physical Properties

Density. 9.22 g/cm^3 (0.333 lb/in.^{3})
Melting range. 1370 to 1418 °C (2500–2585 °F)
Coefficient of thermal expansion. 10.6 μm/m · K at 25 to 100 °C (5.7 μin./in. · °F at 78–200 °F)
Electrical resistivity. 1.37 μΩ · m (53.8 μΩ · in.) at room temperature
Thermal diffusivity. 3.0×10^{-6} m^2/s (4.6×10^{-9} in.^{2}/s)

Chemical Properties

General corrosion behavior. Excellent resistance to hydrochloric acid at all concentrations and temperatures. Alloy B-3 also withstands sulfuric, acetic, formic, and phosphoric acids, and other nonoxidizing media. The chemistry of alloy B-3 has been designed to achieve a level of thermal stability superior to that of alloy B-2. It also resists pitting corrosion, stress-corrosion cracking, and weldment corrosion.
Resistance to specific corroding agents. See Table 63 for data comparing alloys B-3, B-2, type 316L stainless steel, and nickel-copper alloy 400 in various boiling acids.

Table 62 Typical tensile properties of Hastelloy B-3 sheet and plate

Test temperature		Ultimate tensile strength		Yield strength at 0.2% offset		Elongation 50 mm (2 in.), %
°C	°F	MPa	ksi	MPa	ksi	
Sheet(a)						
RT	RT	860	125.0	420	60.6	53.4
95	200	830	120.7	380	55.3	56.9
205	400	760	110.0	325	47.0	59.7
315	600	720	104.4	300	43.5	63.4
425	800	705	102.0	290	42.4	62.0
540	1000	675	97.8	270	39.0	59.0
650	1200	715	103.5	315	45.8	55.8
Plate(b)						
RT	RT	885	128.3	400	58.2	57.8
95	200	845	122.4	375	54.1	58.2
205	400	795	115.1	330	47.6	60.9
315	600	765	111.2	305	44.4	61.6
425	800	745	108.2	285	41.3	61.7
540	1000	730	105.6	275	39.6	61.7
650	1200	735	106.9	290	42.0	64.6

(a) Bright annealed 3.2 mm (0.125 in.) thick sheet. (b) Solution treated 6.4 mm (0.250 in.) thick plate

Table 63 Corrosion rates of Hastelloy B-3 in various boiling acids compared with other corrosion resistant alloys

	Average corrosion rates, mm/yr (mils/yr)			
Acid medium	B-3 alloy	B-2 alloy	Type 316L	Monel 400 alloy
50% acetic acid	0.005 (0.2)	0.010 (0.4)	0.005 (0.2)	…
40% formic acid	0.013 (0.5)	0.018 (0.7)	1.041 (41)	0.053 (2.1)
50–55% phosphoric acid	0.076 (3.0)	0.152 (6)	0.457 (18)	0.114 (4.5)
50% sulfuric acid	0.043 (1.7)	0.030 (1.2)	>500 (>20,000)	4.699 (185)
20% hydrochloric acid	0.305 (12)	0.381 (15)	>500 (>20,000)	40.310 (1587)

Hastelloy C-4

Specifications

ASTM. B 366 (welding fittings), B 574 (rod), B 575 (plate, sheet, and strip), B 619 (welded pipe), B 622 (seamless pipe and tube), B 626 (welded tubes)
ASME. SB-366, SB-574, SB-575, SB-619, SB-622, SB-626
UNS number. N06455

Chemical Composition

Composition limits. 14 to 18 Cr; 14 to 17 Mo; 3.00 max Fe; 2.00 max Co; 1.00 max Mn; 0.70 max Ti; 0.15 max C; 0.08 max Si; 0.04 max P; 0.03 max S; bal Ni

Applications

Typical uses. Outstanding high-temperature stability; exhibits good ductility and corrosion resistance after long-time aging at 650 to 1040 °C (1200–1900 °F). Resists formation of grain-boundary precipitates in weld heat-affected zones, and is suitable for most chemical process applications in the as-welded condition. Has excellent resistance to stress-corrosion cracking and to oxidizing atmospheres up to 1040 °C (1900 °F).

Mechanical Properties

Tensile properties. Average, at room temperature, for material solution treated at 1065 °C (1950 °F) and quenched. Sheet: tensile strength, 785 MPa (114 ksi); yield strength, 400 MPa (58 ksi); elongation in 50 mm or 2 in., 54%. Plate: tensile strength, 785 MPa (114 ksi); yield strength, 345 MPa (50 ksi); elongation in 50 mm or 2 in., 60%
Hardness. At room temperature, for sheet heat treated at 1065 °C (1950 °F) and quenched: 91 HRB
Elastic modulus. In tension, average of three tests at each temperature for 12.7 mm (½ in.) thick plate heat treated at 1065 °C (1950 °F) and quenched:

Temperature		Modulus	
°C	°F	GPa	10^6 psi
RT	RT	211	30.8
93	200	207	30.2
205	400	201	29.3
315	600	194	28.3
425	800	187	27.3
540	1000	179	26.2
650	1200	171	25.0
760	1400	162	23.7
870	1600	152	22.2
980	1800	141	20.6

RT, room temperature

Physical Properties

Density. 8.64 g/cm^3 (0.312 lb/in.^{3}) at 20 °C (68 °F)
Coefficient of thermal expansion (linear):

Temperature		Coefficient	
°C	°F	µm/m · K	µin./in. · °F
20–93	68–200	10.8	6.0
20–205	68–400	11.9	6.6
20–315	68–600	12.6	7.0
20–425	68–800	13.0	7.2
20–540	68–1000	13.3	7.4
20–650	68–1200	13.5	7.5
20–760	68–1400	14.4	8.0
20–870	68–1600	14.9	8.3
20–980	68–1800	15.7	8.7

Specific heat:

Temperature		Specific heat	
°C	°F	J/kg · K	Btu/lb · °F
0	32	406	0.097
100	212	426	0.102
200	390	448	0.107
300	570	465	0.111
400	750	477	0.114
500	930	490	0.117
600	1100	502	0.120

Thermal conductivity:

Temperature		Conductivity	
°C	°F	W/m · K	Btu/ft · h · °F
23	74	10.0	5.8
100	212	11.4	6.6
200	390	13.2	7.7
300	570	14.9	8.7
400	750	16.6	9.7
500	930	18.4	10.7
600	1100	20.4	11.8

Thermal diffusivity:

Temperature		Diffusion coefficient,
°C	°F	10^{-6} m^2/s
23	74	2.8
100	212	3.1
200	390	3.3
300	570	3.7
400	750	4.0
500	930	4.3
600	1100	4.7

Electrical resistivity:

Temperature		
°C	°F	Resistivity, μΩ · m
23	74	1.25
100	212	1.25
200	390	1.26
300	570	1.27
400	750	1.28
500	930	1.29
600	1110	1.32

Chemical Properties

General corrosion behavior. Exceptional resistance to a variety of chemical process environments, including hot contaminated mineral acids, solvents, chlorine, and chlorine-contaminated media (organic and inorganic, dry chlorine, formic and acetic acids, acetic anhydride, seawater, and brine)

Hastelloy C-22

Specifications

ASTM. B 366 (welding fittings), B 564 (forgings), B 574 (rod), B 575 (plate, sheet, and strip), B 619 (welded pipe), B 622 (seamless tubing), B 626 (welded tubing)
ASME. SB-366, SB-564, SB-574, SB-575, SB-619, SB-622, SB-626
NACE International. MR-01-75 (materials for oil field equipment)
UNS number. N06022

Chemical Composition

Nominal composition. 22 Cr; 13 Mo; 3 Fe; 3 W; 2.5 max Co; 0.5 max Mn; 0.35 max V; 0.08 max Si; 0.01 max C; bal Ni

Applications

Typical uses. Some of the areas of use for alloy C-22 are acetic acid/acetic anhydride production, cellophane manufacturing, chlorination systems, complex acid mixtures, electrogalvanizing rolls, expansion bellows, flue gas scrubber systems, hydrogen fluoride scrubber systems, geothermal wells, incineration scrubber systems, nuclear fuel reprocessing, pesticide production, phosphoric acid production, pickling systems, plate heat exchangers, selective leaching systems, sulfur dioxide cooling towers, sulfonation systems, tubular heat exchangers, and weld overlays for valves.

Mechanical Properties

Tensile properties. See Table 64.

Table 64 Typical tensile properties of solution heat treated Hastelloy C-22

Test temperature,	Ultimate tensile strength		Yield strength at 0.2% offset		Elongation in
°C (°F)	MPa	ksi	MPa	ksi	50 mm (2 in.), %
Sheet, 0.71 to 3.2 mm (0.028 to 0.125 in.) thick					
Room temperature	800	116	407	59	57
93 (200)	758	110	372	54	58
204 (400)	703	102	303	44	57
316 (600)	676	98	290	42	62
427(800)	655	95	283	41	67
538 (1000)	627	91	276	40	61
649 (1200)	586	85	248	36	65
760 (1400)	524	76	241	35	63
Plate, 6.4 to 19 mm (¼ to ¾ in.) thick					
Room temperature	786	114	372	54	62
93 (200)	738	107	338	49	65
204 (400)	676	98	283	41	66
316 (600)	655	95	248	36	68
427 (800)	634	92	241	35	68
538 (1000)	607	88	234	34	67
649 (1200)	572	83	221	32	69
760 (1400)	524	76	214	31	68
Bar, 13 to 50 mm (½ to 2 in.) diam					
Room temperature	765	111	359	52	70
93 (200)	724	105	310	45	73
204 (400)	662	96	262	38	74
316 (600)	634	92	234	34	79
427 (800)	614	89	214	31	79
538 (1000)	579	84	200	29	80
649 (1200)	552	80	193	28	80
760 (1400)	496	72	200	29	77

Hardness. Sheet: 93 HRB; plate: 95 HRB
Elastic modulus. For plate, solution treated at 1120 °C (2050 °F) and rapidly quenched: 206 GPa (29.9 × 10^6 psi) at room temperatures, 190 GPa (27.6 × 10^6 psi) at 315 °C (600 °F), and 177 GPa (26.6 × 10^6 psi) at 540 °C (1000 °F)
Impact strength. For plate, solution treated at 1120 °C (2050 °F) and rapidly quenched: 353 J (260 ft · lbf) at room temperature, and 351 J (259 ft · lbf) at –195 °C (–320 °F)

Physical Properties

Density. 8.69 g/cm^3 (0.314 lb/$in.^3$)
Melting range. 1357 to 1399 °C (2475–2550 °F)
Coefficient of thermal expansion. 12.4 μm/m · K at 24 to 93 °C (6.9 μin./in · °F at 75–200 °F)
Thermal conductivity. 10.1 W/m · K at 48 °C (70 Btu · in./ft^2 · h · °F), 11.1 W/m · K at 100 °C (77 Btu · in./ft^2 · h · °F), and 13.4 W/m · K at 200 °C (93 Btu · in./ft^2 · h · °F at 392 °F)
Specific heat. 414 J/kg · K at 52 °C (0.099 Btu/lb · °F at 126 °F) and 423 J/kg · K at 100 °C (0.101 Btu/lb · °F at 212 °F)
Electrical resistivity. 1.14 μΩ · m (44.8 μΩ · in.) at room temperature

Chemical Properties

General corrosion behavior. Alloy C-22 has outstanding resistance to pitting, crevice corrosion, and stress-corrosion cracking. It has excellent resistance to oxidizing aqueous media including wet chlorine and mixtures containing nitric acid or oxidizing acids with chloride ions. Alloy C-22 also offers optimum resistance to environments where reducing and oxidizing conditions are encountered in process streams. Because of this versatility, it can be used where upset conditions are likely to occur or in multipurpose plants.
Resistance to specific corroding agents. Comparative corrosion data for alloy C-22, C-276, C-4, and 625 are given in Table 65.

Table 65 Corrosion rates of Hastelloy C-22 in various corrosive media compared with other corrosion resistant alloys

Media	Concentration, wt%	Test temperature, °C (°F)	Average corrosion rate mils/yr(a)			
			C-22 alloy	C-276 alloy	C-4 alloy	625 alloy
Acetic acid	99	Boiling	Nil	<1	Nil	<1
Ferric chloride	10	Boiling	1	2	140	7325
Formic acid	88	Boiling	<1	1	2	9
Hydrochloric acid	1	Boiling	3	13	25	1
	1.5	Boiling	14	32	64	353
	2	90 (194)	Nil	1	31	Nil
	2	Boiling	61	51	82	557
	2.5	90 (194)	<1	12	34	72
	2.5	Boiling	141	85	44	605
	10	Boiling	400	288	228	642
Hydrochloric acid + 42 g/L $Fe_2(SO_4)_3$	1	93 (200)	2	41	…	238
	5	66 (150)	2	5	3	2
Hydrochloric acid + 2% HF	5	70 (158)	59	26	34	123
Hydrofluoric acid	2	70 (158)	9	9	17	20
	5	70 (158)	14	10	15	16
P_2O_5 (commercial grade)	38	85 (185)	2	9	…	1
	44	116 (240)	21	100	…	23
	52	116 (240)	11	33	…	12
P_2O_5 + 2000 ppm Cl	38	85 (185)	1	12	…	2
P_2O_5 + 0.5% HF	38	85 (185)	7	45	…	9
Nitric acid	10	Boiling	<1	7	7	<1
	65	Boiling	134	888	217	21
Nitric acid + 6% HF	5	60 (140)	67	207	204	73
Nitric acid + 25% H_2SO_4 + 4% NaCl	5	Boiling	12	64	97	713
Nitric acid + 1% HCl	5	Boiling	<1	8	11	1
Nitric acid + 2.5% HCl	5	Boiling	2	21	26	<1
Nitric acid + 15.8% HCl	8.8	52 (126)	4	33	114	>10,000
Sulfuric Acid	2	66 (150)	Nil	<1	Nil	Nil
	2	Boiling	5	6	6	6
	5	79 (174)	<1	1	1	<1
	5	Boiling	9	12	16	16
	10	Boiling	12	19	25	37
	20	66 (150)	<1	<1	<1	<1
	20	79 (174)	1	3	2	13
	20	Boiling	33	39	36	91
	30	66 (150)	<1	1	<1	<1
	30	79 (174)	3	4	3	27
	30	Boiling	64	55	73	227
	40	38 (100)	<1	<1	<1	<1
	40	66 (150)	<1	1	9	1
	40	79 (174)	9	10	15	35
	50	38 (100)	<1	Nil	<1	1
	50	66 (150)	1	4	13	25
	50	79 (174)	16	12	25	58
	60	38 (100)	<1	<1	1	<1
	70	38 (100)	Nil	Nil	2	<1
	80	38 (100)	Nil	<1	<1	<1
Sulfuric acid + 0.1% HCl	5	Boiling	26	33	49	151
Sulfuric acid + 0.5% HCl	5	Boiling	61	49	91	434
Sulfuric acid + 1% HCl	10	70 (158)	<1	11	24	121
Sulfuric acid + 1% HCl	10	90 (194)	94	45	66	326
Sulfuric acid + 1% HCl	10	Boiling	225	116	192	869
Sulfuric acid + 2% HF	10	Boiling	29	22	26	55
Sulfuric acid + 200 ppm Cl^-	25	70 (158)	11	12	37	110
Sulfuric acid + 200 ppm Cl^-	25	Boiling	215	186	182	325
Sulfuric acid + 1.2% HCl + 1% $FeCl_3$ + 1% $CuCl_2$	11.5	Boiling	3	42	837	1815
Sulfuric acid + 1.2% HCl + 1% $FeCl_3$ + 1% $CuCl_2$ (ASTM G 28B)	23	Boiling	8	55	2155	2721
Sulfuric acid + 42 g/L $Fe_2(SO_4)_3$ (ASTM G 28A)	50	Boiling	40	250	143	23

(a) To convert mils/yr to mm/yr, divide by 40.

Hastelloy C-276

Specifications

ASTM. B 366 (welding fittings), B 564 (forgings), B 574 (rod), B 575 (plate, sheet, and strip), B 619 (welded pipe), B 622 (seamless pipe and tube), B 626 (welded tubes)
ASME. SB-366, SB-564, SB-574, SB-575, SB-619, SB-622, SB-626
NACE International. MR-01-75 (materials for oil field equipment)

UNS number. N10276

Chemical Composition

Composition limits. 14.50 to 16.50 Cr; 15.0 to 17.0 Mo; 4.00 to 7.00 Fe; 3.00 to 4.50 W; 2.50 max Co; 1.00 max Mn; 0.35 max V; 0.04 max P; 0.03 max S; 0.08 max Si; 0.02 max C; bal Ni

Applications

Typical uses. Alloy C-276 is used in chemical processing, pollution control, pulp and paper production, industrial and municipal waste treatment, and the recovery of sour natural gas. Applications in air pollution control include stack liners, ducts, dampers, scrubbers, stack-gas reheaters, fans, and fan housings. In chemical processing, the alloy is used in heat

exchangers, reaction vessels, evaporators, and transfer piping.

Mechanical Properties

Tensile properties. Room temperature, average for material solution treated at 1120 °C (2050 °F) and quenched. Sheet: tensile strength, 790 MPa (115 ksi); yield strength, 355 MPa (52 ksi); elongation, 61% in 50 mm (2 in.). Plate: tensile strength, 785 MPa (114 ksi); yield strength, 365 MPa (53 ksi); elongation, 59% in 50 mm (2 in.)
Hardness. Average: sheet, 90 HRB; plate, 87 HRB
Elastic modulus (average, in tension):

Temperature		Modulus	
°C	°F	GPa	10^6 psi
RT	RT	205	29.8
204	400	195	28.3
316	600	188	27.3
427	800	182	26.4
538	1000	176	25.5

RT, room temperature

Physical Properties

Density. 8.89 g/cm^3 (0.321 lb/in.^{3}) at 22 °C (72 °F)
Liquidus temperature. 1370 °C (2500 °F)
Solidus temperature. 1325 °C (2415 °F)
Coefficient of thermal expansion (linear):

Temperature		Coefficient	
°C	°F	μm/m · K	μin./in. · °F
24–93	75–200	11.2	6.2
24–205	75–400	12.0	6.7
24–315	75–600	12.8	7.1
24–425	75–800	13.2	7.3
24–540	75–1000	13.4	7.4
24–650	75–1200	14.1	7.8
24–760	75–1400	14.9	8.3
24–870	75–1600	15.9	8.8
24–925	75–1700	16.0	8.8

Specific heat. 427 J/kg · K (0.102 Btu/lb · °F) at room temperature
Thermal conductivity:

Temperature		Conductivity	
°C	°F	W/m · K	Btu/ft · h · °F
–168	–270	7.2	4.2
–73	–100	8.6	5.0
–18	0	9.4	5.4
+38	+100	10.2	5.9
93	200	11.1	6.4
205	400	13.0	7.5
315	600	15.0	8.7
425	800	16.9	9.75
540	1000	19.0	11.0
650	1200	20.9	12.1
760	1400	23.0	13.3
870	1600	24.9	14.4
980	1800	26.7	15.4
1090	2000	28.2	16.3

Electrical resistivity. 1.30 μΩ · m at 24 °C (75 °F)

Chemical Properties

General corrosion behavior. Alloy C-276 has exceptional resistance to many of the most severe media encountered in chemical processing, including reducing and oxidizing acids, highly oxidizing neutral and acid chlorides, solvents, formic and acetic acids, acetic anhydride, wet chlorine gas, hypochlorites, and chlorine solutions. It has excellent resistance to phosphoric acid. At all temperatures below the boiling point and at concentrations lower than 65 wt%, tests have shown corrosion rates of less than 0.13 mm/yr (5 mils/yr). Alloy C-276 also resists sulfide stress cracking and stress-corrosion cracking in sour gas environments containing hydrogen sulfide, carbon dioxide, and chlorides.
Resistance to specific corroding agents. Data comparing the corrosion resistance of alloy C-276 with other corrosion resistant alloys in various corrosive media are listed in Tables 37, 38, 48, and 65.

Hastelloy C-2000

Specifications

ASTM. B 366 (welding fittings), B 564 (forgings), B 574 (rod), B 575 (plate, sheet, and strip), B 619 (welded pipe), B 622 (seamless pipe and tube), B 626 (welded tubes)
ASME. SB-366, SB-564, SB-574, SB-575, SB-619, SB-622, SB-626
UNS number. Falls into the range of N06200, but has a more restricted composition

Chemical Composition

Nominal composition. 59 Ni; 23 Cr; 16 Mo; 1.6 Cu; 0.01 max C; 0.08 max Si

Applications

Typical uses. Chemical processing plant components (e.g., reactors, heat exchangers, valves, pumps) for both reducing and oxidizing environments

Mechanical Properties

Tensile properties. See Table 66.

Physical Properties

Density. 8.50 g/cm^3 (0.307 lb/in.^{3})
Coefficient of thermal expansion. 12.4 μm/m · K at 25 to 100 °C (6.9 μin./in. · °F at 77–200 °F)
Thermal conductivity. 9.1 W/m · K (63 Btu · in/ft^2 · h · °F) at room temperature
Electrical resistivity. 128 μΩ · cm (50.6 μΩ · in.) at room temperature

Chemical Properties

General corrosion behavior. Alloy C-2000 is one of the most versatile Ni-Cr-Mo alloys. The alloy was designed to resist an extensive

Table 66 Typical room-temperature tensile properties of solution heat treated Hastelloy C-2000

Thickness		Ultimate tensile strength		Yield strength at 0.2% offset		Elongation
mm	in.	MPa	ksi	MPa	ksi	in 50 mm (2 in.), %
1.6	0.063	752	109.0	358	52.0	64.0
3.2	0.125	765	111.0	393	57.0	63.0
6.4	0.250	779	113.0	379	55.0	62.0
13	0.500	758	110.0	345	50.0	68.0
25	1.00	752	109.0	372	54.0	63.0

range of corrosive chemicals, including sulfuric, hydrochloric, and hydrofluoric acids. Unlike other Ni-Cr-Mo alloys, which are optimized for use in either oxidizing or reducing acids, alloy C-2000 extends corrosion resistance in both types of environments. The combination of molybdenum and copper (at levels of 16 and 1.6 wt%, respectively) provides resistance to reducing media (e.g., dilute hydrochloric or sulfuric acids), while oxidizing acid resistance is provided by high chromium content (23 wt%). Alloy C-2000 also resists oxidizing media containing ferric ions, cupric ions, or dissolved oxygen. Figure 22 compares the corrosion rates of alloy C-2000 with other nickel-base alloys in both reducing and oxidizing environments.

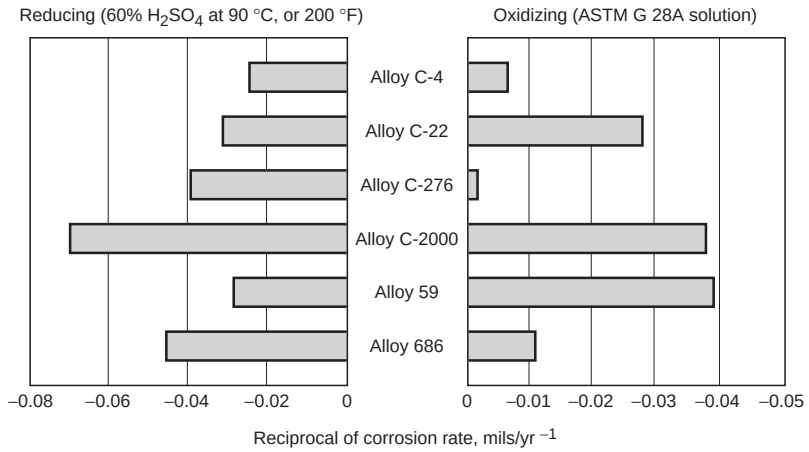


Fig. 22 Application ranges for Hastelloy C-2000 compared to other nickel-chromium-molybdenum alloys

Hastelloy G

Specifications

ASTM. B 366 (welding fittings), B 581 (bar), B 582 (plate, sheet, and strip), B 619 (welded pipe), B 622 (seamless pipe and tube), B 626 (welded tube)
ASME. SB-366, SB-581, SB-582, SB-619, SB-622, SB-626
NACE International. MR-01-75 (materials for oil field equipment)
UNS number. N06007

Chemical Composition

Composition limits. 21 to 23.5 Cr; 18.0 to 21.0 Fe; 5.5 to 7.5 Mo; 1.75 to 2.50 (Nb + Ta); 1.5 to 2.5 Cu; 1.0 to 2.0 Mn; 2.5 max Co; 1.0 max W; 1.0 max Si; 0.05 max C; 0.04 max P; 0.03 max S; bal Ni

Applications

Typical uses. Chemical applications, particularly those involving sulfuric and phosphoric acids, pulp digestion operations, dissolver vessels, and attendant equipment for the dissolution of spent nuclear fuel elements

Mechanical Properties

Tensile properties. See Table 67.
Compressive properties. Compressive yield strength, plate; 25 mm (1 in.) thick: 315 MPa (45.5 ksi); bar, 32 mm (1.25 in.) diameter: 355 MPa (51.5 ksi)
Hardness. Sheet: 0% cold reduction, 84 HRB; 10% reduction, 97 HRB; 20% reduction, 28 HRC; 30% reduction, 31 HRC; 40% reduction, 34 HRC; 50% reduction, 36 HRC. In the aged condition:

Temperature		
°C	°F	Hardness
Aged for 1 h		
650	1200	84 HRB
705	1300	83 HRB
760	1400	84 HRB
815	1500	84 HRB
Aged for 4 h		
650	1200	86 HRB
705	1300	85 HRB
760	1400	86 HRB
815	1500	20 HRC
Aged for 16 h		
650	1200	86 HRB
705	1300	86 HRB
760	1400	94 HRB
815	1500	26 HRC
Aged for 50 h		
650	1200	88 HRB
705	1300	89 HRB
760	1400	21 HRC
815	1500	29 HRC
Aged for 100 h		
650	1200	88 HRB
705	1300	89 HRB
760	1400	25 HRC
815	1500	30 HRC

Elastic modulus:

Temperature		Dynamic modulus of elasticity	
°C	°F	GPa	10^6 psi
21	70	195	28
93	200	185	27
205	400	180	26
315	600	175	25
425	800	165	24
540	1000	160	23
650	1200	150	22
760	1400	145	21

Table 67 Typical tensile properties of solution-treated Hastelloy G

Temperature		Tensile strength		Yield strength		Elongation,
°C	°F	MPa	ksi	MPa	ksi	%
Sheet, 3.1 mm (0.125 in.) thick and under						
…	–320	840	122	450	65	48
…	–150	795	115	400	58	50
21	70	705	102	315	46	61
93	200	670	97	290	42	56
205	400	625	91	255	37	74
315	600	605	88	250	36	82
425	800	585	85	230	33	84
540	1000	565	82	230	33	83
650	1200	525	76	220	32	82
760	1400	425	62	220	32	61
Plate, 9.5 to 16 mm (0.375–0.625 in.) thick						
…	–320	840	122	460	67	60
…	–150	800	116	400	58	55
21	70	690	100	310	45	62
93	200	655	95	260	38	61
205	400	605	88	235	34	63
315	600	580	84	205	30	68
425	800	565	82	200	29	70
540	1000	525	76	195	28	73
650	1200	505	73	200	29	68
760	1400	415	60	195	28	57

Impact strength:

Temperature		Charpy V-notch impact strength	
°C	°F	J	ft · lbf
Aged for 16 h			
650	1200	181	134
705	1300	65	48
760	1400	27	20
815	1500	19	14
Aged for 100 h			
650	1200	49	36
705	1300	39	29
760	1400	11	8
815	1500	7	5

Fatigue strength. Plate, 13 mm (0.5 in.) thick, solution treated, 330 MPa (48 ksi) at 10^6 cycles
Stress-rupture strength:

Temperature		Average initial stress for rupture	
°C	°F	MPa	ksi
At 10 h			
650	1200	385	56
760	1400	195	28
870	1600	90	13
980	1800	41	6
At 100 h			
650	1200	310	45
760	1400	145	21
870	1600	62	9
980	1800	28	4
At 500 h			
650	1200	275	40
760	1400	125	18
870	1600	55	8
980	1800	21	3
At 1000 h			
650	1200	260	38
760	1400	110	16
870	1600	48	7
980	1800	14	2
At 2000 h			
650	1200	235	34
760	1400	105(a)	15(a)
870	1600	41(a)	6(a)
980	1800	14(a)	2(a)

(a) Extrapolated values

Physical Properties

Density. 8.31 g/cm^3 (0.300 lb/in.^{3}) at 22 °C (70 °F)
Melting range. 1260 to 1340 °C (2300–2450 °F)
Coefficient of thermal expansion (linear):

Temperature		Mean coefficient	
°C	°F	μm/m · K	μin./in. · °F
21–93	70–200	13.5	7.5
21–205	70–400	13.9	7.7
21–315	70–600	14.2	7.9
21–425	70–800	14.9	8.3
21–540	70–1000	15.7	8.7
21–650	70–1200	16.4	9.1

Specific heat:

Temperature		Specific heat	
°C	°F	J/kg · K	Btu/lb · °F
0	32	390	0.093
100	212	455	0.109
200	392	480	0.115
300	570	502	0.120
400	750	520	0.124
500	930	535	0.128
600	1110	553	0.132
700	1290	570	0.136
800	1470	586	0.140
900	1650	603	0.144
1000	1830	620	0.148

Thermal conductivity:

Temperature		Conductivity	
°C	°F	W/m · K	Btu/ft · h · °F
25	77	10.1	5.8
100	212	11.2	6.5
200	392	12.8	7.4
300	570	14.3	8.3
400	750	15.9	9.2
500	930	17.5	10.1
600	1110	19.2	11.1
700	1290	20.8	12.0
800	1470	22.4	12.9
900	1650	24.0	13.9

Chemical Properties

Resistance to specific corroding agents. Outstanding resistance to hot sulfuric and phosphoric acids in the as-welded condition. Also resists mixed acids, fluosilicic acid, sulfate compounds, contaminated nitric acid, flue gases, and hydrofluoric acid.

Hastelloy G-3

Specifications

ASTM. B 581 (bar), B 582 (plate, sheet, and strip), B 619 (welded pipe), B 622 (seamless pipe and tube), B 626 (welded tube)
ASME. SB-581, SB-582, SB-619, SB-622, SB-626
NACE International. MR-01-75 (materials for oil field equipment)
UNS number. N06985

Chemical Composition

Nominal composition. 22.2 Cr; 19.5 Fe; 7.0 Mo; 5.0 max Co; 1.9 Cu; 1.5 max W; 0.8 Mn; 0.4 Si; 0.3 Nb + Ta; 0.04 max P; 0.03 max S; 0.015 max C; bal Ni

Applications

Typical uses. Chemical applications, particularly those involving sulfuric and phosphoric acids, pulp digestion operations, dissolver vessels and attendant equipment for the dissolution of spent nuclear fuel elements

Mechanical Properties

Tensile properties. See Table 68.
Hardness. See Table 68.

Physical Properties

Density. 8.31 g/cm^3 (0.300 lb/in.^{3}) at 21 °C (70 °F)

Chemical Properties

General corrosion behavior. Excellent resistance to hot sulfuric and phosphoric acids
Resistance to specific corroding agents. Tables 69 and 70 compare the corrosion resistance of alloy G-3 with that of Hastelloy G-30 and alloy 625 in various acidic media.

Table 68 Typical mechanical properties of Hastelloy G-3 at room temperature

Form	Tensile strength MPa	Tensile strength ksi	Yield strength MPa	Yield strength ksi	Elongation, %	Hardness, HRB
Sheet(a)	690	100	325	47	50	79
Sheet(b)	685	99	305	44	53	83
Plate(c)	740	107	365	53	56	87
Bar(d)	695	101	295	43	59	80
Weld metal(e)	690	100	450	65	46(f)	…

(a) 0.63–0.97 mm (0.025–0.038 in.) thick. (b) 1.4–4.8 mm (0.056–0.187 in.) thick. (c) 6.4–19 mm (0.25–0.75 in.) thick. (d) 13–25 mm (0.5–1.0 in.) diameter. (e) Shielded metal-arc welded. (f) In 57 mm or 2.25 in.

Table 69 Comparison of corrosion rates of Hastelloy G-3, Hastelloy G-30, and alloy 625 in phosphoric acid media

Media	Temperature, °C (°F)	Average corrosion rate, mils/yr(a) G-3 alloy	G-30 alloy	625 alloy
28% P_2O_5 + 2000 ppm Cl^-	85 (185)	0.9	1.0	1.5
42% P_2O_5 + 2000 ppm Cl^-	85 (185)	11	0.9	1.3
44% P_2O_5	116 (241)	22	7.0	23
44% P_2O_5 + 2000 ppm Cl^-	116 (241)	22	7.7	25
44% P_2O_5 + 0.5% HF	116 (241)	49	16	60
52% P_2O_5	116 (241)	11	3.9	12
52% P_2O_5	149 (300)	64	28	79
54% P_2O_5	116 (241)	16	8	16
54% P_2O_5 + 2000 ppm Cl^-	116 (241)	16	7	15

(a) To convert mils/yr to mm/yr, divide by 40.

Table 70 Comparison of corrosion rates of Hastelloy G-3, Hastelloy G-30, and alloy 625 in various acidic media

Media	Concentration, wt%	Test temperature, °C (°F)	Average corrosion rate, mils/yr(a) G-3 alloy	G-30 alloy	625 alloy
Acetic acid	99	Boiling	0.6	1	<1
Formic acid	88	Boiling	5	2	9
Nitric acid	10	Boiling	0.9	0.4	1
	60	Boiling	8.5	5.3	16
	65	Boiling	11	5	20
Nitric acid + 1% HF	20	80 (176)	74	31	123
Nitric acid + 6% HF	20	80 (176)	540	177	2400
Nitric acid + 1% HF	50	80 (176)	420	192	…
Nitric Acid + 0.5% HF	56	110 (230)	110	47	…
Nitric acid + 0.5% HF + 2000 ppm Cl^-	56	110 (230)	113	50	…
Sulfuric acid + 10% nitric acid	50	Boiling	30	16	…
Sulfuric acid	2	Boiling	6	8	6
	10	Boiling	19	31	46, 25
	20	Boiling	30	54	124, 91
	50	107 (225)	37	37	223
	80	52 (125)	23	12	33
	99	130 (266)	74	43	…
	99	140 (284)	57	46	…
Sulfuric acid + 42 g/L $Fe_2(SO_4)_3$ (ASTM G 28A)	50	Boiling	11	7	23,17
Sulfuric acid + 5% nitric acid	70	Boiling	240	133	…
Sulfuric acid + 5% nitric acid	60	Boiling	84	45	105
Sulfuric acid + 8% nitric acid + 4% HF	77	54 (129)	1.5	0.4	…
Nitric acid + 8% HCl	18	80 (176)	18	2	6
Nitric acid + 11% HCl	25	80 (176)	914	23	126
Nitric acid + 3% HCl	59	80 (176)	34	5	20

(a) To convert mils/yr to mm/yr, divide by 40.

Hastelloy G-30

Specifications

ASTM. B 366 (welding fittings), B 581 (bar), B 582 (plate, sheet, and strip), B 619 (welded pipe), B 622 (seamless pipe and tube), B 626 (welded tube)
ASME. SB-366, SB-581, SB-582, SB-619, SB-622, SB-626
NACE International. MR-01-75 (materials for oil field equipment)
UNS number. N06030

Chemical Composition

Composition limits. 28.0 to 31.5 Cr; 13.0 to 17.0 Fe; 4.0 to 6.0 Mo; 5.0 max Co; 1.5 to 4.0 W; 0.8 max Si; 1.5 max Mn; 0.03 max C; 0.3 to 1.5 Nb + Ta; 1.0 to 2.4 Cu; 0.004 max P; 0.02 max S; bal Ni

Applications

Typical uses. Typical applications for alloy G-30 include phosphoric acid service, sulfuric acid service, nitric acid service, nuclear fuel reprocessing, nuclear waste processing, pickling operations, petrochemical operations, fertilizer manufacture, pesticide manufacture, and gold ore extraction.

Table 71 Typical room-temperature tensile properties of solution heat-treated Hastelloy G-30

Form	Ultimate tensile strength MPa	Ultimate tensile strength ksi	Yield strength at 0.2% offset MPa	Yield strength at 0.2% offset ksi	Elongation in 50 mm (2 in.), %	Reduction of area, %
Sheet, 0.71 mm (0.028 in.) thick	690	100	324	47	56	…
Sheet, 3.2 mm (0.125 in.) thick	690	100	352	51	56	…
Plate, 6.4 mm (0.250 in.) thick	676	98	317	46	55	…
Plate, 9.5 mm (0.375 in.) thick	690	100	310	45	65	68
Plate, 12.7 mm (0.500 in.) thick	690	100	317	46	64	77
Plate, 19.1 mm (0.750 in.) thick	676	98	324	47	65	67
Plate, 31.8 mm (1.250 in.) thick	683	99	310	45	60	…
Bar, 25.4 mm (1.0 in.) thick	690	100	317	46	60	…

Table 72 Typical elevated-temperature tensile properties of Hastelloy G-30 plate and bar in thicknesses ranging from 6.4 to 32 mm (0.25 to 1.25 in.)

Test temperature		Ultimate tensile strength		Yield strength at 0.2% offset		Elongation in
°C	°F	MPa	ksi	MPa	ksi	50 mm (2 in.), %
Room temperature		710	103	338	49	53
93	200	655	95	290	42	54
204	400	607	88	248	36	59
316	600	572	83	228	33	59
427	800	552	80	214	31	60
538	1000	524	76	200	29	62

Table 73 Effect of cold work and aging on the hardness of Hastelloy G-30

Cold work, %	Unaged	Aged 200 h at 200 °C (392 °F)	Aged 100 h at 500 °C (932 °F)
As mill annealed	90 HRB	…	…
10	98 HRB	100 HRB	93 HRB
20	29 HRC	26 HRC	25 HRC
30	32 HRC	34 HRC	34 HRC
40	35 HRC	38 HRC	40 HRC
50	36 HRC	39 HRC	41 HRC
60	40 HRC	43 HRC	44 HRC
70	41 HRC	43 HRC	46 HRC

Mechanical Properties

Tensile properties. See Tables 71 (room-temperature data) and 72 (elevated-temperature data).
Hardness. See Table 73.
Elastic modulus. See Table 74.
Impact strength. Charpy V-notch values for mill annealed plate, 13 mm (½ in.) thick, 353 J (260 ft · lbf); for 50% cold-rolled material, 42 J (31 ft · lbf). See Table 75 for the effects of aging on impact strength.

Physical Properties

Density. 8.22 g/cm^3 (0.297 lb/in.^{3})
Coefficient of thermal expansion (linear):

Temperature		Mean coefficient	
°C	°F	μm/m · K	μin./in. · °F
30–93	86–200	12.8	7.1
30–204	86–400	13.9	7.7
30–316	86–600	14.4	8.0
30–427	86–800	14.9	8.3
30–538	86–1000	15.5	8.6
30–649	86–1200	16.0	8.9
30–760	86–1400	16.0	8.9

Thermal conductivity:

Temperature		Conductivity	
°C	°F	W/m · K	Btu · in./ft^2 · h · °F
24	75	10.2	71
100	212	11.9	83
200	392	14.4	100
300	572	16.7	116
400	572	18.7	130
500	932	20.3	141
600	1112	21.4	149

Electrical resistivity:

Temperature		Resistivity	
°C	°F	μΩ · m	μΩ · in.
24	75	1.16	45.7
100	212	1.17	46.1
200	392	1.19	46.9
300	572	1.21	47.6
400	752	1.23	48.4
500	932	1.24	48.8
600	1112	1.25	49.2

Table 74 Effect of temperature on the dynamic elastic modulus of Hastelloy G-30 that was solution heat treated at 1175 °C (2150 °F) and rapidly quenched

Temperature		Modulus	
°C	°F	GPa	10^6 psi
24	75	202	29.3
204	400	196	28.4
316	600	194	28.2
427	800	192	27.8
538	1000	184	26.7

Chemical Properties

General corrosion behavior. Alloy G-30 exhibits superior corrosion resistance in commercial phosphoric acids as well as many complex environments containing highly oxidizing acids, such as nitric/hydrochloric, nitric/hydrofluoric, and sulfuric acids. The resistance of alloy G-30 to the formation of grain-boundary precipitates in the heat-affected zone makes it suitable for use in most chemical process applications in the as-welded condition.
Resistance to specific corroding agents. Table 69 compares the resistance of alloy G-30 in phosphoric acid with that of alloys G-3 and 625. Similar comparative data for a variety of acid media are shown in Table 70.

Table 75 Effect of aging on the impact strength of 13 mm (½ in.) thick Hastelloy G-30 plate

		Charpy V-notch impact strength			
		Room temperature		–196 °C (–320 °F)	
Condition	Orientation	J	ft · lbf	J	ft · lbf
Mill annealed (MA)	Longitudinal	353	260	354	261
MA	Transverse	353	260	355	262
MA + 1 h at 760 °C (1400 °F)	Longitudinal	271	200	…	…
MA + 24 h at 760 °C (1400 °F)	Longitudinal	79	58	…	…
MA + 1 h at 871 °C (1600 °F)	Longitudinal	130	96	…	…

Hastelloy G-50

Specifications

NACE International. MR-01-75 (materials for oil field equipment)
UNS number. N06950

Chemical Composition

Nominal composition. 50 Ni; 20 Cr; 17.5 Fe; 9 Mo; 0.4 Al; 0.5 Nb; 2.5 max Co; 1 max W; 1 max Mn; 0.50 Cu; 0.02 max C

Applications

Typical uses. Developed primarily for use as tubular components in sour gas applications where high hydrogen sulfide is present in combination with carbon dioxide and chlorides, for example. Compared with other alloys used for sour gas service, alloy G-50 is more corrosion resistant than alloy G-3 and less expensive than alloy C-276.

Mechanical Properties

Tensile properties. See Table 76.
Hardness. Ranges from 31 to 38 HRC depending on the strength of the alloy

Elastic modulus. 192 GPa (27.9×10^6 psi) at room temperature

Physical Properties

Density. 8.33 g/cm^3 (0.301 lb/in.^{3})
Coefficient of thermal expansion (linear):

Temperature		Mean coefficient	
°C	°F	μm/m · K	μin./in. · °F
20–95	68–200	13.0	7.21
20–205	68–400	13.5	7.52
20–315	68–600	14.1	7.83

Chemical Properties

General corrosion behavior. Improved performance in sour gas environments when compared with alloy G-3. Slow strain rate and C-ring tests have shown that G-50 provides superior resistance to stress-corrosion cracking and sulfide stress cracking.
Resistance to specific corroding agents. Table 77 compares the general corrosion resistance of alloys G-50, G-3, and C-276 in hydrochloric and hydrochloric/hydrofluoric acid media.

Table 76 Typical tensile properties of Hastelloy G-50 tubular goods

Temperature		Ultimate tensile strength		Yield strength, 90.2% offset		
°C	°F	MPa	ksi	MPa	ksi	Elongation, %
Longitudinal direction						
Room temperature		875	126.9	742	107.6	25.8
95	200	825	119.7	700	101.5	24.8
205	400	761	110.4	631	91.5	24.7
315	600	717	104.0	619	89.8	22.6
Transverse direction						
Room temperature		838	121.6	709	102.9	26.8
95	200	782	113.4	669	97.0	24.3
205	400	712	103.3	587	85.1	24.5
315	600	678	98.4	578	83.8	21.7

Table 77 General corrosion resistance of Hastelloy G-50, G-3, and alloy C-276

Temperature		Corrosion rate, mm/yr (mils/yr)				
		15% HCl			12% HCl + 3% HF	
°C	°F	G-50 alloy	G-3 alloy	C-276 alloy	G-50 alloy	G-3 alloy
66	150	1.4 (55)	1.8 (73)	0.7 (28)	1.4 (57)	0.9 (36)
93	200	5.0 (199)	7.8 (313)	1.7 (67)	8.1 (323)	17 (680)
121	250	28 (1120)	45 (1810)	6.4 (257)	…	…
149	300	172 (6896)	513 (20,516)	…	204 (8170)	439 (17,536)

Hastelloy N

Specifications

ASTM. B 366 (welding fittings), B 434 (plate and sheet), B 573 (bar)
ASME. SB-366, SB-434, SB-573
AMS. 5607 (sheet, strip, and plate), 5771 (bars, forgings, and rings)
UNS number. N10003

Chemical Composition

Composition limits. 15.00 to 18.00 Mo; 6.00 to 8.00 Cr; 5.0 max Fe; 0.80 max Mn; 0.50 max W; 0.35 max Cu; 0.20 max Co; 0.04 to 0.08 C; 0.020 max S; 0.015 max P; 0.010 max B; 0.50 max Al + Ti; 1.00 max Si; bal Ni

Applications

Typical uses. Developed specifically for primary-loop service in molten salt reactors. Especially good for use with hot fluoride salts.

Mechanical Properties

Tensile properties. Room-temperature values for 1.6 mm (0.063 in.) thick sheet: tensile strength, 794 MPa (115,100 psi); yield strength, 314 MPa (45,500 psi); elongation in 50 mm (2 in.), 50.7%
Hardness. 96 HRB for solution-treated 1.6 mm (0.063 in.) sheet
Elastic modulus. 219 GPa (31.7×10^6 psi) for solution-treated sheet at 14 °C (57 °F)
Impact strength. 108 to 119 J (80–88 ft · lbf) at room temperature for solution-treated 13 mm (½ in.) thick plate

Physical Properties

Density. 8.86 g/cm^3 (0.320 lb/in.^{3})
Coefficient of thermal expansion (linear):

Temperature		Coefficient	
°C	°F	μm/m · K	μin./in. · °F
20–315	68–600	12.6	7.0
20–425	68–800	13.0	7.2
20–540	68–1000	13.3	7.4
20–650	68–1200	13.5	7.5
20–760	68–1400	14.2	7.9
20–870	68–1600	14.8	8.2
20–980	68–1800	15.3	8.5
20–1090	68–2000	15.7	8.7

Specific heat:

Temperature		Specific heat	
°C	°F	J/kg · K	Btu/lb · °F
100	212	419	0.100
200	390	440	0.105
300	570	456	0.109
400	750	469	0.112
480	895	477	0.114
540	1005	486	0.116
570	1060	523	0.125
590	1095	565	0.135
620	1150	586	0.140
660	1220	582	0.139
680	1255	578	0.138
700	1290	578	0.138

Thermal conductivity:

Temperature		Conductivity	
°C	°F	W/m · K	Btu/ft · h · °F
100	212	11.5	6.6
200	390	13.1	9.4
300	570	14.4	8.3
400	750	16.5	9.2
500	930	18.0	10.3
600	1110	20.3	11.8
700	1290	23.6	13.6

Electrical resistivity:

Temperature		
°C	°F	Resistivity, μΩ · m
RT	RT	1.20
705	1300	1.26
815	1500	1.24

RT, room temperature

Chemical Properties

General corrosion behavior. Good oxidation resistance; also resists aging and embrittlement. Compares favorably with Hastelloy alloys B, C, and W in various corrosive media.
Resistance to specific corroding agents. Exceptional resistance to hot fluoride salts; it can serve continuously at temperatures to 980 °C (1800 °F). In fluoride salts at 700 °C (1300 °F), corrosion is less than 0.025 mm/yr (1 mil/yr).

Hastelloy S

Specifications

AMS. 5711 (bars, forgings, and rings), 5838 (wire and welding wire), 5873 (sheet, strip, and plate)
UNS number. N06635

Chemical Composition

Composition limits. 14.5 to 17.0 Cr; 14.0 to 16.5 Mo; 2.0 max Co; 3.0 max Fe; 0.20 to 0.75 Si; 0.3 to 1.0 Mn; 0.02 max C; 0.10 to 0.50 Al; 0.015 max B; 0.01 to 0.10 La; bal Ni

Applications

Typical uses. Developed for applications involving severe cyclic heating conditions where components must be capable of retaining strength, ductility, dimensional stability, and metallurgical integrity after long-time exposure

Mechanical Properties

Tensile properties. Average at room temperature. Sheet: tensile strength, 890 MPa (129 ksi); yield strength, 495 MPa (72 ksi); elongation, 51% in 50 mm (2 in.). Plate: tensile strength, 850 MPa (123 ksi); yield strength, 385 MPa (56 ksi); elongation, 55% in 50 mm (2 in.)
Hardness. Solution heat treated: sheet, 52 HRA; plate, 57 HRA
Elastic modulus. Average, in tension, for sheet heat treated at 1065 °C (1950 °F) and air cooled:

Temperature		Modulus	
°C	°F	GPa	10^6 psi
24	75	212	30.8
360	675	194	28.2
540	1000	182	26.4
650	1200	174	25.2
760	1400	166	24.1
815	1495	161	23.3
925	1700	151	21.9
1090	2000	132	19.2

Impact strength. Charpy V-notch, average for solution heat-treated plate: 190 J (140 ft · lbf)
Creep and stress-rupture characteristics. See Tables 78 and 79.

Physical Properties

Density. 8.747 g/cm^3 (0.316 lb/in.^{3}) at 22 °C (72 °F)
Liquidus temperature. 1380 °C (2516 °F)
Solidus temperature. 1335 °C (2435 °F)

Table 78 Average creep date for Hastelloy S

Temperature			Average initial stress to produce specified creep in:					
			10 h		100 h		1000 h	
°C	°F	Creep, %	MPa	ksi	MPa	ksi	MPa	ksi
Plate, 25 mm (1 in.) thick								
650	1200	0.2	310	45.0	217	31.5	145	21.0
		0.5	345	50.0	245	35.5	165	24.0
		1.0	390	56.5	276	40.0	186	27.0
730	1350	0.2	152	22.0	97	14.1	62	9.0
		0.5	172	25.0	112	16.2	72	10.4
		1.0	200	29.0	131	19.0	84	12.2
815	1500	0.2	70	10.2	41	5.9	…	…
		0.5	81	11.8	48	7.0	…	…
		1.0	95	13.8	58	8.4	…	…
Sheet, 1.1 to 1.6 mm (0.045–0.063 in.) thick								
650	1200	0.2	310	45.0	186	27.0	117(a)	17.0(a)
		0.5	372	54.0	225	32.6	131	19.0
		1.0	386	56.0	234	34.0	143	20.8
705	1300	0.2	165	24.0	86	12.5	46(a)	6.7(a)
		0.5	200	29.0	114	16.5	62	9.0
		1.0	234	34.0	138	20.0	83	12.0
760	1400	0.2	90	13.0	45	6.5	23(a)	3.3(a)
		0.5	117	16.9	63	9.2	33	4.8
		1.0	143	20.7	81	11.8	46	6.7
815	1500	0.2	54	7.8	26	3.8	13(a)	1.9(a)
		0.5	69	10.0	39	5.7	21	3.0
		1.0	86	12.5	48	6.9	26	3.8
870	1600	0.2	32	4.7	15	2.2	7.6(a)	1.1(a)
		0.5	43	6.3	24	3.5	13	1.9
		1.0	52	7.6	28	4.1	15	2.2

(a) Extrapolated values

Coefficient of thermal expansion (linear):

Temperature		Coefficient	
°C	°F	μm/m · K	μin./in. · °F
20–93	68–200	11.5	6.4
20–205	68–400	12.2	6.8
20–315	68–600	12.8	7.1
20–425	68–800	13.1	7.3
20–540	68–1000	13.3	7.4
20–650	68–1200	13.7	7.6
20–760	68–1400	14.4	8.0
20–870	68–1600	14.9	8.3
20–980	68–1800	15.5	8.6
20–1090	68–2000	16.0	8.9

Specific heat:

Temperature		Specific heat	
°C	°F	J/kg · K	Btu/lb · °F
0	32	398	0.095
100	212	427	0.102
200	390	448	0.107
300	570	465	0.111
400	750	477	0.114
500	930	490	0.117
600	1110	498	0.119
700	1290	594	0.142
800	1470	590	0.141
900	1650	594	0.142
1000	1830	599	0.143
1100	2010	603	0.144

Thermal conductivity:

Temperature		Conductivity	
°C	°F	W/m · K	Btu/ft · h · °F
200	390	14.0	8.1
300	570	16.1	9.3
400	750	17.9	10.3
500	930	19.5	11.3
600	1110	21.0	12.2
700	1290	26.0	15.1
800	1470	26.0	15.1
900	1650	26.0	15.1
950	1740	27.0	15.7
1000	1830	28.0	16.2

Thermal diffusivity:

Temperature		Diffusion coefficient,
°C	°F	10^{-6} m^2/s
100	212	3.8
200	390	3.8
300	570	3.8
400	750	4.5
500	930	4.5
600	1110	5.1
700	1290	5.1
800	1470	5.1
900	1650	5.1
950	1740	5.1
1000	1830	5.8

Electrical resistivity. 1.28 μΩ · m at 25 °C (77 °F) for material aged 16,000 h at 650 °C (1200 °F)

Chemical Properties

General corrosion behavior. Excellent oxidation resistance to 1090 °C (2000 °F)

Table 79 Stress-rupture data for Hastelloy S

Temperature		Average stress for rupture life of:					
		10 h		100 h		1000 h	
°C	°F	MPa	ksi	MPa	ksi	MPa	ksi
Sheet, 1.1 to 1.6 mm (0.045–0.063 in.) thick							
650	1200	431	62.5	345	50.0	262	38.0
730	1350	269	39.0	194	28.2	139	20.2
815	1500	162	23.5	103	15.0	68	9.9
925	1700	66	9.6	40	5.8	…	…
Plate, 25 mm (1 in.) thick							
650	1200	552	80.0	400	58.0	269	39.0
705	1300	386	56.0	262	38.0	172	25.0
760	1400	262	38.0	169	24.5	107	15.5
815	1500	172	25.0	110	16.0	66	9.6
870	1600	114	16.5	68	9.8	37	5.4

Hastelloy W

Specifications

AMS. 5755 (bar, forgings, and rings), 5786 (welding wire)
AWS. A 5.11 (covered welding electrode ENiMo-3) and A 5.14 (bare welding rod ERNiMo-3)
ASME. SFA 5.11 (covered welding electrode) and SFA 5.14 (bare welding rod)
UNS number. N10004

Chemical Composition

Composition limits. 0.12 max C; 23.0 to 26.0 Mo; 4.0 to 6.0 Cr; 4.0 to 7.0 Fe; 0.60 max V; 2.50 max Co; 1.00 max Mn; 1.00 max Si; 0.040 max P; 0.030 max S; bal Ni

Applications

Typical uses. Primarily a high-temperature alloy for structural applications up to 760 °C (1400 °F). As a weld filler metal, it has excellent characteristics for joining dissimilar high-temperature metals.

Mechanical Properties

Tensile properties. Average at room temperature. Sheet, 2.5 mm (0.109 in.) thick: tensile strength, 850 MPa (123 ksi); yield strength, 370 MPa (53.5 ksi); elongation, 55% in 50 mm (2 in.). Weld metal: tensile strength, 875 MPa (127 ksi); elongation, 37% in 50 mm (2 in.). See also Table 80.

Physical Properties

Density. 9.03 g/cm^3 (0.325 lb/in.^{3}) at 22 °C (72 °F)
Liquidus temperature. 1316 °C (2400 °F)
Coefficient of thermal expansion. Linear: 11.3 µm/m · K (6.28 µin./in. · °F) at 23 to 1000 °C (73–1832 °F)

Table 80 Typical properties of solution-treated Hastelloy W sheet

Temperature		Tensile strength		Yield strength		Elongation in 50 mm
°C	°F	MPa	ksi	MPa	ksi	(2 in.), %
425	800	725	105	260	38	56.0
650	1200	…	…	255	37	29.5
730	1350	465	67	…	…	16.0
815	1500	405	59	250	36	17.0
900	1650	353	52	220	32	14.5
980	1800	…	…	135	20	14.5
1065	1950	180	26	…	…	34.0

Hastelloy X

Specifications

ASTM. B 366 (welding fittings), B 435 (sheet and plate), B 572 (rod), B 619 (welded pipe), B 622 (seamless pipe and tube), B 626 (welded tube)
ASME. SB-435, SB-572, SB-619, SB-622, SB-626
AMS. 5536 (sheet, strip, and plate), 5588 (welded tubing), 5754 (bars, forgings, and rings), 5798 (wire)
UNS number. N06002

Chemical Composition

Composition limits. 0.50 to 2.50 Co; 20.50 to 23.00 C; 8.00 to 10.00 Mo; 0.20 to 1.00 W; 17.00 to 20.00 Fe; 0.05 to 0.15 C; 1.00 max Si; 1.00 max Mn; 0.010 max B; 0.040 max P; 0.030 max S; bal Ni

Applications

Typical uses. Exceptional strength and oxidation resistance up to 1200 °C (2200 °F); used in many industrial furnace applications because of its resistance to oxidizing, neutral and carburizing atmospheres; widely used for aircraft parts, such as jet engine tailpipes, afterburners, turbine blades, and vanes.
Precautions in use. Upper limit of usefulness just above 1200 °C (2200 °F)

Mechanical Properties

Tensile properties. Room temperature, average, for sheet solution treated at 1175 °C (2150 °F)

and rapidly cooled: tensile strength, 785 MPa (114 ksi); yield strength, 360 MPa (52 ksi); elongation, 43% in 50 mm (2 in.)

Hardness. Average, for sheet solution treated at 1175 °C (2150 °F) and rapidly cooled: 89 HRB

Poisson's ratio. 0.320 at 22 °C (72 °F); 0.328 at –78 °C (–108 °F)

Elastic modulus. In tension, average, for sheet solution treated at 1175 °C (2150 °F) and rapidly cooled:

Temperature		Modulus	
°C	°F	GPa	10^6 psi
25	76	196	28.5
100	212	193	28.0
200	390	185	26.9
300	570	179	26.0
400	750	172	25.0
500	930	164	23.8
600	1110	158	22.9
700	1290	150	21.8
800	1470	143	20.7
900	1650	134	19.5
1000	1830	126	18.3

Impact strength. Charpy V-notch, average, for plate solution treated at 1175 °C (2150 °F) and rapidly cooled:

Temperature		Impact strength	
°C	°F	J	ft · lb
–196	–321	50	37
–157	–216	60	44
–78	–108	69	51
–29	–20	76	56
RT	RT	73	54
+815	+1500	79	58

RT, room temperature

Creep and stress-rupture characteristics. See Tables 81 and 82.

Physical Properties

Density. 8.22 g/cm^3 (0.297 lb/in.^{3}) at 22 °C (72 °F)

Melting range. 1260 to 1355 °C (2300–2470 °F)

Coefficient of thermal expansion (linear):

Temperature		Coefficient	
°C	°F	μm/m · K	μin./in. · °F
26–100	79–200	13.8	7.7
26–500	79–1000	14.9	8.4
26–600	79–1200	15.3	8.6
26–700	79–1350	15.7	8.8
26–800	79–1500	16.0	8.9
26–900	79–1650	16.3	9.1
26–1000	79 –1800	16.6	9.2

Specific heat:

Temperature		Specific heat	
°C	°F	J/kg · K	Btu/lb · °F
RT	RT	486	0.116
315	600	498	0.119
650	1200	582	0.139
870	1600	699	0.167
1095	2000	858	0.205

RT, room temperature

Table 81 Average creep data for Hastelloy X

Temperature			Average initial stress to produce specified creep in:					
			10 h		100 h		1000 h	
°C	°F	Creep, %	MPa	ksi	MPa	ksi	MPa	ksi
Sheet, solution heat treated(a)								
650	1200	0.5	276	40	186	27	121	17.5
		1.0	303	44	207	30	145	21
		2.0	331	48	227	33	155	22.5
760	1400	0.5	114	16.5	72	10.5	45	6.5
		1.0	131	19	90	13	62	9
		2.0	145	21	103	15	74	10.8
870	1600	0.5	54	7.8	34	4.9	21	3.1
		1.0	62	9	42	6.1	25	3.6
		2.0	72	10.5	50	7.2	30	4.3
980	1800	0.5	21	3.1	12	1.7	6	0.9
		1.0	25	3.6	13	1.9	7	1.0
		2.0	29	4.2	15	2.2	8	1.1
1090	2000	0.5	…	…	…	…	…	…
		1.0	6	0.8	…	…	…	…
		2.0	8	1.1	…	…	…	…
Plate and bar, solution heat treated(b)								
650	1200	1.0	331	48	220	32	151	22
		5.0	441	64	296	43	200	29
730	1350	1.0	186	27	131	19	89	13
		5.0	234	34	165	24	113	16.5
815	1500	1.0	103	15	71	10.4	50	7.3
		5.0	124	18	89	13	62	9
900	1650	1.0	55	8	37	5.4	25	3.7
		5.0	72	10.5	46	6.8	28	4.2
980	1800	1.0	28	4.2	17	2.6	11	1.6
		5.0	37	5.4	22	3.3	14	2.0

(a) Based on over 100 tests. (b) Based on over 90 tests for 1.0% creep, over 60 tests for 5.0% creep

Table 82 Stress-rupture data for Hastelloy X

Temperature		Average rupture life strength for:							
		10 h		100 h		1000 h		10,000 h	
°C	°F	MPa	ksi	MPa	ksi	MPa	ksi	MPa	ksi
Sheet, solution heat treated(a)									
650	1200	462	67	331	48	234	34	170	24.6
760	1400	221	32	155	22.5	109	15.8	77	11.1
870	1600	117	17	73	10.6	45	6.5	28	4.0
980	1800	45	6.5	26	3.7	14	2.1	8	1.2
1090	2000	17	2.4	8	1.2	4	0.6	…	…
Plate and bar, solution heat treated(b)									
650	1200	496	72	330	47.9	234	34	165	24
730	1350	248	36	172	25	124	18	86	12.5
815	1500	145	21	96	14	69	10	47	6.8
900	1650	83	12	52	7.5	32	4.7	21	3.0
980	1800	48	7.0	29	4.2	17	2.4	10	1.4
1065	1950	26	3.7	13	1.9	7	1.0(c)	…	…
1150	2100	12	1.7	5	0.7	2	0.3(c)	…	…

(a) Based on over 100 tests for sheet. (b) Over 150 tests for plate and bar. (c) Extrapolated

Thermal conductivity:

Temperature		Conductivity	
°C	°F	W/m · K	Btu/ft · h · °F
20	70	9.7(a)	5.25(a)
100	200	11.1	6.3
300	500	14.7	8.2
600	1100	20.6	12.0
700	1300	22.8	13.3
800	1500	25.0	14.5
900	1700	27.4(a)	15.8(a)

(a) Extrapolated values

Electrical resistivity. 1.18 μΩ · m at 22 °C (72 °F)

Magnetic permeability. <1.002 at a field strength of 16 kA/m

Chemical Properties

General corrosion behavior. Resistant to oxidation and carburization; resistant to aqueous solutions at ambient temperatures

ASM Specialty Handbook: Nickel, Cobalt, and Their Alloys
J.R. Davis, editor, p 55-61
DOI:10.1361/ncta2000p055

Copyright © 2000 ASM International®
All rights reserved.
www.asminternational.org

Cast Corrosion-Resistant Nickel Alloys

NICKEL-BASE ALLOY CASTINGS are widely used for handling corrosive media and are regularly produced by high-alloy steel foundries. The principal alloys are identified by Alloy Casting Institute (ACI) designations and are included in ASTM A 494, "Standard Specification for Castings, Nickel and Nickel Alloy." Table 1 lists the compositions of these alloys. In addition, a number of specialized proprietary grades are often used for severe corrosion applications, for example, sulfuric acid service.

As indicated in Table 1, some of the cast nickel-base alloys have wrought counterparts and are frequently specified as the cast components in systems built of both wrought and cast components made from a single alloy. Compositions of cast and equivalent wrought grades differ in minor elements because workability in wrought grades is a dominant factor, whereas castability and soundness are dominant factors in cast grades. The differences in minor elements do not result in significant differences in serviceability.

Nickel-base castings are employed most often in fluid handling systems where they are matched with equivalent wrought alloys. They also are quite commonly used for pump and valve components or where crevices and high-velocity effects require a superior material in a wrought stainless steel system. Because of high cost, nickel-base alloys are usually selected only for severe service conditions where maintenance or product purity is of great importance and where less costly stainless steels or other alternative materials are inadequate.

Standard Grades

Nickel-base castings covered in ASTM A 494 typically contain more than 50% Ni and less than 10% Fe (Table 1). In general, these alloys are produced to optimize corrosion resistance, and mechanical properties are secondary. The property of most interest to the foundry is ductility. A high ductility allows for better weldability and response to water quenching. A low ductility is often an indirect indication that insufficient quantities of precipitates have dissolved in heat treatment, and corrosion properties may be adversely affected. Table 2 lists minimal mechanical property requirements.

Alloy Classifications

Cast nickel-base corrosion resistant alloys described in ASTM A 494 may be classified as follows:

- Nickel
- Nickel-copper (or nickel-copper-silicon) alloys
- Nickel-chromium-iron alloys
- Nickel-chromium-molybdenum alloys
- Nickel-molybdenum alloys

Compositions of these alloys are given in Table 1.

Table 1 Compositions of standard cast corrosion-resistant nickel-base alloys

Alloy	Wrought equivalent	Composition, %									
		C	Si	Mn	Cu	Fe	Cr	P	S	Mo	Others
Cast nickel											
CZ-100	…	1.0 max	2.0 max	1.5	1.25	3.0	…	0.03	0.03	…	…
Nickel-copper											
M-35-1	Monel 400	0.35	1.25	1.5	26.0–33.0	3.50 max	…	0.03	0.03	…	…
M-35-2	…	0.35	2.0	1.5	26.0–33.0	3.50 max	…	0.03	0.03	…	…
M-30H	H Monel	0.30	2.7–3.7	1.50	27.0–33.0	3.50 max	…	0.03	0.03	…	…
M-25S	S Monel	0.25	3.5–4.5	1.50	27.0–33.0	3.50 max	…	0.03	0.03	…	…
M-30C	…	0.30	1.0–2.0	1.50	26.0–33.0	3.50 max	…	0.03	0.03	…	1.0–3.0 Nb
Nickel-chromium-iron											
CY-40	Inconel 600	0.40	3.0	1.5	…	11.0 max	14.0–17.0	0.03	0.03	…	…
Nickel-chromium-molybdenum											
CW-12MW	Hastelloy C	0.12	1.0	1.0	…	4.5–7.5	15.5–17.5	0.04	0.03	16.0–18.0	0.20–0.40 V, 3.75–5.25 W
CW-6M	Hastelloy C (mod)	0.07	1.0	1.0	…	3.0 max	17.0–20.0	0.04	0.03	17.0–20.0	…
CW-2M	Hastelloy C-4	0.02	0.8	1.0	…	2.0 max	15.0–17.5	0.03	0.03	15.0–17.5	0.20–0.60 V
CW-6MC	Inconel 625	0.06	1.0	1.0	…	5.0	20.0–23.0	0.015	0.015	8.0–10.0	3.15–4.50 Nb
CY5SnBiM	…	0.05	0.5	1.5	…	2.0 max	11.0–14.0	0.03	0.03	2.0–3.5	3.0–5.0 Bi, 3.0–5.0 Sn
CX2MW	Hastelloy C-22	0.02	0.8	1.0	…	2.0–6.0	20.0–22.5	0.025	0.025	12.5–14.5	2.5–3.5 W, 0.35 V max
CU5MCuC(a)	…	0.05 max	1.0 max	1.0 max	1.5–3.5	bal	19.5–23.5	0.030 max	0.030 max	2.5–3.5	0.60–1.2 Nb
Nickel-molybdenum											
N-12MV	Hastelloy B	0.12	1.0	1.0	…	4.0–6.0	1.0	0.04	0.03	26.0–30.0	0.20–0.60 V
N-7M	Hastelloy B (mod)	0.07	1.0	1.0	…	3.0 max	1.0	0.04	0.03	30.0–33.0	…

(a) Contains 38.0–44.0% Ni

Cast Nickel. CZ-100 is the ACI designation for the standard grade of cast nickel. A higher-carbon, higher-silicon grade is occasionally specified for greater resistance to wear and galling. Cast nickel is unsurpassed in handling concentrated and anhydrous caustic at elevated temperatures. It is also used in applications where product contamination by elements other than nickel cannot be tolerated.

The minor elements in CZ-100 provide for excellent castability and the production of sound, pressure-tight castings. Usual practice is to aim for 0.75% C and 1.0% Si. Carbon is present as finely distributed spheroidal graphite. A maximum carbon content of 0.10% or less is occasionally specified where castings are welded into wrought nickel systems. Low-carbon CZ-100, however, is a difficult material to cast and has no significant advantage over the higher-carbon option under any known service conditions. CZ-100 is used in the as-cast condition.

Mechanical property requirements for CZ-100 are listed in Table 2. Cast nickel has excellent toughness, thermal resistance, and heat-transfer characteristics.

CZ-100 can be readily repair welded. It can be joined to other castings or to wrought forms using any arc or gas welding process; filler metal is nickel rod or wire. Joints must be prepared very carefully for welding because small amounts of sulfur or lead will embrittle the welds.

The most common application for nickel castings is in the manufacture of caustic soda and in chemical processing with caustic. As temperature and caustic soda concentration increase, austenitic stainless steels are of limited usefulness. Nickel-copper (M-35) and Ni-Cr-Fe (CY-40) alloys often are applied at intermediate concentrations, and cast nickel is selected for higher caustic concentrations including fused anhydrous sodium hydroxide (NaOH). Minor amounts of elements such as oxygen and sulfur can have profound effects on the corrosion rate of nickel in caustic. Detailed corrosion data should be obtained before making a final selection.

Nickel-Copper Alloys. Cast 70Ni-30 alloys (Monels) are listed in ASTM A 494 as M-35-1, M-35-2, M-30H, M-25S, and M-30C. The low-silicon grades M-35-1 (1.25% Si), M-35-2 (2.0% Si), and M-30C (1.5% Si) are commonly used in conjunction with wrought nickel-copper and copper-nickel alloys in pumps, valves, and fittings. A higher-silicon grade, M-30H (3.5% Si), is used in rotating parts and wear rings because it combines corrosion resistance with high strength and wear resistance. Alloy M-25S (4.0% Si) is employed where exceptional resistance to galling is required.

M-35-1, M-35-2, and M-30C are employed in the as-cast condition. Homogenization at 815 to 925 °C (1500–1700 °F) may slightly improve corrosion resistance, but under most corrosive conditions, alloy performance is not affected by the minor segregation present in as-cast metal.

At about 3.5% Si, age hardening becomes possible. At approximately 3.8% Si, the solubility limit for silicon in the nickel-copper matrix is exceeded and hard, brittle silicides are formed. These effects are particularly evident in the high-silicon alloy M-25S. The combination of aging during cooling to room temperature after casting, plus the hard silicides developed when the silicon content exceeds about 3.8% can cause considerable difficulty in machining. Softening of composition M-25S is accomplished by solution heat treatment consisting of heating to 900 °C (1650 °F), holding at temperature 1 h for each 25 mm (1 in.) of section, and oil quenching. Maximum softening is obtained by oil quenching from 900 °C, but it is apt to result in quench cracks in complicated castings or castings with large differences in section size.

In solution heat treating of complicated castings, it is advisable to charge them into a furnace below 315 °C (600 °F) and heat them to 900 °C (1650 °F) at a rate that will limit the maximum temperature difference within any casting to about 55 °C (100 °F). After soaking, castings should be transferred to a furnace held at 730 °C (1350 °F), allowed to equalize in temperature, and then oil quenched. Alternatively, the furnace may be cooled rapidly to 730 °C (1350 °F), the casting temperature equalized, and the castings subsequently quenched in oil.

Table 2 Tensile requirements for standard cast corrosion-resistant nickel-base alloys

Alloy	Tensile strength, MPa	Tensile strength, ksi	Yield strength, MPa	Yield strength, ksi	Elongation in 50 mm (2 in.), %	Hardness, HB
CZ-100	345	50	125	18	10	…
M-35-1	450	65	170	25	25	…
M-35-2	450	65	205	30	25	…
M-30H	690	100	415	60	10	243–294
M-25S	…	…	…	…	…	300 (min)
M-30C	450	65	225	32.5	25	125–150
N-12MV	525	76	275	40	6	…
N-7M	525	76	275	40	20	…
CY-40	485	70	195	28	30	…
CW-12MW	495	72	275	40	4	…
CW-6M	495	72	275	40	25	…
CW-2M	495	72	275	40	20	…
CW-6MC	485	70	275	40	25	…
CX2MW	550	80	280	45	30	…
CU5MCuC	520	75	240	35	20	…

Solution treated castings are age hardened by placing them in a furnace at 315 ° C (600 °F), heating uniformly to 600 °C (1100 °F), holding 4 to 6 h, and cooling in air.

Tensile properties of nickel-copper castings are controlled by the solution-hardening effect of silicon or of silicon plus niobium. Increasing the copper content also has a minor strengthening effect. The tensile properties of M-35-1 and M-35-2 are controlled by a carbon-plus-silicon relationship, and tensile properties of M-30C are controlled by a silicon-plus-niobium relationship.

The combination of aging plus hard silicides in M-25S results in an alloy with exceptional resistance to galling. As the silicon content is increased above 3.8%, the amounts of hard, brittle silicides in a tough nickel-copper matrix increase, ductility decreases sharply, and tensile and yield strengths increase. Because of these effects, strength and ductility cannot be controlled readily, and thus minimum hardness is the only mechanical property specified for M-25S (see Table 2).

The toughness of nickel-copper alloys decreases with increasing silicon content, but all grades retain their room temperature toughness down to at least –195 °C (–320 °F).

Weldability of nickel-copper alloys decreases with increasing silicon content, but is adequate up to at least 1.5% Si. Niobium can enhance weldability of nickel-copper alloys, particularly when small amounts of low-melting-point residuals are present. Careful raw-material selection and good foundry practice, however, have largely eliminated any difference in weldability between niobium-bearing and niobium-free grades.

The high-silicon alloys M-30H and M-25S are considered not weldable. They can be brazed or soldered, as can the low-silicon grades.

Principal advantages of 70Ni-30Cu alloys are high strength and toughness coupled with excellent resistance to reducing mineral acids, organic acids, salt solutions, food acids, strong alkalies, and marine environments.

The most common applications for 70Ni-30Cu alloy castings are in equipment for handling hydrofluoric acid, salt water, neutral and alkaline salt solutions, and reducing acids.

The cast nickel-chromium-iron alloy CY-40 (Inconel 600) differs in composition from the parallel wrought grade in having higher carbon, manganese, and silicon contents, which impart the required qualities of castability and pressure tightness.

CY-40 is used in the as-cast condition because the alloy is insensitive to intergranular attack of the type encountered in as-cast or sensitized stainless steels. A modified cast Ni-Cr-Fe alloy for nuclear applications (0.12% max C) is usually solution treated as an extra precaution.

The minimum mechanical properties in Table 2 are for a typical composition of 0.20 C, 1.50 Si, 1.0 Mn, 15.5 Cr, 8.0 Fe, balance Ni. Lower carbon and silicon contents for

nuclear-grade castings result in a lower yield strength, but do not lower the minimum tensile strength.

CY-40 is frequently used for elevated-temperature fittings in conjunction with a wrought alloy of similar composition. Typical elevated-temperature properties are listed in Tables 3 and 4.

CY-40 castings can be repair welded or joined to other components using any of the standard arc or gas welding processes. Rod and wire whose nickel and chromium contents match those of the castings should be used. Postweld heat treatment is not required after repair welding or fabrication unless residual stresses must be relieved.

CY-40 is commonly used to handle hot corrosives or corrosive vapors under moderately oxidizing conditions, where stainless steels might be subject to intergranular attack or stress corrosion cracking. CY-40 has also been used extensively for components in systems handling hot boiler feedwater in nuclear power plants because it provides a greater margin of safety over stainless steels.

Nickel-Chromium-Molybdenum Alloys. Cast alloys CW-12MW, CW-6M, CW-2M, and CX2MW, which parallel the Hastelloy C wrought series, are widely used in the chemical processing industry because they provide corrosion resistance over a wide range of reducing and oxidizing environments. CW-12MV is similar to the original Hastelloy C grade (high carbon—1.12% C—with a tungsten addition). This alloy has lost favor in wrought products because of its poor performance in some applications and is rarely produced. However, it is still common in castings because of the buyer's habit of ordering Hastelloy C as a generic alloy. Wrought Hastelloy C-276 (low carbon with tungsten) replaced grade "C," but has no cast counterpart in ASTM A 494. Modified versions of CW-12MW alloy include the lower carbon alloys CW-6M (0.07% C with no tungsten addition) and CW-2M (0.02% C with no tungsten addition), which is the cast counterpart to Hastelloy C-4. CX2MW is the most recent alloy addition in this group and is patterned after Hastelloy C-22. This alloy has more chromium than CW-12MW, but less molybdenum and tungsten.

The "C" grade castings resist oxidizing agents such as wet chlorine, chlorine gas, hypochlorite, chlorine dioxide solutions, ferric chloride, and nitric, hydrochloric, and sulfuric acids at moderate temperatures or under oxidizing conditions; have excellent resistance to acetic acid, seawater, and many organic acids and salts; and have good high-temperature properties. Table 5 lists typical corrosion rates for CW-12MW in selected corrosive media.

The "C" grades have relatively high yield strengths (Table 2) due to solution-hardening effect of chromium, molybdenum, tungsten, vanadium, and niobium. Ductility is excellent up to the limits of solid solubility.

The "C" grades can be arc or gas welded, using wire or rod of matching composition. For best weldability, carbon content of the base metal should be as low as practicable. The usual practice is to solution treat and quench prior to repair welding. Heat treatment after welding generally is not necessary because the alloy is not subject to sensitization in the heat-affected zone.

The "C" grades are probably the most common material for upgrading a system where service conditions are too demanding for standard or special stainless steels—most often, service involving combinations of acids and elevated temperatures. These cast alloys may be used in conjunction with similar wrought materials, or they may be used to upgrade pump and valve components in a wrought stainless steel system.

Other Ni-Cr-Mo alloys covered in ASTM A 494 include:

- CW-6MC, a low-molybdenum (9.0% Mo) alloy that is the cast counterpart to wrought Inconel 625. Compared to the "C" grade compositions, this alloy is less resistant to reducing media, but more resistant to oxidizing solutions.
- CU5MCuC, which is a Ni-Fe-Cr-Mo-Cu alloy similar to wrought Incoloy 825 used in sulfuric acid service
- CY5SnBiM, a low molybdenum (3.0% Mo) alloy with tin and bismuth additions for improved galling resistance

Nickel-Molybdenum Alloys. Cast alloys N-12MV and N-7M, which parallel the Hastelloy B wrought series, are frequently used for handling hydrochloric acid in all concentrations at temperatures up to the boiling point. These alloys also resist sulfuric acid, phosphoric acid, acetic acid, and other chemicals. Table 5 lists typical corrosion rates for N-12MV in selected corrosive media.

Slow cooling in the mold is detrimental to corrosion resistance, ductility, and weldability of nickel-molybdenum castings. Because of this, the alloy should be solution treated, at a temperature of at least 1180 °C (2150 °F) for N-12MV and 1120 °C (2050 °F) for N-7M, and water quenched.

The nickel-molybdenum grades have a high yield strength due to the solution-hardening effect of molybdenum (Table 2). Ductility is controlled by the carbon and molybdenum contents. For best ductility, carbon content should be as low as practicable and molybdenum content should be adjusted to avoid the formation of intermetallic phases.

Nickel-molybdenum castings can be arc or gas welded using wire or rod of matching composition. Castings should be solution treated and quenched prior to repair welding. Postweld heat treatment is not necessary because these alloys are not subject to sensitization in the heat-affected zone.

Nickel-Base Proprietary Alloys

In addition to the standard corrosion-resistant nickel-base cast alloys, there are a number of proprietary alloys that are widely used in corrosive service. As is described later, some alloys were developed for specialized applications. Table 6 lists the compositions of proprietary nickel-base cast alloys; mechanical properties are given in Table 7.

Nickel-Molybdenum-Chromium and Nickel-Molybdenum Alloys. Chlorimet alloy 3 is a Ni-Mo-Cr alloy that conforms to the standard CW-6M specification. Chlorimet alloy 3 exhibits excellent resistance to corrosion in all concentrations of sulfuric acid up to 65 °C (150 °F) and has good resistance to all concentrations of the acid, except 60 to 85%, to 95 °C (200 °F) as shown in Fig. 1. In the 60 to 85% range, the good resistance is limited to about 75 °C (165 °F). Table 8 gives corrosion test results for Chlorimet alloy 3 at 80 °C (175 °F) for various acid concentrations. Chlorimet alloy 3 is also resistant to various organic acids.

Chlorimet alloy 2 is a nickel-molybdenum alloy that conforms to the standard N-7M specification. This alloy has excellent resistance to all concentrations of sulfuric acid up to 65 °C (150 °F) and good resistance up to the boiling point in the 10 to 60% concentration range as shown in Fig. 2. At concentrations above 60% sulfuric acid, the maximum temperature should

Table 3 Typical elevated-temperature tensile properties of CY-40

Temperature		Tensile strength		Yield strength		Elongation
°C	°F	MPa	ksi	MPa	ksi	in 25 mm or 1 in., %
RT	RT	486	70.5	293	42	16
480	900	427	62	…	…	20
650	1200	372	54.5	…	…	21
730	1350	314	45.5	…	…	25
815	1500	186	27	…	…	34

Note: Data are typical for investment cast test bars with nominal analysis of 0.20 C and 1.50 Si. RT, room temperature

Table 4 Typical stress-rupture properties of CY-40

Temperature		Stress to rupture in 100 h	
°C	°F	MPa	ksi
650	1200	165	24
730	1350	103	15
815	1500	62	9
925	1700	38	5.5

Note: Data are typical for investment cast test bars with nominal analysis of 0.20 C and 1.50 Si.

Table 5 Typical corrosion rates for CW-12MW and N-12MV in various corrosive media

Concentration, %	Temperature °C	Temperature °F	Penetration rate(a) for: CW-12MW μm/yr	CW-12MW mils/yr	N-12MV μm/yr	N-12MV mils/yr
Acetic acid						
10	65	150	5	0.2	152	6.0
10	Boil.	Boil.	10	0.4	18	0.7
50	65	150	3	0.1	102	4.0
50	Boil.	Boil.	3	0.1	10	0.4
99	65	150	3	0.1	13	0.5
99	Boil.	Boil.	3	0.1	5	0.2
Chlorine, wet						
…	RT	RT	3	0.1	12,140	478
Chromic acid						
2	RT	RT	nil	nil	nil	nil
2	65	150	nil	nil	nil	nil
2	Boil.	Boil.	51	2.0	710(b)	28(b)
20	RT	RT	3	0.1	8	0.3
20	65	150	127	5.0	1,650	65
20	Boil.	Boil.	1,473	58.0	25,400	1,000
Hydrochloric acid						
2	RT	RT	23	0.9	50	2.0
2	65	150	3	0.1	230	9.0
2	Boil.	Boil.	1,510	62	76	3.0
10	RT	RT	50	2.0	50	2.0
10	65	150	560	22	180	7.0
10	Boil.	Boil.	8,430	332	230	9.0
20	RT	RT	50	2.0	50	2.0
20	65	150	635	25	125	5.0
20	Boil.	Boil.	10,338	407	610	24.0
37	RT	RT	25	1.0	8	0.3
37	65	150	280	11	50	2.0
Hydrofluoric acid						
5	RT	RT	25	1.0	100	4.0
25	RT	RT	125	5.0	125	5.0
45	RT	RT	150	6.0	76	3.0
Nitric acid						
10	RT	RT	3	0.1	…	…
10	65	150	25	1.0	…	…
10	Boil.	Boil.	180	7.0	…	…
30	RT	RT	3	0.1	…	…
30	65	150	76	3.0	…	…
30	Boil.	Boil.	3,890	153	…	…
50	RT	RT	25	1.0	…	…
Nitric acid (continued)						
50	65	150	280	11.0	…	…
50	Boil.	Boil.	1,200	473	…	…
70	RT	RT	25	1.0	…	…
70	65	150	585	23	…	…
70	Boil.	Boil.	19,810	780	…	…
Phosphoric acid (chemically pure)						
10	65	150	5	0.2	50	2.0
10	Boil.	Boil.	15	0.6	25	1.0
30	65	150	3	0.1	20	0.8
30	Boil.	Boil.	100	4.0	76	3.0
50	65	150	8	0.3	8	0.3
50	Boil.	Boil.	100	4.0	76	3.0
85	65	150	8	0.3	10	0.4
85	Boil.	Boil.	1,140	45	710	28.0
Sodium hydroxide						
5	65	150	nil	nil	nil	nil
5	Boil.	Boil.	nil	nil	nil	nil
50	65	150	nil	nil	nil	nil
Sulfuric acid						
2	RT	RT	5	0.2	25	1.0
2	65	150	13	0.5	125	5.0
2	Boil.	Boil.	280	11	25	1.0
10	RT	RT	3	0.1	25	1.0
10	65	150	13	0.5	76	3.0
10	Boil.	Boil.	840	33	50	2.0
25	RT	RT	5	0.2	25	1.0
25	65	150	25	1.0	25	1.0
25	Boil.	Boil.	1,625	64	50	2.0
50	RT	RT	25	1.0	10	0.4
50	65	150	100	4.0	25	1.0
50	Boil.	Boil.	8,430	332	50	2.0
60	RT	RT	50	2.0	5	0.2
60	65	150	100	4.0	25	1.0
60	Boil.	Boil.	24,330	958	180	7.0
80	RT	RT	3	0.1	3	0.1
80	65	150	76	3.0	8	0.3
80	Boil.	Boil.	>25,400	>1,000	>25,400	>1,000
96	RT	RT	5	0.2	5	0.2
96	65	150	25	1.0	8	0.3
96	Boil.	Boil.	6,450	254	>25,400	>1,000

Boil., boiling; RT, room temperature. (a) All data are steady-state, as calculated from a minimum of five 24 h test periods, unless otherwise indicated. (b) For the fifth 24 h test period, not steady-state rate.

Table 6 Compositions of proprietary cast corrosion-resistant nickel-base alloys

Alloy	Composition, % Ni	Fe	Cr	Mo	Cu	C	Si	Mn	Others
Chlorimet 2	62.0	2.0	1.0	30–33	…	0.07	1.0	1.0	…
Chlorimet 3	57.0	3.0	17–20	17–20	…	0.07	1.0	1.0	…
Hastelloy D	85.0	2.0	1.0	…	2–4	0.12	8.5–10	0.5–1.25	1.5 Co
Illium G	58.0	5.0	22.0	6.0	6.0	0.2	0.2	1.25 max	…
Illium 98	55.0	1.0	28.0	8.0	5.0	0.05	0.7 max	1.25 max	…
Illium B	49.0	3.0	28.0	8.0	5.0	0.05	4.5	1.25 max	0.05–0.55 B
Lewmet 55	33.0	16.0	32.0	4.0	3.0	0.1 max	3.5	3.0	6.0 Co
Lewmet 66	37.0	16.0	31.0	…	3.0	0.08	3.0	…	6.0 Co
Waukesha 23	80.0	…	…	…	…	…	…	1.50–2.50	7.0–9.0 Sn, 6.0–9.0 Zn, 3.5–4.5 Pb
Waukesha 54C	75.0	1.5	…	…	…	0.21	…	2.0	8.0 Sn, 8.0 Zn, 6.0 Ag
Waukesha 88	70.0	4.0–6.0	11.0–14.0	2.5–3.5	…	0.05 max	0.15–0.50	0.65–1.0	3.0–5.0 Sn, 3.0–4.5 Bi

Table 7 Tensile properties of proprietary cast corrosion-resistant nickel-base alloys

Alloy	Tensile strength MPa	Tensile strength ksi	Yield strength MPa	Yield strength ksi	Elongation in 50 mm (2 in.), %	Hardness
Hastelloy D	790	115	(a)	(a)	1	30–39 HRC
Illium 98	370	54	285	41	18	160 HB
Illium B	420	61	415	60	1	221–420 HB
Illium G	470	68	270	39	7.5	168 HB
Waukesha 23	496–531	72–77	338–365	49–53	9–13	150–175 HB
Waukesha 88	276 min	40 min	245 min	355 min	6 min	140–160 HB
Waukesha 54C	517	75	414	60	5	220 HB

(a) Yield strength is near the ultimate tensile strength.

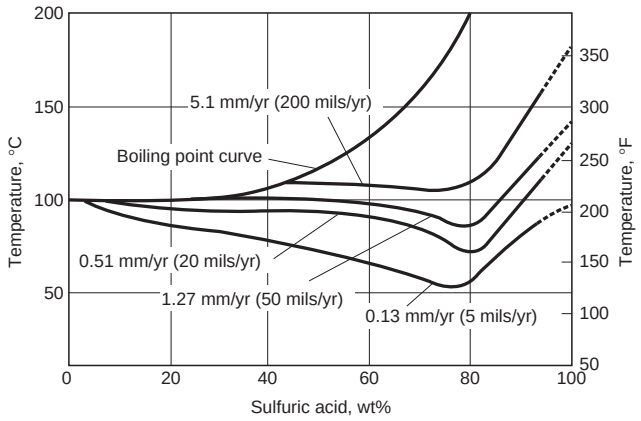


Fig. 1 Isocorrosion diagram for Chlorimet alloy 3 in sulfuric acid. Source: Ref 1

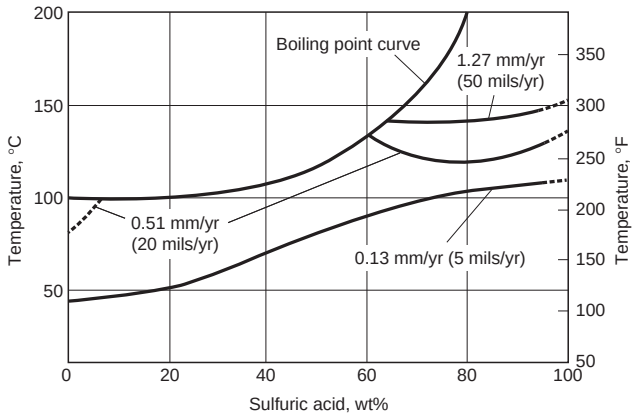


Fig. 2 Isocorrosion diagram for Chlorimet alloy 2 in sulfuric acid. Source: Ref 1

not exceed 120 °C (250 °F). Chlorimet alloy 2 is also highly resistant to acetic acid exposures.

Nickel-Silicon-Copper Alloy. Hastelloy D is a high-silicon (9.5% Si) alloy that is produced only in cast form. The most important property of Hastelloy D is its resistance to all concentrations of hot sulfuric acid. It is also resistant to hydrochloric acid under mild conditions and to other nonoxidizing acids and salts. It should not be used under oxidizing conditions at elevated temperatures. Table 9 lists typical corrosion rates for Hastelloy D in selected corrosive media.

Nickel-chromium-molybdenum-copper-iron alloys were designed to resist sulfuric acid at concentrations to 98% at temperatures to 100 °C (212 °F). They include Illium alloys G, 98, and B.

Illium alloy G is a cast alloy that was originally developed to resist mixtures of sulfuric and nitric acids as encountered in the chamber process manufacture of sulfuric acid and in nitrating operations.

It resists sulfuric acid at all concentrations to 70 °C (160 °F) and is satisfactory at all temperatures from dilute to 40% acid. Other areas exist where satisfactory performance occurs, and these are shown in Fig. 3. The alloy is also used in handling mixtures of sulfuric acid and hydrogen sulfide in viscose rayon and cellophane coagulation baths. It is a highly useful, machinable, and weldable casting alloy for pumps and valves that must resist attack by a great variety of solutions containing sulfuric acid along with other chemicals. It is most corrosion resistant in its annealed state where the carbon and chromium are held in solution.

Illium alloy 98 is a weldable, machinable cast alloy that was originally designed to withstand hot, 98% sulfuric acid. However, it can be used over a wide range of concentrations

Table 8 Corrosion of Chlorimet alloy 3 in sulfuric acid solutions at 80 °C (175 °F)

Acid concentration, wt %	Corrosion rate	
	mm/yr	mils/yr
10	0.02	0.6
25	0.10	4
50	0.33	13
78	1.1	44
93	0.10	4

Source: Ref 1

Table 9 Corrosion rates for Hastelloy D (85Ni-10Si-3Cu) in various corrosive media

Medium	Concentration, %	Temperature		Penetration rate	
		°C	°F	μm/yr	mils/yr
Acetic acid	10	65	150	230	9
	10	Boil.	Boil.	50	2
	50	65	150	455	18
	50	Boil.	Boil.	75	3
	99	65	150	125	5
	99	Boil.	Boil.	23	0.9
Chlorine, wet	…	RT	RT	4,650	183
Chromic acid	2	RT	RT	nil	nil
	2	65	150	2.5	0.1
	2	Boil.	Boil.	230	9
	20	RT	RT	7.5	0.3
	20	65	150	18,540	730
	20	Boil.	Boil.	>25,400	>1,000
Hydrochloric acid	2	RT	RT	50	2
	2	65	150	380	15
	2	Boil.	Boil.	3,325	131
	10	RT	RT	102	4
	10	65	150	2,440	96
	10	Boil.	Boil.	22,325	879
	20	RT	RT	660	26
	20	65	150	1,930	76
	20	Boil.	Boil.	>25,400	>1,000
	37	RT	RT	750	30
	37	65	150	>25,400	>1,000
Hydrofluoric acid	5	RT	RT	150	6
	25	RT	RT	150	6
	45	RT	RT	102	4
Phosphoric acid (chemically pure)	10	65	150	75	3
	10	Boil.	Boil.	25	1
	30	65	150	50	2
Phosphoric acid (continued)	30	Boil.	Boil.	175	7
	50	65	150	75	3
	50	Boil.	Boil.	250	10
	85	65	150	25	1
	85	Boil.	Boil.	2,310	91
Sodium hydroxide	5	65	150	nil	nil
	5	Boil.	Boil.	nil	nil
	50	65	150	nil	nil
Sulfuric acid	2	RT	RT	25	1
	2	65	150	150	6
	2	Boil.	Boil.	102	4
	10	RT	RT	25	1
	10	65	150	125	5
	10	Boil.	Boil.	330	13
	25	RT	RT	25	1
	25	65	150	50	2
	25	Boil.	Boil.	230	9
	50	RT	RT	25	1
	50	65	150	25	1
	50	Boil.	Boil.	280	11
	60	RT	RT	25	1
	60	65	150	150	6
	60	Boil.	Boil.	205	8
	80	RT	RT	25	1
	80	65	150	50	2
	80	Boil.	Boil.	915	36
	96	RT	RT	25	1
	96	65	150	25	1
	96	Boil.	Boil.	2,184	86

Note: Acid strengths are given in percentage by weight. In some instances, no measurable penetration could be observed. These instances are noted by the word "nil." All other data are steady-state, as calculated from a minimum of five 24 h test periods, unless otherwise indicated. For the fifth 24 h test period, not steady-state rate.

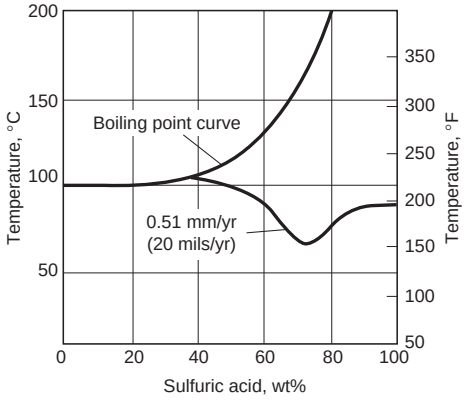


Fig. 3 Isocorrosion diagram for Illium alloy G in sulfuric acid. Source: Ref 1

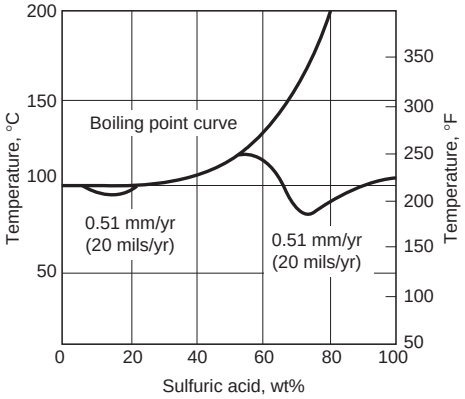


Fig. 4 Isocorrosion diagram for Illium alloy 98 in sulfuric acid. Source: Ref 1

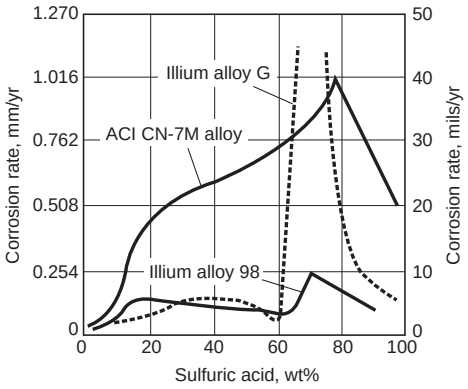


Fig. 5 Corrosion rates of cast alloys in 80 °C (175 °F) sulfuric acid solutions. Source: Ref 1

and temperatures as indicated in Fig. 4. Illium alloy 98 is a preferred material for the very corrosive middle range of sulfuric acid concentration range as shown in Fig. 5 and 6. Note the superiority of Illium alloy 98 over cast ACI CN-7M (Fe-29Ni-20Cr-3.5Cu-2.5Mo). Maximum corrosion resistance with this alloy is obtained after a solution anneal followed by water quenching.

Illium alloy B is a modification of Illium alloy 98 that extends the useful service range in 98% sulfuric acid to higher temperatures, as shown in Fig. 7. Note that aeration of the sulfuric acid enhances the corrosion resistance of the Illium alloys under these conditions. Although aeration has been shown to be beneficial in reducing corrosion with Illium alloy B in 96 to 98% sulfuric acid, the alloy is not recommended where strongly oxidizing conditions are present.

An isocorrosion diagram for Ilium alloy B (Fig. 8) shows the excellent corrosion resistance of this alloy over the entire concentration range, although its outstanding resistance at the higher sulfuric acid concentrations makes it the alloy of choice in that region (see Fig. 6). In addition, Ilium alloy B is hardenable for maximum wear and galling resistance. However, welding operations should be completed before hardening.

Nickel-Chromium-Iron-Molybdenum-Cobalt-Copper-Silicon Alloy. Lewmet alloy 55 is a cast, nickel-base alloy specifically designed for hot, concentrated sulfuric acid service. Isocorrosion curves for acid concentrations from 77 through 99.4% sulfuric acid, where the alloy finds greatest application, are shown in Fig. 9. The effect of temperature on corrosion of

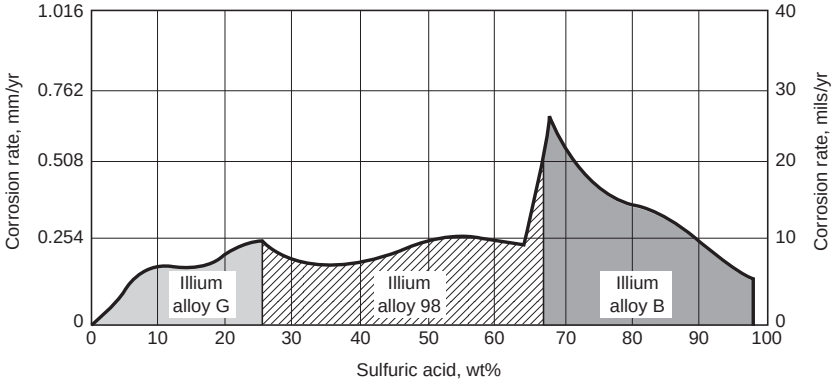


Fig. 6 Corrosion rates of Illium alloys in sulfuric acid at 100 °C (212 °F). Source: Ref 1

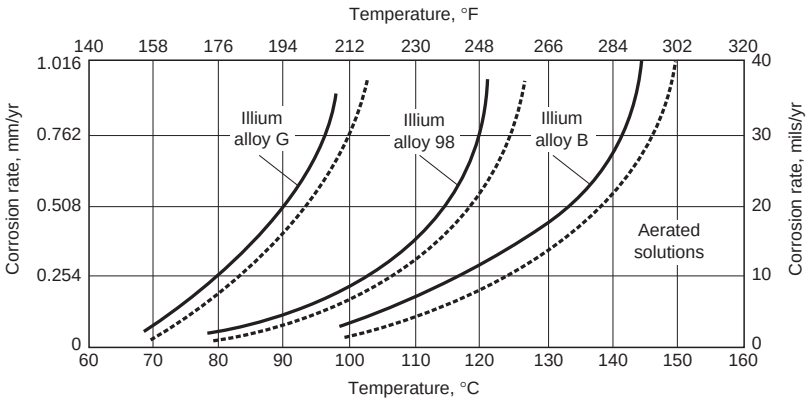


Fig. 7 Corrosion of Illium alloys in 96 to 98% sulfuric acid solutions. Source: Ref 1

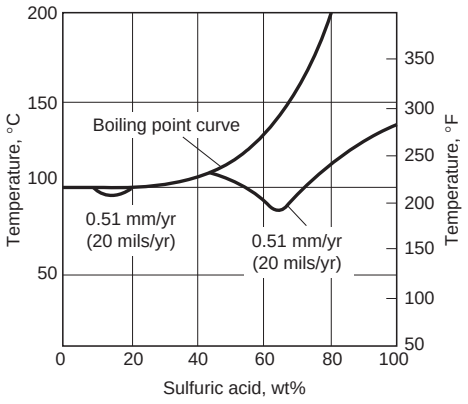


Fig. 8 Isocorrosion diagram for Illium alloy B in sulfuric acid. Source: Ref 1

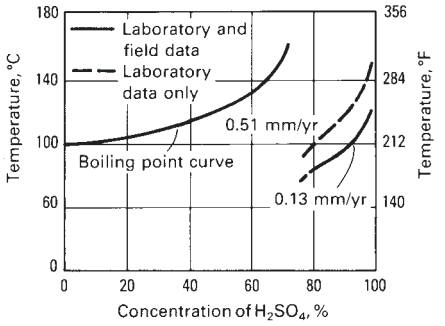


Fig. 9 Isocorrosion diagram for Lewmet alloy 55 in sulfuric acid. Source: Ref 1

Lewmet alloy 55 in 98% sulfuric acid, as determined in laboratory tests, is shown in Fig. 10.

This alloy is age hardenable from about 225 up to 500 HB. In the hardened condition, equivalent corrosion resistance with the unhardened alloy is claimed, but with greater resistance to abrasion, galling, and seizing. However, any necessary welding has to be performed prior to hardening. Lewmet alloy 55 has been used in the soft condition for pump impellers, orifice plates, and so forth, and in the hardened condition as pump-impeller-wear-rings, bearings, and the like.

Nickel-Chromium-Iron-Cobalt-Copper-Silicon Alloy. Lewmet alloy 66 is a ductile, cast, nickel-base alloy that can also be made in wrought form. Both the cast and wrought versions exhibit excellent corrosion resistance in the 0 to 60% and 80 to 98% sulfuric acid concentration range, as shown in Fig. 11. Corrosion rates tend to be erratic and are sometimes high in the range of 60 to 80% sulfuric acid.

Because of the excellent resistance of Lewmet alloy 66 in dilute sulfuric acid, it has been used for dilution pipes and spray nozzles. It has also been used for sulfuric acid concentrations above 80% where its ductility in combination with corrosion resistance was required.

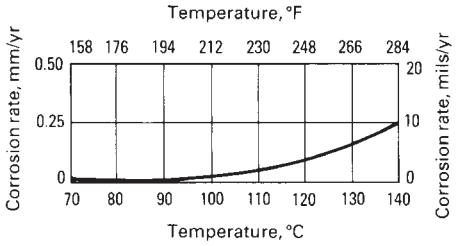


Fig. 10 Corrosion of Lewmet alloy 55 in 98% sulfuric acid. Source: Ref 1

Tin-containing nickel castings include Waukesha alloys No. 88, 23, and 54C. Although these alloys exhibit good corrosion resistance, they were designed to resist seizing and galling when run against stainless steels. Alloy No. 88 is a Ni-Cr-Fe-Mo alloy that contains both tin and bismuth. It is similar to standard alloy CY5SnBiM. Alloy No. 23 is a Ni-Sn-Zn-Pb alloy. Both alloys No. 88 and 23 are used as bushings, bearings, and valves in food and chemical industry equipment. Alloy No. 54C is a Ni-Sn-Zn-Ag alloy that can be used at temperatures up to 870 °C (1600 °F). It is used as valve guides in aircraft engines and nuclear industry bearings.

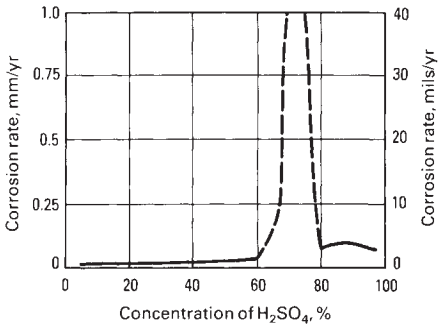


Fig. 11 Corrosion rates of Lewmet alloy 66 in sulfuric acid solutions at 100 °C (212 °F). Source: Ref 1

REFERENCE

1. "The Corrosion Resistance of Nickel-Containing Alloys in Sulfuric Acid and Related Compounds," The International Nickel Company, 1983 (available from the Nickel Development Institute as publication No. 1318)

ASM Specialty Handbook: Nickel, Cobalt, and Their Alloys
J.R. Davis, editor, p 62-67
DOI:10.1361/ncta2000p062

Copyright © 2000 ASM International®
All rights reserved.
www.asminternational.org

Cast Heat Resistant Nickel-Chromium, Nickel-Iron-Chromium, and Nickel-Chromium-Iron Alloys

THE NICKEL-CHROMIUM ALLOYS described in this article are castings containing 40 to 50% Ni and 50 to 60% Cr. These alloys are essentially binary systems where the total alloy content (excluding nickel and chromium) totals less than approximately 2.5%. These alloys are cast into tube supports and other firebox fittings for certain stationary and marine boilers. The chief attribute of the nickel-chromium alloys is their resistance to hot-slag corrosion in boilers that fire oil high in vanadium content. Hot slag high in vanadium pentoxide (V_2O_5) is extremely destructive to most other heat resistant alloys.

The Ni-Fe-Cr alloys described below are an extension of the cast heat resistant (H-type) stainless steels that are used in applications where service temperatures exceed 650 °C (1200 °F) and may reach extremes as high as 1315 °C (2400 °F). Two standard grades, HX and HW, fall into this group. These alloys contain 58 to 68% Ni, 10 to 19% Cr, with the remainder iron.

The Ni-Cr-Fe alloys discussed later in this article are proprietary grades that contain about 45% Ni, 30% Cr, with the remainder iron and other alloying elements. These alloys are intended for high-temperature service where strength and/or carburization resistance are prime considerations. These alloys are also highly resistant to oxidation.

Information on other nickel-chromium alloys, for example, alloys containing 70 to 80% Ni and 20 to 30% Cr used for resistance heating elements or thermocouples, can be found in the article "Special-Purpose Nickel Alloys" in this Handbook. More complex heat resistant casting alloys, such as the solid-solution strengthened or precipitation-strengthened nickel-base alloys, are described in the article "Superalloys" in this Handbook.

Nickel-Chromium Alloys to Resist Fuel Oil Ash Corrosion (Ref 1)

A growing problem over the past 35 years has been corrosion of heat resistant metals and refractories by the ash from combustion of heavy residual fuel oils used in various industrial furnaces. This has stemmed from the growing use of heavy residual fuel oil, owing to its relatively attractive price, and extension of its use in furnaces operating at increasingly higher temperatures. An additional factor is the general trend (often governed by petroleum marketing considerations) toward maximizing production of distillates with corresponding reduction in fuel oil yield. As a result, greater amounts of the ash-forming constituents responsible for high-temperature corrosion, particularly organo-metallic vanadium compounds, are concentrated in the residual fuel oil.

It has been well established for many years that vanadium pentoxide and alkali metal sulfates are the primary ash constituents responsible for oil ash corrosion. Vanadium exists in certain crude oils as an oil-soluble porphyrin complex in variable quantities. While fuel oil derived from some crude oil contains relatively low amounts of vanadium (e.g., 20 ppm)—that from certain Middle Eastern crudes, and particularly from Venezuelan crudes—often contains several hundred parts per million (Table 1).

Various mechanisms have been advanced to explain oil ash corrosion. The simplest explanation is that low-melting constituents formed from vanadium pentoxide and alkali metal sulfates, when molten, exert a fluxing action on the protective oxide films of heat resistant alloys, allowing corrosion to progress in an accelerated manner at temperatures ranging from 500 to 700 °C (930–1300 °F).

Although a number of methods have been used or proposed to mitigate oil ash corrosion, it is best controlled by proper alloy selection. As described later in this article, the 50/50-type nickel-chromium alloys are well-established materials for resisting oil ash corrosion.

Alloy development of cast 50Ni-50Cr and 40Ni-60Cr alloys began in the mid-1950s with an extensive series of laboratory screening tests on established and experimental heat resistant alloys. These tests were conducted by the U.S. Naval Boiler & Turbine Laboratory and the U.S. National Bureau of Standards under contract from the U.S. Navy. This work was undertaken to find materials for service as uncooled tube spacers and supports in marine boiler superheaters that would offer significantly improved resistance to oil ash from Bunker C fuel oil, compared with standard HH (25Cr-12Ni) and HK (25Cr-20Ni) heat-resistant steel castings. The results demonstrated that the cast nickel-chromium alloys had much improved resistance to synthetic oil ash attack (Ref 1). In fact, these alloys exhibited corrosion resistance 12 to 45 times that of 25Cr-20Ni steels.

Further studies by Swales and Ward (Ref 3), McDowell and Mihalisin (Ref 4), and Spafford (Ref 5) confirmed the good performance of cast nickel-chromium in high-temperature oil ash environments. Comparative data for a number of heat resistant alloys, including the 50Ni-50Cr alloy, are presented in Table 2. These alloys have similar resistance to oil ash attack at temperatures up to 900 °C (1650 °F). At temperatures ranging from 900 to 1090 °C (1650–2000 °F), the higher-chromium alloy is

Table 1 Amounts of various constituents found in residual fuel oils from various crudes

Source of crude oil	Content, ppm		
	V	Ni	Na
Africa			
1	5.5	5	22
2	1	5	…
Middle East			
3	7	…	1
4	173	51	…
5	47	10	8
United States			
6	13	…	350
7	6	2.5	120
8	11	…	84
Venezuela			
9	…	6	480
10	57	13	72
11	380	60	70
12	113	21	49
13	93	…	38

Source: Ref 2

recommended. However, due to its superior as-cast ductility, machinability, and weldability, the 50Ni-50Cr alloy is used in the majority of applications in power plants, oil refinery heaters, and marine boilers involving temperatures less than about 900 °C (1650 °F). The 50/50-type alloy also has better foundry characteristics and lower cost.

Both of these alloys, as well as a modified higher-strength alloy containing approximately 1.5% Nb, are covered by ASTM A 560 "Standard Specification for Castings, Chromium-Nickel Alloy." The basic compositional and property requirements of A 560 are given in Tables 3 and 4. Additional information on the higher-strength Ni-Cr-Nb cast alloy is presented later in this article.

Corrosion of Oil-Refinery Heaters. Figure 1 summarizes the results of a number of quantitative field tests in crude oil distillation, platformer, and catalytic-cracking heaters. These tests, which covered a reasonably wide practical range of fuel quality, temperature, and operating conditions, confirmed the general superiority of the nickel-chromium alloys, as far as oil ash corrosion is concerned, over the standard cast heat resistant steels used for tube supports. In cases where residual fuel was used for only a small proportion of the test duration and refinery gas was used for the remainder, high-chromium alloys did not show any advantage over the conventional 25Cr-20Ni and 25Cr-12Ni steels in resisting attack in oxidizing sulfurous gases at high temperatures. Indeed, they may be inferior (e.g., compare the results for oil refinery heaters D and E in Fig. 1). Consequently, there is no point in specifying the more expensive high-chromium alloys for heaters unless it is probable that heavy residual fuel oils will be used for a substantial proportion of the firing operations.

Corrosion in Power Stations. Figure 2 shows the results of a comprehensive test carried out by the Consolidated Edison Company of New York at their Hudson Avenue Generating Station, following simple 500 h rack tests at their Hell Gate station. Seventy-five sets of castings representing 12 different materials were installed in the first-pass zone of the superheater. Gas temperatures were up to 980 °C (1800 °F), and the temperatures of the metal supports averaged about 820 °C (1500 °F). The fuel oil during the test period had vanadium contents of 150 to 250 ppm, sodium contents of 20 to 80 ppm, and sulfur contents of the order of 2.5%. After 4500, 6450, 9429, and 12,000 h, a set of castings, comprising one casting of each material, was removed for examination. After 12,000 h all the castings, with the exception of the nickel-chromium alloys, had to be removed because of their poor condition. Both the 50Ni-50Cr and 40Ni-60Cr alloys were reported to be still in service several years later.

A high-strength nickel-chromium alloy, commonly referred to as IN-657, has been developed that provides the same good resistance to fuel oil ash corrosion exhibited by the standard 50Ni-50Cr alloys, but with improved creep and stress rupture properties. This was achieved by modifying the standard alloy with a controlled addition of niobium and reducing the upper permissible limits of nitrogen and silicon as specified in ASTM A 560. The basic compositional and property requirements for this alloy are given in Tables 3 and 4.

The elevated-temperature strength of IN-657 is better than that of the standard 50Ni-50Cr alloy, as illustrated by the mean stress/rupture relationships shown in Fig. 3(a). These are based on tests made on six commercial and six laboratory heats. Similar comparisons between IN-657 and cast 25Cr-20Ni steel (HK-40), based on published data for the latter material, shows their stress rupture strengths to be roughly equal (Fig. 3b). The stress rupture ductility values of IN-657, an important consideration in high-temperature service, are generally equal or superior to those of 50Ni-50Cr alloy and 25Cr-20Ni steel, depending on the test temperature.

In common with most cast heat resistant alloys, including the standard 50Ni-50Cr type, IN-657 suffers a loss of room-temperature tensile ductility after service at high temperatures. However, the niobium-containing nickel-chromium alloys show less impairment of ductility than the standard 50Ni-50Cr alloy (Ref 6).

Figure 4 compares IN-657, 50Ni-50Cr, and 25Cr-20Ni (HK-40) steel for resistance to oil ash corrosion. The weight losses shown were determined after half-immersion tests in 80% V_2O_5 + 20% Na_2SO_4. The results recorded for HK-40 relate to only 16 h of exposure, compared with 300 h for the other two alloys. Preliminary field service experience of up to about 3 years has supported these laboratory data, indicating that there is essentially no difference between 50Cr-50Ni alloy and IN-657 with respect to oil ash corrosion resistance.

In a field rack test in a crude oil heater at 700 °C (1290 °F), alloy 657 performed 10 times better than HH and HK alloys, as illustrated in Fig. 5. Swales and Ward (Ref 3) reported numerous field experiences for IN-657 as tube supports in refinery heaters. They concluded that the alloy provided satisfactory service at temperatures up to 900 °C (1650 °F). At temperatures higher than 900 °C (165 °F), IN-657 often suffered severe corrosion attack.

Nickel-Iron-Chromium Alloys

As stated in the introductory paragraphs of this article, Ni-Fe-Cr alloys are an extension of stainless steel compositions. As listed in Table 5, these materials, which are recognized in ASTM specifications, fall in the range of 0 to 68% Ni, 8 to 32% Cr, with the balance consisting of iron and carbon plus up to 2.5% Si and 2.0% Mn. Of the alloys listed in Table 5, only alloys HW and HX are classified as nickel-base alloys. The iron-chromium, Fe-Cr-Ni, and Fe-Ni-Cr alloys listed in Table 5 are classified as stainless steels.

Table 2 Results of a field test (uncooled specimens) exposed in the superheater section at 815 °C (1500 °F) in a boiler fired with high vanadium (150–450 ppm) Bunker C fuel

	Corrosion rate	
Alloy	mm/yr	mils/yr
5Cr steel	32–45	1270–1775
406	5.7	224
431	17–23	655–925
446	3.8	149
302B	14–16	533–644
309	5.0	196
321	9–13	346–505
347	6.2	243
310	4.7	187
Incoloy 800	9–12	364–458
Incoloy 804	13–18	495–710
Inconel 600	5.0	196
50Cr-50Ni	3.1	121
HE	4.8	187
HH	12–16	467–645

Source: Ref 4

Table 3 Chemical composition requirements for nickel-chromium alloys described in ASTM A 560

	Composition(a), wt%												
Grade	C	Mn	Si	S	P	N	N + C	Fe	Ti	Al	Nb	Cr	Ni
50Ni-50Cr	0.10	0.30	1.00	0.02	0.02	0.30	…	1.00	0.50	0.25	…	48.0–52.0	bal
40Ni-60Cr	0.10	0.30	1.00	0.02	0.02	0.30	…	1.00	0.50	0.25	…	58.0–62.0	bal
50Ni-50Cr-Nb	0.10	0.30	0.50	0.02	0.02	0.16	0.20	1.00	0.50	0.25	1.4–1.7	47.0–52.0	bal

(a) The total of the nickel, chromium, and niobium contents must exceed 97.5%.

Table 4 Minimum room-temperature property requirements for cast nickel-chromium alloys described in ASTM A 560

	Tensile strength		Yield point		Elongation in 50 mm	Charpy unnotched impact strength	
Alloy	MPa	ksi	MPa	ksi	(2 in.), %	J	ft · lbf
50Ni-50Cr	550	80	340	49	5	78	50
40Ni-60Cr	760	110	590	85	…	14	10
50Ni-50Cr-Nb	550	80	345	50	5	…	…

Room-temperature mechanical properties for HW and HX are compared with other cast heat resistant alloys in Table 6. While possessing moderate high-temperature strength (Table 7), the creep strength of the Ni-Fe-Cr alloys is fairly low (Fig. 6). The high-nickel grades have the highest carburization of the standard H-type castings. Figure 7 shows the effect of nickel content on the carburization resistance of heat resistant cast alloys.

HW alloy (60Ni-12Cr) is especially well suited for applications in which wide and/or rapid fluctuations in temperature are encountered. In addition, HW exhibits excellent resistance to carburization and high-temperature oxidation. HW alloy has good strength at steel-treating temperatures, although it is not as strong as HT (35Ni-17Cr). HW performs satisfactorily at

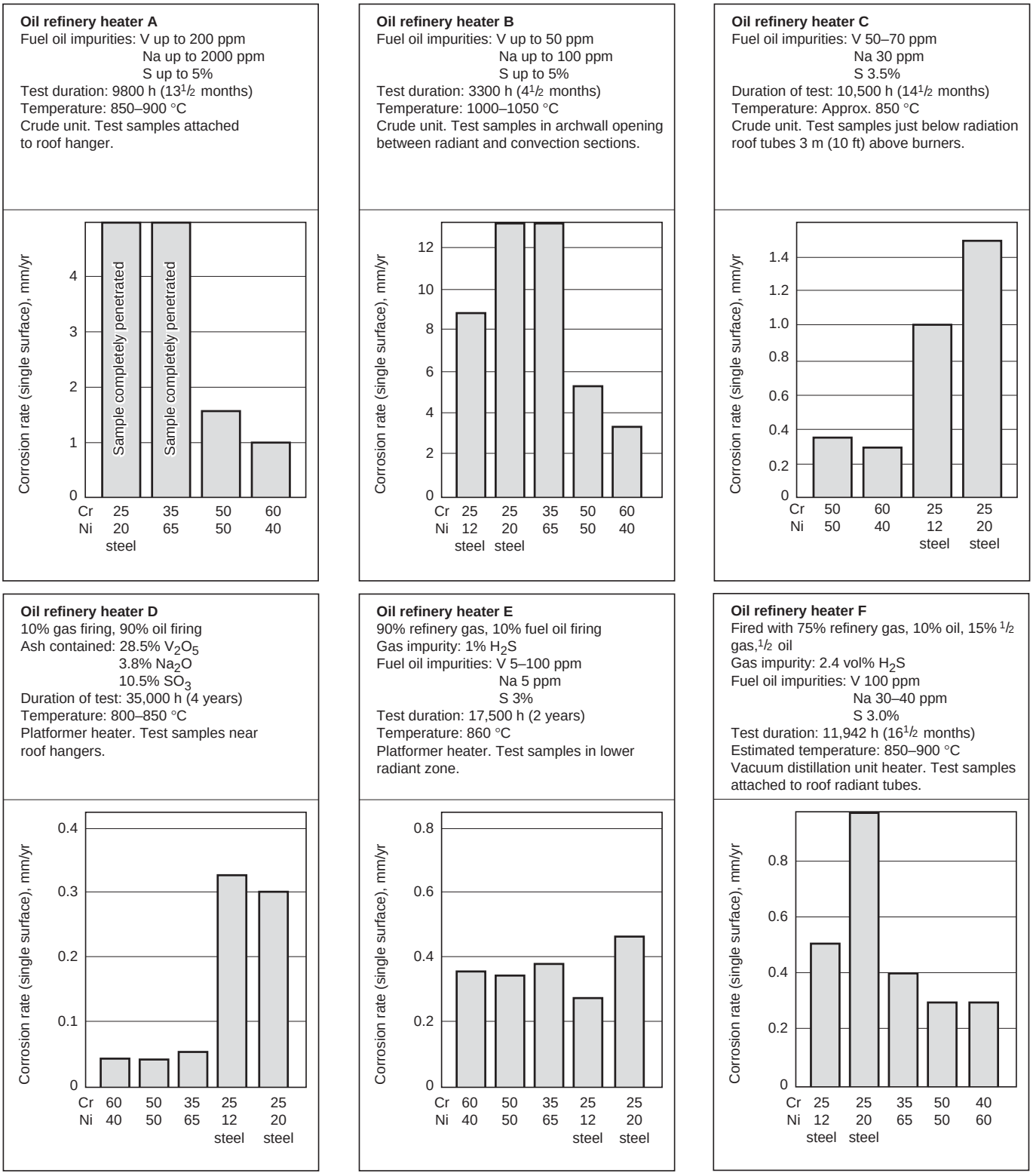


Fig. 1 Results of field tests of oil ash corrosion in oil refinery heaters. Source: Ref 1

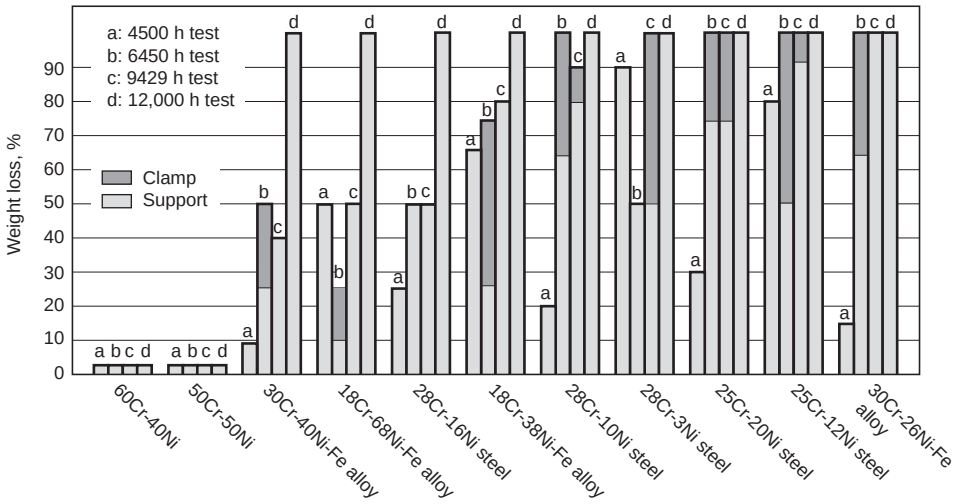


Fig. 2 Results of field tests of oil ash corrosion in power station boiler components. The tests were carried out in Bunker C oil at 815 °C (1500 °F). See text for details. Source: Ref 1

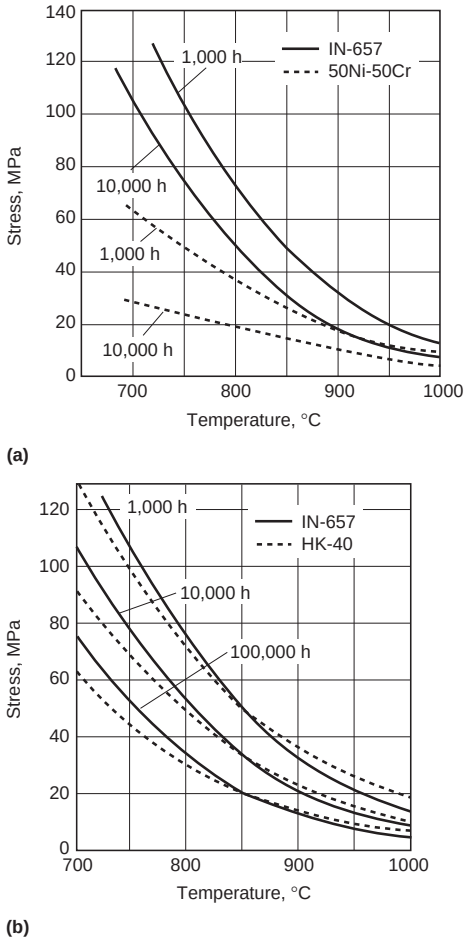


Fig. 3 Stress rupture properties for nickel-chromium and steel castings derived from Larson-Miller curves. (a) IN-657 versus 50Ni-50Cr. (b) IN-657 versus HK-40. Source: Ref 1

Table 5 Compositions of standard heat resistant casting alloys

Wrought alloy type(a)	ACI designation	UNS No.	Composition(b), % C	Cr	Ni	Si (max)
…	HA	…	0.20 max	8–10	…	1.00
446	HC	J92605	0.50 max	26–30	4 max	2.00
327	HD	J93005	0.50 max	26–30	4–7	2.00
312	HE	J93403	0.20–0.50	26–30	8–11	2.00
302B	HF	J92603	0.20–0.40	18–23	8–12	2.00
309	HH	J93503	0.20–0.50	24–28	11–14	2.00
…	HI	J94003	0.20–0.50	26–30	14–18	2.00
310	HK	J94224	0.20–0.60	24–38	18–22	2.00
…	HK-30	J94203	0.25–0.35	23.0–27.0	19.0–22.0	1.75
…	HK-40	J94204	0.35–0.45	23.0–27.0	19.0–22.0	1.75
…	HL	N08604	0.20–0.60	28–32	18–22	2.00
…	HN	J94213	0.20–0.50	19–23	23–27	2.00
…	HP	N08705	0.35–0.75	24–28	33–37	2.00
330	HT	N08605	0.35–0.75	13–17	33–37	2.50
…	HT-30	N08603	0.25–0.35	13.0–17.0	33.0–37.0	2.50
…	HU	N08005	0.35–0.75	17–21	37–41	2.50
…	HW	N08006	0.35–0.75	10–14	58–62	2.50
…	HX	N06050	0.35–0.75	15–19	64–68	2.50

(a) Type numbers of wrought alloys are listed only for nominal identification of corresponding wrought and cast grades. Composition ranges of cast alloys are not the same as for corresponding wrought alloys; cast alloy designations should be used for castings only. (b) Balance Fe in all compositions. Manganese content: 0.35–0.65% for HA, 1% for HC, 1.5% for HD, and 2% for the other alloys. Phosphorus and sulfur contents: 0.04% (max) for all. Molybdenum is intentionally added only to HA, which has 0.90–1.20% Mo; maximum for other alloys is set at 0.5% Mo. HH also contains 0.2% N (max).



Fig. 4 Comparison of fuel oil ash corrosion resistance for nickel-chromium alloys and HK-40 steel. Source: Ref 1

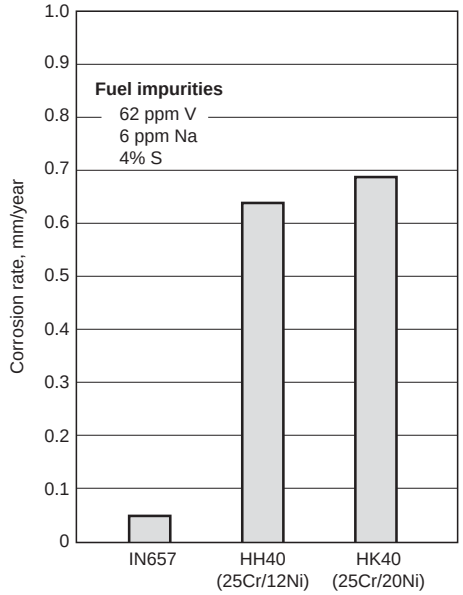


Fig. 5 Results of a field test at 700 °C (1290 °F) for 6 months in a refinery (crude oil) heater comparing IN-657 to HH and HK alloys. Source: Ref 3

temperatures up to about 1120 °C (2050 °F) in strongly oxidizing atmospheres and up to 1040 °C (1900 °F) in oxidizing or reducing products of combustion provided that sulfur is not present in the gas. The generally adherent nature of its oxide scale makes HW suitable for enameling furnace service, where even small flakes of dislodged scale could ruin the work in process.

HW alloy is widely used for intricate heat treating fixtures that are quenched with the load and for many other applications (such as furnace retorts and muffles) that involve thermal shock, steep temperature gradients, and high stresses. Its structure is austenitic and contains carbides in amounts that vary with carbon content and thermal history. In the as-cast condition, the microstructure consists of a continuous interdendritic network of elongated eutectic carbides. Upon prolonged exposure at service temperatures, the austenitic matrix becomes uniformly peppered with small carbide particles except in the immediate vicinity of eutectic carbides. This change in structure is accompanied by an increase in room-temperature strength, but there is no change in ductility.

HX alloy (66Ni-17Cr) is similar to HW, but contains more nickel and chromium. Its higher chromium content gives it substantially better resistance to corrosion by hot gases (even sulfur-bearing gases), which permits it to be used in severe service applications at temperatures up to 1150 °C (2100 °F). However, it has been reported that HX alloy decarburizes rapidly at temperatures from 1100 to 1150 °C (2000–2100 °F). High-temperature strength, resistance to thermal fatigue, and resistance to carburization are essentially the same as for HW. Hence HX is suitable for the same general applications in which its corrosion microstructures, as well as its mechanical properties and fabricating characteristics, are similar to those of HW.

Nickel-Chromium-Iron Alloys

This group of nickel-base alloys does not contain any standard Alloy Casting Institute (ACI) alloys. All of the compositions are proprietary grades based on a 45Ni-30Cr-Fe alloy. The balance of iron can be significantly diminished by various alloying additions. As shown in Table 8, these alloys make use of carbide-forming elements niobium, titanium, and tungsten, together with noncarbide-forming additions of aluminum and cobalt. Tables 6 and 9 list room-temperature mechanical properties

Table 6 Typical room-temperature properties of heat resistant casting alloys

Alloy	Condition	Tensile strength		Yield strength		Elongation,	Hardness,
		MPa	ksi	MPa	ksi	%	HB
Standard grades							
HA	N + T(a)	738	107	558	81	21	220
HC	As-cast	760	110	515	75	19	223
	Aged(b)	790	115	550	80	18	…
HD	As-cast	585	85	330	48	16	90
HE	As-cast	655	95	310	45	20	200
	Aged(b)	620	90	380	55	10	270
HF	As-cast	635	92	310	45	38	165
	Aged(b)	690	100	345	50	25	190
HH, type 1	As-cast	585	85	345	50	25	185
	Aged(b)	595	86	380	55	11	200
HH, type 2	As-cast	550	80	275	40	15	180
	Aged(b)	635	92	310	45	8	200
HI	As-cast	550	80	310	45	12	180
	Aged(b)	620	90	450	65	6	200
HK	As-cast	515	75	345	50	17	170
	Aged(c)	585	85	345	50	10	190
HL	As-cast	565	82	360	52	19	192
HN	As-cast	470	68	260	38	13	160
HP	As-cast	490	71	275	40	11	170
HT	As-cast	485	70	275	40	10	180
	Aged(c)	515	75	310	45	5	200
HU	As-cast	485	70	275	40	9	170
	Aged(d)	505	73	295	43	5	190
HW	As-cast	470	68	250	36	4	185
	Aged(e)	580	84	360	52	4	205
HX	As-cast	450	65	250	36	9	176
	Aged(d)	505	73	305	44	9	185
Nonstandard 45Ni-30Cr-Fe grades							
45Ni-30Cr-Nb-Ti	As-cast	586	85	290	42	10	195
45Ni-30Cr-W	As-cast	517	75	290	42	10	171
45Ni-30Cr-W-Co	As-cast	531	77	303	44	10	…

(a) Normalized and tempered at 675 °C (1250 °F). (b) Aging treatment: 24 h at 760 °C (1400 °F), furnace cool. (c) Aging treatment: 24 h at 760 °C (1400 °F), air cool. (d) Aging treatment: 48 h at 980 °C (1800 °F), air cool. (e)Aging treatment: 48 h at 980 °C (1800 °F), furnace cool.

Table 7 Representative short-term tensile properties of standard cast heat resistant alloys at elevated temperatures

Alloy	Property at indicated temperature														
	760 °C (1400 °F)					870 °C (1600 °F)					980 °C (1800 °F)				
	Ultimate tensile strength		Yield strength at 0.2% offset		Elongation,	Ultimate tensile strength		Yield strength at 0.2% offset		Elongation,	Ultimate tensile strength		Yield strength at 0.2% offset		Elongation,
	MPa	ksi	MPa	ksi	%	MPa	ksi	MPa	ksi	%	MPa	ksi	MPa	ksi	%
HA	462(a)	67(a)	220(b)	32(b)	…	…	…	…	…	…	…	…	…	…	…
HD	248	36	…	…	14	159	23	…	…	18	103	15	…	…	40
HF	262	38	172	25	16	145	21	107	15.5	16	…	…	…	…	…
HH (type I)(c)	228	33	117	17	18	127	18.5	93	13.5	30	62	9	43	6.3	45
HH (type II)(c)	258	37.4	136	19.8	16	148	21.5	110	16	18	75	10.9	50	7.3	31
HI	262	38	…	…	6	179	26	…	…	12	…	…	…	…	…
HK	258	37.5	168	24.4	12	161	23	101	15	16	85.5	12.4	60	8.7	42
HL	345	50	…	…	…	210	30.5	…	…	…	129	18.7	…	…	…
HN	…	…	…	…	…	140	20	100	14.5	37	83	12	66	9.6	51
HP	296	43	200	29	15	179	26	121	17.5	27	100	14.5	76	11	46
HT	240	35	180	26	10	130	19	103	15	24	76	11	55	8	28
HU	275	40	…	…	…	135	19.5	…	…	20	69	10	43	6.2	28
HW	220	32	158	23	…	131	19	103	15	…	69	10	55	8	40
HX	310(d)	45(d)	138(d)	20(d)	8(d)	141	20.5	121	17.5	48	74	10.7	47	6.9	40

(a) In this instance, test temperature was 540 °C (1000 °F). (b) Test temperature was 590 °C (1100 °F). (c) Type I and II per ASTM A 447. (d) Test temperature was 650 °C (1200 °F).

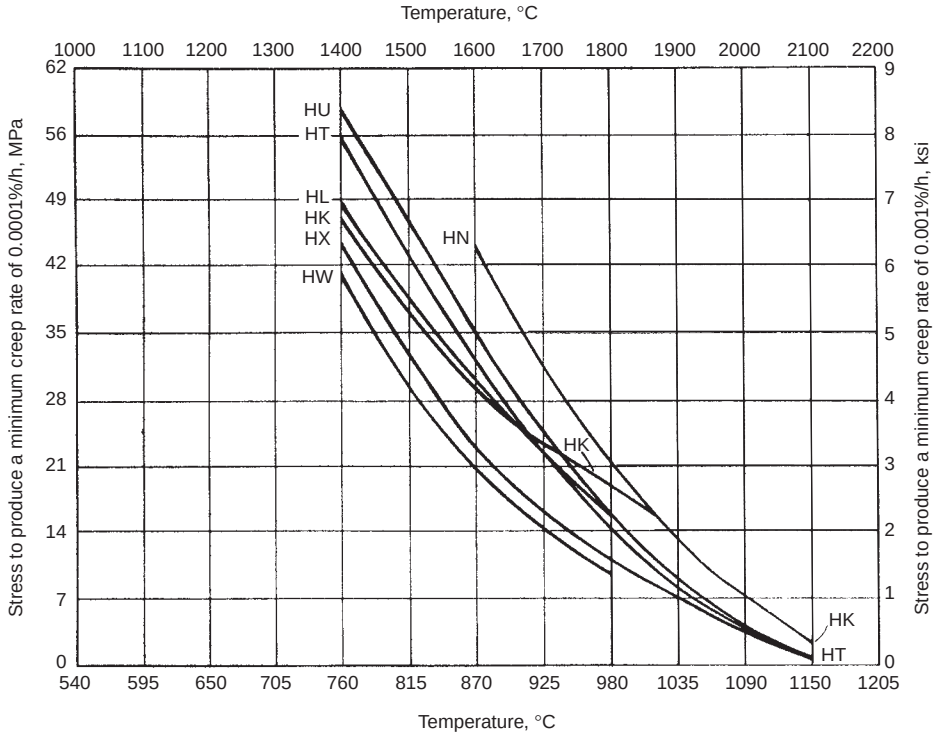


Fig. 6 Creep strength comparison of nickel-base HX and HW alloys and stainless steel heat resistant alloys

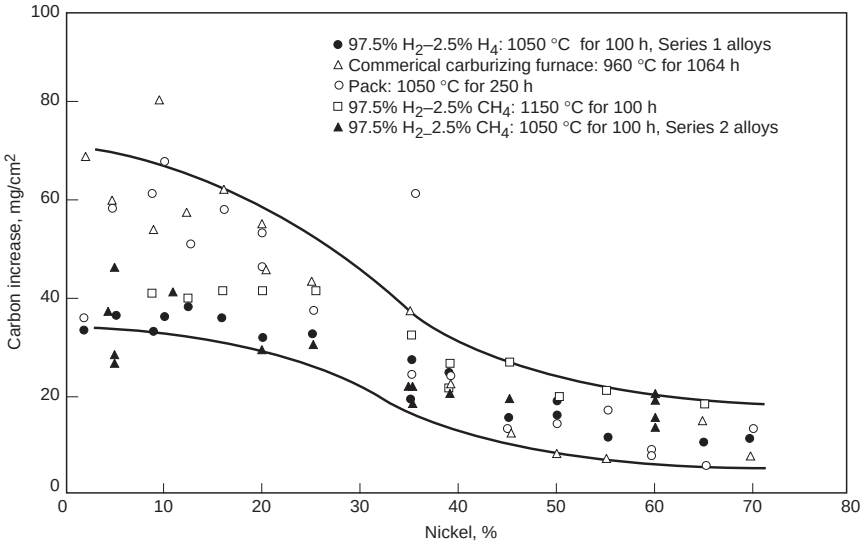


Fig. 7 Effect of nickel on the carburization resistance of heat resistant cast alloys. Source: Ref 7

and creep properties, respectively, for 45-Ni-30Cr-Fe alloys.

Nickel-chromium-iron alloys are used almost exclusively in very-high-strength, high-temperature, high oxidation resistant applications. Alloy uses include hydrocarbon reformers for direct-reduced iron pellet plants, tube and assembly supports and hangers, and skid buttons in steel billet reheating furnaces where surface temperatures of 1260 to 1315 °C (2300–2400 °F) are encountered.

ACKNOWLEDGMENT

This article was adapted from:

- Nickel-Chromium and Nickel-Thoria Alloys, *ASM Specialty Handbook: Heat-Resistant Materials*, J.R. Davis, Ed., ASM International, 1997, p 383–388
- High-Alloy Cast Steels, *ASM Specialty Handbook: Heat-Resistant Materials*, J.R. Davis, Ed., ASM International, 1997, p 200–218

Table 8 Nominal compositions of nonstandard Ni-Cr-Fe heat resistant alloys

Generic alloy base	Composition, wt%									
	C	Mn	Si	Cr	Ni	W	Nb	Co	Ti	Fe
45–30-Nb-W	0.4	1	1	34	44	0.5	0.5	…	…	bal
45–30-Nb-Ti	0.42	1	1	34	45	…	1	…	0.1–0.3	bal
45–30-W	0.5	1	1	28	47	5	…	…	…	bal
45–30-W-Co	0.45	1	1	26	47	5	…	3	…	bal
45–30-W-Al	0.2	0.4	0.2	33	50	16	…	…	…	bal

Note: Sulfur and phosphorus typically specified at less than 0.03% of these alloys. Some alloys may also contain microalloying additions of aluminum.

Table 9 Creep properties of nonstandard nickel-chromium-iron cast heat resistant alloys

Alloy	Temperature		Creep stress to produce 0.0001 %/h creep in 100,000 h		Stess to produce rupture in 100,000 h	
	°C	°F	MPa	ksi	MPa	ksi
45-30-Nb-Ti	760	1400	…	…	57.8	8.39
	870	1600	…	…	31.4	4.55
	980	1800	21.4	3.1	12.3	1.79
	1095	2000	…	…	3.1	0.45
45-30-W	870	1600	…	…	…	…
	980	1800	21.4	3.1	14.5	2.10
	1095	2000	8.8	1.27	4.8	0.69
45-30-W-Co	870	1600	…	…	31.7	4.6
	980	1800	22.1	3.2	13.1	1.90
	1095	2000	11.0	1.6	5.2	0.76
45-30-W-Al	870	1600	…	…	41.4	6.0
	980	1800	…	…	15.7	2.27
	1095	2000	8.6	1.25	5.2	0.75

REFERENCES

1. "High-Chromium Cr-Ni Alloys to Resist Fuel Oil Ash Corrosion: A Review of Developments and Experience 1955–1975," Publication 4299, Nickel Development Institute, 1975
2. Fuel Ash Effects on Boiler Design and Operation, *Steam: Its Generation and Use*, 40th ed., S.C. Stultz and J.B. Kitto, Ed., Babcock & Wilcox Co., 1992
3. G.L. Swales and D.M. Ward, Paper 126, presented at Corrosion/79, National Association of Corrosion Engineers, 1979
4. D.W. McDowell, Jr. and J.R. Mihalisin, Paper 60-WA-260, presented at ASME Winter Annual Meeting (New York), 27 Nov to 2 Dec 1960
5. B.F. Spafford, *Conf. Proc. U.K. Corrosion '83*, Institution of Corrosion Science & Technology, Birmingham, U.K., 1982, p 67
6. P.J. Penrice, A.J. Stapley, and J.A. Towers, Nickel Chromium Alloys with 30–60% Chromium in Relation to Their Resistance to Corrosion by Fuel Ash Deposits, Part II: Mechanical Properties and the Influence of Exposure at High Temperatures on Tensile and Impact Properties. *J. Inst. Fuel*, Vol 39, Jan 1966, p 14–21
7. C. Steel and W. Engel, *AFS Int. Cast Metals J.*, Sept 1981, p 28

ASM Specialty Handbook: Nickel, Cobalt, and Their Alloys
J.R. Davis, editor, p 68-91
DOI:10.1361/ncta2000p068

Copyright © 2000 ASM International®
All rights reserved.
www.asminternational.org

Superalloys

SUPERALLOYS are nickel-, iron-nickel-, and cobalt-base alloys generally used at temperatures above approximately 540 °C (1000 °F). They have a face-centered cubic (fcc, austenitic) structure. Iron, cobalt, and nickel are transition metals with consecutive positions in the periodic table of elements. The iron-nickel-base superalloys are an extension of stainless steel technology and generally are wrought, whereas cobalt- and nickel-base superalloys may be wrought or cast, depending on the application/composition involved.

Appropriate compositions of all superalloy-base metals can be forged, rolled to sheet, or otherwise formed into a variety of shapes. The more highly alloyed compositions normally are processed as castings. Fabricated structures can be built up by welding or brazing, but many highly alloyed compositions containing a high amount of hardening phase are difficult to weld.

Properties can be controlled by adjustments in composition and by processing (including heat treatment), and excellent elevated-temperature strengths are available in finished products. Figure 1 compares stress rupture behavior of the three alloy classes.

General Background

Important Metal Characteristics

Pure iron has a density of 7.87 g/cm^3 (0.284 lb/in.^{3}), and pure nickel and cobalt have densities of approximately 8.9 g/cm^3 (0.322 lb/in.^{3}). Iron-nickel-base superalloys have densities of approximately 7.9 to 8.3 g/cm^3 (0.285–0.300 lb/in.^{3}); cobalt-base superalloys, approximately 8.3 to 9.4 g/cm^3 (0.300–0.340 lb/in.^{3}); and nickel-base superalloys, approximately 7.8 to 8.9 g/cm^3 (0.282–0.322 lb/in.^{3}). Superalloy density is influenced by alloying additions: aluminum, titanium, and chromium reduce density, whereas tungsten, rhenium, and tantalum increase it. The corrosion resistance of superalloys depends primarily on the alloying elements added and the environment experienced.

The melting temperatures of the pure elements are as follows: nickel, 1453 °C (2647 °F); cobalt, 1495 °C (2723 °F); and iron, 1537 °C (2798 °F). Incipient melting temperatures and melting ranges of superalloys are functions of composition and prior processing. Generally, incipient melting temperatures are greater for cobalt-base than for nickel- or iron-nickel-base superalloys. Nickel-base superalloys may show incipient melting at temperatures as low as 1204 °C (2200 °F). Advanced nickel-base single-crystal superalloys with limited amounts of melting-point depressants tend to have incipient melting temperatures equal to or in excess of those of cobalt-base alloys.

Iron and cobalt both undergo allotropic transformations and become fcc at high temperatures; nickel, on the other hand, is fcc at all temperatures. In superalloys based on iron and cobalt, the fcc forms of these elements generally are stabilized by alloying additions. The upper limit of usage for superalloys is not restricted by the occurrence of allotropic transformation reactions, but rather is a function of incipient melting temperature and dissolution of strengthening phases. Some tendency toward transformation of the fcc phase to stable lower-temperature phases occasionally occurs in cobalt-base superalloys. The austenitic fcc matrices of superalloys have extended solubility for some alloying additions, excellent ductility, and favorable characteristics for precipitation of uniquely effective strengthening phases (iron-nickel- and nickel-base superalloys).

Superalloys typically have moduli of elasticity in the vicinity of 207 GPa (30 × 10^6 psi), although moduli of specific polycrystalline alloys can vary from 172 to 241 GPa (25 to 35 × 10^6 psi) at room temperature, depending on the alloy system. Processing that leads to directional grain or crystal orientation can result in moduli of approximately 124 to 310 GPa (about 18 to 45 × 10^6 psi), depending on the relation of grain or crystal orientation to testing direction. Physical properties (electrical conductivity, thermal conductivity, and thermal expansion) tend to be low compared to other metal systems. These properties are influenced by the nature of the base metals (transition elements) and the presence of refractory-metal additions.

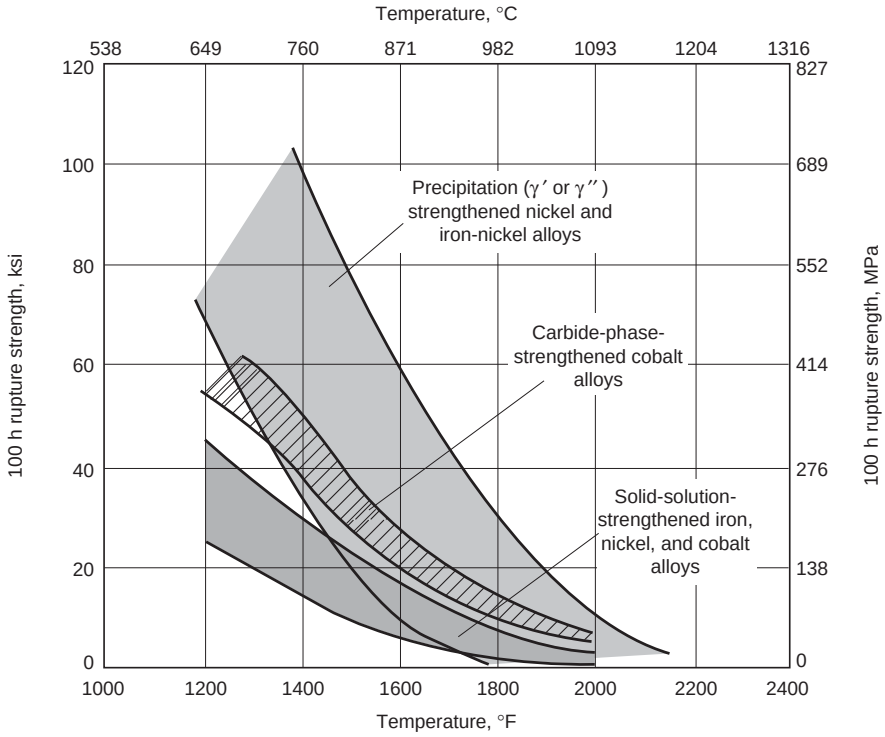


Fig. 1 General stress rutpure behavior of superalloys

The superalloys are relatively ductile, although the ductilities of cobalt-base superalloys generally are less than those of iron-nickel- and nickel-base superalloys. Iron-nickel- and nickel-base superalloys are readily available in extruded, forged, or rolled form; the higher-strength alloys generally are found only in the cast condition. Hot deformation is the preferred forming process, cold forming usually being restricted to thin sections (sheet). Cold rolling may be used to increase short-time strength properties for applications at temperatures below the lower temperature level of 540 °C (1000 °F) established in this article for superalloy use.

Phases and Structures of Superalloys

Superalloys consist of the austenitic fcc matrix phase γ plus a variety of secondary phases. Secondary phases of value in controlling properties are the carbides MC, $M_{23}C_6$, M_6C, and M_7C_3 (rare) in all superalloy types; the γ′ fcc ordered $Ni_3(Al,Ti)$, γ″ bct (body-centered tetragonal) ordered Ni_3Nb, η hexagonal ordered Ni_3Ti, and δ orthorhombic Ni_3Nb intermetallic compounds in nickel- and iron-nickel-base superalloys. The superalloys derive their strength from solid-solution hardeners and precipitated phases. Principal strengthening precipitate phases are γ′ and γ″. Carbides may provide limited strengthening directly (e.g., through dispersion hardening) or, more commonly, indirectly (e.g., by stabilizing grain boundaries against excessive shear). The δ and η phases are useful (along with γ′) in control of structure of wrought superalloys during processing. The extent to which they directly contribute to strengthening depends on the alloy and its processing.

In addition to those elements that produce solid-solution hardening and/or promote carbide and γ′ formation, other elements (e.g., boron, zirconium, and hafnium) are added to enhance mechanical or chemical properties. Some carbide- and γ′-forming elements may contribute significantly to chemical properties as well. Tables 1(a) and (b), respectively, give a generalized list of the ranges of alloying elements and their effects in superalloys. Similar information is provided in Fig. 2. Typical operating microstructures of representative superalloys are shown in Fig. 3.

Table 1(a) Common ranges of major alloying additions in superalloys

Element	Range, %	
	Fe-Ni- and Ni-base	Co-base
Chromium	5–25	19–30
Molybdenum, tungsten	0–12	0–11
Aluminum	0–6	0–4.5
Titanium	0–6	0–4
Cobalt	0–20	…
Nickel	…	0–22
Niobium	0–5	0–4
Tantalum	0–12	0–9
Rhe nium	0–6	0–2

Superalloy Systems

The three types of superalloys—iron-nickel-, nickel-, and cobalt-base—may be further subdivided into cast and wrought. A large number of alloys have been invented and studied; many have been patented. However, the many alloys have been winnowed down over the years, and only a few are extensively used. Alloy usage is a function of industry (gas turbines, steam turbines, etc.). Not all alloys can be mentioned; examples of older and newer alloys are used to demonstrate the physical metallurgy response of superalloy systems. Representative superalloys and compositions emphasizing alloys developed in the United States are listed in Tables 2 to 5. Additional compositions for nickel-base superalloys can be found in the article "Powder Metallurgy Processing of Nickel Alloys" in this Handbook.

Iron-Nickel-Base. The most important class of iron-nickel-base superalloys includes those strengthened by intermetallic compound precipitation in an fcc matrix. The most common precipitate is γ′, typified by A-286, V-57, or Incoloy 901. Some alloys, typified by Inconel (IN)-718, which precipitate γ″, were formerly classed as iron-nickel-base but now are considered to be nickel-base. Other iron-nickel-base superalloys consist of modified stainless steels primarily strengthened by solid-solution hardening. Alloys in this last category vary from

Table 1(b) Role of alloying elements in superalloys

Effect(a)	Iron-base	Cobalt-base	Nickel-base
Solid-solution strengtheners	Cr, Mo	Nb, Cr, Mo, Ni, W, Ta	Co, Cr, Fe, Mo, W, Ta, Re
fcc matrix stabilizers	C, W, Ni	Ni	…
Carbide form:			
MC	Ti	Ti	W, Ta, Ti, Mo, Nb, Hf
M_7C_3	…	Cr	Cr
$M_{23}C_6$	Cr	Cr	Cr, Mo, W
M_6C	Mo	Mo, W	Mo, W, Nb
Carbonitrides: M(CN)	C, N	C, N	C, N
Promotes general precipitation of carbides	P	…	…
Forms γ′ $Ni_3(Al,Ti)$	Al, Ni, Ti	…	Al, Ti
Retards formation of hexagonal η (Ni_3Ti)	Al, Zr	…	…
Raises solvus temperature of γ′	…	…	Co
Hardening precipitates and/or intermetallics	Al, Ti, Nb	Al, Mo, Ti(b), W, Ta	Al, Ti, Nb
Oxidation resistance	Cr	Al, Cr	Al, Cr, Y, La, Ce
Improve hot corrosion resistance	La, Y	La, Y, Th	La, Th
Sulfidation resistance	Cr	Cr	Cr, Co, Si
Improves creep properties	B	…	B, Ta
Increases rupture strength	B	B, Zr	B(c)
Grain-boundary refiners	…	…	B, C, Zr, Hf
Facilitates working	…	Ni_3Ti	…
Retard γ′ coarsening	…	…	Re

(a) Not all these effects necessarily occur in a given alloy. (b) Hardening by precipitation of Ni_3Ti also occurs if sufficient Ni is present. (c) If present in large amounts, borides are formed. Source: Adapted from Ref 1

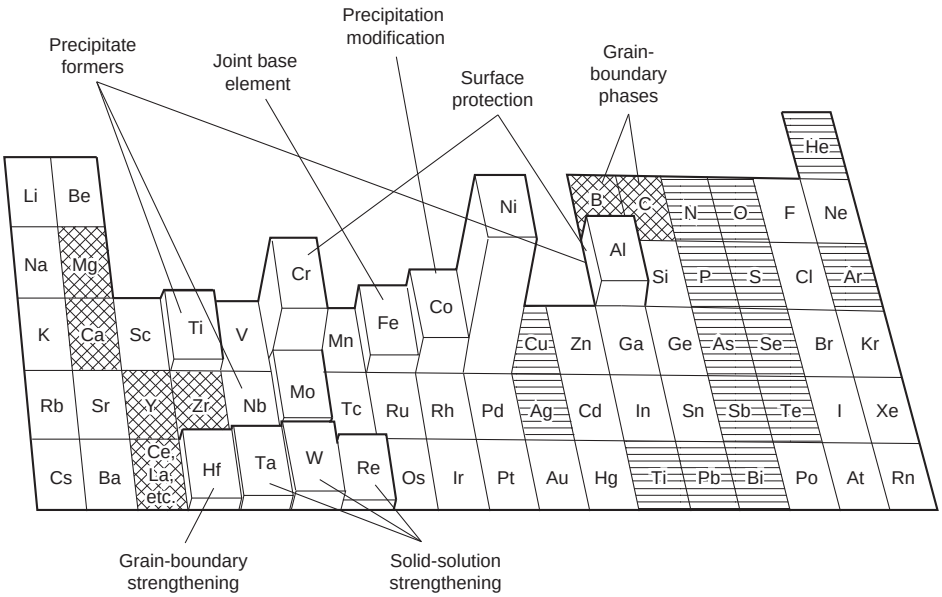


Fig. 2 Alloying elements used in nickel-base superalloys. The height of the element blocks indicates the amount that may be present. Beneficial trace elements are marked with cross hatching and harmful trace elements are marked with horizontal line hatching.

19-9DL (18-8 stainless with slight chromium and nickel adjustments, additional solution hardeners, and higher carbon) to Incoloy 800H (21 chromium, high nickel with small additions of titanium and aluminum, which yields some γ′ phase).

Nickel-Base. The most important class of nickel-base superalloys is that strengthened by intermetallic-compound precipitation in an fcc matrix. For nickel-titanium/aluminum alloys the strengthening precipitate is γ′. Such alloys are typified by the wrought alloys Waspaloy and Udimet (U)-720, or by the cast alloys René 80 and IN-713. For nickel-niobium alloys the strengthening precipitate is γ″. These alloys are typified by IN-718. Some nickel-base alloys may contain both niobium plus titanium and/or aluminum and utilize both γ′ and γ″ precipitates in strengthening. Alloys of this type are IN-706 and IN-909. Another class of nickel-base superalloys is essentially solid-solution strengthened. Such alloys are Hastelloy X and IN-625. The solid-solution-strengthened nickel-base alloys may derive some additional strengthening from carbide and/or intermetallic-compound precipitation. A third class includes oxide-dispersion-strengthened (ODS) alloys such as IN-MA-754 and IN-MA-6000E, which are strengthened by dispersion of inert particles such as yttria, coupled in some cases with γ′ precipitation (MA-6000E).

Nickel-base superalloys are utilized in both cast and wrought forms, although special processing (powder metallurgy/isothermal forging) is frequently used to produce wrought versions of the more highly alloyed compositions

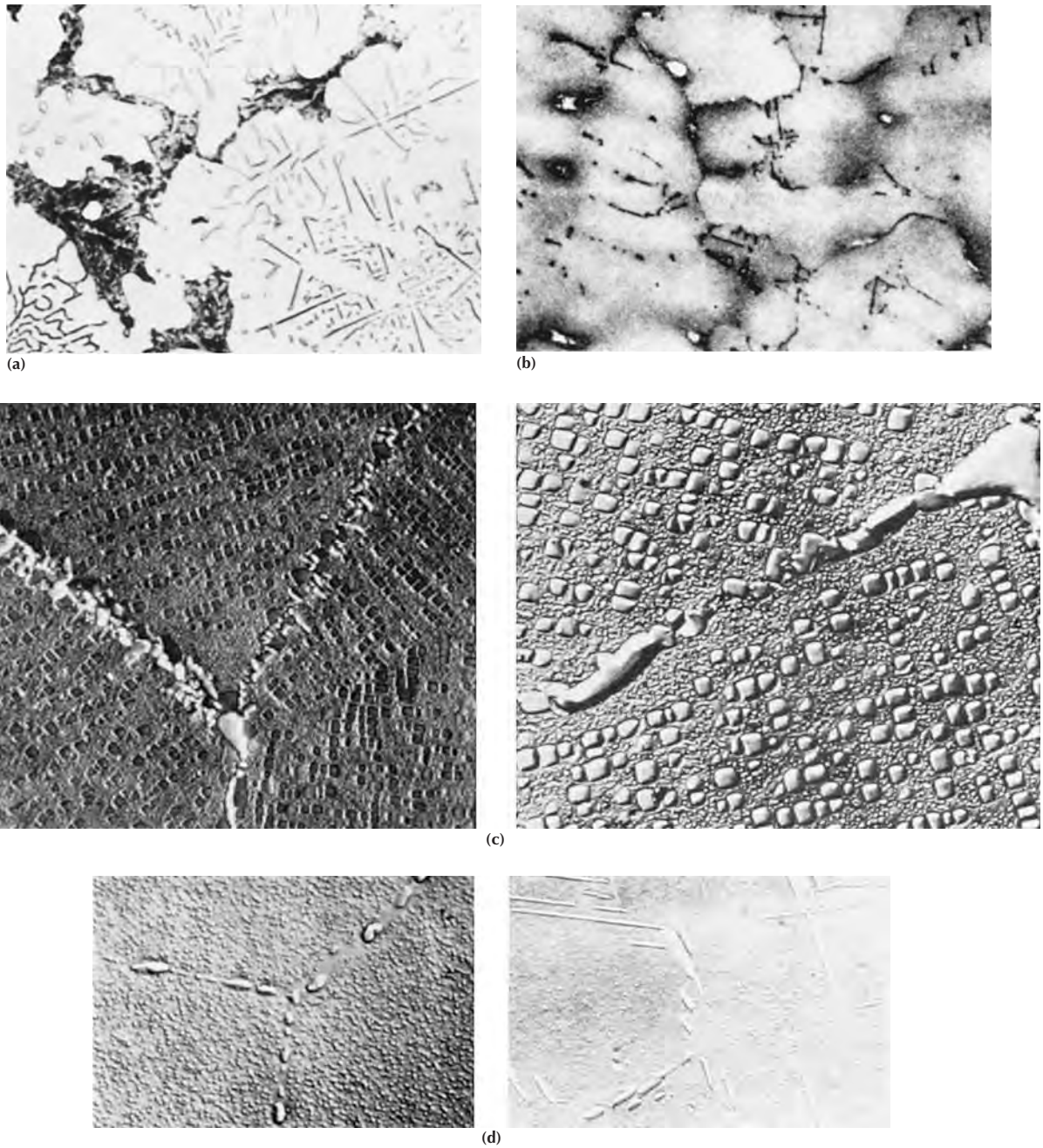


Fig. 3 Typical operating microstructures of representative superalloys. (a) Cast cobalt-base alloy. 250×. (b) Cast nickel-base alloy. 100× (c) Wrought (left, 3300×) and cast (right, 5000×) nickel-base alloys. (d) Two wrought iron-nickel-base alloys (left, 17,000×; right, 3300×). Note script carbides in (a) and (b) as well as eutectic carbide-cobalt grain-boundary structures in (a), spheroidal and cuboidal γ′ as well as grain-boundary carbides in (c), and spheroidal γ′ as well as grain-boundary carbides or grain-boundary and intragranular δ phase in (d). γ″ not obvious but present in (d) (right).

Table 2 Nominal compositions of wrought superalloys

Alloy	UNS No.	Composition, %										
		Cr	Ni	Co	Mo	W	Nb	Ti	Al	Fe	C	Other
Solid-solution alloys												
Iron-nickel-base												
Alloy N-155 (Multimet)	R30155	21.0	20.0	20.0	3.00	2.5	1.0	…	…	32.2	0.15	0.15 N, 0.2 La, 0.02 Zr
Haynes 556	R30556	22.0	21.0	20.0	3.0	2.5	0.1	…	0.3	29.0	0.10	0.50 Ta, 0.02 La, 0.002 Zr
19-9 DL	S63198	19.0	9.0	…	1.25	1.25	0.4	0.3	…	66.8	0.30	1.10 Mn, 0.60 Si
Incoloy 800	N08800	21.0	32.5	…	…	…	…	0.38	0.38	45.7	0.05	…
Incoloy 800H	N08810	21.0	33.0	…	…	…	…	…	…	45.8	0.08	…
Incoloy 800HT	N08811	21.0	32.5	…	…	…	…	0.4	0.4	46.0	0.08	0.8 Mn, 0.5 Si, 0.4 Cu
Incoloy 801	N08801	20.5	32.0	…	…	…	…	1.13	…	46.3	0.05	…
Incoloy 802	N08802	21.0	32.5	…	…	…	…	0.75	0.58	44.8	0.35	…
Nickel-base												
Haynes 214	N07214	16.0	76.5	…	…	…	…	…	4.5	3.0	0.03	
Haynes 230	N06230	22.0	55.0	5.0 max	2.0	14.0	…	…	0.35	3.0 max	0.10	0.015 max B, 0.02 La
Inconel 600	N06600	15.5	76.0	…	…	…	…	…	…	8.0	0.08	0.25 Cu
Inconel 601	N06601	23.0	60.5	…	…	…	…	…	1.35	14.1	0.05	0.5 Cu
Inconel 617	N06617	22.0	55.0	12.5	9.0	…	…	…	1.0	…	0.07	…
Inconel 625	N06625	21.5	61.0	…	9.0	…	3.6	0.2	0.2	2.5	0.05	…
RA 333	N06333	25.0	45.0	3.0	3.0	3.0	…	…	…	18.0	0.05	…
Hastelloy B	N10001	1.0 max	63.0	2.5 max	28.0	…	…	…	…	5.0	0.05 max	0.03 V
Hastelloy N	N10003	7.0	72.0	…	16.0	…	…	0.5 max	…	5.0 max	0.06	
Hastelloy S	N06635	15.5	67.0	…	15.5	…	…	…	0.2	1.0	0.02 max	0.02 La
Hastelloy W	N10004	5.0	61.0	2.5 max	24.5	…	…	…	…	5.5	0.12 max	0.6 V
Hastelloy X	N06002	22.0	49.0	1.5 max	9.0	0.6	…	…	2.0	15.8	0.15	…
Hastelloy C-276	N10276	15.5	59.0	…	16.0	3.7	…	…	…	5.0	0.02 max	…
Haynes HR-120	N08120	25.0	37.0	3.0	2.5	2.5	0.7	…	0.1	33.0	0.05	0.7 Mn, 0.6 Si, 0.2 N, 0.004 B
Haynes HR-160	N12160	28.0	37.0	29.0	…	…	…	…	…	2.0	0.05	2.75 Si, 0.5 Mn
Nimonic 75	N06075	19.5	75.0	…	…	…	…	0.4	0.15	2.5	0.12	0.25 max Cu
Nimonic 86	…	25.0	65.0	…	10.0	…	…	…	…	…	0.05	0.03 Ce, 0.015 Mg
Cobalt-base												
Haynes 25 (L605)	R30605	20.0	10.0	50.0	…	15.0	…	…	…	3.0	0.10	1.5 Mn
Haynes 188	R30188	22.0	22.0	37.0	…	14.5	…	…	…	3.0 max	0.10	0.90 La
Alloy S-816	R30816	20.0	20.0	42.0	4.0	4.0	4.0	…	…	4.0	0.38	…
MP35-N	R30035	20.0	35.0	35.0	10.0	…	…	…	…	…	…	…
MP159	R30159	19.0	25.0	36.0	7.0	…	0.6	3.0	0.2	9.0	…	…
Stellite B	N07718	30.0	1.0	61.5	…	4.5	…	…	…	1.0	1.0	…
UMCo-50	…	28.0	…	49.0	…	…	…	…	…	21.0	0.12	…
Precipitation-hardening alloys												
Iron-nickel-base												
A-286	S66286	15.0	26.0	…	1.25	…	…	2.0	0.2	55.2	0.04	0.005 B, 0.3 V
Discaloy	S66220	14.0	26.0	…	3.0	…	…	1.7	0.25	55.0	0.06	…
Incoloy 903	N19903	0.1 max	38.0	15.0	0.1	…	3.0	1.4	0.7	41.0	0.04	…
Pyromet CTX-1	…	0.1 max	37.7	16.0	0.1	…	3.0	1.7	1.0	39.0	0.03	…
Incoloy 907	N19907	…	38.4	13.0	…	…	4.7	1.5	0.03	42.0	0.01	0.15 Si
Incoloy 909	N19909	…	38.0	13.0	…	…	4.7	1.5	0.03	42.0	0.01	0.4 Si
Incoloy 925	N09925	20.5	44.0	…	2.8	…	…	2.1	0.2	29	0.01	1.8 Cu
V-57	…	14.8	27.0	…	1.25	…	…	3.0	0.25	48.6	0.08 max	0.01 B, 0.5 max V
W-545	S66545	13.5	26.0	…	1.5	…	…	2.85	0.2	55.8	0.08 max	0.05 B
Nickel-base												
Astroloy	N13017	15.0	56.5	15.0	5.25	…	…	3.5	4.4	<0.3	0.06	0.03 B, 0.06 Zr
Custom Age 625 PLUS	N07716	21.0	61.0	…	8.0	…	3.4	1.3	0.2	5.0	0.01	…
Haynes 242	…	8.0	62.5	2.5 max	25.0	…	…	…	0.5 max	2.0 max	0.10 max	0.006 max B
Haynes 263	N07263	20.0	52.0	…	6.0	…	…	2.4	0.6	0.7	0.06	0.6 Mn, 0.4 Si, 0.2 Cu
Haynes R-41	N07041	19.0	52.0	11.0	10.0	…	…	3.1	1.5	5.0	0.09	0.5 Si, 0.1 Mn, 0.006 B
Inconel 100	N13100	10.0	60.0	15.0	3.0	…	…	4.7	5.5	<0.6	0.15	1.0 V, 0.06 Zr, 0.015 B
Inconel 102	N06102	15.0	67.0	…	2.9	3.0	2.9	0.5	0.5	7.0	0.06	0.005 B, 0.02 Mg, 0.03 Zr
Incoloy 901	N09901	12.5	42.5	…	6.0	…	…	2.7	…	36.2	0.10 max	…
Inconel 702	N07702	15.5	79.5	…	…	…	…	0.6	3.2	1.0	0.05	0.5 Mn, 0.2 Cu, 0.4 Si
Inconel 706	N09706	16.0	41.5	…	…	…	…	1.75	0.2	37.5	0.03	2.9 (Nb + Ta), 0.15 max Cu
Inconel 718	N07718	19.0	52.5	…	3.0	…	5.1	0.9	0.5	18.5	0.08 max	0.15 max Cu
Inconel 721	N07721	16.0	71.0	…	…	…	…	3.0	…	6.5	0.04	2.2 Mn, 0.1 Cu
Inconel 722	N07722	15.5	75.0	…	…	…	…	2.4	0.7	7.0	0.04	0.5 Mn, 0.2 Cu, 0.4 Si
Inconel 725	N07725	21.0	57.0	…	8.0	…	3.5	1.5	0.35 max	9.0	0.03 max	
Inconel 751	N07751	15.5	72.5	…	…	…	1.0	2.3	1.2	7.0	0.05	0.25 max Cu
Inconel X-750	N07750	15.5	73.0	…	…	…	1.0	2.5	0.7	7.0	0.04	0.25 max Cu
M-252	N07252	19.0	56.5	10.0	10.0	…	…	2.6	1.0	<0.75	0.15	0.005 B
Nimonic 80A	N07080	19.5	73.0	1.0	…	…	…	2.25	1.4	1.5	0.05	0.10 max Cu
Nimonic 90	N07090	19.5	55.5	18.0	…	…	…	2.4	1.4	1.5	0.06	…
Nimonic 95	…	19.5	53.5	18.0	…	…	…	2.9	2.0	5.0 max	0.15 max	+B, +Zr
Nimonic 100	…	11.0	56.0	20.0	5.0	…	…	1.5	5.0	2.0 max	0.30 max	+B, +Zr
Nimonic 105	…	15.0	54.0	20.0	5.0	…	…	1.2	4.7	…	0.08	0.005 B
Nimonic 115	…	15.0	55.0	15.0	4.0	…	…	4.0	5.0	1.0	0.20	0.04 Zr

(continued)

(René 95, Astroloy, IN-100). An additional dimension of nickel-base superalloys has been the introduction of grain-aspect ratio and orientation as a means of controlling properties. In some instances, in fact, grain boundaries have been removed (see the subsequent discussion of investment casting). Wrought powder metallurgy (P/M) alloys of the ODS class and cast alloys such as MAR-M-247 have demonstrated property improvements owing to control of grain morphology by directional recrystallization or solidification.

Cobalt-Base. The cobalt-base superalloys are invariably strengthened by a combination of carbides and solid-solution hardeners. The essential distinction in these alloys is between cast and wrought structures. Cast alloys are typified by X-40 and wrought alloys by alloy

Table 2 (continued)

Alloy	UNS No.	Composition, %										
		Cr	Ni	Co	Mo	W	Nb	Ti	Al	Fe	C	Other
Precipitation-hardening alloys (continued)												
Nickel-base (continued)												
C-263	N07263	20.0	51.0	20.0	5.9	…	…	2.1	0.45	0.7 max	0.06	…
Pyromet 860	…	13.0	44.0	4.0	6.0	…	…	3.0	1.0	28.9	0.05	0.01 B
Pyromet 31	N07031	22.7	55.5	…	2.0	…	1.1	2.5	1.5	14.5	0.04	0.005 B
Refractaloy 26	…	18.0	38.0	20.0	3.2	…	…	2.6	0.2	16.0	0.03	0.015 B
René 41	N07041	19.0	55.0	11.0	10.0	…	…	3.1	1.5	<0.3	0.09	0.01 B
René 95	…	14.0	61.0	8.0	3.5	3.5	3.5	2.5	3.5	<0.3	0.16	0.01 B, 0.05 Zr
René 100	…	9.5	61.0	15.0	3.0	…	…	4.2	5.5	1.0 max	0.16	0.015 B, 0.06 Zr, 1.0 V
Udimet 500	N07500	19.0	48.0	19.0	4.0	…	…	3.0	3.0	4.0 max	0.08	0.005 B
Udimet 520	…	19.0	57.0	12.0	6.0	1.0	…	3.0	2.0	…	0.08	0.005 B
Udimet 630	…	17.0	50.0	…	3.0	3.0	6.5	1.0	0.7	18.0	0.04	0.004 B
Udimet 700	…	15.0	53.0	18.5	5.0	…	…	3.4	4.3	<1.0	0.07	0.03 B
Udimet 710	…	18.0	55.0	14.8	3.0	1.5	…	5.0	2.5	…	0.07	0.01 B
Unitemp AF2-1DA	N07012	12.0	59.0	10.0	3.0	6.0	…	3.0	4.6	<0.5	0.35	1.5 Ta, 0.015 B, 0.1 Zr
Waspaloy	N07001	19.5	57.0	13.5	4.3	…	…	3.0	1.4	2.0 max	0.07	0.006 B, 0.09 Zr

Table 3 Nominal compositions of cast polycrystalline superalloys

Alloy designation	Nominal composition, %												
	C	Ni	Cr	Co	Mo	Fe	Al	B	Ti	Ta	W	Zr	Other
Nickel-base													
Aerex 350	0.025	44.5	17	25	3	…	1.1	0.025	2.2	4	2	…	1.1 Nb
B-1900	0.1	64	8	10	6	…	6	0.015	1	4(a)	…	0.10	…
Hastelloy X	0.1	50	21	1	9	18	…	…	…	…	1	…	…
Inconel 100	0.18	60.5	10	15	3	…	5.5	0.01	5	…	…	0.06	1 V
Inconel 713C	0.12	74	12.5	…	4.2	…	6	0.012	0.8	1.75	…	0.1	0.9 Nb
Inconel 713LC	0.05	75	12	…	4.5	…	6	0.01	0.6	4	…	0.1	…
Inconel 738	0.17	61.5	16	8.5	1.75	…	3.4	0.01	3.4	…	2.6	0.1	2 Nb
Inconel 792	0.2	60	13	9	2.0	…	3.2	0.02	4.2	…	4	0.1	2 Nb
Inconel 718	0.04	53	19	…	3	18	0.5	…	0.9	…	…	…	0.1 Cu, 5 Nb
X-750	0.04	73	15	…	…	7	0.7	…	2.5	…	…	…	0.25 Cu, 0.9 Nb
M-252	0.15	56	20	10	10	…	1	0.005	2.6	…	…	…	…
MAR-M 200	0.15	59	9	10	…	1	5	0.015	2	…	12.5	0.05	1 Nb(b)
MAR-M 246	0.15	60	9	10	2.5	…	5.5	0.015	1.5	1.5	10	0.05	…
René 41	0.09	55	19	11.0	10.0	…	1.5	0.01	3.1	…	…	…	…
René 77	0.07	58	15	15	4.2	…	4.3	0.015	3.3	…	…	0.04	…
René 80	0.17	60	14	9.5	4	…	3	0.015	5	…	4	0.03	…
René 80 Hf	0.08	60	14	9.5	4	…	3	0.015	4.8	…	4	0.02	0.75 Hf
René 100	0.18	61	9.5	15	3	…	5.5	0.015	4.2	…	…	0.06	1V
René N4	0.06	62	9.8	7.5	1.5	…	4.2	0.004	3.5	4.8	6	…	0.5 Nb, 0.15 Hf
Udimet 500	0.1	53	18	17	4	2	3	…	3	…	…	…	…
Udimet 700	0.1	53.5	15	18.5	5.25	…	4.25	0.03	3.5	…	…	…	…
Udimet 710	0.13	55	18	15	3	…	2.5	…	5	…	1.5	0.08	…
Waspaloy	0.07	57.5	19.5	13.5	4.2	1	1.2	0.005	3	…	…	0.09	…
Cobalt-base													
AiResist 13	0.45	…	21	62	…	…	3.4	…	…	2	11	…	0.1 Y
AiResist 213	0.20	0.5	20	64	…	0.5	3.5	…	…	6.5	4.5	0.1	0.1 Y
AiResist 215	0.35	0.5	19	63	…	0.5	4.3	…	…	7.5	4.5	0.1	0.1 Y
FSX-414	0.25	10	29	52.5	…	1	…	0.010	…	…	7.5	…	…
Haynes 21	0.25	3	27	64	…	1	…	…	…	…	…	…	5 Mo
Haynes 25; L-605	0.1	10	20	54	…	1	…	…	…	…	15	…	…
J-1650	0.20	27	19	36	…	…	…	0.02	3.8	2	12	…	…
MAR-M 302	0.85	…	21.5	58	…	0.5	…	0.005	…	9	10	0.2	…
MAR-M 322	1.0	…	21.5	60.5	…	0.5	…	…	0.75	4.5	9	2	…
MAR-M 509	0.6	10	23.5	54.5	…	…	…	…	0.2	3.5	7	0.5	…
MAR-M 918	0.05	20	20	52	…	…	…	…	…	7.5	…	0.1	…
NASA Co-W-Re	0.40	…	3	67.5	…	…	…	…	1	…	25	1	2 Re
S-816	0.4	20	20	42	…	4	…	…	…	…	4	…	4 Mo, 4 Nb, 1.2 Mn, 0.4 Si
V-36	0.27	20	25	42	…	3	…	…	…	…	2	…	4 Mo, 2 Nb, 1 Mn, 0.4 Si
WI-52	0.45	…	21	63.5	…	2	…	…	…	…	11	…	2 Nb + Ta
X-40 (Stellite alloy 31)	0.50	10	22	57.5	…	1.5	…	…	…	…	7.5	…	0.5 Mn, 0.5 Si

(a) B-1900 + Hf also contains 1.5% Hf. (b) MAR-M 200 + Hf also contains 1.5% Hf.

25 (also known as L605). No intermetallic compound possessing the same degree of utility as the γ′ precipitate in nickel- or iron-nickel-base superalloys has been found to be operative in cobalt-base systems.

Applications

Superalloys have been used in cast, rolled, extruded, forged, and powder-processed forms. Sheet, bar, plate, tubing, shafts, airfoils, disks, and pressure vessels (cases) are some of the shapes that have been produced. These metals have been used in aircraft, industrial, and marine gas turbines; nuclear reactors; aircraft skins; spacecraft structures; petrochemical production; orthopedic and dental prostheses; and environmental protection applications. Although developed for high-temperature use, some are used at cryogenic temperatures and others at body temperature. Applications continue to expand, but at lower rates than in previous decades. Aerospace usage remains the predominant application on a volume basis.

Processing

Primary and Secondary Melting

A number of superalloys, particularly cobalt- and iron-nickel-base alloys, are air melted by various methods applicable to stainless steels. However, for most nickel- or iron-nickel-base superalloys, vacuum induction melting (VIM) is required as the primary melting process.

Vacuum induction melting consists of melting the required components of an alloy under high vacuum and pouring into an ingot or article mold. The use of VIM reduces interstitial gases to low levels, enables higher and more reproducible levels of aluminum and titanium (along with other relatively reactive elements) to be achieved, and results in less contamination from slag or dross formation than air melting. The benefits of reduced gas content and ability to control aluminum plus titanium are shown in Fig. 4 and 5.

Segregation (on a microscale) occurs during the solidification of all superalloys. The solidification region consists of a zone where the alloy is partially solid and partially liquid (the liquid + solid zone). The solidification mode is generally dendritic and the first (primary) dendrites to form are lower in precipitate-forming elements (titanium, aluminum, niobium, and carbon) than the average melt composition. The interdendritic areas are correspondingly enriched in these solute elements. As cooling rates become slower (increasing casting size), the primary dendrites and interdendritic regions become larger. The slower the cooling rate and the more highly alloyed the melt, the larger the interdendritic regions. At some point, the interdendritic regions become large enough to interconnect and form macroscale defects. Driven by density differences between the solute-rich interdendritic liquid and the nominal melt composition, these regions become self-perpetuating continuous channels in the solidification structure. Such channel defects may grow vertically (but not truly perpendicular) from the solidification front for low-density interdendritic fluids or may grow horizontally

Table 4 Chemical compositions of nickel-base directionally solidified castings

	Nominal composition, wt%													
Alloy	C	Cr	Co	Mo	W	Nb	Re	Ta	Al	Ti	B	Zr	Hf	Ni
First generation														
MAR-M 200 Hf	0.13	8.0	9.0	…	12.0	1.0	…	…	5.0	1.9	0.015	0.03	2.0	bal
René 80H	0.16	14.0	9.0	4.0	4.0	…	…	…	3.0	4.7	0.015	0.01	0.8	bal
MAR-M 002	0.15	8.0	10.0	…	10.0	…	…	2.6	5.5	1.5	0.015	0.03	1.5	bal
MAR-M 247	0.15	8.0	10.0	0.6	10.0	…	…	3.0	5.5	1.0	0.015	0.03	1.5	bal
PWA 1422	0.14	9.0	10.0	…	12.0	1.0	…	…	5.0	2.0	0.015	0.10	1.5	bal
Second generation														
CM 247 LC	0.07	8.0	9.0	0.5	10.0	…	…	3.2	5.6	0.7	0.015	0.010	1.4	bal
CM 186 LC	0.07	6.0	9.0	0.5	8.4	…	3.0	3.4	5.7	0.7	0.015	0.005	1.4	bal
PWA 1426	0.10	6.5	10.0	1.7	6.5	…	3.0	4.0	6.0	…	0.015	0.10	1.5	bal
René 142	0.12	6.8	12.0	1.5	4.9	…	2.8	6.35	6.15	…	0.015	0.02	1.5	bal

Table 5 Chemical compositions of nickel-base single-crystal castings

	Compsition, wt%												Density,
Alloy	Cr	Co	Mo	W	Ta	Re	V	Nb	Al	Ti	Hf	Ni	g/cm³
First generation													
PWA 1480	10	5	…	4	12	…	…	…	5.0	1.5	…	bal	8.70
PWA1483	12.8	9	1.9	3.8	4	…	…	…	3.6	4.0	…	bal	…
René N4	9	8	2	6	4	…	…	0.5	3.7	4.2	…	bal	8.56
SRR 99	8	5	…	10	3	…	…	…	5.5	2.2	…	bal	8.56
RR 2000	10	15	3	…	…	…	1	…	5.5	4.0	…	bal	7.87
AM1	8	6	2	6	9	…	…	…	5.2	1.2	…	bal	8.59
AM3	8	6	2	5	4	…	…	…	6.0	2.0	…	bal	8.25
CMSX-2	8	5	0.6	8	6	…	…	…	5.6	1.0	…	bal	8.56
CMSX-3	8	5	0.6	8	6	…	…	…	5.6	1.0	0.1	bal	8.56
CMSX-6	10	5	3	…	2	…	…	…	4.8	4.7	0.1	bal	7.98
CMSX-11B	12.5	7	0.5	5	5	…	…	0.1	3.6	4.2	0.04	bal	8.44
CMSX-11C	14.9	3	0.4	4.5	5	…	…	0.1	3.4	4.2	0.04	bal	8.36
AF 56 (SX 792)	12	8	2	4	5	…	…	…	3.4	4.2	…	bal	8.25
SC 16	16	…	3	…	3.5	…	…	…	3.5	3.5	…	bal	8.21
Second generation													
CMSX-4	6.5	9	0.6	6	6.5	3	…	…	5.6	1.0	0.1	bal	8.70
PWA 1484	5	10	2	6	9	3	…	…	5.6	…	0.1	bal	8.95
SC 180	5	10	2	5	8.5	3	…	…	5.2	1.0	0.1	bal	8.84
MC2	8	5	2	8	6	…	…	…	5.0	1.5	…	bal	8.63
René N5	7	8	2	5	7	3	…	…	6.2	…	0.2	bal	…
Third generation													
CMSX-10	2	3	0.4	5	8	6	…	0.1	5.7	0.2	0.03	bal	9.05
René N6	4.2	12.5	1.4	6	7.2	5.4	…	…	5.75	…	0.15	bal	8.98

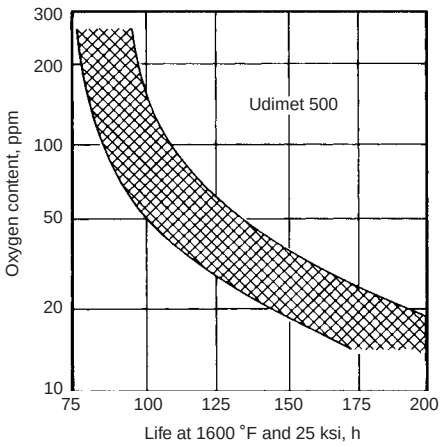


Fig. 4 Improvement of rupture life at 870 °C (1600 °F) and 170 MPa (25 ksi) by reduced oxygen content produced by vacuum melting

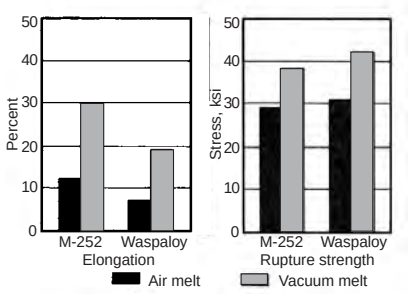


Fig. 5 Effects of vacuum melting, incorporating beneficial modifications in composition, on properties of two nickel-base superalloys

(parallel) to the solidification front for high-density interdendritic liquids.

Solute-rich channel defects are referred to as "freckles" because, when viewed in a cross section perpendicular to their growth axis, they are seen as round, dark, circular spots. Freckle regions may form hard intermetallic compounds that cannot be removed by subsequent processing. The presence of such compounds in wrought alloys is extremely detrimental to fatigue life. If the large ingot sizes required for production of wrought alloys are direct static cast, the formation of unacceptable solute-rich defects is essentially unavoidable. Superalloys for wrought production are thus generally remelted (secondary melting) to control the solidification structure. Three types of secondary melting practices are in use: vacuum arc remelting (VAR), electroslag remelting (ESR), and ESR-VAR.

The vacuum arc remelting process uses a cast (generally VIM) electrode as the cathode in a direct-current (dc) system. Under vacuum, in a water-cooled crucible, an arc is struck between the electrode and the bottom of the crucible. The heat of the arc melts the bottom surface of the electrode at a controlled rate. The molten metal is resolidified in the crucible, with the electrode melt rate being controlled by the applied power. The melting/solidification parameters control the depth and angle of the solidification front (pool shape). Pool shape can be maintained such that unacceptable solute-rich solidification structures do not occur.

In addition to establishing a controlled solidification structure, VAR reduces the amounts of high-vapor-pressure elements in the alloy. Elements such as bismuth and lead (which can be present in low concentrations even after VIM) are highly undesirable, but are reduced to negligible levels by the VAR process. Magnesium, which is considered desirable for improved workability (and is an addition element in VIM), is reduced in concentration but not completely removed. With the exception of high-vapor-pressure elements, the VIM chemistry is representative of the VAR chemistry. The flotation of oxides and nitrides to the melt surface in VAR improves the cleanliness and reduces the gas content of material processed through VAR.

Figure 6 schematically illustrates the relationship among the VAR electrode, the solidifying ingot, and the shape and depth of the solidification front. In VAR, the first metal to solidify against the water-cooled crucible has low solute content (solute lean). The upper part of this solidification layer is built up of splash from the melt pool and is called the "crown." After the crown is melted back by the advancing molten metal front, an alloy-lean layer remains on the outside of the ingot. This is called "shelf." During the remelting operation, the residual oxides/nitrides in the VIM electrode are swept across the top of the molten pool and incorporated into the shelf.

Other important variables of the VAR process are illustrated in Fig. 6. The distance between the side of the electrode and the crucible wall is the annulus. The distance between the bottom of the electrode and the top of the molten pool is the arc gap. As the ingot solidifies, a shrinkage gap is opened between the ingot and the water-cooled crucible. For segregation-sensitive alloys, helium gas is often introduced into the shrinkage gap to improve heat transfer and thus minimize the depth of the molten pool. As shown in Fig. 6, the heat extraction in VAR is concentrated near the top of the molten pool. Vacuum arc remelting is thus a process with low thermal inertia in which very rapid responses (change in pool shape) occur in response to changes in power input.

Freckles, although the most serious defect to occur in secondary melting, are not the only melt-related defect that can be produced. Solute-lean segregation can occur from a number of different sources. The most common mechanism for formation of solute-lean segregation is the undercutting (by the arc) of the shelf, causing a "drop-in" defect. Pieces of the shelf dropping into the pool may not be completely remelted. The result is the incorporation into the structure of a defect with the chemistry of the shelf and which may also contain oxide/nitride stringers. These solute-lean regions are often detected by macroetching of parts/test wafers, where they are seen as light-etching regions in a dark-etching matrix. Thus, they are described as "discrete white spots."

Discrete white spots may also form from drop-in of dendrites from porous regions of the electrode. If the electrode is cracked, pieces larger than dendrites may drop into the melt. While this also produces a light-etching defect, the defect is larger than a discrete white spot and contains dark-etching regions (remnant cast structure). Such structures are often called "dendritic white spots." Although VAR practice and control may be optimized to minimize the frequency of discrete white spot formation, due to the inherent instability of the arc discrete white spots cannot be eliminated. Design of components from VAR-processed material must take into consideration the historical frequency of white spot occurrence for a given process or alloy.

Control of the VAR process is considered from two different aspects: control of pool depth and shape (control of solidification structure) and control of arc stability (control of drop-in defect formation). Pool shape and depth are controlled by regulating heat input and heat extraction. Heat input is determined by the melt rate of the electrode. Melt rate is often monitored and corrected over very short time periods by changes in melt current (melt rate control). Alternatively, control of the median melt rate over the duration of a melt may be maintained by operating at constant melt amperage (amperage control). Heat extraction is a function of the contact surface/ingot volume (ingot size) being melted. Larger ingots have poorer heat extraction (lower surface/volume) and must be melted at proportionately lower melt rates to prevent the formation of large liquid + solid zones and thus the formation of unacceptable positive segregation. While, for a given ingot size, high melt rate may promote positive segregation, a melt rate that is too low may cause the formation of visible solute-lean structures. The mechanism of formation of these "solidification white spots" is not completely understood. They differ from discrete white spots in that they are a solidification effect, not a shelf or electrode drop-in, and therefore do not contain oxide/nitride stringers. Nevertheless, such solute-lean regions are potentially detrimental as they may make it difficult to control grain growth in subsequent processing.

Active control of arc stability is primarily by control of the arc gap throughout the melting of an electrode. (Annulus is a fixed parameter for a given standard process.) For melting of superalloys, arc gaps are generally controlled in the

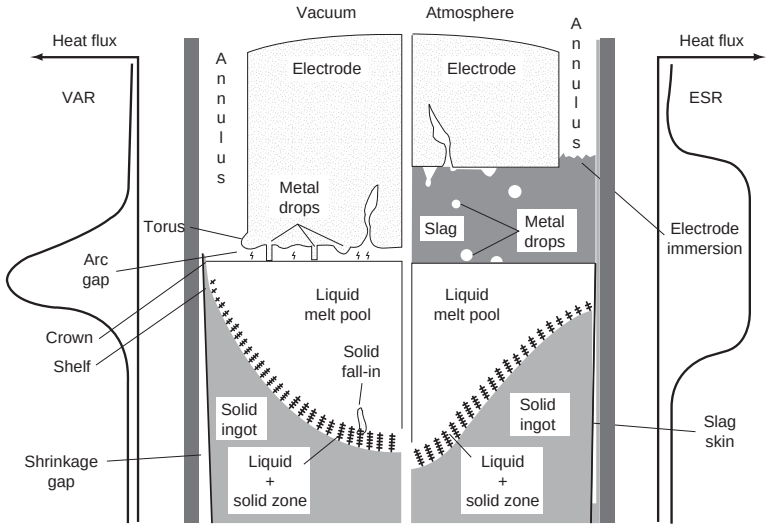


Fig. 6 Schematic of solidification relationships in VAR (left) and ESR (right) melting processes. Source: After Ref 1

range of 6.4 to 12.7 mm (¼–½ in.). To maintain constant arc gap, the electrode is fed into the melt either faster or slower (ram drive) according to the fluctuation in voltage that occurs when the resistance of the system changes in response to changes in the arc gap. Modern control systems for superalloys generally do not use voltage for arc gap control, but rather use a related voltage measurement: the drip short frequency (DSF). A drip short is the transient downward voltage spike that occurs when a molten metal droplet is in contact with both the electrode and the molten pool. The number of shorts occurring in a given time period is proportional to the arc gap. (The relationship for arc gap versus DSF is not melt-rate independent.) Passive control of arc stability is maintained by controlling the annulus and controlling the quality of the electrode being remelted. Electrodes for VIM generally contain porosity and low levels of residual refractory, both of which may act to destabilize the arc. Vacuum induction melting and pouring practice is thus a significant factor in ensuring VAR arc stability and in minimizing the formation of drop-in type defects.

The electroslag remelting process, as applied to superalloys, utilizes a cast (generally VIM) electrode as a consumable element in an alternating-current (ac) system operated open to the atmosphere. A "slag" charge of fluorides and oxides is also part of the system and is kept in a molten state by the passage of electric current through it. The electrode is immersed in the slag and the surface of the electrode melts as droplets, which pass through the slag to solidify (similarly to VAR) in a water-cooled crucible. The melt rate is controlled by the applied power. Heat extraction is controlled by the selection of ingot size. By balancing the melting/solidification parameters, the depth and angle of the liquid + solid zone can be maintained such that unacceptable solute-rich solidification defects do not occur.

Unlike VAR, high-vapor-pressure tramp elements are not removed by ESR. Thus, magnesium may be retained at higher levels than is possible in VAR (with beneficial effects on hot workability). A beneficial chemical reaction related to workability is the removal of sulfur. Detrimental compositional changes may occur in reactive elements (notably titanium and aluminum), as these elements change to attain chemical equilibrium with components of the slag.

Oxides incorporated in the electrode being melted are effectively removed by the ESR process, producing an ingot that is generally cleaner than a VAR ingot. The structures in the solidified ingot are governed by the same principles as those governing a solidifying VAR ingot, but the nature of the heat transfer (through an oxide skin) and the presence of a heat reservoir (the molten slag) at the top of the ingot/molten pool make ESR structure inherently different from that of VAR.

Figure 6 schematically illustrates the relationship among the ESR electrode, the solidifying ingot, and the shape and depth of the molten pool. A major feature of ESR solidification is that a "skin" of oxide is incorporated between the ingot surface and the crucible wall. Similar to VAR, the distance between the side of the electrode and the crucible wall is called the annulus. The depth of the slag pool is an important operating parameter that controls the electrical resistance of the system. The depth of immersion of the electrode into the slag is an important parameter in controlling the molten pool shape. As shown in Fig. 6, the heat extraction in ESR is of a much greater magnitude than for VAR. Due to the insulating characteristic of the ingot slag skin, heat extraction in ESR is inherently less efficient than in VAR. Thus, ESR is a process with high thermal inertia and slow responses (change in pool shape) that occur in response to changes in power input.

The presence of an ingot slag skin not only improves the ingot surface quality, but also, more importantly, eliminates the presence of a solute-lean shelf layer on ESR ingots. (As oxide particles from the electrode are dissolved into the slag, they do not agglomerate on the ingot surface.) Because ESR ingots do not have ingot shelf, they are inherently free of the formation of drop-in (discrete) white spots from this source, but drop-in electrode may still be a source of white spots in ESR. Solidification white spots have not been reported in ESR product. However, one consequence of the ingot slag skin is that heat extraction in ESR is less efficient than for VAR. This is shown schematically in Fig. 6 by the difference in pool shape between the two processes. ESR pools tend to be both deeper and more V-shaped (compared to a U-shaped VAR pool). Deep pools favor freckle formation, which can only be counteracted by reducing ingot size. Consequently, the maximum size of ESR ingot produced (for any given alloy system) is smaller than one that can be produced by VAR.

Control of the ESR process is considered from two different aspects: control of pool depth and shape (control of solidification structure) and development of a satisfactory ingot skin. Pool depth and shape are controlled primarily by melt rate (power input). Electroslag remelting generally is run using melt rate control, with continuous amperage adjustments to maintain a uniform melt rate. Due to the high thermal inertia of the ESR process, the melt rate of ESR is more variable than in VAR. A secondary control of pool depth and shape is effected by maintaining uniform, shallow immersion of the electrode in the slag. The passage of molten metal droplets through the slag affects slag resistivity and thus causes variation in the operating voltage of the system. The operating voltage appears as a band of values due to this variation. The width of that band is called the volt swing. The electrode immersion is proportional to the volt swing, and the ram drive of the ESR advances the electrode to maintain the desired swing value.

Production of satisfactory ingot skin is not actively controlled during the melt, but is due to the choice of variables. The most important of these are melt rate, depth of the slag pool, and choice of slag composition. Higher melt rates produce better ingot surfaces. As higher melt rates also produce deeper molten pools and move the process closer to the conditions for freckle formation, selection of the correct balance of parameters is critical.

Slag compositions are based on CaF_2. Additions of CaO, MgO, and Al_2O_3 are made to modify both the resistance of the slag and its melting point. All commercial-purity CaF_2 contains SiO_2. During melting of titanium-bearing alloys, an exchange will take place between the titanium in the alloy and the silicon in the slag. The slag becomes enriched with TiO_2 and the silicon content of the alloy increases until an equilibrium is established, usually within the first few hundred pounds of melting. To minimize this exchange, some commercial slags are buffered with intentional additions of TiO_2.

ESR-VAR Remelting Process. Comparison of the VAR and ESR processes shows that the ESR process is inherently capable of producing cleaner metal but that the VAR process has the capability to produce larger ingots while retaining freedom from alloy-rich defects. The need to produce larger forging stock for gas turbine components has led to the development of a hybrid process: VIM-ESR-VAR (triple melt). In this process, the ESR operation produces a clean, sound electrode for subsequent remelting. The improved (compared to VIM-VAR) electrode quality facilitates control in the VAR operation, producing material with a greater assurance of freedom from alloy-rich segregation (in very large ingot) and a reduced frequency of white spots for all ingot sizes.

In some advanced nickel-base superalloys with high volume fractions (V_f) of γ', even VIM-VAR or VIM-ESR does not provide a satisfactory ingot structure for subsequent hot working. Such superalloys have been processed by P/M techniques (see the section "Powder Processing" in this article).

Other Melting Processes. Electron-beam remelting/refining (EBR) has been evaluated as an alternative process for improving nickel- and iron-nickel-base superalloy properties and processibility through a further lowering of impurity levels and drastic reductions in dross/inclusion content. This process can help produce improved feedstock for casting operations or provide more workable starting ingot for wrought processing. The expanded use of secondary melt processes such as EBR and argon-oxygen decarburization (AOD) will be governed by the extent to which they each provide an economical means for quality processing of nickel- and iron-nickel-base superalloys.

Cobalt Alloy Melting. Melting of cobalt-base superalloys generally does not require the sophistication of vacuum processing. An air induction melt (AIM) is commonly used, but VIM, VIM-VAR, and ESR also have found

application, the latter being used to produce stock for subsequent deformation processing. Alloys containing aluminum or titanium (J-1570) and tantalum or zirconium (MAR-M 302 and MAR-M 509) must be melted by VIM. Vacuum melting of other cobalt-base superalloys may enhance properties such as strength and ductility because of the improved cleanness and compositional control associated with this process.

Deformation Processing (Conversion)

As noted in the preceding section, the structure of superalloy ingots consists of primary dendrites, which are solute lean, and interdendritic regions, which are solute rich. For those alloys with sufficient aluminum, titanium, or niobium to exhibit commercially useful age-hardening response, it is necessary to thermally treat the ingot prior to deformation processing. The thermal treatment is referred to as "homogenization" and consists of extended exposure (48 h is not uncommon) to temperatures approaching the incipient melting temperature of the alloy. The degree of segregation that must be removed by homogenization is a function of alloy composition and melt practice. While homogenization treatments are generally effective in producing a great leveling of microscale concentration differences in superalloys, some residual minor differences may remain in areas of large primary dendrite formation.

Consumably remelted superalloys generally are processed to either forged parts or to sheet/plate. Forged products are produced through an intermediate (billet) forging process, during which refinement of the cast structure is accomplished and a recrystallized grain size is established. Subsequent die forging of increments cut from the billet may further refine the structure or may simply shape the increment into the desired form while retaining the billet structure.

Similarly, ingots to be processed into sheet are often converted by cogging to the desired input size for the rolling mill. The large reductions of the subsequent sheet-rolling process reduce the need for control of cogged structure compared to that required for forging stock. Thus, for some alloys utilizing ESR as the secondary melt process, the ingot may be "cast" into a slab for direct input into the rolling process.

Workability is affected primarily by composition and secondarily by microstructure. Optimal strain and temperature conditions for working of superalloys can be defined by "processing maps." In superalloys, high sulfur levels may constrict the favorable processing range, while additional elements such as magnesium may counteract the effect of sulfur and expand the process range. Unfavorable microstructure may be formed on grain boundaries at any stage in the processing. An example of carbide films developed on prior-grain boundaries is shown in Fig. 7. Such structures will restrict the range of processing conditions. Some superalloys and their nominal forging temperatures are given in Table 6. Superalloys such as IN-100 may have forging temperatures that vary depending on whether isothermal/superplastic forging is used. Grain-refinement requirements also may affect the forging process.

To refine grain structure (to improve low-cycle fatigue resistance and/or stress rupture resistance) in forgings, it is common to process precipitation-hardening superalloys within a more restricted temperature range than is given in Table 6. The temperature range is restricted so that not all the precipitating elements are in solution during forging, thus causing pinning of grain boundaries and restriction of grain growth. The forging conditions must be chosen and controlled so that sufficient strain and temperature are used to allow recrystallization while not allowing the temperature to exceed the solution temperature for the precipitate. The grain structure obtained by such processing must be retained during heat treatment of the forging by either direct aging of the forged structure or aging after a "pseudo" solution heat treatment that does not exceed the true solution temperature of all the precipitate.

A principal use of such processing is in the production of direct-aged IN-718. Figure 8 shows a time-temperature-transformation (TTT) diagram for the precipitates in IN-718. Note that the TTT diagram does not address the relative volume of each precipitate. In IN-718 the volumes of γ'' and δ greatly exceed the volume of γ'. At low temperatures, the metastable precipitates γ' and γ'' predominate. At temperatures above 925 °C (1700 °F), the dominant phase is δ. At temperatures around 925 °C (1700 °F), the δ phase forms in a needlelike Widmanstätten structure. As the temperature is increased, the morphology of the δ phase becomes more blocky. When δ phase is subjected to strain at higher temperatures (980–1010 °C, or 1800–1850 °F), the δ phase is spheroidized. As the temperature is increased, the volume of stable precipitate is decreased, with complete solution occurring at the δ solvus temperature. Thus, hot working in the range from 980 to 1010 °C (1800–1850 °F) causes the formation



Fig. 7 Continuous or nearly continuous MC film produced in grain boundaries of Waspaloy after high-temperature forging soak with no subsequent reduction, followed by normal solution treating and aging. 2700×

Table 6 Forgeability ratings of superalloys

Alloy	Forging temperature °C	Forging temperature °F	Forgeability
A-286	1065	1950	Excellent
IN-901	1095	2000	Good to excellent
Hastelloy X	1095	2000	Excellent
Waspaloy	1080	1975	Good
IN-718	1065	1950	Excellent
Astroloy	1095	2000	Fair to good

Source: Ref 2

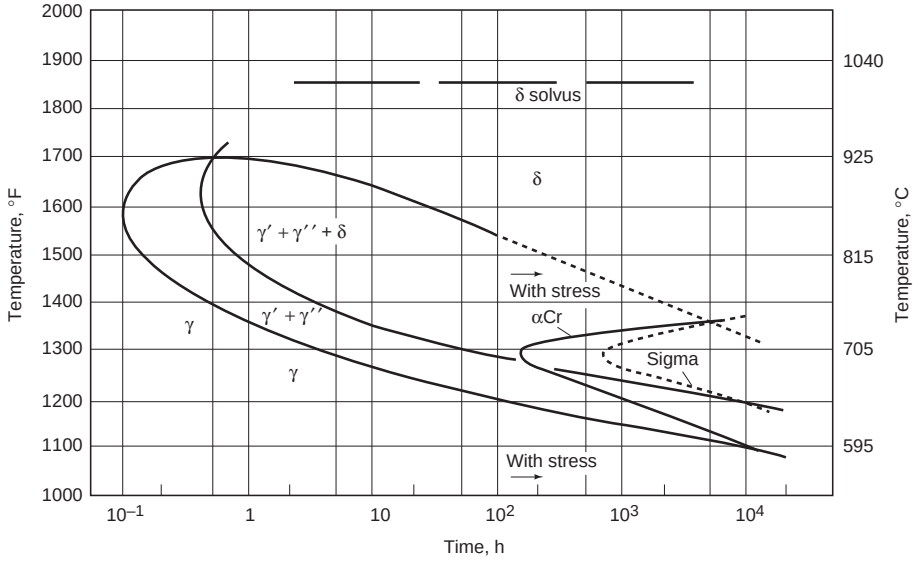


Fig. 8 TTT diagram for IN-718

of a small volume of spheroidized δ phase, which pins grain-boundary growth. The greater percentage of niobium is retained in solution and is available to form the strengthening γ″ precipitate upon subsequent direct heat treatment (aging) of the forged part. Additional information on deformation processing of superalloys can be found in the articles "Forming of Nickel Alloys" and "Forging of Nickel Alloys" in this Handbook.

Powder Processing

As described in the article "Powder-Metallurgy Processing of Nickel Alloys" in this Handbook, powder techniques are being used extensively in superalloy production. Principally, high-strength gas turbine disk alloy compositions such as IN-100 or René 95, which are difficult or impractical to forge by conventional methods, have been powder processed. Inert atmospheres are used in the production of powders, often by gas atomization, and the powders are consolidated by extrusion or hot isostatic pressing (HIP). The latter process has been used either to produce shapes directly for final machining or to consolidate billets for subsequent forging. Extruded or HIP billets often are isothermally forged to configurations for final machining. Minimal segregation, reduced inclusion sizes, ability to use very high V_f γ′ compositions, and ease of grain-size control are significant advantages of the powder process. Reduced costs, particularly through HIP formation of near-net-shape disks, may be possible with powder techniques, but the extent of actual cost savings is a function of alloy and part complexity. An alternative powder-processing technique, the Osprey process (or variants thereof), can create a built-up article by repetitive spraying of powder onto an appropriate mandrel.

Deformation processing of powder-produced articles generally is preferred from a mechanical property standpoint. Designers tend to have more confidence in parts that have been deformation processed to some extent. The deformation processing is thought to enhance the detectability of subsurface imperfections that would limit the fracture mechanics life of the article. It is claimed that Osprey-consolidated parts may be used with or without further deformation processing, but deformation processing would be desirable. Another facet of P/M is the importance of maintaining low gas content in powder products to minimize potential defects. Sources of excessive gas in P/M superalloys include hollow argon-atomized powder particles and container leakage or insufficient evacuation and purging of containers before consolidation.

Powder techniques also have been used to produce turbine blade/vane alloys of the ODS type. Mechanical alloying is the principal technique for introducing the requisite oxide/strain energy combination to achieve maximum properties. Rapid-solidification-rate (RSR) technology has been applied to produce highly alloyed (very high V_f γ′) superalloys and shows promise for advanced gas-turbine applications. Rapid-solidification-rate and ODS alloys can benefit from aligned crystal growth in the same manner as can directionally cast alloys. Directional recrystallization has been used in ODS alloys to produce favorable polycrystalline grain orientations with elongated (high-aspect-ratio) grains parallel to the major loading axis.

Investment Casting

Cobalt-base, high V_f γ′ nickel-base, and IN-718 γ″-hardened superalloys are processed to complex final shapes by investment casting. Iron-nickel-base superalloys are not customarily investment cast. Investment casting permits intricate internal cooling passages and re-entrant angles to be achieved and produces a near-net shape of very precise dimensions. Most investment castings are small random-grain-oriented polycrystalline articles ranging in weight from less than a pound to a few pounds, but columnar-grain and single-crystal parts also are being cast, some as large as 4.5 to 9 kg (10–20 lb). In addition, large investment castings are being made in configurations up to several feet in diameter and hundreds of pounds in weight. A cast alloy commonly used to obtain the economic benefits of large sections is IN-718; a wide range of alloys are cast as smaller parts in polycrystalline, columnar-grain, or single-crystal form. Nickel-base and some cobalt-base superalloy remelting stock for investment casting is produced by VIM. Vacuum induction melted heats of superalloys intended for the investment casting process are much smaller in mass than the VIM heats used to produce stock for wrought alloy processing.

Cast articles are made by creating a pattern in wax or plastic. The pattern is duplicated as many times as necessary, typically using conventionally machined injection tooling. Hollow castings with complex internal features are produced by first creating a ceramic positive replica of the internal hollow passage through injection of a ceramic slurry into a die cavity to form a ceramic core. This core is then placed into the wax injection die and encapsulated with wax. An appropriate number of wax patterns are then attached to a "tree" complete with pourcup, sprue, risers, and so forth to channel metal from the pourcup into the part geometry.

The resulting tree is invested with ceramic of various sizes by dipping the assembled tree into a slurry, applying ceramic granules, and then drying the assembly under controlled conditions. The investing process is performed as many times as needed to build up a satisfactory ceramic coating. The invested tree is dried, and the wax is burned out. Then the investment is fired at a higher temperature to achieve maximum strength through sintering. The resulting mold is ready for use.

Many alloys are investment cast, including VIM superalloys, steels, and aluminum. These metals are melted and poured into the mold and solidified under conditions according to whether the product is to be large or small, and polycrystalline, columnar grained, or single crystal. Grain size in polycrystalline products is controlled by an appropriate primary dip coat in the investment along with mold-metal pour temperatures and selective mold insulation. An example is the Microcast-X method, which makes fine-grained (ASTM 5 to 3) superalloys by utilizing a very low superheat (low pour temperature) and a heated mold. Grain orientation in columnar-grain or single-crystal products is controlled by special furnaces that provide appropriate thermal gradients and by selective filters and/or starter nucleation sites.

After casting, the expendable ceramic shell is removed and the parts are cut from the tree. If the castings possess internal ceramic cores for internal feature fabrication, this core is removed using caustic chemicals. When removed, the positive core gives rise to the negative cavity possessing complex internal features. Most castings are typically heat treated to homogenize the metallurgical structure and precipitation strengthened to optimize mechanical properties. The castings then undergo x-ray inspection (internal defects), fluorescent penetrant inspection (external defects), chemical grain etch (crystal integrity), ultrasonic inspection (wall thickness for hollow parts), and dimensional inspection.

Inclusions, coarse grain size, surface attack in core leaching, core shift, and resulting undersized wall thickness are a few of the problems encountered in investment casting of superalloys. These problems reduce casting yield and cause potential property-level reductions if not properly controlled. Inclusions are controlled by melting technology and the use of filters to eliminate dross. Selective surface attack is controlled by modifying the autoclave leaching processes. In the past several decades, improved shell and core materials and casting mold design plus control of grain size and inclusions have led to improvements in casting yield and, occasionally, improvements in cast part strength. Casting porosity has been a problem in parts having large cross sections and in small parts made of some high V_f γ′ alloys. Hot isostatic pressing techniques used for powder processing have been applied successfully in many instances to eliminate nonsurface-connected porosity, particularly in large castings of iron-nickel- and nickel-base superalloys. Improved fatigue and creep life generally result (Fig. 9), because casting quality is improved by HIP.

Directional-casting technology has become a commonly accepted production process for nickel-base superalloys. Columnar grain directionally solidified (CGDS) structures have been produced by promoting unidirectional heat flow within the furnace during the solidification cycle. Substantial property improvements have resulted for many alloys, Modulus parallel to the natural growth direction is lowered,

leading to improvements in thermal fatigue life, ductility generally is increased, and creep rupture strength (life) is improved through removal of transverse grain-boundary segments. Compositions of CGDS alloys are listed in Table 4.

A logical extension of columnar-grain technology is the production of single crystals of hot-section aircraft gas turbine components. Removal of all grain boundaries and adjustments of alloy composition permitted by the absence of grain boundaries result in single-crystal (SC) article benefits similar to those described for the CGDS process, along with substantial improvements in strength capability. Directional casting to create a SC article provides composition flexibility and opens the possibility of additional alloy development for high-strength nickel-base superalloys. Although initially restricted to relatively small turbine airfoil components of aircraft gas turbines, CGDS, and SC processing has been extended to produce airfoils for large industrial gas turbines. Compositions of alloys designed for SC processing are listed in Table 5. Figure 10 compares the structures of polycrystalline, columnar grain, and SC alloys.

Directional solidification adds problems to those normally encountered in superalloy casting. Increased tendencies for inclusions (owing to the use of hafnium to enhance transverse ductility), separately nucleated grains, grain misorientation, and the tendency for freckle grains (grain nucleation caused by inverse segregation due to dendrite erosion) are causes for casting rejects in CGDS product. Freckles, slivers, low-angle boundaries (LAB), and spurious grains are casting problems in SC production. In both CGDS and SC alloys, surface recrystallization induced by surface strains and excess temperatures in postcast processing can be a cause for casting rejection.

Although cobalt-base superalloys can be directionally solidified in columnar grain structures, they are invariably cast as polycrystalline parts. Single-crystal manufacture of cobalt-base superalloys may be possible but has not been reported. It is doubtful that sufficiently significant property benefits would result from single-crystal or columnar-grain cobalt-base superalloys to warrant the expense of such processing.

A new technology known as rapid prototyping has enabled significant changes within the casting industry by eliminating the need for many of the investment casting process steps. This elimination has led to significant cost and lead-time reduction for development hardware. Processes such as stereolithography, selective laser sintering, and other three-dimensional printing technology can provide casting patterns without the use of costly conventional wax or ceramic injection dies. Special machines can take a three-dimensional computer-aided design (CAD), convert the design into cross-sectional layers, and build a three-dimensional representation of the CAD geometry in plastic, wax, or polymer. Some processes can directly build (from three-dimensional CAD geometry) three-dimensional ceramic shells into which metal can be poured. Other technologies focused on direct metal fabrication from three-dimensional CAD geometry are being developed. These technologies have revolutionized the industry in allowing faster development through low-cost iterative design so that design concepts can be transitioned to production rapidly.

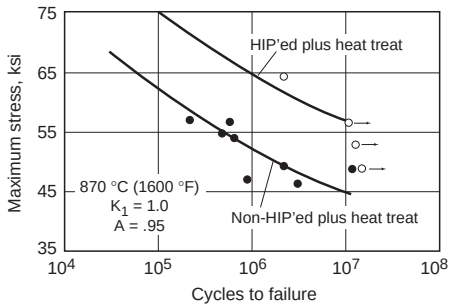


Fig. 9 Beneficial effect of HIP on high-cycle fatigue resistance of René 80

Joining

Cobalt-base superalloys are readily joined by gas metal arc welding (GMAW) or gas tungsten arc welding (GTAW) techniques. Cast alloys such as WI-52 and wrought alloys such as Haynes 188 have been extensively welded. Filler metals generally have been less highly alloyed cobalt-base alloy wire, although parent rod or wire (the same composition as the alloy being welded) have been used. Cobalt-base superalloy sheet also is successfully welded by resistance techniques. Gas turbine vanes that crack in service have been repair welded using the above techniques (e.g., WI-52 vanes using L605 filler rod and 540 °C, or 1000 °F, preheat). Appropriate preheat techniques are needed in GMAW and GTAW to eliminate tendencies for hot cracking. Electron beam welding (EBW) and plasma arc welding (PAW) can be used on cobalt-base superalloys, but usually are not required in most applications because alloys of this class are so readily weldable.

Nickel- and iron-nickel-base superalloys are considerably less weldable than cobalt-base superalloys. Because of the presence of the γ' strengthening phase, the alloys tend to be susceptible to hot cracking (weld cracking) and postweld heat treatment (PWHT) cracking (strain age or delay cracking). The susceptibility to hot cracking is directly related to the aluminum and titanium contents (γ' formers), as shown in Fig. 11. Hot cracking occurs in the weld heat-affected zone (HAZ), and the extent of cracking varies with alloy composition and weldment restraint.

Nickel- and iron-nickel-base superalloys have been welded by GMAW, GTAW, EBW, laser, and PAW techniques. Filler metals, when used, usually are weaker, more ductile austenitic alloys so as to minimize hot cracking. Occasionally, base-metal compositions are employed as fillers. Welding is restricted to the lower V_f γ' ($\leq$0.35) alloys, generally in the wrought condition. Cast alloys of high V_f γ'' have not been consistently welded successfully when filler metal is required, as in weld repair

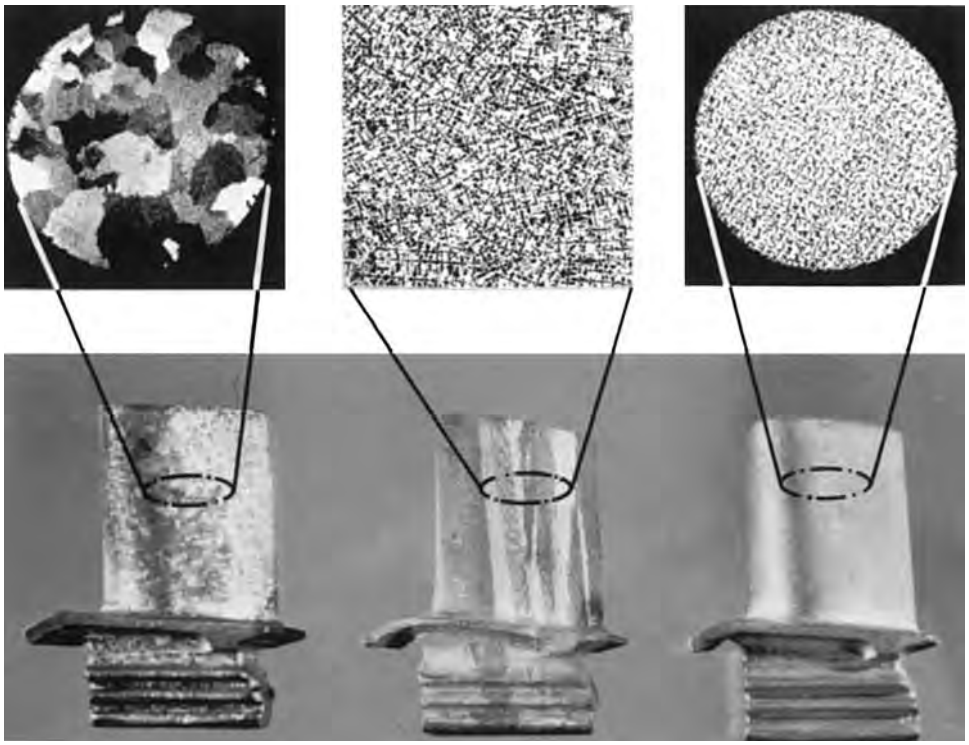


Fig. 10 Comparison of macro- and microstructures in (from left) equiaxed, directionally solidified, and SC turbine blades

of service parts. However, EBW can be used to make structural joints in such alloys. Friction or inertia welding also has been successfully applied to the lower V_f γ' alloys.

Because of their γ' strengthening mechanism and capability, many nickel- and iron-nickel-base superalloys are welded in the solution heat treated condition. Special preweld heat treatments have been used for some alloys. Nickel-niobium alloys, as typified by IN-718, have unique welding characteristics. The hardening phase, γ'', is precipitated more sluggishly at a lower temperature than is γ' so that the attendant welding-associated strains that must be redistributed are more readily accommodated in the weld metal and HAZ. The alloy is welded in the solution-treated condition and then given a postweld stress-relief-and-aging treatment that causes γ' precipitation. Some alloys, such as A-286, are inherently difficult to weld despite only moderate levels of γ' hardeners. There is some evidence that high-titanium alloys may be more difficult to weld than alloys of similar V_f γ' relying on high aluminum/titanium ratios for their strength capabilities.

Weld techniques for superalloys must address not only hot cracking but also PWHT cracking, particularly as it concerns microfissuring (microcracking), which can be subsurface and thus difficult to detect. Tensile and stress rupture strengths may be hardly affected by microfissuring, but fatigue strengths can be drastically reduced.

In addition to being weldable by the usual fusion welding techniques discussed above, nickel- and iron-nickel-base alloys can be resistance welded when in sheet form; brazing, diffusion bonding, and transient liquid phase (TLP) bonding also have been employed to join these alloys. Brazed joints tend to be more ductility limited than welds; diffusion bonding of superalloys has not found consistent application. Transient liquid phase bonding has been found to be very useful, principally in turbine parts of aircraft gas turbine engines. The distinguishing characteristic of TLP bonding that produces its excellent integrity is that, although a lower-temperature bond is made as in brazing, subsequent diffusion occurs at the bonding temperature, leading to a fully solidified joint that has a composition similar to that of the base metal and a microstructure indistinguishable from it. Consequently, the resultant joint can have a melting temperature and properties very similar to those of the base metal. Additional information on welding of precipitation-hardenable nickel-base superalloys can be found in the article "Welding and Brazing of Nickel Alloys" in this Handbook.

Properties and Microstructure

The principal microstructural variables of superalloys are the precipitate amount and its morphology, grain size and shape, and carbide distribution. Nickel and iron-nickel-base alloys of the titanium/aluminum type have their properties controlled by all three variables; nickel-niobium alloys have the additional variable of δ phase distribution; cobalt-base superalloys are not affected by the first variable. Structure control is achieved through composition selection/modification and by processing. For a given nominal composition, there are property advantages and disadvantages of the structures produced by deformation processing and by casting. Cast superalloys generally have coarser grain sizes, more alloy segregation, and improved creep and rupture characteristics. Wrought superalloys generally have more uniform, and usually finer, grain sizes and improved tensile and fatigue properties.

Nickel- and iron-nickel-base superalloys of the Ni-Ti/Al type typically consist of γ' dispersed in a γ matrix, and the strength increases with increasing V_f γ'. The lowest V_f amounts of γ' are found in iron-nickel-base and first-generation nickel-base superalloys, where V_f γ' is generally less than about 0.25 (25 vol%). The γ' is commonly spheroidal in lower V_f γ' alloys but often cuboidal in higher V_f γ' (≥0.35) nickel-base superalloys. The nickel-niobium-type superalloys typically consist of γ'' dispersed in a γ matrix, with some γ' present as well. The inherent strength capability of the γ'- and γ''-hardened superalloys is controlled by the intragranular distribution of the hardening phases; however, the usable strength in polycrystalline alloys is determined by the condition of the grain boundaries, particularly as affected by the carbide-phase morphology and distribution, and in the case of nickel-niobium alloys, additionally by the distribution of the δ phase.

Satisfactory properties in Ni-Ti/Al alloys are achieved by optimizing the γ' V_f and morphology (not necessarily independent characteristics) in conjunction with securing a dispersion of discrete globular carbides along the grain boundaries (Fig. 12). Discontinuous (cellular) carbide or γ' at grain boundaries increases surface area and drastically reduces rupture life, even though tensile and creep strength may be relatively unaffected.

Wrought nickel- and iron-nickel-base superalloys generally are processed to have optimal tensile and fatigue properties. At one time, when wrought alloys were used for creep-limited applications, such as gas turbine high-pressure turbine blades, heat treatments different from those used for tensile-limited uses were applied to the same nominal alloy composition to maximize creep-rupture life. Occasionally, the nominal composition of an alloy such as IN-100 or U-700/Astroloy varies according to whether it is to be used in the cast or the wrought condition.

Evolution of Microstructure

Effects of Alloying Elements on Microstructure. Superalloys contain a variety of elements in a large number of combinations to produce desired effects. Some elements go into solid solution to provide one or more of the following: strength (molybdenum, tantalum, tungsten, rhenium); oxidation resistance (chromium, aluminum); phase stability (nickel); and increased volume fractions of favorable secondary precipitates (cobalt). Other elements are added to form hardening precipitates such as γ' (aluminum, titanium) and γ'' (niobium). Minor

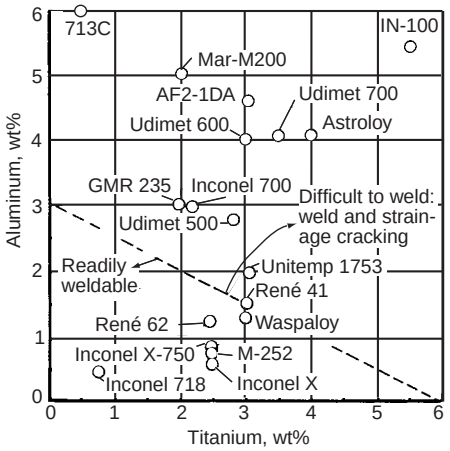


Fig. 11 Weldability diagram for some γ'-strengthened iron-nickel- and nickel-base superalloys, showing influence of total aluminum + titanium hardeners

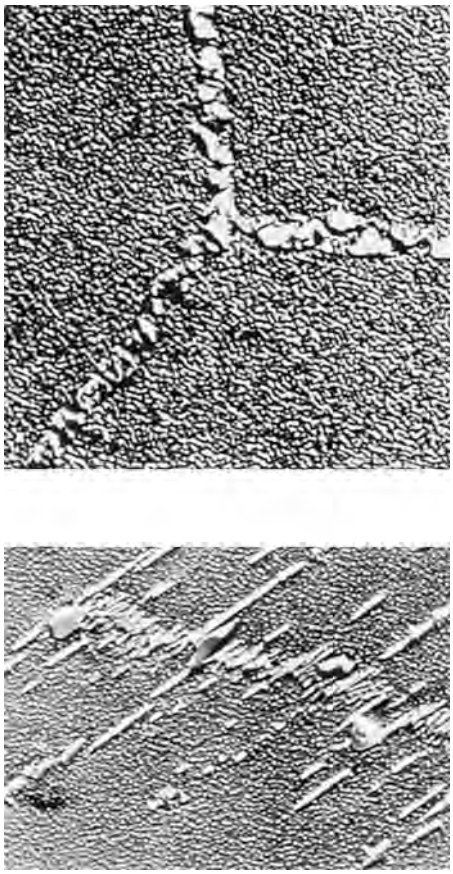


Fig. 12 Carbide precipitation in Waspaloy. (a) Favorable discrete grain-boundary type (10,000×). (b) Less favorable zipperlike, discontinuous type (6800×)

elements (carbon, boron) are added to form carbides and borides; these and other elements (magnesium) are added for purposes of tramp-element control. Some elements (boron, zirconium, hafnium) also are added to promote grain-boundary effects other than precipitation or carbide formation. Lanthanum has been added to some alloys to promote oxidation resistance, and yttrium has been added to coatings to enhance oxidation resistance. A major addition to nickel-base superalloy chemistry in recent years has been the element rhenium, which has extended the temperature capability of the CGDS and SC alloys. Rhenium appears to produce these improvements by significantly reducing the coarsening rate for γ'. Many elements (cobalt, molybdenum, tungsten, rhenium, chromium, etc.), although added for their favorable alloying qualities, can participate, in some circumstances, in undesirable phase formation (σ, μ, Laves, etc.).

Some of these elements produce readily discernible changes in microstructure; others produce more subtle microstructural effects. The precise microstructural effects produced are functions of processing and heat treatment. The most obvious microstructural effects involve precipitation of geometrically close-packed (gcp) phases such as γ', formation of carbides, and formation of topologically close-packed (tcp) phases such as s. Even when the type of phase is specified, microstructure morphology can vary widely—for example, script versus blocky carbides, cuboidal versus spheroidal γ', cellular versus uniform precipitation, acicular versus blocky σ, and discrete γ' versus γ' envelopes. Typical nickel-base superalloy microstructures as they evolved from spheroidal to cuboidal γ' are depicted in Fig. 13.

The γ' phase is an ordered ($L1_2$) intermetallic fcc phase having the basic composition $Ni_3(Al,Ti)$. Alloying elements affect γ' mismatch with the matrix γ phase, γ' antiphase-domain-boundary (APB) energy, γ' morphology, and γ' stability. A related phase, η, is an ordered ($D0_{24}$) hexagonal phase of composition Ni_3Ti that may exist in a metastable form as γ' before transforming to η. Other types of intermetallic phases, such as δ, orthorhombic Ni_3Nb, or γ'', bct ordered ($D0_{22}$) Ni_3Nb strengthening precipitate, have been observed.

Carbides also are an important constituent of superalloys. They are particularly essential in the grain boundaries of cast polycrystalline alloys for production of desired strength and ductility characteristics. Carbide levels in wrought alloys always have been below those in cast alloys, but some carbide has been deemed desirable for achieving optimal strength properties. As cleanliness of superalloys has increased, the carbide levels in wrought alloys have been lowered. Carbides, at least large ones, become the limiting fracture mechanics criteria for modern wrought superalloy application.

Carbides may provide some degree of matrix strengthening, particularly in cobalt-base alloys, and are necessary for grain-size control in some wrought alloys. Some carbides are virtually unaffected by heat treatment, while others require such a step to be present. Various types of carbides are possible depending on alloy composition and processing. Some of the important types are MC, M_6C, $M_{23}C_6$, and M_7C_3, where M stands for one or more types of metal atom. in many cases, the carbides exist jointly; however, they usually are formed by sequential reactions in the solid state following breakdown of the MC that normally is formed in the molten state. The common carbide-reaction sequence for many superalloys is MC to $M_{23}C_6$, and the important carbide-forming elements are chromium ($M_{23}C_6$, M_7C_3); titanium, tantalum, niobium, and hafnium (MC); and molybdenum and tungsten (M_6C). Boron may participate somewhat interchangeably with carbon and produces such phases as MB_{12}, M_3B_2, and others. One claim made for boron is that primary borides formed by adjustment of boron/carbon ratio are more amenable to morphological modification through heat treatment.

Alloying Elements to Improve Oxidation Resistance. All superalloys contain some chromium plus other elements to promote resistance to environmental degradation. The role of chromium is to promote Cr_2O_3 formation on the external surface of an alloy. When sufficient aluminum is present, formation of the more protective oxide Al_2O_3 is promoted when oxidation occurs. A chromium content of 6 to 22 wt% generally is common in nickel-base superalloys, whereas a level of 20 to 30 wt% Cr is characteristic of cobalt-base superalloys, and a level of 15 to 25 wt% Cr is found in iron-nickel-base superalloys. Amounts of aluminum up to approximately 6 wt% can be present in nickel-base superalloys.

Effect of Tramp Elements on Microstructure. A discussion of the function of alloying elements in terms of microstructure would be incomplete without mention of the tramp elements. Elements such as silicon, phosphorus, sulfur, lead, bismuth, tellurium, selenium, and silver, often in amounts as low as the parts per million (ppm) level, have been associated with property-level reductions, but they are not visible optically or with an electron microscope. Microprobe and Auger spectroscopic analyses have determined that grain boundaries can be decorated with tramp elements at high local concentrations. Elements such as magnesium tend to tie up some detrimental elements such as sulfur in the form of a compound, and titanium tends to tie up the element nitrogen as TiN. In such cases, these and other similar compounds often are visible in the microstructure.

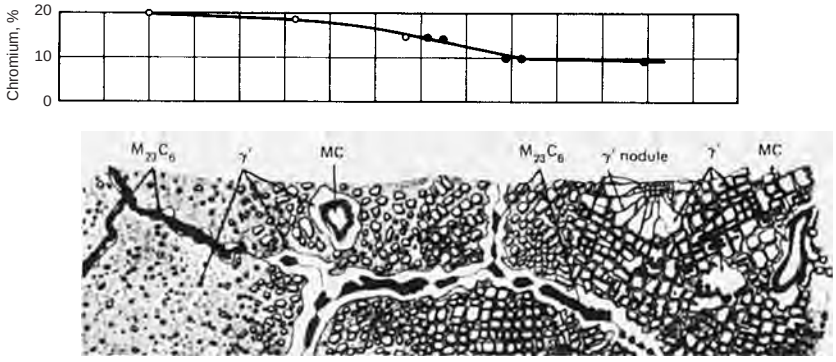


Fig. 13 Qualitative description of the evolution of microstructure and chromium content of nickel-base superalloys. Source: Adapted from Ref 3. Original source: Ref 4

Function of Processing

Processing is considered to be the art/science of rendering the superalloy material into its final form. Processing and alloying elements are interdependent. The general microstructural changes brought about by processing result from the overall alloy composition plus the processing sequence. The role of heat treatment on phases is referred to when prior microstructural effects are considered; the role of composition on phases has been discussed above. Tables 7 and 8 provide information pertaining to typical heat treatment cycles for a variety of common superalloys.

The three most significant process-related microstructural variables other than those resulting from composition/heat treatment interactions are the size, shape, and orientation (in anisotropic structures) of the grains. Grain size varies considerably from cast to wrought structure, generally being significantly smaller for the latter. Special processing—for example, directional solidification or directional recrystallization—can effect changes not only in grain size but also in grain shape and orientation, which significantly alter mechanical and physical properties. Corrosion reactions, however, are primarily functions of composition.

Effects of Prior Microstructure on Properties

Nickel- and iron-nickel-base superalloys may be hardened by γ' or γ'' precipitation (in an fcc γ matrix). The γ' in iron-nickel-base and first-generation nickel-base alloys generally is spheroidal, whereas the γ' in later-generation nickel-base alloys generally is cuboidal (Fig. 14). The γ'' phase is disk shaped. The V_f of γ' is generally approximately 0.2 or less in wrought iron-nickel-base superalloys, but may exceed 0.6 in nickel-base superalloys. There are insufficient alloy compositions to provide knowledge of a range for V_f γ'' in γ''-hardened alloys.

Gamma Prime Precipitation. Strengthening by precipitate particles is related to many factors; in the case of γ', the most direct correlations can be made with V_f of γ' and with γ' particle size. However, the correlation between strength and γ' size may be difficult to prove in commercial alloys over the range of particle sizes available. Before the age-hardening peak is reached during precipitation, the operative strengthening mechanism involves cutting of γ' particles by dislocations, and strength increases with increasing γ' size (Fig. 15) at constant V_f of γ'. After the age-hardening peak is reached, strength decreases with continuing particle growth because dislocations no longer cut γ' particles but rather bypass them. This effect can be demonstrated for tensile or hardness behavior in low V_f γ' alloys (A-286, Incoloy 901, Waspaloy), but is not as readily apparent in high V_f γ' alloys such as MAR-M-246, IN-100, and so forth. For creep rupture, the effects are less well defined; however, uniform fine-to-moderate γ' sizes (0.25–0.5 μm) are preferred to coarse or hyperfine γ' for optimal properties.

Alloy strength in titanium/aluminum hardened alloys clearly depends on V_f γ'. The V_f γ' and thus strength can be increased to a point by adding more hardener elements (aluminum, titanium). Alloy strengths increase as aluminum + titanium content increases (Fig. 16), and also as the aluminum-to-titanium ratio increases. In wrought alloys, the γ' usually exists as a bimodal (duplex) distribution of fine γ', and all of the aluminum + titanium contributes effectively to the hardening process. In cast alloys, the character of the γ' precipitate developed can be extremely variable because of the effects of segregation and cooling rate. Large amounts of γ-γ' eutectic and coarse γ' may be

Table 7 Typical solution-treating and aging cycles for wrought superalloys

	Solution treating				Aging			
	Temperature			Cooling	Temperature			Cooling
Alloy	°C	°F	Time, h	procedure	°C	°F	Time, h	procedure
Iron-base alloys								
A-286	980	1800	1	Oil quench	720	1325	16	Air cool
Discaloy	1010	1850	2	Oil quench	730	1350	20	Air cool
					650	1200	20	Air cool
N-155	1165–1190	2125–2175	1	Water quench	815	1500	4	Air cool
Incoloy 903	845	1550	1	Water quench	720	1325	8	Furnace cool
					620	1150	8	Air cool
Incoloy 907	980	1800	1	Air cool	775	1425	12	Furnace cool
					620	1150	8	Air cool
Incoloy 909	980	1800	1	Air cool	720	1325	8	Furnace cool
					620	1150	8	Air cool
Incoloy 925	1010	1850	1	Air cool	730(a)	1350(a)	8	Furnace cool
					620	1150	8	Air cool
Nickel-base alloys								
Astroloy	1175	2150	4	Air cool	845	1550	24	Air cool
	1080	1975	4	Air cool	760	1400	16	Air cool
Custom Age 625 PLUS	1038	1900	1	Air cool	720	1325	8	Furnace cool
					620	1150	8	Air cool
Inconel 901	1095	2000	2	Water quench	790	1450	2	Air cool
					720	1325	24	Air cool
Inconel 625	1150	2100	2	(b)	…	…	…	…
Inconel 706	925–1010	1700–1850	…	…	845	1550	3	Air cool
					720	1325	8	Furnace cool
					620	1150	8	Air cool
Inconel 706(c)	980	1800	1	Air cool	730	1350	8	Furnace cool
					620	1150	8	Air cool
Inconel 718	980	1800	1	Air cool	720	1325	8	Furnace cool
					620	1150	8	Air cool
Inconel 725	1040	1900	1	Air cool	730(a)	1350	8	Furnace cool
					620	1150	8	Air cool
Inconel X-750	1150	2100	2	Air cool	845	1550	24	Air cool
					705	1300	20	Air cool
Nimonic 80A	1080	1975	8	Air cool	705	1300	16	Air cool
Nimonic 90	1080	1975	8	Air cool	705	1300	16	Air cool
René 41	1065	1950	0.5	Air cool	760	1400	16	Air cool
Udimet 500	1080	1975	4	Air cool	845	1550	24	Air cool
					760	1400	16	Air cool
Udimet 700	1175	2150	4	Air cool	845	1550	24	Air cool
	1080	1975	4	Air cool	760	1400	16	Air cool
Waspaloy	1080	1975	4	Air cool	845	1550	24	Air cool
Cobalt-base alloys								
S 816	1175	2150	1	(b)	760	1400	12	Air cool

Note: Alternate treatments may be used to improve specific properties. (a) If furnace size/load prohibits fast heat up to initial age temperature, a controlled ramp up from 590–730 °C (1100–1350 °F) is recommended. (b) To provide adequate quenching after solution treating, it is necessary to cool below about 540 °C (1000 °F) rapidly enough to prevent precipitation in the intermediate temperature range. For sheet metal parts of most alloys, rapid air cooling will suffice. Oil or water quenching is frequently required for heavier sections that are not subject to cracking. (c) Heat treatment of Inconel 706 to enhance tensile properties instead of creep resistance for tensile-limited applications

Table 8 Typical heat treatments for precipitation-strengthened cast superalloys

Alloy	Heat treatment (temperature/duration in h/cooling)
Polycrystalline (conventional) castings	
B-1900/B-1900 + Hf	1080 °C (1975 °F)/4/AC + 900 °C (1650 °F)/10/AC
IN-100	1080 °C (1975 °F)/4/AC + 870 °C (1600 °F)/12/AC
IN-713	As-cast
IN-718	1095 °C (2000 °F)/1/AC + 955 °C (1750 °F)/1/AC + 720 °C (1325 °F)/8/FC + 620 °C (1150 °F)/8/AC
IN-718 with HIP	1150 °C (2100 °F)/4/FC + 1190 °C (2175 °F)/4/15 ksi (HIP) + 870 °C (1600 °F)/10/AC + 955 °C (1750 °F)/1/AC + 730 °C (1350 °F)/8/FC + 655 °C (1225 °F)/8/AC
IN-738	1120 °C (2050 °F)/2/AC + 845 °C (1550 °F)/24/AC
IN-792	1120 °C (2050 °F)/4/RAC + 1080 °C (1975 °F)/4/AC + 845 °C (1550 °F)/24/AC
IN-939	1160 °C (2120 °F)/4/RAC + 1000 °C (1830 °F)/6/RAC + 900 °C (1650°F)/24/AC + 700 °C (1290 °F)/16/AC
MAR-M 246 + Hf	1220 °C (2230 °F)/2/AC + 870 °C (1600 °F)/24/AC
MAR-M 247	1080 °C (1975 °F)/4/AC + 870 °C (1600 °F)/20/AC
René 41	1065 °C (1950 °F)/3/AC + 1120 °C (2050 °F)/0.5/AC + 900 °C (1650 °F)/4/AC
René 77	1163 °C (2125 °F)/4/AC + 1080 °C (1975 °F)/4/AC + 925 °C (1700 °F)/24/AC + 760 °C (1400 °F)/16/AC
René 80	1220 °C (2225 °F)/2/GFQ + 1095 °C (2000 °F)/4/GFQ + 1050 °C (1925 °F)/4/AC + 845 °C (1550 °F)/16/AC
Udimet 500	1150 °C (2100 °F)/4/AC + 1080 °C (1975 °F)/4/AC + 760 °C (1400 °F)/16/AC
Udimet 700	1175 °C (2150 °F)/4/AC + 1080 °C (1975 °F)/4/AC + 845 °C (1550 °F)/24/AC + 760 °C (1400 °F)/16/AC
Waspaloy	1080 °C (1975 °F)/4/AC + 845 °C (1550 °F)/4/AC + 760 °C (1400 °F)/16/AC
Columnar-grain (CG) castings	
DS MAR-M 247	1230 °C (2250 °F)/2/GFQ + 980 °C (1800 °F)/5/AC + 870 °C (1600 °F)/20/AC
DS MAR-M 200+Hf	1230 °C (2250 °F)/4/GFQ + 1080 °C (1975 °F)/4/AC + 870 °C (1600 °F)/32/AC
DS René 80H	1190 °C (2175)/2/GFQ + 1080 °C (1975 °F)/4/AC + 870 °C (1600 °F)/16/AC
Single-crystal castings	
CMSX-2	1315 °C (2400 °F)/3/GFQ + 980 °C (1800 °F)/5/AC + 870 °C (1600 °F)/20/AC
PWA 1480	1290 °C (2350 °F)/4/GFQ + 1080 °C (1975 °F)/4/AC + 870 °C (1600 °F)/32/AC
René N4	1270 °C (2320 °F)/2/GFQ + 1080 °C (1975 °F)/4/AC + 900 °C (1650 °F)/16/AC

AC, air cooling; FC, furnace cooling; GFQ, gas furnace quench; RAC, rapid air cooling

developed during solidification. Subsequent heat treatment can modify these structures. Bimodal and trimodal γ′ distributions plus γ-γ′ eutectic can be found in cast alloys after heat treatment. Solution heat treatments at temperatures sufficiently high to homogenize the alloy and dissolve coarse γ′ and the eutectic γ-γ′ constituents for subsequent reprecipitation as a uniform fine γ′ have improved creep capability. However, incipient melting temperatures limit the homogenization possible in many polycrystalline or CGDS super-alloys. For a columnar-grain nickel-base superalloy, a direct correlation has been found to exist between creep rupture life at 980 °C (1800 °F) and the V_f of fine γ′ (Fig. 17).

In general, to achieve the greatest hardening in γ′-hardened alloys it is necessary to solution heat treat the alloys above the γ′ solvus. One or more aging treatments are used to optimize the γ′ distribution and to promote transitions in other phases such as carbides. In some alloys, several intermediate and several lower-temperature aging treatments are used; in cast alloys or in very high V_f γ′ wrought alloys, a coating cycle or high-temperature aging treatment may precede the intermediate-temperature aging cycle. When multiple aging treatments are used, a superalloy may show the bimodal or trimodal γ′ distribution described above. An essential feature of γ′ hardening in nickel-base superalloys is that a temperature fluctuation that dissolves some γ′ does not necessarily produce permanent property damage, because subsequent cooling to normal operating conditions reprecipitates γ′ in a useful form.

In the final analysis, it is not possible to judge alloy performance by considering just the γ′ phase. The strength of γ′-hardened grains must be balanced by grain-boundary strength. If the γ′-hardened matrix becomes much stronger relative to grain boundaries, then premature failure occurs because stress relaxation at the grain boundaries becomes difficult.

Gamma Double Prime Precipitation. The γ″ phase relationship to properties has not been studied extensively. Strength will be a function of V_f of γ″; however, any quantitative relationships established for γ′-hardened alloys will not hold for γ″-hardened alloys because of a difference in precipitate morphology (the γ′-hardened alloys use initial precipitates that are cuboids or spheres, while the γ″ precipitates are disks). The nickel-niobium alloys tend to have reversion or dissolution of the strengthening phase at relatively low temperatures. Bimodal γ″ distributions are not necessarily found, but γ″ coupled with γ′ distributions form.

Heat treatments for the nickel-niobium alloys attempt to optimize the distribution of the γ″ phase as well as to control grain size. Although for many years, a sequence of solution treatment followed by two-step aging was the preferred route to an appropriate γ″ distribution after an article was forged, this is no longer the case. This sequence has been replaced in most instances by a direct-age process after cooling of the nickel-niobium alloy article from the forging temperature. Uniform γ″ distributions with attendant γ′ precipitate are formed. See the following discussion and the prior discussion of direct aging in IN-718 in the "Deformation Processing" section.

The practical use of γ″ precipitation is restricted to nickel-base alloys with niobium additions in excess of 4 wt%. IN-718 is the outstanding example of an alloy in which γ″ formation has been commercially exploited. The V_f of γ″ in IN-718 is substantially in excess of that of γ′. Both γ″ and γ′ will be found in alloys where γ″ is present, but γ″ will be the predominant strengthening agent. Although the strengthening behavior of γ″ phase has not been studied, similar considerations to γ′ behavior as described earlier probably pertain; that is, there will be an optimal γ″ size and V_f for strength. The most significant feature of γ″ is probably the ease with which it forms at moderate temperatures after prior solutioning

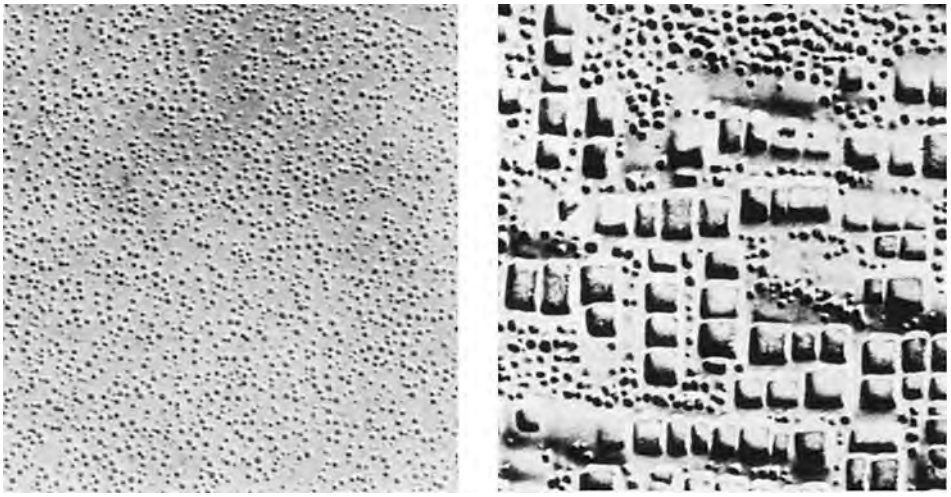


Fig. 14 Wrought nickel-base superalloys showing spheroidal nature of early (low V_fγ′) alloys (Waspaloy, left) and cuboidal nature of later (higher V_fγ′) alloys (U-700, right). Note secondary (cooling) γ′ between primary cuboidal γ′ particles in U-700. Original magnification, 6800×

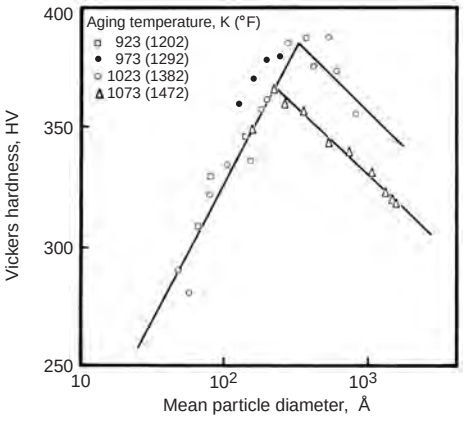


Fig. 15 Strength (hardness) versus particle diameter in a nickel-base superalloy. Cutting occurs at low particle sizes, bypassing at larger sizes. Note that aging temperature also affects strength in conjunction with particle size.

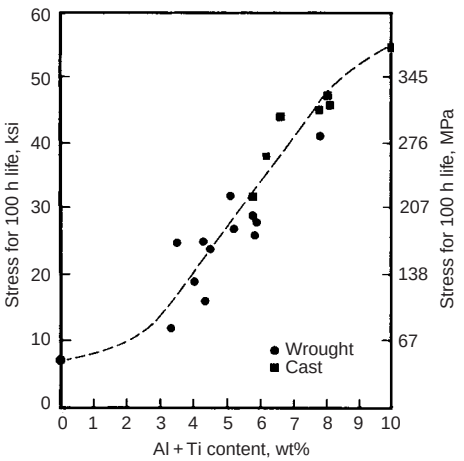


Fig. 16 Effect of aluminum + titanium content on strength of wrought and cast nickel-base superalloys at 870 °C (1600 °F)

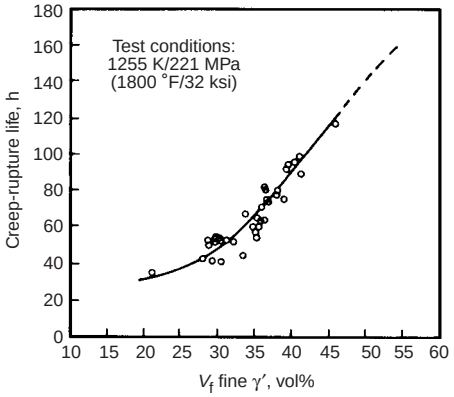


Fig. 17 Increase in creep rupture life with increase in V_f of fine γ′, demonstrated in a columnar-grain, directionally solidified nickel-base superalloy, PWA 1422 (variant of MAR-M 200, with hafnium addition)

by heat treatment or joining processes. Because of this behavior, a γ″-hardened alloy can be aged, after welding, to produce a fully strengthened structure with exceptional ductility.

The γ″ phase, not normally a stable phase, can convert to γ′ and δ Ni_3Nb on longtime exposure. The strength of γ′ is additive to that of γ″ phase. A lack of notch ductility in IN-718 has been associated with a γ″ precipitate-free zone (PFZ); the γ″ PFZ can be eliminated and ductility restored by appropriate heat treatment. Alloys hardened with γ″ phase achieve high tensile strengths and very good creep-rupture properties at lower temperatures, but the conversion of γ″ to γ and δ above approximately 675 °C (1250 °F) causes a sharp reduction in strength.

Carbide Precipitation: Grain-Boundary Hardening. Carbides exert a profound influence on properties by their precipitation on grain boundaries. In most superalloys, $M_{23}C_6$ forms at the grain boundaries after a postcasting or postsolution treatment thermal cycle such as aging. Chains of discrete globular $M_{23}C_6$ carbides were found to optimize creep rupture life by preventing grain-boundary sliding in creep rupture while concurrently providing sufficient ductility in the surrounding grain for stress relaxation to occur without premature failure.

In contrast, if carbides precipitate as a continuous grain-boundary film, properties can be severely degraded. $M_{23}C_6$ films were reported to reduce impact resistance of M252, and MC films were blamed for lowered rupture lives and ductility in forged Waspaloy. At the other extreme, when no grain-boundary carbide precipitate is present, premature failure will also occur because grain-boundary movement essentially is unrestricted, leading to subsequent cracking at grain-boundary triple points.

The role of carbides at grain boundaries in iron-nickel-base superalloys is less well documented than for nickel-base alloys, although detrimental effects of carbide films have been reported. Studies of specific effects of grain-boundary carbides in cobalt-base alloys are even more sparse, because the carbide distribution in cobalt-base alloys arises from the original casting or on cooling after mill annealing for wrought cobalt-base alloys. The significantly greater carbon content of cobalt-base alloys leads to much more extensive grain-boundary carbide precipitation than in nickel- and iron-nickel-base alloys. Carbides at grain boundaries in cast cobalt-base alloys appear as eutectic aggregates of M_6C, $M_{23}C_6$, and fcc γ cobalt-base solid solution. No definitive study of the effects of varied carbide forms in grain boundaries on the mechanical behavior of cobalt-base superalloys has been reported.

The lamellar eutectic (carbides-γ Co) nature of carbides ($M_{23}C_6$-M_6C) in cast cobalt-base superalloys is interesting. A somewhat similar morphology of $M_{23}C_6$, occurring when it is precipitated in cellular form in nickel- and iron-nickel-base alloys, leads to mechanical-property loss in such alloys, but lamellar eutectic does not seem to degrade cast cobalt-base alloy properties. Cellular growth in nickel-base alloys was found to occur when a high supersaturation of carbon produced by solution heat treatment was not relieved by an intermediate precipitation treatment prior to aging at 705 to 760 °C (1300–1400 °F). The ductility of a nickel-base superalloy also was impaired by a different type of precipitation—namely, Widmanstätten M_6C at grain and twin boundaries. However, formation of intragranular Widmanstätten M_6C after exposure of B-1900 nickel-base alloy did not appear to reduce properties.

Another effect produced by grain-boundary $M_{23}C_6$ carbide precipitation is the occasional formation, on either side of the boundary, of a zone depleted in γ′ precipitate. These PFZs may have significant effects on rupture life of nickel- and iron-nickel-base superalloys. If such zones should become wide or much weaker than the matrix, deformation would concentrate there, resulting in early failure. The more complex (higher V_f γ′) alloys do not show significant PFZ effects, probably because of their higher saturation with regard to γ′-forming elements. An effect seen concurrently with PFZ and not clearly separated from it is the γ′ envelope produced by breakdown of TiC and consequent formation of $M_{23}C_6$ or M_6C + γ′ (from the excess titanium). Not only is the role of the γ′ envelope insufficiently established, but there is also the remote possibility that the excess titanium-rich area is really either η or a metastable γ′ that could transform to η in use.

Carbide Precipitation: Matrix or General Hardening. Carbides affect the creep rupture strengths of cobalt-base superalloys and some nickel- and iron-nickel base superalloys by formation within grains. In cobalt-base cast superalloys, script MC carbides are liberally interspersed within grains, causing a form of dispersion hardening that is not of a large magnitude owing to its relative coarseness. The distribution of carbides in cast alloys can be modified by heat treatment, but strength levels attained at all but the highest temperatures are substantially less than those of the γ′-hardened alloys. Consequently, cast cobalt-base alloys generally are not heat treated except in a secondary sense through the coating diffusion heat treatment of 4 h at 1065 to 1120 °C (1950–2050 °F) sometimes applied.

Wrought cobalt-base superalloys have carbide modifications produced during the fabrication sequence. Carbide distributions in wrought alloys result from the mill anneal after final working. Properties are largely a result of grain size, refractory-metal content, and carbon level, which indicates the V_f of carbides available for hardening.

True solutioning, in which all minor constituents are dissolved, is not possible in most cobalt-base superalloys, because melting often occurs before all the carbides are solutioned. Some enhancement of creep rupture behavior has been achieved by heat treatment. Rupture-time improvements can be gained by aging a modified Vitallium alloy (Fig. 18); larger increases have been produced by increasing the carbon content of the alloy. Solution treating and aging is not suitable for producing stable cobalt-base superalloys for use above 815 °C (1500 °F) because of carbide dissolution or overaging.

Matrix carbides in nickel- and iron-nickel-base superalloys also may be partially solutioned. MC carbides will not totally dissolve, however, without incipient melting of the alloy and tend to be unstable, decomposing to $M_{23}C_6$ at temperatures below about 815 to 870 °C (1500–1600 °F) or possibly converting to M_6C at temperatures of 980 to 1040 °C (1800–1900 °F) if the alloy has a sufficiently high molybdenum + tungsten content. Matrix carbides generally contribute very small increments of strengthening to nickel- and iron-nickel-base superalloys.

An interesting microstructural trend has taken place with the advent of single crystals of nickel-base superalloys. Because no grain boundaries exist, there is little need for the normal grain-boundary strengtheners such as carbon. Consequently, very few matrix or subboundary carbides exist in first-generation SC alloys. Although the initial trend was to remove carbon completely from SC nickel-base superalloys, the subsequent realization that subboundaries in single crystals could benefit from carbides has led to a relaxation of carbon restrictions, and low amounts of carbon are now permitted in many single-crystal alloys. (Hafnium, boron, and zirconium in limited amounts also may be permitted.) As noted previously, the trend in wrought nickel-base superalloys continues to be toward reduced carbon and reduced carbide size.

Perhaps the most common other role of matrix carbides (also shared by grain-boundary carbides) is a negative one: They may participate in the fatigue cracking process by premature cracking or by oxidizing at the surface of uncoated alloys to cause a notch effect.

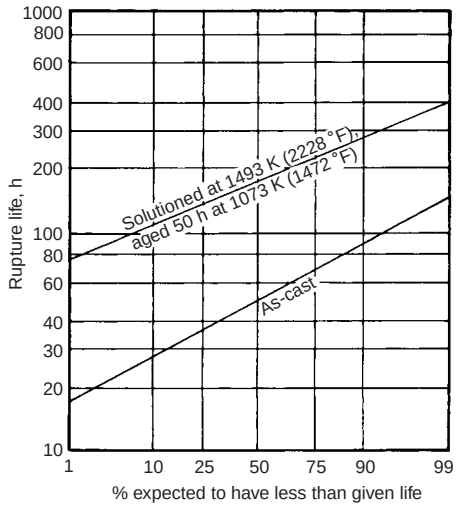


Fig. 18 Effect of heat treatment on a cobalt-base superalloy (HS-31, also known as X-40), showing increase in strength resulting from carbide precipitation

Oxidized carbides or precracked carbides from machining or thermal stresses can initiate fatigue cracks. Precracked carbides can be related to prior casting processes. Carbide size is important, and reduced carbide volumes and sizes in nickel-base alloys result in a reduction in precracked carbides. The longer solidification times and lower gradients of early directional solidification processes often resulted in moderately large carbides. However, improved gradients and the reduced carbon contents of SC alloys (few or no carbides) have resulted in substantial improvements in fatigue resistance, particularly over similarly oriented CGDS alloys with normal carbon levels. This effect is most noticeable in low-cycle fatigue (LCF) and thermomechanical fatigue (TMF). No evidence is available to interpret the effect of the absence of carbides on high-cycle fatigue (HCF), but beneficial effects could be anticipated.

Oxidized carbides can be minimized or prevented by several methods. Casting procedures and/or chemical composition may be modified to produce smaller primary carbides. Powder processing may be used to produce the same result. Carbon content may be reduced if it is not specifically required to enable the alloy to attain the desired strength levels. Reduced carbon is the rule in SC and powdered superalloys. Of course, the alloy may be coated with an appropriate protective coating that leaves the carbides in a subsurface location.

Although there is limited documentation, it frequently is assumed that noncarbide-forming elements do influence the formation of carbides. Cobalt, for example, has been claimed to modify the carbides in nickel-base alloys, and phosphorus has produced a more general, more finely dispersed, and smaller carbide precipitation than carbon alone in a heat-resisting iron-base alloy. The modifying effect on carbides may be intragranular or intergranular depending on the modifier and the base-alloy system.

Boron, Zirconium, and Hafnium. Within limits, significant improvements in mechanical properties can be achieved by additions of boron, zirconium, and hafnium. However, only limited microstructural correlations can be made. The presence of these elements may modify the initial grain-boundary carbides or tie up deleterious elements such as sulfur and lead. Reduced grain-boundary diffusion rates may be obtained, with consequent suppression of carbide agglomeration and creep cracking. Hafnium contributes to the formation of more γ-γ' eutectic in cast alloys; the eutectic at grain boundaries is thought (in modest quantities) to contribute to alloy ductility. The effects of these elements are limited to nickel- and iron-nickel-base alloys; virtually no cobalt-base alloys contain them. Hafnium in particular contributes strongly to improved ductility in transverse boundaries in CGDS alloys.

Processing. Three major processing techniques are used for controlling superalloy properties. Thermomechanical working is used for wrought nickel- and iron-nickel-base alloys to store energy by producing a fine grain size and controlling dislocation density/configuration. Improvements in tensile properties and LCF have resulted.

A second processing route involves the use of powder metallurgy to produce reduced carbide size and greater homogeneity in materials with a resultant improvement in fatigue resistance and fracture mechanics life limits. Furthermore, in conjunction with isothermal processing, alloy grain sizes of ASTM 8 to 12 are being routinely produced in very-high-strength alloys, resulting in additional fatigue-life benefits. (Major benefits result from the ability to form alloys such as IN-100, which are unforgeable by some standard procedures.)

The third area is casting control of grain size and morphology, especially by controlled solidification. Cast-alloy grain sizes have been made more uniform and, in some cases, have been reduced to enhance fatigue or tensile properties. Directional grain structures have improved strength (Fig. 19). Improved creep rupture and fatigue resistance have resulted from the elimination of transverse grain boundaries and the favorable orientation of a low modulus direction to reduce strains. In the extreme, grains have been eliminated in SC alloys with additional gains in creep rupture behavior (Fig. 19).

Porosity in superalloys has led to fatigue and creep rupture failure. Reduced porosity owing to HIP has resulted in improved properties. Efforts to date have centered on nickel-base cast alloys, but the process should enhance properties of any cast alloy with nonsurface-connected casting porosity. (In the biomedical field, use of HIP has provided significant improvements in fatigue life of cast Vitallium alloy hip replacements.)

Effects of Thermal Exposure on Mechanical Properties

Superalloys generally behave much like other alloy systems on thermal exposure during testing or in service, but with some differences due to the nature of the γ' precipitates. Most alloys with secondary hardening phases undergo property degradation due to coalescence of the secondary phases, a process that reduces their effectiveness. This behavior occurs in superalloys and is manifested by such phenomena as γ' agglomeration and coarsening; carbide precipitation and γ' envelope formation also occur. In addition, the superalloys may show a tendency to form less-desirable secondary phases such as σ.

These detrimental phases generally reduce property levels of the superalloys in which they form because of their inherent properties and/or the consumption of elements intended for γ and γ'. Some of these phases can be prevented from forming by application of compositional control guided by the concept of the electron-vacancy number, N_v. Formation of tcp phases such as σ, Laves, and μ is found to be related to excess electron vacancies in the transition-element base metals (iron, nickel, and cobalt). By ascribing N_v values to the alloying elements of the γ matrix, a weighted N_v can be calculated for γ, and, by experiment, upper limits for N_v can be set for a given alloy composition to ensure the absence of tcp phases in reasonable exposure times. Unfortunately, simple calculations of this type have not been found applicable to δ or η formation, which can be detrimental in certain morphologies and/or in excess amounts. Trial-and-error adjustments of composition and processing generally are required to ensure that δ and η precipitation do not occur and cause a significant loss of properties.

In addition to the formation of a singular detrimental phase, a more complex microstructure can appear under coatings. A specific secondary reaction zone (SRZ) was reported for alloys of the N4 and N5 type. This zone produced a transformation front that often occurred as a cellular reaction in which γ and P phase (about 50% Re) formed in a matrix of γ' phase. Strength was dramatically reduced, especially when SRZ formed in dendritic areas. Modified alloys have negated the formation of this complex structure, just as N_v control minimizes formation of detrimental tcp phases.

Transformation of Hardening Phase. In iron-nickel-base superalloys, the strengthening precipitate usually degrades in a moderate tempera ture regime, 650 to 760 °C (1200–1400 °F), forming structures and precipitate morphologies that are less effective in strengthening the alloy. In alloys hardened by large amounts of titanium, η phase replaces γ'. The precipitation of η may occur in two forms: at the grain boundaries as cellular product or intragranularly as Widmanstätten plates. The cellular precipitation is often associated with loss of mechanical properties, particularly notch stress rupture (NSR). Intragranular plates also may cause some property loss, but data are not available. In some nickel-base superalloys with higher titanium/aluminum ratios (e.g., IN-738, IN-792, and IN-939), η has been reported, but no information on property degradation is available.

In a nickel-niobium alloy such as IN-718, plates of orthorhombic δ phase will form on exposure after sufficiently long times at elevated temperatures. Because of its relatively coarse morphology, properties deteriorate when excess amounts of platelike or acicular δ form.

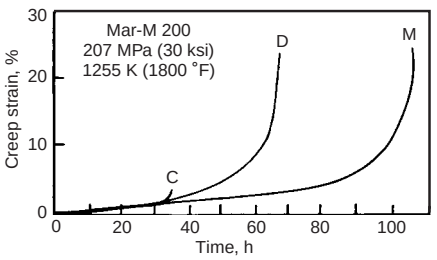


Fig. 19 Comparison of creep properties of MAR-M 200 alloy, polycrystalline conventionally cast (C), columnar-grain directionally solidified (D), and single-crystal directionally solidified (M)

Formation of Transition-Element Phases. Of great concern in all superalloys has been the formation of detrimental secondary phases not directly associated with the primary hardening precipitate phases, γ′ and γ″. Laves phases have been found in the iron-nickel-base superalloys IN-718, Incoloy 901, and A-286. Room-temperature yield strength and ductility of IN-718 are reduced by Laves formation, whereas Laves in A-286 does not affect properties. Laves in the cobalt-base alloy L605 severely degrades room-temperature ductility.

Phases such as Laves, σ, and μ in acicular form generally are detrimental owing to their morphology, lack of ductility, and the tying up of some hardening elements. Sigma-phase formation in several nickel-base alloys has been shown to reduce stress-rupture life (Fig. 20). Sigma generally forms with exposure and is controlled by establishing composition limits (phase control electron vacancy number, N_v) or by preventing an alloy from operating in the σ-forming temperature range. The extent of the effect that tcp and other secondary phases have on properties varies with the type of alloy (cast versus wrought), property being measured, initial microstructure, and environmental effects (coated versus uncoated, test atmosphere).

Morphological Changes in γ′. Changes in γ′ during testing produce effects on properties that may not be readily observed because of the simultaneous occurrence of other microstructural changes. Most commonly, γ′ coarsens following well-established kinetics and agglomerates in a creep rupture test (Fig. 21), tending to form platelets of γ′ on the [001] planes perpendicular to the applied stress. The coarsening of γ′ can cause reduced rupture life (Fig. 22). Overheating can cause accelerated coarsening as well as solutioning of some fine γ′. Properties may be reduced, but reprecipitation of fine γ′ occurs in the case of mild overheating excursions.

Carbide Morphology/Type Changes. As exposure time increases, there is a tendency for further reduction in the primary MC carbide amounts and for further morphological changes together with a tendency to form increased amounts of the secondary carbides $M_{23}C_6$ and M_6C. If carbide films form and/or acicular carbides of the M_6C type form, alloy ductility and strength can be reduced. Agglomeration of carbides, however, can lead to increased ductility accompanied by strength reduction.

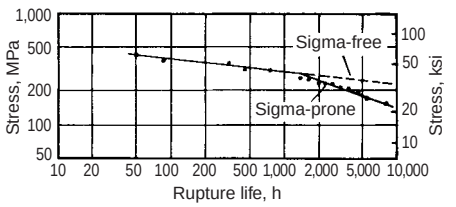


Fig. 20 Stress rupture behavior of U-700, showing reduction in strength that occurs when σ phase forms. Source: Ref 5 (original source: Ref 6)

In cast cobalt-base superalloys, precipitation of additional intragranular carbides during service has led to sharply increased rupture strength and reduced rupture ductility. The precipitation of an intragranular acicular Widmanstätten carbide brought about by aging in another cobalt-base alloy degraded both rupture life and ductility.

Property Recovery after Thermal Exposure. As noted, changes in γ′ occur with exposure to elevated temperatures. Most commonly, γ′ coarsens and agglomerates, particularly under stress. Overheating can cause accelerated coarsening as well as solutioning of some fine γ′. Properties may be reduced in such circumstances, but when the overheating has been mild, reprecipitation of fine γ′ occurs with a return to normal temperatures, and some property recovery occurs. Property recovery, however, does not occur in the case of additional thermal exposure of tcp, δ, or η phases in superalloys. Nor is recovery achieved by thermal exposure after excessive carbide precipitation (as may occur in cobalt-base superalloys) or after extensive γ′ coarsening (as in nickel- and iron-nickel-base superalloys).

Recovery of properties is desired as a means of prolonging component life. If, as above, additional thermal exposure fails to promote better properties, then re-solution heat treatment and aging is required to restore property levels. While this process may be satisfactory in alloys degraded only by thermal exposure, service exposure under stress generally produces property losses (due in part to cavitation or wedge creep cracking), which cannot be recovered by simple heat treatment alone—at least for the more complex commercial superalloys. The use of HIP plus re-solution and aging treatment of exposed superalloys has suggested that some improvements can be achieved under suitable circumstances, but the extent to which such salvage processing is economically viable is uncertain.

Typical Mechanical Properties of Superalloys

In this discussion, "typical" means the most likely value to be reached for a given property in a standard test if one were to conduct random testing. Typical properties are merely a guide for comparison. Exact chemistry, section size, heat treatment, and other processing steps must be known to generate property for design. Tables 9 and 10 summarize property behavior for wrought alloys; Tables 11 and 12 provide similar information for cast alloys.

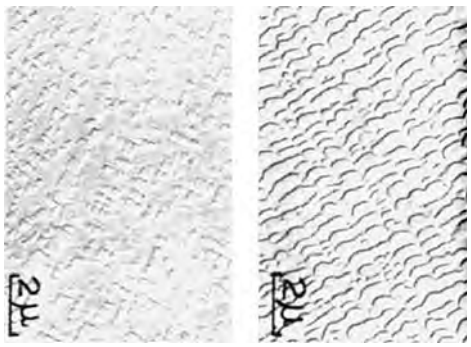


Fig. 21 Agglomeration of γ′ in Udimet 700 resulting from creep testing. Left, as heat treated. Right, after 91.2 h at 252.3 MPa (36.6 ksi) and 893 °C (1640 °F). 4000×

Environmental Effects

A brief discussion of high-temperature corrosion, protective coatings to improve resistance to high-temperature corrosion, and environmentally induced embrittlement is given below. More detailed information can be found in the articles "High-Temperature Corrosion Behavior of Nickel Alloys," "High-Temperature Coatings for Superalloys," and "Stress-Corrosion Cracking and Hydrogen Embrittlement of Nickel Alloys" in this Handbook.

General Oxidation

Superalloys generally react with oxygen, and oxidation is the prime environmental effect on these alloys. At moderate temperatures—approximately 870 °C (1600 °F) and below—general uniform oxidation is not a major problem. At higher temperatures, commercial nickel- and cobalt-base superalloys are attacked by oxygen. The level of oxidation resistance at temperatures below approximately 980 °C (1800 °F) is a function of chromium content (Cr_2O_3 forms as a protective oxide); at temperatures above approximately 980 °C (1800 °F), aluminum content becomes more important in oxidation resistance (Al_2O_3 forms as a protective oxide). Chromium and aluminum can contribute in an interactive fashion to oxidation protection. The higher the chromium level, the less aluminum may be required to form a highly protective Al_2O_3 layer. However, the aluminum contents of many superalloys are insufficient to provide long-term Al_2O_3 protection, and so protective coatings are applied (see below). These coatings also prevent selective attack that occurs along grain boundaries and at

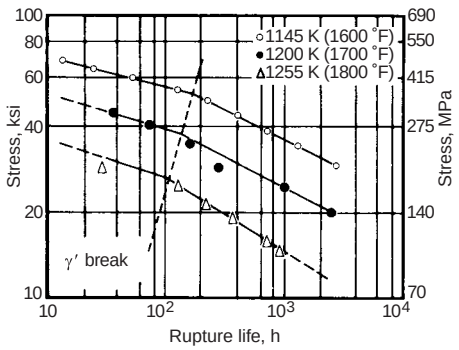


Fig. 22 Stress rupture behavior of B-1900 nickel-base superalloy, showing break in slope believed to be caused by γ′ coarsening

Table 9 Effect of temperature on the mechanical properties of wrought nickel-, iron-, and cobalt-base superalloys

		Ultimate tensile strength at:						Yield strength at 0.2% offset at:						Tensile elongation, % at:		
		21 °C (70 °F)		540 °C (1000 °F)		760 °C (1400 °F)		21 °C (70 °F)		540 °C (1000 °F)		760 °C (1400 °F)		21 °C	540 °C	760 °C
Alloy	Form	MPa	ksi	MPa	ksi	MPa	ksi	MPa	ksi	MPa	ksi	MPa	ksi	(70 °F)	(1000 °F)	(1400 °F)
Nickel-base																
Astroloy	Bar	1415	205	1240	180	1160	168	1050	152	965	140	910	132	16	16	21
Cabot 214	…	915	133	715	104	560	84	560	81	510	74	495	72	38	19	9
D-979	Bar	1410	204	1295	188	720	104	1005	146	925	134	655	95	15	15	17
Hastelloy C-22	Sheet	800	116	625	91	525	76	405	59	275	40	240	35	57	61	63
Hastelloy G-30	Sheet	690	100	490	71	…	…	315	46	170	25	…	…	64	75	…
Hastelloy S	Bar	845	130	775	112	575	84	455	65	340	49	310	45	49	50	70
Hastelloy X	Sheet	785	114	650	94	435	63	360	52	290	42	260	38	43	45	37
Haynes 230	(a) (b)	870	126	720	105	575	84	390	57	275	40	285	41	48	56	46
Inconel 587(c)	Bar	1180	171	1035	150	830	120	705	102	620	90	605	88	28	22	20
Inconel 597(c)	Bar	1220	177	1140	165	930	135	760	110	720	104	665	96	15	15	16
Inconel 600	Bar	660	96	560	81	260	38	285	41	220	32	180	26	45	41	70
Inconel 601	Sheet	740	107	725	105	290	42	455	66	350	51	220	32	40	34	78
Inconel 617	Bar	740	107	580	84	440	64	295	43	200	29	180	26	70	68	84
Inconel 617	Sheet	770	112	590	86	470	68	345	50	230	33	230	33	55	62	59
Inconel 625	Bar	965	140	910	132	550	80	490	71	415	60	415	60	50	50	45
Inconel 706	Bar	1310	190	1145	166	725	105	1005	146	910	132	660	96	20	19	32
Inconel 718	Bar	1435	208	1275	185	950	138	1185	172	1065	154	740	107	21	18	25
Inconel 718 Direct Age	Bar	1530	222	1350	196	…	…	1365	198	1180	171	…	…	16	15	…
Inconel 718 Super	Bar	1350	196	1200	174	…	…	1105	160	1020	148	…	…	16	18	…
Inconel X750	Bar	1200	174	1050	152	…	…	815	118	725	105	…	…	27	26	…
M-252	Bar	1240	180	1230	178	945	137	840	122	765	111	720	104	16	15	10
Nimonic 75	Bar	745	108	675	98	310	45	285	41	200	29	160	23	40	40	67
Nimonic 80A	Bar	1000	145	875	127	600	87	620	90	530	77	505	73	39	37	17
Nimonic 90	Bar	1235	179	1075	156	655	95	810	117	725	105	540	78	33	28	12
Nimonic 105	Bar	1180	171	1130	164	930	135	830	120	775	112	740	107	16	22	25
Nimonic 115	Bar	1240	180	1090	158	1085	157	865	125	795	115	800	116	27	18	24
Nimonic 263	Sheet	970	141	800	116	650	94	580	84	485	70	460	67	39	42	21
Nimonic 942(c)	Bar	1405	204	1300	189	900	131	1060	154	970	141	860	125	37	26	42
Nimonic PE.11(c)	Bar	1080	157	1000	145	760	110	720	105	690	100	560	81	30	30	18
Nimonic PE.16	Bar	885	128	740	107	510	74	530	77	485	70	370	54	37	26	42
Nimonic PK.33	Sheet	1180	171	1000	145	885	128	780	113	725	105	670	97	30	30	18
Pyromet 860(c)	Bar	1295	188	1255	182	910	132	835	121	840	122	835	121	22	15	18
René 41	Bar	1420	206	1400	203	1105	160	1060	154	1020	147	940	136	14	14	11
René 95	Bar	1620	235	1550	224	1170	170	1310	190	1255	182	1100	160	15	12	15
Udimet 400(c)	Bar	1310	190	1185	172	…	…	930	135	830	120	…	…	30	26	…
Udimet 500	Bar	1310	190	1240	180	1040	151	840	122	795	115	730	106	32	28	39
Udimet 520	Bar	1310	190	1240	180	725	105	860	125	825	120	725	105	21	20	15
Udimet 630(c)	Bar	1520	220	1380	200	965	140	1310	190	1170	170	860	125	15	15	5
Udimet 700	Bar	1410	204	1275	185	1035	150	965	140	895	130	825	120	17	16	20
Udimet 710	Bar	1185	172	1150	167	1020	148	910	132	850	123	815	118	7	10	25
Udimet 720	Bar	1570	228	…	…	1455	211	1195	173	…	…	1050	152	13	…	9
Unitemp AF2-1DA6	Bar	1560	226	1480	215	1290	187	1015	147	1040	151	995	144	20	19	16
Waspaloy	Bar	1275	185	1170	170	650	94	795	115	725	105	675	98	25	23	28
Iron-base																
A-286	Bar	1005	146	905	131	440	64	725	105	605	88	430	62	25	19	19
Alloy 901	Bar	1205	175	1030	149	725	105	895	130	780	113	635	92	14	14	19
Discaloy	Bar	1000	145	865	125	485	70	730	106	650	94	430	62	19	16	…
Haynes 556	Sheet	815	118	645	93	470	69	410	60	240	35	220	32	48	54	49
Incoloy 800(c)	Bar	595	86	510	74	235	34	250	36	180	26	150	22	44	38	83
Incoloy 801(c)	Bar	785	114	660	96	325	47	385	56	310	45	290	42	30	28	55
Incoloy 802(c)	Bar	690	100	600	87	400	58	290	42	195	28	200	29	44	39	15
Incoloy 807(c)	Bar	655	95	470	68	350	51	380	55	255	37	225	32.5	48	40	34
Incoloy 825(d)(e)	…	690	100	~590	~86	~275	~40	310	45	~234	~34	180	~26	45	~44	~86
Incoloy 903	Bar	1310	190	…	…	…	…	1105	160	…	…	…	…	14	…	…
Incoloy 907(d)(f)	…	~1365	~198	~1205	~175	~655	~95	~1110	~161	~960	~139	~565	~82	~12	~11	~20
Incoloy 909	Bar	1310	190	1160	168	615	89	1020	148	945	137	540	78	16	14	34
N-155	Bar	815	118	650	94	428	62	400	58	340	49	250	36	40	33	32
V-57	Bar	1170	170	1000	145	620	90	830	120	760	110	485	70	26	19	34
19-9 DL(g)	…	815	118	615	89	…	…	570	83	395	57	…	…	43	30	…
16-25-6(g)	…	980	142	…	…	415	60	770	112	…	…	345	50	23	…	11
Cobalt-base																
AiResist 213(h)	…	1120	162	…	…	485	70	625	91	…	…	385	56	14	…	47
Elgiloy(h)	…	960(e)–2480(i)	100(e)–360(i)	…	…	…	…	480(e)–2000(i)	7–290	…	…	…	…	34	…	…
Haynes 188	Sheet	960	139	740	107	635	92	485	70	305	44	290	42	56	70	43
L-605	Sheet	1005	146	800	116	455	66	460	67	250	36	260	38	64	59	12
MAR-M 918	Sheet	895	130	…	…	…	…	895	130	…	…	…	…	48	…	…
MP35N	Bar	2025	294	…	…	…	…	1620	235	…	…	…	…	10	…	…
MP159	Bar	1895	275	1565	227	…	…	1825	265	1495	217	…	…	8	8	…
Stellite 6B(h)	Sheet	1010	146	…	…	…	…	635	92	…	…	…	…	11	…	…
Haynes 150(h)	…	925	134	…	…	…	…	317	46	…	…	…	…	8	…	…

(a) Cold-rolled and solution-annealed sheet, 1.2–1.6 mm (0.048–0.063 in.) thick. (b) Ref 11. (c) Ref 7. (d) Ref 8. (e) Annealed. (f) Precipitation hardened. (g) Ref 9. (h) Ref 10. (i) Work strengthened and aged. Source: Ref 12, except as noted

surface carbides (Fig. 23) and inhibit internal oxidation or subsurface interaction of O_2/N_2 with γ' envelopes, a process believed to occur in nickel-base superalloys.

Hot Corrosion

In lower-temperature operating conditions, ≤870 °C (≤1600 °F), accelerated oxidation in a gas path may occur in superalloys through the operation of selective fluxing agents. One of the better-documented accelerated oxidation processes is hot corrosion (sometimes known as sulfidation). The hot corrosion process is separated into two regimes: low temperature and high temperature. The principal method for combating hot corrosion is the use of a high chromium content (≥20 wt%) in the base alloy. Although cobalt-base superalloys and many iron-nickel-base alloys have chromium levels in this range, most nickel-base alloys—especially those with high creep-rupture strengths—do not, because a high chromium content is not compatible with the high V_f γ' required.

Higher titanium/aluminum ratios also seem to reduce attack on uncoated superalloys, and alloys with improved resistance to hot corrosion, based on slightly increased chromium contents and appropriate titanium/aluminum modifications, have been produced. For maximum uncoated hot-corrosion resistance, however, chromium contents in excess of 20 wt% appear to be required. Such alloys are not capable of achieving the strengths of the high V_f γ' alloys such as MAR-M-247. Consequently, coatings that protect the base metal (overlay coatings seem to provide the best surface protection), or sometimes environmental inhibitors, are used to suppress hot-corrosion attack in high-strength (high V_f γ') nickel-base superalloys.

Table 10 1000 h rupture strengths of wrought nickel-, cobalt-, and iron-base superalloys

		Rupture strength at:							
		650 °C (1200 °F)		760 °C (1400 °F)		870 °C (1600 °F)		980 °C (1800 °F)	
Alloy	Form	MPa	ksi	MPa	ksi	MPa	ksi	MPa	ksi
Nickel-base									
Astroloy	Bar	770	112	425	62	170	25	55	8
Cabot 214	…	…	…	…	…	30	4	15	2
D-979	Bar	515	75	250	36	70	10	…	…
Hastelloy S	Bar	…	…	90	13	25	4	…	…
Hastelloy X	Sheet	215	31	105	15	40	6	15	2
Haynes 230	…	…	…	125	18	55	8	15	2
Inconel 587(a)	Bar	…	…	285	41	…	…	…	…
Inconel 597(a)	Bar	…	…	340	49	…	…	…	…
Inconel 600	Bar	…	…	…	…	30	4	15	2
Inconel 601	Sheet	195	28	60	9	30	4	15	2
Inconel 617	Bar	360	52	165	24	60	9	30	4
Inconel 617	Sheet	…	…	160	23	60	9	30	4
Inconel 625	Bar	370	54	160	23	50	7	20	3
Inconel 706	Bar	580	84	…	…	…	…	…	…
Inconel 718	Bar	595	86	195	28	…	…	…	…
Inconel 718 Direct Age	Bar	405	59	…	…	…	…	…	…
Inconel 718 Super	Bar	600	87	…	…	…	…	…	…
Inconel X750	Bar	470	68	…	…	50	7	…	…
M-252	Bar	565	82	270	39	95	14	…	…
Nimonic 75	Bar	170	25	50	7	5	1	…	…
Nimonic 80A	Bar	420	61	160	23	…	…	…	…
Nimonic 90	Bar	455	66	205	30	60	9	…	…
Nimonic 105	Bar	…	…	330	48	130	19	30	4
Nimonic 115	Bar	…	…	420	61	185	27	70	10
Nimonic 942(a)	Bar	520	75	270	39	…	…	…	…
Nimonic PE.11(a)	Bar	335	49	145	21	…	…	…	…
Nimonic PE.16	Bar	345	50	150	22	…	…	…	…
Nimonic PK.33	Sheet	655	95	310	45	90	13	…	…
Pyromet 860(a)	Bar	545	79	250	36	…	…	…	…
René 41	Bar	705	102	345	50	115	17	…	…
René 95	Bar	860	125	…	…	…	…	…	…
Udimet 400(a)	Bar	600	87	305	44	110	16	…	…
Udimet 500	Bar	760	110	325	47	125	18	…	…
Udimet 520	Bar	585	85	345	50	150	22	…	…
Udimet 700	Bar	705	102	425	62	200	29	55	8
Udimet 710	Bar	870	126	460	67	200	29	70	10
Udimet 720	Bar	670	97	…	…	…	…	…	…
Unitemp AF2-1DA6	Bar	885	128	360	52	…	…	…	…
Waspaloy	Bar	615	89	290	42	110	16	…	…
Iron-base									
A-286	Bar	315	46	105	15	…	…	…	…
Alloy 901	Sheet	525	76	205	30	…	…	…	…
Discaloy	Bar	275	40	60	9	…	…	…	…
Haynes 556	Sheet	275	40	125	18	55	8	20	3
Incoloy 800(a)	Bar	165	24	66	9.5	30	4.4	13	1.9
Incoloy 801(a)	Bar	…	…	…	…	…	…	…	…
Incoloy 802(a)	Bar	170	25	110	16	69	10	24	3.5
Incoloy 807(a)	Bar	…	…	105	15	43	6.2	19	2.7
Incoloy 903	Bar	510	74	…	…	…	…	…	…
Incoloy 909	Bar	345	50	…	…	…	…	…	…
N-155	Bar	295	43	140	20	70	10	20	3
V-57	Bar	485	70	…	…	…	…	…	…
Cobalt-base									
Haynes 188	Sheet	…	…	165	24	70	10	30	4
L-605	Sheet	270	39	165	24	75	11	30	4
MAR-M 918	Sheet	…	…	60	9	20	3	5	1
Haynes 150(b)	…	…	…	40(c)	5.8	…	…	…	…

(a) Ref 7. (b) Ref 9. (c) At 815 °C (1500 °F). Source: Ref 12, except as noted

Coatings

Development of increased strength (increased V_f γ') in nickel-base superalloys led to reductions in chromium content and to greater oxidation attack and susceptibility to hot corrosion. Although aluminum contents of some alloys were increased in order to enhance resistance to oxidation, intergranular and carbide attack worsened as operating temperatures escalated. Furthermore, some of the more oxidation-resistant alloys were found to be very poor in hot-corrosion resistance. To protect against local oxidation, and later, against hot corrosion and similar fluxing reactions, coatings were applied to superalloys. In recent years, thermal barrier coatings (TBCs) have been developed to provide substantial reductions in temperatures on superalloy surfaces. These coatings are commonly used in conjunction with corrosion protective coatings.

Coatings are of two types: aluminide (diffusion) coatings and overlay coatings. Use of coatings is a preferred method of protecting superalloy surfaces from environmental attack because:

- Coatings (at least overlay coatings) can be tailored to the hostile environment anticipated.
- Development of base alloys for strength is less inhibited, because significant protection (but not all of the protection) is provided by the coating.
- Coatings provide an opportunity to refurbish worn surfaces after exposure and environmental attack without causing significant degradation of the base metal.

Aluminide (Diffusion) Coatings. The most common type of coating for environmental protection of superalloys is the aluminide diffusion coating, which develops an aluminide (CoAl or NiAl) outer layer with enhanced oxidation resistance. This outer layer is developed by the reaction of aluminum with the nickel or cobalt in the base metal.

Some use has been made of aluminides containing chromium or silicon, and in recent years noble metals such as platinum have been used to enhance the oxidation resistance of aluminides. The oxidation resistance of aluminide coatings is derived from formation of protective Al_2O_3 scales. Aluminide diffusion coatings generally are thin—about 50 to 75 μm (2–3 mils). They consume some base metal in their formation and, although deposited at lower temperatures, are invariably diffused at temperatures from approximately 1040 to 1120 °C (1900–2050 °F) prior to being placed in service.

Overlay coatings generally are referred to as MCrAl or MCrAlY coatings, and are derived directly from the deposition process. They do not require diffusion for their formation. The constituent denoted "M" in these designations has at various times been iron, cobalt, nickel, or combinations of nickel and cobalt. A high-temperature heat treatment (at 1040 to 1120 °C, or 1900 to 2050 °F) is performed to homogenize the coating and to ensure its adherence to the substrate.

MCrAl coatings are approximately twice as thick as aluminide coatings, and, through incorporation of yttrium, overlay coatings can be made to have improved corrosion resistance. An advantage of MCrAlY coatings is that their compositions can be tailored to produce greater or lesser amounts of chromium or aluminum within the coating, and thus the protectivity and mechanical properties of the coating can be balanced for optimal performance.

Thermal barrier coatings have provided enough insulation for superalloys to operate in temperature environments as much as 165 °C (300 °F) above their customary operating range. The TBCs are ceramics, most notably plasma sprayed partially stabilized zirconia (PSZ). These ceramic coatings use an underlay of a corrosion-protective layer—typically an overlay coating such as an MCrAlY that provides for oxidation resistance and the necessary roughness for top-coat adherence. Thermal barrier coatings do not provide oxidation protection for superalloys.

Effects of Coatings on Mechanical Behavior. Coatings seem to have little deleterious effect on tensile and creep rupture properties. In fact, creep rupture life may be enhanced by

Table 11 Effect of temperature on the mechanical properties of cast nickel-base and cobalt-base alloys

	Ultimate tensile strength at:						0.2% yield strength at:						Tensile elongation, % at:		
	21 °C (70 °F)		538 °C (1000 °F)		1093 °C (2000 °F)		21 °C (70 °F)		538 °C (1000 °F)		1093 °C (2000 °F)		21 °C	538 °C	1093 °C
Alloy	MPa	ksi	MPa	ksi	MPa	ksi	MPa	ksi	MPa	ksi	MPa	ksi	(70 °F)	(1000 °F)	(2000 °F)
Nickel-base															
IN-713 C	850	123	860	125	…	…	740	107	705	102	…	…	8	10	…
IN-713 LC	895	130	895	130	…	…	750	109	760	110	…	…	15	11	…
B-1900	970	141	1005	146	270	38	825	120	870	126	195	28	8	7	11
IN-625	710	103	510	74	…	…	350	51	235	34	…	…	48	50	…
IN-718	1090	158	…	…	…	…	915	133	…	…	…	…	11	…	…
IN-100	1018	147	1090	150	(380)	(55)	850	123	885	128	(240)	(35)	9	9	…
IN-162	1005	146	1020	148	…	…	815	118	795	115	…	…	7	6.5	…
IN-731	835	121	…	…	275	40	725	105	…	…	170	25	6.5	…	…
IN-738	1095	159	…	…	…	…	950	138	…	…	…	…	…	…	…
IN-792	1170	170	…	…	…	…	1060	154	…	…	…	…	4	…	…
M-22	730	106	780	113	…	…	685	99	730	106	…	…	5.5	4.5	…
MAR-M 200	930	135	945	137	325	47	840	122	880	123	…	…	7	5	…
MAR-M 246	965	140	1000	145	345	50	860	125	860	125	…	…	5	5	…
MAR-M 247	965	140	1035	150	…	…	815	118	825	120	…	…	7	…	…
MAR-M 421	1085	157	995	147	…	…	930	135	815	118	…	…	4.5	3	…
MAR-M 432	1240	180	1105	160	…	…	1070	155	910	132	…	…	6	…	…
MC-102	675	98	655	95	…	…	605	88	540	78	…	…	5	9	…
Nimocast 75	500	72	…	…	…	…	179	26	…	…	…	…	39	…	…
Nimocast 80	730	106	…	…	…	…	520	75	…	…	…	…	15	…	…
Nimocast 90	700	102	595	86	…	…	520	75	420	61	…	…	14	15	…
Nimocast 242	460	67	…	…	…	…	300	44	…	…	…	…	8	…	…
Nimocast 263	730	106	…	…	…	…	510	74	…	…	…	…	18	…	…
René 77	…	…	…	…	…	…	…	…	…	…	…	…	…	…	…
René 80	…	…	…	…	…	…	…	…	…	…	…	…	…	…	…
Udimet 500	930	135	895	130	…	…	815	118	725	105	…	…	13	13	…
Udimet 710	1075	156	…	…	240	35	895	130	…	…	170	25	8	…	…
CMSX-2(a)(b)	1185	172	1295(c)	188(c)	…	…	1135	165	1245(c)	181(c)	…	…	10	17(c)	…
GMR-235(b)	710	103	…	…	…	…	640	93	…	…	…	…	3	…	18(d)
IN-939(b)	1050	152	915(c)	133(c)	325(d)	47(d)	800	116	635(c)	92(c)	205(d)	30(d)	5	7(c)	25(d)
MM 002(b)(e)	1035	150	1035(c)	150(c)	550(d)	80(d)	825	120	860(c)	125(c)	345(d)	50(d)	7	5(c)	12(d)
IN-713 Hf(b)(f)	1000	145	895(c)	130(c)	380(d)	55(d)	760	110	620(c)	90(c)	240(d)	35(d)	11	6(c)	20(d)
René 125 Hf(b)(g)	1070	155	1070(c)	155(c)	550(d)	80(d)	825	120	860(c)	125(c)	345(d)	50(d)	5	5(c)	12(d)
MAR-M 246 Hf(b)(h)	1105	160	1070(c)	155(c)	565(d)	82(d)	860	125	860(c)	125(c)	345(d)	50(d)	6	7(c)	14(d)
MAR-M 200 Hf(b)(i)	1035	150	1035(c)	150(c)	540(d)	78(d)	825	120	860(c)	125(c)	345(d)	50(d)	5	5(c)	10(d)
PWA-1480(a)(b)	…	…	1130(c)	164(c)	685(d)	99(d)	895	130	905(c)	131(c)	495(d)	72(d)	4	8(c)	20(d)
SEL(b)	1020	148	875(c)	127(c)	…	…	905	131	795(c)	115(c)	…	…	6	7(c)	…
UDM 56(b)	945	137	945(c)	137(c)	…	…	850	123	725(c)	105(c)	…	…	3	5(c)	…
SEL-15(b)	1060	154	1090(c)	158(c)	…	…	895	130	815(c)	118(c)	…	…	9	5(c)	…
Cobalt-base															
AiResist 13(j)	600	87	420(c)	61(c)	…	…	530	77	330(c)	48(c)	…	…	1.5	4.5(c)	…
AiResist 215(j)	690	100	570(k)	83(k)	…	…	485	70	315(k)	46(k)	…	…	4	12(k)	…
FSX-414	…	…	…	…	…	…	…	…	…	…	…	…	…	…	…
Haynes 1002	770	112	560	81	115	17	470	68	345	50	95	14	6	8	28
MAR-M 302	930	135	795	115	150	22	690	100	505	73	150	22	2	…	21
MAR-M 322(j)	830	120	595(c)	86(c)	…	…	630	91	345(c)	50(c)	…	…	4	6.5(c)	…
MAR-M 509	785	114	570	83	…	…	570	83	400	58	…	…	4	6	…
WI-52	750	109	745	108	160	23	585	85	440	64	105	15	5	7	35
X-40	745	108	550	80	…	…	525	76	275	40	…	…	9	17	…

(a) Single crystal [001]. (b) Data from Ref 12. (c) At 760 °C (1400 °F). (d) At 980 °C (1800 °F). (e) RR-7080. (f) MM 004. (g) M 005. (h) MM 006. (i) MM 009. (j) Data from Vol 3, 9th ed., *Metals Handbook*, 1980. (k) At 650 °C (1200 °F). Source: Nickel Development Institute, except as noted

protection of the superalloy surface from oxidation or fluxing-agent attack. Thermomechanical fatigue can be greatly affected by a coating because the ductilities of coatings tend to be low at low temperatures. Ductilities of aluminide coatings generally are lower than those of overlay coatings at lower temperatures (≤540 °C, or 1000 °F). However, ductilities of both overlay and diffusion coatings increase sharply at higher temperatures (≥650 °C, or 1200 °F). When TMF cycles have peak tensile strains at lower temperatures, coatings may crack within the first few cycles, and TMF response is related to the crack-propagation rate in the base metal. Some adjustment of ductility is possible, particularly in the overlay coatings. However, because aluminum—the protective element—is a principal cause of reduced ductility, a balance must be achieved between protectivity and resistance to TMF.

Coating Processes. Aluminide diffusion coatings generally are applied by pack processes, but slurry, electrophoretic, and other techniques also have been used. Customarily, deposition is done at an intermediate temperature, followed by diffusion in a controlled-atmosphere furnace at approximately 1040 to 1120 °C (1900–2050 °F).

Overlay coatings are applied by physical vapor deposition (PVD) in vacuum chambers. They also may be applied by plasma spray techniques. Low-pressure plasma spray (LPPS) techniques produce coatings with properties comparable to or better than those of PVD vacuum-produced coatings. (Argon is used in LPPS, in opposition to the air plasma-spray process originally used.) Low-pressure plasma spray has been one of the primary methods of applying TBCs.

Overlay coatings tend to be line-of-sight coatings, whereas pack-diffusion coatings are not. Plasma spray techniques afford more flexibility in application of overlay coatings than do PVD processes, because the angular relationship between the plasma and the part may be varied more or less in a large envelope in order to direct the coating to desired areas. Plasma spray also provides more opportunity for compositional flexibility than does PVD.

General Requirements of a Corrosion Protective Coating. Coating selection will be based on knowledge of oxidation/corrosion behavior in laboratory, pilot-plant, and field tests. Attributes probably required for successful coating selection include:

- High resistance to oxidation and/or hot corrosion
- Ductility sufficient to provide adequate resistance to TMF
- Compatibility with the base alloys
- Low rate of interdiffusion with the base alloy
- Ease of application and low cost relative to improvement in component life
- Ability to be stripped and reapplied without significant reduction of base-metal dimensions or degradation of base-metal properties

Other Environmental Effects

Stress-corrosion cracking can occur in nickel- and iron-nickel-base superalloys at lower temperatures. Hydrogen embrittlement at cryogenic

Table 12 Stress rupture strengths for selected cast nickel-base superalloys

	Rupture stress at:					
	815 °C (1500 °F)		870 °C (1600 °F)		980 °C (1800 °F)	
Alloy	100 h MPa (ksi)	1000 h MPa (ksi)	100 h MPa (ksi)	1000 h MPa (ksi)	100 h MPa (ksi)	1000 h MPa (ksi)
Nickel-base						
IN-713 LC	425 (62)	325 (47)	295 (43)	240 (35)	140 (20)	105 (15)
IN-713 C	370 (54)	305 (44)	305 (44)	215 (31)	130 (19)	70 (10)
IN-738 C	470 (68)	345 (50)	330 (48)	235 (34)	130 (19)	90 (13)
IN-738 LC	430 (62)(a)	315 (46)	295 (43)(a)	215 (31)	140 (20)(a)	90 (13)
IN-100	455 (66)	365 (53)	360 (52)	260 (38)	160 (23)	90 (13)
MAR-M 247 (MM 0011)	585 (85)	415 (60)	455 (66)	290 (42)	185 (27)	125 (18)
MAR-M 246(a)	525 (76)	435 (62)	440 (63)	290 (42)	195 (28)	125 (18)
MAR-M 246 Hf (MM 006)	530 (77)	425 (62)	425 (62)	285 (41)	205 (30)	130 (19)
MAR-M 200	495 (72)(a)	415 (60)(a)	385 (56)(a)	295 (43)(a)	170 (25)	125 (18)
MAR-M 200 Hf (MM 009)(b)	…	…	…	305 (44)	…	125 (18)
B-1900	510 (74)	380 (55)	385 (56)	250 (36)	180 (26)	110 (16)
René 77(a)	…	…	310 (45)	215 (31.5)	130 (19)	62 (9.0)
René 80	…	…	350 (51)	240 (35)	160 (23)	105 (15)
IN-625(a)	130 (19)	110 (16)	97 (14)	76 (11)	34 (5)	28 (4)
IN-162(a)	505 (73)	370 (54)	340 (49)	255 (37)	165 (24)	110 (16)
IN-731(a)	505 (73)	365 (53)	…	…	165 (24)	105 (15)
IN-792(a)	515 (75)	380 (55)	365 (53)	260 (38)	165 (24)	105 (15)
M-22(a)	515 (75)	385 (56)	395 (57)	285 (41)	200 (29)	130 (19)
MAR-M 421(a)	450 (65)	305 (44)	310 (46)	215 (31)	125 (18)	83 (12)
MAR-M 432(a)	435 (63)	330 (48)	295 (40)	215 (31)	140 (20)	97 (14)
MC-102(a)	195 (28)	145 (21)	145 (21)	105 (15)	…	…
Nimocast 90(a)	160 (23)	110 (17)	125 (18)	83 (12)	…	…
Nimocast 242(a)	110 (16)	83 (12)	90 (13)	59 (8.6)	45 (6.5)	…
Udimet 500(a)	330 (48)	240 (35)	230 (33)	165 (24)	90 (13)	…
Udimet 710(a)	420 (61)	325 (47)	305 (44)	215 (31)	150 (22)	76 (11)
CMSX-2(b)	…	…	…	345 (50)	…	170 (25)
GMR-235(b)	…	…	…	180 (26)	…	75 (11)
IN-939(b)	…	…	…	195 (28)	…	60 (9)
MM 002(b)	…	…	…	305 (44)	…	125 (18)
IN-713 Hf (MM 004)(b)	…	…	…	205 (30)	…	90 (13)
René 125 Hf (MM 005)(b)	…	…	…	305 (44)	…	115 (17)
SEL-15(b)	…	…	…	295 (43)	…	75 (11)
UDM 56(b)	…	…	…	270 (39)	…	125 (18)
Cobalt-base						
HS-21	150 (22)	95 (14)	115 (17)	90 (13)	60 (9)	50 (7)
X-40 (HS-31)	180 (26)	140 (20)	130 (19)	105 (15)	75 (11)	55 (8)
MAR-M 509	270 (39)	225 (33)	200 (29)	140 (20)	115 (17)	90 (13)
FSX-414	150 (22)	115 (17)	110 (16)	85 (12)	55 (8)	35 (5)
WI-52	…	195 (28)	175 (25)	150 (22)	90 (13)	70 (10)

(a) Ref 12. (b) Ref 13

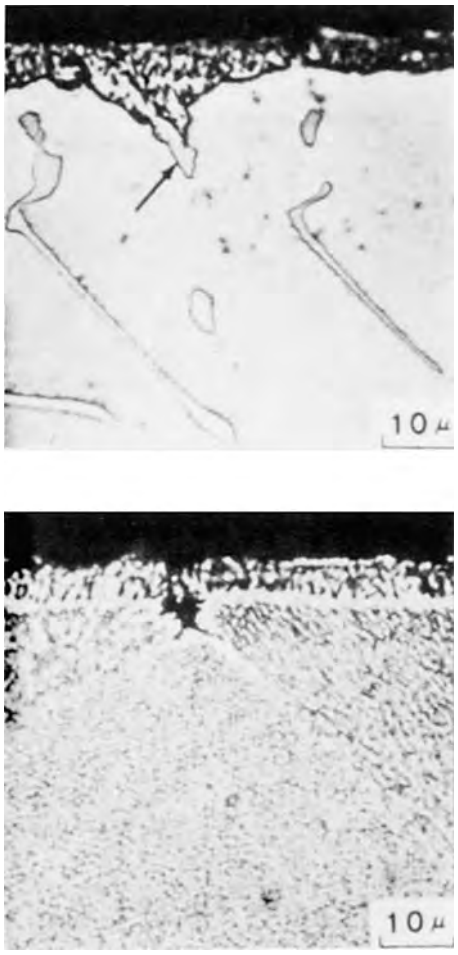


Fig. 23 Effects of oxidation on superalloys. (a) Accelerated oxidation of MC carbide (arrow) at surface of MAR-M 200 at 925 °C (1700 °F). (b) Accelerated oxidation of grain boundary in Udimet 700 at 760 °C (1400 °F). 1000×

temperatures has been reported for such alloys. Furthermore, so-called inert environments—vacuum, for example, or gases such as helium or argon—may produce mechanical behavior substantially different from baseline uncoated properties, which usually are determined in static-air tests.

ACKNOWLEDGEMENT

This article was adapted from M.J. Donachie and S.J. Donachie, Superalloys, *Metals Handbook Desk Edition*, 2nd ed., J.R. Davis, Ed., ASM International, 1998, p 394–414

REFERENCES

1. G.E. Maurer, Primary and Secondary Melt Processing—Superalloys, *Superalloys, Supercomposites and Superceramics*, Academic Press, 1989, p 49–97
2. R. Galipeau and R. Sjoblad, *Mater. Eng.*, Sept 1967
3. C.R. Brooks, *Heat Treatment, Structure and Properties of Nonferrous Alloys*, American Society for Metals, 1982
4. C.T. Sims, "Nickel Alloys—The Heart of Gas Turbine Engines," Paper 70-GT-24, American Society of Mechanical Engineers, 1970
5. M.J. Donachie, Overheating, Creep and Alloy Stability, *Properties and Selection: Stainless Steels, Tool Materials and Special-Purpose Metals*, Vol 3, 9th ed., *Metals Handbook*, American Society for Metals, 1980, p 220–229
6. D.M. Moon and F.J. Wall, The Effect of Phase Instability on the High Temperature Stress Rupture Properties of Representative Nickel Base Superalloys, *Int. Symp. Structural Stability in Superalloys*, Vol 1, TMS-AIME, 1968, p 115–133
7. "High-Temperature High-Strength Nickel Base Alloys," Inco Alloys International Ltd., distributed by Nickel Development Institute
8. "Product Handbook," Publication 1A1-38, Inco Alloys International Inc., 1988
9. *Materials Selector 1988*, Penton, 1987
10. F.R. Morral, Ed., Wrought Superalloys, *Properties and Selection: Stainless Steels, Tool Materials and Special-Purpose Metals*, Vol 3, 9th ed., *Metals Handbook*, American Society for Metals, 1980
11. Alloy 230 product literature, Haynes International
12. Appendix B, compiled by T.P. Gabb and R.L. Dreshfield, *Superalloys II*, C.T. Sims, N.S. Stoloff, and W.C. Hagel, Ed., John Wiley & Sons, 1987, p 575–596
13. R.W. Fawley, Superalloy Progress, *The Superalloys*, C.T. Sims and W.C. Hagel, Ed., John Wiley & Sons, 1972, p 12

SELECTED REFERENCES

General

- W. Betteridge and J. Heslop, Ed., *The Nimonic Alloys*, 2nd ed., Crane, Russak and Co., 1974
- Chapters on heat-resistant materials and superalloys in *Properties and Selection: Irons, Steels, and High-Performance Alloys*, Vol 1, *ASM Handbook*, ASM International, 1990, p 950–1006
- J.R. Davis, Ed., *Heat-Resistant Materials*, ASM International, 1997
- M.J. Donachie, Ed., *Superalloys Source Book*, American Society for Metals, 1984
- G.Y. Lai, *High Temperature Corrosion of Engineering Alloys*, ASM International, 1990
- The proceedings of a continuing series of conferences in the United States, first held at Seven Springs Mountain Resort, Champion, PA, in 1968 and at 4-year intervals thereafter with emphasis on high-temperature materials (initial proceedings published as follows: *International Symposium on Structural Stability in Superalloys*, Vol I & Vol II, AIME, New York, 1968)
- The proceedings of a continuing series of conferences in Europe, first held in 1978 and at 4-year intervals thereafter, with emphasis on gas turbines, power engineering and other applications (initial proceedings published as follows: *High Temperature Alloys for Gas Turbines*, Applied Science Publishers, 1978)
- The proceedings of a continuing series of conferences in the United States, first held in 1989 and at irregular intervals thereafter with emphasis on the metallurgy of IN-718 and related alloys (initial proceedings published as follows: *Superalloy 718—Metallurgy and Applications*, AIME, 1989)
- The proceedings of a series of conferences in the United States published as follows: *Heat-Resistant Materials* and *Heat-Resistant Materials—II*, ASM International, 1991 and 1995
- K.P. Rohrbach, Trends in High-Temperature Alloys, *Adv. Mater. & Process.*, Vol 148 (No. 10), 1995, p 37–40
- C.T. Sims and W.C. Hagel, Ed., *The Superalloys*, John Wiley & Sons, 1972
- C.T. Sims, N.S. Stoloff, and W.C. Hagel, Ed., *Superalloys II*, John Wiley & Sons, 1987
- C.P. Sullivan, M.J. Donachie, and F.R. Morral, *Cobalt-Base Superalloys—1970*, Cobalt Information Center, Brussels, 1970

Microstructure

- M.J. Donachie and O.H. Kriege, Phase Extraction and Analysis in Superalloys—Summary of Investigations by ASTM Committee E-4 Task Group I, *J. Mater.*, Vol 7, 1972, p 269–278
- J.L. Johnson and M.J. Donachie, Jr., "Microstructure of Precipitation Strengthened Nickel-Base Superalloys," Report System Paper C 6-18.1, American Society for Metals, 1966
- E. Kohlhaas and A. Fischer, The Metallography of Superalloys, *Prakt. Metallogr.*, Vol 8, 1971, p 3–25
- P.S. Kotval, The Microstructure of Superalloys, *Metallography*, Vol 1, 1969, p 251–285
- H.F. Merrick, Precipitation in Nickel-Base Alloys, *Precipitation Processes in Solids*, TMS-AIME, 1978, p 161–190
- J.R. Mihalisin, Phase Chemistry and Its Relation to Alloy Behavior in Several Cast Nickel-Base Superalloys, *Rev. High Temp. Mater.*, Vol 2, 1974, p 243–260
- J.F. Radavich and W.H. Couts, Metallography of the Superalloys, *Rev. High Temp. Mater.*, Vol 1, 1971, p 55–96
- G.P. Sabol and R. Stickler, Microstructure of Nickel-Based Superalloys, *Phys. Status Solidi*, Vol 35, 1969, p 11–52

Properties and Microstructure

- S.D. Antolovich and N. Jayaraman, The Effect of Microstructure on the Fatigue Behavior of Ni Base Superalloys, *Fatigue: Environment and Temperature Effects*, Plenum Press, 1983, p 119–144
- R.F. Decker, Strengthening Mechanisms in Nickel-Base Alloys, *Steel Strengthening Mechanisms*, Climax Molybdenum, 1970, p 147–170
- M.J. Donachie, Relationship of Properties to Microstructure in Superalloys, *Superalloys Source Book*, American Society for Metals, 1984, p 102-111
- M.J. Donachie, Overheating, Creep and Alloy Stability, *Properties and Selection: Stainless Steels, Tool Materials and Special--Purpose Metals*, Vol 3, 9th ed., *Metals Handbook*, American Society for Metals, 1980, p 220–229
- R.L. Dreshfield, Understanding Single-Crystal Superalloys, *Met. Prog.*, Vol 130 (No. 2), 1986, p 43–46
- M. Gell et al., The Fatigue Strength of Nickel-Base Alloys, *Achievement of High Fatigue Resistance*, STP 467, ASTM, 1970, p 113–153
- G.W. Goward, Low-Temperature Hot Corrosion in Gas Turbines: A Review of Causes and Coatings Therefor, *J. Eng. Gas Turb. Power (Trans. ASME)*, Vol 108, 1986, p 421–425
- R.T. Holt and W. Wallace, Impurities and Trace Elements in Nickel-Base Superalloys, *Int. Met. Rev.*, Vol 21, 1976, p 1–24
- A.K. Jena and M.C. Chaturvedi, The Role of Alloying Elements in the Design of Nickel-Base Superalloys, *J. Mater. Sci.*, Vol 19, 1984, p 3121–3139
- F.S. Pettit and G.W. Goward, High Temperature Corrosion and Use of Coatings for Protection, *Metallurgical Treatises*, AIME, 1981, p 603–619

- P.N. Quested and S. Ogersby, Mechanical Properties of Conventionally Cast, Directionally Solidified, and Single Crystal Superalloys, *Mater. Sci. Technol.*, Vol 2 (No. 5), 1986, p 461–475
- J.F. Radavich, The Physical Metallurgy of Cast and Wrought Alloy 718, *Superalloy 718—Metallurgy and Applications*, AIME, 1989, p 229–240
- C.T. Sims, a series of articles in *J. Met.*, Vol 18, 1966, p 1119–1134; Vol 21 (No. 12), 1969, p 27–42
- C.P. Sullivan and M.J. Donachie, a series of articles in *Met. Eng. Q.*, Vol 7 (No. 2), 1967, p 36–45; Vol 9 (No. 2), 1969, p 16–29; Vol 11 (No. 4), 1971, p 1–11
- D.A. Woodford and D.F. Mowbray, Effect of Material Characteristic on Thermal Fatigue of Cast Superalloys: A Review, *Mater. Sci. Eng.*, Vol 16, 1974, p 5–45

Processing

- J.L. Bartos, Review of Superalloy Powder Metallurgy Processing for Aircraft Gas Turbine Applications, *MiCon 78*, STP 672, ASTM, 1979, p 564–577
- J.A. Burger and D.K. Hanink, Heat Treating Nickel-Base Superalloys, *Met. Prog.*, Vol 92 (No. 1), 1967, p 61–66
- J.E. Coyne, Microstructural Control in Titanium- and Nickel-Base Forgings: An Overview, *Met. Technol.*, Vol 4, 1977, p 337–345
- D.A. DeAntonio, D. Duhl, T. Howson, and M.F. Rothman, Heat Treating of Superalloys, *Heat Treating*, Vol 4, *ASM Handbook*, ASM International, 1991, p 793–814
- A.J. DeRidder and R.W. Koch, Controlling Variations in Mechanical Properties of Heat Resistant Alloys during Forging, *Met. Eng. Q.*, Vol 5 (No. 3), 1965, p 61–64
- J.D. Destefani, Clean PM Superalloys, *Adv. Mater. Process.*, Vol 136 (No. 3), 1989, p 63–66
- K.A. Ellison, P. Lowden, and J. Liburdi, Powder Metallurgy Repair of Turbine Components, *J. Eng. Gas Turb. Power (Trans. ASME)*, Vol 116, 1994, p 237–242
- G.W. Goward and L.W. Cannon, Pack Cementation Coatings for Superalloys: A Review of History, Theory and Practice, *J. Eng. Gas Turb. Power (Trans. ASME)*, Vol 110, 1988, p 150–154
- W.L. Hallerberg, "Superalloy Investment Castings—Processing and Applications," Paper CM71-160, Society of Manufacturing Engineers, 1971
- Heat Resistant Superalloys, Chapter 11, *Forging Materials and Practices*, Reinhold, 1968, p 254–293
- G. Heckman, "Stabilizing Heat Treatments for Gas Turbine Bucket Alloys," Paper No. 67-GT-55, American Society of Mechanical Engineers, March 1967
- L.A. Jackman, G.E. Maurer, and S. Widge, White Spots in Superalloys, *Superalloy 718—Metallurgy and Applications*, AIME, 1989, p 153–166
- H. Lammermann and G. Kienel, PVD Coatings for Aircraft Turbine Blades, *Adv. Mater. Process.*, Vol 140, 1991, p 18–23
- G.E. Maurer, Primary and Secondary Melt Processing—Superalloys, *Superalloys, Supercomposites and Superceramics*, Academic Press, 1989, p 49–97
- S.M. Meier and D.K. Gupta, The Evolution of Thermal Barrier Coatings in Gas Turbine Engine Applications, *J. Eng. Gas Turb. Power (Trans. ASME)*, Vol 116, 1994, p 250–257
- S.M. Meier, D.K. Gupta, and K.D. Sheffler, Ceramic Thermal Barrier Coatings for Commercial Gas Turbine Engines, *J. Met.*, Vol XX, 1991, p 50–53
- A. Mitchell, Recent Developments in Specialty Melting Processes, *Mater. Technol.*, Vol 9, 1994, p 201–206
- W.J. Molloy, Investment-Cast Superalloys: A Good Investment, *Adv. Mater. Process.*, Vol 138 (No. 4), 1990, p 23–25, 28–30
- D.R. Muzyka, Controlling Microstructures and Properties of Superalloys via Use of Precipitated Phases, *Met. Eng. Q.*, Vol 11 (No. 4), 1971, p 12–20
- D. Muzyka and G.N. Maniar, Microstructure Approach to Property Optimization in Wrought Superalloys, *Metallography—A Practical Tool for Correlating the Structure and Properties of Materials*, STP 557, ASTM, 1974, p 198–219
- J.R. Nichols and D.J. Stephenson, Applications of Coating Technology and HIP to Advanced Materials Processing, *Mater. High Temp.*, Vol 9, 1991, p 110–120
- W.A. Owczarski, Process and Metallurgical Factors in Joining Superalloys and Other High Service Temperature Materials, *Physical Metallurgy of Metal Joining*, AIME, 1980, p 166–189
- C. Olofson et al., "Machining and Grinding of Nickel- and Cobalt-Base Alloys," Report No. TM X-53446, National Aeronautics and Space Administration, 1966
- J.W. Pridgeon, F.N. Darmara, J.S. Huntington, and W.H. Sutton, Principles and Practices of Vacuum Induction Melting and Vacuum Arc Remelting, *Metallurgical Treatises*, AIME, 1981, p 261–276
- J. Rawson, Effect of Temperature on Forgeability of Some Heat-Resistant Alloys, *Reheating for Hot Working*, Iron and Steel Institute, London, 1968, p 65–69
- A.J. Ridder and R. Koch, Forging and Processing of High-Temperature Alloys, *MiCon 78*, STP 672, ASTM, 1979, p 547–563
- S.K. Srivastava, Forging of Heat-Resistant Alloys, *Forming and Forging*, Vol 14, *ASM Handbook*, ASM International, 1988, p 231–236
- R.A. Stevens and P.E.J. Flewitt, Hot Isostatic Pressing to Remove Porosity and Creep Damage, *Mater. Eng.*, Vol 3, 1982, p 461–469
- K.N. Strafford et al., Ed., *Coatings and Surface Treatment for Corrosion and Wear Resistance*, Institution of Corrosion Science and Technology, 1988
- J. Vagi et al., "Joining of Nickel and Nickel-Base Alloys," Report TM X-53447, National Aeronautics and Space Administration, 1966
- F.L. VerSnyder and M.E. Shank, The Development of Columnar Grain and Single Crystal High Temperature Materials through Directional Solidification, *Mater. Sci. Eng.*, Vol 6, 1970, p 213–247
- C.H. White, P.M. Williams, and M. Morley, Cleaner Superalloys via Improved Melting Practices, *Adv. Mater. Process.*, Vol 137 (No. 4), 1990, p 53–57
- N.A. Wilkinson, Forging of 718—The Importance of T.M.P., *Superalloy 718—Metallurgy and Applications*, AIME, 1989, p 119–133

ASM Specialty Handbook: Nickel, Cobalt, and Their Alloys
J.R. Davis, editor, p 92-105
DOI:10.1361/ncta2000p092

Copyright © 2000 ASM International®
All rights reserved.
www.asminternational.org

Special-Purpose Nickel Alloys

NICKEL-BASE ALLOYS have a number of unique properties, or combinations of properties, that allow them to be used in a variety of specialized applications. For example, the high resistivity (resistance to flow of electricity) and heat resistance of nickel-chromium alloys lead to their use as electric resistance heating elements. The soft magnetic properties of nickel-iron alloys are employed in electronic devices and for electromagnetic shielding of computers and communication equipment. Iron-nickel alloys have low expansion characteristics as a result of a balance between thermal expansion and magnetostrictive changes with temperature. Originally used as clock pendulums, these alloys are now widely employed as lead frames in packaging electronic chips and as the shadow-masks in color television tubes. On a larger scale, they provide one solution to coping with the thermal expansion requirements of storage and transportation tanks for the growing liquid natural gas industry.

Other properties of interest that expand the markets and applications of nickel and nickel alloys include those to follow:

- Shape memory characteristics of equiatomic nickel-titanium alloys that allow them to be used as actuators, hydraulic connectors, and eyeglass frames
- The high strength at elevated temperature and resistance to stress relaxation that allow wrought nickel-beryllium-titanium to be used for demanding electrical/electronic applications, for example, springs subjected to elevated temperatures (up to 370 °C, or 700 °F) for short times
- The combination of heat removal (high thermal conductivity) and wear resistance that allows cast nickel-beryllium-carbon alloys to be used for tooling for glass forming operations

These and other special-purpose alloys and applications are described subsequently.

Commercially Pure Nickel for Electronic Applications

Commercially pure nickel is available in several grades, slightly different in composition, to meet special needs. The grades considered in this section include the following:

- Nickel 200 (99.6% Ni, 0.04% C)
- Nickel 201 (99.6% Ni, 0.02% C maximum)
- Nickel 205 (99.6% Ni, 0.04% C, 0.04% Mg)
- Nickel 233 (see composition in table that follows)
- Nickel 270 (99.97% Ni)

Composition limits and property data on several of these grades can be found in the article "Wrought Corrosion-Resistant Nickels and Nickel Alloys" in this Handbook.

Nickel 200 and 201. Wrought Nickel 200 (UNS N02200), the general purpose grade, is used for leads and terminals where good strength and toughness at elevated temperature and subzero temperatures are necessary; for transducers (it being one of three metals demonstrating magnetostrictive properties); and for fuel cell and battery plates.

A low-carbon variant, Nickel 201 (UNS N02201), is ideal for deep drawing, etching, spinning, and coining; its rate of work hardening is also low.

Nickel 205. The selected chemistry of Nickel 205 (UNS N02205) results in a high magnetostrictive coefficient and Curie temperature. Its uses have included grid side rods, base pins, anodes, getter tabs, and cathode shields.

Nickel 233 (UNS N02233) is specially produced to the following closely controlled, low-residual-element levels:

Element	Percentage
Carbon	0.15 max
Copper	0.10 max
Iron	0.10 max
Magnesium	0.01–0.10
Manganese	0.30 max
Sulfur	0.008 max
Silicon	0.10 max
Titanium	0.005 max
Nickel	99.00 min

This grade is especially suitable for active cathodes, vacuum tube anodes, and structural parts of tubes.

Nickel 270 (UNS N02270), a high-purity, powder-produced nickel, is 99.97% nickel with a 0.001% maximum limit on cobalt, magnesium, chromium, titanium, sulfur, silicon, manganese, and copper, a 0.005% limit on iron, and a 0.02% limit on carbon. This high purity results in lower coefficient of expansion, electrical resistivity, Curie temperature, and greater ductility than those of other grades of nickel and makes Nickel 270 especially useful for some electronics applications such as components of hydrogen thyratrons and as a substrate for precious metal cladding.

Resistance Heating Alloys

Resistance heating alloys are used in many varied applications—from small household appliances to large industrial process heating systems and furnaces. In appliances or industrial process heating, the heating elements are usually either open helical coils of resistance wire mounted with ceramic bushings in a suitable metal frame, or enclosed metal-sheathed elements consisting of a smaller-diameter helical coil of resistance wire electrically insulated from the metal sheath by compacted refractory insulation. In industrial furnaces, elements often must operate continuously at temperatures as high as 1300 °C (2350 °F) for furnaces used in metal-treating industries, 1700 °C (3100 °F) for kilns used for firing ceramics, and occasionally 2000 °C (3600 °F) or higher for special applications.

Material Requirements. Materials for electric heating depend on an inherent resistance to the flow of electricity to generate heat. Copper wire does not get appreciably hot when carrying electricity because it has good electrical conductivity. Thus for an alloy—as wire, ribbon, or strip—to perform as an electric heating element, it must resist the flow of electricity.

Most of the common steels and alloys such as stainless steels do resist the flow of electricity. The measure of this characteristic is referred to as "electrical resistivity." It is expressed as either ohm millimeter square per meter ($\Omega \cdot mm^2/m$) in metric units or ohm times circular mils per foot ($\Omega \cdot$ circular mil/ft) in English units.

If resistivity alone was the prime factor for an electric heating element, the choice could be from many alloy candidates in a broad spectrum of cost. However, there are a number of requirements a material must meet in order to avoid failure and provide an extended service

Table 1 Typical properties of resistance heating materials

Basic composition	Resistivity(a), Ω · mm²/m(b)	Average change in resistance(c), %, from 20 °C to: 260 °C	540 °C	815 °C	1095 °C	Thermal expansion, μm · °C, from 20 °C to: 100 °C	540 °C	815 °C	Tensile strength MPa	ksi	Density g/cm³	lb/in.³
Nickel-chromium and nickel-chromium-iron alloys												
78.5Ni-20Cr-1.5Si (80–20)	1.080	4.5	7.0	6.3	7.6	13.5	15.1	17.6	655–1380	95–200	8.41	0.30
77.5Ni-20Cr-1.5Si-1Nb	1.080	4.6	7.0	6.4	7.8	13.5	15.1	17.6	655–1380	95–200	8.41	0.30
68.5Ni-30Cr-1.5Si (70–30)	1.180	2.1	4.8	7.6	9.8	12.2	…	…	825–1380	120–200	8.12	0.29
68Ni-20Cr-8.5Fe-2Si	1.165	3.9	6.7	6.0	7.1	…	12.6	…	895–1240	130–180	8.33	0.30
60Ni-16Cr-22Fe-1.5Si	1.120	3.6	6.5	7.6	10.2	13.5	15.1	17.6	655–1205	95–175	8.25	0.30
37Ni-21Cr-40Fe-2Si	1.08	7.0	15.0	20.0	23.0	14.4	16.5	18.6	585–1135	85–165	7.96	0.288
35Ni-20Cr-43Fe-1.5Si	1.00	8.0	15.4	20.6	23.5	15.7	15.7	…	550–1205	80–175	7.95	0.287
35Ni-20Cr-42.5Fe-1.5Si-1Nb	1.00	8.0	15.4	20.6	23.5	15.7	15.7	…	550–1205	80–175	7.95	0.287
Iron-chromium-aluminum alloys												
83.5Fe-13Cr-3.25Al	1.120	7.0	15.5	…	…	10.6	…	…	620–1035	90–150	7.30	0.26
81Fe-14.5Cr-4.25Al	1.25	3.0	9.7	16.5	…	10.8	11.5	12.2	620–1170	90–170	7.28	0.26
73.5Fe-22Cr-4.5Al	1.35	0.3	2.9	4.3	4.9	10.8	12.6	13.1	620–1035	90–150	7.15	0.26
72.5Fe-22Cr-5.5Al	1.45	0.2	1.0	2.8	4.0	11.3	12.8	14.0	620–1035	90–150	7.10	0.26
Pure metals												
Molybdenum	0.052	110	238	366	508	4.8	5.8	…	690–2160	100–313	10.2	0.369
Platinum	0.105	85	175	257	305	9.0	9.7	10.1	345	50	21.5	0.775
Tantalum	0.125	82	169	243	317	6.5	6.6	…	345–1240	50–180	16.6	0.600
Tungsten	0.055	91	244	396	550	4.3	4.6	4.6	3380–6480	490–940	19.3	0.697
Nonmetallic heating-element materials												
Silicon carbide	0.995–1.995	–33	–33	–28	–13	4.7	…	…	28	4	3.2	0.114
Molybdenum disilicide	0.370	105	222	375	523	9.2	…	…	185	27	6.24	0.225
$MoSi_2$ + 10% ceramic additives	0.270	167	370	597	853	13.1	14.2	14.8	…	…	5.6	0.202
Graphite	9.100	–16	–18	–13	–8	1.3	…	…	1.8	0.26	1.6	0.057

(a) At 20 °C (68 °F). (b) To convert to Ω·circular mil/ft, multiply by 601.53. (c) Changes in resistance may vary somewhat, depending on cooling rate.

Table 2 Recommended maximum furnace operating temperatures for resistance heating materials

Basic composition, %	Approximate melting point °C	°F	Maximum furnace operating temperature in air °C	°F
Nickel-chromium and nickel-chromium-iron alloys				
78.5Ni-20Cr-1.5Si (80–20)	1400	2550	1150	2100
77.5Ni-20Cr-1.5Si-1Nb	1390	2540		
68.5Ni-30Cr-1.5Si (70–30)	1380	2520	1200	2200
68Ni-20Cr-8.5Fe-2Si	1390	2540	1150	2100
60Ni-16Cr-22Fe-1.5Si	1350	2460	1000	1850
35Ni-30Cr-33.5Fe-1.5Si	1400	2550		
35Ni-20Cr-43Fe-1.5Si	1380	2515	925	1700
35Ni-20Cr-42.5Fe-1.5Si-1Nb	1380	2515		
Iron-chromium-aluminum alloys				
83.5Fe-13Cr-3.25Al	1510	2750	1050	1920
81Fe-14.5Cr-4.25Al	1510	2750		
79.5Fe-15Cr-5.2Al	1510	2750	1260	2300
73.5Fe-22Cr-4.5Al	1510	2750	1280	2335
72.5Fe-22Cr-5.5Al	1510	2750	1375	2505
Pure metals				
Molybdenum	2610	4730	400(a)	750(a)
Platinum	1770	3216	1500	2750
Tantalum	3000	5400	500(a)	930(a)
Tungsten	3400	6150	300(a)	570(a)
Nonmetallic heating-element materials				
Silicon carbide	2410	4370	1600	2900
Molybdenum disilicide	(b)	(b)	1700–1800	3100–3270
$MoSi_2$ + 10% ceramic additives	(b)	(b)	1900	3450
Graphite	3650–3700(b)	6610–6690(c)	400(d)	750(d)

Element	Recommended temperatures: Vacuum	Pure H_2	City gas
Mo	1650 °C (3000 °F)	1760 °C (3200 °F)	1700 °C (3100 °F)
Ta	2480 °C (4500 °F)	Not recommended	Not recommended
W	1650 °C (3000 °F)	2480 °C (4500 °F)	1700 °C (3100 °F)

(a) Recommended atmospheres for these metals are a vacuum of 10^{-4} to 10^{-5} mm Hg, pure hydrogen, and partly combusted city gas dried to a dew point of 4 °C (40 °F). In these atmospheres, the recommended temperatures, would be as shown above. (b) Decomposes before melting at approximately 1740 °C (3165 °F) for $MoSi_2$, and 1825 °C (3315 °F) for $MoSi_2$ + 10% ceramic additives. (c) Graphite volatilizes without melting at 3650 to 3700 °C (6610 to 6690 °F). (d) At approximately 400 °C (750 °F) (threshold oxidation temperature), graphite undergoes a weight loss of 1% in 24 h in air. Graphite elements can be operated at surface temperatures up to 2205 °C (4000 °F) in inert atmospheres.

life. The primary requirements of materials used for heating elements are high melting point, high electrical resistivity, reproducible temperature coefficient of resistance, good oxidation resistance, absence of volatile components, and resistance to contamination. Other desirable properties are good elevated-temperature creep strength, high emissivity, low thermal expansion, and low modulus (both of which help minimize thermal fatigue), good resistance to thermal shock, and good strength and ductility at fabrication temperatures.

Property Data. Four groups of materials are commonly used for high-temperature resistance heating elements: (1) nickel-chromium (Ni-Cr) and nickel-chromium-iron (Ni-Cr-Fe) alloys, (2) iron-chromium-aluminum alloys, (3) refractory metals, and (4) nonmetallic (ceramic) materials. Of these four groups, the Ni-Cr and Ni-Cr-Fe alloys serve by far the greatest number of applications. Table 1 compares the physical and mechanical properties of the four groups. Maximum operating temperatures for resistance heating materials for furnace applications are given in Table 2. Additional property data on some of the Ni-Cr and Ni-Cr-Fe alloys listed in Tables 1 and 2 can be found in data sheets published in the section Properties of Electrical Resistance Alloys in the article "Electrical Resistance Alloys" in *Properties and Selection: Nonferrous Alloys and Special-Purpose Materials*, Volume 2 of the *ASM Handbook*.

The resistivities of Ni-Cr and Ni-Cr-Fe alloys are high, ranging from 1000 to 1187 nΩ · m (600 to 714 Ω · circular mil/ft) at 25 °C. Figure 1 shows that the resistance changes more rapidly with temperature for 35Ni-20Cr-

45Fe than for any other alloy in this group. The curve for 35Ni-30Cr-35Fe (which is no longer produced) is similar but slightly lower. The other four curves, which are for alloys with substantially higher nickel contents, reflect relatively low changes in resistance with temperature. For these alloys, rate of change reaches a peak near 540 °C (1000 °F), goes through a minimum at about 760 to 870 °C (1400 to 1600 °F), and then increases again. For Ni-Cr alloys, the change in resistance with temperature depends on section size and cooling rate. Figure 2 presents values for a typical 80Ni-20Cr alloy. The maximum change (curve A) occurs with small sections, which cool rapidly from the last production heat treatment. The smallest change occurs for heavy sections, which cool slowly. The average curve (curve B) is characteristic of medium-size sections.

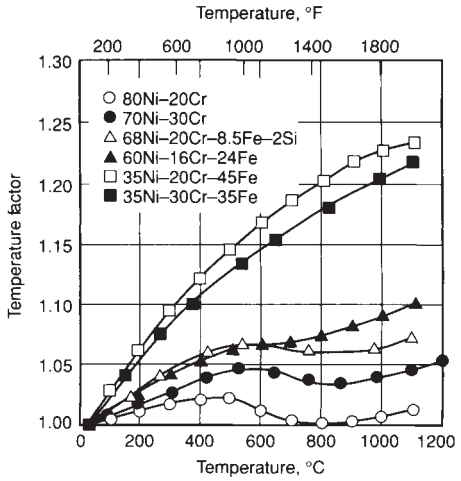


Fig. 1 Variation of resistance with temperature for six Ni-Cr and Ni-Cr-Fe alloys. To calculate resistance at temperature, multiply resistance at room temperature by the temperature factor.

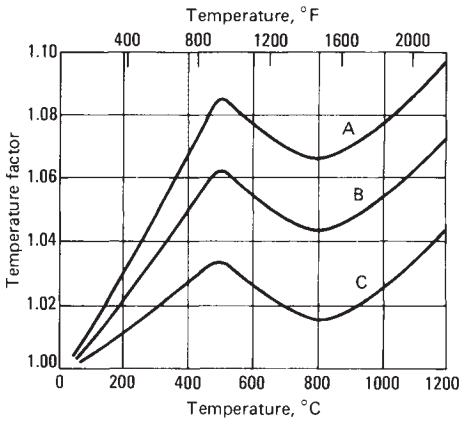


Fig. 2 Variation of resistance with temperature for 80Ni-20Cr heating alloy. Curve A is for a specimen cooled rapidly after the last production heat treatment. Curve C is for a specimen cooled slowly after the last production heat treatment. Curve B represents the average value for material as delivered by the producer. To calculate resistance at temperature, multiply the resistance at room temperature by the temperature factor.

Nickel Alloys for Resistors and Thermostats. In addition to their use as heating elements in furnaces and appliances, nickel electrical resistance alloys are also used in instruments and control equipment to measure and regulate electrical characteristics, for example, resistors, and in applications where heat generated in a metal resistor is converted to mechanical energy, for example, thermostat metals. Resistor alloys include Ni-Cr and Ni-Cr-Fe alloys similar to those used for heating elements and 75Ni-20Cr-3Al alloys containing small amounts of other metals—usually either copper, manganese, or iron. A thermostat metal is a composite material (usually in the form of sheet or strip) that consists of two or more materials bonded together, of which one may be a nonmetal. Nickel-iron, nickel-chromium-iron, and nickel-copper alloys are commonly used. Additional information on resistor and thermostat alloys can be found in the article "Electrical Resistance Alloys" in *Properties and Selection: Nonferrous Alloys and Special-Purpose Materials*, Volume 2 of the *ASM Handbook*.

Thermocouple Alloys

The thermocouple thermometer is one of the most widely used devices for measurement of temperature in the metals industry. Essentially, a thermocouple thermometer is a system consisting of a temperature-sensing element called a thermocouple, which produces an electromotive force (emf) that varies with temperature, a device for sensing emf, which may include a printed scale for converting emf to equivalent temperature units, and an electrical conductor (extension wires) for connecting the thermocouple to the sensing device. Although any combination of two dissimilar metals and/or alloys will generate a thermal emf, only eight thermocouples are in common industrial use today. These eight have been chosen on the basis of such factors as mechanical and chemical properties, stability of emf, reproducibility, and cost.

Table 3 presents base compositions, melting points, and electrical resistivities of the eight standard thermocouples. As indicated in the table, nickel-copper, nickel-chromium, nickel-silicon, and nickel alloys containing various combinations of aluminum, manganese, iron, silicon, and cobalt are used as either the positive (P) or negative (N) thermoelement. The maximum operating temperatures and limiting environmental factors for these alloys are also listed in Table 3. A nonstandard nickel-base thermocouple element consisting of 82Ni-18Mo alloy as the positive themoelement and 99Ni-1Co alloy as the negative thermoelement is also used in hydrogen or reducing atmospheres. More detailed information on thermocouple devices and materials can be found in the article "Thermocouple Materials" in *Properties and Selection: Nonferrous Alloys and Special-Purpose Materials*, Volume 2 of the *ASM Handbook* and in "Thermocouple Materials" in the *Metals Handbook Desk Edition, Second Edition*.

Table 3 Properties of standard thermocouples

Type	Thermoelements	Base composition	Melting point, °C	Resistivity, nΩ · m	Recommended service	Max temperature °C	Max temperature °F
J	JP	Fe	1450	100	Oxidizing or reducing	760	1400
	JN	44Ni-55Cu	1210	500			
K	KP	90Ni-9Cr	1350	700	Oxidizing	1260	2300
	KN	94Ni-Al, Mn, Fe, Si, Co	1400	320			
N	NP	84Ni-14Cr-1.4Si	1410	930	Oxidizing	1260	2300
	NN	95Ni-4.4Si-0.15 Mg	1400	370			
T	TP	OFHC Cu	1083	17	Oxidizing or reducing	370	700
	TN	44Ni-55Cu	1210	500			
E	EP	90Ni-9Cr	1350	700	Oxidizing	870	1600
	EN	44Ni-55Cu	1210	500			
R	RP	87Pt-13Rh	1860	196	Oxidizing or inert	1480	2700
	RN	Pt	1769	104			
S	SP	90Pt-10Rh	1850	189	Oxidizing or inert	1480	2700
	SN	Pt	1769	104			
B	BP	70Pt-30Rh	1927	190	Oxidizing, vacuum or inert	1700	3100
	BN	94Pt-6Rh	1826	175			

Nickel-Iron Soft Magnetic Alloys

Soft magnetic nickel-iron alloys containing from about 30 to 80% Ni are used extensively in applications requiring the following characteristics:

- High permeability
- High saturation magnetostriction
- Low hysteresis-energy loss
- Low eddy-current loss in alternating flux
- Low Curie temperature
- Constant permeability with changing temperature

As shown in Table 4, these include electromagnetic and radio frequency shields, transformers, amplifiers, tape recording head laminations, ground fault interrupter cores, antishoplifting devices, torque motors, and so on.

The nickel-iron alloys are generally manufactured as strip or sheet product; however, billet, bar, and wire can be produced as needed. Strip products are usually supplied in a

cold-rolled condition for stamping laminations or as thin foil for winding of tape toroidal cores. Strip and sheet products may also be supplied in a low-temperature, mill-annealed, fine-grain condition suitable for forming and deep drawing.

Classes of Commercial Alloys

Two broad classes of commercial alloys have been developed in the nickel-iron system. Based on nickel content, these include high-nickel alloys (about 79% Ni) and low-nickel alloys (about 45 to 50% Ni). Some alloys containing even lower nickel contents (~29 to 36%) can be used for measuring instruments requiring magnetic temperature compensation (see Table 4).

The effect of nickel content in nickel-iron alloys on saturation induction (B_s) and on initial permeability (μ_o) after annealing are illustrated in Fig. 3 and 4. Below ~28% Ni, the crystalline structure is body-centered cubic (bcc) low-carbon martensite if cooled rapidly and ferrite and austenite if cooled slowly, and these alloys are not considered useful for soft magnetic applications. Above ~28% Ni, the structure is face-centered cubic (fcc) austenite. The Curie temperature in this system is approximately room temperature at ~28% Ni and increases rapidly up to ~610 °C (1130 °F) at 68% Ni. Thus, these austenitic alloys are ferromagnetic.

The high-nickel alloys containing about 79% Ni have high initial and maximum permeabilities (Fig. 4) and very low hysteresis losses, but they also have a saturation induction of only about 0.8 T (8 kG) as shown in Fig. 3. Alloying additions of 4 to 5% Mo, or of copper and chromium to 79Ni-Fe alloys, serve to accentuate particular magnetic characteristics. Popular high-permeability alloys include the MolyPermalloys (typically 80Ni-4 to 5Mo-bal Fe) and MuMetals (typically 77Ni-5Cu-2Cr-bal Fe).

The magnetic properties of high-nickel alloys are very dependent on processing and heat treatment. Figure 5 illustrates that in ~78.5Ni-Fe, the initial permeability was low after either furnace cooling or baking at 450 °C (840 °F). However, if the same alloy was rapidly cooled from 600 °C (1110 °F), the initial permeability was increased dramatically. High-purity 78.5Ni-Fe can exhibit an initial direct current (dc) permeability of 5×10^4 and a maximum permeability of 3×10^5. These properties are obtained on ring laminations annealed in dry hydrogen at 1175 °C (2150 °F), rapid furnace cooled to room temperature, then reheated to 600 °C (1110 °F), and oil quenched. This alloy has limited commercial use because the complex heat treatment is not easily performed on parts. Also, its electrical resistivity is only 16 $\mu\Omega \cdot$ cm, which allows large eddy-current losses in alternating current (ac) applications.

High-permeability alloys must also be of high commercial purity. Air-melting and vacuum-melting practices are both used to produce low-nickel alloys, but nearly all of the high-nickel alloys are produced by vacuum induction melting (VIM). Figure 6 shows a historical perspective of the change in initial permeability of 80Ni-4Mo-Fe alloys when VIM became

Table 4 Applications for nickel-iron magnetically soft alloys

Application	Specialty alloy	Special property
Instrument transformer	79Ni-4Mo-Fe, 77Ni-5Cu-2Cr-Fe, 49Ni-Fe	High permeability, low noise and losses
Audio transformer	79Ni-4Mo-Fe, 49Ni-Fe, 45Ni-Fe, 45Ni-3Mo-Fe	High permeability, low noise and losses, transformer grade
Hearing aid transformers	79Ni-4Mo-Fe	High initial permeability, low losses
Radar pulse transformers	Oriented 49Ni-Fe, 79Ni-4Mo-Fe, 45Ni-3Mo-Fe	Processed for square hysteresis loop, tape toroidal cores
Magnetic amplifiers	Oriented 49Ni-Fe, 79Ni-4Mo-Fe	Processed for square hysteresis loop, tape toroidal cores
Transducers	45-50Ni-Fe	High saturation magnetostriction
Shielding	79Ni-4Mo-Fe, 77Ni-5Cu-2Cr-Fe, 49Ni-Fe	High permeability at low induction levels
Ground fault (GFI) interruptor core	79Ni-4Mo-Fe	High permeability, temperature stability
Sensitive direct current relays	45 to 49Ni-Fe, 78.5Ni-Fe	High permeability, low losses, low coercive force
Tape recorder head laminations	79Ni-5Mo-Fe	High permeability, low losses (0.05 to 0.03 mm, or 0.002 to 0.001 in.)
Temperature compensator	29 to 36Ni-Fe	Low Curie temperature
Dry reed magnetic switches	51Ni-Fe	Controlled expansion glass/metal sealing
Chart recorder (instrument) motors, synchronous motors	49Ni-Fe	Moderate saturation, low losses, nonoriented grade
Loading coils	81-2 brittle Moly-Permalloy	Constant permeability with changing temperature

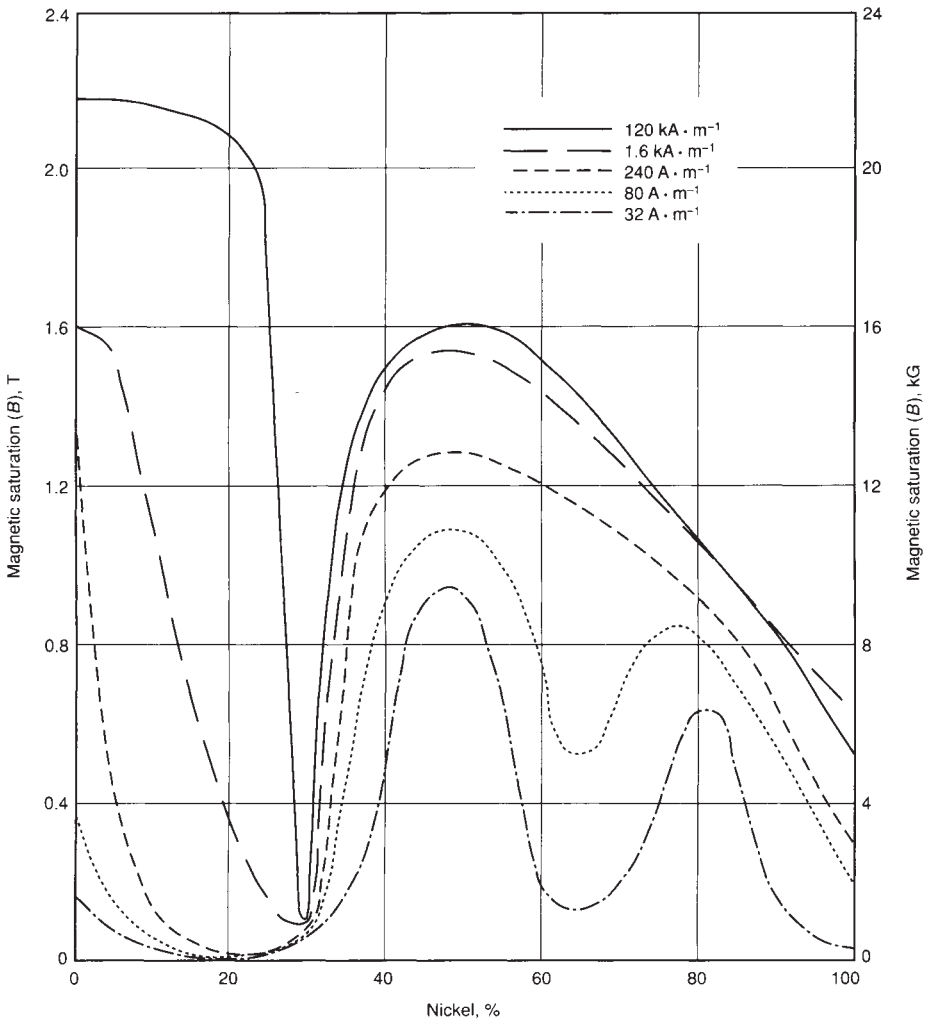


Fig. 3 Magnetic saturation of binary nickel-iron alloys at various field strengths. All samples were annealed at 1000 °C (1830 °F) and cooled in the furnace.

widely used around 1960. Interstitial impurities such as carbon, sulfur, oxygen, and nitrogen must be minimized by special melting procedures and by careful final annealing of laminations and other core configurations. Sulfur contents higher than several ppm and carbon in excess of 20 ppm are detrimental to final-annealed magnetic properties in high-nickel alloys.

Laminations or parts made from these high-nickel alloys are usually commercially annealed in pure dry hydrogen (dew point less than –50 °C, or –58 °F, at ~1000 to 1205 °C, or 1830 to 2200 °F) for several hours to eliminate stresses, to increase grain size, and to provide for alloy purification. They are cooled at any practical rate down to the critical ordering temperature range. The rate of cooling through the ordering range is typically 55 to 350 °C/h (100 to 630 °F/h), depending on the alloy being heat treated. Although the cooling rate below the ordering range is not critical, stresses due to rapid quenching must be avoided.

Vacuum furnaces may be used to anneal some high-nickel soft magnetic alloys if the application does not demand the optimum magnetic properties. However, dry hydrogen is strongly recommended for annealing nickel-iron alloys. Parts must always be thoroughly degreased to remove oils (particularly sulfur-bearing oils) prior to annealing.

The low-nickel alloys containing approximately 45 to 50% Ni are lower in initial and maximum permeability than the 79% Ni alloys (Fig. 4), but the low-nickel alloys have a higher saturation induction (about 1.5 T, or 15 kG, as shown in Fig. 3). Values of initial permeability (at a magnetic induction, *B*, or 4 mT, or 40 G) above 1.2×10^4 are typically obtained in low-nickel alloys, and values above 6×10^4 are typically obtained for 79Ni-4Mo-Fe alloys at 60 Hz using 0.36 mm (0.014 in.) thick laminations.

In alloys containing approximately 45 to 50% Ni, the effect of cooling rate on initial permeability is not great, as evidenced in Fig. 5. The typical annealing cycle to develop high permeability for these low-nickel alloys is similar to the high-nickel cycle, except that any cooling rate between ~55 °C/h (100 °F/h) and ~140 °C/h (252 °F/h) is usually suggested. A dry hydrogen atmosphere is also recommended for annealing low-nickel alloys.

Property Data. The magnetic properties of the nickel-iron soft magnetic alloys are a function of strip thickness, melting procedure, chemical analysis, and freedom from contaminants such as carbon, sulfur, and oxygen that can be picked up during melting, machining, or annealing. As described earlier, these alloys must be annealed in an inert dry hydrogen atmosphere to reduce carbon, to prevent surface oxidation during the annealing cycle, and to promote optimum magnetic properties. Tables 5 and 6 provide typical dc and ac magnetic characteristics of nickel-iron alloys. Table 7 lists recommended heat treatments and the resulting mechanical properties.

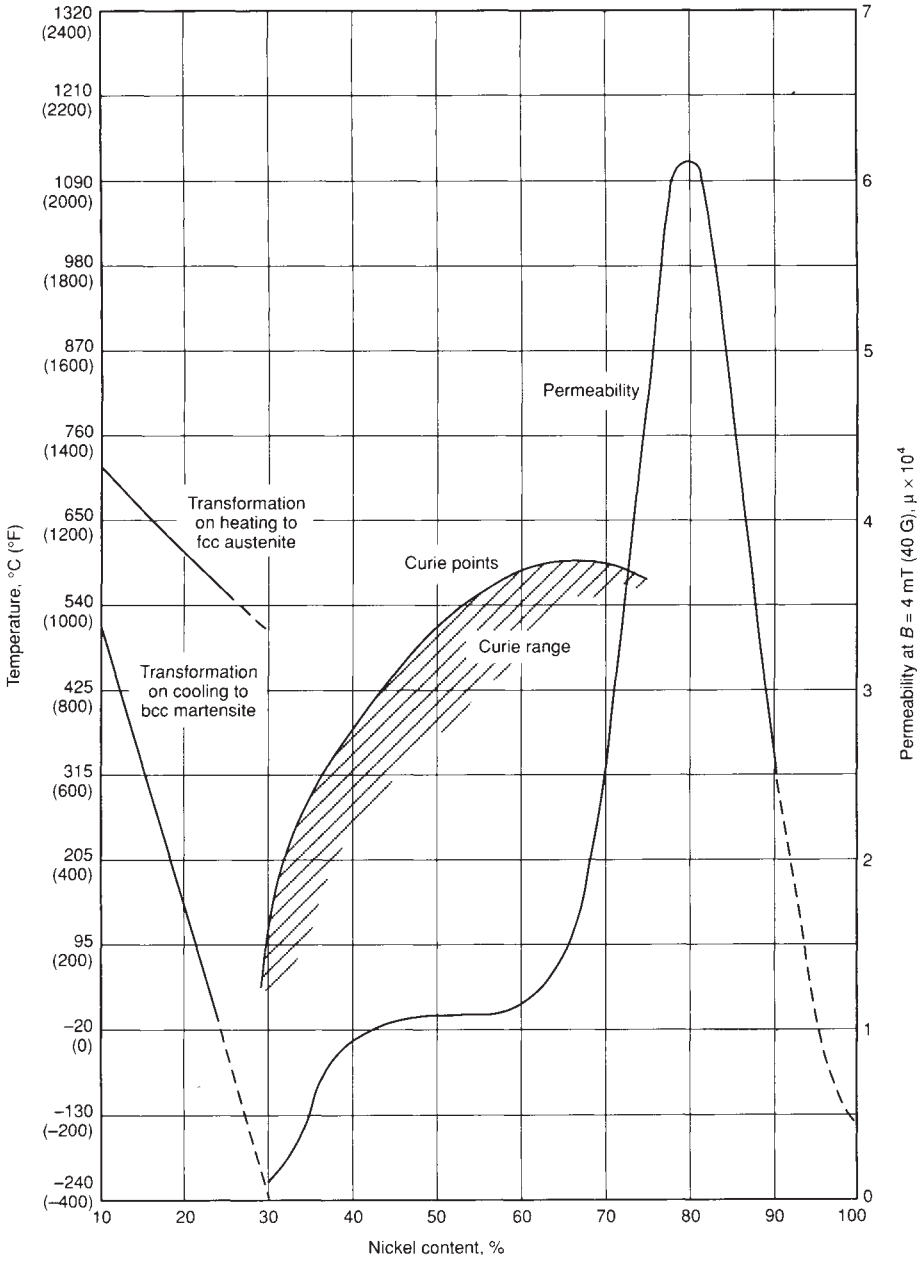


Fig. 4 Effect of nickel content on initial permeability, Curie temperature, and transformation in nickel-iron alloys

Low-Expansion Alloys

The room-temperature coefficients of thermal expansion for most metals and alloys range

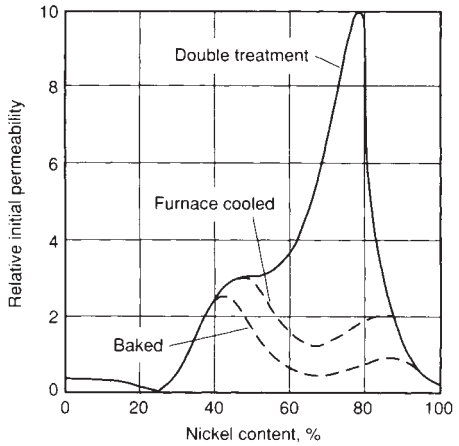


Fig. 5 Relative initial permeability at 2 mT (20 G) for Ni-Fe alloys given various heat treatments. Treatments were as follows: furnace cooled—1 h at 900 to 950 °C (1650 to 1740 °F), cooled at 100 °C/h (180 °F/h); baked—furnace cooled plus 20 h at 450 °C (840 °F); double treatment—furnace cooled plus 1 h at 600 °C (1110 °F) and cooled at 1500 °C/min (2700 °F/min).

from about 5 to 25 μm/m · K. For some applications, however, alloys must be selected that exhibit a very low thermal expansion (0 to 2 μm/m · K) or display uniform and predictable expansion over certain temperature ranges. This has resulted in a family of iron-nickel, iron-nickel-chromium, and iron-nickel-cobalt low-expansion alloys used in applications such as the following:

- Rods and tapes for geodetic surveying
- Compensating pendulums and balance wheels for clocks and watches
- Moving parts that require control of expansion, such as pistons for some internal-combustion engines
- Bimetal strip
- Glass-to-metal seals
- Thermostatic strip
- Vessels and piping for storage and transportation of liquefied natural gas
- Superconducting systems in power transmissions
- Integrated-circuit lead frames
- Components for radios and other electronic devices
- Structural components in optical and laser measuring systems

Low-expansion alloys are also used with high-expansion alloys (65%Fe-27%Ni-5%Mo, or 53%Fe-42%Ni-5%Mo) to produce movements in thermoswitches and other temperature-regulating devices.

Effect of Nickel on the Thermal Expansion of Iron

Nickel has a profound effect on the thermal expansion of iron. Depending on the nickel content, alloys of iron and nickel have coefficients of linear expansion ranging from a small negative value (–0.5 μm/m · K) to a large positive value (20 μm/m · K). Figure 7 shows the effect of nickel content on the linear expansion of iron-nickel alloys at room temperature. In the range of 30 to 60% Ni, alloys with appropriate expansion characteristics can be selected. The alloy containing 36% nickel (with small quantities of manganese, silicon, and carbon amounting to a total of less than 1%) has a coefficient of expansion so low that its length is almost invariable for ordinary changes in temperature. This alloy is known as Invar, meaning invariable.

After the discovery of Invar, an intensive study was made of the thermal and elastic properties of several similar alloys. Iron-nickel alloys that have nickel contents higher than that of Invar retain to some extent the expansion characteristics of Invar. Alloys that contain less than 36% nickel have much higher coefficients of expansion than alloys containing 36% or more nickel.

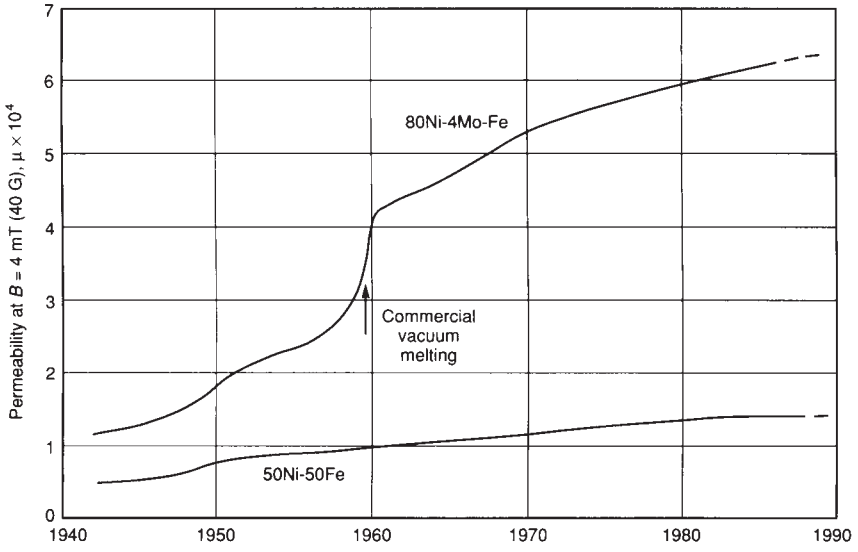


Fig. 6 Progress in initial permeability values of commercial-grade nickel-iron alloys since early 1940s. Frequency, *f*, is 60 Hz. Thickness of annealed laminations was 0.36 mm (0.014 in.).

Invar (Fe-36%Ni Alloy)

Invar (UNS number K93601) and related binary iron-nickel alloys have low coefficients of expansion over only a rather narrow range of temperature (see Fig. 8). At low temperatures in the region from A to B, the coefficient of expansion is high. In the interval between B and C, the coefficient decreases, reaching a minimum in the region from C to D. With increasing temperature, the coefficient begins again to increase from D to E, and thereafter (from E to F), the expansion curve follows a trend similar to that of the nickel or iron of which the alloy is composed. The minimum expansivity prevails only in the range from C to D.

In the region between D and E in Fig. 8, the coefficient is changing rapidly to a higher value. The temperature limits for a well-annealed 36% Ni iron are 162 and 271 °C (324 and 520 °F). These temperatures correspond to the initial and final losses of magnetism in the material (that is, the Curie temperature). The slope of the curve between C and D is, then, a measure of the coefficient of expansion over a limited range of temperature.

Table 8 gives coefficients of linear expansion of iron-nickel alloys between 0 and 38 °C (32 and 100 °F). The expansion behavior of

Table 5 Typical direct current magnetic properties of annealed high-permeability nickel-iron alloys

Data for 0.30 to 1.52 mm (0.012 to 0.060 in.) thickness strip; ring laminations annealed in dry hydrogen at 1175 °C (2150 °F) (unless otherwise noted), 2 to 4 h at temperature. ASTM A 596

	Permeability		Approximate induction at maximum permeability, μ_m		Residual induction B_r		Coercive force, H_c		Saturation, induction, (B_s)		Resistivity,
Alloy	Initial × 10^3	Maximum, $\mu_m \times 10^3$	T	kG	T	kG	A · m^{-1}	Oe	T	kG	μΩ · cm
Low nickel											
45Ni-Fe	7(a)	90	0.6	6	0.68	6.8	4	0.05	1.58	15.8	50
49Ni-Fe(b)	6.1(a)	64	0.8	8	0.96	9.6	8	0.10	1.55	15.5	47
49Ni-Fe(c)	14(a)	140	0.78	7.8	0.97	9.7	4	0.05	1.55	15.5	47
49Ni-Fe	17(a)	180	0.75	7.5	0.90	9.0	2.4	0.03	1.55	15.5	47
45Ni-3Mo-Fe	6(a)	60	0.62	6.2	0.89	8.9	4.8	0.06	1.45	14.5	65
High nickel											
78.5Ni-Fe	50(d)	300	0.35	3.5	0.50	5.0	1.0	0.013	1.05	10.5	16
79Ni-4Mo-Fe	90(d)	400	0.28	2.8	0.35	3.5	0.3	0.004	0.79	7.9	59
75Ni-5Cu-2Cr-Fe	85(d)	375	0.25	2.5	0.34	3.4	0.4	0.005	0.77	7.7	56

(a) Measured at B = 10 mT (100 G). (b) Annealed at 955 °C (1750 °F). (c) Annealed at 1065 °C (1950 °F). (d) Measured at B = 4 mT (40 G)

several iron-nickel alloys over wider ranges of temperature is represented by curves 1 to 5 in Fig. 9. For comparison, Fig. 9 also includes the similar expansion obtained for ordinary steel.

Effects of Composition on Expansion Coefficient. Figure 7 shows the effect of variation in nickel content on linear expansivity. Minimum expansivity occurs at approximately 36% Ni, and small additions of other metals have considerable influences on the position of this minimum. Because further additions of nickel raise the temperature at which the inherent magnetism of the alloy disappears, the inflection temperature in the expansion curve (Fig. 8) also rises with increasing nickel content.

The addition of third and fourth elements to iron-nickel provides useful changes of desired properties (mechanical and physical) but significantly changes thermal expansion characteristics. Minimum expansivity shifts toward higher nickel contents when manganese or chromium is added and toward lower nickel contents when copper, cobalt, or carbon is added. Except for the ternary alloys with Ni-Fe-Co compositions, the value of the minimum expansivity for any of these ternary alloys is, in general, greater than that of a typical Invar alloy.

Figure 10 shows the effects of additions of manganese, chromium, copper, and carbon. Additions of silicon, tungsten, and molybdenum produce effects similar to those caused by additions of manganese and chromium; the composition of minimum expansivity shifts toward higher contents of nickel. Addition of carbon is said to produce instability in Invar, which is attributed to the changing solubility of carbon in the austenitic matrix during heat treatment.

Effects of Processing. Heat treatment and cold work change the expansivity of Invar alloys considerably. Table 9 shows the effect of heat treatment for a 36% Ni Invar alloy. The expansivity is greatest in well-annealed material and least in quenched material.

Annealing is done at 750 to 850 °C (1380 to 1560 °F). When the alloy is quenched in water from these temperatures, expansivity is decreased, but instability is induced both in actual length and in coefficient of expansion. To overcome these deficiencies and to stabilize the material, it is common practice to stress relieve at approximately 315 to 425 °C (600 to 800 °F) and to age at a low temperature 90 °C (200 °F) for 24 to 48 hours.

Cold drawing also decreases the thermal expansion coefficient of Invar alloys. The values for the coefficients in the following table are from experiments on two heats of Invar:

Material condition	Expansivity, ppm/°C
Direct from hot mill	1.4 (heat 1)
	1.4 (heat 2)
Annealed and quenched	0.5 (heat 1)
	0.8 (heat 2)
Quenched and cold drawn (>70% reduction with a diameter of 3.2 to 6.4 mm, or 0.125 to 0.250 in.)	0.14 (heat 1)
	0.3 (heat 2)

By cold working after quenching, it is possible to produce material with a zero, or even a negative, coefficient of expansion. A negative coefficient can be increased to zero by careful annealing at a low temperature.

Magnetic Properties. Invar and all similar iron-nickel alloys are ferromagnetic at room temperature and become paramagnetic at higher temperatures. Because additions in nickel content raise the temperature at which the inherent magnetism of the alloy disappears, the inflection temperature in the expansion curve rises with increasing nickel content. The loss of magnetism in a well-annealed sample of a true Invar begins at 162 °C (324 °F) and ends at 271 °C (520 ° F). In a quenched sample, the loss begins at 205 °C (400 °F) and ends at 271 °C (520 °F).

Table 6 Typical alternating current magnetic properties of annealed high-permeability nickel-iron alloys

Nominal composition	Thickness, mm (in.)	Cyclic frequency, Hz	Impedance permeability, $\mu_z \times 10^3$, at indicated induction, *B*(a)				
			B = 4 mT (40 G)	*B* = 20 mT (200 G)	*B* = 0.2 T (2 kG)	*B* = 0.4 T (4 kG)	*B* = 0.8 T (8 kG)
49Ni-Fe(b)	0.51 (0.020)	60	10.2	16.5	31.3	40.1	...
	0.36 (0.014)	60	12	19.4	37.3	48.2	54.7
	0.25 (0.010)	60	12	20.5	42.5	54.9	68.9
	0.15 (0.006)	60	12	21	47	63.5	85.3
	0.51 (0.020)	400	4.7	5.9	11.7	11.3	...
	0.36 (0.014)	400	6.1	7.9	14.4	17.7	13.3
	0.15 (0.006)	400	8.8	12.6	21.8	28.6	35
79Ni-4Mo-Fe	0.36 (0.014)	60	68	77	100	...	...
79Ni-5Mo-Fe	0.15 (0.006)	60	90	110	170	...	...
	0.10 (0.004)	60	110	135	230	...	...
	0.03 (0.001)	60	100	120	180	...	...
	0.36 (0.014)	400	23.2	25.4	30.5	...	...
	0.15 (0.006)	400	49.7	52.4	64.5	...	...
	0.03 (0.001)	400	89.6	105.2	180.4	...	...
49Ni-Fe(c)	0.36 (0.014)	60	...	...	...	...	...
	0.15 (0.006)	60	...	...	...	...	...
	0.36 (0.014)	400	...	...	...	...	...
	0.15 (0.006)	400	...	...	...	...	...

Nominal composition	Inductance permeability, $\mu_L \times 10^3$, DU laminations(d)				
	B = 4 mT(40 G)	*B* = 20 mT (200 G)	*B* = 0.2 T (2 kG)	*B* = 0.4 T (4 kG)	B = 0.8 T (8 kG)
49Ni-Fe(b)	...	...	...	...	...
	...	...	...	...	...
	...	...	...	...	...
	...	...	...	...	...
	...	...	...	...	...
	...	...	...	...	...
79Ni-4Mo-Fe	...	...	...	...	...
79Ni-5Mo-Fe	...	...	... ...	...	
	...	...	...	...	...
	...	...	...	...	...
	...	...	...	...	...
	...	...	...	...	...
	...	...	...	...	...
	...	...	...	...	...
49Ni-Fe(c)	18.6	35.8	78	110	135
	19.6	39.2	98.5	142	215
	11.8	17.6	36.4	55	30
	12.2	18.5	48.3	95	164

Nominal composition	Core loss in mW/kg (mW/lb) at indicated induction *B*				
	B = 4 mT (40 G)	*B* = 20 mT (200 G)	*B* = 0.2 T (2 kG)	*B* = 0.4 T (4 kG)	B = 0.8 T (8 kG)
49Ni-Fe(b)	...	...	...	...	...
	0.011 (0.005)	0.21 (0.097)	15 (6.7)	48 (21.7)	160 (73)
	...	...	...	...	...
	0.009 (0.004)	0.21 (0.094)	13 (5.8)	44 (19.9)	135 (62)
	...	...	...	...	...
	0.21 (0.094)	4.34 (1.97)	282 (128)	905 (410)	3880 (1760)
	0.15 (0.069)	3.20 (1.45)	238 (108)	705 (320)	2310 (1050)
79Ni-4Mo-Fe	...	0.099 (0.045)	6.50 (2.95)	...	...
79Ni-5Mo-Fe	...	0.051 (0.023)	3.00 (1.36)	...	...
	...	0.024 (0.011)	1.60 (0.73)	...	
	...	...	...	...	...
	0.11 (0.050)	2.20 (1.00)	160 (72.5)	...	...
	0.044 (0.020)	0.99 (0.45)	65.9 (29.9)	...	...
	...	...	...	...	...
49Ni-Fe(c)	0.011 (0.005)	0.22 (0.10)	15 (6.6)	51 (23)	185 (83)
	0.007 (0.003)	0.13 (0.06)	8.6 (3.9)	31 (14)	105 (47)
	0.20 (0.091)	4.4 (2.00)	306 (139)	1010 (460)	4800 (2200)
	0.11 (0.052)	2.38 (1.08)	172 (78.0)	550 (250)	1700 (790)

(a) Tested per ASTM A 772 method: thicknesses >0.13 mm (0.005 in.) tested using ring specimens; <0.13 mm (0.005 in.) tested via tape toroid specimens. (b) Nonoriented rotor or motor grade. (c) Transformer semioriented grade. (d) Per ASTM A 346 method; DU, interleaved U-shape transformer

Table 7 Typical heat treatments and physical properties of nickel-iron alloys

Alloy nominal composition	ASTM standard	Annealing treatment(a)	Hardness	Yield Strength MPa	Yield Strength ksi	Ultimate tensile strength MPa	Ultimate tensile strength ksi	Elongation, %	Specific gravity
45Ni-Fe	A 753 Type 1	Dry hydrogen, 1120 to 1175 °C (2050 to 2150 °F), 2 to 4 h, cool at nominally 85 °C/h (150 °F/h)	48 HRB	165	24	441	64	35	8.17
49Ni-Fe	A 753 type 2	Same as 45Ni-Fe	48 HRB	165	24	441	64	35	8.25
45Ni-3Mo-Fe	...	Same as 45Ni-Fe	...	...	...	...	...	...	8.27
78.5Ni-Fe	...	Dry hydrogen, 1175 °C (2150 °F), 4 h rapid cool to RT(b), reheat to 600 °C (1110 °F), 1 h, oil quench to RT	50 HRB	159	23	455	66	35	8.60
80Ni-4Mo-Fe	A 753 type 4	Dry hydrogen, 1120 to 1175 °C (2050 to 2150 °F), 2 to 4 h cool through critical ordering temperature range, ~760 to400 °C (1400 to 750 °F) at a rate specified for the particular alloy, typically 55 °C/h (100 °F/ h) up to ~390 °C/h (700 °F/h)	58 HRB	172	25	545	79	37	8.74
80Ni-5Mo-Fe	A 753 type 4	Same as 80Ni-4Mo-Fe	58 HRB	172	25	545	79	37	8.75
77Ni-5Cu-2Cr-Fe	A 753 type 3	Same as 80Ni-4Mo-Fe	50 HRB	125	18	441	64	27	8.50

(a) All nickel-iron soft magnetic alloys should be annealed in a dry (–50 °C, or –58 °F) hydrogen atmosphere, typically for 2 to 4 h; cool as recommended by producer. Vacuum annealing generally provides lower properties, which may be acceptable depending upon specific application. (b) RT, room temperature

Table 8 Thermal expansion of iron-nickel alloys between 0 and 38 °C

Ni, %	Mean coefficient, μm/m · K
31.4	3.395 + 0.00885 *t*
34.6	1.373 + 0.00237 *t*
35.6	0.877 + 0.00127 *t*
37.3	3.457 – 0.00647 *t*
39.4	5.357 – 0.00448 *t*
43.6	7.992 – 0.00273 *t*
44.4	8.508 – 0.00251 *t*
48.7	9.901 – 0.00067 *t*
50.7	9.984 + 0.00243 *t*
53.2	10.045 + 0.00031 *t*

Table 9 Effect of heat treatment on coefficient of thermal expansion of Invar

Condition	Mean coefficient, μm/m · K
As forged	
At 17–100 °C (63–212 °F)	1.66
At 17–250 °C (63–480 °F)	3.11
Quenched from 830 °C (1530 °F)	
At 18–100 °C (65–212 °F)	0.64
At 18–250 °C (65–480 °F)	2.53
Quenched from 830 °C and tempered	
At 16–100 °C (60–212 °F)	1.02
At 16–250 °C (60–480 °F)	2.43
Quenched from 830 °C to room temperature in 19 h	
At 16–100 °C (60–212 °F)	2.01
At 16–250 °C (60–480 °F)	2.89

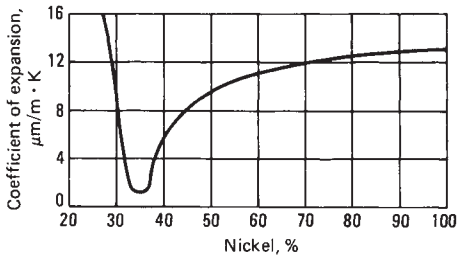


Fig. 7 Coefficient of linear expansion at 20 °C versus Ni content for Fe-Ni alloys containing 0.4% Mn and 0.1% C

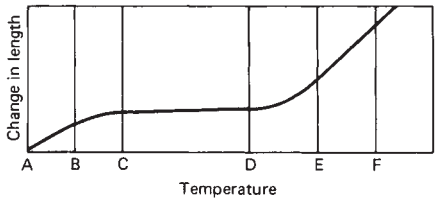


Fig. 8 Change in length of a typical Invar alloy over different ranges of temperature

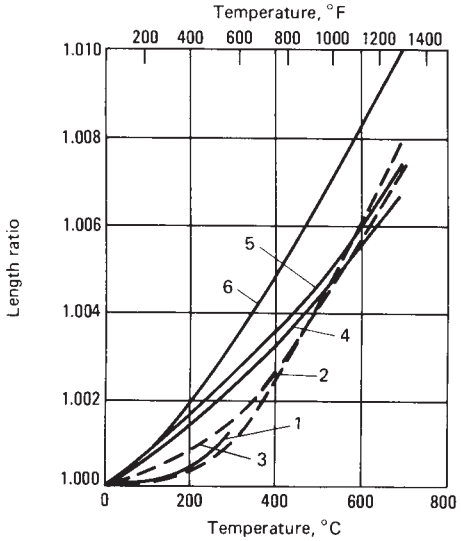


Fig. 9 Thermal expansion of iron-nickel alloys. Curve 1, 64Fe-31Ni-5Co; curve 2, 64Fe-36Ni (Invar); curve 3, 58Fe-42Ni; curve 4, 53Fe-47Ni; curve 5, 48Fe-52Ni; curve 6, carbon steel (0.25% C)

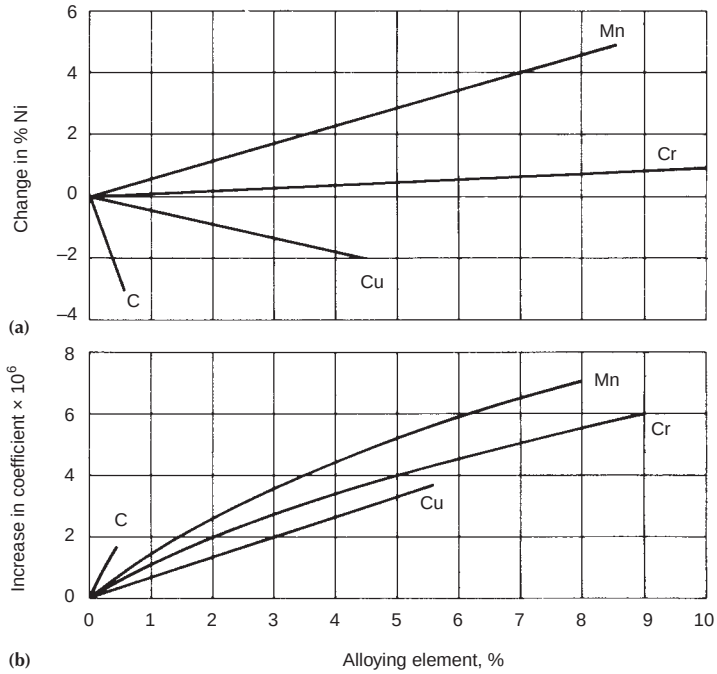


Fig. 10 Effect of alloying elements on expansion characteristics of iron-nickel alloys. (a) Displacement of nickel content caused by additions of manganese, chromium, copper, and carbon to alloy of minimum expansivity. (b) Change in value of minimum coefficient of expansion caused by additions of manganese, chromium, copper, and carbon

Electrical Properties. The electrical resistance of 36Ni-Fe Invar is between 750 and 850 nΩ · m at ordinary temperatures. The temperature coefficient of electrical resistivity is about 1.2 mΩ/Ω · K over the range of low expansivity. As nickel content increases above 36%, the electrical resistivity decreases to approximately 165 nΩ · m at approximately 80% NiFe.

Other Physical and Mechanical Properties. Table 10 presents data on miscellaneous properties of Invar in the hot-rolled and forged conditions. Figure 11 illustrates the effects of temperature on mechanical properties of forged 66Fe-34Ni.

Iron-Nickel Alloys Other Than Invar

Alloys containing less than 36% Ni include temperature compensator alloys (30 to 34% Ni). These exhibit linear changes in magnetic characteristics with temperature change. They are used as compensating shunts in metering devices and speedometers.

Alloys Containing 42 to 50% Ni. Applications for these alloys include semiconductor packaging components, thermostat bimetals, glass-to-metal sealing, and glass sealing of fiber optics. Typical compositions and thermal expansion characteristics for some of these alloys are given in Table 11. Included in this group is Dumet wire, an alloy containing 42% Ni that is clad with copper to provide improved electrical conductivity and to prevent gassing at glass seals.

Table 10 Physical and mechanical properties of Invar

Solidus temperature, °C (°F)	1425 (2600)
Density, g/cm^3	8.1
Tensile strength, MPa (ksi)	450–585 (65–85)
Yield strength, MPa (ksi)	275–415 (40–60)
Elastic limit, MPa (ksi)	140–205 (20–30)
Elongation, %	30–45
Reduction in area, %	55–70
Scleroscope hardness	19
Brinell hardness	160
Modulus of elasticity, GPa (10^6 psi)	150 (21.4)
Thermoelastic coefficient, µm/m · K	500
Specific heat, at 25–100 °C (78–212 °F), J/kg · °C (Btu/lb · °F)	515 (0.123)
Thermal conductivity, at 20–100 °C (68–212 °F), W/m · K (Btu/ft · h · °F)	11 (6.4)
Thermoelectric potential (against copper), at –96 °C (–140 °F), µV/K	9.8

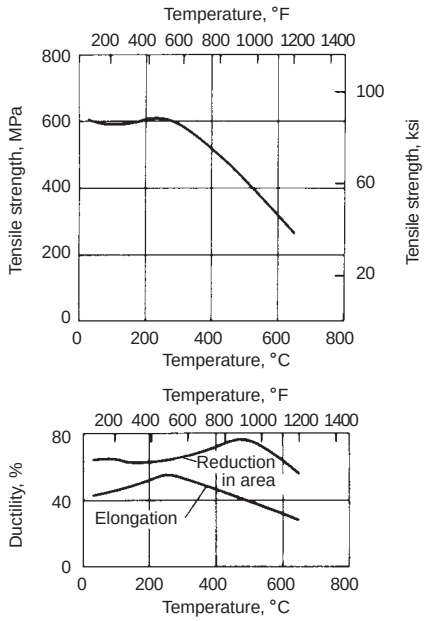


Fig. 11 Mechanical properties of a forged 34% Ni alloy. Alloy composition: 0.25 C, 0.55 Mn, 0.27 Si, 33.9 Ni, bal Fe. Heat treatment: annealed at 800 °C (1475 °F) and furnace cooled

Iron-Nickel-Chromium Alloys

Elinvar is a low-expansion iron-nickel-chromium alloy with a thermoelastic coefficient of zero over a wide temperature range. It is more practical than the straight iron-nickel alloys with a zero thermoelastic coefficient because its thermoelastic coefficient is less susceptible to variations in nickel content expected in commercial melting.

Elinvar is used for such articles as hairsprings and balance wheels for clocks and watches and for tuning forks used in radio synchronization. Particularly beneficial where an invariable modulus of elasticity is required, it has the further advantage of being comparatively rustproof.

The composition of Elinvar has been modified somewhat from its original specification of 36% Ni and 12% Cr. The limits now used are 33 to 35 Ni, 53 to 61 Fe, 4 to 5 Cr, 1 to 3 W, 0.5 to 2 Mn, 0.5 to 2 Si, and 0.5 to 2 C. Elinvar, as created by Guillaume and Chevenard, contains 32% Ni, 10% Cr, 3.5% W, and 0.7% C.

Other iron-nickel-chromium alloys with 40 to 48% Ni and 2 to 8% Cr are useful as glass-sealing alloys because the chromium promotes improved glass-to-metal bonding as a result of its oxide-forming characteristics. The most common of these contain approximately 42 to 48% nickel with chromium of 4 to 6%.

Iron-Nickel-Cobalt Alloys

Super-Invar. Substitution of ~5% Co for some of the nickel content in the 36% Ni (Invar) alloy provides an alloy with an expansion coefficient even lower than Invar. A Super-Invar alloy with a nominal 32% Ni and 4 to 5% Co will exhibit a thermal expansion coefficient close to zero, over a relatively narrow temperature range. This alloy has been used as structural components or bases for optical and laser instruments.

Kovar (UNS K94610) is a nominal 29% Ni-17%Co-54%Fe alloy that is a well-known glass-sealing alloy suitable for sealing to hard (borosilicate) glasses. Kovar has a nominal expansion coefficient of approximately 5 ppm/°C and inflection temperature of ~450 °C (840 °F). Kovar is widely used for making hermetic seals with the harder borosilicate (Pyrex, Corning, Inc., Corning, NY) glass and ceramic materials used in power tubes, microwave tubes, transistors, and diodes, as well as in integrated circuits.

Hardenable Low-Expansion, Controlled-Expansion, and Constant-Modulus Alloys

Hardenable Low-Expansion/Constant-Modulus Alloys. Alloys that have low coefficients of expansion, and alloys with constant modulus of elasticity, can be made age hardenable by adding titanium. In low-expansion alloys, nickel content must be increased when titanium is added. The higher nickel content is required because any titanium that has not combined with the carbon in the alloy will neutralize more than twice its own weight in nickel by forming an intermetallic compound during the hardening operation.

Table 11 Composition and typical thermal expansion coefficients for common iron-nickel low-expansion alloys

Alloy	ASTM specification	Composition(a), % C (max)	Mn (max)	Si (max)	Ni (nom)
42 Ni-Iron	F 30	0.02	0.5	0.25	41
46 Ni-Iron	F 30	0.02	0.5	0.25	46
48 Ni-Iron	F 30	0.02	0.5	0.25	48
52 Ni-Iron	F 30	0.02	0.5	0.25	51
42 Ni-Iron (Dumet)	F 29	0.05	1.0	0.25	42
42 Ni-Iron (Thermostat)	B 753	0.10	0.4	0.25	42

	Typical thermal expansion coefficients from room temperature to:					
	300 °C (570 °F)		400 °C (750 °F)		500 °C (930 °F)	
Alloy	ppm/°C	ppm/°F	ppm/°C	ppm/°F	ppm/°C	ppm/°F
42 Ni-Iron	4.4	2.4	6.0	3.3	7.9	4.4
46 Ni-Iron	7.5	4.2	7.5	4.2	8.5	4.7
48 Ni-Iron	8.8	4.9	8.7	4.8	9.4	5.2
52 Ni-Iron	10.1	5.6	9.9	5.5	9.9	5.5
42 Ni-Iron (Dumet)	...	...	6.6	3.7	...	…
42 Ni-Iron (Thermostat)	5.8(b)	3.2(b)	5.6(c)	3.1(c)	5.7(d)	3.15(d)

(a) Balance of iron with residual impurity limits of 0.25% max Si, 0.015% max P, 0.01% max S, 0.25% max Cr, and 0.5% max Co. (b) From room temperature to 90 °C (200 °F). (c) From room temperature to 150 °C (300 °F). (d) From room temperature to 370 °C (700 °F)

As shown in Table 12, addition of titanium raises the lowest attainable rate of expansion and raises the nickel content at which the minimum expansion occurs. Titanium also lowers the inflection temperature. Mechanical properties of alloys containing 2.4% titanium and 0.06% carbon are given in Table 13.

In alloys of the constant-modulus type containing chromium, addition of titanium allows the thermoelastic coefficients to be varied by adjustment of heat-treating schedules. The alloys in Table 14 are the three most widely used compositions. The recommended solution treatment for the alloys that contain 2.4% Ti is 950 to 1000 °C (1740 to 1830 °F) for 20 to 90 min, depending on section size. Recommended duration of aging varies from 48 h at 600 °C (1110 °F) to 3 h at 730 °C (1345 °F) for solution-treated material.

For material that has been solution treated and subsequently cold worked 50%, aging time varies from 4 h at 600 °C (1100 °F) to 1 h at 730 °C (1350 °F). Table 15 gives mechanical properties of a constant-modulus alloy containing 42% Ni, 5.4% Cr, and 2.4% Ti. Heat treatment and cold work markedly affect these properties.

High-strength controlled-expansion superalloys are based on the iron-nickel-cobalt system. They are strengthened by the addition of the age-hardening elements niobium, titanium, and aluminum. As indicated in Table 16, these alloys exhibit both a low and constant coefficient of expansion up to about 430 °C (800 °F). They also provide high strength at temperatures up to 540 °C (1000 °F). These alloys have been used by the aerospace industry to design near net-shape components and to provide closer clearance between the tips of rotating turbine blades and retainer rings. This allows for greater power output and fuel efficiencies. These high-strength alloys also allow increased strength-to-weight ratios in engine design, resulting in weight savings. Alloy 909 (UNS N19909) offers attractive properties for rocket engine thrust chambers, ordnance hardware, springs, gage blocks, and instrumentation. Additional information on iron-nickel-cobalt controlled expansion alloys can be found in the article "Uses of Cobalt" in this Handbook.

Table 12 Minimum coefficient of expansion in low-expansion Fe-Ni alloys containing titanium

Ti, %	Optimum Ni, %	Minimum coefficient of expansion, m/m · K
0	36.5	1.4
2	40.0	2.9
3	42.5	3.6

Table 13 Mechanical properties of low-expansion Fe-Ni alloys containing 2.4 Ti and 0.06 C

Condition	Tensile strength MPa	Tensile strength ksi	Yield strength MPa	Yield strength ksi	Elongation(a), %	Hardness, HB
42Ni-55.5Fe-2.4Ti-0.06C(b)						
Solution treated	620	90	275	40	32	140
Solution treated and age hardened	1140	165	825	120	14	330
Solution treated, cold rolled 50% and age hardened	1345	195	1140	165	5	385
52Ni-45.5Fe-2.4Ti-0.06C(c)						
Solution treated	585	85	240	35	27	125
Solution treated and age hardened	825	120	655	95	17	305

(a) In 50 mm (2 in.). (b) Inflection temperature, 220 °C (430 °F); minimum coefficient of expansion, 3.2 m/m ·K. (c) Inflection temperature, 440 °C (824 °F); minimum coefficient of expansion, 9.5 m/m ·K

Table 14 Thermoelastic coefficients of constant modulus Fe-Ni-Cr-Ti alloys

Composition, % Ni	Cr	C	Ti	Thermoelastic coefficient, annealed condition, m/m · K	Range of possible coefficients(a), m/m · K
42	5.4	0.06	2.4	0	18 to –23
42	6.0	0.06	2.4	36	54 to 13
42	6.3	0.06	2.4	–36	–18 to –60

(a) Any value in this range can be obtained by varying the heat treatment.

Table 15 Mechanical properties of constant-modulus alloy 50Fe-42Ni-5.4Cr-2.4Ti

Condition	Tensile strength MPa	Tensile strength ksi	Yield strength MPa	Yield strength ksi	Elongation(a), %	Hardness, HB	Modulus of elasticity GPa	Modulus of elasticity 10^6 psi
Solution treated	620	90	240	35	40	145	165	24
Solution treated and aged 3 h at 730 °C (1345 °F)	1240	180	795	115	18	345	185	26.5
Solution treated and cold worked 50%	930	135	895	130	6	275	175	25.5
Solution treated, cold worked 50%, and aged 1 h at 730 °C (1345 °F)	1380	200	1240	180	7	395	185	27

(a) In 50 mm (2 in.)

Table 16 Composition and thermal expansion coefficients of high-strength controlled-expansion alloys

Alloy designation	Composition, %	Coefficient of thermal expansion, from room temperature to: 260 °C (500 °F) ppm/°C	260 °C (500 °F) ppm/°F	370 °C (700 °F) ppm/°C	370 °C (700 °F) ppm/°F	415 °C (780 °F) ppm/°C	415 °C (780 °F) ppm/°F	Inflection temperature °C	Inflection temperature °F
Incoloy 903 and Pyromet CTX-1	0.03 C, 0.20 Si, 37.7 Ni, 16.0 Co, 1.75 Ti, 3.0 (Nb + Ta), 1.0 Al, 0.0075 B, bal Fe	7.51	4.17	7.47	4.15	7.45	4.14	440	820
Incoloy 907 and Pyromet CTX-3	0.06 C max, 0.5 Si, 38.0 Ni, 13.0 Co, 1.5 Ti, 4.8 (Nb + Ta), 0.35 Al max, 0.012 B max, bal Fe	7.65	4.25	7.50	4.15	7.55	4.20	415	780
Incoloy 909 and Pyromet CTX-909	0.06 C max, 0.40 Si, 38.0 Ni, 14.0 Co, 1.6 Ti, 4.9 (Nb + Ta), 0.15 Al max, 0.012 B max, bal Fe	7.75	4.30	7.55	4.20	7.75	4.30	415	780

Nickel-Titanium Shape Memory Alloys

Metallic materials that demonstrate the ability to return to some previously defined shape or size when subjected to the appropriate deformation/thermal procedure are referred to as shape memory alloys (SMA). According to the shape memory effect, an alloy that is shaped at a given temperature and then reshaped at another temperature will return to the original shape when it is brought back to the shaping temperature. The shape memory effect is associated with a martensitic transformation (see "Shape Memory Alloys," *Properties and Selection: Nonferrous Alloys and Special-Purpose Materials*, Volume 2, *ASM Handbook*, for details).

The basis of the nickel-titanium system of SMA is the binary, equiatomic (49 to 51 at.% Ni) intermetallic compound of NiTi. This intermetallic compound is extraordinary because it has a moderate solubility range for excess nickel or titanium, as well as most other metallic elements, and it also exhibits a ductility comparable to most ordinary alloys. This solubility allows alloying with many of the elements to modify both the mechanical properties and the transformation properties of the system. Excess nickel, in amounts up to approximately 1%, is the most common alloying addition. Ex-

cess nickel strongly depresses the martensitic transformation temperature and increases the yield strength of the austenite. Other frequently used elements are iron and chromium (to lower the transformation temperature), and copper (to decrease the hysteresis and lower the deformation stress of the martensite). Because common contaminants such as oxygen and carbon can also shift the transformation temperature and degrade the mechanical properties, it is also desirable to minimize the amount of these elements.

Properties

Table 17 shows the major physical properties of the basic binary Ni-Ti system and some of the mechanical properties of the alloy in the annealed condition. Selective work hardening, which can exceed 50% reduction in some cases, and proper heat treatment can greatly improve the case with which the martensite is deformed, give an austenite with much greater strength, and create material that spontaneously moves itself both on heating and on cooling (two-way shape memory). One of the biggest challenges in using this family of alloys is in developing the proper processing procedures to yield the properties desired.

Table 17 Properties of binary nickel-titanium shape memory alloys

Properties	Property value
Melting temperatures, °C (°F)	1300 (2370)
Density, g/cm^3(lb/in.^{3})	6.45 (0.233)
Resistivity, μΩ · cm	
Austenite	~100
Martensite	~70
Thermal conductivity, W/m · °C (Btu/ft · h · °F)	
Austenite	18 (10)
Martensite	8.5 (4.9)
Corrosion resistance	Similar to 300 series stainless steel or titanium alloys
Young's modulus, GPa (10^6 psi)	
Austenite	~83 (~12)
Martensite	~28–41 (~4–6)
Yield strength, MPa (ksi)	
Austenite	195–690 (28–100)
Martensite	70–140 (10–20)
Ultimate tensile strength, MPa (ksi)	895 (130)
Transformation temperatures, °C (°F)	–200 to 110 (–325 to 230)
Hysteresis, Δ°C (Δ°F)	~30 (~55)
Latent heat of transformation, kJ/kg · atom (cal/g · atom)	167 (40)
Shape memory strain	8.5% maximum

Processing

Because of the reactivity of the titanium in these alloys, all melting of them must be done in a vacuum or an inert atmosphere. Methods such as plasma-arc melting, electron-beam melting, and vacuum-induction melting are all used commercially. After ingots are melted, standard hot-forming processes such as forging, bar rolling, and extrusion can be used for initial breakdown. The alloys react slowly with air, so hot working in air is quite successful. Most cold-working processes can also be applied to these alloys, but they work harden extremely rapidly, and frequent annealing is required. Wire drawing is probably the most widely used of the techniques, and excellent surface properties and sizes as small as 0.05 mm (0.002 in.) are made routinely.

Heat treating to impart the desired memory shape is often done at 500 to 800 °C (950 to 1450 °F), but it can be done as low as 300 to 350 °C (600 to 650 °F) if sufficient time is allowed. The SMA component may need to be restrained in the desired memory shape during the heat treatment; otherwise, it may not remain there.

Applications

Applications for NiTi alloys can be grouped into four broad categories: actuation devices, constrained recovery devices, superelastic devices, and martensitic devices.

Actuation Devices. Shape memory actuation devices utilize the shape memory effect to recover a particular shape upon heating above their transformation temperatures. Shape memory actuation devices can act without constraint to freely recover their trained shape, can be fully constrained so that they provide a force, or can be partially constrained so that they perform work. The transformation temperatures of the NiTi alloy can be adjusted to activate at precisely the required temperature. Common actuation temperatures are human body temperature and boiling water temperature. Examples of shape memory actuation devices include blood-clot filters (NiTi wire is shaped to anchor itself in a vein and catch passing clots), vascular stents to reinforce blood vessels, and coffeepot themostats.

Constrained Recovery Devices. The most successful example of constrained recovery devices is hydraulic pipe couplings. These fittings are manufactured as cylindrical sleeves slightly smaller than the metal tubing they join. Their diameters are then expanded while martensitic, and on warming to austenite, these fittings shrink in diameter and strongly hold the tube ends. The tubes prevent the coupling from fully recovering its manufactured shape, and the stresses created as the coupling attempts to do so are great enough to create a joint that, in many ways, is superior to a weld.

Superelastic devices are used for applications that demand the extraordinary flexibility of NiTi. Nickel-titanium has the ability to absorb large amounts of strain energy and release it as the applied strain is removed. The elasticity of NiTi is approximately ten times that of steel. Nickel-titanium also has excellent torqueability and kink resistance, which are important for medical guidewires. Further, superelastic NiTi alloys provide a constant force over a large strain range. This has been exploited in the field of orthodontics (arch wires) where a constant force enhances tooth movement with greater patient comfort. Eyeglass frames represent another important superelastic application.

Martensitic Devices. The martensitic phase of NiTi has some unique properties that have made it an ideal material for many applications. First, the martensitic phase transformation has excellent damping characteristics due to the energy absorption characteristics of its twinned phase structure. Second, the martensitic form of NiTi has remarkable fatigue resistance. Finally, the martensitic phase is easily deformed, yet will recover its shape on heating above its transformation temperatures. Examples of martensitic devices include vibration dampers, bendable surgical tools for open heart surgery, and highly fatigue resistant wires.

Nickel-Beryllium Alloys

Beryllium additions up to about 2 wt% in nickel promote strengthening through precipitation hardening. These alloys are distinguished by very high strength, excellent formability, and excellent resistance to fatigue, elevated temperature softening, stress relaxation, and corrosion. Wrought nickel-beryllium is available in strip, rod, and wire forms. The wrought product is used primarily as mechanical and electrical/electronic components that must exhibit good spring properties at elevated temperatures (for example, thermostats, bellows, diaphragms, burn-in connectors, and sockets).

A variety of nickel-beryllium casting alloys exhibit strengths nearly as high as those of the wrought products, and they have the advantage of excellent castability. Many of the casting alloys are used in molds and cores for glass and

Table 18 Nominal compositions of commercial nickel-beryllium alloys

		Composition, wt%			
Product form	Alloy	Be	Cr	Other	Ni
Wrought	360 (UNS N03360)	1.85–2.05	...	0.4–0.6 Ti	bal(a)
Cast	M220C (UNS N03220)	2.0	...	0.5 C	bal
Cast	41C	2.75	0.5	...	bal(b)
Cast	42C	2.75	12.0	...	bal(b)
Cast	43C	2.75	6.0	...	bal(b)
Cast	44C	2.0	0.5	...	bal(b)
Cast	46C	2.0	12.0	...	bal(b)
Cast	Master	6	...	...	bal(c)

(a) 99.4 Ni + Be + Ti + Cu min, 0.25 Cu max. (b) 0.1 C max. (c) Master alloys with 10, 25, and 50 wt% Be are also available.

polymer molding, other glass-forming tools (e.g., bottle plungers and neck rings), diamond drill bit matrices, and cast turbine parts. Some casting alloys are also used in jewelry and dental applications by virtue of their high replication of detail in the investment casting process.

Compositions of the wrought and cast nickel-beryllium alloys are shown in Table 18. Only one composition is supplied in wrought form, alloy 360 (UNS N03360), which contains 1.85 to 2.05 wt% Be, 0.4 to 0.6 wt% Ti, and a balance of nickel. The most commonly employed cast composition is alloy M220C (UNS N03220), which contains 1.80 to 2.30% Be, 0.30 to 0.50% C, and a balance of nickel. Other commercially available cast alloys include a series of ternary nickel-chromiumberyllium alloys with up to 2.75% Be and 0.5 to 12.0% Cr and a 6 wt% Be master alloy.



Fig. 12 Alloy 360 (UNS N03360) strip, solution annealed at 990 °C (1800 °F), water quenched, and aged at 510 °C (950 °F) for 1.5 h. The structure shows nickel-beryllium compound particles dispersed uniformly through the nickel-rich matrix. Hardening precipitates are not resolved, but equilibrium γ (NiBe) precipitates are present in grain boundaries. Modified Marble's etchant. 800×

Physical Metallurgy. The metallurgy of nickel-beryllium alloys is analogous to that of the high-strength copper-beryllium alloys. The alloys are solution annealed at a temperature high in the α-nickel region to dissolve a maximum amount of beryllium, then rapidly quenched to room temperature to create a supersaturated solid solution. Precipitation hardening involves heating the alloy to a temperature below the equilibrium solvus to nucleate and grow metastable beryllium-rich precipitates, which harden the matrix. In the high-strength copper-beryllium alloys, the equilibrium γ-precipitate forms at grain boundaries only at higher-age-hardening temperatures; commercial nickel-beryllium alloys, on the other hand, exhibit a degree of equilibrium grain-boundary precipitate formation at all temperatures in the age-hardening range.

Microstructure. Wrought unaged nickel-beryllium microstructures exhibit nickel-beryllide intermetallic compound particles containing titanium in a nickel-rich matrix of equiaxed or deformed grains, depending on whether the alloy is in the solution-annealed or a cold-worked temper. After age hardening, a small volume fraction of equilibrium nickel-beryllium phase is generally observed at the grain boundaries. In other respects, unaged and aged beryllium-nickel microstructures are essentially indistinguishable when viewed in an optical microscope. The typical microstructure of a solution annealed and aged wrought microstructure is shown in Fig. 12.

Cast nickel-beryllium alloys containing carbon exhibit graphite nodules in a matrix of nickel-rich dendrites with an interdendritic nickel-beryllium phase. Cast chromium-containing alloys exhibit primary dendrites of nickel-chromium-beryllium solid solution and an interdendritic nickel-beryllium phase. Solution annealing cast nickel-beryllium partially spheroidizes but does not appreciably dissolve the interdendritic nickel-beryllium phase.

Heat Treatment. Wrought UNS N03360 is typically solution annealed at about 1000 °C (1830 °F). Cold work up to about 40% can be imparted between solution annealing and aging to increase the rate and magnitude of the age-hardening response. Aging to peak strength is performed at 510 °C (950 °F) for up to 2.5 h for annealed material and for up to 1.5 h for cold-worked material.

The cast binary alloys are solution annealed at about 1065 °C (1950 °F) and aged at 510 °C (950 °F) for 3 h. Cast ternary alloys are annealed at a temperature of approximately 1090 °C (1990 °F) and given the same aging treatment. Castings are typically used in the solution-annealed and aged (AT) temper for maximum strength. The cast plus aged (CT) temper is not employed.

Mechanical and Physical Properties. Annealed wrought nickel-beryllium is designated the A temper and cold worked material is designated ¼ H through H temper. As with the wrought copper-beryllium alloys, increasing cold work through about a 40% reduction in area increases the rate and magnitude of the age-hardening response. User age-hardened materials are designated the AT through HT tempers. As with the high-strength copper-beryllium alloys, nickel-beryllium strip is processed by proprietary cold-working and age-hardening techniques to provide a series of ascending-strength mill-hardened tempers designated MH2 through MH12; these tempers do not require heat treatment by the user after stamping and forming.

Mechanical properties of nickel-beryllium strip and casting alloys are given in Tables 19 and 20, respectively. The ultimate tensile strengths of wrought materials range from a minimum of 1480 MPa (215 ksi) in the annealed and aged AT temper to a minimum of 1860 MPa (270 ksi) in the cold-rolled and aged HT temper. Tensile strengths of mill-hardened strip range from 1065 MPa (155 ksi) to over 1790 MPa (260 ksi). Ductility decreases with increasing strength in both the heat-treatable and age-hardened conditions. In addition to high strength in tension, nickel-beryllium strip exhibits high fatigue strength in fully reversed bending (Fig. 13). A significant fraction of

Table 19 Mechanical properties of wrought nickel-beryllium alloy 360 strip

Temper designations		Heat	Tensile strength		Yield strength at 0.2% offset		Minimum elongation	Rockwell
ASTM	Commercial	treatment(a)	MPa	ksi	MPa	ksi	in 50 mm (2 in.), %	hardness
TB00	A	...	655–895	95–130	275–485	40–70	30	39–57 HRA
TD01	¼H	...	760–1035	110–150	445–860	65–125	15	50–65 HRA
TD02	½H	...	895–1205	130–175	790–1170	115–170	4	51–70 HRA
TD04	H	...	1065–1310	154–190	1035–1310	150–190	1	55–75 HRA
TF00	AT	2.5 h at 510 °C	1480 min	215 min	1035 min	150 min	12	78–86 HRN
TH01	¼HT	2.5 h at 510 °C	1585 min	230 min	1205 min	175 min	10	80–88 HRN
TH02	½HT	1.5 h at 510 °C	1690 min	245 min	1380 min	200 min	9	81–90 HRN
TH04	HT	1.5 h at 510 °C	1860 min	270 min	1585 min	230 min	8	83–90 HRN
…	MH2	M	1065–1240	154–180	690–860	100–125	14	...
…	MH4	M	1240–1415	180–205	825–1065	120–154	12	...
…	MH6	M	1380–1550	200–225	1035–1205	150–175	10	...
…	MH8	M	1515–1690	220–245	1170–1415	170–205	9	...
…	MH10	M	1655–1860	240–270	1380–1550	200–225	8	...
…	MH12	M	1790–2000	260–290	1515–1690	20–245	8	...

(a) M, heat treatment performed at mill

Table 20 Typical mechanical properties of selected nickel-beryllium casting alloys

Alloy	Condition	Ultimate tensile strength MPa	Ultimate tensile strength ksi	0.2% yield strength MPa	0.2% yield strength ksi	Elongation in 50 mm (2 in.), %	Hardness, HRC
M220C	Annealed(a)	760	110	345	50	35	95
	Annealed and aged(b)	1620	235	1380	200	4	54
41C	Annealed and aged(b)	1585	230	...	...	...	55
42C	Annealed and aged(c)	1035	150	...	...	6	38
43C	Annealed and aged(b)	1310	190	...	...	...	45
44C	Annealed and aged(b)	1310	190	...	...	...	48
46C	Annealed and aged(b)	1035	150	...	...	...	35

(a) Solution annealed at 1065 °C (1950 °F) for 1 h and water quenched. (b) Solution annealed and aged at 510 °C (950 °F) for 3 h. (c) Solution annealed at 1093 °C (2000 °F) for 10 h, water quenched, and then aged at 510 °C (950 °F) for 3 h

room-temperature strength is maintained through short exposure to temperatures as high as 540 °C (1000 °F).

Physical and electrical properties of selected nickel-beryllium alloys are given in Table 21. Electrical conductivity is about 6% IACS in the age-hardened condition. Nickel-beryllium displays only a fraction of the conductivity of the copper-beryllium alloys, but nickel-beryllium conductivity exceeds that of stainless steel.

Ordered Intermetallic Alloys of Ni_3Al

The ordered intermetallic compound Ni_3Al is of interest because of its excellent strength and oxidation resistance at elevated temperature. This nickel aluminide has long been used as a strengthening constituent in high-temperature nickel-base superalloys, which owe their outstanding strength properties to a fine dispersion of precipitation particles of the ordered γ′ phase (Ni_3Al) embedded in a ductile matrix (see the article "Superalloys" in this Handbook).

Despite their great promise, the commercial success of nickel aluminides has not been achieved because of their tendency to exhibit brittle fracture and low ductility at ambient temperatures. Much of the research on these materials has centered around microalloying and macroalloying additions that would eliminate brittle behavior. The compositions, structures, and properties of alloys based on the intermetallic compound Ni_3Al are briefly outlined subsequently. More detailed information on the processing and properties of nickel aluminides can be found in the *ASM Handbook Specialty Handbook: Heat-Resistant Materials* (see the article "Structural Intermetallics").

Composition and Structure. During the latter part of the 1970s, it was found that small boron additions were critical for achieving reasonable levels of ductility in the alloys. Boron is thought to increase grain boundary cohesiveness, thereby reducing the tendency for brittle intergranular fracture. Other alloying additions were made to improve strength, castability, hot workability, and corrosion resistance. As shown in Table 22, these include chromium, iron, zirconium, and molybdenum.

Ordered nickel aluminide (Ni_3Al) alloys are based on an $L1_2$ crystal structure. The unit cell consists of an fcc arrangement in which the aluminum atoms occupy the corner positions and the nickel atoms preferentially occupy the face-centered positions. The fact that atoms occupy preferred positions in the crystal structure imparts unusual mechanical properties to the nickel aluminide alloys.

Mechanical Properties. Among the most striking properties of nickel aluminide alloys, and that which captured initial interest among metal producers, is their rising yield strength with rising temperature. Figure 14 shows that the yield strength of four nickel aluminide alloys tends to rise to a maximum in the temperature range of ~400 to 650 °C (~750 to 1200 °F). Above this temperature range, the yield strength declines. The effect of cold working on the yield strength of IC-50 alloy is shown in Fig. 15. Up to test temperatures of ~600 °C (~1110 °F), cold working had an effect on the yield strength, but at a test temperature of 800 °C (1470 °F), there was no significant enhancement of yield strength.

Corrosion Resistance. The oxidation and carburization resistance of Ni_3Al alloys are compared in Fig. 16 and 17. It is clear from Fig. 16 that the Ni_3Al alloys that form a protective Al_2O_3 scale on the surface have significantly better oxidation resistance than aluminum-free alloy 800. Carburization resistance is also high under both oxidizing or reducing environment (Fig. 17).

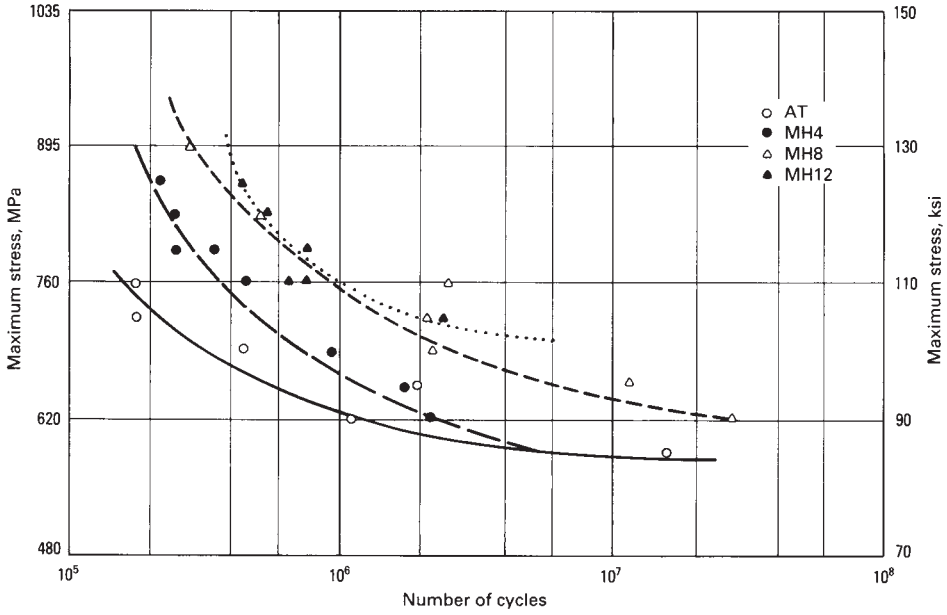


Fig. 13 Fatigue behavior of nickel-beryllium alloy N03360 strip in fully reversed bending (stress ratio, $R = -1$)

Table 21 Typical physical and electrical properties of selected nickel-beryllium alloys

Product form	Alloy	Condition	Density, g/cm^3	Thermal expansion from 20–550 °C (70–1020 °F), 10^{-6}/°C	Thermal conductivity, W/m · K	Electrical resistivity, μΩ · cm	Electrical conductivity, %IACS	Elastic modulus GPa	Elastic modulus 10^6 psi
Wrought	360 (UNS N03360)	Aged(a)	8.27	4.5	28 (at 20 °C)	28.7 max	6 min	193–206	28–30
		Mill hardened(b)	...	...	...	34.5 max	5 min	...	...
		Unaged(c)	...	...	...	43.1 max	4 min	...	...
Cast	M220C (UNS N03220)	Aged(a)	8.08–8.19	4.8	36.9 (at 38 °C) 51.1 (at 538 °C)	21.0	...	179–193	26–28
Cast	42C	Aged(a)	7.8	...	34.6 (at 93 °C)	34.5	5 min	193	28

(a) Solution annealed and aged at 510 °C (950 °F) for 3 h. (b) Heat treated by producing mill. (c) Solution annealed with 0 to 37% cold work

Table 22 Nominal compositions of selected nickel aluminide alloys

Alloy(a)	Composition, wt% Al	Cr	Fe	Zr	Mo	B	Ni
IC-50	11.3	...	...	0.6	...	0.02	bal
IC-74M	12.4	...	...	...	...	0.05	bal
IC-218	8.5	7.8	...	0.8	...	0.02	bal
IC-218 LZr	8.7	8.1	...	0.2	...	0.02	bal
IC-221	8.5	7.8	...	1.7	...	0.02	bal
IC-357	9.5	7.0	11.2	0.4	1.3	0.02	bal
IC-396M	8.0	7.7	...	0.8	3.0	0.01	bal

(a) Designations used by Oak Ridge National Laboratory, Oak Ridge, TN

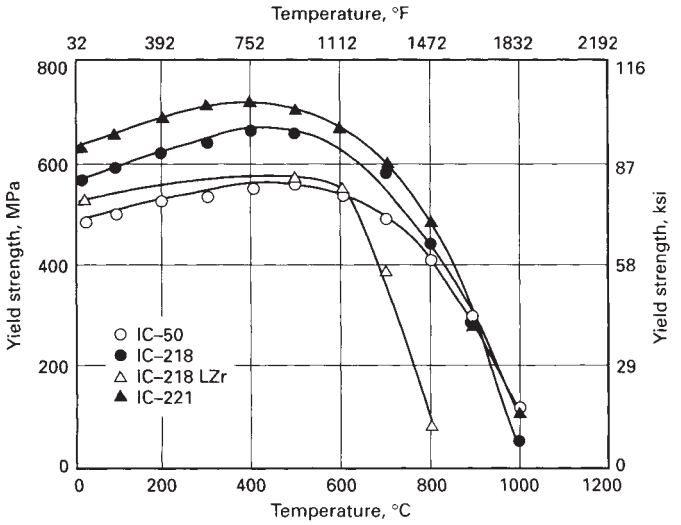


Fig. 14 Variation of yield strength with test temperature for selected nickel aluminide alloys. Strain rate, 0.5 mm/mm/min

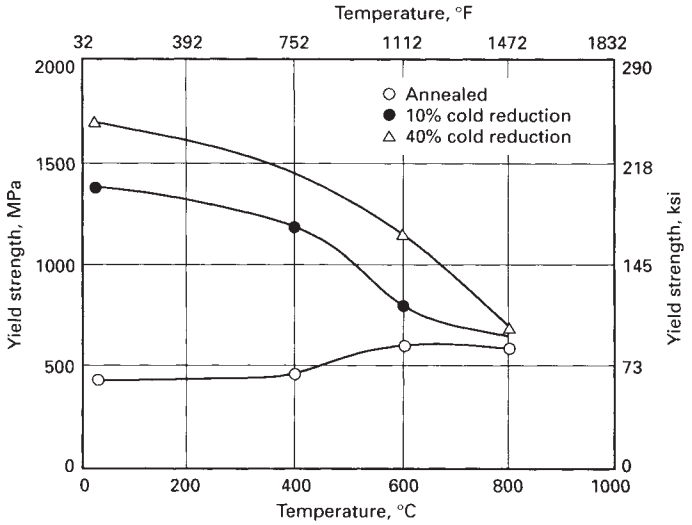


Fig. 15 Plot of yield strength versus test temperature of IC-50 nickel aluminide alloy as a function of cold working

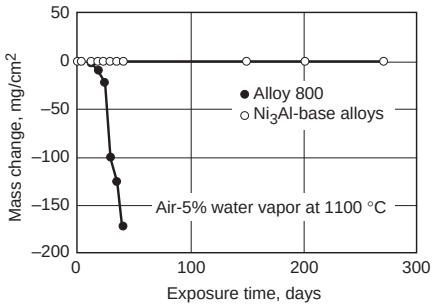


Fig. 16 Comparison of the oxidation resistance of Ni_3Al alloys with that of alloy 800 in air with 5% water vapor at 1100 °C (2010 °F)

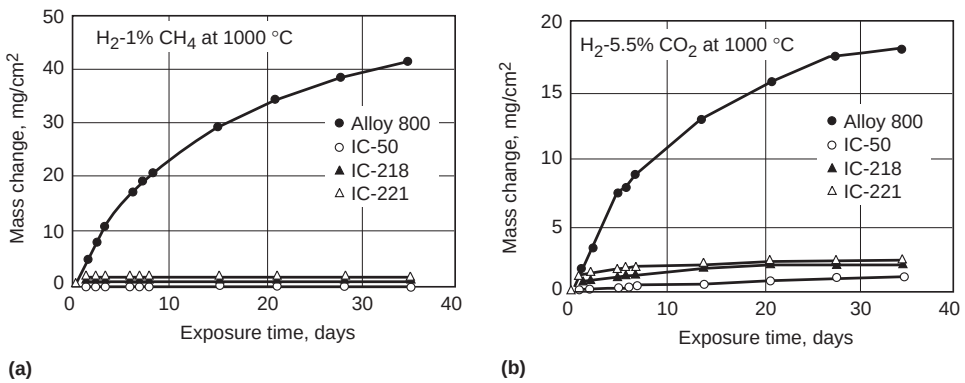


Fig. 17 Comparison of the carburization resistance of Ni_3Al alloys with that of alloy 800. (a) Oxidizing carburizing environment. (b) Reducing carburizing environment

Applications. The potential applications (and the properties they would exploit) for nickel aluminide alloys include:

- Heat-treating furnace parts (superior carburization resistance, high-temperature strength, and thermal fatigue resistance)
- Gas, water, and steam turbines (the excellent cavitation, erosion, and oxidation resistance of the alloys)
- Aircraft fasteners (low density and ease of achieving the desired strength)
- Automotive turbochargers (high fatigue resistance and low density)
- Pistons and valves (wear resistance and capability of developing a thermal barrier by high-temperature oxidation treatment)
- Bellows for expansion joints to be used in corrosive environments (good aqueous corrosion resistance)
- Tooling (high-temperature strength and wear resistance developed through preoxidation)
- Permanent molds (the ability to develop a thermal barrier coating by high-temperature oxidation)

ACKNOWLEDGMENTS

Portions of this article were adapted from the following:

- D.W. Dietrich, Magnetically Soft Materials, *Properties and Selection: Nonferrous Alloys and Special-Purpose Materials*, Vol 2, *ASM Handbook*, ASM International, 1990, p 761–781
- E.L. Frantz, Low-Expansion Alloys, *Properties and Selection: Nonferrous Alloys and Special-Purpose Materials*, Vol 2, *ASM Handbook*, ASM International, 1990, p 889–896
- J.C. Harkness, Beryllium-Copper and Other Beryllium-Containing Alloys, *Properties and Selection: Nonferrous Alloys and Special-Purpose Materials*, Vol 2, *ASM Handbook*, ASM International, 1990, p 403–427
- Shape Memory Alloys, *Metals Handbook Desk Edition*, 2nd ed., J.R. Davis, Ed., ASM International, 1998, p 668–669
- R.A. Watson, et al., Electrical Resistance Alloys, *Properties and Selection: Nonferrous Alloys and Special-Purpose Materials*, Vol 2, *ASM Handbook*, ASM International, 1990, p 822–839

ASM Specialty Handbook: Nickel, Cobalt, and Their Alloys
J.R. Davis, editor, p 106-123
DOI:10.1361/ncta2000p106

Copyright © 2000 ASM International®
All rights reserved.
www.asminternational.org

Nickel Coatings

NICKEL AND NICKEL ALLOY COATINGS are commonly deposited by electroplating (the most commercially important process), electroless plating, thermal spraying, weld surfacing, and solid-state cladding techniques (e.g., roll bonding). Each of these processes is discussed in this article with emphasis placed on electroplating and electroless plating.

For specialized applications, nickel can also be deposited by selective plating, also known as brush plating, pulsed-current plating, and chemical vapor deposition (CVD). The first two of these processes are variations of the traditional tank or bath electroplating process. Chemical vapor deposition involves the decomposition of nickel carbonyl at 180 °C (360 °F). More detailed information on these alternative nickel coating procedures can be found in *Surface Engineering*, Volume 5 of *ASM Handbook*.

Nickel Plating

Nickel is one of the most important metals applied by electrodeposition. Nickel electrodeposits are used extensively as a foundation for a highly lustrous finish on many manufactured metallic and plastic articles. Protection of the base metal and permanence of a stain-free surface are the primary requisites of such decorative coatings. Decorative applications account for approximately 80% of the nickel consumed in plating; the remaining 20% is consumed for engineering and electroforming purposes. The annual worldwide consumption of nickel for electroplating is approximately 180 million pounds (81,700 tonnes) and accounts for about 10% of world nickel consumption. Some basic information about nickel and common nickel salts for plating is given in the following table:

Nickel	Atomic weight 58.69. Valency 2. Specific gravity 8.90. Plating rate, at 100% cathode efficiency, 1.095 g/A · h (0.039 oz/A · h)
Nickel salts	
Nickel chloride	Formula is $NiCl_2 \cdot 6H_2O$. Contains 24.7% Ni.
Nickel sulfate	Formula is $NiSO_4 \cdot 6H_2O$. Contains 22.3% Ni.
Nickel sulfamate	Formula is $Ni(NH_2SO_3)_2$. Contains 23.2% Ni.
Nickel carbonate	Formula is $NiCO_3$. Contains about 46% Ni.

General Overview

Decorative Plating. Modern decorative nickel plating solutions contain organic additives that modify the electrocrystallization process so that mirror-bright, highly leveled nickel coatings are deposited directly from solution. Prior to the introduction of "organic" baths, decorative nickel coatings were produced by polishing nickel-plated parts mechanically, a practice that continued from 1870 to about 1945. Thin layers of chromium were electrodeposited over polished nickel coatings for the first time in 1927 to prevent the "yellowing" or tarnishing of nickel in outdoor atmospheres, and that practice continues with the "as-deposited" bright nickel coatings now available. An effort to develop improved decorative, electroplated nickel coatings began in the late 1940s and led to the development of multilayer nickel coatings (early 1950s) and microdiscontinuous chromium coatings (mid to late 1960s). Modern multilayer nickel coatings in combination with microdiscontinuous chromium are capable of protecting and enhancing the appearance of most metals and alloys, plateable plastics, and other materials for extended periods of time.

Figure 1 shows a history of the development and use of decorative nickel and nickel-plus-chromium coatings. The major result of these developments has been a significant improvement in the corrosion performance of decorative nickel-plus-chromium coatings without the need to increase deposit thickness.

Engineering Plating. The engineering applications of nickel plating include those where a fully bright appearance is not required. Engineering nickel deposits are usually sulfur-free and matte in appearance. These deposits may be specified to improve corrosion and wear resistance, to salvage or build up worn or undersized parts, to modify magnetic properties, to prepare surfaces for enameling or for organic coating, to function as diffusion barriers in electronic applications, and for other purposes. Engineering applications exist in the chemical, nuclear, telecommunications, consumer electronics, and computer industries.

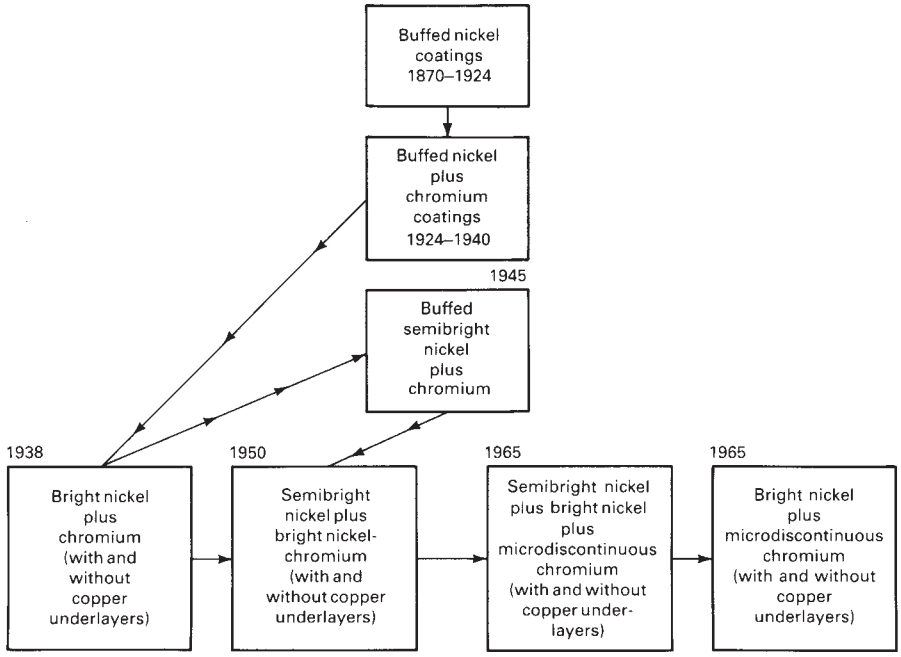


Fig. 1 History of the development of nickel and nickel-chromium coatings showing time of introduction and periods of use

Electroforming. Nickel electroforming is electrodeposition applied to the manufacture of nickel products of various kinds, and it differs from electroplating in one major respect. In electroplating, the coating is metallurgically bonded to the substrate and is an integral part of the surface. In electroforming, nickel is deposited onto a mandrel or mold nonadherently so that the nickel can be separated from the mandrel when it is removed from the plating solution. Electroforming applications include the fabrication of molds and dies, mesh, and other products that are indispensable to operations in the textile, aerospace, communication, electronics, automotive, photocopying, and entertainment industries. Additional information is available in the section "Electroforming" in this article.

Basic Process Considerations

Before describing decorative, engineering, and electroforming plating processes, some basic facts are reviewed that make it possible to control the nickel plating process, predict the amount of nickel deposited, and estimate nickel coating thickness.

The Basic Process. Nickel plating is similar to other electroplating processes that employ soluble metal anodes. It requires the passage of direct current between two electrodes that are immersed in a conductive, aqueous solution of nickel salts. The flow of direct current causes one of the electrodes (the anode) to dissolve and the other electrode (the cathode) to become covered with nickel. The nickel in solution is present in the form of divalent positively charged ions (Ni^{++}). When current flows, the positive ions react with two electrons ($2e^-$) and are converted to metallic nickel (Ni^0) at the cathode surface. The reverse occurs at the anode, where metallic nickel is dissolved to form divalent positively charged ions, which enter the solution. The nickel ions discharged at the cathode are replenished by those formed at the anode.

Hydrogen Evolution and Cathode Efficiency. The discharge of nickel ions is not the only reaction that can occur at the cathode; a small percentage of the current is consumed in the discharge of hydrogen ions from water. This reduces the cathode efficiency for nickel deposition from 100% to 92 to 97%, depending on the nature of the electrolyte. The discharged hydrogen atoms form bubbles of hydrogen gas at the cathode surface.

Anode Efficiency. Under normal conditions the efficiency of dissolution at the anode is 100% and no hydroxyl ions are discharged from the water. If the pH of the solution is too high, however, hydroxyl ions may be discharged in preference to the dissolution of nickel, and oxygen will be evolved. Under those conditions, the nickel anode becomes passive and ceases to dissolve nickel. Activated nickel anode materials are available commercially that resist the onset of passivity and replenish the solution with nickel ions over a wide range of plating conditions.

Nickel Ion and pH Changes. Under normal operating conditions, the nickel ion concentration and the pH of the solution will slowly increase as plating proceeds. The rate of increase in nickel ion concentration depends on the difference between cathode and anode efficiencies. Because cathode efficiencies may vary from 92 to 97%, whereas anode efficiency is always 100%, the rate of increase in nickel ion concentration depends on the nature of the plating solution and not on the type of soluble nickel anode material that is used.

Faraday's Law for Nickel. The amount of nickel deposited at the cathode and the amount dissolved at the anode are directly proportional to the product of the current and time (Faraday's law). The proportionality constant is equal to M divided by nF, where M is the molecular weight, n is the number of electrons involved in the electrochemical reaction, and F is Faraday's constant, equal to 96,500 coulombs (ampere-seconds). For nickel, the constant is 1.095 g/A·h. The constant for nickel deposition is calculated assuming that cathode efficiency is 100%; because a small part of the current goes to discharge hydrogen, the constant must be adjusted by multiplying by the cathode efficiency (for example, 1.095 × 0.955 = 1.046).

Faraday's law for nickel may be expressed as $m = 1.095\ (a)\ (l)\ (t)$, where m is the amount of nickel deposited at the cathode (or dissolved at the anode), in grams; l is the current that flows through the plating tank, in amperes; t is the time that the current flows , in hours; and a is the current efficiency ratio for the reaction of interest. In almost all cases, the anode efficiency is 100% ($a = 1$). The cathode efficiency may vary from 92 to 97% and accordingly, a will vary from 0.92 to 0.97.

Average Nickel Thickness. The nickel electrodeposition data compiled in Table 1 have been calculated on the assumption that cathode efficiency is 95.5%, which approximates the case for most nickel plating solutions. From the table, one can estimate the time required to deposit a specified thickness of nickel at a specified current density. If the plating process is operated at 5 A/dm^2, for example, it takes about 20 min to deposit a nickel coating with an average thickness of 20 μm.

The data in Table 1 provide a means of estimating the average coating thickness. The actual thickness on an individual part depends on the uniformity of current density distribution. Under practical plating conditions, the thickness of the nickel on a batch of parts is measured in one or more trials, and adjustments are made, if necessary, as to how the parts are placed in the tank relative to the anode and how they are positioned on the plating racks. In some cases, shields and auxiliary anodes may be required to obtain acceptable thickness uniformity. Shields are made of nonconductive materials and may be placed on the anode, on the cathode, or between electrodes to block or control current flow. Auxiliary anodes may be either soluble or insoluble, and they are placed closer to the cathode than principal anodes so as to direct current to a recessed or relatively small area on the cathode. With care, current density distribution and coating thickness can be made reasonably uniform and predictable.

The Watts Solution and Deposit Properties

The nickel plating solution described by Watts in 1916 was a major milestone in the development of nickel plating technology. The solution eventually replaced all others in use up to that time. It remains the basis of most decorative nickel plating processes, and it is used for engineering applications and for electroforming. Operated at elevated temperatures, the solution described by Watts is capable of being used with high current densities.

The composition of the modern Watts bath is included in Table 2. The constituents of the Watts bath have several functions.

- *Nickel sulfate:* Available in commercially pure forms, nickel sulfate is relatively inexpensive and is the major source of the nickel ions in solution. A high nickel sulfate concentration is used when high current densities are required.

Table 1 Nickel electrodeposition data

Deposit thickness, μm	Weight per unit area, g/dm^2	Amp hours per unit, A · h/dm^2	Time (min) required to obtain deposit at current density (A/dm^2) of:									
			0.5	1	1.5	2	3	4	5	6	8	10
2	0.18	0.17	20	10	6.8	5.1	3.4	2.6	2.0	1.7	1.3	1
4	0.36	0.34	41	20	14	10	6.8	5.1	4.1	3.4	2.6	2
6	0.53	0.51	61	31	20	15	10	7.7	6.1	5.1	3.8	3.1
8	0.71	0.68	82	41	27	20	13	10	8.2	6.8	5.1	4.1
10	0.89	0.85	100	51	34	26	17	13	10	8.5	6.4	5.1
12	1.1	1.0	120	61	41	31	20	15	12	10	7.7	6.1
14	1.2	1.2	140	71	48	36	24	18	14	12	8.9	7.1
16	1.4	1.4	160	82	54	41	27	20	16	14	10	8.2
18	1.6	1.5	180	92	61	46	31	23	18	15	11	9.2
20	1.8	1.7	200	100	68	51	34	26	20	17	13	10
40	3.6	3.4	410	200	140	100	68	51	41	34	26	20

Note: Values are based on 95.5% cathode efficiency

- *Nickel chloride:* Serving primarily to improve anode corrosion, nickel chloride also increases conductivity and uniformity of coating thickness distribution. Excessive amounts of chloride increase the corrosivity of the solution and the internal stress of the deposits. (*Internal stress* refers to forces created within the deposit as a result of the electrocrystallization process and/or the codeposition of impurities such as hydrogen, sulfur, and other elements. Internal stress is either tensile [contractile] or compressive [expansive] and may cause plating problems if excessively high.)
- *Boric acid:* Used in nickel plating solutions for buffering purposes, boric acid concentration may affect the appearance of the deposits. The deposit may first become frosty in high current density areas at 30 g/L (4 oz/gal) of boric acid, and then, as the boric acid concentration approaches 15 to 23 g/L (2 to 3 oz/gal), the deposit may be burnt and cracked. No effect on appearance is observed at high boric acid concentrations up to saturation (45 g/L, or 6 oz/gal).
- *Wetting agents or surfactants:* Formulated specifically for nickel plating solutions, wetting agents or surfactants are almost always added to control pitting. Their function is to lower the surface tension of the plating solution so that air and hydrogen bubbles do not cling to the parts being plated.

Good-quality nickel deposits can be produced within the ranges of solution pH, temperature, and current density given in Table 2. Although the maximum current density given in the table is 11 A/dm^2, higher rates of plating are possible with increased solution agitation and flow rates.

The physical and mechanical properties of nickel deposited from Watts solutions are affected by the operating conditions and chloride content of the solution as shown in Fig. 2 to 5. Figures 2 to 4 show how pH, current density, and temperature affect properties such as internal stress, hardness, percent elongation, and tensile strength. Figure 5 shows how the chloride content affects those properties; the maximum ductility and softest deposits are produced when 25% of the nickel in solution is present as nickel chloride.

Table 2 Nickel electroplating solutions

Parameter	Watts nickel	Nickel sulfamate	Typical semibright bath(a)
Electrolyte composition(b), g/L			
Nickel sulfate, $NiSO_4 \cdot 6H_2O$	225 to 400	…	300
Nickel sulfamate, $Ni(SO_3NH_2)_2$	…	300 to 450	…
Nickel chloride, $NiCl_2 \cdot 6H_2O$	30 to 60	0 to 30	35
Boric acid, H_3BO_3	30 to 45	30 to 45	45
Operating conditions			
Temperature, °C	44 to 66	32 to 60	54
Agitation	Air or mechanical	Air or mechanical	Air or mechanical
Cathode current density, A/dm^2	3 to 11	0.5 to 30	3 to 10
Anodes	Nickel	Nickel	Nickel
pH	2 to 4.5	3.5 to 5.0	3.5 to 4.5
Mechanical properties(c)			
Tensile strength, MPa	345 to 485	415 to 610	…
Elongation, %	10 to 30	5 to 30	8 to 20
Vickers hardness, 100 g load	130 to 200	170 to 230	300 to 400
Internal stress, MPa	125 to 210 (tensile)	0 to 55 (tensile)	35 to 200 (tensile)

(a) Organic additives available from plating supply houses are required for semibright nickel plating. (b) Antipitting agents formulated for nickel plating are often added to control pitting. (c) Typical properties of *bright* nickel deposits are as follows: elongation, 2 to 5%; Vickers hardness, 100 g load, 600 to 800; internal stress, 12 to 25 MPa (compressive)

Decorative Bright Nickel Plating

Bright nickel plating solutions are modifications of the Watts formulation given in Table 2, but bright nickel plating solutions contain organic and other additives that act to produce a fully bright finish suitable for immediate chromium plating without mechanical finishing. Portions of the addition agent molecules may be incorporated into the deposit, resulting in a hard, fine-grain coating that contains incorporated sulfur. The sulfur causes the deposit to be electrochemically more reactive than sulfur-free matte, polished, or semibright nickel deposits. Decomposition products of the additives accumulate in solution with time and are removed by purification with activated carbon. In modern solutions, continuous filtration through active carbon removes deleterious decomposition products without significant removal of the addition agents themselves.

Several substances—organic and inorganic—are used at appropriate concentrations to achieve brightness, leveling, and control of internal stress. (Leveling is the ability of the deposit to become smoother than the surface on which it is deposited as the thickness of the nickel is increased.) The substances used as additives in bright nickel plating solutions may be described by the following three terms: *carriers*, *auxiliary brighteners*, and *brighteners*. The terminology is not standardized, however, and alternative terms mentioned in the literature are shown in parentheses.

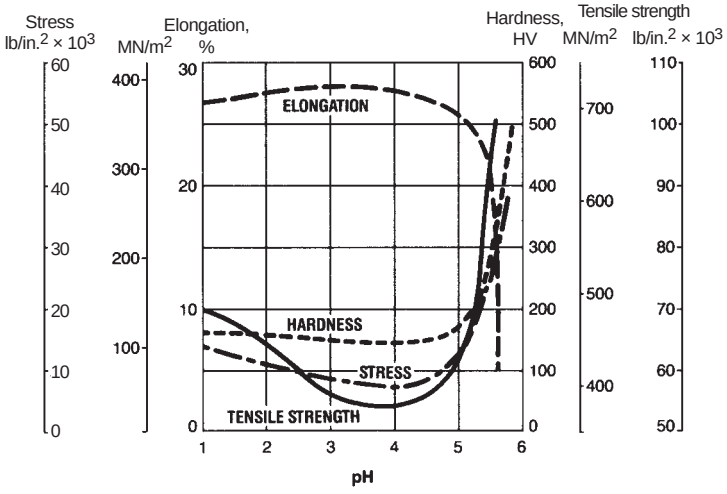


Fig. 2 Variation in internal stress, tensile strength, ductility, and hardness with pH. Watts bath operated at 55 °C (130 °F) and 5 A/dm^2. Internal stress is tensile (indicated by a positive number).

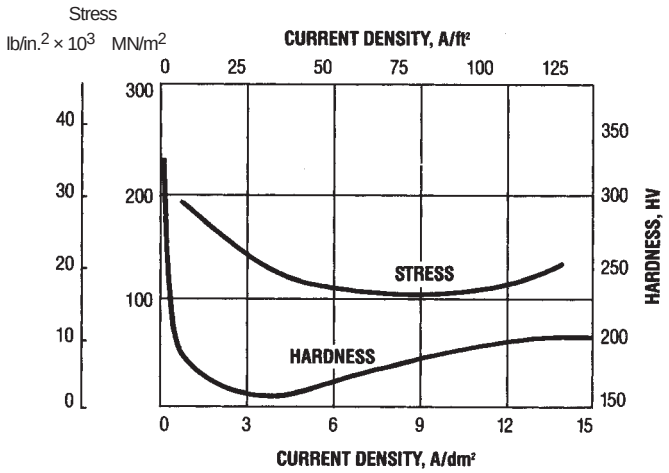


Fig. 3 Variation in internal stress and hardness with current density. Watts bath operated at 55 °C (130 °F) and pH 3.0. Internal stress is tensile (indicated by a positive number).

Carriers (brighteners of the first class, secondary brighteners, control agents, ductilizers) are usually aromatic organic compounds. They are the principal source of the sulfur codeposited with the nickel. Their main function is to refine grain structure and provide deposits with increased luster compared with matte or full deposits from baths without additives. Some of these additives can be used in Watts solution or high-chloride versions of the Watts solution (for example, solutions with 115 g/L, or 15 oz/gal, nickel chloride). This class of brightener widens the bright range when used in combination with the auxiliary brighteners and brighteners discussed below. Some examples of carriers are saccharin (o-sulfobenzoic imide), paratoluene sulfonamide, benzene sulfonamide, benzene monosulfonate (sodium salt), ortho sulfobenzaldehyde (sodium salt), and naphthalene 1,3,6-trisulfonate (sodium salt). Carriers are used in concentrations of about 1 to 25 g/L (0.1 to 3 oz/gal), either singly or in combination. They are not consumed rapidly by electrolysis, and consumption is primarily by dragout and by losses during batch carbon treatment. (Batch treatment involves interrupting production and transferring the plating solution to a separate treatment tank where it is treated with activated carbon, filtered, and returned to the main tank.) The stress-reducing property of carriers is increased if they contain amido or imido nitrogen. For example, saccharin is a most effective stress reducer and often helps to decrease or eliminate hazes. It is generally used as sodium saccharin at a concentration of 0.5 to 4.0 g/L (0.07 to 0.5 oz/gal).

Auxiliary brighteners may be either organic or inorganic. Their functions are to augment the luster attainable with the carriers and brighteners and to increase the rate of brightening and leveling. Some examples are sodium allyl sulfonate; zinc, cobalt, cadmium (for rack and barrel plating); and 1,4-butyne 2-diol. The concentration of these additives may vary from about 0.1 to 4 g/L (0.01 to 0.5 oz/gal). The rate of consumption depends on the type of compound and may vary widely. These compounds may be of aromatic or aliphatic types and usually are heterocyclic or unsaturated. The inorganic metallic ions—zinc, cobalt, and cadmium—are not often used anymore as auxiliary brighteners.

Brighteners (brighteners of the second class, primary brighteners, leveling agents), when used in combination with carriers and auxiliary brighteners, produce bright to brilliant deposits having good ductility and leveling characteristics over a wide range of current densities. Some of the compounds used as brighteners include reduced fuchsin, phenosafranin, thiourea, 1,4-butyne diol, n-allylquinolinium bromide and 5-aminobenzimidazolethiol-2. Materials of this type generally are used in concentrations of 0.005 to 0.2 g/L (0.0006 to 0.02 oz/gal); an excess of brighteners may cause serious embrittlement. The rates of consumption of these materials may vary within wide limits.

Modern bright nickel plating solutions employ combinations of additives similar to those described and are formulated to produce bright deposits over a wide range of current densities. The deposits have excellent leveling or scratch-filling characteristics, produce deposits with fair ductility and low internal stress, produce bright deposits in areas of low current density, permit use of high average current densities and bath temperatures, are less sensitive to metallic contaminants than some of the solutions first commercialized, permit continuous purification of the plating solution by use of activated carbon on filters, produce breakdown products that can be removed by activated carbon, and are not overly sensitive to anode effects.

Multilayer Decorative Plating

The single-layer, bright nickel coatings produced from solutions containing organic additives are less resistant to corrosion than polished nickel coatings. The lower corrosion resistance is due to the presence of small amounts of sulfur that originate from the organic additives present in solution. The amount of sulfur that is incorporated depends on exactly how the process is formulated and controlled. Single-layer bright nickel coatings are suitable for use in mildly corrosive service using a nickel thickness of 10 to 20 μm (0.39 to 0.79 mil). For severe and very severe conditions of exposure, especially where longtime resistance to corrosion is required, multilayer nickel coatings with microdiscontinuous chromium are used. The principal types are double-layer and triple-layer coatings.

Double-layer coatings involve the electrode position of two layers of nickel, one semibright and one bright, before the application of chromium. The first layer (semibright) is deposited from a Watts-type formulation containing one or more sulfur-free organic additives. Semibright nickel deposits contain less than 0.005 wt% S and are semilustrous, smooth, and fine-grain over a wide current density range. The deposits have a columnar structure and good ductility. The typical composition and operating conditions for a semibright nickel plating bath are given in Table 2. Deposit internal stress increases with increasing nickel chloride content; deposits also tend to be nonuniform in color and leveling at high chloride levels. The concentrations of the

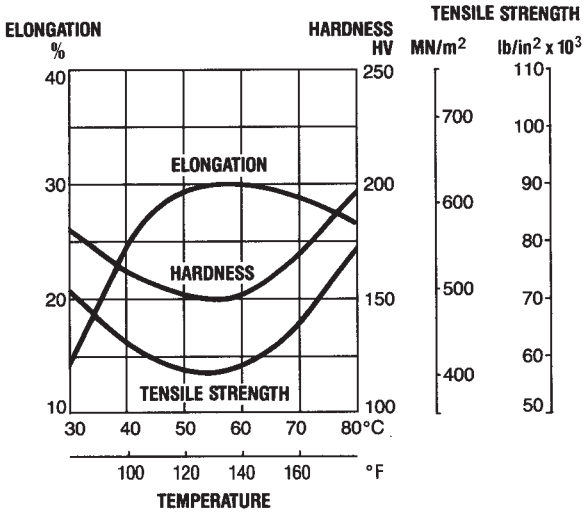


Fig. 4 Variation in elongation, tensile strength, and hardness with temperature. Watts bath operated at 55 °C (130 °F) and 5 A/dm²

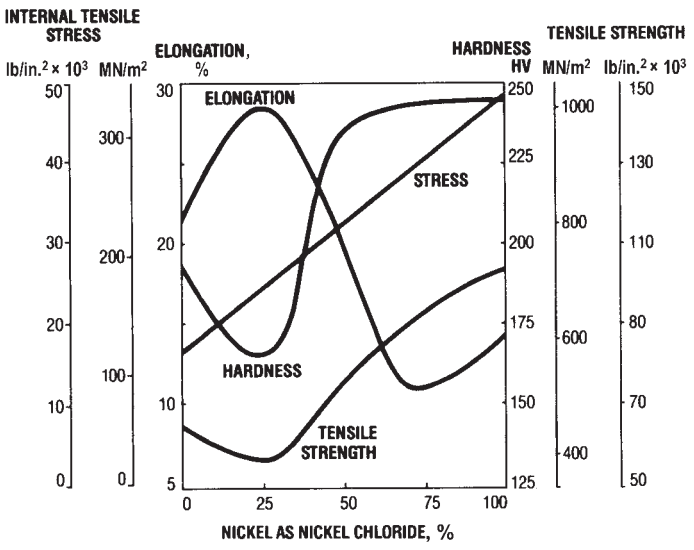


Fig. 5 Variation in internal stress, elongation, tensile strength, and hardness with chloride content in deposits from Watts solutions operated at 55 °C (130 °F), pH 3.0, and 5 A/dm². Internal stress is tensile (indicated by a positive number).

organic additives for semibright nickel solutions are usually fairly low, from 0.05 to 0.5 g/L (0.006 to 0.06 oz/gal). Examples of these additives are 1,4-butyne diol (or other aliphatic compounds with olefinic or acetylenic unsaturation), formaldehyde, coumarin, and ethylene cyanohydrin. There are two families of semibright nickel plating processes that are usually referred to as *coumarin* and *noncoumarin* types. The latter were introduced more recently and offer advantages. Semibright nickel plating solutions usually contain anionic surfactants and antipitting agents, singly or in combination.

The bright nickel layer deposited on top of the semibright one may range in thickness from 5 to 8 μm (0.2 to 0.3 mil), or about 20 to 35% of the total nickel thickness. Ideally, it should be plated from a bath that is compatible with the semibright additive, or additives, because in most double-layer systems the semibright additive functions as either a brightener or an auxiliary brightener in the bright nickel bath.

Triple-layer coatings are similar to double-layer coatings except that a thin, high-sulfur-containing layer is deposited between the semibright and bright layers. The thin layer must contain greater than 0.15 wt% S. Some of the requirements for double-layer and triple-layer nickel coatings are summarized in Table 3. Why multilayer coatings improve corrosion performance is discussed subsequently in the section "Corrosion Performance of Decorative Coatings."

Microdiscontinuous Chromium

Decorative electrodeposited nickel coatings, whether single-layer or multilayer, are most often used in combination with electrodeposited chromium. The thin layer of chromium, initially applied over nickel to prevent tarnishing, now provides added resistance to corrosion because of the developments discussed in this and the next section.

Conventional or regular chromium deposits are low-porosity coatings, whereas microdiscontinuous chromium deposits have a high, controlled degree of microporosity or microcracking. Controlled microporosity or microcracking in the chromium is achieved by depositing a special nickel strike on top of the bright nickel layer just prior to chromium plating. When it is plated over with chromium, the thin layer of nickel, usually about 1 to 2 μm (0.04 to 0.08 mil), helps create microcracks or micropores in the chromium. Microporosity may also be achieved without the use of a special nickel layer by means of the Pixie process, a patented process that involves postplating treatment of the chromium to increase porosity on a microscopic scale. Traditionally, the chromium is deposited from conventional hexavalent processes, but within the last ten years, trivalent chromium plating processes have grown in popularity.

Microcracked chromium is produced by depositing the thin layer of nickel from a special bath formulated to produce nickel with a high internal tensile stress. When the chromium deposit is chromium plated, the thin nickel and the chromium then crack. Varying the conditions under which the nickel layer is deposited can provide variations in the crack density over a range of from 30 cracks/mm (750 cracks/in.) to 80 cracks/mm (2000 cracks/in.). The nickel bath usually consists of a basic nickel chloride electrolyte with additives that provide additional stress, such as the ammonium ion. Boric acid is not used, but other buffers such as the acetate ion may be added. Proprietary organic additives are also used to enhance the brightness and the ability of the deposit to crack, especially in the low-current-density areas. Temperature and pH are controlled to vary the crack density; low temperature (23 °C, or 73 °F) and high pH (4.5) favor higher crack densities; high temperature (36 °C, or 97 °F) and low pH (3.5) favor lower crack densities. Cracking of the chromium deposit must occur subsequent to chromium plating. Aging or the use of a hot water dip may be necessary to promote the formation of all microcracks.

Microcracked chromium deposits can also be produced directly from chromium baths by increasing thickness, or by depositing chromium over chromium. The latter, dual-layer chromium technique is no longer popular.

Microporous chromium is produced from Watts-type nickel baths using air agitation and containing very fine inert particles, usually inorganic, and the normal additives used for bright nickel plating. Chromium, plated over the resulting nickel-particle matrix, deposits around the particles, creating pores. The nickel baths are operated much like bright nickel solutions, with the exception that filtration cannot be performed. In some instances, auxiliary additives permit reduction of the particle concentration in the plating bath and still provide high pore densities. Pore densities can vary according to the concentration of particles, agitation rates, and additives. Generally, a minimum pore density of 100 pores/mm^2 (64,000 pores/in.^{2}) is specified. In either case, chromium thicknesses should not be allowed to exceed about 0.5 μm (0.02 mil) or the cracks and pores will start to heal.

Corrosion Performance of Decorative Coatings

The remarkable corrosion resistance of modern decorative nickel-plus-chromium coatings depends on the use of multilayer nickel in combination with microdiscontinuous chromium. The improved performance of multilayer nickel coatings is due to the fact that the combination of layers of nickel have different electrochemical reactivities. If one measures the corrosion potentials of various nickel deposits in the same electrolyte, one finds that the bright nickel deposits display more active dissolution potentials than do the semibright nickels. If bright and semibright nickel deposits (for example, in the form of foils separated from the substrate) are electrically connected in the electrolyte, electrons will flow from the bright nickel to the semibright nickel. The result is that the rate of corrosion of the bright nickel is increased, whereas the rate of corrosion of the semibright nickel is decreased. In a composite coating consisting of bright nickel over semibright nickel, this is manifested by enhanced lateral corrosion of the bright nickel layer and delayed penetration of the semibright nickel layer.

Effect of Multilayer Corrosion Potentials. The extent to which bright nickel protects the underlying semibright nickel layer by sacrificial action is dependent on the difference between the corrosion potentials of the semibright and bright nickel. The difference should be at least 100 mV (as measured by the simultaneous thickness and electrochemical potential, or STEP, test described in ASTM B 764). Differences in potential are beneficial, especially in low-current-density areas of complicated parts. If the difference becomes too great, appearance suffers because of the accelerated corrosion of the bright nickel layer; that is, there is an optimum value that represents a compromise between preventing basis metal attack and controlling superficial corrosion. The result is that penetration of the coating and exposure of the underlying substrate occur slowly. Multilayer nickel coatings are thus more protective than single-layer bright nickel coatings of equal thickness.

The rate of pit penetration through the nickel layers varies inversely with the number of microdiscontinuities in the chromium layer. Pit penetration may occur rapidly with low-porosity, conventional chromium. When corrosion takes place at a pore in conventional chromium, the large cathodic area of chromium surrounding the pore accelerates the corrosion of the nickel, and pitting may occur rapidly. With microdiscontinuous chromium, a large number of microscopic pores or cracks are deliberately induced in the chromium deposit so that corrosion can start at many sites. The available corrosion current has to be spread

Table 3 Requirements for double-layer or triple-layer nickel coatings

Type of nickel coating(a)	Specific elongation, %	Sulfur content, wt%	Thickness as a percentageof total nickel thickness	
			Double-layer	Triple-layer
Bottom (s—semibright)	>8	<0.005	>60 (≥75 for steel)	>50 (but not >70)
Middle (b—high-sulfur bright)	…	> 0.15	…	10 max
Top (b—bright)	…	0.04–0.15	>10 but <40	≥30

(a) s, semibright nickel layer applied prior to bright nickel; b, fully bright nickel layer that contains the amount of sulfur specified

over a myriad number of tiny corrosion cells, so that the rate of corrosion of the nickel is greatly reduced. For example, the approximate depth of pitting of nickel after 16 h of CASS testing (ASTM B 368, "Copper-Accelerated Acetic Acid Salt Spray [Fog] Testing") was 10 to 20 μm with conventional chromium and 1 to 6 μm with microdiscontinuous chromium.

Test Results. Corrosion studies conducted by plating suppliers, nickel producers, and groups such as ASTM Committee B-8 have confirmed that multilayer nickel coatings are significantly more protective than single-layer, bright nickel coatings, that microdiscontinuous chromium coatings provide more protection than conventional chromium coatings, and that the corrosion protection of decorative, electroplated nickel-plus-chromium coatings is directly proportional to nickel thickness and to the ratio of semibright and bright nickel in multilayer coatings. Table 4 is based on the results of a study conducted at the LaQue Center for Corrosion Technology, Wrightsville Beach, NC, and it summarizes the types of coatings that protected standard panels from corrosion for more than 15 years outdoors in a severe marine atmosphere.

Standards and Recommended Thicknesses

ASTM B 456 "Standard Specification for Electrodeposited Coatings of Copper plus Nickel plus Chromium and Nickel plus Chromium," provides information on specific requirements for decorative nickel-plus-chromium coatings to achieve acceptable performance under five different conditions of service. The standard defines several classes of coatings that differ in thickness and type, and it classifies the various coating systems according to their resistance to corrosion. The standard specifies the requirements for double-layer and triple-layer nickel coatings (Table 3), and it gives the classification numbers of coatings appropriate for each service condition number. For example, Table 5 specifies decorative nickel-plus-chromium coatings on steel.

The service condition number characterizes the severity of the corrosion environment, 5 being the most severe and 1 being the least severe. The classification number is a way to specify the details of the coating in an abbreviated fashion. For example, the classification number Fe/Ni30d Cr mp indicates that the coating is applied to steel (Fe) and consists of 30 μm of double-layer nickel (d) with a top layer of microporous (mp) chromium that is 0.3 μm thick. (The thickness value of the chromium is not included in the classification number unless its thickness is different from 0.3 μm.) The type of nickel is designated by the following symbols: "b" for electrodeposited single-layer bright nickel, "d" for double- or multilayer nickel coatings, "p" for dull, satin, or semibright nickel deposits, and "s" for polished dull or semibright electrodeposited nickel. The type of chromium is given by the following symbols: "r" for regular or conventional chromium, "mp" for microporous chromium, and "mc" for microcracked chromium.

Table 4 Coating systems on steel giving best performance after 15 years of outdoor marine exposure and 96 h of CASS testing

Type and thickness of coating, μm			ASTM performance ratings(a)	
Copper	Nickel(b)	Chromium(c)	Outdoor marine, 15 years	CASS, 96 h
...	38d	1.5 mc	10/8	10/8
12	26d	1.5 mc	10/9	10/8
...	38d	0.25 mp	10/7	10/7
12	26d	0.25 mp	10/9	10/7

Note: CASS testing ("Copper-Accelerated Acetic Salt Spray [Fog] Testing") is conducted according to ASTM B 368. (a) A two-number system has been adopted by ASTM for rating panels after corrosion testing. The first, the protection number, is based on the percentage of the base metal that is defective due to corrosion. A rating of 10 on steel indicates that the panel did not rust. The second, the appearance number, is similarly based on percentage of defective area, but it rates the extent to which corrosion of the base metal, as well as superficial corrosion, detract from the overall appearance. Appearance ratings of 7, 8, or 9 indicate that 0.25 to 0.5%, 0.1 to 0.25%, or 0 to 0.1% of the area, respectively, is defective due to superficial staining and corrosion. (b) d, double layer. The double-layer nickel coatings in the program differed in reactivity. For details see G.A. DiBari and F.X. Carlin, Decorative Nickel/Chromium Electrodeposits on Steel—15 Years Corrosion Performance Data, *Plating and Surface Finishing*, May 1985, p 128. (c) mc, microcracked; mp, microporous. The type of microcracked chromium used in this study is based on the addition of selenium compounds to a conventional chromium bath to obtain microcracking. Consistent crack patterns were obtained at the chromium thicknesses given in the table.

Table 5 Decorative nickel-plus-chromium coatings on steel

Service condition number (typical applications)	Coating designation(a)	Minimum nickel thickness, μm
SC 5—Extended very severe (exterior automotive where longtime corrosion protection is a requirement)	Fe/Ni35d Cr mc	35
	Fe/Ni35d Cr mp	35
SC 4—Very severe (exterior automotive, boat fittings)	Fe/Ni40d Cr r	40
	Fe/Ni30d Cr mp	30
	Fe/Ni30d Cr mc	30
SC 3—Severe (patio and lawn furniture, bicycles, hospital furniture, and cabinets)	Fe/Ni30d Cr r	30
	Fe/Ni25d Cr mp	25
	Fe/Ni25d Cr mc	25
	Fe/Ni40p Cr r	40
	Fe/Ni30p Cr mp	30
	Fe/Ni30p Cr mc	30
SC 2—Moderate service (stove tops, oven liners, office furniture, golf club shafts, plumbing fixtures, and bathroom accessories)	Fe/Ni20p Cr r	20
	Fe/Ni15b Cr mp	15
	Fe/Ni15b Cr mc	15
SC 1—Mild (toaster bodies, interior automotive accessories, trim for major appliances, fans, light fixtures)	Fe/Ni10b Cr r	10

(a) b, electrodeposited single-layer bright nickel; d, double-layer or multilayer nickel coating; r, regular or conventional chromium; mc, microcracked chromium; mp, microporous chromium. The numerals in the designations denote the thickness of the nickel coating in microns. The thickness of the chromium is assumed to be 0.3 μm unless otherwise specified. When permitted by the purchaser, copper may be used as an undercoat for nickel, but it cannot be substituted for any of the part of the nickel specified. Results of several test programs have raised doubt about whether coating systems involving regular chromium are satisfactory for SC 4 and SC 3.

Decorative Nickel Alloy Plating

Decorative nickel-iron alloy plating processes were introduced to conserve nickel and to lower anode material costs by substituting a portion of the nickel with iron. Decorative nickel-iron alloy deposits have full brightness, high leveling, excellent ductility, and good receptivity for chromium. Nickel-iron can be plated on steel, brass, aluminum, zinc die castings, or plastic substrates in either barrel or rack equipment. The operation and the proprietary additives used in commercially available processes are similar to those in conventional bright nickel plating. In addition, the bath requires special additives to stabilize the ferrous and ferric ions so that hydroxide compounds do not form and precipitate. The stabilizers are either complexers or reducing agents, depending on the nature of the proprietary process. The processes should be controlled within the limits recommended by plating supply houses. Deposits on steel or copper that is subsequently chromium plated have had good acceptance for interior applications as a substitute for bright nickel. Decorative nickel-iron alloy deposits are not often used for outdoor applications where corrosion conditions are severe, because the deposits tend to form a fine, superficial brown stain relatively quickly. The rate at which this occurs depends on the iron content of the deposits, and those with less than 15% Fe have been used in outdoor applications.

Watts and Nickel Sulfamate Solutions for Engineering Applications

Electrodeposited nickel coatings are applied in engineering applications to modify or improve surface properties, such as corrosion resistance, hardness, wear, and magnetic properties. Although the appearance of the coating is important and the plated surface should be defect-free, the lustrous, mirror-like deposits described in previous sections are not usually required. Nickel electroforming is the specialized use of the nickel plating process to produce or reproduce articles by electroplating onto a

mandrel that is subsequently separated from the deposit.

Watts and Nickel Sulfamate Processes. The two most popular solutions for depositing engineering nickel coatings and for electroforming, Watts nickel and nickel sulfamate, have been included in Table 2. The table summarizes the chemical composition, operating conditions, and typical mechanical property data for deposits from these solutions. The Watts solution is relatively inexpensive and easy to control; it has already been discussed.

Nickel sulfamate solutions are widely used for electroforming because of the low internal stress of the deposits, high rates of deposition, and superior throwing power. Throwing power is the relationship between current distribution and uniformity of coating thickness, as influenced by geometric factors (the shape and relative positioning of anode and cathode), and by the electrochemical characteristics of the solution (conductivity, cathode polarization, and cathode efficiency). Throwing power is a measure of the extent to which a solution will produce deposits that are more uniform than those that would be produced in the absence of cathode polarization and cathode efficiency effects. Because of the very high solubility of nickel sulfamate, a higher nickel metal concentration is possible than in other nickel electrolytes, permitting lower operating temperatures and higher plating rates.

A small amount of nickel chloride is usually added to nickel sulfamate solutions to minimize anode passivity, especially at high current densities. If nickel chloride is not added, sulfur-containing nickel anode materials with about 0.02% S are essential to avoid anodic oxidation of the sulfamate ion, which can result in the uncontrolled and unpredictable production of sulfur-containing compounds that act as stress reducers and that cannot easily be removed from solution. Bromide ions, instead of chloride, are sometimes added to nickel sulfamate solutions to promote anode dissolution.

Nickel sulfamate is so soluble that it cannot be readily recrystallized from solution. It is commercially available as a concentrated solution, usually prepared by reacting high-purity nickel powder with sulfamic acid under controlled conditions. Nickel sulfamate plating solutions are more expensive than those based on commercial grades of nickel sulfate and nickel chloride. The extra cost of using solutions that are as pure as possible is more than offset by savings in the preliminary purification procedures necessary otherwise.

Prolonged use of sulfamate solutions at temperatures above 60 °C (140 °F) or at a pH of less than 3.0 can hydrolyze the nickel sulfamate to the less soluble form of nickel ammonium sulfate. The ammonium and sulfate ions produced from the hydrolysis increase the internal tensile stress and hardness of the deposits.

Nickel electrodeposited from a well-purified sulfamate bath containing no stress-reducing agent and operated at 46 °C (115 °F), a pH of 4.0, and a current density of 2.0 A/dm^2 (20 A/ft^2) has a residual tensile stress varying from 15 to 40 MPa (2 to 6 ksi). The stress in a deposit produced from a similarly operated Watts bath would be about 170 MPa (25 ksi).

Sulfamate nickel plating baths are especially useful for applications requiring low residual stress in the electrodeposited nickel, such as in electroforming, and for coating objects that are susceptible to fatigue cracking. Steel crankshafts that are nickel plated for resistance to corrosion and wear should be coated with a low-stress nickel deposit, such as sulfamate nickel, to minimize loss of fatigue strength. The fatigue limit of nickel-plated steel is reduced almost proportionally to the amount of residual tensile stress in the nickel plate, and the use of compressively stressed deposits provides additional benefits.

Alternative Nickel Plating Solutions for Engineering Applications

Although used to a lesser extent than Watts and nickel sulfamate solutions, a number of alternative plating solutions have been developed for specific engineering applications. Examples of these are listed in Table 6, along with available mechanical properties.

Fluoborate. The fluoborate solution listed in Table 6 can be used over a wide range of nickel concentrations, temperatures, and current densities. The fluoborate anion is aggressive, and

Table 6 Alternative nickel plating solutions for specific engineering applications

Type	Composition(a), g/L	pH	Temperature		Cathode current density, A/dm^2	Vickers hardness, 100 g load	Tensile strength		Elongation, %	Internal stress	
			°C	°F			MPa	ksi		MPa	ksi
Fluoborate	Nickel fluoborate, 225–300 Nickel chloride, 0–15 Boric acid, 15–30	2.5–4	38–70	100–158	3–30	125–300	380–600	55–87	5–30	90–200	13–29
Hard nickel	Nickel sulfate, 180 Ammonium chloride, 25 Boric acid, 30	5.6–5.9	43–60	100–140	2–10	350–500	990–1100	144–160	5–8	300	44
All–chloride	Nickel chloride, 225–300 Boric acid, 30–35	1–4	50–70	122–158	2.5–10	230–260	620–930	90–135	4–20	275–340	40–49
All–sulfate	Nickel sulfate, 225–410 Boric acid, 30–45	1.5–4	38–70	100–158	1–10	180–275	410–480	59–70	20	120	17
Sulfate chloride	Nickel sulfate, 150–225 Nickel chloride, 150–225 Boric acid, 30–45	1.5–2.5	43–52	109–126	2.5–15	150–280	480–720	70–104	5–25	210–280	30–41
High sulfate	Nickel sulfate, 75–110 Sodium sulfate, 75–110 Ammonium chloride, 15–35 Boric acid, 15	5.3–5.8	20–32	68–90	0.5–2.5	…	…	…	…	…	…
Black nickel (sulfate bath)	Nickel sulfate, 75 Zinc sulfate, 30 Ammonium sulfate, 35 Sodium thiocyanate, 15	5.6	24–32	75–90	0.15	…	…	…	…	…	…
Black nickel (chloride bath)	Nickel chloride, 75 Zinc chloride, 30 Ammonium chloride, 30 Sodium thiocyanate, 15	5.0	24–32	75–90	0.15–0.6	…	…	…	…	…	…
Nickel phosphorus	Nickel sulfate, 170 or 330 Nickel chloride, 35–55 Boric acid, 0 or 4 Phosphoric acid, 50 or 0 Phosphorous acid, 2–40	0.5–3.0	60–95	140–203	2–5	…	…	…	…	…	…

(a) The formulas of the compounds in the table are as follows: nickel fluoborate, $Ni(BF_4)_2$; nickel sulfate, $NiSO_4 \cdot 6H_2O$; nickel chloride, $NiCl_2 \cdot 6H_2O$; boric acid, H_3BO_3; ammonium chloride, NH_4Cl; ammonium sulfate, $(NH_4)_2SO_4$; sodium sulfate, Na_2SO_4; phosphoric acid, H_3PO_4; phosphorous acid, H_3PO_3; zinc sulfate, $ZnSO_4 \cdot 7H_2O$; zinc chloride, $ZnCl_2$; sodium thiocyanate, NaSCN.

some materials that contact the solution are chemically attacked. Silica filter aids cannot be used on a continuous basis, although cellulose filters are satisfactory. Lead, titanium, and high-silicon cast iron are readily attacked. Stainless steels containing 20% Cr, 25 to 30% Ni, and 2 to 3% Mo are resistant. Anode materials can be encased in Vinyon, polypropylene, or Orlon anode bags to prevent insoluble particles and anode residues from entering the plating solution; nylon bags are unsuitable. Only sleeve-type glass electrodes for pH measurement should be used because of the formation of relatively insoluble potassium fluoborate with permanent junction types. The mechanical and physical properties of deposits produced by the fluoborate bath are similar to those from Watts solutions. The nickel fluoborate solution has been used primarily for high-speed deposition of thick nickel.

Hard Nickel. Developed especially for engineering applications, this solution is applied where controlled hardness, improved abrasion resistance, greater tensile strength, and good ductility are required (without the use of sulfur-containing organic addition agents). Close control of pH, temperature, and current density is necessary for this bath to maintain the desired hardness values. The tensile strength increases and the ductility decreases with an increase in pH and a decrease in temperature. The internal stress is slightly higher than in deposits from Watts solutions. The disadvantages of the hard nickel bath are its tendency to form nodules on edges and the low annealing temperature (230 °C, or 450 °F) of its deposits. Hard nickel deposits are used primarily for buildup or salvage purposes. For optimum results, the ammonium ion concentration should be maintained at 8 g/L (1.1 oz/gal). In those applications where the part being plated is not going to be exposed to elevated temperatures in service, it is simpler to add organic compounds such as saccharin, p-toluene sulfonamide, p-benzene sulfonamide, or other carriers to Watts or sulfamate solutions to achieve hardness without increased internal stress. Because the additives introduce 0.03% S (or more), this approach cannot be used for parts that will be exposed to high temperatures where sulfur severely embrittles the nickel deposit.

All-Chloride. The principal advantage of the all-chloride bath (Table 6) is its ability to operate effectively at high cathode current densities. Other advantages include its high conductivity, its slightly better throwing power, and a reduced tendency to form nodular growths on edges. Deposits from this electrolyte are smoother, finer-grain, harder, and stronger than those from Watts solutions, and more highly stressed. Because of the partial solubility of lead chloride, lead cannot be used in contact with the all-chloride solution. Mists from this solution are corrosive to the superstructure, vents, and other plant equipment, if not well protected. The solution has been used to some extent for salvaging underside or worn shafts and gears.

All-sulfate has been applied for electrodepositing nickel where the principal or auxiliary anodes are insoluble. For example, insoluble auxiliary or conforming anodes may be required to plate the insides of steel pipes and fittings. To prevent pitting, hydrogen peroxide may be added to all-sulfate solutions, provided they contain no wetting agents or organic stress reducers. Oxygen is evolved at insoluble anodes in the all-sulfate solution, and as a result, the nickel concentration and pH decrease during plating. The pH is controlled and the nickel ion concentration is maintained by adding nickel carbonate. Another procedure that has been used in low-pH solutions replenishes the nickel electrolytically by employing a replenishment tank with nickel anodes; the current in the replenishment tank is periodically reversed to keep the nickel anodes actively dissolving in the absence of chlorides. The insoluble anodes in all-sulfate solutions may be lead, carbon, graphite, or platinum. If a small anode area is required, solid platinum (in the form of wire) may be used; for large anode areas, platinum-plated or platinum-clad titanium is recommended. In some forms, carbon and graphite are too fragile; lead has the disadvantage of forming loose oxide layers, especially if it is immersed in other solutions in the course of a plating cycle. In chloride-free solution, pure nickel is almost insoluble and may function as an internal anode if properly bagged.

Sulfate/Chloride. The sulfate/chloride solution given in Table 6 has roughly equivalent amounts of nickel sulfate and nickel chloride and was developed to overcome some of the disadvantages of the all-chloride solution. It has high conductivity and can be operated at high current densities. Although the internal stress of the deposits is higher than in deposits from Watts solutions, the stress is lower than in the all-chloride solution. The other properties are about midway between those for deposits from Watts and all-chloride solutions. Lead may not be used for equipment in contact with this solution because of the high chloride content.

High Sulfate. The high-sulfate bath was developed for plating nickel directly on zinc-base die castings. It may also be used to plate nickel on aluminum that has been given a zincate or comparable surface preparation treatment. The high sulfate and low nickel contents, together with the high pH, provide good throwing power with little attack of the zinc. The deposits are less ductile and more highly stressed than nickel deposited from a Watts bath. For this reason, high sulfate nickel is sometimes used as a thin undercoating for more ductile nickel. In general, the deposition of copper from a cyanide solution directly on zinc-base die castings prior to the deposition of nickel is simpler and more reliable.

Black Nickel. There are at least two formulations for producing black nickel deposits; these incorporate zinc and thiocyanate (CNS^-) ions. Table 6 gives the composition and operating conditions for a sulfate and a chloride black nickel plating bath. The process was developed for decorative reasons—color matching and blending. The black nickel deposit has little wear or corrosion resistance and is usually deposited over a layer of nickel deposited from a bright or dull nickel plating solution. It is in commercial use, but it is limited in its applications.

Nickel phosphorus solutions result in the electrodeposition of nickel phosphorus alloys that are analogous to electroless deposits using sodium hypophosphite as the reducing agent. The hardness of the electrolytic deposits can be increased by heat treatment in the same way that the hardness of electroless nickel deposits can be increased, with maximum hardness occurring at 400 °C (750 °F). The phosphorus content of the deposits is best controlled by frequent additions of phosphite or phosphorous acid. The electrodeposition of nickel phosphorus alloys is receiving increased attention because deposits with greater than 10% P are amorphous and therefore have enhanced resistance to corrosion.

Nickel Alloy Plating for Engineering Applications

Nickel alloys electroplated for engineering applications include nickel-iron, nickel-cobalt, nickel-manganese, nickel-molybdenum, nickel-chromium, zinc-nickel, and tin-nickel. A brief summary of each of these alloy coatings is given in subsequent sections. It should be noted that alloy electrodeposition is far less commercially important than unalloyed nickel decorative and engineering plating or electroforming. Nevertheless, alloy coatings are used for some specialized applications. More detailed information on these alloy electrodeposits can be found in *Surface Engineering,* Volume 5 of *ASM Handbook.*

Nickel-Iron. Iron is an inexpensive metal, and solutions for plating nickel-iron alloys were developed mainly in order to reduce the cost of the metal used to produce a layer of a given thickness. Up to 35 % of the nickel is replaced by iron in these coatings. Alloys containing 18 to 25% Fe are soft magnetic materials with low coercive force, low remanence, and high maximum permeabilities. A typical nickel-iron plating solution is given in Table 7.

Nickel-iron coatings have not achieved commercial success because the organic addition agents are more expensive than those needed for bright nickel, substantially negating the saving on metal. In addition, nickel-iron is less resistant to corrosion than nickel, and the higher the iron content, the lower its resistance. The corrosion product is rust colored.

Nickel-Cobalt. Cobalt additions to nickel plating solutions increase the hardness and strength of the nickel plating, especially in electroforming applications. Adding 6 g/L Co (0.8 oz/gal) to a 600 g/L (75 oz/gal) nickel sulfamate solution produces an alloy containing about 34% Co with a peak hardness of 520 HV.

However, at peak hardness, internal tensile stress is too high for electroforming applications, although the alloy can be used as a coating on a solid substrate. For electroforming purposes, the limit of tolerable deposit stress is reached with alloys containing about 15% Co that have hardnesses around 350 to 400 HV.

Nickel Manganese. Embrittlement of nickel by incorporated sulfur when heated above 200 °C (390 °F) can arise by formation of brittle grain boundary films. In electrodeposits, the sulfur incorporation can result from the use of organic addition agents put into the solution in order to control-internal stress in the plating. In these circumstances, manganese ions can be added to the solution so as to allow deposition of a nickel-manganese alloy resistant to sulfur embrittlement. Strength is also superior to that of pure nickel coatings.

The disadvantages of these alloy coatings is that manganese does not codeposit as readily as iron or cobalt with nickel, and so nickel-manganese alloys contain much less manganese for a given concentration in solution of the second metal (manganese contents range from only 0.02 to 0.27%). Nickel-manganese alloys containing a useful amount of manganese tend to have high tensile internal stress and to be brittle.

Nickel-Molybdenum. Alloy layers about 20 to 30 μm thick of nickel with about 15% Mo exhibit higher hardness and resistance to corrosion than pure nickel. However, these property improvements come at the expense of a reduction in ductility to about 1%.

Nickel-Chromium. There are many references in the published literature describing the deposition of nickel-chromium and nickel-chromium-iron alloys from simple salt solutions, but these solutions for the most part have not achieved commercial success. Chromium contents in these alloy coatings can range from 1 to 60%. Interest in ternary nickel-chromium-iron continues because the development of a stainless steel coating would conserve strategic metals and lower cost if they could be applied to plain carbon-steel strip or sheet or to a component that has been fabricated to the required size and shape.

Zinc-nickel alloys produce the highest corrosion resistance of electroplated zinc alloys. These alloys contain from 5 to 15% Ni. Corrosion resistance improves with nickel content up to 15 to 18%. Beyond this range the alloy becomes more noble than steel and loses its sacrificial protection property. An alloy containing 10 to 13 wt% Ni is electroplated on steel strip and coil as an alternative to zinc-iron or electrogalvanizing. An advantage of this composition is the formability of the steel after coiling.

Tin-Nickel. The intermetallic compound 65Sn-35Ni can be plated from several commercial electrolyte solutions. The finish has high lubricity and a bright, chromelike appearance with excellent corrosion resistance, especially in seawater environments. It is used more often for general industrial applications than for electronic components, because it is more difficult to solder than other tin-alloy coatings.

Table 7 Typical nickel-iron solution composition

Constituent	Amount, g/L (oz/gal)
Ni^{+2}	56 (7.46)
Iron (total)	4 (0.53)
$NiSO_4 \cdot 6H_2O$	150 (20.00)
$NiCl_2 \cdot 6H_2O$	90 (12.00)
$FeSO_4 \cdot 7H_2O$	20 (2.67)
H_3BO_3	45 (6.00)
Stabilizer(a)	15 (2.00)

(a) Concentration will vary between 10 and 25 g/L (1.3 and 3.3 oz/gal), depending on the type of stabilizer used.

Electroforming

Electroforming is the process by which articles or shapes can be exactly reproduced by electrodeposition on a mandrel or form that is later removed, leaving a precise duplicate of the original. In certain applications, the mandrel is designed to remain as an integral part of the final electroformed object. Electroforms themselves may be used as parents or masters, usually with special passivating treatments so the secondary electroform can be easily removed. The same or similar electrodeposition additives as those used for electroplating are required for electroforming to control deposit stress, grain size, and other resultant mechanical properties in order to produce high-quality electroforms.

Applications

The clectroforming industry uses nickel to electrofabricate critical components such as the main combustion chamber for the *Space Shuttle*, heart pump components, body joint implants (prosthetic devices), hypodermic needles, high-precision optical scanners and holographic masters (for credit cards, etc.), and recording masters. Fabrication of duplicating plates such as electrotypes, video disc stampers, and currency embossing plates is manufacturing technology that employs electroforming. High-precision parts such as molds and dies, where tolerances of internal surfaces are critical, are pieces for which electroforming can be used advantageously. Optical memory disc mold cavities, including those for compact disc (CD and video discs) rely on the virtually perfect surface reproduction found with the electroforming process. The average optical disc requires impressions having a mean diameter of about 0.2 μm, which is well within the range of the electroforming processes practiced today.

Process Advantages and Disadvantages

Advantages. Once the conceptual design for a part or component is developed, it is necessary to determine the fabrication process that best meets the functional requirements of the hardware with least cost impact. The following advantages of electroforming might be weighed:

- Parts can be mass produced with identical tolerances from one part to the next, provided that mandrels can be made with adequate replication.
- Fine detail reproduction is unmatched by any other method of mass fabrication. Examples are the electroforming of microgroove masters and stampers for the record and compact disc industries, surface roughness standards, and masters and stampers for holographic image reproduction.
- Mechanical properties of electroformed articles can be varied over a wide range by selecting a suitable plating electrolyte and adjusting operating conditions. In some instances properties can be created in electroformed metals that are difficult, if not impossible, to duplicate in wrought counterparts.
- Some shapes, particularly those with complex internal surfaces or passages, cannot be made by any other method without excessive machining costs and scrap losses. These shapes are often easily electroformed. Examples of such hardware are regeneratively cooled thrust chambers and waveguides with compound curves.
- Gearing up to high-volume production is relatively easy in many electroforming applications. For example, a number of first-generation positive replicas can be made from which a large number of second-generation negatives can be electroformed. Such technology lends itself to many molds, stamping devices, and optical surfaces requiring volume production.
- The size and thickness of parts electroformed is not limited. Larger size can be accommodated by increasing the tank volume in which the electrolyte is contained. Thickness may vary from micrometers, as in foils, to one or more centimeters, as is common in rocket thrust chamber shells.
- Without the use of thermal joining techniques, metal layers can be applied by electroforming to provide sandwich composites having a variety of functional properties. Waveguides having an inner silver electroformed layer for high electrical conductivity and an outer electroformed structural layer of copper, nickel, nickel-cobalt, or other electrodepositable alloys are examples.

Disadvantages. There are also some disadvantages of electroforming that must be considered, such as these:

- Electroforming is generally an expensive manufacturing method and is chosen when other methods are more expensive or impractical to produce the desired hardware.
- Thick electroforming is very time-consuming. Some deposits require days, or even weeks, to produce the desired thickness.

However, unlike precision machining, which is also very time-consuming, electroforming is not labor-intensive once the deposition process is started.
- Design limitations exist in that deep or narrow recesses and sharp angles cause problems. Sudden and severe change in cross section or wall thickness must be avoided unless subsequent machining can be permitted.
- Most electrodeposits have some degree of stress in the as-deposited condition that may cause distortion after the mandrel is separated. Stress relieving and special attention to electrolyte chemistries and operating parameters can lessen this problem.
- Any degradation in the mandrel surface quality will be reproduced in the electroform made from it.

The Electroforming Process

Electroforming is very similar to conventional electroplating as far as facilities and electrolytes are concerned. However, the controls are more stringent because the process consumes much more time and the product must be mechanically sound and have low internal stress for dimensional acceptance. With long deposition times, high current densities at edges and surfaces closer to the anodes result in significant buildup, leading to nodules and uncontrolled growth. This results in further current density variations that can seriously affect the mechanical properties of the deposit.

Mandrels are either permanent or expendable. Permanent mandrels are usually metallic, but they can also be made of a conductive plastic. They can be used repeatedly until surface wear or scratching renders them useless. The most widely used permanent mandrels are made of 300 series stainless steels. Expendable mandrels may consist of cast fusible metals, aluminum, plaster, plastics, waxes, or wood.

Nickel Electroforming Solutions. Nickel, the most commonly electroformed metal, is plated from Watts, fluoborate, and sulfamate solutions. The last is the most widely used due to lower stresses in the deposits and ease of operation. Nickel is deposited from most baths with moderate to high tensile stress. If uncontrolled, this stress can make removal of the mandrel difficult, can result in distorted parts after mandrel separation, and can even result in deposit cracking. In general, the chloride-free sulfamate bath produces the lowest internal stresses of all the nickel baths. Typical nickel sulfamate electrolyte compositions, operating conditions, and deposit mechanical properties are shown in Table 2. Effects of changes in operating variables on mechanical properties of nickel sulfamate deposits are described in Table 8. Similar information for all commonly used nickel electroforming baths is given in ASTM B 503, "Standard Practice for Use of Copper and Nickel Electroplating Solutions for Electroforming."

Electroless Nickel Plating

Electroless nickel plating is used to deposit nickel without the use of an electric current. The coating is deposited by an autocatalytic chemical reduction of nickel ions by hypophosphite, aminoborane, or borohydride compounds. Nickel-phosphorus (1 to 12% P), nickel-boron (~5% B), and composite (cermet) electroless coatings are deposited on carbon on carbon and alloy steels, 300 and 400 series stainless steels, aluminum alloys, copper alloys, and plastics.

Electroless nickel is an engineering coating, normally used because of excellent corrosion and wear resistance. Electroless nickel coatings are also frequently applied on aluminum to provide a solderable surface and are used with molds and dies to improve lubricity and part release. Because of these properties, electroless nickel coatings have found many applications, including those in petroleum, chemicals, plastics, optics, printing, mining, aerospace, nuclear, automotive, electronics, computers, textiles, paper, and food machinery. Some advantages and limitations of electroless nickel coatings include the following:

Advantages

- Good resistance to corrosion and wear
- Excellent uniformity
- Solderability and brazability
- Low labor costs

Limitations

- Higher chemical cost than electroplating
- Brittleness
- Poor welding characteristics due to contamination of nickel plate with nickel-phosphorus deposits
- Need to copper-strike the plate alloys containing significant amounts of lead, tin, cadmium, and zinc before electroless nickel can be applied
- Slower plating rate, as compared to the rates of electrolytic methods

Bath Composition and Characteristics

Electroless nickel coatings are produced by the controlled chemical reduction of nickel ions onto a catalytic surface. The deposit itself is catalytic to reduction, and the reaction continues as long as the surface remains in contact with the electroless nickel solution. Because the deposit is applied without an electric current, its thickness is uniform on all areas of an article in contact with fresh solution.

Electroless nickel solutions are blends of different chemicals, each performing an important function. Electroless nickel solutions contain the following:

- A source of nickel, usually nickel sulfate
- A reducing agent to supply electrons for the reduction of nickel
- Energy (heat)
- Complexing agents (chelators) to control the free nickel available to the reaction
- Buffering agents to resist the pH changes caused by the hydrogen generated during deposition
- Accelerators (exultants) to help increase the speed of the reaction
- Inhibitors (stabilizers) to help control reduction

The characteristics of an electroless nickel bath and its deposit are determined by the composition of these components.

Reducing agents include sodium hypophosphite, aminoboranes, sodium borohydride, and hydrazine.

Sodium Hypophosphite Baths. The majority of electroless nickel used commercially is deposited from solutions reduced with sodium hypophosphite. The principal advantages of these solutions over those reduced with boron compounds or hydrazine include lower cost, greater ease of control, and better corrosion resistance of the deposit. Early electroless nickel formulations were ammoniacal and operated at high pH. Later acid solutions were found to have several advantages over alkaline solutions. Among these are (a) higher plating rate, (b) better stability, (c) greater ease of control, and (d) improved deposit corrosion resistance. Accordingly, most hypophosphite reduced electroless nickel solutions are operated between

Table 8 Variables affecting mechanical properties of electroformed deposits from nickel sulfamate electrolytes

Property	Operational effects	Solution composition effects
Tensile strength	Decreases with increasing temperature to 49 °C (120 °F); then increases slowly with further temperature increase. Increases with increasing pH. Decreases with increasing current density	Decreases slightly with increasing nickel content
Elongation	Decreases as the temperature varies in either direction from 43 °C (120 °F). Decreases with increasing pH. Increases moderately with increasing current density	Increases slightly with increasing nickel content. Increases slightly with increasing chloride content
Hardness	Increases with increasing temperature within operating range suggested. Increases with increasing solution pH. Reaches a minimum at about 13 A/dm^2	Decreases slightly with increasing concentration of nickel ion. Decreases slightly with increasing chloride content
Internal stress	Decreases with increasing solution temperature. Reaches a minimum at pH 4.0–4.2. Increases with increasing current density	Relatively independent of variation in nickel ion content within range. Increases significantly with increasing chloride content

4 and 5.5 pH. Table 9 lists compositions of alkaline and acid plating solutions.

Aminoborane Baths. The use of aminoboranes in commercial electroless nickel plating solutions has generally been limited to two compounds: (a) N-dimethylamine borane (DMAB)—$(CH_3)_2$ $NHBH_3$, and (b) N-diethylamine borane (DEAB)—$(C_2H_5)_2$ $NHBH_3$. Compositions and operating conditions for aminoborane baths are listed in Table 10.

Sodium Borohydride Baths. The borohydride ion is the most powerful reducing agent available for electroless nickel plating. Any water-soluble borohydride can be used, although sodium borohydride is preferred. Compositions of borohydride-reduced electroless nickel baths are also shown in Table 10.

Hydrazine Baths. Hydrazine has also been used to produce electroless nickel deposits. These baths operate at 90 to 95 °C (195 to 205 °F) and 10 to 11 pH. Their plating rate is approximately 12 μm/h (0.5 mil/h). Because of the instability of hydrazine at high temperatures, however, these baths tend to be very unstable and difficult to control.

Energy. The amount of energy or heat present in an electroless nickel solution is one of the most important variables affecting coating deposition. In a plating bath, temperature is a measure of the energy content of the bath.

Temperature has a strong effect on the deposition rate of acid hypophosphite-reduced solutions. The rate of deposition is usually very low (~4 μm/h) at temperatures below 65 °C (150 °F). At the preferred operating range for most solutions (85 to 95 °C, or 185 to 205 °F), deposition rates range from 12 to 20 μm/h.

Complexing Agents. To avoid spontaneous decomposition of electroless nickel solutions and to control the reaction so that it occurs only on the catalytic surface, complexing agents are added. Complexing agents are organic acids or their salts, added to control the amount of free nickel available for reaction. They act to stabilize the solution and to retard precipitation of nickel phosphite.

Accelerators. Complexing agents reduce the speed of deposition and can cause the plating rate to become uneconomically slow. To overcome this, organic additives called accelerators or exultants are often a added to the plating solution in small amounts. In hypophosphite-reduced solutions, succinic acid is the accelerator most frequently used. Other carbonic acids, soluble fluorides, and some solvents, however, have also been used.

Inhibitors. Traditionally, inhibitors used with hypophosphite reduced electroless nickel have been of three types: sulfur compounds, such as thiourea; oxy anions, such as molybdates or iodates; and heavy metals, such as lead, bismuth, tin, or cadmium. More recently, organic compounds, including oleates and some unsaturated acids, have been used for some functional solutions. Organic sulfide, thio-compounds, and metals, such as selenium and thallium, are used to inhibit aminoborane-reduced and borohydride-reduced electroless nickel solutions.

Table 9 Hypophosphite-reduced electroless nickel plating solutions

Constituent or condition	Alkaline			Acid		
	Bath 1	Bath 2	Bath 3	Bath 4	Bath 5	Bath 6
Composition						
Nickel chloride, g/L (oz/gal)	45 (6)	30 (4)	30 (4)	…	…	…
Nickel sulfate, g/L (oz/gal)	…	…	…	21 (2.8)	34 (4.5)	45 (6)
Sodium hypophosphite, g/L (oz/gal)	11 (1.5)	10 (1.3)	10 (1.3)	24 (3.2)	35 (4.7)	10 (1.3)
Ammonium chloride, g/L (oz/gal)	50 (6.7)	50 (6.7)	…	…	…	…
Sodium citrate, g/L (oz/gal)	100 (13.3)	…	…	…	…	…
Ammonium citrate, g/L (oz/gal)	…	65 (8.6)	…	…	…	…
Ammonium hydroxide	To pH	To pH	…	…	…	…
Lactic acid, g/L (oz/gal)	…	…	…	28 (3.7)	…	…
Malic acid, g/L (oz/gal)	…	…	…	…	35 (4.7)	…
Amino-acetic acid, g/L (oz/gal)	…	…	…	…	…	40 (5.3)
Sodium hydroxyacetate, g/L (oz/gal)	…	…	10 (1.3)	…	…	…
Propionic acid, g/L (oz/gal)	…	…	…	2.2 (0.3)	…	…
Acetic acid, g/L (oz/gal)	…	…	…	…	…	10 (1.3)
Succinic acid, g/L (oz/gal)	…	…	…	…	10 (1.3)	…
Lead, ppm	…	…	…	1	…	…
Thiourea, ppm	…	…	…	…	1	…
Operating conditions						
pH	8.5–10	8–10	4–6	4.3–4.6	4.5–5.5	4.5–5.5
Temperature, °C (°F)	90–95 (195–205)	90–95 (195–205)	88–95 (190–205)	88–95 (190–205)	88–95 (190–205)	88–95 (190–205)
Plating rate, μm/h (mil/h)	10 (0.4)	8 (0.3)	10 (0.4)	25 (1)	25 (1)	25 (1)

Table 10 Aminoborane- and borohydride-reduced electroless nickel plating solutions

Constituent or condition	Aminoborane		Borohydride	
	Bath 7	Bath 8	Bath 9	Bath 10
Composition				
Nickel chloride, g/L (oz/gal)	30 (4)	24–48 (3.2–6.4)	…	20 (2.7)
Nickel sulfate, g/L (oz/gal)	…	…	50 (6.7)	…
DMAB, g/L (oz/gal)	…	3–4.8 (0.4–0.64)	3 (0.4)	…
DEAB, g/L (oz/gal)	3 (0.4)	…	…	…
Isopropanol, mL (fluid oz)	50 (1.7)	…	…	…
Sodium citrate, g/L (oz/gal)	10 (1.3)	…	…	…
Sodium succinate, g/L (oz/gal)	20 (2.7)	…	…	…
Potassium acetate, g/L (oz/gal)	…	18–37 (2.4–4.9)	…	…
Sodium pyrophosphate, g/L (oz/gal)	…	…	100 (13.3)	…
Sodium borohydride, g/L (oz/gal)	…	…	…	0.4 (0.05)
Sodium hydroxide, g/L (oz/gal)	…	…	…	90 (12)
Ethylene diamine, 98%, g/L (oz/gal)	…	…	…	90 (12)
Thallium sulfate, g/L (oz/gal)	…	…	…	0.4 (0.05)
Operating conditions				
pH	5–7	5.5	10	14
Temperature, °C (°F)	65 (150)	70 (160)	25 (77)	95 (205)
Plating rate, μm/h (mil/h)	7–12 (0.5)	7–12 (0.5)	…	15–20 (0.6–0.8)

DMAB, N-dimethylamine borane, $(CH_3)_2$ $NHBH_3$; DEAB, N-diethylamine borane, $(C_2H_5)_2$ $NHBH_3$

Properties of Electroless Nickel-Phosphorus Coatings

Hypophosphite-reduced electroless nickel is an unusual engineering material, because of both its method of application and its unique properties. As applied, nickel-phosphorus coatings are uniform, hard, relatively brittle, lubricious, easily solderable, and highly corrosion resistant. They can be precipitation hardened to very high levels through the use of low-temperature treatments, producing wear resistance equal to that of commercial hard chromium coatings. This combination of properties makes the coating well suited for many severe applications and often allows it to be used in place of more expensive or less readily-available alloys. Table 11 provides a summary of the properties of nickel-phosphorus as well as nickel-boron electroless deposits.

Structure. Hypophosphite-reduced electroless is one of the very few metallic glasses used as an engineering material. Depending on the formulation of the plating solution, commercial coatings generally contain 6 to 12% P dissolved in nickel, and as much as 0.25% of other elements. As applied, most of these coatings are amorphous; they have no crystal or phase structure. Their continuity, however, depends on their composition. Coatings containing more than 10% P and less than 0.05% impurities are

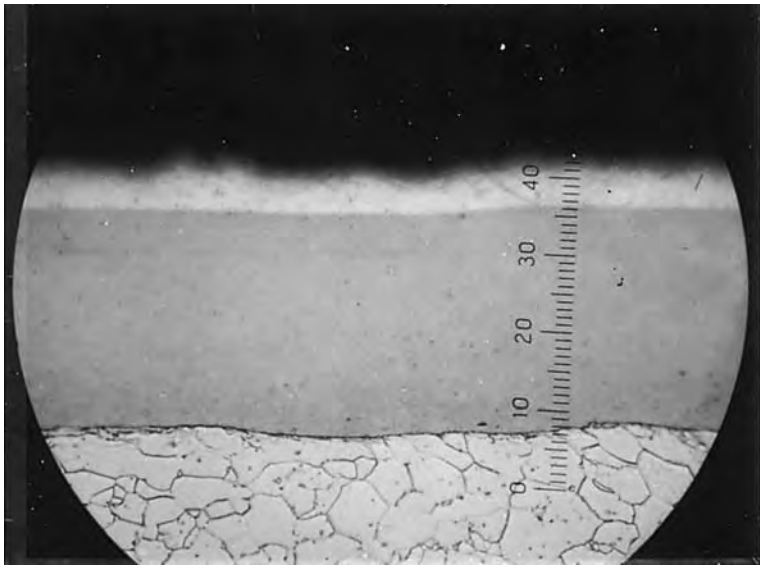


Fig. 6 Cross section of a 75 μm (3 mils) thick electroless nickel deposit. Contains approximately 10% phosphorus and less than 0.05% other elements. 400×

typically continuous. A cross section of one of these coatings is shown in Fig. 6.

Coatings with lower phosphorus content, especially those applied from baths stabilized with heavy metals or sulfur compounds, are often porous. These deposits consist of columns of amorphous material separated by cracks and holes. The presence of such discontinuities has a severe effect on the properties of the deposit, especially on ductility and corrosion resistance.

Mechanical Properties. The mechanical properties of electroless nickel deposits are similar to those of other glasses. They have high strength, limited ductility, and a high modulus of elasticity. The ultimate tensile strength of commercial coatings exceeds 700 MPa (102 ksi) and allows the coating to withstand a considerable amount of abuse without damage. The effect of phosphorus content on the strength and strain at fracture of electroless nickel deposits is shown in Fig. 7.

The ductility of electroless nickel coatings also varies with composition. High-phosphorus, high-purity coatings have a ductility of about 1 to 1½% (as elongation). Although this is less ductile than most engineering materials, it is adequate for most coating applications. Thin films of deposit can be bent completely around themselves without fracture. With lower phosphorus deposits, or with deposits containing metallic or sulfur impurities, ductility is greatly reduced and can approach zero.

Hardening type heat treatments reduce both the strength and ductility of electroless nickel deposits. Exposure to temperatures above 220 °C (428 °F) causes an 80 to 90% reduction in strength and can destroy ductility. This is illustrated by Fig. 8, which shows the effect of different 1 h heat treatments on the elongation at fracture of brass panels coated with 6% P electroless nickel.

Hardness and wear resistance are extremely important properties for many applications. As deposited, the microhardness of electroless nickel coatings is about 500 to 600 HV_{100}, which is approximately equal to 48 to 52 HRC and equivalent to many hardened alloy steels. Heat treatment causes these alloys to age harden and can produce hardness values as high as 1100 HV_{100}, equal to most commercial hard chromium coatings. Figure 9 shows the effect of different 1 h heat treatments on the hardness of electroless nickel containing 10½% P.

Because of their high hardness, electroless nickel coatings have excellent resistance to wear and abrasion, both in the as-deposited and hardened conditions. Taber Abraser Index values for electroless nickel and for electrodeposited

Table 11 Physical and mechanical properties of electroless nickel-phosphorus and nickel-boron deposits

Properties are for coatings in the as-deposited condition, unless noted.

Property	Electroless nickel-phosphorus(a)	Electroless nickel-boron(b)
Density, g/cm^3 (lb/in.^{3})	7.75 (2.8)	8.25 (2.98)
Melting point, °C (°F)	890 (1630)	1080 (1980)
Electrical resistivity, μΩ · cm	90	89
Thermal conductivity, W/m · K (cal/cm · s · °C)	4 (0.01)	…
Coefficient of thermal expansion (22–100 °C, or 72–212 °F), μm/m · °C (μin./in. · °F)	12 (6.7)	12.6 (7.1)
Magnetic properties	Nonmagnetic	Very weakly ferromagnetic
Internal stress, MPa (ksi)	Nil	110 (16)
Tensile strength	700 (100)	110 (16)
Ductility, % elongation	1.0	0.2
Modulus of elasticity, GPa (10^6 psi)	200 (29)	120 (17)
As-deposited hardness, HV_{100}	500	700
Heat-treated hardness, 400 °C (750 °F) for 1 h, HV_{100}	1100	1200
Coefficient of friction vs steel, lubricated	0.13	0.12
Wear resistance, as-deposited, Taber mg/1000 cycles	18	9
Wear resistance, heat treated 400 °C (750 °F) for 1 h, Taber mg/1000 cycles	9	3

(a) Hypophosphite-reduced electroless nickel containing approximately 10.5% P. (b) Borohydride-reduced electroless nickel containing approximately 5% B.

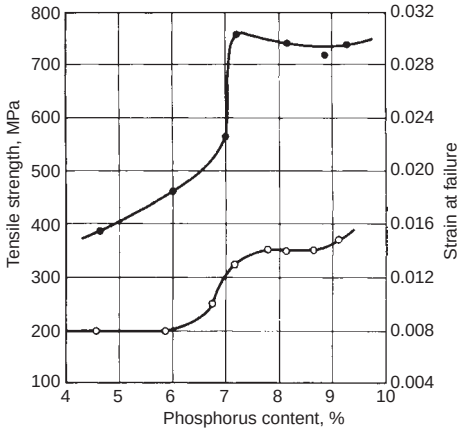


Fig. 7 Effect of deposit phosphorus content on strength (top curve) and strain (bottom curve) at fracture

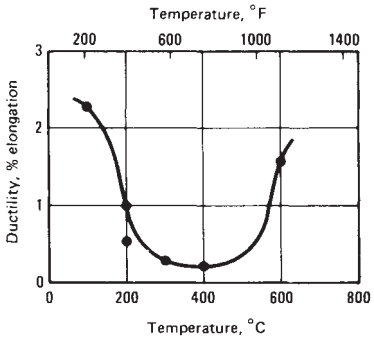


Fig. 8 Effect of heat treatment on the ductility of a 6% P electroless nickel coating

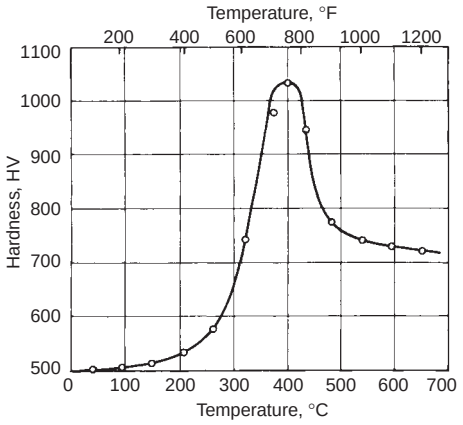


Fig. 9 Effect of heat treatment on hardness of 10.5% P electroless nickel coating

Table 12 Comparison of the Taber abraser resistance of different engineering coatings

Coating	Heat treatment for 1 h		Taber wear index(a), mg/1000 cycles
	°C	°F	
Watts nickel	None	None	25
Electroless Ni-P(b)	None	None	17
	300	570	10
	500	930	6
	650	1200	4
Electroless Ni-B(c)	None	None	9
	400	750	3
Hard chromium	None	None	2

(a) CS-10 abraser wheels, 1000 g load, determined as average weight loss per 1000 cycles for total test of 6000 cycles. (b) Hypophosphite-reduced electroless nickel containing approximately 9% P. (c) Borohydride-reduced electroless nickel containing approximately 5% B

nickel and chromium are summarized in Table 12.

Corrosion Resistance. Electroless nickel is a barrier coating, protecting the substrate by sealing it off from the environment, rather than using sacrificial action. Therefore, the deposit must be free of pores and defects. Because of its amorphous nature and passivity, the coating's corrosion resistance is excellent and, in many environments, superior to that of pure nickel or chromium alloys. Amorphous alloys have better resistance to attack than equivalent polycrystalline materials, because of their freedom from grain or phase boundaries, and because of the glassy films that form on and passivate their surfaces. Some examples of the corrosion experienced in different environments are shown in Table 13. The resistance to attack in neutral and acidic environments is increased as the phosphorus content is increased in the deposit. The reverse is true in alkaline corrosive environments. The effect of phosphorus content on the corrosion rate of electroless coatings is shown in Tables 14 and 15. Where corrosion resistance is required, hardened (heat treated) coatings should not be used.

Properties of Electroless Nickel-Boron Coatings

The properties of deposits from borohydride-reduced or aminoborane-reduced baths are similar to those of electroless nickel-phosphorus alloys with a few exceptions. The hardness of nickel-boron alloys is very high, and these alloys can be heat treated to levels equal to or greater than that of hard chromium. Nickel-boron coatings have outstanding resistance to wear and abrasion. These coatings, however, are not completely amorphous and have reduced resistance to corrosive environments; furthermore, they are much more costly than nickel-phosphorus coatings. The physical and mechanical properties of borohydride-reduced electroless nickel are summarized in Table 11.

Structure. The boron content of electroless nickel reduced with DMAB or DEAB can vary from 0.2 to 4% depending on bath formulation and operation. Commercial borohydride-reduced coatings typically contain 3 to 5% B. Unlike nickel-phosphorus coatings in the as-deposited condition, electroless nickel-boron contains crystalline nickel mixed with nickel-boron (typically Ni_2B) glass. These coatings are not totally homogeneous and consist of phases of different composition.

Mechanical Properties. The strength and ductility of nickel-boron coatings containing 5% B is only about one fifth that of high-phosphorus deposits. Table 11 compares mechanical properties of nickel-boron and nickel-phosphorus deposits.

Hardness and Wear Resistance. The principal advantage of electroless nickel-boron is its high hardness and superior wear resistance. In the as-deposited condition, microhardness values of 650 to 750 HV_{100} are typical for borohydride-reduced and aminoborane-reduced coatings. After 1 h heat treatments at 350 to 400 °C (660 to 750 °F), hardness values of 1200 HV_{100} can be produced.

The wear resistance of electroless nickel-boron is exceptional and after heat treatment

Table 13 Corrosion of electroless nickel coatings in various environments

Environment	Temperature		Corrosion rate: Electroless nickel-phosphorus(a)		Corrosion rate: Electroless nickel-boron(b)	
	°C	°F	μm/yr	mil/yr	μm/yr	mil/yr
Acetic acid, glacial	20	68	0.8	0.03	84	3.3
Acetone	20	68	0.08	0.003	Nil	Nil
Aluminum sulfate, 27%	20	68	5	0.2	…	…
Ammonia, 25%	20	68	16	0.6	40	1.6
Ammonia nitrate, 20%	20	68	15	0.6	(c)	(c)
Ammonium sulfate, saturated	20	68	3	0.1	3.5	0.14
Benzene	20	68	Nil	Nil	Nil	Nil
Brine, 3.5% salt, CO_2 saturated	95	205	5	0.2	…	…
Brine, 3.5% salt, H_2S saturated	95	205	Nil	Nil	…	…
Calcium chloride, 42%	20	68	0.2	0.008	…	…
Carbon tetrachloride	20	68	Nil	Nil	Nil	Nil
Citric acid, saturated	20	68	7	0.3	42	1.7
Cupric chloride, 5%	20	68	25	1	…	…
Ethylene glycol	20	68	0.6	0.02	0.2	0.008
Ferric chloride, 1%	20	68	200	8	…	…
Formic acid, 88%	20	68	13	0.5	90	3.5
Hydrochloric acid, 5%	20	68	24	0.9	…	…
Hydrochloric acid, 2%	20	68	27	1.1	…	…
Lactic acid, 85%	20	68	1	0.04	…	…
Lead acetate, 36%	20	68	0.2	0.008	…	…
Nitric acid, 1%	20	68	25	2	…	…
Oxalic acid, 10%	20	68	3	0.1	…	…
Phenol, 90%	20	68	0.2	0.008	Nil	Nil
Phosphoric acid, 85%	20	68	3	0.1	(c)	(c)
Potassium hydroxide, 50%	20	68	Nil	Nil	Nil	Nil
Sodium carbonate, saturated	20	68	1	0.04	Nil	Nil
Sodium hydroxide, 45%	20	68	Nil	Nil	Nil	Nil
Sodium hydroxide, 50%	95	205	0.2	0.008	…	…
Sodium sulfate, 10%	20	68	0.8	0.03	11	0.4
Sulfuric acid, 65%	20	68	9	0.4	…	…
Water, acid mine, 3.3 pH	20	68	7	0.3	…	…,
Water, distilled, N_2 deaerated	100	212	Nil	Nil	Nil	Nil
Water, distilled, O_2 saturated	95	205	Nil	Nil	Nil	Nil
Water, sea (3.5% salt)	95	205	Nil	Nil	…	…

(a) Hypophosphite reduced electroless nickel containing approximately 10.5% P. (b) Borohydride reduced electroless nickel containing approximately 5% B. (c) Very rapid. Specimen dissolved during test

Table 14 Comparison of the corrosion rates of electroless nickel-phosphorus coatings in chemical process environments with other commonly used materials

Corrodent	Corrosion rate(a), μm/yr: Nickel 200 (UNS N02200)	Ni-P Coatings(b): LP	MP	HP	Mild steel	Type 316 stainless steel (UNS S31600)
Thionyl chloride	7.0	900.0	1.8	2.5	200.0	5.1
Orthochlorobenzyl chloride (crude)	12.7	3.8	7.4	7.1	NA(c)	25.0
Orthochlorobenzyl chloride	12.7	5.3	13.5	9.4	NA(c)	2.5
Phosphoric acid	10.0	900.0	193.0	19.3	1270.0	2.5
Phosphorus oxychloride	10.0	28.4	1.5	2.5	100.0	18.8
Benzotrichloride	5.1	2.5	5.6	6.1	9.0	5.1
Benzoyl chloride	5.1	1.0	0.8	0.5	8.6	5.1

(a) 60 days exposure at 40 ± 2 °C (105 ± 4 °F). (b) LP, low-phosphorus (1 to 4%) coating; MP, medium-phosphorus (5 to 8%) coating; HP, high-phosphorus (9 to 12%) coating. (c) NA, no data available

Table 15 Comparison of the corrosion rates of electroless nickel-phosphorus coatings in caustic solutions with other commonly used materials

Corrodent	Corrosion rate(a), μm/yr					
	Nickel 200 (UNS N02200)	Ni-P coatings(b)			Mild steel	Type 316 stainless steel (UNS S31600)
		LP	MP	HP		
45% NaOH + 5% NaCl at 40 ± 2 °C (105 ± 5 °F)	2.5	0.3	0.3	0.8	35.6	6.4
45% NaOH + 5% NaCl at 140 ± 2 °C (285 ± 5 °F)	80.0	5.3	11.9	F(c)	NA(d)	27.9
35% NaOH at 93 ± 2 °C (200 ± 5 °F)	5.1	5.3	17.8	13.2	94.0	52.0
50% NaOH at 93 ± 2 °C (200 ± 5 °F)	5.1	6.1	4.8	533.4	83.8	…
73% NaOH at 120 ± 2 °C (250 ± 5 °F)	5.1	2.3	7.4	F(c)	1448.0	332.7

(a) 100 days exposure temperature indicated. (b) LP, low-phosphorus (1 to 4%) coating; MP, medium-phosphorus (5 to 8%) coating; HP, high-phosphorus (9 to 12%) coating. (c) Failed. (d) NA, no data available

equals or exceeds that of hard chromium coatings. Typical Taber wear test results for a 5% B coating is shown in Tables 11 and 12.

Corrosion Resistance. In general, the corrosion resistance of electroless nickel-boron coatings is less than that of high-phosphorus alloys. That is illustrated by Table 13, which compares the attack experience by hypophosphite-reduced and borohydride-reduced coatings in different media. In environments that cause little corrosion of nickel-phosphorus, such as alkalis and solvents, electroless nickel-boron is also very resistant. In environments, however, that cause moderate attack of nickel-phosphorus, such as acids and ammonia solutions, nickel-boron coatings can be severely corroded. In strongly oxidizing media, of course, neither coating is satisfactory.

Ternary Electroless Nickel Alloy Coatings

Ternary alloy coatings are used to provide higher performance in specific properties over conventional nickel-phosphorus and nickel-boron coating systems. By incorporating a third element in significant levels, the basic structure and physical properties of the coating can be altered. As shown in Table 16, ternary alloy systems include Ni-P-Mo, Ni-Cu-P, Ni-Co-P, Ni-Fe-P, Ni-Re-P, Ni-W-P, Ni-Tl-B, and Ni-Sn-B. Figure 10 shows the microstructure of an electroless Ni-Tl-B plating deposit.

Electroless Nickel Composite Coatings

Composites are one of the most recently developed types of electroless nickel coatings. These cermet deposits consist of small particles of intermetallic compounds, fluorocarbons, or diamonds dispersed in an electroless nickel-phosphorus matrix. These coatings have a high apparent hardness and superior wear and abrasion resistance.

Chemistry. Most composite coatings are applied from proprietary baths. Typically, they consist of 20 to 30 vol% of particles entrapped in an electroless nickel containing 4 to 11% P. Most commonly silicon carbide, diamond particles, fluorinated carbon powders, and polytetrafluoroethylene (PTFE) are used, although calcium fluoride is also occasionally co-deposited. The particles are carefully sized and are normally 1 to 3 μm in diameter for silicon carbide and diamonds and 0.35 μm for PTFE. A micrograph of a typical silicon carbide composite coating is shown in Fig. 11. The baths used for composite plating are conventional sodium hypophosphite reduced electroless nickel solutions, with the desired particles suspended in them. These baths, however, are heavily stabilized to overcome or inhibit the very high surface area produced by the particles. The baths otherwise are operated normally and the nickel-phosphorus matrix is produced by the traditional hypophosphite reduction of nickel. The particles are merely caught or trapped in the coating as it forms. Their bond to the coatings is purely mechanical.

Hardness and Wear. The primary use for electroless nickel composite coating is for applications requiring maximum resistance to wear and abrasion. The hardnesses of diamond and silicon carbide are 10,000 and 4,500 HV, respectively. In addition, the coatings are normally heat treated to provide maximum hardness (1000 to 1100 HV_{100}) of the electroless nickel matrix. The resulting apparent surface hardness of the composite is 1300 HV_{100} or more.

The wear surface of a composite coating consists of very hard mounds separated by lower areas of hard electroless nickel. During wear, the mating surface usually rides on the particles and slides over the matrix. Thus, the wear characteristics of these coatings approach that of the particle material. Typical wear test

Table 16 Electroless ternary nickel alloy plating systems

Alloy	Hardness, HK_{100}	Environments in which plating has demonstrated corrosion resistance	Significant properties and applications	Availability
Hypophosphite-reduced alloys				
Nickel-phosphorus-molybdenum (5–9% P, 0.5–1% Mo, bal Ni)	550–650	Alkali, brine, caustics, weak acid solutions	Pitting corrosion protection	Laboratory
Nickel-copper-phosphorus (4–8% P, 1–3% Cu, bal Ni)	430–520	Alkali, brine, caustic solutions	Nonmagnetic, conductive, high modulus	Production
Nickel-cobalt-phosphorus (15–40% Co, 3–8% P, bal Ni)	…	…	High-coercivity coating for use in magnetic memory applications	Laboratory, limited production
Nickel-iron-phosphorus (1–4% Fe, 2–4% P, bal Ni)	…	…	Magnetic applications in electronics	Laboratory
Nickel-rhenium-phosphorus (1–45% Re, 3–8% P, bal Ni)	…	…	High melting point (1700 °C, or 3090 °F); high-temperature wear resistance	Laboratory
Nickel-tungsten-phosphorus (4–8% P, 1–4% W, bal Ni)	550–620	…	High melting point (1550 °C, or 2820 °F); high-temperature wear resistance	Laboratory
Boron-reduced alloys				
Nickel-thallium-boron (3–5% Tl, 3–5% B, bal Ni)	650–850	…	Wear applications requiring resistance to galling, fretting, and erosion; coating is self-lubricating in contact with ferrous materials	Production
Nickel-tin-boron (3–5% B, 1–3% Sn, bal Ni)	650–850	…	Wear applications requiring resistance to galling, fretting, and erosion; this coating is also self-lubricating	Production

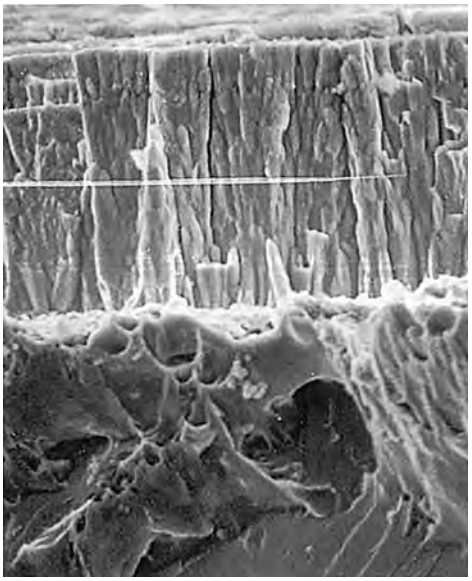


Fig. 10 Electroless nickel-thallium-boron deposit. The hard columnar structure increases resistance to fretting wear and the ability of the deposit to retain oil. Additional lubrication is provided with the presence of thallium, which interferes with the galling process between nickel and a mating iron/steel surface.

results for a silicon carbide composite coating are shown in Table 17.

Corrosion Resistance. In general, the corrosion resistance of composite coatings is significantly less than that of other electroless nickel coatings. The electroless nickel matrix contains large amounts of codeposited inhibitor, which reduces the passivity and corrosion resistance of the alloy. Also, heat treated coatings are less protective than are as-applied coatings, both because of the conversion of the amorphous deposit to crystalline nickel and Ni_3P and because of cracking of the coating. With composites, this problem is amplified because of the presence of the diamond or intermetallic particles. The mixture of phosphides, nickel, and particles creates a very strong galvanic couple accelerating attack. For applications requiring good corrosion resistance, electroless nickel composite coatings are not normally used.

Thermal Spray Coatings

Thermal spraying comprises a group of processes in which divided molten metallic or nonmetallic material is sprayed onto a prepared substrate to form a coating. The sprayed material is originally in the form of wire, rod, or powder. As the coating materials are fed through the spray unit, they are heated to a molten or plastic state and propelled by a stream of compressed gas onto the substrate. As the particles strike the surface, they flatten and form thin platelets that conform and adhere to the irregularities of the prepared surface and to each other. They cool and accumulate, particle by particle, into a lamellar, castlike structure (Fig. 12). In general, the substrate temperature can be kept below approximately 200 °C (400 °F), eliminating metallurgical change of the substrate material.

A wide variety of nickel alloys can be deposited using various thermal spray methods, including flame spraying, high-velocity oxyfuel (HVOF) spraying, and plasma spraying. Examples include the following:

- Commercially pure nickel, Inconel alloys 600, 625, and 718, and Hastelloy alloys B, C, and C-276 for corrosion-resistant applications
- Nickel-chromium, nickel aluminide, and NiCrCoAlY coatings for high-temperature corrosion protection
- Nickel-base alloys containing chromium boride, tungsten carbide, and chromium carbide for wear-resistant applications

Table 18 provides a list of alloys available from one producer of wear-resistant products and services. Many of these alloys are deposited by the spray-and-fuse process. This is a two-step process in which powdered coating material is deposited by conventional thermal spraying, usually using either a combustion gun (or torch) or a plasma spray gun, and subsequently fused using either a heating torch or a furnace. The spray-and-fuse process usually employs self-fluxing hardfacing alloys that contain silicon and boron. These elements act as fluxing agents, which, during fusion, permit the coating to react with any oxide film on the workpiece or individual powder particle surfaces, allowing the coating to wet and interdiffuse with the substrate and result in virtually full densification of the coating. Hard particles, such as tungsten carbide, may be added for increased wear resistance.

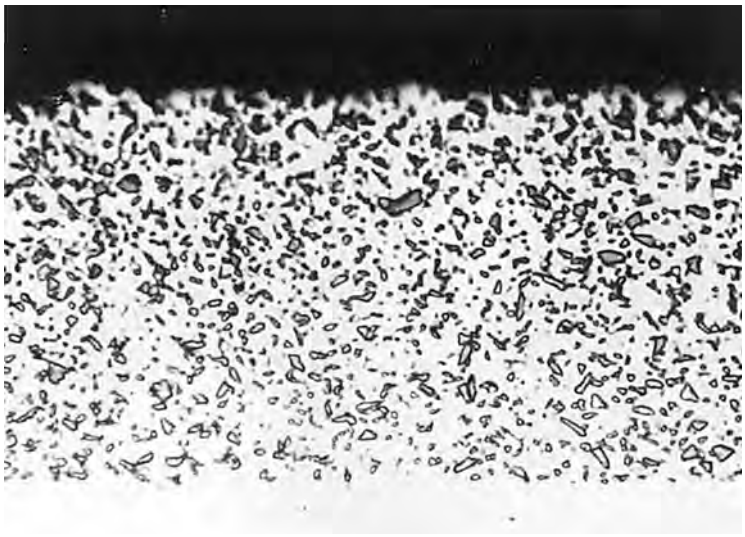


Fig. 11 Cross-sectional view of a typical silicon carbide composite coating.

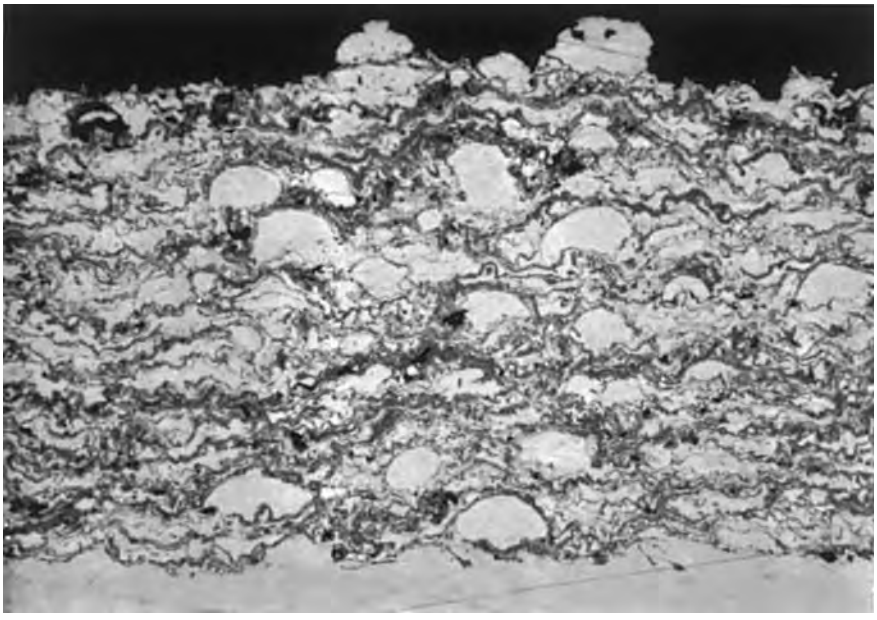


Fig. 12 Micrograph showing the microstructure of a thermally sprayed 80Ni-20Cr alloy. The microstructure includes partially melted particles and dark oxide inclusions that are characteristic of many metallic coatings sprayed in air

Weld-Overlay Coatings

Nickel weld overlay coatings include both wear-resistant (hardfacing) alloys and corrosion-

Table 17 Comparison of the Taber abraser resistance of silicon carbide composite coatings with other engineering materials

Material	Hardness	Taber wear index, Mg 11,000 cycles
400-C stainless steel	57 HRC	5.6
A2 tool steel	60–62 HRC	5.0
Electroless nickel (hardened)	900–1000 HV	3.7
Hard chromium	1000–1100 HV	3.0
Tungsten carbide	1300 HV	2.0
Electroless nickel and silicon carbide composite	1300 HV	0.18–0.22

Note: Taber wear index determined for an average of three 5000 cycle runs with 100 g load and CS17 abrasive test wheels

resistant (weld cladding) alloys. These coatings can be applied by oxyfuel gas welding and various arc welding methods, for example, gas-tungsten arc welding (GTAW), shielded metal arc welding (SMAW), and plasma-transferred arc (PTA) welding.

Hardfacing Alloys

Most commercially available nickel-base hardfacing alloys can be divided into two groups: boride-containing alloys and Laves phase-containing alloys. The compositions of some typical nickel-base hardfacing alloys are listed in Table 19.

The boride-containing nickel-base alloys were first commercially produced as spray-and-fuse powders. The alloys are currently available from most manufacturers of hardfacing products under various tradenames and in a variety of forms, such as bare cast rod, tube wires, and powders for plasma weld and manual torch.

Of all the various ferrous and nonferrous hardfacing alloys, the boride-containing nickel-base alloys are microstructurally the most complex. The complexity of this type of alloy structure is evident in Fig. 13, which shows a two-layer PTA deposit of ERNiCr-C (see Table 19 for composition). The alloy compositions represent a progression in terms of iron, chromium, boron, and carbon contents. Iron content is largely incidental, allowing the use of ferrocompounds during manufacture. Together with nickel, the other three elements determine the level and type of hard phase within the structure upon solidification, boron being the primary hard-phase forming element (for which nickel and chromium compete) and carbon being the secondary hard-phase former. The actual phases that form in boride-containing nickel-base alloys are listed in Table 20 on the basis of chromium content.

Table 18 Nickel-base wear-resistant coatings deposited by thermal spraying or weld overlays

Alloy	Nominal composition(a), wt%	Hardness, HRC	Density, g/cm^3	Approximate fusing temperature °C	Approximate fusing temperature °F	Supplied as	Method of application(b)
Nickel-base with chromium boride							
Colmonoy 6	C 0.70, Cr 14.3, B 3.0, Si 4.25, Fe 4.0	56–61	8.10	1030	1890	Crushed powder, bare rods, castings, ingot	Oxyacetylene, dc electric arc, GTAW, spraywelder
Colmonoy 6PTA(c)	C 1.10, Cr 20.0, B 2.1, Si 5.6, Fe 5.7	Double pass 56–61/ single pass 49–54	7.93	1065	1950	Atomized powder	PTA
Colmonoy 56	C 0.60, Cr 13.1, B 2.6, Si 3.8, Fe 4.4	50–55	8.18	1030	1885	Crushed powder, bare rods, castings, ingot	Oxyacetylene, dc electric arc, GTAW, spraywelder
Colmonoy 56 PTA	C 0.90, Cr 18.0, B 1.9, Si 5.3, Fe 5.4	Double pass 53–58/ single pass 46–51	8.01	1060	1940	Atomized powder	PTA
Colmonoy 5	C 0.45, Cr 13.8, B 2.1, Si 3.3, Fe 4.8	45–50	8.24	1025	1880	Crushed powder, bare rods, castings, ingot	Oxyacetylene, dc electric arc, GTAW, spraywelder
Colmonoy 5PTA(c)	C 0.75, Cr 14.25, B 1.6, Si 4.8, Fe 4.9	Double pass 47–52/ single pass 40–45	8.14	1095	2000	Atomized powder	PTA
Colmonoy 4	C 0.40, Cr 10.0, B 2.1, Si 2.4, Fe 2.8	35–40	8.39	1050	1925	Crushed powder, bare rods, castings, ingot	Oxyacetylene, dc electric arc, GTAW, spraywelder
Colmonoy 4PTA(c)	C 0.55, Cr 13.0, B 1.3, Si 3.9, Fe 4.0	Double pass 37–42/ single pass 30–35	8.28	1120	2050	Atomized powder	PTA
Nickel-base with chromium carbide							
Colmonoy 69SC	C 0.55, Cr 16.5, B 3.6, Si 4.8, Fe 3.0, Cu 2.1, Mo 3.5	58–63	8.06	1030	1890	Atomized powder	Spraywelder, HVOF
Colmonoy 62SA	C 0.60, Cr 15.0, B 2.9, Si 4.80, Fe 4.0	56–61	8.07	1025	1875	Atomized powder	Spraywelder, fusewelder, HVOF
Colmonoy 52SA	C 0.55, Cr 12.3, B 2.2, Si 3.7, Fe 3.8	45–50	8.24	1065	1950	Atomized powder	Spraywelder, fusewelder, HVOF
Colmonoy 42SA	C 0.15, Si 2.8, Cr 4.0, B 1.15, Fe 0.10, Mo 3.0	35–40	8.50	980	1800	Atomized powder	Spraywelder, fusewelder, HVOF
Colmonoy 98	C 0.06, Cr 7.9, Si 4.2, Cu 2.5, B 3.2, Mo 2.0, Nb 2.0	55–60	8.31	1015	1860	Atomized powder	Spraywelder, HVOF, fusewelder, PTA
Colmonoy 88	C 0.80, Si 4.0, Cr 15.0, B 3.0, Fe 3.5, W 17.3	59–64	9.89	1055	1930	Atomized powder, bare rods, cored wire-GTAW, oxy, GMAW	Spraywelder, HVOF, fusewelder, PTA
Colmonoy 84	C 1.15, Si 2.4, Cr 29.0, B 1.4, Fe 2.0, W 7.5	40–45	8.84	1095	2000	Atomized powder, castings, ingot	Spraywelder, PTA, HVOF
Colmonoy 72	C 0.70, Si 3.8, Cr 13.0, B 2.9, Fe 4.0, W 13.0	57–62	9.51	1060	1940	Atomized powder, bare rods, castings, ingot	Oxyacetylene, dc electric arc, GTAW, spraywelder, PTA
Colmonoy 21A PTA(c)	C 0.30, Cr 5.80, B 0.95, Si 4.10, Fe 1.30	28–32	8.45	1120	2050	Atomized powder	PTA
Colmonoy 22	C 0.02, Cr 0.08, B 1.5, Si 3.4, Fe 0.12	28–33	8.58	1050	1925	Atomized powder, bare rods, ingot, castings	Oxyacetylene, fusewelder
Colmonoy 23A and 24	C 0.02, Cr 0.08, B 1.5, Si 2.5, Fe 0.12	16–23	8.64	1065	1950	Atomized powder, bare rods, ingot, castings	Fusewelder
Nickel-base with tungsten carbide							
Colmonoy 75	C 1.90, Cr 9.30, B 2.0, W 29.50, Si 2.8, Fe 2.60, Co 4.2	58–63	11.25	1050	1920	Crushed powder	Spraywelder
Colmonoy 83PTA(c)	C 2.00, Cr 20.30, B 0.90, Si 1.40, Fe 1.40, W 34.00	Double pass 50–55/ single pass 43–48	11.78	1115	2040	Crushed and atomized powder	PTA
Colmonoy 635	C 2.3, Cr 8.2, B 1.9, W 30.8, Si 3.1, Fe 2.4, Co 2.1	58–63	11.46	1025	1875	Crushed and atomized powder	Spraywelder
Colmonoy 705	C 2.20, Cr 7.00, B 1.50, W 48.20, Si 1.90, Fe 2.20, Co 0.10	58–63	13.38	1025	1875	Crushed and atomized powder	Fusewelder
Colmonoy 730	C 2.4, Cr 8.6, B 1.9, W 38.9, Si 2.5, Fe 2.8, Co 2.4	58–63	12.36	1060	1940	Crushed and atomized powder	Spraywelder, HVOF
Colmonoy 750	C 2.05, Cr 8.45, B 1.95, W 37.30, Si 2.34, Fe 2.60, Co 4.20	58–63	12.17	1060	1940	Crushed and atomized powder	Spraywelder
Coltung 1	C 1.75, Cr 7.00, B 1.90, W 38.50, Si 2.65, Fe 2.20, Co 0.12	58–63	12.33	1040	1900	Bare rods	Oxyacetylene, GTAW

(a) Balanced nickel. (b) dc, direct current; GTAW, gas-tungsten arc welding; PTA, plasma transferred arc; HVOF, high-velocity oxyfuel (thermal spray). (c) Composition specially formulated for plasma transferred arc deposition. Source: Wall Colmonoy Corporation

The chief purpose of silicon in the material is to provide, in conjunction with boron, self-fluxing characteristics. However, as an important matrix element and as a potential promoter of intermetallic precipitates, it also has a powerful influence on the wear properties of the alloys.

Boron content influences the level of silicon required for silicide (Ni_3Si) formation. The higher the boron content, the lower is the silicon contest required to form silicides.

Because of the boride and carbide dispersions within their microstructures, the boride-containing nickel-base alloys exhibit excellent resistance to abrasion. Low-stress abrasion resistance generally increases with boron and carbon contents, hence the hard-phase volume fraction for these materials. Although their performance is not as good under self-mated sliding conditions as that of cobalt-base materials, the boride-containing nickel-base alloys possess moderate resistance to galling. Of the nonferrous materials, the boride-containing nickel-base alloys are the least resistant to corrosion. This is attributed to the lack of chromium in the matrix that follows boride and carbide formation. Selected properties of nickel-base hardfacing alloys are given in Table 21. Additional wear data on nickel-base hardfacing alloys can be found in the article "Wear Behavior of Cobalt Alloys" in this Handbook.

Laves Phase Alloys. Only one Laves phase-containing nickel-base alloy is commercially available: Ni-33Mo-16Cr-3.5Si (T-700 in Table 19). This alloy is difficult to weld using the oxyacetylene process, but it can be readily welded using GTAW or the PTA process. It can also be applied using the plasma or high-velocity oxygen fuel thermal spray techniques. Although it has excellent metal-to-metal wear resistance and moderate abrasive wear resistance, the alloy T-700 possesses poor impact resistance. Selected properties of alloy T-700 are listed in Table 21.

Table 19 Chemical compositions of nickel-base hardfacing alloys

	Composition, wt%								
Alloy	B	C	Co	Cr	Fe	Se	Si	Mo	Ni
Boride-containing alloys									
ER NiCr-A	2.00–3.00	0.30–0.60	1.50 max	8.0–14.0	1.25–3.25	0.005 max	1.25–3.25	…	bal
ER NiCr-B	2.00–4.00	0.40–0.80	1.25 max	10.0–16.0	3.00–5.00	0.005 max	3.00–5.00	…	bal
ER NiCr-C	2.50–4.50	0.50–1.00	1.00 max	12.0–18.0	3.50–5.50	0.005 max	3.50–5.50	…	bal
Laves phase alloy									
T-700	…	…	…	16	…	…	3.5	33	bal

Table 20 Phases formed in boride-containing nickel-base hardfacing alloys

	Secondary phases		
Chromium content	Compound formed	Required conditions	Dominant hard phase
Low (~5 wt%)	Ni_3Si	>3 wt% Si	Ni_3B
Medium (~15 wt%)	Ni_3Si	>2.5 wt% Si	Ni_3B and chromium boride (usually CrB although Cr_2B and Cr_3B_2 may also be present)
High (~25 wt%)	Ni_3Si	>3 wt% Si	CrB and Cr_5B_3
All levels	...	...	Complex carbides of $M_{23}C_6$ and M_7C_3 types

Table 21 Properties of selected nickel-base hardfacing alloys

Property	RNiCrC	RNiCrB	Hastelloy C (Ni-17Cr-17Mo-0.12C)	Tribaloy T-700
Density, g/cm^3 (lb/in.^{3})	7.8 (0.28)	8.0 (0.29)	8.6 (0.32)	8.6 (0.32)
Coefficient of thermal expansion, °C^{-1} (°F^{-1})	14.3 (8.0)	14.3 (8.0)	13.7 (7.6)	11.9 (6.6)
Hot hardness DPH at:				
425 °C (800 °F)	555	...	190	500
540 °C (1000 °F)	440	...	185	485
650 °C (1200 °F)	250	...	170	400
760 °C (1400 °F)	115	...	145	280
Wear				
Unlubricated sliding wear(a), mm^3 (in.^{3} × 10^{-3}) at:				
670 N (150 lbf)	0.15 (0.009)	0.3 (0.018)	0.4 (0.024)	0.1 (0.006)
1330 N (300 lbf)	0.3 (0.018)	0.4 (0.024)	...	0.3 (0.018)
Abrasive wear(b), mm^3 (in.^{3} × 10^{-3})				
OAW	12 (0.73)	18 (1.10)	...	...
GTAW	11 (0.67)	12 (0.73)	105 (6.40)	43 (2.62)
Unnotched Charpy impact strength, J (ft · lbf)	3 (2)	3 (2)	39 (29)	1.4 (1)
Corrosion resistance at 65 °C (150 °F)(c):				
65% nitric acid	U	U	E	E
5% sulfuric acid	U	U	E	E
50% phosphoric acid	U	U	E	E

DPH, diamond pyramid hardness; OAW, oxyacetylene welding.(a) Wear measured from tests conducted on Dow-Corning LFW-1 against 4620 steel ring at 80 rev/min for 2000 rev varying the applied loads. (b) Wear measured from dry sand rubber wheel abrasion tests. Tested for 2000 rev at a load of 135 N (30 lbf) using a 230 mm (9 in.) diam rubber wheel and American Foundrymen's Society test sand. (c) E, less than 2 mils/year; U, more than 50 mils/year

Weld Cladding Alloys

The term weld cladding usually denotes the application of a relatively thick layer (≥3 mm, or ⅛ in.) of weld metal for the purpose of providing a corrosion-resistant surface. Weld cladding is usually performed using the submerged arc welding (SAW) process, but flux-cored, plasma arc, and electroslag welding methods can also produce weld claddings. Typically the base metals for weld cladding are carbon and low-alloy steels. The cladding material is usually an austenitic stainless steel or a nickel-base alloy. Nickel, nickel-copper (Monels), nickel-chromium-iron (Inconels), and nickel-molybdenum and nickel-chromium-molybdenum (Hastelloys) filler metals are used for weld cladding of steels. These alloys are covered by American Welding Society specifications A5.11 (covered electrodes) and A5.14 (bare rods or electrodes).

Solid-State Nickel Cladding

The cladding process described in this section is differentiated from the weld cladding process by the fact that none of the metals to be joined is molten when a metal-to-metal bond is achieved. Also, there are no intermediate layers, such as adhesives. The principle solid-state



Fig. 13 Microstructure of ERNiCr-C (two-layer PTA deposit) nickel-base/boride-type nonferrous alloy. 425×

cladding techniques include cold-roll bonding, hot-roll bonding, hot pressing, explosion bonding, and extrusion bonding.

A wide range of corrosion-resistant alloys clad to steel substrates have been used in industrial applications. Clad metals of this type are typically used in the form of strip, plate, and tubing. Some typical nickel alloys that are bonded to steel substrates include Nickel 201, Monel 400, Inconel 625, and Hastelloy C-276. High-nickel alloy clad metals find various applications in the marine, chemical processing, power, and pollution control industries.

ACKNOWLEDGMENTS

Portions of this article were adapted from the following:

- G.A. Di Bari, Nickel Plating, *Surface Engineering*, Vol 5, *ASM Handbook*, ASM International, 1994, p 201–212
- D. W. Baudrand, Electroless Nickel Plating, *Surface Engineering*, Vol 5, *ASM Handbook*, ASM International, 1994, p 290–310

SELECTED REFERENCES

Electroplating

- G.A. DiBari and S.A. Watson, "A Review of Recent Trends in Nickel Electroplating Technology in North America," NiDI publication No. 14 024, Nickel Development Institute
- L.J. Durney, Ed., *Electroplating Engineering Handbook*, 4th ed., Van Nostrand Reinhold, 1984
- R. Parkinson and T. Hart, "Electroplating on Plastics," NiDI publication No. 10 078, Nickel Development Institute
- W.H. Safranek, *The Properties of Electrodeposited Metals and Alloys-A Handbook*, 2nd ed., American Electroplaters and Surface Finishers Society, 1986
- S.A. Watson, "Nickel Electroplating Solutions," NiDI publication No. 10 047, Nickel Development Institute
- S.A. Watson, "Organic Addition Agents for Nickel Electroplating Solutions," NiDI publication No. 10 048, Nickel Development Institute
- S.A. Watson, "Anodes for Electrodeposition of Nickel," NiDI publication No. 10 049, Nickel Development Institute
- S.A. Watson, "Applications of Decorative Nickel Plating," NiDI publication No. 10 050, Nickel Development Institute
- S.A. Watson, "Applications of Engineering Nickel Plating," NiDI publication No. 10 051, Nickel Development Institute
- S.A. Watson, "Nickel Sulphamate Solutions," NiDI publication No. 10 052, Nickel Development Institute
- S.A. Watson, "Additions to Sulphamate Solutions, NiDI publication No. 10 053, Nickel Development Institute

Electroforming

- R. Parkinson, "Electroforming—A Unique Metal Fabrication Process," NiDI publication No. 10 084, Nickel Development Institute
- S.A. Watson, "Applications of Electroforming," NiDI publication No. 10 054, Nickel Development Institute
- S.A. Watson, "Modern Electroforming," NiDI publication No. 14 005, Nickel Development Institute
- S.A. Watson, "Electroforming Today," NiDI publication No. 14 012, Nickel Development Institute

Electroless Coating

- G.O. Mallory and J.B. Hajda, *Electroless Plating: Fundamentals and Applications*, American Electroplaters Society, 1990
- R. Parkinson, "Properties and Applications of Electroless Nickel," NiDI publication No. 10 081, Nickel Development Institute
- S.A. Watson, "Electroless Nickel Coatings," NiDI publication No. 10 055, Nickel Development Institute

ASM Specialty Handbook: Nickel, Cobalt, and Their Alloys
J.R. Davis, editor, p 127-140
DOI:10.1361/ncta2000p127

Copyright © 2000 ASM International®
All rights reserved.
www.asminternational.org

Corrosion Behavior of Nickel Alloys in Specific Environments

NICKEL and its alloys, like the stainless steels, offer a wide range of corrosion resistance. However, nickel can accommodate larger amounts of alloying elements, chiefly chromium, molybdenum, copper, and tungsten, in solid solution than can iron. Therefore, nickel-base alloys in general can be used in more severe environments and offer greater resistance to general corrosion, pitting, crevice corrosion, intergranular attack, and stress-corrosion cracking (SCC). Nickel and nickel alloys are widely used in the chemical processing industry, pulp and paper mills, flue gas desulfurization pollution control systems, sour gas applications, and petrochemical and refining applications.

Alloy Characteristics

The common corrosion resistant wrought nickel alloy families include commercially pure nickels, nickel-copper alloys, nickel-molybdenum alloys, Ni-Cr-Fe alloys, Ni-Cr-Mo alloys, and Ni-Cr-Fe-Mo alloys. Similar alloy categories are applicable for cast alloys (see the article "Cast Corrosion-Resistant Nickel Alloys" in this Handbook). Table 1 lists nominal compositions and corrosion resistant applications for nickel and nickel alloys.

Commercially Pure Nickels. The most significant attribute of the commercially pure nickel grades is their outstanding resistance to caustic alkalies—for example, sodium hydroxide (caustic soda)—over a wide range of temperatures and concentrations. They are also resistant to corrosion by high-temperature halogens, reducing salts and other oxidizing halides, and foods, in which these alloys are particularly suited for maintaining product purity. Unalloyed nickel is not a suitable choice for strong oxidizing environments such as nitric acid.

Nickel-Copper Alloys. The corrosion behavior of nickel-copper alloys, like that of commercially pure nickel, is best under reducing conditions and can be compromised by aeration and oxidizing chemicals. Alloy 400 possesses very good resistance to halogen acids and compounds, particularly hydrofluoric acid and hot gases rich in fluorine or hydrogen fluoride.

Table 1 Compositions and characteristics/applications of the nickel and nickel-base alloys described in this article

Alloy	Nominal composition	Characteristics/major applications
Commercially pure nickels		
Nickel 200	99.6Ni-0.04C	Commercially pure wrought nickel with good mechanical properties and corrosion resistance. Used for chemical and process plants such as caustic soda and synthetic fiber production, and for food handling
Nickel 201	99.6Ni-0.02C max	Similar to Nickel 200 but with the carbon content controlled to prevent intergranular embrittlement at service temperatures above 315 °C (600 °F). Used for chemical and process plants
Nickel-copper alloys		
Monel 400	65.1Ni-32Cu-1.6Fe-1.1Mn	A nickel-copper alloy with high strength and excellent resistance to a range of media including seawater, dilute hydrofluoric and sulfuric acids, and alkalies. Used in marine and offshore engineering, salt production, feedwater heater tubing, and chemical and hydrocarbon processing
Monel K-500	64.7Ni-30.2Cu-2.7Al-1Fe-0.6Ti	Similar to Monel 400 but age hardenable for improved strength and hardness. Used for pump shafts, oil well tools, doctor blades, springs, fasteners, and marine propeller shafts
Nickel-molybdenum alloys		
Hastelloy B	62Ni-28Mo-5Fe-2Co-1Cr-1Mn-1Si-0.12C	Higher carbon content predecessor to Hastelloy alloys B-2 or B-3 that was originally developed to resist hydrochloric acid in all concentrations up to the boiling point. Susceptible intergranular attack (sensitization) of weld HAZs
Hastelloy B-2	69Ni-28Mo-2Fe-1Co-1Cr-1Mn-0.1Si-0.01C	Lower carbon version of Hastelloy B that exhibits superior resistance to hydrochloric acid, aluminum chloride catalysts, and other strongly reducing chemicals. Does not exhibit propensity to weld corrosion
Hastelloy B-3	65Ni-28.5Mo-1.5Cr-1.5Fe-3Co-3Mn-3W-0.5Al-0.2Ti-0.1Si-0.01C	Same excellent resistance to hydrochloric acid and other strongly reducing chemicals as B-2 alloy, but with significantly better thermal stability, fabricability, and SCC resistance
Nickel-chromium-iron alloys		
Inconel 600	76Ni-15Cr-8Fe	Combines good high-temperature strength and oxidation resistance with resistance to SCC and caustic corrosion. Used for chemical and petrochemical processing, heat treatment applications, and nuclear and automobile engineering
Inconel 601	60.5Ni-23Cr-14.4Fe-1.4Al	An alloy with outstanding high-temperature strength and oxidation resistance. Used in a range of thermal processing applications
Inconel 690	61.5Ni-29Cr-9Fe	An alloy with excellent resistance to high-temperature corrosion in applications such as nuclear steam generators, coal gasification, and sulfuric, nitric/hydrofluoric acid processing
Incoloy 800	46.0Fe-32.5Ni-21.0Cr-0.05C	An Fe-Ni-Cr alloy with high strength and corrosion resistance used in chemical, petrochemical and food processing, in nuclear engineering, and for the sheathing of electric heating elements. Applications generally at temperatures below 650 °C (1200 °F)
Incoloy 800H	46.0Fe-32.5Ni-21.0Cr-0.3-1.2Al + Ti-0.08C	Similar to alloy 800 but with improved creep and stress-rupture properties for applications above 650 °C (1200 °F). Resistant to high-temperature oxidation, carburization, and nitridation, it is widely used in petrochemical and thermal processing
Incoloy 800HT	46Fe-32.5Ni-21Cr-0.85-1.2Al + Ti-0.08C	Similar to alloy 800H but with even more precisely controlled composition and higher ASME design stress allowables
Nickel-chromium-molybdenum alloys		
Inconel 617	52Ni-22Cr-12.5Co-9.5Mo-1.5Fe-1.2Al	A cobalt-containing alloy with an exceptional combination of high-temperature strength, stability, and oxidation resistance. Also resistant to carburizing gases and a range of aqueous environments, it is used in petrochemical and thermal processing, nitric acid production, and gas turbine engineering.

(continued)

Table 1 (continued)

Alloy	Nominal composition	Characteristics/major applications
Nickel-chromium-molybdenum alloys (continued)		
Inconel 625	61Ni-21.5Cr-9Mo-3.6Nb-2.5Fe	An alloy with resistance to severely corrosive environments, particularly to pitting, crevice corrosion, and high-temperature oxidation, and with high strength from cryogenic temperatures up to 815 °C (1500 °F). Used in aerospace engineering, gas turbines, chemical processing, oil and gas extraction, pollution control, and marine and nuclear engineering
Hastelloy C	54Ni-17Mo-15Cr-5Fe-4W	The "grandfather" of the nickel-chromium-molybdenum family of corrosion-resistant alloys developed to resist a wide range of both reducing and oxidizing environments. Advances in melt processing and corrosion research has prompted the evolution of various lower carbon C-type alloys (see alloys C-276, C-4, C-22, and C-2000 listed below).
Hastelloy C-276	57Ni-16Mo-16Cr-5Fe-4W	An alloy with excellent resistance to reducing and mildly oxidizing environments. Resistant to localized attack and SCC. Used extensively in pollution control applications and throughout the chemical and process industries
Hastelloy C-4	65Ni-16Mo-16Cr-3Fe-2Co	An alloy with high-temperature stability in 650–1040 °C (1200–1900 °F) range as evidenced by good ductility and corrosion resistance. Virtually the same corrosion resistance as alloy C-276
Hastelloy C-22	56Ni-22Cr-13Mo-3Fe-3W-2.5Co	Better overall corrosion in oxidizing environments than C-276, C-4, and 625 alloys. Outstanding resistance to localized corrosion and excellent resistance to SCC. Best alloy to use as universal weld filler metal to resist corrosion of weldments
Hastelloy C-2000	59Ni-23Cr-16Mo-1.6Cu	Most versatile corrosion resistant Ni-Cr-Mo alloy with excellent resistance to uniform corrosion in oxidizing or reducing environments. Excellent resistance to SCC and superior resistance to localized corrosion as compared to alloy C-276
Allcorr	56Ni-31Cr-10Mo-2W	High pitting resistance in chloride-containing oxidizing environments. Used for deep sour gas wells, flue gas desulfurization, chemical and hydrocarbon processing, and pulp and paper mill equipment
Nickel-chromium-iron-molybdenum alloys		
Incoloy 825	42Ni-28Fe-21.5Cr-3Mo-2Cu	An alloy with excellent resistance to sulfuric and phosphoric acids. Resistant to oxidizing and reducing acids, SCC, pitting, and intergranular corrosion, it is used in chemical and petrochemical processing, oil and gas extraction, pollution control, waste processing, and pickling applications
Hastelloy G	44Ni-22Cr-19.5Fe-6.5Mo-2Cu-0.05C	Original member of the G-type Ni-Cr-Fe-Mo family introduced primarily for handling phosphoric acid. Has been largely replaced by the lower-carbon alloy G-3 and higher-chromium alloy G-30 listed below
Hastelloy G-3	44Ni-22Cr-19.5Fe-7Mo-2Cu-0.015C	Lower carbon version of alloy G used in chemical applications, particularly those involving sulfuric and phosphoric acids, and pulp digestion operations. Exhibits improved resistance to HAZ carbide precipitation when compared to alloy G
Hastelloy G-30	43Ni-30Cr-15Fe-5.5Mo-2.5W-5Co-2Cu-0.03C	High chromium-content alloy designed to possess even greater resistance to HAZ corrosion attack. Used for handling phosphoric acid, sulfuric acid, nitric acid, fluoride environments, and oxidizing acid mixtures
Hastelloy D-205	65Ni-20Cr-6Fe-5Si-2.5Mo-2Cu	A Ni-Cr-Fe-Si-Mo alloy with outstanding resistance to hot concentrated sulfuric acid, and other highly concentrated oxidizing media. Can also be aged hardened for higher strength
Hastelloy N	71Ni-16Mo-7Cr-5Fe	A Ni-Mo-Cr-Fe alloy with good resistance to aging and embrittlement and good fabricability. It also has excellent resistance to hot fluoride salts in the temperature range of 705–870 °C (1300–1600 °F).
Nicrofer 3033 (Alloy 33)	33Cr-32Fe-31Ni-2Mo-0.5N	A Cr-Fe-Ni-Mo-N alloy developed to have the highest possible corrosion resistance to oxidizing media such as highly concentrated sulfuric acid. It is also very resistant to nitric acid and to nitric/hydrofluoric acid mixtures.

Nickel-copper alloys are used widely for handling sulfuric acid solutions, seawater, and brines.

Nickel-molybdenum alloys are noted for their superior resistance to sulfuric, phosphoric, and hydrochloric acids under reducing conditions. They are particularly suited for equipment handling hydrochloric acid at all concentrations and temperatures up to the boiling point. As with commercially pure nickels and nickel-copper alloys, corrosion rates of nickel-molybdenum alloys in acid solutions can be greatly increased by the presence of strong oxidizers in the acid.

Nickel-Chromium-Iron Alloys. The addition of chromium to the nickel matrix extends the suitability of alloy 600 into the oxidizing range. Though only satisfactory for mineral acids, alloy 600 has excellent resistance to organic acids and is used extensively in fatty acid processing. It is also employed widely in the production and handling of caustic soda and alkali chemicals. Alloy 600 is also an excellent material for high-temperature applications requiring a combination of heat and corrosion resistance. The excellent performance of the alloy in hot halogen environments makes it a popular choice for organic chlorination processes. Alloy 600 also resists oxidation, carburization, and nitridation.

Alloy 690 has the highest chromium content (29% Cr) among nickel alloys suitable for fabrication of pressure equipment, which confers exceptional resistance to oxidizing media. It is used for hot sulfuric acid, nitric acid, and nitric/hydrofluoric acid mixtures, as well as for oxidizing salts. The high chromium content also improves resistance in hot sulfidizing environments.

Alloys 800, 800H, and 800HT are high nickel iron-base alloys. Although resistant to many aqueous media, they are used primarily for their oxidation and carburization resistance and strength at elevated temperature. These 46Fe-32.5Ni-2lCr alloys are sometimes referred to as superaustenitic stainless steels, but this is not accurate because these alloys contain no molybdenum. Superaustenitic stainless steels contain about 6% Mo. More accurately, these alloys should be considered solid-solution-strengthened iron-base superalloys.

Nickel-chromium-molybdenum-alloys are among the most versatile of the nickel-base alloys and are used in a broad range of environments, both oxidizing and reducing. Alloy 625, which contains 9% Mo, serves effectively as both a corrosion resistant and heat resistant material. The combination of high-temperature strength and resistance to halogen attack, oxidation, and carburization has made alloy 625 a popular choice for chemical and petrochemical process equipment exposed to hostile, high-temperature environments.

The other Ni-Cr-Mo alloys contain higher molybdenum contents (~15% Mo) and have outstanding resistance to acids, salts, and a wide spectrum of other substances encountered in chemical processing. They are also resistant to chloride ion SCC. The high molybdenum alloys are used when sulfuric acid becomes contaminated with halides. They are also specified when sulfuric acid is used in the production of other chemicals such as phosphoric acid, hydrofluoric acid, titanium dioxide, ammonium sulfate, and in the refining of nickel and copper ores.

Nickel-Chromium-Iron-Molybdenum Alloys. Alloy 825 excels in sulfuric and phosphoric acid applications. Though reasonably resistant to hydrochloric acid, alloy 825 is subject to pitting and crevice corrosion, particularly in stagnant, unaerated solutions. Its high iron content (~30% Fe) makes it less resistant than higher-nickel-containing alloys to alkalis and halogens.

The lower iron content alloys G-3 and G-30 are especially resistant to sulfuric acid and contaminated phosphoric acid and can withstand both reducing and oxidizing conditions. Alloy G-30 has better weldability and offers improved all-round corrosion resistance, notably in weld heat-affected zones.

Silicon-modified (5% Si) alloy D-205 is recommended for strongly oxidizing environments. Its primary use is as a plate-heat-exchanger material in sulfuric acid service.

Alloy N is a Ni-Mo-Cr-Fe alloy that was developed to resist attack by molten fluoride salts at temperatures up to 700 °C (1300 °F). It also compares favorably to other Ni-Cr-Mo and Ni-Cr-Fe-Mo alloys in various other corrosive media.

Alloy 33 is actually a chromium-base alloy with a nominal composition of 33Cr-32Fe-31Ni-1.6Mo. It was developed to withstand oxidizing environments such as highly concentrated sulfuric acid. Its resistance to localized corrosion in chloride-bearing media is

equivalent or superior to that of the 6% Mo superaustenitic stainless steels.

Effects of Major Alloying Elements

The roles of the major alloying elements used to promote corrosion resistance in nickel-base alloys are summarized below. Figure 1 shows some compositional modifications that result in improved corrosion resistance.

Copper. Additions of copper provide improvement in the resistance of nickel to nonoxidizing acids. In particular, alloys containing 30 to 40% Cu offer useful resistance to nonaerated sulfuric acid (H_2SO_4) and offer excellent resistance to all concentrations of nonaerated hydrofluoric acid (HF). Additions of 2 to 3% Cu to Ni-Cr-Mo-Fe alloys have also been found to improve resistance to hydrochloric acid (HCl) H_2SO_4, and phosphoric acid (H_3PO_4).

Chromium additions impart improved resistance to oxidizing media such as nitric (HNO_3) and chromic (H_2CrO_4) acids. Improved resistance to hot H_3PO_4 has also been shown. Chromium also improves resistance to high-temperature oxidation and to attack by hot sulfur-bearing gases. Although alloys have been formulated containing up to 50% Cr, alloying additions are usually in the range of 15 to 30%.

Iron is typically used in nickel-base alloys to reduce costs, not to promote corrosion resistance. However, iron does provide nickel with improved resistance to H_2SO_4 in concentrations above 50%. Iron also increases the solubility of carbon in nickel; this improves resistance to high-temperature carburizing environments.

Molybdenum in nickel substantially improves resistance to nonoxidizing acids. Commercial alloys containing up to 28% Mo have been developed for service in nonoxidizing solutions of HCl, H_3PO_4, and HF, as well as in H_2SO_4 in concentrations below 60%. Molybdenum also markedly improves the pitting and crevice corrosion resistance of nickel-base alloys. In addition, it is an important alloying element for imparting strength in metallic materials designed for high-temperature service.

Tungsten behaves similarly to molybdenum in providing improved resistance to nonoxidizing acids and to localized corrosion. However, because of its atomic weight, approximately twice as much tungsten as molybdenum must be added by weight to achieve atomically equivalent effects. Because of the negative impact this would have on alloy density and because of the typically higher cost and lower availability of tungsten, additions of molybdenum are generally preferred. However, additions of tungsten of the order of 3 to 4% in combination with 13 to 16% Mo in a nickel-chromium base result in alloys with outstanding resistance to localized corrosion.

Silicon is typically present only in minor amounts in most nickel-base alloys as a residual element from deoxidation practices or as an intentional addition to promote high-temperature oxidation resistance. In alloys containing significant amounts of iron, cobalt, molybdenum, tungsten, or other refractory elements, the level of silicon must be carefully controlled because it can stabilize carbides and harmful intermetallic phases. On the other hand, the use of silicon as a major alloying element has been found to improve greatly the resistance of nickel to hot, concentrated H_2SO_4. Alloys containing 9 to 11% Si are produced for such service in the form of castings.

Cobalt. The corrosion resistance of cobalt is similar to that of nickel in most environments. Because of this and because of its higher cost and lower availability, cobalt is not generally used as a primary alloying element in materials designed for aqueous corrosion resistance. On the other hand, cobalt imparts unique strengthening characteristics to alloys designed for high-temperature service. Cobalt, like iron, increases the solubility of carbon in nickel-base alloys, and this increases resistance to carburization. Further, the melting point of cobalt sulfide is higher than that of nickel sulfide; therefore, alloying with cobalt also tends to improve high-temperature sulfidation resistance.

Niobium and Tantalum. In corrosion resistant alloys, both niobium and tantalum were originally added as stabilizing elements to tie up carbon and prevent intergranular corrosion attack due to grain-boundary carbide precipitation. However, the advent of argon-oxygen decarburization melting technology made it possible to achieve very low levels of residual carbon, and such additions of niobium and tantalum are no longer necessary. In high-temperature alloys, both elements are used to promote high-temperature strength through solid-solution and precipitation-hardening mechanisms. Additions of these elements are also considered to be beneficial in reducing the tendency of nickel-base alloys toward hot cracking during welding.

Aluminum and titanium are often used in minor amounts in corrosion resistant alloys for the purpose of deoxidation or to tie up carbon and/or nitrogen, respectively. When added

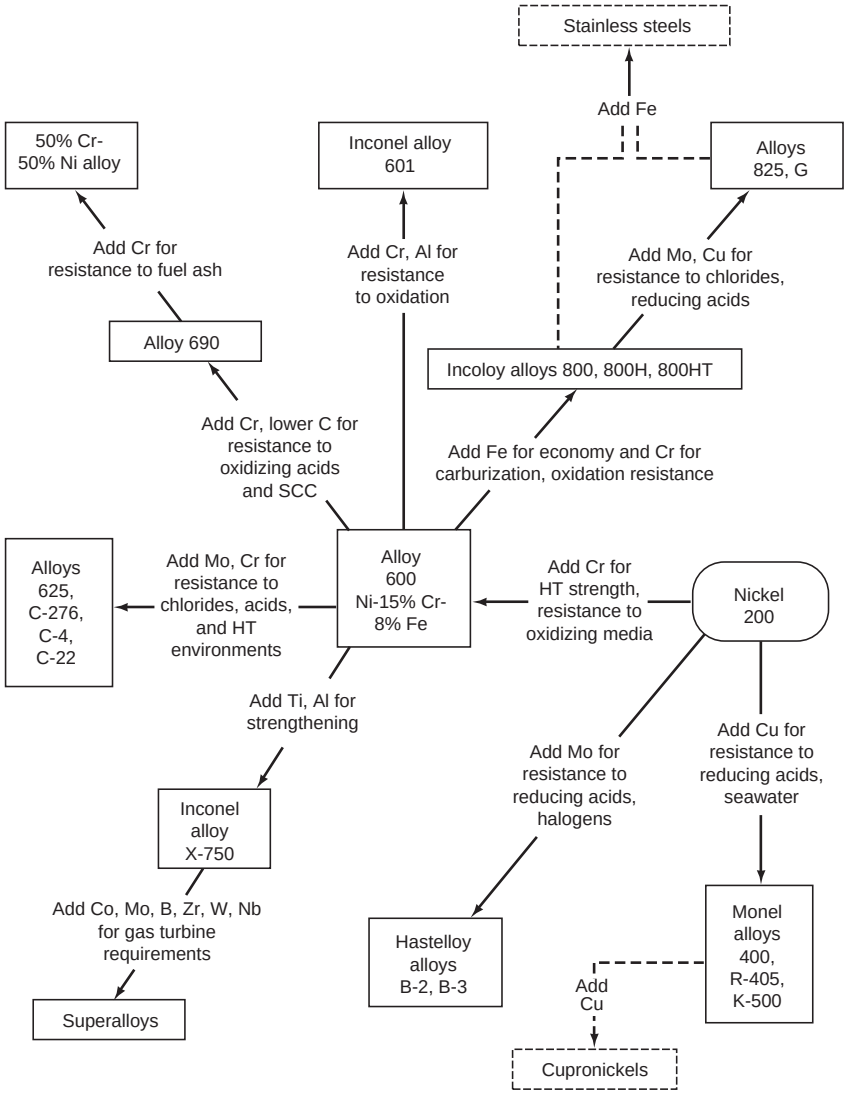


Fig. 1 Effects of alloying additions on the corrosion resistance of nickel alloys. HT, high-temperature

together, these elements enable the formulation of age-hardenable high-strength alloys for low- and elevated-temperature service. Additions of aluminum can also be used to promote the formation of a tightly adherent alumina scale at high temperature that resists attack by oxidation, carburization, and chlorination.

Carbides. In corrosion resistant alloys, many types of carbides are considered harmful because they can precipitate at grain boundaries during heat treatment or weld fabrication and subsequently promote intergranular corrosion or cracking in service. This results from the depletion of matrix elements essential to corrosion resistance during the carbide precipitation process. In high-temperature alloys, the presence of carbides is generally desired to control grain size and to enhance elevated-temperature strength and ductility. However, careful attention must be paid to the carbide types and morphologies after solution heat treatment or postfabrication heat treatment in order to avoid cracking during component manufacture or loss of strength and/or ductility in service.

Carbides that have a deleterious effect on weld fabrication are discussed in the section "Corrosion of Nickel and High-Nickel Alloy Weldments" in this article. Additional information on carbide precipitation can be found in the article "Stress-Corrosion Cracking and Hydrogen Embrittlement of Nickel Alloys" in this Handbook.

Intermetallic Phases. The occurrence of intermetallic phases in nickel-base alloys carries both good and bad connotations. On the positive side, the nickel-base system has been the most widely and successfully exploited of any alloy base in the development of high-strength high-temperature alloys because of the occurrence of unique intermetallic phases such as gamma prime (γ') and gamma double prime (γ''). On the negative side, the precipitation of certain intermetallic phases such as sigma (σ), mu (μ), and Laves phase can seriously degrade ductility and corrosion resistance. This latter effect results from the fact that intermetallics, like carbides, can rob the matrix of elements vital to service performance.

In the case of corrosion resistant alloys, especially the solid-solution type, the formulation of alloy chemistry to avoid intermetallic precipitation altogether is not necessary, because service temperatures are usually well below those at which precipitation kinetics become important. In such cases, it is necessary only to restrict alloy composition sufficiently to ensure successful manufacturing, fabrication, and use capabilities. For high-temperature alloys, the precipitation of undesired intertmetallics can be a major concern, especially for applications requiring a long service life or ease of repair. Therefore, much effort has been devoted to understanding intermetallics and their effects on properties and to determining how to avoid their occurrence through alloy design.

The effect of μ phase on weld fabrication is described in the section "Corrosion of Nickel and High-Nickel Alloy Weldments" in this article. Additional information on intermetallic phases in nickel alloys can be found in the articles "Superalloys" and "Stress-Corrosion Cracking and Hydrogen Embrittlement of Nickel Alloys" in this Handbook.

Corrosion in Specific Environments

The corrosive environments described in this section involve both aqueous and nonaqueous environments at relatively low temperatures (<260 °C, or 500 °F). High-temperature applications of nickel alloys involving hot gases are discussed in the article "High-Temperature Corrosion Behavior of Nickel Alloys" in this Handbook.

Atmospheric Corrosion

Nickel and nickel-base alloys have very good resistance to atmospheric corrosion. Corrosion rates are typically less than 0.0025 mm/yr (0.1 mil/yr), with varying degrees of surface discoloration depending on the alloy (Table 2). Nickel 200 will become dull and acquire a thin adherent corrosion film, which is usually a sulfate. A greater tarnish will result in industrial sulfur-containing atmospheres than in rural or marine atmospheres.

Corrosion of alloy 400 is negligible in all types of atmospheres, although a thin gray-green patina will develop. In sulfurous atmospheres, a brown patina may be produced. Because of its low corrosion rate and pleasing patina, alloy 400 has been used for architectural service, such as roofs, gutters, and flashings, and for outdoor sculpture.

Nickel alloys containing chromium and iron, such as alloys 600 and 800, also have very good atmospheric corrosion resistance, but may develop a slight tarnish after prolonged exposure, especially in industrial atmospheres. Nickel-chromium-molybdenum materials such as alloys 825, 625, G, C-276, and C-22 develop very thin and protective passive oxide films that prevent even significant tarnishing. A mirror finish can be maintained after extended exposure to the atmosphere.

Although alloy 400 has been used for atmospheric service in the past, atmospheric exposures requiring nickel alloys are now relatively infrequent. Less costly stainless steels or plated materials are normally used.

Corrosion in Waters

Distilled Water and Freshwater. Nickel and nickel-base alloys generally have very good resistance to corrosion in distilled water and freshwater. Typical corrosion rates for Nickel 200 (commercially pure nickel) in a distilled water storage tank at ambient temperature and domestic hot water service are <0.0025 mm/yr (<0.1 mil/yr) and <0.005 mm/yr (<0.2 mil/yr), respectively. Nickel-copper alloys such as 400 and R-405 also have very low corrosion rates and are used in freshwater systems for valve seats and other fittings. Because of the cost of nickel alloys, less expensive stainless steels or other materials are usually specified for pure or freshwater applications unless increased resistance to SCC or pitting is required. Alloys 600 and 690, for example, are used for increased SCC resistance in high-purity water nuclear steam generators.

In steam/hot water systems, such as condensers, appreciable corrosion of Nickel 200 and alloy 400 may occur if noncondensables (CO_2 and air) in the steam exist in certain proportions. Deaeration of the feedwater or venting of the noncondensable gases will prevent this attack. Alloy 600 is resistant to all mixtures of steam, air, and CO_2 and is particularly useful in contact with steam at high temperatures.

Seawater. Nickel 200 and alloy 400 and nickel-base alloys containing chromium and iron are very resistant to flowing seawater, but in stagnant or very low velocity seawater pitting or crevice corrosion can occur, especially under fouling organisms or other deposits. In moderate- and high-velocity seawater or brackish water, alloy 400 is frequently used for pump and valve trim and transfer piping. It has excellent resistance to cavitation erosion and exhibits corrosion rates less than 0.025 mm/year (1 mil/yr). Alloy 400 sheathing also provides economical seawater splash zone protection to steel offshore oil and gas platforms, pilings, and other structures. Although pitting can occur in alloy 400 under stagnant conditions, such pitting tends to slow down after fairly rapid initial attack and rarely exceeds 1.3 mm (50 mils) in depth. Age-hardened alloy K-500, with corrosion resistance similar to that of alloy 400, is frequently used for high-strength fasteners and pump and propeller shafting in freshwater and seawater applications.

Other nickel-base alloys containing chromium and molybdenum offer increased resistance to localized corrosion in stagnant seawater. Corrosion resistance of some nickel-base alloys and type 316 stainless steel in ambient temperature seawater is compared in Table 3. In hot seawater applications, such as heat exchangers, highly alloyed materials such as alloys 625 or C-276 may be required. In addition,

Table 2 Atmospheric corrosion and pitting of nickel-base alloys

Results of a 20 year exposure 24.4 m (80 ft) from the ocean at Kure Beach, NC

Alloy	Average weight loss, mg/dm^2	Average corrosion rate(a) mm/yr	mils/yr
Nickel 200	468.6	<0.0025	<0.1
Alloy 800	27.9	<0.0025	<0.1
Alloy 600	19.7	<0.0025	<0.1
Alloy 400	644.7	<0.0025	<0.1
Alloy 825	8.7	<0.0025	<0.1

(a) No pitting recorded for Nickel 200 and alloy 600. The average of the four deepest pit depths for the other three alloys was less than 0.025 mm (0.001 in.).

Table 3 Resistance of various alloys to stagnant seawater

3-year exposure tests

Alloy	Maximum pit depth	
	mm	mils
625	Nil	Nil
825	0.025	0.98
K-500	0.864	34
400	1.067	42
AISI type 316	1.575	62

alloys 625, 400, and K-500 are frequently specified for U.S. Naval wetted components in contact with seawater. Specific high tensile strength requirements are met with alloy 718.

Corrosion in Sulfuric Acid

Sulfuric acid is the most ubiquitous environment in the chemical industry. The electrochemical nature of the acid varies a great deal, depending on the concentration of the acid and the impurity content. The pure acid is considered to be a nonoxidizing acid up to a concentration of about 50 to 60% by weight, beyond which it is generally considered to be oxidizing. The corrosion rates of nickel-base alloys, in general, increase with acid concentration up to about 90% weight. Higher concentrations of the acid are generally less corrosive. The corrosion resistance of nickel alloys in H_2SO_4 and related compounds is reviewed in Ref 1.

A broad view of the relative performance of various alloys in reagent grade H_2SO_4 is illustrated in Fig. 2. In this graph, the temperatures at which the corrosion rate of an alloy in a given concentration of the acid exceeds 0.5 mm/yr (20 mils/yr) are plotted as isocorrosion curves. At low acid concentrations, the Ni-Cr-Mo alloys show a significantly higher resistance than type 316 stainless steel. Alloy 20, a high-nickel stainless steel, shows similar behavior. These high-Ni-Cr-Mo alloys can be used only to moderate temperatures in the intermediate and high concentrations of H_2SO_4. The nickel-molybdenum alloys B-2 and B-3 can be used to higher temperatures for all concentrations of acid. However, in the presence of oxidizing species and in aqueous acid systems, alloys B-2 and B-3 suffer serious corrosion. This effect is shown in Fig. 3 for alloy B-2.

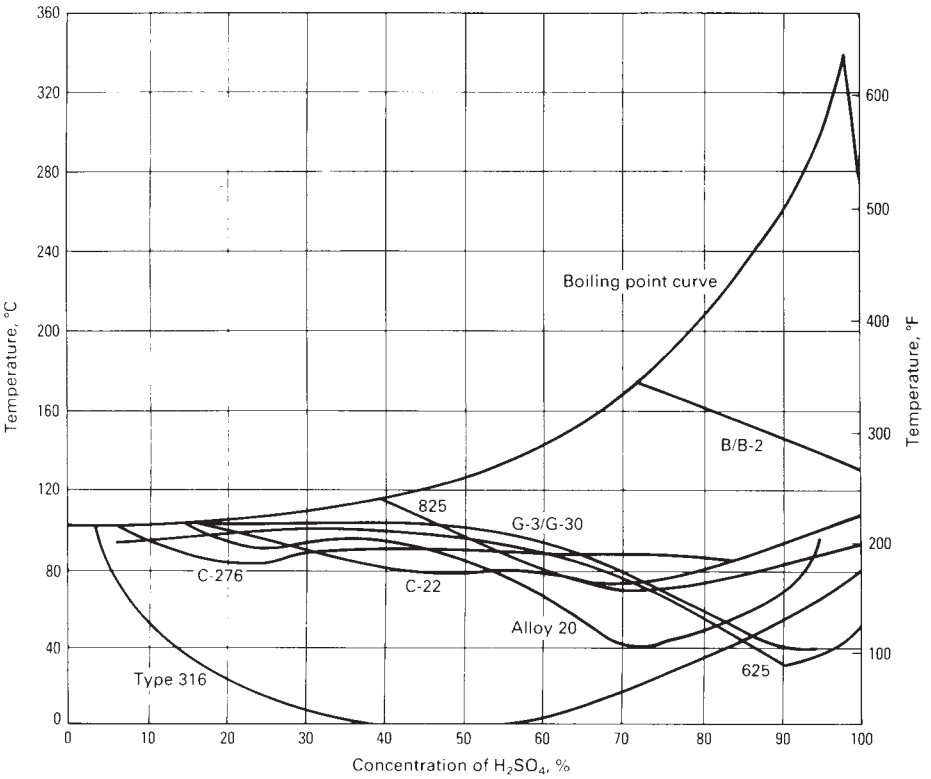


Fig. 2 Comparative behavior of several nickel-base alloys in pure H_2SO_4. The isocorrosion lines indicate a corrosion rate of 0.5 mm/yr (20 mils/yr). Source: Ref 2–4

The presence of oxidizing impurities can be beneficial to Ni-Cr-Mo alloys shown in Fig. 2 because these impurities can aid in the formation of passive films that retard corrosion. Another important consideration is the presence of chlorides (Cl^-). Chlorides generally accelerate the attack; the extent of acceleration differs for various alloys. This is shown in Fig. 4 in terms of the 0.13 mm/yr (5 mils/yr) isocorrosion curves for alloys C-276 and G.

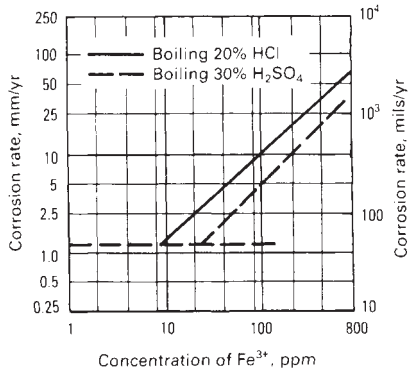


Fig. 3 Effect of Fe^{3+} in boiling H_2SO_4 and HCl on the corrosion rate of alloy B-2

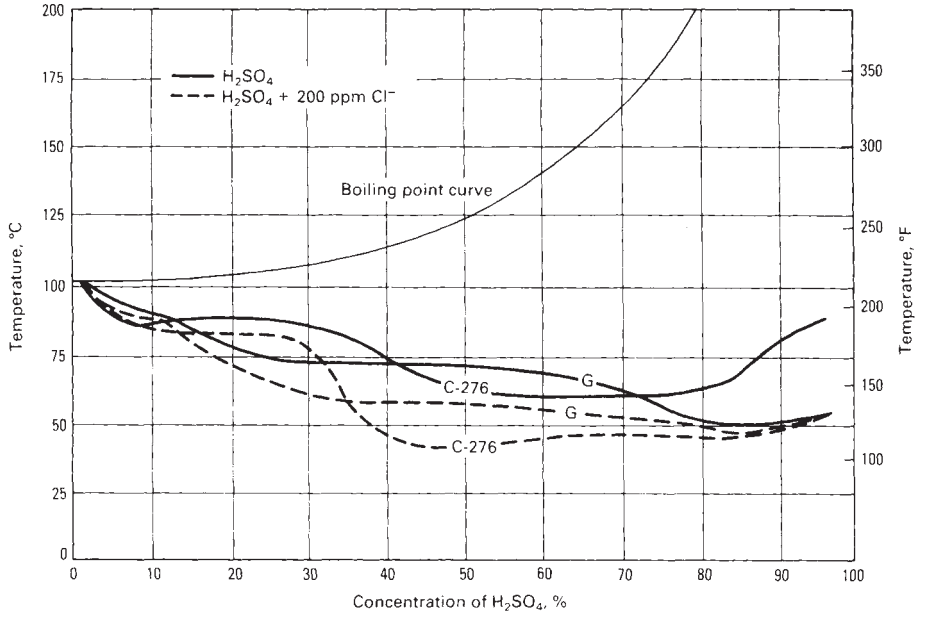


Fig. 4 Effect of dissolved chlorides on the corrosion resistance of nickel-base alloys in H_2SO_4. The isocorrosion lines indicate a corrosion rate of 0.13 mm/yr (5 mils/yr).

Corrosion in Hydrochloric Acid

The corrosion resistance of several nickel-base alloys in HCl and related environments is reviewed in Ref 5. Commercially pure nickel (200 and 201) and nickel-copper alloys (alloy 400) have room-temperature corrosion rates below 0.25 mm/yr (10 mils/yr) in air-free HCl at concentrations up to 10%. In HCl concentrations of less than 0.5%, these alloys have been used at temperatures up to about 200 °C (390 °F) (Ref 5). Oxidizing agents, such as cupric (Cu^{2+}), Fe^{3+}, and chromate (CrO_4^{2-}) ions or aeration, raise the corrosion rate considerably. Under these conditions Ni-Cr-Mo alloys such as 625 or C-276 offer better corrosion resistance. They can be passivated by the presence of oxidizing agents.

The Ni-Cr-Mo alloys also show higher resistance to uncontaminated HCl (Fig. 5). For example, alloys C-276, 625, and C-22 show very good resistance to dilute HCl at elevated temperatures and to a wide range of HCl concentrations at ambient temperature. The corrosion resistance of these alloys depends on the molybdenum content. The alloys with the highest molybdenum content—Hastelloy alloys B-2 and B-3—show the highest resistance in HCl of all the nickel-base alloys. Accordingly, these alloys are used in a variety of processes involving hot HCl or nonoxidizing chloride salts hydrolyzing to produce HCl. In Fig. 5, alloy B-2 shows two isocorrosion curves—one at high temperatures near the boiling point and one at low temperature. This is due to variations in the oxygen content of the solutions. At the higher temperatures, the oxygen solubility is lower, and therefore the corrosion rate is lower. The major weakness of the alloy is that its corrosion resistance decreases dramatically under oxidizing conditions (Fig. 3). Chromium-containing alloys such as C-276 or 625 can be passivated when oxidizers are present and thus display much lower corrosion rates.

Pitting Corrosion in Chloride Environments. The Ni-Cr-Mo alloys, such as alloys C-276, 625, ALLCORR, and C-22, exhibit very high resistance to pitting in oxidizing chloride environments. The critical pitting temperatures of various Ni-Cr-Mo alloys in an oxidizing chloride solution are shown in Table 4. Pitting corrosion is most prevalent in chloride-containing environments, although other halides and sometimes sulfides have been known to cause pitting. There are several techniques that can be used to evaluate resistance to pitting. Critical pitting potential and pitting protection potential indicate the electrochemical potentials at which pitting can be initiated and at which a propagating pit can be stopped, respectively. These values are functions of the solution concentration, pH, and temperature for a given alloy; the higher the potentials, the better the alloy. The critical pitting temperature (below which pitting does not initiate) is often used as an indicator of resistance to pitting, especially in the case of highly corrosion resistant alloys (Table 4). Chromium and molybdenum have been shown to be extremely beneficial to pitting resistance.

Corrosion in Nitric Acid

Chromium is an essential alloying element for corrosion resistance in HNO_3 environments because it readily forms a passive film in these environments. Thus, the higher chromium alloys show better resistance in HNO_3 (Fig. 6). In these types of environments, the highest chromium alloys, G-30 and 690, seem to show the highest corrosion resistance. Molybdenum is generally detrimental to corrosion resistance in HNO_3. For example, alloy C-22 (with 13% Mo) is not as good as alloy G-3 (with 7% Mo). In pure HNO_3, stainless steels find the greatest application. In concentrated (98%) HNO_3, stainless steels containing both chromium and silicon are finding greater use. Because of its oxidizing nature, HNO_3 streams are too severe for nickel-molybdenum alloys. The behavior of nickel-silicon alloys in HNO_3 seems to depend on their microstructure and composition. Cast Hastelloy alloy D, which consists of two phases (the nickel-silicon solid solution and the eutectic), does not show good resistance to any concentration of HNO_3. The Ni-9.5Si-2.5Cu-3Mo-2.75Ti cast alloy, which consists of a single phase, showed high resistance to boiling concentrated HNO_3 above 60% and to fuming (99%) HNO_3 up to 80 °C (175 °F). However, the corrosion rates in more dilute acid were very high.

Corrosion in Phosphoric Acid

Phosphoric acid is obtained by two different routes. The wet-process acid is obtained by reacting phosphate rock with concentrated H_2SO_4 and concentrating the resulting dilute acid by evaporation. The furnace acid is obtained by calcining the phosphate rock to produce elemental phosphorus, which is then oxidized and reacted with water to produce H_3PO_4. This latter acid is very pure and is used as reagent grade. The wet-process acid is used to make phosphatic fertilizers and usually contains a number of impurities, such as HF, H_2SO_4, and SiO_2. The percentage of these impurities depends on the source of the rock, the process of reaction with H_2SO_4, and the stage of concentration of the H_3PO_4.

The corrosion rates of various alloys in pure and wet-process acids are compared in Table 5. It is interesting to note the variation in corrosion rate of the same alloy in wet-process acid from two different manufacturers. Because of these differences, it is imperative that any comparison between alloys in this type of acid be made from tests conducted in the same batch of acid from the same source. It can also be seen that the wet-process acid can be considerably more corrosive than the reagent grade acid. It has been shown that in wet-process acid a high chromium content, such as in alloy G-30, is beneficial. In addition, Cl^- is inevitably present in these acids; therefore, molybdenum and tungsten additions are beneficial.

The plant test results shown in Table 6 indicate that alloys 20Cb3, 825, and C have the highest corrosion resistance in dilute H_3PO_4 process solutions. In very high-concentration H_3PO_4 at high temperatures, alloy B-2 shows the highest resistance (Table 7). The corrosion resistance in these acids seems to depend on molybdenum content.

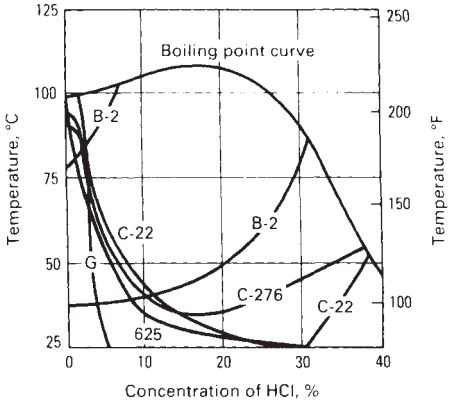


Fig. 5 Comparative isocorrosion plots of various nickel-base alloys in HCl. The lines indicate a corrosion rate of 0.13 mm/yr (5 mils/yr).

Table 4 Critical pitting temperatures for nickel alloys evaluated in 6% $FeCl_3$ for 24 h periods

Alloy	Critical pitting temperature °C	°F
825	0.0, 0.0	32.0, 32.0
904L	2.5, 5.0	36.5, 41
Type 317LM stainless steel	2.5, 2.5	36.5, 36.5
G	23.0, 25.0	73.5, 77
G-3	25.0, 25.0	77, 77
C-4	37.5, 37.5	99.5, 99.5
625	35.0, 40.0	95, 104
ALLCORR	52.5, 52.5	126.5, 126.5
C-276	60.0, 65.0	140, 149
C-22	70.0, 70.0	158, 158

Source: Ref 6

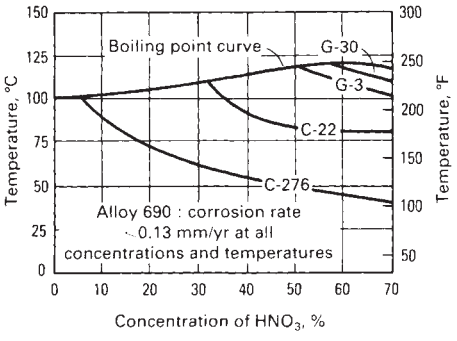


Fig. 6 Comparative behavior of nickel-base alloys in HNO_3. Isocorrosion curves indicate a corrosion rate of 0.13 mm/yr (5 mils/yr).

Table 5 Corrosion of various alloys in reagent grade and wet-process H_3PO_4

	Corrosion rate					
	Reagent grade 75% H_3PO_4,		Wet-process 75% H_3PO_4 (54% P_2O_5), 115 °C (240 °F)			
	115 °C (240 °F)		Source A		Source B	
Alloy	mm/yr	mils/yr	mm/yr	mils/yr	mm/yr	mils/yr
Type 316 stainless steel	0.76	30	29	1140	1.7	67
825	…	…	14	550	0.64	25
C-276	0.38	15	1.9	74	0.71	28
C-22	0.3	12	0.84	33	0.28	11
625	0.3	12	0.91	36	0.3	12
690	0.13	5	0.5	20	0.18	7
G-30	0.13	5	0.46	18	0.15	6

Table 6 Results of plant corrosion test in a H_3PO_4 evaporator

Specimens were exposed for 42 days to 53% H_3PO_4 containing 1–2% H_2SO_4 and 1.2–1.5% fluoride at 120 °C (250 °F). No pitting was observed.

	Corrosion rate	
Alloy	mm/yr	mils/yr
20Cb3	0.12	4.7
C	0.13	5
825	0.16	6.2
Type 317 stainless steel	0.26	10.4
400	0.64	25
Type 316 stainless steel	1.1	44
600	>33(a)	>1300(a)
B	>33(a)	>1300(a)

(a) Specimen was destroyed. Source: Ref 7

Corrosion in Hydrofluoric Acid

Hydrofluoric acid is commercially available in concentrations ranging from 30 to 70% and as anhydrous HF. Plain carbon steel can withstand the anhydrous acid and is extensively used in rail cars carrying anhydrous HF. Of the nickel-base alloys, alloy 400 has been the most extensively examined. The alloy possesses good corrosion resistance in all concentrations of HF up to a temperature of about 120 °C (250 °F). However, the presence of oxygen in the solution is detrimental (Table 8).

In another investigation, alloy 400 showed transgranular SCC in the vapor phase of dilute HF solutions (up to 0.5% HF) at temperatures up to 95 °C (200 °F) (Ref 8). The cracking susceptibility did not depend on the presence of oxygen, and no cracking was found in the liquid phase. The nickel-molybdenum alloys B and B-2 show good corrosion resistance at low temperatures. However, in one case, increasing the temperature from 25 to 95 °C (75 to 200 °F) in a 0.5% HF solution resulted in an increase in the corrosion rate of alloy B from 0.025 to 0.05 mm/yr (1–2 mils/yr) to 7.1 mm/yr (280 mils/yr). Alloy C-276 showed a low corrosion rate at all temperatures in HF up to 0.5% (Ref 8). The corrosion resistance of a variety of nickel-base alloys in various concentrations of HF is shown in Table 9. No control of aeration was attempted in these tests. The presence of aeration may be detrimental to the corrosion resistance of alloy C-276, as shown in Table 10 for 70% HF solution.

Corrosion in Organic Acids

The organic acids are generally not as corrosive as the mineral acids because of their lower acidity. Of the organic acids, acetic and formic acids form the bulk of the corrosion data on nickel-base alloys. Corrosion data on other organic acids can be found in Ref 9 and 10.

Acetic Acid. The corrosion rates of Nickel 200, alloy 400, and alloy 600 are shown in Table 11. The detrimental effects of aeration can be seen for alloy 400 and Nickel 200. The corrosion rates of a variety of alloys in boiling 10 and 99% acetic acids are given in Tables 12 and 13. No deliberate aeration or deaeration was done in these tests. The corrosion rates of all the alloys are quite low in these environments. Even though pure acetic acid is not very aggressive, the addition of contaminants can increase the corrosion rates. This is shown for Nickel 200 and alloy 400 in Table 14. The detrimental effects of aeration and oxidizing ions are indicated, especially in the dilute acid.

Formic acid is generally more corrosive than acetic acid. This is partly because the dielectric constant of formic acid (56.1 at 25 °C,

Table 7 Corrosion of various nickel-base alloys in pure H_3PO_4

Acid was nitrogen purged before the test, which was conducted at 280 °C (535 °F).

		Corrosion rate			
	Molybdenum	108% H_3PO_4		112% H_3PO_4	
Alloy	content, %	mm/yr	mils/yr	mm/yr	mils/yr
G-30	5.5	9.4	372	32.5	1280
G-3	7	7.9	310	24.4	961
625	9	4.6	180	14.9	590
C-22	13	2.6	102	3.9	152
C-276	16	1.4	54	1.8	72
B-2	28	0.23	9	0.05	2

Table 8 Effect of oxygen on corrosion of alloy 400 in HF solutions

The acids were purged with nitrogen containing various amounts of oxygen.

	Corrosion rate							
	Boiling (112 °C, or 234 °F) 38% HF				Boiling (108 °C, or 226 °F) 48% HF			
	Liquid phase		Vapor phase		Liquid phase		Vapor phase	
Concentration of oxygen in purge gas, ppm	mm/yr	mils/yr	mm/yr	mils/yr	mm/yr	mils/yr	mm/yr	mils/yr
<5	0.24	9.5	0.17	6.8	0.28	11	0.076	3
<500	0.43	17	0.3	12	0.56	22	0.1	4
1,500	0.79	31	1.24	49	0.7	28	0.61	24
2,500	0.74	29	0.46	18	0.69	27	0.23	9
3,500	0.86	34	1.37	54	0.86	34	0.74	29
4,700	1.3	53	2.7	107	1.1	43	2.1	83
10,000	1.2	46	0.64	25	1.2	48	1.9	75

Source: Ref 7

Table 9 Corrosion of various nickel-base alloys in HF

24 h tests with no control of aeration

	Corrosion rate, mm/yr (mils/yr)			
	2% HF		5% HF	
Alloy	70 °C (160 °F)	Boiling	70 °C (160 °F)	Boiling
C-276	0.24 (9.5)	0.076 (3)	0.25 (10)	0.1 (4)
C-22	0.23 (9.4)	0.94 (37)	0.34 (13.5)	0.84 (33)
625	0.5 (20)	…	0.4 (16)	…
C-4	0.43 (17)	…	0.38 (15)	…
200	…	…	0.46 (18)	…
600	…	…	0.23 (9)	…
B-2	…	…	0.38 (15)	…
G-3	…	…	0.5 (20)	…
G-30	0.25 (10)	…	0.76 (30)	…

Table 10 Effect of aeration on corrosion of two nickel-base alloys in 70% HF

Welded samples were tested from 14–36 days

	Corrosion rate			
	Nitrogen blanket		Oxygen blanket	
Alloy	mm/yr	mils/yr	mm/yr	mils/yr
C-276	0.008	0.3	0.94	37
400	0.013	0.5	0.58	23

Table 11 Corrosion of high-nickel alloy in acetic acid

Concentration of acetic acid, %	Temperature °C	Temperature °F	Corrosion rate, mm/yr (mils/yr) Alloy 400 Aerated	Alloy 400 Unaerated	Nickel 200 Aerated	Nickel 200 Unaerated	Alloy 600 Aerated	Alloy 600 Unaerated
2	30	86	…	0.0008 (0.03)	…	…	…	0.0013 (0.05)
5	116	240	…	0.0008 (0.03)	…	0.007 (0.28)	…	0.002 (0.08)
10	30	86	0.008 (0.33)	0.002 (0.08)	…	0.0025 (0.1)	…	0.0005 (0.02)
25	30	86	0.01 (0.41)	0.002 (0.08)	…	…	…	…
30	30	86	…	…	0.084 (3.3)	…	…	…
50	30	86	0.019 (0.74)	0.0025 (0.1)	0.11 (4.3)	0.006 (0.25)	…	…
75	30	86	0.009 (0.36)	0.0013 (0.05)	…	…	…	…
99.9	30	86	0.006 (0.23)	0.002 (0.08)	…	0.003 (0.13)	…	…
99.9	116	240	0.004 (0.15)	…	0.009 (0.36)	…	…	…

Source: Ref 8

Table 12 Corrosion of various mill-annealed alloys in boiling 10% acetic acid

Results are based on four 24 h test periods.

Alloy	Corrosion rate mm/yr	Corrosion rate mils/yr
Type 316L stainless steel	0.015–0.018	0.58–0.72
Alloy 825	0.0152–0.016	0.60–0.63
Alloy G	0.011–0.014	0.43–0.54
Alloy 625	0.01–0.019	0.39–0.77
Alloy C-276	0.011–0.0114	0.41–0.45
Alloy B-2	0.0112–0.013	0.44–0.50

Table 13 Corrosion of various mill-annealed nickel-base alloys in boiling 99% acetic acid

Results are based on four 24 h tests.

Alloy	Corrosion rate mm/yr	Corrosion rate mils/yr
200	0.11	4.5
400	0.015	0.6
G	0.03	1.2
G-2	0.005	0.2
G-3	0.015	0.6
625	0.01	0.4
C-4	0.0005	0.02
C-276	0.0076	0.3
B-2	0.03	1.2

Table 14 Effect of oxidizing ions on corrosion of Nickel 200 and alloy 400 in boiling acetic acid

Alloy	Concentration of acetic acid, %	Corrosion rate: No air mm/yr	No air mils/yr	Air sparge mm/yr	Air sparge mils/yr	3200 ppm Cu^{2+}(a) mm/yr	3200 ppm Cu^{2+}(a) mils/yr
Nickel 200	100	0.036	1.4	0.025	1	0.81	32
Alloy 400	100	0.0025	0.1	0.05	2	2.97	117
Nickel 200	50	0.076	3	1.6	63	0.71	28
Alloy 400	50	0.025	1	2.1	84	0.9	36

(a) Added as acetate. Source: Ref 9

or 75 °F) is higher than that of acetic acid (6.2 at the same temperature); therefore, the ionic dissociation is higher in the former. Formic acid is also much more acidic than acetic acid. The corrosion rates of a variety of nickel-base alloys in boiling 40 and 88% formic acid are given in Tables 15 and 16. Among the Ni-Cr-Mo-Fe alloys, the higher-molybdenum alloys generally tended to show higher resistance to corrosion. The isocorrosion curves for alloys C-276, B, and 400 and AISI type 316 stainless steel are shown in Fig. 7. For alloys 400 and B, the data shown in Fig. 7 and in boiling acids (Tables 15 and 16) do not agree. It is possible that these discrepancies are due to differences in aeration, because boiling acids are expected to have low aeration after a certain period of time.

Table 15 Corrosion of various mill-annealed nickel-base alloys in 40% formic acid

Results are based on four 24 h test periods.

Alloy	Corrosion rate mm/yr	Corrosion rate mils/yr
825	0.2	7.9
200	0.26–0.27	10.3–10.5
400	0.038–0.068	1.5–2.7
600	0.25	10.0
G	0.013–0.0132	5.0–5.2
G-3	0.046–0.05	1.8–2.1
625	0.17–0.19	6.8–7.8
C-4	0.07–0.076	2.9–3.0
C-276	0.07–0.074	2.8–2.9
B-2	0.008–0.01	0.31–0.40

Propionic Acid. The corrosion rates of several alloys in boiling propionic acid are shown in Fig. 8. Lowering the temperature from the boiling point can increase the corrosion rates of those alloys that are sensitive to the degree of aeration (Table 17).

Other Organic Acids. The higher organic acids, such as acrylic acid, and the fatty acids, such as lauric and stearic acids, are generally not very corrosive to nickel-base alloys (Ref 9). The corrosion rates in these acids, as in other organic acids, are determined by the inorganic impurities present in the acids (for example, chlorides and oxidizing salts).

Corrosion in Acid Mixtures

In many processes, mixtures of several acids or acids and salts are encountered. Corrosion resistance in these types of environments is sometimes predictable qualitatively. In some cases, anomalous effects can be produced. Although it is impossible to list the corrosion rates of alloys in a wide range of acid mixtures within the constraints of this section, an attempt is made to present those mixtures that are of greatest importance or that show surprising features.

Table 16 Corrosion of various mill-annealed nickel-base alloys in boiling 88% formic acid

Results are based on four 24 h test periods.

Alloy	Corrosion rate mm/yr	Corrosion rate mils/yr
825	0.064–0.08	2.5–3.1
200	0.31–0.34	12.2–13.2
400	0.024–0.028	0.97–1.1
G	0.099–0.12	3.9–4.6
G-2	0.05–0.067	2.0–2.6
G-3	0.14–0.15	5.4–5.9
625	0.236–0.238	9.3–9.4
C-4	0.05–0.076	2.0–3.0
C-276	0.043–0.048	1.7–1.9
B-2	0.00025–0.001	0.01–0.04
C-22	0.023	0.9

Sulfuric + Nitric Acid Mixtures. In alloys that contain chromium and exhibit active-passive behavior, addition of HNO_3 or nitrates to H_2SO_4 will reduce the corrosion rate (Fig. 9). In nonchromium-containing alloys (for example, alloys B-2 or 400), addition of HNO_3 will increase the corrosion rates. The nitrate reduction reaction increases the redox potential in H_2SO_4 solution; the redox potential of H_2SO_4 solution is normally controlled by the H^+ reduction reaction. In nonpassivating alloys, for example, alloy B-2, in which the corrosion current increases monotonically with potential, an increase in potential will increase the corrosion rate. In passivating alloys, an increase in potential can move the alloy from the active state to the passive state, thus reducing the corrosion rate. For high nitrate concentrations, the pas-

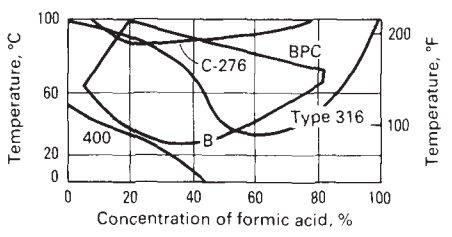


Fig. 7 Isocorrosion curves (0.1 mm/yr, or 4 mils/yr) of various nickel-base alloys in formic acid. BPC, boiling point curve. Source: Ref 9

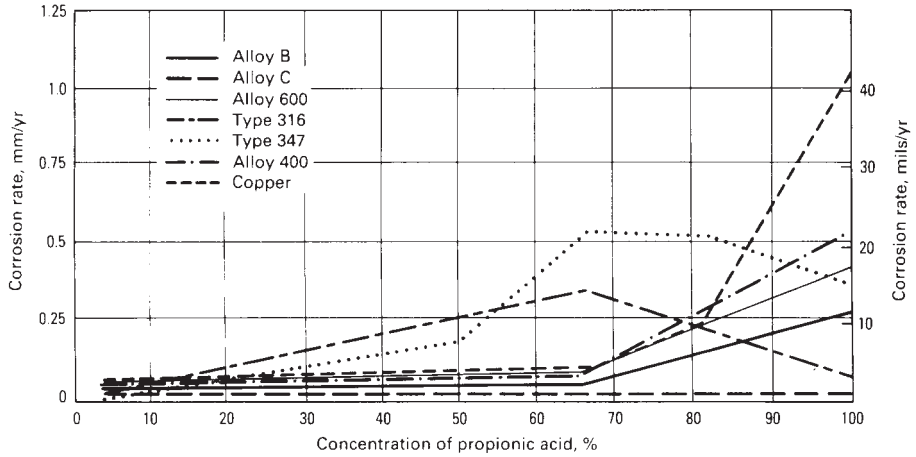


Fig. 8 Corrosion of various alloys in boiling propionic acid. Source: Ref 11

sive current density itself can increase, or the corrosion potential can move into the transpassive region, which results in an increase in corrosion rate. In the case of alloy C-276 in Fig. 9, only an increase in corrosion rate is observed with the HNO_3 addition. It is possible that for lower concentrations (<10%) of HNO_3 a decrease in corrosion rate could have been observed.

Sulfuric + Hydrochloric (or Chloride) Mixtures. The addition of alkali chloride salts or HCl to H_2SO_4 increases the corrosion rates of all alloys. The behavior of three of the nickel-base alloys is shown in Fig. 4 and Fig. 10. For deaerated conditions, alloys B and B-2 are the most versatile, with alloys C-276 and C-22 following in that order. Generally, the higher the molybdenum, the better the performance of the alloy in H_2SO_4 + HCl mixtures.

Nitric + Hydrochloric Acid Mixtures. The effects of HNO_3 additions to HCl are similar to the effects of HNO_3 additions to H_2SO_4 (Fig. 11). However, in HNO_3 + HCl mixtures, pitting is the mechanism of corrosion, rather than uniform corrosion, which occurs in H_2SO_4 + HNO_3 mixtures. In addition, small changes in HCl concentration can result in enormous changes in corrosion rates (Fig. 12).

Nitric + Hydrofluoric Acid Mixtures. The addition of HNO_3 to HF reduces the corrosion rate initially, but beyond 10% HNO_3, the corrosion rate increases. Increasing the HF concentration results in an increasing corrosion rate (Fig. 13). However, unlike the case of HCl addition, the higher-chromium alloys generally showed lower rates, irrespective of molybdenum level. Intergranular corrosion was also observed in many of these alloys. In all of the above cases, increasing temperature caused increased corrosion rates.

Corrosion in Alkalies

Nickel 200 and 201 are used extensively in caustic production and processes involving all concentrations and temperatures of sodium hydroxide (NaOH) and potassium hydroxide (KOH). This resistance prevails even when these alkalies are molten. The lower-carbon Nickel 201 is used at temperatures above 315

Table 17 Effect of test temperature on corrosion of various nickel-base alloys in propionic acid

No attempt was made to control aeration.

Alloy	Acid concentration, %	Corrosion rate: 50 °C (120 °F) mm/yr	50 °C (120 °F) mils/yr	75 °C (165 °F) mm/yr	75 °C (165 °F) mils/yr	Boiling mm/yr	Boiling mils/yr
Alloy 400	50	0.28	11	0.13	5	0.076	3
	80	0.4	16	0.15	6	0.25	10
	99	0.48	19	1.19	47	0.53	21
Alloy B	50	0.38	15	0.1	4	0.05	2
	80	0.61	24	0.3	12	0.13	5
	99	0.15	6	0.64	25	0.28	11
Alloy C	50	Nil	Nil	Nil	Nil	0.025	1
	80	Nil	Nil	Nil	Nil	0.025	1
	99	Nil	Nil	Nil	Nil	0.025	1

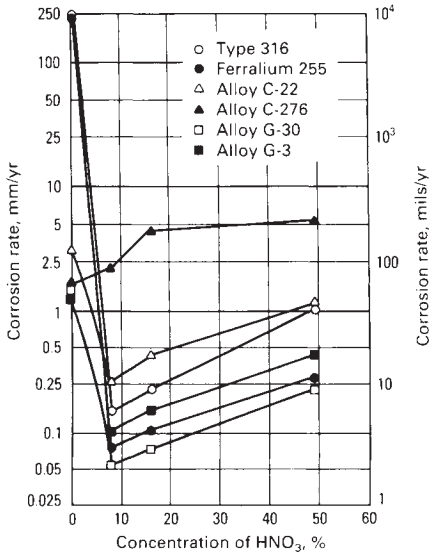


Fig. 9 Effect of HNO_3 on the corrosion of various alloys in a boiling 30% H_2SO_4 solution. Source: Ref 12

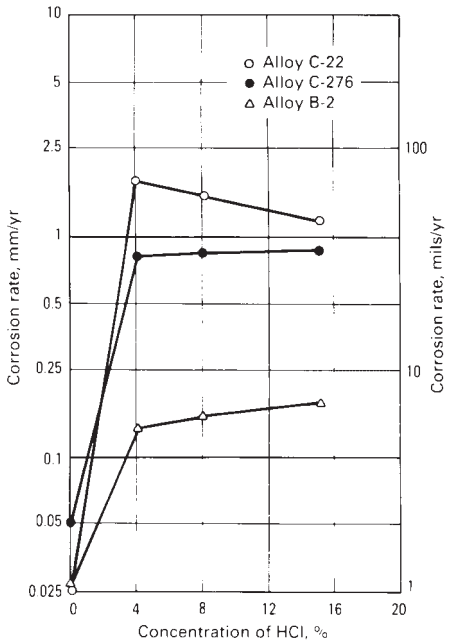


Fig. 10 Effect of HCl on the corrosion of various alloys in 15% H_2SO_4 at 80 °C (175 °F). Source: Ref 12

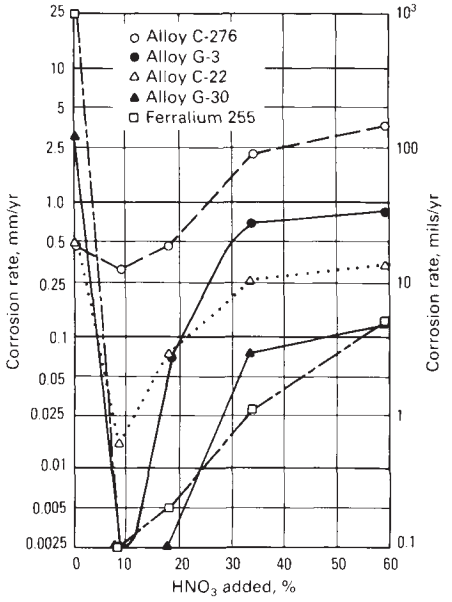


Fig. 11 Effect of HNO_3 on the corrosion of various alloys and Ferralium 255 in a 4% HCl solution at 80 °C (175 °F). Source: Ref 12

°C (600 °F) to avoid graphite precipitation. Isocorrosion curves for Nickel 200 and 201 are shown in Fig. 14. Nickel 200 is used extensively in caustic evaporator service where dilute caustic is concentrated up to 50%. In this service, contaminants such as chlorates, hypochlorites, and chlorides can cause increased corrosion rates, especially under velocity conditions. Though nickel is resistant to most alkalies, it is not resistant to ammonium hydroxide (NH_4OH) solutions.

The resistance of nickel alloys to general corrosion and SCC increases with increasing nickel content. In some caustic applications where higher strength or resistance to other corrodents is required, alloys 400, 600, C-276, and others are used. These alloys are highly resistant to general corrosion and SCC, but can be attacked at high caustic concentrations and temperatures.

Alloys 600 and 800 have been used extensively in nuclear steam generator service at about 300 °C (570 °F). In this service, resistance to caustic, which can be formed and concentrated at tube sheets, is of concern. The higher-chromium alloy 690 is more resistant to SCC under some conditions.

Corrosion in Pulp and Paper Mill Environments

Nickel alloys are used in pulp and paper mills generally where conditions are the most corrosive. Alloys 600 and 800 have been utilized for more than 35 years for digester liquor heater tubing because their high nickel content provides excellent resistance to chloride SCC. In the disposal of organic wastes in unevaporated black liquor, alloy 600 has been used for the reactor vessel, transfer lines, and piping.

A major problem in this industry has been the cracking of steel digesters in the weld area. A practical solution to the problem is to weld overlay the weld area with alloy 600 or 625 filler metals. Other methods are the use of alloy 600 or 625 sheet liners to cover repaired weld areas or the use of alloy clad steel plate in the initial digester fabrication.

One of the oldest applications of nickel alloys ran the pulp and paper industry is alloy K-500 doctor blades. Alloy K-500 provides high corrosion resistance with the abrasive and wear resistance needed for good service even in wet creping operations.

The bleaching circuit and pollution control areas are the most demanding corrosive environments in the pulp and paper mill process. Alloys needed in this area must be resistant to oxidizing conditions of high-temperature low-pH liquors containing chlorine, chlorine dioxide, oxygen, hypochlorate, peroxides, and chlorides. Only the high-molybdenum alloys 625, C-276, and C-22 have the required corrosion

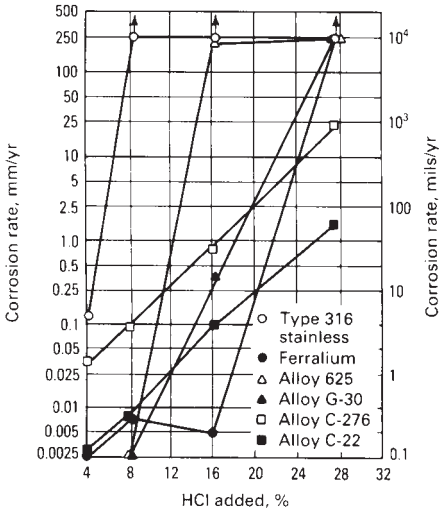


Fig. 12 Effect of HCl additions on the corrosion rates of various alloys in 9% HNO_3 at 52 °C (125 °F)

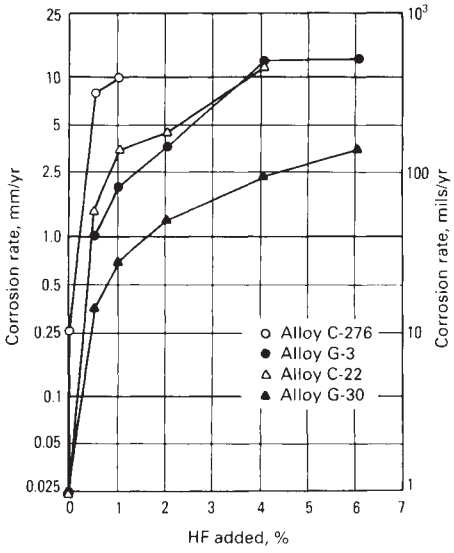


Fig. 13 Effect of HF additions on the corrosion of various alloys in 20% HNO_3 solutions at 80 °C (175 °F)

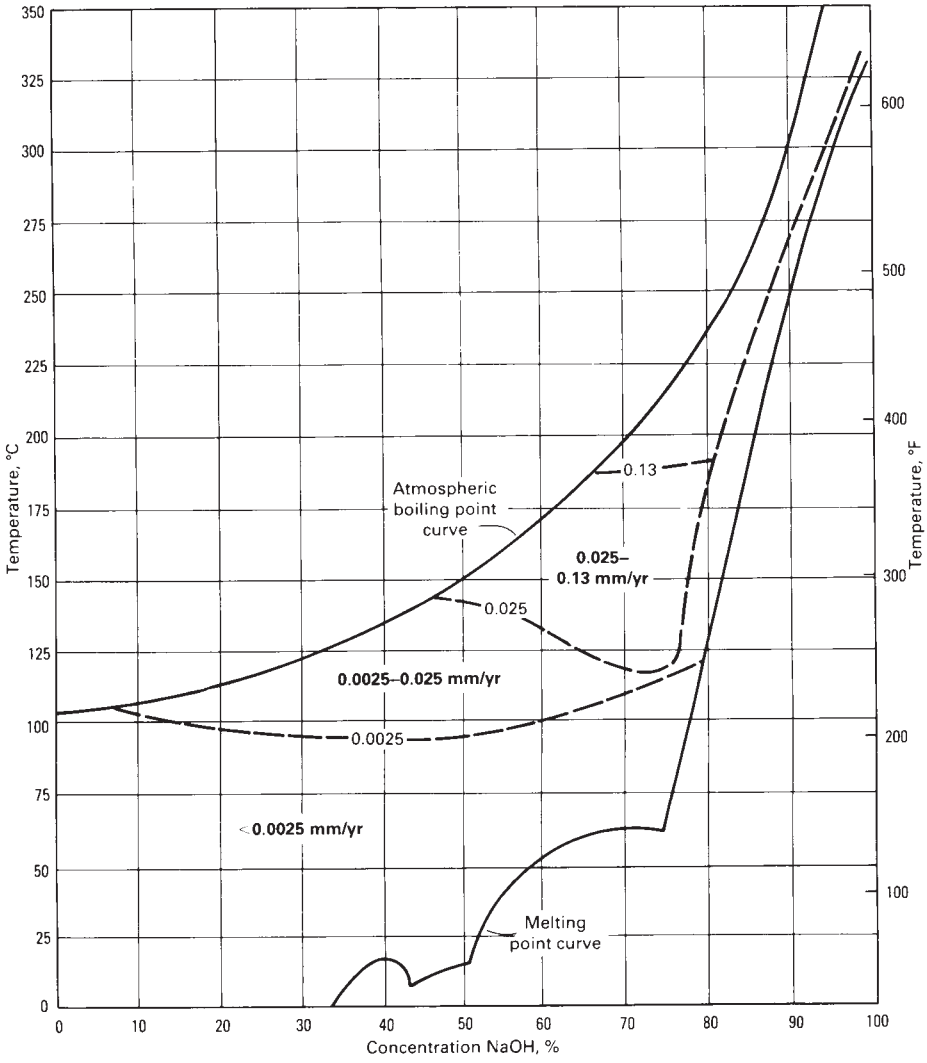


Fig. 14 Isocorrosion diagram for Nickel 200 and Nickel 201 in NaOH. Source: Ref 13

resistance to resist these aggressive liquors. In equipment used to clean off-gas from the recovery boiler, alloys 825, 625, G, and C-276 have been used, depending on the severity of the conditions. Typical conditions found are acid mists, low-pH liquors containing chlorides and organics, and sometimes high temperatures. Alloy G scrubbers have given more than 10 years of good service at one pulp and paper mill. Other plants have used alloys 625 and C-276 for internal components of scrubbers, fans, ducting, and so on.

Corrosion in Flue Gas Desulfurization Environments

Nickel alloys were first used in flue gas desulfurization (FGD) systems in wet-induced draft fans in a particulate scrubber system in 1972. Alloy 625 replaced type 316 stainless steel because of the inadequate mechanical properties of type 316. Construction of FGD equipment increased greatly after the Clean Air Act Amendments were enacted in 1977. Nickel alloys saw limited use during the early years because of their high initial cost.

During the period of rapid growth in the utilization of FGD equipment, the industry experienced severe corrosion problems at nearly every operating FGD system. Catastrophic failures were reported for coatings and linings on carbon steel, nonmetallics, stainless steel, and occasionally of nickel alloys. The corrosion problems were due to hot acids (nitric, sulfurous, sulfuric, hydrochloric, and hydrofluoric), chlorides, fluorides, and crevice conditions.

A wide variety of nickel alloys are available for use in FGD applications. Alloys 825 and G are significantly more corrosion resistant in sulfurous and sulfuric acids than austenitic stainless steels. With increasing molybdenum levels, alloys 625, ALLCORR, G, and C-276 are used to combat pitting and crevice corrosion. These nickel alloys have been successfully used in FGD components, such as quenchers, absorber towers, dampers, stack gas reheaters, wet induced draft fans and fan housings, outlet ducting, and stack liners. Some innovative FGD applications include the use of alloy 625 in a unique heat recovery system, all-alloy scrubber towers constructed with alloy 625, the application of thin-gage nickel alloy clad steel in new construction, and nickel alloy sheet liners to repair existing FGD components. Severe corrosion problems in FGD systems can be prevented and long life achieved economically by the proper application of nickel alloys in FGD systems.

Corrosion in Sour Gas Environments

Sour gas is defined by NACE International Material Recommendation MR-01-75 as gas being handled at an absolute pressure in excess of 0.45 MPa (65 psi) with a partial pressure of H_2S greater than 345 Pa (0.05 psi). This combination can cause sulfide stress cracking. Sulfide stress cracking can be controlled by using resistant alloys, by controlling the environment, or by isolating the component from the sour environment. The sulfide stress cracking problem is complicated because the environment normally also contains brackish water and CO_2 and is found at 65 to 245 °C (150–475 °F), depending on the depth and location of the well

The best nickel alloys to use in these environments are those containing a minimum of 42% Ni (to resist chlorides), high chromium, and at least 3% Mo. Alloys 825, 925, 2550, 28, G-3, and C-276 are good examples. These are normally furnished for production tubing with minimum yield strengths of 758 or 862 MPa (110 or 125 ksi). Yield strengths up to 1030 MPa (150 ksi) minimum have been used. These strengths are obtained through cold work.

Similar strengths are required for tools and components. These can be much larger in cross section and therefore cannot be cold worked to derive strength. In these cases, precipitation-hardenable alloys are used. The same basic guidelines for composition—high nickel, high chromium, and at least 3% Mo—hold true for these components. The best alloy for use in each environment is usually determined by corrosion testing in that environment. The NACE specification MR-01-75 includes a list of alloys that have passed their initial corrosion screening tests. A list is also provided of the maximum hardness that an alloy can have and still resist sulfide stress cracking.

Corrosion in Petrochemical and Refining Environments

The petrochemical and refining industries are defined as those involved in the production of basic organic chemicals and fuels from petroleum-base feedstocks. Examples include fuels and lubricants, ethylene and ethylene derivatives, steam hydrocarbon reforming, NH_3, methanol, and the many organic chemicals. In general, most petrochemical and refining applications are endothermic, requiring temperatures from 425 to 1000 °C (800–1830 °F) and higher. Typical environmental conditions include oxidizing, carburizing, nitriding, sulfidizing, and halogen gases (chlorine, hydrogen chloride, fluorine, and so on). Materials used in these applications must exhibit corrosion resistance, metallurgical stability, and strength in these high-temperature environments.

Alloys 800H and 800HT are the standard materials for intermediate temperatures (620–925 °C, or 1150–1700 °F). These alloys combine corrosion resistance with strength and metallurgical stability (Fig. 15). Major applications include hydrogen reformer manifolds and pigtail piping, ethylene dichloride furnace tubing, transfer piping, and high-temperature pressure vessels.

As the environments become more aggressive and high-temperature strength requirements more demanding, alloys 600, 601, 617, 625, and X are utilized. High-temperature halogenations require alloys 600 and 625, while high-temperature oxygen requires alloy 601. Aggressive carburizing and nitriding environments utilize alloys 600 and 617. Expansion joints for high-temperature applications require alloys with good fatigue resistance such as alloys 617 or 625.

Corrosion in Fused Salts

Most applications for nickel alloys in fused salts occur in the heat treating of metals with salt baths. Common heat treating applications and temperature ranges are:

- *Cyaniding:* 760 to 870 °C (1400–1600 °F)
- *Austempering:* 205 to 595 °C (400–1100 °F)
- *Martempering:* 205 to 370 °C (400–700 °F)
- *Tempering:* 165 to 760 °C (325–1400 °F)
- *Heat treating of tool steels, stainless steels, aluminum, and copper alloys:* 205 to 1095 °C (400–2000 °F)

At temperatures in the range of 205 to 815 °C (400–1500 °F), cyanides, nitrates, and nitrites are employed. As the temperature requirements increase beyond 705 °C (1300 °F), various chloride mixtures of sodium, potassium, and barium are utilized. It is in the higher-temperature chloride mixtures that high-nickel alloys find significant applications. Increasing the temperatures and basic oxide contents normally increase corrosion rates.

Alloy 600 has proved to be one of the most resistant alloys to high-temperature chloride salt attack. Alloys 601, 617, 690, RA330, 800, and 825 also provide useful resistance.

Corrosion of Nickel and High-Nickel Alloy Weldments

The corrosion resistance of weldments is related to the microstructural and microchemical changes resulting from thermal cycling. The effects of welding on the corrosion resistance of nickel-base alloys are similar to the effects on the corrosion resistance of austenitic stainless steels. For example, sensitization due to carbide precipitation in the heat-affected zone (HAZ) is a potential problem in both classes of alloys. However, in the case of nickel-base alloys, the high content of such alloying elements as chromium, molybdenum, tungsten, and niobium can result in the precipitation of other intermetallic phases, such as μ, σ, and η.

Therefore, this section is concerned with the characteristics of the various nickel-base alloys and the evolution of these alloys. The corrosion resistance of weldments is dictated not only by the HAZ but also by the weld metal itself. The effect of elemental segregation on weld metal corrosion must also be examined. The

nickel-base alloys discussed in this section are the solid-solution alloys.

The nickel-molybdenum alloys, represented by Hastelloy alloys B, B-2, and B-3, have been primarily used for their resistance to corrosion in nonoxidizing environments such as HCl. Hastelloy alloy B has been used since about 1929 and has suffered from one significant limitation: weld decay. The welded structure has shown high susceptibility to knife-line attack adjacent to the weld metal and to HAZ attack at some distance from the weld. The former has been attributed to the precipitation of molybdenum carbide (Mo_2C); the latter, to the formation of M_6C-type carbides. This necessitated postweld annealing, a serious shortcoming when large structures are involved. The knife-line attack on an alloy B weldment is shown in Fig. 16. Many approaches to this problem were attempted, including the addition of carbide-stabilizing elements, such as vanadium, titanium, zirconium, and tantalum, as well as the lowering of carbon.

The addition of 1% V to an alloy B-type composition was first patented in 1959. The resultant commercial alloys—Corronel 220 and Hastelloy alloy B-282—were found to be superior to alloy B in resisting knife-line attack, but were not immune to it. In fact, it was demonstrated that the addition of 2% V decreased the corrosion resistance of the base metal in HCl solutions. During this time, improvements in melting techniques led to the development of a low-carbon low-iron version of alloy B called alloy B-2. This alloy did not exhibit any propensity to knife-line attack (Fig. 17).

Segregation of molybdenum in weld metal can be detrimental to corrosion resistance in some environments. In the case of boiling HCl solutions, the weld metal does not corrode preferentially. However, in H_2SO_4 + HCl and $H_2SO_4 + H_3PO_4$ acid mixtures, preferential corrosion of as-welded alloy B-2 has been observed (Fig. 18). No knife-line or HAZ attack was noted in these tests. During solidification, the initial solid is poorer in molybdenum and therefore can corrode preferentially. This is shown in Fig. 18 for an autogenous gas tungsten arc (GTA) weld in alloy B-2. In such cases, postweld annealing at 1120 °C (2050 °F) will be beneficial.

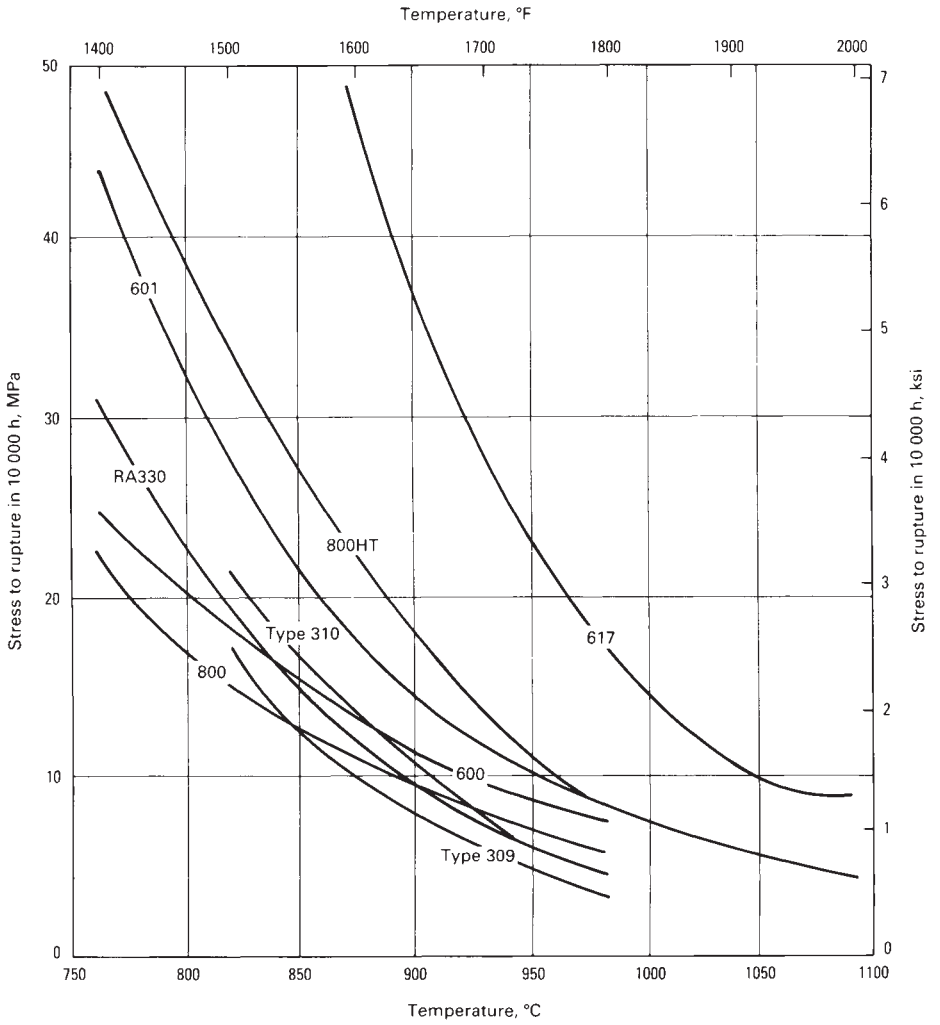


Fig. 15 High-temperature stress rupture data for various nickel-base and stainless alloys. Test duration was up to 10,000 h. Data are from manufacturers' published data.

The Ni-Cr-Mo alloys represented by the Hastelloy C family of alloys and by Inconel 625 have also undergone evolution because of the need to improve the corrosion resistance of



Fig. 16 Cross section of a Hastelloy alloy B weldment corroded after 16 days of exposure in boiling 20% HCl. 80×. Source: Ref 14

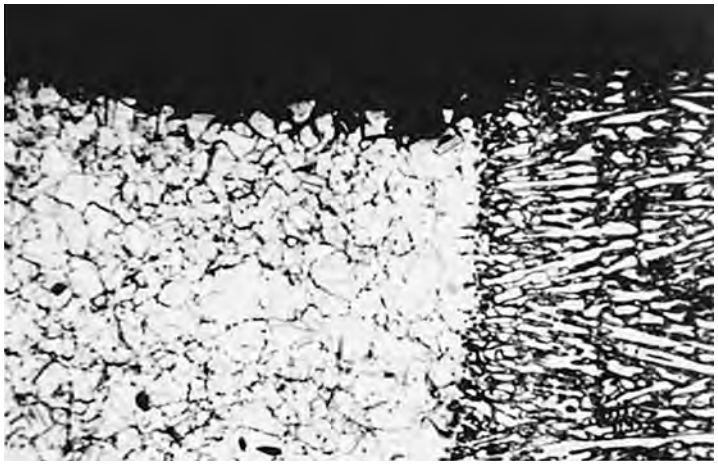


Fig. 17 Cross section of a Hastelloy alloy B-2 weldment after 16 days of exposure to boiling 20% HCl. 80×. Source: Ref 14



Fig. 18 Preferential corrosion of autogenous GTA weld in Hastelloy alloy B-2 exposed to boiling 60% H_2SO_4 + 8% HCl

weldments. Hastelloy alloy C (UNS N10002) containing nominally 16% Cr, 16% Mo, 4% W, 0.04% C, and 0.5% Si had been in use for some time, but had required the use of postweld annealing to prevent preferential weld and HAZ attack. Many investigations were carried out on the nature of precipitates formed in alloy C, and two main types of precipitates were identified. The first is a Ni_7Mo_6 intermetallic phase called μ, and the second consists of carbides of the Mo_6C type. Other carbides of the $M_{23}C_6$ and M_2C were also reported. Another type, an ordered Ni_2Cr-type precipitate, occurs mainly at lower temperatures and after a long aging time; it is not of great concern from a welding viewpoint.

Both the intermetallic phases and the carbides are rich in molybdenum, tungsten, and chromium and therefore create adjacent areas of alloy depletion that can be selectively attacked. Carbide precipitation can be retarded considerably by lowering carbon and silicon; this is the principle behind Hastelloy alloy C-276. The time-temperature behaviors of alloys C and C-276 are compared in Fig. 19, which shows much slower precipitation kinetics in alloy C-276. Therefore, the evolution of alloy C-276 from alloy C enabled the use of this alloy system in the as-welded condition. However, because only carbon and silicon were controlled in C-276, there remained the problem of intermetallic μ-phase precipitation, which occurred at longer times of aging. Alloy C-4 was developed with lower iron, cobalt, and tungsten levels to prevent precipitation of μ phases.

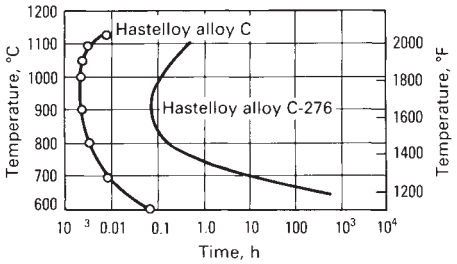


Fig. 19 Time-temperature transformation curves for Hastelloy alloys C and C-276. Intermetallics and carbide phases precipitate in the regions to the right of the curves. Source: Ref 15

The effect of aging on sensitization of alloys C, C-276, and C-4 is shown in Fig. 20. For alloy C, sensitization occurs in two temperature ranges (700–800 °C, or 1290–1470 °F, and 900–1100 °C, or 1650–2010 °F) corresponding to carbide and μ phase precipitation, respectively. For alloy C-276, sensitization occurs essentially in the higher temperature region because of μ-phase precipitation. Also, the μ-phase precipitation kinetics in alloy C-276 are slow enough not to cause sensitization problems in many high heat input weldments; however, precipitation can occur in the HAZ of alloy C-276 welds (Fig. 21). Because C-4 has lower tungsten than C-276, it has lower pitting and crevice corrosion resistance, for which tungsten is beneficial. Therefore, an alternate solution to alloy C-4 was needed in which both corrosion resistance and thermal stability are preserved. Hastelloy alloy C-22 has demonstrated improved corrosion resistance and thermal stability.

Because of the low carbon content of alloy C-22, the precipitation kinetics of carbides were slowed. Because alloy C-22 has lower molybdenum and tungsten levels than alloy C-276, μ-phase precipitation was also retarded.

From a weld HAZ point of view, this difference is reflected in lower grain-boundary precipitation even in a high heat input weld (Fig. 22). The HAZ microstructure of alloy C-4 was similar to this. This difference in the sensitization of the HAZ is also illustrated in Fig. 23, which shows that the HAZ and weld metal of alloy C-276 are attacked to a considerable extent in an oxidizing mixture of H_2SO_4, ferric sulfate ($Fe_2(SO_4)_3$), and other chemicals.

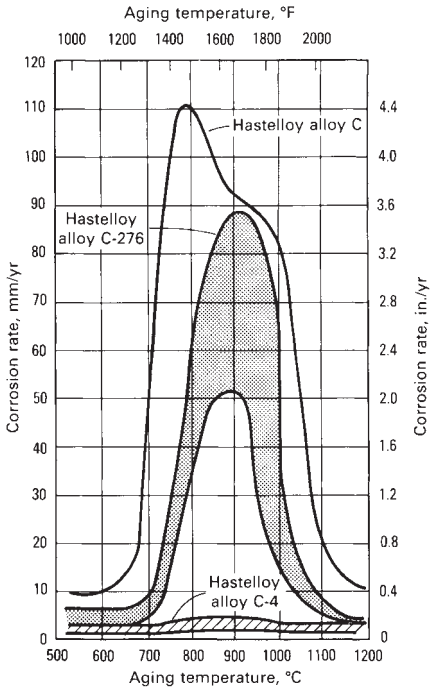


Fig. 20 Effect of 1 h aging treatment on corrosion resistance of three Hastelloy alloys in 50% H_2SO_4 + 42 g/L $Fe_2(SO_4)_3$. Source: Ref 16

ACKNOWLEDGMENTS

This article was adapted from:

- A.I. Asphahani et al., Corrosion of Nickel-Base Alloys, *Corrosion*, Vol 13, *ASM Handbook*, ASM International, 1987, p 641–657
- K.F. Krysiak, Corrosion of Weldments, *Corrosion*, Vol 13, *ASM Handbook*, ASM International, 1987, p 344–368



Fig. 21 Typical microstructure of the HAZ of a multipass submerged-arc weld in Hastelloy alloy C-276. Source: Ref 17



Fig. 22 Typical microstructure of the HAZ of a multipass submerged-arc weld in Hastelloy alloy C-22. Matching filler metal was used. Source: Ref 17

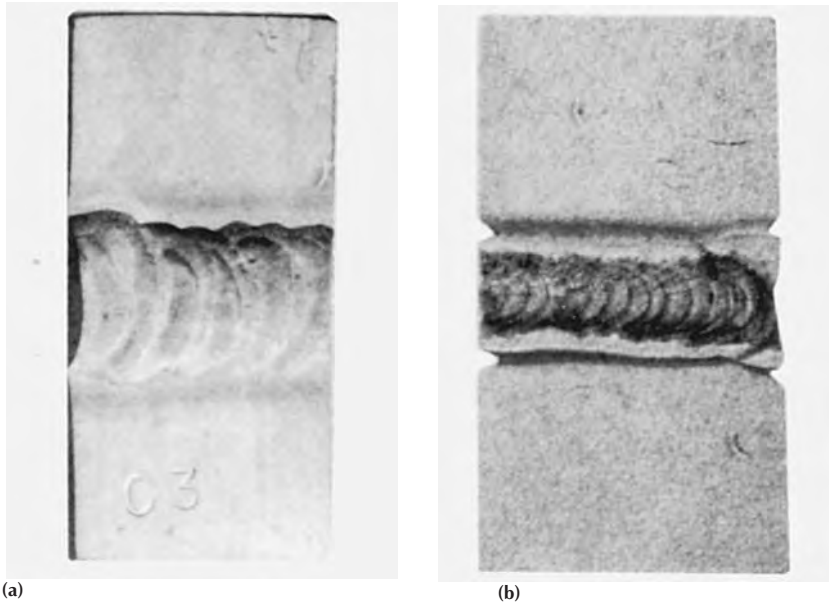


Fig. 23 Corrosion of the weld metal and the HAZ in Hastelloy alloys C-22 (a) and C-276 (b) in an aerated mixture of 6 vol% H_2SO_4 + 3.9% $Fe_2(SO_4)_3$ + other chemicals at 150 °C (300 °F). Source: Ref 17

REFERENCES

1. "The Corrosion Resistance of Nickel-Containing Alloys in Sulfuric Acid and Related Compounds," The International Nickel Company, 1983 (Available from the Nickel Development Institute as publication No. 1318)
2. Data Brochures H2002, H2006, H2007, H2009, H2019. H2028, and H2043, Haynes International, Inc.
3. "Materials of Construction for Handling Sulfuric Acid," Publication 5A151, National Association of Corrosion Engineers
4. J.R. Crum and M.E. Atkins, *Mater Perform.*, Vol 25 (No. 2), 1986, p 27–32
5. Corrosion Engineering Bulletin 3, International Nickel Company, Inc.
6. E. Hibner, Paper 181, presented at Corrosion/86 (Houston, TX), National Association of Corrosion Engineers, 1986
7. Corrosion Engineering Bulletin 4, International Nickel Company, Inc.
8. S.W. Ciaraldi, M.R. Berry, and J.M. Johnson, Paper 98, presented at Corrosion/82 (Houston, TX), National Association of Corrosion Engineers, 1982
9. Corrosion Engineering Bulletin 6, International Nickel Company, Inc., 1979
10. D.L. Graver, Ed., *Corrosion Data Survey—Metals Section*, National Association of Corrosion Engineers, 1985
11. G.B. Elder, in *Process Industries Corrosion*, National Association of Corrosion Engineers, 1975, p 247
12. N. Sridhar, Paper 182, presented at Corrosion/86 (Houston, TX), National Association of Corrosion Engineers, 1986
13. Corrosion Engineering Bulletin 2, International Nickel Company, Inc.
14. F.G. Hodge and R.W Kirchner, Paper 60, presented at Corrosion/75, (Toronto, Canada), National Association of Corrosion Engineers, April 1975
15. R.B. Leonard, *Corrosion*, Vol 25 (No. 5), 1969, p 222–228
16. F.G. Hodge and R.W. Kirchner, Paper presented at the Fifth European Congress on Corrosion (Paris), Sept 1973
17. P.E. Manning and J.D. Schobel, Paper presented at ACHEMA '85 (Frankfurt, West Germany), 1985; See also *Werkst. Korros.*, March 1986

SELECTED REFERENCES

- W. Betteridge, *Nickel and Its Alloys*, Ellis Horwood Ltd., 1984
- J. Brown and B. Montford "Nickel-Base Alloys in the Power Industry," NiDi Technical Series No. 10012, Nickel Development Institute
- W.Z. Friend, *Corrosion of Nickel and Nickel-Base Alloys*, John Wiley & Sons, 1980
- "Resistance of Nickel and High Nickel Alloys to Corrosion by Hydrochloric Acid, Hydrogen Chloride, and Chlorine," NiDi Technical Series No. 279, Nickel Development Institute
- C.M. Schillmoller, "Alloy Selection in Wet-Process Phosphoric Acid Plants," NiDi Technical Series No. 10015, Nickel Development Institute
- C.M. Schillmoller, "Alloys to Resist Chlorine, Hydrogen Chloride, and Hydrochloric Acid," NiDi Technical Series No. 10020, Nickel Development Institute
- G. Sorell, Corrosion- and Heat-Resistant Nickel Alloys, *Chemical Processing*, Part I, Nov 1997, Part II, Oct 1998 (Available from the Nickel Development Institute as publication No. 10086)
- "The Corrosion Resistance of Nickel-Containing Alloys in Flue Gas Desulfurization and Other Scrubbing Processes," NiDi Technical Series No. 1300, Nickel Development Institute
- B. Todd, "Nickel-Containing Materials in Marine and Related Environments," NiDi Technical Series No. 10011, Nickel Development Institute

ASM Specialty Handbook: Nickel, Cobalt, and Their Alloys
J.R. Davis, editor, p 141-166
DOI:10.1361/ncta2000p141

Copyright © 2000 ASM International®
All rights reserved.
www.asminternational.org

Stress-Corrosion Cracking and Hydrogen Embrittlement of Nickel Alloys

NICKEL AND NICKEL-BASE ALLOYS are specified for many critical service applications because of their fabricability, their fracture toughness, and their ability to be designed by alloying, for a wide variety of environments. Additionally, unique intermetallic phases can form between nickel and some of its alloying elements, enabling formulation of alloys that exhibit high strength even at high temperatures. They are often used because of their resistance to stress-corrosion cracking (SCC). However, SCC of nickel-base alloys can occur under particular combinations of environment, microstructure, and stress. The number of environments that can cause SCC of nickel-base alloys (indeed of almost any alloy system) has grown with time (Table 1). This can be attributed to the increasing diversity of the application of nickel-base alloys, greater knowledge of service performance, and greater recognition of SCC problems. It is no longer necessary to think of SCC as a manifestation of specific alloy/environment combinations, and attempts have been made to generalize various SCC systems within a potential-pH framework for a given metal such as nickel (Ref 1). Unfortunately, this approach is limited by:

- The paucity of systematic SCC data in terms of potential and pH
- The fact that SCC is not always controlled by the electrochemical stability of nickel, even in a single environment

Table 1 Evolution of environments that cause SCC of nickel and nickel-base alloys

Period	Environment
About 1950	H_2O-HF
	Fluosilicic acid
About 1978	H_2O-Cl^-
	H_2O-OH^-
	Polythionic acid
	Chromic acid
	Acetic acid
	Molten caustics
	Steam
	Organic liquids
	Liquid Li, Hg, Sn, Zn, Bi, Pb
	H_2O
	H_2
Late 1970s to present	H_2O-Cl^--CO_2-H_2S-S_8
	H_2O-Br^-
	H_2O-I^-
	Thiocyanates, tetrathionate, thiosulfate
	Sulfurous acid

Hence, for the present, one must be content to examine the various types of environments in which SCC has been observed in nickel-base alloys.

In the following sections, the physical metallurgy of nickel-base alloys is briefly discussed and then SCC is described in terms of various types of environments. The emphasis is on SCC at relatively moderate temperatures (less than 350 °C, or 660 °F). The information in this article is intended to provide the reader with an overview of the types of environment/alloy combinations that may lead to SCC. No attempt is made to synthesize the results in terms of various mechanisms. The reader is referred to other sources (e.g., Ref 2) for more in-depth discussion of the mechanistic aspects of SCC in nickel-base alloys. The test techniques that have typically been used to study SCC and hydrogen embrittlement of nickel-base alloys are outlined in the last section. Approaches for the mitigation of SCC are intertwined with the discussion of the phenomenon in various environments.

Physical Metallurgy of Nickel-Base Alloys

Effect of Alloy Composition on Corrosion Behavior. Nickel-base alloys range from simple binary systems (e.g., nickel-copper alloys) to multicomponent systems containing up to 10 (or more) intentional alloying elements. Additionally, various impurities, such as carbon, nitrogen, silicon, sulfur, and phosphorus, are present in varying concentrations. This section briefly reviews the primary role major alloying elements play in the corrosion resistance of nickel-base alloys. More detailed information can be found in the preceding article "Corrosion Behavior of Nickel Alloys in Specific Environments" and in Ref 3.

Copper and molybdenum are added to increase corrosion resistance to reducing environments, molybdenum being more effective. Chromium is added to provide resistance to oxidizing environments. Molybdenum and tungsten are added to chromium-containing alloys to increase resistance to oxidizing environments that contain halides. Silicon is typically present in small amounts and is considered detrimental. However, a cast Ni-9Si alloy has been used for its resistance to H_2SO_4 of all concentrations. Niobium and titanium are added to stabilize the chromium-containing alloys against precipitation of chromium carbides. In the precipitation-hardenable grades, niobium, aluminum, and titanium also combine with nickel to form coherent intermetallic phases that increase strength. Iron is typically used in nickel-base alloys to reduce cost. However, iron also increases the erosion resistance of copper-nickel alloys, increases the solubility of carbon and nitrogen, and inhibits the formation of the intermetallic phase Ni_4Mo.

Effect of Carbide Precipitation on SCC Behavior. Carbide precipitation is an important factor affecting SCC of nickel-base alloys. In nickel, carbon is known to form Ni_3C, but it decomposes to graphite, which weakens the grain boundaries (Ref 4, 5). The addition of copper reduces the tendency to graphitization. In the other nickel-base alloys, the type and composition of carbides depend on the composition of the alloy (Ref 4).

Carbides in these alloys can be classified as either primary or secondary. Primary carbides form during solidification in the interdendritic areas, which are generally rich in alloying elements. These carbides include the MC types, where M is niobium, tantalum, or titanium, and the M_6C types, where M is usually molybdenum or tungsten. Primary carbides are not easily dissolved during subsequent processing of the alloys and thus will be present as stringers along the rolling direction. A small amount of stringers must be tolerated in commercial alloys because they cannot be economically removed, but large amounts of stringers can be detrimental to fabricability and performance.

Secondary carbides precipitate as a result of thermal exposures during processing, heat treatment, fabrication, and service. They are usually intergranular, although in extreme cases precipitation inside the grains along slip lines and twin boundaries may occur. The amount of precipitation depends on the concentration

of carbon in solution, the stability of the alloy, time, temperature, presence of cold work, and grain size. Secondary carbides are often extremely detrimental to corrosion and SCC resistance because of their associated depletion zones (Fig. 1). For example, in alloy 600, precipitation of Cr_7C_3 carbide at the grain boundary results in a depletion of chromium adjoining the grain boundaries (Ref 6), the extent of which increases initially, then decreases at longer time periods due to back-diffusion of chromium from the bulk.

Carbides also can be classified as those that are rich in chromium and those that are rich in refractory elements (molybdenum, tungsten, niobium, titanium, and tantalum). One study (Ref 7) has shown that the chromium-rich carbides occur in alloys whose Cr/(Mo + 0.4W) ratio exceeds approximately 3.5. The chromium-rich carbides can be either Cr_7C_3 or $Cr_{23}C_6$, although the latter occurs in most alloys. In low-chromium alloys, such as alloy 600, that also contain low concentrations of other alloying elements, the predominant carbide that forms is Cr_7C_3, although $Cr_{23}C_6$ also has been reported (Ref 8). In more complex alloys, molybdenum, tungsten, iron, or nickel can substitute for chromium, and carbides of the form $Cr_{21}(Mo,W)_2C_6$ have been observed. The $M_{23}C_6$ carbides can occur at the grain boundaries as discrete globular particles, continuous films, or cellular precipitates. The temperature range of stability depends on alloy composition, with higher chromium, molybdenum, and tungsten contents increasing the stability to higher temperatures.

Time-temperature sensitization diagrams for two alloys that form $M_{23}C_6$ carbides are shown in Fig. 2 and 3 (Ref 9, 10). Although sensitization diagrams indicate the kinetics of the effect of carbide precipitation on intergranular corrosion and not the kinetics of carbide precipitation (as do transformation diagrams), it can be seen that alloy 825, which contains 3% Mo, exhibits sensitization at higher temperatures than does alloy 800, which contains no molybdenum.

The refractory-metal carbides take on the form of MC, M_6C, or $M_{12}C$, depending on alloy composition. In the MC-type carbides, M is a mixture of niobium, titanium, and tantalum, but may also contain some molybdenum or tungsten. If nitrogen is present in the alloy, it

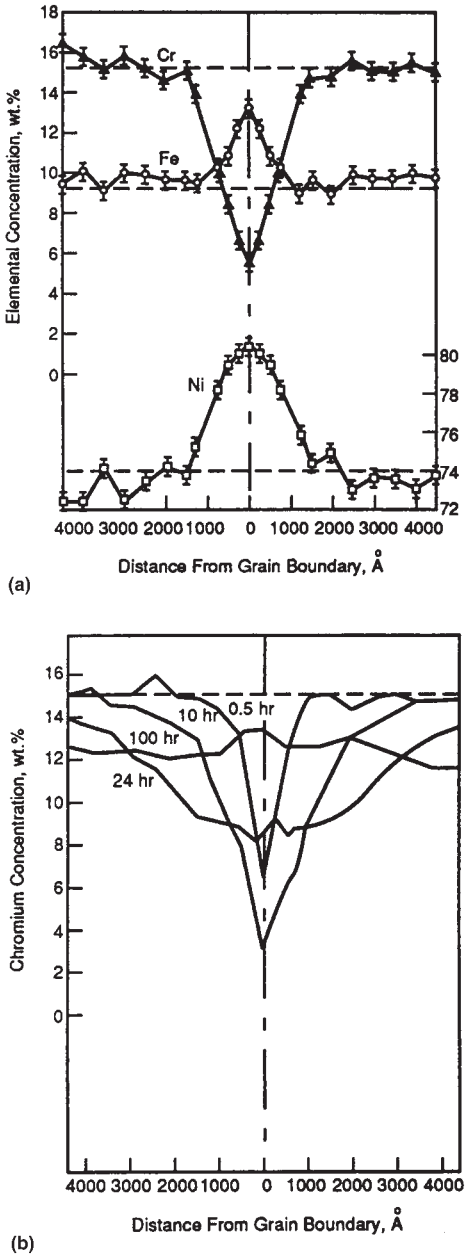


Fig. 1 (a) Grain-boundary chemistry of alloy 600, annealed 30 min at 1100 °C (2010 °F) and heated for 5 h at 700 °C (1290 °F). (b) Grain-boundary chromium depletion in alloy 600, annealed 30 min at 1100 °C (2010 °F) and heated at 700 °C (1290 °F) for various times. Source: Ref 6

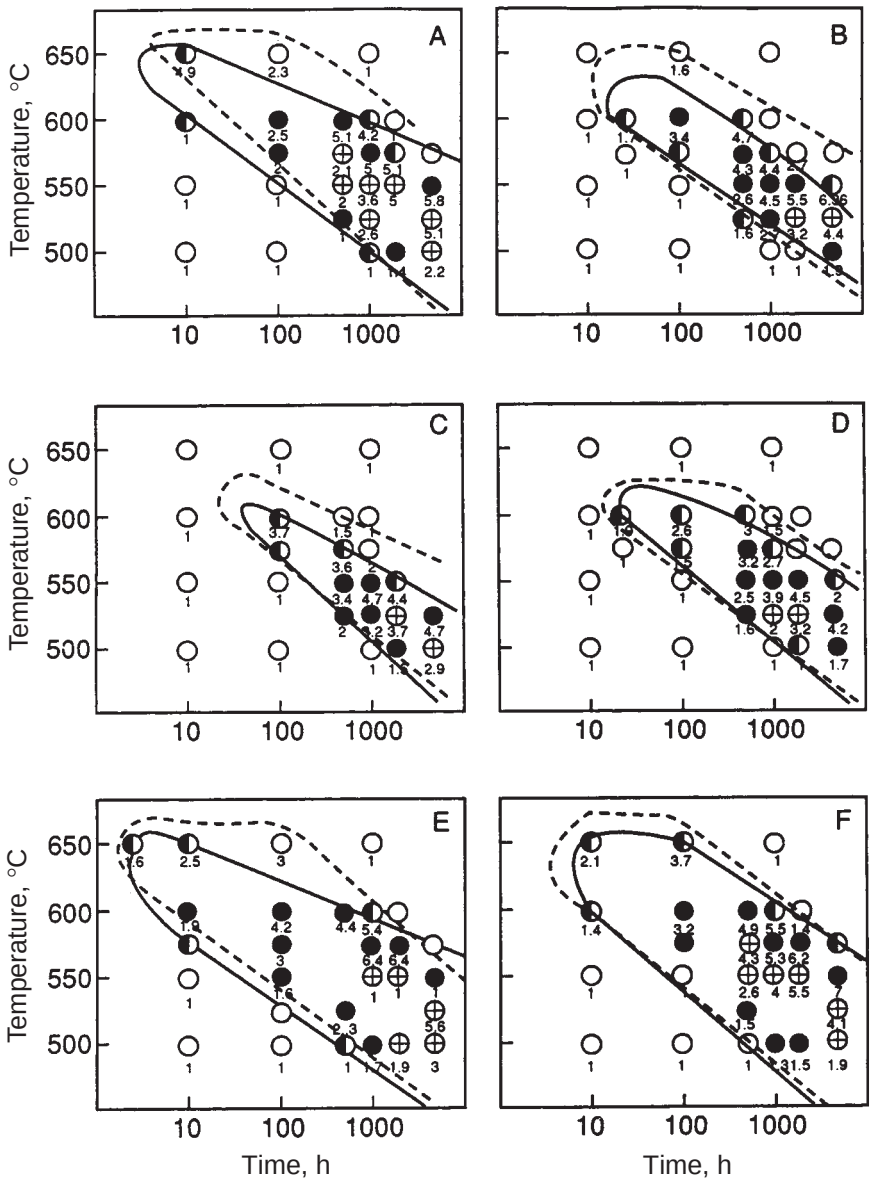


Fig. 2 Time-temperature sensitization diagrams for various heats of alloy 800. The relative change of the magnetic susceptibility is reported below each point. The dotted lines define the conditions for chromium depletion. Source: Ref 9

may substitute for some of the carbon, and the resulting carbonitrides may appear yellow or orange when examined metallographically, in contrast to the grayish color of the carbides. The MC-type carbides are extremely stable and generally do not break down. The M_6C-type carbides, also known as η-carbides, are formed by molybdenum and tungsten. However, major substitutional alloying elements, such as nickel, iron, and chromium, also are present in these carbides (Ref 11). Some typical compositions include Mo_6C, $(Ni,Co)_3Mo_3C_6$, and $(Mo,Ni,Cr,W)_6C$. Typically, these carbides dissolve at higher temperatures than the $M_{23}C_6$-type carbides. It must be noted that since these carbides are not usually rich in chromium, the depletion zones associated with them are molybdenum or tungsten depletion zones. "Sensitization" in these alloys means enhanced intergranular corrosion as a result of depletion of molybdenum or tungsten. Other types of refractory carbides are $Mo_{12}C$ and Mo_2C, which may form in a nickel-molybdenum system depending on the carbon and molybdenum contents (Ref 12).

Effect of Intermetallic Phases on SCC Behavior. The intermetallic phases in nickel-base alloys can be coherent phases such as γ′ and γ″, which are often desirable for increased strength, or noncoherent phases, which are detrimental to toughness and corrosion resistance. The detrimental intermetallic phases are primarily the topologically close-packed (TCP) phases—σ, μ, and Laves—which form in the temperature range of 1100 to 800 °C (2010–1470 °F), depending on alloy composition.

Sigma phase typically occurs in alloys that contain large amounts of chromium, and in iron-chromium alloys it has the approximate composition of FeCr. Although σ-phase formation is not common in the nickel-chromium system, it can form in nickel-base alloys that contain moderate concentrations of molybdenum and iron. Other alloying elements that tend to stabilize σ-phase include silicon and tungsten. Sigma phase has a complex, tetragonal, layered structure (Ref 13) and tends to nucleate from $M_{23}C_6$ carbides, to which it is structurally and compositionally related.

Mu phase, which has a complex, rhombohedral structure, occurs in chromium-containing alloys with large amounts of molybdenum and tungsten and is stabilized by iron. In the iron-molybdenum system, μ-phase has a composition similar to Fe_7Mo_6, but has not been observed in the nickel-molybdenum system. In Ni-Cr-Mo-Fe alloys, it has been found to have a composition similar to $(Ni_{0.36}Cr_{0.16}Fe_{0.04}Co_{0.02})(Mo_{0.39}W_{0.03})$ (Ref 11). Mu phase tends to nucleate on M_6C-type carbides, which are structurally and compositionally similar to it.

Laves phases have complex, hexagonal structures and are compounds of iron and molybdenum, tungsten, niobium, or tantalum. Other intermetallic compounds that are detrimental to corrosion or SCC include the ordered Ni_4Mo that forms in the commercial nickel-molybdenum alloy in the temperature range of 800 to 650 °C (1470–1200 °F) and the Ni_2Cr-type ordered particles that form in commercial Ni-Cr-Mo alloys in the temperature range of 550 to 200 °C (1020–390 °F).

Some intermetallic compounds can also be beneficial to properties such as strength. These are usually coherent precipitates with relatively low lattice mismatch, such as γ′, which is a metastable form of $Ni_3(Al,Ti,Si)$, and γ″, which is a metastable version of Ni_3Nb. In both types of coherent precipitates, other alloying elements, such as chromium, molybdenum, and tungsten, tend to substitute for some of the nickel, although the γ′ precipitates have been shown to be leaner in these alloying elements than the matrix phase (Ref 14).

A typical time-temperature-transformation diagram for alloy 625 (Ni-Cr-Mo) is shown in Fig. 4 (Ref 15). It can be seen that a variety of precipitates, including various types of carbides, metastable phases (γ″), and intermetallic phases, can form in a single alloy. In the absence of phase diagrams for the multicomponent alloys, semiempirical correlations have been used. For example, based on Pauling's analysis of the electronic structure of transition metals, Beck and others (Ref 16) developed a computerized calculation scheme known as PHACOMP. In this approach, the residual matrix alloying element concentrations are calculated after accounting for carbides, borides, and γ′, which are then used to calculate an electron vacancy number. This is compared to a critical electron vacancy number for σ-phase precipitation. Similar approaches include SIGMA-SAFE (Ref 17) and New PHACOMP (Ref 18).

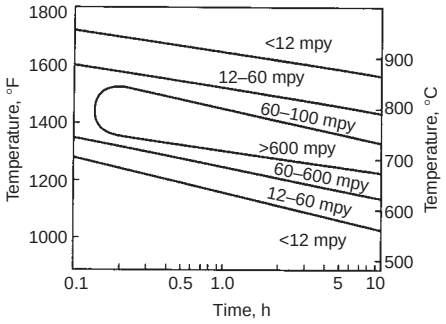


Fig. 3 Time-temperature sensitization diagram for alloy 825, annealed at 1205 °C (2200 °F) for 1 h prior to sensitizing treatment. Source: Ref 10

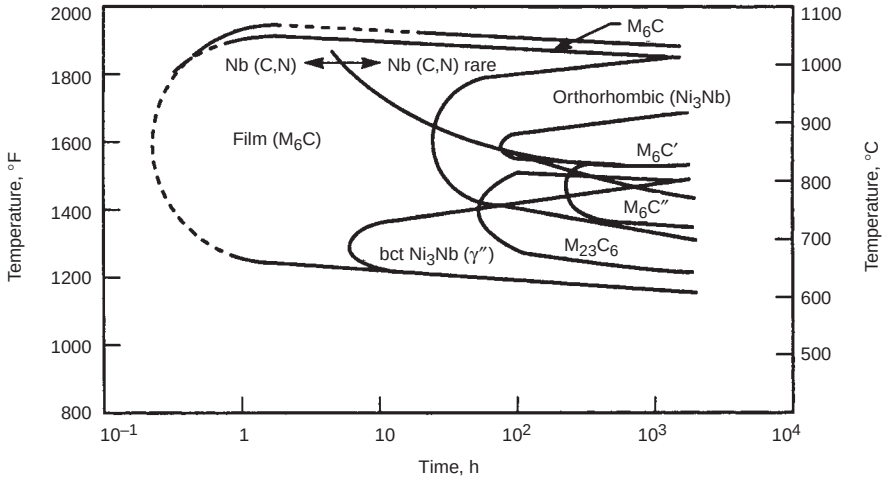


Fig. 4 Time-temperature-transformation diagram for solution-treated alloy 625. Lower γ″ limit determined by hardness measurement. Source: Ref 15

SCC in Halide Environments

Halide environments are those that contain chloride, bromide, iodide, or fluoride ion solutions. Each is described below. Table 2 lists alloy-halide environment combinations known to cause SCC in nickel-base alloys.

Table 2 SCC of nickel-base alloys in halogen ion containing environments

Alloy	Environment
800, 825, 718	Boiling (155 °C, or 310 °F) 42% $MgCl_2$
800, 825, G-3, G, X, C-276	20% $MgCl_2$, 230 °C (450 °F)
800, C-276, MP35N	Boiling 85–89% $ZnCl_2$
825, G, G-3, C-276	47% $ZnBr_2$, 205 °C (400 °F)
400, 600	Seawater, 285 °C (550 °F)
400, alloy 20	Salton sea brine, deaerated, 230 °C (450 °F)
625, C-276	Salton sea brine, aerated, 230 °C (450 °F)
825, G, G-3	Aerated NaCl, $CaCl_2$, 230 °C (450 °F)
825, G-3	25% NaCl + H_2S + CH_3COOH
400, X-750, 600, K500	HF and H_2SiF_6, 50 °C (120 °F)
804, 825	H_2O + 100 ppm Cl + 50 ppm O_2, 300 °C (570 °F)
825, G-3	10% HCl + H_2S, 20 °C (70 °F)
825, 625, C-276, 718, G-3	1% HCl, 205 °C (400 °F)
B	1% HBr, 230 °C (450 °F)
B	1% Hl, 205 °C (400 °F)
625, 718, C-276, G, 825	HAc + Cl^- + H_2S, 205 °C (400 °F)
B-2	HCl + H_2S, 175 °C (350 °F)

Source: Ref 3

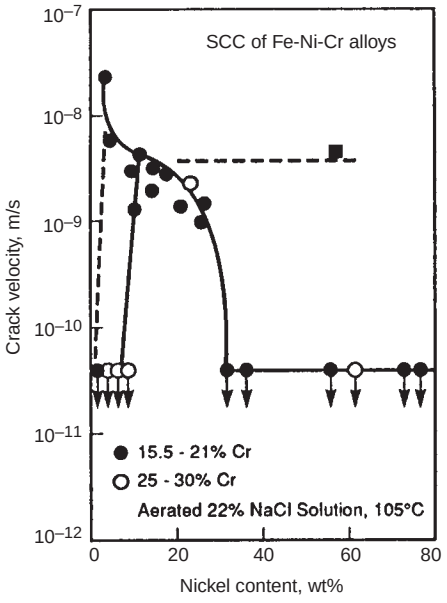
SCC in Chlorides

Effect of Nickel Content. The beneficial effect of nickel on the SCC resistance of Fe-Ni-Cr-Mo alloys to chloride solutions has been well established since the publication of the now-famous "Copson Curve" (Ref 19). This classic work was performed on wire samples in boiling 45% $MgCl_2$ solution and indicated that alloys containing above about 45% Ni did not crack in 30 days of testing. However, Staehle et al. (Ref 20) have shown that cracking can occur in the same nominal environment in nickel-base alloys that contain 32 to 52% Ni (Ref 20). They have also demonstrated the statistical nature of SCC.

The beneficial effect of nickel has been demonstrated in other chloride solutions using precracked samples (Fig. 5) (Ref 21) and, at higher temperatures, using two-point bend samples (Fig. 6) (Ref 22). At temperatures slightly above the boiling point (Fig. 5), essentially no cracking is observed in alloys with nickel contents above approximately 35% over a range of chromium contents. The corresponding stage 2 (stress-intensity independent) crack-growth rates are too low to be measurable. The lowest threshold stress intensity (highest susceptibility for SCC) in this study was observed for alloys containing ~20% Ni—unless the chromium content was higher than 25%, in which case the nickel content for the lowest threshold stress intensity was close to 4% (ferritic or duplex stainless steels). However, it must be noted that the stage 2 crack growth for the low-nickel ferritic/duplex stainless steels was low. It is likely that the presence of aeration enhanced SCC in these alloys.

Stress-corrosion cracking can be observed even in high-nickel alloys, if the temperature is sufficiently high (Fig. 6). The critical temperature at and above which cracking was observed in this study (Ref 22) depended mainly on nickel content and not on chromium or molybdenum content. In the same study, similar response to temperature was noted in the same alloys in 25% NaCl and 23.7% $CaCl_2$, with the severity of the environment roughly following the sequence: $MgCl_2$ > NaCl > $CaCl_2$. All cracking was transgranular. It was also noted that the effect of cold working was not as significant as that of temperature. Since the critical temperature for cracking depended only on nickel content, it is difficult to envision localized corrosion as a precursor to cracking in this environment.

Effect of Environmental Variables. Nickel may be beneficial in terms of either controlling the deformation mode or changing the corrosion potential away from the cracking potential. Further study using controlled-potential tests at various temperatures is needed. Chiang and Streicher (Ref 23) tested alloy 825 U-bend samples in boiling 42 and 45% $MgCl_2$ solutions (Table 3). Since finger-type condensers allow greater air intrusion into the flask, SCC occurred more readily. No cracking was found in a 50% $MgCl_2$ solution, suggesting that the lower oxygen solubility probably affected the test results. The effect of applied potential on SCC of sensitized nickel-base alloys in boiling dilute chloride and sulfate solutions was examined by Herbsleb (Ref 24). All cracking was intergranular and, as shown in Fig. 7 and 8, was observed only at high potentials well beyond the pitting potential.



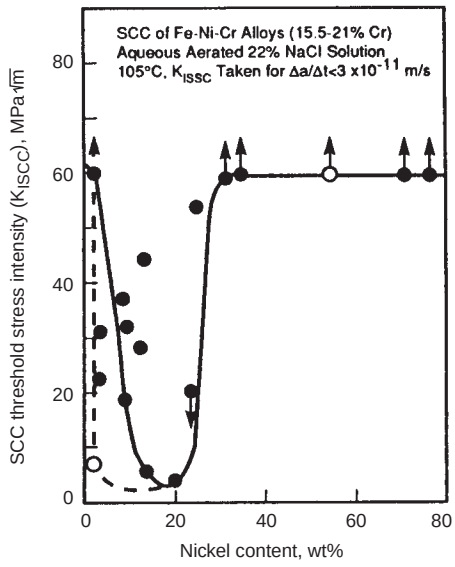


Fig. 5 Effect of nickel content on maximum crack-growth rate and threshold stress-intensity factor for Fe-Ni-Cr alloys in hot chloride solutions. Source: Ref 21

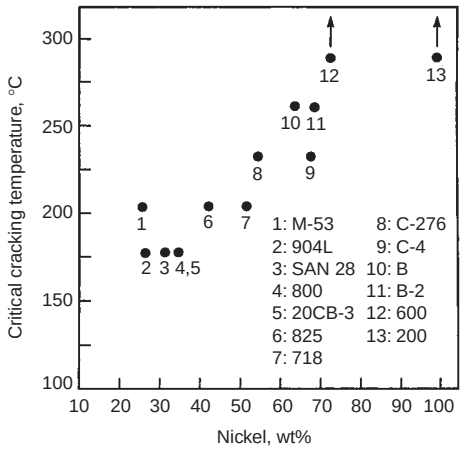


Fig. 6 Effect of nickel on SCC in 20.4% $MgCl_2$ deaerated with nitrogen. Source: Ref 22

Table 3 SCC of mill-annealed alloy 825 in boiling $MgCl_2$ solutions

$MgCl_2$,	Boiling temperature		Time to failure, h		
			Finger condenser	Modified Allihn condenser	
wt%	°C	°F		No purge	Oxygen
42	145	293	155	1100	…
45	155	311	…	80	80
50	170	338	50(a)	1000(a)	…

Tests performed according to ASTM G 30 using two different types of condensers. (a) No cracking. Source: Ref 23

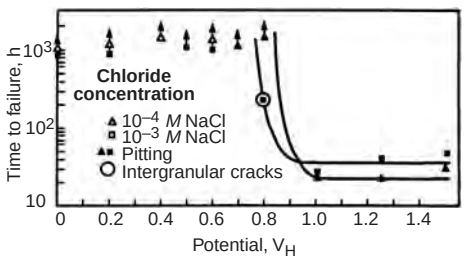


Fig. 7 Effect of chloride concentration on time-to-failure/potential curves of sensitized (1 h at 650 °C, or 1200 °F) alloy 800 tensile specimens (σ_a = 1.75 $\sigma_{0.2}$) in boiling 10^{-2} *M* and 10^{-4} *M* NaCl. σ_a, applied stress; $\sigma_{0.2}$, yield strength. Source: Ref 24

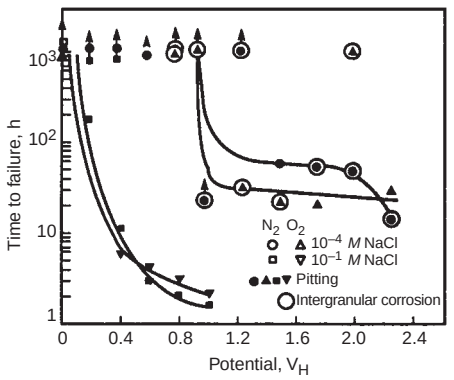


Fig. 8 Effect of chloride concentration on time to failure of sensitized (1 h at 600 °C, or 1110 °F) alloy 600 tensile specimens (σ_a = 1.75 $\sigma_{0.2}$) in boiling NaCl (H_2 and O_2 atmosphere). Source: Ref 24

Humphries and Nelson (Ref 25) observed that in a moist 3.5% NaCl environment, under alternating wet (10 min) and dry (50 min) conditions at room temperature, no cracking was observed in alloy 718, alloy C (high-carbon C-276), and type 304 stainless steel. Cracking in concentrated HCl at room temperature has been observed in several nickel-base alloys (Fig. 9) (Ref 26). Cracking was observed only in precipitation-hardenable alloys and not in solid-solution-strengthened alloys (Ref 26). Stress-corrosion cracking can occur in alloys that do not exhibit any passive behavior. This is shown in Table 4 for a variety of Ni-Cr-Mo-Fe alloys. In all the cases where cracking was observed, considerable corrosion was also observed. The addition of H_2S to 17% HCl has been shown to induce transgranular cracking in alloys 825, C-276, and C-22 even at room temperature (Ref 27).

Table 4 SCC of nickel-base alloys in 1% HCl

Alloy	Results of triplicate tests(a)
Type 316 stainless steel	C, C, C
Alloy 718	C, C, C
Alloy 825	C, C, C
Alloy G-30	C, C, C
Alloy 625	C, C, C
Alloy C-276	C, C, C
Alloy C-22	C, C, C
Titanium, grade 2	NC, NC, NC

Tests were conducted on two-point bend samples for 1000 h at 204 °C (400 °F); no deaeration. All alloys in mill-annealed condition except alloy 718, which was double aged (1 h at 968 °C/WQ/aged 8 h at 732 °C/cooled to 621 °C/aged 8 h/AC).(a) C, cracking; NC, no cracking. Source: Ref 27

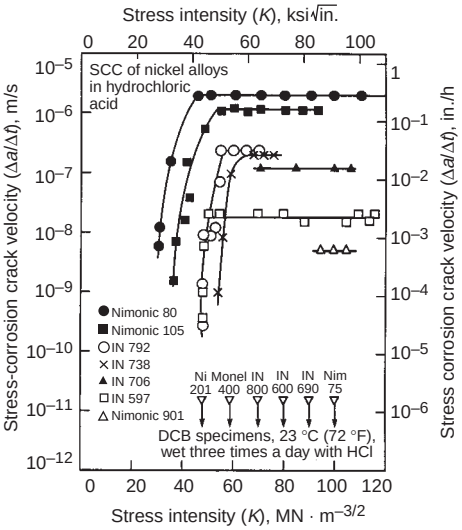


Fig. 9 Effect of stress intensity on SCC velocity of nickel alloys in concentrated aerated HCl at ambient temperature. Note that precipitation-hardened alloys crack, while solid-solution-strengthened alloys and pure nickel (Ni 201) resist cracking. Source: Ref 26

The effect of precipitation hardening on SCC in boiling chloride solutions is shown in Table 5 (Ref 28). Both alloys 718 and R-41 suffered increased SCC upon aging. From the data on R-41, it can be seen that hardness is not necessarily the determining factor, since the cold-rolled material did not suffer from SCC. A combination of changes in distribution of alloying elements between the γ- and γ′-phases, chromium depletion at the brain boundaries due to carbide precipitation, and changes in the deformation mode from cross slip to a more planar mode may be responsible for the increased SCC susceptibility.

The effect of sensitization on SCC of Ni-Cr-Mo-W alloys with varying degrees of susceptibility to carbide and μ-phase precipitation was studied by Streicher (Ref 29). His results are summarized in Table 6. No cracking was observed in the solution-annealed alloys. The precipitation of M_6C carbide, which was observed in alloys with a carbon content greater than 0.008 wt%, was much more detrimental to SCC resistance in $MgCl_2$ than the precipitation of μ-phase, which was observed in low-carbon alloys but not low-tungsten alloys. Cracking in all cases was intergranular.

SCC in Bromides, Iodides, and Fluorides

Bromides. Bromide solutions are encountered in chemical process industries (e.g., flame-retardant chemicals) and the oil and gas industry (e.g., packer and completion fluids). Due to the proprietary nature of both of these applications, extensive data are not available, especially for accurate comparison to SCC in chloride environments. In many plant failures related to SCC of stainless steels in bromide environments, some chloride is inevitably present. None of the Ni-Fe-Cr-Mo alloys suffered from SCC in two-point bend tests in 1% HBr. Among the nickel-molybdenum alloys, only alloy B cracked within 168 h in the same test. Stress-corrosion cracking has been observed in a number of nickel-base alloys in concentrated bromide solutions used as packer fluids. This is illustrated in Table 7 (Ref 30). Cracking in 4.7% $ZnBr_2$ is more severe than in 43% $CaBr_2$, probably because of the greater acidity of the former solution, especially in the presence of

Table 5 Effect of precipitation hardening on SCC of alloy 718 (UNS N07718) and alloy R-41 (UNS N07041) in chloride environments

Alloy	Thermal treatment	Hardness	Time to failure, h: 20.4% $MgCl_2$, 177 °C (350 °F)	Time to failure, h: 25% NaCl, 204 °C (400 °F)
718	Mill annealed (MA)	80 HRB	408/408/408	48/48/504
	Aged 8 h at 663 °C	26 HRC	72/144/240	48/48/48
	MA + 8 h/718 °C + 8 h/621 °C	42 HRC	72/72/144	48/48/48
R-41	Mill annealed	100 HRB	…	NC/NC/NC(a)
	Cold rolled	45 HRC	…	NC/NC/NC
	1080 °C + 30 min 1066 °C/AC 16 h 760 °C	42 HRC	…	48/96/NC

Two-point bend samples, tested for 1008 h. (a) NC, no cracking. Source: Ref 28

Table 6 Effect of grain-boundary precipitation on SCC of Ni-Cr-Mo-W alloys in boiling 45% $MgCl_2$

Alloy	Analysis, wt%: Carbon	Analysis, wt%: Silicon	Treatment	Type of precipitate	SCC in 45% $MgCl_2$ at 154 °C (310 °F)(a)
Alloy C	0.05	0.70	Solution annealed	None	NC, 2407 h
			1 h/704 °C	M_6C	IGC, 107–552 h
			1 h/871 °C	M_6C, μ	IGC, 90 h
			1 h/1038 °C	M_6C, μ	IGC, 552–625 h
C-276	0.01	0.01	1 h/704 °C	μ, small M_6C	NC, 6536 h
			1 h/871 °C	μ, M_6C	IGC, 905–2100 h
			1 h/1038 °C	Small μ and M_6C	NC, 6536 h
	0.008	0.004	1 h/1149 °C	None	NC, 2847 h
			1 h/704 °C	μ, small M_6C	Cracking, 2252 h
			1 h/ 871 °C	μ, small M_6C	IGC, 957 h
			1 h/1038 °C	μ, small M_6C	IGC, 4539 h
	0.004	0.01	Mill annealed	None	NC, 2407 h
			1 h/704 °C	μ	NC, 2407 h
			1 h/871 °C	μ	NC, 2407 h
			1 h/1038 °C	Small μ	NC, 2407 h

(a) NC, no cracking in the stated time period; IGC, intergranular cracking. Source: Ref 29

Table 7 SCC in simulated packer fluids

Alloy	Time to failure(a), months: 4.7% $ZnBr_2$	Time to failure(a), months: 43% $CaBr_2$
255 (Fe-25Cr-5.5Ni-3Mo-2Cu-0.2N)	1, 1, 2	4, 4, 4
825	1, 1, 2	>12, >12, >12,
G-3	1, 2, 2	>12, >12, >12,
C-276	1, 1, 2	>12, >12, >12,
C-22	>12, >12, >12,	>12, >12, >12,

(a) Indicates no cracking within the stated time period. Solutions were deaerated and backfilled with nitrogen (1 atm); two-point bend testing of all mill-annealed samples at 204 °C (400 °F). Source: Ref 30

H_2S. Fricke (Ref 31) investigated the SCC of a variety of materials in highly concentrated NaBr (1.5 g/mL) and $CaCl_2$ (1.49 g/mL) in the presence of H_2S using both C-ring and double-cantilever-beam (DCB) tests. His results (Table 8) indicate that the nickel-base alloy with low iron (alloy 625) suffered SCC when coupled to carbon steel at room temperature, which is probably related to hydrogen embrittlement rather than SCC. In a NaBr + H_2S environment at 232 °C (500 °F), all the highly alloyed materials underwent SCC, while the 9Cr and 13Cr alloys exhibited high rates of general and localized corrosion.

Iodides. Stress-corrosion cracking in iodide environments has been encountered in the manufacture of acetic acid (CH_3COOH), where potassium iodide is used as a promoter for the formation of acetic acid. The data to date indicate that cracking is specific to the nickel-molybdenum alloys (Table 9) and that cracking in mill-annealed alloys is transgranular.

Fluorides. Nickel-base alloys have been used quite successfully in fluoride-containing environments. Examples include alkylation in the refinery industry, semiconductor etching, and the manufacture of organic fluorides. However, intergranular cracking of cold-worked alloy 400 in fluosilicic acid was one of the earliest reported instances of SCC in nickel-base alloys (Ref 32). Since then, rather extensive data have been collected, mainly for nickel-copper alloys—for example, by Copson and Cheng (Ref 33), who showed that cracking occurred only in the vapor space in the presence of air, and by Graf and Wittich (Ref 34), who examined the SCC of nickel-copper alloys in hydrogen fluoride containing CuF_2 as the oxidizer. Everhart and Price (Ref 35) have examined the effect of strain rate, air, $CuCl_2$, and CuF_2 on SCC of alloys 400 and K-500. Stress-corrosion cracking of alloy 400 is found at the liquid-vapor interface or in the vapor phase because of the formation of a thin film of concentrated hydrogen fluoride and the easy access of oxygen to the surface, which increases the corrosion potential. Other oxidizers such as CuF_2 and $CuCl_2$ serve the same purpose. The effect of increasing applied stress and increasing concentrations of CuF_2 is shown in Fig. 10(a) and (b) (Ref 34). In slow-strain-rate tests (Ref 35), where the samples were partially immersed in HF + CuF_2 solutions, considerable interfacial corrosion and deposition of copper-rich product were noted along with cracking. However, the cracking was not associated with pitting. Intergranular cracking was observed at lower strains and

Table 8 SCC in packer fluids

	K_{ISCC}(a), MPa$\sqrt{m}$ (ksi$\sqrt{in.}$)			
	1.5 g/mL NaBr 6.89 MPa H_2S + 4 MPa CO_2		1.49 g/mL $CaCl_2$ 6.89 MPa H_2 + 4.1 MPa CO_2	
Alloy	24 °C (75 °F)	232 °C (500 °F)	24 °C (75 °F)	232 °C (500 °F)
9Cr-1Mo steel	>81.7 (74.3)	>85.1 (77.4)	>68.2 (62)	>80.8 (73.5)
13Cr steel	33.1 (30.1),C	>119.7 (108.9)	25.8 (23.5), C	<86.3 (78.5)
22Cr duplex stainless steel	C	27.5 (25), C	<34.8 (31.7), C	28.6 (26), C
Sanicro 28	>114.7 (104.4)	<78.6 (71.5)	>124.3 (113.1)	>108.7 (98.9)
625	67.8* (61.7)	84.3 (76.7)	68.1* (62), C	51.1 (46.5)

Note: K_{ISCC} determined by DCB tests; 28-day C-ring exposure; stress = 90% longitudinal yield strength. (a) < indicates crack branching; > indicates no crack growth; * indicates that the specimen was coupled to steel; C indicates C-ring cracking. Source: Ref 31

Table 9 SCC in 1% HI

	Time to failure(a), h		
Alloy	177 °C (350 °F)	204 °C (400 °F)	232 °C (450 °F)
B-2	168, 168, 366	48, 168, 168	48, 48, 48
200	NC, NC, NC	NC, NC, NC	NC, NC
400	NC, NC, NC	NC, NC, NC	NC, NC
600	NC, NC, NC	NC, NC	NC, NC, NC
825	NC, NC, NC	NC, NC, NC	NC, NC, NC
G-3	NC, NC, NC	NC, NC, NC	NC, NC, NC
C-276	NC, NC, NC	NC, NC, NC	NC, NC, NC

Two-point bend samples tested for 1000 h max. (a) NC, denotes no cracking in 1000 h

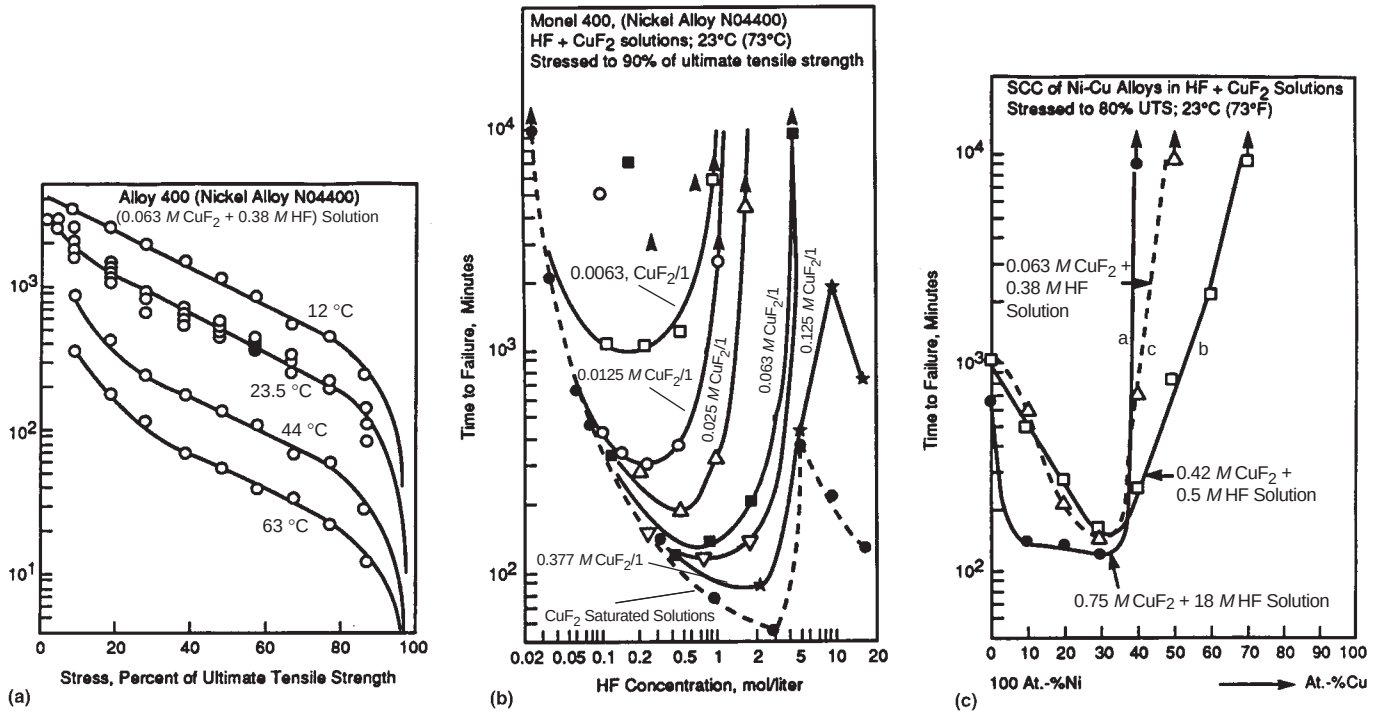


Fig. 10 SCC of nickel-copper alloys in fluoride environments. Source: Ref 34

strain rates, while transgranular cracking was observed at higher strains and strain rates. The effects of temperature and stress level are shown in Fig. 10(b). In a series of binary nickel-copper alloys, Ni-30Cu exhibits the greatest sensitivity to cracking in these environments (Fig. 10b). Nickel-chromium alloys, such as alloy 600, have been used in components exposed to hydrogen fluoride vapors to minimize SCC.

SCC in Environments Containing Sulfur Species

Environments that contain sulfur species are encountered in oil and gas production, both in downhole and surface components, and in refinery operations. Such environments can be divided into two major classifications:

- $Cl^- + H_2S + CO_2$ + elemental sulfur environments
- Other sulfur-containing environments (thiosulfate, tetrathionate, polythionic acid)

Environmentally induced cracking has been observed in the first type of environment, both at low and high temperatures. However, in low-temperature H_2S environments, cracking has been observed only when the nickel-base alloys have been coupled to carbon steel, thus cathodically polarizing them. Hence, this is discussed under hydrogen-embrittlement phenomena.

SCC in $Cl^- + H_2S + CO_2$ Environments

Nickel-base alloys have come into prominence in the oil and gas industry because of the need to go to greater depths to find oil and natural gas. Because most of the nickel-base alloys used as downhole components (tubing, casing, valves) are solid-solution-strengthened alloys, the required strength levels (yield strengths ranging from 758 to 1103 MPa, or 110 to 160 ksi) can be achieved mainly through cold working. These are seldom welded, although some surface components such as flow lines can be joined by circumferential welding. Thick-wall components such as safety valves and tubing hangers, which cannot be cold worked economically or uniformly, are manufactured from precipitation-strengthened nickel-base alloys.

The behavior of solid-solution-strengthened alloys is discussed first, followed by precipitation-strengthened alloys. The discussion is, of necessity, brief, and the interested reader is referred to several reviews (Ref 36–39). Investigation of the SCC of nickel-base alloys in $H_2S + CO_2 + Cl^-$ environments began in the late 1970s (Ref 40). These early investigations emphasized low-temperature embrittlement under cathodic polarization conditions. However, initial data on anodic cracking in 5% NaCl + 0.1% CH_3COOH + H_2S (saturated at room temperature) at up to 204 °C (400 °F) showed that some of the high-carbon nickel-base alloys, precipitation-hardenable nickel-base alloys, and cobalt-base alloys were susceptible to cracking (Ref 40). The cracking was transgranular, in contrast to the intergranular low-temperature cracking under cathodic polarization. Watkins et al. (Ref 41) reported the results of SCC in alloy C-276 in a H_2S environment containing elemental sulfur (referred to in this article as S_8, although at the temperatures of interest in downhole applications, sulfur does not exist as a ring of eight atoms but as long chains of many lengths that contain biradicals of sulfur). Since then, many investigations of the effects of H_2S, S_8, Cl^-, CO_2, and pH have been carried out.

Effect of Temperature. In the absence of galvanic coupling with carbon steel, increasing the temperature increases the SCC susceptibility of nickel-base alloys. This is shown in Fig. 11 for alloy C-276 in a $H_2S + S_8$ environment. Watkins et al. (Ref 41) showed that the percentage of samples that cracked in the slow-strain-rate tests increased with temperature and that duplicate tests may not be sufficient to detect cracking. They also compared the results of slow-strain-rate tests to constant-deflection tests. Their results, shown in Table 10, indicate that slow-strain-rate tests are more severe than constant-deflection tests. This has not always been found to be the case, and cracking susceptibility may be controlled by a variety of factors, such as corrosion potential, surface effects, and sample orientation. In the same environment, Watkins et al. (Ref 41) found cracking at temperatures as low as 204 °C (400 °F).

The detrimental effect of temperature has also been used to rank alloys in terms of their critical temperature for SCC in a given environment. This is illustrated for a variety of experimental alloys in Fig. 12 (Ref 42). It can be seen that increasing molybdenum content results in increased temperature above which cracking occurs in C-ring tests. In contrast, Ciaraldi (Ref 43) concluded, from DCB precracked specimens, that nickel exerts the dominant beneficial effect and chromium and molybdenum a lesser one. These may not be contradictory results, because the higher-nickel alloys (above 45% Ni) examined by Ciaraldi also contained higher molybdenum content.

Effect of H_2S. It has been well established that H_2S promotes cracking in nickel-base alloys. For example, Asphahani (Ref 44) showed that the addition of CO_2 to 5% NaCl did not cause cracking of nickel-base alloys, whereas H_2S additions resulted in SCC of 25% Ni at 177 °C (350 °F). No cracking was found in alloys containing higher amounts of nickel. However, unlike the cases of steels and duplex stainless steels, no systematic study to establish the minimum concentration of H_2S needed for cracking has been reported. Kolts (Ref 30) showed that for a 25Cr-5.5Ni-3Mo duplex stainless steel, 9 psia H_2S was sufficient to cause cracking (two-point bend tests) even at room temperature, whereas no cracking was reported in nickel-base alloys (31–56% Ni) in 100 psia H_2S + 25% NaCl at 204 °C (400 °F). Ikeda et al. (Ref 45) reported that a minimum

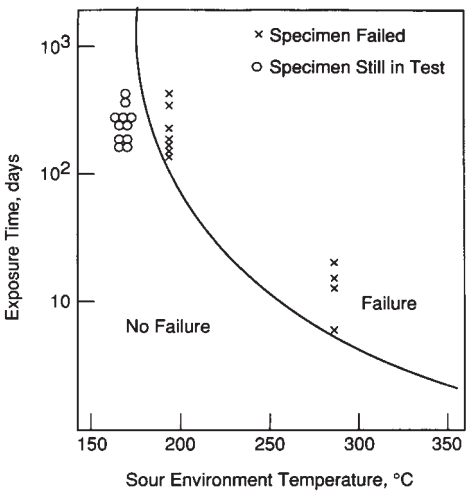


Fig. 11 SCC behavior of alloy C-276 versus testing temperature. Heat treatment: 260 °C (500 °F) for 250 h; environment: 25% NaCl + 0.5% CH_3COOH + 1 g/L S_8 + H_2S; yield strength: 1050 to 1160 MPa (152–168 ksi); stress level: 70 and 90% of yield strength. Source: Ref 41

Table 10 Effect of test technique on observed SCC in a H_2S environment

Test technique	Temperature °C	Temperature °F	No. cracked/Total
C-ring, constant deflection(a)	232	450	0/3
Slow strain rate(b)	232	450	3/6
	214	417	1/3
	204	400	0/3

Solution: 25% NaCl + 2.4 MPa H_2S (RT) + 1.7 MPa CO_2 (RT). Alloy: 50Ni-24Cr-15Fe-6Mo-1Cu-1Ti-1Mn. (a) Stressed to 90% longitudinal yield strength; exposed for a total of 6 months; same alloy bolt. (b) Extension rate, 4×10^{-6}/s; SCC based on secondary crack observation. Source: Ref 41

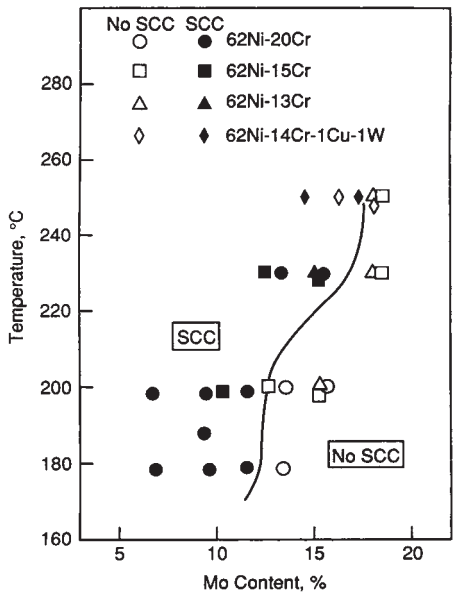


Fig. 12 Effect of molybdenum content on SCC resistance of Ni-Cr-Mo alloys in 20% NaCl + 0.5% CH_3COOH + 10 atm H_2S + 10 atm CO_2 + 1 g/L S_8. Source: Ref 42

of 10 atm H_2S (25% NaCl + 0.5% CH_3COOH + 10 atm CO_2) was needed to cause cracking under slow-strain-rate testing conditions (4×10^{-6}/s) in a 30Ni-22Cr-4Mo alloy at 150 °C (300 °F). Unlike the case of steels, cracking of nickel-base alloys in H_2S solutions at high temperatures is related to anodic dissolution mechanisms.

The effect of H_2S on localized corrosion has been studied more systematically than cracking. Tsujikawa (Ref 46) showed that the addition of 0.01 atm H_2S to a 20% NaCl solution at 80 °C (175 °F) and atmospheric pressure lowered the pitting potential from –25 to –200 mV (SCE). He also showed that the effect of H_2S on localized corrosion can be reproduced by the addition of $K_2S_2O_3$. The ranking of various alloys in terms of their localized corrosion resistance in NaCl + H_2S solution did not correspond to their ranking in an oxidizing chloride solution such as 6% $FeCl_3$. Similar results have been reported by Rhodes (Ref 39) and Kolts (Ref 30). As is mentioned later, in environments containing S_8, H_2S does not seem to be necessary to cause localized corrosion or cracking, perhaps due to local generation of H_2S from electrolytic reduction of sulfur. The detrimental effect of H_2S may be related to adsorption of sulfur atoms in the passive film and eventual depassivation, as shown for nickel by Marcus (Ref 47).

Effect of CO_2. Carbon dioxide has been shown to have no significant effect on cracking of nickel-base alloys in chloride environments (Ref 30, 40, 44). In environments that contain H_2S and S_8, CO_2 may also inhibit cracking slightly (Ref 48). The role of CO_2 in inhibiting cracking is not clear. Bicarbonate has been shown to be a much greater inhibitor in a NaCl + H_2S + S_8 environment (Ref 48), perhaps due to its buffering action.

Effect of Elemental Sulfur (S_8). Most recent studies of nickel-base alloy in sour-gas environments have focused on the effect of S_8. It is clear from all the studies, dating back to the late 1970s, that S_8 is extremely detrimental to localized corrosion and cracking of nickel-base alloys in brine. What has not been clear until now is the mechanism by which S_8 affects cracking in these environments.

The structure and chemistry of sulfur as it pertains to sour-gas environments have been reviewed by Schmidt (Ref 49). Sulfur exists at room temperature in the α-form, which has a nonplanar ring structure consisting of eight atoms. In this configuration it is quite stable. When heated above 95 °C (203 °F), the α-phase transforms to a monoclinic β-phase, which also has an eight-atom ring structure. The β-phase melts at 119.5 °C (247 °F) to form the λ-phase, which retains the ring structure. The easy displacement of the ring structure results in rather low viscosity. However, above 160 °C (320 °F), the λ-phase transforms mostly to μ-phase, with a small percentage of π-phase. The μ-phase has a zigzag chain structure with biradical ends. Because of formation of long polymeric structures, the viscosity increases above 160 °C (320 °F) rather dramatically Above 160 °C (320 °F), H_2S and Cl^- can combine with the biradicals and reduce the viscosity (Ref 49).

The melting point of sulfur can also be decreased by an increase in H_2S pressure, significant changes occurring only beyond 0.1 MPa (0.015 ksi). Ueda et al. (Ref 50) have shown that the melting point and viscosity changes are the same in aqueous brine solutions containing 0.1 MPa (0.015 ksi) H_2S and 1 MPa (0.15 ksi) CO_2 as in pure sulfur. This agrees with the data given by Schmidt (Ref 49). It is well known that α-, β-, and λ-sulfur are insoluble in water. Sulfur solubility has been shown to be increased by an increase in H_2S pressure in hydrocarbon gases due to the formation of polysulfide chains. However, very little solubility data in aqueous systems are available. Ueda et al. (Ref 50) have calculated the sulfur solubility in H_2O + H_2S systems, based on thermodynamic self-oxidation and reduction reactions of sulfur:

$$S + 2H^+ + 2e^- = H_2S \quad \text{(Eq 1)}$$

$$S + 4H_2O = SO_4^{2-} + 8H^+ + 6e^- \quad \text{(Eq 2)}$$

Based on these reactions, the sulfur solubility in H_2O at a pH of 3 and a temperature of 200 °C (390 °F) will be about 1 g/L and will be expected to be decreased by the presence of H_2S and increased by an increase in pH. Ueda et al. offer, as evidence for the validity of the above reactions, detection of H_2S in the gas phase and SO_4^{2-} in the aqueous phase after reaction of sulfur in a 5% NaCl solution in the presence of a platinum electrode at 250 °C (480 °F). Additionally, an increase in pH consistent with Eq 1 was noted upon exposure of a corroding Ni-Fe-Cr-Mo alloy in a Cl^--H_2S-S_8 environment. Schmidt (Ref 49) has proposed that chemisorption of sulfide molecules on molten sulfur particles serves to increase their electrical conductivity and thus facilitate electron-exchange reactions.

The effect of sulfur on SCC of two nickel-base alloys is illustrated in Fig. 13 (Ref 51). It can be seen that at 204 °C (400 °F) as little as 0.02 g/L of S_8 was sufficient to induce cracking of alloy G-3 in a 25% NaCl + 0.7 MPa (0.1 ksi) H_2S environment. Greater amounts of S_8 were required to crack alloy C-276. Cracking was transgranular in all the alloys and was invariably associated with deposits of dark sulfides, underneath which considerable corrosion also occurred. Miyasaka et al. (Ref 52) showed that H_2S is not necessary to cause cracking in the presence of S_8 because of the local H_2S created by the reduction of sulfur.

The mechanism of the effect of sulfur on cracking and the electrochemical behavior of nickel-base alloys is still being debated. Both Kolts (Ref 30) and Ciaraldi (Ref 43) have shown that the effect of elemental sulfur is similar to that of oxygen (Table 11). In Ciaraldi's experiments, it is possible that oxygen converted H_2S to sulfur. However, no H_2S was used in the experiments reported by Kolts. Thus, the effect of sulfur may be viewed as that of an oxidizer or cathodic depolarizer. Rhodes (Ref 39) showed that sulfur increased the corrosion potential of alloy MP35N (35Co-35Ni-20Cr-10Mo). However, his potential measurements were carried out with reference to a platinum electrode immersed in the same solution. Since the platinum electrode also tends to be polarized by sulfur, the effect of sulfur on the corrosion potential of the alloy cannot be estimated accurately. Ueda et al. (Ref 50) showed that sulfur in a NaCl solution increased the open-circuit potential of platinum and a Ni-Fe-Cr-Mo alloy at 200 °C (390 °F) (measured against a pressure-balanced Ag/AgCl electrode at room temperature). However, in the presence of H_2S, no effect of sulfur on open-circuit potential was observed. They also found that sulfur increased the anodic currents and decreased the pitting potential even in the presence of H_2S. Miyasaka et al. (Ref 52) showed that sulfur increased the cathodic reaction kinetics but not the open-circuit potential or the anodic currents of Ni-Fe-Cr-Mo alloys and platinum. Wilhelm (Ref 48) found a slight decrease in the corrosion potential of alloy 825 with the addition of sulfur but an increase in cathodic reaction kinetics. He found a small decrease in anodic current density due to the addition of sulfur.

Sulfur may also affect cracking by increasing the anodic reaction or preventing repassivation of the alloy surface. Marcus (Ref 47) has examined the effect of adsorbed sulfur on the anodic reaction kinetics of nickel, nickel-iron, and Fe-Ni-Cr-Mo alloys and has shown that adsorbed sulfur prevents passivation of the surface by excluding OH^- adsorption. However, his measurements have been carried out under conditions where atomic adsorption of sulfur at the surface was ensured and at low temperatures in nonchloride environments.

Effect of Inhibitors. Wilhelm (Ref 48) has shown that addition of bicarbonate inhibits cracking of alloy G-3 in a Cl^--H_2S-S_8 environment at 232 °C (450 °F). Similarly, addition of

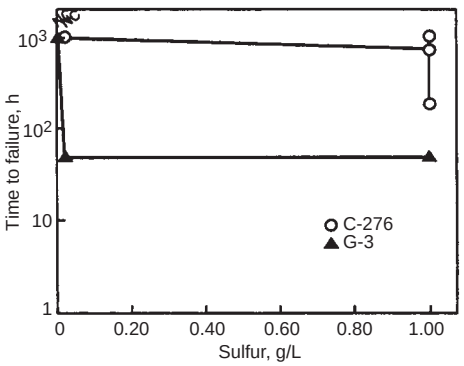


Fig. 13 Effect of sulfur on SCC of two-point bend samples of Ni-Fe-Cr-Mo alloys, in 25% NaCl + 0.7 MPa H_2S (RT) at 204 °C (400 °F). NC, no cracking. Source: Ref 51

Table 11 Effects of elemental sulfur and oxygen on SCC of nickel-base alloys

	1 g/L S_8			0.07 MPa O_2		
	K_{ISCC}			K_{ISCC}		
Alloy, nominal composition	MPa$\sqrt{m}$	ksi$\sqrt{in.}$	SCC	MPa$\sqrt{m}$	ksi$\sqrt{in.}$	SCC
25Cr-7Ni	45.0	40.9	Yes	47.7	43.4	Yes
20Cr-26Ni	27.5	25.0	Yes	22.0	20.0	Yes
27Cr-31Ni	66.2	60.2	Yes	67.8	61.6	Yes
21Cr-36Ni	72.5	65.9	Yes	76.0	69.1	Yes
23Cr-42Ni	…	…	No	…	…	No
22Cr-45Ni	…	…	No	…	…	No

DCB samples (7 to 10.4 mm, or 0.28 to 0.4 in., thick) with side grooves tested at 204 °C (400 °F) in a solution of 20% NaCl + 0.1% CH_3COOH + 1.72 MPa H_2S + 1.72 MPa CO_2. Note: Applied stress intensity ranged from 66–100 MPa$\sqrt{m}$ (60–91 ksi$\sqrt{in.}$). Source: Ref 43

the sulfur solvents diethylamine and monoethanolamine has been shown (Ref 30, 51) to inhibit cracking of Ni-Cr-Mo alloys (Table 12).

Effect of Electrode Potential. It is possible that cracking in $Cl^- + H_2S$ environments occurs in specific ranges of potential depending on the environmental and alloy compositions. The effect of applied potential on SCC of alloy 825 is shown in Fig. 14 (Ref 53). It is interesting to note that only a 10 mV increase in potential from the corrosion potential is needed to cause cracking in this environment. Such small differences can be easily caused by differences in deaeration and incidental galvanic contact of the sample with autoclaves and other metallic test accessories (Ref 53). These differences may account for the irreproducibility of slow-strain-rate data between various laboratories on identical materials and environments. For example, Ciaraldi (Ref 43) noted that no cracking occurred when the environment was completely deaerated, whereas even a slight exposure to air caused increased cracking. Kolts (Ref 30) also noted the adverse effect of aeration. Wilhelm (Ref 48) measured the corrosion potentials of alloy 825 in 15% Cl^-+ 2.76 MPa (0.4 ksi) H_2S + 5.5 MPa (0.8 ksi) CO_2 environment at 204 °C (400 °F). The measured potentials were significantly higher than those measured by Ueda et al. (Ref 50), and cracking was noted in all the samples.

Effect of pH. Acidification by HCl or CH_3COOH has been shown to increase cracking susceptibility in both H_2S and $H_2S + S_8$ environments (Ref 30, 43, 48, 51). Conversely, increasing the pH by the addition of NaOH has been shown to prevent cracking in these environments (Ref 30, 48).

Table 12 Effect of sulfur solvents on SCC

	Time to failure, h(a)		
Alloy	No solvent	5% diethylamine (pH 10–11)	5% diethylamine (pH 3.3–5.5)
825	960	>1440	>1440
G-3	1440	>1440	>1440
C-276	>8640	8640	8640

Mill-annealed two-point bend samples tested (2.6 to 4% strain) at 232 °C (450 °F) in a solution of 25% NaCl + 0.5% CH_3COOH + 0.7 MPa H_2S + 1 g/L S8. (a) > indicates no cracking. Source: Ref 51

Effect of Chloride. Wilhelm (Ref 48) showed that chloride concentrations below approximately 9% did not cause cracking of alloys 825 and G-3 in a 2.76 MPa (0.4 ksi) H_2S + 5.5 MPa (0.8 ksi) CO_2 + 1 g/L S_8 environment at 204 °C (400 °F). Ikeda et at. (Ref 45) showed that cracking of a 31Ni-22Cr-4Mo alloy did not occur below 15% Cl^- when tested by the slow-strain-rate method in a 1 MPa (0.15 ksi) H_2S + 1 MPa (0.15 ksi) CO_2 environment at 150 °C (300 °F).

Effect of Alloy Composition. As shown in Fig. 12, the higher-molybdenum alloys exhibit superior SCC resistance, especially in environments containing elemental sulfur. This finding has been confirmed by many investigators (Ref 40–42, 45, 46, 48, 50, 51, 53, 54). In contrast, Ciaraldi (Ref 43) has indicated that nickel is the most beneficial element, with chromium less beneficial and molybdenum having no effect. However, since the high-nickel alloys (above 45% Ni) also contained significantly higher molybdenum than the lower-nickel alloys, the effect of molybdenum cannot be separated from that of nickel in his studies. It must be emphasized that increasing the contents of molybdenum and tungsten, as well as chromium and other refractory elements, increases the possibility of formation of intermetallic phases such as μ and Laves. Hence, metallurgical stability considerations limit the design of alloys. This is indicated in Fig. 15 (Ref 55), where the alloys of interest in $H_2S + S_8$ environments are plotted in terms of chromium versus molybdenum + 0.5 W. At Mo + 0.5 W levels (the factor 0.5 indicates a rough accounting for the relative atomic weight of tungsten with respect to molybdenum) below about 12% (line 1), the alloys do not possess adequate SCC resistance. Line 3, outside which the alloys are unstable, is calculated using the concept of M_d (Ref 18), which relates alloy composition to stability in terms of electron concentration. Line 2 refers to an area outside which the alloys will not be resistant to hydrogen embrittlement in H_2S environment. While this type of diagram is useful, its limitations are: (1) material stability is considered in terms of observed second-phase stringers after solution annealing rather than in terms of grain-boundary precipitation or sensitization, and (2) the authors did not present any data to justify the delineation of hydrogen embrittlement resistance by line 2.

Effect of Alloy Strength. As shown in Table 13, increasing the yield strength by cold work generally decreases the resistance to SCC (Ref 51). However, this relationship is not always monotonic and depends on the severity of the environment for a given alloy. Ikeda et al. (Ref 45) have shown that, in an environment of 25% NaCl + 0.5% CH_3COOH + 7 atm H_2S at 150 °C (300 °F), slow-strain-rate testing of alloys C-276 and 2550 showed no cracking at any strength level ranging from 758 to 1310 MPa (110–190 ksi). Asphahani (Ref 44) has shown that increased cold working increased the cracking tendency of 25 to 30% Ni stainless steels but not of the higher-nickel alloys in a 5% NaCl + 0.5% CH_3COOH + 1 atm H_2S (saturated at room temperature) at 177 °C (350 °F).

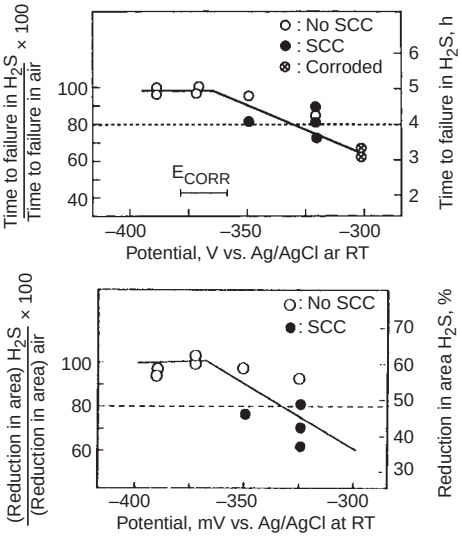


Fig. 14 Effect of potential on SCC resistance of alloy 825 in 25% NaCl + 0.5% CH_3COOH + 0.7 MPa H_2S, at 150 °C (300 °F): strain rate, $\dot{\varepsilon} = 4 \times 10^{-6}$/s. Source: Ref 53

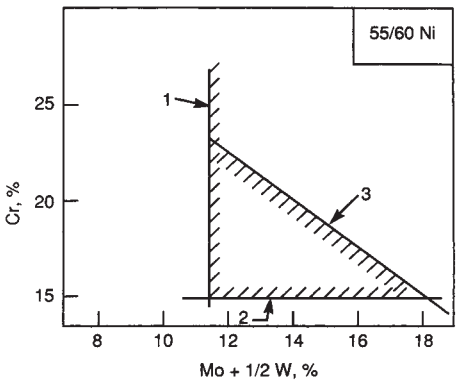


Fig. 15 Recommended region of chromium and molybdenum content of nickel-base alloy with approximately 55 to 60 wt% Ni in H_2S-CO_2-Cl^- -S environment. Line 1: SCC; 230 °C (450 °F), 1 MPa H_2S + 1 MPa CO_2 + 25 wt% NaCl + 1 g/L S_8, 336 h; four-point bent beam. Line 2: hydrogen embrittlement; 25 °C (77 °F), 5% NaCl + 0.5% CH_3COOH + 0.1 MPa H_2S, 720 h, $\sigma = \sigma_{0.2}$, iron coupling; four-point bent beam. Line 3: phase stability. Source: Ref 55

Effect of Precipitation. Incoherent, intermetallic precipitates such as μ-, σ-, and Laves phases are generally detrimental to the mechanical properties and corrosion resistance of nickel-base alloys. However, their effect on SCC in H_2S environments has not been clearly established. The detrimental effect of σ-phase is illustrated in Fig. 16 (Ref 56). In this alloy, precipitation of both coherent phases (γ′ and γ″) and incoherent phases (σ, η, carbides) occurs, depending on the time at temperature. Precipitation of σ-phase occurred above 704 °C (1300 °F) and caused SCC at 730 °C (1350 °F), but not at the higher temperatures. This may have been because of the low ductility in air that resulted in low times of exposure to the environment or due to "healing" of the sensitized regions. The precipitation of coherent phases at lower temperatures did not cause SCC. Precipitation of coherent or semicoherent γ″-phases in alloy 625 Plus (Ref 57) and alloy 725 (Ref 58) also did not result in loss of SCC resistance in 25% NaCl + 0.5% CH_3COOH + S_8+ H_2S environments at temperatures up to 232 °C (450 °F). Igarashi et al. (Ref 59) have suggested that alloys that are strengthened by γ″ (by addition of niobium) are more resistant than alloys strengthened by γ′ (by addition of titanium or aluminum) or by a mixture of γ″ + γ′. Their slow-strain-rate data in 25% NaCl + 0.5% CH_3COOH + 0.7 MPa (0.1 ksi) H_2S are presented in Table 14. They suggest that the γ′ alloys showed a greater planarity of slip because of dislocations cutting the precipitates, which led to strain localization and cracking. On the other hand, heterogeneous slip was not observed in the γ″ alloy. They also showed that pitting susceptibility of the γ′ alloy was greater, which is probably related to partitioning of alloying elements between the matrix and precipitates.

Carbide precipitation has been shown to be detrimental to SCC in sulfide environments. The results of lshizawa et al. (Ref 60) are shown in Table 15. They annealed 42Ni-22Cr-3Mo-2Cu (similar to alloy 825) specimens at two temperatures and then cold worked them to various degrees. The lower annealing temperature produced grain-boundary $M_{23}C_6$-type carbides and chromium depletion, as measured by scanning transmission electron microscopy (STEM). Although the investigators did not test multiple samples, the results in Cl^- + H_2S indicate that the presence of carbides resulted in cracking at a lower temperature. Cracking in both the sensitized and non-sensitized samples was intergranular. However, tests on the same alloy in a Cl^- + H_2S + S_8 environment did not show any effect of sensitization, and the cracking was all transgranular.

Table 13 Effect of yield strength on sulfide stress cracking of alloy C-276

	Yield stress		Time to failure(a), h	
			177 °C	232 °C
Yield stress, %	MPa	ksi	(350 °F)	(450 °F)
70	1069	155	>8600	528
	1262	183	>8640	300
	1317	191	>8640	144
90	1069	155	>8688	528
	1262	183	>8688	312
	1317	191	>8688	168

C-ring samples (cold pilgered + aged at 204 °C, or 400 °F, for 200 h) tested in a solution of 5% NaCl + 0.1% CH_3COOH + 0.7 MPa H_2S (RT) + 1 g/L S_8. (a) > indicates no cracking within the stated time period

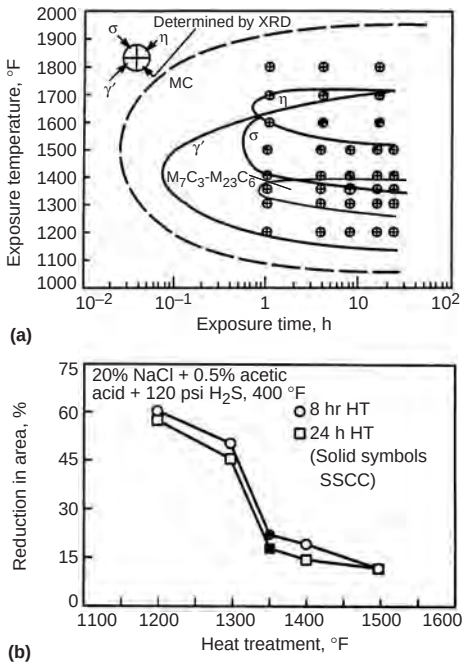


Fig. 16 (a) Time-temperature-transformation diagrams for annealed (1010 °C, or 1850 °F) alloy 925. (b) Slow-strain-rate test results for hot-rolled + annealed (1010 °C, or 1850 °F) + aged samples. XRD, x-ray diffraction; SSCC, sulfide SCC. Source: Ref 56

SCC in Sulfur-Oxyanions Solutions

Another class of aggressive sulfur-bearing species that can induce intergranular SCC of sensitized, single-phase Ni-Cr-Fe alloys is the family of metastable oxyanions, which includes polythionates ($S_xO_6^{2-}$, x = 3, 4, 5, 6) and thiosulfate ($S_2O_3^{2-}$).

SCC in Polythionic Acid Solutions. Initial observations were related to the so-called "polythionic acid cracking" that affected sensitized stainless steels in catalytic reformers used in the petroleum industry in the early 1950s (Ref 61, 62). Samans (Ref 63) was the first to report the intergranular cracking in a polythionic acid solution at room temperature of alloys 600 and 800 after being sensitized at 650 °C (1200 °F) for 4 h. Samans observed no cracking in mill-annealed specimens.

Polythionic acid solutions are commonly prepared by bubbling H_2S into a cold solution of SO_2 in water (Wackenroder's solution). These solutions contain a mixture of the different polythionic acids. Solutions prepared according to ASTM Standard Practice G35-88 have a pH of about 1.15 and approximately 0.13 mol/L of polythionic acids, in addition to 1.62% H_2SO_4 and 3.02% of H_2SO_3 (Ref 64, 65). The predominant species is tetrathionic acid at a concentration of approximately 0.074 mol/L, which represents around 57% of the total content of polythionic acids. Ahmad et al. (Ref 65) also showed that of all the polythionic acids, only tetrathionic acid is a potent cracking agent for sensitized AISI 304 stainless steel.

Scarberry et al. (Ref 66) confirmed that annealed alloy 600 was not susceptible to cracking in polythionic acid solution after 1000 h of exposure under constant-load conditions over a

Table 14 Effect of precipitation hardening on SCC

	Room-temperature yield strength		(Time to failure in H_2S)/(Time to failure in air), h		
Alloy	MPa	ksi	149 °C (300 °F)	177 °C (350 °F)	204 °C (400 °F)
23Cr-3.5Mo-4.7Nb (γ″alloy)	896	130	16.7/16.8	16.3/16.9	4.0/17.0
19Cr-3Mo-0.9Ti-5.1Nb (γ′ + γ″55 alloy)	931	135	6.3/17.7	6.9/17.2	…
22Cr-3Mo-2.67Ti (γ′ alloy)	690	100	4.5/19.6	4.4/18.2	…

Samples (solutionized at 1149 °C + 699 °C/20 h + AC) tested at a strain rate of 4×10^{-6}/s in a solution of 25% NaCl + 0.5% CH_3COOH + 0.7 MPa H_2S. Source: Ref 59

Table 15 Effect of grain-boundary carbides on SCC of an alloy similar to alloy 825

Annealing temperature		Yield strength		Test temperature(a)			
°C	°F	MPa	ksi	200 °C (390 °F)	250 °C (480 °F)	275 °C (525 °F)	300 °C (570 °F)
950	1740	296	43	NC	NC	…	NC
		775	112	NC	NC	…	NC
		764	111	NC	NC	…	…
		859	125	NC	IGC	…	…
		924	134	NC	IGC	…	IGC
		937	136	NC	IGC	…	IGC
1100	2010	856	124	…	NC	IGC	…
		871	126	…	NC	IGC	…

C-ring samples of 42Ni-22Cr-3Mo-1.7Cu-0.7Ti-0.016C tested at 100% of transverse yield strength in a solution of 20% NaCl + 1 MPa H_2S + 1 MPa CO_2. (a) NC, no cracking in 30 days; IGC, intergranular cracking. Source: Ref 60

wide range of nominal stress, whereas a sensitization treatment at 593 °C (1100 °F) for 4 h induced intergranular cracking in less than 10 h. As expected, the time to failure increased with decreasing stress, and an apparent threshold stress value as low as 69 MPa (10 ksi) was reported.

Similar behavior was observed in alloy 800 U-bend specimens exposed to polythionic acid solution (Ref 67). In relatively short times (4–48 h), cracks were detected in specimens solution annealed at 955 °C (1750 °F) for 1 h and heat treated at 650 °C (1200 °F) for 1 and 2 h. Prolonged heat treatment times did not lead to cracking in 1000 h of exposure. As suggested by all these authors, susceptibility to intergranular SCC is related to the existence of a chromium-depleted region along grain boundaries caused by the intergranular precipitation of chromium carbides. However, correlation with the results of boiling nitric acid tests (Ref 66, 67) was not entirely satisfactory since this test leads to relatively high corrosion rates even for microstructures that are not prone to cracking. This was more evident in the case of stabilized alloys, such as alloy 801 (a titanium-stabilized version of alloy 800), which was found to be resistant to cracking even though high corrosion rates (30.5 mm/yr, or 1200 mil/yr) were measured in the boiling nitric acid test.

SCC in Tetrathionate- and Thiosulfate-Containing Solutions. Intergranular SCC of these sensitized Ni-Cr-Fe alloys is by no means confined to the very acidic polythionic acid solutions. Berge and Donati (Ref 68) reported the intergranular SCC of alloy 600, sensitized at 700 °C (1290 °F) for 1 h, in 0.1 mol/L sodium tetrathionate (pH 3) at room temperature. A threshold stress of about 100 MPa (14.5 ksi), which is almost identical to that obtained in the presence of polythionic acids, was determined in that solution. However, at higher stress levels the failure time was found to be shorter in polythionic acids.

The discovery of extensive intergranular cracking of alloy 600 tubing in the once-through steam generators at the Three Mile Island Unit 1 Nuclear Power Plant, following a prolonged shutdown, prompted an intensive investigation (Ref 69). As previously reported for sensitized AISI 304 stainless steel (Ref 62, 70) the thiosulfate ($S_2O_3^{2-}$) anion was identified as one of the primary causative species for the failure. Furthermore, very small concentrations (of the order of parts per million of equivalent sulfur) were sufficient to induce cracking. In a series of publications, Newman and coworkers (Ref 71–74) examined mechanical, material, and environmental factors relevant to the intergranular cracking of alloy 600 in dilute thiosulfate and tetrathionate solutions.

The threshold stress for intergranular SCC of sensitized alloy 600 in thiosulfate-containing solutions, as measured in constant-load tests, was found to be about 95% of the yield strength (Ref 73). However, this value was obtained at 22 °C (72 °F) in a relatively mild environment containing 1.3% boric acid, thiosulfate equivalent to 0.7 ppm sulfur and 0.7 ppm lithium added as LiOH. In more aggressive solutions, such as polythionic acid (Ref 66) or concentrated tetrathionate (Ref 68), the apparent threshold stress for alloy 600 is close to 30% of the yield strength. It has been suggested (Ref 73) that the threshold stress may approach zero for conditions at which deep intergranular corrosion occurs (low-pH solutions or inside crevices). Although no fracture-mechanics tests have been conducted, it can be concluded that, under a wide range of environmental conditions in terms of anion concentration, pH, and temperature, crack growth occurs primarily in the stage 2 (stress-intensity independent) region.

The degree of sensitization of alloy 600 is a critical factor in the intergranular SCC of this alloy in thiosulfate and tetrathionate solutions. Whereas solution- or mill-annealed material is not susceptible to cracking even in relatively concentrated thiosulfate and tetrathionate solutions, sensitization as a result of heat treatment at 600 to 700 °C (1110–1290 °F) for a short period induces severe cracking (Ref 73, 75). On the other hand, prolonged heat treatment at those temperatures renders the alloy immune to cracking because of replenishment of the chromium-depleted regions along grain boundaries.

The initial microstructure of alloy 600 before sensitization heat treatment is extremely important in determining its SCC susceptibility in the presence of metastable sulfur oxyanions. Solution-annealed material contains more available carbon in solid solution than does mill-annealed material and will therefore experience more severe chromium depletion along grain boundaries after a sensitization heat treatment. This was confirmed (Ref 73) by comparing the behaviors of solution- and mill-annealed samples with a further heat treatment at 621 °C (1150 °F) for 18 h. The solution-annealed and sensitized (SAS) alloy was found to be susceptible to intergranular SCC in neutral thiosulfate solution, which was not the case for the mill-annealed and sensitized (MAS) alloy. However, in more aggressive environments (tetrathionate or acidified thiosulfate), both materials cracked. In order to differentiate the degree of sensitization of the MAS and SAS materials, electrochemical potentiokinetic reactivation (EPR) tests were performed in 0.5 *M* H_2SO_4 + 0.01 *M* KSCN solution. A semiquantitative correlation with the tendency to SCC was observed, since the reactivation charges per unit grain-boundary area for the mill-annealed, MAS, and SAS materials were found to be 111, 209, and 774 C/cm^2, respectively.

However, as noted by Was and Rajan (Ref 76), degree of sensitization is a rather ambiguous concept that arises from the fact that sensitization is defined in terms of the tendency to intergranular corrosion experienced by a material in a given environment, generally evaluated according to the EPR test or other standardized ASTM A 262 test methods. Different responses are obtain according to the test environment. By conducting slow-strain-rate tests in $Na_2S_4O_6$ solutions using a high-purity Ni-16Cr-9Fe alloy heat treated under different time and temperature conditions, Was and Rajan (Ref 77) showed that the level of chromium depletion at the grain boundary (see Fig. 1) is the determining factor in the propensity to intergranular SCC. They noted that, irrespective of heat treatment conditions, a grain-boundary chromium level below 5 wt% resulted in 100% intergranular fracture, whereas levels above 8.3 wt% produced no intergranular fracture. In addition, the variation in the slope of the chromium concentration profile at the grain boundary had no effect on the propensity to intergranular SCC. On the other hand, the EPR test in H_2SO_4 + KSCN solutions is more sensitive to broad, shallow, chromium-depleted regions in which the chromium concentration can be as high as 13 wt%. From these observations, it can be concluded that the results of EPR tests cannot be used to quantitatively predict the SCC susceptibility of sensitized alloy 600.

Effect of Heat Treatment. From the previous discussion, it is apparent that intergranular SCC of Ni-Cr-Fe alloys in the presence of metastable sulfur oxyanions can be avoided by using prolonged heat treatments (i.e., 15 h at 700 °C, or 1290 °F, for alloy 600) that replenish the chromium-depleted regions. For nickel-base alloys, the decrease in the carbon content does not provide adequate improvement, as in the case of austenitic stainless steels (i.e., types 304L and 316L), because of the low solubility of carbon in nickel. It is expected that stabilized alloys, such as alloys 801, 601, and 625, and those containing higher chromium levels, such as alloy 690, are resistant to cracking. However, no systematic investigation has been reported for the stabilized alloys. In the case of alloy 690, even though chromium depletion down to a concentration of 15 wt% has been measured at grain boundaries for certain heat treatments, no SCC was detected in 0.001 *M* $Na_2S_2O_3$ solution at pH 3 (Ref 78). It is obvious that the level of chromium depletion attained, even for prolonged heat treatments at 600 to 700 °C (1110–1290 °F), is insufficient to induce intergranular SCC in this alloy. It is worthwhile to note that Berge and Donati (Ref 68) have reported that high-purity heats (carbon content below 0.003%) of Ni-*x*Cr-8Fe alloys, where $7 < x < 16$, were immune to cracking in the solution-annealed condition, with the exception of the alloy containing 7% Cr, which exhibited transgranular cracking in polythionic acid solution.

Effect of Environmental Variables. Environmental factors are also extremely important in the intergranular SCC of these alloys in sulfur-oxyanions solutions. Very low concentrations of either thiosulfate or tetrathionate anions (about 10^{-5} mol/L) are sufficient to promote cracking in severely sensitized materials. Bandy et al. (Ref 73) have determined threshold concentrations of ~2×10^{-6} mol/L thiosulfate and 1×10^{-6} mol/L tetrathionate in air-saturated solutions at 22 °C (72 °F).

Although the effects of both metastable sulfur oxyanions are similar, it appears that the propensity to cracking initiation in thiosulfate is lower than in tetrathionate. The presence of oxygen seems to be necessary to initiate intergranular SCC in thiosulfate solutions. Oxygen is not necessary in the case of tetrathionate, presumably because of the higher oxidizing ability of tetrathionate with respect to thiosulfate. In a related study (Ref 72) using reverse U-bend specimens of alloy 600, no cracking was observed in 0.1 *M* thiosulfate, whereas tetrathionate caused cracking down to 10^{-5} *M* concentration. However, rapid cracking occurred when the pH of the thiosulfate solution was reduced to 3.

Intergranular SCC of sensitized alloy 600 in 0.5 *M* $Na_2S_2O_3$ at 22 °C (72 °F) occurs in a potential range that extends from –300 to 300 mV (SCE) (Ref 71). Very rapid crack-growth rates (4×10^{-7} m/s) were measured at approximately 0 mV (SCE), whereas under open-circuit conditions, crack velocities up to 1.5×10^{-8} m/s were observed over a wide range of $S_2O_3^{2-}$ concentrations (10^{-2} to 10^{-4} mol/L) in air-saturated H_3BO_3 at 40 °C (104 °F), as shown in Fig. 17. Crack velocity also increased with temperature, but it leveled off at ~80 °C (~175 °F), presumably due to the decrease in the concentration of oxygen dissolved in the solution and the concurrent decrease in the potential. An important observation in the studies of Newman et al. (Ref 71, 74) is that cracking in solutions containing H_3BO_3 and a low concentration of $Na_2S_2O_3$ can be prevented by the addition of LiOH. Although it is not shown in Fig. 17, the addition of 20 ppm Li^+ to the boric acid solution containing 7 ppm sulfur as $S_2O_3^{2-}$ decreases the mean crack velocity to values lower than 1 nm/s. The same inhibiting effect was exhibited when 5.6 ppm Li^+ were added to a solution containing 0.7 ppm sulfur, as shown in Fig. 17. In the presence of LiOH, the concentration of $H_2BO_3^-$ increases, and cracking is prevented by the competitive electromigration of this anion with $S_2O_3^{2-}$.

It appears that the intergranular cracking of alloy 600 in tetrathionate and thiosulfate solutions is a true SCC phenomenon in the presence of low concentrations of these anions. However, with increasing concentrations, intergranular corrosion assisted by stress seems to be the dominant phenomenon. Under certain low-pH conditions or in crevices, intergranular corrosion rather than intergranular SCC predominates. Localized attack in the form of pitting near grain boundaries has been identified by Bandy et al. (Ref 72, 73) as the initial step in the nucleation of intergranular cracks.

Finally, it should be noted that other sulfur-bearing compounds may be involved directly or indirectly in the intergranular SCC of sensitized Ni-Cr-Fe alloys. As in the case of sensitized austenitic stainless steels, the SCN^- anion may be a cracking agent under certain environmental conditions, and SO_2 and/or H_2S dissolved in water in the presence of air and a catalytic metal surface are known to generate polythionates as predominant ionic species. On the other hand, a thermodynamically stable sulfur-oxyanion such as sulfate does not promote intergranular SCC, even in heavily sensitized alloys. As reported by Herbsleb (Ref 24), sensitized alloys 600 and 800 were found to be resistant to intergranular cracking in boiling Na_2SO_4 solutions over a wide range of applied potentials.

SCC in High-Temperature Water and Dilute Aqueous Solutions

It is now well recognized that solid-solution-strengthened nickel alloys, such as alloy 600, and precipitation-hardened alloys, such as alloys X-750 and 718, are susceptible to intergranular SCC in deaerated high-purity water at ~300 to 350 °C (~570–660 °F). For alloy 600, very long initiation times (of the order of months) and relatively high stress levels (above macroscopic yielding) are required to develop intergranular cracks at the lower end of that temperature range. Under identical environmental and stress conditions, the same phenomenon has not been observed in alloys 800 or 690, which are used, as is alloy 600, as tubing materials in steam generators of pressurized nuclear water reactors.

SCC of Alloy 600 in High-Temperature Water

Coriou and coworkers were the first to report the intergranular SCC of alloy 600 in deaerated high-temperature pure water (Ref 79). For nearly 20 years, the general validity of their observation was questioned, but the widespread occurrence of intergranular cracking originating from the primary side of recirculating steam generators in many nuclear power plants has eliminated any doubts about the generic character of the phenomenon (Ref 80, 81).

Most of the testing has employed reverse U-bend specimens cut from split tubing, since this is the main product form for alloy 600. Significant variations in failure times have been observed by comparing different heats, reflecting the important influence of relatively minor differences in thermomechanical treatments. Bandy and Van Rooyen (Ref 82) found that for mill-annealed material and cold-worked material tested under constant-load conditions in both pure water and primary water (H_3BO_3 + LiOH) at 365 °C (690 °F), time to failure is related to applied stress by the following expression:

$$t_f = k\sigma^{-4.0} \qquad \text{(Eq 3)}$$

indicating a strong dependence of failure time on applied stress.

Intergranular SCC has also been observed in slow-strain-rate tests at strain rates ranging from 3×10^{-8}/s to 1×10^{-6}/s over the range 290 to 365 °C (555–690 °F) (Ref 83, 84). Although crack-initiation times are usually shortened under dynamic straining conditions, it is difficult to initiate cracking of alloy 600 in high-temperature water within the duration of slow-strain-rate tests. It has been shown (Ref 85) that tensile specimens with a pressed hump, which introduces high levels of cold work locally, exhibit short initiation times.

Effect of Alloy Composition. A singular aspect of the intergranular SCC of alloy 600, in addition to the fact that it occurs in apparently innocuous environments such as deaerated high-purity water, is associated with alloy composition. As noted previously, Ni-Cr-Fe alloys with lower nickel contents, such as alloys 800 and 690, are not susceptible to this form of cracking. However, results of constant-load tests in a hydrogenated H_3BO_3 + LiOH solution at 360 °C (680 °F) (Fig. 18) indicate that the resistance to cracking of solution-annealed Ni-Cr-Fe alloys increases with increasing chromium content (Ref 86). It can be inferred, therefore, that the higher chromium content is the factor that renders alloys 800 and 690 immune to intergranular SCC under those environmental conditions. The presence of carbon and other impurities, such as phosphorus and boron, does not necessarily play a detrimental role, since high-purity alloys of similar composition are also susceptible to cracking (Ref 87–89).

Effect of Microstructure. One of the most important factors affecting intergranular SCC of alloy 600 is microstructure, which depends on the thermomechanical history and carbon content of the material. As noted by several authors (Ref 90, 91), alloy 600 tubing subjected to mill-annealing treatments below 950 °C (1740 °F) exhibits a fine-grained microstructure with relatively heavy transgranular carbide precipitation and almost no carbide precipitation on grain boundaries. This microstructure is characteristic of a material highly susceptible to intergranular SCC in high-temperature water. On the other hand, a higher-temperature annealing (>1000 °C, or 1830 °F) increases the grain size, decreases the transgranular precipitation, and induces preferential grain-boundary carbide precipitation, leading to a microstructure that, although not immune, is more

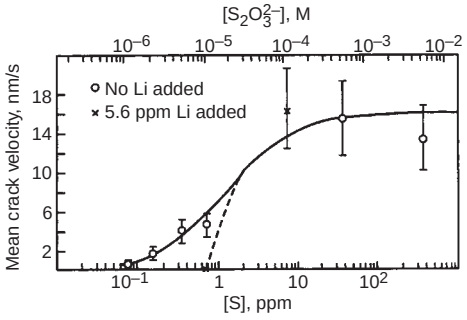


Fig. 17 Mean crack velocity of constant-extension-rate tests on sensitized alloy 600 as a function of $S_2O_3^{2-}$ concentration in air-saturated 1.3% H_3BO_3 at 40 °C (104 °F). Source: Ref 71

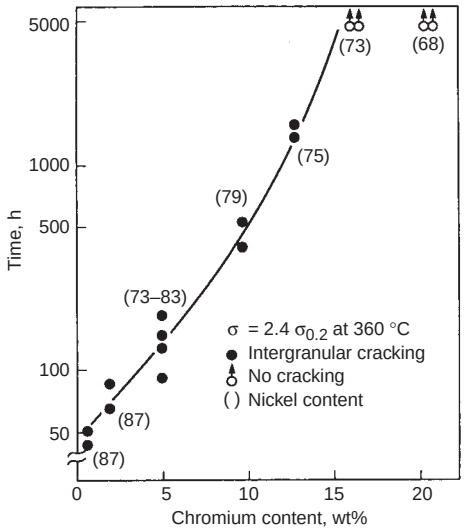


Fig. 18 Effect of chromium content on the time to failure of solution-annealed Ni-Cr-Fe alloys tested in H_3BO_3 + LiOH solutions containing hydrogen at 360 °C (680 °F). Source: Ref 86

resistant to intergranular SCC. In this regard, a carbon content of at least 0.02 wt% in the commercial alloy seems necessary for improving SCC resistance in high-temperature water. By heat treatment at 700 °C (1290 °F) for several hours, a semicontinuous grain-boundary precipitation of Cr_7C_3 occurs. This treatment renders the alloy more resistant to intergranular SCC (Ref 87, 92, 93). The degree of improvement is extremely dependent on the prior microstructure of the mill-annealed material. This implies that mill annealing should be done at a temperature sufficiently high (>1000 °C, or 1830 °F) to maintain enough carbon in solid solution. In addition, the treatment at 700 °C (1290 °F) should be extended for a period long enough (>15 h) to replenish, at least partially, the chromium-depleted region along grain boundaries to avoid intergranular cracking in the presence of acidic contaminants or metastable sulfur oxyanions.

Effect of Environmental Variables. Environmental variables also have an important effect on the intergranular SCC of alloy 600 in high-temperature water. However, very little effort has been made to evaluate systematically the effect of compositional variables in the medium, including pH, concentration of dissolved gases (such as hydrogen and oxygen), and, above all, potential.

Van Rooyen and coworkers (Ref 82–84) found that the environment did not significantly affect crack velocity as measured in slow-strain-rate tests at 345 °C (653 °F) comparing deaerated water, water containing hydrazine (to scavenge oxygen) and morpholine (to adjust the pH to 9), and primary water, which contains H_3BO_3, LiOH, and an overpressure of hydrogen gas. A slightly accelerating effect was noted for primary water with respect to pure water. Using U-bend specimens, they found that crack-initiation time was shorter for the pH-adjusted waters than for pure water. It appears that variations of the pH_{25C} within the range of 7 to 9 did not affect the susceptibility to intergranular SCC.

Effect of Hydrogen Additions. Slow-strain-rates and reverse U-bend tests conducted in pure water and in water containing H_3BO_3 and LiOH showed a definite accelerating effect on SCC susceptibility or rate upon addition of hydrogen to the environment at partial pressures of the order of a few bars, followed by a decrease at higher pressures, as summarized by Smialowska (Ref 94). Tests for a 12-week period on U-bend specimens from nine heats of alloy 600 produced approximately 2% failure in pure deaerated water at 365 °C (690 °F) without hydrogen, but 83% failure in water containing hydrogen at concentrations typical of primary water in pressurized water reactors (PWRs) (Ref 82). Airey (Ref 93) found that the crack-initiation time decreases by a factor of 5 due to the presence of hydrogen in high-temperature (360 °C, or 680 °F) pure water. These initial observations were confirmed for pure water and also for steam at 360 to 400 °C (680–750 °F) (Ref 95, 96). In both environments, the percentage of failed U-bend specimens increased with the partial pressure of hydrogen up to 0.27 MPa (0.04 ksi), but decreased at higher pressures. On the other hand, no intergranular SCC has been observed in alloy 600 exposed to dry hydrogen, even at 35 MPa (5 ksi) at 300 to 400 °C (570–750 °F) (Ref 94). As noted previously, the detrimental effect of hydrogen has also been observed in 0.01 *M* H_3BO_3,+ 0.001 *M* LiOH at 350 °C (660 °F) using slow-strain-rate tests. The percentage of intergranular SCC in the fracture surface increased from approximately 10 to 60% by increasing the hydrogen partial pressure from 0.005 to 0.1 MPa (0.0007–0.015 ksi) (Ref 96, 97). A high hydrogen content was measured in the most strained volume of the specimens (close to the fracture surface) at the highest hydrogen partial pressure, but absorption of hydrogen was also noted at the lowest pressure.

The effect of dissolved oxygen on the intergranular SCC susceptibility of mill-annealed alloy 600 in high-temperature water has been reviewed in detail (Ref 98, 99). The accelerating effect of oxygen is well documented, and it is even more significant in creviced specimens (Ref 100). However, the effect of heat treatment on cracking susceptibility is precisely the opposite of that found in deaerated water. Alloy 600, with a carbon content of approximately 0.05%, exhibited the greatest susceptibility when sensitized at 677 °C (1250 °F). The time required to nucleate cracks decreases with increasing oxygen concentration (from 5 to 100 ppm) in pH 10 ammoniated water at 315 °C (600 °F) (Ref 100). It appears that, depending on the oxygen concentration and, therefore, on the electrode potential, two different mechanisms are operative. At high oxygen levels, the behavior is similar to that observed in high-temperature acidic solutions. In high-temperature (290 °C, or 555 °F) dilute H_2SO_4 solutions, sensitized alloy 600 is extremely susceptible to intergranular SCC at potentials above 0 V (SHE), whereas annealed and annealed plus cold-drawn materials are slightly susceptible (Ref 101, 102). These observations have been confirmed and extended by several authors (Ref 103–105) to a range of environmental conditions in terms of pH and solution composition. Under the same testing conditions, alloy 690 is not susceptible to cracking (Ref 103).

Effect of Electrode Potential. In this context, it is worth noting that the variation of the corrosion potential of alloy 600 as a function of dissolved oxygen concentration and temperature has been studied (Ref 106, 107). Sigmoidal curves showing a potential difference of approximately 600 mV between deaerated (<10 ppb O) and air-saturated (8 ppm O) solutions have been determined at 250 °C (480 °F). As in the case of other passive Fe-Cr-Ni alloys, as well as for platinum, alloy 600 attains a corrosion potential in high-temperature deoxygenated solutions that is close to the reversible value for the hydrogen evolution reaction. Over a wide range of dissolved hydrogen concentrations, the corrosion potential depends on the partial pressure of hydrogen, as expected for the reversible hydrogen electrode, and therefore will decrease (become more negative) with increasing hydrogen overpressure.

The effect of applied potential on the intergranular SCC of as-received alloy 600, as determined by slow-strain-rate tests conducted at 350 °C (660 °F) in solutions containing H_3BO_3 + LiOH at two different partial pressures of hydrogen, is shown in Fig. 19 (Ref 97). A small decrease of potential in the proximity of the corrosion potential measured in the solution with a partial pressure of hydrogen equal to 0.005 MPa (0.0007 ksi) produces a significant increase in the intergranular SCC susceptibility. A further decrease to more cathodic potentials has almost no effect. On the other hand, no intergranular SCC was detected at anodic potentials, at least up to potentials 400 mV higher than the corrosion potential. It is apparent from Fig. 19 that the major effect produced by the increase in the partial pressure of hydrogen is the displacement of the corrosion potential to lower potential values where susceptibility is higher.

Effect of Temperature. Temperature is another environmental variable that strongly affects crack initiation and propagation. Temperature dependence has been represented according to an Arrhenius plot with an apparent activation energy that varies from 125 to 290 kJ/mol within 325 to 365 °C (615–690 °F), according to the results of different authors (Ref 82, 83, 95, 108). A lowest value of 74 kJ/mol has been reported by Totsuka et al. (Ref 109) between 310 and 350 °C (590–660 °F). Putting aside mechanistic interpretations and the wide variability in the data that make such interpretations difficult, it should be noted that the high value of the apparent activation energy indicates that both crack propagation and initiation become very slow processes below 300 °C (570 °F).

Avoiding SCC. The principal remedial measures for mitigating and controlling intergranular SCC of alloy 600 in existing steam generators have been the application of local stress-relief heat treatments to reduce the level of residual stress and the introduction of compressive stresses in the inner tubing surface by shot peening and rotopeening.

SCC of Other Nickel Alloys in High-Temperature Water

Other nickel-base alloys that are susceptible to intergranular SCC in high-temperature deaerated water are precipitation-hardened alloys X-750 and 718 (Ref 110, 111). These alloys are used in water-cooled nuclear reactors in hold-down springs in fuel assemblies, high-strength pins and bolts in reactor cores, and other structural components. A larger number of failures in service have been reported for alloy X-750 than for alloy 718, probably because of the widespread use of alloy X-750 and the fact that it has been more extensively studied.

SCC of Alloy X-750. In several studies on the cracking of alloy X-750 (Ref 112–115), a pronounced effect of heat treatment on intergranular SCC susceptibility has been reported. A heat treatment that causes less susceptibility consists of solution annealing at a relatively high temperature (>1050 °C, or 1920 °F), followed by a single-step aging treatment of approximately 20 h at about 700 °C (1290 °F). This heat treatment, although it improves cracking resistance in deaerated high-temperature water, produces a microstructure that is susceptible to intergranular SCC under oxidizing conditions, as a result of chromium depletion at the grain boundaries. On the other hand, a two-step aging heat treatment, originally adopted from previous applications in the aircraft industry, was found to promote intergranular SCC in both deaerated and aerated water—typical of PWR and boiling water reactor (BWR) environments, respectively.

As shown in Fig. 20, crack velocity of alloy X-750 in oxygenated water depends on the stress-intensity factor, as for other alloys, but a *K*-independent region is not discernible due to the limited number of data points at high *K* values (Ref 116). In this type of oxidizing environment, crack-growth rates are not affected significantly by heat treatment. Under deaerated conditions, even though the crack-growth rates are comparable to those shown in Fig. 20, a lower value of K_{ISCC} is observed (Ref 111). Also, K_{ISCC} is very sensitive to the effect of heat treatment. While work conducted with U-bend specimens suggests that alloy 718 is more resistant than alloy X-750 to intergranular SCC in deoxygenated water at 360 °C (680 °F) (Ref 113), fracture-mechanics tests using wedge-loaded compact tension specimens indicated that K_{ISCC} is lower for alloy 718 (Ref 117). Miglin et al. (Ref 118) reported that the presence of a heterogeneous, banded microstructure containing δ and Laves phases in a commercial heat of alloy 718 gives rise to a lower K_{ISCC} than a homogeneous microstructure.

The significant effect of potential on the intergranular SCC behavior of different heats and heat treatments of alloy X-750 is shown in Fig. 21 (Ref 115). While in the case of heat A the pronounced susceptibility at high potentials is noticeable, the beneficial effect of the single-step heat treatment for heat B is apparent over a wide range of potentials.

Chromium content is also important to the SCC resistance of alloy X-750 in high-purity water containing dissolved hydrogen. As clearly illustrated in Fig. 22, a modified alloy with an increased chromium content of 19% is significantly more resistant to cracking (Ref 119). The effect of chromium, in this regard, is similar to that observed in single-phase Ni-Cr-Fe alloys. A Ni-20Cr-15Fe alloy containing 1.5% Ti, 3.7% Nb, and 3.1% Mo was found to be extremely resistant to intergranular SCC even in oxidizing environments (Ref 120).

SCC in Caustic Environments

Stress-corrosion cracking of solid-solution-strengthened nickel-base alloys in caustic environments has been extensively studied as a result of many service failures experienced in the nuclear power industry. Most of the studies concentrated on alloy 600 because of its extensive use as steam generator tubing in PWRs. Intergranular SCC of this alloy, initiated in the outer surface of the tubing, has been attributed to the formation of highly concentrated alkaline solutions in the annular gap between the tube and the tube sheet and also within the sludge pile in the secondary side of recirculating steam generators.

The threshold stress for the SCC of nickel alloys in high-temperature NaOH solutions has not been determined precisely. However, as illustrated in Fig. 23(a), it appears that at a given NaOH concentration the threshold stress is lower for alloy 600 than it is for alloy 800 (Ref 121, 122). Additionally, the exposure time required to observe cracks of a given length (~100 μm) is far less dependent on stress for alloy 600 than for alloy 800. As reported by Theus (Ref 123), cracking of as-received alloy 600 has been observed at stress levels as low as 20% of the room-temperature yield strength in deaerated 10% NaOH solution at 288 °C (550 °F). The threshold stress for cracking of alloy 690 is significantly higher than those for the other two alloys.

The effect of stress intensity on the crack-growth rate of alloy 600 in NaOH solutions at

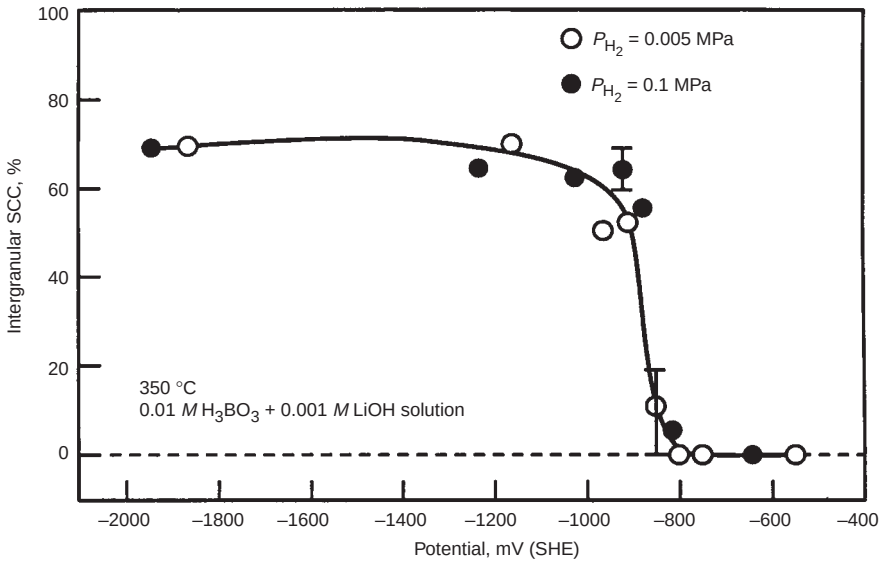


Fig. 19 Percentage of intergranular SCC on the fracture surface of alloy 600 as a function of applied potential in 0.01 *M* H_3BO_3 + 0.001 *M* LiOH solution at 350 °C (660 °F). Corrosion potentials for both hydrogen partial pressures are indicated by vertical bars. The extent of the bars shows the variation of percentage of intergranular SCC for three independent tests. Source: Ref 97

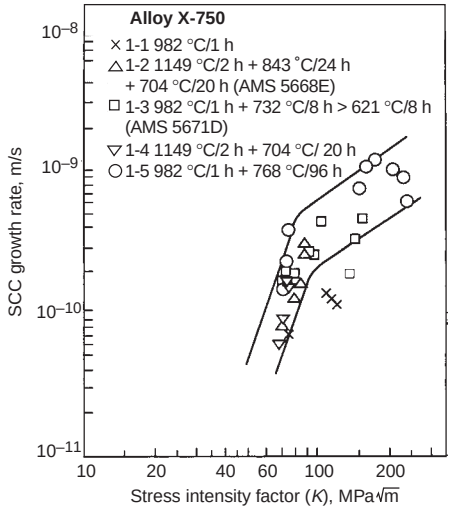


Fig. 20 Effect of stress intensity on crack-growth rates of alloy X-750 in oxygenated pure water at 300 °C (570 °F). Source: Ref 116

350 °C (660 °F) is shown in Fig. 24(a) (Ref 68, 122). It is seen that K_{ISCC} increases slightly with decreasing NaOH concentration. Additionally, heat treatment at 700 °C (1290 °F) increases K_{ISCC} and decreases crack velocity in the plateau region. On the other hand, alloy 690 exhibited a higher K_{ISCC} in the most concentrated NaOH solution than alloy 600 (Fig. 24b) and no crack growth in 4 g/L NaOH. The beneficial effect of heat treatment is noticeable in Fig. 24(b).

Effect of Alloy Composition. As shown in Fig. 23 and 24, alloy composition is extremely important in determining the susceptibility of austenitic Ni-Cr-Fe alloys to intergranular SCC in caustic solutions. For deaerated, concentrated NaOH solutions at 280 to 350 °C (535–660 °F), stainless steels and alloys 800 and 600 are far less resistant to cracking than alloy 690, while nickel 201 (low-carbon nickel) is immune. However, it is not nickel content alone that determines cracking susceptibility. A high chromium content, as in alloy 690, is required to reduce the susceptibility of Ni-Cr-Fe alloys to caustic cracking. In addition, molybdenum-containing alloys, such as alloys C-276 and 825, were found to be susceptible to cracking in concentrated caustic solutions (Ref 124). While transgranular cracking of both alloys was observed in 50% NaOH solution, a higher temperature (>150 °C, or 300 °F) was required for alloy 825, indicating that this alloy is slightly more resistant to cracking in this environment than alloy C-276.

Effect of Heat Treatment. As shown in Fig. 24(a), prolonged heat treatment within the carbide-precipitation temperature range renders alloy 600 more resistant to intergranular SCC in hot caustic solutions (Ref 125–128). The same effect has been observed in the case of alloy 690 (Fig. 24b). However, as pointed out by Crum (Ref 129), the inherently greater SCC resistance of alloy 690 makes the effect of heat treatment less important than in the case of alloy 600. Although there are conflicting results, it seems (Ref 130) that heat treatment at a temperature ranging from 700 to 850 °C (1290–1560 °F) is beneficial for alloy 800. However, Mignone et al. (Ref 131) found that a sensitized material (heat treated at 575 °C, or 1065 °F, for 100 h) is more susceptible to intergranular SCC than the mill-annealed alloy.

Effect of Environmental Variables. In general, the severity of SCC in caustic solutions is a function of concentration and temperature. Nevertheless, according to Fig. 23(b), NaOH concentration has a minor influence on the cracking of alloy 600 in deaerated NaOH

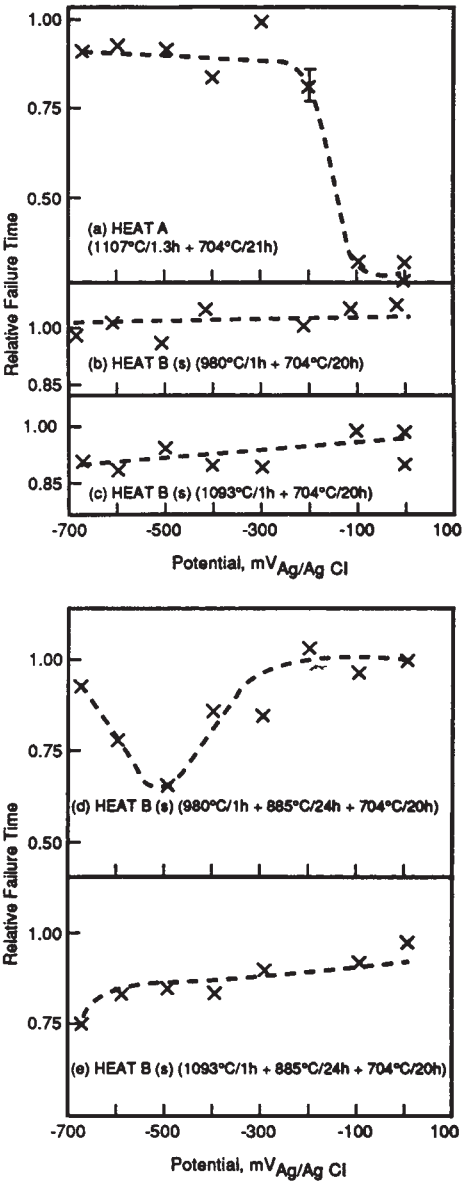


Fig. 21 Effect of potential on relative failure time for alloy X-750 (different heats and thermal treatments) in H_3BO_3 + LiOH solution at 340 °C (645 °F); $\dot{\varepsilon} = 1.5 \times 10^{-6}$/s. Source: Ref 115

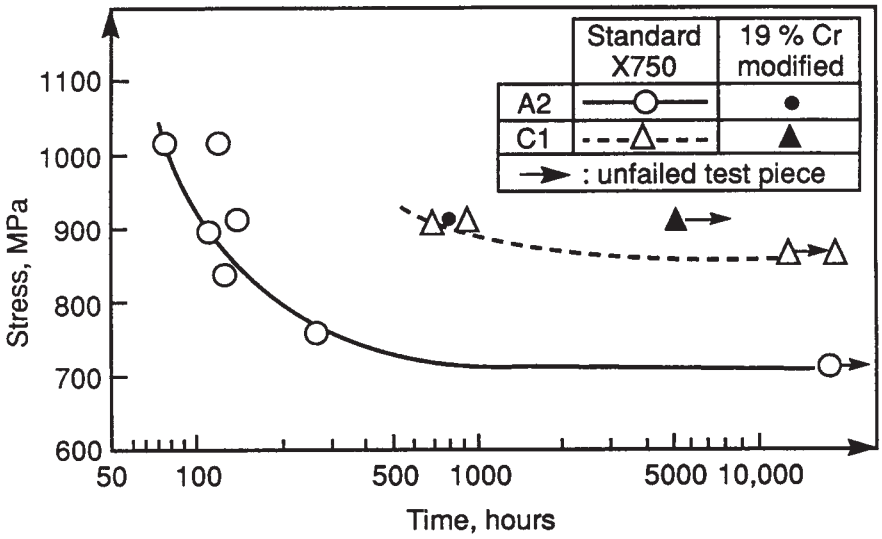


Fig. 22 SCC tests on tensile specimens of standard and modified alloy X-750 in pure water with 25 to 50 mL H_2 (STP)/kg H_2O at 350 °C (660 °F). A2: 885 °C/24 h, AC + 730 °C/8 h; furnace cooled at 14 °C/h down to 620 °C/8 h, AC. C1: 1093 °C/1 h, AC + 704 °C/20 h, AC. STP, standard temperature and pressure. Source: Ref 119

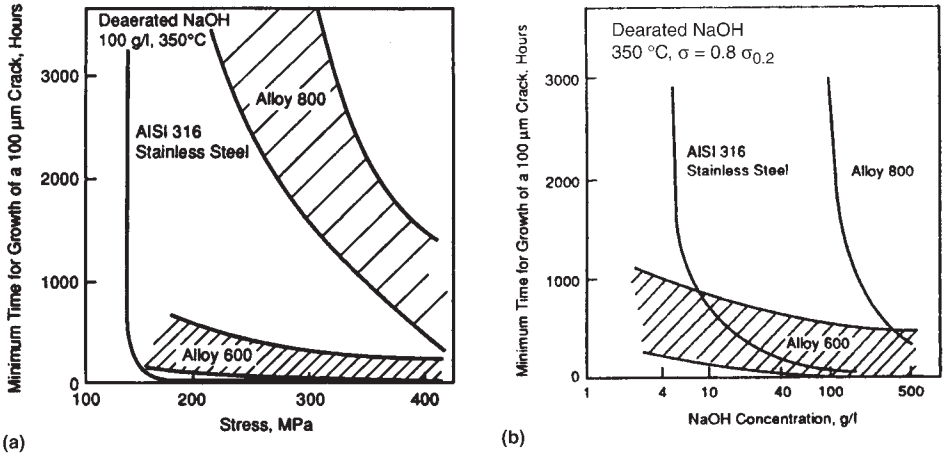


Fig. 23 Comparison of the SCC resistance of alloy 600, alloy 800, and type 316 stainless steel in deaerated caustic soda solutions at 350 °C (660 °F). (a) Effect of stress (NaOH = 100 g/L). (b) Effect of caustic soda concentration ($\sigma \approx 0.8\ \sigma_{0.2}$). Source: Ref 121, 122

solutions at 350 °C (660 °F). On the other hand, the susceptibility to cracking of alloys 800 and 690 seems to be more dependent on NaOH concentration. The effect of temperature on the intergranular SCC of alloy 600 is apparently not as strong as it is in pure water. Some authors (Ref 121, 132) have observed only a minor temperature effect in deaerated, concentrated NaOH solutions at 284 to 350 °C (543–660 °F). However, by comparing results obtained at 316 and 343 °C (600 and 650 °F), Airey (Ref 93) found temperature to have an accelerating effect in 10% NaOH solutions for both mill-annealed and thermally treated alloy 600.

Effect of Electrode Potential. Potential is a dominant factor in the intergranular SCC susceptibility of alloy 600 in hot caustic solutions. Many authors (Ref 133–137) have conducted potentiostatic SCC tests in concentrated NaOH solutions to identify potential ranges over which cracking occurs. With minor variations, most authors have observed intergranular SCC above 300 °C (570 °F) within an anodic potential region that extends from 80 to 250 mV with respect to the open-circuit potential (corrosion-potential), as shown in Fig. 25 (Ref 135). This potential range corresponds to the active-passive transition observed in the anodic polarization curve. At even higher potentials, within the passive region, no cracking has been observed, whereas at potentials near the corrosion potential, extended intergranular attack has been detected (Ref 137, 138). Several anions, such as SO_4^{2-}, CO_3^{2-}, and PO_4^{3-}, increase SCC susceptibility, whereas SO_3^{2-} acts as an inhibitor (Ref 137).

Most workers who have conducted potentiostatic tests in solutions containing approximately 10% NaOH at about 320 °C (610 °F) (Ref 126, 133–137) have found that prolonged heat treatment at the sensitization temperature (i.e., 620 °C for 18 h or 700 °C for 15–24 h) significantly improves cracking resistance at the potential of maximum susceptibility (~90–150 mV anodic with respect to the open circuit potential). At lower temperatures (140 °C, or 285 °F) in more concentrated NaOH solutions, cracking behavior is more complex (Ref 128, 139). Regions of intergranular SCC have been identified over most of the range of primary passivity, whereas transgranular SCC has been observed at the open-circuit potential and within the secondary passivation region. The beneficial effect of heat treatment on intergranular SCC was also confirmed at this high NaOH concentration.

The effect of potential on the cracking behavior of alloys 800 and 690 has been studied less extensively. Mill-annealed alloy 800 seems to be more resistant to intergranular SCC than alloy 600 at potentials close to the active-passive transition in 50% NaOH solution at 140 °C (285 °F) (Ref 139). However, it is more susceptible to SCC in the secondary passivation region. The addition of SiO_2 to 50% NaOH solution at 140 °C (285 °F) seems to inhibit cracking of alloy 600, but does not affect the tendency to intergranular cracking of alloy 800 (Ref 140). At higher temperatures (300 °C, or 570 °F) in a more dilute solution (deaerated 10% NaOH), no cracking of alloy 800 was found at the open-circuit potential, but transgranular SCC was observed at anodic potentials ranging from 70 to 300 mV with respect to the open-circuit potential. Maximum susceptibility was observed at 200 to 250 mV (Ref 134). However, intergranular SCC at a

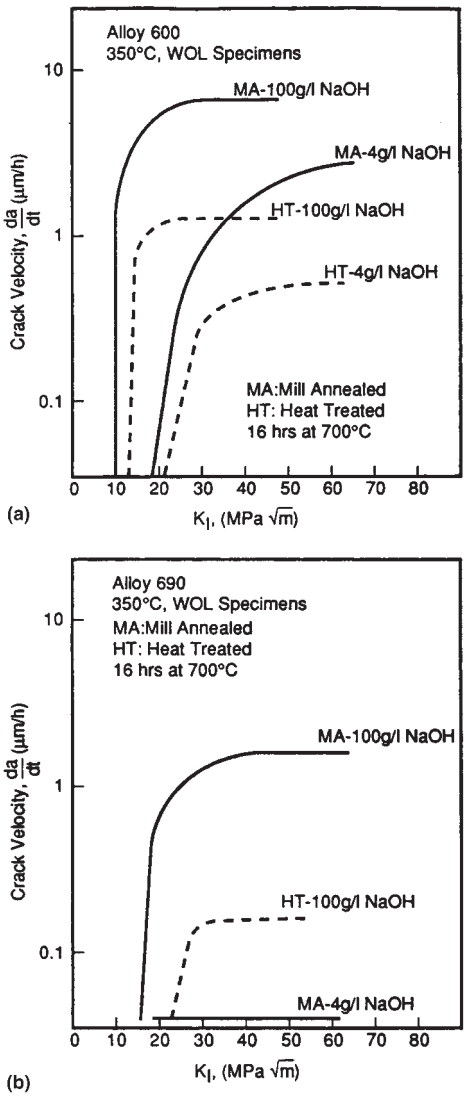


Fig. 24 Effect of stress intensity on crack velocity in deaerated NaOH at 350 °C (660 °F). WOL, wedge opening loaded. MA, mill annealed; HT, heat treated 16 h at 700 °C. (a) Alloy 600. (b) Alloy 690. Source: Ref 68

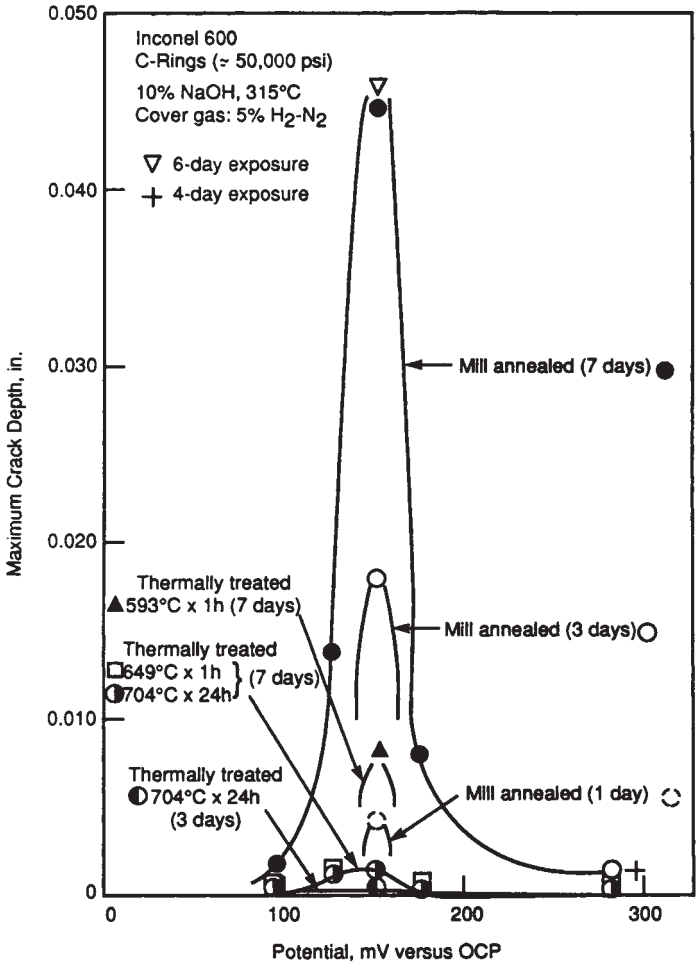


Fig. 25 Variation of maximum SCC depth with specimen potential for mill-annealed and thermally treated alloy 600 exposed to 10% NaOH at 315 °C (600 °F). OCP, open-circuit potential. Source: Ref 135

potential of 60 mV anodic with respect to the open-circuit potential has been reported (Ref 130) in a more concentrated solution (15% NaOH). Cracking was also observed at the open-circuit potential. For alloy 690, few studies on the effect of potential have been reported. Very short, intergranular cracks (>130 μm) were detected in annealed alloy 690 using the slow-strain-rate technique in 10% NaOH solution at 316 °C (600 °F) under an applied potential of 150 mV above the open-circuit potential (Ref 129). Under the same conditions, alloy 600 exhibited crack depths close to 900 μm. Sarver et al. (Ref 141) found that the cracking range for alloy 690 is narrower than that for alloy 600 in 10% NaOH solution at 288 °C (550 °F). Tests were conducted at potentials ranging from 150 to 250 mV above the open-circuit potential, but intergranular cracks were detected only at 170 mV.

In summary, all the austenitic Ni-Cr-Fe alloys are susceptible to SCC in hot, concentrated caustic solutions. Alloy 690 is probably the most resistant of the commercial alloys, but only pure nickel seems to be immune to cracking. Most of these alloys crack intergranularly; however, alloys with a lower nickel content, such as alloy 800, frequently exhibit transgranular cracking.

Cracking in Other Environments

Liquid-Metal Embrittlement. Although liquid-metal embrittlement does not fall under the restricted category of SCC, a brief summary of the liquid metals that have been shown to embrittle nickel and its alloys is presented here. Shunk and Warke (Ref 142) summarized the combinations of metal-embrittler couples for various metals discussed in literature up to 1974. Nickel and its alloys were shown to be embrittled by mercury, lithium, lead, and tin. However, Johnson et al. (Ref 143) examined several commercial Ni-Cr-Mo-Fe alloys as well as a Co-Cr-Mo alloy and found that tin did not wet the alloys, while lead and zinc wetted but did not embrittle the alloys. Molten zinc reacted profusely with the nickel-base alloys and formed brittle corrosion products. Sadigh (Ref 144) also reported that molten zinc or its vapor did not cause cracking of commercial nickel-base alloys such as 825, C-276, 400, 600, 800, and 200, but did cause brittle nickel-zinc corrosion products. He also confirmed the well-known susceptibility of type 304 stainless steel to crack rapidly in molten zinc. An intermediate nickel-containing stainless steel (alloy 20Cb-3) also showed a slight susceptibility to cracking in molten zinc. Kelly (Ref 145) reported that molten calcium that occurs in the processing of ferrites for the electronic industry caused cracking of retorts built of alloy RA 330 (36Ni-19Cr-1.1Si-0.05C). He also reported cracking of some nickel-base alloys in molten lead, lithium, and probably samarium, neodymium, and promethium. Hemsworth et al. (Ref 146) have reported cracking of type 316 stainless steel in molten tellurium, particularly when tellurium is mixed with cerium. The most systematic investigation by far has been conducted in mercury cracking of alloy 400 (Ni-30Cu) (Ref 147, 148).

Organic Environments. Takizawa and Sekine (Ref 149) reported cracking of a nickel-molybdenum alloy (alloy B-2) in an organic environment of unknown composition that contained small amounts of sulfuric acid and water. Intergranular cracking was found near welds on alloys whose compositions tended to form Ni_4Mo phase. Laboratory tests on the plant solution at 130 °C (265 °F) of samples that were aged at 750 °C (1380 °F) for various times ranging from 1 to 30 min also showed susceptibility to intergranular cracking.

Hydrogen Embrittlement

Embrittlement due to hydrogen in nickel-base alloys can manifest itself in a variety of ways, including embrittlement due to absorbed atomic hydrogen either from a gaseous or an aqueous source, hydrogen reaction with carbides or other reactive phases, and pressure buildup due to hydrogen gas formation inside defects. Of these, hydrogen embrittlement due to absorption of hydrogen from an aqueous phase is discussed here, because it is closely allied to many SCC processes and has been postulated as a mechanism for SCC in some cases. Nickel-base alloys embrittle in hydrogen, although not to the same extent as iron-base alloys. This is illustrated in Fig. 26 (Ref 150) for a series of nickel-copper and nickel-iron alloys. As the iron content of the nickel alloys increases, the tendency toward hydrogen embrittlement decreases until sufficient iron is added to change the alloy from a face-centered cubic (fcc) to a body-centered cubic (bcc) crystal structure.

Hydrogen embrittlement in nickel-base alloys is predominately intergranular, although some embrittlement has also been observed to be by dimpled rupture (Ref 151). In contrast, hydrogen embrittlement in iron-base alloys is predominantly transgranular, although in some cases cracking has occurred along prior-austenitic grain boundaries. The addition of copper to nickel also decreases the tendency toward hydrogen embrittlement. Pure copper has not been shown to be embrittled by hydrogen. The three most important environmental variables affecting hydrogen embrittlement are (1) hydrogen fugacity, as dictated by the cathodic current density in aqueous systems, (2) recombination poisons such as sulfur, and (3) temperature. The metallurgical variables that control embrittlement include (1) alloy composition (e.g., iron content), (2) deformation mode, as controlled by stacking-fault energy and coherent precipitation, (3) segregation of metalloid elements to the grain boundaries, (4) grain size and orientation, and (5) strength level.

Effect of Environmental Variables

Effect of Hydrogen Fugacity. Hydrogen fugacity in aqueous systems is controlled by the cathodic current density, which in turn can be controlled by factors such as galvanic coupling between nickel-base alloy and carbon steel components and the potential-pH conditions prevailing in defects such as cracks, pits, or crevices. Galvanic effects often occur, for example, in oil and gas production operations when a steel liner comes in contact with high-nickel tubing and in offshore structures when nickel alloy bolts come in contact with steel structural elements. The effect of cathodic current density on time to failure is shown for two nickel-base alloys in Fig. 27 (Ref 152). Its effect on stage 2 (stress-intensity independent) crack-growth rate for alloy C-276 is shown in Fig. 28 (Ref 153).

Effect of Recombination Poisons. Minor concentrations of impurities in the environment or alloy can greatly increase the entry of hydrogen into the metal by preventing recombination of adsorbed hydrogen atoms, resulting in the evolution of hydrogen gas. A rather extensive review of the recombination poisons was performed by McCright (Ref 154). These include sulfur, phosphorus, arsenic, antimony, and tin. In sour-gas environments, H_2S has been shown (Ref 37) to increase hydrogen permeation (related to the concentration of adsorbed hydrogen) in steels. Some of these elements are also present as impurities in alloys and can influence hydrogen entry into the metal. However, these alloyed impurities may also influence embrittlement directly by reducing the grain-boundary cohesion synergistically with hydrogen. The effect of these internal impurity elements is discussed in the section on metallurgical variables.

The effect of temperature on hydrogen embrittlement depends on temperature range, alloy composition, and the environmental conditions under which hydrogen entry takes place. Wilcox and Smith (Ref 155) examined the delayed failure of prestrained, hydrogen-charged nickel between –50 and 0 °C (–58 and 32 °F) and found that increasing the temperature decreased the time to failure (increased embrittlement), with an activation energy of 6.8 kcal/mol. Chandler and Walter (Ref

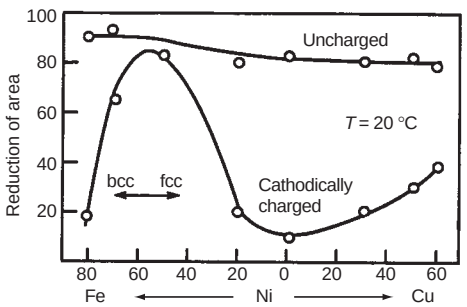


Fig. 26 Fracture behavior of cathodically charged nickel containing iron or copper. Source: Ref 150

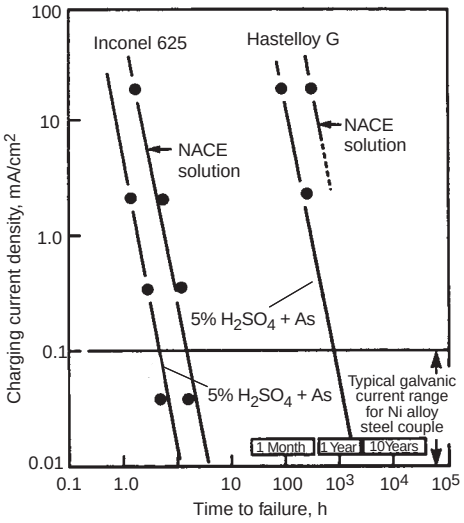


Fig. 27 Effect of test environment and charging current density on the failure time of stressed C-ring specimens of alloy 625 (59% cold rolled + 500 °C for 50 h) and alloy G (59% cold rolled + 260 °C for 250 h). Room temperature; 100% yield stress. Source: 152

156), however, showed that when electroformed nickel was tested in high-pressure gaseous hydrogen over a wider temperature range (–73 to 170 °C, or –100 to 340 °F), embrittlement initially increased with temperature up to 24 °C (75 °F), but decreased thereafter. Most investigations of hydrogen ernbrittlement at temperatures close to 0 °C (32 °F) and above have found that increasing the temperature decreases embrittlement. This is illustrated in Fig. 29 and 30. In the case of the Ni-Cr-Mo alloy (C-276), embrittlement in a NaCl + H_2S solution occurs only upon cathodic polarization, either by galvanic coupling to carbon steel (Fig. 29) or by applying a cathodic current. The embrittling tendency decreases at temperatures above approximately 120 °C (250 °F) (Ref 41). Similar results have been observed for other nickel-base alloys in this type of H_2S test (Ref 30, 40). In the case of alloy 400 (Fig. 30), the loss in ductility (percentage of reduction in area of a tensile sample) from air to hydrogen increases initially with temperature and then decreases above 20 °C (68 °F). Some exceptions to the above trends include the delayed failure of alloy K-500 (Ni-30Cu-3Al), where embrittlement due to precharged hydrogen has been found to increase with temperature even at temperatures as high as 177 °C (350 °F) (Ref 157), and in hydrogen-purged high-purity water, where cracking of alloy 600 has been shown to increase with temperatures of up to 350 °C (660 °F) (Ref 158).

Effect of Metallurgical Variables

Impurity segregation and its associated effects of grain size have been examined for a number of alloys and for pure nickel. Impurities include sulfur, phosphorus, antimony, tin, and carbon. In pure nickel, sulfur segregation to

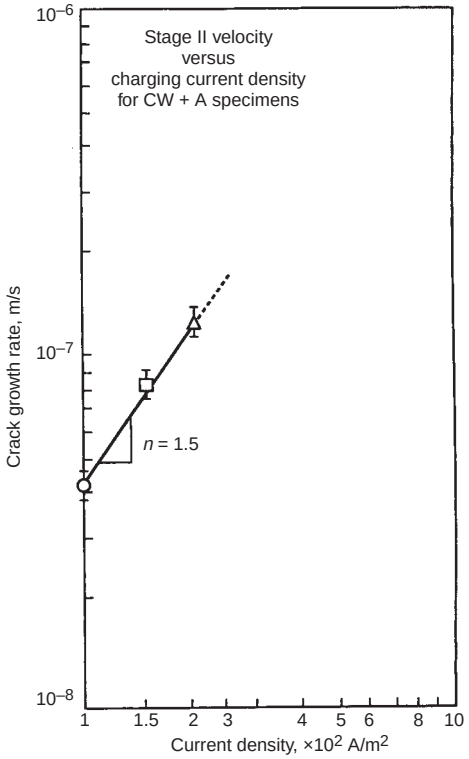


Fig. 28 Stage 2 (stress-intensity independent) crack velocity as a function of charging current density for cold-worked and aged specimens of alloy C-276 at room temperature. Source: Ref 153

the grain boundaries is the dominant factor (Ref 2). This is illustrated in Fig. 31 (Ref 159). Intergranular fracture is observed when the grain-boundary concentration of sulfur exceeds approximately 0.1 monolayers at an applied cathodic potential of –0.3 V (SHE). However, sulfur can have an interactive effect with hydrogen fugacity; at more negative cathodic potentials (greater hydrogen charging current or fugacity), less sulfur is needed at grain boundaries in order for intergranular cracking to occur. Jones and Bruemmer (Ref 2) report a very high tendency for sulfur segregation to grain boundaries, such that even 1 ppm bulk concentration can result in 10% monolayer concentration.

Phosphorus segregation has been reported to be more of a problem in nickel-base alloys, although not all the reported results agree on this point (Ref 160–168). Unlike the case of pure nickel, however, increased embrittlement cannot be attributed solely to grain-boundary segregation; other metallurgical changes can occur simultaneously. For example, Berkowitz and Kane (Ref 160) showed that hydrogen embrittlement and grain-boundary phosphorus concentration of a Ni-Cr-Mo-W alloy (alloy C-276) increased with low-temperature aging at 500 °C (930 °F). A low-phosphorus alloy exhibited less sensitivity toward aging-induced increase in hydrogen embrittlement (Table 16).

In contrast, Asphahani (Ref 161) tested the same Ni-Cr-Mo-W alloys, varying in bulk phosphorus concentration from 0.003 to 0.086%, and showed no link between bulk phosphorus increase and the tendency toward hydrogen embrittlement. However, he used a much greater hydrogen fugacity than Berkowitz and Kane (cathodic current density of 40 mA/cm^2). It must be noted that an ordering reaction of the type Ni_2Cr occurs in the same temperature region in these alloys. Ladna and Kargol (Ref 162), using a Ni-22Cr-6Mo-20Fe alloy (alloy G), which does not undergo ordering, showed that only a small increase in crack growth (in a ductile mode) occurred due to aging at 500 °C (930 °F). Hence, increased crack growth due to low-temperature aging in these alloys cannot be attributed to phosphorus segregation alone. The effect of phosphorus versus ordering in this alloy system has been a matter of considerable controversy, because the prescription for aging-enhanced hydrogen embrittlement depends heavily on which factor is considered important.

Berkowitz et al. (Ref 163) and Kurkela et al. (Ref 169) further examined this issue by testing pure Ni_2Cr after various aging treatments to produce various degrees of long-range ordering. They showed that the alloy was most susceptible to hydrogen embrittlement in the completely disordered and completely ordered conditions and that susceptibility decreased as the percent ordering (calculated from aging time) increased (Fig. 32). On the other hand, Lehman et al. (Ref 164) tested Ni_2Cr with various phosphorus contents and showed that high

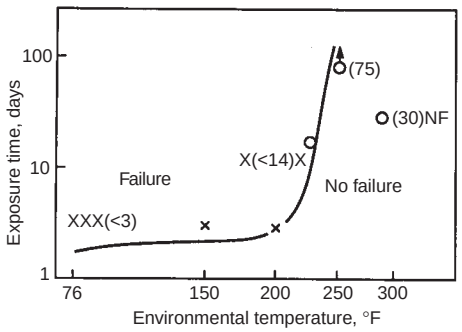


Fig. 29 Effect of environmental temperature on hydrogen embrittlement of alloy C-276. Environment: 4% NaCl + 0.5% CH_3COOH + H_2S (1 atm), coupled to carbon steel. Stressed to 90% yield. Alloy aged at 500 °C (930 °F) for 100 h. Source: Ref 41

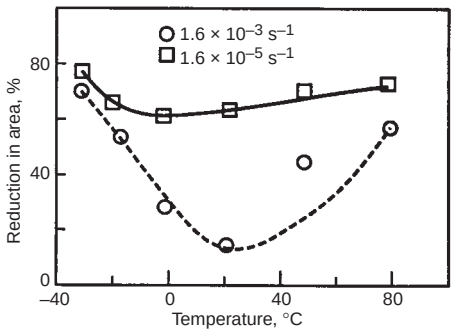


Fig. 30 Reduction in area at fracture of alloy 400 tested in the presence of hydrogen. Source: Ref 148

levels of phosphorus increased ordering kinetics significantly. From a practical perspective, it is difficult to reach bulk phosphorus levels below approximately 3 ppm economically, and most commercial alloys contain approximately 10 ppm phosphorus. Ordering reactions in the nickel-base alloys can be prevented by increasing the iron content above approximately 10%; however, some corrosion resistance will be sacrificed because alloys containing that amount of iron cannot sustain as much molybdenum and tungsten.

Cornet et al. (Ref 165) showed that addition of phosphorus to a high-purity Ni-16Cr-8Fe alloy (residual phosphorus level was 0.004%) may actually lower hydrogen embrittlement susceptibility. Their investigation was carried out on alloys that were solution annealed at 1100 °C (2010 °F) but not aged. In a more recent investigation (Ref 166), Ni-20Cr alloy was doped with 0.015% bulk P and tested under cathodic hydrogen charging conditions. The authors contend that the effect of phosphorus is more complex than portrayed by previous reports. Phosphorus can be detrimental if its segregation to the grain boundaries occurs without coprecipitation of carbides; it can be beneficial at temperatures that allow carbide precipitation. Other species shown to be detrimental to hydrogen-embrittlement resistance of nickel-base alloys include antimony and tin (Ref 165, 168, 170).

Deformation mode in nickel-base alloys depends on stacking-fault energy and precipitation of second phases. Stacking faults are created in fcc crystal structures by alteration of the sequence of the stacked layers of atoms (Ref 171). Stacking faults are enclosed by partial dislocations—the type of dislocation depending on the type of stacking fault as well as the crystal structure. Because stacking faults are internal surfaces, energy is required to alter their area. The lower the stacking-fault energy, the larger the area of the stacking fault or the higher the stacking-fault probability. Because of energy constraints, dislocations that contain stacking faults must move along a given slip plane (the plane along which shear deformation occurs). This type of deformation, termed *planar deformation*, creates large inhomogeneities in slip as well as great stress concentrations at obstacles such as grain boundaries. It has been shown that lower stacking-fault energies can lead to greater hydrogen embrittlement and SCC (Ref 172). This relationship becomes especially obvious in nickel-base alloys as cobalt concentration becomes progressively larger. Cobalt reduces the stacking-fault energy of nickel, and the hydrogen ernbrittlement resistance of nickel-cobalt alloys decreases with increasing cobalt content. However, stacking-fault energy is not the only factor affecting hydrogen embrittlement; the addition of iron decreases stacking-fault energy, but increases resistance to hydrogen embrittlement.

As mentioned before, short- and long-range ordering reactions can also cause the planar deformation mode. In the case of short-range ordering, plastic deformation by dislocation motion tends to disorder the material, thus raising the energy. This in turn tends to force dislocation motion along certain planes. In the case of long-range ordering, several mechanisms can come into play to force planar deformation. For example, in alloy C-276 long-range ordering of the type Ni_2Cr forces the alloy to deform by twinning. The effect of low-temperature aging on hydrogen-induced crack-growth rate in alloy C-276 is shown in Fig. 33 (Ref 173). Two stages of increase in crack growth can be seen: one at time periods of a few minutes to 100 h, and the second after 500 h or more of aging. The first increase has been attributed to a combination of phosphorus segregation and short-range ordering and the second to long-range ordering.

Coherent precipitates such as γ' and γ'' also induce planar deformation, as mentioned earlier. The effects of coherent precipitation on hydrogen ernbrittlement of alloys K-500 and X-750 have been experienced in oil and gas production processes (Ref 157, 174–176). For example, in offshore platforms, alloy K-500 bolts, which were threaded after precipitation hardening, failed when cathodically coupled to carbon steel (Ref 175). Failure analysis suggested that hydrogen embrittlement was the failure mechanism and that threading after

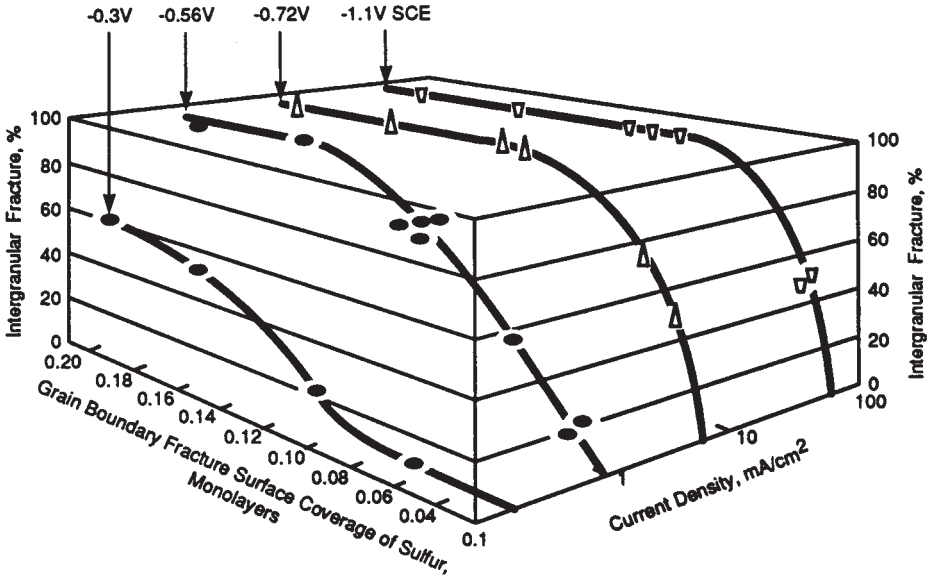


Fig. 31 Interrelationships among cathodic current density, grain-boundary sulfur composition, and fracture mode in straining electrode tests of nickel. Source: Ref 159

Table 16 Effect of bulk phosphorus content on hydrogen embrittlement in a chloride + H_2S environment

Condition	Aging temperature °C	Aging temperature °F	Aging time, h	Time to failure(a), days 0.023% P	Time to failure(a), days 0.002% P
50% cold-rolled sheet	Unaged	Unaged	…	>36	>36
	204	400	200	13	>36
	371	700	20	<3	9
	482	900	0.16	<3	>36
	482	900	900	<3	<3
60% cold-rolled sheet	Unaged	Unaged	…	>36	>36
	204	400	200	<3	>36
	371	700	20	<3	>36
	482	900	0.016	<3	>36
	482	900	900	<3	<3

Bent sheet samples coupled to carbon steel tested at room temperature in a solution of 5% NaCl + 0.5% CH_3COOH + 1 atm H_2S (saturated at RT). (a) > indicates no cracking in the stated time period; < indicates cracking. Source: Ref 160

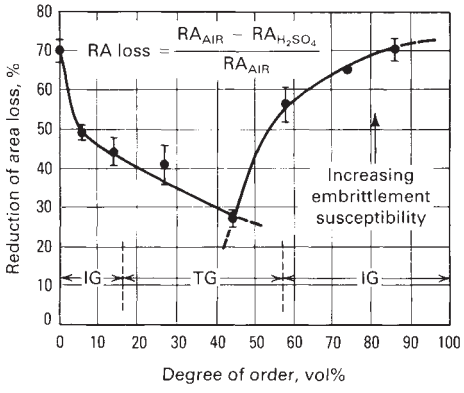


Fig. 32 Effect of the degree of order on the embrittlement susceptibility of Ni_2Cr. Regions of intergranular (IG) and ductile transgranular fracture (TG) are shown. Source: Ref 163

precipitation hardening caused the hardness at the thread roots to exceed 35 HRC. It was recommended that the bolts be solution annealed after threading and then hardened to a maximum of 35 HRC. However, even after being treated in accordance with the recommendations, and with a hardness of 25 HRC, the bolts still failed in service. This was shown (Ref 176) to be caused by polarization to a more negative potential, which resulted from the bolts being coupled to steel cathodically protected by aluminum anodes. Results of laboratory slow-strain-rate tests that reproduced this type of cracking are shown in Table 17. While these cracking occurrences have been at ambient temperatures, hydrogen embrittlement of alloy K-500 and other precipitation-hardenable alloys, such as alloy 925, has been shown to occur at temperatures up to 125 °C (257 °F) (Ref 175) in $MgCl_2$ brines under cathodic polarization.

Another example of failure in oil and gas production is cracking of tubing hangers made of alloy X-750, a γ′ precipitation-hardened alloy, which was shown to be related to hydrogen embrittlement in combination with hardnesses above 35 HRC (Ref 177). Hydrogen embrittlement of alloy 718, a γ″-type precipitation-hardenable alloy has occurred in high-pressure hydrogen gas when the alloy was double-aged to produce hardnesses above 40 HRC (Ref 178). However, hydrogen embrittlement in H_2S-containing solutions has not generally been observed in this alloy, with the exception of a result from slow-strain-rate testing (Ref 179). Precipitation-hardenable alloys with higher molybdenum contents, such as alloys 625 Plus and 725, have been shown to be resistant to hydrogen embrittlement, even when subjected to a combination of precipitation-hardening and low-temperature aging treatments (Ref 180).

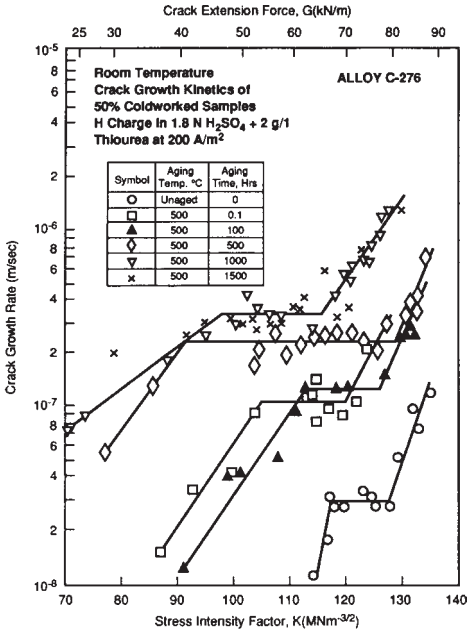


Fig. 33 Effect of stress intensity on crack-growth rate of alloy C-276 as a function of aging time at 500 °C (930 °F). Source: Ref 173

SCC Testing Methods

This section summarizes the test techniques that are used to study SCC and hydrogen embrittlement of nickel-base alloys. A more detailed discussion of SCC test methods can be found in the article "Evaluation of Stress-Corrosion Cracking" in *Corrosion*, Volume 13 of the *ASM Handbook*.

Environmental Conditions. While the environmental conditions are specific to the aims of a particular study, certain general considerations apply. In SCC tests, it is desirable to monitor the open-circuit or corrosion potential of the stressed sample and, if possible, test under a variety of applied potentials. Small variations in potential that may be produced by relatively small differences in deaeration or in experimental arrangements (e.g., galvanic contacts with test apparatus) can substantially affect the measured cracking susceptibility of nickel-base alloys (Ref 53). However, when monitoring or control of the potential is not possible, concentrations of oxidizing species must be maintained at relatively constant levels. For example, oxygen is detrimental in many SCC environments because its presence generally increases the corrosion potential. The oxygen concentration in a solution can be affected by a variety of factors, including condenser design, temperature, chloride concentration, and any unintentional deaeration performed prior to or during the test (Ref 23).

Constant-deflection tests are the most common type of SCC test and use a variety of configurations: U-bend, C-ring, two-point bend, four-point bend, and so on. Constant-deflection tests do not require elaborate loading apparatus and can be adapted to a wide range of product forms. The C-ring test has been used widely in the oil and gas industry for testing seamless tubular products. One of the most important variables in this test is surface condition. The usual procedure is to grind the outer surface, which will be stressed in tension to a given finish—typically 120 grit, wet ground. However, grinding or machining may remove any surface chromium depletion, thus affecting SCC evaluation of a given alloy product (Ref 181). Removing oxide films, altering the rest potential, or introducing surface stresses by grinding may affect crack initiation.

In some cases, a crevice is formed at the apex of the stressed sample by spot welding another strip of the same alloy onto the stressed sample. In elemental sulfur environments, it has been shown that cracking occurs under crevices formed either intentionally or unintentionally. Another important factor in constant-deflection tests is the assumed stress level. Typically, samples are stressed to a given percent of the yield strength. In the case of tubular products, yield strength in the transverse direction is difficult to measure and is usually assumed to be about 90% of the longitudinal yield strength. In the case of other types of products, it is important to specify the direction of stress relative to the rolling direction. It has been shown (Ref 182) that the hydrogen embrittlement tendency of highly cold-worked nickel-base alloys is more pronounced when a sample is stressed in the transverse direction, which is the usual stressing direction.

Constant-Load Tests. Some of the earliest testing of nickel-base alloys was performed on wire samples using constant load (Ref 19). Wire samples offer the advantage of simplicity in experimental design, but they cannot be used to examine the behavior of the products used in most applications (sheet, plate, tubing, and bar). A commonly used constant-load test is the NACE TM-01-77 tensile test (Ref 183). In this test, a cylindrical sample, usually 6.3 mm (0.25 in.) in gage diameter is spring loaded in a proof-ring apparatus and the time to failure monitored. Because samples are machined, the effect of surface condition cannot be tested. An advantage of the constant-load test over the constant-deflection test is that cracking is accelerated once it is initiated, because the cross section available to sustain the load decreases and the stress level increases.

Precracked samples offer the advantage of separating crack-initiation processes from crack growth, and they usually allow more accelerated testing than do smooth samples. Because of the well-defined stress conditions at the crack tip, precracked samples are more amenable to modeling than smooth samples, in which multiple cracking can occur. The types

Table 17 Results of slow-strain-rate tests on samples from 50 mm (2 in.) diam alloy K-500 bolts

Environment	Time to failure, h	Elongation, %	Reduction in in area, %	Fracture type
Air	36.3	24.6	36	Ductile
Seawater, no anode	39.8	27.4	42	Ductile
Seawater, steel anode, –620 mV (AgCl)	28.0	19.0	45	Ductile
Seawater, steel anode precoupled 8 days, –620 mV (AgCl)	30.0	21.0	46	Ductile
Seawater, aluminum anode, –900 mV (AgCl)	6.1	4.2	8	Intergranular
Seawater, aluminum anode precoupled 8 days, –900 mV (AgCl)	4.1	3.5	7	Intergranular
Seawater, potentiostat, –800 mV (AgCl)	5.8	4.0	…	Intergranular

Hardness of precipitation-hardened samples: 25 HRC. Source: Ref 176

of samples that have been used in testing nickel-base alloys include compact tension, wedge-opening-loaded (WOL), modified WOL (bolt-loaded), double-cantilever-beam, and double torsion samples. Selection of a particular type of sample depends on the particular test apparatus, economics, the availability of suitably sized material, and the type of information sought.

Because most corrosion-resistant nickel-base alloys exhibit high fracture toughness (K_{Ic} > 1000 MPa$\sqrt{m}$, or 910 ksi$\sqrt{in.}$) and relatively low yield strengths (300–1000 MPa, or 43.5–145 ksi), the thickness requirements for plane-strain conditions over a wide range of crack-growth rates may not be met by the material sizes that are available. In many tests, significant crack branching occurs, which can sometimes be overcome by using side grooves. The double torsion test was initially developed to test ceramic materials (Ref 153, 173), but has also been used to study nickel-base alloys. Although the test is not well established, its advantages include constant stress intensity at constant applied load and ease of monitoring crack-growth rate through load changes.

Slow-strain-rate testing or constant-extension-rate testing involves slow straining of a tensile sample to failure while it is exposed to the environment of interest. The susceptibility to embrittlement depends on the strain rate, but the optimal strain rate for nickel-base alloys appears to be lower for SCC than for hydrogen embrittlement. For example, Ueda et al. (Ref 53) showed that the highest embrittlement for a Fe-21Cr-31Ni-4Mo-1.5Cu alloy in a 25% NaCl + 0.5% CH_3COOH + 1 MPa (0.15 ksi) H_2S + 1 MPa (0.15 ksi) CO_2 environment at 150 °C (300 °F) occurred at a nominal strain rate of 4×10^{-6}/s. Most testing in H_2S, chloride, and caustic environments has used strain rates ranging from 1×10^{-6}/s to 4×10^{-6}/s. In high-purity water, strain rates of 1×10^{-7}/s have been used (Ref 184), although some evidence indicates that even this strain rate is not low enough to cause cracking. Introduction of cold work in the gage section of tensile specimens overcomes this problem (Ref 85). For hydrogen embrittlement, much higher strain rates (10^{-4}/s to 10^{-2}/s) may be used (Ref 165, 185).

ACKNOWLEDGMENT

This article was adapted from N. Sridhar and G. Cragnolino, Stress-Corrosion Cracking of Nickel-Base Alloys, *Stress-Corrosion Cracking: Materials Performance and Evaluation*, R.H. Jones, Ed., ASM International, 1992, p 131–179.

REFERENCES

1. R.W. Staehle, Understanding "Situation Dependent Strength:" A Fundamental Objective in Assessing the History of Stress Corrosion Cracking, *Environment Induced Cracking of Metals*, R.P. Gangloff and M.B. Ives, Ed., National Association of Corrosion Engineers, 1990, p 561
2. R.H. Jones and S.M. Bruemmer, Environment-Induced Crack Growth Processes in Ni-Base Alloys, *Environment Induced Cracking of Metals*, R.P. Gangloff and M.B. Ives, Ed., National Association of Corrosion Engineers, 1990, p 287
3. A.I. Asphahani, Corrosion of Nickel-Base Alloys, *Corrosion*, Vol 13, 19th ed., *Metals Handbook*, ASM International, 1987
4. W.Z Freind, *Corrosion of Nickel and Ni-Base Alloys*, John Wiley & Sons, 1980
5. W. Betteridge, *Nickel and Its Alloys*, Ellis Horwood Ltd., 1984
6. G.S. Was, H.H. Tischner, and R.M. Latanision, The Influence of Thermal Treatment on the Chemistry and Structure of Grain Boundaries in Inconel 600, *Metall. Trans. A*, Vol 12, 1981, p 1397
7. R.L. Dreshfield, The Effect of Refractory Elements on the Stability of Complex Carbides in Ni-Base Superalloys, *Trans. ASM*, Vol 51, 1968, p 352
8. C.L. Briant, C.S. O'Toole, and E.L. Hall, The Effect of Microstructure on the Corrosion and Stress Corrosion Cracking of Alloy 600 in Acidic and Neutral Environments, *Corrosion*, Vol 42, 1986, p 15
9. A. Borello, S. Casadio, A. Saltelli, and G. Scibona, Susceptibility to the Intergranular Corrosion of Alloy 800, *Corrosion*, Vol 37, 1981, p 498
10. E.L. Raymond, Mechanisms of Sensitization and Stabilization of Incoloy Ni-Fe-Cr Alloy 825, *Corrosion*, Vol 24, 1968, p 180
11. M. Raghavan, B.J. Berkowitz, and J.C. Scanlon, Electron Microscopic Analysis of Heterogeneous Precipitates in Hastelloy Alloy C-276, *Metall. Trans. A*, Vol 13, 1982, p 979
12. C.R. Brooks, J.E. Spruiell, and E.E. Stansbury, Physical Metallurgy of Nickel-Molybdenum Alloys, *Int. Met. Rev.*, Vol 29, 1984, p 210
13. H.J. Wernik, Topologically Close Packed Structures, in *Intermetallic Compounds*, John Wiley & Sons, 1967
14. Y.C. Fayman, γ-γ′ Partitioning Behavior in Waspaloy, *Mater. Sci. Eng.*, Vol 82, 1986, p 203
15. J.R. Crum, M.E. Adkins, and W.G. Lipscomb, Performance of High Nickel Alloys in Refinery and Petrochemical Environments, *Mater. Perform.*, Vol 25, 1986, p 27
16. C.T Sims, Occurrence of Topologically Close-Packed Phases, *The Superalloys*, C.T. Sims, Ed., John Wiley & Sons, 1972
17. E.S. Machlin and J. Shao, SIGMA-SAFE: A Phase Diagram Approach to the Sigma Problem in Superalloys, *Metall. Trans. A*, Vol 9, 1978, p 561
18. M. Morinaga, N. Yukawa, H. Adachi, and H. Ezaki, New PHACOMP and Its Application to Alloy Design, *Superalloys Source Book*, American Society for Metals, 1984.
19. H.R. Copson, *Physical Metallurgy of Stress Corrosion Fracture*, T.N. Rhodin, Ed., Interscience, 1959, p 247
20. R.W. Staehle, J.J. Royuela, T.L. Raredon, E. Serrate, C.R. Morin, and R.V. Farrar, Effect of Alloy Composition on SCC on Fe-Cr-Ni Base Alloys, *Corrosion*, Vol 26, 1970, p 451
21. M.O. Speidel, Stress Corrosion Cracking of Stainless Steels in NaCl Solutions, *Metall. Trans. A*, Vol 12, 1981, p 779
22. J. Kolts, "Temperature Limits for Stress Corrosion Cracking of Selected Stainless Steels and Ni-Base Alloys in Chloride-Containing Environments," Paper No. 241, presented at Corrosion/82, National Association of Corrosion Engineers, 1982
23. Y.L. Chiang and M.A. Streicher, "The Effect of Condenser Design on Stress Corrosion Cracking of Stainless Alloys in Boiling Chloride Solutions," Paper No. 353, presented at Corrosion/85, National Association of Corrosion Engineers, 1985
24. G. Herbsleb, The Stress Corrosion Cracking of Sensitized Austenitic Stainless Steels and Nickel-Base Alloys, *Corros. Sci.*, Vol 20, 1980, p 243
25. T.S. Humphries and E.E. Nelson, "Stress Corrosion Evaluation of Several Ferrous and Nickel Alloys," TM X-64511, National Aeronautics and Space Administration, April 1970
26. M.O. Speidel and R.W. Staehle, Ed., *ARPA Handbook of Stress Corrosion Cracking and Corrosion Fatigue*, to be published
27. J. Kolts, C.C. Burnette, and M.W. Joosten, Stress Corrosion Cracking of Nickel-Base Alloys in Room-Temperature HCl Containing H_2S, *Environment Induced Cracking of Metals*, R.P. Gangloff and M.B. Ives, Ed., National Association of Corrosion Engineers, 1990
28. J. Kolts, "Heat Treatment and Environmental Embrittlement of High Performance Alloys," Paper No. 407, presented at Corrosion/86, National Association of Corrosion Engineers, 1986
29. M.A. Streicher, Effect of Composition and Structure on Crevice, Intergranular, and Stress Corrosion of Some Wrought Ni-Cr-Mo Alloys, *Corrosion*, Vol 32, 1976, p 79
30. J. Kolts, "Laboratory Evaluation of Corrosion Resistant Alloys for the Oil and Gas Industry," Paper No. 323, presented at Corrosion/86, National Association of Corrosion Engineers, 1986
31. J. Fricke, "Corrosion in Packer and Completion Fluids," Paper No. 300, presented at Corrosion/87, National Association of Corrosion Engineers, 1987
32. W.K. Boyd and W.E. Berry, Stress Corrosion Cracking of Nickel and Nickel Alloys, *Stress Corrosion Cracking of*

Metals—A State of the Art, STP 518, ASTM, 1972, p 58
33. H.R. Copson and C.F. Cheng, *Corrosion*, Vol 12, 1956, p 71t
34. L. Graf and W. Wittich, *Werkst. Korros.*, Vol 5, 1966, p 385
35. L.G. Everhart and C.E. Price, Stress Corrosion Cracking in Monel at Room Temperature, *Corrosion Testing and Evaluation*, STP 1000, R. Baboian and S.W. Dean, Ed., ASTM, 1990
36. R.N. Tuttle and R.D. Kane, Ed., *H_2S Corrosion in Oil and Gas Production—A Compilation of Classic Papers*, National Association of Corrosion Engineers, 1981
37. R.D. Kane, Roles of H_2S in Behavior of Engineering Alloys, *Int. Met. Rev.*, Vol 30, 1985, p 291
38. I. Matsushima, T. Shimada, Y. Ishizawa, K. Masamura, J. Sakai and M. Tanimura, "Effects of Alloy Composition and SCC Resistance of High Alloys OCTG in Sour Well Environments," Paper No. 233, presented at Corrosion/85, National Association of Corrosion Engineers, 1985
39. P.R. Rhodes, "Stress Cracking Risks in Corrosive Oil and Gas Wells," Paper No. 322, presented at Corrosion/86, National Association of Corrosion Engineers, 1986
40. A.I. Asphahani, "High Performance Alloys for Deep Sour Gas Wells," Paper No. 42, presented at Corrosion/78, National Association of Corrosion Engineers, 1978; also published in Ref 36
41. M. Watkins, H.E. Chaung. and G.A. Vaughn, "Laboratory Testing of the SCC Resistance of Stainless Alloys," Paper No. 283, presented at Corrosion/87, National Association of Corrosion Engineers, 1987
42. Y. Ishizawa, T. Takaoka, H. Misao, K. Masamura, and J. Matsushima, Development of Ni-Base Corrosion Resistant Alloy OCTG, *NKK Tech. Rev.*, No. 55, 1989
43. S.W. Ciaraldi, "Stress Corrosion Cracking of Corrosion-Resistant Alloy Tubulars in Highly Sour Environments," Paper No. 284, presented at Corrosion/97, National Association of Corrosion Engineers, 1987
44. A.I. Asphahani, Evaluation of Highly Alloyed Stainless Materials for CO_2/H_2S Environments, *Corrosion*, Vol 37 (No. 6), 1981, p 327
45. A. Ikeda, M. Ueda, and H. Tsuge, "Environmental Cracking Evaluation of Corrosion Resistant Alloys in H_2S-CO_2-Cl^- Environment by Slow Strain Rate Test," Paper No. 7, presented at Corrosion/89, National Association of Corrosion Engineers, 1989
46. S. Tsujikawa, "A New Test Method for Predicting Pitting Corrosion Resistance of CRA's in Sour Environments," Paper No. 64, presented at Corrosion/88, National Association of Corrosion Engineers, 1988
47. P. Marcus, The Mechanisms of Sulfur-Induced Corrosion of Nickel and Nickel Alloys, *Advances in Localized Corrosion*, H. Isaacs, U. Bertocci, J. Kruger, and S. Smialowska, Ed., National Association of Corrosion Engineers, 1990, p 289
48. S.M. Wilhelm, "Effect of Elemental Sulfur on Stress Corrosion Cracking of Nickel Base Alloys in Deep Sour Gas Well Production," Paper No. 77, presented at Corrosion/88, National Association of Corrosion Engineers, 1988
49. G. Schmidt, Effect of Elemental Sulfur on Corrosion in Sour Gas Systems, *Corrosion*, Vol 47, 1991, p 285
50. M. Ueda, H. Tsuge, and A. Ikeda, "Influence of Elemental S on Corrosion Behavior of CRA in H_2S-CO_2-Cl^- Environment," Paper No. 8, presented at Corrosion/89, National Association of Corrosion Engineers, 1989
51. N. Sridhar and S.M. Corey, "The Effect of Elemental Sulfur on Stress Cracking of Ni-Base Alloys," Paper No. 12, presented at Corrosion/89, National Association of Corrosion Engineers, 1989
52. A. Miyasaka, K. Denpo, and H. Ogawa, "Environmental Aspects of SCC of High Alloys in Sour Environments," Paper No. 70, presented at Corrosion/88, National Association of Corrosion Engineers, 1988
53. M. Ueda and T. Kudo, "Evaluation of SCC Resistance of CRA's in Sour Service," Paper No. 2, presented at Corrosion/91, National Association of Corrosion Engineers, 1991
54. T. Takaoka, Y. lshizawa, K. Masamura, H. Misao, and T. Inazumi, "Effect of Alloying Elements on Environmental Cracking of Ni-Base Alloys in Sour Gas Environments," Paper No. 73, presented at Corrosion/88, National Association of Corrosion Engineers, 1988
55. A. Ikeda, M. Igerashi, M. Ueda, Y. Okada, and H. Tsuge, "On the Evaluation Methods of Ni-Ease Corrosion Resistant Alloys for Sour Gas Exploration and Production," Paper No. 65, presented at Corrosion/88, National Association of Corrosion Engineers, 1988
56. P. Ganesan, E.F. Clatworthy, and J.A. Harris, "Development of a Time-Temperature-Transformation Diagram for Alloy 925," Paper No. 286, presented at Corrosion/87, National Association of Corrosion Engineers, 1987
57. R.B. Frank and T.A. DeBold, "Heat-Treatment of an Age-Hardenable Corrosion Resistant Alloy—UNS N07716," Paper No. 59, presented at Corrosion/90, National Association of Corrosion Engineers, 1990
58. E.L. Hibner, Corrosion Behavior of Age-Hardenable Alloy UNS N07725 for Oil Field and Other Applications, *Environmental Effects on Advanced Materials*, R.D. Kane, Ed., National Association of Corrosion Engineers, 1991
59. M. Igarashi, S. Mukai, T. Kudo, Y. Okada, and A. Ikeda, "Precipitation Hardened Nickel-Base Alloys for Sour Gas Environments," Paper No. 287, presented at Corrosion/87, National Association of Corrosion Engineers, 1987
60. Y. lshizawa, T. Shimada, T. Inazumi, T. Takaoka, and M. Tankmura, Effects of Heat Treatment and Microstructure on Stress Corrosion Cracking of High Nickel Austenitic Alloys in Sour Gas Environments," Paper No. 234, presented at Corrosion/85, National Association of Corrosion Engineers, 1985
61. A.J. Sedriks, *Corrosion of Stainless Steels*, John Wiley & Sons, 1979
62. G.A. Cragnolino and D.D. Macdonald, Intergranular Stress Corrosion Cracking of Austenitic Stainless Steel at Temperatures Below 100 °C—A Review, *Corrosion*, Vol 38, 1982, p 406–424
63. C.H. Samans, Stress Corrosion Cracking Susceptibility of Stainless Steels and Nickel-Base Alloys in Polythionic Acids and Acid Copper Sulfate Solution, *Corrosion*, Vol 20, 1964, p 256t–262t
64. S. Ahmad, M.L. Mehta, S.K. Saraf, and I.P. Saraswat, Stress Corrosion Cracking of Sensitized 304 Austenitic Stainless Steel in Petroleum Refinery Environment, *Corrosion*, Vol 38, 1982, p 347–353
65. S. Ahmad, M.L. Mehta, S.K. Saraf, and I.P. Saraswat, Effect of Polythionic Acid Concentration on Stress Corrosion Cracking of Sensitized Austenitic Stainless Steel, *Corrosion*, Vol 39, 1983, p 333–338
66. R.C. Scarberry, S.C. Pearman, and J.R. Crum, Precipitation Reactions on Inconel Alloy 600 and Their Effect on Corrosion Behavior, *Corrosion*, Vol 32, 1976, p 401–406
67. C.D. Stephens and R.C. Scarberry, The Relation of Sensitization to Polythionic Acid Cracking of Incoloy Alloys 800 and 801, *Proc. 25th Conf. NACE*, 1969, p 583–586
68. P. Berge and J.R. Donati, Materials Requirements for Pressurized Water Reactor Steam Generator Tubing, *Nucl. Technol.*, Vol 55, 1981, p 88–104
69. R.L. Jones, R.L. Long, and J.S. Olszewski, "The Origin of the Extensive Cracking of the Steam Generator Tubing at TMI Unit 1," Paper No. 141, presented at Corrosion/83, National Association of Corrosion Engineers, 1983
70. H.S. Isaacs, B. Vyas, and M.W. Kendig, The Stress Corrosion Cracking of Sensitized Stainless Steel in Thiosulfate Solutions, *Corrosion*, Vol 38, 1982, p 130–136
71. R.C. Newman, R. Roberge, and R. Bandy, Environmental Variables in the Low Temperature Stress Corrosion Cracking of Inconel 600, *Corrosion*, Vol 39, 1983, p 386–390
72. R. Bandy, R. Roberge, and R.C. Newman, Low Temperature Stress Corrosion Cracking of Sensitized Inconel 600 in Tetrathionate and Thiosulfate Solutions, *Corrosion*, Vol 39, 1983, p 391–398

73. R. Bandy, R. Roberge, and R.C. Newman, Low Temperature Stress Corrosion Cracking of Inconel 600 under Two Different Conditions of Sensitization, *Corros. Sci.*, Vol 23, 1983, p 995–1006
74. R.C. Newman, R. Roberge, and R. Bandy, Evaluation of SCC Test Methods for Inconel 600 in Low-Temperature Aqueous Solutions, *Environment-Sensitive Fracture: Evaluation and Comparison of Test Methods*, STP 821, ASTM, 1984, p 310–322
75. K.H. Lee, G.A. Cragnolino, and D.D. Macdonald, Effect of Heat Treatment and Applied Potential on the Caustic Stress Corrosion Cracking of Inconel 600, *Corrosion*, Vol 41, 1985, p 540–553
76. G.S. Was and V.B. Rajan, On the Relationship between the EPR Test, Sensitization, and IGSCC Susceptibility, *Corrosion*, Vol 43, 1987, p 576–579
77. G.S. Was and V.B. Rajan, The Mechanism of Intergranular Cracking of Ni-Cr-Fe Alloys in Sodium Tetrathionate, *Metall. Trans. A*, Vol 18, 1987, p 1313–1323
78. G.-P. Yu and H.-C. Yao, The Relation between the Resistance of IGA and IGSCC and the Chromium Depletion of Alloy 690, *Corrosion*, Vol 46, 1990, p 391–402
79. H. Coriou, L. Grall, and S. Vettier, Corrosion sous contrainte de l'Inconel dans l'eau a haute temperature, *Third Saclay Metallurgy Colloquium*, North Holland, 1960, p 161 (in French)
80. P. Berge, Can PWR U-Tube Steam Generators Work Safely?, *Third Int. Symp. Environmental Degradation of Materials in Nuclear Power Systems—Water Reactors*, G.J. Theus and J.R. Weeks, Ed., The Metallurgical Society, 1988, p 49–54
81. C.S. Welty, Jr. and J.C. Blomgren, Steam Generator Issues, *Proc. Fourth Int. Symp. Environmental Degradation of Materials in Nuclear Power Systems—Water Reactors*, D. Cubicciotti, Ed., National Association of Corrosion Engineers, 1990, p 1.27–1.36
82. R. Bandy and D. Van Rooyen, Stress Corrosion Cracking of Inconel Alloy 600 in High Temperature Water—An Update, *Corrosion*, Vol 40, 1984, p 425–430
83. T.S. Bulischek and D. Van Rooyen, Stress Corrosion Cracking of Alloy 600 Using the Constant Strain Rate Test, *Corrosion*, Vol 37, 1981, p 597–607
84. R. Bandy and D. Van Rooyen, Mechanisms of Intergranular Failures in Alloy 600 in High-Temperature Environments, *Proc. Ninth Int. Cong. Metallic Corrosion*, Vol 2, National Research Council of Canada, 1984, p 202–209
85. N. Totsuka, E. Lunarska, G. Cragnolino, and Z. Szklarska-Smialowska, A Sensitive Technique for Evaluating Susceptibility to IGSCC of Alloy 600 in High Temperature Water, *Scr. Metall.*, Vol 20, 1986, p 1035–1040
86. T. Yonezawa and K. Onimura, "Effect of Chemical Composition and Microstructure on the Stress Corrosion Cracking Resistance of Nickel Base Alloys," presented at EPRI Meeting on Intergranular Stress Corrosion Cracking Mechanisms (Washington, DC), April 27–May 1, 1987, Electric Power Research Institute
87. J. Blanchet, H. Coriou, L. Grall, C. Mahhiew, C. Otter, and G. Turler, Historical Review of the Principal Research Concerning the Phenomenon of Cracking of Nickel-Base Austenitic Alloys, *Stress Corrosion Cracking and Hydrogen Embrittlement of Iron-Base Alloys*, R.W. Staehle, J. Hochmann, R.D. McCright, and J.E. Slater, Ed., National Association of Corrosion Engineers, 1977, p 1149–1160
88. V.B. Rajan, J.K. Sung, and G.S. Was, Stress Corrosion Cracking of Controlled Purity Inconel 600-Type Alloys in High Purity Water and Caustic Solutions, *Proc. Third Int. Symp. Environmental Degradation of Materials in Nuclear Power Systems–Water Reactors*, G.J. Theus and J.R. Weeks, Ed., The Metallurgical Society, 1988, p 545–550
89. J.K. Sung and G.S. Was, The Role of Grain Boundary Chemistry in Pure Water Intergranular Stress Corrosion Cracking of Ni-16Cr-9Fe Alloys, *Proc. Fourth Int. Symp. Environmental Degradation of Materials in Nuclear Power Systems–Water Reactors*, D. Cubicciotti, Ed., National Association of Corrosion Engineers, 1990, p 6.25–6.37
90. A.A. Stein, A. Deleon, and A.R. McIlree, "Relationship of Annealing Temperature and Microstructure to Primary Side Cracking of Alloy 600 Steam Generator Tubing," EPRI Steam Generator Owners Group, SCC Contractors Workshop (San Diego, CA), March, 1985, Electric Power Research Institute
91. D. Garriga Majo, J.M. Gras, Y. Rouillon, F. Vaillant, J.C. VanDuysen, and G. Zacharie, "Prediction of the Stress Corrosion Cracking Resistance of Alloy 600 in Pure/Primary Water," Paper No. 56, presented at Int. Symp. Life Prediction of Corrodible Structures, Cambridge, UK, Sept 1991
92. H.A. Domian, R.H. Samuelson, L.W. Sarver, G.J. Theus, and L. Katz, Effect of Microstructure on Stress Corrosion Cracking of Alloy 600 in High Purity Water, *Corrosion*, Vol 33, 1977, p 26–37
93. G. Airey, "Optimization of Metallurgical Variables to Improve Corrosion Resistance on Inconel 600," NP-3051, Electric Power Research Institute, 1983
94. Z. Szklarska-Smialowska, Factors Influencing IGSCC of Alloy 600 in Primary and Second Waters of PWR Steam Generators, *Proc. Fourth Int. Symp. Environmental Degradation of Materials in Nuclear Power Systems–Water Reactors*, D. Cubicciotti, Ed., National Association of Corrosion Engineers, 1990, p 6.1–6.24
95. G. Economy, R.J. Jacko, and F.W. Pement, IGSCC Behavior of Alloy 600 Steam Generator Tubing in Water or Steam Tests Above 360 °C, *Corrosion*, Vol 43, 1987, p 727–734
96. N. Totsuka, E. Lunarska, G. Cragnolino, and Z. Szklarska-Smialowska, Effect of Hydrogen on the Intergranular Stress Corrosion Cracking of Alloy 600 in High Temperature Aqueous Environments, *Corrosion*, Vol 43, 1987, p 505–514
97. N. Totsuka and Z. Szklarska-Smialowska, Effect of Electrode Potential on the Hydrogen-Induced IGSCC of Alloy 600 in an Aqueous Solution at 350 °C, *Corrosion*, Vol 43, 1987, p 734–738
98. R.L. Cowan and G.M. Gordon, Intergranular Stress Corrosion Cracking and Grain Boundary Composition in Fe-Ni-Cr Alloys, *Stress Corrosion Cracking and Hydrogen Embrittlement of Iron Base Alloys*, R.W. Staehle, J. Hochmann, R.D. McCright, and J.E. Slater, Ed., National Association of Corrosion Engineers, 1977, p 1023–1070
99. D. Van Rooyen, Review of the Stress Corrosion Cracking of Inconel 600, *Corrosion*, Vol 31, 1975, p 327–337
100. H.R. Copson and G. Economy, Effect of Some Environment Conditions on Stress Corrosion Behavior of Ni-Cr-Fe Alloys in Pressurized Water, *Corrosion*, Vol 24, 1968, p 55–65
101. D.A. Vermilyea, Stress Corrosion Cracking of Iron- and Nickel-Base Alloys in Sulfate Solutions at 289 °C, *Corrosion*, Vol 29, 1973, p 442–448
102. D.A. Vermilyea, Susceptibility of Iron- and Nickel-Base Alloys to SCC in pH 2.5 H_2SO_4 at 289 °C, *Corrosion*, Vol 31, 1975, p 421–424
103. J.F. Newman, "Stress Corrosion of Alloys 600 and 690 in Acidic Sulfate Solutions at Elevated Temperatures," NP-3043, Electric Power Research Institute, 1983
104. P.L. Andresen, "The Effects of Sulfate Impurities in 288 °C Water on IGSCC of Inconel 600 in Constant Load and SSRT Experiments," Paper No. 177, presented at Corrosion/84, National Association of Corrosion Engineers, 1984
105. C.A. Caraminhas and D.F. Taylor, Constant Extension Rate Tensile (CERT) Tests of Creviced Alloy 600 Specimens in Aqueous Environments at 288 °C, *Corrosion*, Vol 40, 1984, p 382–385
106. R.W. Staehle, J.A. Begley, A.K. Agrawal, F.H. Beck, and J.B. Lumsden, "Corrosion and Corrosion Cracking of Materials for Water Cooled Reactors," NP-1741, Electric Power Research Institute, 1981
107. D.D. Macdonald, Z. Szklarska-Smialowska, G. Cragnolino, F.H. Beck, A. Boateng, A. Moccari, and S.P. Pednekar, "Corrosion and Corrosion Cracking of Materials for Water Cooled Reactors,"

Progress Reports FCC7805 (Jan–June 1980), Electric Power Research Institute
108. P. Berge, "Modeling Corrosion for Life Prediction of Nuclear Reactor Components," Paper No. l, presented at Int. Symp. Life Prediction of Corrodible Structures, Cambridge, UK, Sept 1991
109. N. Totsuka and Z. Szklarska-Smialowska, Hydrogen Induced IGSCC of Ni-Containing FCC Alloys in High Temperature Water, *Proc. Third Int. Symp. Environmental Degradation of Materials in Nuclear Power Systems–Water Reactors,* G.J. Theus and J.R. Weeks, Ed., The Metallurgical Society, 1988, p 691–696
110. A.R. McIlree, Degradation of High Strength Austenitic Alloys X-750, 718, and A-285 in Nuclear Power Systems, *Proc. Int. Symp. Environmental Degradation of Materials in Nuclear Power Systems–Water Reactors,* National Association of Corrosion Engineers, 1984, p 838–850
111. H. Hanninen and I. Aho-Mantila, Environment-Sensitive Cracking of Reactor Internals, *Proc. Third Int. Symp. Environmental Degradation of Materials in Nuclear Power Systems–Water Reactors,* G.J. Theus and J.R. Weeks, Ed., The Metallurgical Society, 1988, p 77–92
112. K. Hosoi, S. Hattori, Y. Urayama, I. Masaoka, and R. Sasaki, Relation between Susceptibility to Stress Corrosion Cracking in High Temperature Water and Microstructure of Inconel Alloy X-750, *Proc. Int. Symp. Environmental Degradation of Materials in Nuclear Power Systems–Water Reactors,* National Association of Corrosion Engineers, 1984, p 334–344
113. T. Yonezawa, K. Onimura, N. Sakamoto, N. Sasaguri, H. Nakata, and H. Susukida, Effect of Heat Treatment on Stress Corrosion Cracking Resistance of High Nickel Alloys in High Temperature Water, *Proc. Int. Symp. Environmental Degradation of Materials in Nuclear Power Systems–Water Reactors,* National Association of Corrosion Engineers, 1984, p 345–367
114. C.A. Grove and L.D. Petzold, Mechanisms of Stress Corrosion Cracking of Alloy X-750 in High Purity Water, *Proc. Conf. Corrosion of Nickel-Base Alloys,* R.C. Scarberry, Ed., American Society for Metals, 1985, p 165–180
115. P. Skeldon and P. Hurst, Environmentally Assisted Cracking of Inconel X-750, *Proc. Third Int. Symp. Environmental Degradation of Materials in Nuclear Power Systems–Water Reactors,* G.J. Theus and J.R. Weeks, Ed., The Metallurgical Society, 1988, p 703–710
116. T. Kawakubo and B. Rosborg, Stress Corrosion Cracking Threshold Testing—SCC Growth Behavior of Alloy X-750 and Type 304 Stainless Steel under Slow Rising Load, *Proc. Second Int. Atomic Energy Agency Specialists Meeting on Subcritical Crack Growth,* Vol 1, NUREG/CP-0067, U.S. Nuclear Regulatory Commission, 1986, p 477–485
117. I.L. Wilson and T.R. Mager, Stress Corrosion of Age-Hardenable Ni-Fe-Cr Alloys, *Corrosion,* Vol 42, 1986, p 352–361
118. B.P. Miglin, M.T. Miglin, J.V. Monter, T. Sato, and K. Aoki, Stress Corrosion Cracking of Commercial-Grade Alloy 718 in Pressurized Water-Reactor Primary Water, *Proc. Fourth Int. Symp. Environmental Degradation of Materials in Nuclear Power Systems–Water Reactors,* D. Cubicciotti, Ed., National Association of Corrosion Engineers, 1990, p 11.32–11.44
119. J.R. Donati, M. Guttman, Y. Rouillon, P. Saint-Paul, and J.C. VanDuysen, Stress Corrosion Cracking Behavior of Nickel-Base Alloys with 19% Chromium in High Temperature Water, *Proc. Third Int. Symp. Environmental Degradation of Materials in Nuclear Power Systems–Water Reactors,* G.J. Theus and J.R. Weeks, Ed., The Metallurgical Society, 1988, p 697–701
120. S. Hattori, K. Yamauchi, Y. Urayama, J. Kuniya, and H. Itow, Evaluation of Stress Corrosion Margin of Precipitation Hardenable Nickel Base Alloys in High Temperature Water, *Proc. Fourth Int. Symp. Environmental Degradation of Materials in Nuclear Power Systems–Water Reactors,* D. Cubicciotti, Ed., National Association of Corrosion Engineers, 1990, p 11.1–11.11
121. P. Berge and J.R. Donati, An Evaluation of PWR Steam Generator Tubing Alloys, *Nucl. Energy,* Vol 17, 1978, p 291–299
122. P. Berge, J.R. Donati, B. Prieux, and D. Villard, Caustic Stress Corrosion of Fe-Cr-Ni Austenitic Alloys, *Corrosion,* Vol 33, 1977, p 425–435
123. G.J. Theus, "Summary of the Babcock and Wilcox Company's Stress Corrosion Cracking Tests of Alloy 600," EPRI Workshop on Cracking of Alloy 600 U-Bend Tubes in Steam Generators, EPRI-WS-80-0136, Electric Power Research Institute, 1980
124. A.I. Asphahani, Slow-Strain-Rate Technique and Its Applications to the Environmental Stress Cracking of Nickel-Base and Cobalt-Base Alloys, *Stress Corrosion Cracking—The Slow Strain Rate Technique,* STP 665, G.M. Ugianski and J. Payer, Ed., ASTM, 1979, p 279–293
125. I.L. W. Wilson and R.G. Aspden, Caustic Stress Corrosion Cracking of Iron-Nickel-Chromium Alloys, *Stress Corrosion Cracking and Hydrogen Embrittlement of Iron Base Alloys,* R.W. Staehle, J. Hochmann, R.D. McCright, and J.E. Slater, Ed., National Association of Corrosion Engineers, 1977, p 1189–1204
126. G. Theus, Caustic Stress Corrosion Cracking of Inconel 600, Incoloy 800 and Type 304 Stainless Steel, *Nucl. Technol.,* Vol 28,1976, p 388–397
127. J.R. Crum, Effect of Composition and Heat Treatment on Stress Corrosion Cracking of Alloy 600 Steam Generator Tubing in Sodium Hydroxide, *Corrosion,* Vol 38, 1982, p 40–45
128. K.H. Lee, G. Cragnolino, and D.D. Macdonald, Effect of Heat Treatment and Applied Potential on the Caustic Stress Corrosion Cracking of Inconel 600, *Corrosion,* Vol 41, 1985, p 540–553
129. J.R. Crum, Stress Corrosion Cracking Testing of Inconel Alloys 600 and 690 in High Temperature Caustic, *Corrosion,* Vol 42, 1986, p 368–372
130. R.S. Pathania and R.D. Cleland, The Effect of Thermal Treatments on Stress Corrosion Cracking of Alloy 800 in a Caustic Environment, *Corrosion,* Vol 41, 1985, p 575–581
131. A. Mignone, M.F. Maday, A. Borello, and M. Vittori, Effect of Chemical Composition, Thermal Treatment and Caustic Concentration on the SCC Behavior of Alloy 800, *Corrosion,* Vol 46, 1990, p 57–65
132. A.R. McIlree and H.T. Michels, Stress Corrosion Behavior of Fe-Cr-Ni and Other Alloys in High Temperature Caustic Solutions, *Corrosion,* Vol 33, 1977, p 60–67
133. J.R. Cels, Stress Corrosion Cracking of Stainless Steels and Nickel Alloys at Controlled Potential in 10% Caustic Soda Solutions at 550 °F, *J. Electrochem. Soc.,* Vol 12, 1976, p 1152–1156
134. J.R. Cels, Caustic Stress Corrosion Studies at 288 °C (550 °F) Using the Straining Electrode Potential Technique—Comparison of Alloy 600, Alloy 800 and Type 304 Stainless Steel, *Corrosion,* Vol 34, 1978, p 198–209
135. N. Pessal, G.P. Airey, and B.P. Lingenfelter, The Influence of Thermal Treatment on the Stress Corrosion Cracking Behavior of Inconel 600 at Controlled Potential in 10% Caustic Soda Solutions at 315 °C, *Corrosion,* Vol 35,1979, p 100–107
136. R. Roberge, R. Bandy, and D. Van Rooyen, "IGA of Alloy 600 in High Temperature Solutions of Sodium Hydroxide Contaminated with Carbonate," NP-3059, Electric Power Research Institute, 1983
137. G. Pinard Legry and G. Plante, "Intergranular Attack of Alloy 600: High Temperature Electrochemical Tests," NP-3062, Electric Power Research Institute, 1983
138. D. Van Rooyen and R. Bandy, "Mechanism of Intergranular Attack and Stress Corrosion Cracking of Alloy 600 by High Temperature Caustic Solutions Containing Impurities," NP-5129, Electric Power Research Institute, 1987
139. A. Kawashima and M. Takano, Stress Corrosion Cracking of Inconel 600 and Incoloy 800 in 50% NaOH Aqueous Solutions at 140 °C, *Boshuku Gijutsu,* Vol 27, 1978, p 340–347
140. H. Hickling and N. Wieling, Electrochemical Aspects of the Stress Corrosion Cracking of Fe-Ni-Cr Alloys in Caustic Solutions, *Corros. Sci.,* Vol 20, 1980, p 269–279

141. J.M. Sarver, J.V. Monter, and B.P. Miglin, The Effect of Thermal Treatment on the Microstructure and SCC Behavior of Alloy 690, *Proc. Fourth Int. Symp. Environmental Degradation of Materials in Nuclear Power Systems–Water Reactors*, D. Cubicciotti, Ed., National Association of Corrosion Engineers, 1990, p 5.47–5.63
142. F.A. Shunk and W.R. Warke, Specificity as an Aspect of Liquid Metal Embrittlement, *Scr. Metall.*, Vol 8, 1974, p 519
143. P.D. Johnson, A.I. Asphahani, and C.W. Allen, "Response of Several Nickel and cobalt Base Alloys to Molten Pb, Sn, and Zn," Paper No. 128, presented at Corrosion/79, National Association of Corrosion Engineers, 1979
144. S. Sadigh, Stress Cracking of Stainless Steel and High Alloys in Molten Zinc at High Temperature, *Mater. Perform.*, July 1981, p 16
145. J. Kelly, Rolled Alloys Inc., private communication, Nov 1986
146. J.A. Hemsworth, M.G. Nicholas, and R.M. Crispin, Tellurium Embrittlement of Type 316 Steel, *J. Mater. Sci.*, Vol 25, 1990, p 5248
147. C.E. Price and R.S. Fredell, A Comparative Study of the Embrittlement of Monel 400 at Room Temperature by Hydrogen and by Mercury, *Metall. Trans. A*, Vol 17, 1986, p 889
148. C.E. Price and R.N. King, The Embrittlement of Monel 400 by Hydrogen and Mercury as a Function of Temperature, *Corrosion Cracking*, V.S. Goel, Ed., American Society for Metals, 1985
149. Y. Takizawa and I. Sekine, "Stress Corrosion Cracking Phenomena on Ni-Mo Alloys in High Temperature Nonaqueous Solution," Paper No. 355, presented at Corrosion/85, National Association of Corrosion Engineers, 1985
150. G.C. Smith, *Hydrogen in Metals*, I.M. Bernstein and A.W. Thompson, Ed., American Society for Metals, 1974, p 485
151. A.W. Thompson, Hydrogen Assisted Fracture in Single-Phase Nickel Alloys, *Scr. Metall.*, Vol 16, 1982, p 1189
152. R.D. Kane, Accelerated Hydrogen Charging of Ni-Base and Co-Base Alloys, *Corrosion*, Vol 34, 1978, p 442
153. N. Sridhar, J.A. Kargol, and N.F. Fiore, Hydrogen-Induced Crack Growth in a Ni-Base Superalloy, *Scr. Metall.*, Vol 14, 1980, p 225
154. R.D. McCright, Effects of Environmental Species and Metallurgical Structure on the Hydrogen Entry Into Steel, *Stress Corrosion Cracking and Hydrogen Embrittlement of Iron-Base Alloys*, R.W. Staehle, J. Hochmann, R.D. McCright, and J.E. Slater, Ed., National Association of Corrosion Engineers, 1977, p 306
155. B.A. Wilcox and G.C. Smith, *Acta Metall.*, Vol 13, 1964, p 331
156. W.T. Chandler and R.J. Walter, Testing to Determine the Effect of High Pressure Hydrogen Environments on the Mechanical Properties of Metals, *Hydrogen Embrittlement Testing*, STP 543, ASTM, 1974
157. J. Papp, R.F. Hehemann, and A.R. Troiano, Hydrogen Embrittlement of High-Strength FCC Alloys, *Hydrogen in Metals*, A.W. Thompson and I.M. Bernstein, Ed., American Society for Metals, 1974, p 657
158. N. Totsuka and Z. Szklarska-Smialowska, Activation Energy for IGSCC of Alloy 600 in an Aqueous Solution Containing Dissolved H_2 at 300 to 350 °C, *Scr. Metall.*, Vol 21, 1987, p 45–47
159. S.M. Bruemmer, "Grain Boundary Composition Effects on Environmentally Induced Cracking of Engineering Materials," Paper No. 185, presented at Corrosion/87, National Association of Corrosion Engineers, 1987
160. B.J. Berkowitz and R.D. Kane, The Effect of Impurity Segregation on the Hydrogen Embrittlement of a High-Strength Ni-Base Alloy in H_2S Environment, *Corrosion*, Vol 36, 1980, p 24
161. A.I. Asphahani, "Hydrogen Cracking of Ni-Base Alloys," Second Int. Cong. Hydrogen in Metals, Paris, 1977
162. J.A. Kargol and B. Ladna, The Roles of Ordering and Impurity Segregation on the Hydrogen-Assisted Propagation in Ni-Base Stainless Alloys, *Sci. Metall.*, Vol 16, 1982, p 191
163. B.J. Berkowitz, M. Kurkela, and R.M. Latanision, Effect of Ordering on the Hydrogen Permeation and Embrittlement of Ni_2Cr, in *Effect of Hydrogen on Behavior of Metals*, The Metallurgical Society, 1980, p 411
164. L.P. Lehman and T.H. Kosel, Influence of Phosphorus on the Kinetics of Ordering in Ni_2Cr, *High Temperature Ordered Intermetallic Alloys*, C.C. Koch et al., Ed., Materials Research Society Symposia Proceedings, Vol 39, 1985
165. M. Comet, C. Bertrand, and M. Da Cunha Belo, Hydrogen Embrittlement of Ultra--Pure Alloys of the Inconel 600 Type: Influence of the Additions of Elements (C, P, Sn, Sb), *Metall. Trans. A*, Vol 13, 1982, p 141
166. J. Kupper-Feser and H.J. Grabke, Effect of Grain Boundary Composition on Tensile Strength and Hydrogen Induced Stress Corrosion Cracking of Ni-20Cr, *Mater. Sci. Technol.*, Vol 7, 1991, p 111
167. A.W. Funkenbusch, L.A. Heldt, and D.F. Stein, *Metall. Trans. A*, Vol 13, 1982, p 611
168. S. Hinotani, Y. Ohmori, and F. Terasaki, *Mater. Sci. Technol.*, Vol 1, 1985, p 297
169. M. Kurkela, R. Latanision, and B.J. Berkowitz, Effect of Ordering on the Hydrogen Permeation and Embrittlement of Ni_2Cr, in *Effect of Hydrogen on Behavior of Metals*, The Minerals, Metals, and Materials Society, 1980
170. R.M. Latanision and H. Opperhauser, The Intergranular Embrittlement of Nickel by Hydrogen: The Effect of Grain Boundary Segregation, *Metall. Trans.*, Vol 5, 1974, p 483
171. J.P. Hirth and J. Lothe, *Theory of Dislocations*, 2nd ed., Wiley-Interscience, 1982
172. A.W. Thompson and I.M. Bernstein, The Role of Metallurgical Variables in Hydrogen-Assisted Environmental Fracture, *Advances in Corrosion Science and Technology*, Vol 7, R.W. Staehle and M.G. Fontana, Ed., Plenum Press, 1977
173. N. Sridhar, J.A. Kargol, and N.F. Fiore, Effect of Low Temperature Aging on Hydrogen-Induced Crack Growth in a Ni-Base Superalloy, *Scr. Metall.*, Vol 14, 1980, p 1257
174. J.G. Erlings, H.W. deGroot, and J.F.M. van Roy, Stress Corrosion Cracking and Hydrogen Embrittlement of High-Strength Nonmagnetic Alloys in Brines, *Mater. Perform.*, Oct 1986, p 28
175. K.D. Efird, Failure of Monel Ni-Cu-Al Alloy K-500 Bolts in Seawater, *Mater. Perform.*, April 1985, p 37
176. L.H. Wolfe and M.W. Joosten, Failures of Nickel/Copper Bolts in Subsea Applications, *SPE Prod. Eng.*, Aug 1988, p 382
177. J.W. Kochera, A.K. Dunlop, and J.P. Tralmer, Experience with Stress Corrosion Cracking of Nickel Base Alloys in Sour Hydrocarbon Production, *H_2S Corrosion in Oil and Gas Production—A Compilation of Classic Papers*, R.N. Tuttle and R.D. Kane, Ed., National Association of Corrosion Engineers, 1981, p 413
178. J. Kolts, Alloy 718 for Oil and Gas Industry, *Superalloy 718—Metallurgy and Applications*, E.A. Loria, Ed., The Minerals, Metals, and Materials Society, 1989, p 329
179. O.A. Onyewuenyi, Alloy 718—Alloy Optimization for Applications in Oil and Gas Production, *Superalloy 718—Metallurgy and Applications*, E.A. Loria, Ed., The Minerals, Metals, and Materials Society, 1989, p 345
180. R.B. Frank and T.A. DeBold, "Heat Treatment of an Age-Hardenable Corrosion-Resistant Alloy—UNS N07716," Paper No. 59, presented at Corrosion/90, National Association of Corrosion Engineers, 1990
181. M.C. Place, P.R. Rhodes, and R.D. Mack, "Qualifications of Corrosion Resistant Alloys for Sour Service," Paper No. 1, presented at Corrosion/91, National Association of Corrosion Engineers, 1991
182. R.D. Kane, M. Watkins, D.F. Jacobs, and G.L. Hancock, Factors Influencing the Embrittlement of Cold Worked High Alloy Materials in H_2S Environments, *Corrosion*, Vol 33, 1977, p 309
183. "Laboratory Testing of Metals for Resistance to Sulfide Stress Cracking and Stress

Corrosion Cracking in H_2S Environments," NACE Standard Test Method TM0177-96, NACE International, 1996
184. T.S. Bulischeck and D. Van Rooyen, "Experimental Investigation of the SCC of Inconel 600 and a Predictive Model for Evaluating Service Performance," NUREG/CR-1675, Brookhaven National Laboratory, 1980
185. R.J. Coyle, J.A. Kargol, and N.F. Fiore, The Effect of Aging on Hydrogen Embrittlement of a Nickel Alloy, *Metall. Trans. A,* Vol 12, 1981, p 653

SELECTED REFERENCES

- P. Gangloff and M.B. Ives, *Environment Induced Cracking of Metals,* National Association of Corrosion Engineers, 1990
- D.D. Macdonald and G.A. Cragnolino, Corrosion of Steam Cycle Materials, *The ASME Handbook on Water Technology for Thermal Power Systems,* P. Cohen, Ed., American Society of Mechanical Engineers, 1989, Chap 9
- A.J. McEvily, Jr., Ed., *Atlas of Stress Corrosion and Corrosion Fatigue Curves,* ASM International, 1990
- R.W. Staehle, A.J. Forty, and D. Van Rooyen, Ed., *Fundamental Aspects of Stress Corrosion Cracking,* National Association of Corrosion Engineers, 1969
- R.N. Tuttle and R.D. Kane, Ed., *H_2S Corrosion in Oil and Gas Production—A Compilation of Classic Papers,* National Association of Corrosion Engineers, 1981
- G.M. Ugianski and J.H. Payer, Ed., *Stress Corrosion Cracking—The Slow Strain Rate Technique,* STP 665, American Society for Testing and Materials, 1979

ASM Specialty Handbook: Nickel, Cobalt, and Their Alloys
J.R. Davis, editor, p 167-188
DOI:10.1361/ncta2000p167

Copyright © 2000 ASM International®
All rights reserved.
www.asminternational.org

High-Temperature Corrosion Behavior of Nickel Alloys

HIGH-TEMPERATURE DEGRADATION of heat resistant nickel-, cobalt-, and iron-base alloys (commonly referred to as superalloys), as well as stainless steels, is typically caused by oxidation, carburization, nitridation, sulfidation, and or halogenation. Each type of high-temperature corrosion is caused by specific corrosive media and may be minimized by the addition of appropriate alloying elements as summarized in Table 1. Most heat resistant alloys have sufficient amounts of chromium (with or without the additions of aluminum or silicon) to form chromia (Cr_2O_3), alumina (Al_2O_3), and/or silica (SiO_2) protective oxide scales, which provide resistance to environmental degradation.

Although emphasis in this article has been placed on heat resistant nickel alloys, comparative data are also presented for cobalt alloys, iron-base superalloys, and stainless steels. Additional information on the high-temperature corrosion resistance of cobalt alloys can be found in the article "Corrosion Behavior of Cobalt Alloys" in this Handbook. For information pertaining to stainless steels, the reader is referred to the *ASM Specialty Handbook: Stainless Steels,* or the *ASM Specialty Handbook: Heat-Resistant Materials.*

Oxidation

Alloying Effects. Resistance to oxidizing environments at high temperatures is a primary requirement for superalloys, whether they are used coated or uncoated. Therefore, an understanding of superalloy oxidation and how it is influenced by alloy characteristics and exposure conditions is essential for effective design and application of superalloys. As the nickel content in the Fe-Ni-Cr system increases from austenitic stainless steels to 800-type alloys, and to 600-type Ni-Cr alloys, the alloys become more stable in terms of metallurgical structure and more resistant to creep deformation. The alloys also become more resistant to scaling as nickel content increases. Figure 1 illustrates that the scaling resistance of several high-nickel alloys was better than that of austenitic stainless steels when cycled to 980 °C (1800 °F) in air (Ref 1).

A majority of high-temperature alloys rely on chromia scale to resist oxidation attack. Chromium has a very high affinity for oxygen, so it can readily react with oxygen to form chromia. A sufficiently high level of chromium is needed in the alloy to develop an external chromia scale for oxidation protection. The iron-chromium, nickel-chromium, and cobalt-chromium alloys exhibit the lowest oxidation rates when chromium concentration is about 15 to 30% (Ref 2). Therefore, most iron-, nickel-, and cobalt-base commercial austenitic alloys contain about 16 to 25% Cr. Because of the high solubility of chromium in austenitic alloys, these commercial alloys have been developed without melting and processing difficulties. Excessive amounts of chromium tend to promote embrittling intermetallic phases, such as σ-phase, or even α-ferrite.

Aluminum is also very effective in improving alloy oxidation resistance. Cyclic oxidation in air to 1090 °C (2000 °F) showed that alloy 601 (about 1.3% Al) was better than alloy 600 (0% Al), as illustrated in Fig. 2. As temperature increases, the amount of aluminum needed in the alloy to resist cyclic oxidation also increases. Figure 3 shows a linear weight loss for alloy 601 when cycled to 1150 °C (2100 °F) in air for 42 days (Ref 4). In contrast, alloy 214 (about 4.5% Al) showed essentially no changes in weight (Ref 4). With only about 1.3% Al, alloy 601 forms a chromia scale when heated to elevated temperatures. The chromia begins to convert to volatile CrO_3 as the temperature exceeds about 1000 °C (1830 °F), thus losing its protective capability against oxidation attack (Ref 5, 6). Alloy 214, with about 4.5% Al, on the other hand, forms an alumina scale that is significantly more protective. The excellent oxidation resistance of alloy 214 might also be due partially to yttrium in the alloy. The beneficial effects of rare earth elements (e.g., Y, La, Ce, etc.) on the oxidation resistance of alloys have been extensively studied for alumina or chromia formers (Ref 7–13).

Many mechanisms have been proposed to explain these effects. One widely accepted mechanism is the formation of oxide intrusions

Table 1 Alloying elements and their effects in nickel- and iron-base superalloys

Element	Effects on alloy
Chromium	Improves oxidation resistance provided temperature does not exceed 950 °C (1740 °F) for long periods; decreases carbon ingress—helps carburization resistance; detrimental to fluorine-containing environment at high temperatures; detrimental to nitridation resistance; high chromium beneficial to oil ash corrosion and attack by molten glass; improves sulfidation resistance
Silicon	Improves resistance to oxidation, nitridation, sulfidation, and carburization; synergistically acts with chromium to improve scale resilience; detrimental to non-oxidizing chlorination process
Aluminum	Independently and synergistically with chromium raises oxidation resistance; helps sulfidizing and carburization resistance; detrimental to nitridation resistance
Titanium	Detrimental to nitridation resistance
Niobium	Increases short-term creep strength; may be beneficial in carburization resistance; detrimental to nitridation resistance
Molybdenum, tungsten	Improves high-temperature strength, good in reducing chlorination resistance; improves creep strength; detrimental for oxidation resistance at higher temperatures
Nickel	Improves carburization, nitridation, and chlorination resistance; detrimental to sulfidation resistance
Carbon	Improves strength; helps nitridation resistance; beneficial to carburization resistance; oxidation resistance adversely affected
Yttrium, rare earths	Improves adherence and spalling resistance of oxide layer, hence improves oxidation, sulfidation, and carburization resistance
Manganese	Slight positive effect on high-temperature strength and creep; detrimental to oxidation resistance, increases solubility of nitrogen
Cobalt	Reduces rate of sulfur diffusion, hence helps with sulfidation resistance; improves solid-solution strength

Source: VDM Technologies Corp.

(or pegs), which mechanically key the scale to the substrate (Ref 8). Funkenbusch et al. (Ref 14) proposed that rare earth elements (and other reactive elements), which are strong sulfide formers, reduce the segregation of sulfur to the oxide scale-metal interface, thereby improving scale adherence. Rare earth elements have been used in the development of superalloys in recent years. Some of these commercial alloys include alloy 214 using yttrium, and alloys 188, S, and 230 using lanthanum.

Long-term oxidation data in air at an intermediate temperature were generated by Barrett (Ref 15) for 33 high-temperature alloys, from ferritic stainless steels to superalloys. Tests were performed at 815 °C (1500 °F) for 10,000 h with 10,000 h cycles (a total of 10 cycles). The results are shown in Fig. 4. Also included for comparison is the maximum metal loss value for chromia formers in isothermal tests (10,000 h in air at 815 °C, or 1500 °F). As expected, many alloys suffered more attack in cyclic tests than in isothermal tests. Alloys with no chromium or low chromium content, such as alloy B (Ni-Mo), alloy N (Ni-Mo-Cr), and type 409 stainless steel, suffered severe oxidation. It was surprising to find that type 321 exhibited severe metal loss, significantly more than types 304, 316, and 347. No explanation of this was offered in the study. It may be due to titanium, which is generally detrimental to alloy oxidation resistance, as discussed below.

An oxidation database for a wide variety of commercial alloys, including stainless steels, high-nickel alloys, and superalloys, has also been generated (Ref 16). Tests were conducted in flowing air (30 cm/min) at 980, 1095, 1150, and 1200 °C (1800, 2000, 2100, and 2200 °F)

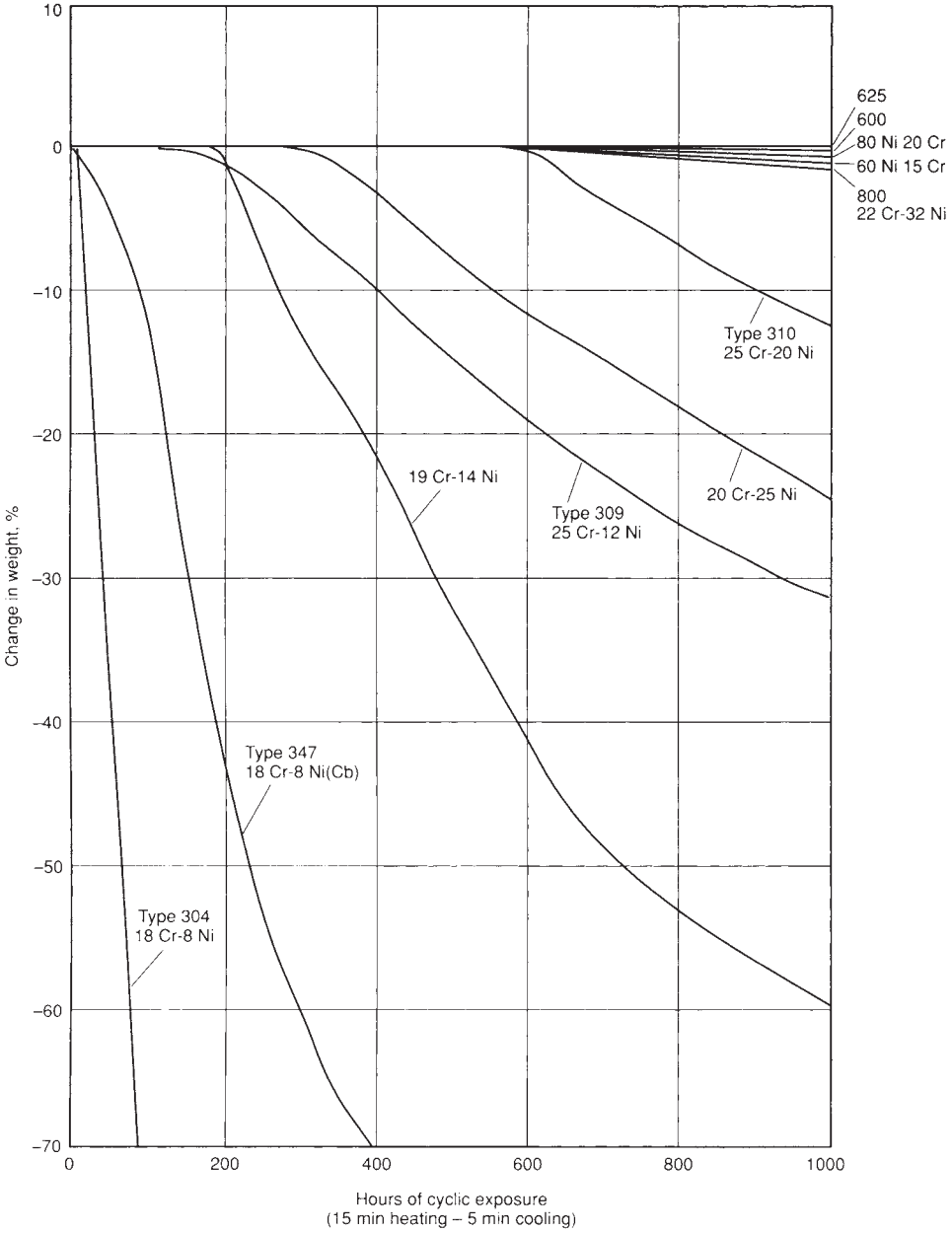


Fig. 1 Cyclic oxidation resistance of several stainless steels and nickel-base alloys in air at 980 °C (1800 °F). Source: Ref 1

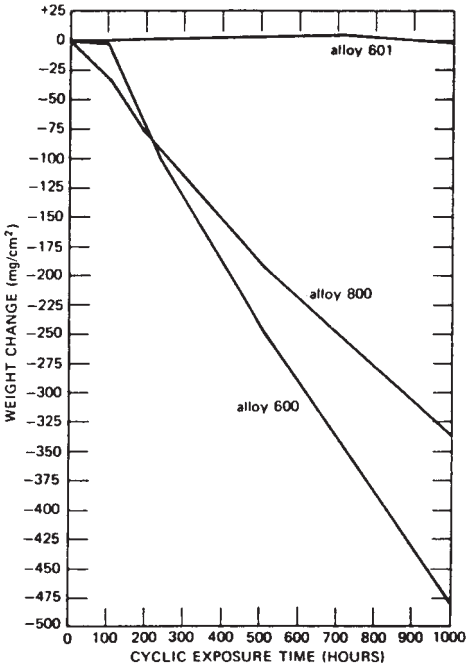


Fig. 2 Cyclic oxidation resistance of alloy 601 compared to alloys 600 and 800 in air at 1090 °C (2000 °F) (15 min in hot zone and 5 min out of hot zone). Source: Ref 3

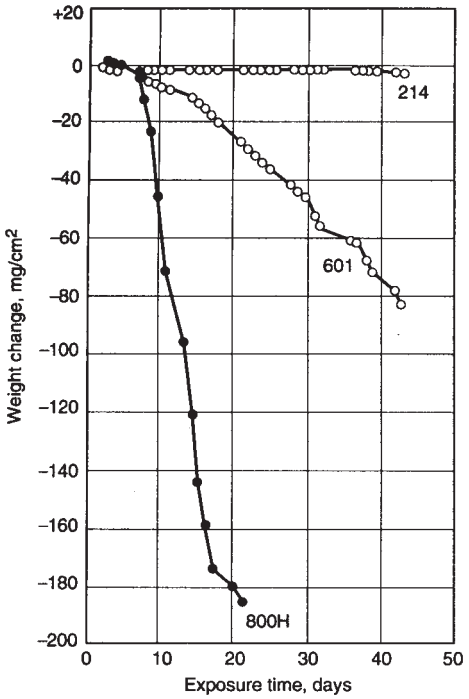


Fig. 3 Cyclic oxidation resistance of alloy 214 compared to alloys 601 and 800H in still air at 1150 °C (2100 °F) cycled once a day every day except weekends. Source: Ref 4

for 1008 h. The samples were cooled to room temperature for visual examination once a week (168 h). The results, presented in terms of metal loss and average metal affected (metal loss plus internal penetration), are summarized in Table 2.

For Fe-Cr and Fe-Ni-Cr alloys, types 304 and 316 stainless steel (SS) were found to be the least resistant to oxidation, both suffering severe attack at 980 °C (1800 °F). As the temperature was increased to 1095 °C (2000 °F) or higher, the oxidation rates of these two alloys became so high that the samples were consumed before the end of the 1008 h test. Type 304 performed slightly better than type 316, presumably due to a slightly higher chromium level. The high-chromium ferritic stainless steel type 446 (Fe-27Cr) exhibited good oxidation resistance at 980 °C (1800 °F), but suffered very severe oxidation attack at 1095 °C (2000 °F) and higher. Types 310, RA330, and alloy 800H were, in general, better than types 446, 304, and 316, particularly at higher temperatures. This may be attributed to higher nickel contents.

The oxidation resistance of alloy 556 is significantly better than that of Multimet alloy, even though both are iron-base superalloys with molybdenum and tungsten additions for solid solution strengthening. Multimet alloy begins suffering rapid oxidation at 1095 °C (2000 °F), and the rates become unacceptably high at higher temperatures. Alloy 556 shows excellent oxidation resistance up to 1095 °C (2000 °F). Oxidation attack becomes high at 1150 °C (2100 °F) and unacceptably high at 1200 °C (2200 °F).

Alloy 556 and Multimet alloy have similar chemical compositions. Alloy 556 was developed by making minute changes of minor alloying elements in Multimet alloy. The improved oxidation resistance resulted from replacement of niobium (columbium) with tantalum as well as the controlled addition of reactive elements, such as lanthanum and aluminum (Ref 17). Irving et al. (Ref 18) found that tantalum is beneficial and niobium is detrimental to oxidation resistance in Co-20Cr-base alloys.

Among the cobalt-base superalloys tested, alloy 188 was best. However, oxidation attack for this alloy became severe when the temperature was increased to 1150 °C (2100 °F). At 1200 °C (2200 °F) the attack was so severe that the alloy should not be considered for long-term service at this temperature. Alloy 188 is significantly better than alloy 25 in oxidation resistance. This improvement was attributed to the addition of lanthanum and the control of minor elements such as silicon, aluminum, titanium, and so forth. Higher nickel content may also have contributed to improved oxidation resistance. Irving et al. (Ref 19) observed a noticeable reduction in oxide scale thickness when the nickel content in Co-15Cr-Ni alloys was increased to 20% and higher. Alloy 150 (or UMCo 50) exhibited unacceptably high oxidation rates at 1150 °C (2100 °F) and higher, while alloy 6B, widely used for wear applications, suffered rapid oxidation at 1095 °C (2000 °F) and higher.

Among the three groups of nickel-base alloys, the precipitation-strengthened alloys, particularly γ'-strengthened alloys, are overall the least resistant to oxidation. These alloys contain relatively high levels of titanium. Titanium is very active in scale formation. The formation of titanium-rich oxides apparently disrupts the chromia scale. The poor oxidation resistance of type 321 stainless steel as compared to types 304, 316, and 347 (Ref 15) may also be attributed to titanium. Nagai et al. (Ref 11) found that titanium was detrimental to the oxidation resistance of Ni-20Cr alloy. In the Fe-Cr-Al system, however, the addition of 1% Ti to Fe-18Cr-6Al was found to improve resistance to cyclic oxidation at 950 °C (1740 °F) in air (Ref 20). Niobium is another alloying element that is detrimental to alloy oxidation resistance. The relatively poor oxidation resistance of alloy 625 at 1095 and 1150 °C (2000 and 2100 °F) may be attributed to niobium.

For Ni-Cr-Fe alloys with various amounts of aluminum, alloy 600 (which generally contains 0.2 or 0.3% Al from melting practices) exhibits

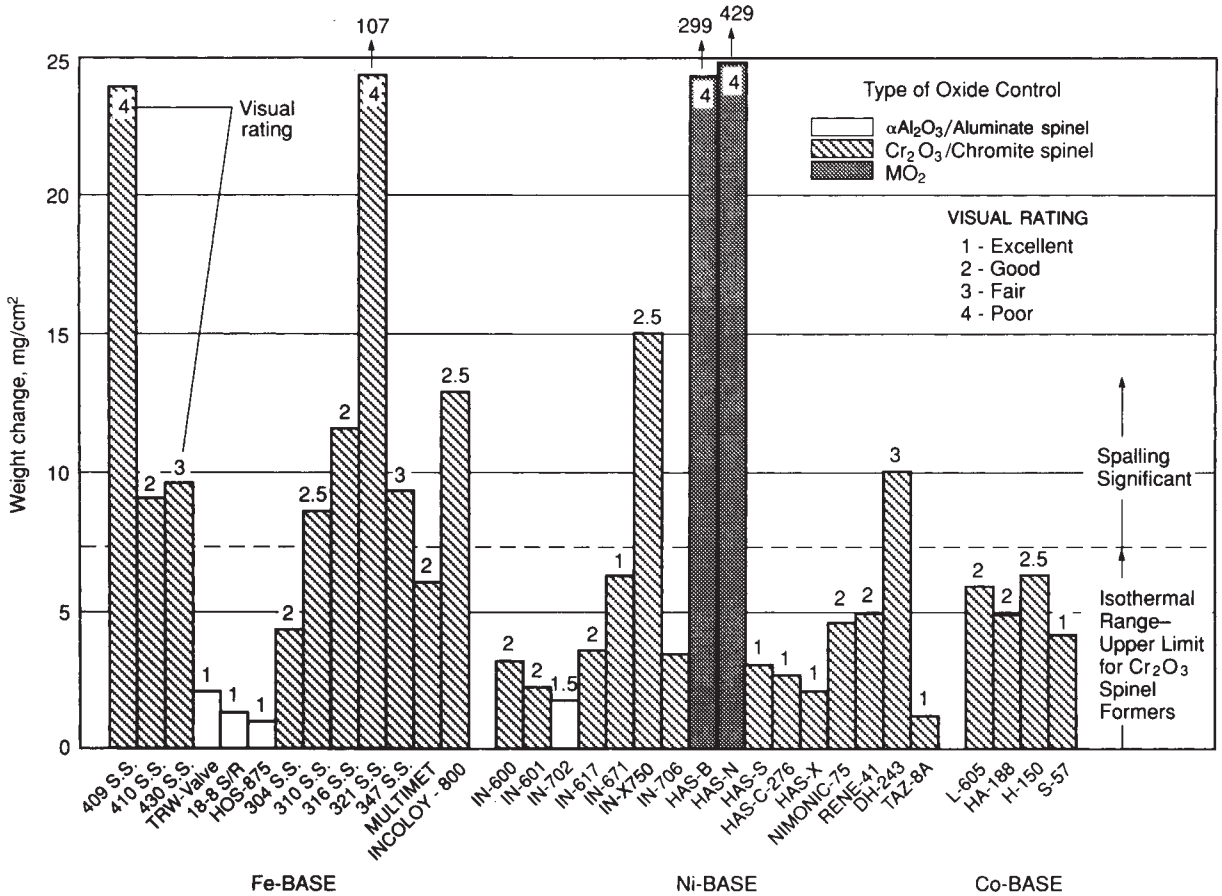


Fig. 4 Long-term oxidation tests (10,000 h) in air at 815 °C (1500 °F) with 1000 h cycles for iron-, nickel-, and cobalt-base alloys. Also included is the upper limit of the metal loss for isothermal tests (i.e., 10,000 without cycling) for same alloys. Source: Ref 15

oxidation attack similar to that of alloy 601, with about 1.4% Al. The level of aluminum in alloy 601 is well below the level needed to form a continuous alumina scale. Thus, alloy 601 is still a chromia former. Because of insufficient aluminum in alloy 601 to form a continuous alumina scale, aluminum tends to segregate to form internal oxides as well as internal nitrides. This sometimes results in much deeper internal penetration. With about 4.5% Al, alloy 214 readily forms an alumina scale. It is clearly shown in Table 2 that alloy 214, exhibiting less than 0.025 mm (1 mil) of total depth of attack at temperatures up to 1200 °C (2200 °F), is significantly better than all the other alloys tested. With a continuous alumina scale, alloy 214 showed little or no internal oxidation attack.

Cyclic Oxidation. Very few industrial processes are able to operate without intermittent shutdowns. Therefore, studies on oxidation should always include the cyclic effect. The oxide scales of some alloys may be more susceptible to cracking or spalling during cooling, thus increasing subsequent oxidation attack when the system resumes operation. The oxidation data presented in Table 2 were generated with a weekly cycle (168 h) to room temperature. When the cyclic frequency was increased to 25 h cycles, oxidation rates were increased for all the alloys tested. However, some alloys are more sensitive to cyclic oxidation than others. The effect of thermal cycling on the oxidation resistance of various alloys in air at 1095 °C (2000 °F) is illustrated in Table 3, which compares once-a-week (168 h) cycle data (Ref 16) with 25 h cycle data (Ref 21). Alloy 214 (an

Table 2 Results of 1008 h static oxidation tests on iron-, nickel-, and cobalt-base alloys in flowing air at indicated temperatures

	980 °C (1800 °F)				1095 °C (2000 °F)				1150 °C (2100 °F)				1205 °C (2200 °F)			
	Metal loss		Average metal affected		Metal loss		Average metal affected		Metal loss		Average metal affected		Metal loss		Average metal affected	
Alloy	mm	mils	mm	mils	mm	mils	mm	mils	mm	mils	mm	mils	mm	mils	mm	mils
214	0.0025	0.1	0.005	0.2	0.0025	0.1	0.0025	0.1	0.005	0.2	0.0075	0.3	0.005	0.2	0.018	0.7
601	0.013	0.5	0.033	1.3	0.03	1.2	0.067	2.6	0.061	2.4	0.135	5.3	0.11	4.4	0.19	7.5
600	0.0075	0.3	0.023	0.9	0.028	1.1	0.041	1.6	0.043	1.7	0.074	2.9	0.13	5.1	0.21	8.9
230	0.0075	0.3	0.018	0.7	0.013	0.5	0.033	1.3	0.058	2.3	0.086	3.4	0.11	4.5	0.20	7.9
S	0.005	0.2	0.013	0.5	0.01	0.4	0.033	1.3	0.025	1.0	0.043	1.7	>0.81	31.7	>0.81	31.7
617	0.0075	0.3	0.033	1.3	0.015	0.6	0.046	1.8	0.028	1.1	0.086	3.4	0.27	10.6	0.32	12.5
333	0.0075	0.3	0.025	1.0	0.025	1.0	0.058	2.3	0.05	2.0	0.1	4.0	0.18	7.1	0.45	17.7
X	0.0075	0.3	0.023	0.9	0.038	1.5	0.069	2.7	0.11	4.5	0.147	5.8	>0.9	35.4	>0.9	35.4
671	0.0229	0.9	0.043	1.7	0.038	1.5	0.061	2.4	0.066	2.6	0.099	3.9	0.086	3.4	0.42	16.4
625	0.0075	0.3	0.018	0.7	0.084	3.3	0.12	4.8	0.41	16.0	0.46	18.2	>1.2	47.6	>1.2	47.6
Waspaloy	0.0152	0.6	0.079	3.1	0.036	1.4	0.14	5.4	0.079	3.1	0.33	13.0	>0.40	15.9	>0.40	15.9
R-41	0.0178	0.7	0.122	4.8	0.086	3.4	0.30	11.6	0.21	8.2	0.44	17.4	>0.73	28.6	>0.73	28.6
263	0.0178	0.7	0.145	5.7	0.089	3.5	0.36	14.2	0.18	6.9	0.41	16.1	>0.91	35.7	>0.91	35.7
188	0.005	0.2	0.015	0.6	0.01	0.4	0.033	1.3	0.18	7.2	0.2	8.0	>0.55	21.7	>0.55	21.7
25	0.01	0.4	0.018	0.7	0.23	9.2	0.26	10.2	0.43	16.8	0.49	19.2	>0.96	37.9	>0.96	37.9
150	0.01	0.4	0.025	1.0	0.058	2.3	0.097	3.8	>0.68	26.8	>0.68	26.8	>1.17	46.1	>1.17	46.1
6B	0.01	0.4	0.025	1.0	0.35	13.7	0.39	15.2	>0.94	36.9	>0.94	36.9	>0.94	36.8	>0.94	36.8
556	0.01	0.4	0.028	1.1	0.025	1.0	0.067	2.6	0.24	9.3	0.29	11.6	>3.8	150.0	>3.8	150.0
Multimet	0.01	0.4	0.033	1.3	0.226	8.9	0.29	11.6	>1.2	47.2	>1.2	47.2	>3.7	146.4	>3.7	146.4
800H	0.023	0.9	0.046	1.8	0.14	5.4	0.19	7.4	0.19	7.5	0.23	8.9	0.29	11.3	0.35	13.6
RA330	0.01	0.4	0.11	4.3	0.02	0.8	0.17	6.7	0.041	1.6	0.22	8.7	0.096	3.8	0.21	8.3
310	0.01	0.4	0.028	1.1	0.025	1.0	0.058	2.3	0.075	3.0	0.11	4.4	0.2	8.0	0.26	10.3
316	0.315	12.4	0.36	14.3	>1.7	68.4	>1.7	68.4	>2.7	105.0	>2.7	105.0	>3.57	140.4	>3.57	140.4
304	0.14	5.5	0.21	8.1	>0.69	27.1	>0.69	27.1	>0.6	23.6	>0.6	23.6	>1.7	68.0	>1.73	68.0
446	0.033	1.3	0.058	2.3	0.33	13.1	0.37	14.5	>0.55	21.7	>0.55	21.7	>0.59	23.3	>0.59	23.3

Source: Ref 16

Table 3 Comparative oxidation resistance of iron-, nickel-, and cobalt-base alloys in flowing air between 168 and 25 h cycles at 1095 °C (2000 °F)

	Metal loss, mm (mils)		Extrapolated metal loss, mm/yr (mils/yr)		Average metal affected, mm (mils)		Extrapolated oxidation rate, mm/yr (mils/yr)	
Alloy	1008 h/168 h	1050 h/25 h	168 h cycle	25 h cycle	1008 h/168 h	1050 h/25 h	168 h cycle	25 h cycle
214	0.003 (0.1)	0.003 (0.1)	0.025 (1)	0.025 (1)	0.003 (1.0)	0.025 (1)	0.025 (1)	0.20 (8)
601	0.030 (1.2)	0.231 (9.1)	0.25 (10)	1.93 (76)	0.066 (2.6)	0.297 (11.7)	0.58 (23)	2.49 (98)
600	0.028 (1.1)	0.079 (3.1)	0.25 (10)	0.66 (26)	0.041 (1.6)	0.185 (7.3)	0.36 (14)	1.55 (61)
671	0.038 (1.5)	0.462 (18.2)	0.33 (13)	3.86 (152)	0.061 (2.4)	0.584 (23.0)	0.53 (21)	4.88 (192)
230	0.013 (0.5)	0.015 (0.6)	0.10 (4)	0.13 (5)	0.003 (1.3)	0.086 (3.4)	0.28 (11)	0.71 (28)
S	0.010 (0.4)	0.013 (0.5)	0.10 (4)	0.10 (4)	0.003 (1.3)	0.061 (2.4)	0.28 (11)	0.51 (20)
G-30	0.038 (1.5)	0.036 (1.4)	0.33 (13)	0.30 (12)	0.122 (4.8)	0.203 (8.0)	1.07 (42)	1.70 (67)
617	0.015 (0.6)	0.168 (6.6)	0.13 (5)	1.40 (55)	0.046 (1.8)	0.267 (10.5)	0.41 (16)	2.24 (88)
333	0.025 (1.0)	0.033 (1.3)	0.23 (9)	0.28 (11)	0.058 (2.3)	0.130 (5.1)	0.51 (20)	1.09 (43)
625	0.084 (3.3)	0.353 (13.9)	0.74 (29)	2.95 (116)	0.122 (4.8)	0.414 (16.3)	1.07 (42)	3.45 (136)
Waspaloy	0.036 (1.4)	0.279 (10.9)	0.30 (12)	2.31 (91)	0.137 (5.4)	0.414 (16.3)	1.19 (47)	3.15 (136)
263	0.089 (3.5)	0.439 (17.3)	0.76 (30)	3.66 (144)	0.361 (14.2)	0.478 (18.8)	3.12 (123)	3.99 (157)
188	0.010 (0.4)	0.028 (1.1)	0.10 (4)	0.23 (9)	0.003 (1.3)	0.058 (2.3)	0.28 (11)	0.48 (19)
25	0.234 (9.2)	0.419 (16.5)	2.03 (80)	3.51 (138)	0.259 (10.2)	0.490 (19.3)	2.26 (89)	4.09 (161)
150	0.058 (2.3)	0.223 (8.8)	0.51 (20)	1.85 (73)	0.097 (3.8)	0.353 (13.9)	0.84 (33)	2.95 (116)
6B	0.348 (13.7)	>0.800 (31.5)	3.02 (119)	>6.68 (263)	0.394 (15.5)	>0.800 (31.5)	3.43 (135)	>6.68 (263)
556	0.025 (1.0)	0.038 (1.5)	0.23 (9)	0.33 (13)	0.066 (2.6)	0.117 (4.6)	0.58 (23)	0.97 (38)
Multimet	0.223 (8.9)	0.328 (12.9)	1.96 (77)	2.74 (108)	0.295 (11.6)	0.381 (15.0)	2.57 (101)	3.18 (125)
800H	0.137 (5.4)	0.328 (12.9)	1.19 (47)	2.74 (108)	0.188 (7.4)	0.406 (16.0)	1.63 (64)	3.40 (134)
RA330	0.020 (0.8)	0.269 (10.6)	0.18 (7)	2.24 (88)	0.170 (6.7)	0.442 (17.4)	1.47 (58)	3.68 (145)
310	0.025 (1.0)	0.058 (2.3)	0.23 (9)	0.48 (19)	0.058 (2.3)	0.112 (4.4)	0.51 (20)	0.94 (37)
446	0.333 (13.1)	0.579 (22.8)	2.92 (115)	4.83 (190)	0.368 (14.5)	0.655 (25.8)	3.20 (126)	5.46 (215)

alumina former) was found to suffer little or no attack in tests with either 168 h or 25 h cycling. Some chromia formers (230, S, 333, 188, 556, and type 310) showed good resistance to thermal cycling. It is not possible to correlate the performance of these alloys with their chemical compositions. However, most of these alloys (i.e., alloys 230, S, 188, and 556) contain many minor reactive elements as well as a rare earth element, lanthanum.

Kane et al. (Ref 22) studied the cyclic oxidation resistance of several high-temperature alloys in air-5H_2O at 1100 °C (2010 °F) for exposure times up to 2016 h with 24 h cycles. Their results in terms of weight change as a function of exposure time are shown in Fig. 5. The alumina-forming MA956 alloy (about 4.5% Al) exhibited no changes in weight, while all chromia formers (alloy 601, HK alloy, alloy 800, and type 310) suffered weight losses, with type 310 being the worst. This was in contrast to the 25 h cyclic test results observed by Lai (Ref 21), where type 310 was found to be more resistant to cyclic oxidation than some nickel-base alloys, (such as alloy 601) and Fe-Ni-Cr alloys (such as alloy 800H). There was a difference between the two test environments. The air environment used by Kane et al. (Ref 22) contained 5% H_2O, while that used by Lai (Ref 21) was basically dry air (the air was passed through an air filter prior to entering the test retort). Table 4 shows the results of another cyclic oxidation study, done by Kane et al. (Ref 23) in air-5H_2O at 1100 °C (2010 °F) for 504 h with 15 min cycles. Two alumina formers, MA956 and IN-814, were the best performers, followed by cobalt- and nickel-base alloys (alloys 188, 601, 617, X, and 333). Three iron-base alloys (HK alloy, type 310, and alloy 800) were not as good as the nickel-base alloys.

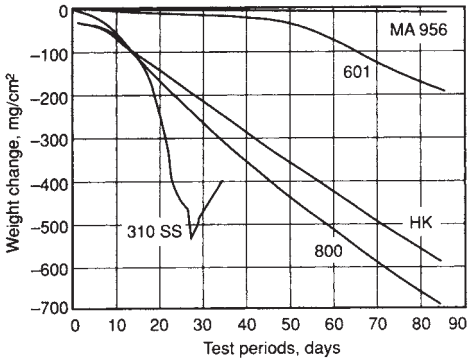


Fig. 5 Cyclic oxidation resistance of several high-temperature alloys in air-5H_2O at 1100 °C (2010 °F) for times up to 2016 h with 24 h cycles. Source: Ref 22

Oxidation Behavior in Combustion Atmospheres. Many industrial processes involve combustion. The burner rig test system has been quite popular in the gas turbine industry to study the oxidation of gas turbine alloys in combustion atmospheres. It has also been routinely used during the development of new alloys for gas turbines. Lai (Ref 21) studied the oxidation behavior of a wide variety of alloys, from stainless steels to superalloys, in combustion atmospheres using a burner rig test system. The combustion of fuel oil with preheated, pressurized air results in a high-velocity gas stream (0.3 mach, or 225 mph). Because of this high-velocity stream, the test is also referred to as a "dynamic" oxidation test. The sample holder, which can hold as many as 24 samples, is rotated during testing to ensure that all samples are subjected to identical conditions. Furthermore, severe thermal cycling is imposed, which involves automatically lowering the samples every 30 min, blasting them with fan air to cool them to below 260 °C (500 °F) in 2 min, then returning them to the combustion test tunnel. The air-to-fuel ratio is 50 to 1, and the fuel oil (mixture of two parts No. 1 and one part No. 2) typically contains about 0.15% S. Table 5 tabulates the test results generated at 1090 °C (2000 °F) for 500 h with 30 min cycles for iron-, nickel-, and cobalt-base alloys.

With an alumina scale, alloy 214 suffered very little attack. The alloy showed no sign of breakaway corrosion after 500 h, and the scale consisted of aluminum-rich oxides. After 1000 h (2000 cycles) of testing, the scale remained aluminum-rich. The maximum metal affected (metal loss plus maximum internal penetration) remained about the same after 1000 h compared to after 500 h. All the other alloys tested were chromia formers, with performance varying quite significantly from alloy to alloy.

In general, the Fe-Ni-Cr and Ni-Cr-Fe alloys were the poorest performers; however, RA330 was the best in the group. Alloys containing about 1% Al are generally susceptible to the formation of internal aluminum nitrides in air or highly oxidizing combustion atmospheres. For example, alloy 601, which suffered a metal loss similar to that of RA330, exhibited internal aluminum nitrides throughout the sample thickness. Alloy 617 is another alloy that frequently suffers the formation of internal aluminum nitrides.

Of all the alloys tested at 1090 °C (2000 °F), Multimet alloy was one of the worst. The specimen (about 1.4 mm, or 0.056 in., thick) was consumed in only about 225 h. Alloy 556, a modified version of Multimet alloy with some changes of minor alloying elements (Ref 17), exhibited significantly better oxidation resistance. This is a good example of how the addition and modification of minor alloying elements can improve oxidation resistance.

The results of dynamic oxidation tests at 980 °C (1800 °F) for 1000 h (2000 cycles) are presented in Table 6. The performance ranking was similar to that of 1090 °C (2000 °F) tests, with the exception of alloy 625, which was ranked higher. RA330 continued to be the best among the Fe-Ni-Cr and Ni-Cr-Fe alloys. The 18Cr-8Ni steels suffered extremely rapid oxidation attack. Types 304 and 316 stainless steel samples (1.17 mm, or 0.046 in., thick) were consumed in about 65 h.

Very limited field test data generated in "clean" combustion atmospheres have been reported. Table 7 summarizes the results of a field test performed inside a radiant tube fired with natural gas with an average temperature of 1010 °C (1850 °F) (Ref 24). The rack containing coupons of various alloys was exposed for

Table 4 Cyclic oxidation resistance of several iron-, nickel-, and cobalt-base alloys at 1100 °C (2010 °F) for 504 h in air-5H_2O

	Specific weight change (descaled), mg/cm²		Metal loss		Maximum attack	
Alloy	Mean	Range	mm	mils	mm	mils
AC1 grade HK	–105.8	–98 to –124	0.25	9.9	0.35	13.8
310SS	–149.0	–92 to –235	0.31	12.2	0.38	15.0
800	–168.6	–83 to –223	0.39	15.4	0.59	23.2
601	–11.0	–6.3 to –17.2	<0.02	0.8	0.12	4.7
617	–13.5	–6.5 to –17.5	…	…	…	…
X	–20.0	–10.0 to –29.5	0.05	2.0	0.25	9.9
RA333	–30.5	…	…	…	…	…
IN-814	–3.5	–2.5 to –4.9	0	0	<0.01	0.4
188	–25.0	–13.0 to –40.5	0.03	1.2	0.15	5.9
MA956	–1.0	–0.3 to –1.5	<0.01	0.4	0.02	0.8

Note: 15 min in furnace and 5 min out of furnace. Source: Ref 23

Table 5 Dynamic oxidation resistance of iron-, nickel-, and cobalt-base alloys in high-velocity combustion gas stream at 1090 °C (2000 °F) for 500 h

	Metal loss		Maximum metal affected(a)	
Alloy	mm	mils	mm	mils
214	0.013	0.5	0.046	1.8
230	0.056	2.2	0.15	5.7
RA333	0.10	4.0	0.22	8.7
188	0.19	7.5	0.27	10.7
556	0.22	8.7	0.30	11.7
X	0.23	9.0	0.34	13.5
RA330	0.28	10.9	0.35	13.6
S	0.30	11.8	0.39	15.2
600	0.44	17.2	0.53	20.7
310	0.54	21.2	0.61	24.1
601	0.27	10.7	0.61(b)	24.0(b)
617	0.32	12.4	0.61(b)	24.0(b)
800H	0.77(c)	30.5(c)	0.86(c)	34.0(c)
625	>0.79(d)	31.0(d)	>0.79(d)	31.0(d)
Multimet	1.25(e)	49.1(e)	1.42(e)	55.8(e)

Note: Gas velocity was 0.3 mach (100 m/s, or 225 mph); samples were cycled to less than 260 °C (500 °F) once every 30 min; 50-to-1 air-to-fuel ratio; two parts No. 1 fuel oil and one part No. 2 fuel oil. (a) Metal loss plus maximum internal penetration. (b) Internal nitrides through thickness. (c) Extrapolated from 400 h; sample was about to be consumed after 400 h. (d) Sample was consumed in 500 h. (e) Extrapolated from 225 h; sample was about to be consumed after 225 h. Source: Ref 21

Table 6 Dynamic oxidation resistance of iron-, nickel-, and cobalt-base alloys in high-velocity combustion gas stream at 980 °C (1800 °F) for 1000 h

	Metal loss		Maximum metal affected(a)	
Alloy	mm	mils	mm	mils
214	0.010	0.4	0.031	1.2
230	0.020	0.8	0.089	3.5
188	0.028	1.1	0.107	4.2
556	0.043	1.7	0.158	6.2
X	0.069	2.7	0.163	6.4
S	0.079	3.1	0.17	6.6
RA333	0.064	2.5	0.18	7.0
625	0.12	4.9	0.19	7.6
617	0.069	2.7	0.27	10.7
RA330	0.20	7.8	0.30	11.8
Multimet	0.30	11.8	0.38	14.8
800H	0.31	12.3	0.39	15.3
310	0.35	13.7	0.42	16.5
600	0.31(b)	12.3(b)	0.45(b)	17.8(b)
601	0.076	3.0	0.51	20.0
304	>9.0(c)	354(c)	>9.0(c)	354(c)
316	>9.0(c)	354(c)	>9.0(c)	354(c)

Note: Gas velocity was 0.3 mach (100 m/s, or 225 mph); samples were cycled to less than 260 °C (500 °F) once every 30 min; 50-to-1 air-to-fuel ratio; two parts No. 1 fuel oil and one part No. 2 fuel oil. (a) Metal loss plus maximum internal penetration. (b) Extrapolated from 917 h; sample was about to be consumed after 917 h. (c) Extrapolated from 65 h; sample was consumed in 65 h. Source: Ref 21

about 3000 h. Many chromia formers, such as alloys 601, 230, 556, 310SS, 600, and 330, were found to perform well, with oxidation rates of less than 0.5 mm/yr (20 mils/yr). The test also showed that the temperature of 1010 °C (1850 °F) was too high for type 304 stainless steel. Similar to the results of air oxidation tests and burner rig dynamic oxidation tests, the alumina former (alloy 214) was found to be the best performer. In another field test (Ref 25) performed in a natural gas-fired furnace used for reheating ingots and slabs of nickel- and cobalt-base alloys, samples of various alloys were exposed for about 113 days at temperatures from 1090 to 1230 °C (2000–2250 °F) with frequent cycles to 540 °C (1000 °F). The results are summarized in Table 8. All of the chromia formers tested suffered severe oxidation attack. On the other hand, the alumina former (alloy 214) exhibited little attack. The scales formed on alloy 214 consisted of essentially aluminum-rich oxides (Ref 25).

The alumina scale formed on alloy 214 is very protective in both laboratory and field tests at temperatures up to 1230 °C (2250 °F). This oxide scale remains protective even when the temperature is increased to 1320 °C (2400 °F). The sample showed no sign of breakaway corrosion after testing in air at 1320 °C (2400 °F) for 200 h with 25 h cycles (Ref 21). The scale consisted of mainly aluminum-rich oxides and showed no sign of cracking.

Carburization

In addition to oxygen attack, high-temperature alloys are frequently subjected to attack by carbon compounds (carburization). Materials problems due to carburization are quite common in heat treating components associated with carburizing furnaces. The environment in the carburizing furnace typically has a carbon activity that is significantly higher than that in the alloy of the furnace component. Therefore, carbon is transferred from the environment to the alloy. This results in the carburization of the alloy, and the carburized alloy becomes embrittled.

Lai (Ref 26) studied the carburization resistance of more than 20 commercial wrought alloys, ranging from stainless steels to superalloys. The test environments were characterized by a unit carbon activity and oxygen potentials such that a chromia scale was not expected to form on the metal surface. Oxides of silicon, titanium, and aluminum were expected to be stable under the test conditions. The relative performance rankings for alloys tested at 870, 930, and 980 °C (1600, 1700, and 1800 °F) are shown in Fig. 6. No obvious correlations between performance and alloy composition were noted, perhaps because most of the alloys contained many alloying elements, including solid-solution-strengthening elements (e.g., molybdenum, tungsten, niobium), precipitate-forming elements (e.g., aluminum, titanium, niobium), and other minor elements for oxidation resistance, melting control, and so forth. Some of these alloying elements may play an important role in affecting the performance of an alloy.

One alloy that was found to be consistently better than the others was alloy 214, containing about 4.5% Al. The excellent resistance of this alloy was attributed to the alumina film formed on the metal surface. The existence of this film was confirmed by Auger analysis (Ref 26). Figure 7 illustrates the microstructure of alloy 214 compared to those of alloys X, 601, and 150 after exposure to the test environment at 980 °C (1800 °F) for 55 h (Ref 26). Tests in the same gas mixture at 1090 °C (2000 °F) showed that the mass of carbon absorbed by alloy 214 was only about one-third of that by the best chromia former (Table 9). A similar observation was made by Kane et al. (Ref 28), who compared MA956 (an oxide dispersion strengthened alloy with about 4.5% Al) with alloys 601, 800H, 310, and cast alloy HK (Fe-26Cr-20Ni). MA956 (an alumina former) was significantly better than the other alloys tested (chromia formers), as shown in Table 10.

Metal dusting, which is sometimes referred to as catastrophic carburization, is another frequently encountered mode of corrosion that is associated with carburizing furnaces. Metal dusting tends to occur in a region where the carbonaceous gas atmosphere becomes stagnant. The alloy normally suffers rapid metal wastage. The corrosion products (or wastage) generally consist of carbon soots, metal, metal carbides, and metal oxides. The attack is nor-

Table 7 Results of field test in a natural gas-fired tube at 1010 °C (1850 °F) for 3000 h

	Metal loss		Maximum metal affected(a)		Oxidation rate	
Alloy	mm	mils	mm	mils	mm/yr	mils/yr
214	0.003	0.1	0.025	1	0.076	3
601	0.023	0.9	0.076	3	0.23	9
230	0.028	1.1	0.10	4	0.30	12
556	0.018	0.7	0.10	4	0.30	12
310	0.041	1.6	0.10	4	0.30	12
600	0.018	0.7	0.15	6	0.46	18
RA330	0.048	1.9	0.15	6	0.46	18
800H	0.12	4.7	0.30	12	0.89	35
309	0.50	19.7	0.51	20	1.5	58
304	>1.5(b)	60(b)	>1.5	60(b)	>4.4	175

(a) Metal loss plus maximum internal penetration. (b) Sample was consumed. Source: Ref 24

Table 8 Results of field test in a natural gas-fired furnace for reheating nickel- and cobalt-base alloy ingots and slabs for 113 days at 1090–1230 °C (2000–2250 °F) with frequent cycles to 540 °C (1000 °F)

	Metal loss		Maximum affected(a)	
Alloy	mm	mils	mm	mils
214	0.013	0.5	0.11	4.5
RA330	0.39	15.5	0.65	25.5
601	0.18	7.2	0.95	37.2
600	0.64	25.0	1.1	45.0
800H	>0.79(b)	31.0(b)	>0.79(b)	31.0(b)
310SS	>1.0(b)	41.0(b)	>1.0(b)	41.0(b)
304SS	>1.5(b)	60.0(b)	>1.5(b)	60.0(b)
316SS	>1.6(b)	63.0 (b)	>1.6(b)	63.0 (b)
446SS	>0.61(b)	24.0(b)	>0.61(b)	24.0(b)

(a) Metal loss plus internal penetration. (b) Samples were consumed. Source: Ref 25

Table 9 Carburization resistance of various alloys in Ar-5H_2-5CO-5CH_4 at 1090 °C (2000 °F) for 24 h

Alloy	Carbon absorption, mg/cm^2
214	3.4
600	9.9
625	9.9
230	10.3
X	10.6
S	10.6
304	10.6
617	11.5
316	12.0
333	12.4
800H	12.6
330	12.7
25	14.4

Source: Ref 27

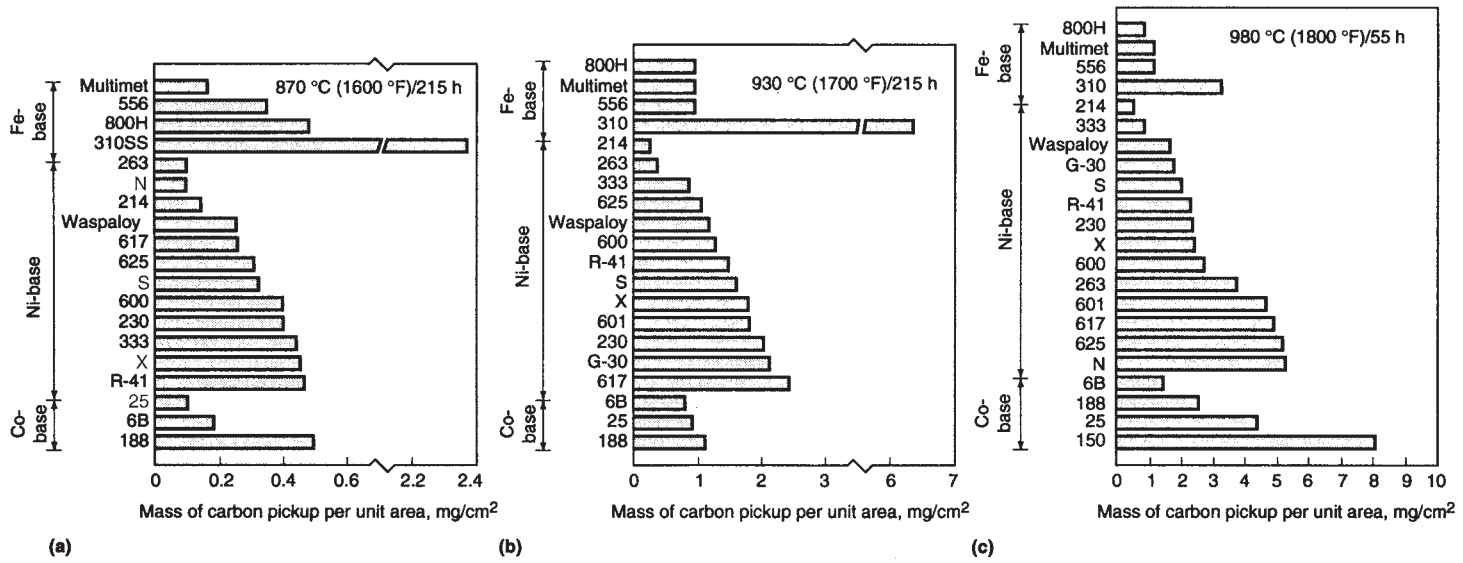


Fig. 6 Carburization resistance of various iron-, nickel-, and cobalt-base alloys tested in Ar-5H_2-5CO-5CH_4 at (a) 870 °C/215 h, (b) 930 °C/215 h, and (c) 980 °C/55 h. Source: Ref 26

mally initiated from the metal surface that is in contact with the furnace refractory. The furnace components that suffer metal dusting include thermowells, probes, and anchors. Figure 8 illustrates the metal dusting attack on Multimet alloy. The component was perforated as a result of metal dusting.

Metal dusting has been encountered with straight chromium steels, austenitic stainless steels, and nickel- and cobalt-base alloys. All of these alloys are chromia formers. Because metal dusting is a form of carburization, it would appear that alumina formers, such as alloy 214, would also be more resistant to metal dusting.

Nitridation

Metals or alloys are generally susceptible to nitridation when exposed to ammonia-bearing or nitrogen-base atmospheres at elevated temperatures. Nitridation typically results in the formation of nitrides. As a result, the alloy can become embrittled.

Ammonia-Base Atmospheres. Studies by Barnes and Lai (Ref 29) have examined the nitridation behavior of a variety of commercial alloys in ammonia. The alloys studied included stainless steels, Fe-Ni-Cr alloys, and nickel- and cobalt-base superalloys. The superalloys under study contained many alloying elements,

Table 10 Carburization in H_2-2CH_4 at 1000 °C (1830 °F) for 100 h

Alloy	Weight gain, mg/cm^2
MA956	<0.3
601	10
800	19
310SS	36
HK (1.07% Si)	34
HK (2.54% Si)	29

Source: Ref 28

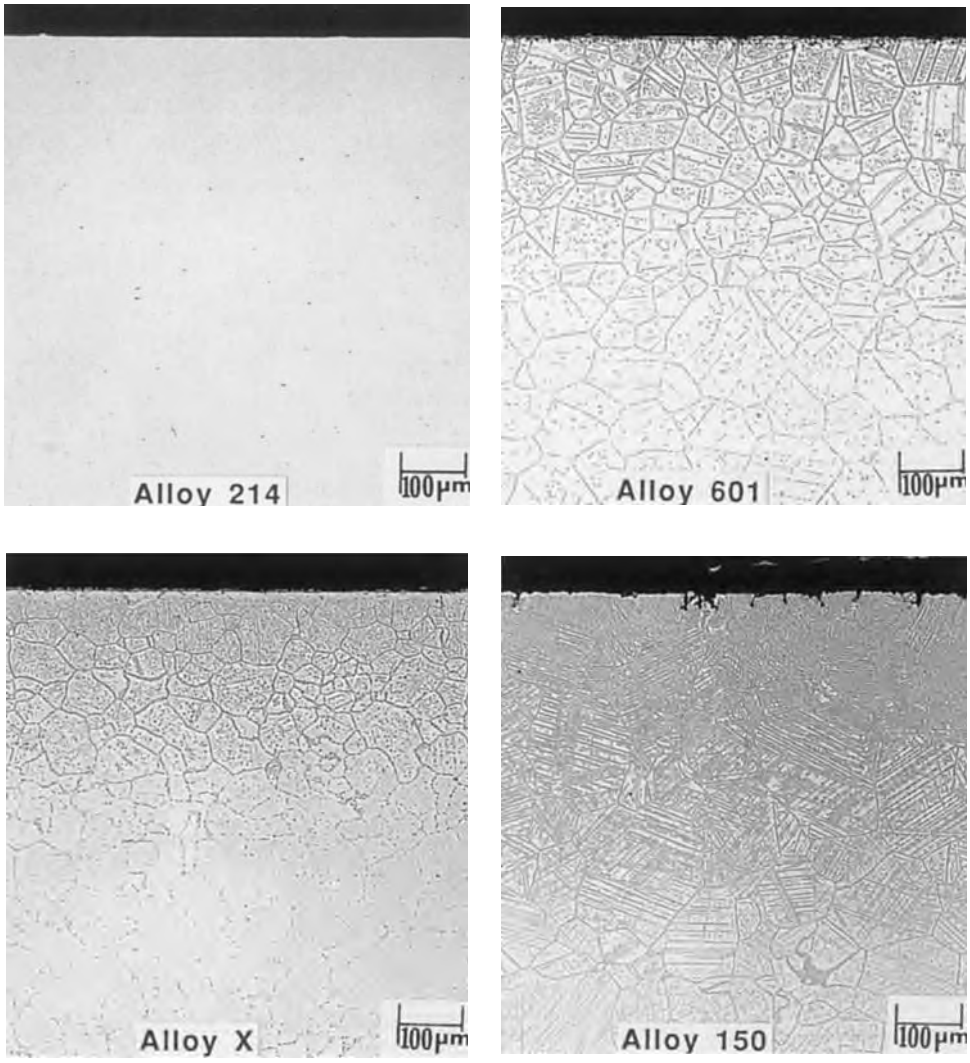
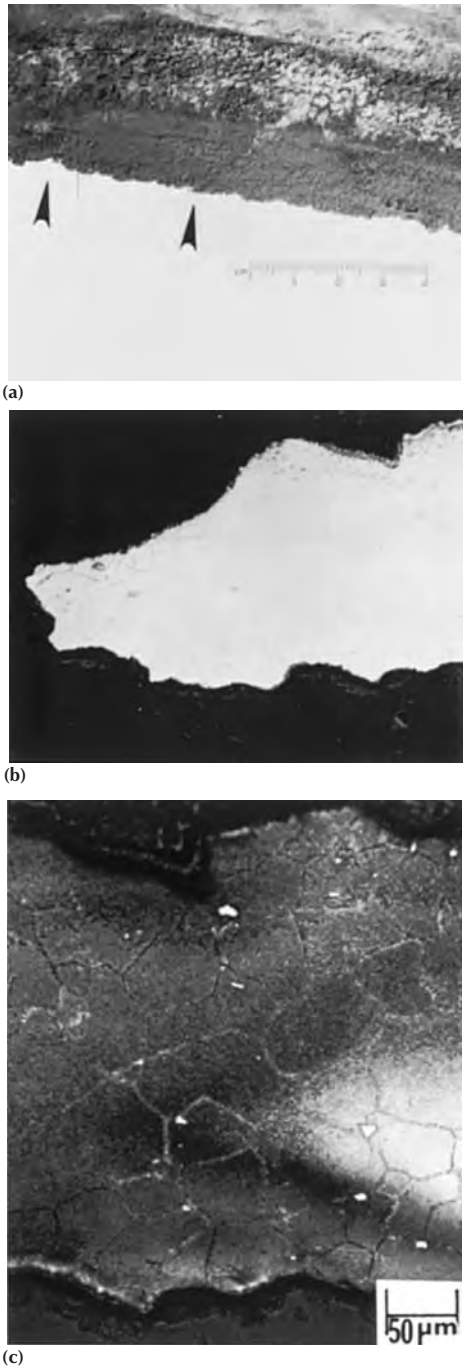


Fig. 7 Microstructure of several high-temperature alloys tested at 980 °C (1800 °F) for 55 h in Ar-5H_2-5CO-5CH_4

such as aluminum, titanium, zirconium, niobium, chromium, molybdenum, tungsten, and iron. These are all nitride formers. The test results generated at 650, 980, and 1090 °C (1200, 1800, and 2000 °F) are summarized in Tables 11 to 13. Again, it was found that nickel-base alloys are generally better than iron-base alloys and that increasing nickel content generally improves the resistance of an alloy to nitridation attack. Increased cobalt content appears to have the same effect. When nitrogen absorption was plotted against Ni + Co content in the alloy for the 650 °C (1200 °F) test data (Fig. 9), resistance to nitridation improved with increasing Ni + Co content up to about 50 wt%. Further increases up to about 75% did not seem to affect the nitridation resistance of an alloy. For maximum resistance to nitridation attack at 650 °C (1200 °F), it appears that alloys with at least 50% Ni or 50% (Ni + Co) are most suitable.

This finding is in general agreement with the results reported by Moran et al. (Ref 30). Their results suggested that improvement in nitridation resistance begins to level off at about 40% Ni, with no improvement resulting from further increases in nickel up to 80%. Pure nickel, however, showed significantly lower nitridation resistance (Ref 30).

At higher temperatures (e.g., 980 °C, or 1800 °F), a slightly different relationship was observed, as shown in Fig. 10. Nitrogen absorption was reduced dramatically with an initial 15% Ni or 15% (Ni + Co). As Ni + Co content increased from 15 to 50%, no dramatic improvement in nitridation resistance was noted. Further increases in Ni + Co content in excess of about 50% caused a sharp improvement. Alloys with Ni (or Ni + Co) in excess of about



(a) (b) (c)

Fig. 8 Metal dusting of a Multimet alloy component at the refractory interface in a carburizing furnace. Perforation of the component (arrows). (b) Cross section of the sample showing severe pitting. (c) Severe carburization beneath the pitted area

Table 11 Nitridation resistance of various alloys at 650 °C (1200 °F) for 168 h in ammonia

Alloy	Alloy base	Nitrogen absorption, mg/cm^2	Depth of nitride penetration	
			mm	mils
C-276	Nickel	0.7	0.02	0.6
230	Nickel	0.7	0.03	1.2
HR-160	Nickel	0.8	0.01	0.5
600	Nickel	0.8	0.03	1.3
625	Nickel	0.9	0.01	0.5
RA333	Nickel	1.0	0.03	1.0
601	Nickel	1.1	0.03	1.0
188	Cobalt	1.2	0.02	0.6
S	Nickel	1.3	0.03	1.1
617	Nickel	1.3	0.03	1.0
214	Nickel	1.5	0.04	1.5
X	Nickel	1.7	0.04	1.5
825	Nickel	2.5	0.06	2.2
800H	Iron	4.3	0.10	4.1
556	Iron	4.9	0.09	3.5
316	Iron	6.9	0.19	7.3
310	Iron	7.4	0.15	6.0
304	Iron	9.8	0.21	8.4

Note: 100% NH_3 in the inlet gas and 30% NH_3 in the exhaust gas. Source: Ref 29

Table 12 Nitridation resistance of various alloys at 980 °C (1800 °F) for 168 h in ammonia

Alloy	Alloy base	Nitrogen absorption, mg/cm^2	Depth of nitride penetration	
			mm	mils
214	Nickel	0.3	0.04	1.4
600	Nickel	0.9	0.12	4.8
S	Nickel	0.9	0.18	7.2
601	Nickel	1.2	0.17	6.6
230	Nickel	1.4	0.12	4.9
617	Nickel	1.5	0.38	15.0
HR-160	Nickel	1.7	0.18	7.2
188	Cobalt	2.3	0.19	7.4
625	Nickel	2.5	0.17	6.9
6B	Cobalt	3.1	0.15	5.8
253MA	Iron	3.3	0.48	19.0
25	Cobalt	3.6	0.26	10.4
X	Nickel	3.2	0.19	7.4
RA333	Nickel	3.7	0.42	16.4
RA330	Iron	3.9	0.52	20.6
800H	Iron	4.0	0.28	11.1
825	Nickel	4.3	0.58	23.0
150	Cobalt	5.3	0.38	15.1
Multimet	Iron	5.6	0.35	13.6
316	Iron	6.0	0.52	20.3
556	Iron	6.7	0.37	14.7
304	Iron	7.3	>0.58	23.0
310	Iron	7.7	0.38	15.1
446	Iron	12.9	>0.58	23.0

Note: 100% NH_3 in the inlet gas and less than 5% NH_3 in the exhaust gas. Source: Ref 29

Table 13 Nitridation resistance of various alloys at 1090 °C (2000 °F) for 168 h in ammonia

Alloy	Alloy base	Nitrogen absorption, mg/cm^2	Depth of nitride penetration	
			mm	mils
600	Nickel	0.2	0	0
214	Nickel	0.2	0.02	0.7
S	Nickel	1.0	0.34	13.4
230	Nickel	1.5	0.39	15.3
25	Cobalt	1.7	>0.65	25.5
617	Nickel	1.9	>0.56	22
188	Cobalt	2.0	>0.53	21
HR-160	Nickel	2.5	0.46	18
601	Nickel	2.6	>0.58	23
RA330	Iron	3.1	>0.56	22
625	Nickel	3.3	>0.56	22
316	Iron	3.3	>0.91	36
304	Iron	3.5	>0.58	23
X	Nickel	3.8	>0.58	23
150	Cobalt	4.1	0.51	20
556	Iron	4.2	>0.51	20
446	Iron	4.5	>0.58	23
6B	Cobalt	4.7	>0.64	25
Multimet	Iron	5.0	>0.64	25
825	Nickel	5.2	0.58	23
RA333	Nickel	5.2	>0.71	28
800H	Iron	5.5	>0.76	30
253MA	Iron	6.3	>1.5	60
310	Iron	9.5	>0.79	31

Note: 100% NH_3 in the inlet gas and less than 5% in the exhaust gas. Source: Ref 29

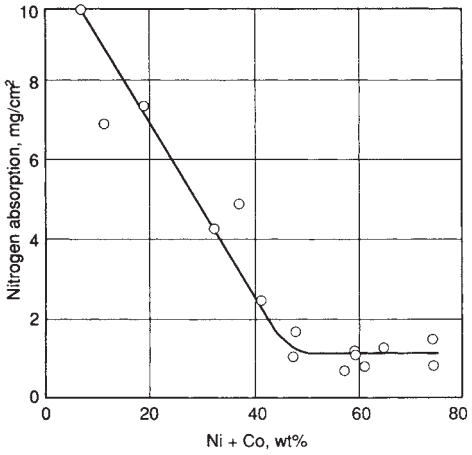


Fig. 9 Effect of Ni + Co content in iron-, nickel-, and cobalt-base alloys on nitridation resistance at 650 °C (1200 °F) for 168 h in ammonia (100% NH_3 in the inlet gas and 30% NH_3 in the exhaust). Source: Ref 29

60% showed the most resistance to nitridation. No data are available for alloys with 80% Ni (or Ni + Co) and higher. It is generally believed that the beneficial effect of nickel or cobalt in increasing nitridation resistance is due to the reduced solubility of nitrogen in the alloy. Nickel and cobalt were found to reduce the solubility of nitrogen in iron (Ref 31, 32).

Nitridation at low temperatures (e.g., 650 °C, or 1200 °F) generally results in a surface nitride layer consisting of mostly iron nitrides (Fe_2N or Fe_4N). High temperatures, on the other hand, result in internal nitrides, mostly CrN, Cr_2N, and/or $(Fe,Cr)_2N$. Figure 11 illustrates the morphology of nitrides formed at both low and high temperatures. In addition to iron and chromium nitrides, aluminum nitrides, which are needle phases, are frequently observed in some alloys containing aluminum. Aluminum is a very strong nitride former. When alloys contain relatively low aluminum (e.g., about 1%), such as alloys 601 and 617, a significant amount of internal aluminum nitrides is generally formed, as shown in Fig. 12(a). For alloys containing relatively high aluminum (e.g., 4.5% Al in alloy 214), very few aluminum nitrides are formed, as illustrated in Fig. 12(b). This may be related to the alumina film developed in alloy 214. Alloys such as alloy 601, with only about 1.3% Al, are generally not capable of developing an alumina continuous surface film. It is believed that alumina is thermodynamically stable in the test environments used in the studies by Barnes and Lai (Ref 29). It should be noted that alumina scale formation is favored kinetically at high temperatures, such as 980 °C (1800 °F) or above. Higher temperatures generally produce a more protective alumina scale.

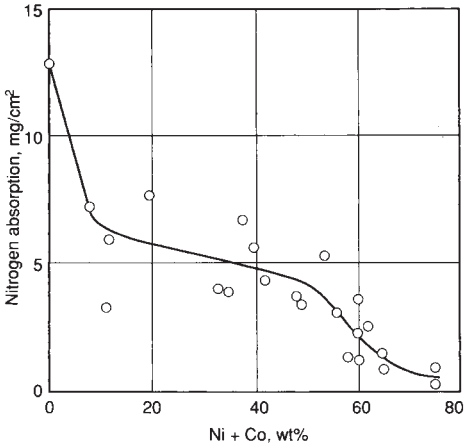


Fig. 10 Effect of Ni + Co content in iron-, nickel-, and cobalt-base alloys on nitridation resistance at 980 °C (1800 °F) for 168 h in ammonia (100% NH_3 inlet gas and <NH_3 in the exhaust). Source: Ref 29

Nitrogen-Base Atmospheres. There have been very few studies on the nitridation behavior of alloys in nitrogen-base atmospheres. This type of atmosphere is becoming more popular as a protective atmosphere in heat treating and sintering operations. Smith and Bucklin (Ref 33) investigated the gas-metal reactions for several iron- and nickel-base alloys in several nitrogen-base atmospheres. Their test results, generated in nitrogen at 980, 1090, and 1200 °C (1800, 2000, and 2200 °F), are shown in Table 14. Both AlN and Cr_2N were found in alloys 600 and 800 after exposure to nitrogen at 1200 °C (2200 °F) for 100 h. For RA330, only Cr_2N was detected after exposure to the same test conditions.

The nitridation attack was surprisingly severe in pure nitrogen. Alloys 601, 800, and 330 suffered more than 3.8 mm (150 mils) of penetration depth after only 100 h of exposure at 1200 °C (2200 °F). Even the best performer, alloy 600, suffered a penetration depth of 2.2 mm (85 mils) in 100 h. When the temperature was lowered to 1090 °C (2000 °F), nitridation attack was still quite severe. For exposure of 960 h at 1090 °C (2000 °F), alloys 800, 520, 330, and 314 suffered more than 3.8 mm (150 mils) of penetration. Alloys 600 and 601 exhibited 1.9 mm (73 mils) and 2.8 mm (110 mils) of attack, respectively. The nitridation attack remained quite severe even at 980 °C (1800 °F). After 1008 h, alloys 600 and 601 showed 1.3 and 1.6 mm (51 and 61 mils) of attack, respectively, whereas iron-base alloys suffered much more attack.

According to the above results, generated by Smith and Bucklin (Ref 33), it appears that stainless steels, Fe-Ni-Cr alloys, and Ni-Cr-Fe alloys may not be suitable for long-term service in pure nitrogen at temperatures above 980 °C (1800 °F). The pure nitrogen environments employed in these studies had a dew point of –66 °C (–86.8 °F) and 1 ppm O_2. Oxygen potentials may play a significant role in nitridation behavior. Odelstam et al. (Ref 34) found that nitride penetration was significantly increased in pure nitrogen when the level of oxygen was reduced

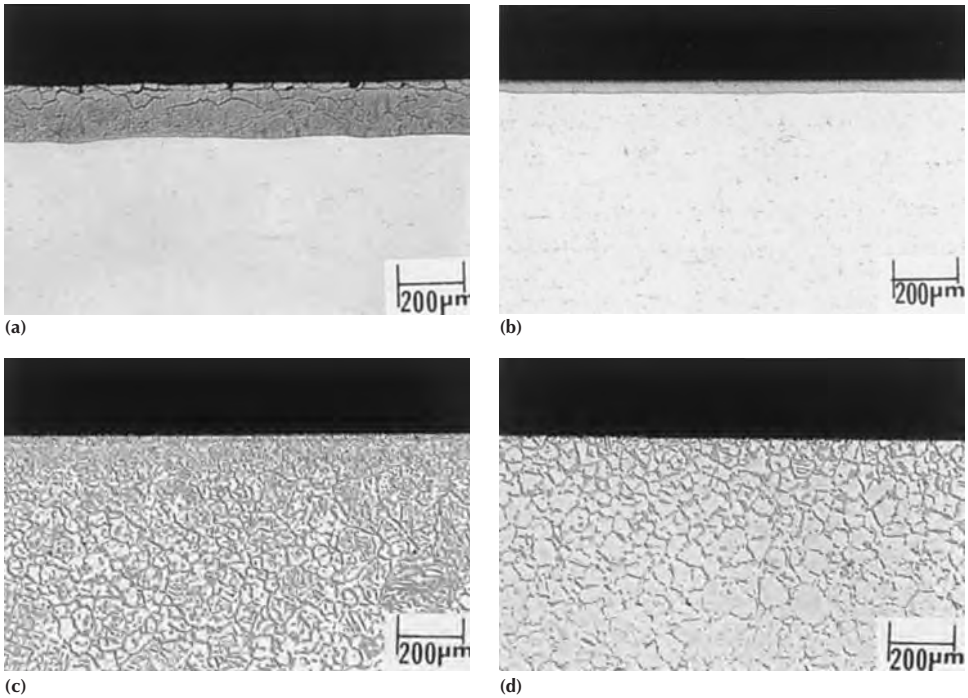


Fig. 11 Typical morphology of nitrides formed in ammonia at 650 °C (1200 °F) for 168 h for (a) type 310 stainless steel and (b) alloy X, and at 1090 °C (2000 °F) for 168 h for (c) type 310 and (d) alloy X

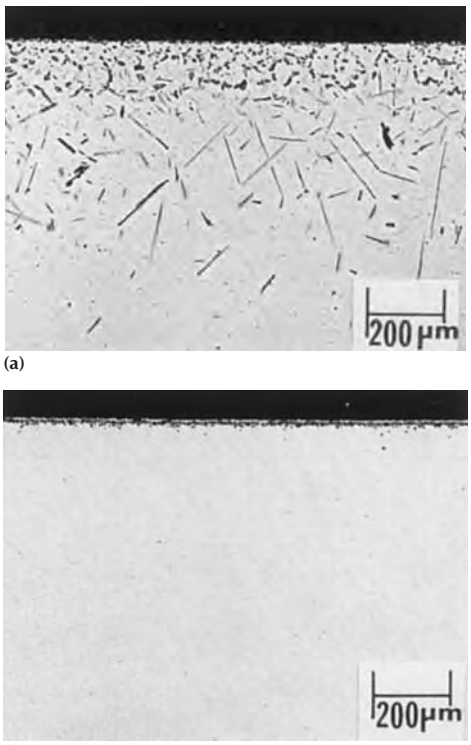


Fig. 12 (a) Extensive internal AlN formation (needle phases) in alloy 601 (about 1.3% Al) and (b) insignificant AlN formation in alloy 214 (about 4.5 Al) after nitriding at 1090 °C (2000 °F) for 168 h in 100% NH_3 (inlet gas)

Table 14 Nitridation resistance of several iron- and nickel-base alloys in pure nitrogen

	982 °C (1800 °F)/1008 h(a) nitrided depth		1093 °C (2000 °F)/900 h(b) nitrided depth		1204 °C (2200 °F)/100 h(c) nitrided depth	
Alloy	mm	mils	mm	mils	mm	mils
600	1.30	51	1.85	73	2.16	85
601	1.55	61	2.79	110	>3.81	150
800	1.85	73	>3.81	150	>3.81	150
520	…	…	>3.81	150	…	…
RA330	2.57	101	>3.81	150	>3.81	150
314SS	>3.81	150	>3.81	150	…	…

(a) Specimens were cycled to room temperature once every 24 h for the first three days and then weekly for the remainder of the test. (b) Specimens were cycled to room temperature once every 96 h (four days). (c) Isothermal exposure. Source: Ref 33

from 205 to 43 ppm for alloy 253MA, as illustrated in Fig. 13. Other higher-nickel alloys, such as alloy 800H, showed no significant changes. Smith and Bucklin (Ref 33) found that in nitrogen containing 1% H_2 with a dew point of 5.6 °C (42 °F), none of the alloys tested (314, 330, 800, 601, and 600) showed signs of nitridation after exposure at 930 °C (1700 °F) for 1032 h. It is not clear whether this was due to a lower temperature (100 °F lower in this case) or to a higher dew point. It is reasonable to assume that an oxide scale tends to reduce nitridation kinetics. It may reduce the rate of surface absorption of nitrogen molecules and/or the diffusion of nitrogen into the metal. Nevertheless, more studies in pure nitrogen are needed, with emphasis on the effect of oxygen potentials and other alloy systems, such as alumina formers.

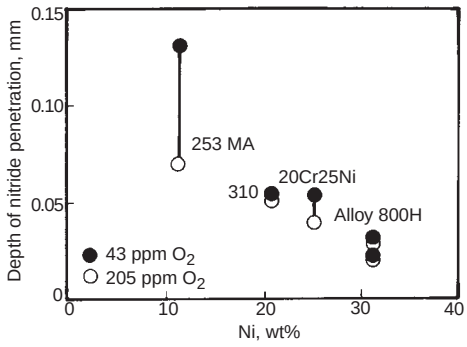


Fig. 13 Results of nitridation tests in nitrogen with two different levels of oxygen contamination at 825 °C (1500 °F) for 400 h. Source: Ref 34

Sulfidation

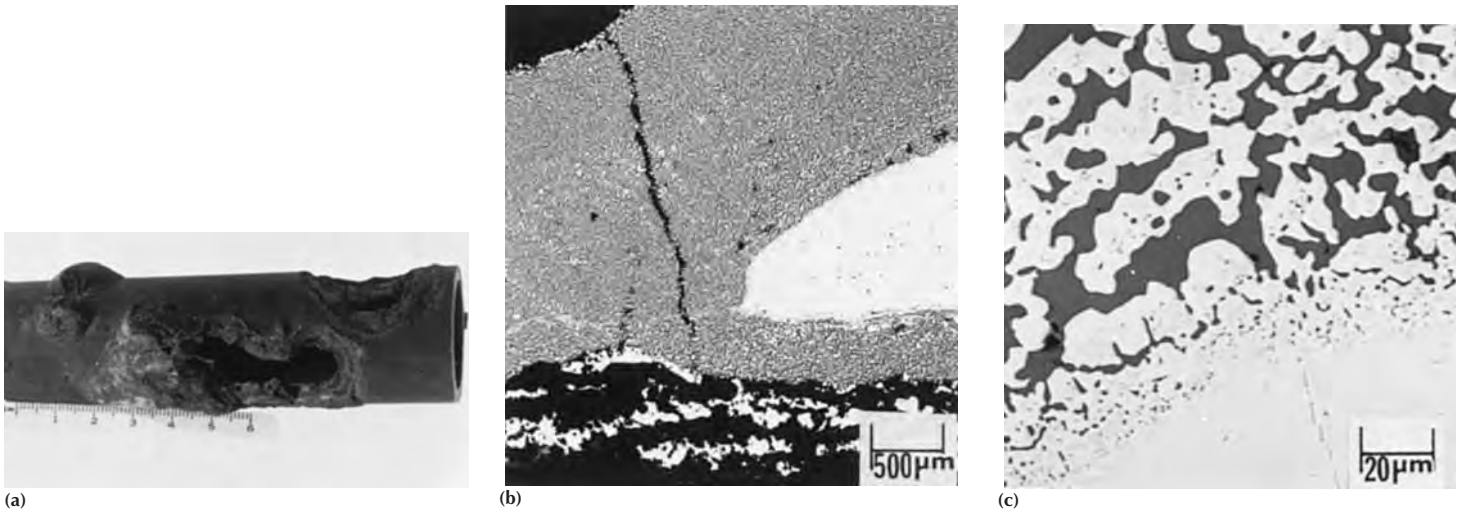
Sulfidation involves the interaction of metal with sulfur to form sulfide scale. Because sulfur is one of the most common corrosive contaminants in high-temperature industrial environments (it is generally present in fuels or feedstocks), this mode of attack is frequently encountered. Sulfidation is influenced by both sulfur and oxygen activities, and formation of metal sulfides leads to severe damage. One example of this damage is development of porous layers offering little protection. Because the volume of metal sulfides is 2.5 to 2.9 times greater than that of the corresponding metal oxides, the resulting stresses lead to severe flaking. Another reason they are so damaging is that the metal sulfides have lower melting points than corresponding oxides or carbides. As a result, corrosive attack is catastrophic because of the increase in the diffusion rate by several orders of magnitude via the liquid phase.

Figure 14 illustrates catastrophic failure of a Ni-Cr-Fe alloy tube used in a furnace. The liquid-appearing nickel-rich sulfide phase, which melts at about 650 °C (1200 °F), is clearly visible. Figure 14 also shows that sulfidation attack is quite localized in many cases. In this particular case, the high-nickel alloy suffered sulfidation attack at about 930 °C (1700 °F) in a furnace that was firing ceramic tiles. The cross section at the corroded area showed sulfides through the section of the component. The breakdown of a protective oxide scale (i.e., the chromia scale for most high-temperature alloys) usually signifies the initiation of breakaway corrosion, which is generally followed by rapid corrosion attack.

Breakaway corrosion is illustrated in Fig. 15 for both type 310 stainless steel and alloy 800H tested in a coal gasification atmosphere. Both of these alloys followed a parabolic reaction rate prior to rapid corrosion attack. Figure 16 shows the oxide scales formed on alloy 800H during the protective stage and after breakaway corrosion in a coal gasification environment.

High-nickel alloys such as 600/601 are particularly susceptible to sulfidation (Fig. 17). However, resistance to sulfidation can generally be improved by increasing chromium levels to ≥25%. It can also be improved by the presence of cobalt: cobalt-base alloys, as well as cobalt-containing alloys, provide higher resistance to sulfidation attack. In addition, high cobalt levels in nickel-base alloys reduce the rate of diffusion of sulfur in the matrix, and they reduce the risk of developing low-melting-point eutectics, because the CO-CO_4S_3 eutectic forms only above 880 °C (1620 °F). By comparison, the Ni-Ni_3S_2 eutectic occurs at 635 °C (1180 °F). Results generated by Lai (Ref 38) at 760, 870, and 980 °C (1400, 1600, and 1800 °F) also revealed that cobalt-base alloys were more sulfidation resistant than nickel-base and Fe-Ni-Cr alloys with similar chromium contents (Fig. 18).

The beneficial effect of titanium was also demonstrated in the Lai study (Ref 38). As



(a) (b) (c)

Fig. 14 Catastrophic sulfidation of an alloy 601 furnace tube. The furnace atmosphere was contaminated with sulfur; the component failed after less than 1 month at 930 °C (1700 °F). (a) General view. (b) Cross section of the perforated area showing liquid-like nickel-rich sulfides. (c) Higher-magnification view of nickel-rich sulfides

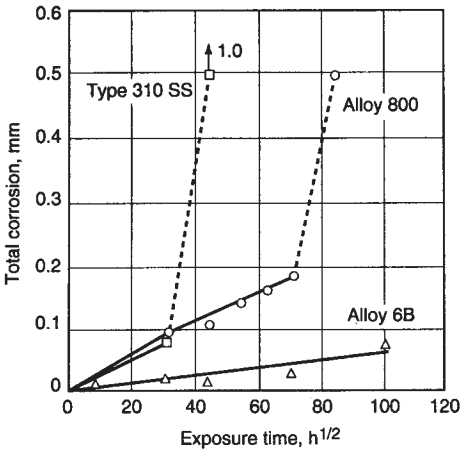


Fig. 15 Corrosion behavior of type 310 stainless steel, alloy 800, and alloy 6B at 980 °C (1800 °F) in a coal gasification atmosphere. Inlet gas: $24H_2$-$18CO$-$12CO_2$-$5CH_4$-$1NH_3$-$0.5H_2S$ (balance H_2O) at 6.9 MPa, or 100 psig. Source: Ref 35

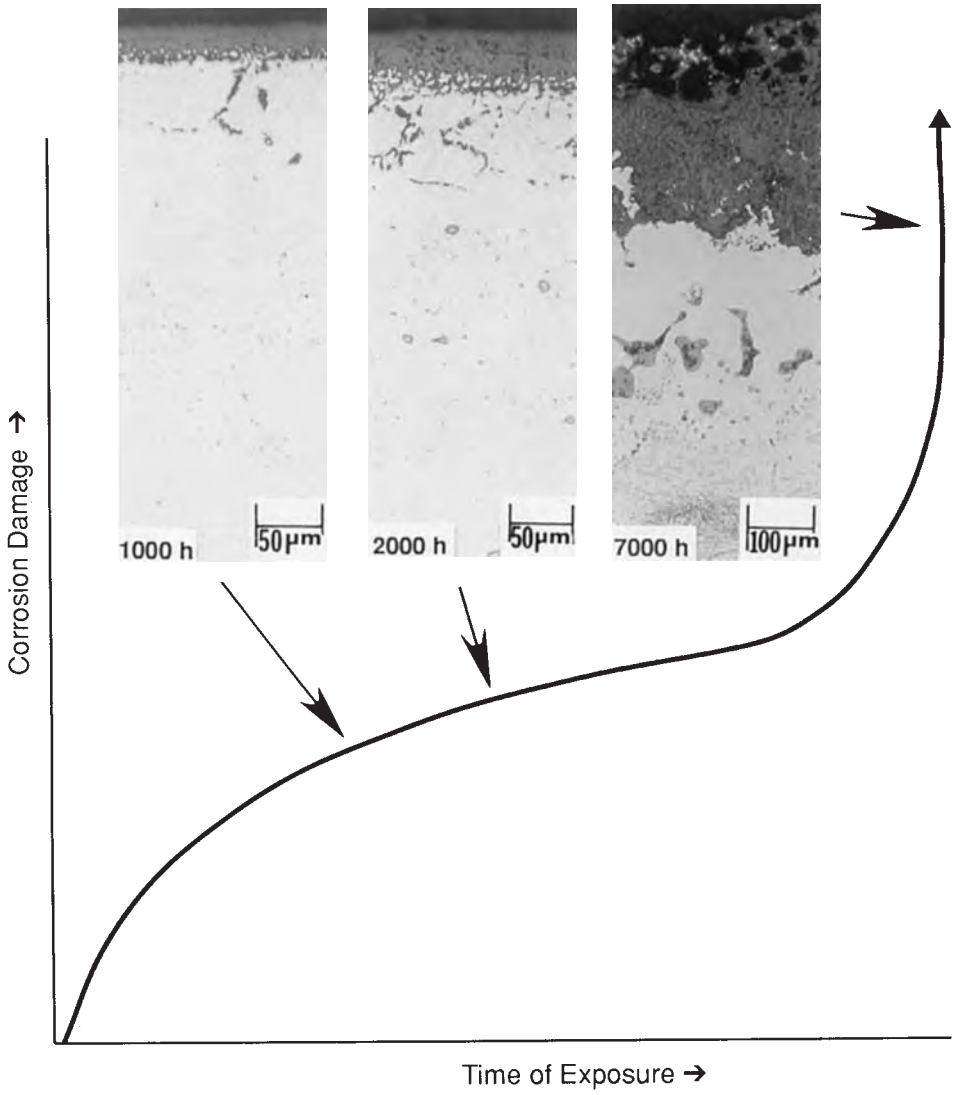


Fig. 16 Corrosion behavior of alloy 800H in a coal gasification atmosphere (0.5% H_2S at 900 °C, or 1650 °F, and 6.9 MPa, or 1000 psig), showing oxide scales during the protective stage and after breakaway corrosion. Source: Ref 36

shown in Fig. 18, alloy R-41 and Waspaloy alloy (both contain about 3% Ti) were the best of the nickel-base alloys tested. In fact, their performance approached that of some cobalt-base alloys. Alloy 263 (2.5% Ti), while performing well at 760 °C (1400 °F), suffered severe sulfidation attack at 870 and 980 °C (1600 and 1800 °F).

More recently developed alloys for resisting sulfidation attack are based on the nickel-cobalt system with high chromium and silicon contents. For example, alloy HR-160 combines high chromium (28%) with relatively high silicon (2.75%) to form a very protective oxide scale (Ref 39–41). Silicon is also effective in improving sulfidation resistance. Increasing cobalt in the Ni-Co-Cr-Fe-Si alloy by replacing iron significantly improved sulfidation resistance. Figure 19 shows the sulfidation resistance of alloy HR-160 compared to that of some existing commercial alloys such as 556, 800H, and 600 (Ref 41). Norton (Ref 42) conducted corrosion tests on several Fe-Ni-Cr alloys and alloy HR-160 at 700 °C (1290 °F) for up to 1000 h in H_2-$7CO$-$1.5H_2O$-$0.6H_2S$. After exposure for 1000 h, alloy HR-160 exhibited about 1.0 mg/cm^2 weight gain compared to about 7 mg/cm^2 for alloys 556 and HR-120, and about 200 to 300 mg/cm^2 for type 321, type 347, and alloy 800H. The gravimetric data are shown in Fig. 20. Comparison of alloy HR-160 with cobalt-base alloys is shown in Table 15. The alloy is significantly better than alloys 188, 25, and 150 (or UMCo-50) and approaches alloy 6B in performance.

Halogenation

Halogen and halogen compounds generally attack via the gaseous phase or molten salt compounds. Salts cause slagging and disintegration of the oxide layer; the gas-phase halogens penetrate deeply into the material without destroying the oxide layer. Therefore, preoxidation is of no benefit.

Corrosion in Chlorine-Bearing Environments. Nickel and nickel-base alloys are widely used in chlorine-bearing environments. Nickel reacts with chlorine to form $NiCl_2$, which has a relatively high melting point (1030 °C, or 1886 °F) compared to $FeCl_2$ and $FeCl_3$ (676 and 303 °C, or 1249 and 577 °F, respectively). This may be an important factor, making nickel more resistant to chlorination attack than iron. Brown et al. (Ref 43) conducted short-term laboratory tests in chlorine on various commercial alloys. The results (see Table 16) suggested that, in an environment of 100% Cl_2, carbon steel and cast iron are useful at temperatures up to 150 to 200 °C (300–400 °F) only. The 18-8 stainless steels can be used at higher temperatures, up to 320 to 430 °C (600–800 °F). Nickel and nickel-base alloys (e.g., Ni-Cr-Fe, Ni-Mo, and Ni-Cr-Mo) were most resistant. The beneficial effect of nickel on the resistance of chlorination attack in chlorine environments is illustrated in Fig. 21. This trend is also reflected in long-term tests (Table 17).

Corrosion in Oxygen-Chlorine Environments. Many industrial environments may contain both chlorine and oxygen. Metals generally

Table 15 Sulfidation resistance of alloy HR-160 compared to that of alloy 556 and cobalt-base alloys at 870 °C (1600 °F) for 500 h

Alloy	Weight change, mg/cm^2	Metal loss		Maximum metal affected(a)	
		mm	mils	mm	mils
HR-160	–0.5	0.01	0.2	0.13	5.2
556	183.6	0.52	20.6	0.90	35.6
188	40.6	0.19	7.6	0.60	23.6
25	33.0	0.10	4.1	0.37	14.6
150	131.7	0.26	10.3	0.72	28.3
6B	10.7	0.01	0.3	0.08	3.3

Note: Ar-$5H_2$-$5CO$-$1CO_2$-$0.15H_2S$; $P_{O_2} = 3 \times 10^{-19}$ atm. $P_{S_2} = 0.9 \times 10^{-6}$ atm. (a) Metal loss plus maximum internal penetration. Source: Ref 40

follow a parabolic rate law by forming condensed phases of oxides, if the environment is free of chlorine. With the presence of both oxygen and chlorine, corrosion of metals then involves a combination of condensed and volatile chlorides. Depending on the relative amounts of oxides and chlorides formed, corrosion can follow either a paralinear rate law (a combination of weight gain due to oxidation and weight loss due to chlorination) or a linear rate law due to chlorination. This is illustrated by the results of Maloney and McNallan (Ref 45) on corrosion of cobalt in Ar-$50O_2$-Cl_2 mixtures (Fig. 22).

A number of studies have examined the corrosion behavior of commercial alloys in mixed oxygen-chlorine environments. Short-term test results generated in Ar-$20O_2$-$2Cl_2$ at 900 °C (1650 °F) for 8 h are summarized in Table 18. The results indicate several interesting trends. Two aluminum-containing nickel-base alloys (214 and R-41) performed best. The two worst alloys were cobalt-base alloys containing tungsten. Molybdenum-containing nickel-base alloys did not perform well at all. Accordingly, alloy 188 (14% W), alloy C-276 (16% Mo, 4% W), alloy 6B (4.5% W, 1.5% Mo), alloy X (9% Mo), and alloy S (14.5% Mo) suffered relatively high rates of corrosion attack. Simple

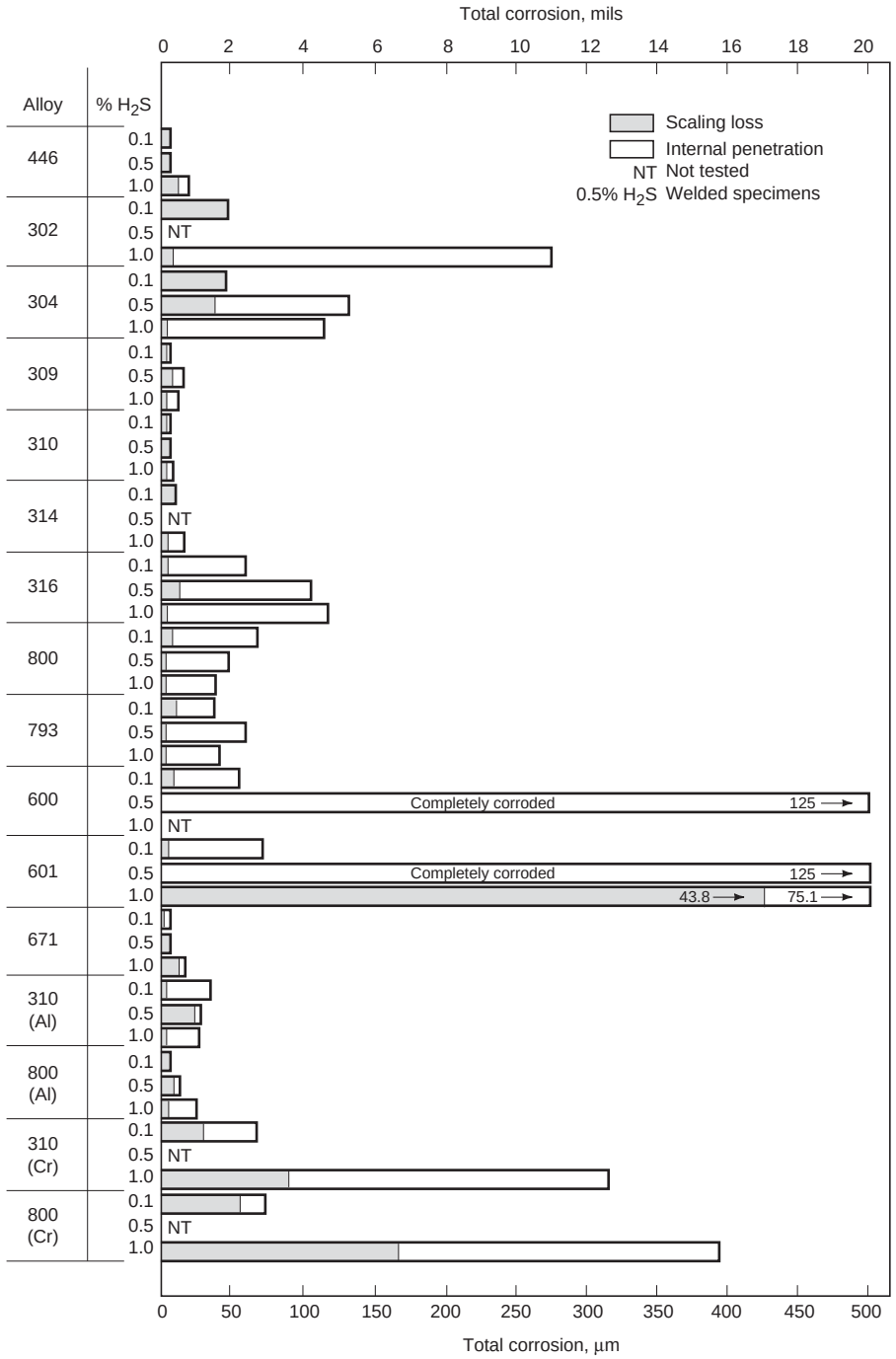


Fig. 17 Corrosion of stainless steels and nickel-base alloys at 816 °C (1500 °F) for 100 h in a coal gasification atmosphere with 0.1, 0.5, and 1.0% H_2S. Source: Ref 37

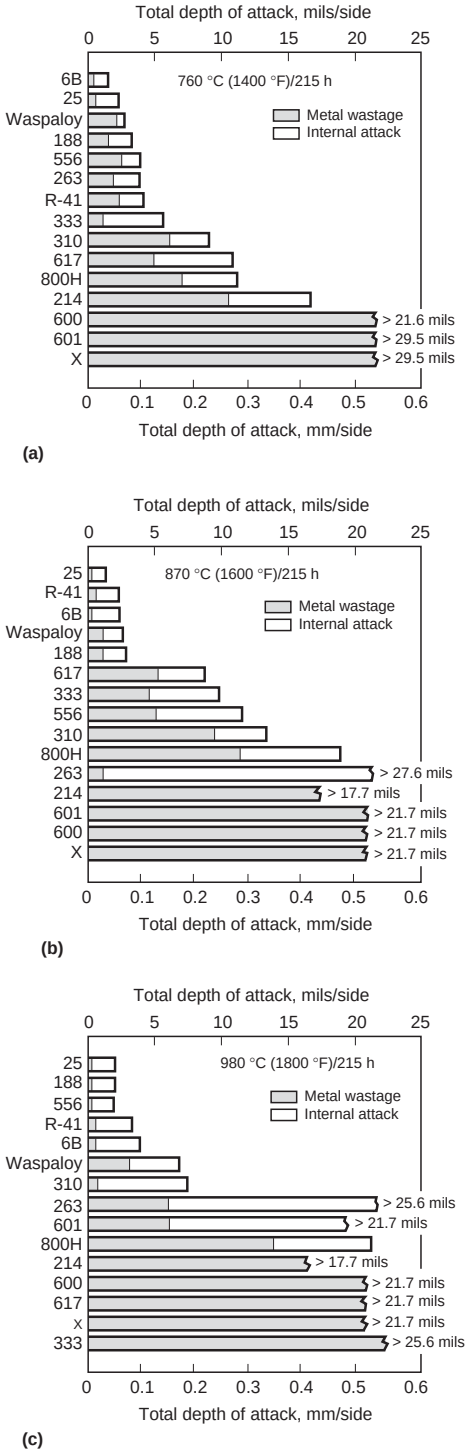


Fig. 18 Corrosion of iron-, nickel-, and cobalt-base alloys after 215 h at (a) 760 °C (1400 °F), (b)870 °C (1600 °F), and (c) 980 °C (1800 °F) in Ar-$5H_2$-5CO-$1CO_2$-$0.15H_2S$. Source: Ref 38

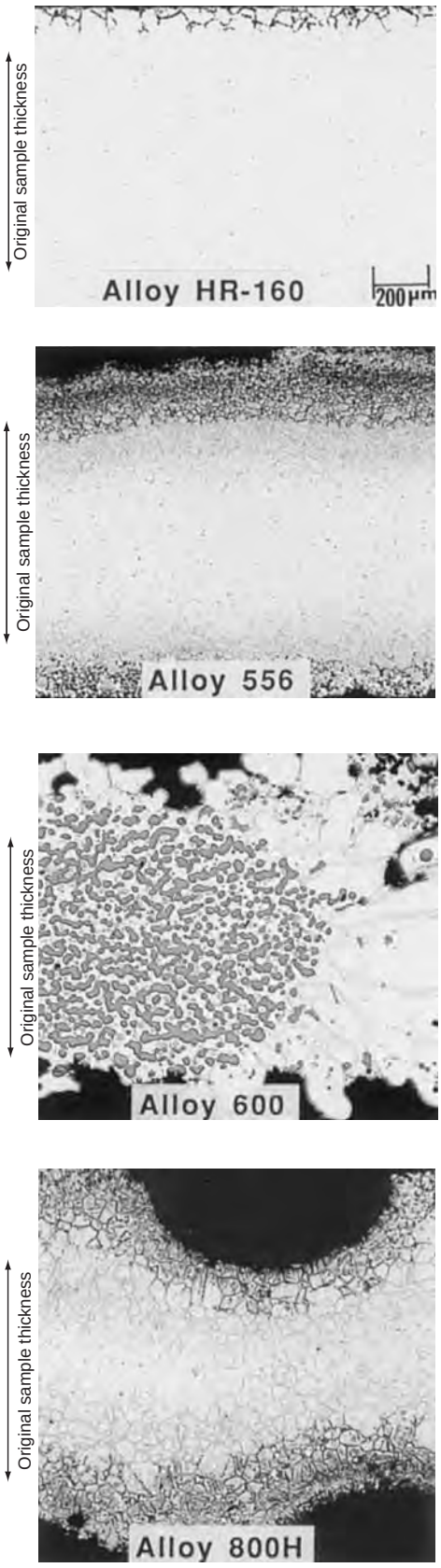


Fig. 19 Sulfidation resistance of alloy HR-160 compared to those of alloys 556, 800H, and 600 after 215 h at 870 °C (1600 °F) in Ar-5H_2-5CO-1CO_2-0.15H_2S. Samples were cathodically descaled before mounting for metallographic examination.

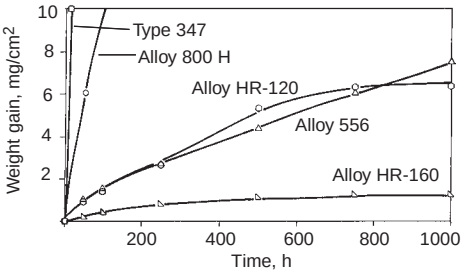


Fig. 20 Corrosion behavior of type 347 stainless steel, alloy 800H, alloy HR-120, alloy 556, and alloy HR-160 at 700 °C (1290 °F) in H_2O-7CO-1.5H_2O-0.6H_2S. Source: Ref 42

Table 16 Corrosion of selected alloys in chlorine

Alloy	Approximate temperature, °C (°F), at which given corrosion rate is exceeded			
	0.8 mm/yr (30 mils/yr)	1.5 mm/yr (60 mils/yr)	3.0 mm/yr (120 mils/yr)	15 mm/yr (600 mils/yr)
Nickel	510 (950)	538 (1000)	593 (1100)	650 (1200)
Alloy 600	510 (950)	538 (1000)	565 (1050)	650 (1200)
Alloy B	510 (950)	538 (1000)	593 (1100)	650 (1200)
Alloy C	480 (900)	538 (1000)	565 (1050)	650 (1200)
Chromel A	425 (800)	480 (900)	538 (1000)	650 (1150)
Alloy 400	400 (750)	455 (850)	480 (900)	538 (1000)
18-8Mo	315 (600)	345 (650)	400 (750)	455 (850)
18-8	288 (550)	315 (600)	345 (650)	400 (750)
Carbon steel	120 (250)	175 (350)	205 (400)	230 (450)
Cast iron	93 (200)	120 (250)	175 (350)	230 (450)

Source: Ref 43

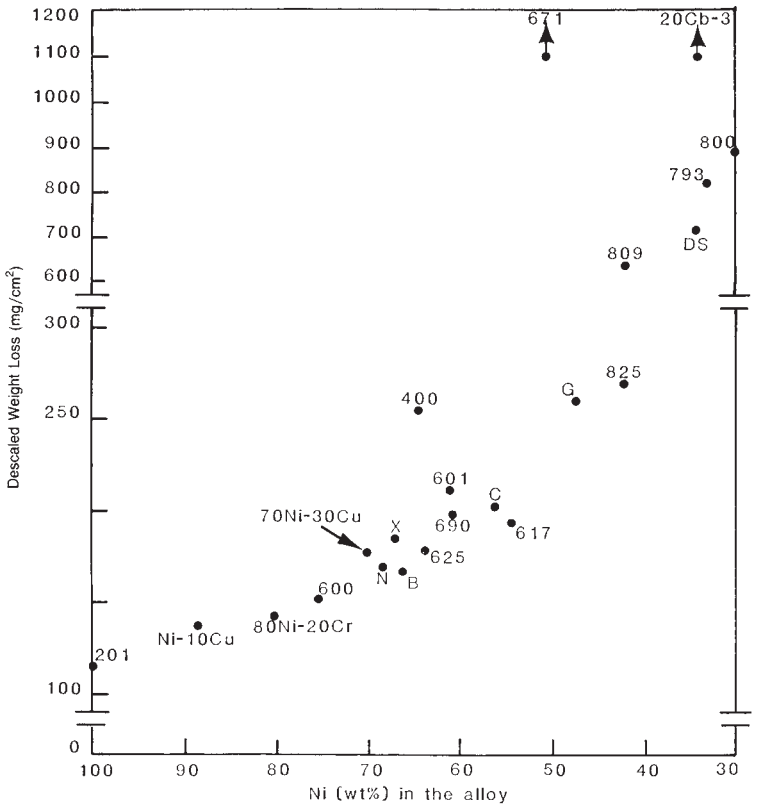


Fig. 21 Effect of nickel on the corrosion resistance of alloys in Ar-30Cl_2 at 704 °C (1300 °F) for 24 h. Source: Ref 44

Table 17 Corrosion of selected alloys in Ar-30Cl_2 after 500 h at 400–705 °C (750–1300 °F)

Alloy	Descaled weight loss, mg/cm²			
	400 °C (750 °F)	500 °C (930 °F)	600 °C (1110 °F)	705 °C (1300 °F)(a)
Ni-201	0.2	0.3	47–101	97
600	0.02	5	127–180	160
601	0.3	3	85–200	215
625	0.7	7	…	180
617	0.6	7	…	190
800	6	13	200–270	890
310	28	370	…	820
304	108	1100	…	>1000
347	215	Total	…	Total

(a) 24 h test period. Source: Ref 44

Table 18 Corrosion of selected alloys in Ar-20O_2-2Cl_2 at 900 °C (1650 °F) for 8 h

Alloy	Metal loss		Average metal affected(a)	
	mm	mils	mm	mils
214	0	0	0.012	0.48
R-41	0.004	0.16	0.028	1.12
600	0.012	0.48	0.035	1.36
310SS	0.012	0.48	0.041	1.60
S	0.053	2.08	0.063	2.48
X	0.020	0.80	0.071	2.80
C-276	0.079	3.12	0.079	3.12
6B	0.014	0.56	0.098	3.84
188	0.014	0.56	0.116	4.56

(a) Metal loss plus average internal penetration. Source: Ref 46

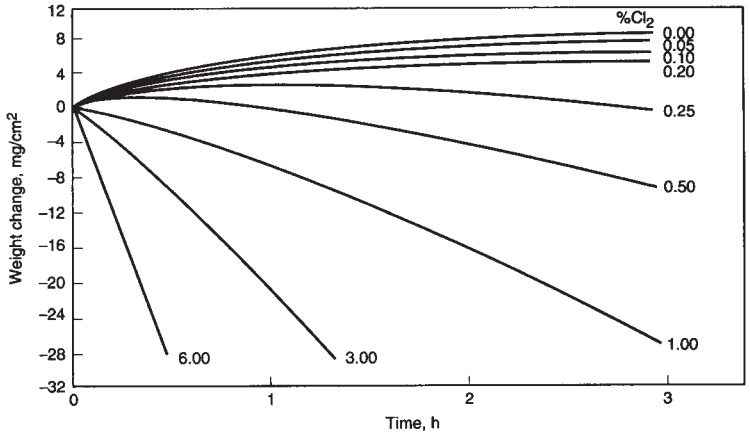


Fig. 22 Corrosion of cobalt in Ar-50O_2-Cl_2 mixtures at 927 °C (1700 °F). Source: Ref 45

iron- and nickel-base alloys, such as type 310 stainless steel (Fe-Ni-Cr) and alloy 600 (Ni-Cr-Fe), performed better than molybdenum- or tungsten-containing alloys. The thermogravimetric results for representative alloys are summarized in Fig. 23.

With about 1.5% Al and 3% Ti, alloy R-41 exhibited good resistance to chlorination attack in a short-term test despite a relatively high molybdenum content (about 10%). The results of long-term tests in Ar-20O_2-0.25Cl_2 by Rhee et al. (Ref 48) and McNallan et al. (Ref 49) showed that these nickel-base alloys with molybdenum, such as alloys R-41 and 263 (6% Mo, 2.4% Ti, and 0.6% Al), eventually suffered severe attack despite the presence of aluminum and titanium. Figure 24 shows gravimetric data for aluminum-containing nickel-base alloys with and without molybdenum, tested at 900 °C (1650 °F). Test results for all the alloys tested at 900 and 1000 °C (1650 and 1830 °F) are summarized in Tables 19 and 20.

The beneficial effect of aluminum, as well as the detrimental effect of molybdenum and tungsten, on resistance to chlorination attack in oxidizing environments is further substantiated by the results of long-term tests in another environment with a higher concentration of chlorine, as shown in Fig. 25. Similar results were obtained by Elliott et al. (Ref 50) from tests conducted in air-2Cl_2 at 900 °C (1650 °F) for 50 h (Fig. 26).

McNallan et al. (Ref 49) reported corrosion behavior in Ar-20O_2-0.25Cl_2 at 900 and 1000 °C (1650 and 1830 °F). This was followed by a study (Ref 51) using the same environment to investigate the same alloys at lower temperatures: 700, 800, and 850 °C (1290, 1470, and 1560 °F) (see Table 21). The corrosion behavior of alloys at temperatures from 700 to 1000 °C (1290–1830 °F) are summarized in Fig. 27 using three alloy systems:

- Ni-Cr-Mo (alloy S)
- Fe-Ni-Cr (alloy 800H)
- Ni-Cr-Al (alloy 214)

As discussed earlier, refractory metals, such as molybdenum and tungsten, are detrimental to chlorination resistance in oxidizing environments. Alloy S was less corrosion resistant than alloy 900H. Both alloys suffered increasing corrosion attack with increasing temperatures. This represents a typical trend for most alloys in oxidizing environments. One exception is

Table 19 Corrosion of selected alloys in Ar-20O_2-0.25Cl_2 for 400 h at 900 and 1000 °C (1650 and 1830 °F)

Alloy	Weight loss, mg/cm^2	
	900 °C (1650 °F)	1000 °C (1830 °F)
214	4.28	9.05
601	20.67	124.99
600	72.08	254.96
800H	26.91	87.05
310SS	47.15	97.40
556	40.29	82.74
X	54.41	153.49
625	99.07	220.09
R-41	63.83	207.32
263	82.57	229.53
188	139.77	156.30
S	228.21	248.98
C-276	132.05	298.85

Source: Ref 49

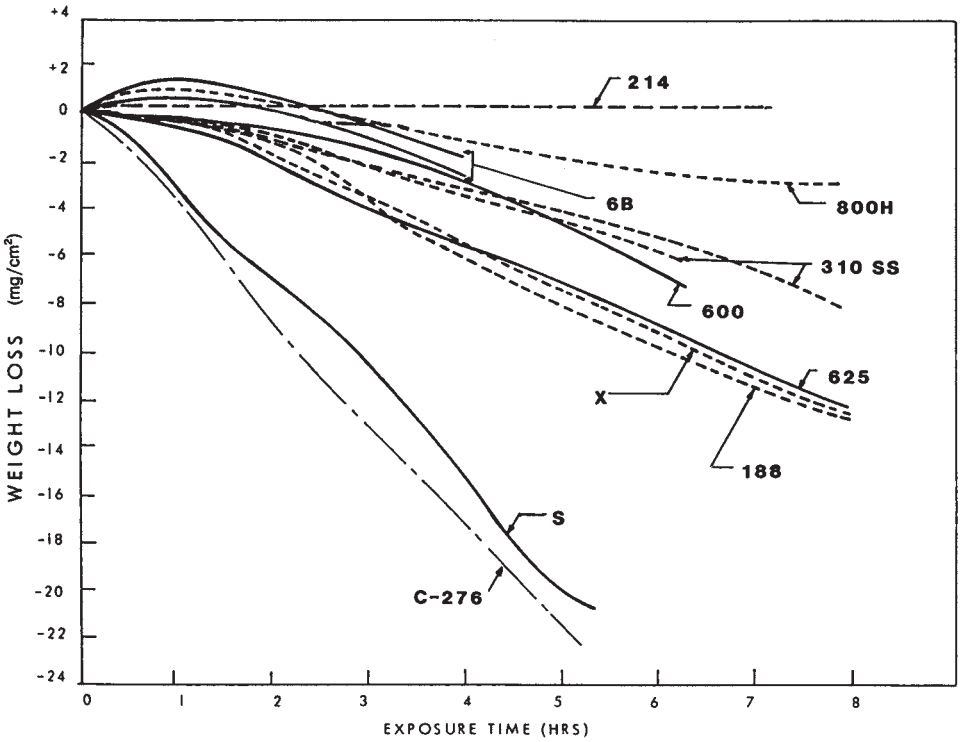


Fig. 23 Corrosion of selected commercial alloys in Ar-20O_2-2Cl_2 at 900 °C (1650 °F) in terms of weight change of specimen as a function of time. Source: Ref 47

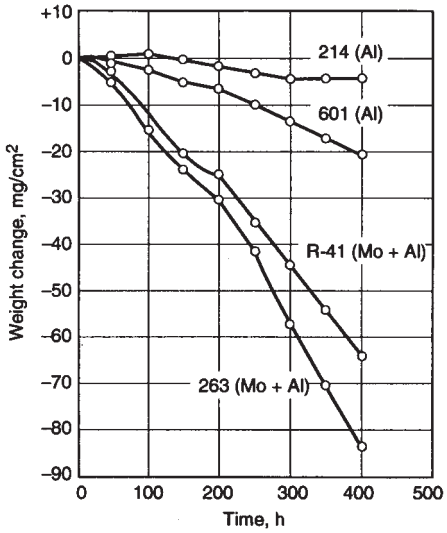


Fig. 24 Corrosion of several aluminum-containing nickel-base alloys with and without molybdenum in Ar-20O_2-0.25Cl_2 at 900 °C (1650 °F). Source: Ref 49

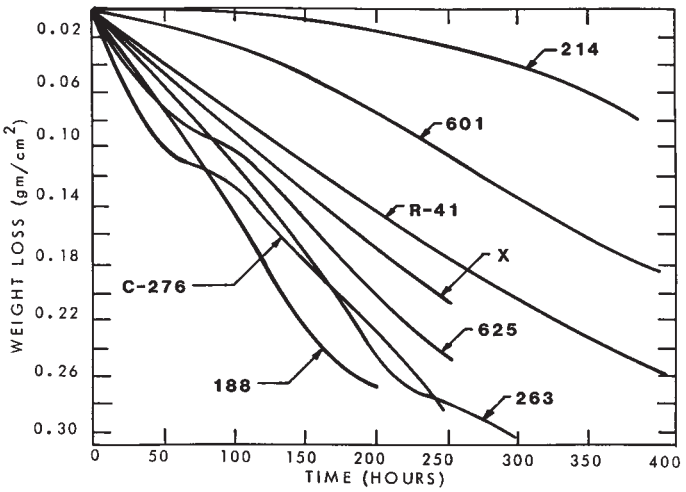


Fig. 25 Corrosion of several nickel- and cobalt-base alloys in Ar-20O_2-1Cl_2 at 900 °C (1650 °F). Source: Ref 46

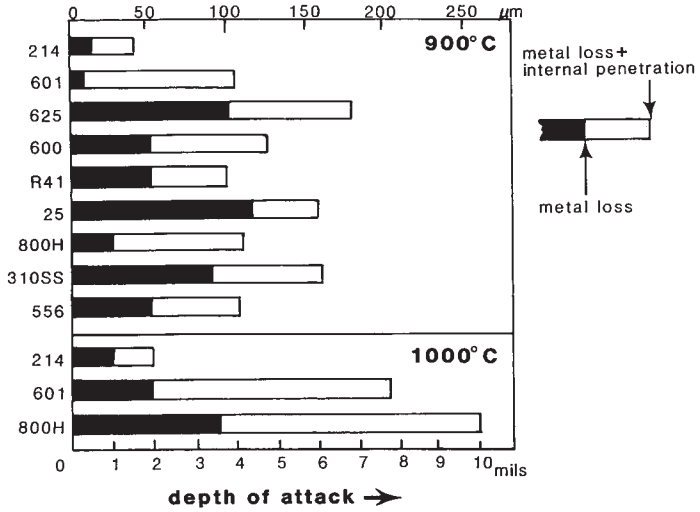


Fig. 26 Corrosion of several iron- and nickel-base alloys in air-2Cl_2 at 900 and 1000° C (1650 and 1830 °F) for 50 h. Source: Ref 50

the Ni-Cr-Al system. As illustrated in Fig. 27, alloy 214 showed a sudden decrease in corrosion attack as the temperature was increased from 900 to 1000 °C (1650–1830 °F). This sharp reduction in corrosion attack at 1000 °C (1830 °F) was attributed to the formation of a protective alumina scale. At lower temperatures, such as ≤900 °C (≤1650 °F), the kinetics of alumina formation were not fast enough to form a protective oxide scale.

Corrosion in HCl Environments. Hossain et al. (Ref 52) performed long-term tests in HCl on several commercial alloys. Their results are summarized in Table 22 and Fig. 28. Type 310 stainless steel was the worst among the alloys tested. The molybdenum-containing nickel-chromium alloys, such as alloys 625 and C-4, were the best performers. This is in contrast to the discussion above about oxygen-chlorine environments, where molybdenum- or tungsten-containing nickel-base alloys performed poorly. Table 22 also shows that unalloyed nickel performed reasonably well in HCl until the temperature reached 700 °C (1290 °F). At 700 °C, nickel was inferior to many nickel-base alloys, such as alloys 600, 625, and C-4.

In reducing environments, such as Ar-4HCl-4H_2 investigated by Baranow et al. (Ref 46), Ni-Cr-Mo alloys, such as alloys C-276 and S, were significantly better than alloys 600, 625, 188, and X. Nickel and nickel alloys also exhibit excellent high-temperature corrosion resistance in dilute HCl environments.

Corrosion in Fluorine-Bearing Environments. Additions of alloying elements to nickel generally are detrimental to fluorine corrosion resistance. Many nickel-base alloys have been found to be significantly more susceptible than commercially pure nickel (e.g., Nickel 200) to fluorine corrosion or corrosion in fluorine-

Table 20 Depth of attack after 400 h at 900 and 1000 °C (1650 and 1830 °F) in Ar-20O_2-0.25Cl_2

	900 °C (1650 °F)				1000 °C (1830 °F)			
	Metal loss		Total depth(a)		Metal loss		Total depth(a)	
Alloy	mm	mils	mm	mils	mm	mils	mm	mils
214	0.023	0.9	0.150	5.9	0.013	0.5	0.051	2.0
601	0.061	2.4	0.264	10.4	0.203	8.0	0.295	11.6
600	0.127	5.0	0.252	9.9	0.330	13.0	0.386	15.2
800H	0.043	1.7	0.191	7.5	0.203	8.0	0.424	16.7
301SS	0.086	3.4	0.152	6.0	0.191	7.5	0.246	9.7
556	0.046	1.8	0.152	6.0	0.152	6.0	0.300	11.8
X	0.099	3.9	0.218	8.6	0.318	12.5	0.434	17.1
625	0.208	8.2	0.272	10.7	0.356	14.0	0.437	17.2
R-41	0.114	4.5	0.244	9.6	0.381	15.0	0.457	18.0
263	0.130	5.1	0.193	7.6	0.368	14.5	0.424	16.7
188	0.216	8.5	>0.356	14.0	0.254	10.0	0.417	16.4
S	0.315	12.4	0.353	13.9	0.419	16.5	0.472	18.6
C-276	0.300	11.8	0.320	12.6	0.419	16.5	0.450	17.7

(a) Metal loss plus internal penetration. Source: Ref 49

Table 21 Depth of attack after 400 h at 700, 800, and 850 °C (1290, 1470, and 1560 °F) in Ar-20O_2-0.25Cl_2

	700 °C (1290 °F)				800 °C (1470 °F)				850 °C (1560 °F)			
	Metal loss		Total depth		Metal loss		Total depth		Metal loss		Total depth	
Alloy	mm	mils	mm	mils	mm	mils	mm	mils	mm	mils	mm	mils
214	0.010	0.4	0.010	0.4	0.018	0.7	0.061	2.4	0.018	0.7	0.066	2.6
600	…	…	…	…	0.020	0.8	0.086	3.4	0.038	1.5	0.132	5.2
800H	0.025	1.0	0.033	1.3	0.023	0.9	0.046	1.8	0.031	1.2	0.097	3.8
310SS	…	…	…	…	0.036	1.4	0.053	2.1	0.031	1.2	0.061	2.4
556	…	…	…	…	0.020	0.8	0.051	2.0	0.020	0.8	0.079	3.1
S	0.079	3.1	0.081	3.2	0.145	5.7	0.150	5.9	0.224	8.8	0.257	10.1
C-276	0.033	1.3	0.046	1.8	0.066	2.6	0.071	2.8	0.163	6.4	0.175	6.9
188	…	…	…	…	0.058	2.3	0.074	2.9	0.025	1.0	0.264	10.4

Source: Ref 51

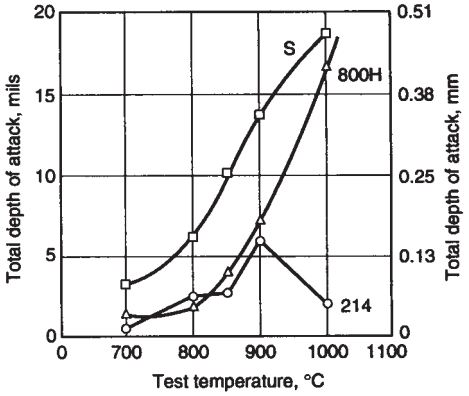


Fig. 27 Corrosion behavior of alloy 214 (Ni-Cr-Al-Y), alloy S (Ni-Cr-Mo), and alloy 800H (Fe-Ni-Cr) in Ar-20O_2-0.25Cl_2 for 400 h at 700 to 1000 °C (1290–1830 °F). Source: Ref 49, 51

Table 22 Corrosion of selected alloys in HCl at 400, 500, 600, and 700 °C (750, 930, 1110, and 1290 °F)

	Metal loss, mg/cm^2							
	400 °C (750 °F)		500 °C (930 °F)			600 °C (1110 °F)		700 °C (1290 °F)
Alloy	300 h	1000 h	100 h	300 h	1000 h	100 h	300 h	96 h
Ni-201	1.19	0.91	1.60	2.89	4.86	11.46	37.7	377
601	1.58	1.47	2.57	4.14	9.38	9.01	19.46	102.5
310	3.26	5.16	6.74	13.65	46.60	15.65	32.6	102.5
625	0.74	1.1	2.42	3.78	8.64	6.79	14.6	26.5
C-4	0.55	1.12	2.09	3.36	7.24	7.31	19.14	34.9
B-2	0.75	0.76	2.10	2.65	5.87	12.93	62.3	126.4
600	0.93	0.81	1.69	3.31	7.81	7.67	17.3	49.6

Source: Ref 52

bearing environments such as hydrogen fluoride (Ref 53, 54).

Hot Corrosion

Hot corrosion is generally described as a form of accelerated attack experienced by the hot gas components of gas turbine engines. As described below, two forms of hot corrosion can be distinguished.

Type I Hot Corrosion. Most of the corrosion encountered in turbines burning fuels can be described as type I hot corrosion, which occurs primarily in the metal temperature range of 850 to 950 °C (1550–1750 °F). This is a sulfidation-based attack on the hot gas path parts involving the formation of condensed salts, which are often molten at the turbine operating temperature. The major components of such salts are sodium sulfate (Na_2SO_4) and/or potassium sulfate (K_2SO_4), apparently formed in the combustion process from sulfur from the fuel and sodium from the fuel or the ingested air. Because potassium salts act very much like sodium salts, alkali specifications for fuel or air are usually taken to the sum total of sodium plus potassium. An example of the corrosion morphology typical of type I hot corrosion is shown in Fig. 29.

Very small amounts of sulfur and sodium or potassium in the fuel and air can produce sufficient Na_2SO_4 in the turbine to cause extensive corrosion problems because of the concentrating effect of turbine pressure ratio. For example, a threshold level has been suggested for sodium in air of 0.008 ppm by weight, below which hot corrosion will not occur. Type I hot corrosion, therefore, is possible even when premium fuels are used. Other fuel (or air) impurities, such as vanadium, phosphorus, lead, and chlorides, may combine with Na_2SO_4 to form mixed salts having reduced melting temperature, thus broadening the range of conditions over which this form of attack can occur. Also, agents such as unburned carbon can promote deleterious interactions in the salt deposits.

Hot corrosion generally proceeds in two stages: an incubation period exhibiting low corrosion rates, followed by accelerated corrosion attack. The incubation period is related to the formation of a protective oxide scale. Initiation of accelerated corrosion attack is believed to be related to the breakdown of the protective oxide scale. Many mechanisms have been proposed to explain accelerated corrosion attack; the salt fluxing model is probably the most widely accepted. Oxides may dissolve in Na_2SO_4 as anionic species (basic fluxing) or cationic species (acid fluxing), depending on the salt composition. Salt is acidic when it is high in SO_3 and basic when low in SO_3. More detailed information on the hot corrosion mechanism by salt fluxing can be found in Ref 55 to 60.

Research has led to greater definition of the relationships among temperature, pressure, salt concentration, and salt vapor-liquid equilibria so that the location and rate of salt deposition in an engine can be predicted. Additionally, it has been demonstrated that a high chromium content is required in an alloy for good resistance to type I hot corrosion (Table 23). The trend to lower chromium levels with increasing alloy strength has therefore rendered most superalloys

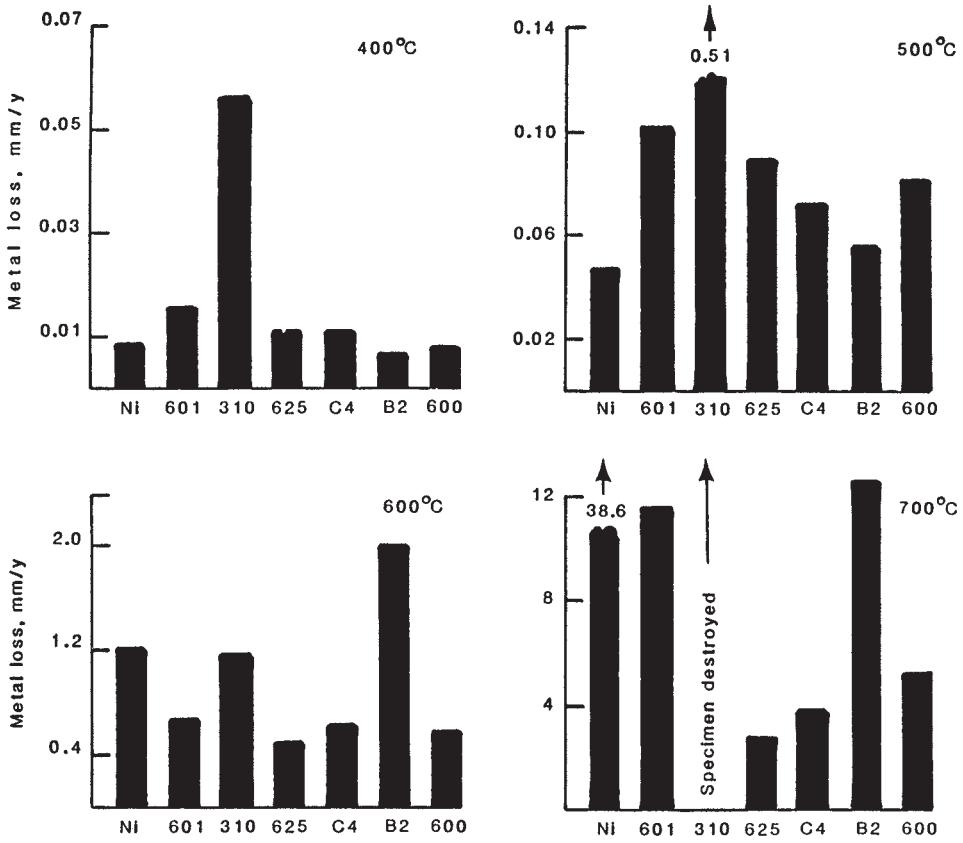


Fig. 28 Corrosion rates of several iron- and nickel-base alloys in HCl at 400 to 700 °C (750–1290 °F). Source: Ref 52

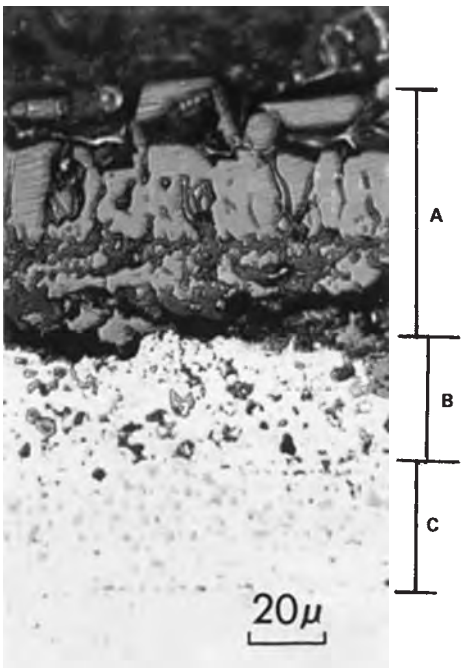


Fig. 29 Ni-20Cr-2ThO_2 after simulated type 1 hot corrosion exposure (coated with Na_2SO_4 and oxidized in air at 1000 °C, or 1832 °F). A, nickel-rich scale; B, Cr_2O_3 subscale; C, chromium sulfides

Table 23 Effect of chromium content on the hot corrosion resistance of nickel- and cobalt-base alloys

Alloy	Chromium content in alloy, %	Loss in sample diameter(a), mm (mils) 870 °C (1600 °F) 500 h	950 °C (1750 °F) 1000 h	980 °C (1800 °F) 1000 h	1040 °C (1900 °F) 1000 h
SM-200	9.0	1.6 (64.4)	3.3+ (130+)	…	…
IN-100	10.0	3.3+ (130+)	3.3+ (130+)	…	…
SEL-15	11.0	3.3+ (130+)	3.3+ (130+)	…	…
IN-713	13.0	3.3+ (130+)	2.0+ (77+)	…	…
U-700	14.8	1.7+ (66+)	1.6 (63.9)	…	…
SEL	15.0	1.2 (45.8)	1.3 (51.8)	0.3 (11.4)	…
U-500	18.5	0.2 (7.6)	0.8 (31.7)	0.7 (29.3)	…
René 41	19.0	0.3 (10.3)	…	0.8 (30.8)	
Hastelloy alloy X	22.0	…	0.3 (12.0)	0.4 (15.2)	…
L-605 (alloy 25)	20.0	…	0.4 (15.3)	0.3 (11.3)	1.1 (41.9)
WI-52	21.0	0.5 (21.4)	0.5 (18.2)	…	1.9 (73.9)
MM-509	21.5	…	0.3 (10.9)	…	0.8 (31.8)
SM-302	21.5	0.14 (5.4)	0.3 (10.0)	…	0.6 (23.1)
X-40	25.0	0.11 (4.2)	0.3 (11.6)	…	0.5 (18.5)

(a) Results of burner rig tests with 5 ppm sea salt injection. Source: Ref 61

inherently susceptible to this type of corrosion. The effects of other alloying additions, such as tungsten, molybdenum, and tantalum, have been documented, and their effects on rendering an alloy more or less susceptible to type I hot corrosion are known and mostly understood (Ref 61–66).

Although various attempts have been made to develop figures of merit to compare superalloys, these have not been universally accepted. Nonetheless, the near standardization of such alloys as IN-738 and IN-939 for first-stage blades/buckets and FSX-414 for first-stage vanes/nozzles, implies that these are the accepted best compromises between high-temperature strength and hot corrosion resistance. It has also been possible to devise coatings with alloying levels adjusted to resist this form of hot corrosion. The use of such coatings is essential for the protection of most modern superalloys intended for duty as first-stage blades or buckets. Coatings to prevent hot corrosion are described in the article "High-Temperature Coatings for Superalloys" in this Handbook.

Type II, or low-temperature hot corrosion, occurs in the metal temperature range of 650 to 700 °C (1200 to 1400 °F), well below the melting temperature of Na_2SO_4, which is 884 °C (1623 °F). This form of corrosion produces characteristic pitting, which results from the formation of low-melting mixtures of essentially Na_2SO_4 and cobalt sulfate ($CoSO_4$), a corrosion product resulting from the reaction of the blade/bucket surface with sulfur trioxide (SO_3) in the combustion gas. The melting point of the Na_2SO_4-$CoSO_4$) eutectic is 540 °C (1004 °F). Unlike type I hot corrosion, a partial pressure of SO_3 in the gas is critical for the reactions to occur. Knowledge of the SO_3 partial pressure-temperature relationships inside a turbine allows some prediction of where type II hot corrosion can occur. Cobalt-free nickel-base alloys (and coatings) may be more resistant to type II hot corrosion than cobalt-base alloys; it has also been observed that resistance to type II hot corrosion increases with the chromium content of the alloy or coating.

Ash/Salt Deposit Corrosion

Deposition of ashes and salts on the surfaces of process components is quite common in some industrial environments, such as fossil-fuel-fired power plants. The corrosion process under these conditions involves both the deposit and the corrosive gases. The deposit may alter the thermodynamic potentials of the environment on the metal surface beneath the deposit. In an environment with both oxygen and sulfur activities, for example, the deposit tends to lower the oxygen activity and raise the sulfur activity beneath the deposit. As a result, formation of a protective oxide scale on the metal surface may become more difficult for most alloys. In most cases, the deposit involves some type of salt. This may lead to chemical reactions between the protective oxide scale and the salt, resulting in the breakdown of the scale. A salt deposit that becomes liquid is particularly damaging.

Table 24 Temperatures and principal contaminants encountered in various types of incinerators

Incinerator type	Temperatures and principal contaminants
Municipal waste incinerators	980–1090 °C (1800–2000 °F), S, Cl, K, Zn, etc. 700–760 °C (1300–1400 °F), S, Cl, K, Zn, Pb
Industrial waste incinerator	870–903 °C (1600–1700 °F), S, Cl, K, etc.
Hospital waste incinerator	650–760 °C (1200–1400 °F), S, Cl, Zn, etc.
Low-level radioactive waste incinerator	590–760 °C (1100–1400 °F), S, Cl, Zn, P, Pb, etc.
Chemical waste incinerator	480 °C (900 °F), Pb, K, S, P, Zn, and Ca

Source: Ref 67, 68

Fireside corrosion of components such as superheaters and reheaters in fossil-fired boilers is commonly referred to as "fuel ash corrosion." The corrosion process in fuel ash corrosion is related to alkali-iron trisulfates for coal-fired boilers and vanadium salts (a mixture of vanadium pentoxide and sodium oxide or sodium sulfate) for oil-fired boilers. Hot corrosion in oil-fired boilers is referred to as "oil ash corrosion."

Material Selection. Components used in coal-fired boilers are generally made from chromium-molybdenum steels (e.g., 1.25Cr-0.25Mo, 2.25Cr-1Mo, 5Cr-0.5Mo, and 9Cr-1Mo) and austenitic stainless steels. Nickel-base alloys are not utilized although Fe-Ni-Cr alloys like 800H have been used extensively.

Components used in oil-fired boilers include austenitic stainless steels, both wrought and cast, and cast nickel-chromium alloys containing from 40 to 50% Ni. The performance of nickel-chromium and high-strength Ni-Cr-Nb alloys in oil ash environments is described in the article "Cast Heat Resistant Nickel-Chromium and Nickel-Chromium-Iron Alloys" in this Handbook.

Corrosion in Waste Incineration Environments

As shown in Table 24, combustion environments generated by incineration of municipal, hospital, chemical, and hazardous wastes contain common corrosive contaminants such as sulfur and chlorine. At temperatures higher than 650 °C (1200 °F), sulfidation and/or chloride attack are frequently responsible for the corrosion reaction. Figure 30 illustrates sulfidation and chloride attack of an Fe-Ni-Co-Cr alloy used in an industrial waste incinerator. Thus, alloys resistant to both sulfidation and chloride attack are preferred for applications at temperatures higher than 650 °C (1200 °F). In addition to sulfur and chlorine, other constituents frequently detected in significant amounts in deposits on incinerator components include potassium, sodium, zinc, and

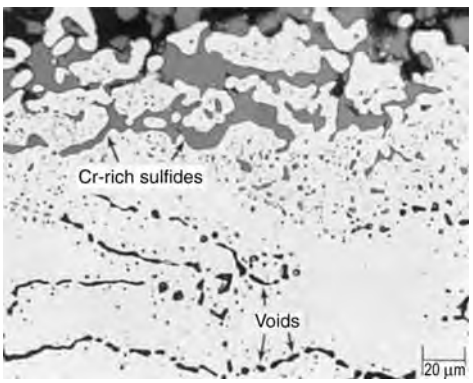


Fig. 30 Fe-Ni-Co-Cr alloy showing both sulfidation and chloride attack. Internal voids were formed by volatile metal chlorides.

lead (Table 24). These elements may contribute to the formation of low-melting-point salts. Many salt mixtures become molten in the temperature range of the furnace wall tubes and superheater tubes. Thus, molten salt deposit corrosion may also be a likely corrosion mechanism.

Molten Salt Corrosion

Molten salts generally are a good fluxing agent, effectively removing oxide scale from a metal surface. The corrosion reaction proceeds primarily by oxidation, which is then followed by dissolution of metal oxides in the melt. Oxygen and water vapor in the salt thus often accelerate molten salt corrosion.

Corrosion can also take place through mass transfer due to thermal gradient in the melt. This mode of corrosion involves dissolution of an alloying element at hot spots and deposition of that element at cooler spots. This can result in severe fouling and plugging in a circulating system. Corrosion is also strongly dependent on temperature and velocity of the salt.

Corrosion can take the form of uniform thinning, pitting, or internal or intergranular attack. In general, molten salt corrosion is quite similar to aqueous corrosion. A more complete discussion on the mechanisms of molten salt corrosion can be found in *Corrosion*, Volume 13 of *ASM Handbook*.

Corrosion in Molten Chlorides. Chloride salts are widely used in the heat treating industry for annealing and normalizing of steels. These salts are commonly referred to as neutral salt baths. The most common neutral salt baths are barium, sodium, and potassium chlorides, used separately or in combination in the temperature range of 760 to 980 °C (1400–1800 °F).

Lai et al. (Ref 69) evaluated various wrought iron-, nickel-, and cobalt-base alloys in a NaCl-KCl-$BaCl_2$ salt bath at 840 °C (1550 °F) for 1 month (Fig. 31). Surprisingly, two high-nickel alloys (alloys 600 and 617) suffered more corrosion attack than stainless steels such as types 304 and 310. The Co-Fe-Ni-W, Fe-Ni-Co-Cr, and Ni-Cr-Fe-Mo alloys performed best. Laboratory testing in a simple salt bath failed to reveal the correlation between alloying elements and performance. Tests were conducted at 840 °C (1550 °F) for 100 h in a NaCl salt bath with fresh salt for each test run. Results are tabulated in Table 25. Similar to the field test results, Co-Ni-Cr-W and Fe-Ni-Co-Cr alloys performed best.

Intergranular corrosion is the major corrosion morphology by molten chloride salts. Figures 32 and 33 show typical intergranular corrosion by molten chloride salt. Figure 32 shows the intergranular attack of a Ni-Cr-Fe alloy (alloy 600) coupon welded to a heat treating basket that underwent heat treat cycles involving a molten KCl salt bath at 870 °C (1600 °F) and a quenching salt bath of molten sodium nitrate and sodium nitrite at 430 °C (800 °F) for 1 month (Ref 71). Figure 33 shows the intergranular attack of a heat treating basket made of the same alloy after service for 6 months in the same heat treating cycling operation (Ref 71).

Corrosion in Molten Nitrates/Nitrites. Molten nitrates or nitrate-nitrite mixtures are widely used for heat treat salt baths, typically operating from 160 to 590 °C (325–1100 °F). They are also used as a medium for heat transfer or energy storage.

Table 25 Results of laboratory tests in a NaCl salt bath at 840 °C (1550 °F) for 100 h

	Total depth of attack(a)	
Alloy	mm	mils
188	0.051	2.0
25	0.064	2.5
556	0.066	2.6
601	0.066	2.6
Multimet	0.069	2.7
150	0.076	3.0
214	0.079	3.1
304	0.081	3.2
446	0.081	3.2
316	0.081	3.2
X	0.097	3.8
310	0.107	4.2
800H	0.109	4.3
625	0.112	4.4
RA330	0.117	4.6
617	0.122	4.8
230	0.140	5.5
S	0.168	6.6
RA330	0.191	7.5
600	0.196	7.7

Note: A fresh salt bath was used for each test run; air was used for the cover gas. (a) Mainly intergranular attack; no metal wastage. Source: Ref 69, 70

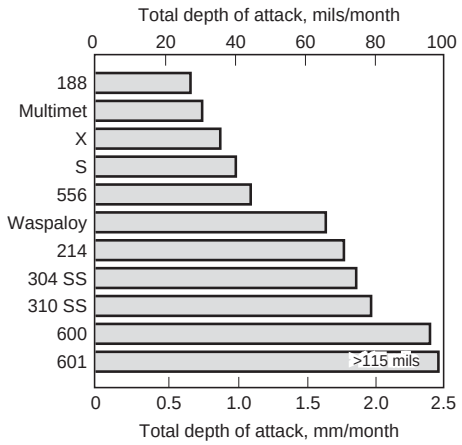


Fig. 31 Results of a field rack test in a NaCl-KCl-$BaCl_2$ salt bath at 840 °C (1550 °F) for 1 month. Source: Ref 69

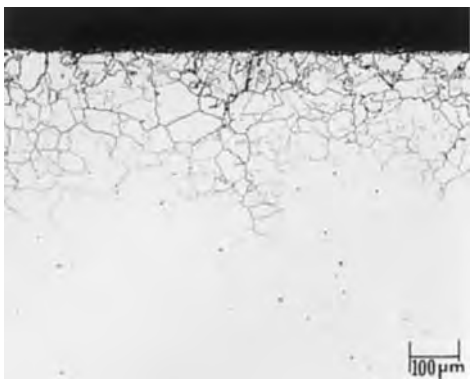


Fig. 32 Intergranular attack of an alloy 600 coupon welded to a heat treating basket after service for 1 month in a heat treating operation cycling between a molten KCl bath at 870 °C (1600 °F) and a quenching salt bath of molten sodium nitrite-nitrate at 430 °C (800 °F). Source: Ref 71



Fig. 33 Intergranular attack of an alloy 600 heat treating basket after service for 6 months in the same heat treating cycling operation described in Fig. 32. Source: Ref 71

Numerous studies have been carried out to determine potential candidate containment materials for handling molten drawsalt ($NaNO_3$-KNO_3). Bradshaw and Carling (Ref 72) summarized these studies as well as the results of their own study in Table 26. The data suggest that, for temperatures up to 630 °C (1170 °F), many alloys are adequate for handling molten $NaNO_3$-KNO_3 salt. Carbon steel and 2.25Cr-1Mo steel exhibited low corrosion rates (mm/yr, or 5 mils/yr) at 460 °C (860 °F). At 500 °C (932 °F), 2.25Cr-1Mo steel exhibited a corrosion rate of about 0.026 mm/yr (1 mil/yr). Aluminized chromium-molybdenum steel showed higher resistance, with a corrosion rate of less than 0.004 mm/yr (0.2 mils/yr) at 600 °C (1110 °F). Austenitic stainless steels, alloy 800, and alloy 600 were more resistant than carbon steel and chromium-molybdenum steels. Unalloyed nickel, however, suffered high corrosion rates.

Slusser et al. (Ref 73) evaluated the corrosion behavior of a variety of alloys in molten $NaNO_3$-KNO_3 (equimolar volume) salt with an equilibrium nitrite concentration (about 6 to 12 wt%) at 675 °C (1250 °F) for 336 h. A constant purge of air in the melt was maintained during testing. Nickel-base alloys were generally much more resistant than iron-base alloys. Increasing nickel content improved alloy corrosion resistance to molten nitrate-nitrite salt. However, pure nickel suffered rapid corrosion attack. Figure 34 shows the corrosion rates of various alloys as a function of nickel content (Ref 73). Silicon-containing alloys, such as RA330 and Nicrofer 3718, performed poorly. A long-term test (1920 h exposure) at 675 °C (1250 °F) was performed on selected alloys, showing corrosion rates similar to those obtained from 336 h exposure tests (Table 27). Alloy 800, however, exhibited a higher corrosion rate in the 1920 h test than in the 336 h test. As the temperature was increased to 700 °C (1300 °F), corrosion rates became much higher, particularly for iron-base alloy 800, which suffered an unacceptably high rate (Table 27). Boehme and Bradshaw (Ref 74) attributed the increased corrosion rate with increasing temperature to higher alkali oxide concentration.

Slusser et al. (Ref 73) found that adding sodium peroxide (Na_2O_2) to the salt increased the salt corrosivity.

Corrosion in Molten Sodium Hydroxide (Caustic Soda). The reaction of metals with molten sodium hydroxide (NaOH) leads to metal oxide, sodium oxide, and hydrogen. Nickel is most resistant to molten NaOH, particularly low-carbon nickel such as Ni 201 (Ref 74). Gregory et al. (Ref 75) reported several nickel-base alloys obtained from static tests at 400 to 680 °C (750–1260 °F) (Table 28). Molybdenum and silicon appear to be detrimental alloying elements in molten NaOH salt. Iron may also be detrimental. Molybdenum and iron were found to be selectively removed from nickel-base alloys with less than 90% Ni, leading to the formation of internal voids (Ref 76).

Corrosion in Molten Fluorides. Corrosion of alloys in molten fluoride salts has been extensively studied for nuclear reactor applications. The nuclear reactor uses a LiF-BeF_2 base salt as a fuel salt, containing various amounts of UF_4, ThF_4, and ZrF_4 (Ref 77). The reactor coolant salt is a $NaBF_4$-NaF mixture. A nickel-base alloy, Hastelloy N, has proved to be the most corrosion resistant in molten fluoride salts (Ref 78). The alloy was the primary containment material for a molten salt test reactor successfully operated from 1965 to 1969 (Ref 79). Koger (Ref 77) reported a corrosion rate of less than 0.0025 mm/yr (0.1 mil/yr) at 704 °C (1300 °F) in the LiF-BeF_2 base salt (fuel salt) and about 0.015 mm/yr (0.6 mil/yr) at 607 °C (1125 °F) in the $NaBF_4$-NaF coolant salt for alloy N.

Corrosion in Molten Carbonates. Molten carbonates are generally less corrosive than molten chlorides or hydroxides. Corrosion data generated in molten carbonate salt at 900 °C (1650 °F) for 504 h are summarized in Table 29. The best performer was Ni-Cr-Fe-Mo alloy (alloy X), followed by Ni-Cr-Fe-Al alloy (214 alloy) and Co-Ni-Cr-W alloy (alloy 188). Ni-Cr-Mo alloy (alloy S) was severely corroded. There was no evidence of a systematic trend in the correlation between alloying elements and

Table 26 Corrosion rates of selected metals and alloys in molten $NaNO_3$-KNO_3

Alloy	Temperature °C	Temperature °F	Corrosion rate mm/yr	Corrosion rate mils/yr
Carbon steel	460	860	0.120	4.7
2.25Cr-1Mo	460	860	0.101	4.0
	500	932	0.026	1.0
9Cr-1Mo	550	1020	0.006	0.2
	600	1110	0.023	0.9
Aluminized Cr-Mo steel	600	1110	<0.004	0.2
12Cr steel	600	1110	0.022	0.9
304SS	600	1110	0.012	0.5
316SS	600	1110	0.007–0.010	0.03–0.4
	630	1170	0.106	4.2
800	565	1050	0.005	0.2
	600	1110	0.006–0.01	0.02–0.4
	630	1170	0.075	3.0
600	600	1110	0.007–0.01	0.3–0.4
	630	1170	0.106	4.2
Nickel	565	1050	>0.5	20
Titanium	565	1050	0.04	1.6
Aluminum	565	1050	<0.004	0.2

Source: Ref 72

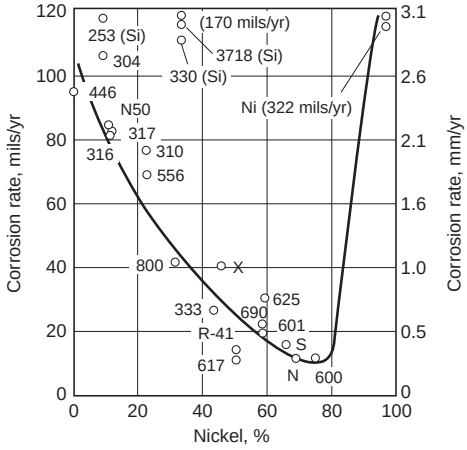


Fig. 34 Corrosion rates of various alloys as a function of nickel content in molten $NaNO_3$-KNO_3 salt at 675 °C (1250 °F). Source: Ref 73

Table 27 Corrosion rates of selected alloys at 675 and 700 °C (1250 and 1300 °F) in sodium-potassium nitrate-nitrite salt

Alloy	Corrosion rate, mm/yr (mils/yr) 675 °C (1250 °F), 1920 h	Corrosion rate, mm/yr (mils/yr) 700 °C (1300 °F), 720 h
214	0.41 (16)	0.53 (21)
600	0.25 (10)	0.99 (39)
N	0.23 (9.1)	1.22 (48)
601	0.48 (19)	1.25 (49)
800	1.85 (73)	6.6 (259)

Source: Ref 73

Table 28 Corrosion rates of selected nickel-base alloys obtained from static tests in molten sodium hydroxide

Alloy	Corrosion rate, mm/yr (mils/yr) 400 °C (750 °F)	500 °C (930 °F)	580 °C (1080 °F)	680°C (1260 °F)
Ni-201	0.023 (0.9)	0.033 (1.3)	0.06 (2.5)	0.96 (37.8)
C	…	2.54 (100)	(a)	…
D	0.018 (0.7)	0.056 (2.2)	0.25 (9.9)	(a)
400	0.046 (1.8)	0.13 (5.1)	0.45 (17.6)	…
600	0.028 (1.1)	0.06 (2.4)	0.13 (5.1)	1.69 (66.4)
301SS	0.043 (1.7)	0.08 (3.2)	0.26 (10.4)	1.03 (40.7)
75	0.028 (1.1)	0.36 (14.3)	0.53 (20.8)	1.21 (47.6)

(a) Severe corrosion. Source: Ref 75

Table 29 Results of corrosion tests in molten eutectic sodium-potassium carbonate at 900 °C (1650 °F) for 504 h

Alloy	Total depth of corrosion attack(a) mm	Total depth of corrosion attack(a) mils
X	0.12	4.7
214	0.19	7.5
188	0.22	8.7
556	0.26	10.2
X-750	0.27	10.6
600(b)	0.34	13.4
600(b)	0.44	17.3
R-41	0.42	16.5
N	0.51	20.1
304SS	0.54	21.3
316SS	0.63	24.8
230	0.77	30.3
Nickel	>0.30	11.8
800(b)	0.25	9.8
800(b)	>0.8	31.5
S	>1.43	56.3

Note: N_2-1CO_2-(1–10O_2) was used for the cover gas. (a) All alloys showed metal loss only except nickel, which suffered 0.2 mm (7.9 mils) metal loss and more than 0.11 mm (4.3 mils) intergranular attack. (b) Two samples from two different suppliers. Source: Ref 80

Table 30 Results of static immersion tests in molten aluminum at 760 °C (1400 °F) for 4 h

Alloy	Maximum depth of corrosion attack	
	mm	mils
Titanium	0.22	8.5
6B	0.43	16.8
188	0.51	20.2
150	0.73	28.9
556	>0.5(a)	20.6(a)
X	>0.6(a)	23.8(a)
671	>0.7(a)	26.3(a)
Carbon steel	>1.6(a)	63.1(a)

(a) Sample was consumed. Source: Ref 81

Table 31 Results of static immersion tests in molten zinc at 454 °C (850 °F) for 50 h

Alloy	Depth of corrosion attack	
	mm	mils
556	0.04	1.6
25	0.06	2.3
188	0.06	2.5
446SS	0.24	9.3
800H	0.28	11.0
304SS	0.36	14.1
625	>0.61	24.0(a)
X	>0.61	24.0(a)

(a) Complete alloying. Source: Ref 81

performance. There was, however, an anomaly in the test results. A significant difference in corrosion was observed between two samples of alloy 800 obtained from different suppliers. This marked difference could not be attributed to the different suppliers. Two samples of alloy 600, however, showed good agreement.

Molten Metal Corrosion

Molten metal corrosion of containment metal is most often related to its solubility in the molten metal. This type of corrosion is simply a dissolution-type attack. A containment metal with a higher solubility in the molten metal generally exhibits a higher corrosion rate. In the case of an alloy, the solubilities of the major alloying elements could dictate the corrosion rate. The solubility of an alloying element in a molten metal typically increases with increasing temperature. As the temperature increases, the diffusion rate also increases. Thus, the alloy corrosion rate increases with increasing temperature.

Corrosion by molten metal can also proceed by alloying of the containment metal (or its major alloying elements) with the molten metal to form an intermetallic compound. This requires some solubility of the liquid metal in the containment metal.

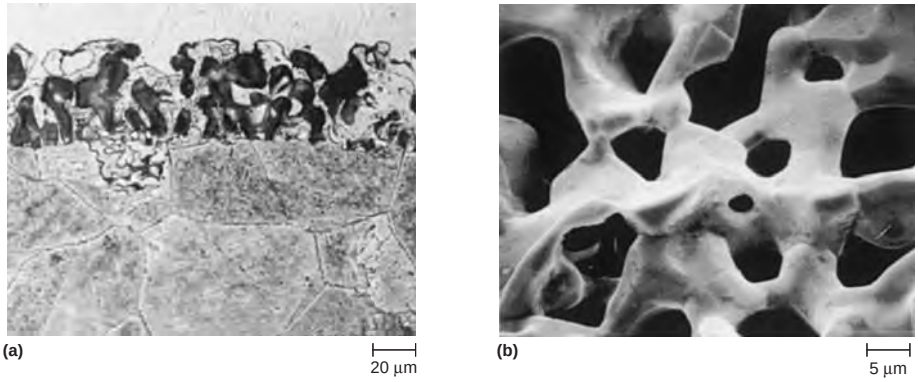


Fig. 35 Corrosion of alloy 706 exposed to liquid sodium for 8000 h at 700 °C (1290 °F); hot leg of circulating system. A porous surface layer has formed with a composition of ~95% Fe, 2% Cr, and %Ni. The majority of the weight loss encountered can be accounted for by this subsurface degradation. Total damage depth: 45 μm. (a) Light micrograph. (b) SEM of the surface of the porous layer

Corrosion in Molten Aluminum. Aluminum melts at 660 °C (1220 °F). Iron, nickel, and cobalt, along with their alloys, are readily attacked by molten aluminum. Extremely high corrosion rates of iron-, nickel-, and cobalt-base alloys in molten aluminum are illustrated by the laboratory test results shown in Table 30.

Corrosion in Molten Zinc. Zinc melts at 420 °C (787 °F). Molten zinc is widely used in the hot dip galvanizing process to coat steel for corrosion protection. Galvanizing tanks, along with baskets, fixtures, and other accessories, require materials resistant to molten zinc corrosion.

Nickel and high-nickel alloys react readily with molten zinc by direct alloying. Iron- and cobalt-base alloys are generally corroded by dissolution, even those containing up to 33% Ni, such as alloy 800H. The results of static tests in molten zinc for selected iron-, nickel-, and cobalt-base alloys are summarized in Table 31. Nickel-base alloys suffered the worst attack, followed by austenitic stainless steels, Fe-Ni-Cr alloys, and iron-chromium alloys. Cobalt-base alloys generally performed better. However, an Fe-Ni-Co-Cr alloy (556 alloy) performed as well as cobalt-base alloys.

Corrosion in Molten Lead. Lead melts at 327 °C (621 °F). Nickel and nickel-base alloys generally have poor resistance to molten lead corrosion (Ref 82, 83). The solubility of nickel in molten lead is higher than that of iron. Cast iron, steels, and stainless steels are commonly used for handling molten lead.

Corrosion in Liquid Lithium. Nickel has a very high solubility in liquid lithium. Thus, nickel and nickel-base alloys are not considered good candidates for handling liquid lithium (Ref 84). Cobalt-base alloys are only slightly more resistant than nickel-base alloys (Ref 85, 86).

Corrosion in Liquid Sodium. High-nickel alloys do not exhibit good resistance to liquid sodium. Exposure can lead to the development of a highly porous surface layer (Fig. 35) and/or intergranular corrosion.

ACKNOWLEDGMENT

This article was adapted from:

- G.Y. Lai, *High-Temperature Corrosion of Engineering Alloys*, ASM International, 1990
- I.G. Wright, High-Temperature Corrosion, *Corrosion*, Vol 13, *ASM Handbook*, 1987, p 97–103

REFERENCES

1. H.E. Eiselstein and E.N. Skinner, in STP No. 165, ASTM, 1954, p 162
2. G.C. Wood, I.G. Wright, T. Hodgkiess, and D.P. Whittle, *Werkst. Korros.*, Vol 21, 1970, p 900
3. "Inconel Alloy 601," booklet, Huntington Alloys, Inc., 1969
4. G.Y. Lai, *J. Met.*, Vol 37 (No. 7), July 1985, p 14
5. E.A. Gulbranson and K.F. Andrew, *J. Electrochem. Soc.*, Vol 104, 1957, p 334
6. E.A. Gulbranson and S.A. Jansson, *Heterogeneous Kinetics at Elevated Temperatures*, G.R. Belton and W.L. Worrell, Ed., Plenum Press, 1970, p 181
7. K.N. Strafford, *High Temp. Technol.*, Nov 1983, p 307
8. D.P. Whittle and J. Stringer, *Philos. Trans. R. Soc.*, Vol A295, 1980, p 309
9. K.N. Strafford and J.M. Harrison, *Oxid. Met.*, Vol 10, 1976, p 347
10. C.C. Wood and J. Bonstead, *Corros. Sci.*, Vol 8, 1968, p 719
11. H. Nagai, M. Okaboyashi, and H. Mitani, *Trans. Jpn. Inst. Met.*, Vol 21, 1980, p 341
12. M.H. Lagrange, A.M. Huntz, and J.H. Davidson, *Corros. Sci.*, Vol 24 (No. 7), 1984, p 617
13. J.C. Pivin, D. Delaunay, C. Rogues-Carmes, A.M. Huntz, and P. Lacombe, *Corros. Sci.*, Vol 20, 1980, p, 351
14. A.W. Funkenbusch, J.G. Smeggil, and N.S. Borstein, *Metall. Trans. A.*, Vol 16, 1985, p 1164

15. C.A. Barrett, *Proc. Conf. Environmental Degradation of Engineering Materials*, M.R. Louthan, Jr. and R.P. McNitt, Ed., Virginia Polytechnic Institute, Blacksburg, VA, 1977, p 319
16. M.F. Rothman, internal report, Cabot Corporation, 1985
17. R.B. Herchenroeder, *Behavior of High Temperature Alloys in Aggressive Environments*, Proc. Petten Int. Conf. (The Netherlands), 15–18 Oct 1979, The Metals Society, London
18. G.N. Irving, J. Stringer, and D.P. Whittle, *Corros. Sci.*, Vol 15, 1975, p 337
19. G.N. Irving, J. Stringer, and D.P. Whittle, *Oxid. Met.*, Vol 8 (No. 6), 1974, p 393
20. G.M. Kim, E.A. Gulbranson, and G.H. Meier, *Proc. Conf. Fossil Energy Materials Program*, ORNL/FMP 87/4, compiled by R.R. Judkins, Oak Ridge National Laboratory, 19–21 May 1987, p 343
21. G.Y. Lai, unpublished results, Haynes International, Inc., 1988
22. R.H. Kane, G.M. McColvin, T.J. Kelly, and J.M. Davidson, Paper 12, presented at Corrosion/84, National Association of Corrosion Engineers, 1984
23. R.H. Kane, J.W. Schultz, H.T. Michels, R.L. McCarron, and F.R. Mazzotta, Ref 30 of the paper by R.H. Kane in *Process Industries Corrosion*, B.J. Moniz and W.I. Pollock, Ed., National Association of Corrosion Engineers, 1986, p 45
24. G.Y. Lai, M.F. Rothman, and D.E. Fluck, Paper 14, presented at Corrosion/85, National Association of Corrosion Engineers, 1985
25. J.J. Barnes and S.K. Srivastava, Paper 527, presented at Corrosion/89, National Association of Corrosion Engineers, 1989
26. G.Y. Lai, *High Temperature Corrosion in Energy Systems*, Proc. TMS-AIME Symposium, M.F. Rothman, Ed., The Metallurgical Society of AIME, 1985, p 551
27. G.Y. Lai and C.R. Patriarca, *Corrosion*, Vol 13, *ASM Handbook*, ASM International, 1987, p 1311
28. R.H. Kane, G.M. McColvin, T.J. Kelly, and J.M. Davison, Paper 12, presented at Corrosion/84, National Association of Corrosion Engineers, 1984
29. J.J. Barnes and G.Y. Lai, paper presented at TMS Annual Meeting (Las Vegas, NV), 1989
30. J.J. Moran, J.R. Mihalisin, and E.N. Skinner, *Corrosion*, Vol 17 (No. 4), 1961, p 191t
31. H. Schenck, M.G. Frohberg, and F. Reinders, *Stahl Eisen*, Vol 83, 1963, p 93
32. H.A. Wriedt and O.D. Gonzalez, *Trans. Met. Soc. AIME*, Vol 221, 1961, p 532
33. G.D. Smith and P.J. Bucklin, Paper 375, presented at Corrosion/86, National Association of Corrosion Engineers, 1986
34. T. Odelstam, B. Larsson, C. Martensson, and M. Tynell, Paper 367, presented at Corrosion/86, National Association of Corrosion Engineers, 1986
35. M.A.H. Howes, "High Temperature Corrosion in Coal Gasification Systems," Final Report GRI-8710152, Gas Research Institute, Chicago, Aug 1987
36. S.K. Verma, Paper 336, presented at Corrosion/85, National Association of Corrosion Engineers, 1985
37. J.L. Blough, V.L. Hill, and B.A. Humphreys, *The Properties and Performance of Materials in the Coal Gasification Environment*, V.L. Hill and H.L. Black, Ed., American Society for Metals, 1981, p 225
38. G.Y. Lai, *High Temperature Corrosion in Energy Systems*, M.F. Rothman, Ed., The Metallurgical Society of AIME, 1985, p 227
39. G.Y. Lai, "Sulfidation-Resistant Co-Cr-Ni Alloy with Critical Contents of Silicon and Cobalt," U.S. Patent No. 4711763, Dec 1987
40. G.Y. Lai, Paper 209, presented at Corrosion/89, National Association of Corrosion Engineers, 1989
41. G.Y. Lai, *J. Met.*, Vol 41 (No. 7), 1989, p 21
42. J.F. Norton, unpublished data, Joint Research Centre, Petten Establishment, Petten, The Netherlands, 1989
43. W.M.H. Brown, W.B. DeLong, and J.R. Auld, *Ind. Eng. Chem.*, Vol 39 (No. 7), 1947, p 839
44. R.H. Kane, *Process Industries Corrosion*, B.J. Moritz and W.I. Pollock, Ed., National Association of Corrosion Engineers, 1986, p 45
45. M.J. Maloney and M.J. McNallan, *Met. Trans. B*, Vol 16, 1995, p 751
46. S. Baranow, G.Y. Lai, M.F. Rothman, J.M. Oh, M.J. McNallan, and M.H. Rhee, Paper 16, presented at Corrosion/84, National Association of Corrosion Engineers, 1984
47. J.M. Oh, M.J. McNallan, G.Y. Lai, and M.F. Rothman, *Metall. Trans. A*, Vol 17, June 1986, p 1087
48. M.H. Rhee, M.J. McNallan, and M.F. Rothman, *High Temperature Corrosion in Energy Systems*, M.F. Rothman, Ed., The Metallurgical Society of AIME, 1985, p 483
49. M.J. McNallan, M.H. Rhee, S. Thongtem, and T. Hensler, Paper 11, presented at Corrosion/85, National Association of Corrosion Engineers, 1985
50. P. Elliott, A.A. Ansari, R. Prescott, and M.F. Rothman, Paper 13, presented at Corrosion/85, National Association of Corrosion Engineers, 1985
51. S. Thongtem, M.J. McNallan, and G.Y. Lai, Paper 372, presented at Corrosion/86, National Association of Corrosion Engineers, 1986
52. M.K. Hossain, J.E. Rhoades-Brown, S.R.J. Saunders, and K. Ball, *Proc. UK Corrosion/83*, p 61
53. C.F. Hale, E.J. Barber, H.A. Bernhardt, and K.E. Rapp, "High Temperature Corrosion of Some Metals and Ceramics in Fluorinating Atmospheres," Report K-1459, Union Carbide Nuclear Co., Sept 1960
54. M.J. Steindler and R.C. Vogel, "Corrosion of Materials in the Presence of Fluorine at Elevated Temperatures," ANL-5662, Argonne National Laboratory, Jan 1957
55. F.S. Pettit and C.S. Giggons, Hot Corrosion, *Superalloys II*, C.T. Sims, N.S. Stoloff, and W.C. Hagel, Ed., John Wiley & Sons, 1987, p 327–358
56. J.A. Goebel, F.S. Pettit, and G.W. Goward, *Metall. Trans.*, Vol 4, 1973, p 261
57. J. Stringer, *Am. Rev. Mater. Sci.*, Vol 7, 1977, p 477
58. R.A. Rapp, *Corrosion*, Vol 42 (No. 10), 1986, p 568
59. J. Stringer, R.I. Jaffee, and T.F. Kearns, Ed., *High Temperature Corrosion of Aerospace Alloys*, AGARD-CP120, Advisory Group for Aerospace Research and Development, North Atlantic Treaty Organizations, 1973
60. *Hot Corrosion Problems Associated with Gas Turbines*, STP 421, ASTM, 1967
61. P.A. Bergman, A.M. Beltran, and C.T. Sims, "Development of Hot Corrosion-Resistant Alloys for Marine Gas Turbine Service," Final Summary Report to Marine Engineering Lab., Navy Ship R&D Center, Annapolis, MD, Contract N600 (61533) 65661, 1 Oct 1967
62. J. Clelland, A.F. Taylor, and L. Wortley, *Proc. 1974 Gas Turbine Materials in the Marine Environment Conf.*, MCIC-75-27, J.W. Fairbanks and I. Machlin, Ed., Battelle Columbus Laboratories, 1974, p 397
63. M.J. Zetlmeisl, D.F. Laurence, and K.J. McCarthy, *Mater. Perform.*, June 1984, p 41
64. J. Stringer, *Proc. Symp. Properties of High Temperature Alloys with Emphasis on Environmental Defects*, Z.A. Foroulis and F.S. Pettit, Ed., The Electrochemical Society, 1976, p 513
65. A.M. Beltran, *Cobalt*, Vol 46, March 1970, p 3
66. P.A. Bergman, C.T. Sims, and A.M. Beltran, *Hot Corrosion Problems Associated with Gas Turbines*, STP 421, ASTM, 1967, p 38
67. G.R. Smolik and J.D. Dalton, Paper 207, presented at Corrosion/89, National Association of Corrosion Engineers, 1989
68. G.Y. Lai, "Alloy Performance in Incineration Plants," paper presented at Chemical Waste Incineration Conference, 12–13 March 1990, (Manchester, UK)
69. G.Y. Lai, M.F. Rothman, and D.E. Fluck, Paper 14, presented at Corrosion/85, National Association of Corrosion Engineers, 1985
70. G.Y. Lai, unpublished results, Haynes International, Inc., 1986
71. S.K. Srivastava, unpublished results, Haynes International, Inc., 1989
72. R.W. Bradshaw and R.W. Carling, "A Review of the Chemical and Physical Properties of Molten Alkali Nitrate Salts and Their Effect on Materials Used for Solar Central Receivers," SAND 87-8005, Sandia Laboratory, April 1987

73. J.W. Slusser, J.B. Titcomb, M.T. Heffelfinger, and B.R. Dunbobbin, *J. Met.*, July 1985, p 24
74. R.R. Miller, "Thermal Properties of Hydroxide and Lithium Metal," Quarterly Progress Report 1 May–1 Aug 1952, NRL-3230-201/52, 1952
75. J.N. Gregory, N. Hodge, and J.V.G. Iredale, "The Static Corrosion of Nickel and Other Materials in Molten Caustic Soda," AERE-C/M-272, March 1956
76. G.P. Smith and E.E. Hoffman, *Corrosion*, Vol 13, 1957, p 627t
77. J.W. Koger, *Corrosion*, Vol 29 (No. 3), 1973, p 115
78. J.W. Koger, *Corrosion*, Vol 30 (No. 4), 1974, p 125
79. J.R. Keiser, D.L. Manning, and R.E. Clausing, *Proc. Int. Symp. Molten Salts*, J.P. Pemsler, et al., Ed., Electrochemical Society, 1976, p 315
80. R.T. Coyle, T.M. Thomas, and G.Y. Lai, *High Temperature Corrosion in Energy Systems*, M.F. Rothman, Ed., The Metallurgical Society of AIME, 1985, p 627
81. G.Y. Lai, unpublished results, Haynes International, Inc., 1985
82. F.R. Morrall, *Wire and Wire Products*, Vol 23, 1948, p. 484, 571
83. L.R. Kelman, W.D. Wilkinson, and F.L. Yaggee, "Resistance of Materials to Attack by Liquid Metals," Report ANL-4417, Argonne National Laboratory, July 1950
84. R.E. Cleary, S.S. Blecherman, and J.E. Corliss, "Solubility of Refractory Metals in Lithium and Potassium," USAEC Report TIM-950, Nov 1965
85. M.S. Freed and K.J. Kelly, "Corrosion of Columbium Base and Other Structural Alloys in High Temperature Lithium," Report PWAC-355, Pratt and Whitney Aircraft-CANEL, Division of United Aircraft Corp., June 1961 (declassified in June 1965)
86. E.E. Hoffman, "Corrosion of Materials by Lithium at Elevated Temperatures," USAEC Report ORNL-2924, Oct 1960

ASM Specialty Handbook: Nickel, Cobalt, and Their Alloys
J.R. Davis, editor, p 191-197
DOI:10.1361/ncta2000p191

Copyright © 2000 ASM International®
All rights reserved.
www.asminternational.org

Forming of Nickel Alloys

THE DUCTILITY of nickel-base alloys in the annealed condition makes them adaptable to virtually all methods of cold forming. Within this group of alloys, which includes the commercially pure nickels, the nickel-coppers, and the more highly alloyed solid-solution-strengthened and precipitation-hardenable (PH) alloys, other engineering properties vary sufficiently to cause the alloys to range from moderately easy to difficult to form, compared to other materials.

Factors Influencing Formability

Strain Hardening. Because strain hardening is related to the solid-solution strengthening afforded by alloying elements, strain-hardening rate generally increases with the complexity of the alloy. Accordingly, strain-hardening rates range from moderately low for nickel and nickel-copper alloys to moderately high for the nickel-chromium, nickel-chromium-cobalt, and nickel-iron-chromium alloys. Similarly, the PH alloys have higher strain-hardening rates than their solid-solution equivalents. Figure 1 compares the strain-hardening rates of six nickel alloys, in terms of the increase in hardness with increasing cold reduction, with those of four other materials. Note that the strain-hardening rates of the nickel-base alloys are greater than that of 1020 steel, and most are less than that of AISI-type 304 stainless steel.

Because the modulus of elasticity of the high-nickel alloys is relatively high (similar to that of steel), a small amount of springback in cold-forming operations might be expected. However, springback is also a function of proportional limit, which can increase greatly during cold working of strain-hardenable materials. For instance, a yield strength of 170 MPa (25 ksi) of an alloy in the annealed condition might increase to 520 MPa (75 ksi), during a drawing operation. Therefore, the amount of springback for this alloy must be computed from the 520 MPa (75 ksi) flow stress, rather than from the initial value of the yield strength.

Temper. Most cold-forming operations require the use of annealed material. However, the softer alloys, such as Nickel 200, the nickel-iron NILO alloys, and alloy 400, are frequently used in $\frac{1}{8}$-hard and $\frac{1}{4}$-hard tempers for improved shearing and piercing. For similar reasons, alloy 400 is usually cold headed in No. 1 or 0 temper for fastener applications.

Galling. Because high-nickel alloys do not readily develop an oxide film that would present a barrier to diffusion bonding, they cold weld (gall) easily to materials of similar atomic diameter. When a cold weld is formed, the high shear strength and ductility of the alloys prevent the weld from being easily broken. For these reasons, the coefficient of friction between nickel-base alloys and other metals, including most die materials, is usually high.

Alloying with highly reactive elements that readily form oxide films, such as chromium, reduces the galling (or cold welding) propensity of nickel alloys. Accordingly, the nickel-chromium and nickel-iron-chromium alloys are less likely to gall than are the nickel and nickel-copper alloys. However, chromium oxide films are thin and brittle and provide only limited protection because they are easily broken when the substrate is deformed. The use of heavy-duty lubricants will minimize galling in most cold forming.

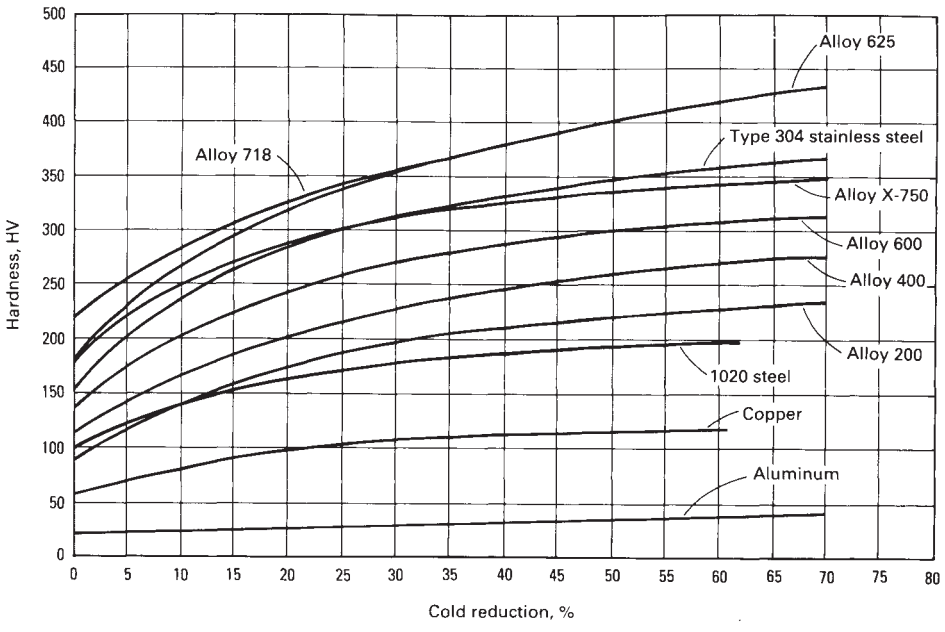


Fig. 1 Effect of cold work on the hardness of various nickel-base alloy sheet materials

Special Considerations for Heat-Resistant Alloys

Effect of Composition on Formability. The differences in composition of the various heat-resistant alloys cause differences in their formability. Most alloys that contain substantial amounts of molybdenum or tungsten for strengthening, such as alloy 230 (UNS N06230), which contains 14% W and 2% Mo, or alloy 41 (UNS N07041), which contains 10% Mo, are harder to form than alloys containing lesser amounts of these elements. Alloys that contain aluminum and titanium are strengthened by precipitation of the γ' phase. The volume fraction γ' depends strongly on the amounts of aluminum and titanium present and an overall composition. Examples of alloys that contain γ' include alloy 80A (UNS N07080), Waspaloy alloy (UNS N07011), and alloy 214 (UNS N07214). These typically contain 15, 20, and 33% γ', respectively. Many PH alloys require complex production steps to produce satisfactory components. Most of the iron-base and nickel-base alloys contain less than 0.15% C; more carbon than this causes excessive carbide

precipitation, which can severely reduce ductility. Small amounts of boron (up to 0.03% B) are used in some of the heat treatable nickel-base alloys, such as alloy 41 and Udimet 700, to prevent carbide precipitation at grain boundaries; to much boron, however, can cause cracking during forming.

Sulfur causes hot shortness of nickel-base alloys. Silicon content should be below 0.60% and preferably less than 0.30%. More than 0.60% Si causes cracking of cold-drawn alloys and may cause weld cracking in others. Silicon at levels of less than 0.30% usually does not contribute to difficulties in forming.

Cold versus Hot Forming. Cold forming is preferred for heat-resistant alloys, especially in thin sheets. Most of these alloys can be hot formed effectively only in a narrow temperature range (between approximately 925 and 1260 °C, or 1700 and 2300 °F). Intermediate annealing between cold-forming operations is usually preferred to hot forming.

Effect of Alloy Condition on Formability. For the fine grain structure that is best for cold forming, heat-resistant alloys must be cold worked (reduced) beyond a critical percentage reduction and then annealed. The critical amount of cold work varies with the alloy and with the annealing temperature but is usually 8 to 10%. Reheating metal that is only slightly cold worked can result in abnormal grain growth, which can cause orange peel or alligator hide effects in subsequent forming.

For example, an alloy X (UNS N06002) workpiece, partly formed, stress relieved, and then given the final form, had severe orange peel on much of its surface. The partial forming resulted in approximately 5% cold working, and during stress relief, an abnormally coarse grain structure developed. The difficulty was corrected by making certain that the metal was stretched 10% or more before it was stress relieved. In addition, stress relieving was done at the lowest temperature and shortest time that could be used, because higher temperatures and longer times increased grain growth. Optimal time and temperature were determined by hardness testing.

Severely cold-formed parts should be fully annealed after final forming. If annealing causes distortion, the work can be formed within 10% of the intended shape, annealed, pickled, and then given the final forming.

Solution annealed products are usually soft enough to permit mild forming. If the solution annealed alloy is not soft enough for the forming operation, an annealing treatment must be used that will remove the effects of cold work and dissolve the precipitation-hardening and other secondary phases. Some control of grain size is sacrificed, but if cooling from the annealing temperature is very rapid, the precipitation-hardening elements will be retained in solution. Further annealing after forming can be done at a lower temperature to decrease the risk of abnormal grain growth. Several process anneals may be required in severe forming, but the high-temperature anneal need not be repeated. Annealing should be performed at a temperature that produces optimal ductility for the specific metal.

Effect of Rolling Direction on Formability. Depending on the size, amount, and dispersion of secondary phases, the PH alloys show greater directional effects (Fig. 2) than alloys that are not PH. However, vacuum melting and solution annealing serve to reduce directional effects (anisotropy). As shown by data for press-brake bending in Fig. 2, directional effects contribute erratically to cracking and surface defects.

Annealing Practices for Precipitation-Hardenable Alloys. Two types of annealing treatments are used to soften the PH nickel-base alloys for forming, based on the ductility needed for forming and, if subsequent welding is required, on the avoidance of adverse metallurgical effects during and after welding. A high-temperature anneal is used to obtain maximum ductility and when no welding will be done on the formed part. A lower-temperature anneal, resulting in some sacrifice in ductility, is used when the part will be welded.

For example, solution annealing of alloy 41 at 1175 °C (2150 °F) followed by quenching in water gives maximum ductility. However, parts formed from sheet annealed in this way should not be welded; during welding or subsequent heat treatment, they are likely to crack at the brittle carbide network developed in the grain boundaries. A lower annealing temperature, preferably 1065 to 1080 °C (1950 to 1975 °F), results in less sensitization during welding and decreases the likelihood of grain-boundary cracking. Formability is reduced by 10 to 20% but is adequate for most forming operations.

Lubricants

Heavy-duty lubricants are required in most cold forming of nickel-base alloys. Although sulfur-containing and chlorine-containing additives can improve lubricants, they can also have harmful effects if not completely removed after forming. Sulfur will embrittle nickel-base alloys at elevated temperatures such as those that might be encountered in annealing or age hardening, and chlorine can cause pitting of the alloys after long exposure. Therefore, sulfurized and chlorinated lubricants should not be used if any difficulty is anticipated in cleaning the formed part. Neither are these lubricants recommended for use in spinning, as this operation may burnish the lubricant into the surface of the metal. Similarly, molybdenum disulfide is seldom recommended for use with nickel alloys because of difficulty in removal.

Pigmented oils and greases should be selected with care, because the pigment may be white lead (lead carbonate), zinc oxide, or similar metallic compounds that have low melting points. These elements can embrittle nickel alloys if the compounds are left on the metal during heat treatment. Inert fillers such as talc can be used safely.

Metallic Coatings. Maximum film strength can be obtained by using a coating of copper. However, because application and removal are expensive, metallic coatings are used as lubricants only in severe cold-forming operations and then only when they can be properly removed.

Ordinary petroleum greases are seldom used in forming nickel-base alloys. These greases do not necessarily have the film strength indicated by their viscosity, and they do not have a strong polar attraction for metals.

Phosphates do not form usable surface compounds on nickel-base alloys and cannot be used as lubricant carriers.

Light mineral oils and water-base lubricants have limited film strength and lubricity and can be used only in light forming operations.

Tools and Equipment

Nickel-base alloys do not require special equipment for cold forming. However, the physical and mechanical properties of these materials frequently necessitate modification of tools and dies used for cold forming other metals. These modifications are discussed in this section. Information applying to specific forming operations is presented in the sections covering those operations.

Die materials used in forming austenitic stainless steels are suitable for similar operations on nickel-base alloys. Examples include the following:

- O1, A2, D2, and D4 tools and cemented carbides for blanking and piercing dies
- Cemented carbide, D2 tool steel, or high-strength aluminum bronze for press forming dies
- D2 tool steel (short runs) and cemented carbides (long runs) for deep drawing dies

Soft die materials such as aluminum bronze, nickel-aluminum bronze, and zinc alloys are

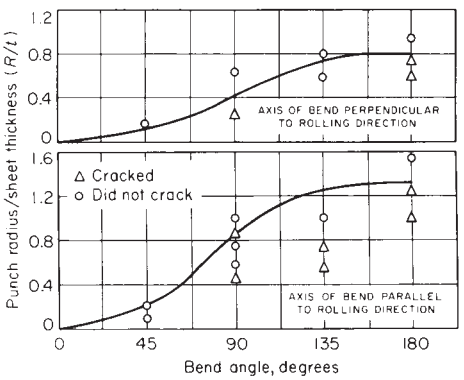


Fig. 2 Effect of forming direction relative to rolling direction on the formability of alloy 41 sheet 0.5 to 4.75 mm (0.02 to 0.187 in.) thick in press brake bending

used when superior surface finishes are desired. However, these materials have a relatively short service life. Parts formed with zinc alloy dies should be flash-pickled in dilute nitric acid to remove any traces of zinc picked up from the dies during forming. Zinc can cause embrittlement of nickel alloys during heat treatment or high-temperature service. For similar reasons, parts formed with brass or bronze dies should be pickled if the dies impart a bronze color to the workpiece.

Tool Design. Because nickel-base alloys are likely to gall, and because of the high pressures developed in forming, tooling should be designed with liberal radii, fillets, and clearances. The radii and clearances used in the cold forming of nickel-base alloys are usually larger than those for brass and low-carbon steel and about equal to those for the austenitic stainless steels.

Because nickel-base alloys, particularly the nickel-chromium alloys, have higher yield strengths and strain-hardening rates, they require stronger and harder dies and more powerful forming equipment than low-carbon steel requires. Generally, 30 to 50% more power is required for nickel-base alloys than is needed for low-carbon steel.

Equipment Operation. The strain-rate sensitivity and frictional characteristics of nickel-base alloys dictate that all forming operations be performed at relatively slow speeds. For instance, the slide speed in shearing, deep drawing, and press-brake bending is usually 9 to 15 m/min (30 to 50 ft/min). Cold heading, piercing, and similar operations are normally done at speeds of 60 to 100 strokes per minutes.

Shearing, Blanking, and Piercing

The optimum temper of nickel-base alloys for shearing, blanking, and piercing varies from skin hard to full hard, depending on the alloy and thickness. For instance, thin strip of Nickel 200 and the low-expansion nickel-iron alloys should be blanked in full-hard temper for maximum die life and minimum edge burr, but alloy 600 (UNS N06600) usually gives best results in skin-hard temper. Annealed temper is usually suitable for blanking of the PH alloys such as alloy X-750 (UNS N07750).

Punch-to-die clearance per side should be 3 to 5% of stock thickness for thin material and 5 to 10% of stock thickness for thick (≥3.2 mm, or ⅛ in.) material. The clearance between the punch and the stripper plate should be as small as is practicable.

Shears should have a low-carbon steel rating of 50% greater than the size of the nickel alloy material to be sheared. For example, a shear with a low-carbon steel rating of 9.5 mm (⅜ in.) should be used to cut 6.4 mm (¼ in.) thick alloy 400 (UNS N04400) plate.

Lubricants are not usually used in shearing but should be used in blanking and piercing. A light mineral oil fortified with lard oil can be used for material less than 3.2 mm (⅛ in.) thick. A heavier sulfurized oil should be used for material that is thicker than 3.2 mm (⅛ in.).

Procedure. In piercing, the minimum hole diameter is usually equal to or greater than the thickness of the material, depending on the thickness, temper, and specific alloy. Minimum hole diameters for given thicknesses of alloys 200, 400, and 600 are as follows:

Sheet thickness, *t*		Minimum hole diameter
mm	in.	
0.46 – 0.86	0.018 – 0.034	1.5*t*
0.94 – 1.78	0.037 – 0.070	1.3*t*
1.98 – 3.56	0.078 – 0.140	1.2*t*
3.97	0.156	1*t*

Hole diameters equal to the thickness of the sheet have been produced in material as thin as 0.46 mm (0.018 in.), but only after considerable experience and with proper equipment.

The softer alloys, such as Nickel 200, have greater impact strength than do the harder, chromium-containing alloys. Consequently, the softer alloys are more sensitive to the condition of dies and equipment. Shear knives may penetrate 65 to 75% of the material thickness before separation occurs in shearing Nickel 200, whereas penetration may be only 20 to 30% in shearing the harder alloys.

Laboratory tests have indicated that the shear strength of nickel-base alloys in double shear averages about 65% of the tensile strength. However, these values were obtained under essentially ideal conditions using laboratory testing equipment with sharp edges and controlled clearances. Shear loads on nickel-base alloys ranged from 113 to 131% of those on low-carbon steel in production shearing based on tests using a power shear with a rake of 31 mm/m (⅜ in./ft) of blade length.

Deep Drawing

Nickel-base alloys can be drawn into any shape that is feasible with deep drawing steel. The physical characteristics of nickel-base alloys differ from those of deep drawing steel, but not so much as to require different manipulation of dies for the average deep-drawing operation.

Most simple shapes can be deep drawn in nickel-base alloys using dies and tools designed for use on steel or copper alloys. However, when intricate shapes with accurate finished dimensions are required, minor die alterations are necessary. These alterations usually involve increasing clearances and enlarging the radius of the draw ring or of the punch nose.

Double-Action Drawing. In drawing and redrawing of thin stock (≤1.6 mm, or 1/16 in.) into cylindrical shells with no ironing, the diameter reduction should be 35 to 40% on the first operation and 15 to 25% on redraws. If the walls are held to size, the first and second operations may be the same as suggested above, but the amount of reduction should be diminished by about 5% on each successive redraw.

Although reductions of up to 50% can be made in one operation, this is not advisable because of the possibility of excessive shell breakage. Also, large reductions may open the surface of the metal and cause difficulty in finishing.

The number of redraws that can be made before annealing is necessary depends on the alloy being drawn. The alloys with the lower rates of work hardening (Fig. 1) can often be redrawn more than once without intermediate annealing. Trial runs may be needed to determine when annealing is necessary.

Single-Action Drawing. As with all metals, the depth to which nickel-base alloys can be drawn in single-action presses without some means of blank restraint is controlled by the blank-thickness-to-diameter ratio. For single-action drawing without holddown pressure, the blank thickness should be at least 2% of the blank or workpiece diameter for reductions of up to 35%. With properly designed dies and sufficiently thick material, the reduction on the first (cupping) operation with a single-action setup may be made equal to those recommended for double-action dies—that is, 35 to 40%. Redraws should not exceed a 20% reduction.

If the shell wall is to be ironed, the increased pressure on the bottom of the shell usually necessitates a decrease in the amount of reduction to prevent shell breakage. With reductions of 5% or less, the shell wall may be thinned by as much as 30% in one draw. With medium reductions of about 12%, the thickness of the shell wall can be decreased by about 15%. If the wall is to be reduced by a large amount, the shell should first be drawn to the approximate size with little or no wall thinning and the ironing done last. If a good surface finish is desired, the final operation should have a burnishing effect with only a slight change in wall thickness.

Clearances. Because nickel-base alloys have higher strengths than does low-carbon steel of drawing quality, nickel alloys have greater resistance to the wall thinning caused by the pressure of the punch on the bottom of the shell. Consequently, greater die clearance is required than is the case for steel if the natural flow of the metal is not to be resisted. However, the clearances required for nickel-base alloys are only slightly greater than those required for steel, and if dies used for steel have greater-than-minimum clearances, they are usually satisfactory for drawing nickel-base alloys, depending primarily on the mechanical properties of the alloy.

For ordinary deep drawing of cylindrical shells, a punch-die clearance per side of 120 to 125% of the blank thickness is sufficient and will prevent the formation of wrinkles. In the drawing of sheet thicker than 1.6 mm (1/16 in.), it is general practice to have the inside diameter of the draw ring larger than the diameter of the punch by three times the thickness of the blank (150% of stock thickness per side).

Draw-Ring and Punch Radii. Because nickel-base alloys work harden rapidly, relatively large draw-ring and punch radii should be used, especially for the early operations in a series of draws. Nickel-base alloys require more power to draw than does steel; consequently, the punch imposes a greater stress on the bottom corner of the shell. Small punch radii cause thinning of the shell at the line of contact, and if such a shell is further reduced, the thinned areas will appear farther up the shell wall and may result in visible necking or rupture. Also, buffing a shell having thinned areas will cause the shell wall to have a wavy appearance. For redraws, it is preferable to draw over a beveled edge and to avoid round-edged punches except for the final draw.

The draw-ring radius for a circular die is principally governed by the thickness of the material to be drawn and the amount of reduction to be made. A general rule for light-gage material is to have the draw-ring radius from 5 to 12 times the thickness of the metal. Insufficient draw-ring radius may result in galling and excessive thinning of the wall.

Drawing Rectangular Shells. As with other materials, the depth to which rectangular shapes can be drawn in nickel-base alloys in one operation is principally governed by the corner radius. To permit drawing to substantial depths, the corner radii should be as large as possible. Even with large corner radii, the depth of draw should be limited to from two to five times the corner radius for alloys 400, 200, and 201, and to four times the corner radius for alloy 600 and alloy 75 (UNS N06075). The permissible depth also depends on the dimensions of the shape and on whether the shape has straight or tapered sides The depth of draw for sheet less than 0.64 mm (0.025 in.) thick should not exceed an amount equal to three times the corner radius for alloys 400, 200, and 201 and should be less than that for alloy 600.

The corner radius on the drawing edge of the die should be as large as possible—approximately four to ten times the thickness of the material. To avoid wrinkles around the top corner of the shape, it is essential that the blank not be released prematurely.

In redrawing for the purpose of sharpening the corners or smoothing out wrinkles along the sides, only a small amount of metal should be left in the corners.

Frequently, it is necessary to draw shapes on dies designed to make a deeper single draw than is practical for nickel-base alloys. With such dies, the general practice is to draw about two-thirds of the full depth, to anneal the shape after this draw, and to complete the draw to full depth on the same dies. This same practice can be used to avoid wrinkling in drawing to lesser depths.

Spinning

Power spinning is preferred over manual spinning for nickel-base alloys. However, thin material, particularly alloys 200 and 400, can be manually spun with no difficulty. Table 1 gives practical limits on blank thickness for manual spinning of seven nickel-base alloys.

Tools. Except for small, light shapes, the required pressure cannot be exerted with the ordinary bar or hand tool pivoted on a fixed pin. Most shapes require the use of a tool that is mechanically adapted for the application of greater force, such as a compound-lever tool or roller tools that are operated by a screw. For small jobs, a ball-bearing assembly can be used on the end of a compound lever to make a good roller tool. Roller tools should be used whenever practical in order to keep friction at a minimum and exert maximum pressure. Roller tools should also be used to perfect contours in the spinning of press-drawn shapes.

When possible, tools used for spinning nickel-base alloys should be broader and flatter than those used for softer materials. The broader tool distributes plastic flow over a greater area and reduces overstraining. Except for this consideration, bar and roller tools should be designed the same as those used for spinning copper or brass.

Correct tool materials are essential for successful spinning. The most suitable material for bar tools is a highly polished, hard alloy bronze. Hardened tool steels are preferred for roller and beading tools. Chromium-plated hardened tool steel is recommended, as it decreases metal pickup by the tool. Tools of common brass and carbon steel, which are used for spinning softer materials, are unsatisfactory for use with nickel-base alloys.

Rotary cutting shears are preferred for edge trimming. If rotary shears are not available, hand trimming bars, hard faced with cobalt-base alloy, may be used, but the trimming speed must be reduced. Hand trimming bars should be ground so that they have a back-rake angle of 15 to 20° from the cutting edge, and the edge must be kept sharp. A tool shaped like a thread-cutting lathe tool can be used for trimming. This tool also has a back rake from the cutting edge. With this type of tool, the material is not sheared off the edge; instead, the tool is fed into the side of the workpiece. A narrow ring is cut from the edge. The workpiece should be supported at the back during all trimming operations.

Mandrels. Hardened-alloy cast iron and steel mandrels give longer life and better results than softer materials such as wood. Hard maple or birch mandrels may be used for intermediate operations if production quantities are small and tolerances are liberal.

Spinning nickel-base alloys over mandrels that are the same as those used for copper alloys will not necessarily result in spun shapes of exactly the same dimensions as those of the softer metal. Most nickel-base alloy shapes will have slightly larger peripheries than those of softer metals spun over the same mandrel. This is caused by the greater springback of the nickel-base alloys.

Lubricants. Heavy-bodied, solid lubricants, such as yellow laundry soap, beeswax, and tallow, are recommended for spinning. These lubricants can be manually applied to the blank as it rotates. Blanks can be electroplated with 5 to 18 μm (0.2 to 0.7 mils) of copper to improve lubrication on difficult shapes.

Procedure for spinning nickel-base alloys is essentially the same as that used for other metals. As a general rule, in laying out a spinning sequence for alloy 400, an increase in height of 25 to 38 mm (1 to 1½ in.) on the article being spun constitutes an operation if spinning is being done in the usual way with a bar tool. Approximately twice that depth per operation may be obtained with a compound-lever or roller tool. The workpiece should be trimmed and annealed before it is spun to greater depths.

A hard-surfaced mandrel should be provided for each operation so that the metal can always be pushed firmly against the surface of the mandrel. This procedure keeps the workpiece surface smooth and dense, and ensures the best results in annealing. With an insufficient number of intermediate mandrels, the material is subjected to an excessive amount of cold working. This may result in either spinning a buckle into the material or formation of a pebbled surface. It is virtually impossible to smooth out the former by additional cold work or to correct the latter by annealing.

Figure 3 illustrates the number of mandrels and annealing operations necessary for spinning deep cups from 0.94 mm (0.037 in.) thick alloy 200, 400, and 600 blanks using hand tools. Figure 3 also shows the amount of forming that can be done before annealing and between intermediate anneals. The spinnability of other alloys can be estimated from their relative work-hardening rates (Fig. 1) and from their tensile properties.

In spinning, the optimum speed of the rotating blank is governed by its diameter and thickness. Small, thin blanks can be spun at greater speeds than larger or thicker pieces. Nickel-base alloys are often spun at speeds of one-half to three-fourths those normally used in spinning the same shape from softer metals. Lathe speeds of 250 to 1000 rpm are usually satisfactory. Trimming speeds must necessarily be slow; ordinarily, trimming is done at the minimum speed of the lathe.

Table 1 Maximum blank hardness and thickness for manual spinning of nickel-base alloys

Alloy	Maximum hardness	Maximum thickness	
	HRB	mm	in.
Nickel 200	64	1.57	0.062
Nickel 201	55	1.98	0.078
Alloy 400	68	1.27	0.050
Alloy 600	80	0.94	0.037
Alloy 722	94	0.94	0.037
Alloy X-750	94	0.94	0.037
Alloy 801	88	0.94	0.037

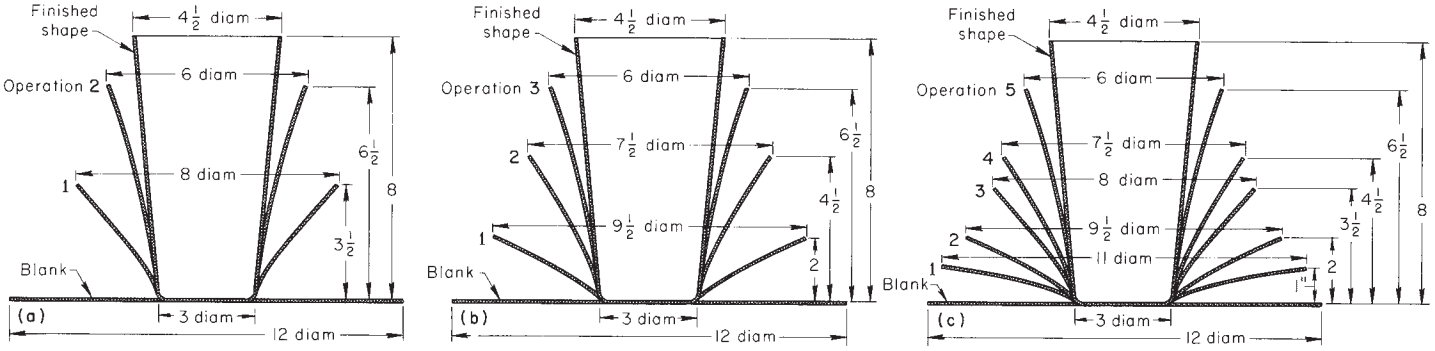


Fig. 3 Spinnability of three nickel-base alloys, as shown by the number of operations required for manual spinning of a deep cup from a 0.94 mm (0.037 in.) thick blank of each alloy. Workpieces were annealed between all operations. Dimensions given in inches. (a) Alloy 200. (b) Alloy 400. (c) Alloy 600

Bending Tube and Pipe

All common forming operations such as bending, coiling, and expanding can be performed readily on nickel-base alloy tube and pipe, using the same type of equipment as is used for other metals. In general, material in the annealed condition is recommended. Alloys 400, 200, and 201 can be formed in the stress-relieved temper; however, the amount of deformation will be limited by the higher tensile strength and lower ductility. In bending, the minimum radius to which stress-relieved tubing can be bent is 25 to 50% greater than it is for annealed tubing of the same size.

The minimum radii to which nickel-base alloy tubing can be bent by various methods are given in Table 2. Depending on equipment design, tube size, and quality of the finished bend, it is possible to bend to radii smaller than those listed; however, trial bends should be made to determine whether the smaller radii are practicable.

Bending without Mandrels or Fillers. When bending with no internal support, the dies should be slightly smaller than those used for bending with a mandrel or filler. Bending without use of a mandrel or filler is suitable only for tube and pipe that have a wall thickness greater than 7% of the outside diameter, or for large-radius bends. Nickel-base alloy tube in sizes within the above ratio can be bent with no mandrel or filler to a minimum mean radius of three times the outside diameter of the tube (3*D*) through 180°.

Table 2 Minimum bend radii for nickel-base alloy tubes

Bending method	Minimum mean bend radius(a)	Maximum included angle of bend, degrees
Press bending, unfilled tube	6*D*	120
Roll bending, filled tube	4*D*	360
Compression bending		
Unfilled tube	2.5*D*	180
Filled tube(b)	2*D*	180
Draw bending		
Unfilled tube	3*D*	180
Filled tube(b)	2*D*	180

(a) *D*, tube outside diameter. (b) Or using mandrel

Bending with Mandrels or Fillers. Thin-wall tubing can be bent to small radii with freedom from wrinkles by use of a mandrel or filler. Thin-wall tubing of nickel alloys can be mandrel-bent through 180° to a minimum mean radius of 2*D*.

To minimize galling of the inside surface of the tube, mandrels should be made of hard-alloy bronze rather than of steel. If steel mandrels are used, they should be chromium plated to reduce galling.

Mandrels must be lubricated before use; chlorinated oils with extreme-pressure (EP) additives are recommended for severe bending. For less severe bending or for ease of removal, water-soluble lubricants are used.

Any conventional filler material, such as sand, resin, and low-melting alloy, can be used. Sand is the least desirable because it is difficult to pack tightly and, thus, can lead to the formation of wrinkles or kinks during bending.

Low-melting alloy fillers produce the best bends. The expansion characteristics of these fillers ensure that voids are eliminated and a sound carrier is created.

Alloy fillers are removed by heating the bent tube in steam or hot water. Metallic fillers must not be removed by direct torch heating, because they contain elements such as lead, tin, and bismuth that will embrittle nickel alloys at elevated temperatures. It is imperative that all traces of metallic fillers be removed if the tube is to be subjected to elevated temperatures during subsequent fabrication or during service.

Press Bending. Press or ram bending, in which the tube is held by two supporting dies and a force is applied between the dies, is normally used only for heavy-wall tubing in which some flattening is tolerable. This method does not provide close tolerances and is applicable only to large-radius bends. The bend is limited to 120°, and the radius of the bend should not be less than six times the outside diameter of the tube (6*D*) if a smooth bend is desired. A filler material should be used for bends of radii less than 6*D*.

Pressure dies used in press bending should be at least two times longer than the outside diameter of the tube. Press bending with wing dies is used for unfilled, thin-wall, large-diameter tube.

Annealed tubing is not always preferred for press bending. Annealed tubing of low base hardness is not stiff enough to withstand deformation without excessive flattening. Consequently, nickel and nickel-copper alloys are usually press-bent in the stress-relieved temper. Nickel-chromium alloys have higher mechanical properties in the annealed condition than do nickel and nickel-copper alloys and should be press-bent in the annealed temper. Ideally, the choice of temper for a specific bend should be determined form the results of several trial bends.

Roll bending is the principal method of producing helical coils, spirals, and circular configurations, because an included angle of 360° can be obtained. Bending may be done on either unfilled or filled tube. The minimum bend radius that can be attained on unfilled tube is approximately six times the outside diameter of the tube.

Compression bending uses a stationary bending form and a movable wiper shoe. This method is unsuitable for thin-wall tubing and is generally used with no mandrel support.

Compression bending can produce bend radii down to 2½ *D* but is normally used only for large-radius bends. The maximum included angle that can be produced is 180°.

Draw bending is the most common bending process and the preferred method for bending nickel-base alloy tube. The process is similar to compression bending, except that the bending form revolves and the pressure due either remains stationary or slides along a straight line. The sliding pressure die is preferred because it distributes the applied stresses more evenly.

Bends of up to 180° with a minimum radius of 2*D* can be produced by draw bending. Bending can be done with or without a mandrel. In general, a mandrel is preferred and must be used when the ratio of tube diameter to wall thickness is above the limit suitable for bending without tube wrinkling or collapsing. Various types of mandrels are used, including ball and plug types.

Hot Bending. When possible, tube and pipe should be formed by cold bending. If hot bending is necessary, it is performed by standard hot bending methods.

Hot bending is normally limited to tube and pipe larger than 2 in. schedule 80 (60.5 mm, or

2.375 in., OD and 5.54 mm, or 0.218 in., wall thickness). Thin-wall tubing should not be bent hot, because it is difficult to retain sufficient heat to make the bend.

Hot bending should be done on filled tube only. Sand is the normal filler material. The sand must be free of sulfur, because contamination of nickel-base alloys by sulfur causes cracking during bending. Sulfur can be removed from sand by heating to about 1150 °C (2100 °F) in an oxidizing atmosphere. Tubing must be cleaned thoroughly before filling or heating.

Sand-filled tube and pipe in small sizes (60.2 to 72.9 mm, or 2.37 to 2.87 in., OD) can be bent hot to a minimum mean radius of two times the outside diameter of the tube. Larger sizes require greater bend radii.

In hot bending, the metal should be worked as soon as possible after removal from the furnace, to avoid cooling before bending is completed.

Bending of Plate, Sheet, and Strip

Table 3 lists minimum bend diameters for hot-rolled and annealed nickel-base alloy sheet, plate, and strip. In compiling these data, a sample was judged to have passed the 180° bend test if its surface showed no ductile fracturing. Because of the effects of various surface conditions and heat treatments on bendability, the data in Table 3 should be regarded as general guidelines. Many of the materials can in fact be bent in stages to tighter radii than those suggested provided initial bending is not too severe.

The importance of surface condition is demonstrated by the alloys from which scale or oxides must be removed to ensure successful bending. Scale can be removed either by chemical or mechanical means, depending on the alloy.

Expanding

Nickel-base alloy tubing can be expanded into tube sheets for heat exchanger applications by any conventional method. The oversize allowance on tube sheet holes to the nominal outside diameter of the tube should be kept to a minimum. The tube sheet hole should be 0.10 to 0.20 mm (0.004 to 0.008 in.) larger than the nominal outside diameter of the tube for tubing less than 38 mm (1½ in.) in outside diameter. For tubing 38 mm (1½ in.) or larger in outside diameter, the oversize allowance should be 0.23 to 0.25 mm (0.009 to 0.010 in.).

Procedure. Expanding may be done by drifting with sectional expanders or by rolling with three-roll expanders. Three-roll expanders are preferred. The ends of rolled-in tubing are flared in the conventional manner.

The tube sheet hole and both the outside and inside surfaces of the tube must be free of all foreign matter such as oxides, dirt, and oil. The ends of the tube should also be deburred before rolling.

Lubrication should be provided between the rollers of the tool and the inside surface of the tube. Any sulfur-free mineral oil or lard oil, either diluted or straight, can be used. Lubricants that contain embrittling or contaminating elements such as sulfur or lead should be avoided, because of the difficulty in cleaning the finished assembly.

Controlled rolling equipment should be used to prevent overexpanding, which may distort the tube sheet and deform the tube sheet ligaments, causing loose-fitting tubes. This is particularly true when the tube has a higher hardness than the tube sheet or a significantly higher rate of work hardening.

Temper. The tube sheet should be harder than the tube being rolled into it. Otherwise, springback in the tube may be greater than in the tube sheet, causing a gap between the two when the expanding tool is removed. For this reason, tube sheets are usually supplied in the as-rolled or as-forged temper, and tube is supplied in the annealed temper. The need for the tube sheet to be harder than the tube is greatest when the thickness of the tube sheet is less than the outside diameter of the tube, and when the center-to-center spacing of the tubes (tube pitch) is less than 1¼ times the OD of the tube or the OD plus 6.4 mm (¼ in.), whichever is greater.

Stress-relieved tubing may be slightly harder than the tube sheet but can be expanded to form a satisfactory connection if greater care is exercised in expanding. For greater assurance of pressure tightness, a seal weld may be placed around the end of the tube after expanding. The stress-relieved temper is suitable for either welding or silver brazing.

Tubing in the annealed condition is used when optimum rolling or expanding characteristics are desired or for severe cold bending and flaring.

Forming of Rod and Bar

Rod and bar in the annealed condition are preferred for cold forming. Material in other tempers may be required for some forming operations or when properties that cannot be obtained by heat treatment after forming are desired in the end product.

Bending. Rod and bar may be bent in the same manner as tubing. The possibility of collapsing or wrinkling is eliminated, because the solid section provides its own internal support.

Most nickel-base alloys have suitable mechanical properties in the hot-finished condition for moderate bending. The annealed temper should always be used for extremely small-bend radii or low radius-to-thickness ratios. Cold drawn, annealed material should be used if surface roughening (orange peeling) related to coarse grain structure is undesirable.

Coiling of rod and bar is limited almost entirely to the production of springs. Nickel-base alloy springs for high-temperature service are usually annealed or solution treated and aged after forming. Consequently, they may be produced from annealed material (or even produced by hot coiling) with no adverse effect on final properties.

If the desired properties cannot be obtained by heat treating after forming, the spring must be coiled from tempered, cold-worked material. The use of tempered material greatly increases the minimum radius to which the rod or bar can be coiled.

Pressures and speeds encountered in production coiling usually require the use of high-grade lubricants with good film strength. Wire rod is often coated with copper to reduce friction and improve retention of organic lubricants.

Table 3 Minimum bend diameters for annealed sheet and strip and hot-rolled, annealed plate

Alloys were bent 180°; minimum bend diameters are given in terms of material thickness.

Alloy	Product form	Thickness, *t*		Minimum bend diameter(a)
		mm	in.	
Nickel 200	Sheet, strip	0.30–6.35	0.012–0.250	1*t*
	Plate	4.75–6.35	0.187–0.250	2*t*
Alloy 400	Sheet, strip	0.30–2.77(b)	0.012–0.109(b)	1*t*
		2.79–6.35	0.110–0.250	2*t*
	Plate	4.75–6.35(c)	0.187–0.250(c)	2*t*
Alloy 600	Sheet, strip	0.30–6.35	0.012–0.250	1*t*
	Plate	4.75–6.35	0.187–0.250	2*t*
Alloy 625(d)	Sheet, strip	0.30–6.35	0.012–0.250	2*t*
	Plate	4.75–6.35	0.187–0.250	2*t*
Alloy 718(d)	Sheet, strip	0.30–1.24	0.012–0.049	1*t*
		1.27–6.35	0.050–0.250	2*t*
Alloy X-750	Sheet, strip	0.30–1.24	0.012–0.049	1*t*
		1.27–6.35	0.050–0.250	2*t*
Alloy 800	Sheet, strip	0.30–6.35(b)	0.012–0.250(b)	1*t*
	Plate	4.75–6.35(b)	0.187–0.250(b)	2*t*
Alloy 825	Sheet, strip	0.30–6.35(b)	0.012–0.250(b)	2*t*
	Plate	4.75–6.35(b)	0.187–0.250(b)	2*t*

(a) Bend tests performed according to ASTM E 290 with a guide bend jig as described in ASTM E 190. (b) Successful bending depended on surface condition of the samples, with particular regard to freedom from oxidation. (c) Samples were descaled. (d) Sheared edges were ground or meachined.

The severe cold forming involved in producing coils and the severe service conditions in which these products are often used demand a high-grade starting product. Centerless-ground or ground and cold-drawn material is used to obtain the necessary quality.

Cold Heading and Cold Extrusion

Cold heading and cold extrusion are most often used in the production of fasteners and similar cold upset parts. Cold extrusion is rarely done except in conjunction with cold heading.

The high strength and galling characteristics of nickel-base alloys require slow operating speeds and high-alloy die materials. Cold heading machines should be operated at a ram speed of about 10 to 15 m/min (35 to 50 ft/min). These ram speeds correspond to operating speeds of 60 to 100 strokes per minute on medium-size equipment.

Tools should be made of oil-hardening or air-hardening die steel. The air-hardening types, such as AISI D2, D4, or high-speed steel (M2 or T1), tempered to 60 to 63 HRC, are preferred.

Material. Rod stock (usually less than 25 mm, or 1 in., in diameter) in coils is used for starting material, as cold heading is done on high-speed automatic or semiautomatic equipment. Although alloy 400 is sometimes cold headed in larger sizes, 22 mm (⅞ in.) is the maximum diameter in which alloys 400 and K-500 can be cold headed by most equipment. Limiting sizes in harder alloys are proportionately smaller, depending on their hardness and yield strength in the annealed condition. Stock sizes in excess of these limits are normally hot formed.

Cold-heading equipment requires wire rod with diameter tolerances in the range of 0.076 to 0.127 mm (0.003 to 0.005 in.). Because alloy 400 should be cold headed in the 0 or No. 1 temper to provide resistance to crushing and buckling during forming, these tolerances can normally be obtained with the drawing pass used to develop this temper. For tighter tolerances or harder alloys, fully cold-drawn material must be used.

The surface quality of regular hot-rolled wire rod, even with a cold sizing pass, may not be adequate for cold heading. Consequently, a special cold heading quality wire rod is usually recommended. Configurations that are especially susceptible to splitting, such as rivets, flat-head screws, and sockethead bolts, require shaved or centerless-ground material.

Lubricants. To prevent galling, high-grade lubricants must be used in cold heading of nickel-base alloys.

Lime and soap are usually used as a base coating on alloy 400. Better finish and die life can be obtained by using copper plating 7.5 to 18 μm (0.3 to 0.7 mils) thick as a lubricant carrier. Copper plating may be used also on the chromium-containing alloys 600 and 800, but oxalate coatings serve as an adequate substitute.

Regardless of the type of carrier, a base lubricant is best applied by drawing it on in a light sizing pass to obtain a dry film of the lubricant. Any of the dry soap powders of the sodium, calcium, or aluminum stearate types can be applied this way.

If the wire rod is to be given a sizing or tempering pass before the cold-heading operations, the heading lubricant should be applied during drawing.

Lubrication for cold heading is completed by dripping a heavy, sulfurized mineral oil or a sulfurized and chlorinated paraffin on the blank as it passes through the heading stations.

Straightening

Rod and bar in straight lengths are usually straightened by conical rolls, stretchers, or punch presses. Material in coil form is straightened with staggered-roll straighteners or rotating-die straighteners.

Like other forming equipment, straighteners require about 50% more power for nickel-base alloys than they do for low-carbon steel; a straightener having a capacity of 12.7 mm (½ in.) diameter in steel will be limited to about 9.5 mm (⅜ in.) diam in nickel alloys.

A lubricant should be used with rotating-die straighteners to reduce scratching and scoring and to improve die life. Spiral scoring may become quite severe on large sizes of harder alloys. If scoring cannot be held to an acceptable level by the use of lubricants, material in the softest temper available should be used.

Staggered-roll straightening involves lower contact velocities than do rotating-die types, and lubrication is less critical. Coil stock is often straightened without lubricant, for better grip on rolls.

Dies for rotary-die straighteners may be either bronze or cast iron. Cast iron dies must be used if contamination from rubbed-off bronze occurs in the end product, and no pickling is done after straightening.

Cold-Formed Parts for High-Temperature Service

A part that is highly stressed from cold forming may require heat treatment to avoid excessive creep in service above its recrystallization temperature. Recrystallization of a specific alloy is determined largely by the extent of cold work and the temperature to which the part is exposed during service. The grain size and exact composition of the material also complicate prediction of the recrystallization temperature.

The nickel-base alloys most likely to be subjected to high temperatures in service are the iron-nickel-chromium and nickel-chromium alloys. These alloys are frequently used in the grain-coarsened condition at service temperatures above 595 °C (1100 °F).

Generally, cold-formed nickel-base alloys should be heat treated if they have been strained in either tension or compression by more than 10% and will be subject to service temperatures above 650 °C (1200 °F). Producers should be consulted for the proper thermal treatments.

In certain alloys, heavy cold working (for example, highly restrained bending) followed by exposure at moderate to high temperatures (for example, stress relieving or age hardening) can lead to cracking. In age-hardenable alloys, for example, the combination of high residual tensile stress and the stress associated with the aging response may exceed the stress-rupture strength of the material. In nonage-hardenable alloys, excessive cold working of coarse-grain material (grain size of ASTM No. 5 or coarser) without the recommended intermediate annealing can cause cracking during subsequent exposure at stress-relieving or annealing temperatures. Testing the material under actual conditions of forming and heating will determine its susceptibility to cracking.

Springs can be cold formed from PH alloys in the annealed or cold-drawn temper. For service at temperatures above 315 °C (600 °F), springs should be solution annealed before aging to prevent loss of strength from relaxation.

ACKNOWLEDGMENTS

This article was adapted from the following:

- R.W. Breitzig, Forming of Nickel-Base Alloys, *Forming and Forging,* Vol 14, *ASM Handbook,* ASM International, 1988, p 831–837
- S.K. Srivastava and E.W. Kelley, Forming of Heat-Resistant Alloys, *Forming and Forging,* Vol 14, *ASM Handbook,* ASM International, 1988, p 779–784

ASM Specialty Handbook: Nickel, Cobalt, and Their Alloys
J.R. Davis, editor, p 198-202
DOI:10.1361/ncta2000p198

Copyright © 2000 ASM International®
All rights reserved.
www.asminternational.org

Forging of Nickel Alloys

NICKEL ALLOYS are often closed-die forged into turbine blades, turbine disks, exhaust valves, chain hooks, heat-exchanger headers, valve bodies, and pump bodies. Shafts and seamless rings are made by open-die forging. Seamless rings are also made by ring rolling. Each of these forging methods are described in greater detail in *Forming and Forging,* Volume 14, of the *ASM Handbook.*

Most nickel-base alloys are stronger and stiffer than steel. Commercially pure alloy 200 (UNS N02200) and nickel-copper alloy 400 (UNS N04400), however, are softer than many steels. As an indication of the relative resistance to hot deformation, Table 1 lists the pressures developed in the roll gap at 20% reduction in hot rolling for five nickel-base alloys and two steels at four hot-working temperatures. Higher pressures indicate greater resistance. Sufficiently powerful equipment is of particular importance when forging alloys 800 (UNS N08800), 600 (UNS N06600), 625 (UNS N06625), and the precipitation-hardenable alloys such as 718 (UNS N07718) and X-750 (UNS N07750). These alloys were specifically developed to resist deformation at elevated temperatures.

Die Materials and Lubrication

The die materials used to forge nickel-base alloys are similar to those used for stainless steel and include hot-work tool steels such as H11, H12, and H13. For the softer nickel alloys, the service lives of steel dies usually range from 3000 to 10,000 pieces. Die life is a major problem, however, in forging some heat-resistant superalloys, and dies often must be reworked after forging as few as 400 pieces.

Isothermal forging (see discussion below) requires strength and integrity of the dies at temperatures of the workpiece. For such applications, TZM molybdenum has very good strength and stability as a die material at service temperatures up to 1200 °C (2190 °F). However, this alloy requires either a vacuum or an inert atmosphere to prevent oxidation of the die.

Lubrication. Dies can be lubricated to facilitate removal of the workpiece after forging. Sulfur-free lubricants are necessary; those made with colloidal graphite give good results.

Lubricants can be applied by swabbing or spraying. Spraying is preferred because it produces more uniform coverage.

Heating for Forging

Nickel-base alloy billets can be induction heated or furnace heated before hot forging. Regardless of the heating method used, the material must be cleaned of all foreign substances. Although nickel-base alloys have greater resistance to scaling at hot-working temperatures than steels, they are more susceptible to attack by sulfur during heating. Exposure of hot metal to sulfur must be avoided. Marking paints and crayons, die lubricants, pickling liquids, and slag and cinder that accumulate on furnace hearths are all possible sources of sulfur and should be removed from the metal before heating. Metal surfaces that have been attacked by sulfur at high temperatures have a distinctly burned appearance. If the attack is severe, the material is mechanically weakened and rendered useless.

If furnace heating is used, nickel-base alloy forging preforms should be supported on metal rails or by other means in order to avoid contamination. The metal should not touch the furnace bottom or sides. Protection against spalls from the roof may also be necessary.

Fuels

Many standard fuels are suitable for the furnace heating of nickel-base alloys. An important requirement is that they be of low sulfur content.

Gaseous fuels such as natural gas, manufactured gas, butane, and propane are the best fuels and should always be used if available. They must not contain more than 2 g (30 grains) of total sulfur per 2.8 m^3 (100 ft^3) of gas and preferably not more than 1 g (15 grains) of total sulfur per 2.8 m^3 (100 ft^3) of gas.

Oil is a satisfactory fuel provided it has a low sulfur content. Oil containing more than 0.5% S should not be used. Coal and coke are generally unsatisfactory because of the difficulty in providing for proper heating conditions, inflexibility in heat control, and excessive sulfur content.

Furnace Atmosphere

The furnace atmosphere should be sulfur free and should be continuously maintained in a slightly reducing condition, with 2% or more carbon monoxide. The atmosphere should not be permitted to alternate from reducing to oxidizing. The slightly reducing condition is obtained by reducing the air supply until there is a tendency to smoke, which indicates an excess of fuel and a reducing atmosphere. The air supply should then be increased slightly to produce a hazy atmosphere or a soft flame. Excessive amounts of carbon monoxide or free carbon are not harmful; nickel-base alloys, unlike steels, will not carburize under these conditions. However, a slight excess of fuel over air is all that is required, and the closer the atmosphere is to the neutral condition, the easier it is to maintain the required temperature. The true condition of the atmosphere is determined by analyzing gas

Table 1 Hot-forming pressures for several nickel-base alloys

Pressures developed in the hot forming of 1020 steel and AISI type 302 stainless steel are shown for comparison.

		Pressure developed at working temperature(a)							
		870 °C (1800 °F)		1040 °C (1900 °F)		1095 °C (2000 °F)		1150 °C (2100 °F)	
Alloy	UNS No.	MPa	ksi	MPa	ksi	MPa	ksi	MPa	ksi
400	N04400	124	18	106	15.3	83	12	68	9.8
600	N06600	281	40.8	239	34.6	195	28.3	154	22.3
625	N06625	463	67.2	379	55	297	43	214	31
718	N07718	437	63.3	385	55.8	333	48.3	283	41
X-750	N07750	335	48.6	299	43.3	265	38.4	230	33.3
1020 steel	G10200	154	22.4	126	18.3	99	14.3	71	10.3
Type 302 stainless steel	S30200	192	27.8	168	24.3	148	21.4	124	18

(a) Pressure developed in the roll gap at 20% reduction in hot rolling.

samples taken at various points near the metal surface.

It is important that combustion take place before the mixture of fuel and air contacts the work, or the metal may be embrittled. Proper combustion is ensured by providing ample space to burn the fuel completely before the hot gases enter the furnace chamber.

General Guidelines for Ingot Breakdown (Ref 1)

Because of their high alloy content and generally narrow working temperature range, nickel-base alloys must be converted from cast ingots with care. Initial breakdown operations are generally conducted well above the γ′ solvus temperature, with subsequent deformation completed below it but still high enough to avoid excessive warm working and an unrecrystallized microstructure. The original cast structure must be completely refined during breakdown, that is, before final forging, particularly when substantial levels of reduction are not imposed during closed-die forging.

Good heat retention practice during ingot breakdown is an important factor in obtaining a desirable billet microstructure. Rapid transfer of the ingot from the furnace to the forging press, as well as the use of such techniques as reheating during breakdown, is necessary to promote sufficient recrystallization during each forging pass. In addition, it has been found that diffusion of precipitation-hardening elements is associated with recrystallization during ingot conversion. Mechanical factors such as cycling speed (which affects heat losses), reduction, length of pass, die design, and press capacity all influence the degree of work penetration through the billet cross section and therefore the rate of ingot conversion.

General Guidelines for Finish Forging

Figure 1 shows the temperature ranges for the safe forging of 12 nickel-base alloys. Use of the lower part of the temperature range may be required for the development of specific mechanical properties.

Closed-die forging of nickel-base alloys is generally done below the γ′ solvus temperature in order to avoid excessive grain growth. Approximately 80% of the reduction is scheduled in the recrystallization temperature range, with the remaining 20% done at lower temperatures to introduce a certain amount of warm work for improved mechanical properties. Preheating of all tools and dies to about 260 °C (500 °F) is recommended to avoid chilling the metal during working.

Forging Rate. A very rapid rate of forging often causes heat buildup (due to friction and deformation heating), a nonuniform recrystallized grain size, and mechanical property variations. Susceptibility to free surface ruptures also increases with forging rate (and forging temperature). Therefore, slow strain rates are typically used during the initial closed-die reductions of such alloys as Astroloy (UNS N13017) and René 95 (Ni-14Cr-8Co-3.5Mo-3.5W-3.5Nb-3.5Al-2.5Ti). With proper selection of starting stock and forging temperature, however, the forging rate is less critical. For example, some Astroloy turbine components are currently hammer forged.

Forging Reduction. A sufficient amount of recrystallization is necessary in each of a series of closed-die forging operations to achieve the desired grain size and to reduce the effects of the continuous grain-boundary or twin-boundary carbide networks that develop during heating and cooling. This condition contributes more to mechanical-property and other problems than any other single factor. Poor weldability, low-cycle fatigue, and stress rupture properties are associated with continuous grain-boundary carbide networks. Heat treatment can do very little to correct this problem without creating equally undesirable mechanical-property problems when higher solution treatment temperatures are used. All portions of a part must receive some hot work after the final heating operation in order to achieve uniform mechanical properties.

In open-die forging, a series of moderate reduction passes along the entire length of the forging is preferred. In working a square section into a round, the piece should be worked down in the square form until it approaches the final size. It should then be converted to an oversize octagon before finishing into the round. Billet corners that will be in contact with dies should be chamfered rather than left square. The work should be lifted away from the dies occasionally to permit relief of local cold areas.

Other Considerations. The precipitation-hardenable nickel alloys are subject to thermal cracking. Therefore, localized heating is not recommended. The entire part should be heated to the forging temperature.

If any ruptures appear on the surface of the metal during hot working, they must be removed at once, either by hot grinding or by cooling the work and cold overhauling. If the ruptures are not removed, they may extend into the body of the part.

For sections equal to or larger than 405 mm (16 in.) square, precautions should be taken in heating precipitation-hardenable alloys. They should be charged into a furnace at 870 °C (1600 °F) or colder and brought up to forging temperature at a controlled rate of 40 °C/h (100 °F/h).

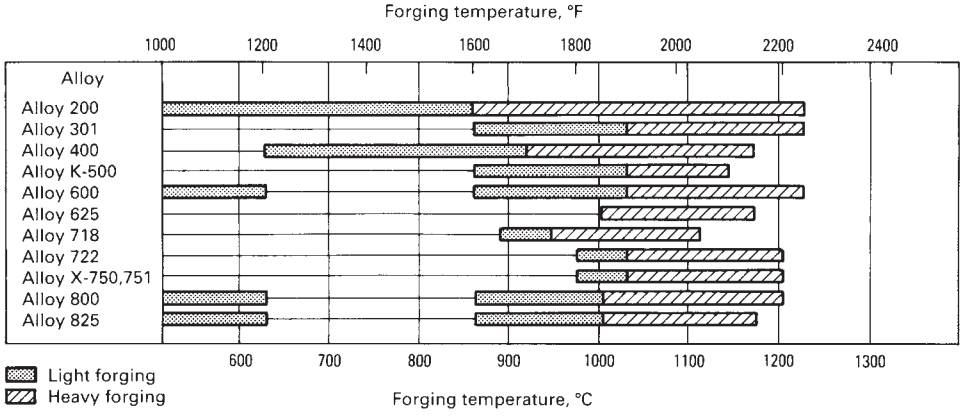


Fig. 1 Forging temperature for 12 nickel-base alloys

Cooling after Forging

The rate of cooling after forging is not critical for alloys 200, 400, and 625. Alloys K-500 (UNS N05500) and 301 (UNS N03301) should be water quenched from forging temperatures to avoid the excessive hardening and cracking that could occur if they were cooled slowly through the age-hardening range and to maintain good response to subsequent aging. Alloy 825 (UNS N08825) should be cooled at a rate equal to or faster than air cooling.

Alloys 800 and 600 are subject to carbide precipitation during heating in or slow cooling through the temperature range of 540 to 760 °C (1000–1400 °F). If sensitization is likely to prove disadvantageous in the end use, parts made of these alloys should be water quenched or cooled rapidly in air.

The precipitation-hardenable alloys should, in general, be cooled in air after forging. Water quenching is not recommended because of the possibility of thermal cracking, which can occur during subsequent heating for further forging or heat treating.

Forging Practice for Specific Alloys

The following practices are used in the forging of nickel-base alloys. Variations from these procedures may be necessary for some specialized applications.

Alloy 200 should be charged to a hot furnace, withdrawn as soon as the desired temperature has been reached, and worked rapidly. The recommended range of forging temperatures

is 650 to 1230 °C (1200–2250 °F). Because the metal stiffens rapidly when cooled to about 870 °C (1650 °F), all heavy work and hot bending should be done above that temperature. High mechanical properties can be produced by working lightly below 650 °C (1200 °F). The best range for hot bending is 870 to 1230 °C (1600–2250 °F).

Alloy 301. The optimal temperature range for the forging of alloy 301 is 1065 to 1230 °C (1900–2250 °F). Light finishing work can be done down to 870 °C (1600 °F). Finer grain size is produced in forgings by using 1175 °C (2150 °F) for the final reheat temperature and by taking at least 30% reduction of area in the last forging operation.

After hot working, the alloy should be quenched from 790 °C (1450 °F) or above. Quenching retains the strain hardening imparted by the forging operation and produces better response to subsequent age hardening. Quenching in water containing about 2 vol% alcohol results in less surface oxidation.

Material that must be cooled prior to subsequent hot working should also be quenched. Slow cooling may cause age hardening, which sets up stresses in the workpiece that can cause cracking during subsequent reheating.

Alloy 400. The maximum heating temperature for forging alloy 400 is 1175 °C (2150 °F). Prolonged soaking at the working temperature is detrimental. If a delay occurs during processing, the furnace temperature should be reduced to 1040 °C (1900 °F) and not brought to 1175 °C (2150 °F) until operations are resumed.

The recommended metal temperature for heavy reductions is 925 to 1175 °C (1700–2150 °F). Light reductions may be taken down to 650 °C (1200 °F). Working at the lower temperatures produces higher mechanical properties and smaller grain size.

A controlled forging procedure is necessary to meet the requirements of some specifications for forged hot-finished parts. Both the amount of reduction and the finishing temperature must be controlled in order to develop the desired properties.

One procedure for producing forgings to such specifications consists of taking a 30 to 35% reduction after the final reheat. This is done as follows:

- Reheat
- Forge to a section having about 5% larger area than the final shape (take at least 25% reduction)
- Cool to 705 °C (1300 °F)
- Finish to size (5% reduction)

High-tensile forgings, as described in certain military specifications, also require a minimum of 30 to 35% reduction after the last reheat. This is taken in the following manner:

- Reheat
- Forge to a section having an area about 25% larger than the final shape (take about 5% reduction)
- Cool to 705 °C (1300 °F)
- Finish to size (25% reduction)

Grain refinement is achieved by using 1095 °C (2000 °F) for the final reheat and by increasing the amount of reduction taken after the last reheat.

Alloy K-500. The maximum recommended heating temperature for the forging of alloy K-500 is 1150 °C (2100 °F). Metal should be charged into a hot furnace and withdrawn when uniformly heated. Prolonged soaking at this temperature is harmful. If a delay occurs such that the material would be subject to prolonged soaking, the temperature should be reduced to or held at 1040 °C (1900 °F) until shortly before working is to begin, then brought to 1150 °C (2100 °F). When the piece is uniformly heated, it should be withdrawn. In the event of a long delay, the work should be removed from the furnace and water quenched.

The forging temperature range is 870 to 1150 °C (1600–2100 °F). Heavy work is best done between 1040 and 1150 °C (1900 and 2100 °F), and working below 870 °C (1600 °F) is not recommended. To produce finer grain in forgings, 1095 °C (2000 °F) should be used for the final reheat temperature, and at least 30% reduction of area should be taken in the last forging operation.

When forging has been completed or when it is necessary to allow alloy K-500 to cool before further hot working, it should not be allowed to cool in air, but should be quenched from a temperature of 790 °C (1450 °F) or higher. If the piece is allowed to cool slowly, it will age harden to some extent, and stress will be set up that may lead to thermal splitting or tearing during subsequent reheating. In addition, quenched material has better response to age hardening because more of the age-hardening constituent is retained in solution.

Alloy 600. The normal forging temperature range for alloy 600 is 870 to 1230 °C (1600–2250 °F). Heavy hot work should be done in the range from 1040 to 1230 °C (1900–2250 °F). Light working can be continued down to 870 °C (1600 °F). Generally, forging should not be done between 650 and 870 °C (1200 and 1600 °F) because of the low ductility of the alloy in this temperature range. Judicious working below 650 °C (1200 °F) will develop higher tensile properties.

The rate of cooling after forging is not critical with respect to thermal cracking. However, alloy 600 is subject to carbide precipitation in the range between 540 and 760 °C (1000 and 1400 °F), and if subsequent use dictates freedom from sensitization, the part should be rapidly cooled through this temperature range.

Alloy 625 should be heated in a furnace held at 1175 °C (2150 °F) but no higher. The work should be brought as close to this temperature as conditions permit. Forging is done from this temperature down to 1010 °C (1850 °F); below 1010 °C (1850 °F) the metal is stiff and hard to move and attempts to forge it may cause hammer splits at the colder areas. The work should be returned to the furnace and reheated to 1175 °C (2150 °F) whenever its temperature drops below 1010 °C (1850 °F). To guard against duplex grain structure, the work should be given uniform reductions. For open-die work, final reductions of a minimum of 20% are recommended.

Alloy 718 is strong and offers considerable resistance to deformation during forging. The forces required for hot deformation are somewhat higher than those employed for alloy X-750. Alloy 718 is forged in the range from 900 to 1120 °C (1650–2050 °F). In the last operation, the metal should be worked uniformly with a gradually decreasing temperature, finishing with some light reduction below 955 °C (1750 °F). Figure 2 shows a forged and machined alloy 718 marine propeller blade. In heating for forging, the material should be brought up to temperature, allowed to soak a short time to ensure uniformity, and withdrawn.

Alloy 718 should be given uniform reductions in order to avoid duplex grain structure. Final reductions of 20% minimum should be used for open-die work, and 10% minimum for closed-die work. Parts should generally be air cooled from the forging temperature, rather than water quenched.

Alloy 706 (UNS N09706) is similar to alloy 718, except that alloy 706 is more readily fabricated, particularly by machining. Forging should be done using the same procedures and temperatures as those for alloy 718.



Fig. 2 Forged and machined alloy 718 marine propeller blade. Courtesy of Ladish Company

Alloy X-750. The forging range for alloy X-750 is 980 to 1205 °C (1800–2200 °F). Below 980 °C (1800 °F), the metal is stiff and hard to move, and attempts to work it may cause splitting. All heavy forging should be done at about 1040 °C (1900 °F), and the metal should be reheated whenever it cools to below that temperature. Forgings can be finished with some light reduction in the range between 980 and 1040 °C (1800 and 1900 °F).

As a general rule, alloy X-750 should be air cooled rather than liquid quenched from the forging temperature. Liquid quenching can cause high residual stresses that may result in cracking during subsequent heating for further hot work or for heat treatment. Parts with large cross sections and pieces with variable cross sections are especially susceptible to thermal cracking during cooling. In very large cross sections, furnace cooling may be necessary to prevent thermal cracking.

Alloy 800. Hot working of alloy 800 is started at 1205 °C (2200 °F), and heavy forging is done at temperatures down to 1010 °C (1850 °F). Light working can be accomplished down to 870 °C (1600 °F). No working should be done between 870 and 650 °C (1600 and 1200 °F). As with alloy 600, thermal cracking is not a problem, and workpieces should be cooled rapidly through the range between 540 and 760 °C (1000 and 1400 °F) to ensure freedom from sensitization.

Alloy 825. The forging range for alloy 825 is 870 to 1175 °C (1600–2150 °F). It is imperative that some reduction be accomplished between 870 and 980 °C (1600 and 1800 °F) during final forging in order to ensure maximum corrosion resistance.

Cooling after forging should be done at a rate equal to or faster than air cooling. Heavy sections may become sensitized during cooling from the forging temperature and therefore be subject to intergranular corrosion in certain media. A stabilizing anneal of 1 h at 940 °C (1725 °F) restores corrosion resistance. If the forged piece is to be welded and used in an environment that could cause intergranular corrosion, the piece should be given a stabilizing anneal to prevent sensitization from the heat of welding, regardless of the cooling rate after forging.

Alloy 925. The hot-working characteristics of alloy 925 (UNS N09925) are similar to those of alloy 825 at temperatures to 1095 °C (2000 °F). At higher temperatures, alloy 925 has lower ductility and higher strength. The forging range is 870 to 1175 °C (1600–2150 °F). For maximum corrosion resistance and highest mechanical properties after direct aging, final hot working should be done in the range of 870 to 980 °C (1600–1800 °F).

Alloys 722 and 751 (UNS N07722 and N07751, respectively) are forged using the same procedures and temperatures as those for alloy X-750.

Alloys 903, 907, and 909 (UNS N19903, N19907, and N19909, respectively) are best forged in three stages in order to obtain the desired properties after aging. The initial breakdown of 40% minimum reduction should be performed at 1060 to 1120 °C (1940–2050 °F). For intermediate forging at a minimum of 25% reduction, these alloys should be heated between 995 and 1050 °C (1825 and 1925 °F). The final heating for alloys 907 and 909 should be 980 to 1025 °C (1800–1875 °F) for a minimum reduction of 20% over a falling temperature range (finishing at ≤925 °C, or 1700 °F). The final heating for alloy 903 should be 870 °C (1600 °F) with a final forging reduction of 40% minimum.

Thermal-Mechanical Processing (TMP)

Thermal-mechanical processing refers to the control of temperature and deformation during processing to enhance specific properties. Special TMP sequences have been developed for a number of nickel-base alloys.

The design of TMP sequences relies on a knowledge of the melting and precipitation temperatures for the alloy of interest. Table 2 lists these temperatures for several nickel-base alloys. Although nickel-base (as well as iron- and cobalt-base) alloys form various carbides—for example, MC (M = titanium, niobium, etc.), M_6C (M = molybdenum and/or tungsten), or $M_{23}C_6$ (M = chromium)—primary precipitate of concern in the processing of such materials is the γ'-strengthening precipitate. Gamma prime is an ordered face-centered cubic (fcc) compound in which aluminum and titanium combine with nickel to form $Ni_3(Al, Ti)$. In nickel-iron alloys such as alloy 718, titanium, niobium, and to a lesser extent, aluminum combine with nickel to form ordered fcc γ' or ordered body-centered tetragonal γ''. Nickel-iron base alloys are also prone to the formation of other phases, such as hexagonal close-packed Ni_3Ti (η), as in titanium-rich alloy 901, or orthorhombic Ni_3Nb (δ) in niobium-rich alloy 718.

Early forging practice of nickel- and nickel-iron base alloys consisted of forging from and solution heat treating at temperatures well in excess of the γ' solvus temperature. High-temperature solution treatment dissolved all of the γ', annealed the matrix, and promoted grain growth (typical grain size ≈ ASTM 3 or coarser). This was followed by one or more aging treatments that promoted controlled precipitation of γ' and carbide phases. Optimal creep and stress rupture properties above 760 °C (1400 °F) were thus achieved. Later in the development of forging practice, it was found that using preheat furnace temperatures slightly above the recrystallization temperature led to the development of finer grain sizes (ASTM 5 to 6). Coupling this with modified heat treating practices resulted in excellent combinations of tensile, fatigue, and creep properties.

State-of-the art forging practices for nickel-base alloys rely on the following microstructural effects (Ref 3):

- Dynamic recrystallization is the most important softening mechanism during hot working.
- Grain boundaries are preferred nucleation sites for recrystallization.
- The rate of recrystallization decreases with the temperature and/or the extent of deformation.
- Precipitation that may occur during the recrystallization can inhibit the softening process. Recrystallization cannot be completed until the precipitate coarsens to a relatively ineffective morphology.

Forging temperature is carefully controlled during TMP of nickel- and nickel-iron-base alloys to make use of the structure control effects of second phases such as γ'. Above the optimal forging temperature range (Table 3), the structure control phase goes into solution and loses its effect. Below this range, extensive fine precipitates are formed, and the alloy becomes too stiff to process. Several examples of specific TMP sequences are given in the following paragraphs.

Waspaloy. A typical TMP treatment of nickel-base alloys is that used for Waspaloy (UNS N07001) to obtain good tensile and creep properties. This consists of initial forging at 1120 °C (2050 °F) and finish forging below approximately 1010 °C (1850 °F) to produce a fine, equiaxed grain size of ASTM 5 to 6. Solution treatment is then done at 1010 °C (1850 °F), and aging is conducted at 845 °C (1550 °F) for 4 h, followed by air cooling plus 760 °C (1400 °F) for 16 h and then air cooling.

René 95. Initial forging of René 95 is done at a temperature between 1095 and 1140 °C (2000 and 2080 °F). Following an in-process recrystallization anneal at 1175 °C (2150 °F), finish forging (reduction ~40–50%) is then imposed below the γ' solvus, typically at temperatures between 1080 and 1105 °C (1975 and 2025 °F). The large grains formed during high-temperature recrystallization are elongated and

Table 2 Critical melting and precipitation temperatures for several nickel-base alloys

		First melting temperature		Precipitation temperature	
Alloy	UNS No.	°C	°F	°C	°F
Alloy X	N06002	1260	2300	760	1400
Alloy 718	N07718	1260	2300	845	1550
Waspaloy	N07001	1230	2250	980	1800
Alloy 901	N09901	1200	2200	980	1800
Alloy X-750	N07750	1290	2350	955	1750
M-252	N07252	1200	2200	1010	1850
Alloy R-235	…	1260	2300	1040	1900
René 41	N07041	1230	2250	1065	1950
U500	N07500	1230	2250	1095	2000
U700	…	1230	2250	1120	2050
Astroloy	N13017	1230	2250	1120	2050

Source: Ref 2

Table 3 Structure control phases and working temperature ranges for various heat-resistant alloys

Alloy	UNS No.	Phases for structure control	Working temperature range	
			°C	°F
Nickel-base alloys				
Waspaloy	N07001	γ' $Ni_3(Al,Ti)$	955–1025	1750–1875
Astroloy	N13017	γ' $Ni_3(Al,Ti)$	1010–1120	1850–2050
IN-100	…	γ' $Ni_3(Al,Ti)$	1040–1175	1900–2150
René 95	…	γ' $Ni_3(Al,Ti)$	1025–1135	1875–2075
Nickel-iron-base alloys				
901	N09901	η (Ni_3Ti)	940–995	1725–1825
718	N07718	δ (Ni_3Nb)	915–995	1675–1825
Pyromet CTX-1	…	η (Ni_3Ti), δ (Ni_3Nb), or both	855–915	1575–1675

Source: Ref 4

surrounded by small recrystallized grains that form during finish forging.

Alloy 901. The TMP of alloy 901 is often done to produce a fine-grain structure that enhances fatigue strength (Ref 5). This is accomplished by using the η (Ni_3Ti) phase, which is introduced in a Widmanstätten form at the beginning of processing by a heat treatment at 900 °C (1650 °F) for 8 h. Forging is then conducted at 955 °C (1750 °F), which is below the η solvus; the forging deformation is completed below the recrystallization temperature. A fine-grain structure is generated by a subsequent recrystallization treatment below the η solvus. The needlelike η phase will become spherical during forging and will restrict grain growth. Aging is then conducted according to standard procedures.

Isothermal Forging

Nickel-base alloys that are hard to work or are typically used in the cast condition can be readily forged when in a powder-consolidated form. The most common forging technique using powder preforms is isothermal forging. In this process, powder is produced by inert gas atomization and is compacted into billet form by extrusion. The billets are fabricated below the γ' solvus temperature for alloys such as IN-100 in order to maintain a fine grain size and a fine distribution of precipitates. In this condition, the material exhibits superplastic properties that are characterized by large tensile elongations (during sheet forming) and good die-filling capacity (during forging). Multiples of the extruded bar are then isothermally forged into a variety of complex turbine engine and other high-temperature parts.

The key to successful isothermal forging of nickel-base alloys is the ability to develop a fine grain size before forging and to maintain it during forging. With regard to the latter, a high volume percentage of second phase is useful in preventing grain growth. Therefore, alloys such as IN-100, René 95, and Astroloy, which contain large amounts of γ', are readily capable of developing the superplastic properties necessary in isothermal forging. In contrast, Waspaloy, which contains less than 25 vol% γ' at isothermal forging temperatures, is only marginally superplastic. Nickel-iron base alloys such as alloys 718 and 901 have even lower volume fractions of precipitate and are therefore even less frequently used in isothermal forging.

As the term implies, isothermal forging consists of forging with the workpiece and the dies at the same temperature. Because this temperature is often of the order of 980 to 1095 °C (1800–2000 °F), the dies are usually made of molybdenum for elevated-temperature strength. The isothermal forging system must be operated in a vacuum or inert atmosphere in order to protect such die materials from oxidation.

Compared to conventional forging, isothermal forging deformation rates are slow; hydraulic press speeds of approximately 2.5 mm/min (0.1 in./min) are typical. However, the slower production rate is largely offset by the ability to forge complex shapes to closer tolerances, which leads to less machining and substantial material savings. In addition, a large amount of deformation is accomplished in one operation, pressures are low, and uniform microstructures are achieved. For example, the as-forged weight of a finish-machined 68 kg (150 lb) Astroloy disk is about 110 kg (245 lb) for a conventional forging versus 72 kg (160 lb) for the corresponding isothermal forging.

ACKNOWLEDGMENT

This article was adapted from H.H. Ruble and S.L. Semiatin, Forging of Nickel-Base Alloys, *Forming and Forging*, Vol 14, *ASM Handbook*, ASM International, 1988, p 261–266.

REFERENCES

1. A.J. DeRidder and R. Koch, *MiCon 78: Optimization of Processing, Properties, and Service Performance Through Microstructural Control*, H. Abrams et al., Ed., ASTM, 1979, p 547
2. T. Altan, F.W. Boulger, J.R. Becker, N. Akgerman, and H.J. Henning, *Forging Equipment, Materials, and Practices*, MCIC-HB-03, Metals and Ceramics Information Center, 1973
3. T.G. Byrer, Ed., *Forging Handbook*, Forging Industry Association and American Society for Metals, 1985
4. D.R. Muzyka, *MiCon 78: Optimization of Processing, Properties, and Service Performance Through Microstructural Control*, H. Abrams et al., Ed., ASTM, 1979, p 526
5. L.A. Jackman, *Proc. Symposium on Properties of High Temperature Alloys*, The Electrochemical Society, 1976, p 42

ASM Specialty Handbook: Nickel, Cobalt, and Their Alloys
J.R. Davis, editor, p 203-229
DOI:10.1361/ncta2000p203

Copyright © 2000 ASM International®
All rights reserved.
www.asminternational.org

Powder Metallurgy Processing of Nickel Alloys

POWDER METALLURGY (P/M) PROCESSING of nickel and nickel alloys, as in other P/M systems, begins with the powder production process. Both vapormetallurgical and hydrometallurgical methods are used for producing pure nickel powders. The end use of the powder dictates the method used. Alloyed powders are produced by either atomization techniques or high-energy ball milling (mechanical alloying). Consolidation of powders into nickel-base or nickel-containing parts is accomplished by:

- Conventional P/M processing, that is, die compaction followed by sintering
- Roll compaction plus sintering
- Full density processing, for example, extrusion, hot isostatic pressing (HIP), isothermal forging, and/or combinations of these processes

Each of the powder processing and consolidation methods listed above is described in this article. In addition, a number of unique alloy (primarily superalloy) compositions with improved properties made possible by P/M processing is discussed.

Production of Nickel Powders

Nickel-base powders are produced by the decomposition of nickel carbonyl, by the reduction of aqueous solution of a nickel salt with hydrogen under pressure (the Sherritt process), by inert gas or water atomization, and by mechanical alloying. Of these, decomposition of nickel carbonyl and the Sherritt process, which produce metallic from its ore, are the most important commercially.

Carbonyl Vapormetallurgy

Historical Development. The production of nickel powders by the decomposition of nickel carbonyl dates back to a process developed in 1889 by Ludwig Mond and his coworker Carl Langer and Friedrich Quincke. According to Mond (Ref 1), the firm of Brunner, Mond, and Company was endeavoring to prepare chlorine from ammonium chloride, which in turn was obtained as a by-product of the ammonia-soda process, widely known as the Solvay process.

One of the obstacles to the successful production of chlorine was the unusually rapid corrosion of the nickel valves on the brick-lined tanks in which ammonium chloride was vaporized. Laboratory study of this corrosion proved that it resulted form the small amount of carbon monoxide used to sweep ammonia from the vaporizing tanks. Carbon monoxide was partially converted into carbon dioxide, and a black mixture of nickel and amorphous carbon was deposited. This observation led to a more elaborate study of the reaction of carbon monoxide with finely divided nickel.

Mond and coworkers found that four molecules of carbon monoxide at atmospheric pressure and at temperatures between 40 and 100 °C (105 and 212 °F) react with active nickel to form a colorless gas, nickel tetracarbonyl:

$$Ni + 4CO \xleftarrow{50\ ^\circ C} Ni(CO)_4$$

They further demonstrated that the reaction is readily reversible by heating the nickel tetracarbonyl to temperatures in the 150 to 300 °C (300 to 570 °F) range to yield pure nickel and carbon monoxide:

$$Ni(CO)_4 \xleftarrow{230\ ^\circ C} Ni + 4CO$$

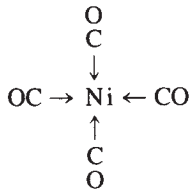
Nickel that has been in contact with air does not react with carbon monoxide, which is why carbonyls were not discovered earlier.

Encouraged by their success in preparing nickel tetracarbonyl, Mond and coworkers immediately attempted to prepare carbonyls from all the metals at their disposal. However, it was Berthelot who first announced the formation of a volatile compound of carbon monoxide and iron, iron pentacarbonyl, in June 1891. Subsequent discoveries were made of many metal carbonyls, including cobalt, iron, molybdenum, and ruthenium carbonyls.

After preliminary laboratory trials, Mond built an experimental plant near Birmingham, England, and subsequently developed the Mond-Langer process for separating nickel from Canadian matte. By 1895, the plant successfully produced 1½ tons of nickel weekly from Canadian matte containing 40% Ni. Mond subsequently opened a refinery in Clydach, Wales (Mond Nickel Company), and during the 27 years the refinery operated, the plant processed more than 82,000 metric tons (90,000 tons) of nickel in the form of pellets that exhibited greater purity than nickel produced by any other commercial process at that time.

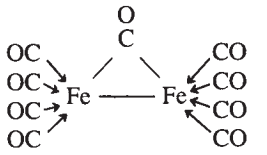
In this process, which in modified form is still used at the refinery in Clydach, nickel oxide produced from roasting nickel sulfide is reduced to nickel sponge by hydrogen, activated by sulfiding, and volatilized as carbonyl in an atmospheric reactor. Nickel carbonyl produced in this manner is decomposed directly in the powder and pellet units as part of a continuous process of refining.

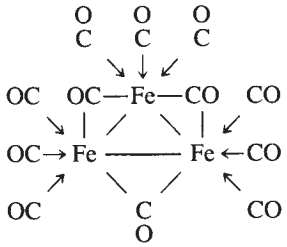
Metal Carbonyls. Many metals form carbonyls; in fact, all of the metals of the first, second, and third transition metal series have been converted into one or more types of carbonyls. Additionally, several of the lanthanides and actinides have formed carbonyls. Nickel forms a single carbonyl, $Ni(CO)_4$, in its zero valent form:



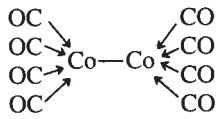
Nickel also forms a hydridocarbonyl, $H_2Ni_2(CO)_6$, where nickel has an oxidation number of –1. The carbon monoxide ligands in nickel carbonyl can be replaced by other ligands such as phosphines, phosphites, and certain unsaturated hydrocarbons where a high degree of electron density is capable of allowing "back bonding π," as well as the conventional σ bonding typical of donor ligands.

The iron penta compound, iron pentacarbonyl or $Fe(CO)_5$, rapidly condenses into the bimetallic species diiron nonacarbonyl $Fe_2(CO)_9$, which on heating further condenses into the trimetallic triiron dodecacarbonyl $Fe_3(CO)_{12}$. The nonacarbonyl compound exhibits two types of carbonyl bonding, the donor σ type and the bonding bridge type (π):

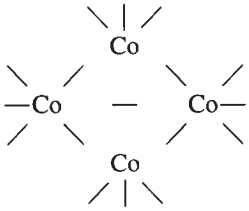




Chromium, molybdenum, and tungsten each form a single hexacarbonyl, a hexacoordinated octahedron. Cobalt forms a binuclear carbonyl, dicobalt octacarbonyl, $Co_2(CO)_8$:



which condenses to the tetranuclear species, containing bridged cobalt atoms:



The condensing continues with the formation of what is known as a cluster carbonyl:

$$Co_8(CO)_{18}C^{2-}$$

Several types of carbonyl clusters exist; one of the largest is the tetracapped pentagonal prism:

$$Rh_{15}(CO)_{28}C_2^-$$

Some metals have avoided becoming "pure" carbonyls to date, but halo derivatives of copper, gold, platinum, and palladium have been synthesized:

$$Cu(CO)Cl \quad Pt(CO)_2Cl_2$$

$$Au(CO)Cl \quad Pd_2(CO)_2Cl_4$$

Heterocarbonyls also have been produced, including:

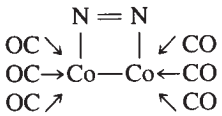
$$(CO)_5MnCo(CO)_4$$

$$[(CO)_5Re]_2Fe(CO)_4$$

$$Re_2Ru(CO)_{12}$$

$$Ru_2Os(CO)_{12}$$

Metal carbonyl carbides also exist, such as $Fe_5(CO)_{15}C$ and the dicarbide clusters $Ru_{10}C_2(CO)_{24}$, $Co_{13}C_2(CO)_{24}$, and $Rh_{15}C_2(CO)_{23}$. Another example of metal carbonyl is the dinitrogen derivative:



A complete list of all the metal carbonyls that can be formed is beyond the scope of this article. The previous examples are provided to illustrate the diversity of the chemical forms of metal carbonyls.

Metal Carbonyl Formation and Decomposition. While the equation for metal carbonyls is generally written as follows, the mechanism is far more complex than the equation implies:

$$xMe + yCO \leftrightarrow Me_x(CO)_y$$

At room temperature, carbonyls typically form liquids, vapors, and colored crystals. Carbonyls may be formed, volatilized, and condensed in a continuous process to separate them from the inert constituents of the feed. Some must be separated with elaborate techniques, while still others are intractable materials. They may be formed as liquids or as solutions in organic solvents and separated from inert solids by filtration. Crude carbonyls are separated from each other and residual impurities by distillation, sublimation, recrystallization, or selective solution of the carbonyl. Purified carbonyls are decomposed by heating into the carbon monoxide and pure metal. When a metal carbonyl can be separated from its impurities, subsequent decomposition generally results in high-purity metals. Exceptions to this include the formation of carbides.

Nickel tetracarbonyl was the first carbonyl discovered in the 1890s. Iron pentacarbonyl and cobalt octacarbonyl followed soon after; these remain the only carbonyls whose singular chemical properties have been applied commercially to extractive metallurgy, although it is speculated that ruthenium separation by carbonyl formation should ensue. In the formation of nickel tetracarbonyl, a mixture of freshly prepared nickel metal and nickel sulfide is heated in the presence of carbon monoxide.

Thermal decomposition reactions of commercial interest for cobalt, iron, and nickel carbonyls occur at temperatures of about 200 °C (390 °F), where carbonyls can be handled in vapor form. Under these conditions, reaction kinetics permit acceptable powder production rates to be maintained. Carbonyls are heated rapidly to the desired decomposition temperature; at this temperature, nuclei form in the vapor to provide the required sites for metal deposition.

Decomposition products are the pure metal and carbon monoxide. During decomposition in commercial decomposers, the disproportionation reaction of carbon monoxide is catalyzed by the freshly formed metals. Iron is much more active as a catalyst than either nickel or cobalt, and therefore carbon contents in nickel carbonyl-derived powder are related to the trace iron content:

$$2\,CO \xrightarrow[Fe]{} CO_2 + C$$

Nickel Tetracarbonyl. The versatility of the carbonyl extraction of nickel is characterized not only by selectivity in formation, but also by the relative ease of separation and decomposition to high-purity metal. Under the conditions employed for reaction at atmospheric pressure, carbonyl-forming impurities in crude nickel metal do not enter the gas phase. Thus, extraction of nickel by its volatilization from crude metal as carbonyl vapor is a highly selective process.

For a given condition of surface activity, the rate of gaseous or liquid carbonyl formation is determined by the temperature of the reaction and increases with increasing partial pressure of carbon monoxide. Whereas the rate of carbonyl formation increases with increasing temperature, the equilibrium mole fraction of carbonyl formed decreases sharply with increasing temperature. At a given total pressure, there is an optimal temperature at which metal carbonyl will form, as shown in Fig. 1.

Kinetic data for the nickel tetracarbonyl reaction can be correlated by means of a modified first-order rate equation. The ultimate degree of

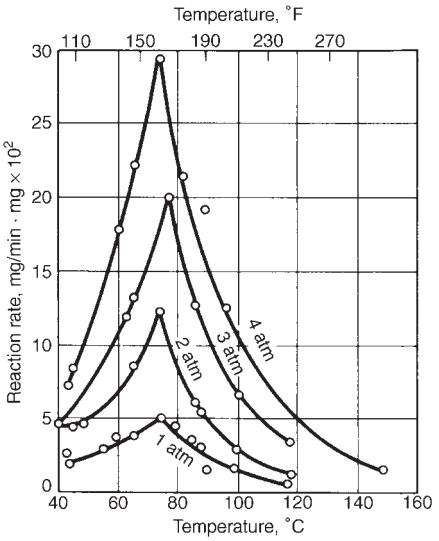


Fig. 1 Influence of system pressure and temperature on reaction rate in the formation of nickel tetracarbonyl. Source: Ref 2

metal conversion of "initial surface activity" has a definite value at a given temperature and pressure, which permits the derivation of a functional relationship between surface activity and metal conversion. Substituting this relationship and integrating the first-order rate equation yields a semiempirical model for correlating nickel tetracarbonyl formation rate data at a given temperature (Ref 3):

$$\ln \frac{a^o}{a^o - x} = K_o \left(P_{coi} - \sqrt[b]{\frac{P_{cai}}{K_e}} \right) t$$

where a^o is the initial activity of the surface, b is the number of moles of carbon monoxide per mole of carbonyl, K_o is the rate constant in grams per square centimeter per hour, K_e is the equilibrium constant, P_{cai} is the partial pressure of carbonyl at the interface in torr, P_{coi} is the partial pressure of carbon monoxide at the interface in torr, t is time in seconds, and x is the fraction of metal reacted.

From an engineering design viewpoint, conversion of nickel to a carbonyl at a fixed temperature depends primarily on the partial pressure of the carbon monoxide present. The effect of increased system pressure on the conversion of nickel to a carbonyl has been shown experimentally and demonstrated commercially. The volume change inherent in the carbonyl reaction—four carbon monoxide molecules combining in one molecule of nickel tetracarbonyl—also points to an increase in carbon monoxide pressure as a means of improving reaction kinetics. In addition to directly increasing the rate of reaction, increased pressure stabilizes the carbonyl, thus permitting reaction at higher temperatures for a further increase in rate. The nickel tetracarbonyl formation reaction is highly exothermic:

$$Ni + 4CO \rightarrow Ni(CO)_4$$
$$\Delta_f H^{298} = +160.4 \text{ kJ/g} \cdot \text{mol} \ (38.4 \text{ kcal/g} \cdot \text{mol})$$

Accordingly, high conversion-rate commercial nickel carbonylation processes require large heat removal systems.

At room temperature, nickel tetracarbonyl is a colorless volatile liquid with a high vapor pressure. It boils at about 43 °C (109.4 °F) and begins to decompose at 60 °C (140 °F) or less, depending on conditions. It is only slightly soluble in water, but is highly miscible with many organic solvents. Some physical properties of nickel tetracarbonyl include:

Chemical formula	$Ni(CO)_4$
Color and state	Colorless liquid
Molecular weight	170.75
Nickel, %	34.37
Melting point	–25 °C (–13 °F)
Boiling point	43 °C (109.4 °F) at 101.1 kPa (751 mm Hg) 42.1 °C (107.8 °F) at atmospheric pressure
Specific gravity	1.36153 at 0 °C (32 °F) 1.27132 at 36 °C (97 °F)
Heat of formation ($\Delta_f H^{298}$)	–602.5 kJ/g · mol (–144.0 kcal/g · mol)

Nickel tetracarbonyl vapor is exceedingly toxic when inhaled; 50 ppb of the compound in the air is the maximum allowable concentration designated by the American Conference of Governmental and Industrial Hygienists. Nickel tetracarbonyl should be handled only by personnel who are familiar with its toxic properties.

The stability of metal carbonyls varies considerably. Nickel tetracarbonyl begins to liberate carbon monoxide and nickel at 0 °C (32 °F) in a vacuum, and the decomposition becomes rapid above 60 °C (140 °F) in an inert gas under atmospheric pressure. Thermal decomposition is endothermic and is markedly inhibited by the presence of carbon monoxide. The mechanism of formation of nickel powder by the thermal decomposition of nickel tetracarbonyl is complex. In the formation of powder particles from the gaseous phase, several simultaneously occurring processes exert an influence. These include the formation of complex nuclei, secondary crystallization of nickel on the surfaces of the finest particles, the interaction of particles sin the crystallization process, and side reactions such as the decomposition of carbon monoxide. At a given temperature, the homogeneous part of the decomposition of nickel tetracarbonyl follows the rate equation (Ref 3):

$$r = \frac{K_o P_{ca}}{1 + K_g P_{co}}$$

where r is the decomposition rate in grams per cubic centimeter per hour, K_g is the adsorption constant of carbon monoxide on metal in $torr^{-1}$, K_o is the rate constant in grams per square centimeter per hour, P_{ca} is the partial pressure of carbonyl in torr, and P_{co} is the partial pressure of carbon monoxide in torr. The decomposition rate for nickel tetracarbonyl is directly proportional to the partial pressure of the carbonyl and inversely proportional to the partial pressure of the liberated carbon monoxide.

Conditions that influence the formation of the self-nucleating nickel particles during carbonyl decomposition (such as process temperature and the concentration and rate of the nickel tetracarbonyl supply to the decomposer) can vary greatly, which affects the physical and technical properties of the powders produced. Additions to the nickel tetracarbonyl gas stream sent to the decomposer can alter the mechanism by which the powder is formed, as well as its resulting morphology. For example, hydroquinone vaporized with the carbonyl acts as a free radical trap, resulting in the formation of macroparticles of nickel metal. Nickel tetracarbonyl can be photochemically decomposed to form elemental nickel by light of wavelengths shorter than 390 nm (3900 Å).

The most important industrial application of nickel tetracarbonyl is for refining nickel, in which nickel pellets and powder products are formed. Gas-plated products and a wide range of metallic and nonmetallic (nickel-coated graphite) powders can be produced by forming coatings of nickel on various surfaces by decomposing the carbonyl under special conditions. Nickel tetracarbonyl is manufactured on a limited basis to serve the chemical industry. The carbonyl serves as a catalyst for organic synthesis, as well as providing a means for the manufacture of other organonickel compounds. It also is used for vapor plating on smooth surfaces (such as plastic and metal) and to form nickel molds for the glass industry.

Commercial Processes. Currently, Inco Ltd. produces high-purity nickel powders by the thermal decomposition of nickel tetracarbonyl. Gaseous nickel tetracarbonyl is formed by reacting carbon monoxide with nickel concentrates under controlled conditions; subsequent thermal decomposition of the gas permits recovery of the nickel as a fine metallic powder and nickel pellets. The process, which affords a high degree of purity with respect to metallic elements other than nickel, produces nickel powders with extremely uniform particle size and structure.

The original Mond-Langer process has been greatly improved during its continued use. Commercial nickel refineries employing the carbonyl process to produce nickel powder are located on the site of the original Mond facility in Clydach, Wales, and in Copper Cliff, a subdivision of Sudbury, Ontario.

The Clydach refinery began nickel output from Sudbury cupriferrous nickel matte in 1902. Current plate feed matte is granular nickel oxide that contains small amounts of copper, cobalt, and iron, as well as siliceous matter. This refinery still uses the basic concept of the Mond-Langer process and produces nickel products using atmospheric pressure carbonyl processing. The latest innovations involve replacement of the many small heath-type reducers and volatilizers of the original works by large rotary kilns arranged in trains of two kilns with a smaller sulfiding unit. In the initial unit of each train, the nickel feed matte is reduced to metal by a countercurrent flow of preheated hydrogen. The reduced nickel matte is then activated by sulfiding and is volatilized as carbonyl in the final kiln by a countercurrent flow of carbon monoxide. The resulting nickel tetracarbonyl vapor is decomposed directly into pure nickel pellets and powders in reactors or decomposers.

The Copper Cliff Nickel Refinery began operations in 1973 with two newly developed techniques, including the use of top-blown rotary converters that take 64 metric ton (70 ton) charge of feed materials. The other manufacturing method uses the Inco pressure carbonyl process for the recovery of nickel from a variety of nickel-bearing feed materials, including the removal of nickel from copper, cobalt, and precious metal concentrates. The refinery produces pellets and powder of 99.9+% nickel purity and a codecomposed iron-nickel powder.

Environmental controls at the plant include a totally enclosed process that constantly recycles all process reagents. The Copper Cliff refinery uses the same basic process chemistries,

but forms nickel tetracarbonyl at high pressure, which is necessary to extract nickel in the presence of high copper concentrations.

The plant feed is a mixture of oxides and sulfides of nickel, copper, iron, and cobalt, other crude metallics, and partially processed precious metals and refinery residues that contain nickel. This mixture is charged along with coke into one of two 64 metric ton (70 ton) capacity, top-blown rotary converters, where it is melted and partly blown to slag silicates and some of the iron. The converter-treated hot material is subsequently granulated by pouring it through high-velocity water jets. At this point, the granules contain 65 to 75% Ni, 15 to 20% Cu, 2 to 3% Fe, and 3% S present as sulfides.

The metallic granules are batch-reacted with carbon monoxide at temperatures up to 180 °C (360 °F) and pressure up to 70 atm (1030 psi) in one of three 136 metric ton (150 ton) capacity rotating reactors. Nickel, and some iron, is extracted as a crude carbonyl vapor, while copper, cobalt, previous metals, and impurities are retained in the residue. Removal of iron is controlled to between 20 and 50% of the input iron level. Iron concentration in the granules rarely exceeds 4%. Cobalt in the feed does not form $Co_2(CO)_8$ or $Co_3(CO)_{12}$, because these compounds occur only when carbon monoxide pressures of 150 atm (2205 psi) are achieved.

Formation of nickel tetracarbonyl is quite exothermic; consequently, the reactors are water cooled. Extracted carbonyl vapor is liquefied and stored at atmospheric pressure. The carbon monoxide carrier gas also is recycled. The liquefied product stream, containing mutually soluble nickel and iron carbonyls, subsequently is pumped to distillation columns, where it is separated into nickel tetracarbonyl vapor and an iron-rich liquid carbonyl. Fractionating the crude carbonyl liquid is achieved easily, because the boiling points of the nickel and iron carbonyls are 43 °C (109.4 °F) and 102.8 °C (217 °F), respectively. The system produces nickel tetracarbonyl vapor of 99.998% purity, with the bottom liquor having nickel-to-iron ratios of up to 3 to 7. At the top of the column, nickel tetracarbonyl vapor is siphoned off and fed directly into powder decomposers. Somewhat below the top of the column, liquid nickel tetracarbonyl is taken off and either held in storage or used to feed the nickel pellet decomposers.

The powder decomposers are steel cylinders, the walls of which are heated with high-capacity electrical resistance heaters. Nickel carbonyl vapor is introduced into the top of the decomposer chamber slightly above atmospheric pressure, where it contacts the heated decomposer walls that are preset at a temperature between 250 and 350 °C (480 and 660 °F). The thermal shock decomposes nickel tetracarbonyl into nickel powder, with the release of carbon monoxide. The latter is recycled through filters to the main gas compressor to be recycled to the pressure carbonyl reactors, while the powder is collected, gas purged, stabilized with an oxide coating, and transferred to storage completely free from carbonyl and carbon monoxide.

The dangerous nature of the gaseous and liquid carbonyl compounds formed in the Inco processes is fully countered by established, effective, and practical safety measures. All product discharge systems are purged completely prior to powder and pellet packaging.

Powder Properties and Applications. Currently, there are four types of nickel powders produced by thermally decomposing nickel tetracarbonyl—single spikey particles, filaments, high-surface-area powders, and high-density semismooth particles. These powders exhibit uniform size and structure and high surface areas, and the method of production affords a high degree of purity with respect to other metallic elements.

Spikey particles are a general-purpose type of nickel powder (Inco type 123). They are fine and regular in shape, with rough surface projections (Fig. 2). The powder typically contains 700 to 900 mL/m^3 (700–900 ppm) oxygen, 3 to 5 mL/m^3 (3–5 ppm) iron, 1 mL/m^3 (1 ppm) sulfur or less, and 600 to 700 mL/m^3 (600–700 ppm) of graphitic carbon. The Fisher subsieve size is 3 to 7 μm, and apparent density is 1.8 to 2.7 g/cm^3. Surface area is on the order of 0.4 m^2/g as determined by the Brunauer-Emmett-Teller (BET) method.

Filimentary nickel powders (Inco types 255, 287, etc.) are characterized by their unique, spikey, chainlike structure of relatively fine particles, which makes them fluffy in nature, with low apparent density (0.5–1.0 g/cm^3) and large specific surface area (0.6–0.7 m^2/g). The structure and asymmetrical filament shape of this powder type are illustrated in Fig. 3.

Extra fine nickel powders (e.g., Inco type 210) also have filamental morphology, but the filaments are finer and specific areas range from 1.5 to 6 m^2/g depending on the grade.

Semismooth high-density nickel powders are available in fine and coarse sizes. The fine is 10 to 20 μm in diameter (Fig. 4); the coarse is –16+40 mesh. Powder apparent density ranges from 3.5 to 4.2 g/cm^3.

The properties of these high-purity nickel powders have been tailored to meet the demanding requirements of the chemical, energy, and metal industries. Currently, these products provide the basic nickel source for a wide range of specialized products. Application areas for these powders include:

- Batteries and fuel-cell electrodes
- P/M structural parts
- P/M porous parts, for example, filter systems (Fig. 5) and flow-control devices
- Ferrites
- Carbide cutting tools
- Catalysts
- Welding products
- Pigments and coatings
- Chemicals
- Electronic alloys
- Getters
- Conductive resins and plastics
- Electromagnetic shielding

Production of Nickel Powder by Hydrometallurgical Processing

The production of nickel powders by hydrometallurgical processing incorporates leaching, solution purification, and metal recovery operations. The Sherritt (Corefco) refinery in Fort Saskatchewan, Alberta, Canada, provides an example of hydrometallurgical processing used in the production of nickel powder. This refinery commenced operations in 1954, at which time the feedstock for the plant was nickel concentrate from Sherritt's Lynn Lake mining operations in Manitoba. The Sherritt refinery was the first successful commercialization of a hydrometallurgical process for the treatment of a nickel sulfide concentrate. The refinery has

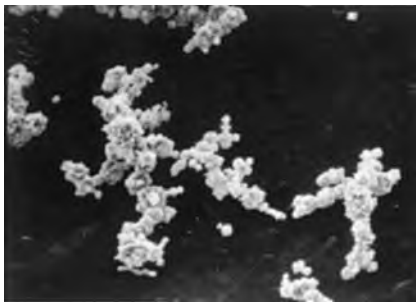


Fig. 3 Scanning electron micrograph of the filamentary-type nickel powder produced by carbonyl decomposition. 1000×

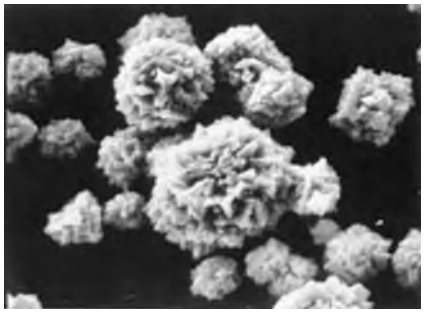


Fig. 2 Scanning electron micrograph of general-purpose nickel powder produced by carbonyl decomposition. 3000×

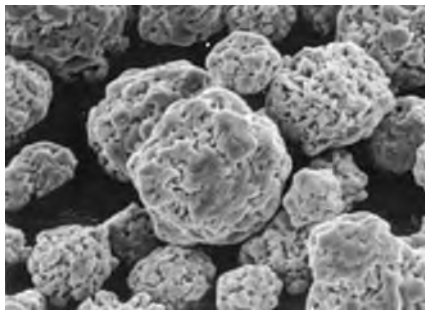


Fig. 4 Scanning electron micrograph of high-density (fine) nickel powder produced by carbonyl decomposition. 1000×

undergone process and equipment modifications in recent years to increase its capacity and enable the acceptance and treatment of different feedstocks. At present, the primary feed to the refinery is a high-grade nickel cobalt sulfide from Moa, Cuba.

A flow diagram of the Sherritt process is shown in Fig. 6. The Sherritt process is adaptable to handle a wide variety of different feedstocks. It has been adopted by Western Mining Corporation in a refinery at Kwinana, Western Australia. Further information regarding the Sherritt process is containing in Ref 4 to 8.

Feed to Process. At present, the principal feed to the Sherritt refinery is a nickel and cobalt sulfide produced in Moa, Cuba. The Moa Bay lateritic deposits contain ore that is high in iron and also relatively rich in cobalt. The processing of this ore is accomplished through pressure leaching with sulfuric acid. The key step in this process is the separation of nickel and cobalt from iron. Iron, which typically constitutes 50% of the ore, is separated by precipitation at high temperature and pressure in an acid leaching step. It is possible to achieve the selective dissolution of nickel and cobalt with less than 1 g/L iron in the leach liquor. The leach liquor is neutralized using limestone mud, and the metal values in the leach liquor are then precipitated with hydrogen sulfide. The chemical analysis of the cobalt-nickel sulfide produced at Moa is given in Table 1. This material is packaged, as a wet filter cake, in bulk bags and transported to the refinery in Fort Saskatchewan. A schematic flowsheet for the Moa Bay process is shown in Fig. 7.

Leaching. At Fort Saskatchewan, the first stage in the refining process is the leaching of the metal values from the sulfide feeds into solution. The fine sulfide concentrate feed materials are blended with an ammonium sulfate leaching liquor in a repulp tank and are then fed into the leach autoclaves. In the leaching process, air, ammonia, and the sulfidic minerals react in a series of interrelated steps. The leaching process is carried out at elevated temperature and pressure in a continuous process. The typical conditions in the leach autoclaves are given in Table 2.

Table 1 Chemical composition of Moa sulfides

Component	Analysis, wt%
Nickel	51–56
Cobalt	5.0–6.0
Iron	0.5–0.8
Copper	0.1–0.2
Sulfur	32–37
Zinc	1.0–1.3

Table 2 Leaching conditions for the Sherritt process

Parameter	Value
Temperature, °C (°F)	90–95 (195–205)
Pressure, psig	110–120
Ammonia, g/L	80–110
Ammonium sulfate, g/L	150–200

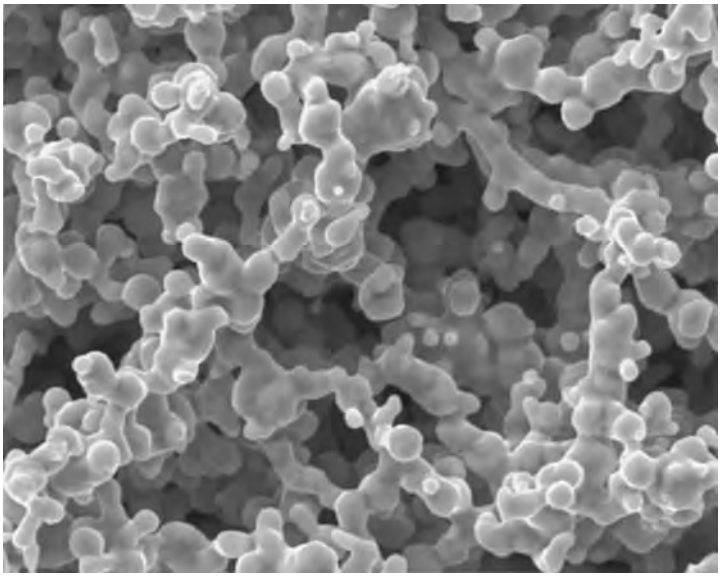


Fig. 5 Carbonyl nickel powder particles with a size range of 2 to 4 μm that are compacted and sintered to 35% dense in order to yield a 0.1 μm filter grade cup. Note that the particles are attached in a filamentary chain-type structure. 2000×

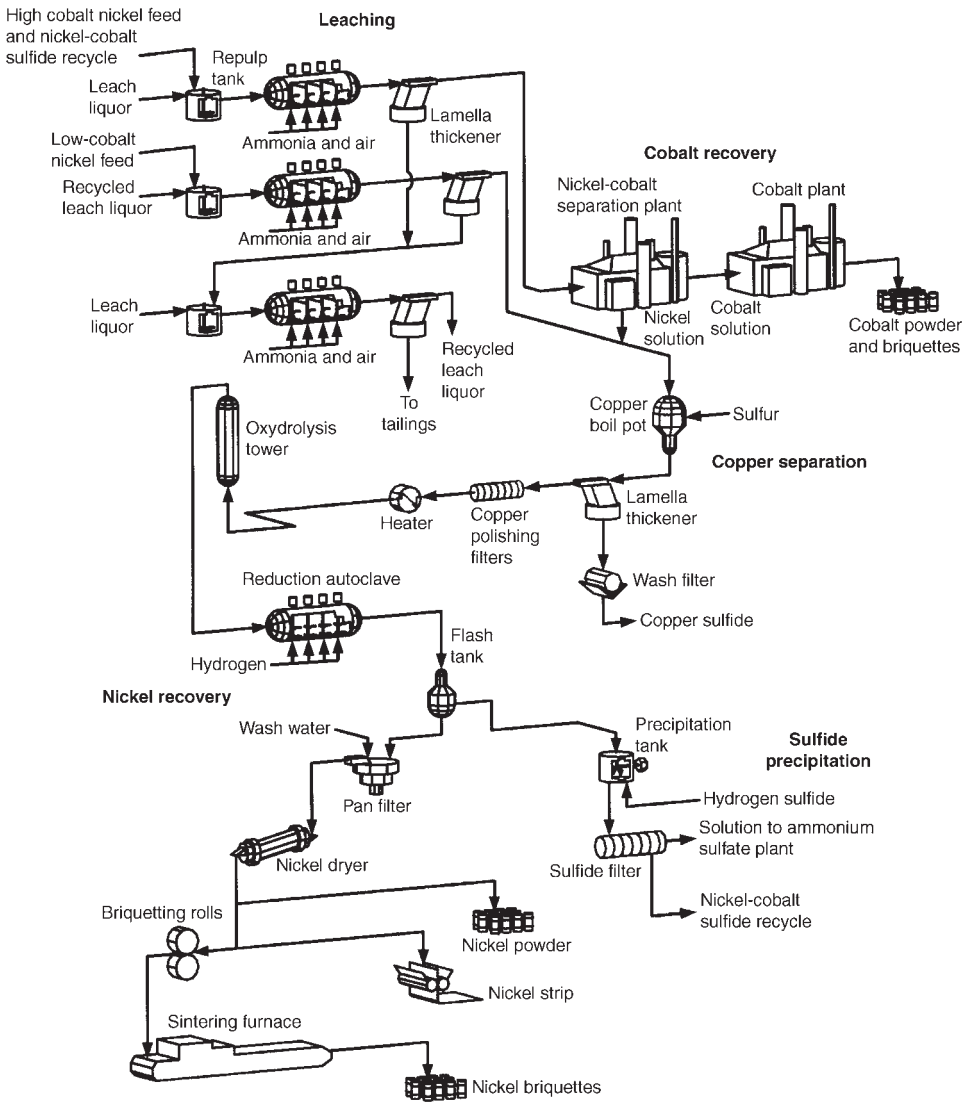


Fig. 6 Flowsheet of the Sherritt ammonia pressure leach process

The net leach reaction is the oxidative dissolution of the metal sulfides to soluble ammine complexes with the simultaneous oxidation of sulfide sulfur (S^{2-}) to form a series of soluble thiosalts including sulfate (SO_4^{2-}). The general equation for the ammoniacal leaching of sulfides may be represented as:

$$MS + n NH_3 + 2O_2 \longrightarrow M(NH_3)_n^{2+} + SO_4^{2-}$$

where M = nickel, cobalt, iron, copper, zinc, and n = 2 to 6.

The leaching process takes advantage of the differing stability of the ammine complexes. The iron ammine complex is the least stable and is completely hydrolyzed to a hydrated iron oxide, $Fe_2O_3 \cdot H_2O$ (hematite), which is reprecipitated. The leach slurry passes to a lamella thickener where the leach liquor is separated from the solid residue.

In fact, the actual reaction chemistry of the leaching process is much more complex due to the behavior of sulfur in alkaline solutions. The reactions sequence of the oxidation of sulfur to form sulfate, sulfamate, and a range of ammonium thiosalts may be represented as follows:

$$S^{2-} \rightarrow S_2O_3^{2-} \rightarrow S_nO_6^{2-} \rightarrow SO_4^{2-} + SO_3NH_2^-$$

where n = 2 to 6. At any given time, the leach liquor will contain sulfur in several forms. The amounts of these species present depend on the leach conditions and duration (Fig. 8). The leach solution typically contains 60 to 70 g/L Ni, 6 to 9 g/L Co, 1 to 2 g/L Cu, 130 g/L NH_3, 200 g/L $(NH_4)_2SO_4$, and varying amounts of other sulfur oxyanions.

Before it is possible to reduce the nickel from the leach solution as the pure metal, several solution purification steps must be completed.

Cobalt Separation. The leach liquor is transferred to the nickel-cobalt separation plant. There cobalt is separated from the nickel as pure crystalline cobaltic hexammine salt. After the removal of cobalt, the nickel-rich, or "pregnant," solution proceeds through the copper-removal circuit.

Copper Removal. Copper is removed from the leach liquors and pregnant solution from cobalt separation in a unit operation referred to as the "copper boil." In the copper boil, the combination of lowering the ammonia level by boiling to distill off the free ammonia and the addition of elemental sulfur and sulfur dioxide at elevated temperature results in the precipitation of copper sulfide. The copper sulfide is a mixture of cupric sulfide (CuS) and cuprous sulfide (Cu_2S) and is prepared by the reaction of soluble copper with thiosulfate ($S_2O_3^{2-}$):

$$Cu^{2+} + S_2O_3^{2-} + H_2O \rightarrow CuS + SO_4^{2-} + 2H^+$$

$$2Cu^{+} + S_2O_3^{2-} + H_2O \rightarrow Cu_2S + SO_4^{2-} + 2H^+$$

The selectivity for copper is achieved by the fact that copper sulfide is less soluble than nickel sulfide. This copper sulfide by-product is filtered, washed, and then sold to a copper smelter.

Oxidation and Hydrolysis. The solution remaining after copper removal contains appreciable amounts of sulfamate ($SO_3NH_2^-$) and other forms of unsaturated sulfur. The removal of all unsaturated sulfur compounds is necessary before the nickel can be recovered. If these sulfur compounds are not fully converted to sulfate, the nickel powder product would contain unacceptably high levels of sulfur. These are removed by hydrolizing the sulfamate to sulfate at 245 °C (473 °F) and oxidizing the thionates to sulfate with air at 4800 kPa (700 psi) in one combined step referred to as "oxydrolysis." The major reactions taking place in oxydrolysis are:

$$(NH_4)_2S_2O_3 + 2O_2 + H_2O + 2NH_3 \rightarrow 2(NH_4)_2SO_4$$
$$(NH_4)_2S_3O_6 + 2O_2 + 2H_2O + 4NH_3 \rightarrow 3(NH_4)_2SO_4$$
$$(NH_4)SO_3(NH_2) + H_2O \rightarrow (NH_4)_2SO_4$$

Ammonium sulfamate is a herbicide and must be hydrolyzed to sulfate to avoid contamination of the ammonium sulfate fertilizer. Ammonium sulfate is crystallized from the reduction end solution, following sulfide precipitation of the minor amounts of metal remaining in solution after hydrogen reduction.

Metal Recovery. In the final step of the Sherritt process, nickel is precipitated from solution as a metal powder through a process referred to as hydrogen reduction. The objective of the hydrogen reduction process is to precipitate the nickel ions present in the purified solution to nickel powder using hydrogen gas as a reductant. The reduction of metals from solution by hydrogen requires that the hydrogen potential of the system should exceed the electrode potential of the metal ions, in which case hydrogen will go into solution and the metal precipitates. The hydrogen potential is governed by the pH of the solution and by the partial pressure of hydrogen applied as shown in Fig. 9. The electrode potential of the metal ions is, however, little affected by concentration.

The reduction process is carried out in mechanically agitated horizontal autoclaves at elevated temperatures and pressures. This is a batch process consisting of two distinct stages, initial nucleation and subsequent densifications. In the initial nucleation stage. Fine nickel seed powder is formed in the autoclave. The densification refers to the process whereby nickel from solution is reduced onto the seed powder, which then grows in size. The reduction process, where 1 mole of hydrogen reduces 1 mole of nickelous ions to metallic nickel and yields 2 moles of ammonium ions as by-product, can be written:

$$Ni^{2+} + 2NH_3 + H_2 \rightarrow Ni^{o} + 2NH_4^+$$

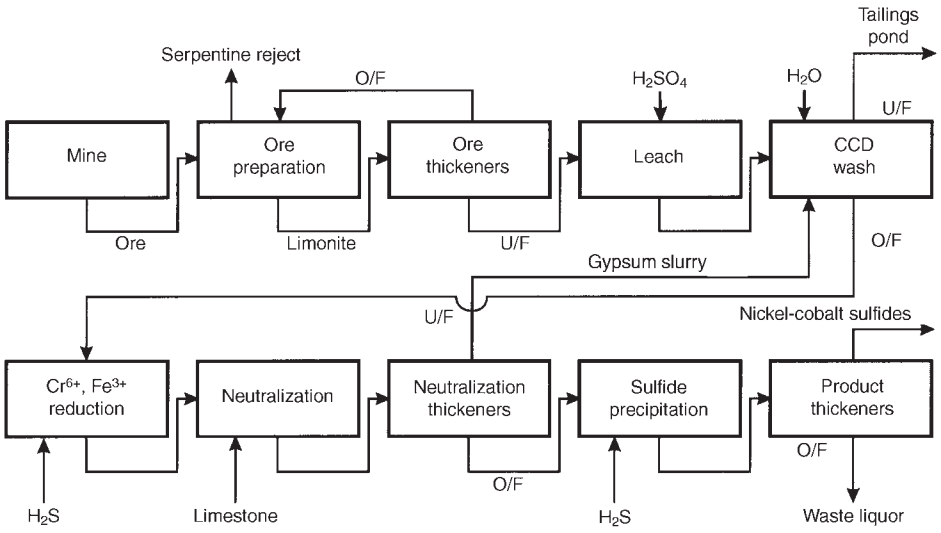


Fig. 7 Flowsheet for the Moa Bay hydrometallurgical process. O/F, thickener overflow; U/F, thickener underflow; CCD, counter-current decantation

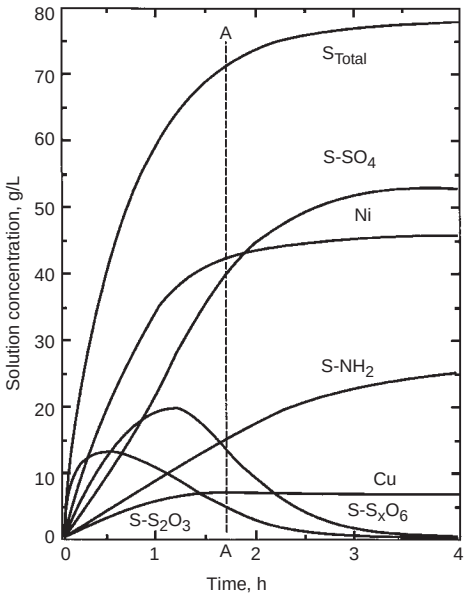


Fig. 8 A representation of the Sherritt process leach solution composition as determined in batch leaching tests

The presence of free ammonia is necessary to neutralize the hydrogen ions produced during reduction. At low pH and lower hydrogen potentials the reduction of the metal ions effectively ceases. During the reduction process, the slurry in the autoclave is agitated by impellers; however, once reduction is complete the agitation is stopped and the nickel powder is allowed to settle. The spent solution (or reduction end solution) is then pumped out and the autoclave is filled with fresh nickel solution; the agitators are restarted and hydrogen pressure is applied. This batch reduction process is repeated 50 to 60 times to build up consecutive coatings of nickel on the powder particles. The overall process is stopped when the powder has reached the desired size. During the final discharge, the agitators are kept running and the entire contents of the autoclave are pumped to the flash tank.

In addition to nickel, the feed solution to reduction also contains significant quantities of cobalt and zinc. Zinc does not present a problem with respect to contamination of the product powder because zinc will not be reduced to the metallic state under the conditions employed. Cobalt on the other hand has a similar standard reduction potential to that of nickel (–0.267 V for cobalt compared to –0.241 V for nickel). In order to effect the preferential reduction of nickel, the ammonia concentration is adjusted in the nickel reduction feed solution to give a NH_3-to-total metals molar ratio of 1.9 to 1.

In practice, the reduction feed solution contains 65 g/L Ni, 2.5 g/L Co, and 2 g/L Zn. The reduction of nickel ions to metal occurs rapidly only as a heterogeneous reaction, in which nickel is precipitated onto an existing surface. Figure 10 shows the change of particle size and apparent density with the number of reduction cycles or densifications. Figure 11 shows a scanning electron micrograph of a Sherritt-produced nickel powder. The analysis of Sherritt's standard grade nickel powder is given in Table 3.

The additional of various organic additives to the densification reductions can also be used to provide the means of controlling the size, shape, and surface morphology of the powder produced.

The slurry of powder and reduction end solution is discharged from the autoclave and collected in flash tanks. The solution is allowed to overflow into a holding tank and is then pumped to sulfide precipitation. The nickel powder is then drawn off from the flash tank cone as a 90% solids slurry and is filtered and washed on a rotary pan filter. From the pan filter the wet powder (typically 5% moisture) is fed by a screw feeder into a gas-fired rotary dryer.

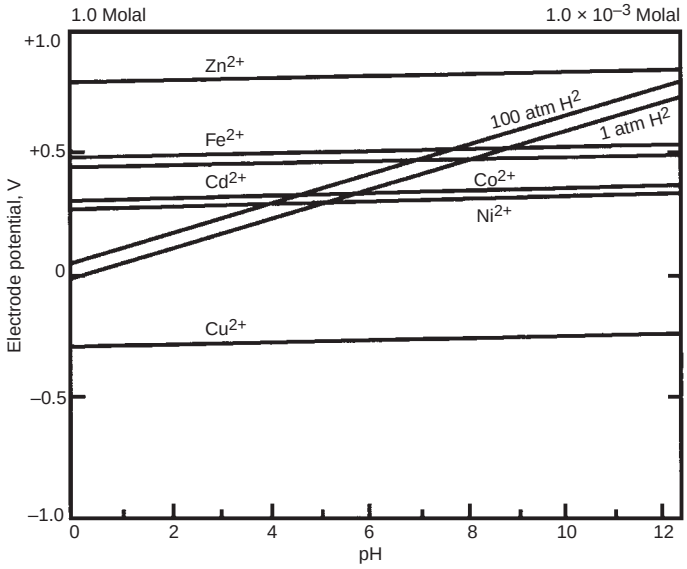


Fig. 9 Hydrogen and metal electrode potentials in solution (Sherritt process)

Table 3 Typical properties of Sherritt's standard grade nickel powder

Chemical composition, %	
Nickel	99.9
Cobalt	0.08
Copper	0.003
Iron	0.010
Sulfur	0.025
Carbon	0.006
Mesh screen size, %	
+100	0–10
–100+150	5–30
–150+200	20–45
–200+250	10–25
–250+325	10–35
–325	5–25
Apparent density, g/cm^3	3.5–4.5

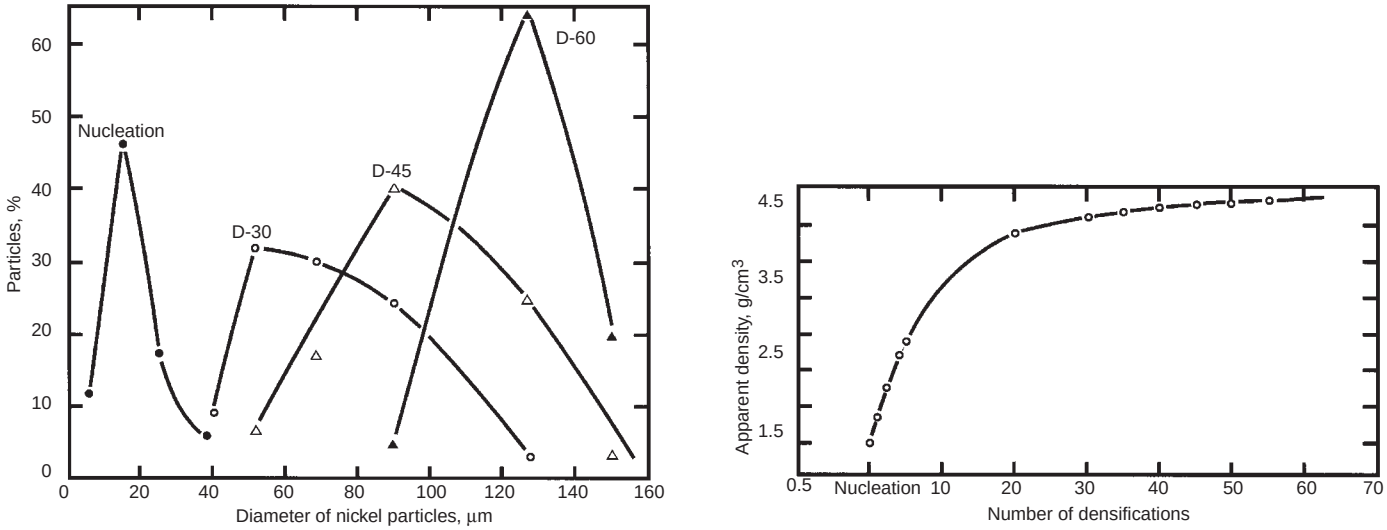


Fig. 10 Physical characteristics of nickel powder produced in a commercial hydrometallurgical operation

The dried-and-cooled nickel powder is either packaged as a powder product, or it can be directed to the briquetting operation. For briquetting, the nickel powder is first blended with an organic binder in a pug mill and is then compressed using a roll-briquette device. The briquettes are fed through a sintering furnace to effect carbon and sulfur removal and, through sintering at high temperature, impart structural integrity to the briquettes. The removal of carbon from the briquettes relied on the oxidation of carbon and its release as either CO or CO_2. In contrast to this, the mechanism for sulfur removal depends on the maintenance of reductive conditions through hydrogen injection, with the release of H_2S. The sintering furnace therefore consists of three distinct zones: the oxidizing "preheat zone" for carbon removal, the reducing "hot zone" for sulfur removal, and finally a "cooling zone." After exiting the furnace, the briquettes are packaged as the finished product (Fig. 12).

Sulfide Precipitation. The liquor from hydrogen reduction contains residual nickel, cobalt, and zinc. These metal ions are precipitated using hydrogen sulfide and recovered as sulfide precipitates. The general precipitation reaction is:

$$M^{2+}(aq) + H_2S \rightarrow MS(s) + 2H^+(aq)$$

where M = nickel, cobalt, zinc. Metals can be selectively removed from solution by controlling pH of the sulfide precipitation reaction. The pH is controlled by the addition of ammonia to neutralize the acid generated in the precipitation reaction:

$$NH_3 + H^+ \rightarrow NH_4^+$$

The nickel and cobalt sulfides are then returned to the leach, the zinc sulfide (which is precipitated independently of nickel and cobalt sulfide) is sold as a by-product, and the barren liquor (metal-free ammonium sulfate solution) proceeds to ammonium sulfate recovery.

Ammonium Sulfate Recovery. The solution obtained after removal of the metal values as metal sulfides contains only ammonium sulfate. This solution, referred to as "barren solution," is then evaporated and ammonium sulfate, which is formed as an overall refinery by-product, is recovered in a crystalline form. The ammonium sulfate recovery consists of crystallization followed by centrifuging, drying, and screening. The crystalline ammonium sulfate is then sold as a fertilizer.

Applications. Most hydrometallurgically produced nickel powder is compacted into briquettes or rondelles for consumption as an alloying additive in the steel industry. Smaller amounts of powder are roll compacted into nickel strip or dissolved to produce various nickel salts.

Atomization

Atomization is simply the breakup of a liquid into fine droplets. Any material available in liquid form can be atomized. In the case of high melting materials, the result is frozen droplets, that is, powder. Typically, the size of atomized powders is smaller than 150 μm, although larger-sized powders can be produced (in which case atomization is referred to as "shotting" or "granulation").

The general types of atomization processes encompass a number of industrial and research methods. Industrial methods include:

- Two-fluid atomization, where a liquid metal is broken up into droplets by impingement with water, oil, or an inert gas (Fig. 13a and b)
- Centrifugal atomization, where a liquid stream is dispersed into droplets by the centrifugal force of a rotating disk, cup, or electrode (Fig. 13c)
- Vacuum or soluble gas atomization, where a molten metal is supersaturated with a gas that causes atomization of the metal in a vacuum (Fig. 13d)
- Ultrasonic atomization, where a liquid metal film is agitated by ultrasonic vibration (Fig. 13e)

Application to Nickel Alloy Powders. Of these methods, only oil atomization and ultrasonic atomization are not used to produce nickel alloy powders. Inert gas atomization, centrifugal atomization, and vacuum atomization are used to produce prealloyed superalloy powders. Each of these methods is described in greater detail in the section "Conventional P/M Superalloy Processing" in this article. Both water and gas atomization are used to produce nickel-base hardfacing alloys, including the weld overlays and the thermal spray coatings described in the article "Nickel Coatings" in this Handbook. Nickel alloy powders used to fabricate porous P/M parts are also produced by water and gas atomization. Examples include Hastelloy C-22, Inconel 600, Monel 400, and Hastelloy X alloys used in filtration and fluid flow control applications where improved corrosion resistance, temperature resistance, and/or strength is required.

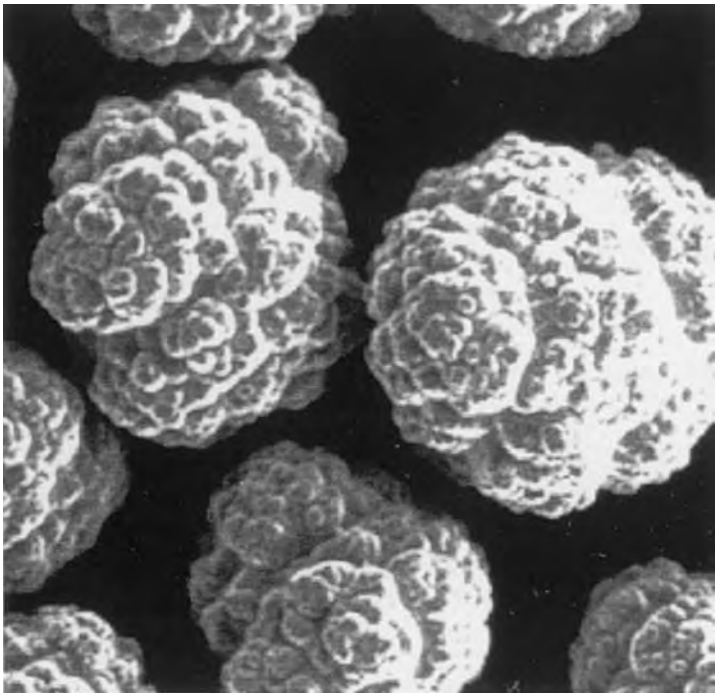


Fig. 11 Scanning electron micrograph (1000×) of nickel powder produced by the Sherritt process



Fig. 12 Nickel briquettes (each briquette is ~38 by 25 by 18 mm, or 1.5 by 1.0 by 0.7 in.) produced by the Sherritt process

Water-atomized nickel powder are also roll compacted into strip. Following sintering, the strip is hot and/or cold worked to full density and to the desired thickness of the final product.

Mechanical Alloying

Mechanical alloying is a dry, high-energy ball-milling operation that can be used to produce composite metal alloy powders with a uniform dispersion of refractory metal oxide particles in a complex metal matrix. The process occurs by repeated welding, fracturing, and rewelding of powder metal particles. The resulting mechanically alloyed powder is subsequently consolidated and then thermomechanically treated to optimize grain structure and properties. A more detailed account of the mechanical alloying process can be found in the section "Specialized P/M Superalloy Processes" in this article.

Sintering of Nickel and Nickel Alloys

Sintered nickel-base materials enjoy wide commercial usage due to their unique properties, such as corrosion resistance, wear resistance, mechanical strength at low and elevated temperatures, thermal expansion, electrical conductivity, and magnetic permeability. Commercial products represent a wide range of shapes, sizes, and microstructures. Sintered products with ≤90% porosity are technologically as important as fully dense products. Sintering practices aimed at achieving such diverse properties represent a variety of manufacturing technologies.

Depending on the end product, sintering operations can be performed on a loose power bed, a thin layer applied to a substrate, a lightly compacted coating, a roll-compacted strip, or die-compacted preforms. Sintering temperatures range from those at which the material is completely solid to those at which ≤60% of the material is in the liquid state.

Conventional sintering practices generally are useful, although more recent techniques such as HIP are required in specialized applications. Sintering atmospheres are generally reducing; in some applications, however, nonreactive environments such as vacuum or an inert gas are required. Physical and chemical characteristics of the starting powders, such as moisture content, degree of oxidation, segregation, morphology, and purity, are equally as important as the green compact microstructure prior to sintering.

Sintered porous nickel products of commercial interest include electrodes of alkaline nickel-cadmium, nickel-zinc, and nickel-iron rechargeable batteries, electrodes of alkaline

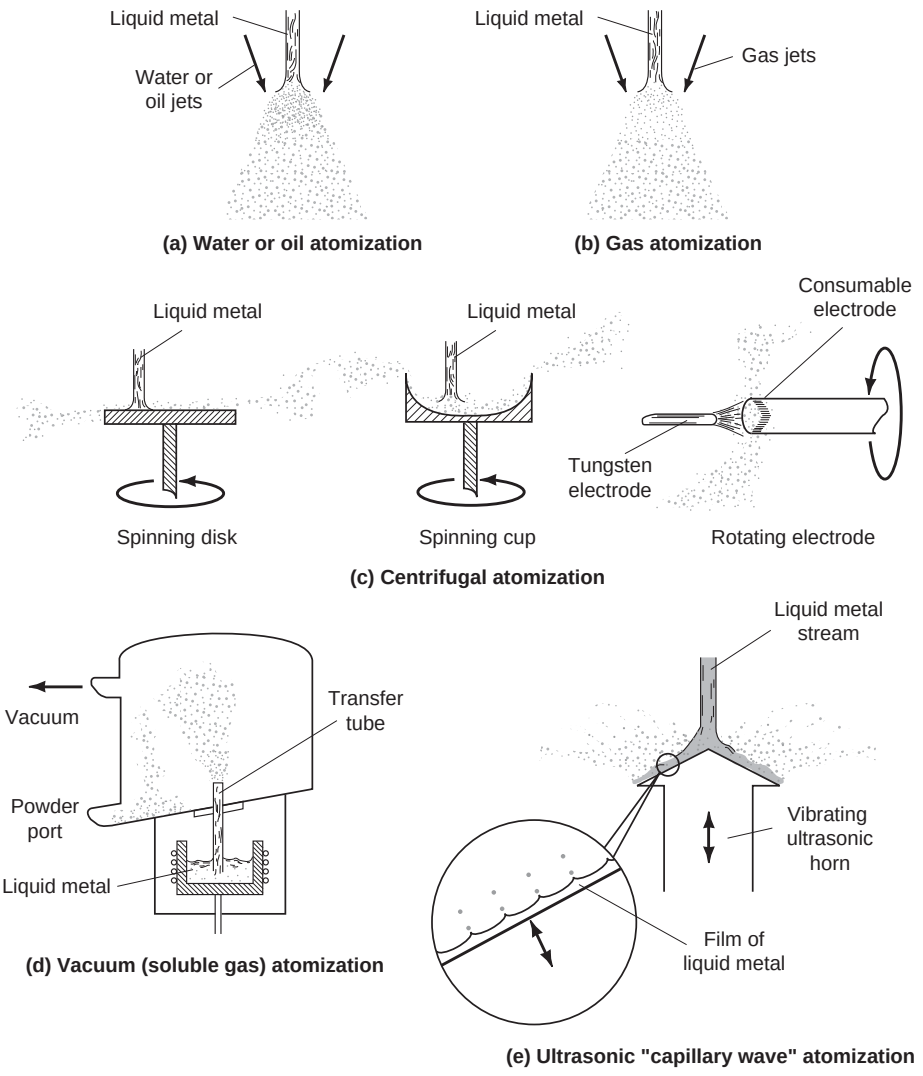


Fig. 13 Schematic of industrial atomization processes

Table 4 Functional, service, and structural requirements for sintered porous nickel products

Product	Function	Service conditions of service requirements	Structural requirements
Electrodes of alkaline nickel-cadmium, nickel-zinc, and nickel-iron rechargeable batteries	Hold active mass (nickel hydroxide or cadmium hydroxide) of the battery	Pores in the electrodes are impregnated with the active mass before battery assembly. Electrodes are in contact with a highly caustic solution of potassium hydroxide. Contraction and expansion of the active mass during discharge and charge cycles leads to ~25 vol% change.	75–85% porosity for holding the active mass, mechanical strength to withstand handling during assembly and volume changes during battery operation
Electrodes of alkaline fuel cells and metal-air cells	Provide a barrier between the electrolyte and gases	Must provide the largest electrolyte/gas interface. Must avoid complete wetting of pores or bubbling of gases through pores	Small pore sizes; very narrow pore size distribution; total pore volume of about 48%
Filter elements	Filter highly caustic solutions	Depends on specific applications	Depends on specific applications. Both pore volume and pore size distribution are important.

fuel cells and metal-air (zinc-air or iron-air) cells, electrolyzers, and filter elements. Table 4 lists the functions and structural requirements these components must meet for efficient operation.

Highly porous electrodes for alkaline rechargeable batteries are made from nickel powders that have low bulk densities (<1 g/cm^3). These powders are produced by carbonyl processes. Slurries made from these powders are coated onto a support strip and then sintered. Alternatively, loosely packed beds of powder can be sintered. For all other porous structures, a carbonyl nickel powder with higher bulk density is suitable. Finer nickel powders can also be used by lightly compacting in a die or by roll compacting to produce the desired high green density.

Sintering temperatures between 850 and 1050 °C (1560 and 1920 °F) are commonly used to produce porous nickel products. The reducing conditions required for sintering are obtained easily with nitrogen-hydrogen gas mixtures or a burnt natural gas with low combustibles.

During sintering, loosely packed beds or compacted preforms of carbonyl nickel powders do not densify at <600 °C (<1110 °F). However, considerable strengthening of compacted materials occurs at <600 °C (<1110 °F) due to surface diffusion. As the temperature increases above 600 °F (1110 °F), volume diffusion increases. At ~950 °C (~1740 °F), filaments in the porous structures become smooth and broadened, while in consolidated structures the pores become rounded. To attain adequate strength without excessive loss of porosity, sintering temperatures between 950 and 1000 °C (1740 and 1830 °F) are optimal.

Table 5 gives typical porosity, strength, and electrical resistivity values for loose sintered and pressed-and-sintered materials. Table 6 shows reduction in surface area as a result of sintering. Figure 14 shows pore size distributions of sintered porous nickel structures. A micrograph of a sintered porous filter element made from nickel carbonyl powder is shown in Fig. 5.

Sintered dense nickel products (high-density) generally are used as preforms for further working operations. Additional densification occurs as the preform is hot and/or cold worked into a useful commercial shape. Preforms can be round or square billets or strips. Conventional compacting and sintering of individual small components is also used commercially.

A typical example of a high-density billet for further hot working involves extremely high-purity (99.97% Ni), inclusion-free nickel for electronic applications. Commercial melting and casting practices previously used could not guarantee the high purity and freedom from inclusions required for this application. Powder metallurgy processing, however, provides extremely high-purity nickel powders produced by techniques other than atomization. As a result, various mill shapes such as plates, rod, bar, and tube were manufactured from sintered billet stock.

The optimal starting powder for this application is a high-purity nickel powder with a carbon content below 0.1%, oxygen content below 0.15%, and sulfur content below 7 ppm. A high degree of compressibility is desirable. Powder is typically compacted by cold isostatic pressing to a density of approximately 6 g/cm^3. Sintering is carried out in a sulfur-free, reducing atmosphere such as hydrogen, dissociated ammonia, or a mixture of 90% N and 10% H. The prime objectives of the sintering operation are densification, development of strength (for subsequent hot working operations), and reduction of carbon and oxygen levels to below 0.01% and 0.005%, respectively.

During heatup of the green billet, gases adsorbed on powder surfaces are liberated. Carbon and oxygen in the powder then begin to react and produce gaseous products such as carbon dioxide and carbon monoxide. Sufficient time must be allowed at low and intermediate temperatures to permit the escape of these gases and the resulting decarburization before densification begins. For billets to reach a density above 96% of theoretical, sintering temperature is raised to 1100 to 1200 °C (2010–1290 °F) following decarburization. Depending on sintering temperature, sintering time may vary from 4 to 12 h.

The same considerations that apply to high-purity, electronic-grade nickel (high purity and freedom from inclusions) are responsible for commercial interest in the production of magnetic and low-expansion P/M alloys. Soft magnetic alloys such as Ni-50Fe, Ni-17Fe-4Mo, and Ni-17Fe-5Cu-4Mo are commercially produced from high-purity elemental metal powders. Carbonyl nickel and iron powders and high-purity copper and/or molybdenum powders are mechanically blended, isostatically compacted, and sintered in hydrogen at 1200 to 1400 °C (2190–2550 °F). During sintering, the density increases from ~70% in the as-pressed condition to 90 to 95% in the sintered condition. Bulk liquid hydrogen gas with an incoming dew point of approximately –73 °C (–99 °F) is used for sintering. Sintered billet is subsequently converted to a wrought product by hot and cold working.

Selection of Sintering Atmosphere. Composition and dew point of a sintering atmosphere determine whether reducing or oxidizing conditions prevail during sintering of a given material. The Richardson free-energy chart (Fig. 15) should be consulted for proper conditions. For example, in sintering of nickel at 1000 °C (1830 °F), according to the Richardson free-energy chart, the hydrogen-to-water and carbon monoxide-to-carbon dioxide ratios must be >0.01 to prevent oxidation of nickel. A reducing gas containing approximately 5% H, 5% CO, 8% CO_2, and the remainder nitrogen easily meets these requirements.

However, if nickel is alloyed with reactive elements such as silicon, manganese, chromium, vanadium, titanium, aluminum, zirconium, magnesium, and calcium, much higher ratios must be maintained to prevent oxidation of the reactive elements. Thus, for instance, the hydrogen-to-water and carbon monoxide-to-carbon dioxide ratios must be greater than 8×10^3 to prevent oxidation of chromium. Very pure hydrogen with a dew point of –45 °C (–49 °F) or lower is required for sintering nickel-chromium alloys. Also, time and temperature during heatup to sintering temperature must be carefully controlled so that the material being sintered is surrounded by an atmosphere with the required ratios. Additionally, alloys containing nitride-forming elements (chromium, titanium, and zirconium, for example), must be sintered in nitrogen-free atmospheres. In some cases, vacuum sintering may be necessary.

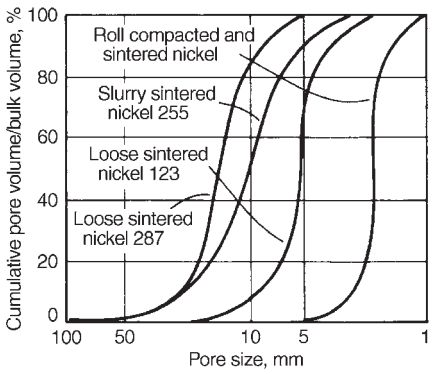


Fig. 14 Pore size distributions in sintered porous nickel structures

Table 5 Typical physical properties of sintered porous nickel structures

Material	Condition	Porosity, %	Electrical resistivity, μΩ · cm	Bend strength	
				MPa	psi
Nickel 287	Loose sintered	83	150–200	5.8	840
Nickel 255	Slurry sintered	82	100–150	12.7	1,840
Roll compacted strip	Sintered (49% porosity)	38	30–40	137	19,865
Nickel 123	Loose sintered	60	60–70	24.5	3,550

All materials were sintered at 950 °C (1740 °F) for 5 min.

Table 6 Surface area of sintered porous nickel structures

Powder type	Surface area, m^2/g		
	Loose powder	As sintered at 850 °C (1560 °F) for 5 min	As sintered at 950 °C (1740 °F) for 5 min
Nickel 255	0.6	0.18	0.16
Nickel 123	0.3	0.11	0.10

Surface area determined by BET method using krypton

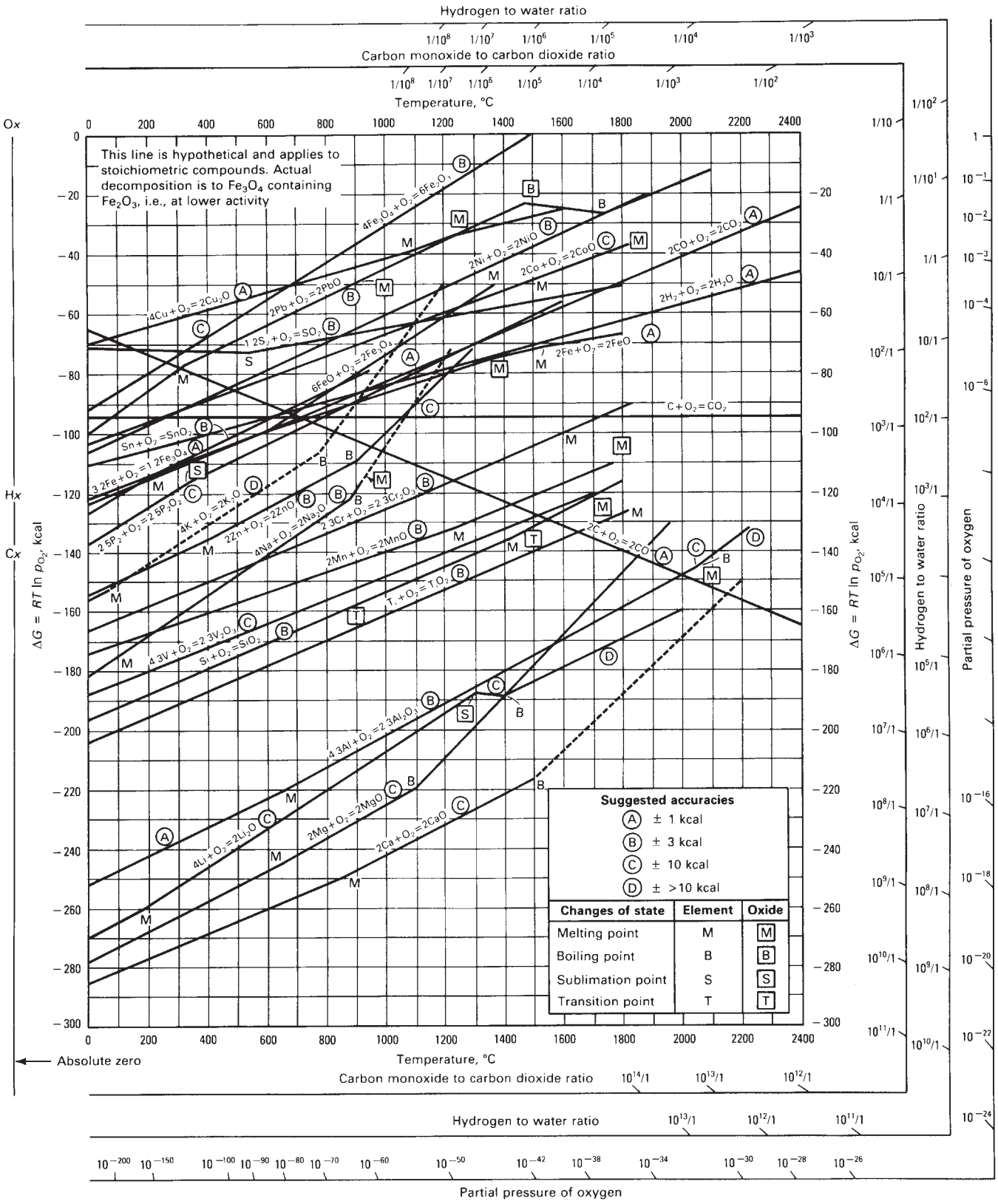


Fig. 15 Standard free energy of formation of metal oxides. To convert kcal to kJ, multiply kcal by 4.184. Source: Ref 9

Roll Compacting of Nickel and Nickel Alloys

Roll compacting, or powder rolling, refers to the continuous compaction of metal powders by a rolling mill. In this process, metal powders are fed from a hopper to a set of compacting rolls that produce a continuous green (unsintered) strip or sheet. These materials undergo further processing by sintering and rerolling to produce an end product with the desired mechanical properties. Material can be produced fully dense or with a desired porosity and pore size.

Production of Fully Dense Nickel Strip

The first successful application of rolling nickel powders into strip was the Sherritt Gordon process (Ref 10). This strip was used to make coinage blanks for the Canadian Mint. Typical mechanical properties of roll-compacted nickel strip at various stages of manufacturing are given in Table 7. Typical physical properties for strip made from nickel powder are listed in Table 8.

Strip Densification. After nickel powder is compacted into a green strip, the strip is sintered between 1000 and 1200 °C (1830 and 2190 °F) in a muffled furnace. Hydrogen, dissociated ammonia, or even less reducing gases provide a suitable atmosphere. Strip is conveyed through the furnace on a mesh belt or rollers.

Densification of the roll-compacted nickel strip can be achieved by hot or cold rolling. Hot rolling of nickel strip is performed above 800 °C (1470 °F), with a reduction in thickness of approximately 50%. Because of its porous nature, the sintered strip should be protected from oxidation when heating for hot rolling. This can be accomplished by using an inert or exothermic atmosphere.

Cold rolling and annealing cycles also may be used to densify the sintered strip. To be successful, sintering must be performed at 1100 °C (2010 °F) or higher. Limited reduction is achieved on the first cold mill pass. The strip must then be fed directly to a furnace without coiling, where it is annealed and cold rolled to full density. Reductions in excess of 35% are necessary to achieve full density.

Powders Used. Nickel powders with consistent high flow rates and compressibility are required so that high-volume production units with automatic powder-feeding mechanisms can be used. Water-atomized nickel powders usually are used for this purpose, although powders produced by the Sherritt process (Fig. 11) are also used commercially.

Advantages. Several advantages are gained from producing high-purity nickel strip by roll compacting. Lower electrical resistivity is possible ($73–79 \times 10^{-6}$ Ω · m, or 44–48 Ω · cir mil/ft). Stability can be maintained at ±2% throughout the coil and from heat to heat. Wrought nickel offers an erratic ±6% tolerance. Work-hardening rates for roll-compacted nickel strip are 25% less than for wrought nickel strip.

The lower softening (annealing) temperature coupled with high purity makes this nickel useful in clad metal combinations. In these applications, low and closely controlled annealing temperatures are required to minimize interdiffusion and to prevent incipient melting reactions.

Finished nickel strip produced from powder is virtually indistinguishable from strip produced from an ingot. Differences in physical properties are the result of compositonal variance, rather than the method of fabrication.

Specialty Applications. Specialty full-density strip produced by roll compacting includes various compositions of nickel-iron alloys produced for applications requiring controlled expansion properties. Examples include:

- High-purity nickel strip parts for heart pacemaker batteries
- Nickel-iron strip for resistor caps (Fig. 16)
- Nickel-iron lead frames (Fig. 16)
- Ni-Fe-Co cans for glass-sealed electronic parts

Production of Porous Nickel Strip

Roll compaction of porous nickel sheet materials has been commonly used in the production of battery materials (Ref 11, 12). Nickel and other powders are rolled to a thickness ranging from 0.13 to 3.8 mm (0.005–0.150 in.)

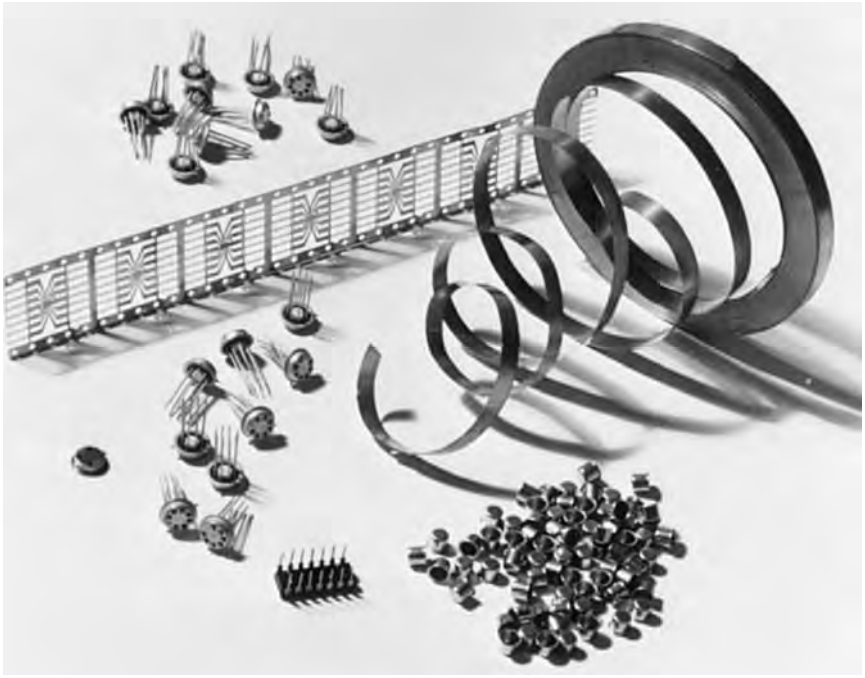


Fig. 16 Typical roll-compacted nickel strip applications. (a) Pure nickel semiconductor caps. (b) Nickel-iron lead frame. (c) Nickel-iron dual inline package integrated circuit. (d) Nickel-iron resistor end caps

Table 7 Typical mechanical properties of powder-rolled nickel strip

Strip	Strip thickness		Strip density, %	Ultimate tensile strength		Yield strength		Elongation, %
	mm	in.		MPa	ksi	MPa	ksi	
Green strip	4.0	0.158	79	4	0.6	4	0.6	0
Sintered strip	4.1	0.161	79	138	20	136	19	0
Hot rolled strip	2.1	0.084	100	358	52	165	24	38
Cold rolled strip	1.3	0.052	100	579	84	572	83	5
Annealed strip	1.3	0.052	100	362	53	83	12	48

Note: Compacting roll diameter, 560 mm (22 in.). Roll speed, 2.2 rpm. Roll gap (green strip), 3.5 mm (0.140 in.)

Table 8 Typical physical properties of powder-rolled nickel strip

Density	8.90 g/cm^3
Coefficient of thermal expansion at 20–100 °C	14 µm/m · °C
Coefficient of thermal expansion at 20–500 °C	15 µm/m · °C
Thermal conductivity	86.23 W/m · K (0.206 cal/cm · s · °C)
Cold-working capacity	Good
Hot-forming capacity	Good
Hot-work temperature	800–900 °C (1470–1650 °F)
Annealing temperature	700–900 °C (1300–1650 °F)
Magnetic properties	
Curie temperature	353 °C (667 °F)
Initial permeability	130
Maximum permeability	1240
Saturation induction	6.05 T
Remanance	3.25 T
Coercivity	23.87 A/m
Magnetostriction (soft) 1590 A/m	0.000032 mm/mm

and widths up to 1 m (39.37 in.), depending on the green strength and requirements of the application. Controlling the powder feed is critical to the process to obtain the best uniformity of the final product. Attempting to roll sheet with larger cross-sectional thickness can lead to delamination or low-density center regions that cause poor mechanical properties. Thin cross sections or powders with low green strength limit the handling of the porous sheet prior to sintering. The rolled sheet can be directly fed into a sintering furnace to minimize handling problems in certain high-volume applications. Roll compaction is used to produce an economical, uniform density material with good mechanical properties and tight dimensional tolerances (±2% on thickness). Width and length tolerances are determined by secondary machining, cutting, or shearing operations. Shapes or patterns can often be designed into the rolls, or parts can be stamped from the finished porous sheet.

Conventional P/M Superalloy Processing

Conventional processing of P/M superalloys involves production of spherical prealloyed powder, screening to a suitable maximum particle size, blending the powder to homogenize the powder size distribution, loading the powder into containers, vacuum outgassing and sealing the containers, and then consolidating the powder to full density. For most applications, the consolidated powder is consolidated by extrusion and subsequently forged to enhance mechanical properties, particularly high-temperature strength and ductility. For some applications, powder consolidated by HIP it utilized without further thermomechanical processing. In either case, the resulting product is fully dense and has properties that are generally superior to cast and wrought material.

Powder Production

Virtually all powder used to produce P/M superalloys is prealloyed, meaning that the powder is made from the molten state and each powder particle is essentially a mini-ingot with the same composition as the molten alloy. The principal commercial powdermaking processes are inert gas atomization and vacuum (soluble gas) atomization. Less commonly used processes include the rotating electrode process and centrifugal atomization.

In gas atomization, high-purity raw materials are vacuum induction melted and subsequently atomized using gas (Fig. 13b). Typically, the equipment consists of a top-melt chamber where high-purity raw materials are vacuum induction melted. The metal is delivered to a nozzle to form a small metal stream that is atomized by high-pressure gas using either a continuous annular-type nozzle or discrete individual nozzles. The resulting powder, which is highly spherical, is collected in a bottom chamber and/or cyclone collector. Argon gas is normally used to atomize superalloys. Nitrogen gas atomization can also be used to reduce cost and to eliminate entrapped argon. The use of nitrogen usually requires slight modifications in composition, such as lower carbon content, to accommodate the nitrogen increase associated with the atomization process.

Vacuum atomization is a commercial practice based on the principle that, when a molten metal is supersaturated with gas under pressure and is then suddenly exposed to a lower pressure, the gas expands, comes out of solution, and causes the liquid metal to be atomized. The equipment consists of two vertical chambers connected by a transfer tube (Fig. 13d and 17). The metal is vacuum induction melted in the lower chamber. When the lower chamber is pressurized with gas, the molten metal is forced upward through the transfer tube. As the metal rises into the upper chamber, it is atomized by escaping gases. The resulting powder falls to the bottom of the upper chamber and then through a powder drain into a collection container (Fig. 17).

Other Methods. Superalloy powder can also be produced using the plasma rotating electrode process (PREP) and the centrifugal atomization process. In PREP, a plasma arc is used to melt the end of a rapidly rotating prealloyed bar. The high-speed rotation of the bar causes liquid droplets to spin from the end of the bar and solidify in flight through a helium atmosphere. In centrifugal atomization, a molten stream of prealloyed metal is poured onto a spinning disk and atomized by centrifugal force. The emitted liquid particles are further broken up and subsequently cooled by high-pressure helium gas.

Powder Processing

Screening. Following powder production, the powders are screened to remove oversized particles and then blended to obtain a uniform size distribution. All powder handling is performed to minimize the possibility of introducing foreign material into the powder. This involves the use of specially designed stainless steel containers, valves, and inert handling or air handling of powder in clean rooms. Powder is normally screened to minimize the inclusion size in the final part. Depending on the application, powder sizes ranging from –60 to –325 mesh (–250 to –45 μm) are typically used.

Powder Cleanliness Evaluation. Prior to being loaded into containers for consolidation, superalloy powders are evaluated for cleanliness by techniques such as water elutriation, which separates nonmetallic inclusions from the powder for counting, sizing, and identification. A consolidated sample of the powder can also be evaluated by conducting large bar (e.g., 1.27 mm, or 0.500 in., diameter × 5.08 mm, or 2.0 in., gage section) fatigue tests. Cleanliness is evaluated on the basis of fatigue life and fracture origin.

Powder Outgassing. Containers for consolidation are made from stainless steel or mild steel. Exhaustive procedures are used to ensure that the containers are clean before powder loading. A "final filter" is commonly used to rescreen the powder as it enters the container as a final in-process control to ensure that no oversized particles are in the consolidated part. At some point in the processing, the powder is subjected to a vacuum and heated to remove air and adsorbed moisture. This can be accomplished during loading or after loading the powder into a container. In the former case, powder is loaded from an evacuated container into an evacuated consolidation container and then the container is sealed. In the latter case, powder is loaded in air into a consolidation container that is subsequently cold and hot outgassed and then sealed. Various combinations or modifications of these two outgassing techniques are used by different manufacturers.

Powder Consolidation

Superalloy powders are consolidated to full density using a combination of high temperature and high pressure. The primary consolidation methods for superalloys are HIP, extrusion, or a combination of the two.

Hot Isostatic Pressing. For HIP, the powder containers can be simple geometric shapes or complex near-net shapes. The product can be a billet suitable for subsequent extrusion and/or forging. The HIP product can also be a near-net forging preform or a near-net machining preform to be used without additional hot working. The HIP parameters generally used are 1040 to

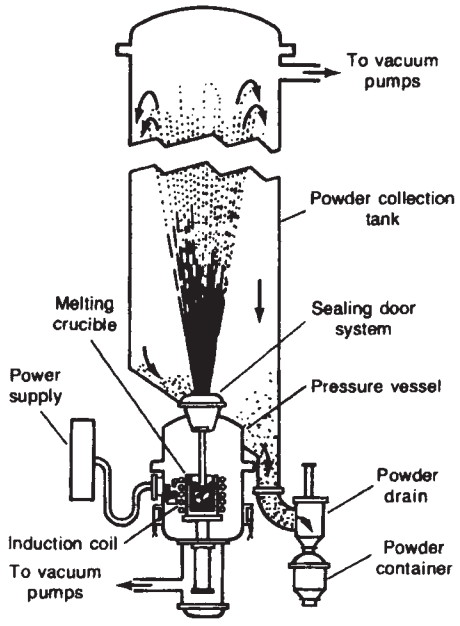


Fig. 17 Vacuum atomization system for producing superalloy powder

1205 °C (1900–2200 °F) at 105 to 205 MPa (15–30 ksi) for 3 to 5 h. An example of a HIP near-net sonic shape and the resulting turbine disk is shown in Fig. 18.

Extrusion of superalloy powders can be done either as the extrusion of loose powder or extrusion of a preconsolidated billet. The extrusion of loose powder requires a specialized container with a nose plug designed to protect the evacuation stem on the container from rupturing prior to entering the extrusion die. Extrusion ratios used for direct extrusion of powder are at least 7 to 1. With extrusion of preconsolidated billet, the powder may be preconsolidated by HIP, a separate forging press, or in the extrusion press against a blank die. Extrusion ratios for solid billet are normally at least 3 to 1. Typical extrusion temperatures for P/M superalloys range from 1040 to 1175 °C (1900–2150 °F).



Fig. 18 As-HIP René 95 turbine disks. As-HIP shape (upper left), sonic shape (upper right), finished machined disks (bottom). Courtesy Crucible Compaction Metals

Postconsolidation Processing

The postconsolidation processing of P/M superalloys is similar to that used for ingot products, but the P/M material has a number of advantages. The uniform grain size and lack of segregation in P/M material generally improves forgeability, machinability, and ultrasonic inspectability. Most P/M superalloys exhibit superplasticity and are normally isothermally forged at low strain rates to reduce force requirements and to produce close-tolerance forgings. Conventional high-strain forging is difficult to accomplish due to the high strength and cracking tendencies of these materials. However, recent work has shown that the high-strain-rate formability of Udimet 720 can be markedly improved by HIP at a temperature slightly below the solidus of the alloy (Ref 13). The improvement is attributed to the elimination of grain boundaries, which are coincident with prior-particle boundaries. As a result, conventional forging and ring rolling of P/M billet is deemed practical. The ultrasonic inspectability (background noise level) of P/M alloys, due to their homogeneity, is superior to most conventional cast plus wrought superalloys. As a result, smaller flaws can be detected in the P/M alloys.

Heat treatments applied to P/M materials are also similar to those used for ingot product. In general, this involves a solution treatment followed by multistep aging treatments to stabilize carbides and precipitate and stabilize γ' (generally, a precipitate of the form Ni_3Al). Maximum short-time strength is developed with a "subsolvus" solution treatment at a temperature slightly below the γ' solvus temperature. Fatigue crack growth resistance and creep strength of P/M superalloys can be significantly improved with a "supersolvus" solution treatment slightly above the γ' solvus temperature. The result is improved defect tolerance in these high-strength materials. The supersolvus treatment is being applied to a number of P/M alloys.

Composition and Mechanical Properties of P/M Superalloys

Table 9 gives the compositions of P/M superalloys. Alloys that are in commercial production include René 95, IN-100, LC Astroloy, N18, and René 88DT. A number of alloys are in earlier stages of P/M development. These include Udimet 720, Inconel 706, Inconel 718, AF115, and KM4. Other alloys, such as PA101, MERL 76, and AF2-1DA, where originally considered for P/M applications but are not currently being used commercially. The characteristics and properties of individual alloys are discussed in the following paragraphs. More detailed information on the metallurgy of superalloys, including the strengthening effect of the γ' precipitate, can be found in the article "Superalloys" in this Handbook.

René 95 is one of the highest-strength alloys available for service in the range of 425 to 650 °C (800–1200 °F). The alloy also provides

Table 9 Composition of P/M superalloys

	Composition, wt%													
Alloy	C	Cr	Mo	W	Ta	Ti	Nb	Co	Al	Hf	Zr	B	Ni	Other
René 95	0.07	13.0	3.5	3.5	…	2.5	3.5	8.0	3.5	…	0.05	0.01	bal	…
IN-100	0.07	12.5	3.2	…	…	4.3	…	18.5	5.0	…	0.04	0.02	bal	0.75V
LC Astroloy	0.04	15.0	5.0	…	…	3.5	…	17.0	4.0	…	0.04	0.025	bal	…
N18	0.02	11.5	6.5	…	…	4.3	…	15.5	4.3	0.5	…	0.015	bal	…
René 88DT	0.03	16.0	4.0	4.0	…	3.7	0.7	13.0	2.1	…	0.03	0.015	bal	…
Udimet 720	0.025	16.0	3.0	1.25	…	5.0	…	14.7	2.0	…	0.03	0.020	bal	…
IN-706	0.02	16.0	…	…	…	1.7	3.0	…	0.15	…	…	…	bal	38Fe
IN-718	0.02	18.0	3.0	…	…	0.9	5.0	…	0.45	…	…	0.004	bal	18Fe
AF 115	0.05	10.5	2.8	6.0	…	3.9	1.7	15.0	3.8	2.0	…	…	bal	…
AF2-1DA-6	0.04	12.0	2.75	6.5	1.5	2.8	…	10.0	4.6	…	0.10	0.015	bal	…
PA101	0.10	12.5	…	4.0	4.0	4.0	…	9.0	3.5	1.0	…	…	bal	…
MERL 76	0.02	12.4	3.2	…	…	4.3	1.4	18.5	5.0	0.4	0.06	0.02	bal	…
TMP-3	0.07	10.8	3.1	3.4	…	2.8	3.9	6.9	3.9	…	0.05	0.01	bal	…
SR3	0.03	13.0	5.1	…	…	4.9	1.6	12.0	2.6	0.2	0.03	0.015	bal	…
KM4	0.03	12.0	4.0	…	…	4.0	2.0	18.0	4.0	…	0.03	0.03	bal	…

excellent high-temperature creep resistance and low-cycle fatigue life. René 95 was originally developed as a cast and wrought material, but was soon changed to a P/M material due to forging difficulties and inconsistent mechanical properties. Initially, the P/M version was developed for use in the as-HIP (i.e., no hot working) plus heat treated condition (Ref 14). For maximum short-time strength, HIP René 95 is solution treated slightly below the γ′ solvus temperature (subsolvus treatment) and rapidly cooled using a molten salt quench followed by two-step aging. This treatment results in a fine equiaxed structure (ASTM 11) with a fine dispersion of γ′. Solution treatment above the γ′ solvus (supersolvus treatment) provides increase creep resistance and stress rupture strength through a slightly increased grain size (ASTM 7–8). Tensile and creep rupture properties for HIP René 95 are given in Tables 10 and 11.

Although as-HIP René 95 is in current use, most René 95 production involves extrusion of preconsolidated powder followed by isothermal forging and heat treatment. Tensile and creep rupture properties for thermomechanically processed P/M René 95 are given in Tables 12 and 13. Typical low-cycle fatigue properties are given in Table 14.

IN-100. Powder metallurgy IN-100 is a modified version of what was originally a casting alloy (Ref 17). It is now widely used as a compressor and turbine disk material by Pratt & Whitney Aircraft. Powder metallurgy IN-100 hardware is produced by extrusion of preconsolidated powder followed by isothermal forging and heat treatment. Typical properties are given in Table 15 (Ref 18, 19).

LC Astroloy is a low-carbon version of cast plus wrought Astroloy. The alloy offers a unique combination of excellent ductility and high-temperature strength. As-HIP Astroloy is used by AlliedSignal in dual-alloy turbine disks as well as one-piece hubs with inserted blades for aircraft auxiliary power units (Ref 20, 21). Processing of the alloy usually involves powder consolidation by HIP or direct extrusion plus heat treatment. Typical properties of HIP plus heat treated LC Astroloy are given in Tables 16 and 17.

N18 is a defect tolerant modification of LC Astroloy developed by Societe Nationale d'Etude et de Construction de Moteurs (SNECMA) for high-pressure turbine engine disks (Ref 23, 24). The alloy exhibits high strength as well as good creep resistance and excellent creep fatigue crack growth behavior up to 650 °C (1200 °F).

Alloy N18 is useful in both bore and rim locations at temperatures up to ~650 °C (1200 °F). The alloy is normally produced by extrusion followed by isothermal forging and a subsolvus (1165 °C, or 2130 °F) heat treatment. Under these processing conditions, the resulting grain size is 12 μm (ASTM 10). Typical tensile, creep rupture, and crack growth rate properties are compared with those of LC Astroloy and IN-100 in Fig. 19 to 21. The properties of the alloy are markedly affected by grain size (Ref 25, 26). Increasing the grain size to 60 μm (ASTM 6) using a supersolvus treatment (1200 °C, or 2190 °F) increases creep

Table 10 Tensile properties of as-HIP P/M René 95

Temperature		0.2% yield strength		Tensile strength		Elongation,	Reduction
°C	°F	MPa	ksi	MPa	ksi	%	of area, %
Subsolvus treated(a)							
21	70	1260	183	1653	240	18	18
204	400	1233	179	1591	231	12	12
427	800	1205	175	1571	228	11	11
537	1000	1192	173	1619	235	13	14
649	1200	1171	170	1515	220	14	16
Supersolvus treated(b)							
21	70	1171	170	1592	231	14	16
204	400	1137	165	1481	215	9	12
427	800	1109	161	1557	226	12	14
537	1000	1075	156	1551	225	14	16
649	1200	1027	149	1433	208	14	15
760	1400	951	138	1158	168	10	12

(a) Heat treatment: 1135 °C (2075 °F) + 760 °C (1400 °F)/8 h. (b) Heat treatment: 1175 °C (2150 °F) + 760 °C (1400 °F)/8 h. Source: Ref 15

Table 11 Creep rupture properties of as-HIP P/M René 95

Temperature		Stress		Time to 0.2%	Time to
°C	°F	MPa	ksi	creep, h	rupture, h
Subsolvus treated(a)					
649	1200	847	123	50	340
740	1300	551	80	20	340
Supersolvus treated(b)					
649	1200	847	123	80	1500
704	1300	551	80	280	3000

(a) Heat treatment: 1135 °C (2075 °F) + 760 °C (1400 °F)/8 h. (b) Heat treatment: 1175 °C (2150 °F) + 760 °C (1400 °F)/8 h. Source: Ref 15

Table 12 Tensile properties of extruded and isothermally forged P/M René 95

Temperature		2% yield strength		Tensile strength			Reduction
°C	°F	MPa	ksi	MPa	ksi	Elongation, %	of area, %
21	70	1254	182	1675	243	20	23
204	400	1233	179	1578	229	22	25
427	800	1206	175	1627	236	21	23
538	1000	1192	173	1599	232	17	18
649	1200	1172	170	1454	211	11	13
760	1400	1068	155	1137	165	6	8

Note: Heat treatment: 1120 °C (2050 °F) + 760 °C (1400 °F)/8 h. Source: Ref 15

Table 13 Creep rupture properties of extruded and isothermally forged P/M René 95

Temperature		Stress		Time to 0.2%	Time to
°C	°F	MPa	ksi	creep, h	rupture, h
649	1200	847	123	10	600
704	1300	551	80	90	270

Note: Heat treatment: 1120 °C (2050 °F) + 760 °C (1400 °F)/8 h. Source: Ref 15

Table 14 Typical low-cycle fatigue data for extruded plus isothermally forged P/M

Temperature		Cycles to failure
°C	°F	(N_f)
400	750	130,000
540	1000	160,000

Note: Heat treatment: 1107 °C (2025 °F)/1 h/oil quench + 760 °C (1400 °F)/8 h/air cool. Tested at 0.7% strain, 30 CPM. Source: Ref 16

Table 15 Mechanical properties of P/M IN-100 disk made by extrusion and isothermal forging

Room-temperature tensile properties	
Tensile strength, MPa (ksi)	1591 (231)
Yield strength, MPa (ksi)	1102 (160)
Elongation, %	26
Reduction of area, %	26
Tensile properties at 700 °C (1300 °F)	
Tensile strength, MPa (ksi)	1267 (184)
Yield strength, MPa (ksi)	1068 (155)
Elongation, %	18
Reduction of area, %	20
Stress-rupture properties at 732 °C (1350 °F) and 654 MPa (95 ksi)	
Life, h	35
Elongation, %	13
Creep properties at 700 °C (1300 °F) and 551 MPa (80 ksi)	
Time to 0.1%, h	102
Time to 0.2%, h	134

Note: Heat treatment: 1121 °C (2050 °F/2 h/oil quench + 871 °C (1600 °F)/40 min/air cool + 982 °C (1800 °F)/45 min/air cool + 760 °C (1400 °F)/4 h/air cool. Source: Ref 18, 19

(Fig. 22) and fatigue crack growth resistance (Fig. 23) without major change in low-cycle fatigue resistance. Larger grains can decrease low-cycle fatigue resistance; thus grain size control during processing is most important.

René 88DT (damage tolerant) is a nickel-base P/M superalloy that was developed by General Electric to meet the higher temperature requirements of advanced engines (Ref 27). The specific goals relative to René 95 were 50% reduction in cyclic fatigue crack growth rate, a 13 °C (23 °F) minimum improvement in creep and stress rupture strength, and a maximum 10% reduction in tensile strength. The alloy is currently used in production engine disk hardware (e.g., high- and low-pressure turbine disks and forward outer seals). Typical properties of René 88DT are given in Tables 18 and 19.

Udimet 720 was originally developed as a wrought turbine blade alloy for industrial turbines. In the cast and wrought form it is being used as a turbine disk alloy. More recently, the alloy has been evaluated as a P/M material (Ref 28, 29). Reportedly, P/M Udimet 720 has excellent fatigue crack growth resistance and is being strongly considered as a disk material in small to medium gas turbine engines as well as aircraft auxiliary power units. Udimet 720 can be produced by HIP or by extrusion plus isothermal forging. Figure 24 shows a fully

Table 16 Tensile properties of as-HIP P/M LC Astroloy

Test temperature		Yield strength		Tensile strength		Elongation,	Reduction of area,
°C	°F	MPa	ksi	MPa	ksi	%	%
22	72	930	135	1345	195	22	24
540	1000	861	125	1240	180	22	24
650	1200	827	120	1137	165	22	32
760	1400	792	115	1068	155	22	34

Note: HIP: 1205 °C (2200 °F)/100 MPa (15 ksi)/4 h. Heat treatment: 1115 °C (2040 °F)/2–4 h/AC + 870 °C (1000 °F)/8 h AC + 980 °C (1800 °F)/4 h/AC + 650 °C (1200 °F) 24 h/AC + 760 °C (1400 °F)/8 h/AC. Source: Ref 22

Table 17 Stress rupture properties of as-HIP P/M LC Astroloy

Test temperature		100 h rupture stress	
°C	°F	MPa	ksi
650	1200	889	129
700	1300	703	102
760	1400	496	72

Note: HIP: 1205 °C (2200 °F)/100 MPa (15 ksi)/4 h. Heat treatment: 1115 °C (2040 °F)/2–4 h/AC + 870 °C (1000 °F)/8 h AC + 980 °C (1800 °F)/4 h/AC + 650 °C (1200 °F) 24 h/AC + 760 °C (1400 °F)/8 h/AC. Source: Ref 22

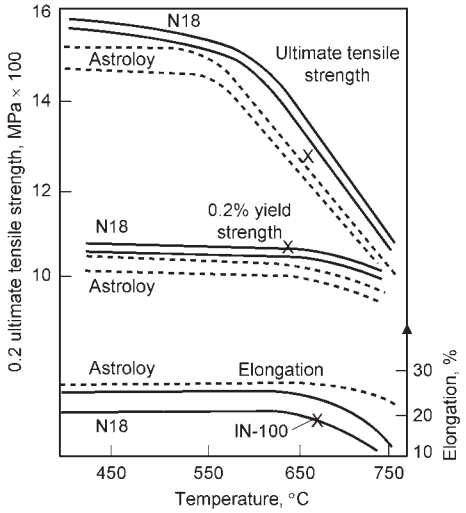


Fig. 19 Tensile properties of extruded plus isothermally forged P/M N18 compared to P/M Astroloy and P/M IN-100 (N18 heat treatment: 1165 °C (2130 °F)/4 h/cooled at 100 °C/min + 700 °C (1292 °F)/24 h/air cool + 800 °C (1472 °F/4 h/air cool). Source: Ref 23

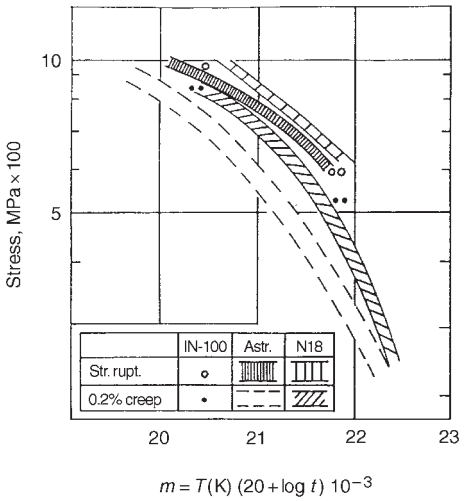


Fig. 20 Larson-Miller creep rupture curves for extruded plus isothermally forged P/M N18 compared to P/M Astroloy and P/M IN-100 (N18 heat treatment: 1165 °C (2130 °F)/4 h/cooled at 100 °C/min + 700 °C (1292 °F)/24 h/air cool + 800 °C (1472 °F)/4 h/air cool). Astr., Astroloy; Str. rupt., stress rupture. Source: Ref 23

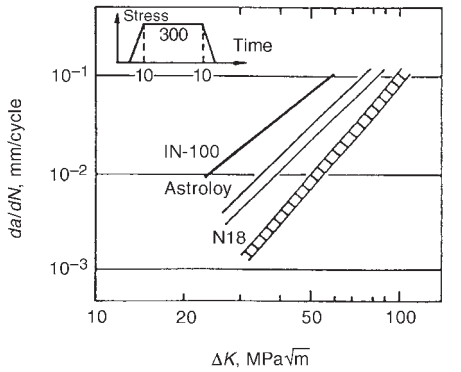


Fig. 21 Crack growth rates at 650 °C (1202 °F) for extruded plus isothermally forged P/M N18 compared to P/M Astroloy and P/M IN-100 (N18 heat treatment: 1165 °C (2130 °F)/4 h/cooled at 100 °C/min + 700 °C (1292 °F)/24 h/air cool + 800 °C (1472 °F)/4 h/air cool). Source: Ref 23

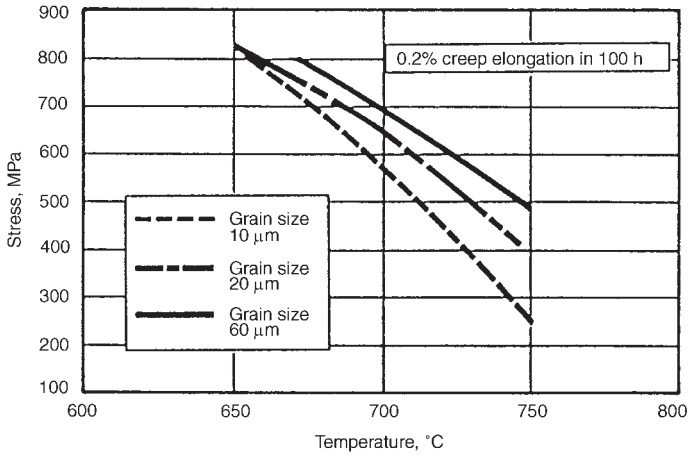


Fig. 22 Effect of grain size on the creep capability of extruded plus isothermally forged P/M N18. Source: Ref 25

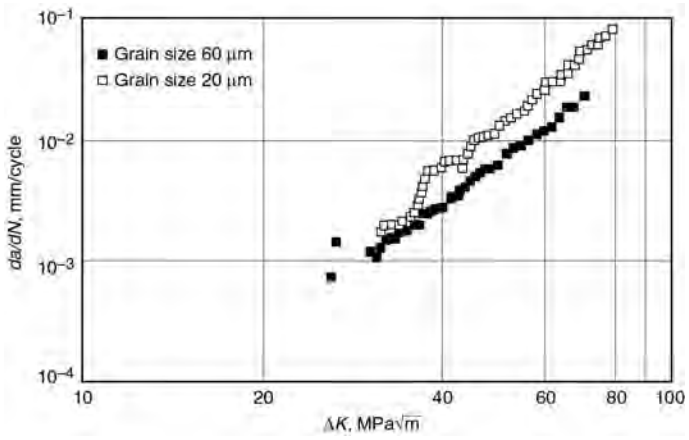


Fig. 23 Effect of grain size on the 750 °C (1382 °F) fatigue crack growth rate of extruded plus isothermally forged P/M N18. Source: Ref 25

machined P/M Udimet 720 turbine disk produced by extrusion plus isothermal forging. A comparison of the costs for P/M and cast and wrought Udimet 720 disks showed more than 20% cost reduction with the P/M process (Ref 28). Tensile properties for P/M Udimet 720 are shown in Fig. 25, and the results of fatigue crack growth rate tests of P/M and cast and wrought material are shown in Fig. 26. Low-cycle fatigue tests (R = 0.0, K_t = 1.0, F = 20 cpm at 425, 540, and 650 °C, or 800, 1000, and 1200 °F) have shown that the P/M Udimet 720 has mean lives that are higher than cast and wrought Udimet 720.

Table 18 Tensile properties of extruded + isothermally forged P/M René 88DT

Temperature		0.2% yield strength		Tensile strength			
°C	°F	MPa	ksi	MPa	ksi	Elongation, %	Reduction of area, %
22	72	1143	166	1232	179	20	25
200	400	1074	156	1143	166	15	19
425	800	1067	155	1053	153	18	20
540	1000	1046	152	1088	158	17	20
650	1200	1019	148	1377	200	18	21
760	1400	971	141	1170	170	13	17

Note: Heat treatment: 1150 °C (2100 °F) + 760 °C (1400 °F)/8 h. Source: Ref 15

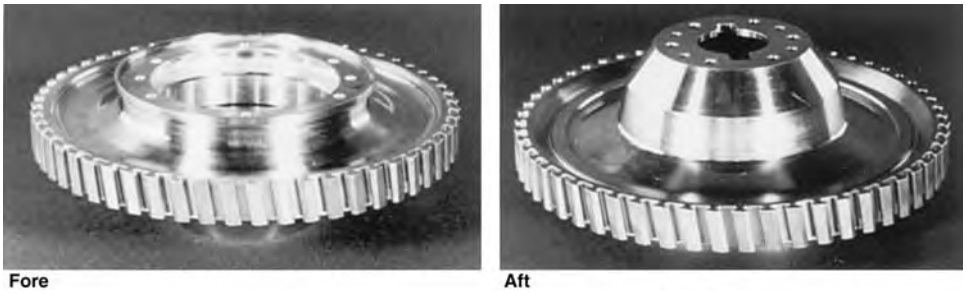


Fig. 24 Fully machined P/M Udimet 720 turbine disk produced by extrusion plus isothermal forging. Courtesy of Allison Engine Company

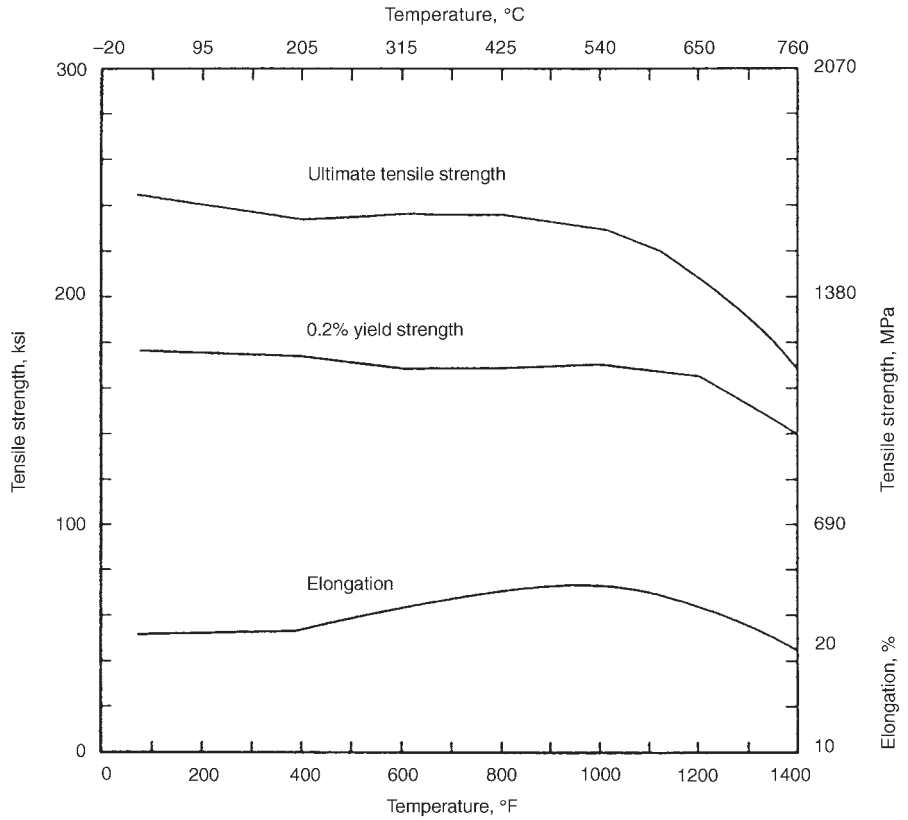


Fig. 25 Tensile properties of P/M Udimet 720 turbine disk produced by extrusion plus isothermal forging (heat treatment: 1090 °C (2000 °F) + two-step age). Source: Ref 28

IN-706 is an iron-nickel-base superalloy that is used for very large forged turbine disks in land-based turbine engines for power generation. Cast and wrought processing for these applications includes vacuum induction melting plus electroslag remelting plus vacuum arc remelting to minimize melt-related defects and segregation. Powder metallurgy is being developed for IN-706 in an effort to further minimize segregation and to lower the cost of these large forgings (Ref 30, 31).

In the P/M work, the effects of varying process parameters (argon and nitrogen atomization, powder size, HIP temperature, forging conditions, and heat treatment) have been studied. Tables 20 and 21 give the results of room-temperature tensile and Charpy V-notch tests of P/M IN-706 in the HIP plus heat treated and HIP forged plus heat treated conditions, respectively. Typical data for cast plus wrought IN-706 are included for comparison. Table 22 gives fracture toughness and low-cycle fatigue data for forged P/M IN-706. Compared to cast

Table 19 Creep rupture properties of extruded plus isothermally forged René 88DT

Temperature		Stress		Time to 0.2% creep, h	Time to rupture, h
°C	°F	MPa	ksi		
650	1200	847	123	1200	2000
700	1300	550	80	820	7000

Note: Heat treatment: 1150 °C (2100 °F) + 760 °C (1400 °F)/8 h. Source: Ref 15

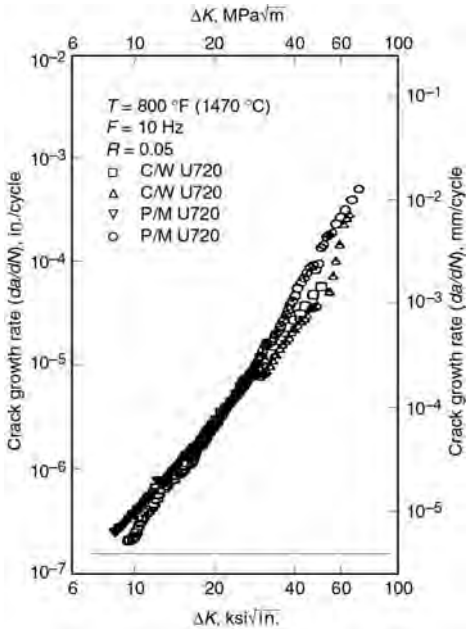


Fig. 26 Fatigue crack growth rates for P/M Udimet 720 turbine disk produced by extrusion plus isothermal forging (heat treatment: 1090 °C (2000 °F) + two-step age) compared to cast and wrought (C/W) Udimet 720. Source: Ref 28

and wrought material, the P/M material exhibits good fracture toughness and excellent fatigue resistance. The work conducted to date indicates that P/M IN-706 ages more rapidly than cast and wrought IN-706. As a result, some heat treatment modifications may be required for the P/M version of IN-706.

In addition to excellent mechanical properties, P/M IN-706 is highly resistant to grain growth at elevated temperatures. This is shown in Fig. 27, which compares the grain growth characteristics of IN-706 with cast and wrought IN-706. The grain growth resistance of P/M IN-706 may permit the use of higher forging temperatures and lower forging forces than that used for cast and wrought material. Powder metallurgy would also permit larger finish cross sections and more reliable ultrasonic inspection.

Table 20 Room-temperature properties of as-HIP P/M 706

Grade(a)	Mesh size	HIP temperature °C	HIP temperature °F	0.2% yield strength MPa	0.2% yield strength ksi	Ultimate tensile strength MPa	Ultimate tensile strength ksi	Tensile elongation, %	Reduction of area, %	Impact energy J	Impact energy ft · lbf
N706	–60	1130	2065	1025	149	1325	192	23	30	35	26
N706	–60	1065	1950	1035	150	1325	192	19	25	27	20
A706	–140	1130	2065	1035	150	1330	193	20	27	26	19
A706	–140	1065	1950	1040	151	1345	195	21	29	27	20

Note: Heat treatment: 980 °C (1800 °F)/ 1 h + 732 °C (1350 °F)/10 h + 620 °C (1150 °F)/8 h. (a) N706, nitrogen atomized; A706, argon atomized. Source: Ref 31

Table 21 Room-temperature properties of as-HIP plus forged P/M 706

Grade(a)	Mesh size	HIP temperature °C	HIP temperature °F	0.2% yield strength MPa	0.2% yield strength ksi	Ultimate tensile strength MPa	Ultimate tensile strength ksi	Tensile elongation, %	Reduction of area, %	Impact energy J	Impact energy ft · lbf
N706	–60	1130	2065	860	125	1205	177	23	44	50	37
N706	–60	1065	1950	855	125	1206	177	23	44	49	36
A706	–140	1130	2065	855	124	1205	177	22	40	41	30
A706	–140	1065	1950	845	123	1190	175	23	39	38	28

Note: Heat treatment: 980 °C (1800 °F)/ 1 h + 732 °C (1350 °F)/10 h + 620 °C (1150 °F)/8 h. (a) N706, nitrogen atomized; A706, argon atomized. Source: Ref 31

Table 22 Room-temperature fracture toughness and 750 °C (1380 °F) and 900 °C (1650 °F) low-cycle fatigue properties of HIP plus forged P/M 706

Alloy(a)	Mesh size	HIP temperature °C	HIP temperature °F	J_{Ic} 10^{-2} · Nm/m²	J_{Ic} in · lb/in.²	K_{Ic} MPa$\sqrt{m}$	K_{Ic} ksi$\sqrt{in.}$	Low-cycle fatigue(b) Cycles to failure at 750 °C (1380 °F)	Low-cycle fatigue(b) Cycles to failure at 900 °C (1650 °F)
N706	–60	1130	2065	…	…	…	…	34,312	32,820
N706	–60	1065	1950	9.3	533	145	133	26,515	52,423
A706	–140	1130	2065	7.5	426	130	119	41,846	64,055
A706	–140	1065	1950	7.4	420	129	118	27,623	45,916

Note: Heat treatment: 980 °C (1800 °F)/ 1 h + 732 °C (1350 °F)/10 h + 620 °C (1150 °F)/8 h. (a) N706, nitrogen atomized; A706, argon atomized. (b) Tested at 0.7% strain. Source: Ref 31

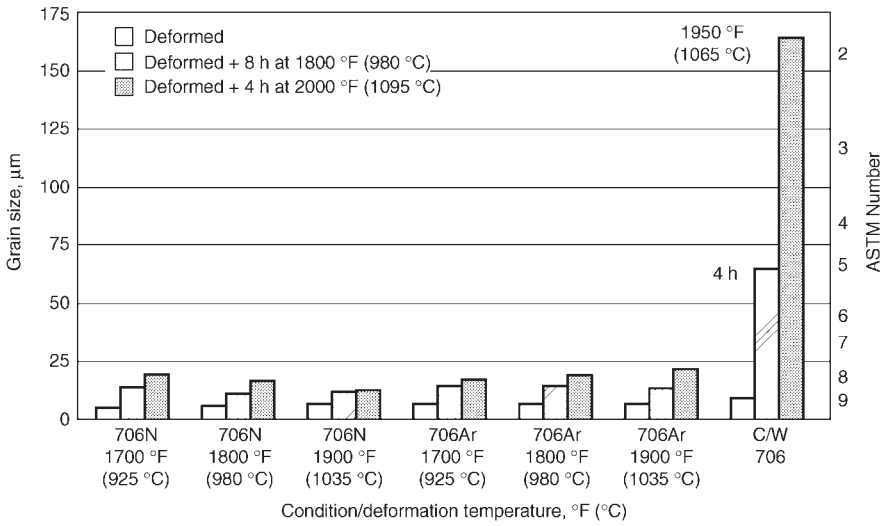


Fig. 27 Grain size of HIP plus forged P/M 706 and cast and wrought (C/W) 706 after heat treating. Source: Ref 31

IN-718 is similar to IN-706, but has higher elevated-temperature strength. Powder metallurgy IN 718 is being considered as a disk material in the next generation of land-based power generation turbine engines (Ref 32). The potential advantages of P/M IN-718 are similar to those described above for P/M IN-706.

AF115 was developed in the 1970s as a very high-strength P/M disk alloy for 760 °C (1400 °F) service (Ref 33), but the alloy is not currently specified for any engine systems. However, a lower-carbon version of the alloy (0.05% versus the original 0.15%) continues to be considered for disk application in the as-HIP and HIP plus forged conditions (Ref 34–36). Properties in HIP plus forged condition are discussed later in the section "Dual-Alloy Turbine Disks/Wheels" in this article.

AF2-1DA-6 is one of the strongest nickel-base superalloys available for use in the temperature range of 650 to 980 °C (1200–1800 °F). Typical tensile rupture properties are given in Tables 23 and 24. Powder metallurgy AF2-1DA-6 has been evaluated as a turbine disk material (Ref 38). However, the alloy is not currently specified for any turbine engine application.

PA101 is a hafnium-containing modification of the cast alloy IN-792 (Ref 39). The alloy is not currently specified for any engine system, but it has been successfully evaluated as one component of a dual-alloy turbine wheel for small turbine engines (Ref 40, 41). Tensile and stress rupture properties of as-HIP PA101 in a dual-property wheel are given in Tables 25 and 26.

MERL 76 is a P/M alloy that was developed for as-HIP fabrication of turbine engine components (Ref 42). It was designed to have properties in the HIP condition similar to those of isothermally forged IN-100. There are no current applications for MERL 76. Figures 28 and 29 give tensile and stress rupture properties, respectively, for the alloy in the as-HIP plus heat treated condition.

Specialized P/M Superalloy Processing

Specialized processing of P/M superalloys includes the mechanical alloying process for producing oxide-dispersion strengthened (ODS) alloys, solid-state bonding techniques for producing dual-alloy turbine disk/wheels, and more recently developed P/M methods such as laser-assisted rapid prototyping, powder injection molding, and spray forming.

Mechanical Alloying

Mechanical alloying (MA) is a dry, high-energy ball-milling process for producing composite metallic powders with a controlled, fine microstructure (Ref 43–45). It is carried out in a highly agitated ball charge by repeated cold welding and fracturing of a mixture of metal powders to which some nonmetal powders may be added. Its widest use has been in the production of dispersion-strengthened nickel- and iron-base superalloys for service at 1000 °C (1830 °F) and above.

Unlike mechanical mixing processes, MA produces a material whose internal homogeneity is independent of starting powder particle size. Thus, ultrafine dispersions (<1 μm interparticle spacing) can be obtained with relatively coarse initial powder (50–100 μm average diameter).

The Processing Path. Figure 30 is a schematic showing the path of raw materials using the MA process. The raw materials, the type of mill used, the process of consolidation, and the details of heat treatment differ depending on the type of product desired, but the processing route remains essentially the same. It is possible that some minor steps are either added or deleted in some special circumstances. The actual process of MA starts with mixing of powders in the right proportion and loading the powder into the mill along with the grinding medium (generally steel balls). This mix is then milled for the desired length of time until a steady state is reached. A steady state occur when the composition of every powder particle is the same as the proportion of the elements in the starting powder mix. Sometimes the powder is milled to an intermediate state either to form metastable phases or to achieve certain desired properties. The milled powder is then consolidated into a bulk shape and heat treated to obtain the desired microstructure and properties.

Equipment. The machinery used for mechanical alloying consists of one of several types of high-energy ball mills. These are selected on the basis of given processing times, ranging from hours to tens of hours. The types of ball mills employed include shaker mills, vibratory mills, stirred ball mills, centrifugal ball mills, and conventional large-capacity ball mills. The restriction on conventional ball mills arises from the relatively low-energy density of

Table 23 Tensile properties of P/M AF2-1DA-6 produced by extrusion plus isothermal forging

Temperature		0.2% yield strength		Tensile strength			Reduction of
°C	°F	MPa	ksi	MPa	ksi	Elongation, %	area, %
21	70	1138	165	1586	230	12	12
760	1400	1000	145	1227	178	8	10
870	1600	793	115	1206	175	10	10

Note: Heat treatment: 1204 °C (2200 °F)/2 h/air cool + 1066 °C (1950 °F)/2 h air cool + 760 °C (1400 °F)/16 h/air cool. Source: Ref 37

Table 24 Stress rupture properties of P/M AF2-1DA-6 produced by extrusion plus isothermal forging

Temperature		Stress		Rupture	Elongation,	Reduction
°C	°F	MPa	ksi	life, h	%	of area, %
760	1400	662	96	50	6	7
816	1500	483	70	55	7	7

Note: Heat treatment: 1204 °C (2200 °F)/2 h/air cool + 1066 °C (1950 °F)/2 h air cool + 760 °C (1400 °F)/16 h/air cool. Source: Ref 37

Table 25 Tensile properties of as-HIP P/M PA101 produced as part of a dual-property wheel

Temperature		0.2% yield strength		Tensile strength			Reduction of
°C	°F	MPa	ksi	MPa	ksi	Elongation, %	area, %
20	70	945	137	1472	213	15	14
650	1200	896	130	1315	191	10	13
760	1400	875	127	1088	159	11	15

Note: Heat treatment: 1120 °C (2050 °F)/2 h/fan cool + 840 °C (1550 °F)/4 h/air cool + 760 °C (1400 °F)/16 h/air cool. Source: Ref 41

Table 26 Stress rupture properties of as-HIP P/M PA101 produced as part of a dual-alloy wheel

Temperature		Stress		Rupture	
°C	°F	MPa	ksi	life, h	Elongation, %
650	1200	862	125	98	5
760	1400	586	85	70	10

Note: Heat treatment: 1120 °C (2050 °F)/2 h/gas fan cool + 840 °C (1550 °F)/4 h/air cool + 760 °C (1400 °F)/16 h/air cool. Source: Ref 41

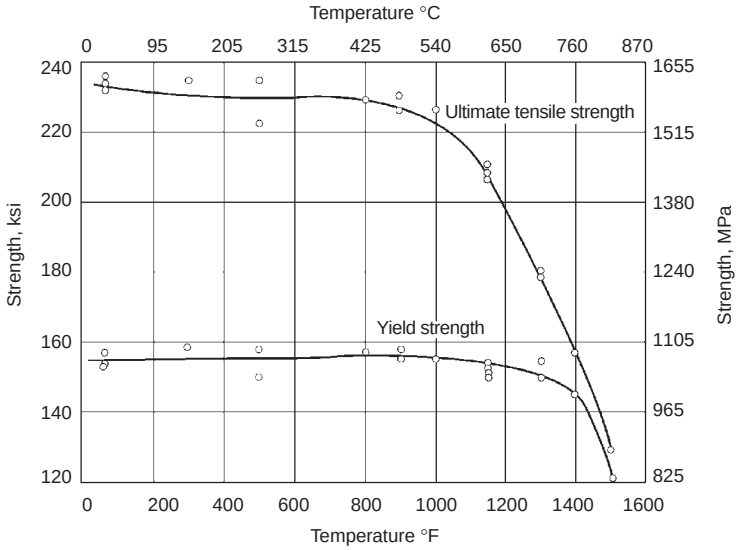


Fig. 28 Tensile and yield strength for as-HIP MERL 76. Heat treatment: 1105 °C (2125 °F)/2 h/oil quench + 870 °C (1600 °F)/40 min/air cool + 982 °C (1800 °F)/45 min/air cool + 650 °C (1200 °F)/24 h/air cool + 760 °C (1400 °F)/16 h/air cool. Source: Ref 42

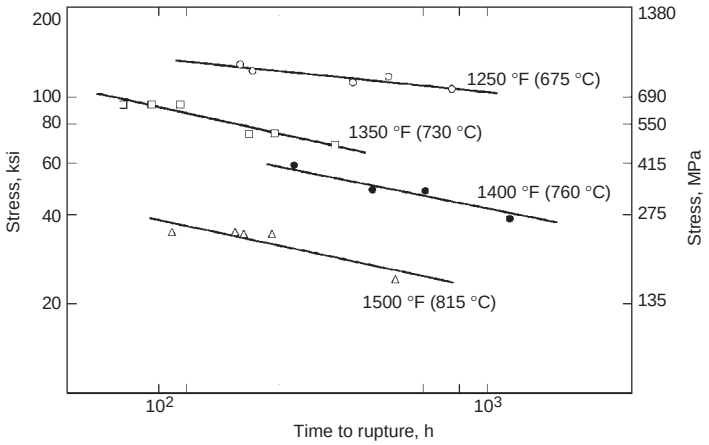


Fig. 29 Stress rupture properties of as-HIP MERL 76. Heat treatment: 1105 °C (2125 °F)/2 h/oil quench + 870 °C (1600 °F)/40 min/air cool + 982 °C (1800 °F)/45 min/air cool + 650 °C (1200 °F)/24 h/air cool + 760 °C (1400 °F)/16 h/air cool. Source: Ref 42

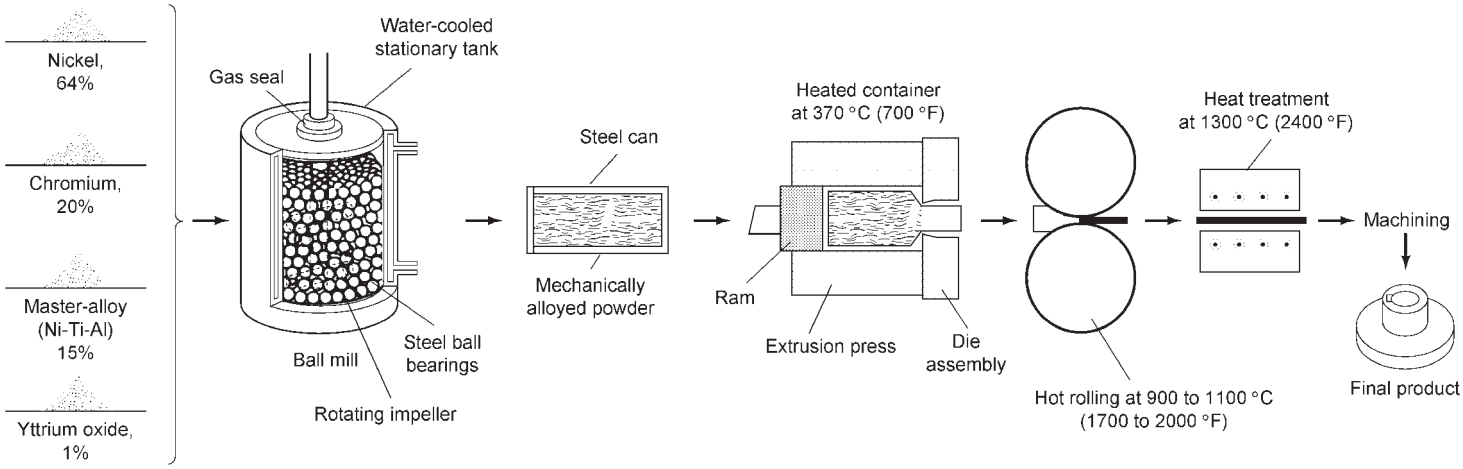


Fig. 30 Processing path in producing a product from powders by mechanical alloying. Source: Ref 43

operation of smaller mills, which leads to excessive processing times.

Unlike the procedure used in ball milling for comminution, the ratio of balls to powder in mechanical alloying is relatively high. These ratios range from 6:1 by weight to as high as 30:1, but most commonly are in the range of 10:1 to 20:1. The balls themselves range from 4 to 20 mm (0.16–0.8 in.) in diameter, but are usually 8 to 10 mm (0.32–0.4 in.) in diameter and are made of a through-hardened steel, such as 52100. The environment within the grinding machine is controlled wherever practical; water cooling and atmosphere control are employed. The milling atmosphere consists of either nitrogen or argon with measured trace amounts of oxygen. Liquids can also be used.

Production of Oxide-Dispersion-Strengthened (ODS) Superalloy Powders. The raw materials used for mechanically alloyed dispersion-strengthened superalloys are widely available commercially pure powders that have particle sizes that vary from about 1 to 200 μm. These powders fall into the broad categories of pure metals, master alloys, and refractory compounds. The pure metals include nickel, chromium, iron, cobalt, tungsten, molybdenum, and niobium. The master alloys include nickel-base alloys with relatively large amounts of combinations of aluminum, titanium, zirconium, or hafnium.

These master alloys are relatively brittle when cast and easily milled into powder. In addition, because they consist of relatively exothermic intermetallic compounds, the thermodynamic activity of the reactive alloying elements, such as aluminum and titanium, is considerably reduced compared to that of the pure metals.

A typical powder mixture may consist of fine (4–7 μm) nickel powder, –150 μm chromium, and –150 μm master alloy. The master alloy may contain a wide range of elements selected for their role as alloying constituents or for gettering of contaminants. About 2 vol% of very fine yttria, Y_2O_3 (25 nm, or 250 Å) is added to form the dispersoid. The yttria becomes entrapped along the weld interfaces between fragments in the composite metal powders. After completion of the powder milling, a uniform interparticle spacing of about 0.5 μm is achieved.

The oxygen contents of the commercially pure metal powders and the master alloys range from 0.05 to 0.2 wt%. The refractory compounds that can be added include carbides, nitrides, and oxides. For the production of dispersion-strengthened materials, such additions are limited to very stable oxides, such as yttria, alumina, or less frequently thoria. These oxides, which are prepared by calcination of oxalate precipitates, consist of crystallites of about 50 nm agglomerated into pseudomorphs of about 1 μm.

The only restriction on the mixture of powder particles for mechanical alloying (other than the particle size range mentioned above and the need to minimize excessive oxygen) is that at least 15 vol% of the mix should consist of a compressibly deformable metal powder. The function of this component, which can consist of any one or all of the pure metals, is to act as a host or binder for the other constituents during the process.

Powder Characteristics. A uniform distribution of submicron refractory oxide particles must be developed in a highly alloyed matrix for the production of ODS alloys. A given sample of mechanically alloyed superalloy powder may contain particles ranging from 10 to 500 μm, with an average particle size between 50 and 200 μm. The internal structure of the powder is independent of particle size once the steady state is achieved.

Because of the severe plastic deformation that occurs during MA, very high hardnesses are achieved in the powders. Hardness increases almost linearly during the initial stages of the process (Fig. 31), reaching a saturation value, after which time it is presumed that work softening balances further cold work.

It has also been noted by magnetic measurements (Fig. 31) that true alloying occurs, as evidenced by the loss of saturation magnetic moment, with increasing processing time in a nigh-nickel composition. This may be due to a combination of factors. First, the extreme amount of cold work leads to low activation energy and pipe diffusion. Second the temperature is moderately elevated to approximately 150 °C (300 °F) during the process. Third, relatively short interdiffusion distances (less than 1 μm) exist toward the end of the process.

Commercial Alloys. The most commercially important nickel-base mechanically alloyed ODS alloys include MA 754, MA 758, MA 6000, and, to a lesser extent MA 760 (the latter alloy is in limited production). Compositions and elevated-temperature tensile properties of these alloys are given in Tables 27 and 28, respectively.

The most significant advantage of ODS superalloys is the increased stress rupture properties. Figure 32 compares the 1000 h specific rupture strength (strength/density) for two ODS alloys (MA 6000 and thoria-dispersed nickel) and two cast alloys (directionally solidified

Table 27 Nominal compositions (wt%) of mechanically alloyed nickel-base superalloys

Alloy	Ni	Cr	Al	Ti	Mo	W	Y_2O_3	Ta
MA 754	bal	20	0.3	0.5	…	…	0.6	…
MA 757	bal	16	4.0	0.5	…	…	0.6	…
MA 758	bal	30	0.3	0.5	…	…	0.6	…
MA 760	bal	20	6.0	…	2.0	3.5	0.95	…
MA 6000	bal	15	4.5	0.5	2.0	4.0	1.1	2.0
TMO-2(a)	bal	6	4.2	0.8	2.0	12.4	1.1	4.7

(a) This alloy additionally contains 9.7 wt% cobalt.

Table 28 Longitudinal tensile properties of mechanically alloyed nickel-base superalloys

Alloy	Temperature °C	Temperature °F	Tensile strength MPa	Tensile strength ksi	Yield strength MPa	Yield strength ksi	Elongation, %	Reduction of area, %
MA 754	21	70	965	140	586	85	21	33
	649	1200	600	87	476	69	25	44
	871	1600	248	36	214	41	31	58
	1093	2000	148	22	134	19	12	24
MA 6000	21	70	1294	188	1284	186	4	3
	760	1400	1156	168	781	113	6	12
	982	1800	407	59	344	50	12	35
	1093	2000	222	32	192	28	9	31
MA 758	21	70	949	138	560	81	27	…
	700	1292	546	79	371	54	29	…
	800	1472	339	49	214	31	47	…
	1000	1832	173	25	151	22	29	…

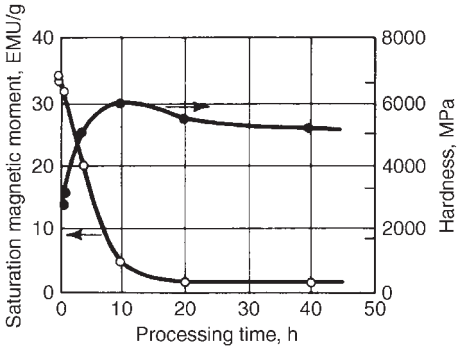


Fig. 31 Change of hardness and magnetic response during mechanical alloying

Mar-M200 + Hf) and single-crystal PWA 454). It is clear from this figure that the MA 6000 alloy can maintain a given stress for a much longer time than a casting alloy for similar vane applications. This is mainly due to the benefits of the combined strengthening modes (γ′ and ODS) in the mechanically alloyed material. Characteristics of various nickel-base ODS alloys are described below.

Alloy MA 754 was the first mechanically alloyed ODS superalloy to be produced on a large scale. This material is basically a Ni-20Cr alloy strengthened by about 1 vol% Y_2O_3. It is comparable to TD NiCr (an earlier ODS material strengthened by thoria, ThO_2), but has a nonradioactive dispersoid.

Alloy MA 758 is a higher-chromium version of MA 754. This alloy was developed for applications in which the higher chromium content is needed for greater oxidation resistance. The mechanical properties of this alloy are similar to those of MA 754 when identical product forms and grain structures are compared (see Table 28).

Alloy MA 6000 has a composition based on an alloy-development philosophy similar to that of the more sophisticated cast and wrought superalloys. This is because it contains a critical balance of elements to produce strength at intermediate and elevated temperatures, along with oxidation and hot-corrosion resistance. Alloy MA 6000 combines γ′ hardening from its aluminum, titanium, and tantalum content for intermediate strength, with ODS from the yttria addition for strength and stability at very high temperatures. Oxidation resistance comes from its aluminum and chromium contents, while titanium, tantalum, chromium, and tungsten act in concert to provide sulfidation resistance. The tungsten and molybdenum also act as solid-solution strengtheners in this alloy.

Alloy MA 760 is an age-hardened nickel-base alloy with a composition designed to provide a balance of high-temperature strength, long-term structural stability, and oxidation resistance. Its primary use is expected to be for industrial gas turbines. It is similar to MA 6000 in that its strength is supplemented by γ′ age hardening. Its properties also benefit from zone annealing to give coarse elongated grains. The stress rupture properties of alloy MA 760 exceed those of MA 754 but are exceeded by those of MA 6000.

Applications. The mechanically alloyed superalloys are considered mainly for three groups of applications—gas turbine vanes, turbine blades, and sheets for use in oxidizing/corrosive atmospheres. The largest use of MA 754 is as vanes and bands for aircraft gas turbine engines (Fig. 33). For applications requiring

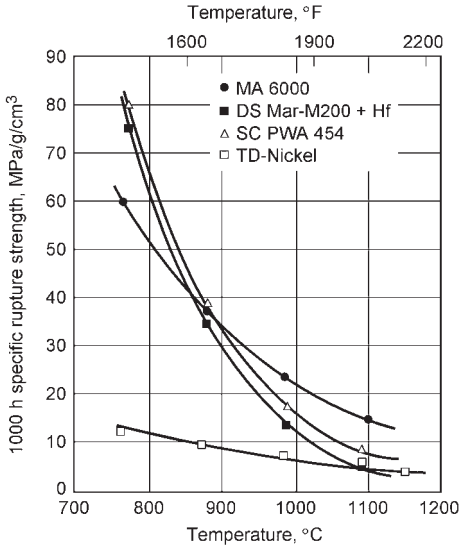


Fig. 32 Comparison of 1000 h specific rupture strength of MA 6000 with directionally solidified Mar-M200 + Hf, TD-Ni, and single-crystal PWA 454



Fig. 33 Some typical gas turbine engine components made of alloy MA 754

good resistance to thermal fatigue, such as gas turbine vanes, Inconel MA 754 is given a strong texture. The majority of the grains are aligned so that their ⟨100⟩ axes are parallel to the principal working direction and along the length of the bar. Such texture results in low modulus of elasticity (149 GPa, or 21.6×10^3 ksi) in the longitudinal direction. The low modulus improves resistance to thermal fatigue by lowering stresses for given thermal strains. Components are fabricated from bar stock using state-of-the-art machining and brazing processes typical for conventional wrought superalloys. Alloy MA 758 is used in a number of industrial applications where its high chromium content makes it resistant to extremes of temperature and environment. The alloy is used in the glass industry for high-temperature components requiring both elevated-temperature strength and resistance to extremely corrosive molten glass. Alloy MA 758 is also used for internal combustion engine components, mainly in critical fuel injection parts. One novel industrial application of alloy MA 754 is a high-temperature atmosphere-circulation fan in a "floating" furnace design being commercialized in Japan. Large rounds are used for the hub, and plate material is used for blades of the fan, which operates at temperatures >1100 °C (>2000 °F).

New product forms of the commercial alloys continue to be developed. Large-diameter, thin-wall tubing of alloy MA 754 has been produced and evaluated for radiant-tube applications, and alloy MA 758 has been used as tubing in heat exchangers and process equipment operating at very high temperatures.

Alloy MA 754 is used for brazed nozzle guide vane and band assemblies in U.S. military aero engines. The principal advantages of the alloy for these applications are thermal fatigue resistance, long-term creep strength, and high melting point.

Alloy MA 6000 is a more complex alloy developed as a blade material for advanced gas turbines. It is used for first- and second-stage turbine vanes and blades machined from solid bar. Unlike cast alloys, MA 6000 exhibits nearly flat rupture-life curves at high temperatures due to the combination of ODS and high grain-to-width ratios (typically >10 to 1). Because of its composition, MA 6000 has excellent resistance to oxidation and sulfidation. The characteristics of this alloy allow blade cooling to be reduced or eliminated as the metal temperature can be increased by 100 ° (180 °F) or more in engines where the stresses are medium or low.

Dual-Alloy Turbine Disk/Wheels

There are significantly different operating conditions for various locations in gas turbine wheels and disks (Ref 46). The rims of these parts operate in the 650 to 750 °C (1202–1382 °F) temperature range where creep and rupture strength are limiting properties. The bores of these parts operate at temperatures below 550 °C (990 °F). In this temperature region, high tensile strength and low-cycle fatigue resistance are required. Conventional processing of disks and wheels uses a single alloy to meet these varied requirements. As a result, some compromise in properties in either the rim or the bore often has to be tolerated, thereby limiting the service conditions of these parts. Several P/M approaches have been developed to resolve this problem.

AlliedSignal has developed one such process and qualified it for use in auxiliary power unit engines (Ref 20). The process involves a preconsolidated P/M LC Astroloy hub that is HIP bonded to a cast IN713LC blade ring to produce an axial turbine wheel (Fig. 34). The development allowed the high-cycle fatigue requirements of the engine to be met. A similar process has been reported for manufacturing a small axial wheel by HIP bonding a P/M PA101 bore to a cast MAR-M246 blade ring (Ref 41).

Kobe Steel has developed a process that uses two P/M superalloys: AF 115 for the rim and TMP-3 for the bore (Ref 47). In this process, the bore alloy is HIP consolidated. The rim is then consolidated and bonded to the bore in a second HIP cycle. The resulting assembly is isothermally forged to a turbine disk configuration. Subsequent heat treatment develops the required coarse-grained microstructure in the rim alloy and retains the fine-grained structure in the bore alloy. Figures 35 to 37 give the tensile, stress rupture, and low-cycle fatigue properties of the resulting forging. The tensile properties of the bore and rim section are very similar. As desired, the rim section (AF 115) had the highest strength, whereas the bore section TMP-3 exhibited the highest resistance to low-cycle fatigue.

General Electric has developed a dual-alloy disk process that utilizes two advanced high-strength P/M superalloys designated KM4 and SR3 as bore and rim alloys, respectively (Ref 48). The process involves forge bonding to join the two components. The advantages of

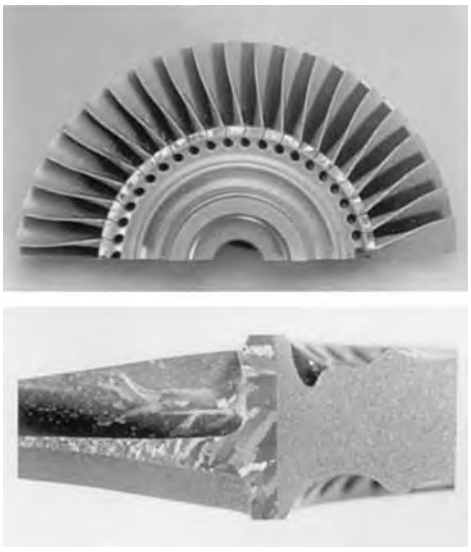


Fig. 34 Section of a dual-alloy property turbine wheel produced by HIP bonding a cast IN-713C blade ring to a P/M LC Astroloy hub. Courtesy of AlliedSignal Engine Division

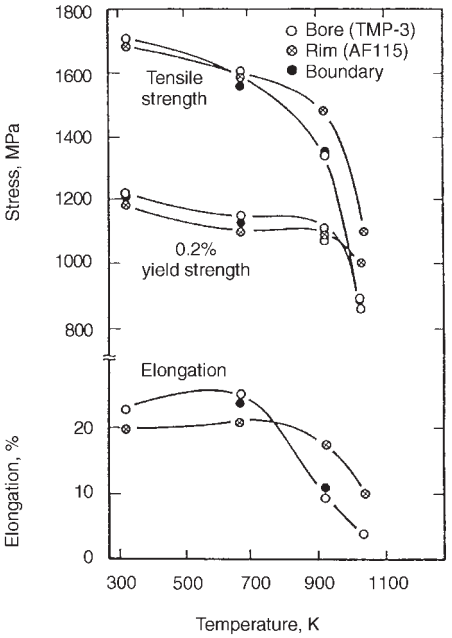


Fig. 35 Tensile properties of a TMP-3 (bore)/AF115 (rim) dual-alloy turbine disk. Source: Ref 47

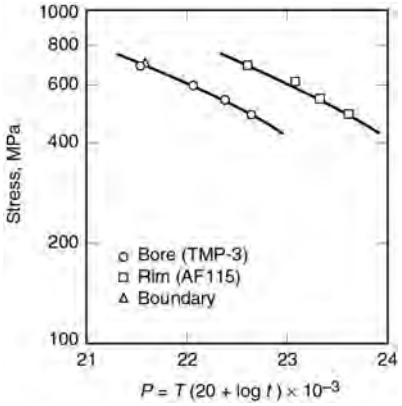


Fig. 36 Stress rupture strength of a TMP-3 (bore)/AF115 (rim) dual-alloy turbine disk. *T,* in K; *t,* in h. Source: Ref 47

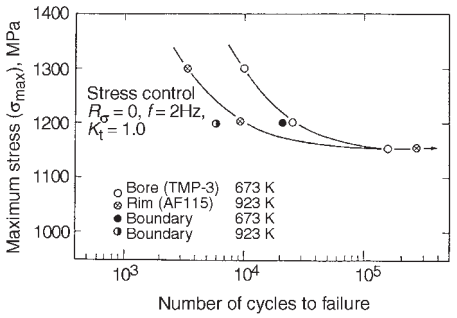


Fig. 37 Low-cycle fatigue life of a TMP-3 (bore)/AF115 (rim) dual-alloy turbine disk. Source: Ref 47

the process are the high degree of mechanical work at the joint and the expulsion of bondline material, which are key factors in developing a high-integrity joint. Figures 38 to 40 give the results of tensile and creep tests of the dual-alloy wheel. The results indicate no loss in strength in the joint region.

Other dual-alloy processing scenarios include various combinations of alloys and various solid-state joining techniques such as friction inertia welding, hot uniaxial pressing, HIP, and extrusion (Ref 49).

Laser-Assisted Rapid Protyping and Manufacturing

Several processes are being developed that produce a part directly from a three-dimensional computer-aided design (CAD) model. The attraction for these processes is that they require no hard tooling and, as a result, considerable time and cost can be saved in prototyping or manufacturing a metal article. In these processes, a laser is used to sinter or melt input powder one layer at a time until the entire part is built up layer upon layer. Two basic techniques are used: selective laser sintering and direct metal deposition.

In selective laser sintering (Ref 50), a thin layer of powder is laid out on a substrate. A computer-guided laser then traces the first planar layer of the part and sinters only that powder that lies in that plane of the part. The part is then indexed downward the equivalent of one powder layer. Anew layer of powder is then placed on the part and the laser traces the second plane of the part and sinters only the powder that lies in that plane of the part. The process is repeated until the part is complete. Figure 41 shows the major components of selective laser sintering equipment.

Heating the metal to sintering temperatures can adversely affect the mechanical properties of the material, and residual stresses developing upon cooling can induce distortion. An alternate approach has been developed to minimize these difficulties using polymer-coated metal powder as the raw material. The laser is then used only to soften the polymer and form necks with other coated particles that then hold the metal particles in the desired shape. The "green" parts are porous and must be further treated to remove the polymer and sinter the metal. Full density can then be attained by HIP (Ref 51).

Direct metal deposition is similar to selective laser sintering with the exception that the powder is introduced into the laser beam, melted, and deposited. The CAD-based model is used to index the laser and/or the part as the metal is laid down one layer at a time. Variations of the process are referred to as directed light fabrication (DLF) (Ref 52, 53), laser-engineered net shaping (LENS) (Ref 54), laser-aided direct metal deposition (LADMD) (Ref 55), or laser-aided direct deposition of metals (Ref 56). Figure 42 shows a schematic of the DLF process. Figure 43 shows an Inconel 690 hexagon shape made by DLF.

Alloys under Development. Trials utilizing laser-assisted rapid prototyping and manufacturing have been conducted on nickel-base alloys such as Inconel 690, Inconel 625, IN-100, and IN-718. Table 29 gives the properties of Inconel 690 bar produced by the DLF process. Some cracking difficulties have been encountered with the γ'-strengthened alloys, indicating that some specialized techniques may be required for precipitation-hardened alloys.

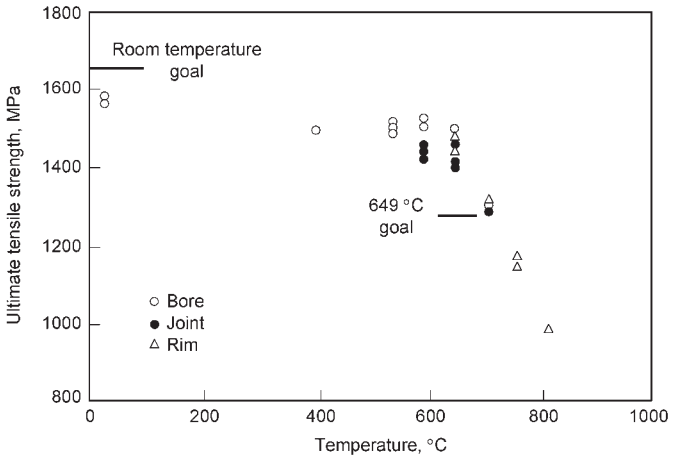


Fig. 38 Tensile strength of a KM4 (bore)/SR3 (rim) dual-alloy turbine disk produced by forge bonding. Source: Ref 48

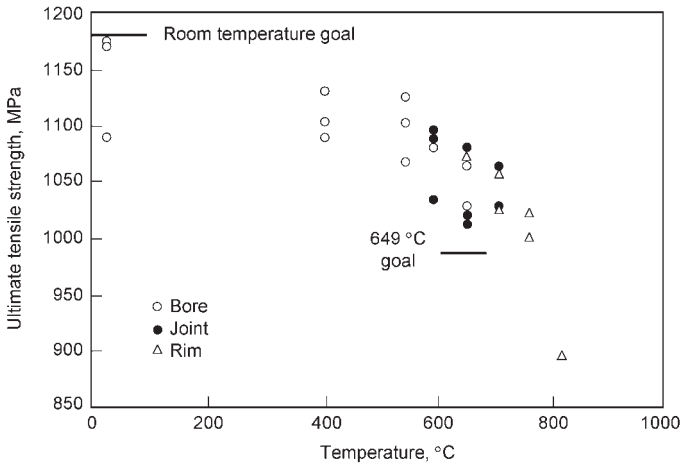


Fig. 39 Yield strength of a KM4 (bore)/SR3 (rim) dual-alloy turbine disk produced by forge bonding. Source: Ref 48

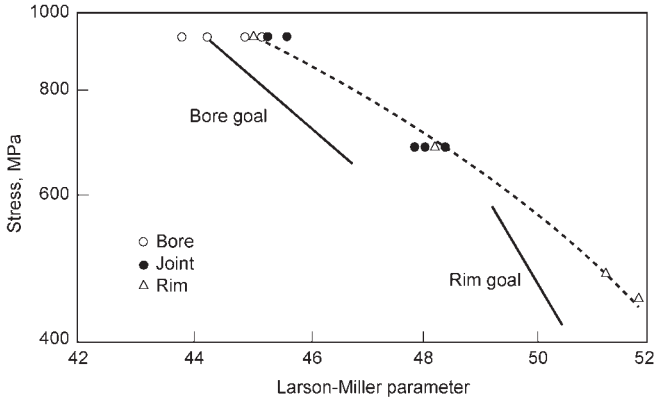


Fig. 40 Time to 0.2% creep data for a KM4 (bore)/SR3 (rim) dual-alloy turbine disk produced by forge bonding. Source: Ref 48

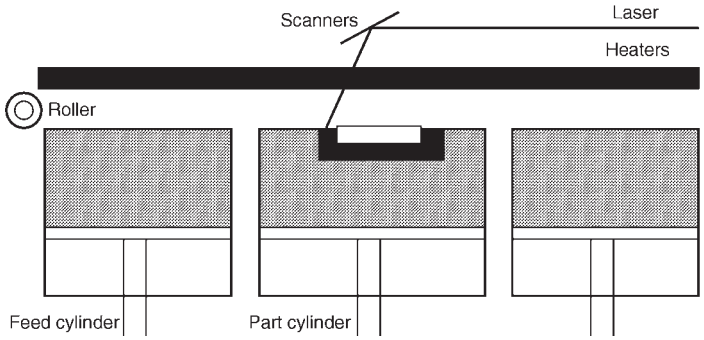


Fig. 41 Major hardware components of selected laser sintering equipment. Source: Ref 50

Powder Injection Molding

Powder injection molding (PIM) is a relatively low-cost process for producing large quantities of small net-shape complex parts. The process involves mixing powder with a suitable binder, pelletizing the mixture, injection molding into a die, debinding, sintering (plus HIP if required), and heat treatment. The process is used to produce a wide variety of parts from steels and stainless steels, but has been only recently considered for use with superalloys for aerospace applications. This work has centered primarily on IN-718 (Ref 57–60). As shown in Table 30, the tensile, stress rupture, creep, and high-cycle fatigue properties of PIM IN-718 can meet the minimum requirements of aerospace materials specification ASM 5596. Based on the results of this work, PIM IN-718 is believed to be a viable process for demanding applications with an expected cost reduction of 50% (Ref 59). In another study (Ref 61), PIM was evaluated using MERL 76 and Udimet 700. After HIP, densities of nearly 100% were attained and tensile strengths were at acceptable levels. The oxygen and carbon contents were relatively high, but the distribution of nonmetallic inclusions was fine and uniform.

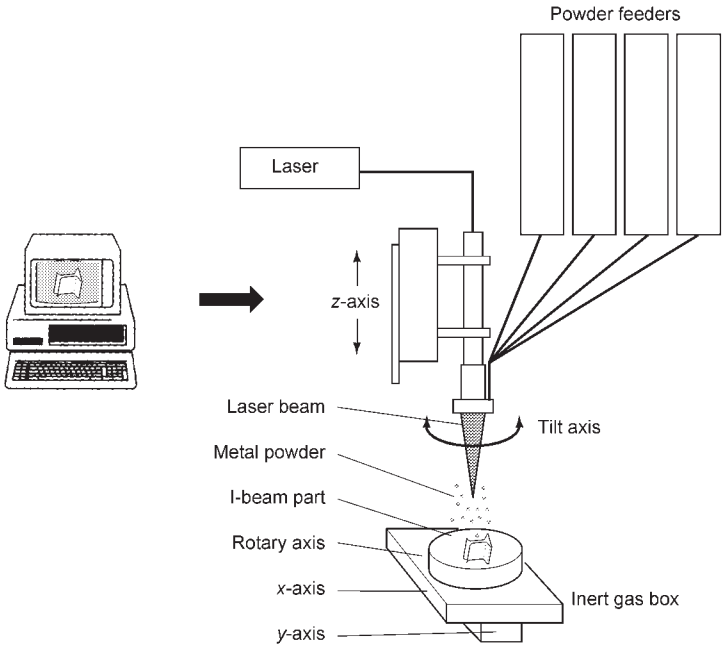


Fig. 42 Schematic of DLF system. Source: Ref 53

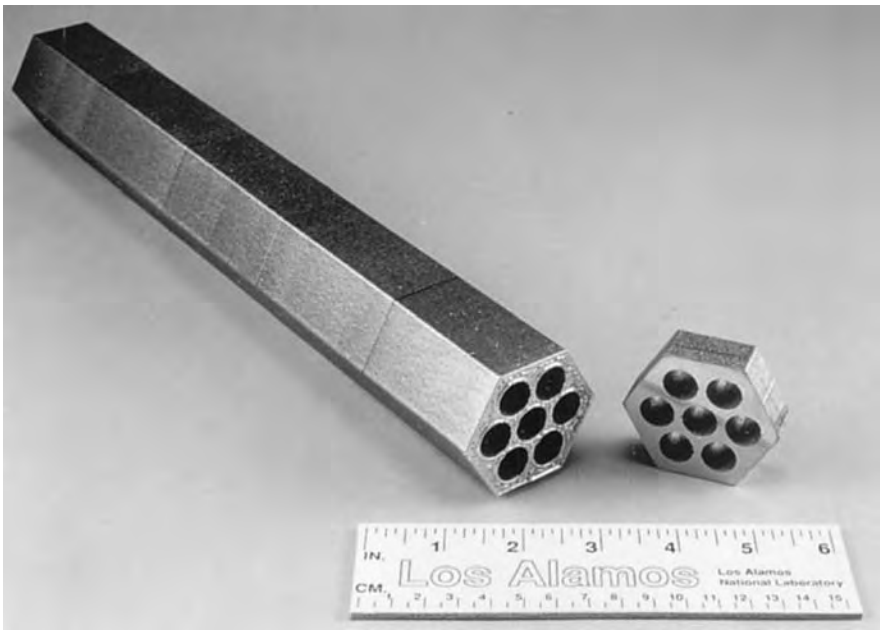


Fig. 43 Inconel 690 hexagon shape with hole array made by DLF. Courtesy of Los Alamos National Laboratories

Spray Forming

Spray forming involves atomizing a stream of molten metal into droplets and collecting the droplets, an approximately 50/50 mixture of liquid and solid, on a substrate before they fully solidify. The process is capable of producing various shapes such as billet, tubes, disks, and sheet (Ref 62–69). Spray-formed preforms can have a density up to about 99.8% of theoretical, but the material is normally HIP and/or hot worked to fully densify and improve properties. Compared to conventional P/M, the advantage of the process is the potential of lower cost because powder handling, canning, and the initial consolidation step are eliminated. Disadvantages of the process are a coarser structure and

Table 29 Tensile properties of Inconel 690 bar produced from powder by directed light fabrication

	0.2% yield strength		Tensile strength		Elongation,
Material condition	MPa	ksi	MPa	ksi	%
DLF, as deposited	448	65	668	97	49
DLF + 930 °C (1700 °F)/ 1 h	489	71	689	100	46
DLF + 980 °C (1800 °F)/ 1 h	475	69	682	99	46
DLF + 1040 °C (1900 °F)/ 1 h	448	65	668	97	47
DLF + 1090 °C (2000 °F)/ 1 h	385	56	648	94	52
Conventionally processed hot-rolled rod	372	54	737	107	50

Source: Ref 53

Table 30 Mechanical properties of PIM IN-718

Property	PIM IN-718	AMS 5596
Room-temperature tensile		
Tensile strength, MPa (ksi)	1350 (196)	1241 (180)
Yield strength, MPa (ksi)	1139 (165)	1034 (150)
Elongation, %	14	12
540 °C (1000 °F) tensile		
Tensile strength, MPa (ksi)	1119 (162)	…
Yield strength, MPa (ksi)	975 (141)	…
Elongation, %	14	…
650 °C (1200 °F) tensile		
Tensile strength, MPa (ksi)	1049 (152)	999 (145)
Yield strength, MPa (ksi)	904 (131)	827 (120)
Elongation, %	10	5
650 °C (1200 °F) stress rupture		
Rupture life, h	50	…
Rupture elongation, %	4	…
High-cycle fatigue (R = –1)		
Runout stress(a) at 430 °C (800 °F), MPa (ksi)	379 (55)	333 (48)
Runout stress(a) at 540 °C (1000 °F), MPa (ksi)	379 (55)	54 (369)
Runout stress(a) at 650 °C (1200 °F), MPa (ksi)	448 (65)	47 (326)

Note: Heat treatment: 950 °C (1750 °F)/1 h/air cool + 718 °C (1315 °F)/8 h/furnace cool at 100 °F per h to 620 °C (1150 °F)/6 h/air cool. (a) Runout = 10^7 cycles. Source: Ref 59

the inability to control inclusion size through particle sizing. The process was originally developed by Osprey Metals and is currently being commercially used to produce billet and tubular shapes of steels and corrosion-resistant alloys.

The application of spray forming to superalloys is currently being developed. The process is being considered for producing engine hardware such as disks and ring-shaped components. For superalloys, the process utilizes vacuum induction melting or electroslag melting to minimize inclusions.

Howmet Process. In a process developed by Howmet, designated Spraycast-X, metal is vacuum induction melted, argon atomized to a spray, and deposited onto a preheated rotating mild-steel mandrel. The resulting preform is then fully densified by HIP. Further processing may involve ring rolling or forging. In conjunction with Pratt & Whitney, the process is being evaluated for use in manufacturing engine hardware. A spray plus HIP plus ring-rolled IN-718 PW4000 high-pressure turbine case has been successfully tested (Ref 69).

General Electric Process. A process developed by General Electric (Ref 63) uses electroslag remelting of a vacuum induction electrode and a ceramic free-metal delivery system to minimize inclusion content (Fig. 44). Argon gas can be used for atomization, but gas entrapped in the structure can lead to pore formation with subsequent high-temperature exposure such as that encountered in forging, heat treatment, or welding. For this reason, nitrogen gas atomization is being explored (Ref 67, 68). Nitrogen reacts with most superalloys to form stable nitrides. As a results, pore formation does not occur during high-temperature exposure.

Alloys under Development. A number of different alloys have been spray formed and evaluated. These include René 95 (Ref 67), IN-718 (Ref 64, 68, 69), René 41 (Ref 64, 66), MERL 76 (Ref 67), Astroloy (Ref 67), Waspaloy (Ref 64), AF2-IDA (Ref 67), and AF115 (Ref 67). In most instances, the properties of spray-formed plus HIP and/or hot working are equal to or improved over those of cast and wrought material. For example, Fig. 45(a) to (c) compare the properties of spray-formed IN-718 with conventional wrought material. Figure 46 compares low-cycle fatigue data of spray formed plus electron beam welded René 41 with that of conventional wrought material. The low-cycle fatigue strength of the base metal was excellent, but that of the weld material was

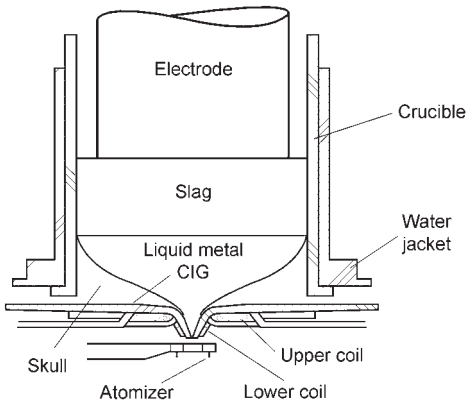


Fig. 44 Schematic of General Electric's clean metal spray forming concept. Source: Ref 63

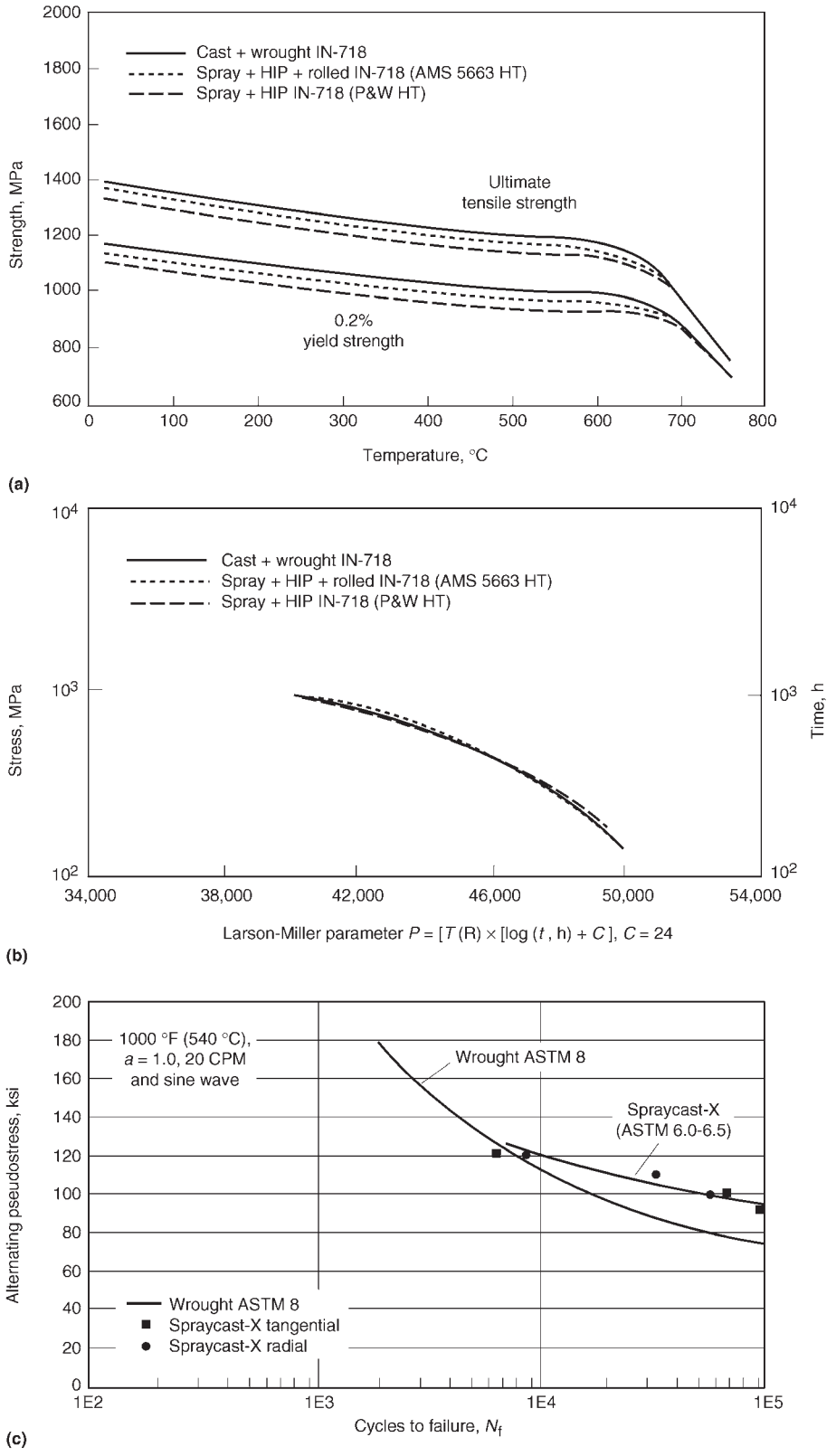


Fig. 45 Comparison of Spraycast-X and conventional cast and wrought IN-718. (a) Tensile properties. (b) Stress rupture properties. (c) Low-cycle fatigue properties. Source: Ref 69

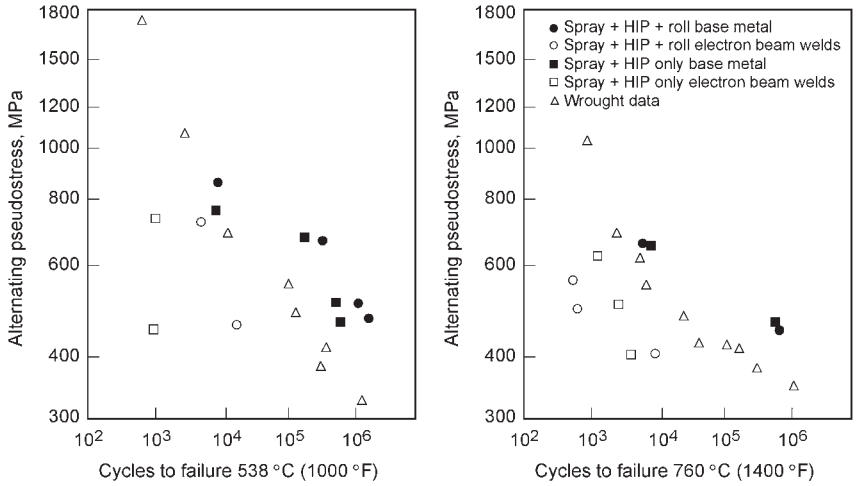


Fig. 46 Low-cycle fatigue data for spray formed René 41 (alternating pseudostress = strain range × Young's modulus/2). Source: Ref 66

low, apparently due to argon pore formation during welding.

ACKNOWLEDGMENT

This article was adapted from:

- M. Eisenmann, Porous Powder Metallurgy Technology, *Powder Metal Technologies and Applications,* Vol 7, *ASM Handbook,* ASM International, 1998, p 1031–1042
- G. Freeman, Production of Nickel Powder by Hydrometallurgical Processing, *Powder Metal Technologies and Applications,* Vol 7, *ASM Handbook,* ASM International, 1998, p 171–174
- W.V. Knopp, Roll Compacting of Metal Powders, *Powder Metal Technologies and Applications,* Vol 7, *ASM Handbook,* ASM International, 1998, p 389–395
- Mechanical Alloying, *Powder Metal Technologies and Applications,* Vol 7, *ASM Handbook,* ASM International, 1998, p 176–178
- J.H. Moll and B.J. McTiernan, Powder Metallurgy Superalloys, *Powder Metal Technologies and Applications,* Vol 7, *ASM Handbook,* ASM International, 1998, p 887–902
- Sintering of Nickel and Nickel Alloys, *Powder Metal Technologies and Applications,* Vol 7, *ASM Handbook,* ASM International, 1998, p 501–502
- C. Suryanarayana, Mechanical Alloying, *Powder Metal Technologies and Applications,* Vol 7, *ASM Handbook,* ASM International, 1998, p 80–90
- H.H. Tundermann, Carbonyl Vapor-metallurgy, *Powder Metal Technologies and Applications,* Vol 7, *ASM Handbook,* ASM International, 1998, p 167–171

REFERENCES

1. L. Mond, C. Langer, and F. Quinke, *Proc. Chem. Soc.*, Vol 86, 1890, p 112
2. W.M. Goldberger and D.F. Othmer, The Kinetics of Nickel Carbonyl Formation, *Ind. Eng. Chem., Process Des. Dev.*, July 1963, p 202–209
3. H.E. Carlton and W.M. Goldberger, Fundamental Considerations of Carbonyl Metallurgy, *J. Met.*, June 1965, p 611–615
4. D.G.E. Kerfoot, *CIM Bull.*, Vol 82 (No. 926), June 1997, p 136–141
5. M.T. Anthony and D.S. Flett, *Min. Ind. Int.*, Jan 1997, p 26–42
6. D.G.E. Kerfoot, *Ullmann's Encyclopedia of Industrial Chemistry*, Vol A 17, VCH, 1991, p 157–219
7. J.R. Boldt and P.E. Queneau, *The Winning of Nickel*, Longman Group, 1967
8. D.J.I. Evans, "The Production of Metals by Gaseous Reduction from Solution, I. Processes and Chemistry," Symposium on Advances in Extractive Metallurgy, Institution of Mining and Metallurgy, London, April 1967
9. F.D. Richardson and J.H.E. Jeffes, The Thermodynamics of Substances of Interest in Iron and Steelmaking from 0 °C to 2400 °C, *J. Iron Steel Inst.*, Vol 160, 1948, p 261
10. M.H.D. Blore et al., Pure Nickel Strip by Powder Rolling, *Met. Eng. Quart.*, Vol 6 (No. 2), 1966, p 54–60
11. V. Tracey, The Roll-Compaction of Metal Powders, *Powder Metall.*, Vol 12 (No. 24), 1969, p 598–612
12. N. Williams and V. Tracey, Porous Nickel for Alkaline Battery and Fuel Cell Electrodes: Production by Roll-Compaction, *Int. J. Powder Metall.*, Vol 4 (No. 2), 1968, p 47–62
13. G.E. Maurer, W. Castledine, F.A. Schweizer, and S. Mancuso, *Development of HIP Consolidated P/M Superalloys for Conventional Forging to Gas Turbine Engine Components*, Superalloys 1996, R.D. Kissinger et al., Ed., The Minerals, Metals and Materials Society, 1996 p 645–652
14. J.L. Bartos and P.S. Mathur, Development of Hot Isostatically Pressed (As-HIP) Powder Metallurgy René 95 Turbine Hardware, *Superalloys: Metallurgy and Manufacture, Proc. of the Third Int. Symp.*, B.H. Kear et al., Ed., Claitor's Publishing Division, 1976, p 495–508
15. General Electric Aircraft Engines
16. Crucible Compaction Metals, Oakdale, PA
17. M.M. Allen, R.L. Athey, and J.B. Moore, Nickel-Base Superalloy Powder Metallurgy—State of the Art, *Progress in Powder Metallurgy*, Vol 31, Metal Powder Industries Federation, 1975
18. J.E. Coyne, W.H. Couts, C.C. Chen, and R.P. Roehm, Superalloy Turbine Components—Which is the Superior Manufacturing Process: As-HIP, HIP + Isoforge or Gatorizing of Extrusion, *Powder Metallurgy Superalloys—Aerospace Materials for the 1980's*, Vol 1, MPR Publishing, 1980
19. Pratt & Whitney Aircraft, private communication, 1997
20. G.S. Hoppin, III and W.P. Danesi, Manufacturing Processes for Long-Life Gas Turbines, *J. Metal.*, July 1986, p 20–23
21. AlliedSignal Engine Division, private communication, Sept 1997
22. "Crucible Nickel Base Superalloy; Low Carbon Astroloy," Crucible Compaction Metals, Oakdale, PA
23. C. Ducrocq, A. Lasalmonie, and Y. Honnorat, N 18, A New Damage Tolerant PM Superalloy for High Temperature, *Superalloys 1988*, The Metallurgical Society, 1988
24. J.H. Davidson, G. Raisson, and O. Farel, The Industrial Development of a New PM Superalloy for Critical High Temperature Aeronautical Gas Turbine Components, *Int. Conf. on PM Aerospace Materials 1991*, MPR Publishing, 1992
25. J.C. Lautridou and J.Y. Guedou, Heat Treatment Upgrading on PM Superalloy N18 for High Temperature Applications, *Materials for Advanced Powder Engineering*, Part II, D. Coutsouradis et al., Ed., *SNECMA*, 1994, p 951–960
26. M. Soucail, M. Marty, and H. Octor, Development of Coarse Grain Structures in a Powder Metallurgy Nickel Base Superalloy N18, *Scr. Mater.*, Vol 34 (No. 4), 1996, p 519–525
27. D.D. Krueger, R.D. Kissinger, and R.G. Menzies, Development and Introduction of a Damage Tolerant High Temperature Nickel-Base Disk Alloy, René 88 DT, *Superalloys 1992*, S.D. Antolovich et al., Ed., The Minerals, Metals and Materials Society, 1992
28. K.A. Green, J.A. Lemsky, and R.M. Gasior, Development of Isothermally Forged P/M Udimet 720 for Turbine Disk Applications, *Superalloys 1996*, R.D. Kissinger et al., Ed., The Minerals, Metals and Materials Society, 1996, p 697–703
29. H. Hattory, M. Takekawa, D. Furrer, and R.J. Noel, Evaluation of P/M U720 for Gas Turbine Application, *Superalloys 1996*, R.D. Kissinger et al., Ed., The Minerals, Metals and Materials Society, 1996, p 705–711
30. U. Habel, J.H. Moll, F.J. Rizzo, and J.J. Conway, Microstructure and Properties

of HIP P/M 706, *Advanced Particulate Materials and Processes*, F.H. Froes et al., Ed., Metal Powder Industries Federation, 1997, p 447–455
31. U. Habel, F.J. Rizzo, J.J. Conway, R. Pishco, V.M. Sample, and G.W. Kuhlman, First and Second Tier Properties of HIP and Forged P/M 706, *Superalloys 718, 625, 706 and Various Derivatives*, E.A. Loria, Ed., TMS, 1997, p 247–256
32. A.S. Watwe, J.M. Hyzak, and D.M. Weaver, Effect of Processing Parameters on the Kinetics of Grain Coarsening in P/M 718, *Superalloys 718, 625, 706 and Various Derivatives*, E.A. Loria, Ed., TMS, 1997, p 237–246
33. J.L. Bartos, "Development of a Very High Strength Disk Alloy for 1400F Service," Air Force Materials Laboratory, Wright-Patterson Air Force Base, Dec 1974
34. H. Takigawa, N. Kawai, K. Iwai, S. Furuta, and N. Nagata, Process Development for Low-Cost, High-Strength PM Ni-Base Superalloy Turbine Disk, *Met. Powder Rep.*, Vol 44 (No. 9), Sept. 1989
35. K. Iwai, S. Furuta, and T. Yokomaku, Mechanical Properties of Ni-Base Superalloy Disks Produced by Powder Metallurgy, *Met. Powder Rep.*, Vol 43 (No. 10), Oct. 1988, p 664–666
36. K. Iwai, S. Furuta, T. Yokomaku, and H. Murai, Mechanical Properties of Ni-Base Superalloy Disks Produced by Powder Metallurgy, *R&D Kobe Steel Eng. Rep.*, Vol 37 (No. 3), 1987, p 11–14
37. "P/M CAP AF 2-IDA-6," Cytemp Specialty Steel Div., Preliminary Data Sheet, 11 May 1972
38. D.F. Gray, Mechanical Properties of Thick Section AF2-IDA-6 Powder Metal Turbine Rotors, *Rapidly Solidified Materials*, American Society for Metals, 1985, p 387–395
39. B. Ewing, F. Rizzo, and C. ZurLippe, Powder Metallurgy Products for Advanced Gas Turbine Applications, *Superalloys Processing, Proc. Second Int. Conf.*, Metals & Ceramic Info. Center, 1972
40. PM Aerospace Materials, *Met. Powder Rep.*, Vol 38 (No. 10), Oct 1983
41. B.A. Ewing, A Solid-to-Solid HIP-Bond Processing Concept for the Manufacture of Dual-Property Turbine Wheels for Small Gas Turbines, *Superalloys 1980*, J.K. Tien et al., Ed., American Society for Metals, 1980, p 169–178
42. D.J. Evans and R.D. Eng, Development of a High Strength Hot-Isostatically-Pressed Disk Alloy, MERL 76, *Modern Developments in Powder Metallurgy*, Vol 14, Metal Powder Industries Federation, 1980, p 51–63
43. J.S. Benjamin, *Sci. Amer.*, Vol 234 (No. 5), 1976, p 40–48
44. J.S. Benjamin, *Met. Powder Rep.*, Vol 45, 1990, p 122–127
45. J.S. Benjamin, Dispersion Strengthened Superalloys by Mechanical Alloying, *Metall. Trans.*, Vol 1, Oct 1970, p 2943–2951
46. J.M. Hyzak and S.H. Reichman, *Advances in High Temperature Structural Materials and Protective Coatings*, National Research Council of Canada, 1994, p 126–146
47. K. Iwai, S. Furuta, H. Takigawa, O. Tsuda, and N. Kanamaru, Dual-Structure PM Ni-Base Superalloy Turbine Disk; *PM Aerosp. Mater., 1991*, MPR Publishing, 1992, p 3-1
48. D.P. Mourer, E. Raymond, S. Ganesh, and J. Hyzak, Dual Alloy Disk Development, *Superalloys 1996*, R.D. Kissinger et al., Ed., The Minerals, Metals and Materials Society, 1996, p 637–643
49. Y. Bienvenu, M.L. Dupont, G. Lemaître, and F. Schwartz, A Study of the Powder Metallurgy Processing of Hybrid Nickel Based Superalloy Components, *Powder Metall.*, 1994, p 2053–2056
50. U. Lakshminarayan and K.P. McAlea, Advances in Manufacturing Metal Objects by Selective Laser Sintering (SLS™), *Advances in Powder Metallurgy & Particulate Materials—1996*, Vol 4, compiled by T.M. Cadle and K.S. Narasimhan, Metal Powder Industries Federation, p 15-129 to 15-138
51. B. Badrinarayan and J.W. Barlow, Effect of Processing Parameters in SLS of Metal-Polymer Powders, *Solid Freeform Fabrication Symposium Proc.*, University of Texas, Austin, 1995, p 55–63
52. G.K. Lewis, D.J. Thoma, R.B. Nemec, and J.O. Milewski, Directed Light Fabrication of Near-Net Shape Metal Components, *Advances in Powder Metallurgy & Particulate Materials—1996*, Vol 4, Parts 13–15, compiled by T.M. Cadle and K.S. Narasimhan, Metal Powder Industries Federation, p 15-65 to 15-76
53. G.K. Lewis, J.O. Milewski, D.J. Thoma, and R.B. Nemec, Properties of Near-Net Shape Metallic Components Made by the Directed Light Fabrication Process, Eighth Solid Freeform Fabrication Symposium, University of Texas, Austin, 11–13 Aug 1997
54. D.M. Keicher, J.A. Romero, C.L. Atwood, J.E. Smugeresky, M.L. Griffith, F.P. Jeantette, L.D. Harwell, and D.L. Greene, Free Form Fabrication Using the Laser Engineered Net Shaping (LENS™) Process, *Advances in Powder Metallurgy & Particulate Materials—1996*, Vol 4, Parts 13–15, compiled by T.M. Cadle and K.S. Narasimhan, Metal Powder Industries Federation, p 15-119 to 15-127
55. D.M. Keicher and J.E. Smugeresky, The Laser Forming of Metallic Components Using Particulate Materials, *JOM*, May 1997, p 51–54
56. J. Mazumder, J. Koch, K. Nagarthnam, and J. Choi, Rapid Manufacturing by Laser Aided Direct Deposition of Metals, *Advances in Powder Metallurgy & Particulate Materials—1996*, Vol 4, Parts 13–15, compiled by T.M. Cadle and K.S. Narasimhan, Metal Powder Industries Federation, p 15-107 to 15-118
57. J.J. Valencia, J. Spirko, and R. Schmees, Sintering Effect on the Microstructure and Mechanical Properties of Alloy 718 Processed by Powder Injection Molding, *Superalloys 718, 625, 706, and Various Derivatives*, E.A. Loria, Ed., the Minerals, Metals, and Materials Society, 1997, p 753–762
58. A. Bose, J.J. Valencia, J. Spirko, and R. Schmees, "Powder Injection Molding of Inconel 718 Alloy," National Center for Excellence in Metalworking Technology, Operated by Concurrent Technologies Corporation under contract No. N00140-92-C-BC49 to the U.S. Navy
59. R. Schmees, J. Spirko, and Dr. J. Valencia, "Powder Injection Molding (PIM) of Inconel 718 Aerospace Components," Pratt & Whitney, West Palm Beach, FL, and Concurrent Technologies Corporation, Johnstown, PA
60. K.F. Hens, J.A. Grohowski, R.M. German, J.J. Valencia, and T. McCabe, Processing of Superalloys via Powder Injection Molding, *Advances in Powder Metallurgy and Particulate Materials*, Vol 4, compiled by C. Lall and A.J. Neupaver, MPIF/APMI Int., 1994, p 137–148
61. E. Lang and M. Poniatowski, Production of Metallic Turbine Parts by the Powder Metallurgical Injection Molding Technique, *Mater. Technol. Testing*, Vol 18 (No. 10), Oct 1987, p 337–344
62. Spray Casting: A Review of Technological and Scientific Aspects, Book Series on Power Metallurgy, Vol 3, *Current Status of P/M Technology*, I. Jenkins and J.V. Wood, Ed., Institute of Metals, 1990
63. M. Hull, Spray Forming Poised to Enter Mainstream, *Powder Metall.*, Vol 40 (No. 1), 1997, p 23–26
64. R.P. Dalal and P.D. Prichard, Thermomechanical Processing of Spraycast-X Superalloys, *Spray Forming 2*, Woodhead Publishing, 1993, p 141–153
65. W. Reichelt et al., *Spray Deposition—An Innovative Method for Innovatory Products 49th International Congress on the Technology of Metals and Materials* (Brazil), Vol 5, Associacao Brasileira deMetalurgia e Materiais, 1995, p 161–170
66. E.S. Huron, Properties of Sprayformed Superalloy Rings, *Spray Forming 2*, Woohead Publishing, 1993, p 155–164
67. K.M. Chang and H.C. Fiedler, Spray-Formed High-Strength Superalloys, *Sixth Int. Symposium on Superalloys*, D.N. Duhl et al., Ed., TMS, Sept 1988
68. M.G. Benz, T.F. Sawyer, F.W. Clark, and P.L. Dupree, *Properties of Superalloys Spray Formed at Process Flow Rates of Less than 20 cm³/S*, GE Research & Development Center, Physical Metallurgy Laboratory 90CRD145, Aug 1990
69. N. Paton, T. Cabral, K. Bowen, and T. Tom, SPRAYCAST IN718 Processing Benefits, *Superalloys 718, 625, 706, and Various Derivatives*, E.A. Loria, Ed., TMS, 1997, p 1–16

ASM Specialty Handbook: Nickel, Cobalt, and Their Alloys
J.R. Davis, editor, p 230-234
DOI:10.1361/ncta2000p230

Copyright © 2000 ASM International®
All rights reserved.
www.asminternational.org

Heat Treating of Nickel Alloys

NICKEL AND NICKEL ALLOYS are, in some ways, easier to heat treat than many of the iron-base alloys that depend on carbon-related microstructural changes to achieve desired properties. Nickel is an austenite former, and in the nickel and high-nickel family of alloys, no allotropic phase transformations occur—the alloys are austenitic from the melting temperature down to absolute zero. While some precipitates such as carbides and the γ′ hardening phase may form, these do not change the basic austenitic-type structure of the matrix.

Because nickel is found in nature as nickel sulfide and nickel oxide ores, it has a natural tendency to combine with sulfur and/or oxygen. One of the most important factors to consider when heat treating nickel or the nickel alloys is to minimize exposure to sulfur, whether in solid form (such as lubricants, grease, or temperature-indicating sticks) or in gaseous form (such as SO_2 or H_2S). When embrittlement by sulfur occurs, there are no techniques that can be used to reclaim the affected material; the contaminated area must be either removed, such as by grinding, or scrapped.

Because nickel has a very low solubility for carbon in the solid state, it does not readily carburize. For this reason the nickel-chromium alloys, most notably Inconel 600, are used as fixtures in carburizing furnaces. Almost all heat treatment methods used with nickel and the nickel alloys are employed either to soften them, such as annealing, or to increase their strength, such as age hardening.

Types of Heat Treatment

Nickel and the nickel alloys may be subjected to one or more of six principal types of heat treatment, depending on chemical composition, fabrication requirements, and intended service. These methods include:

- *Annealing.* A heat treatment designed to produce a recrystallized grain structure and softening in work-hardened alloys. Annealing usually requires temperatures between 705 and 1205 °C (1300 and 2200 °F), depending on alloy composition and degree of work hardening
- *Solution annealing.* A high-temperature anneal (1150–1315 °C, or 2100–2400 °F) of certain nickel alloys to put carbides in solid solution and produce a coarse grain size for enhanced stress-rupture properties
- *Stress relieving.* A heat treatment used to remove or reduce stresses in work-hardened non-age-hardenable alloys without producing a recrystallized grain structure. Stress-relieving temperatures for nickel and nickel alloys range from 425 to 870 °C (800–1600 °F), depending on alloy composition and degree of work hardening
- *Stress equalizing.* A low-temperature heat treatment used to balance stresses in cold-worked material without an appreciable decrease in the mechanical strength produced by cold working
- *Solution treating.* A high-temperature heat treatment designed to put age-hardening constituents into solid solution. Normally applied to age-hardenable materials before the aging treatment
- *Age hardening* (precipitation hardening). A treatment performed at intermediate temperatures (425–870 °C, or 800–1600 °F) on certain alloys to develop maximum strength by precipitation of a dispersed phase throughout the matrix

Figure 1 shows the effect on room-temperature mechanical properties of cold-drawn Monel 400 rod when the rod is held for 3 h at various temperatures. Heating at 700 °C (1300 °F) or above produces the soft annealed condition, heating in the range of 400 to 595 °C (750–1100 °F) results in stress relieving, and heating in the range of 260 to 480 °C (500–900 °F) results in stress equalization, which produces an increase in the proportional limit, a slight increase in tensile strength, and no significant change in elongation. Figure 2 shows schematically the effect of annealing temperature on both the properties and grain structure of cold-worked nickel and nickel alloys.

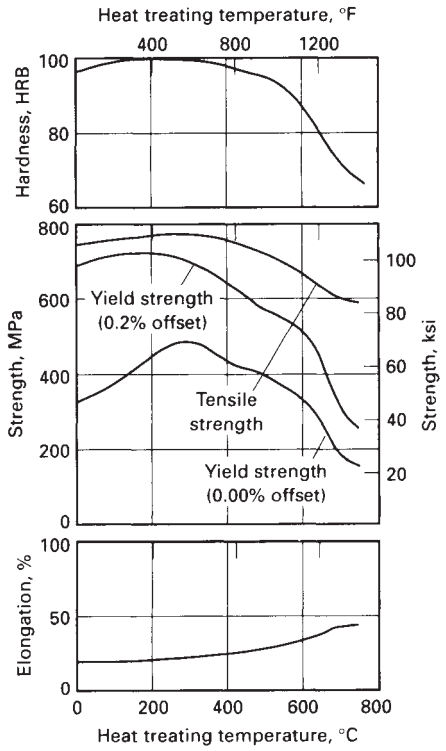


Fig. 1 Effects on room-temperature properties of cold-drawn Monel 400 rod held for 3 h at various temperatures

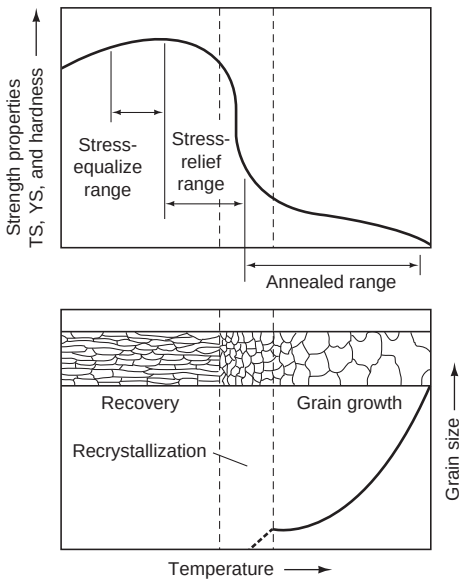


Fig. 2 Schematic representation of the effect of annealing temperature on the properties and grain structure/size of nickel alloys. TS, tensile strength; YS, yield strength

Annealing

The annealing of nickel and nickel alloys consists of heating the metal at a predetermined temperature for a definite time and then slowly or rapidly cooling it to produce a change in mechanical properties, usually a complete softening, as the result of recrystallization. Nickel and nickel alloys that have been hardened by cold-working operations, such as rolling, deep drawing, spinning, or severe bending, require softening before cold working can be continued. The thermal treatment used for softening is known as annealing, or soft annealing.

The differences in chemical composition among nickel and nickel alloys necessitate modifications in annealing temperatures (Table 1) and furnace atmospheres. The precipitation-hardening alloys must be cooled rapidly after annealing if maximum softness is desired. Annealing methods may be divided into three categories: batch, continuous, and specialty. These are described in the following paragraphs.

Batch annealing is a frequently used method of annealing because of its simplicity. It is the method of choice if the material requires a period of soak at temperature. The furnaces can be open (material exposed to products of combustion or direct radiant heat from electrical elements) or closed (material indirectly heated, that is, a muffle is used). Open annealing is used most often. The material to be annealed is heated at the selected temperature and protected from oxidation, in a fuel-heated furnace by the products of combustion and in an electric furnace by a reducing gas. During preliminary heating of the furnace, the burners may be adjusted for optimal combustion, but, before charging, the air supply should be reduced to provide the excess of reducing gases required. Also the top vents or dampers should be partly or fully closed to provide a positive gas pressure over the hearth, thereby preventing air leakage. Closed-annealing temperature control is just as critical as in open annealing. What dictates closed as opposed to open annealing is usually the undesirability of oxide on the work. Closed annealing invariably has a protective atmosphere within the enclosure to minimize oxidation during heat treatment. In most instances, the weight of the protective cover exceeds that of the work; consequently, the amount of fuel required, heat times, and cost are greater than in open annealing. Parts are usually carried into the furnace in alloy trays, and a protective atmosphere is introduced. The atmosphere flows continuously during annealing, pressurizing the furnace and preventing the infiltration of outside air. If the protective atmosphere is carbon monoxide (CO) or hydrogen (H_2), the gas should be flared off as it escapes the enclosure.

Continuous Annealing. A continuous-annealing facility is used when large volumes of product are involved and high throughput desired. Continuous furnaces are complex, requiring more frequent inspections and maintenance than a batch-type furnace, and the initial capital outlay is usually higher than for a comparable batch unit. Most continuous furnaces are of the open variety in which the nickel parts are exposed directly to the products of combustion. Temperature control is critical because the annealing period is short (Table 1). Continuous furnaces are not used for extended soaks; the hot-zone dwell time is quite short compared to a batch furnace. Also, temperature uniformity within the hot zone is more difficult to achieve because of the constant introduction of cold metal into the furnace. Closed annealing in a continuous furnace has the same characteristics as batch furnace annealing. The necessity to minimize oxidation is critical; the reducing atmosphere is continually introduced into the furnace, creating a positive furnace pressure. Most heat treatments of this nature take place in an alloy muffle or supertight furnace lined with high-quality alumina brick for better control of atmosphere and quality.

Specialty Annealing. These processes are so specialized and/or difficult that a separate category has been established to fully recognize their uniqueness. Specialty annealing methods include the use of vacuum furnaces, salt baths, and fluidized-bed furnaces. The percentage of nickel alloys heat treated in these types of facilities is small but growing. Brief descriptions are given below.

Vacuum Furnace. This type of furnace is used extensively for small parts. The furnace is usually heated electrically, and the hot zone evacuated to about 5 to 6 μm. A small amount of hydrogen is then added to maintain the low oxygen pressures needed to prevent oxidation. The hot zone is sometimes back-flushed with an inert or reducing gas for cooling purposes. Material must be very clean prior to annealing.

Salt Bath Furnace. Salt bath annealing is used for special work with small parts. Inorganic salts, such as chlorides and carbonates of sodium, potassium, and barium, which are relatively stable at temperatures considerably above their respective melting points, are fused in large metallic or refractory containers at

Table 1 Annealing, stress-relieving, and stress-equalizing schedules for nickels and nickel alloys

	Soft annealing							
	Continuous				Batch			
	Temperature				Temperature			
Material	°C	°F	Time(a), min	Cooling method(b)	°C	°F	Time, h	Cooling method
Nickel 200	815–925	1500–1700	½–5	AC or WQ	705–760	1300–1400	2–6	AC
Nickel 201	760–870	1400–1600	½–5	AC or WQ	705–760	1300–1400	2–6	AC
Monel 400	870–980	1600–1800	½–15	AC or WQ	760–815	1400–1500	1–3	AC
Monel R-405	870–980	1600–1800	½–15	AC or WQ	760–815	1400–1500	1–3	AC
Monel K-500	870–1040	1600–1900	½–20	WQ	870–1040	1600–1900	1–3	WQ
Inconel 600	925–1040	1700–1900	½–60	AC or WQ	925–980	1700–1800	1–3	AC
Inconel 601	1095–1175	2000–2150	½–60	AC or WQ	1095–1175	2000–2150	1–3	AC
Inconel 617	1120–1175	2050–2150	½–60	AC or WQ	1120–1175	2050–2150	1–3	AC
Inconel 625	980–1150	1800–2100	½–60	AC or WQ	980–1150	1800–2100	1–3	AC
Inconel 718	955–1065	1750–1950	½–60	AC	955–1065	1750–1950	1–3	AC
Inconel X-750	955–1150	1750–2100	½–60	AC	955–1150	1750–2100	1–3	AC
Hastelloy B-2	1095–1185	2000–2165	5–10	AC or WQ	1095–1175	2000–2150	1	AC or WQ
Hastelloy C-276	1215	2220	5–10	WQ	1215	2220	1	WQ
Hastelloy X	1175	2150	½–15	AC or WQ	1175	2150	1	AC or WQ

	Stress relieving				Stress equalizing			
	Temperature				Temperature			
Material	°C	°F	Time, min	Cooling method	°C	°F	Time, h	Cooling method
Nickel 200	480–705	900–1300	½–120	AC	260–480	500–900	1–2	AC
Nickel 201	480–705	900–1300	½–120	AC	260–480	500–900	1–2	AC
Monel 400	540–650	1000–1200	½–120	AC	230–315	450–600	1–3	AC
Inconel 600	760–870	1400–1600	5–60	AC	760–870	1400–1600	1–2	AC

(a) Times given represent actual ranges that thin sheet/strip products and heavy cross sections would receive in continuous furnaces. (b) AC, air cool; WQ, water quench

temperatures up to about 700 °C (1300 °F); at higher temperatures, heat resisting Fe-Ni-Cr alloy pots or refractory containers should be used. Excessive fuming of the bath is an indication that its maximum usable temperature has been exceeded.

Particular care must be exercised to remove all traces of sulfur from the fused salts in order to prevent embrittlement of the work. This may be accomplished in 2 to 3 h by adding to the fused chlorides and carbonates a small amount (≥0.5 kg, or 1 lb) of a mixture consisting (by volume) of three parts powdered borax and one part powdered charcoal. If testpieces of nickel strip or wire do not embrittle after 3 or 4 h in the purified salt bath, the desulfurizing treatment has been sufficient.

The material to be annealed is placed in the molten salts and absorbs heat rapidly. After being annealed, the work metal is quenched in water to free it from particles of the salt mixture. The annealed material will not be bright and may be flash pickled to achieve a bright surface.

Fluidized-bed furnace is a relatively new development. It has the excellent temperature uniformity and rapid heat-up features of the salt bath furnace, without the safety hazards associated with molten salt. Typically, a bed of 80 mesh alumina powder is fluidized by flowing a gas up through the material at 140 MPa (20 psig) pressure. The fluidizing gas is usually either air or metallurgical-grade nitrogen.

Dead-Soft Annealing. When the nickel alloys are annealed at higher temperatures and for longer periods, a condition commonly described as dead-soft is obtained, and the hardness numbers that result are 10 to 20% lower than those of the so-called soft condition. Because this treatment is accompanied by an increase in the grain size of the metal, it should be used only for those few applications in which grain size is of little importance.

Torch Annealing. Some large equipment is hardened locally by fabricating operations. If the available annealing furnace is too small to hold the workpiece, the hardened sections can be annealed with the flames of oil or acetylene torches adjusted so that they are highly reducing. The work should first be warmed gently with sweeping motions of the torch and should not be brought to the annealing temperature until sufficient preheating has been done to prevent cracking as a result of the sudden release of stress. (It should be noted that torch annealing is a poor method for general use because it provides irregular and insufficient annealing and produces heavily oxidized surfaces.)

Process Control Factors in Annealing

Among the more important process control factors in annealing nickel and nickel alloys are the selection of suitably sulfur-free fuels for heating, control of furnace temperature, effects of prior cold working and of cooling rates, control of grain size, control of protective atmospheres, and protection from contamination by foreign material.

Fuels for Heating. Nickel and nickel alloys are subject to intergranular attack when heated in the presence of sulfur or sulfur compounds. Fuels for heating must be low in sulfur content.

Gas is the best fuel for heating nickel alloys and should be used if available. Good heating is achieved readily with gas because of the ease with which gas can be mixed with air and its supply controlled. Gaseous fuels require little combustion space, and the automatic control of temperature and furnace atmosphere is easily accomplished.

Natural gas—consisting chiefly of methane (CH_4) and smaller amounts of ethane (C_2H_6), propane (C_3H_8), and butane (C_4H_{10}), and essentially free of sulfur compounds—is available in many areas.

Bright Annealing. The temperatures required for the soft annealing of nickel and nickel alloys are sufficiently high to cause slight surface oxidation unless the materials are heated in vacuum or in a furnace provided with a reducing atmosphere. Nickel 200, Monel 400, and similar alloys remain bright and free from discoloration when heated and cooled in a reducing atmosphere. However, nickel alloys containing chromium, titanium, and aluminum form a thin oxide film. Even if oxidation is not important, the furnace atmosphere must be suitably sulfur-free and not strongly oxidizing.

The protective atmosphere most commonly used in heating nickel and nickel alloys is that provided by controlling the ratio between the fuel and air supplied to burners firing directly into the furnace. A desirable reducing condition may be obtained by using a slight excess of fuel so that the products of combustion contain at least 4% carbon monoxide plus 4% hydrogen with no more than 0.05% uncombined oxygen. This is considered an 8% reducing atmosphere and can be obtained by burning an air-to-gas ratio of 9.25 to 1 of 1160 kJ (1100 Btu) natural gas.

Another method of maintaining desired conditions of furnace atmosphere is to introduce a prepared atmosphere into the heating and cooling chambers. This can be added to the products of combustion in a direct-fired furnace, although the introduction of prepared atmospheres is more commonly practiced with indirectly heated equipment.

Prepared atmospheres suitable for use with nickel and nickel alloys include dried hydrogen, dried nitrogen, dissociated ammonia, and cracked or partially reacted natural gas. Properties of various protective atmospheres are shown in Table 2. Nickels, modified nickels, and nickel-copper alloys can be bright annealed in all of these atmospheres (except for the first one listed in Table 2, that is, completely burned fuel, lean atmosphere) provided the dew point is 4.4 °C (40 °F) or lower. Inconel 600 and other alloys containing chromium, molybdenum, or both, require completely dissociated ammonia or dried hydrogen for bright annealing. A dew point of –51 °C (–60 °F) or lower is necessary with a positive furnace pressure.

The conditions for bright annealing should be maintained during heating, regardless of the method used for cooling. If facilities for cooling under protective atmosphere are not available, nickel and nickel alloys may be quenched in a 2% (by volume) solution of denatured

Table 2 Prepared atmospheres suitable for annealing of nickels and nickel alloys

Atmosphere 2 through 7 can be used for bright annealing of nickel, modified nickels, and nickel-copper alloys; atmosphere 4 or atmosphere 7 must be used for bright annealing of nickel alloys that contain chromium, molybdenum, or both.

	Atmosphere	Air-to-gas ratio(a)	Composition, vol %						Dew point (approximate)	
			H_2	CO	CO_2	CH_4	O_2	N_2	°C	°F
1	Completely burned fuel, lean atmosphere	10:1	0.5	0.5	10.0	0.0	0.0	89.0	Saturated(b)	Saturated(b)
2	Partially burned fuel, medium-rich atmosphere	6:1	15.0	10.0	5.0	1.0	0.0	69.0	Saturated(b)	Saturated(b)
3	Reacted fuel, rich atmosphere	3:1	38.0	19.0	1.0	2.0	0.0	40.0	20	70
4	Dissociated ammonia (complete dissociation)	No air	75.0	0.0	0.0	0.0	0.0	25.0	–55 to –75	–70 to –100
5	Dissociated ammonia, partially burned	1.25:1(c)	15.0	0.0	0.0	0.0	0.0	85.0	Saturated(b)	Saturated(b)
6	Dissociated ammonia, completely burned	1.8:1(c)	1.0	0.0	0.0	0.0	0.0	99.0	Saturated(b)	Saturated(b)
7	Electrolytic hydrogen, dried(d)	No air	100.0	0.0	0.0	0.0	0.0	0.0	–55 to –75	–70 to –100

(a) Based on use of natural gas containing nearly 100% methane and rated at 37 MJ/m^3 (1000 Btu/ft^3). For high-hydrogen manufactured gas (20 MJ/m^3, or 550 Btu/ft^3), ratios are about 50% of values listed. For manufactured gas with lower hydrogen and high carbon monoxide contents (17 MJ/m^3, or 450 Btu/ft^3), ratios are about 40% of values listed. For propane, ratios are about twice those listed. For butane, multiply listed values by three. (b) When atmosphere is cooled by tap water heat exchangers, dew point will be about 6–8 °C (10–15 °F) above the temperature of the tap water. Dew point may be reduced to about 5 °C (40 °F) by refrigeration equipment and to –55 °C (–70 °F) or lower by activated-absorption equipment. (c) Ratio of air to dissociated ammonia. (d) Dried to a dew point of –55 to –75 °C (–70 to –100 °F) by alumina plus molecular sieve

alcohol. This will reduce the oxide flash formed by the oxygen of the air during transfer from the furnace to the quenching tank.

Manufactured gases are produced from coal or oil, both of which may contain substantial amounts of sulfur. These gases should not be used unless the sulfur compounds are effectively removed during gas manufacture. Sulfur occurs in these manufactured gases as hydrogen sulfide (H_2S) and organic sulfides.

Suppliers of manufactured gas try to keep the total sulfur content of their product to a value below the maximum set by state regulatory agencies. Thus, manufactured gas supplied to consumers usually contains less than 6.9 g of total sulfur per 10 m^3 of gas (less than 30 gr per 100 ft^3). This sulfur content may vary considerably from day to day, but, where adequate maintenance of sulfur removal is observed by the gas supplier, total sulfur content will average 2.3 to 3.4 g per 10 m^3 (10–15 gr per 100 ft^3) or lower. This sulfur content is acceptable for heating nickel alloys; however, the generally accepted statutory limit (6.9 g per 10 m^3, or 30 gr per 100 ft^3) is marginal.

Two other satisfactory gaseous fuels are butane and propane, which are components of natural gas that liquefy and separate out when the gas is compressed. Both fuels are stored and shipped in tank cars that range in capacity from 30 to 57 m^3 (8,000–15,000 gal); the fuels may be distributed throughout a plant in pipelines as liquids under their own vapor pressures. Butane can be considered in a sense an oil fuel of high volatility, and proper means must be provided for gasifying it by heating, before it is mixed with air for combustion. Propane is more volatile and does not require the application of heat to convert it from liquid to gas. It is obtainable in cylinders equipped with pressure regulators to control the flow of gas. These cylinders are useful for occasional work in heating small objects.

Control of Furnace Temperature. The importance of the accurate control of annealing temperature cannot be overemphasized. Satisfactory indicating, controlling, recording, and controlling-recording pyrometers are available. Iron-Constantan and Chromel-Alumel thermocouples should be changed every three months (or more often, if required). Noble metal thermocouples such as platinum are the preferred method of measuring and monitoring temperature because of their inherent ability to resist diseasing at elevated temperatures. Their accuracy and sensitivity are equal to or better than those of the nonplatinum thermocouples. All thermocouples should be checked daily for accuracy.

Effect of Prior Cold Work. The greater the amount of cold work to which the material has been subjected before annealing, the lower the temperature required to produce the same degree of softness without increasing grain size and the shorter the time required at any one temperature.

The amount of any type of previous cold work also has a critical influence on the ductility of nickel and nickel alloys after annealing. If only a small amount of cold work is done (for example, ~10% reduction), full ductility for deep drawing and spinning cannot be restored by annealing because of excessive grain growth due to critical strain, even though the hardness is reduced to that of soft material. A minimum of approximately 20% cold working is required between anneals to ensure maximum ductility and softness following annealing.

Effect of Cooling Rate. Neither slow cooling, whether in or out of the furnace, nor rapid cooling by quenching has any specific effect on the softness of the annealed, solid-solution nickel materials. Therefore, rapid cooling is preferable (except for heavy sections, in which it may set up excessive thermal stresses), both as a time-saver and to minimize the amount of oxidation. Some of the age-hardenable alloys, such as Monel K-500, must be cooled rapidly by quenching from the annealing temperature to ensure the maximum response to subsequent age-hardening treatment.

Control of Grain Size. Coarse-grained material is unsuitable for most cold-working operations. A coarse grain in high-nickel materials cannot be refined by thermal treatment. It can be removed only by cold working sufficiently to effect recrystallization to a smaller grain size during a subsequent annealing treatment. Maximum workability is obtained with material that has been annealed without allowing appreciable grain growth to occur. The average grain diameter should not exceed 0.064 mm (0.0025 in.) (ASTM No. 5). This gives the best combination of ductility to permit extensive deformation, strength to withstand the action of tools, and surface quality to facilitate polishing.

Effect of Fluctuating Atmospheres. If nickel and nickel alloys are annealed in atmospheres that fluctuate between oxidizing (excess of air) and reducing (excess of carbon monoxide or hydrogen), severe intercrystalline attack will occur, with resulting embrittlement, even though the atmosphere is sulfur-free. This type of embrittlement can be prevented by maintaining a constant and sufficient excess of reducing atmosphere during heating and cooling. Alloys containing chromium or molybdenum are affected less than are nickel and nickel-copper alloys.

Protection from Contamination by Foreign Material. Many of the new lubricants used for deep drawing and spinning contain sulfur or lead and are removable with alkaline cleaner solutions at 80 °C (180 °F). Unless these elements are removed before annealing, they will cause embrittlement. The chlorohydrocarbons used in the past will no longer be permitted due to safety and ecological considerations. Alternate methods, such as water-soluble lubricants, will be required as more restrictive laws are enacted. Lubricants of any type should be removed entirely from the material before annealing. Paints and other adherent substances that may contain sulfur, as well as lead or similarly harmful ingredients, should be removed by appropriate methods before annealing.

Stress Relieving

In stress relieving, careful regulation of time and temperature is required. These variables are usually determined experimentally for each application; some typical ranges are given in Table 1. Figure 1 shows the effect of stress relief, at temperatures from about 400 to about 600 °C (750–1100 °F), on the room-temperature properties of Monel 400. Figure 2 shows the effect of stress relief on both properties and grain structure.

Stress Equalizing

Stress equalizing is a low-temperature heat treatment (Table 1) that results in what is known as partial recovery. This recovery, which precedes any detectable microscopic structural change, consists of a considerable increase in the proportional limit, slight increases in hardness and tensile strength (Fig. 2), no significant change in elongation or reduction of area, a balancing of stresses, and the return of electrical conductivity toward its characteristic value for the alloy in the annealed condition.

The temperature required for stress equalizing depends on the composition of the alloy. Figure 1 shows an optimal temperature range of approximately 230 to 315 °C (450–600 °F) for cold-drawn Monel 400 rod. A temperature of approximately 275 °C (525 °F) is recommended for commercial use. Long treatment time at this temperature has no detrimental effect.

Stress equalizing is usually applied to coil springs, wire forms, and flat spring stampings. If coil springs are to be given a cold "set," or cold pressing, after coiling, the stress equalization should be carried out *before* the setting operation, which involves stressing the material beyond the elastic limit. Any cold-working stresses set up by this operation are in a direction such that the stresses will benefit, rather than harm, the material. If stress is equalized *after* cold pressing, part of the beneficial cold-working stress is removed.

Age Hardening

The addition of niobium, aluminum, silicon, titanium, and certain other alloying elements to nickel and nickel alloys, separately or in combinations, produces an appreciable response to age hardening. The effect is dependent on both chemical composition and aging temperature; it is caused by the precipitation of submicroscopic particles throughout the grains, which results in a marked increase in hardness and strength.

Principal aging phases in the more highly alloyed nickel-base superalloys usually include one or more of the following: γ′ (Ni_3Al or Ni_3Al,Ti), η (Ni_3Ti), or γ″ (body-centered tetragonal Ni_3Nb). Secondary phases that may be present include: carbides ($M_{23}C_6$, M_7C_3, M_6C, and MC), nitrides (MN), carbonitrides (MCN), and borides (M_3B_2), as well as Laves phase (M_2Ti) and δ phase (orthorhombic Ni_3Nb). A more complete description of these phases can be found in the articles "Superalloys" and "Metallography and Microstructures of Heat Resistant Alloys" in this Handbook.

Prior Solution Treating. Unlike precipitation-hardening stainless steels and aluminum-base alloys, the nickel alloys normally do not require solution treating in the upper annealing temperature range prior to age hardening. However, solution treating may be used to enhance special properties (Table 3). For example, Inconel X-750 may be solution treated for 2 to 4 h at 1150 °C (2100 °F) and air cooled prior to a double (high and low temperature) aging cycle to develop maximum creep, relaxation, and rupture strength at temperatures above about 600 °C (1100 °F). This combination of heat treatments is considered essential for high-temperature springs and turbine blades made of Inconel X-750. Many aerospace applications require high tensile strength and fatigue strength, as well as good stress rupture properties. To achieve this combination in Inconel 718, the alloy is solution treated 1 to 2 h at 925 to 1010 °C (1700–1850 °F) and air cooled prior to a single aging cycle.

Age-hardening practices for several nickel alloys are summarized in Table 3 and in the article "Superalloys" in this Handbook. In general, nickel alloys are soft when quenched from temperatures ranging from 790 to 1220 °C (1450–2225 °F); however, they may be hardened by holding at 480 to 870 °C (900–1600 °F) or above and then furnace or air cooling. Quenching is not a prerequisite to aging; the alloys can be hardened from the hot-worked and cold-worked conditions, as well as from the soft condition.

Hardening Techniques. Nickel alloy parts are sometimes hardened in sealed boxes placed inside a furnace, although small horizontal or vertical furnaces without boxes may be used also. The box or furnace should hold the parts loosely packed, yet afford a minimum of excess space. Electric furnaces with hot fans provide the optimal temperature uniformity of ±6 °C (±10 °F) and the freedom from contamination required for this work. Gas-heated furnaces, particularly those of the radiant-tube type, can be made so that they give satisfactory results. It is difficult to obtain good results from oil heating, even with muffle furnaces. All lubricants should be removed from the work before hardening.

Because of the long aging time and the difficulty of excluding air from the box or furnace, truly bright hardening cannot be accomplished commercially. For semibright hardening, dry hydrogen (see atmosphere 7 in Table 2) or cracked and dried ammonia (see atmosphere 4 in Table 2) should be used. Care should be exercised in the use and handling of these gases in the age-hardening temperature range that happens to span the minimum ignition temperature of hydrogen, 575 °C (1065 °F). When bright or semibright hardening is not required, other atmospheres may be used, such as nitrogen, cracked natural gas free of sulfur, cracked city gas, cracked hydrocarbons, or a generated gas. The use of sulfur-free gases is necessary to avoid embrittlement.

Salt baths are used occasionally for small parts. The hardened material is never bright and must be flash pickled to restore the natural color. Inorganic salts are used, such as chlorides and carbonates of sodium and potassium, which are relatively stable at temperatures considerably above their respective melting points. It is extremely important that the salts be free of all trace of sulfur so that the work does not become embrittled. Fluidized beds can also be used for this process and are viable substitutes for salt baths without the hazards of molten salts.

Table 3 Solution-treating and age-hardening schedules for selected nickel alloys

	Solution treating				
	Temperature				
Alloy	°C	°F	Time, h	Cooling method	Age hardening
Monel K-500	980	1800	½–1	WQ	Heat to 595 °C (1100 °F), hold 16 h; furnace cool to 540 °C (1000 °F), hold to 6 h; furnace cool to 480 °C (900 °F), hold 8 h; air cool
Inconel 718 (AMS 5662)	980	1800	1	AC	Heat to 720 °C (1325 °F), hold 8 h; furnace cool to 620 °C (1150 °F), hold until furnace time for entire age-hardening cycle equals 18 h; air cool
Inconel 718 (AMS 5664)	1065	1950	1	AC	Heat to 760 °C (1400 °F), hold 10 h; furnace cool to 650 °C (1200 °F), hold until furnace time for entire age-hardening cycle equals 20 h; air cool
Inconel X-750 (AMS 5668)	1150	2100	2–4	AC	Heat to 845 °C (1550 °F), hold 24 h; air cool; reheat to 705 °C (1300 °F), hold 20 h; air cool
Inconel X-750 (AMS 5671)	980	1800	1	AC	Heat to 730 °C (1350 °F), hold 8 h; furnace cool to 620 °C (1150 °F), hold until furnace time for entire age-hardening cycle equals 18 h; air cool

WQ, water quench; AC, air cool

Thermomechanical Processing

In recent years there has been more interest in the interdependence of hot working and heat treating operations. In many critical applications, the desired final properties are not attainable via heat treatment if the hot-working operation has not been conducted under controlled temperature and deformation parameters. This requires a study of hot working and heat treating, known as thermomechanical processing. One application of thermomechanical processing is the development of direct age Inconel 718 for turbine disk applications. Proper heating temperatures and forging operations also influence the microstructure and distribution of phases in alloys such as 718.

Grain Size Control. An important objective of thermomechanical processing is grain size control. For example, grain structure may be controlled by thermomechanical processing in several iron-nickel-base alloys that have two precipitates present, such as the primary strengthening precipitate (γ″ Ni_3Nb in Inconel 718 and γ′ Ni_3Ti in Inconel 901) and a secondary precipitate (δ in Inconel 718 and η Ni_3Ti in Inconel 901). The secondary precipitate is produced first, by an appropriate heat treatment (8 h at 900 °C, or 1650 °F, for 901), followed by working at about 950 °C (1740 °F), below the η solvus. Final working is carried out below the recrystallization temperature, and the alloy is subsequently recrystallized below the η solvus. Finally, the alloy is aged by standard procedures. The result is a fine-grain alloy with higher tensile strength and improved fatigue resistance.

ACKNOWLEDGMENT

This article was adapted from D.J. Tillack, J.M. Manning, and J.R. Hensley, Heat Treating of Nickel and Nickel Alloys, *Heat Treating*, Vol 4, *ASM Handbook*, ASM International, 1991, p 907–912.

SELECTED REFERENCES

- C.R. Brooks, Nickel-Base Alloys, Chapter 5, *Heat Treatment, Structure and Properties of Nonferrous Alloys*, American Society for Metals, 1982, p 139–227
- D.A. DeAntonio, D. Duhl, T. Howson, and M.F. Rothman, Heat Treating of Superalloys, *Heat Treating*, Vol 4, *ASM Handbook*, ASM International, 1991, p 793–814

ASM Specialty Handbook: Nickel, Cobalt, and Their Alloys
J.R. Davis, editor, p 235-244
DOI:10.1361/ncta2000p235

Copyright © 2000 ASM International®
All rights reserved.
www.asminternational.org

Machining of Nickel Alloys*

THE MACHINING of nickel and nickel-base alloys can be readily accomplished providing fundamental principles affecting their machinability are understood and considered. Compared to other materials, the most significant characteristic of nickel alloys is that they are usually much stronger at metal cutting temperatures. Consequently, powerful and rigid machines provide the best results and often are essential for successful machining. Corollary to these property and machine requirements is that tooling be selected to minimize cutting forces, to have maximum edge strength, and to withstand the highest possible cutting temperatures.

In addition to an appreciation of the basic properties of nickel alloys themselves, of paramount importance to successful machining is an understanding of basic principles that come into play in relation to the particular alloy and the method of machining or tooling that is employed. For example, tooling that is optimum for the annealed condition may not be the best choice for hardened material.

In recent years there have been a number of advances in cutting tools and methods applicable to the machining of nickel alloys. This article gives an overview on machining nickel alloys using traditional and nontraditional methods and describes the advances that have been made. A number of very good and useful guides and reference books on the machining of nickel alloys have appeared over the years. They are listed in the Selected References and should be consulted for detailed information on machining conditions. The information in this article is based on the experience of producers and users of nickel alloys and of suppliers of cutting tools. This information should be considered only as a starting point in developing a machining program which then may require optimization to suit specific conditions.

Machinability Categories

Nickel alloys are used primarily in applications involving electrical properties or requiring good corrosion resistance or high strength and oxidation resistance at elevated temperatures. A great many alloys exist to meet these demanding applications, but they all have some properties in common that affect their machinability to a varying degree. They all have an austenitic structure which imparts properties of high ductility and work hardening producing a gummy machining behavior similar to that of austenitic stainless steels. In addition, those alloys designed for high temperature applications remain strong at the temperatures of chip formation during machining, and thermal conductivity is much less than that of steel and many other materials. The age hardening nickel alloys also contain abrasive titanium and aluminum particles. It is these factors that make nickel alloys more difficult to machine than steel, and it is an understanding of the extent to which each nickel alloy is affected by these factors that is the key to their successful machining.

Nickel alloys are classified into different categories according to their relative machining behavior as shown in Table 1. A different set of machining conditions is applicable to each category, and the first step for successful machining is for the programmer/machinist to identify the applicable category for the alloy to be machined. A listing of the common nickel alloys found in each category is also provided in Table 1. The metallurgical condition for some alloys must also be known for proper category classification. As can be seen from Table 1, many factors that define each category are those discussed previously in relation to nickel alloys in general. The relative importance of each factor, however, changes from category to category. This is illustrated for mechanical properties in Fig. 1, where a comparison is made to stainless and carbon steel. As one moves from steel to stainless and then to the nickel alloys, ductility, work hardening, and high-temperature strength gradually increase, denoting more difficult machining and, correspondingly, altered machining conditions.

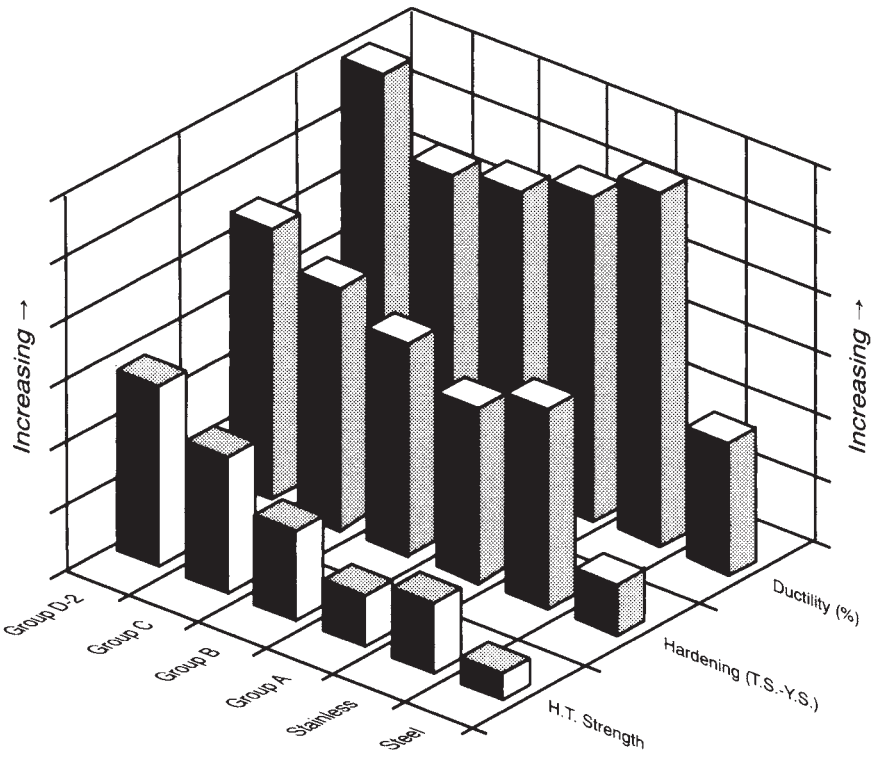


Fig. 1 Nickel alloys grouped according to increasing mechanical properties and resultant increasing difficulty to machine. H.T., high temperature; T.S., tensile strength; Y.S., yield strength

*Adapted from *Machining Nickel Alloys*, NiDI Publication No. 11 008, Nickel Development Institute, Toronto, Ontario, Canada. Used with permission.

Basic Principles Applicable to All Machining Operations

The avoidance of work hardening is of fundamental importance to the successful machining of all nickel alloys. Work hardening occurs when the metal ahead of the cutting tool, especially one that is cutting poorly, is plastically deformed. This hardened layer is very difficult to penetrate in subsequent passes or operations.

Techniques that minimize work hardening include the use of sharp cutting edges, positive rake angles, adequate clearance angles, avoidance of dwelling, and machines and setups having sufficient power and rigidity to keep vibration to a minimum. Feed rate and cutting depth should be set so that in following passes, cutting is done below the previously work hardened layer. For example, in turning, a depth of cut at least 0.38 mm (0.015 in.) is recommended if a following operation is planned, and the feed rate should be 0.13 mm (0.005 in.) or

Table 1 Nickel alloys grouped according to machining characteristics

Group	Group characteristic	Alloy	UNS No.	Ni	Cu	Fe	Cr	Mo	Co	Al	Ti	Nb	Other
A	Alloys containing essentially nickel for caustic alkali chemical and electrical applications. Lowest strength and work hardening of the nickel alloys. Exhibit gummy behavior in the annealed condition; hardenable only by cold working, which provides the best condition for machining	200	N02200	99.6	…	…	…	…	…	…	…	…	0.08 C
		201	N02201	99.6	…	…	…	…	…	…	…	…	0.01 C
		205	N02205	99.6	…	…	…	…	…	…	…	…	0.04 Mg, 0.04 C
		212	…	97.0	…	…	…	…	…	…	…	…	2.0 Mn, 0.05 C
		222	…	99.5	…	…	…	…	…	…	…	…	0.075 Mg
B	Nickel-copper and nickel-iron alloys for sulfuric acid and water corrosion and for electrical applications. Have higher strength, work hardened, than group A alloys have. Most alloys cannot be hardened by heat treatment, and best machining is obtained in cold-drawn or cold-drawn and stress-relieved conditions.	400	N04400	66.5	31.5	…	…	…	…	…	…	…	…
		401	N04401	42.5	55.5	0.3	…	…	…	…	…	…	1.6 Mn
		450	C71500	30.0	68.0	0.7	…	…	…	…	…	…	0.7 Mn
		36	K93600	36.0	…	64.0	…	…	…	…	…	…	…
		K	K94610	29.5	…	53.0	…	…	17.0	…	…	…	…
		MS 250	…	19.0	…	76.0	…	3.0	…	…	1.4	…	…
C	Mainly nickel-chromium and nickel-iron-chromium alloys for acid and high temperature corrosion applications. Similar in mechanical properties to austenitic stainless steels except for greater high temperature strength. These alloys are best machined in the cold-drawn or cold-drawn and stress-relieved conditions.	600	N06600	76.0	…	8.0	15.5	…	…	…	…	…	…
		690	N06690	61.0	…	9.0	29.0	…	…	…	…	…	…
		601	N06601	60.5	…	14.0	23.0	…	…	1.4	…	…	…
		825	N08825	42.0	2.2	30.0	21.5	3.0	…	…	1.0	…	…
		DS	…	37.0	…	41.0	18.0	…	…	…	…	…	2.3 Si
		330	N08330	35.5	…	44.0	18.5	…	…	…	…	…	1.1 Si
		20	N08020	35.0	3.5	37.0	20.0	2.5	…	…	…	0.6	…
		800	N08800	32.5	…	46.0	21.0	…	…	…	…	…	0.05 C
		800HT	N08811	32.5	…	46.0	21.0	…	…	Al + Ti	1.0	…	0.08 C
		802	N08802	32.5	…	46.0	21.0	…	…	…	…	…	0.4 C
		270	N02270	99.98	…	…	…	…	…	…	…	…	0.01 C
		K-500 (unaged)	N05500	65.5	29.5	1.0	…	…	…	2.7	0.6	…	…
		75	N06075	80.0	…	…	19.5	…	…	…	…	…	…
		86	…	64.0	…	…	25.0	10.0	…	…	…	…	0.03 Ce
D-1	This group consists of a limited number of age-hardened alloys in the solution annealed condition. These alloys are relatively easily machined.	301	N03301	94.0	…	…	…	…	…	4.4	0.6	…	…
		925	N09925	42.0	2.2	32.0	21.0	3.0	…	0.3	2.1	…	…
		902	N09902	42.5	…	49.0	5.3	…	…	0.5	2.4	…	…
D-2	This group consists of group D-1 alloys in the age-hardened condition. Most other age-hardenable alloys in both the solution annealed and hardened conditions, and some highly solution-strengthened alloys. They contain strong solution strengtheners and hard abrasive precipitates, which make machining difficult. These alloys should be rough machined in the solution annealed condition and then finish machined after aging. A size contraction up to about 0.07% takes place upon aging, which must be allowed for in rough machining.	301 (aged)	…	94.0	…	…	…	…	…	4.4	0.6	…	…
		K-500 (aged)	N05500	65.5	29.5	1.0	…	…	…	2.7	0.6	…	…
		902 (aged)	N09902	42.5	…	49.0	5.3	…	…	0.5	2.4	…	…
		81	…	67.0	…	…	30.0	…	…	0.9	1.8	…	…
		G-3	N06985	44.0	2.0	19.5	22.0	7.0	2.5	…	…	0.3	0.05 W
		HX	N06002	47.5	…	18.5	21.8	9.0	1.5	…	…	…	…
		625	N06625	61.0	…	2.5	21.5	9.0	…	…	…	3.6	…
		925 (aged)	N09925	42.0	2.2	32.0	21.0	3.0	…	0.3	2.1	…	…
		716	N07716	57.5	…	…	19.2	8.2	…	…	1.4	3.4	…
		725	N07725	57.0	…	9.0	20.8	8.2	…	…	1.4	3.4	…
		MA 754	N07754	77.5	…	1.0	20.0	…	…	0.3	0.5	…	0.6 Y_2O_3
		80A	N07080	76.0	…	…	19.5	…	…	1.4	2.4	…	…
		718	N07718	54.0	…	18.5	18.0	3.0	…	…	…	5.1	…
		PE11	…	39.0	…	34.0	18.0	5.2	…	0.8	2.3	…	…
		706	N09706	42.0	…	36.5	16.0	…	…	…	1.8	3.1	…
		PE16	…	43.5	…	…	16.5	3.3	…	1.2	1.2	…	…
		C-276	N10276	57.0	…	5.5	15.5	16.0	1.2	…	…	…	3.8 W, 0.5 Mn
		751	N07751	73.0	…	7.0	15.5	…	…	1.1	2.5	1.0	…
		X-750	N07750	73.0	…	7.0	15.5	…	…	0.7	2.5	1.0	…
		901	N09901	42.5	…	34.0	12.5	5.8	…	…	2.9	…	…
		617	N06617	52.0	…	1.5	22.0	9.0	12.5	1.2	…	…	…
		263	N07263	51.0	…	36.0	20.0	5.8	20.0	0.5	2.2	…	…
		105	…	54.0	…	…	15.0	5.0	20.0	4.7	1.3	…	…
		90	N07090	60.0	…	…	19.0	…	16.5	1.5	2.5	…	…
		PK50	…	58.0	…	…	19.5	4.25	13.5	1.4	3.0	…	…
		115	…	60.0	…	…	14.2	3.2	13.2	4.9	3.8	…	…
		B-2	N10665	66.0	…	1.0	0.5	27.5	…	0.1	0.1	…	0.05 Si
		903	N19903	38.0	…	41.5	…	…	15.0	0.9	1.4	3.0	…
		907	N19907	38.4	…	42.0	…	…	13.0	0.0	1.5	4.7	0.15 Si
		909	N19909	38.4	…	42.0	…	…	13.0	0.0	1.5	4.7	0.4 Si
E	A special alloy 400 designed to be free machining for high production on automatic screw machines	R-405	…	66.5	31.5	1.2	…	…	…	…	…	…	1.1 Mn, 0.04 S

larger. Vibration can be minimized by using the largest possible tools and holders and by limiting overhang. Power requirements should be determined whenever possible, but a rule of thumb is to operate at only up to approximately 50% of machine capacity. If, when machining nickel alloys, one finds that apparently the material "cannot be cut," the problem usually can be solved by addressing one or more of the preceding factors related to work hardening.

Choice of Cutting Tools. The cutting tool material choice must be consistent with the machining operation, the specific nickel alloy, and its metallurgical condition. Because of the high strength and work hardening of nickel alloys, small size drills, taps, reamers, and grooving tools, or operations involving interrupted cuts, usually require high-speed tools chosen on the basis of toughness. These tools must be run at quite low speeds, but they are often the only choice available with small tooling. When the operation allows for larger tools, carbide provides a good first choice for turning and some milling and drilling operations. The selection of a reasonably strong carbide grade used in conjunction with a positive rake angle will usually give good results in turning, provided machine horsepower and setup rigidity are adequate. Relatively large diameter short holes can be handled with carbide drills on rigid machining centers and numerically controlled (NC) lathes.

High-speed steel (HSS) tooling generally should be the initial choice for most milling operations because of resistance to shock, but carbide can be considered in some instances. The newer ceramic materials definitely have a place in turning the more difficult group C and D nickel alloys. They work very well and can give high metal removal rates providing they are used on very powerful and rigid machines.

The specific nickel alloy and its metallurgical condition also dictate the choice of tooling because of the wide range in hardness, strength and abrasiveness that can be encountered. The softer group A and B alloys lend themselves more to carbide tooling in interrupted roughing operations. For milling the harder alloys and for general finishing, HSS tooling with a sharp cutting edge often gives the best results. An exception is that ceramic tools can give very good turning results in finishing, again providing that the machine is adequate.

Lubricants and Coolants. In cutting nickel alloys, the choice of a cutting fluid is first based on whether cooling or lubrication is the primary consideration. Soluble water-based fluids are used in high-metal-removal-rate turning operations where heat removal is essential. These fluids are also used in turning with ceramics, but some ceramics cannot withstand thermal shock and require cutting without a cutting fluid. Oils are not recommended for ceramic tooling because of the danger of ignition. In low-speed cutting with HSS tools, a sulfur-chlorinated oil that has a viscosity adjusted to the operation is preferred. Normally, a high viscosity provides best tool life, but a lighter fluid aids in providing chip flushing in small deep holes. When using oil, the high temperatures of cutting may produce a brown sulfur stain. This stain is easily removed with various sodium cyanide or chromic-sulfuric acid cleaning solutions. The stain should be removed before any subsequent thermal treatment, including welding, or before use in high-temperature applications, because the sulfur could cause intergranular attack of the metal surface.

Recommendations for Machining

Turning, Boring, and Grooving

High-Speed Steel Tooling. Nickel alloys may be turned with most conventional cutting tool materials, but the programmer/machinist should know that productivity and economics will be highly dependent on an optimization of machine, tool, and cutting parameters. Table 2 gives speed and feed suggestions for the various alloy groups and the various cutting tool materials. Because of its relatively low cutting-speed limitation, HSS tooling only should be considered where high toughness is required,

Table 2 Turning and boring nickel alloys

			High speed steel (T15, M33, etc.)				Carbide					Other				
			Speed		Feed		Speed		Feed			Speed		Feed		
Alloy	Condition	Operation	m/min	sfm	mm/rev	ipr	m/min	sfm	mm/rev	ipr	Grade	m/min	sfm	mm/rev	ipr	Grade
Group A (nickel)	Annealed (45 HRB)	Finishing	18	60	0.21	0.008	…	…	…	…	…	…	…	…	…	…
		Roughing	15	50	0.76	0.030	…	…	…	…	…	…	…	…	…	…
	Cold drawn (95 HRB)	Finishing	61	200	0.10	0.004	…	…	…	…	…	117	385	0.20	0.008	Cast alloy
		Roughing	52	170	0.20	0.008	…	…	…	…	…	…	…	…	…	…
Group B (nickel-copper)	Annealed (65 HRB)	Finishing	21	70	0.20	0.008	99	325	0.20	0.008	C-6, 7	…	…	…	…	…
							99	325	0.20	0.008	C-2, 3	…	…	…	…	…
		Roughing	18	60	0.76	0.030	84	275	0.51	0.020	C-5, 6	…	…	…	…	…
							84	275	0.51	0.020	C-1, 2	…	…	…	…	…
	Cold drawn (100 HRB)	Finishing	30	100	0.13	0.005	122	400	1.02	0.040	C-5, 6, 7	53	175	0.20	0.008	Cast alloy
							91	300	1.02	0.040	C-3, 4	335	1100	0.15	0.006	Ceramic
		Roughing	27	90	0.25	0.010	107	350	0.20	0.008	C-2, 5, 6	244	800	0.20	0.008	Ceramic
Group C (Nickel-Cr & Ni-Cr-Fe)	Annealed (75 HRB)	Finishing	10	35	0.20	0.008	69	225	0.20	0.008	C-6	213	700	0.15	0.006	Ceramic
							40	130	0.20	0.008	C-2, 3	…	…	…	…	…
		Roughing	8	25	0.76	0.030	53	175	0.51	0.020	C-6	244	800	0.20	0.008	Ceramic
							27	90	0.51	0.020	C-1, 2	…	…	…	…	…
	Cold drawn (30 HRC)	Finishing	18	60	0.13	0.005	130	425	0.10	0.004	C-2	38	125	0.20	0.008	Cast alloy
							130	425	0.10	0.004	C-2	183	600	0.15	0.006	Ceramic
		Roughing	15	50	0.25	0.010	114	375	0.20	0.008	C-2	152	500	0.36	0.014	Ceramic
Group D-1 (age hardenable, unaged)	Annealed (80 HRB)	Finishing	15	50	0.20	0.008	76	250	0.02	0.006	C-7	…	…	…	…	…
		Roughing	12	40	0.76	0.030	61	200	0.51	0.020	C-6	…	…	…	…	…
Group D-1 (age hardenable)	Cold drawn (35 HRC)	Finishing	21	70	0.13	0.005	91	300	0.02	0.006	C-7	38	125	0.20	0.008	Cast alloy
		Roughing	18	60	0.25	0.010	76	250	0.25	0.010	C-6	…	…	…	…	…
Group D-2 (age hardenable)	Annealed (85 HRB)	Finishing	6	20	0.13	0.005	40	130	0.13	0.005	C-2	183–488	600–1600	0.15	0.006	Ceramic
		Roughing	5	15	0.25	0.010	23	75	0.20	0.008	C-2	76–305	250–1000	0.25	0.010	Ceramic
	Cold drawn (45 HRC)	Finishing	5	18	0.10	0.004	34	110	0.13	0.005	C-2	122–396	400–1300	0.10	0.004	Ceramic
		Roughing	4	12	0.20	0.008	21	70	0.18	0.007	C-2	91–213	300–700	0.20	0.008	Ceramic
Group E (free machining)	Annealed (65 HRB)	Finishing	24	80	0.20	0.008	99	325	0.02	0.006	C-6	…	…	…	…	…
		Roughing	21	70	0.76	0.030	84	275	0.51	0.020	C-6	…	…	…	…	…
	Cold drawn (100 HRB)	Finishing	40	130	0.13	0.005	122	400	0.10	0.004	C-7	61	200	0.20	0.008	Cast alloy
		Roughing	37	120	0.25	0.010	107	350	0.20	0.008	C-7	…	…	…	…	…

as in the case of interrupted cuts, or where a very fine surface finish is required. High-speed steel tooling can provide reasonable productivity when used with the softer group A and group B alloys but is severely limited when working with nickel alloys in the age-hardened condition. With HSS, good advantage can be taken with positive rake angles to facilitate cutting and to minimize work hardening. Relief angles should be generous enough to avoid rubbing and consequent work hardening and yet not so large as to inadequately support the cutting edge. Positive back-rake angles will range from 0 to 8° for roughing and finishing, respectively, and clearance angles will be in the range of 6 to 8°. The premium grades of HSS that provide the maximum combination of strength, wear, and heat resistance, will be cost effective in relation to the value of the nickel alloys machined.

Carbide tooling should be considered for the general machining of the stronger alloys in groups B and above. The key to success with carbide is to use powerful machines and rigid setups to minimize vibration. Generally, it is found that a positive cutting angle can be used if sufficient rigidity and power are available. The selection of carbide grade will then be a matter of obtaining adequate edge strength for any given set of cutting conditions. The premium coated grades with chip breakers will generally prove economical. Because of the high strength of the nickel alloys, close attention should be paid to factors which affect edge strength, honing, and nose radius. The benefits of positive rake and adequate relief angles also apply to carbide cutting tools.

Ceramic Tooling. For the purpose of this article, *ceramics* are defined as all of the advanced cutting-tool materials beyond coated carbides. These ceramics are described and their properties compared to conventional materials in Table 3, which also gives representative cutting conditions. With the exception of polycrystalline diamond, all of the ceramics have application in the machining of nickel alloys. The greatest field of application for ceramics is in turning, because they perform best at high cutting speeds under conditions where high toughness and impact strength are less important. The limited toughness of ceramics requires the use of very rigid, precision, and powerful machine tools that have minimal high-speed vibration capacity. However, accepting these limitations, nickel alloys can be very efficiently machined with these materials.

Figures 2 and 3 illustrate the cutting speeds that can be obtained with the various ceramic tool materials in turning annealed and hardened group D-2 alloy. Speeds of 5 to 15 times that of carbide are possible depending on the particular ceramic. The two most versatile classes of ceramic used with nickel alloys are the Sialon and whisker-reinforced alumina types, which can be run at speeds of 244 to 488 m/min. (800 to 1600 sfm) on the very difficult to machine group D-2 alloys. The other ceramic classes fall into more specialized niches such as high-speed finishing with cermets or machining very hard alloys with composite alumina or cubic boron nitride. There are also variations in machinability among the group D-2 alloys, which also need to be taken into consideration. A

Table 3 Comparison of tool materials for turning group D-2 nickel alloys

Tool material	Tool characteristics	Machining condition	Annealed (180–250 HB)		Aged (250–375 (HB)	
			Roughing	Finishing	Roughing	Finishing
High-speed steel (HSS)	Steel with alloy carbides; good strength and toughness; poor heat resistance; for small tools, interrupted cuts, and low rigidity applications	DOC, mm (in.)	6.35 (0.22)	1.52 (0.06)	6.35 (0.25)	152 (0.06)
		mm/rev	0.25	0.13	0.20	0.10
		ipr	0.010	0.005	0.008	0.004
		m/min	5	6	4	5
		sfm	15	20	12	18
Carbide	Cobalt binder containing W, Ti, and Ta carbides; combine good toughness and good high-temperature resistance; for general purpose, use on machines of limited power	DOC, mm (in.)	6.35 (0.25)	1.52 (0.06)	0.51 (0.02)	1.02 (0.04)
		mm/rev	0.38	0.18	0.20	0.13
		ipr	0.015	0.007	0.008	0.005
		m/min	30	40	21	32
		sfm	100	130	70	105
Coated carbide	Combine tough carbide base and wear resistant coatings; improved tool life compared to basic carbide grades; improved productivity compared to uncoated carbide	DOC, mm (in.)	6.35 (0.25)	1.52 (0.06)	0.51 (0.02)	1.02 (0.04)
		mm/rev	0.25	0.18	0.20	0.13
		ipr	0.010	0.005	0.008	0.005
		m/min	244	46	183	35
		sfm	120	150	80	115
Silicon aluminum nitride (Sialon)	Hot pressed monolithic silicon aluminum oxynitride; excellent toughness and thermal resistance; good overall performance	DOC, mm (in.)	6.35 (0.25)	1.52 (0.06)	2.54 (0.10)	0.51 (0.02)
		mm/rev	0.25	0.18	0.20	0.13
		ipr	0.010	0.007	0.008	0.005
		m/min	244	395	183	244
		sfm	800	1000	600	800
Whisker-reinforced alumina (Re alumina)	Aluminum oxide with silicon whiskers; best combination of edge strength, shock, and thermal resistance; excellent overall performance in roughing and finishing	DOC, mm (in.)	6.35 (0.25)	1.52 (0.06)	3.18 (0.125)	0.51 (0.02)
		mm/rev	0.20	0.15	0.18	0.10
		ipr	0.008	0.006	0.007	0.004
		m/min	305	488	213	396
		sfm	1000	1600	700	1300
Cermet	Composite titanium carbide and titanium nitride; excellent abrasion and crater resistance, poor toughness; limited to high-speed finishing at light feed and DOC	DOC, mm (in.)	1.52 (0.06)	1.02 (0.04)	NR	0.51 (0.02)
		mm/rev	0.15	0.13	NR	0.08
		ipr	0.006	0.005	NR	0.003
		m/min	76	183	NR	122
		sfm	250	600	NR	400
Composite alumina	Cold or hot pressed alumina and titanium carbide; hot pressed grades have high edge strength; primarily for machining materials over 35 HRC in hardness	DOC, mm (in.)	152 (0.06)	0.51 (0.02)	1.02 (0.04)	0.51 (0.02)
		mm/rev	0.36	0.13	0.25	0.10
		ipr	0.014	0.005	0.010	0.004
		m/min	213	395	152	213
		sfm	700	1000	500	700
Cubic boron nitride (CBN)	Composite of cubic boron nitride in a metal binder; combines highest hardness with excellent toughness; primarily for machining materials over 45 HRC	DOC, mm (in.)	3.18 (0.125)	0.51 (0.02)	1.52 (0.06)	0.51 (0.02)
		mm/rev	0.36	0.15	0.20	0.10
		ipr	0.014	0.006	0.008	0.004
		m/min	152	244	91	152
		sfm	500	800	300	500
Polycrystalline diamond	Composite of diamond crystals; highest hardness and wear resistance; not recommended for nickel alloys due to chemical incompatibility	DOC, mm (in.)	NR	NR	NR	NR
		mm/rev	NR	NR	NR	NR
		ipr	NR	NR	NR	NR
		m/min	NR	NR	NR	NR
		sfm	NR	NR	NR	NR

DOC, depth of cut; NR, not recommended

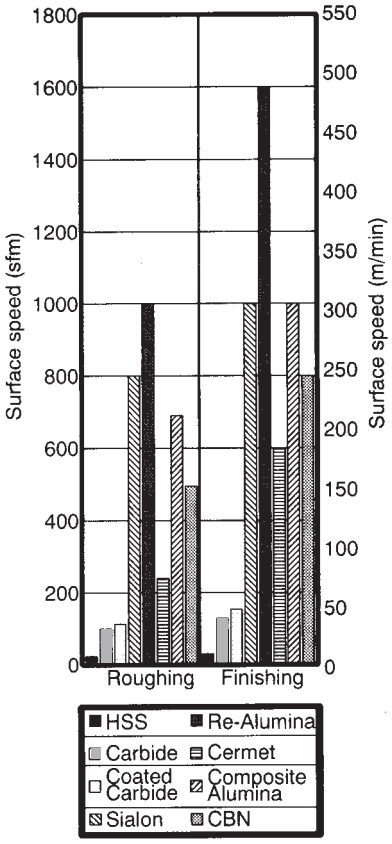


Fig. 2 Typical cutting speeds for cutting tool materials when turning annealed group D-2 nickel alloys

machinability index for turning some of these alloys with whisker-reinforced alumina tooling is given in Fig. 4. It is apparent from Fig. 4 that substantial adjustments in cutting conditions from general recommendations for group D-2 alloys have to be made in some cases.

Each of the ceramic classes have different properties and require somewhat different machining practices, and this may at times be true for ceramics within the same class produced by different manufacturers. Because of the large number of ceramics now available, it is impossible to make specific machining practice suggestions other than that the manufacturer recommendations should always be closely followed as a starting point.

Consideration of the characteristics of a whisker-reinforced alumina ceramic illustrates some important points involved. This material is characterized as having very good fracture and temperature resistance, as well as resistance to thermal shock.

It is paramount in working with ceramics of this kind to recognize that having a high cutting temperature is desirable and that notching of the insert at the cutting line is to be avoided for maximum insert life. Recognizing that the programmer is a key element in the efficient use of ceramics is most important, and programs should take into consideration all practices which maximize ceramic performance. Therefore, the first step for the programmer is to plan speeds and feeds that generate a high metal cutting temperature and that are consistent with the hardness of the material. In this situation, hardness is more important than chemical variations between different nickel alloys. Nomograms (see Fig. 5) taking these factors into consideration have been developed to aid the programmer. In addition to the effect of hardness, Fig. 5 demonstrates the critical relationship between speed and feed. Any reduction in speed must be accompanied by a corresponding reduction in feed. This allows the heat to be concentrated in the chip, thus maintaining a high cutting temperature and low cutting force. The only exception to this is that if the chip becomes too thin to carry away the required heat, the temperature rises excessively. In this case, coolants that can be used with whisker-reinforced alumina will carry away the excessive heat without damage to the tool because of the excellent thermal shock resistance of the whisker-reinforced alumina.

Insert selection and method of use are of extreme importance in realizing the potential of ceramic inserts with nickel alloys. The two primary rules of insert selection are the following:

- Use round inserts
- Use the largest lead angle whenever possible

Both of these rules help to minimize the depth-of-cut (DOC) notch effect that is a weakness of ceramics. A larger lead angle will reduce cutting pressure, and a round insert will have a larger lead angle for a given DOC. It is important to realize that relationships exist between insert diameter or nose radius and the depth of cut that maintains the maximum effective lead angle. The choice of a round insert is also advantageous because it can be rotated to

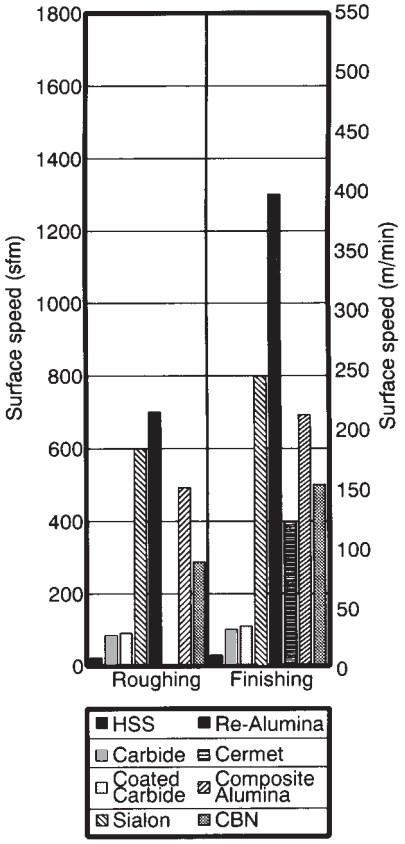


Fig. 3 Typical cutting speeds for cutting tool materials when turning hardening group D-2 nickel alloys

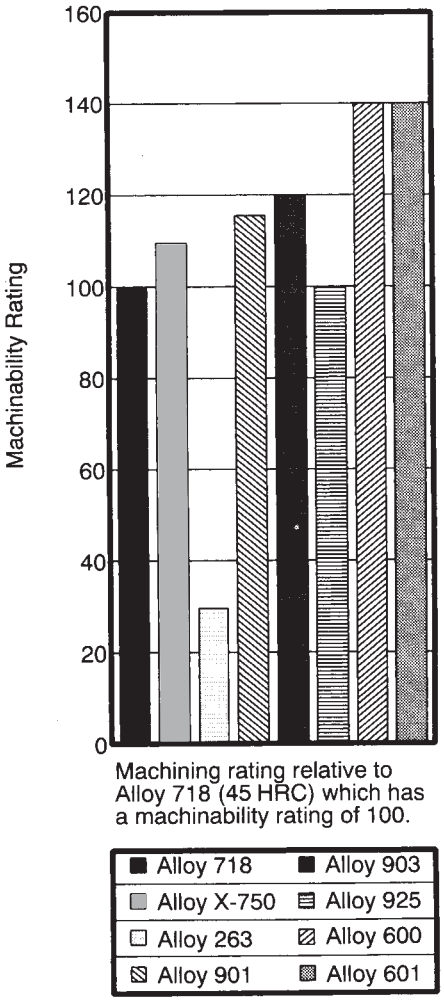


Fig. 4 Machinability rating of nickel alloys in turning with whisker-reinforced alumina tooling

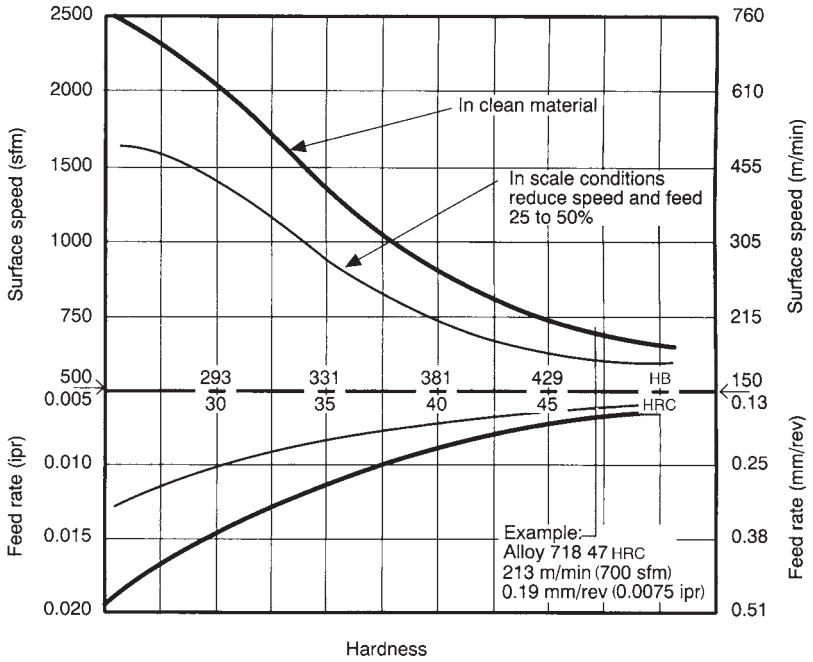


Fig. 5 Nomogram showing the balance in speed and feed required to obtain the high cutting temperature necessary for machining nickel alloys with whisker-reinforced alumina inserts

move the DOC notch away from the line of cut numerous times to extend the insert life beyond that obtainable in an angular insert. This advantage of round inserts compared to square inserts is shown in Fig. 6(a). When a round insert is indexed repeatedly for maximum edge utilization, as shown in Fig. 7, the DOC notch is minimized significantly.

Taking the correct tool path is the most important action that the programmer can take to eliminate notching. There are many techniques for doing this depending on the particular part geometry and machining operation. For example, in prechamfering the corner entry point, the normally selected direction of tool movement will exacerbate the notch effect and be undesirable, as shown in Fig. 6(b). If the direction of feed is aligned at 90° to the chamfer, the depth of cut line continually moves along the insert edge, eliminating any notch effect.

In turning long surfaces, ramping is a very effective technique for extending insert life. This technique involves programming a gradual change in DOC as the insert traverses the length of the cut. This is illustrated in Fig. 6(c), which shows that the DOC line again continually moves along the insert edge. An alternative but less effective method than ramping is to simply avoid taking multiple passes at a constant depth of cut. These are just two of the many ways that the programmer can choose an optimum tool path that will greatly facilitate the machining of nickel alloys with all kinds of tooling.

Other Factors Related to Ceramic Tooling. A number of other factors should be considered in machining nickel alloys with ceramic tooling. Work hardening should be avoided, although this is not quite as important as with other types of tooling because of the higher cutting temperature. Some ceramics, such as whisker-reinforced alumina, can be used without an edge hone; the sharper edge reduces work hardening and produces the best obtainable surface finish. A larger clearance angle minimizes work hardening effects, and some ceramics can be used at larger clearance angles than others. Cutting conditions should be adjusted to avoid impinging the hot chip directly onto the machined surface because the high temperature of the chip may cause it to weld to the surface. Coolants should not be used with most ceramics because of their generally low resistance to thermal shock. However, in the case of the ceramics that do have good thermal shock resistance (for example, whisker-reinforced alumina), the coolant will be helpful in managing the hot chip and in providing part size control.

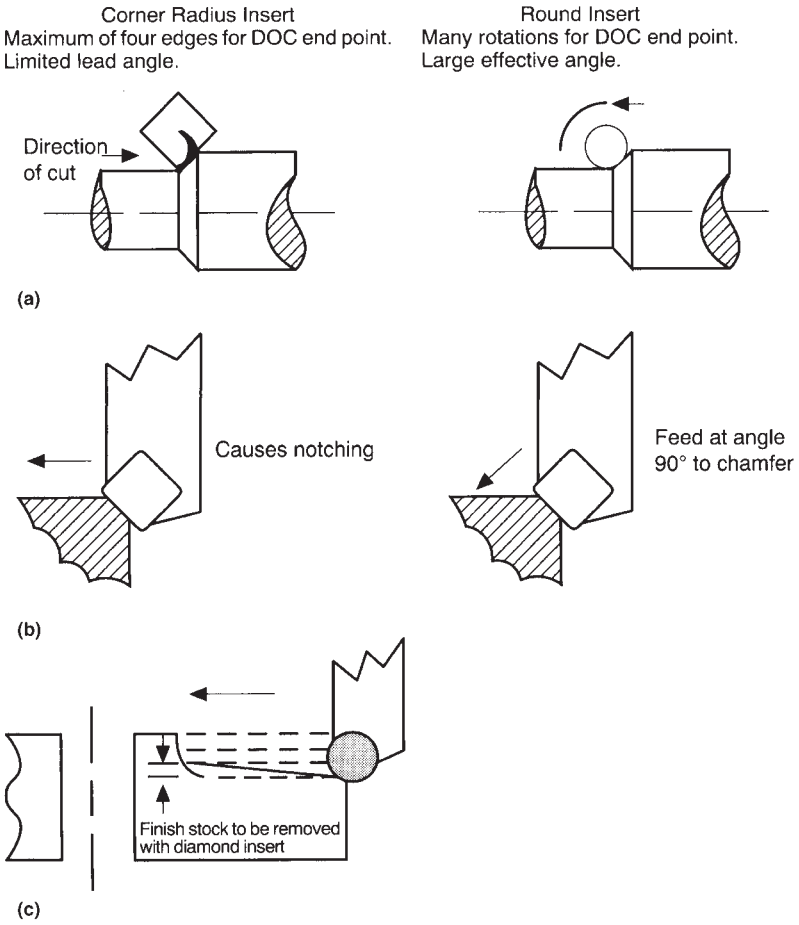


Fig. 6 Programming and tooling techniques that will increase tool life when machining nickel alloys with carbide and ceramic tooling. DOC, depth of cut. (a) Turning: A round insert will produce maximum tool life by giving a large lead angle and many rotations to avoid depth of cut failures. (b) Chamfering: Feeding perpendicular to a chamfer produces maximum tool life by distributing the depth of cut wear across the cutting edge. (c) Ramping: This technique will continually move the depth of cut line along the cutting edge, eliminating the notch effect and increasing tool life. Courtesy of Greenleaf Corporation

Drilling

Twist Drills. For the successful drilling of nickel alloys with twist drills, the most important consideration is to provide positive cutting and to minimize dwell to avoid work hardening. Satisfactory results can be obtained with conventional high-speed twist drills, and work hardening can be minimized if careful attention is given to the considerations known to affect twist-drill performance. Setups should be rigid, and short drills or guides should be used. A typical drill geometry would be 118° point angle, 29° helix, 12° lip relief angle, and a chisel angle of 125 to 135°. Drills should always be machine sharpened, and as the drill is shortened from resharpening, the web should be thinned to maintain a positive effective rake and reduce cutting pressure. The tougher high-speed steel grades should be selected for smaller diameter holes, while in larger drills, the cobalt grades will give better tool life. Solid carbide drills are not normally recommended because of their toughness limitation, but carbide tipped drills may prove satisfactory. Oil-hole drills are useful, and in all cases, a high quality, sulfurized oil flooding the hole should be used. Suggested starting conditions for twist drilling are given in Table 4.

Insert Drills. Large diameter, short holes may be drilled with insert drills on computer numerically controlled (CNC) lathes and machining centers of adequate rigidity and power. A rigid setup and accurate alignment are essential for good performance. With a good setup, tooling and inserts giving a positive rake angle are recommended to minimize cutting forces and work hardening. Through-the-tool lubricant at a pressure of 0.31 to 0.52 MPa (45 to 75 psi) and 45 L (10 gal) per minute flow is recommended, although lower flow rates may be used in some horizontal situations involving shallow holes. Suggested insert drilling conditions are given in Table 5.

Deep-Hole Drilling. Depending on hole diameter and depth, crankshaft, spade, and gun drills are all options for deep-hole drilling in nickel alloys. However, again because of high strength and work hardening, the need to provide positive feed is extremely important with these types of drills. Under the best of conditions, drilling rates will be low, as suggested by the deep hole drilling conditions given in Tables 6 and 7.

Deep-Hole Drilling by Nontraditional Methods. For production or semiproduction work involving a large number of deep or small diameter holes, one of the newer nontraditional machining methods should be considered. These methods are not sensitive to material mechanical properties and, so, are ideal for nickel

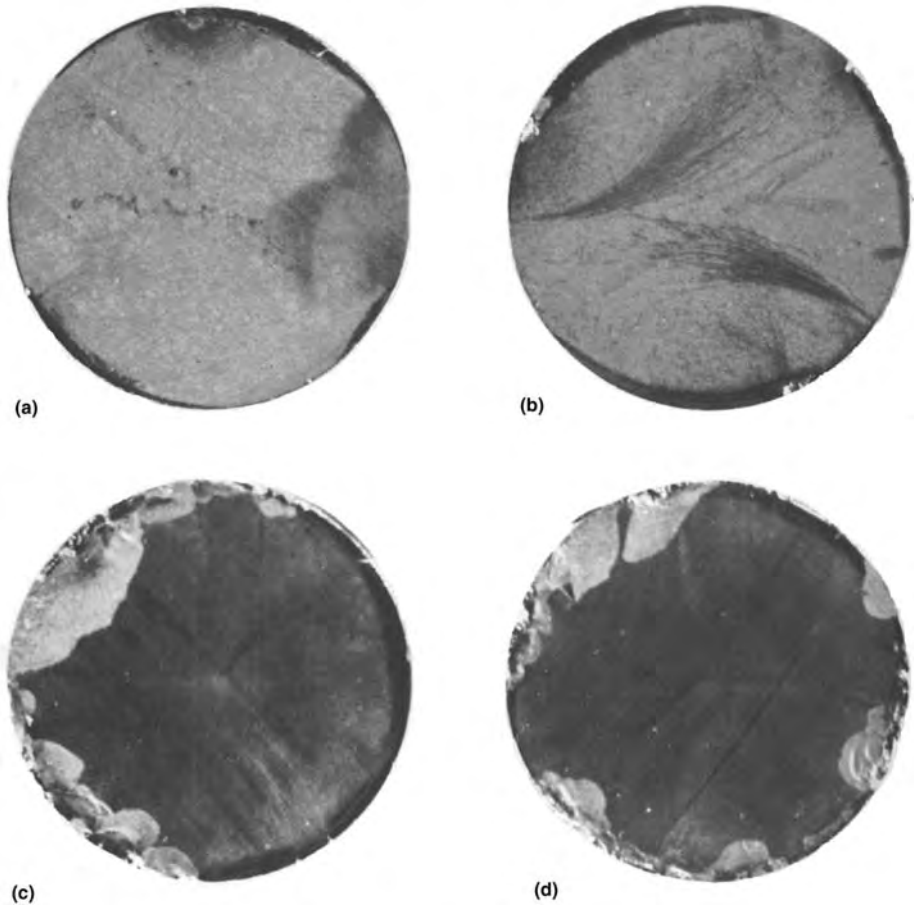


Fig. 7 Appearance of whisker-reinforced alumina ceramic inserts showing that characteristic flaking allows continued useful life and the advantage of indexing round inserts. (a) Insert used for finishing, showing very light wear and minimum depth-of-cut notch. Has considerable remaining life. (b) Insert used for finishing. Displays some notching and small flaked areas. May be used for roughing with much remaining life. (c) Typical appearance of insert used for roughing with almost 50% of edge usable for roughing. (d) Appearance of insert used for roughing and indexed for maximum edge utilization. This should be fairly typical appearance for the insert as used for roughing before it is discarded. Courtesy of Greenleaf Corporation

alloys if their high setup and operating costs can be justified. Electrical discharge, electron beam, and laser machining are all methods capable of producing deep or irregularly shaped holes in nickel alloys. Holes as small as 0.05 mm (0.002 in.) diameter can be drilled up to approximately 12.7 mm (0.5 in.) deep, depending on the process employed. Drilling rates run up to approximately 25 mm/min (1 in. per min) with electric discharge and laser drilling, and an order of magnitude higher with the electron beam method. In addition to the obvious small hole drilling capability, an advantage of these methods is that they can be used on material in the aged condition, thus avoiding distortion problems that can occur with material aged after conventional drilling.

Except for high equipment and engineering costs, there are few drawbacks to drilling employing these methods. They do produce a thin heat-affected surface layer, the depth of which is dependent on the drilling method and heat input. Areas of application have been primarily in the drilling of cooling passages in jet engine and other aerospace components where the high cost can be justified. However, as these processes move more into the general industrial sector and become more refined, they should be considered for general small-hole drilling in nickel alloys.

Reaming

Successful reaming of nickel alloys begins with good holes having a minimum work hardened layer. Therefore, good drilling practices are an essential requirement for successful reaming. The objective when reaming is to penetrate below this layer so that nonhardened material is cut using conditions that avoid further hardening (or glazing). Essential to achieving this are that the reamer be kept sharp at all times, that adequate feeds be used, that chatter be absolutely avoided, and that positive reamers, which are characterized by the following, be used:

- High-speed steel tool material of adequate toughness
- Right-hand cut
- Right-hand helix (positive axial rake)
- Positive radial rake

Speeds for reaming should be about two-thirds of those used for drilling, but not so high as to cause chatter. Feed rates are about 0.04 to 0.10 mm (0.0015 to 0.004 in.) per flute per revolution. Too low a feed will cause glazing and excessive wear, while an excessive feed rate will reduce the hole accuracy and finish. The stock removal needed to cut below the work hardened layer will increase with the diameter of the hole and typical values are 0.25 mm (0.010 in.) on a 6 mm (0.25 in.) diameter hole, 0.38 mm (0.015 in.) on a 12 mm (0.50 in.) diameter hole, and up to 0.64 mm (0.025 in.) on a 38 mm (1.5 in.) diameter hole.

The tool steels used for conventional reamers are normally the molybdenum grades of high-speed steel (such as types M-2 and M-10) selected because of their toughness. Reamers with carbide cutters can also be used and are recommended for the group D-2 alloys. Types C-2 and C-6 (ISO K20 and M,P20) carbides give good results.

Tapping

In tapping nickel alloys, the most important factor is selection of the proper hole size. Decreasing the thread engagement decreases the torque necessary to drive the tap and markedly reduces tap breakage. Conventional thread engagement values of 75% have been found to be unnecessary with high-strength materials; usually, engagements of 50 to 60% are sufficient for most requirements. Recommended tapping speeds and thread engagements for the various alloy groups are given in Table 8. The age-hardenable alloys should be tapped in the unaged condition whenever possible. Ample

Table 4 Twist drilling nickel alloys with high-speed steel drills

	Drill diameter		Surface speed		Feed(a)	
Alloy group	mm	in.	m/min	sfm	mm/rev	ipr
A	<1.6	<1/16	17–23	55–75	0.01–0.03	0.0005–0.001
B	1.6–3.2	1/16–1/8	14–17	45–55	0.03–0.05	0.001–0.002
C	3.2–4.8	1/8–3/16	8–11	25–35	0.05–0.10	0.002–0.004
D-1	6.4–7.9	1/4–5/16	6–9	20–30	0.08–0.13	0.003–0.005
D-2 unaged	9.5–11	3/8–7/16	3–4	10–12	0.10–0.18	0.004–0.007
D-2 aged	13–17	1/2–11/16	2–3	8–10	0.15–0.25	0.006–0.010
E	19–25	3/4–1	15–21	50–70	0.20–0.38	0.008–0.015

(a) Use the lower value for smaller drills in the range or for harder material.

lubricant, preferably with liquid chlorinated wax, is essential for both hand and machine tapping.

Threading

The principles used in lathe threading nickel alloys are similar to those used in turning. Positive tool-cutting angles are helpful but must be slightly less than those in turning in order that the small nose of the tool is supported. Because of the small size of the cutting nose, it is necessary to cut at lower speeds than in straight turning and to flood with sulfurized oil in order to adequately dissipate heat when threading with high-speed tooling. Tough, high-speed steel tooling (such as the M-2 and M-10 grades) should be selected for both threading and tapping. Carbide may also be used for threading, and typical speed is in the range of 26 to 30 m/min (85 to 100 sfm).

Die threading should use self-opening dies because threads may be torn when reversing solid dies. A chamfer angle of 15 to 20° is recommended for producing V-threads in which no shoulder is involved. The rake ankle is 15° for threading material of hardness 30 HRC, and it is increased to 30° for material as soft as hardness 65 HRB. The workpiece diameter should be 1 to 1.5% undersize to prevent binding in the die. The speeds given for lathe threading also apply to die threading.

Threads may be ground using aluminum oxide (150 to 320 grit), vitrified-bonded grinding wheels (medium-hard, open structure), which are effective with the group D-2 alloys in any condition. The recommended grinding fluid is a filtered oil of approximately 300 Saybolt Universal seconds (SUS) viscosity at 20 °C (70 °F). Care should be taken to avoid overheating because of the possibility of heat checking.

Threads can be rolled on material up to approximately hardness 30 HRC while die life decreases rapidly at higher hardness. It is usually preferable to roll material in the as-drawn or annealed condition and then age harden.

Planing and Shaping

Tooling and conditions used for planing and shaping are similar to those used for turning except that the speeds are about 80 to 85% of those in turning. In using high-speed steel tooling, the top rake angle is most important; it must be extremely positive to achieve good cutting action. The optimum chip, resulting from a suitable combination of side cutting angle of about 4 to 6° and top rake angle of 10 to 20°, is a small curl that curves before the tool and breaks upon hitting the work.

The gooseneck type of planer tool should be used for finishing because its spring action affects smooth cuts. It is important that the cutting edge of a gooseneck tool be located behind the centerline of the clapper box pin so that the tool will spring away from the cut and not dig in. Sulfurized oil lubrication should be used to obtain the best finish in finishing operations while soluble oil coolants are adequate for roughing.

Heavy sections may be parted on a planer using a gooseneck finishing tool. However, only light cuts of about 0.13 to 0.25 mm (0.005 to 0.010 in.) may be taken. Shaping operations are similar to planing; therefore, tooling and cutting conditions are the same. High-speed tooling will need good toughness and, so, such grades as M-2 and M-10 are suggested. Carbide tooling also should incorporate a positive cutting geometry with a C-6 type (ISO M,P20) grade. Recommended conditions for planing are given in Table 9.

Broaching

A key element in broaching nickel alloys is to make sure that the teeth are kept sharp. They should be reground frequently and polished or honed after grinding. Chip breakers (nicked teeth) are recommended, and they should be staggered from tooth to tooth and slightly larger than the depth of cut. It is also necessary that the lubricant flows to the cutting edge of the teeth. A generous supply of free-flowing lubricant is necessary, but it should have sufficient body to provide good lubricity to the chips. Sulfurized mineral oil is recommended.

For nickel alloys, a well-designed broach will have a step per tooth (feed) of 0.005 to 0.10 mm (0.002 to 0.004 in.) for surface or spline broaches and 0.04 to 0.08 mm (0.0015 to 0.003 in.) for round broaches. The pitch should provide for at least two teeth cutting simultaneously, and the rake angle will range between 12 and 18° depending on the nickel alloy group. Table 10 gives recommended speeds and rake angles. Types T-1, T-4, and M-4 are suitable high-speed steel broach materials, and they should be hardened and tempered to about 64 HRC.

Milling

Conventional Milling Cutters. The rule that optimal milling results can only be obtained through a careful balance of cutter diameter, number of teeth, feed per tooth, cutting speed, and chip space, applies very strongly to the nickel alloys. In addition, such factors as machine power, condition, and setup that affect chatter are extremely important because of the high strength and work hardening characteristics of these materials. Machines should have adequate power and rigidity. Climb milling is preferred, because the cutting edge enters the workpiece below the work hardened layer. In general, tooling should have positive cutting angles, should be kept sharp, and light feeds

Table 5 Insert drilling annealed group D-2 nickel alloys on CNC lathe or machining center

	Diameter		Feed		Surface speed	
Insert	mm	in.	mm/rev	ipr	m/min	sfm
C-2	15.9–23.8	5/8–15/16	0.10–0.15	0.004–0.006	12–21	40–70
	25.4–38.1	1–1 1/2	0.15–0.23	0.006–0.009	21–30	70–100
Coated	25.4–38.1	1–1 1/2	0.15–0.23	0.006–0.009	30–43	100–140
	41.3–53.9	1 5/8–2 1/8	0.23–0.31	0.009–0.120	43–55	140–80

CNC, computer numerical control

Table 6 Gun drilling nickel alloys with carbide tooling

Alloy group	Feed(a)		Surface speed(a)	
	mm/rev	ipr	m/min	sfm
A	0.003–0.050	0.0001–0.002	67	220
B	0.005–0.100	0.0002–0.004	91	300
C	0.005–0.013	0.0002–0.005	98	320
D-1	0.003–0.075	0.001–0.003	67	220
D-2 unaged	0.003–0.075	0.001–0.003	30	100
D-2 aged	0.003–0.075	0.001–0.003	18	60

CNC, computer numerical control. (a) For drill sizes 1.6–50 mm (1/16–2 in.)

Table 7 Spade drilling nickel alloys

	Feed		Surface speed	
Alloy group	mm/rev	ipr	m/min	sfm
High-speed steel tooling				
A	0.013–0.018	0.005–0.007	17–23	55–75
B	0.013–0.018	0.005–0.007	14–17	45–55
C	0.013–0.018	0.005–0.007	7.6–11	25–35
Coated high-speed steel tooling				
D-2 annealed	0.013–0.305	0.005–0.012	15–21	50–70
D-2 aged	0.013–0.305	0.005–0.012	9–15	30–50

Table 8 Tapping and threading nickel alloys

	High-speed steel tapping			High-speed steel single point or die threading surface speed	
	Surface speed				
Alloy group	mm/rev	ipr	Thread engagement, %	m/min	sfm
A	5–8	15–25	60	7.6–9.1	25–30
B	5–8	15–25	60	7.6–9.1	25–30
C	3–5	10–15	55	3.7–5.5	12–18
D-1	3–5	10–15	55	3.7–5.5	12–18
D-2 unaged	1.5–3	5–10	50	0.9–1.1	3.0–3.5
D-2 aged	1.5–3	5–10	50	0.9–1.1	3.0–3.5

should be avoided to minimize formation of a work hardened layer.

With high-speed steel tooling, the tool material should be a premium grade that combines good toughness and wear resistance so that the cutting edge remains sharp as long as possible. Roughing cutters should have a 12° positive radial rake and 45° axial rake for all alloys except those of group D-2. Light duty cutters with 12° positive axial rake and 18° axial rake (helical flutes) are best for the high-strength alloys of this group. Finishing cutters for all alloys should be of the high helix type with 15° positive radial rake and 52 to 65° helical flutes (positive axial rake). Staggered tooth cutters, with alternate teeth of opposite helix, are best for milling grooves.

With carbide tooling, the choice of insert grade is limited because high toughness is essential and, therefore, wear resistance must be sacrificed. However, this situation can be somewhat improved by the use of chipbreaker designs to produce a more positive cutting angle, coated inserts to improve wear and cratering resistance, and round shape to provide maximum toughness. The machining program is also important from the standpoint of minimizing impact loading on the inserts, avoiding entry into work hardened layers, and allowing the chips to be thrown clear of the cut. Some of the techniques that have been described for turning with ceramic tooling can be used to accomplish these objectives in milling with carbide. Unfortunately, ceramics cannot be recommended for general milling applications with nickel alloys because of their toughness limitations.

Recommendations for milling speeds and feeds are given for high-speed steel and carbide tooling in Table 11. The speeds used in milling with carbide are considerably less than those used in turning because a tougher insert grade must be used in milling.

Electrochemical, Electrical Discharge, and Chemical Milling. The first two of these processes are capable of machining precision intricate cavities, as well as producing general metal removal in nickel alloys, and, so, these first two processes fit well a definition for milling. Chemical milling, however, is limited primarily to light surface removal requirements and is used mainly to produce large thin sections to close tolerances that cannot be machined with conventional milling techniques. These processes have the distinct advantage with nickel alloys that they are essentially unaffected by material strength or heat treatment condition and, therefore, can be used to solve problems where conventional milling is not feasible.

In electrochemical machining, the nickel alloy is made the anode in an electrolytic cell, and metal is removed by passing direct current between a cathode and the workpiece. The equipment, tooling and setup costs are high because of the need to precisely control current and electrolyte purity and hydraulic pressure. For nickel alloys, electrolytes are generally neutral salt solutions of sodium chloride, potassium chloride, or sodium nitrate. Metal removal rates in the range of 1.6 cm^3 (0.1 $in.^3$) per minute can be obtained, and tolerances to ±0.03 mm (0.001 in.) are possible. Surface finish depends on many process variables but generally is in the range of 0.30 to 1.9 μm (12 to 75 μin.) for the frontal gap and as rough as 5 μm (200 μin.) in the side gap area. Metallurgical variations in the workpiece can cause surface defects such as intergranular attack from grain boundary precipitates. These defects can be minimized with high current densities. Electrical discharge machining uses a spark to remove metal from the workpiece that is immersed in a dielectric fluid. The essential equipment and cost elements of this process are otherwise similar to electrochemical machining. This process will produce a very thin heat-affected surface layer approximately 0.01 to 0.125 mm (0.0004 to 0.005 in.) thick, but it will be relatively independent of underlying metallurgical features.

Chemical milling the nickel alloys requires strong acids to achieve practical metal removal rates. The etchants consist of nitric, hydrochloric, and hydrofluoric acids. A disadvantage of this process is the handling and disposal of spent etch and rinse solutions. Unfortunately, these acids can also etch grain-boundaries and cause pitting in the chromium bearing nickel alloys if they have been aged in the 540 to 760 °C (1000 to 1400 °F) temperature range. Therefore, it is preferable to chemical mill the age hardening alloys in the solution annealed condition. Quality control should include a metallographic examination of the finished surface. Even in the best of conditions, chemical milling will lower fatigue life slightly, probably because it removes work hardened surface layers and because incipient grain-boundary attack has occurred.

Sawing

Hacksawing and band sawing are appropriate for all alloys except group D-2. The group D-2 alloys are not readily cut by these tools, although some limited cutting with them may be possible. Hand hacksawing blades should be high-speed steel and have 0.7 to 1.0 tooth/mm (18 to 24 teeth per in.), raker set, for general work. Power hacksaws can be operated at 90 strokes per min for the groups A and B alloys and about 60 strokes per min for groups C and D-1. Recommended speeds for band sawing are given in Table 12. For both types of sawing, it is important that positive feed pressure be used so that the teeth constantly bite into the work.

Friction sawing can be used on material up to about 25 mm (1 in.) thick. Blades with raker-set teeth should be used having 0.4 to 0.71 mm (10 to 18 teeth per in.) depending on material thickness. A blade about 3 mm (0.125 in.) wider than the material to be cut is preferred. Representative saw speeds are given in Table 13.

Abrasive cutoff can be used for all nickel alloys. For dry cutting small sections up to about 25 mm (1 in.), aluminum oxide resinoid wheels such as A-301-R6-B and A-602-Q8-B are satisfactory. Wet cutting is preferred for thicknesses over 25 mm (1 in.) and for the groups D-1 and D-2 alloys in all thicknesses. Aluminum oxide rubber-bonded wheels such as A-602-M-R are recommended. Water with an inhibitor is an adequate cutoff fluid. Speeds should be approximately 1525 to 1675 m/min (5000-5500 sfm) and feed the maximum permitted by machining capability.

Plasma-arc cutting, as well as a number of advanced methods including laser, electron beam, and abrasive waterjet machining, may be used on nickel alloys. All of these methods avoid the difficulties associated with machining these strong, work-hardening materials and should be considered under appropriate conditions.

Table 9 Planing and shaping nickel alloys

Alloy group	Roughing						Finishing					
	Depth		Feed		Speed		Depth		Feed		Speed	
	mm	in.	mm	in.	m/min	sfm	mm	in.	mm	in.	m/min	sfm
High speed tooling (M-2, M-10)												
A	16	5/8	0.13	0.050	15–18	50–60	0.25	0.010	6.35	0.250	15	50
B	16	5/8	0.13	0.050	12–15	40–50	0.25	0.010	6.35	0.250	12	40
C	10	3/8	0.13	0.050	5–6	15–20	0.25	0.010	6.35	0.250	5	15
D-1	10	3/8	0.13	0.050	6–9	20–30	0.25	0.010	6.35	0.250	6	20
D-2 unaged	10	3/8	0.13	0.040	1.5–3	5–10	0.25	0.010	6.35	0.250	1.5	5
D-2 aged	10	3/8	0.13	0.040	1.5–3	5–10	0.25	0.010	6.35	0.250	1.5	5
Carbide tooling (C-6)												
A	13	1/2	1.27	0.050	61	200	0.13	0.005	(a)	(a)	69	225
B	13	1/2	1.14	0.0045	38	125	0.13	0.005	(a)	(a)	46	150
C	3	1/8	1.52	0.060	37	120	0.13	0.005	(a)	(a)	34	110
D-1	13	1/2	1.14	0.045	26	85	0.13	0.005	(a)	(a)	30	100

(a) 3/4 width of square-nose finishing tool

Table 10 Broaching nickel alloys with high-speed steel tooling

Alloy group	Surface speed		Rake angle, degrees
	m/min	sfm	
A	3.1–5.5	10–18	12–18
B	3.1–5.5	10–18	12–18
C	1.5–3.7	5–12	10–15
D-1	1.5–3.7	5–12	10–15
D-2	1.8	6	8–10

Table 11 Milling conditions for nickel alloys

			Roughing				Finishing			
			Feed		Speed		Feed		Speed	
Alloy group	Condition	Tool material	mm/tooth	in./tooth	m/min	sfm	mm/tooth	in./tooth	m/min	sfm
Face and side milling										
A	Annealed or drawn	M-2, 7, 10, C-6	0.08–0.15	0.003–0.006	21–32	70–105	0.10–0.20	0.004–0.008	41–67	135–220
B	Annealed or drawn	M-2, 42, T-15, C-6	0.18–0.25	0.007–0.010	17–26	55–85	0.15–0.25	0.006–0.100	24–53	80–175
C	Annealed or drawn	M-2, 42, T-15, C-2	0.08–0.15	0.003–0.006	6–11	20–35	0.01–0.15	0.004–0.006	20–23	65–75
D-1	Annealed or drawn	M-2, 42, T-10, C-6	0.08–0.15	0.003–0.006	6–11	20–35	0.10–0.15	0.004–0.006	12–24	40–80
D-2	Unaged	M-2, 42, T-15, C-2	0.08–0.13	0.003–0.005	3–8	10–25	0.20–0.30	0.008–0.012	23–30	75–100
D-2	Aged	M-2, 10, T-15, C-2	0.08–0.13	0.003–0.005	2–6	5–20	0.20–0.30	0.008–0.012	20–21	65–70
End and slot milling										
A	Annealed or drawn	M-2, 7, 10, C-6	0.03–0.10	0.001–0.004	12–21	40–70	…	…	…	…
B	Annealed or drawn	M-2, 42, T-15, C-6	0.03–0.010	0.001–0.004	12.5–20	45–65	0.03–0.10	0.001–0.004	46–76	150–250
C	Annealed or drawn	M-2, 42, T-15, C-2	0.03–0.08	0.001–0.003	5–8	15–25	0.03–0.10	0.001–0.004	17–29	55–95
D-1	Annealed or drawn	M-2, 42, T-10, C-6	0.03–0.08	0.001–0.003	5–11	15–35	0.03–0.10	0.001–0.004	34–58	110–190
D-2	Unaged	M-2, 42, T-15, C-2	0.03–0.08	0.001–0.003	3–6	10–20	0.03–0.10	0.001–0.004	14–24	45–80
D-2	Aged	M-2, 10, T-15, C-2	0.03–0.08	0.001–0.003	2–5	5–15	0.03–0.10	0.001–0.004	20–34	65–110

Table 12 Band sawing nickel alloys

	Work thickness		Teeth		Surface speed	
Alloy group	mm	in.	per mm	per in.	m/min	sfm
A	1.6	1/16	0.6	14.0	32	105
	6.4	1/4	0.4	10.0	23	75
	25	1	0.3	8.0	15	50
	76	3	0.2	6.0	15	50
B	1.6	1/16	0.7	18.0	38	125
	6.4	1/4	0.6	14.0	23	75
	25	1	0.4	10.0	15	50
	76	3	0.3	8.0	15	50
C	1.6	1/16	0.6	14.0	27	90
	6.4	1/4	0.5	12.0	23	75
	25	1	0.4	10.0	15	50
	76	3	0.3	8.0	15	50
D	1.6	1/16	0.7	18.0	23	75
	6.4	1/4	0.5	12.0	12	40
	25	1	0.4	10.0	9	30
	76	3	0.3	8.0	9	30

Table 13 Friction sawing nickel alloys

	Speed		Material thickness	
Alloy group	m/min	sfm	mm	in.
A	3.1–5.5	10–18	0.8	1/32
B	3.1–5.5	10–18	5	3/16
C	1.5–3.7	5–12	13	1/2
D-1	1.8	6	25	1

Grinding and Surface Finishing

The grinding of nickel alloys is done by practices similar to those used for steel. Grinding can be conducted on the difficult to machine group D-1 and D-2 alloys in the aged conditions and is a satisfactory alternative to finish machining. This practice has the further advantage that thermal distortion from the aging treatment can be eliminated provided that an allowance is made for the size contraction on aging. All alloys should be in the stress-equalized condition before grinding to avoid warpage.

For best productivity and to avoid surface metallurgical damage, grinding should be done wet to avoid overheating the surface. A solution of 95 L (25 gal) of water and 0.5 kg (1 lb) of sal soda, or 50 parts of water to one part soluble oil, is suitable for all operations other than crush form and thread grinding, which call for a good grinding oil. An inhibitor of sodium chromate can be used in sal soda solutions. Silicon carbide grinding wheels give the best results on the groups A, B, D-1, and E alloys while aluminum oxide wheels traditionally have been used for groups C and D-2. Cubic boron nitride (CBN) with oil coolant is now being used to grind these difficult alloy groups with very good results. In surface grinding, coarse-grit (46 to 60) aluminum oxide produces the best finish. Vitrified-bond, medium-grade aluminum oxide wheels with medium-to-open structures produce the best results with crush form grinding. In all cases, grinding pressures should be great enough to produce slight wheel breakdown. When accurate final dimensions are required, the material should be allowed to cool to room temperature before the finishing pass so that thermally induced distortion is corrected.

In surface grinding, low wheel contact and low pressure help prevent distortion, especially with annealed material. Reciprocating tables are preferred over rotary tables, because wheel contact is reduced. Less heat is generated and, therefore, less distortion. In centerless grinding, the desired slight breakdown of the wheel is controlled by the diameter of the work, in-feed per pass, and the angle and speed of the regulating wheel. By taking light cuts, finish grinding can be done without redressing the wheel after the roughing operation.

In belt grinding, abrasive practice is the same as for wheels. Rough grinding can be conducted dry, but finishing requires a lubricant such as cottonseed oil to which kerosene can be added to impart a high-flowing characteristic.

Honing is done with aluminum oxide, vitrified bond honing stones of medium-to-soft grade. Ample coolant must be used, usually of a proprietary oil that can be diluted by two to three parts of kerosene. Surface speeds are between 45 to 75 m/min (150 to 250 sfm), and reciprocation speeds are between 11 to 15 m/min (35 to 50 sfm). Honing pressure should be about 3100 kPa (450 psi).

Chemical milling and abrasive flow machining are methods that may be considered for such requirements as edge finishing and burr removal on nickel alloys.

SELECTED REFERENCES

- *Machinery's Handbook,* 26th ed., Industrial Press, 2000
- *Machining,* Vol 16, *ASM Handbook,* ASM International, 1989
- *Machining,* Vol 1, 4th ed., *Tool and Manufacturing Engineers Handbook,* Society of Manufacturing Engineers, 1983
- *Machining Data Handbook,* Vol 1 and 2, 3rd ed., Metcut Research Associates, 1980
- R.A. Walsh, *McGraw-Hill Machining and Metalworking Handbook,* 2nd ed., McGraw-Hill Inc., 1998

ASM Specialty Handbook: Nickel, Cobalt, and Their Alloys
J.R. Davis, editor, p 245-272
DOI:10.1361/ncta2000p245

Copyright © 2000 ASM International®
All rights reserved.
www.asminternational.org

Welding and Brazing of Nickel Alloys

NICKEL AND nickel alloys can be joined reliably by a wide variety of welding processes. The more ductile solid solution-strengthened nickels and nickel alloys are the more readily welded, and, to these, almost all welding processes have been successfully applied at some time. The weld fabrication of these materials is straightforward in that they usually do not require preheat or postheat, and interpass temperature control during welding is normally not critical. The precipitation-hardenable alloys are less weldable and, because of the presence of the gamma prime (γ') strengthening phase, tend to be susceptible to what is called "strain-age cracking." These materials are usually welded in the annealed (or solution-annealed condition) and are postweld heat treated to precipitate the γ' phase as a final or near-final production step. The precipitation-hardenable alloys are also frequently joined by brazing.

This article reviews the joining technology associated with nickel and nickel alloys in the following five sections:

- "Welding Metallurgy of Corrosion-Resistant Alloys" addresses solid-solution corrosion-resistant alloys that contain little or no molybdenum. The Monels, Inconels, and Incoloys are well-known members of this group of alloys.
- "Welding Metallurgy of Corrosion-Resistant Alloys Containing Molybdenum" addresses solid-solution corrosion-resistant alloys not covered in the previous section. The Hastelloys make up this alloy group.
- "Welding Metallurgy of Heat-Resistant Alloys" discusses the special challenges of welding precipitation-hardening alloys, with emphasis on the heat-resistant superalloys.
- "Consumable Selection, Procedure Development, and Practice Considerations" describes specific welding practices for both solid-solution and precipitation-hardenable nickel alloys.
- "Brazing of Heat-Resistant Nickel Alloys" covers procedures and practice considerations for brazing this category of nickel alloys.

Additional information on nickel weldments, including guidelines for weld fabrication in corrosive environments, can be found in the article "Corrosion Behavior of Nickel Alloys in Specific Environments" in this Handbook.

Welding Metallurgy of Corrosion Resistant Alloys

This section addresses a family of solid solution-strengthened materials that includes pure nickel, nickel-copper alloys, nickel-chromium alloys, and nickel-chromium-iron alloys. The compositions of some of the more popular, commercially important, wrought alloys in this group are given in Table 1. Although the nickel and nickel-copper alloys listed in Table 1 are used exclusively for corrosion resistant applications, it should be noted that some nickel-chromium and nickel-chromium-iron alloys are used in applications requiring both corrosion resistance and heat resistance. For example, the nickel-chromium-iron alloys are typically used in high-temperature oxidizing and carburizing applications because of their resistance to these environments and their high strength. Typical applications include furnace components, extruded piping for ethylene and steam methane reforming furnaces, and chemical processing equipment.

General Welding Characteristics

Thermal Conductivity. Nickel is quite conductive, and copper is extremely conductive. However, the addition of chromium or iron decreases the thermal conductivity of nickel or nickel-copper. Conductivity, whether thermal or electrical, always decreases when the solvent accepts solute atoms, as in alloying. The data in Table 2 illustrate this fact. Note that nickel has a thermal conductivity value of 75 W/m · K (45 Btu/ft · h · °F) and copper (not shown in Table 2) has a value of 391 W/m · K (225 Btu/ft · h · °F), but alloy 400, which contains roughly two-thirds nickel and one-third copper, has a lower thermal conductivity value (22 W/m · K, or 13 Btu/ft · h · °F) than either nickel or copper.

Thermal conductivity plays an important function during welding because it influences heat flow and the amount of heat required to melt material into the weld puddle. A base

Table 1 Compositions of selected nickel-base corrosion resistant alloys

Alloy	Composition, wt%								
	Ni	Cr	Fe	Cu	C	Si	Al	Ti	Mo
Nickel alloys									
200	99.5	···	···	···	0.08	0.2	···	···	···
201	99.5	···	···	···	0.01	0.2	···	···	···
Nickel-copper alloy									
400	66.5	···	···	31.5	0.15	0.2	···	···	···
Nickel-chromium alloys									
600	76.0	15.5	8	···	0.08	0.2	···	···	···
601	60.5	23	14	···	0.08	0.2	1.3	···	···
690	60.0	30	9.3	···	0.03	0.2	0.3	0.2	···
Nickel-chromium-iron alloys									
800	32.5	21	46	···	0.05	0.5	0.3	0.3	···
825	42	21	30	···	0.03	0.2	0.1	0.9	3

Table 2 Properties of selected nickel-base corrosion resistant alloys

Alloy	Density, g/cm^3	Melting range		Coefficient of thermal expansion(a), 10^{-6}/K	Thermal conductivity		Electrical resisitivity, $10^{-8}\Omega$/m
		°C	°F		W/m^2 · K	Btu/ft^2 · h · °F	
1020 carbon steel (b)	7.9	1470–1530	2680–2790	12	46	27	19
304 stainless steel(b)	8.0	1390–1450	2535–2640	17	16	9.3	72
200	8.9	1435–1502	2615–2735	14	75	45	9
201	8.9	1435–1502	2615–2735	14	79	46	8
400	8.8	1299–1349	2370–2460	16	22	13	51
600	8.4	1354–1413	2470–2575	14	15	8.7	103
601	8.1	1301–1368	2375–2495	15	11	6.4	119
690	8.2	1343–1377	2450–2510	14	12	7	115
800	7.9	1357–1385	2475–2525	16	12	7	99
825	8.1	1371–1399	2500–2550	15	11	6.4	113

(a) In range from 20 to 260°C (68 to 500 °F). (b) Data are provided for purpose of comparison.

material composition with a high level of thermal conductivity will conduct heat away from the fusion zone and, therefore, requires slightly more heat input during welding than would an alloy with low thermal conductivity, which retains the local heat of welding for a longer time.

The nickel-base alloys vary considerably in their thermal conductivity characteristics. The nickel-chromium and nickel-chromium-iron alloys have values lower than those of both the carbon steels and the austenitic stainless steels, whereas nickel and the nickel-copper alloys have values considerably higher than those of the steels.

The electrical resistivity of a material is especially important in the welding process itself, because the melting rate of an electrode or wire is influenced by the electrical characteristics of the material (Table 2). Usually, solid-solution alloys are not very good electrical conductors, because the solute and solvent atoms are of different sizes. This condition distorts the crystal lattice structure of the material and impedes the passage of electrons. The alloys that are composed primarily of one element, such as 1020 steel and nickel-base alloys 200 and 201, have the lowest electrical resistivity values of the alloys listed in Table 2.

The thermal expansion characteristics of a material are important because the heat that is applied to weld joints causes localized expansion and/or contraction during heating and/or cooling. A material with a greater thermal expansion value will expand and contract more during the welding operation, thus creating a greater amount of stress on the weld joint. This is particularly important when the weld deposit is marginally crack sensitive. It is also a consideration when dissimilar metals are welded together, especially when there is a large difference in expansion characteristics. The section "Special Welding Considerations" in this article provides more details on this topic. The nickel-base alloys have thermal expansion values that are between those of carbon steel and the austenitic stainless steels, as shown in Table 2.

Liquidus-Solidus Temperature. The cracking resistance of a material is often associated with the difference in the liquidus and solidus temperatures, particularly when stress is involved. When a highly restrained structure is welded, considerable stress is generated during the welding operation. If a material has a relatively large spread between its liquidus and solidus temperatures, then there is more time that the material is in a vulnerable situation in terms of cracking. However, a material with a relatively narrow liquidus-solidus range will cool down fairly rapidly through the temperature range, and there will be less time for stress-related cracking to occur. This example assumes that other factors that influence cracking, such as grain size or structural mass, are equal. Table 2 lists the liquidus-solidus temperatures, or melting ranges, of several solid-solution nickel alloys.

Welding Metallurgy of the Heat-Affected Zone

The heat-affected zone (HAZ) is defined as that portion of the base metal that has not been melted but whose mechanical properties or microstructure have been altered by the heat of welding. Figure 1 shows the true HAZ in a typical weld. The HAZ is discussed subsequently in terms of grain boundary precipitation, grain growth, and hot cracking.

Grain Boundary Precipitation. Grain boundaries are the weak link in a microstructure that is exposed to elevated temperature, whether that exposure occurs during service or, in the case of welding, during the thermal cycles that are part of the welding operation. Precipitates that form in the grain boundaries can vary in size and composition and can be either harmful or beneficial. Intermetallic compounds such as carbides act as barriers to grain growth and can be very beneficial. Intergranular carbides in alloys 600 and 690 can also deter stress-corrosion cracking (SCC) during high-purity water exposure in nuclear reactor steam generator, primary side environments (Ref 1).

Grain Growth. Generally, it is easier to make defect-free welds in material with a relatively fine grain size, because there is less of an undesirable element concentration that contributes to grain boundary cracking in a fine-grain network. With larger grains, there are fewer grain boundaries, and the deleterious elements are more concentrated in them. However, it is not always possible to have a fine-grain structure to weld. Most high-temperature applications, for example, need a large grain size material to ensure elevated-temperature creep and rupture strength.

Even when a fine-grain material is welded, grain growth will occur in the HAZ. The width of this grain-growth band depends on numerous variables, such as the welding process used, the heat input and travel speed, and the heat transfer characteristics of the base material. The electron-beam (EB) welding process, for example, will produce a narrower HAZ and a smaller band of grain growth than the gas-metal arc welding (GMAW) process. Figure 2 shows grain growth in the HAZ of a gas-tungsten arc welded wrought nickel sample.

Hot Cracking. In terms of constitutional liquation, HAZ fissures are seldom a problem in the nickel or nickel-copper alloys, but they have been the subject of considerable study in nickel-chromium and nickel-chromium-iron alloys.

Such fissures have been observed in alloy 600, for example, when relatively high heat inputs (2.4 MJ/m, or 45×10^3 J/in., and higher) were used. These fissures are typically narrow, linear intergranular separations that are perpendicular to the direction of weld travel. Fissures have been found in the HAZ of welds made by the GMAW, gas-tungsten arc welding (GTAW), and EB welding processes. An example of a typical fissure found in a nickel-chromium HAZ is shown in Fig. 3.

Grain boundary liquation is one of the proposed mechanisms that causes fissuring (Ref 2). Grain boundary liquation occurs when a phase or particle causes the grain boundary to melt at a temperature below the bulk melting point. Because the liquated grain boundary has practically no strength, separation at the liquated grain boundary can occur, causing the fissure.

Constitutional liquation was proposed as a mechanism for hot cracking by Savage in 1959 and was described in detail in subsequent papers (Ref 3). In this theory, a relatively stable second-phase particle begins to dissolve during nonequilibrium, or rapid, heating and forms an intermediate phase with the matrix, which has a solidus temperature that is lower than that of

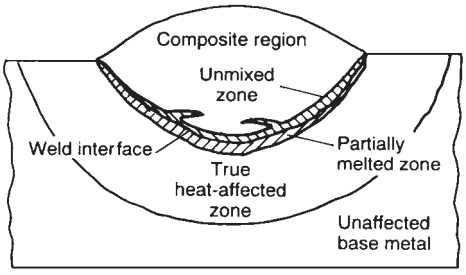


Fig. 1 Metallurgical zones in a typical weld

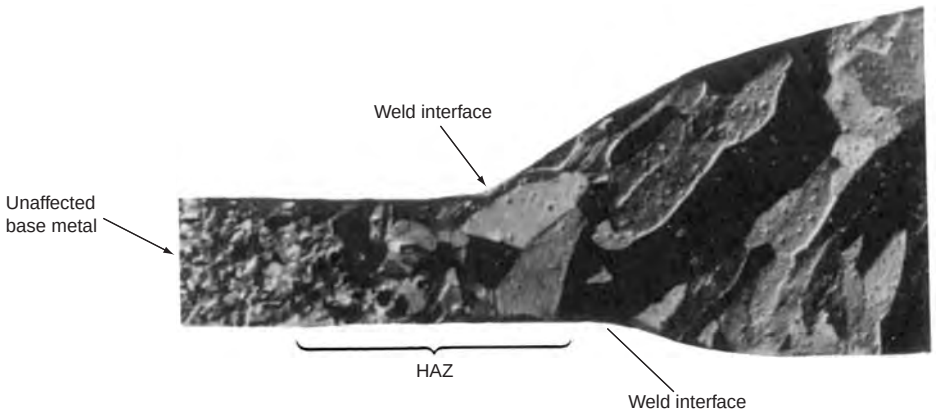


Fig. 2 Gas-tungsten arc weld of pure nickel deposited with matching nickel filler metal. Note the steadily increasing grain size from the outer extremity of the HAZ to a maximum grain size at the weld interface. Etchant: aqua regia. Magnification: 20×

either the second-phase particle or the matrix. In alloy 600, some experimenters have identified the precipitation of Cr_7C_3 at the grain boundary as the second-phase particle around which constitutional liquation occurs.

Chemical segregation at a grain boundary can also cause grain boundary liquation. Boron and sulfur are two elements that form lower melting point eutectics that can contribute to HAZ fissuring. Manganese segregation in alloy 600 has been identified as forming a binary compound (Mn-38Ni) with a 1000 °C (1830 °F) solidus temperature, which is considerably below the bulk melting range of the alloy.

Several approaches can be made to minimize the occurrence of HAZ fissuring, including control of the following:

- Heat input during welding
- Microstructure, to obtain fairly small grain sizes
- Chemistry, to minimize the amount of deleterious minor elements that are known to contribute to fissuring

Many minor elements can contribute to HAZ fissuring in nickel-base alloys, including some that are intentionally added to enhance properties. Although these elements are considered minor because they are present in small amounts, they are far from being minor in their effect on fissuring. These elements include, but are not limited to, sulfur, phosphorus, lead, boron, zirconium, tin, zinc, selenium, tellurium, antimony, bismuth, silver, and gold. Boron and zirconium are two elements that are intentionally added to nickel-base alloys to enhance hot workability and elevated-temperature strength, but they can be detrimental during welding operations. More details on the effects of many of these elements are provided subsequently in the discussion "Effects of Alloying Elements on Weldability."

Welding Metallurgy of the Fusion Zone

The fusion zone is the area of the base metal melted during the welding process, as determined on the cross section of the weld. The fusion zone of autogenous welds (no filler metal added) is discussed below in terms of sensitivity to porosity formation, hot-cracking susceptibility, and microsegregation.

In terms of sensitivity to porosity, the nickel-base alloys can be divided into two groups: those that contain chromium and those that do not. Chromium has a natural affinity for the gases that form during the welding operation, notably oxygen, nitrogen, and hydrogen. Because the nickel and nickel-copper alloys lack chromium, they are sensitive to porosity formation during autogenous welding. Therefore, the protection of the weld puddle during melting and solidification is critical to the achievement of porosity-free autogenous welds in these two alloy classes. Dry torch gases and adequate gas protection are necessities. Although the use of filler metals helps in porosity control, because of the additions of gas-absorbing elements such as titanium and aluminum, proper precautions are still necessary.

Porosity control is much easier in the nickel-chromium and nickel-chromium-iron alloys because of their high chromium levels. This is not meant to imply that gas coverage is not important when autogenously welding the chromium-containing alloys, but it certainly is not as critical, compared with nickel and nickel-copper alloys.

Hot-Cracking Susceptibility. Hot cracking, or fissuring, is a grain-boundary-related mechanism that can occur, primarily, in the nickel-chromium and nickel-chromium-iron families of alloys. Although the nickel and nickel-copper alloys are not immune to this phenomenon, there have been more occurrences in the chromium-bearing nickel-base alloy materials.

A study of the weldability of alloy 800 (Ref 4) found that reducing the aluminum plus titanium content to extremely low levels (<0.06%) essentially eliminated hot cracking. It was noted that when normal levels of these elements were present, segregation of titanium and alu minum resulted in grain-boundary embrittlement and banding that was sufficiently severe to exhibit liquation during heating through a weld cycle. There also appeared to be a strong association between sulfur and titanium in the discrete inclusions observed in sulfur-bearing alloys.

Microsegregation. When a weld solidifies, an inhomogeneous dendritic structure forms. Solidification begins with the highest-melting-point liquid and continues until the whole structure is solid. A condition called microsegregation, or coring, occurs during this solidification process, and areas of the solidified microstructure can have great differences in composition. This becomes a problem in corrosion situations where an alloy was chosen for its particular resistance to corrosion. For example, because the dendritic weld material can have vastly different chromium and molybdenum levels, preferential corrosion may initiate and propagate at those areas of the microstructure that are lean in the element responsible for providing the corrosion resistance.

Microsegregation cannot be eliminated in a weld, but it can be minimized by judicious selection of welding parameters, such as the control of heat input. High-temperature heat treatments for several hours can partially equalize the composition gradients by diffusion. Cold working the weld structure, followed by annealing, can also break down this microsegregation, if the component lends itself to this type of treatment. Thin-sheet welds can be planished, for example. In addition to improving the corrosion resistance of the welds, cold working and annealing the weld area also increases weld ductility. Figure 4 illustrates how a dendritic weld structure can be reduced by cold working and annealing. After a 20% cold reduction followed by an anneal, the cast structure of the weld has been refined substantially, and the wrought grain structure can be seen easily.

Welding Metallurgy of the Unmixed Zone

For many years, it was assumed that there was complete mixing in the weld pool and that the composition of a fusion weld was homogeneous throughout. Now it is known that there are areas adjacent to the fusion line where mixing does not occur (Ref 6). This unmixed zone

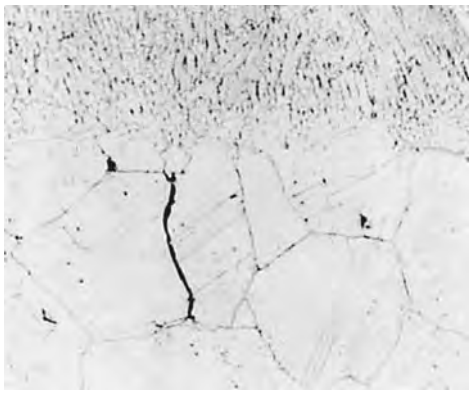
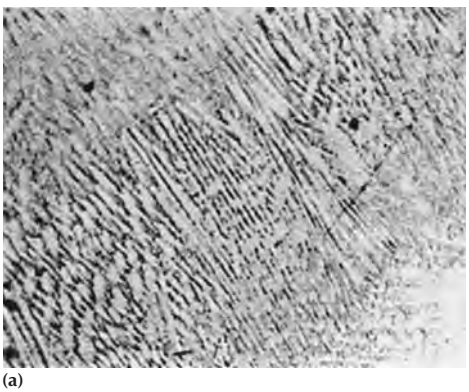


Fig. 3 Micrograph showing a heat-affected zone microfissure in a nickel-chromium alloy. Specimen is a GMAW 44.4 mm (1.75 in.) plate. Electrolytic phosphoric acid etchant. 75×



(a)



(b)

Fig. 4 Microstructures of alloy 400 (UNS N04400) welded with filler metal 60. (a) As welded: cyanide persulfate etchant, 70×. (b) Welded, plus 20% cold reduction, plus anneal at 871 °C (1600 °F)/2 h: cyanide persulfate etchant, 150×. Source: Ref 5

has been the subject of considerable research and is of concern to corrosion engineers because of the adverse effect that a cast base-metal structure can have on weld-associated corrosion. These zones are base material undiluted by filler metal and are, essentially, narrow bands of autogenous welds situated on the fusion line. Figure 1 shows an unmixed zone in a typical weld. There is a greater tendency for unmixed zones to be present in nickel-base welds, compared with steel and stainless steel welds. The sluggish nature of the molten nickel alloy weld metal tends to deter complete mixing during welding.

These unmixed zones can be reduced or practically eliminated by controlling the welding procedures to ensure adequate mixing of the weld pool during welding. As an example, excessively fast travel speed promotes the formation of these zones. Slowing the travel speed and adjusting the other welding parameters to compensate for the slower travel speed will do a great deal to minimize the formation of unmixed zones.

Effects of Alloying Elements on Weldability

Copper forms a complete series of solid-solution alloys with nickel and has little effect on the weldability of nickel. Metallurgically, the binary high-nickel-content alloys that contain from 15 to 40% Cu behave much like commercially pure nickel when welded. The nickel-copper alloys have about the same susceptibility to embrittlement by elements such as sulfur as does commercially pure nickel. The need for alloying to control gaseous porosity is not significantly reduced in the nickel-copper alloys, compared to that required for commercially pure nickel. As copper is increased up to the range of the copper-nickel alloys, such as 70Cu-30Ni and 80Cu-20Ni, the alloy behaves more like a copper alloy, and reduced amounts of deoxidizers can be used. The presence of copper changes the high-temperature solubility of carbon to the point where graphitization is not encountered.

Chromium. The chromium addition in alloys of commercial importance does not exceed the limit of solid-solution alloys and presents an attractively narrow freezing range. Chromium has the ability to form stable oxides and nitrides, which, in turn, greatly reduce the tendency for weld porosity compared to that encountered in commercially pure nickel and nickel-copper welds. The chromium-bearing alloys are more susceptible than other high-nickel-content alloys to hot cracking when other elements, notably silicon, are present. For example, the hot-cracking susceptibility of a nickel-base weld metal containing 15% Cr is sharply increased as silicon increases from a few tenths of a percent to 1% and higher, whereas levels on the order of 1% Si are relatively innocuous in nickel and nickel-copper alloys.

Iron is commonly present in the nickel-chromium alloys, such as alloy 600, in amounts up to 8 wt%. It is not intended to enhance mechanical properties or weldability but is added as a ferroalloy (along with other additives) and helps keep the cost of these alloys down. Up to this level, iron is not believed to appreciably affect welding behavior. As the amount of iron increases to the composition range of nickel-chromium-iron alloys (such as alloy 800, which contains about 46% Fe), the alloy becomes increasingly hot-crack sensitive. When steel is melted into a high-nickel-content alloy weld, such as in an overlay or in dissimilar metal welding, there is some reason to believe that residual elements such as sulfur and phosphorus, which are normally present in more abundant quantities in steel than in nickel-base alloys, are more damaging to the properties of the weld than the iron itself.

Carbon is usually present in nickel and high-nickel-content weld metals in amounts ranging from 0.01 to 0.15 or 0.20%. The effect of carbon is a major concern with commercially pure nickel. The limit of carbon solubility in the temperature range from 370 to 650 °C (700 to 1200 °F) is about 0.02 to 0.03%. During welding, any graphitic carbon present in the HAZ is dissolved and held in a super-saturated solution as the metal rapidly cools. Subsequent exposure to the temperature range from 370 to 650 °C (700 to 1200 °F) causes carbon to precipitate in the form of intergranular graphite. Unwelded high-carbon commercially pure nickel would be similarly embrittled in this temperature range by carbon migration to the grain boundaries, but it would require a much longer time. Therefore, when the wrought commercially pure alloys are to be used at temperatures above 370 °C (700 °F), a maximum of 0.02% carbon is used, as in alloy 201. In weld metal, titanium is added to tie carbon up in the form of titanium carbide, thus preventing the formation of graphitic carbon.

In the nickel-base alloys, copper alters solubility to the point where graphitic embrittlement is not encountered up to carbon levels of 0.15 to 0.20%. The carbon content in nickel-copper alloys does have an effect on hot-cracking tendencies when iron is present. For example, nickel-copper alloys with over 0.20% C can tolerate only about 5% Fe; hot cracking may result at higher levels. Low-carbon nickel-copper alloys with less than 0.10% C can tolerate up to about 30 wt% Fe.

In nickel-chromium alloys, carbon combines with chromium to form chromium carbides, unless titanium or niobium are present to form their respective carbides. Although chromium depletion may occur in the HAZ of welds, as it does with the iron-base alloys in the absence of titanium or niobium, corrosion resistance is impaired only in extremely corrosive media.

Manganese was considered to be relatively unimportant to welding metallurgy for many years. It is now well established that in both the nickel-chromium and nickel-copper alloys, manganese is beneficial in minimizing fissuring and in preventing hot cracking in welds of heavy sections, as well as in cases where excessive iron dilution may be encountered. Additions of up to 9 wt% Mn have been used in some commercially available welding electrodes.

Magnesium in wrought materials forms a stable high-melting-point magnesium sulfide preferentially to the extremely low-melting-point nickel-nickel sulfide eutectic. In welding, magnesium in the base metal serves to prevent hot cracking in the HAZ.

Silicon may be present in nickel-base alloys in amounts ranging from 0.01 to 4.0%. However, it is generally considered to have an adverse effect on welding because it increases the tendency for hot cracking. Therefore, wrought materials generally have less than 1% Si. The adverse behavior is associated with a eutectic melting that is more damaging to weld metal than to base metal. Pure nickel is most resistant, followed by nickel-copper alloys. Nickel-chromium alloys are the least resistant to the effects of silicon.

Both titanium and aluminum can be added to the weld metal and the base material to promote age hardening. In smaller amounts, the addition of titanium to nickel and nonchromium-bearing nickel-base alloys helps control gas porosity. Aluminum is added to wrought alloys as a deoxidizer. If substantial amounts of titanium and aluminum are added, the sensitivity of the weld metal to hot cracking increases.

Boron amounts that range from 0.003 to 0.10% improve the high-temperature mechanical properties of certain wrought and cast nickel-base alloys. These alloys are usually intended for elevated-temperature service, where grain boundary strengths are enhanced by boron additions. Unfortunately, boron contents of 0.03% or higher have a grossly damaging effect on weldability. At higher boron levels, the weld metal and HAZ are extremely hot-crack sensitive, and considerable care must be exercised with respect to heat input and stress levels.

Zirconium acts similarly to boron in nickel-base alloys by promoting hot cracking in the weld metal and HAZ. However, the tolerance for zirconium is somewhat higher than it is for boron.

Sulfur is perhaps the most damaging of all elements that are involved in the welding metallurgy of nickel and high-nickel-content alloys. Sulfur is particularly damaging to nickel because of its extremely limited solid solubility and because of a nickel-nickel sulfide eutectic reaction that occurs at 649 °C (1200 °F).

Sulfur is different from most other elements that adversely affect weldability because it affects both the HAZ and the weld metal. Penetration occurs at the weld HAZ area that is heated above a threshold temperature while being in contact with sulfur-bearing material. The threshold temperature varies from 316 °C (600 °F) for pure nickel to about 649 °C (1200 °F) for chromium-bearing alloys. Magnesium and manganese are alloying additions that are used to control the effects of sulfur. Unusual

diligence is required when handling the nickel-base alloys to avoid contamination from sulfur-containing compounds, which can include such commonly used materials as machining lubricants, marking crayons, temperature-indicating sticks, and shop dirt. Figure 5 shows the type of cracking that can occur when a sheet of alloy 200 is wiped with a dirty cloth containing sulfur compounds and then welded.

Lead causes hot shortness in high-nickel-content weld metal at about the same level as sulfur does. The metallurgical explanation of the subversive effect of lead is very similar to that of sulfur. In practice, lead contamination is less common than sulfur contamination, but probably only because there are fewer common sources of lead-containing contaminants in fabricating shops than there are sources of sulfur-containing contaminants.

Phosphorus can exhibit an effect similar to lead and sulfur in high-nickel-content weld metals. The solubility of phosphorus is quite limited and undergoes a eutectic reaction at about 870 °C (1600 °F). Severe weld metal cracking has been attributed to as little as a few hundredths of a percent of phosphorus.

Postweld Heat Treatment

Postweld heat treatments are usually not required for the non-precipitation-hardenable nickel and nickel-base alloy weldments. For example, the ASME boiler and pressure vessel code for unfired pressure vessels does not require postweld heat treatment, except as agreed on between the user and the manufacturer. However, a dissimilar weldment between a nickel-base alloy and a steel is postweld heat treated because the steel side of the joint requires it. In this case, the heat treatment will normally have little consequence on the nickel-base alloy. Table 3 lists the typical annealing temperatures for many of the solid-solution nickel-base alloys.

In certain environments, it has been beneficial to perform a postweld heat treatment on some of the nickel-base alloy weldments. Alloys 200, 201, and 600 receive this treatment for caustic service applications, as does alloy 400 for hydrofluoric acid service applications. The recommended heat treatment procedures for these materials in these service environments are given in Table 4.

Although determining the rates of heating and cooling after postweld heat treating is seldom a problem with the solid-solution nickel-base alloys, the cooling rate should generally be at least as fast as the rate of an air cool. When there are large differences in cross-sectional areas in a welded structure, the heating and cooling rates may have to be controlled in order to minimize the distortion that might occur with a rapid rate of heating or cooling. Such structures could experience enough distortion to cause fit-up or assembly problems, particularly if a too-rapid cooling rate causes excessive stresses that are due to the mass differences in the structure.

The usual precautions regarding furnace atmosphere and temperature control should be followed when postweld heat treating these alloys. Because cracking caused by contaminants is always a concern, all surfaces should be thoroughly cleaned prior to being postweld heat treated.

Special Welding Considerations

Dissimilar Welding of Plate-to-Plate Specimens. There can be drastic consequences related to complex metallurgical considerations when butt welding plates of different composition. The composition of the weld deposit is controlled not only by the filler metal, but also by the amount of dilution from the two base metals. Many different dissimilar-metal combinations are possible, and the amount of dilution varies with the welding process, the operator technique, and the joint design.

In many cases, more than one welding product will satisfy the requirement of metallurgical compatibility. Selection should be based on the strength required, service environment, or the cost of the welding product. Table 5 lists the recommended filler metals to use when welding numerous dissimilar metal combinations.

The selection of the welding product involves extra considerations when dissimilar materials are being welded. In addition to dilution factors, the thermal expansion of the two metals being joined and of the filler metal should be reviewed in order to achieve a weld that will not fail prematurely.

In the power industry, for example, an austenitic stainless steel and a low-alloy steel represent a common joint. The expansion rate of the stainless steel side is higher than that of the low-alloy side (see Table 2). If this joint were welded with a stainless steel electrode, then both the weld and the stainless steel side of the joint would expand and contract during heating and cooling at the same rate, thus putting stress on the low-alloy side of the weld. Because the low-alloy steel has less strength than the stainless steel, the shifting of stress to this side of the joint is undesirable and could lead to premature fatigue or stress failure.

On the other hand, if a nickel-base alloy filler metal were used to weld this combination, both the weld and the low-alloy side of the joint would expand and contract together during temperature swings in the service environment, and any stresses induced would be shifted to the stainless steel side of the joint, which is stronger than the low-alloy side. This would result in a longer service life for this weld.

Welding Nickel-Clad Steel. Most clad specimens consist of a highly alloyed material (such as a nickel-base alloy) clad to a less-expensive material, usually steel. The nickel-base alloy provides corrosion resistance, whereas the steel, which usually constitutes at least 80% of the total thickness, provides backing strength and reduced costs. Because clad steels are frequently joined by welding, it is important to ensure that any weld-joint surface that is exposed to corrosive media is at least as corrosion resistant as the cladding. This requirement influences both joint design and welding technique.

Butt joints should be used whenever possible. Figure 6 shows recommended designs for



Fig. 5 Sulfur embrittlement of a joint in alloy 200 (UNS N02200). Prior to welding, the cracked side of joint was wiped with dirty cloth on which sulfur-containing residue had accumulated.

Table 3 Typical annealing temperatures for corrosion resistant nickel, nickel-copper, nickel-chromium, and nickel-chromium-iron alloys

All alloys air cooled or water quenched

Alloy	UNS No.	Temperature(a) °C	Temperature(a) °F
200	N02200	830–871	1525–1600
201	N02201	830–871	1525–1600
400	N04400	871	1600
600	N06600	925–1040	1700–1900
601	N06601	1175	2150
690	···	1040	1900
800	N08800	1010–1175	1850–2150
825	N08825	940	1725

(a) ±14 °C (±25 °F)

Table 4 Recommended heat treatment procedures for selected nickel-base corrosion resistant alloys

Alloys 200 and 201 for caustic service

1. Hold at 704 °C (1300 °F) for a minimum of 0.5 h/25.4 mm (1 in.) of thickness.
2. Determine the heating and cooling rates, which will vary with the shape of the part. Complex shapes with nonuniform thicknesses should have heating and cooling rates of 111 °C (200 °F)/h. Shapes with uniform thicknesses can use fast heating and air cooling.

Alloy 600 for caustic service

1. Hold at 899 °C (1650 °F) for a minimum of 1 h/25.4 mm (1 in.) of thickness or at 788 °C (1450 °F) for a minimum of 4 h/25.4 mm (1 in.) of thickness.
2. Determine heating and cooling rates per guidelines for alloys 200 and 201.

Alloy 400 for hydrofluoric acid service

1. Hold at 593 °C (1100 °F) for a minimum of 0.5 h/25.4 mm (1 in.) of thickness.
2. Determine heating and cooling rates per guidelines for alloys 200 and 201.

Table 5 Welding products for dissimilar-metal joints between nickel-base alloys and other metals

	Welding product for dissimilar-metal joint with:									
	Stainless steel		Carbon and low-alloy steel		5–9% Ni steel		Copper		Nickel-copper	
Nickel-base alloy	Electrode	Filler metal	Electrode	Filler metal	Electrode	Filler metal	Electrode	Filler metal	Electrode	Filler metal
200, 201	ENiCrFe-2 (lnco Weld A)	ERNiCr-3 (FM 82)	ENiCrFe-2 (lnco Weld A)	ERNiCr-3 (FM 82)	ERNiCrFe-2 (lnco Weld A)	ERNiCr-3 (FM 82)	ENiCu-7 (WE 190)	ERNiCu-7 (FM 60)	ENiCu-7 (WE 190)	ERNiCu-7 (FM 60)
400	ENiCrFe-2 (Inco Weld A)	ERNiCr-3 (FM 82)	ENiCu-7 (WE 190)	ERNi-1 (FM 61)	ENiCu-7 (WE 190)	ERNi-1 (FM 61)	ENiCu-7 (WE 190)	ERNiCu-7 (FM 60)	ENiCu-7 (WE 190)	ERNiCu-7 (FM 60)
600, 601	ENiCrFe-2 (Inco Weld A)	ERNiCr-3 (FM 82)	ENiCrFe-2 (Inco Weld A)	ERNiCr-3 (Fm 82)	ENiCrFe-2 (Inco Weld A)	ERNiCr-3 (FM 82)	ENi-1 (WE 741)	ERNi-1 (FM 61)	ENi-1 (WE 141)	ERNi-1 (FM 61)
690	ENiCrFe-2 (Inco Weld A)	ERNiCr-3 (FM 82)	ENiCrFe-2 (Inco Weld A)	ERNiCr-3 (FM 82)	ENiCrFe-2 (Inco Weld A)	ERNiCr-3 (FM 82)	ENi-1(a) (WE 141)	ERNi-1 (FM 61)	ENi-1(a) (WE 141)	ERNi-1(a) (FM 61)
800	ENiCrFe-2 (Inco Weld A)	ERNiCr-3 (FM 82)	ENiCrFe-2 (Inco Weld A)	ERNiCr-3 (FM 82)	ENiCrFe-2 (Inco Weld A)	ERNiCr-3 (FM 82)	ENi-1 (WE 141)	ERNi-1 (FM 61)	ENi-1 (WE 141)	ERNi-1 (FM 61)
825	ENiCrMo-3 (WE 112)	ERNiCrMo-3 (FM 625)	ENiCrMo-3 (WE 112)	ERNiCrMo-3 (FM 625)	(WE 113)	ERNiCrMo-3 (FM 625)	ENi-1 (We 141)	ERNi-1 (FM 61)	ENi-1 (WE 141)	ERNi-1 (FM 61)

(a) Precaution is required to minimize copper dilution in the weld, because of the high chromium level of alloy 690. "Buttering" the copper or copper-nickel side of the joint with nickel weld metal prior to welding may be advisable.

two thickness ranges. Both designs include a small edge of unbeveled steel above the cladding to protect the cladding when the steel is welded. The steel side should be welded first, using a low-hydrogen welding product. It is important to avoid cladding penetration during the first welding pass. Dilution of the steel weld with the nickel-alloy cladding can cause the deposit to crack. The clad side of the joint should be prepared by grinding or chipping, and it should be welded using the welding product that is recommended for solid sections of the cladding alloy. The weld metal will be diluted with steel. To maintain corrosion resistance, at least two layers should be applied, although three or more layers are preferable.

The strip-back method is sometimes used instead of the procedure described above. The cladding is removed from the vicinity of the joint, as shown in Fig. 7. The remaining steel is then welded using a standard steel joint design and technique, and the nickel-alloy cladding is reapplied by weld overlaying. The advantage of the strip-back method is that it eliminates the possibility of cracking caused by steel weld metal penetration into the cladding (Ref 7).

Some joints, such as those in closed vessels or tubular products, are accessible only from the steel side. In such cases, a standard steel joint design is used, and the cladding at the bottom of the joint is welded first with nickel-base alloy weld metal. After the cladding is welded, the joint can either be completed with nickel-base alloy weld metal, or, after a barrier layer of carbon-free iron is applied, the joint can be completed with steel weld metal. If the steel thickness is 8.0 mm (5/16 in.) or less, it is generally more economical to complete the joint with nickel-base alloy weld metal.

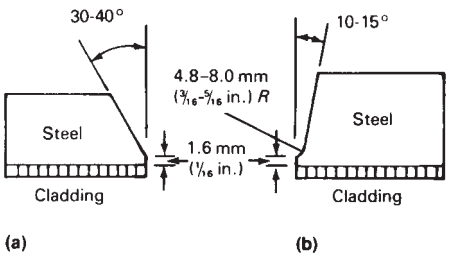


Fig. 6 Joint designs for clad steel. (a) Material of 4.8 to 16 mm (3/16 to 5/8 in.) thickness. (b) Material of 16 to 25 mm (5/8 to 1 in.) thickness. Source: Ref 7

Weld Overlay Cladding. Nickel-base alloy weld metals are readily applied as overlays on carbon steels, low-alloy steels, and other materials. The cleanliness of the surface to be overlaid is extremely important. All oxides and foreign materials must be removed prior to welding to ensure crack-free results and to minimize the possibility of oxide inclusions in the deposited weld metal. If the material being overlaid has a high sulfur or phosphorus content, then cracking is possible in the deposited nickel-base alloy weld layer. If this occurs, then the cracked layer should be ground or machined away and another layer deposited.

This sacrificial layer approach is just one solution to this situation. Other approaches would be to deposit the first layer with a more-tolerant weld metal composition or, if possible, to design the structure with a lower sulfur/phosphorus base material. Using a welding process and welding parameters that minimize dilution also is very helpful in avoiding problems in this type of situation.

Welding of Castings. Many of the wrought solid-solution nickel alloys discussed in this article have equivalent cast compositions that are modified slightly to enhance castability and properties. The largest modification usually is the increase in silicon content, which unfortunately has an adverse effect on weldability. It is not unusual to find silicon levels that exceed 1.5% in cast nickel-base alloys. Depending on other influences, such as restraint, amount of other minor elements, and the welding process used, this level of silicon may result in weld cracking. When welding surface defects that occurred during the casting process, which is a common welding procedure with castings, the welder can use most welding methods with most of the solid-solution nickel-base alloy castings.

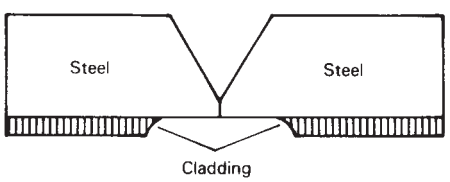


Fig. 7 Strip-back method of joint preparation. Source: Ref 7

Repair Welding. The solid-solution nickel-base alloy system does not undergo drastic metallurgical changes during either thermal cycling or exposure to commonly encountered service temperatures, as do many of the ferrous alloys. This is a definite benefit when it becomes necessary to repair weld a component. Except for exposure to surface-modifying environments, such as carburization, nickel-base alloys generally retain their excellent weldability, even after prolonged service exposure. In those cases where a general condition renders a component unusable, such as overall carburization or oxidation attack, very little can be done to repair weld the part. However, if a localized area fails, then there usually is a good chance that a repair weld can salvage the component.

There are occasions when a carburized area is the site of a failure, and, if the carburization was not the primary reason for the failure, then sometimes the localized area can be ground free of the carburized layer and a successful repair weld made. If the carburization did cause the failure, then localized repair welding would probably result in only a short extension of component life, because failure in another area of the carburized surface would undoubtedly occur quickly. This example illustrates how inspection and examination of the component is an important aspect when deciding whether or not to make a weld repair. Once the decision has been made that repair welding is feasible, an area of the component should be ground clean and a test weld made to determine whether the material can be successfully welded. If this test is positive, then the component should be thoroughly prepared by grinding the surface, if necessary, and cleaning it prior to actual repair welding. If groove welding is necessary, then the previously described precautions concerning joint design should be followed in order to provide room for electrode manipulation.

Welding Metallurgy of Corrosion Resistant Alloys Containing Molybdenum

This section addresses a family of solid solution-strengthened materials that contain appreciable amounts of molybdenum (5 to 28% Mo). Molybdenum additions to nickel substantially improve resistance to nonoxidizing acid environments.

The Hastelloy Family of Alloys

Table 6 gives the nominal compositions of the most widely used materials in the Hastelloy family. Although other molybdenum-bearing nickel-base alloys exist, the information presented below is relative to the joining of similar alloys.

Alloy C Family. Hastelloy alloy C, developed in the early 1930s, is the grandfather of the nickel-chromium-molybdenum family of corrosion-resistant materials. Advances in process metallurgy and corrosion research have prompted the evolution of various C-type alloys. The minimum carbon content of the original alloy C composition was limited to about 0.05% C by the arc-melting practices of the time.

The nickel-chromium-molybdenum alloys proved to be extremely important in the chemical processing industry, because they provided corrosion resistance over a wide range of reducing and oxidizing environments. However, grain boundary precipitation of carbides in the as-welded condition required a postweld solution heat treatment to restore optimum corrosion resistance. The deleterious effect of both carbon and silicon on corrosion resistance led to the development of alloy C-276.

An important factor in this new alloy was the development of a reliable quantitative method for determining susceptibility to intergranular attack in the original C-type alloy and the newer C-276 and C-4 alloys (Ref 8). The introduction of the argon-oxygen decarburization (AOD) process in the late 1960s made the production of alloy C-276 commercially viable. The maximum carbon content of alloy C-276 is 0.01% C with typical production compositions of about 0.005% C (Ref 2). Unfortunately, the optimum corrosion resistance of alloy C-276 was found to be hampered by the precipitation of an intermetallic compound rich in molybdenum and tungsten. The alloy is particularly susceptible to μ-phase formation when exposed to temperatures ranging from 650 to 1095 °C (1200 to 2000 °F).

Advances in alloy development theory, specifically the concept of electron vacancy number (N_V), led to the evolution of alloy C-4 in 1975. Alloy C-4 is essentially a tungsten-free, low-carbon, low-silicon ternary alloy of nickel, chromium, and molybdenum. Secondary carbide precipitation was further controlled by the addition of titanium to stabilize residual carbon that was not totally removed by argon oxygen decarburization (AOD) refining. Unfortunately, the removal of tungsten in order to reduce μ-phase precipitation also reduced the resistance of the alloy to localized corrosion attack, namely pitting and crevice corrosion (Ref 9).

A relatively recent (1985) development in the alloy C family is alloy C-22. Because it was recognized that molybdenum and tungsten had an opposing role to that of chromium in reducing versus oxidizing acid environments, alloy C-22 was developed with the proper balance of both elements to achieve versatility in a wide range of corrosive environments. The reduction of the molybdenum and tungsten content in alloy C-22, versus their content in alloy C-276, also resulted in improved thermal stability (that is, resistance to intermetallic compound formation). An example of an alloy C-type application is in the lining of inlet and outlet ducts that are associated with the flue gas desulfurization (FGD) systems being installed by electric power utility companies.

Alloy B Family. Hastelloy alloy B-2 is unique in that it contains essentially no chromium, an element common to nearly all other corrosion resistant alloys (Ref 10). It was originally developed to resist hydrochloric acid in all concentrations up to the boiling point and is used in many applications involving the production of this acid, as well as acetic acid and other chemicals. The alloy also resists sulfuric acid and pure phosphoric acid. Without chromium, however, this alloy is vulnerable to corrosion attack in reducing acids when oxidizing salts such as ferric or cupric chloride are present, even in the parts-per-million range.

Not unlike the old alloy C, which required postweld heat treatment to restore optimum corrosion properties, alloy B (the predecessor to alloy B-2) was improved by the evolution of a low-carbon (0.02% C maximum) and low-silicon version (0.08% Si maximum). Alloy B-2 is close to being a commercially "pure" binary alloy of nickel and molybdenum. It has a face-centered cubic (fcc) crystal structure and is quite ductile in the solution-annealed condition (that is, 60% room-temperature tensile elongation). However, the alloy forms intermetallic phases, Ni_3Mo and Ni_4Mo, with modest exposure to the intermediate temperature range from 595 to 850 °C (1100 to 1560 °F). Precipitation of these intermetallic compounds can render alloy B-2 quite brittle. For example, its room-temperature ductility can drop to less than 5% elongation if it is exposed to 760 °C (1400 °F) for a period of 10 min.

A third-generation B-type alloy (B-3) has recently been developed. Its composition was specially formulated to provide improved thermal stability while retaining the corrosion resistance of alloy B-2. This means that the reaction kinetics that drive the formation of Ni_3Mo and Ni_4Mo have been significantly retarded, greatly improving the fabricability of this family of alloys.

The alloy G family of alloys has excellent resistance to phosphoric acid and has been used in wet-process phosphoric acid evaporators, agitator shafts, pumps, and in the handling of superphosphoric acid (76% P_2O_5). Alloys G-3 and G-30 are newer versions of predecessor alloy G. Alloy G-3 is a lower-carbon version (0.015% C maximum versus 0.05% C maximum) and, hence, has improved resistance to HAZ carbide precipitation. Improved resistance to hot cracking and improved weld metal bend ductility were also achieved by reducing the niobium plus tantalum content from nominally 2.0% (alloy G) to 0.5% maximum (alloy G-3). Alloy G-30 is a high-chromium (30% Cr) alloy designed to possess even greater resistance to HAZ corrosion attack. Because the phenomenon of sensitization involves the type and amount of HAZ precipitation but also the depleted zones associated with the precipitates, the resistance of alloy G-30 to HAZ corrosion degradation is achieved by higher available chromium, even in the depleted zones. Alloy G-30 resists highly oxidizing acids such as the nitric plus hydrofluoric acid mixtures used in metal pickling baths and in nuclear waste reprocessing.

General Welding Characteristics

Physical Properties. Because of similarities in heat capacity, density, and other physical properties, the welding characteristics of

Table 6 Nominal composition of selected molybdenum-bearing nickel-base corrosion resistant alloys

			Composition, wt%										
Alloy type	Alloy	UNS No.	Ni	Co	Fe	Cr	Mo	W	Mn	Si	C	Cu	Others
Ni-Mo	B-2	N10665	69	1 max	2 max	1 max	28	···	1 max	0.1 max	0.01 max	···	···
	B-3	N10675	65	3 max	1.5	1.5	28.5	3 max	3 max	0.1 max	0.01 max	…	0.5 Al max; 0.2 Ti max
Low C, Ni-Mo-Cr	C-4	N06455	65	2 max	3 max	16	16	···	1 max	0.08 max	0.01 max	···	0.7 Ti max
	C-22	N06022	56	2.5 max	3	22	13	3	0.5 max	0.08 max	0.010	···	0.35 V max
	C-276	N10276	57	2.5 max	5	16	16	4	1	0.08 max	0.01 max	···	0.35 V max
	G-3	N06985	44	5 max	19.5	22	7	1.5 max	1 max	1 max	0.015 max	2.5	0.5 Nb max
Ni-Cr-Fe-Mo-Cu	G-30	N06030	43	5 max	15	30	5.5	2.5	1.5 max	1 max	0.03 max	2	1.5 Nb max
Ni-Mo-Cr-Fe	N	N10003	71	0.2 max	5 max	7	16	0.5 max	0.8 max	1 max	0.08 max	0.35 max	0.5 (Al + Ti) max

the alloys described in this section are quite similar to properties of austenitic stainless steels. The major differences between these alloys and stainless steel are lower thermal expansion, lower thermal conductivity, and higher electrical resistivity. Generally, solidus temperatures are approximately 55 °C (100 °F) lower than those of type 304 stainless. Table 7 summarizes the comparative physical properties relevant to welding and joining operations.

Welding Processes. Gas-tungsten arc welding (GTAW), gas-metal arc welding (GMAW), and shielded metal arc welding (SMAW) processes are commonly used to join this family of corrosion resistant alloys.

A filler metal that matches the composition of the base material is usually recommended when welding the nickel-chromium-molybdenum alloys. Other processes, such as plasma arc welding (PAW), resistance spot welding (RSW), laser-beam welding (LBW), electron-beam welding (EBW), and friction welding, can be used. The plasma arc cutting process is commonly used to cut alloy plate into desired shapes and to prepare weld angles. Oxyacetylene cutting is not recommended, nor is the use of oxyacetylene welding (OAW) and submerged arc welding (SAW). Oxyacetylene welding is not recommended because of the possibility of carbon pickup from the flame, whereas submerged arc welding is not recommended because of its high heat input, chromium loss across the arc, and silicon pickup from the welding flux.

Generally, welding heat input is controlled in the low-to-moderate range. Wide weave beads are not recommended. Stringer bead welding techniques, with some electrode manipulation, are preferred. The nickel-chromium-molybdenum alloy weld metal is not as fluid as carbon steel and does not flow out as readily to "wet" the sidewalls. Therefore, the welding arc and filler metal must be manipulated so as to place the molten metal where it is needed. In addition to sluggishness, the penetration pattern of this alloy type is less than that of a typical carbon or stainless steel weld, and incomplete fusion is more likely to occur. Therefore, care must be taken to ensure that the groove opening is wide enough to allow proper torch or electrode manipulation and proper placement of the weld bead.

Cleaning, Edge Preparation, and Fit-Up. Proper penetration of the weld angles is a very important part of welding these nickel-base corrosion resistant alloys. It is necessary to condition all thermal-cut edges to bright, shiny metal prior to welding. This is particularly important if air arc gouging is being used, because of the possibility of carbon pickup from the carbon electrode.

In addition to the weld angle, a 25 mm (1 in.) wide band on both the top and bottom (face and root) surface of the weld zone should be conditioned to bright metal with approximately an 80-grit flapper wheel or disk. This procedure is particularly important for the SMAW of alloy B-2. If the mill scale is not removed, then the B-2 alloy welding flux can interact with it and cause cracking at the toe of the weld in the base material.

The welding surface and adjacent regions should be thoroughly cleaned with an appropriate solvent prior to any welding operation. All greases, oils, cutting oils, crayon marks, machining solutions, corrosion products, paints, scale, dye-penetrant solutions, and other foreign matter should be completely removed.

Stainless steel wire brushing is normally sufficient for interpass cleaning of GTAW and GMAW weldments. The grinding of starts and stops is recommended for all fusion welding processes. When the GMAW process is used, light grinding may be necessary between passes prior to wire brushing, depending on the composition of the shielding gas. Slag removal during SMAW will require chipping and grinding, followed by wire brushing.

Preheating the nickel-molybdenum and nickel-chromium-molybdenum alloys is not required. A preheat is generally specified as room temperature (typical shop conditions). Interpass temperature should be maintained below 95 °C (200 °F). Auxiliary cooling methods can be used to control the interpass temperature. Water quenching is acceptable. However, care must be taken to avoid contaminating the weld zone with traces of oil from shop air lines, grit/dirt from soiled water-soaked rags, or mineral deposits from hard water used to cool the weld joint. The safest way to maintain a low interpass temperature is to allow the assembly to cool naturally. When attaching hardware to the outside of a thin-walled vessel, it is good practice to provide auxiliary cooling to the inside (process side) to minimize the extent of the HAZ.

Welding Metallurgy of the HAZ

Carbide Precipitation in the HAZ. The corrosion resistance of weldments is related to the microstructural and microchemical changes resulting from thermal cycling. The effects of welding on the corrosion resistance of nickel-base alloys are similar to the effects on the corrosion resistance of stainless steels. For example, sensitization due to carbide precipitation in the HAZ is a potential problem in both classes of alloys. However, it should be noted here that the solid solubility of carbon is considerably lower in nickel-base alloys than in stainless steels. The net effect is that during the welding of low-carbon, nickel-molybdenum and nickel-chromium-molybdenum, corrosion resistant alloys, HAZ grain boundary precipitation is still a potential reality, despite the relatively low carbon content of these alloys. The amount and severity of precipitation will depend on the cooling rate through the intermediate temperature range from 1000 to 600 °C (1830 to 1110 °F). Some heat-to-heat variations in grain boundary precipitation have also been observed during simulated HAZ studies in alloy B-2 (Ref 11). The adverse effects of minor grain boundary precipitation depend on the severity of the corrosive environment. For example, the maximum corrosion penetration after testing in boiling 10% hydrochloric acid (HCl) varied little for simulated heat-affected zones in alloy B-2. However, when harsher autoclave testing environments were used (20% HCl at 150 °C, or 300 °F), penetration by corrosion increased as the simulated HAZ cooling rate decreased from 20 to 120 s through the critical intermediate temperature range (Ref 11). Despite these laboratory findings, most low-carbon nickel-molybdenum and nickel-chromium- molybdenum alloys have been put into corrosion service in the as-welded condition with good results. Occasionally, poor results are encountered. Metallographic examination of the corroded part will usually reveal evidence of grain boundary precipitation in the HAZ (Fig. 8).

Other HAZ Problems. Aside from the possibility of grain growth, few other metallurgical HAZ problems have been reported for these alloys. HAZ hot cracking, especially of the type created by constitutional liquation of primary carbide particles, is not a problem.

Welding Metallurgy of the Fusion Zone

Fusion zone welding metallurgy of the nickel-molybdenum and nickel-chromium-molybde-

Table 7 Physical properties of nickel-base molybdenum-bearing corrosion resistant alloys relative to carbon steel and stainless steels

	Melting temperature range		Density		Thermal conductivity		Coefficient of thermal expansion		Electrical resistivity,
Material	°C	°F	g/cm^3	lb/in.^{3}	W/m · K	Btu · in./ft^2 · h · °F	10^{-6}/K	10^{-6}/ °F	10^{-8} Ω · m
Carbon steel	1470–1530	2670–2785	7.9	0.285	0.46	3.2	11.7	6.51	19
Austenitic stainless steel	1390–1450	2535–2640	8.0	0.289	0.16	1.1	17.0	9.45	72
Nickel-base corrosion resistant alloys									
Alloy B-2	1350–1390	2460–2535	9.2	0.332	0.11	0.76	10.3	5.73	137
Alloy C-22	1350–1390	2460–2535	8.7	0.314	0.10	0.69	12.4	6.89	114
Alloy G-30	1300–1350	2370–2460	8.2	0.296	0.10	0.69	12.8	7.12	116

alloy family is important, because base materials are usually welded with filler metals of matching composition and because these alloys can be welded autogeneously (no filler added), as in the case of welded tubular products. Three issues should be considered in terms of the fusion zone:

- Effect of weld metal segregation on corrosion resistance
- Propensity to form porosity
- Solidification hot-crick sensitivity

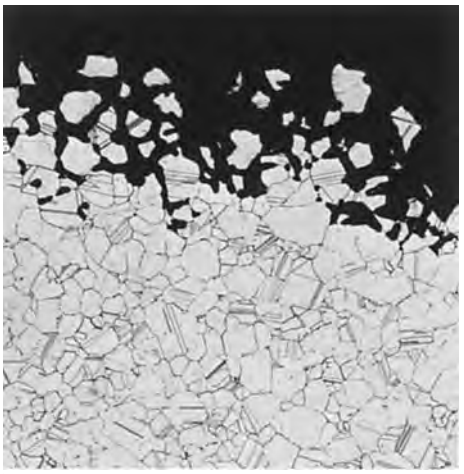
Segregation. Because of the segregation of solute elements on solidification (principally molybdenum, which segregates to the cellular dendritic boundaries of the fusion zone), it is generally accepted that the corrosion resistance of the weld metal will be marginally less than that of the more homogeneous wrought-base material. Differences in corrosion performance, however, depend heavily on the severity of the corrosion environment. In mild corrosion environments, little difference is observed. In severe environments, the fusion zone may be preferentially attacked, as illustrated in Fig. 9, a cross section of an as-welded alloy B-2 coupon exposed for about 1 year in a chemical plant process stream. Figure 10(a) is a high-magnification view of the surface attack on alloy B-2 weld metal when tested for 96 h in 20% HCl at 150 °C (300 °F) in an autoclave. Under these conditions, corrosion attack appears to be the most aggressive at the dendrite cores (molybdenum lean). Figure 10(b) shows the lack of corrosion attack on weld metal from a specially devised overalloyed B-type filler material (Ref 12). This alloy consists of 42% Mo, rather than the nominal 28% Mo. The higher-molybdenum nickel alloy solidifies as a nonequilibrium hypoeutectic structure consisting of a metastable α phase, with Ni_3Mo and NiMo in the interdendritic regions. In this case, despite solidification segregation, the dendrite core regions are sufficiently saturated with molybdenum to resist preferential fusion zone attack.

It should be noted that although the microstructure of the Ni-42Mo material in Fig. 10(b) offers high corrosion resistance, the alloy is characterized by limited weld ductility (Ref 13). However, the use of overalloyed filler metals as a solution to preferential weld metal corrosion attack has been demonstrated elsewhere. For example, alloy C-22 (22% Cr) has been used successfully to refurbish corroded welds in an alloy C-276 (16% Cr) pulp and paper mill bleach-mixing device. Alloy G-30 (30% Cr) is also a logical choice as an overalloyed filler for certain alloy G-3 components.

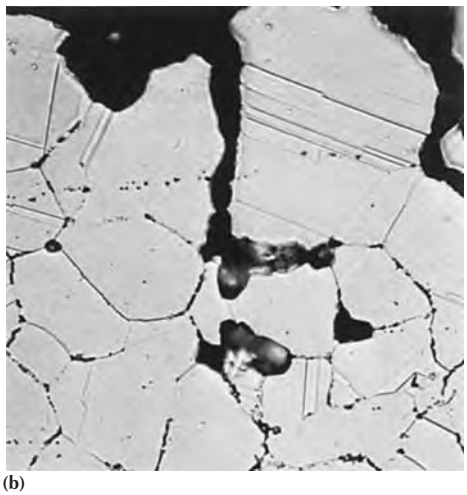
Porosity. Recognizing that the solubility of gas is greater in the liquid state than in the solid state, the subject of weld porosity is relevant to fusion zone discussion. The three most logical origins of gas-generated porosity are carbon monoxide, hydrogen, and nitrogen. However, in welding the low-carbon nickel-molybdenum and nickel-chromium-molybdenum alloys, the cause of porosity is not believed to be from the formation of carbon monoxide. As long as there is a residual silicon or aluminum content in the weld deposit, the oxygen potential is too low for the formation of carbon monoxide. In order to produce a carbon monoxide "carbon boil" during welding, it would be necessary first to deplete all the aluminum, silicon, and any other deoxidizers that may be present,

Gas hole formation can be caused by hydrogen evolution. As is well known, even the smallest amount of water will be reduced by metal deoxidizers, releasing a sufficient volume of gas to create porosity. Hydrocarbons can also dissociate and go into solution. The lower the carbon content of the alloy, the more likely it is to pick up hydrogen from hydrocarbons. These reactions are favored as the carbon content of the alloy decreases. Gas hole formation that is due to hydrogen can be minimized by the well-known methods of keeping the joint area and the weld filler metal dry and oil-free. This approach is especially true when welding with coated electrodes. The ceramic coating ingredients can absorb sufficient moisture in humid weather to cause potential problems. It is because of this behavior that unused electrodes should be stored in a warm oven (110 °C, or 230 °F, minimum).

The third and only other possible cause of gas hole formation is nitrogen. As is well documented in the literature, a large quantity of nitrogen is capable of being picked up by the molten metal during are welding processes whenever the gas in the arc contains any nitrogen.



(a)

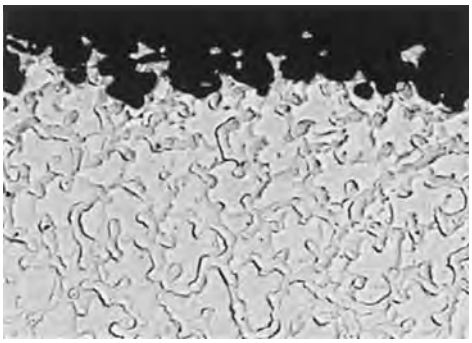


(b)

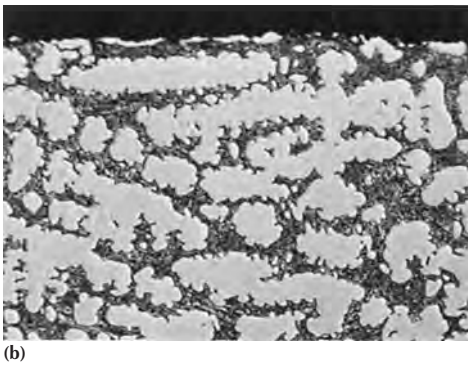
Fig. 8 Micrographs showing corrosion attack in Hastelloy C-276 (UNS N10276) caused by grain boundary precipitation in the heat-affected zone of the weld. The sample was taken from a pipe removed after 18 months of service in a hydrochloric acid vapor environment in a chemical plant. Sample was etched in HCl and oxalic acid. (a) 75×. (b) 375×



Fig. 9 Metallographic cross section showing preferential fusion zone attack in Hastelloy B-2 (UNS N10665). Sample was a welded coupon placed in a chemical plant process stream for approximately 1 year. Hydrochloric and chromic acid etch. 75×



(a)



(b)

Fig. 10 Metallographic cross sections of the corroded surface of weld deposits on Hastelloy B-2 (UNS N10665) after testing in an autoclave at 150 °C (300 °F) for 96 h in a 20% HCl environment. (a) Ni-28Mo (UNS N10665) alloy filler metal. 375×. (b) Ni-42Mo filler metal. 375×. Both samples were etched in hydrochloric acid and chromic acid. See text for explanation.

Nitrogen pickup from air, for example, might prove to be a problem whenever the weld pool is improperly shielded. Different alloys would be expected to have different susceptibilities to nitrogen-induced porosity. The ability of the solidified matrix plus secondary solid phases to hold or carry nitrogen is the primary difference between alloys. Alloys with a greater nitrogen-carrying capacity are apparently less susceptible to nitrogen-induced porosity. For example, a nickel-chromium alloy would be less susceptible to nitrogen porosity than pure nickel because of the increased solubility of nitrogen. Furthermore, because alloy B-2 contains no chromium, it possesses a lower nitrogen solubility than alloy C-22, and, thus, would be more prone to nitrogen porosity.

Hot-Crack Sensitivity. The final fusion zone issue is hot-crack sensitivity. Hot cracking of C-type alloys during solidification has been studied in depth by researchers equipped with sophisticated microanalysis equipment (Ref 14). Solidification hot cracking, as generated by the varestraint hot-cracking device, was found to increase as the tendency to form intermetallic, secondary-solidification constituents increased. In terms of general weldability ranking, alloy C-4 was found to be the least sensitive to solidification cracking, followed by alloy C-22, and then alloy C-276. It should be noted that all of the low-carbon nickel-chromium-molybdenum alloys of the C family are characterized by high weld metal ductility. Hot-cracking problems have rarely been reported under actual fabrication conditions.

Postweld Heat Treatment

Because of their very low carbon contents (<0.02% C), the newer-generation corrosion resistant alloys do not require heat treatment after welding. However, for certain critical corrosion environments, proper postweld annealing will maximize corrosion resistance of the HAZ. Annealing can also be performed to reduce residual stresses, which play a role in the susceptibility to stress-corrosion cracking in some environments. Annealing can be used to increase the corrosion resistance of the weld fusion zone by promoting diffusion of some elements.

Corrosion resistant alloys are usually supplied in the mill-annealed condition, unless otherwise specified. The mill-annealing procedure has been designed to place the material in the optimum condition with respect to ductility and corrosion resistance. During fabrication of a vessel or component, several operations or conditions may require an anneal. For example, following any hot-forming operation, a reanneal of the material should be done to restore ductility and corrosion properties. Annealing is also performed after cold working to restore ductility. Generally, annealing is not required if the total cold work is below 7% outer fiber elongation. In general, the only heat treatment that is acceptable for these alloys is a full solution anneal. Table 8 lists the proper heat treating temperatures and type of quench. Intermediate temperatures commonly used for stress-relieving steels, stainless steels, and other alloys are not effective and could promote precipitation that would be detrimental to corrosion resistance.

Before heat treatment, grease, graphite, and other foreign materials must be removed from all surfaces. Tube products may require special care for complete removal of these contaminants from interior surfaces. Carburization of these materials at the heat-treating temperatures can reduce corrosion resistance, and sulfur embrittlement can cause severe cracking. Proper control of the temperature and time cycle are also critical. A flexible set of rules governing soaking-annealing time is generally followed, because of the many variations in furnace type, furnace operation, facilities for loading and unloading the furnace, and so on. The temperature should be monitored using thermocouples attached to the piece being annealed. The actual holding time should be measured beginning when the entire section is at the specified annealing temperature. It is important to remember that the center of a section does not reach the solutioning temperature as soon as the surface does.

Normally, hold time should be in the range from 10 to 30 min, depending on section thickness. Thin-sheet components are held at the shorter time, whereas heavier sections are held at the longer time. Shorter annealing times can be used if the sole purpose is to remove the effect of cold work. Longer annealing times might be required if the objective is to promote homogenization of the fusion zone.

Rapid cooling is essential after solution heat treatment to prevent the precipitation of secondary phases and the resultant lowering of the corrosion resistance of these alloys. Water quenching is recommended on material thicker than 9.5 mm ($\frac{3}{8}$ in.). Although rapid air cooling can be used on sections thinner than 9.5 mm ($\frac{3}{8}$ in.), water quenching is preferred. The time from the furnace to the quench tank or to the start of rapid air cooling must be as short as possible (less than 3 min).

The requirements for proper annealing of alloy B-2 (UNS N10665) are quite demanding. In addition to the guidelines established above, the following factors should be considered very carefully. It is strongly recommended that the part being heat treated be charged into a furnace that is at the annealing temperature, and that the heating rate be as fast as possible. In addition, the thermal capacity of the furnace should be large to allow the temperature of the furnace to recover quickly after the part is charged into it. These steps are designed to shorten the time in the intermediate temperature range from 595 to 815 °C (1100 to 1500 °F). Extended exposure (greater than 15 min) at these intermediate temperatures can cause intergranular cracking because of phase transformations, especially if the part is in the cold-worked condition. Under certain conditions, shot peening prior to heat treatment may be beneficial to the elimination of residual tensile stresses. For example, it has been observed that shot peening the knuckle radius and straight flange regions of a cold-formed head prior to heat treatment can help reduce intermediate temperature intergranular cracking by lowering the residual stress patterns at the surface of the cold-formed component.

Special Welding Considerations

Dissimilar Metal Welding. Welding of dissimilar metals to nickel-base corrosion resistant alloys does not present a problem in most cases. The nature of nickel as a "forgiving" solvent element renders most industrially encountered dissimilar metal combinations as metallurgically compatible. Filler materials designed to join the nickel-base side of the joint are usually recommended.

When joining a nickel-base alloy to a ferrous alloy (for example, mild steel or a stainless steel), electrodes of the nickel-base alloy should be used as filler metal, rather than steel or stainless electrodes, because excess superheat caused by melting temperature differences (Table 7) tend to aggravate the HAZ on the nickel-base side of the joint.

The joining of clad plate (that is, steel plate that has been explosion clad or roll clad with a thinner nickel-base corrosion resistant alloy) has been successfully performed. However, proper welding procedures need to be developed to ensure minimum iron dilution in the weld zone facing the corrosion environment.

Welding of Castings. The welding of cast molybdenum-containing nickel-base alloys presents no unusual problems, as long as the integrity of the casting is sound (that is, free from shrinkage cavity and inclusions). Welding is often used to repair casting defects. Generally, the defective area is thoroughly removed by grinding, which eventually forms a cavity. The prepared cavity should be dye-penetrant inspected to ensure that all objectionable defects have been removed and then thoroughly cleaned prior to welding repair. Because these alloys have low-penetration characteristics, the ground cavity must be broad enough and have sufficient sidewall clearance in the weld groove

Table 8 Solution annealing temperatures for corrosion-resistant nickel-base alloys containing molybdenum

Data are applicable for either water quench (WQ) or rapid air cool (RAC) quench.

Alloy	UNS No.	Temperature	
		°C ± 14°	°F ± 25°
B-2	N10665	1065	1950
C-4	N06455	1065	1950
C-22	N06022	1120	2050
C-276	N10276	1120	2150
G-3	N06905	1150	2100
G-30	N06030	1175	2150
N	N10003	1175	2150

to allow weld rod/weld bead manipulation. It is not recommended to heal cracks or wash out defects by autogeneously remelting weld beads or by depositing additional filler metal over the defect.

Repair welding of wrought alloy components and structures is accomplished using a similar technique. The good thermal stability of low-carbon corrosion resistant alloys is such that solution annealing of material that has been in corrosion service for many years is generally not required prior to repair welding. In these situations, the repair is usually required because of accelerated corrosion of a localized area. The selection of higher-alloyed filler metals for such repairs should be considered.

Welding Metallurgy of Heat Resistant Alloys

Some heat resistant nickel-base alloys are solid solution-strengthened, while others are strengthened by the precipitation of a second phase (γ' or γ'') from a supersaturated solid solution. The welding metallurgy of many of the solid solution-strengthened alloys, for example, the Inconels and Incoloys, was described earlier in this article (see the discussions of nickel-chromium and nickel-chromium-iron alloys). In this section, emphasis is placed on special problems associated with welding precipitation-hardened nickel-base superalloys. Compositions of widely used alloys are listed in Table 9.

Welding Problems and Solutions

Nickel-base superalloys have a very high creep resistance, making them attractive for critical high-temperature applications such as gas turbines. The high creep strength in these alloys is obtained by forming fine precipitates of γ' $Ni_3(Al,Ti)$ or γ'' (Ni_3Nb) in them. However, this very characteristic can give rise to problems (or solutions) in welding. Table 10 summarizes the typical welding problems in precipitation-hardenable (PH) nickel-base alloys and their solutions. These include loss of strength in the HAZ, postweld-heat-treatment (strain-age) cracking, and hot cracking in the HAZ and fusion zone. Since hot cracking during welding has already been treated in earlier sections of this article, it will not be repeated here.

Table 9 Nominal compositions of selected precipitation-hardenable nickel-base superalloys

	Composition, %									
Alloy	Ni	Cr	Co	Fe	Mo	Ti	Nb	Al	C	Other
GMR-235	63.0	15.5	···	10.0	5.25	2.0	···	3.0	0.15	0.06 B
Inconel 702	79.5	15.5	···	0.4	···	0.7	···	3.4	0.04	···
Inconel 706	41.5	16.0	···	37.5	···	1.75	2.9(a)	0.2	0.03	···
IN-713C	74.0	12.5	···	···	4.2	0.8	2.0	6.0	0.12	0.012 B, 0.10 Zr
Inconel 718	52.5	19.0	···	18.5	3.0	0.9	5.0	0.5	0.08 max	0.15 Cu max
Inconel 722	75.0	15.5	···	7.0	···	2.5	···	0.7	0.04	···
Inconel X-750	73.0	15.5	···	7.0	···	2.5	1.0	0.7	0.04	0.25 Cu max
Incoloy 901	42.5	12.5	···	36.2	6.0	2.7	···	···	0.10 max	···
M-252	56.5	19.0	10.0	<0.75	10.0	2.6	···	1.0	0.15	0.005 B
René 41	55.0	19.0	11.0	<0.3	10.0	3.1	···	1.5	0.09	0.01 B
Udimet 700	53.0	15.0	18.5	<1.0	5.0	3.4	···	4.3	0.07	0.03 B
Waspaloy	57.0	19.5	13.5	2.0 max	4.3	3.0	···	1.4	0.07	0.006 B, 0.09 Zr

(a) Nb + Ta

Table 10 Typical problems and practical solutions associated with welding precipitation-hardening nickel-base superalloys

Typical problems	Practical solutions
Low strength in HAZ	Re-solution and age harden after welding
Reheat cracking	Use less susceptible grade (Inconel 718)
	Heat-treat in vacuum or inert atmosphere
	Welding in overaged condition (good for René 41)
	Rapid heating through critical temperature range, if possible
Hot cracking in HAZ or fusion zone	Reduce restraint
	Avoid coarse-grain structure and Laves phase

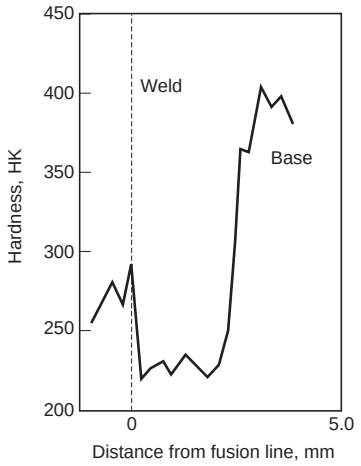


Fig. 11 Hardness profile of alloy 718 welded in the aged condition. Source: Ref 15

Loss of Strength in the HAZ

Welding a PH nickel-base alloy in its aged condition can result in a severe loss of strength in the HAZ. Figure 11, for example, shows the hardness profile of alloy 718 that was welded in the aged condition. The excessive softening of the HAZ due to solutionizing of the precipitates is apparent. In addition to the softening of the HAZ, welding an aged nickel-base alloy can also result in cracking in the areas adjacent to the weld metal. This is because, owing to the softening of the HAZ, these areas become the weakest part of the entire weldment. Unless relatively ductile weld metal is used and severe restraints are avoided, cracking can occur easily in these areas. One way of avoiding the softening of the HAZ is to weld the alloy in its solution-annealed condition first and then postweld-age the entire weldment to develop high strength. Unless this procedure is carried out properly, postweld-heat-treatment cracking can occur, as will be discussed next.

Postweld Heat-Treatment (Strain-Age) Cracking

Precipitation-hardenable (PH) nickel-base alloys are often postweld heat treated for two important reasons: to relieve stress and to develop the maximum strength. In order to develop maximum strength, the weldment is solution annealed and then aged. During solution annealing, the residual stresses in the weldment are also relieved. However, it should be emphasized that aging may occur in the weldment while it is being heated up to the solution annealing temperature, simply because the aging temperature range is lower than the solution annealing temperature. Since this aging action occurs before the residual stresses are relieved, the aging action is harmful and, in fact, often results in cracking during postweld heat treatment. Such postweld-heat-treatment cracking is also called *strain-age cracking* or simply reheat cracking. The term strain-age cracking arises from the fact that cracking occurs in highly restrained weldments as they are heated through the temperature range in which aging occurs. Figure 12 illustrates the welding and postweld heat treating of a heat treatable nickel-base alloy and the occurrence of postweld-heat-treatment cracking.

When strain-age cracking occurs in PH alloys, the results are catastrophic. Figure 13 shows a failure in a 50 mm (2 in.) thick, alloy X-750 plate that was welded in the age-hardened condition and re-aged after welding without intermediate stress relief.

Susceptible Alloys. Figure 14 shows a plot of weldability as a function of (Al + Ti) content. Those alloys with low aluminum and titanium contents, shown below the shaded diagonal line, are more readily weldable and less susceptible to strain-age cracking. However, as combined aluminum and titanium is increased, welding becomes more difficult, and strain-age

cracking is more likely. Alloys like René 41 and Waspaloy are borderline; they weld with relatively little difficulty but sometimes crack during postweld heat treating. Casting alloys with high aluminum and titanium, like 713C and IN-100, have low ductility at all temperatures and usually crack during welding, although repair welding (e.g., turbine-blade and vane-tip restoration) can be carried out if nonhardenable filler metal is used.

Alloy 718 does not undergo strain-age cracking. The age hardening develops around a Ni_3Nb, γ'', precipitate. The γ'' precipitates at a much slower rate than the γ'. This allows alloys to be heated into the solution temperature range without suffering aging and the resultant strain-age cracking. Figure 15 compares the aging rates of several γ' alloys with those of alloy 718, which is strengthened with the γ'' precipitate.

Strain-Age Cracking Susceptibility Curves. Several different methods of avoiding strain-age cracking have been recommended so far. Most of these methods are based on experimentally observed crack susceptibility C-curves. A strain-age crack susceptibility C-curve is a curve indicating the onset of postweld-heat-treatment or strain-age cracking in a temperature-time plot. It is usually obtained by isothermal heat treating of welded circle patches at different temperatures for different periods of time and checking to see if the patches have cracked after heat-treating. Such a curve usually resembles the shape of a "C" and, therefore, is called a strain-age crack susceptibility C-curve. Since the aging rate at the lower end of the aging temperature range is relatively slow, the occurrence of strain-age cracking approaches a symptotically some lower temperature limit. Likewise, since residual stresses are relaxed at the higher temperature end of the aging temperature range and precipitates formed at lower temperature are dissolved, the occurrence of strain-age cracking approaches some higher temperature limit asymptotically. At any temperature between the upper and lower asymptotic limits, there exists a minimum time prior to which no cracking is possible and beyond which cracking is certain to occur (Ref 15).

Shown in Fig. 16 are the crack susceptibility C-curves of Waspaloy and alloy 718. As shown in Fig. 15, alloy 718 ages much more sluggishly than γ'-strengthened nickel-base alloys. As a result, the C-curve of alloy 718 is far to the right of that of Waspaloy, meaning that the former material is much more resistant to strain-age cracking. In fact, alloy 718 is a material designed specifically to minimize strain-age cracking; therefore, when strain-age cracking is of major concern, alloy 718 should be considered.

Other Solutions to Strain-Age Cracking. Although the use of alloy 718 is very effective in avoiding strain-age cracking, it is often necessary to weld other alloys that are more susceptible to strain-age cracking because their properties or specific characteristics are required for an application. In such cases the susceptibility of the particular weldment to strain-age cracking can be reduced in several different ways, as described below. Preweld overaging, either by multistep-type overaging or simply by cooling slowly from the solution annealing temperature, has been observed to significantly reduce postweld heat treatment cracking in René 41 (Ref 15). Figure 17 is an example of such observations.

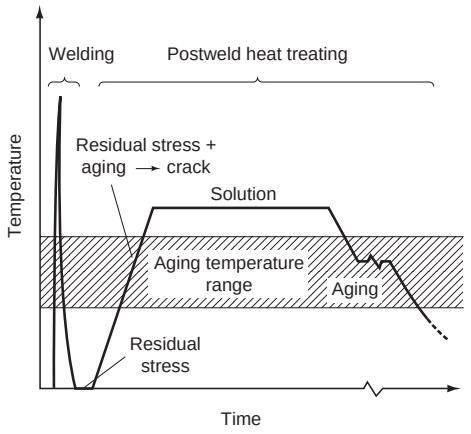


Fig. 12 Schematic illustration for strain-age cracking in precipitation-hardenable nickel-base alloys. Source: Ref 15



Fig. 13 Postweld strain-age cracking failure in Alloy X-750 induced by residual welding stress at a 50 mm (2 in.) thick joint. Alloy was welded in the age-hardened condition and re-aged at 705 °C (1300 °F) for 20 h after welding.

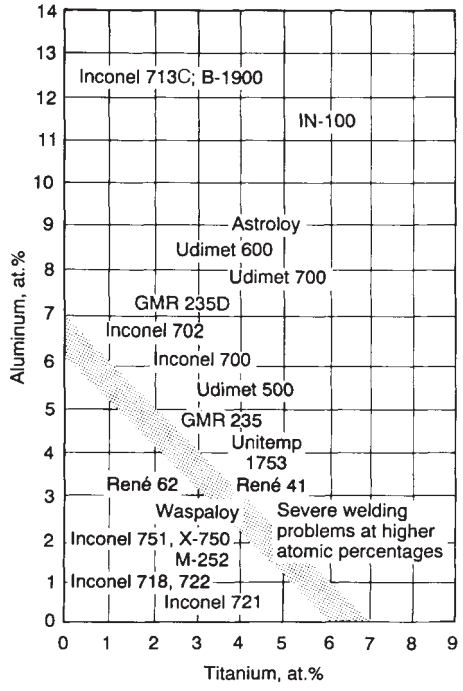


Fig. 14 Plot of aluminum content versus titanium content to indicate commercial nickel-base alloys that present weldability problems when (Al + Ti) content exceeds 6%. Source: Ref 16

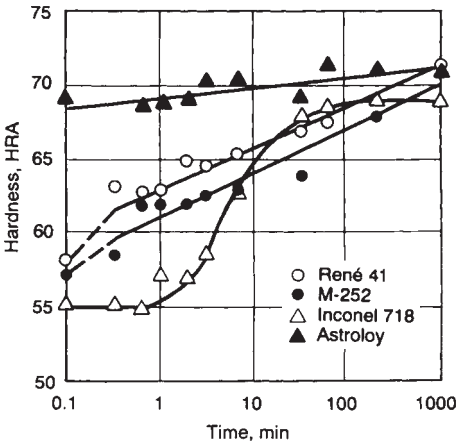


Fig. 15 Plot of hardness versus time to show age-hardening kinetics of selected nickel-base alloys. Source: Ref 17

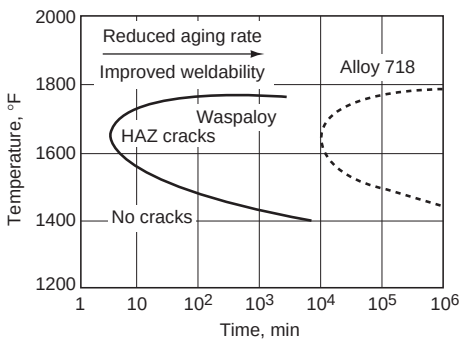


Fig. 16 Strain-age crack susceptibility C-curves for Waspaloy and alloy 718. See text for details. Source: Ref 15

The base metal of a solution-annealed workpiece can age-contract as well as harden during postweld heat treatment, thus preventing effective stress relief in the weldment. If the same weldment is heated up rapidly during postweld heat treatment, effective stress relief can be achieved before it has a chance to harden and age contract, thus avoiding strain-age cracking. As can be seen in Fig. 18, no cracking occurs if the weldment is heated up rapidly to avoid intersecting the crack susceptibility C-curve. This approach is feasible when it is possible to rapidly heat in a furnace or to have a structure that will not excessively distort owing to nonuniform heating. Another way of avoiding strain-age cracking is to use vacuum or inert atmospheres for heat treating. This technique is effective since there is no oxygen present to embrittle the grain boundary during postweld heat treatment. Other approaches that have been recommended include the use of low welding heat inputs, the use of a small grain-size materials, and the control of alloy composition (Fig. 19). Of course, the use of low-restraint joint designs is also recommended.

Summary. The major problem that occurs when postweld heat treating the precipitation-hardenable (PH) alloys is strain-age cracking. The susceptibility of an alloy to strain-age cracking tends to increase with an increasing aluminum and titanium content. Alloys that contain niobium as a hardening element exhibit a sluggish aging response and are therefore less sensitive to strain-age cracking. Strain-age cracking is more prevalent in highly restrained weldments or in the presence of high residual stresses. Cracking is caused by the combination of stress, precipitation strengthening, and the volumetric contraction associated with γ' precipitation. Guidelines to follow to avoid strain-age cracking include these:

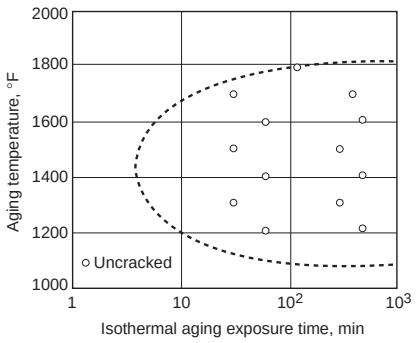


Fig. 17 Comparison of strain-age crack susceptibility for a René 41 specimen that was overaged before welding (circular data points) and a René 41 specimen that was solution annealed before welding (dashed C-curve). The overaging thermal cycle consisted of: 1080 °C (1975 °F), hold for 0.5 h, cool at 2 to 5 °C/min (3 to 8 °F/min) to 980 °C (1800 °F), hold for 4 h, cool at 2 to 5 °C/min (3 to 8 °F/min) to 870 °C (1600 °F) hold for 4 h, cool at 2 to 5 °C/min (3 to 8 °F/min) to 760 °C (1400 °F), hold for 16 h, air cool to room temperature. The result of this overaging treatment is to shift the nose of the C-curve from approximately 4 min in the solution-annealed condition to something in excess of 500 min when overaged. Source: Ref 18

- Minimize residual and thermally induced stresses by using the appropriate joint design, welding process, and filler metal.
- Heat as rapidly as possible through the region of aging temperatures when stress-relief annealing.
- Minimize heat input during welding to avoid partial melting of grain boundaries adjacent to the fusion line.
- Heat treat in an inert atmosphere if possible; the presence of oxygen tends to increase intergranular embrittlement, which can result in cracking.
- Always stress-relief anneal before aging. For heavy-section weldments in aluminum-titanium aged materials, multiple stress-relief anneals may be necessary during welding. Table 11 lists examples of typical stress-relief solution treatment and aging cycles for various PH nickel-base alloys.

Consumable Selection, Procedure Development, and Practice Considerations

Nickel alloys can be joined reliably by all types of welding processes or methods, with the exception of forge welding and oxyacetylene welding. Because the majority of consumables are used with arc welding processes, it is those processes that are discussed in this section. Although some wrought nickel alloys can be welded under conditions similar to those used to weld austenitic stainless steels, there are differences between high-nickel alloys and iron-base alloys that necessitate different techniques. Cast nickel alloys, particularly those with a high silicon content, present difficulties in welding.

The most widely employed processes for welding the non-age-hardenable (solid solution-strengthened) wrought nickel alloys are gas tungsten arc welding (GTAW), gas metal arc welding (GMAW), and shielded metal arc welding (SMAW). Submerged arc welding (SAW) and electroslag welding (ESW) have limited applicability, as does plasma arc welding (PAW). Although the GTAW process is preferred for welding the PH alloys, both the GMAW and SMAW processes are also used.

Heat Treatment of Nickel Alloys

A brief overview of key points that must be considered when heat treating nickel alloy weldments follows. More detailed information can be found in the earlier sections of this article, which dealt with the welding metallurgy of corrosion resistant and heat resistant alloys.

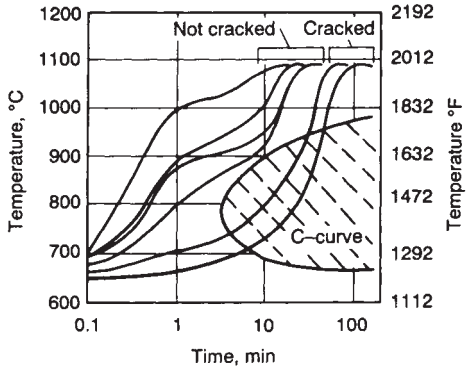


Fig. 18 Effect of heating rate on the cracking tendency of solution-annealed (before welding) René 41 during postweld heat treatment. Source: Ref 19

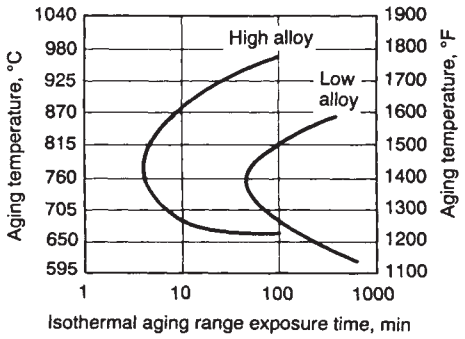


Fig. 19 Effect of alloy composition (high-alloy versus low-alloy concentrations of iron, silicon, manganese, and sulfur taken collectively) on the cracking tendency of postweld heat treated René 41. Source: Ref 19

Table 11 Typical solution treatment and aging cycles for precipitation-strengthened high-temperature alloys

	Solution treatment				Aging			
	Temperature			Cooling	Temperature			Cooling
Alloy	°C	°F	Time, h	procedure	°C	°F	Time, h	procedure
Inconel 718	980	1800	1	Air cool	720	1325	8	Furnace cool
					620	1150	8	Air cool
Inconel X-750	1150	2100	2	Air cool	845	1550	24	Air cool
					705	1300	20	Air cool
Nimonic 80A	1080	1975	8	Air cool	705	1300	16	Air cool
Nimonic 90	1080	1975	8	Air cool	705	1300	16	Air cool
René 41	1065	1950	½	Air cool	760	1400	16	Air cool
Udimet 500	1080	1975	4	Air cool	845	1550	24	Air cool
					760	1400	16	Air cool
Waspaloy	1080	1975	4	Air cool	845	1550	24	Air cool
					760	1400	16	Air cool

Preweld Heating and Heat Treating. Preweld heating of wrought alloys is not required, unless the base metal is below 15 °C (60 °F), in which case a path that is 255 to 305 mm (10 to 12 in.) wide on both sides of the joint should be warmed to 15 to 20 °C (60 to 70 °F) to avoid the condensation of moisture that can cause porosity in the weld metal.

Nickel alloys are usually welded in the solution-treated condition. Precipitation-hardenable alloys should be annealed before welding if they have undergone any operations that introduce high residual stresses.

Postweld Treatment. No postweld treatment, either thermal or chemical, is required to maintain or restore corrosion resistance, although in some cases a full solution anneal will improve corrosion resistance. Heat treatment may be necessary to meet specification requirements, such as stress relief of a fabricated structure to avoid age hardening or stress-corrosion cracking (SCC) of the weldment in hydrofluoric acid vapor or caustic soda. If welding induces moderate-to-high residual stresses, then the PH alloys would require a stress-relief anneal after welding and before aging.

Cleaning of Workpieces

Nickel and nickel alloys are susceptible to embrittlement by lead, sulfur, phosphorus, and other low-melting-point elements. These materials can exist in grease, oil, paint, marking crayons or inks, forming lubricants, cutting fluids, shop dirt, and processing chemicals. Workpieces must be completely free of foreign material before they are heated or welded. Both sides of the workpiece should be cleaned in the area that will be heated by the welding operations. When no subsequent heating is involved, the cleaned area may be restricted to 50 mm (2 in.) on each side of the joint.

Shop dirt, oil, and grease can be removed by either vapor degreasing or swabbing with acetone or another nontoxic solvent. Paint and other materials that are not soluble in degreasing solvents may require the use of methylene chloride, alkaline cleaners, or special proprietary compounds. If alkaline cleaners that contain sodium carbonate are used, then the cleaners themselves must be removed prior to welding. Spraying or scrubbing with hot water is recommended. Marking ink can usually be removed with alcohol. Processing material that has become embedded in the work metal can be removed by grinding, abrasive blasting, and swabbing with a 10 vol% HCl solution, followed by a thorough water wash. Further information on the cleaning of nickel and nickel alloys is given in the article "Cleaning and Finishing of Nickel Alloys" in this Handbook.

Oxides must also be removed from the area involved in the welding operation, primarily because of the difference between the oxide and base metal melting points. Oxides are normally removed by grinding, machining, abrasive blasting, or pickling. Entrapped oxides in weld metal can lead to lack-of-fusion defects at the weld metal/base metal interface.

Joint Design

Various joint designs are used in the arc welding of nickel alloys (Fig. 20). Although the same design can be used for GTAW and SMAW processes, the GMAW and SAW processes require special considerations. A joint design developed for other metals is not necessarily suitable for nickel alloys and should not be used unless it proves to be satisfactory, based on either experience or testing.

Beveled Joints. Beveling is usually not required for metal that is 2.4 mm (0.093 in.) or less in thickness, although thinner sections of certain alloys are sometimes beveled. Metal thicker than 2.4 mm (0.093 in.) should be beveled to form a V-shaped, U-shaped, or J-shaped groove and should be welded using either a backing material or a gas, unless welding from both sides. Otherwise, erratic penetration can result, leading to crevices and voids that are potential areas for joint weakness and accelerated corrosion in the underside of the joint. To attain the best underbead contour on joints that cannot be welded from both sides, the GTAW process should be used for the root pass.

For metal that is more than 9.5 mm (3⁄8 in.) thick, a double U-shaped or V-shaped groove design is preferred. The added cost of preparation is justified, because less welding time and material are required and less residual stress is developed than with a single-groove design.

Beveling is best accomplished by machine, usually a plate planer or other machine tool. Plasma arc and electric arc cutting can be used for joint penetration, but all oxidized metal must be removed from the joint area by grinding or chipping for a depth of 0.8 to 1.6 m (1⁄32 to 1⁄16 in.)

Corner and lap joints can be welded when service stresses will not be excessive. However, corner and lap joints should be avoided if service temperatures are high or if service conditions involve thermal or mechanical cycling. When corner joints are used, a full-penetration weld must be made, usually with a fillet weld on the root side. Lap joints should be welded on both sides.

Design Considerations. Molten nickel alloy weld metal does not flow as easily as steel weld metal. This characteristic cannot be compensated for by using extra heat input or pooling, because serious loss of residual deoxidizers may result. For joints in metal up to 16 mm (5⁄8 in.) thick, ample accessibility is provided by V-groove butt joints beveled to a 60° groove angle. For thicker metal, U-groove butt joints are machined to a 15° bevel angle and a 4.8 to 7.9 mm (3⁄16 to 5⁄16 in.) radius. Single bevels used to form T-joints should have an angle of 45°. The bottom radius of a J-shaped groove for T-joints should be at least 9.5 mm (3⁄8 in.), and the bevel angle previously described should be used for J-shaped and U-shaped grooves. For full-penetration welds, the bevel and groove angles should be about 30% more than those used for carbon steels.

Wetting Profiles and Bead Contour. The increased weld pool viscosity (lack of fluidity) of high-nickel alloys can result in poor wetting or in lack-of-fusion defects along bead edges. Also, if no weave is used, rollover or a very poor wetting profile is sometimes encountered. Because penetration is naturally low with high-alloy materials, the angle formed between the base alloy and the weld bead edge should be greater than 100° to facilitate good tie-ins with subsequent beads. Figure 21 shows acceptable and unacceptable wetting profiles for nickel alloy weldments.

In Fig. 21(a) and (c), the highly convex weld with poor wetting can be caused by too slow a travel speed, too low a voltage, lack of weave. or the wrong polarity. Oxidized or dirty base metal can also inhibit wetting. It is very difficult to fuse these profiles into subsequent beads. Entrapped slag or lack-of-fusion defects often result from attempts to tie into these profiles.

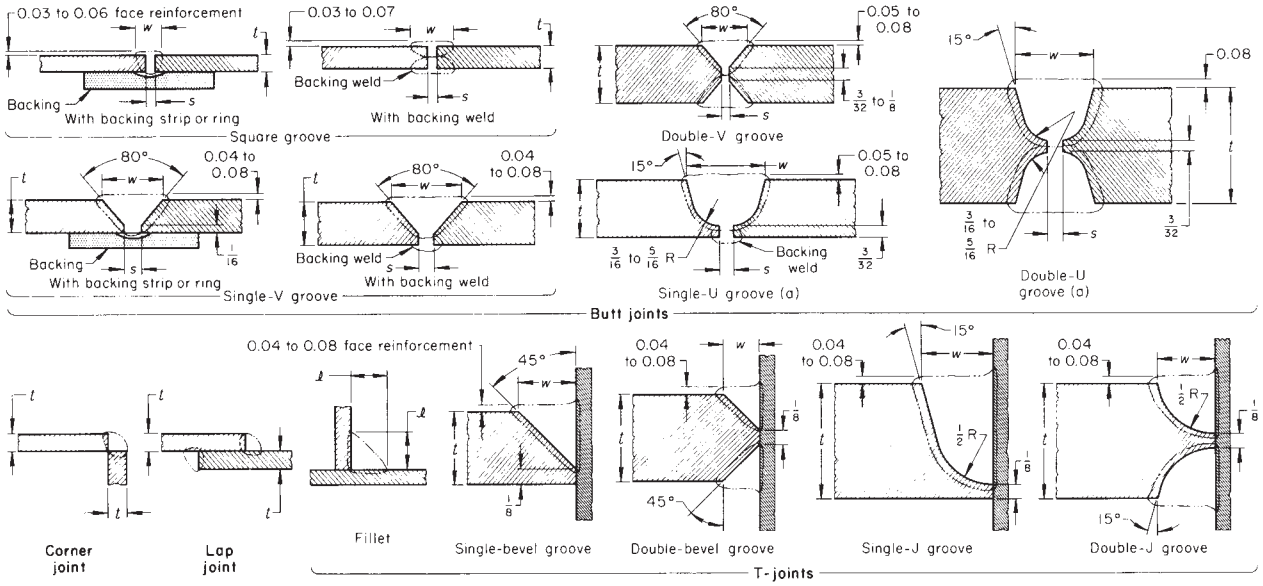
Figures 21(b) and (d) illustrate good wetting profiles that easily accommodate subsequent beads. These profiles are produced by a proper balance of travel speed, parameters, weave, and base plate preparation. Also, greater viscosity usually requires increased included angles for butt joints (75 ± 5° is recommended for nickel-base alloys).

With regard to the subject of bead contour, it should be noted that each bead produced should be slightly convex. Highly stressed flat or concave weldments are prone to centerline cracking. Particular care should also be devoted to producing slightly convex stops. Convex welds can be produced by reducing voltage or by reducing travel speed; convex stops are made by back filling the crater area.

Welding Fixtures

Proper fixturing and clamping hold the workpieces firmly in place, minimize buckling, maintain alignment, and, when needed, provide compressive stress in the weld metal. A backing bar, or any portion of a fixture that might contact the workpiece, should be made of copper. This metal has such a high thermal conductivity that inadvertent welding against the copper will reduce the chance that the bar will fuse to the weldment. In addition, the grooves in copper bars are often used to contour, without sticking, the side underneath the weld.

Backing bars, when used, should incorporate a groove of suitable contour to permit penetration of weld metal and avoid the possibility of trapping gas or flux at the bottom of the weld. Grooves in backing bars used in the GMAW process usually have a shallow semielliptical shape that is 0.38 to 0.89 mm (0.015 to 0.035



Base-metal thickness (*t*)		Width of groove or bead (*w*)		Maximum root opening (*s*)		Approximate amount of metal deposited		Approximate weight of electrode	
mm	in.	mm	in.	mm	in.	kg/m	lb/ft	kg/m	lb/ft(a)
Square-groove butt joint with backing strip or ring									
0.94	0.037	3.2	1/8	0	0	0.03	0.02	0.038	0.025
1.27	0.050	4.0	5/32	0	0	0.06	0.04	0.07	0.05
1.57	0.062	4.8	3/16	0	0	0.06	0.04	0.09	0.06
2.36	0.093	4.8–6.4	3/16–1/4	0.8	1/32	0.09	0.06	0.12	0.08
3.18	0.125	6.4	1/4	1.6	1/16	0.10	0.07	0.13	0.09
Square-groove butt joint with backing weld									
3.2	1/8	6.4	1/4	0.8	1/32	0.16	0.11	0.22	0.15
4.8	3/16	9.5	3/8	1.6	1/16	0.36	0.24	0.48	0.32
6.4	1/4	22	7/8	2.4	3/32	0.46	0.31	0.62	0.42
Single-V-groove butt joint with backing strip or ring									
4.8	3/16	8.89	0.35	3.2	1/8	0.338	0.227	0.46	0.31
6.4	1/4	12.9	0.51	4.8	3/16	0.659	0.443	0.91	0.61
7.9	5/16	15.5	0.61	4.8	3/16	0.866	0.582	1.19	0.80
9.5	3/8	18.0	0.71	4.8	3/16	1.11	0.745	1.52	1.02
13	1/2	23.1	0.91	4.8	3/16	1.73	1.16	2.37	1.59
16	5/8	29.5	1.16	4.8	3/16	2.40	1.61	3.29	2.21
Single-V-groove butt joint with backing weld									
6.4	1/4	10.4	0.41	2.4	3/32	0.62	0.42	0.86	0.58
7.9	5/16	12.9	0.51	2.4	3/32	0.80	0.54	1.10	0.74
9.5	3/8	16.5	0.65	3.2	1/8	1.09	0.73	1.49	1.00
13	1/2	21.6	0.85	3.2	1/8	1.80	1.21	2.48	1.67
16	5/8	26.9	1.06	3.2	1/8	2.17	1.46	2.98	2.00
Double-V-groove butt joint									
13	1/2	10.2	0.40	3.2	1/8	1.32	0.89	1.73	1.16
16	5/8	12.4	0.49	3.2	1/8	1.61	1.08	2.20	1.48
19	3/4	15.7	0.62	3.2	1/8	2.17	1.46	2.98	2.00
25	1	20.6	0.81	3.2	1/8	3.60	2.42	4.97	3.34
32	1 1/4	26.2	1.03	3.2	1/8	4.34	2.92	5.95	4.00
Single-bevel-groove T-joint									
6.4	1/4	3.18	0.125	...	...	0.10	0.07	0.13	0.09
7.9	5/16	4.78	0.188	...	...	0.19	0.13	0.25	0.17
9.5	3/8	6.35	0.250	...	...	0.28	0.19	0.39	0.26
13	1/2	9.52	0.375	...	...	0.57	0.38	0.77	0.52
16	5/8	12.7	0.500	...	...	0.94	0.63	1.28	0.86
19	3/4	15.9	0.625	...	...	1.38	0.93	1.90	1.28
25	1	22.2	0.875	...	...	2.64	1.77	3.60	2.42
Double-bevel-groove T-joint									
13	1/2	4.78	0.188	...	...	0.37	0.25	0.51	0.34
16	5/8	6.35	0.250	...	...	0.58	0.39	0.80	0.54
19	3/4	7.95	0.313	...	...	0.83	0.56	1.15	0.77
25	1	11.1	0.438	...	...	1.47	0.99	2.02	1.36
32	1 1/4	14.3	0.563	...	...	2.29	1.54	3.20	2.15
38	1 1/2	17.5	0.688	...	...	3.29	2.21	4.51	3.03
44	1 3/4	20.7	0.813	...	...	4.46	3.00	6.09	4.09
50	2	23.8	0.938	...	...	5.80	3.90	7.96	5.35
Single-U-groove butt joint(b)									
13	1/2	17.2	0.679	3.2	1/8	1.53	1.03	2.10	1.41
16	5/8	18.9	0.745	3.2	1/8	2.05	1.38	2.83	1.90
19	3/4	20.7	0.813	3.2	1/8	2.50	1.68	3.42	2.30
25	1	24.3	0.957	3.2	1/8	3.91	2.63	5.36	3.60
32	1 1/4	27.3	1.073	3.2	1/8	5.39	3.62	7.38	4.96
38	1 1/2	30.9	1.215	3.2	1/8	7.13	4.79	9.75	6.55
44	1 3/4	34.3	1.349	3.2	1/8	8.90	5.98	12.2	8.19
50	2	37.7	1.485	3.2	1/8	11.0	7.40	15.1	10.12
Double-U-groove butt joint(b)									
25	1	17.2	0.679	3.2	1/8	3.07	2.06	4.20	2.82
32	1 1/4	18.9	0.745	3.2	1/8	4.11	2.76	5.65	3.80
38	1 1/2	20.7	0.813	3.2	1/8	5.00	3.36	6.84	4.60
50	2	24.3	0.957	3.2	1/8	7.83	5.26	10.7	7.20
64	2 1/2	27.3	1.073	3.2	1/8	10.8	7.24	14.8	9.92
Corner and lap joint									
1.6	1/16	...	...	...	...	0.03	0.02	0.06	0.04
3.2	1/8	...	...	...	...	0.07	0.05	0.10	0.07
4.8	3/16	...	...	...	...	0.15	0.10	0.21	0.14
6.4	1/4	...	...	...	...	0.28	0.19	0.39	0.26
9.5	3/8	...	...	...	...	0.62	0.42	0.85	0.57
13	1/2	...	...	...	...	1.04	0.74	1.52	1.02
T-joint with fillet									
...	...	...	...	3.2	1/8	0.04	0.03	0.06	0.04
...	...	...	...	4.8	3/16	0.10	0 .07	0.15	0.10
...	...	...	...	6.4	1/4	0.18	0.12	0.24	0.16
...	...	...	...	7.9	5/16	0.28	0.19	0.39	0.26
...	...	...	...	9.5	3/8	0.40	0.27	0.55	0.37
...	...	...	...	13	1/2	0.70	0.47	0.95	0.64
...	...	...	...	16	5/8	1.10	0.74	1.50	1.01
...	...	...	...	19	3/4	1.59	1.07	2.17	1.46
...	...	...	...	25	1	2.83	1.90	3.87	2.60
Single-J-groove T-joint									
25	1	15.9	0.625	...	...	2.65	1.78	3.6	2.4
32	1 1/4	18.3	0.719	...	...	3.72	2.50	5.1	3.4
38	1 1/2	19.8	0.781	...	...	4.81	3.23	6.5	4.4
44	1 3/4	22.2	0.875	...	...	6.09	4.09	8.3	5.6
50	2	24.6	0.969	...	...	7.34	4.93	10.1	6.8
57	2 1/4	26.2	1.031	...	...	8.63	5.80	11.9	8.0
64	2 1/2	27.8	1.094	...	...	10.3	6.94	14.1	9.5
Double-J-groove T-joint									
25	1	12.7	0.500	...	...	2.20	1.48	3.0	2.0
32	1 1/4	14.3	0.563	...	...	2.83	1.90	3.9	2.6
38	1 1/2	15.1	0.594	...	...	3.81	2.56	5.2	3.5
44	1 3/4	15.9	0.625	...	...	4.63	3.11	6.4	4.3
50	2	16.7	0.656	...	...	5.67	3.81	7.7	5.2
57	2 1/4	17.5	0.688	...	...	6.71	4.51	9.2	6.2
64	2 1/2	19.1	0.750	...	...	7.84	5.27	10.7	7.2

(a) To obtain linear feet of weld per pound of consumable electrode, take the reciprocal of pounds per linear foot. If the underside of the first bead is chipped out and welded, add 0.31 kg/m (0.21 lb/ft) of metal deposited (equivalent to 0.43 kg/m, or 0.29 lb/ft, of consumable electrode). (b) For GMAW (except with the short-circuiting arc), root radius should be one-half the value shown and bevel angle should be twice as great.

Fig. 20 Typical joint configurations and dimensions for GTAW, GMAW, and SMAW applications. Dimensions in schematic are given in inches.

in.) deep and 4.8 to 6.4 mm ($\frac{3}{16}$ to $\frac{1}{4}$ in.) wide. Square corner grooves are used with the GMAW and GTAW processes to accommodate the backing gas. A machined passageway is connected to the gas supply, and holes that are 1.6 mm ($\frac{1}{16}$ in.) in diameter are drilled 75 mm (3 in.) apart from the bottom of the groove to the passageway, permitting the backing gas to flow along the weld. The gas flows out of the groove at the ends of the bar. Figure 22 shows groove designs for backing bars.

The clamping and restraint requirements for nickel alloys are about the same as those for low-carbon steel. The hold-down bars should be located close enough to the line of the weld to maintain alignment and provide the proper degree of heat transfer. Generally, hold-down pressure should be just enough to maintain alignment, but high restraint can be advantageous when welding square groove joints in thin metals using the GMAW process without a filler metal. When the pieces to be welded are positioned with a zero root opening and hold-down bars are brought very close to the line of welding, and when a high hold-down pressure is used, the heat of welding creates an expansive force that results in compression in the line of the weld. This compression will have an upsetting effect on the hot weld metal and can cause the weld to develop a slight top and bottom crown, or weld reinforcement, without the use of filler metal.

Welding of Precipitation-Hardenable (PH) Alloys

The PH alloys require special welding procedures because of their susceptibility to cracking. Cracks can occur in the base-metal HAZ on aging or in service at temperatures above the aging temperature, as a result of residual welding stress and stress induced by precipitation. Before welding these alloys, a full-solution anneal is usually performed. After welding, the appropriate aging heat treatment is performed. To further improve alloy properties, a full anneal after welding, followed by a postweld heat treatment, can be incorporated in the welding procedure.

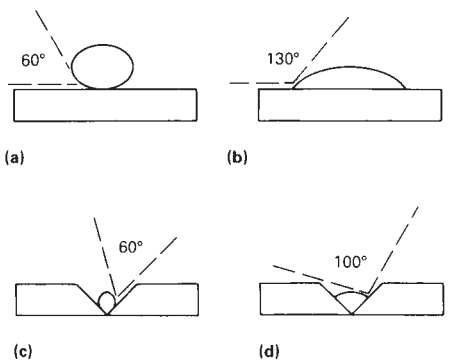


Fig. 21 Acceptable (b and d) and unacceptable (a and c) wetting profiles for nickel alloy weldments. (a) and (b) Overlay welds. (c) and (d) Butt welds

Preweld and Postweld Treatments. Any part that has been subjected to severe bending, drawing, or other forming operations should be annealed before welding. If possible, heating should be done in a controlled-atmosphere furnace to limit oxidation and minimize subsequent surface cleaning.

The aluminum and titanium hardened alloys must be stress relieved (solution treated) after welding and before precipitation hardening. To avoid prolonged exposure of the welded structure to temperatures within the PH range, rapid heating in a furnace preheated to the appropriate temperature is recommended. When the workpiece is large, compared with the furnace area, it may be necessary to preheat the furnace to a temperature that is 110 to 280 °C (200 to 500 °F) above the solution-treatment temperature and then to reset the furnace controls when the workpiece has reached the solution-treatment temperature. The stresses created by repair or alteration welding must be relieved in a similar fashion by rapid heating to the solution-treating temperature prior to re-aging. If satisfactory stress relief of the weldment is not feasible, particularly if the structure is complicated, then preweld overaging treatments may be helpful. Preheating, however, is not a satisfactory substitute for postweld heat treatment. Although PH alloys can be welded in the aged condition, if temperatures encountered in service are in the PH range, then the weldment must be solution treated and re-aged.

General Welding Procedures. Precipitation-hardenable alloys are usually welded by the GTAW process, but SMAW and GMAW processes are also applicable. Heat input during the welding operations should be held to a moderately low level in order to obtain the highest possible joint efficiency and minimize the extent of the HAZ. For multiple-bead or multiple-layer welds, many narrow stringer beads should be used, rather than a few large, heavy beads.

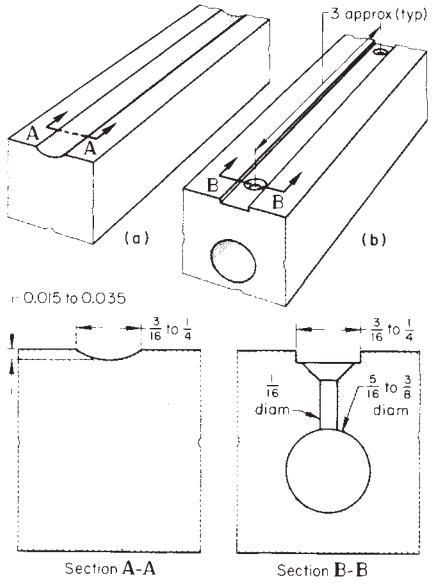


Fig. 22 Groove configurations for backing bars. (a) Standard groove for use without a backing gas. (b) Square-corner groove employed with backing gas (groove depth depends on gas flow required and length of bar). Dimensions given in inches

Either a PH or a solid-solution filler metal may be used for welding nickel-base PH alloys. Maximum mechanical properties, particularly in thick metal, are obtained when PH filler metals are used, because most of the weld deposit is composed of filler metal. The solid-solution filler metals produce welds with lower mechanical properties, but they can be used where maximum strength is not needed. For example, welding alloy 718 with a solid-solution filler metal (Inconel FM82, AWS A5.14 ERNiCr-3) gives tensile properties about one-third lower than those of the base metal. Alloy producers should always be consulted for weld filler metal recommendations.

Any oxides that form during welding should be removed by abrasive blasting or grinding. If such films are not removed as they accumulate on multiple-pass welds, then they can become thick enough to inhibit weld fusion and produce unacceptable laminar-type oxide stringers along the weld axis.

Welding of Cast Nickel Alloys

Cast nickel alloys can be joined by the GTAW, GMAW, and SMAW processes. For optimum results, castings should be solution annealed before welding to relieve some of the casting stresses and provide some homogenization of the cast structure.

Light peening of solidified metal after the first pass will relieve stresses and, thus, reduce cracking at the junction of the weld metal and the cast metal. The peening of subsequent passes is of little, if any, benefit. Stress relieving after welding is also desirable.

Gas-Tungsten Arc Welding

Nickel alloys, both cast and wrought and either solid-solution-strengthened or precipitation-hardenable, can be welded by the GTAW process. The addition of filler metal is usually recommended. Direct current electrode negative (DCEN) is recommended for both manual and machine welding. Parameters for manual GTAW of alloy 400 are given in Table 12.

The welding torch should be set or held at an angle of 90° to the work. A slight deviation is permissible to provide a better view of the work, but an acute angle can lead to aspiration of the surrounding air and contamination of the shielding gas. The largest gas nozzle size applicable to the job should be used, and a minimum practical distance between the nozzle and the work should be maintained. A gas lens should be used to improve shielding gas flow and coverage.

Shielding Gas. Either argon or helium, or a mixture of the two, is used as a shielding gas for welding nickel and nickel alloys. Additions

of oxygen, carbon dioxide, or nitrogen to argon gas will usually cause porosity or erosion of the electrode. Argon with small quantities of hydrogen (typically 5%) can be used and may help avoid porosity in pure nickel, as well as aid in reducing oxide formation during welding. The advantages and disadvantages of using helium, rather than argon, when welding thin metal without the addition of filler metal, are as follows:

- *Improved soundness:* Porosity-free welds are more easily obtained in alloy 400, and the porosity of welds in Nickel 200 is less.
- *Increased welding speed:* With DCEN, welding speed can be increased as much as 40% over that achieved with argon at the same current setting, because welding speed is a function of heat input and heat input is considerably greater with helium.
- *Decreased arc stability:* At lower current levels (<120 A), arc stability is lowered as helium content is increased. Mixtures of argon and helium help stabilize the arc while maintaining the benefits of the helium shielding gas.

Table 12 Parameters for manual GTAW of 1.6 mm (0.062 in.) thick alloy 400

Joint type	Beveled butt, 1.6 mm (1/16 in.) root opening
Electrode	2.4 mm (3/32 in.) diam EWTh-2, tapered to .04 mm (1/64 in.) diam
Filler metal	1.6 mm (1/16 in.) diam ERNiCu-7
Number of passes	3
Welding current, A	70–90 (DCEN)
Voltage, V	10–12
Shielding gas:	
At torch, m^3/h (ft^3/h)	0.6 (20)
Backing gas, m^3/h (ft^3/h)	0.08–0.14 (3–5)
Preheat and postheat treatment	None
Interpass temperature, °C (°F)	175 (350) maximum

DCEN, direct current electrode negative.

Because the purity and dryness of the welding gas are important, welding-grade shielding gas should be used. Furthermore, the welding area should be screened to avoid drafts, because disruption of the shielding atmosphere and drawing in of air can cause porosity in the weld metal.

Electrodes. Pure-tungsten electrodes or tungsten alloyed with thoria or zirconia can be used. The alloyed electrodes are more economical, because of their lower vaporization loss. Overheating that is due to the use of excessive amperage must be avoided at all times.

The best arc stability and penetration control are achieved by tapering the electrode tip. The taper angle should be approximately 30°, with a flat land of about 0.38 mm (0.015 in.) diameter on the tip end. Larger taper angles are used to produce a narrower bead and deeper penetration. After selection, the taper angle should be maintained, because changes in the angle can affect penetration and bead width.

Electrode extension (stick out) should be short, and the amount should be based on joint design. For example, a maximum extension of 4.8 mm (3/16 in.) can be used for butt welds in thin metal, but a 9.5 to 13 mm (3/8 to 1/2 in.) extension is required for some fillet welds or for reaching the bottom of the groove welds.

The electrode should be inclined slightly in the forehand position. Filler metal, when used, should be added carefully at the leading edge of the weld pool to avoid contact with and contamination of the electrode. If contamination occurs, then the electrode should be cleaned and reshaped.

Filler Metals. Compositions of the filler metals used with the GTAW process are, in general, similar to those of the base metals with which they are used. Because of high welding temperatures, filler metals are alloyed to resist porosity and hot cracking of the weld metal. Filler-metal additions and dilution ratios should be adjusted to ensure that the weld metal contains about 75% filler metal.

Table 13 lists the compositions of filler metals used for the GTAW of nickel and nickel alloys. Filler metals of the ERNi-1 classification are used for welding the high-nickel-content alloys (for example, Nickel 200 and 201), whereas those of the ERNiCu-7 classification are used for welding nickel-copper alloys (for example, alloys 400 and 404). The more highly alloyed filler metals are used for welding nickel-chromium, nickel-chromium-iron, nickel-molybdenum alloys, and their variations as well as the PH alloys.

Joint Design. All joint designs shown in Fig. 20 can be used when welding nickel alloys by the GTAW process. If no filler metal is used, then the sections to be joined must be held tightly together to promote satisfactory fusion.

Welding Techniques. When a filler metal is used, the wire diameter should be related to the work-metal thickness. For example, a 1.6 mm (1/16 in.) diameter wire is generally used to weld 1.6 mm (1/16 in.) thick sheet. During welding, the hot end of the wire must remain under the shielding gas to avoid oxidation. A short arc length should be maintained to ensure that deoxidizing elements transfer to the weld pool.

To ensure a sound weld, the arc should be maintained at the shortest possible length. When no filler metal is added, the arc length should be 1.3 mm (0.05 in.), maximum, and preferably 0.5 to 0.8 mm (0.02 to 0.03 in.). When filler metal is used, the arc should be kept as short as possible, consistent with filler-metal diameter, to avoid loss of gas coverage. This loss can result in oxidation and reduced penetration. A short arc also reduces weld spatter with filler wire.

Table 13 Composition of filler metals for GTAW, GMAW, and SAW applications of nickel alloys

		Composition(a), wt%													
UNS No.	Electrode	C max	Mn	Fe	S	Si	Cu	Ni + Co	Al max	Ti	P	Nb + Ta	Mo	Cr	Other
N02061	ERNi-1	0.15	1.0	1.0	0.015	0.75	0.25	93.0 min	1.5	2.0–3.5	0.03	···	···	···	···
N04060	ERNiCu-7	0.15	4.0	2.5	0.015	1.25	bal	62.0–69.0	1.25	1.5–3.0	0.02	···	···	···	···
N08065	ERNiFeCr-1	0.05	1.0	22.0 min	0.03	0.50	1.5–3.0	38.0–46.0	0.20	0.60–1.2	0.03	···	2.50–3.50	19.5–23.5	···
N07092	ERNiCrFe-6	0.03	2.0–2.7	8.0	0.015	0.35	0.50	67.0 min	···	2.5–3.5	0.03	···	···	14.0–17.0	···
N06082	ERNiCr-3	0.10	2.5–3.5	3.0	0.015	0.50	0.50	67.0 min	···	0.75	0.03	2.0–3.0	···	18.0–22.0	···
N06062	ERNiCrFe-5	0.08	1.0	6.0–10.0	0.015	0.35	0.50	70.0 min	···	···	···	1.5–3.0	···	14.0–17.0	···
N06052	ERNiCrFe-7	0.04	1.0	7.0–11.0	0.015	0.50	0.30	bal	1.10	1.0	0.020	0.10	0.50	28.0–31.5	···
N06007	ERNiCrMo-1	0.05	1.0–2.0	18.0–21.0	0.04	1.0	1.5–2.5	bal	···	···	0.04	1.75–2.50	5.5–7.5	21.0–23.5	···
N06625	ERNiCrMo-3	0.10	0.50	5.0	0.015	0.50	0.50	58 min	0.40	0.40	0.02	3.15–4.15	8.0–10.0	20.0–23.0	···
N10276	ERNiCrMo-4	0.02	1.0	4.0–7.0	0.03	0.08	0.50	bal	···	···	0.04	2.5	15.0–17.0	14.5–16.5	2.5 Co, 0.35 V, 3.0–4.5 W
N06985	ERNiCrMo-9	0.015	1.0	18.0–21.0	0.03	1.0	1.5–2.5	bal	···	···	0.04	···	6.0–8.0	21.0–23.5	1.5 W, 5.0 Co
N06022	ERNiCrMo-10	0.02	1.0	2.0–6.0	0.015	0.20	···	bal	···	···	0.03	···	12.5–14.5	20–22.5	2.5–3.5 W
N07718	ERNiFeCr-2	0.08	0.35	bal	0.015	0.35	0.30	50–55	0.2–0.8	0.65–1.15	0.015	4.75–5.50	2.8–3.3	17.0–21.0	0.006 B
N06617	ERNiCrCoMo-1	0.05–0.15	1.0	3.0 max	0.015	1.0	0.50	bal	0.8–1.5	0.60	0.03	···	8.0–10.0	20.0–24.0	···
N10665	ERNiMo-7	0.02	8.0	2.0	0.03	0.10	0.50	bal	···	···	0.04	···	26.0–30.0	1.0	1.0 Co
N06030	ERNiCrMo-11	0.03	1.5	13.0–17.0	0.02	0.80	1.0–2.4	bal	···	···	0.04	0.30–1.50	4.0–6.0	28.0–31.5	5.0 Co, 1.5–4.0 W
N10004	ERNiMo-3	0.12	1.00	4.0–7.0	0.03	1.00	0.50	bal	···	···	0.04	···	23.0–26.0	4.0–6.0	2.5 Co, 0.60 V
N10001	ERNiMo-1	0.08	1.00	4.0–7.0	0.025	1.00	0.50	bal	···	···	0.03	···	26.0–30.0	1.00	2.5 Co, 0.20–0.40 V

(a) Single values are maximum (except where otherwise specified).

The speed of welding affects penetration, weld width, and weld soundness, especially when no filler metal is added. For a given thickness of metal, there is a range of welding speeds that results in minimum porosity. Speeds outside this range, either faster or slower, can result in increased porosity. When welding thinner-gage material, the required heat input is considerably lower. This contributes to increased porosity, which is due to the increased solidification rate of the molten weld pool.

Complete-penetration welds require the use of grooved backing bars that permit local gas shielding (Fig. 22b), or the purging of the inside of the workpiece. The surface condition affects the porosity level in thin sheet material to a much larger degree, because the surface layer makes up a larger percentage of the overall thickness of material.

Table 14 Typical parameters for GMAW applications of Nickel 200 and alloy 400

	Spray metal transfer(a)		Short-circuiting metal transfer(b)		Pulsed-arc metal transfer(c)	
Parameter	Nickel 200	Alloy 400	Nickel 200	Alloy 400	Nickel 200	Alloy 400
Electrode wire designation	ERNi-1	ERNiCu-7	ERNi-1	ERNiCu-7	ERNi-1	ERNiCu-7
Average voltage, V	29–31	28–30	20–21	16–18	21–22	21–22
Peak voltage, V	···	···	···	···	46	40
Average current, A	375	290	160	130–135	150	110
Wire feed rate, mm/s (in./min)	87 (205)	85 (200)	152 (360)	116–123 (275–290)	68 (160)	59 (140)

(a) Argon shielding gas flow rate at 1.7 m^3/h (60 ft^3/h); flat welding position; 1.57 mm (0.062 in.) diam electrode wire. (b) Argon-helium shielding gas flow rate at 1.4 m^3/h (50 ft^3/h); vertical welding position; 0.89 mm (0.035 in.) diam wire. (c) Argon or argon-helium shielding gas flow rate at 0.71 to 0.99 m^3/h (25 to 35 ft^3/h); vertical welding position, 1.14 mm (0.045 in.) diam electrode

Table 15 Typical parameters for spray transfer GMAW of nickel-base alloys

Workpiece was flat welded with argon shielding gas (flow rate of 1.7 m^3/h, or 60 ft^3/h).

	Wire diameter		Wire feed rate		Voltage,	Current,
Filler metal	mm	in.	m/min	in./min	V	A
ERNi-1	0.9	0.035	10.8–13.2	425–520	26–32	200–300
	1.1	0.045	7.0–8.1	275–320	26–32	250–325
	1.6	0.062	4.4–5.6	175–220	27–33	275–350
ERNiCu-7	0.9	0.035	12.1–13.2	475–520	26–32	175–230
	1.1	0.045	6.4–7.6	250–300	26–32	225–300
	1.6	0.062	3.8–5.1	150–200	27–33	250–300
ERCuNi	0.9	0.035	12.1–14.6	475–575	26–32	200–300
	1.1	0.045	6.4–8.1	250–320	26–32	250–325
	1.6	0.062	4.4–5.8	175–230	27–33	275–350
ERNiCrFe-5	0.9	0.035	10.8–13.2	425–520	26–32	175–240
	1.1	0.045	6.4–7.9	250–310	26–32	225–300
	1.6	0.062	4.4–5.6	175–220	27–33	250–330
ERNiCr-3, ERNiFeCr-1, ERNiCrMo-1	0.9	0.035	11.4–13.2	450–520	26–32	175–240
	1.1	0.045	6.4–7.9	250–310	26–32	225–300
	1.6	0.062	3.2–5.1	125–200	27–33	250–330
ERNiCrFe-6	0.9	0.035	11.4–13.2	450–520	26–32	175–240
	1.1	0.045	6.4–8.1	250–320	26–32	225–300
	1.6	0.062	3.2–5.1	125–200	27–33	250–330
ERNiCrCoMo-1, ERNiCrMo-3, ERNiCrMo-4 through -11	0.9	0.035	11.4–15.2	450–600	26–32	180–245
	1.1	0.045	6.4–8.9	250–350	26–32	225–300
	1.6	0.062	3.2–5.7	125–225	27–33	250–330

Gas-Metal Arc Welding

The solid-solution nickel-base alloys can be joined by the GMAW process. In addition, the use of special procedures allows PH alloys (for example, alloy K-500) to be gas-metal arc welded.

Spray, globular, and short-circuiting metal transfer methods are suitable. Varying the power input produces the different types of metal transfer. The pulsed arc process is also used. In these methods, the filler metal is a current-carrying consumable and is typically 0.89, 1.14, or 1.57 mm (0.035, 0.045, or 0.062 in.) in diameter. Table 14 lists typical conditions for the welding of nickel-base alloys using spray-type metal transfer (Table 15), short-circuiting metal transfer (Table 16), and pulsed-arc transfer (Table 17) with various nickel-base filler metals.

Welding current is most often provided by constant-voltage power supplies, although all standard direct current (dc) power supplies are satisfactory. Direct current electrode positive (DCEP) is used because it is virtually impossible to transfer metal in a controlled manner when using DCEN. The amperage should be well within the maximum rating of the equipment, but it should be sufficient to obtain the desired melting rate.

The shielding gas used in the GMAW of nickel alloys by spray or globular transfer can be argon, which yields good results. The addition of 15 to 20% He is beneficial when welding nickel alloys with short-circuiting arc or pulsed-arc transfer methods. As the helium content increases from 0 to 20%, the weld beads become progressively wider and flatter, and penetration decreases. The addition of oxygen or carbon dioxide to argon stabilizes the arc but results in heavily oxidized and irregular bead surfaces. With standard constant-voltage GMAW power sources, helium alone has been used as a shielding gas, but it creates an unsteady arc with excessive weld spatter and is a difficult atmosphere in which to initiate an arc. With pulsed GMAW power sources in which the waveform can be controlled, helium can be very effective for overlaying, resulting in low base metal dilution.

Gas flow rates vary from 0.71 to 2.8 m^3/h (25 to 100 ft^3/h), depending on joint design and position. A flow rate of 1.4 m^3/h (50 ft^3/h) is

Table 16 Typical parameters for short-circuiting transfer GMAW of nickel-base alloys

Data applicable to vertical welding of 3.18 mm (0.125 in.) thick base metal using 65Ar-35H_2 shielding gas at a flow rate of 0.99 m^3/h (35 ft^3/h)

							Wire feed rate							
	Open-circuit voltage, V		Welding voltage, V		Welding current, A		m/min		in./min		Secondary inductance(b)		Slope(b)	
Filler metal(a)	Range	Typical	Range	Typical	Range	Typical	Range	Typical	Range	Typical	Range	Typical	Range	Typical
ERNi-1	28–34	30	20–24	22	90–150	110	5.1–11.4	6.0	200–450	235	5–12	10	6½–8½	7½
ERNiCu-7	27–33	30	19–24	22	90–150	110	5.1–11.4	7.0	200–450	275	7–12	10	6½–8½	8
ERCuNi	27–36	28	19–25	20	100–175	130	5.7–11.4	7.0	225–450	275	5–14	7½	6–7½	6½
ERNiCr-3	29–36	33	21–26	23	90–150	115	4.4–9.5	7.0	175–375	275	10–17	15	7–9½	9½
ERNiCrMo-3	29-36	33	21–26	23	90–150	110	4.4–9.5	7.0	175–375	275	10–17	15	7–9½	9½

(a) Rod diameter of 0.9 mm (0.035 in.). (b) Relative values only. Higher numbers denote greater secondary inductance or slope.

used most frequently. The choice of gas used with short-circuiting metal transfer is influenced by the type of equipment available. Argon, without additions, is suitable for use with equipment that has both inductance and slope control. Argon gas produces convex beads, which may cause cold lapping (lack of fusion), but it also provides a pronounced pinch effect that can be controlled by inductance. The addition of helium is helpful when induction and slope cannot be varied. Helium imparts a wetting action, and the arc is hotter. These factors greatly decrease the possibility of cold lapping. As the percentage of helium increases, the gas flow rate must be increased to ensure adequate protection.

The size of the gas nozzle is important when using a short-circuiting arc. When a 1:1 mixture of argon and helium is used at a flow rate of 1.1 m^3/h (40 ft^3/h) through a 9.5 mm (3/8 in.) diameter nozzle, at a wire feed rate of 6.4 m/min (250 in./min), and a wire diameter of 1.1 mm (0.045 in.), the current can be increased to 160 to 180 A without adversely affecting weld quality. An argon-helium mixture is recommended as the shielding gas with the pulsed-arc GMAW process. The gas flow rate should range from 0.42 to 1.3 m^3/h (15 to 45 ft^3/h). An excessive flow rate can interfere with the arc.

Filler metals used in the GMAW process are listed in Table 13. The appropriate wire diameter depends on the method used and the thickness of the base metal. With globular or spray transfer, 0.89, 1.14, and 1.57 mm (0.035, 0.045, and 0.062 in.) diameter wire is used. The short-circuiting and pulsed-arc processes generally require wire that is 1.14 mm (0.045 in.) or less in diameter.

Joint designs recommended for the GMAW process are shown in Fig. 20. For U-shaped groove designs that use globular or spray transfer methods, the root radius should be decreased by about 50%, and the bevel angle should be doubled. With these transfer methods, the use of high amperage on small-diameter wire produces a high level of arc force. As a result, the arc cannot be deflected from a straight line, as is possible when the welding process utilizes covered electrodes. Because the arc must contact all areas to be fused, the joint design must provide an intersection with the arc force line. When a short-circuiting arc is used, the U-shaped groove designs are the same as those employed with the other arc welding processes.

Welding Techniques. Positioning the electrode holder vertically along the centerline of the joint yields the best results. Some inclination is permissible to allow a better view of the work, but excessive displacement can cause the surrounding atmosphere to be drawn into the shielding gas, causing porous or heavily oxidized welds. Arc length is also important. Too short an arc causes spatter, and too long an arc results in loss of control and reduced penetration.

Because arc length is directly proportional to voltage, particular care must be paid to the voltage setting to ensure properly controlled arc length. In addition, once a procedure has been qualified, consistent torch-to-work positioning should be maintained to prevent possible changes in transfer mode caused by loss (or gain) of energy available at the arc. The alteration in energy at the arc is caused by I^2R energy changes corresponding to wire extension changes.

Cold lapping (lack of fusion) can occur with the short-circuiting, globular, and pulsed-arc processes if manipulation is faulty. The torch should be advanced at a rate that will keep the arc in contact with the base metal, just ahead of the weld pool. The manipulation and angle used with the pulsed-arc torch are similar to those used in the SMAW process. To avoid undercutting, a slight pause should be made at the limit of the weave. Excessive welding speeds and improper torch positioning can cause oxides on the surface of underlying passes to become entrapped between weld passes. Slower welding speeds and good torch positioning allow the arc to reduce certain oxides and/or allow time to float the oxides to the surface of the molten weld pool.

Plasma Arc Welding

Using the keyholing mode, the PAW process can produce acceptable welds in nickel alloys that are up to about 7.5 mm (0.3 in.) thick. Argon-hydrogen mixtures are used as orifice and shielding gases. Levels from 5 to 8% H_2 are optimum. The amount of current needed for keyholing decreases as hydrogen content increases (up to about 7% H_2). Above this level, torch starting becomes more difficult. If helium or hydrogen is used, then the arc starting ability is subsequently reduced.

Typical travel speed and current parameters for keyhole welding are the following:

Travel speed		Current, A	
mm/min	in./min	Nickel 200	Alloy 400
205	8	185	155
255	10	200	175
305	12	220	195
355	14	235	215

Typical conditions for welding 5.97 mm (0.235 in.) thick Nickel 200 using 95% Ar-5%

Table 17 Typical parameters for pulsed-arc transfer GMAW of nickel-base alloys

Data applicable for vertical welding with 1.1 mm (0.045 in.) wire and argon shielding gas flowing at 0.8 m^3/h (30 ft^3/h)

	Typical wire feed rate		Peak voltage, V		Average voltage, V		Current, A	
Filler metal	m/min	in./min	Range	Typical	Range	Typical	Range	Typical
ERNi- 1	4.1	160	45–46	46	21–22	21	90–150	130
ERNiCu-7	3.6	140	39–40	40	21–22	21	90–150	125
ERNiCr-3	3.6	140	43–44	44	20–22	21	90–150	110

Table 18 Composition of electrodes used for SMAW of nickel-alloys, high-nickel content alloys, and nickel-copper alloys

		Composition(a), wt%														
UNS No	Electrode	C	Mn	Fe	S	Si	Cu	Ni + Co	Al	Ti	Nb + Ta	Cr	Mo	P	W	Other
W82141	ENi-1	0.10	0.75	0.75	0.02	1.25	0.25	92.0 min	1.0	1.0–4.0	···	···	···	···	···	···
W84190	ENiCu-7	0.15	4.00	2.5	0.015	1.5	bal	62.0–69.0	0.75	1.0	···	···	···	0.02	···	···
W60715	ECuNi	0.15	1–2.5	0.4–0.75	0.015	0.5	bal	29 min	···	0.5	···	···	···	0.02	···	···
W86112	ENiCrMo-3	0.10	1.0	7.0	0.02	0.75	0.50	55.0 min	···	···	3.15–4.15	20.0–23.0	8.0–10.0	0.03	···	2.5 Co, 0.35 V
W80276	ENiCrMo-4	0.02	1.0	4.0–7.0	0.03	0.2	0.50	bal	···	···	···	14.5–16.5	15.0–17.0	0.04	3.0–4.5	···
W86985	ENiCrMo-9	0.02	1.0	18.0–21.0	0.03	1.0	1.5–2.5	bal	···	···	0.5	21.0–23.5	6.0–8.0	0.04	1.5	5.0 Co
W86022	ENiCrMo-10	0.02	1.0	2.0–6.0	0.015	0.2	0.5	bal	···	···	···	20.0–22.5	12.5–14.5	0.03	2.5–3.5	0.35 V, 2.5 Co
W86030	ENiCrMo-11	0.03	1.5	13.0–17.0	0.02	1.0	1.0–2.4	bal	···	1.5–4.0	0.3–1.5	28.0–31.5	4.0–6.0	0.04	1.5–4.0	5.0 Co
W86040	ENiCrMo-12	0.03	2.2	5.0	0.02	0.7	0.50	bal	···	···	1.0–2.8	20.5–22.5	8.8–10.0	0.03	···	···
W86132	ENiCrFe-1	0.08	3.5	11.0	0.015	0.75	0.50	62.0 min	···	···	1.5–4.0	13.0–17.0	···	0.03	···	···
W86133	ENiCrFe-2	0.10	1.0–3.5	12.0	0.02	0.75	0.50	62.0 min	···	···	0.5–3.0	13.0–17.0	0.50–2.50	0.03	···	0.50–2.50 V
W86134	ENiCrFe-3	0.10	5.0–9.5	10.0	0.015	1.0	0.50	59.0 min	···	1.0	1.0–2.5	13.0–17.0	···	0.03	···	···
W80001	ENiMo-1	0.07	1.0	4.0–7.0	0.03	1.0	0.50	bal	···	···	···	1.0	26.0–30.0	0.04	1.0	0.60 V, 2.5 Co
W80665	ENiMo-7	0.02	1.75	2.0	0.03	0.2	0.50	bal	···	···	···	1.0	26.0–30.0	0.04	1.0	1.0 Co
W86152	ENiCrFe-7	0.05	5.0	7.0–12.0	0.015	0.75	0.5	bal	0.50	0.50	1.0–2.5	28–31.5	0.50	0.030	···	···
W86117	ENiCrCoMo-1	0.05–0.15	0.3–2.5	5.0	0.015	0.75	0.50	bal	···	···	1.0	21.0–26.0	8.0–10.0	0.03	···	9.0–15.0 Co

(a) Single values are maximum (except where otherwise specified).

H_2 gas are as follows: current, 245 A; voltage, 31.5 V; feed rate, 355 mm/min (14 in./min); and gas flow, 0.28 m^3/h (10 ft^3/h) (orifice) and 1.3 m^3/h (45 ft^3/h) (shielding).

Shielded Metal Arc Welding

The SMAW process can be used for welding nickel and nickel alloys. Although the minimum metal thickness is usually about 1.3 mm (0.050 in.), thinner metal can be welded when appropriate fixtures are provided. The types of joints used, as well as bead and groove dimensions, are given in Fig. 20.

Electrodes. The composition of electrodes used in the SMAW process are given in Table 18. Electrode composition is selected to be similar to that of the base metal with which the electrode is to be used. Electrodes of the ENi-1 classification are used to weld wrought and cast forms of nickel and nickel alloys to themselves and to steel. ENiCu electrodes can be used to weld nickel-copper alloys to themselves, to surface steel with a nickel-copper alloy, to weld the clad side of a nickel-copper-clad steel, and to weld nickel-copper alloys to steel. ECuNi electrodes can be used to weld nickel-copper, copper-nickel, and nickel wrought alloys when overlaying steel. A buttering layer of ENi-1 is usually placed onto the steel surface before a copper-nickel surface layer is made.

ENiCrMo-3 electrodes typically are used to join a wide range of pitting and crevice corrosion-resistant alloys. The lowest alloyed materials employed with these electrodes are the molybdenum-modified type 317 stainless steels. ENiCrMo-3 electrodes are used for richer alloy compositions of the nickel-chromium-iron-molybdenum families, up to and including alloy 625. Intermediate alloys welded with ENiCrMo-3 include alloy 825, alloy 20, alloy G, and alloy G-3. This type of electrode is widely used because its high nickel content allows good dissimilar weldability, whereas the high molybdenum content matches or exceeds the pitting resistance of the base alloys being welded. Because of the strength of the ENiCrMo-3 electrode, welding to many high-strength low-alloy (HSLA) grade steels can be performed without sacrificing strength.

Other electrodes in this alloy group, such as ENiCrMo-4 and ENiCrMo-10, are used to join alloys to themselves or to steel. They are also used to join alloys in the ENi-Cr-Mo group to each other. Usually, the base metal is welded with a higher alloyed welding electrode to counteract the microsegregation that occurs in the weld deposit. For example, in a pitting environment, such as the SO_2 environments found in flue gas desulfurization (FGD) applications, the choice would be a nickel-chromium-molybdenum alloy group with a higher molybdenum-containing welding electrode family.

Nickel-chromium-iron electrodes, such as ENiCrFe-2 and ENiCrFe-3, are designed to weld the same family of alloys, as well as dissimilar metal joints involving carbon steel, stainless steel, nickel, and nickel-base alloys. Other welding electrodes with the ENi-Cr-Fe electrode grouping are special-application chemistry electrodes, such as ENi-Cr-Fe-7, which are used to weld alloy 690 to itself, to alloy 600, and to butt weld alloy 690 to steel or to overlay certain grades of steel in nuclear boiler and pressure water reactor applications.

Nickel-chromium-cobalt-molybdenum electrodes, such as ENi-Cr-Co-Mo-1, are readily used to join nickel-chromium-iron alloys, especially when service temperatures will exceed 790 °C (1450 °F) and could reach up to 1150 °C (2100 °F) in oxidizing atmospheres.

Nickel-molybdenum electrodes, such as ENMo-1, are designed to weld nickel-molybdenum alloys to themselves and to other nickel-base, cobalt-base, and iron-base metals. They are normally used in the flat position only.

Covered electrodes should be kept in sealed, moisture-proof containers in a dry storage area prior to their use. All opened containers of unused electrodes should be stored in a cabinet equipped with a dessicant or heated to 6 to 8 °C (10 to 15 °F) above ambient temperature prior to use. If the electrodes are exposed to excessive moisture, then they can be reclaimed by rebaking at 260 °C (500 °F) for 2 h or at 315 °C (600 °F) for 1 h. The electrode diameter should be chosen on the basis of quality requirements and position of welding, rather than on speed of production.

Welding Current. The SMAW process utilizes DCEP. Each electrode size has an optimum amperage range in which good arcing characteristics prevail and outside of which the arc becomes unstable or the electrode overheats. Suggested electrode diameters and current settings for various metal thicknesses are shown in Table 19. Variables such as type of backing, tightness of clamping, and joint design influence the required amount of current density. Actual welding currents should be developed by making sample welds in metal of the same composition and thickness as the metal to be welded.

Welding Position. Flat-position welding should be used whenever possible, because it is faster, more economical, and produces a weld of good quality. The recommended electrode position for flat-position welding is an inclination of about 20° from the vertical, ahead of the weld pool. This position facilitates control of the molten flux and prevents slag entrapment. A short arc must be maintained to prevent atmospheric contamination of the arc and weld and to prevent porosity.

For vertical welding, the arc should be slightly shorter than for flat-position welding, and the amperage should be 10 to 20% lower than the values in Table 19. The electrode should be approximately a 90° angle to the joint. For overhead welding, the arc should be slightly shorter than for flat-position welding, and the welding current should be reduced by 5 to 15 A from the values shown in Table 19.

Welding Techniques. Because molten nickel alloy weld metal is not as free flowing as iron-base alloys, it must be deposited where it is needed. Therefore, a slight weave is required. The amount of weave will depend on joint design, welding position, and type of electrode. Although a straight stringer bead made without weaving can be used for single-pass work and is satisfactory at the bottom of a deep groove on thicker sections, a weave is generally desirable.

When a weave is used, it should be no wider than approximately three times the electrode diameter. Some deviation from this rule may be necessary during vertical welding. A slight weave, if it is not excessive, can help prevent possible centerline solidification cracking problems.

Weld spatter should be avoided. Spatter indicates that the arc is too long, that excessive amperage is being used, or that the current is straight polarity (DCEN). Other causes of spatter are wet electrodes or base metal and slag that run under the arc during welding.

Arc blow may occur when one or both of the metals being welded is magnetic. The arc is deflected from its normal path by a magnetic force in the base metal. One method of overcoming arc blow is to change the location of the

Table 19 Recommended electrode diameter and welding current for SMAW of selected thicknesses of high-nickel-content alloys and nickel-copper alloys in the flat position

Base-metal thickness		Electrode diameter(a)		Current(b),
mm	in.	mm	in.	A
High-nickel-content alloys				
0.94	0.037	2.4	3/32	(c)
1.09	0.043	2.4	3/32	(c)
1.27	0.050	2.4	3/32	(c)
1.57	0.062	2.4	3/32	75
1.98	0.078	2.4	3/32	80
2.36	0.093	2.4	3/32	85
2.77	0.109	3.2	1/8	105
3.18	0.125	3.2	1/8	150
3.18	0.125	2.4–4.0	3/32–5/32	80–150
3.56	0.140	4.0	5/32	130
3.96	0.156	4.0	5/32	135
≥4.75	≥0.187	4.0	5/32	150
Nickel-copper alloys				
0.94	0.037	2.4	3/32	(c)
1.09	0.043	2.4	3/32	(c)
1.27	0.050	2.4	3/32	(c)
1.57	0.062	2.4	3/32	50
1.98	0.078	2.4	3/32	55
2.36	0.093	2.4	3/32	60
2.77	0.109	2.4	3/32	60
2.77	0.109	3.2	1/8	65
3.18	0.125	2.4–4.0	3/32–5/32	60–140
3.56	0.140	2.4–4.0	3/32–5/32	60–140
3.96	0.156	2.4–4.0	3/32–5/32	60–140
6.35	0.250	2.4–4.0	3/32–5/32	60–140
9.53	0.375	2.4–4.8	3/32–3/16	60–180
≥12.7	≥0.500	2.4–4.8	3/32–3/16	60–180

(a) Where a range is shown, the smaller diameter electrodes are used for the first passes at the bottom of the groove, and the joints are completed with the larger diameter electrodes. (b) Current should be in the range recommended by the electrode manufacturer. (c) Use minimum amperage at which arc control can be maintained.

ground connection on the workpiece or to change the direction of the electrical path to the arc. A dissimilar joint (for example, steel welded to a nickel-base alloy) can cause considerable arc blow toward the steel side of the joint.

When the arc is to be broken, it should be shortened slightly, and the rate of travel should be increased to reduce the size of the weld pool. This practice reduces the probability of crater cracking, ensures that the crater does not develop a rolled leading edge, and prepares the way for restriking the arc. Another technique to prevent crater cracking is called crater filling, in which the weld pool is held stationary for a short period of time before the arc is broken. This technique is usually incorporated at the end of a weld.

The manner in which the arc is restruck has a significant effect on the soundness of the weld. A reverse (or T) restrike is recommended. The arc should be struck at the leading edge of the crater and carried back to the extreme rear of the crater at a normal welding speed. The direction is then reversed, weaving is commenced, and the weld is continued. Advantages of this procedure are the following:

- The welder has an opportunity to establish the correct arc length before actual welding commences.
- Some preheat is applied to the cold crater.
- The first drops of rapidly cooled weld metal are deposited where they will be remelted, thus restricting the porosity to a minimum.

Another technique is to make the restrike where the weld metal can be readily removed (for example, 13 to 25 mm, or ½ to 1 in., behind the crater on top of the previous pass). Later, the restrike area can be ground to be level with the rest of the bead. This technique is used when the weld must meet rigid radiographic standards and calls for less welder skill than the reverse-restrike method.

Welding procedures should be qualified before production begins. In one plant where this was not done, qualifying tests of the welding procedure were conducted before further welds were made when cracks appeared in the weld metal of a joint in a 13 mm (½ in.) thick Nickel 200 cylinder.

The original procedure for this weld specified a V-shaped groove butt joint with a 60° included angle, a 3.2 mm (⅛ in.) root face, and zero root opening (Fig. 23a). An ENi-1 electrode that was 355 mm (14 in.) long by 48 mm (3⁄16 in.) wide was used with a welding current of 235 A. On the first pass, a weld bead that was 165 mm (6½ in.) long was deposited with each electrode. On the second pass, a weld bead that was 75 mm (3 in.) long was deposited with each electrode. A cross section of the completed weld is shown in Fig. 23(b). An investigation showed that cracks in the weld metal were caused by the high welding current and low travel speed, which had resulted in the weld pool being held in a superheated condition for an excessively long time.

Therefore, a qualified procedure was established, specifying a welding current of 210 A and an increased travel speed, which resulted in a 305 mm (12 in.) long weld for each electrode on the first pass and 230 mm (9 in.) long welds per electrode on the second pass. Electrode type and length, and all other welding conditions, were unchanged. An included angle of 80° and a 1.6 to 2.4 mm (1⁄16 to 3⁄32 in.) root face would have produced a better welded joint, but the workpieces had been machined and roll formed before the problem arose.

Cleaning the Weld Bead. In multiple-pass welding, all flux and slag must be removed before each succeeding bead is deposited. All slag should be completely removed from completed welds, especially if service involves high temperatures. The slag is easily removed with either hand tools or a hand or power wire brush.

Submerged Arc Welding

Submerged arc welding can be used to join solid-solution nickel alloys. Alloy 400, Nickel 200, and several Ni-Cr-Fe alloys are most frequently welded by this process. Joints in metal up to 75 mm (3 in.) thick have met American Society of Mechanical Engineers (ASME) codes and other specification requirements. The SAW process cannot be used to weld the PH nickel alloys.

Joint Design. Some joint designs used in the submerged arc welding of nickel-alloy plate are shown in Fig. 24. Single compound-angle grooves, single U-grooves, and double U-grooves are used for metal that is 19 mm (¾ in.) or more thick. The double U-groove is usually preferred, because it results in a lower level of residual stress and can be completed in less time with less filler metal. A single V-groove is used for stock up to 13 mm (1 in.) thick.

Electrodes. The compositions of the electrode wires used in the SAW process are the same as those of the filler metals or electrode wires used in GTAW and GMAW processes (Table 13). Submerged arc welding is possible with the following electrodes: ERNi-1, ER-CuNi, ERNiCu-7, ERNiCr-3, ERNiCrFe-5, and ERNiCrMo-3.

Wire that ranges from 1.14 to 2.36 mm (0.045 to 0.093 in.) in diameter can be used for all nickel alloys. The 1.6 mm (1⁄16 in.) diameter wire is generally preferred. Small-diameter wires are used to weld metal that is up to 13 mm (½ in.) thick, and 2.4 mm (3⁄32 in.) diameter wires are used for heavier sections. The approximate amounts of filler metal needed for a single compound angle, a single U-groove, and a single V-groove are given in Table 20.

Fluxes. The fluxes used in the SAW of carbon and stainless steels are not satisfactory when welding nickel alloys. Special proprietary fluxes are available and must be used. Loss of alloy elements (especially chromium), poor weld contour, flux entrapment, weld cracking, and inclusions can result when the wrong flux is used.

Only enough flux cover to prevent arc flashing should be used because excessive flux can cause a deformed bead surface. Slag entrapment can be prevented by appropriate joint design and by correct placement of beads. Slag is easily removed from welds in the bottom of grooves. Fused flux is self-lifting from exposed welds and should be discarded. Unfused flux can be recovered by means of a vacuum system, and it can be reused, if clean. Screening to adjust particle size is not required.

Fluxes should be stored in dry storage areas. Opened containers should be resealed to prevent moisture pickup. However, flux that has absorbed moisture can be reclaimed by drying at 315 °C (600 °F) for 1 h. Hoppers used for fluxes appropriate for the welding of steel and other metals should be thoroughly cleaned before being filled with flux appropriate for the welding of nickel alloys.

Welding Current. Direct current electrode negative (DCEN, typically used for groove plus cladding applications) or direct current electrode positive (DCEP, typically used for cladding applications) can be used. Reverse polarity (DCEP) is preferred for butt welding,

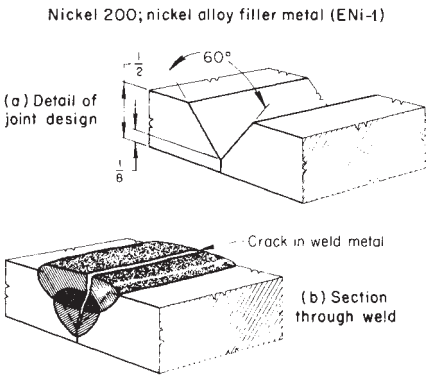


Fig. 23 Joint configurations for welding 13 mm (½ in.) Nickel 200 and subsequent crack in weld metal caused by excessive heat input. Dimensions given in inches

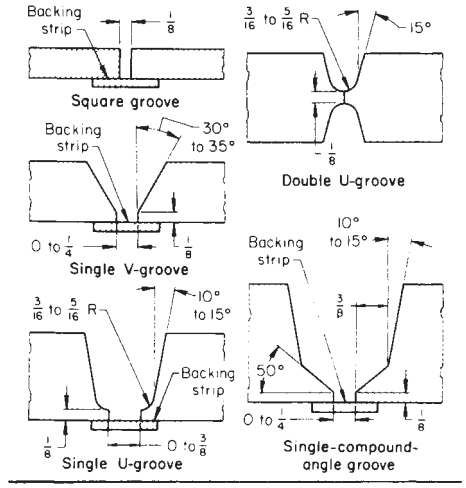


Fig. 24 Typical dimensions for SAW of nickel alloys. Backing strips are optional with zero root openings. Dimensions given in inches

because it produces a flatter bead with deeper penetration at a rather low arc voltage (30 to 33 V). Straight polarity (DCEN) results in a slightly higher rate (typically 30% higher) of deposition at increased voltage (over 35 V) and requires oscillation. The flux covering, however, must be appreciably deeper. Consequently, flux consumption and the risk of slag entrapment increase. Alternating current and the two wire series technique for multiple arc welding are not suitable for use with the available fluxes.

Bead Deposition. The bead location in a multiple-pass layer should provide an open, or reasonably wide, root area for the next bead. Slightly convex beads are preferred to concave beads. Bead contour is controlled by voltage, travel speed, and the position of the electrode.

Minimizing Weld Defects

The defects and metallurgical difficulties encountered in the arc welding of nickel alloys include these:

- Porosity
- Susceptibility to high-temperature embrittlement by sulfur and other contaminants
- Cracking in the weld bead, caused by high heat input and excessive welding speeds
- Stress-corrosion cracking in service
- Strain-age cracking (see the section "Welding Metallurgy of Heat Resistant Alloys" in this article)

Porosity. Oxygen, carbon dioxide, nitrogen, or hydrogen can cause porosity in welds. In the SMAW and SAW processes, porosity can be minimized by using electrodes that contain deoxidizing or nitride-forming elements, such as aluminum and titanium. These elements have a strong affinity for oxygen and nitrogen and form stable compounds with them. Presence of deoxidizers in either type of electrode serves to reduce porosity. In addition, porosity is much less likely to occur in chromium-bearing nickel alloys than in non-chromium-bearing alloys.

In the GMAW and GTAW processes, porosity can be avoided by preventing the access of air to the molten weld metal. Gas backing on the underside of the weld is sometimes used.

In the GTAW process, the use of argon with up to 10% H_2 as a shielding gas helps to prevent porosity. Bubbles of hydrogen that form in the weld pool gather the diffusing nitrogen. Too much hydrogen (>15%) in the shielding gas can result in hydrogen porosity.

Cracking. Hot shortness of welds can result from contamination by sulfur, lead, phosphorus, cadmium, zinc, tin, silver, boron, bismuth, or any other low-melting-point elements, which form intergranular films and cause severe liquid-metal embrittlement at elevated temperatures. Many of these elements are found in soldering and brazing filler metals. Hot cracking of the weld metal usually results from such contamination. Cracking in the HAZ is often caused by intergranular penetration of contaminants from the base-metal surface. Sulfur, which is present in most cutting oils used for machining, is a common cause of cracking in nickel alloys. The removal of foreign material from the surfaces of the work metal is imperative (see "Cleaning of Workpieces" earlier in this section). Weld metal cracking also can be caused by heat input that is too high as a result of high welding current and low welding speed (Fig. 23). Welding speeds have a large effect on the solidification pattern of the weld. High welding speeds create a teardrop molten weld pool, which leads to uncompetitive grain solidification at the center of the weld. At the weld centerline, residual elements will collect and cause centerline hot cracking or lower transverse tensile properties.

In addition, cracking may result from undue restraint. When conditions of high restraint are present, as in circumferential welds that are self restraining, all bead surfaces should be slightly convex. Although convex beads are virtually immune to centerline splitting, concave beads are particularly susceptible to centerline cracking. In addition, excessive width-to-depth or depth-to-width ratios can result in cracking that may be internal (that is, subsurface cracking).

Stress-Corrosion Cracking (SCC). Nickel and nickel alloys do not experience any metallurgical changes, either in the weld metal or in the HAZ, that affect normal corrosion resistance. When the alloys are intended to contact substances such as concentrated caustic soda, fluorosilicates, and some mercury salts, however, the welds may need to be stress relieved to avoid SCC. Nickel alloys have good resistance to dilute alkali and chloride solutions. Because resistance to SCC increases with nickel content, the stress relieving of welds in the high-nickel-content alloys is not usually needed.

Effect of Slag on Weld Metal. Because fabricated nickel alloys are ordinarily used in high-temperature service and in aqueous corrosive environments, all slag should be removed from finished weldments. If slag is not removed in the latter type of application, then crevices and accelerated corrosion can result. Slag inclusions between weld beads reduce the strength of the weld. If the service temperature approximates the melting point of the slag, then severe corrosion can occur when slag is present on the weld surfaces, particularly in oxygen-containing atmospheres. Fluorides in the slag can react with moisture or elements in the environment to create highly corrosive compounds.

Slag also acts as an accumulator of sulfur, particularly in reducing atmospheres, which

Table 20 Quantity of filler metal required to produce submerged arc welds in three types of grooves

Joint design								Approximate amount of metal required (in pounds per linear foot) for indicated plate thickness (in inches) of:								
		Radius (*r*)		Root opening (*s*)		Dimensions (s_1)										
Angle, °	Angle ß, °	mm	in.	mm	in.	mm	in.	1	1¼	1½	1¾	2	2½	3	3½	4
Single-compound-angle groove																
10	40	···	···	0	0	9.5	3/8	2.19	3.10	4.10	5.17	6.33	8.90	11.77	14.95	18.50
10	40	···	···	0	0	13	1/2	2.74	3.56	4.84	6.16	7.61	10.45	13.73	17.32	21.00
10	50	···	···	0	0	9.5	3/8	1.95	2.83	3.79	4.82	5.93	8.40	11.18	14.00	17.70
15	50	···	···	0	0	9.5	3/8	2.03	2.95	4.08	5.29	6.62	9.68	13.20	17.30	21.78
10	50	···	···	6.4	1/4	9.5	3/8	2.87	3.98	5.17	6.43	7.77	10.70	13.94	17.22	21.38
10	40	···	···	6.4	1/4	9.5	3/8	3.11	4.25	5.48	6.78	8.17	11.20	14.53	18.17	22.18
Single U-groove																
10	···	4.8	3/16	0	0	···	···	1.46	2.07	2.76	3.53	4.37	6.33	8.60	11.20	14.10
10	···	6.4	1/4	0	0	···	···	1.77	2.47	3.25	4.12	5.06	7.20	9.67	12.45	15.60
10	···	7.9	5/16	0	0	···	···	2.03	2.86	3.68	4.71	5.76	8.10	10.70	13.70	17.00
15	···	4.8	3/16	0	0	···	···	1.60	2.36	3.23	4.22	5.34	7.94	11.00	14.60	18.68
15	···	6.4	1/4	0	0	···	···	1.90	2.73	3.68	4.76	5.96	8.74	12.00	15.78	20.00
15	···	7.9	5/16	0	0	···	···	2.17	3.08	4.14	5.30	6.60	9.55	12.90	16.90	21.40
10	···	4.8	3/16	6.4	1/4	···	···	2.38	3.22	4.14	5.14	6.21	8.63	11.36	14.42	17.78
10	···	6.4	1/4	6.4	1/4	···	···	2.69	3.62	4.63	5.73	6.90	9.50	12.43	15.67	19.28
Single V-groove																
30	···	···	···	0	0	···	···	1.63	···	···	···	···	···	···	···	···
35	···	···	···	0	0	···	···	1.96	···	···	···	···	···	···	···	···
30	···	···	···	6.4	1/4	···	···	2.55	···	···	···	···	···	···	···	···

can lead to service failure in atmospheres that would be considered adequately low in sulfur. In one instance, although only 0.01% S was present in the atmosphere, the sulfur content of the slag on the weld surface rose from 0.02% to 2 or 3% after a one-month exposure. Sulfur pickup also depresses the melting temperature of the weld slag and, consequently, the maximum safe operating temperature of the weldment.

Joining of Dissimilar Metals

Nickel and nickel alloys have been successfully joined to other nickel alloys and carbon and low-alloy steels, stainless steel, and a number of copper alloys. Filler metal, or consumable electrode, must be selected to ensure a compatible metallurgical relationship between the two base metals. Several factors are involved:

- Differences in thermal expansion of the base metals
- Possibility of permanent changes in volume after extended service at elevated temperature
- Effect of weld-metal dilution at the interfaces with the base metal

All of these factors influence the choice of filler metal and welding process.

An example of a good metallurgical combination is the welding of nickel to alloy 400. Because these metals are completely compatible, they can be welded to each other by any welding process, using any compatible filler metal.

Dilution of Weld Metal. The composition of the weld metal can be expected to differ from that of the filler metal, or consumable electrode, and the base metals being joined, because some elements are lost through the arc when they are transferred from the filler-metal electrode to the weld metal during welding. Filler metal and base metal mixing results in the formation of a unique alloy. The composition of the weld metal is fairly uniform for a given bead, except in a narrow band at the edge of the weld, just adjacent to the fusion line in the near heat-affected zone of the weld. This area is sometimes referred to as the "unmixed zone." Although this region can never entirely be eliminated, its size can be minimized by lowering the overall heat input during welding. The amount of dilution varies from bead to bead. The welding process, current density, deposition rate, welding speed, weld-metal thickness, and welding technique have a significant influence on the amount of base-metal dilution that occurs in the weld deposit. Another region that forms in the near HAZ of the weld is the "partially melted zone." This region can lower the overall corrosion resistance of the weldment but can be controlled by lowering or limiting the heat input during welding.

The dilution of a nickel-base alloy by a dissimilar metal can be tolerated only to a limited degree. When a stainless steel filler metal is used to weld alloy 400 to an austenitic stainless steel, any significant amount of copper pickup from the alloy 400 causes the weld metal to become hot short and to crack. Thus, stainless steel filler metal should not be used when the welding process can cause a considerable amount of dilution. Neither nickel-copper nor copper-nickel types of filler metal can be used in this instance, because chromium from the stainless steel dilutes the weld metal and causes cracking. Although nickel or a nickel-chromium-iron or nickel-chromium-molybdenum filler metal is best, they should only be used after the welding procedure has been qualified by tests.

Filler Metals/Welding Electrodes. Selection of the correct filler metal helps produce a weld that meets the service requirements for strength, corrosion resistance, and soundness and tolerates dilution without causing cracking susceptibility in the weld metal. Crack sensitivity of the weld metal is proportional to the amount of dilution, especially when there is a considerable difference in the composition of a base metal and a filler metal.

Some combinations of base metal and filler metal produce undesirable weld-metal compositions:

- A ferritic weld-metal deposit diluted by nickel, chromium, or copper
- An 18-8 stainless steel weld-metal deposit diluted by more than 3% Cu
- An 18-8 type of weld-metal deposit sufficiently diluted by nickel or chromium to result in the fully austenitic crack-sensitive weld-metal composition (for example, 35% Ni and 15% Cr)
- Any nickel-copper or copper-nickel alloy weld-metal deposit diluted by more than 6 to 8% Cr

Manipulation of the welding arc so that it impinges primarily on the base metal nearest in composition to the filler metal helps reduce dilution. For most combinations of dissimilar metals, filler-metal suppliers should be consulted before a filler metal is selected. The addition of ample filler metal to the root pass helps lower the amount of base-metal dilution and also prevents the probability of producing a concave weld deposit profile, instead of the preferred convex shape.

The coefficients of thermal expansion (CTEs) of the base metals must be considered when selecting filler metals for joining dissimilar metal combinations. CTE differences are a major factor in situations where there is temperature cycling (for example, welding of 300-series stainless steel to carbon or low-alloy steel at temperatures above 425 °C, or 800 °F). A large difference in CTE values can induce stresses of sufficient magnitude to produce cracking in the weld metal. Some of the nickel-base electrodes (ENiCr, ENiCrFe, ERNiCr, and ERNiCrFe) and matching filler metals can be used to weld a wide range of base-metal combinations. These electrodes and filler metals can tolerate considerable dilution without loss of strength or ductility. Filler-metal ERNiMo-6 can be used to join nickel-base alloys, cobalt-base alloys, and stainless steels to themselves and to other metals and alloys. The low chromium content of this filler metal, however, should be carefully considered when welding oxidation-resistant materials.

Although GTAW and GMAW processes can be employed, the SMAW process is the most widely used to join nickel and nickel alloys to dissimilar metals. The welding current should be maintained near the middle of the recommended range for the electrode in order to control dilution. Dilution usually can be kept below 25% by manipulating the electrode to dissipate the arc force on already-deposited weld metal. When depositing the first bead, the arc should be directed toward the member from which dilution of the weld metal will be least detrimental. Welding procedures that reduce the amount of penetration, which can cause dilution of the weld metal by the base metal, will increase the probability of securing a good weld. Table 21 gives recommended welding consumables for joining selected nickel-base alloys.

Brazing of Heat Resistant Nickel-Base Alloys

The heat resistant alloys discussed in this section include cast and wrought solid-solution and PH alloys as well as oxide-dispersion strengthened (ODS) alloys made by powder metallurgy (P/M) techniques. Almost any metal, as well as nonmetallics, can be brazed to these heat resistant alloys, if it can withstand the heat of brazing.

Brazing Filler Metal Compositions

The American Welding Society (AWS) has classified several gold-base and nickel-base brazing filler metals that can be used for elevated-temperature service (Table 22). These brazing filler metals are suitable for high-temperature service; however, if the application is for temperatures above 980 °C (1800 °F) or in severe environments, the required brazing filler metal may not be in Table 22. It should be noted that for lower service temperatures, copper (BCu) (below 480 °C, or 900 °F) and silver (BAg) (below 425 and 200 °C, or 800 and 400 °F) brazing filler metals have been used for many successful applications.

Generally, heat resistant alloys are brazed with nickel-base alloys containing boron and/or silicon, which serve as melting-point depressants. In many commercial brazing filler metals, the levels are 2 to 3.5 % B and 3 to 10% Si. Phosphorus is another effective melting-point depressant for nickel and is used in filler metals from 0.02 to 10%. It is also used where good flow is important in applications of low

Table 21 Selection of welding consumables for nickel-base alloy joining applications

Welding electrode or filler metal	Primary applications
Coated electrodes	
ENi-1	Nickel 200 and Nickel 201; the clad side of nickel-clad steel; joining of steels to nickel alloys
ENiCu-7	Alloy 400 to itself, to low-alloy and carbon steels, to copper and copper-nickel alloys; surfacing of steels
ECuNi	Alloy 450; weldable grades of cast and wrought 70/30, 80/20, and 90/10 copper-nickel alloys
ENiCrFe-1	Alloy 600; alloy 330
ENiCrFe-3	Alloys 600 and 601, surfacing of steel; dissimilar combinations of steels and nickel alloys
ENiCrMo-3	Alloys 625 and 601; pit-resistant alloys; dissimilar combinations of steels and nickel alloys; surfacing of steels
ENiCrCoMo-1	Alloy 617; alloy 800HT; dissimilar combinations of high-temperature alloys
ENiCrMo-3	Alloy 825; alloy 686, alloy 622, alloy C-276; other pit-resistant alloys; surfacing of steels
ENiCrMo-3, ENiCrMo-9	Alloys G and G-3; other pit-resistant alloys; dissimilar combinations of steels and nickel alloys; surfacing of steels
ENiCrFe-3, ENiCrFe-7	Alloy 600 and alloy 690 to themselves and to dissimilar combinations with steel; surfacing of steels
Filler metals	
ERNi-1	Nickel 200 and Nickel 201; dissimilar combinations of nickel alloys and steels; surfacing of steels
ERNiCu-7	Alloys 400, R-405, and K-500; surfacing of steel
ERCuNi	Alloy 450; weldable grades of 70/30, 80/20, and 90/10 copper-nickel alloys
ERNiCr-3, ERNiCrFe-7	Alloy 600, alloy 690; dissimilar combination to steels; surfacing of steels
ERNiCr-3	Alloys 600 and 601; alloys 800 and 800HT; alloy 330; dissimilar combinations of steels and nickel alloys; surfacing of steels
ERNiCr-3, ERNiCrMo-3	Dissimilar combinations of steels and nickel alloys
ERNiCrCoMo-1	Alloy 617; alloy 800HT; dissimilar combinations of high-temperature alloys
ERNiCrMo-3	Alloys 625 and 601; pit-resistant alloys; dissimilar combinations of steels and nickel alloys; surfacing of steels
ERNiFeCr-2	Alloys 718 and X-750
ERNiCrMo-3	Alloy 825
ERNiCrMo-4 through -10	Alloy 686, alloy 622, alloy C-276; other pit-resistant alloys; surfacing of steels

stress, where service temperatures do not exceed 760 °C (1400 °F).

In addition to boron, silicon, and phosphorus, chromium is often present to provide oxidation and corrosion resistance. The amount may be as high as 20%, depending on the service conditions. Higher amounts, however, tend to lower brazement strength.

Many nickel-palladium-base brazing filler metals exhibiting good wetting and flow are not classified by AWS but are also available. These filler metals have been developed to replace gold-containing (BAu) brazing filler metals, which are more expensive.

Another group of brazing filler metals not classified by AWS is used for repair and overhaul of nickel-base superalloy aerospace and industrial turbine engine components. Many of these brazing filler metals are proprietary compositions of the engine manufacturer for which they were developed. However, a good variety of these filler metals are commercially available. These "diffusion braze" filler metals do not contain silicon. However, they do contain boron, which acts as a melting-point suppressant. Both boron and silicon react with metals (such as chromium and molybdenum) to form intermetallic phases. These intermetallic phases are very hard and brittle and can seriously weaken a brazed joint. It is possible to perform annealing heat treatments on diffusion brazed joints that result in the diffusion of the boron out of the brazed joint and into the base metal. The result is a brazed joint in which intermetallic phases are partially dissolved or eliminated completely (Fig. 25). Diffusion heat treatment increases the strength and ductility of the brazed joint.

Silicon atoms do not diffuse as easily as boron atoms (because silicon atoms are larger and sit on a regular lattice site, whereas boron atoms sit on interstitial sites, providing much faster diffusion paths). Therefore, similar heat treatments do not tend to dissolve or eliminate silicon intermetallic phases.

These boron-containing filler metals (used on their own or mixed with base metal powder to act as a gap filler) are used to fill cracks and eroded areas on turbine engine components. Some type of cleaning operation (such as hydrogen fluoride cleaning or mechanical cleaning) is employed before the brazing operation in order to remove oxides on the components and thus facilitate brazing filler metal wetting.

A second group of filler metals not classified by AWS is used for wide gaps (1.52 mm, or 0.060 in., and greater) and eroded areas. These filler metals are generally nickel-base or cobalt-base superalloys that have additions of a melting-point suppressant. These filler metals do not tend to flow away from the area in which they are placed. The microstructure of the joint formed using these filler metals is homogeneous and more closely approximates the base metal microstructure (Fig. 26).

Brazing Filler Metal Product Forms

Available forms of AWS classified and proprietary brazing filler metals include wire, foil,

Table 22 AWS brazing alloys for elevated-temperature service

	Composition, wt%														Solidus		Liquidus		Brazing range	
AWS classification	Cr	B	Si	Fe	C	P	S	Al	Ti	Mn	Cu	Zr	Ni	Total other elements	°C	°F	°C	°F	°C	°F
Nickel-base alloy filler metals(a)																				
BNi-1	13.0–15.0	2.75–3.50	4.0–5.0	4.0–5.0	0.6–0.9	0.02	0.02	0.05	0.05	···	···	0.05	bal	0.50	975	1790	975	1900	1065–1205	1950–2200
BNi-1a	13.0–15.0	2.75–3.50	4.0–5.0	4.0–5.0	0.06	0.02	0.02	0.05	0.05	···	···	0.05	bal	0.50	975	1790	1075	1970	1075–1205	1970–2200
BNi-2	6.0–8.0	2.75–3.50	4.0–5.0	2.5–3.5	0.06	0.02	0.02	0.05	0.05	···	···	0.05	bal	0.50	970	1780	1000	1830	1010–1175	1850–2150
BNi-3	···	2.75–3.50	4.0–5.0	0.5	0.06	0.02	0.02	0.05	0.05	···	···	0.05	bal	0.50	980	1800	1040	1900	1010–1175	1850–2150
BNi-4	···	1.5–2.2	3.0–4.0	1.5	0.06	0.02	0.02	0.05	0.05	···	···	0.05	bal	0.50	980	1800	1065	1950	1010–1175	1850–2150
BNi-5	18.5–19.5	0.03	9.75–10.50	···	0.10	0.02	0.02	0.05	0.05	···	···	0.05	bal	0.50	1080	1975	1135	2075	1150–1205	2100–2200
BNi-6	···	···	···	···	0.10	10.0–12.0	0.02	0.05	0.05	···	···	0.05	bal	0.50	875	1610	875	1610	925–1095	1700–2000
BNi-7	13.0–15.0	0.01	0.10	0.2	0.08	9.7–10.5	0.02	0.05	0.05	0.04	···	0.05	bal	0.50	890	1630	890	1630	925–1095	1700–2000
BNi-8	···	···	6.0–8.0	···	0.10	0.02	0.02	0.05	0.05	21.5–24.5	4.0–5.0	0.05	bal	0.50	980	1800	1010	1850	1010–1095	1850–2000

	Composition, wt%					Solidus		Liquidus		Brazing range	
AWS classification	Au	Cu	Pd	Ni	Total other elements	°C	°F	°C	°F	°C	°F
Precious metals											
BAu-1	37.0–38.0	bal	···	···	0.15	990	1815	1015	1860	1015–1095	1860–2000
BAu-2	79.5–80.5	bal	···	···	0.15	890	1635	890	1635	890–1010	1635–1850
BAu-3	34.5–35.5	bal	···	2.5–3.5	0.15	975	1785	1030	1885	1030–1090	1885–1995
BAu-4	81.5–82.5	···	···	bal	0.15	950	1740	950	1740	950–1005	1740–1840
BAu-5	29.5–30.5	···	33.5–34.5	35.5–36.5	0.15	1135	2075	1165	2130	1165–1230	2130–2250

AWS, American Welding Society. (a) If determined, cobalt is 0.1% max unless otherwise specified. Source: AWS 5.8

tape, paste, and powder. The form used can be dictated by the application or by the composition of the filler metal. If the filler metal required for a specific application is only available as a dry powder, then brazing aids such as cements and pastes are available to help position the brazing filler metal.

Brazing filler metal powders usually are gas atomized and sold in a range of specified particle sizes, which ensures uniform heating and melting of the brazing filler metal during the brazing cycle. These powders can be mixed with plasticizers or organic cements to facilitate positioning. If the mixture must support its own weight until the brazing cycle begins, an organic binder or cement is required. These binders burn off in atmosphere brazing, and little or no residue results. When the brazing filler metal is supplied as a paste. it is simply a premixed powder and binder.

Brazing Tapes and Foils. Brazing filler metals in the form of tapes and amorphous foils appear similar, but the foils are usually made by rapid solidification during melt spinning operations and tend to exhibit homogeneous amorphous structures. Brazing tapes are made of powder that is held together by a binder and formed into a rather fragile sheet. Most amorphous foils have a high metalloid (phosphorus, silicon, boron) content, while tapes can be made from brazing filler metals that have no metalloid content. The metalloids usually are melting-point depressants and frequently form brittle phases. In some cases, where the composition is workable, such as BAu, foils can be made by cold rolling. Foil products can also be produced by rolling an alloy of suitable composition into a foil before adding the metalloids. Tapes and foils are best suited for applications requiring a large area joint, good fit-up, or where brazing flow and wetting may be a problem.

Brazing wires of nonfabricable alloys usually are made by P/M processes from gas atomized powder, which is held together by a binder or by extruding powder into wire and sintering. This form of brazing filler metal is better able to support itself than are pastes and powders of filler metal, but is not used to replace tapes or amorphous foils where precision is needed in preplacing the filler metal, such as joint gaps less than 0.13 mm (0.005 in.).

Surface Cleaning and Preparation

Cleaning of all surfaces that are involved in the formation of the desired brazed joint is necessary to achieve successful and repeatable brazed joints. All obstruction to wetting, flow, and diffusion of the molten brazing filler metal must be removed from both surfaces to be brazed prior to assembly. The presence of contaminants on one or both surfaces to be brazed may result in void formation, restricted or misdirected filler-metal flow, and contaminants included within the solidified brazed area, which reduces the mechanical properties of the resulting brazed joint. Common contaminants are oils, greases, residual liquid penetrant fluids, pigmented markings, residual casting or coring materials, and oxides formed either through previous thermal exposures or by exposures to contaminating environments or engine service.

Chemical cleaning methods are most widely used. As part of any chemical cleaning procedure for preprocessing assemblies for brazing, a degreasing solvent should be used to remove all oils and greases and to ensure wettability of the chemicals used for cleaning. Oils and greases form a very thin film on metals, which prevents wettability by both the subsequent chemical cleaning and/or the molten filler metals. Oil and grease removers that are widely used include degreasing solutions such as stabilized perchloroethylene or stabilized trichloroethylenes. These may be used as simple manual soaks, sprays, or by suspending the parts in a hot vapor of the aforementioned chemicals, commonly referred to as a vapor degreasing process. In conjunction with these processes, anodic and cathodic electrolytic cleaning can be used.

Other cleaning methods include alkaline-based cleaners and emulsion-type cleaners. Alkaline-based cleaners use mixtures of phosphates, carbonates, silicates, soaps, detergents, and hydroxides. Emulsion-type cleaners contain wetting agents, surface actuators, fatty acids, and hydrocarbons.

A chemical cleaning procedure can be a simple single-step process or may involve multistep operations. If the surfaces of the brazed joint are in the machined condition, vapor degreasing may be sufficient to remove machining oils, handling oils, and liquid penetrant fluids to yield a sound, clean surface for brazing. If, on the other hand, one or both of the surfaces to be brazed is not a machined surface, then additional chemical cleanings should be employed. Once vapor degreasing is accomplished, care must be taken to maintain the surface cleanliness of the brazed components by handling in an environmentally clean atmosphere. Additional methods of chemical cleaning to remove oxides and other adherent metallic contaminants include immersion in phosphate acid cleaners or acid pickling solutions, which are comprised of nitric, hydrochloric, or sulfuric acids or combinations of these.

Care must be taken in time of exposure for both acid cleaning and acid pickling of heat resistant base metals. Overexposure during chemical cleaning can lead to excessive metal loss, grain-boundary attack, and selective attack on microstructural phases. As the last step in chemical cleaning, an ultrasonic cleaning in alcohol or clean hot water is recommended to ensure removal of all traces of previous cleaning solutions.

If no subsequent mechanical cleaning is used, the components to be brazed should be stored and transported to the braze preparation areas in dry, clean containers, such as plastic bags. The time between cleaning and braze application to the assembled joints should be kept as short as manufacturing processes allow.

Mechanical cleaning usually is confined to those metals with heavy tenacious oxide films or to repair brazing on components exposed to service. (Nickel-base or cobalt-base superalloy components that require repair brazing can be processed in hydrogen fluoride atmospheres in order to remove oxide films.) Mechanical methods are standard machining processes—abrasive grinding, grit blasting, filing, or wire brushing (stainless steel bristles must be used). These are used not only to remove surface contaminants but to slightly roughen or fray the surfaces to be brazed.

Care must be taken that the surfaces are not burnished and that mechanical cleaning materials are not embedded in the metals to be brazed. In grit blasting, choice of the blasting medium is critical. Wet and dry grit blasting commonly are used, but wet media are subject to additional cleaning requirements to remove the embedded grit. The media used are iron grits, silicon carbide grits, and grits composed of brazing filler metals. Grit sizes as coarse as No. 30 (0.589 mm, or 0.0232 in.) are recommended for cleaning forgings and castings. Finer grits (No. 90 and No. 100, 0.165 and 0.150 mm [0.0065 and 0.0059 in.], respectively) are used

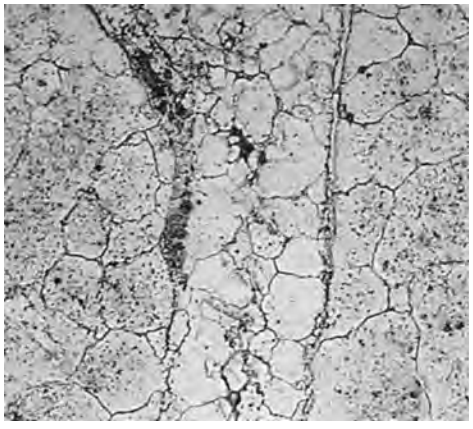


Fig. 25 Micrograph of the crack repair of a diffusion brazed joint by heat treating of the IN-792 base metal. Sample was etched with Kalling's reagent. 76×

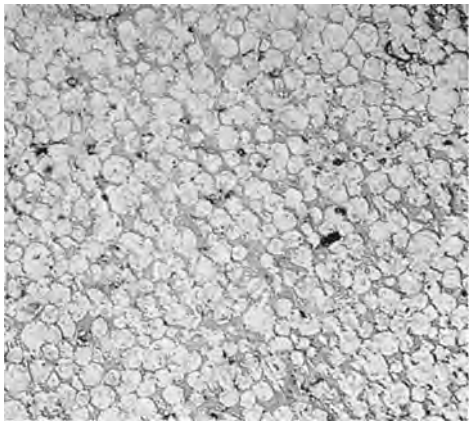


Fig. 26 Microstructure of a wide gap filler metal braze repair. Sample was etched with Kalling's reagent. 40×

for general blasting. All grit mediums should be changed frequently, as extensive reuse of the same medium results in loss of sharp angles or facets. Once these configurations are lost or markedly reduced in the grit medium, burnishing rather than cleaning occurs. Overused medium results in the entrapment of oxides in the metal. If possible, the angle of grit blasting should be less than 90° to the surfaces to be cleaned. This also reduces the chances of embedding the oxides or medium in the surfaces to be brazed.

Care must be taken to remove all blasting medium from the surface after mechanical cleaning, as these media will contaminate the braze. Iron grit may impart an iron film that oxidizes as a rust. Aluminum oxides, if not removed, prevent wetting and flow of the brazing filler metal; thus, use of aluminum oxides is not recommended. Silicon carbide is extremely hard and has sharp facets. Consequently, it becomes embedded if an improper blasting angle is used. Blasting with a nickel-base brazing filler metal or similar alloy gives the best results; stainless steel blasting medium is also acceptable.

After mechanical cleaning, air blasting or ultrasonic cleaning should be used to remove all traces of loosened oxides or cleaning medium. Care must be taken to ensure maintenance of the clean surfaces and components; once cleaned, they should be assembled and brazed as soon as possible.

Hydrogen Fluoride Cleaning. The successful repair of superalloy components requires that oxides formed during service, on external surfaces and within cracks, be removed prior to brazing to ensure proper wetting and flow of the braze material. For cobalt-base superalloy parts, heating in a hydrogen-rich atmosphere (hydrogen reduction) is generally successful in this regard. However, hydrogen reduction is not effective in reducing oxides of aluminum and titanium that are formed on nickel-base superalloy parts in service because these oxides exhibit a high degree of thermodynamic stability. Hydrogen fluoride reduction, on the other hand, has been shown capable of reducing these oxides from the surfaces of nickel-base parts.

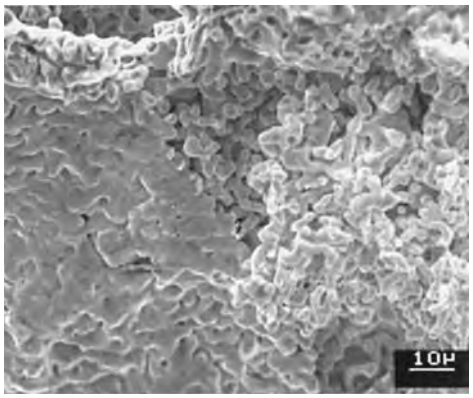


Fig. 27 SEM micrograph of a René 125 aerospace engine component that was cleaned with hydrogen fluoride to deplete the elements at the surface

Oxides of aluminum and titanium are changed to their respective metallic fluorides by the fluoride ions created in the hydrogen fluoride process. Oxides of chromium are also changed to chromium fluoride by the fluoride ions. In addition, workpiece surfaces are depleted of aluminum and titanium so that oxides of theses metals do not tend to reform during subsequent operations, such as braze repair (Fig. 27).

Nickel Flashing. Certain heat resistant alloys that are used as base metals in brazed assemblies—particularly nickel-base alloys containing high percentages of aluminum and titanium—may require a surface pretreatment to ensure maintenance of the cleaned surfaces. This surface pretreatment after cleaning is generally an electroplate of nickel, commonly referred to as nickel flashing. Thickness of the plate flashing is kept under 0.015 mm (0.0006 in.) for alloys with less than 4% (Ti + Al) and 0.020 to 0.030 mm (0.0008 to 0.0012 in.) for alloys with greater than 4% (Ti + Al). This promotes wettability in the braze joint without seriously affecting the braze strength and other mechanical properties of the braze. The thickness of nickel plating may have to be increased as the brazing temperature is increased and as the time above 980 °C (1800 °F) is increased. Titanium and aluminum will diffuse to the surface of the nickel plating upon heating.

Fixturing

One prerequisite to successful brazing that is often neglected is proper fixturing. Two types of fixtures are used: "cold" fixtures and "hot" fixtures.

Cold fixtures are used primarily for assembly purposes. In most cases, cold fixtures are made of hot or cold rolled iron, stainless alloys, nonferrous alloys, or nonmetals, such as phenolics and laminates. These fixtures are used for assembly and subsequent tack welding of parts to be brazed. They need not be massive or heavy, but should be sturdy enough to assemble components as required by design.

Hot fixtures (fixtures used in the furnace for brazing) must have good stability at elevated temperatures and the ability to cool rapidly. Metals can be used but generally are not stable enough to maintain tolerances during the brazing cycle. Therefore, ceramic, carbon, or graphite assemblies often are used for hot fixturing. Ceramics, due to their high processing cost, are used for small fixtures and for spacer blocks to maintain gaps during brazing of small components. Graphite has been found to be the most suitable material for maintaining flatness in a high vacuum or argon atmosphere, and it provides faster cooling because of its high thermal conductivity, which is partially due to its porosity. Graphite should be coated with an Al_2O_3 slurry to prevent carburization of parts during the brazing cycle. It should not be used in a pure dry hydrogen atmosphere as it will cause carburization of the base metals by gaseous transfer. Molybdenum and tungsten may be used, but they are generally avoided because of their cost.

Controlled Atmospheres

Controlled atmospheres (including vacuum) are used to prevent the formation of oxides during brazing and to reduce the oxides present so that the brazing filler metal can wet and flow on clean base metal. Controlled-atmosphere brazing is widely used for the production of high-quality joints. Large tonnages of assemblies of a wide variety of base metals are mass produced by this process.

Controlled atmospheres are not intended to perform the primary cleaning operation for the removal of oxides, coatings, grease, oil, dirt, or other foreign materials from the parts to be brazed. All parts for brazing must be subjected to appropriate prebraze cleaning operations as dictated by the particular metals. Controlled atmospheres commonly are employed in furnace brazing; however, they may also be used with brazing processes that utilize induction, resistance, infrared, laser, and electron-beam heat sources. In applications where a controlled atmosphere is used, postbraze cleaning is generally not necessary. In special cases, flux may be used with a controlled atmosphere (a) to prevent the formation of oxides of titanium and aluminum when brazing in a gaseous atmosphere, (b) to extend the useful life of the flux, and (c) to minimize postbraze cleaning. Fluxes should not be used in a vacuum environment. Some types of equipment, such as metallic muffle furnaces and vacuum systems, may be damaged or contaminated by the use of flux.

The use of controlled atmospheres inhibits the formation of oxides and scale over the whole part and permits finish machining to be done before brazing in many applications. In some applications, such as the manufacture of electronic tubes, eliminating flux is tremendously important.

Pure dry hydrogen is used as a protective atmosphere because it dissociates the oxides of many elements. Hydrogen with a dew point of –51 °C (–60 °F) dissociates the oxides of most elements found in heat resistant alloys, with the notable exception of aluminum and titanium, which are found in most of the high-strength heat resistant base metals.

Inert gases, such as helium and argon, do not form compounds with metals. In equipment designed for brazing at ambient pressure, inert gases reduce the evaporation rate of volatile elements, in contrast to brazing in a vacuum. Inert gases permit the use of weaker retorts than those required for vacuum brazing. Elements such as zinc and cadmium, however, vaporize in pure dry inert atmospheres.

Vacuum. An increasing amount of brazing of heat resistant alloys, particularly PH alloys that contain titanium and aluminum, is done in a vacuum. Vacuum brazing in the range of 13 mPa (10^{-4} torr) has proved adequate for braz-

ing most of the nickel-base superalloys. By removal of gases to a suitably low pressure, including gases that are evolved during heating to brazing temperature, very clean surfaces are obtainable. A vacuum is particularly useful in the manufacture of parts for the aerospace, electronic tube, and nuclear fields, and where metals that react chemically with a hydrogen atmosphere are used or where entrapped fluxes or gases are intolerable. The maximum tolerable pressure for successful brazing depends on a number of factors that are primarily determined by the composition of the base metals, the brazing filler metal, and the gas that remains in the evacuated chamber.

Vacuum brazing is economical for fluxless brazing of many similar and dissimilar base-metal combinations. Vacuums are especially suited for brazing very large, continuous areas where (a) solid or liquid fluxes cannot be removed adequately from the interfaces after brazing, and (b) gaseous atmospheres are not completely efficient because of their inability to purge occluded gases evolved from close-fitting brazing interfaces. It is interesting to note that a vacuum system evacuated to 1.3 mPa (10^{-5} torr) contains only 0.00000132% residual gases based on a starting pressure of 100 kPa (760 torr).

Vacuum brazing has the following advantages and disadvantages compared with brazing that is carried out under other high-purity brazing atmospheres:

- Vacuum removes essentially all gases from the brazing area, thereby eliminating the necessity for purifying the supplied atmosphere. Commercial vacuum brazing generally is done at pressure varying from 0.0013 to 13 Pa (10^{-5} to 10^{-1} torr), depending on the materials brazed, the filler metals being used, the area of the brazing interfaces, and the degree to which gases are expelled by the base metals during the brazing cycle.
- Certain oxides that form on base metals (particularly on copper-base metals) dissociate in vacuum at brazing temperatures.
- Difficulties sometimes experienced with contamination of brazing interfaces, due to expulsion of gases from the parts to be brazed, are negligible in vacuum brazing.
- Low pressure existing around the base and filler metals at elevated temperatures removes volatile impurities and gases from the metals. Frequently, the properties of base metals are improved. This characteristic is also a disadvantage when elements in the filler metal or base metals volatilize at brazing temperatures, thus changing the melting point of the filler metal or properties of the base metal. This tendency may, however, be corrected by employing partial-pressure vacuum brazing techniques.

Special Brazing Considerations

In the selection of a brazing process for a nickel-base alloy, the characteristics of the alloy must be carefully considered. The nickel-base alloy family includes alloys that differ significantly in physical metallurgy (such as the mechanism of strengthening) and in process history (cast versus wrought). These characteristics can have a profound effect on their brazeability.

Precipitation-hardening alloys present several difficulties not normally encountered with solid-solution alloys. Precipitation-hardening alloys often contain appreciable (greater than 1%) quantities of aluminum and titanium for improved strength and corrosion resistance. The oxides of these elements are almost impossible to reduce in a controlled (vacuum or hydrogen) atmosphere. Therefore, nickel plating or the use of a flux is necessary to obtain a surface that allows wetting by the filler metal.

Because these alloys are hardened at temperatures of 540 to 815 °C (1000 to 1500 °F), brazing at or above these temperatures may alter the alloy properties. This frequently occurs when using silver-copper filler metals, which occasionally are used on heat resistant alloys.

Liquid metal embrittlement is another difficulty encountered in brazing of precipitation-hardening alloys. Many nickel-base, iron-base, and cobalt-base alloys crack when stressed parts are exposed to molten metals. This is usually confined to the silver-copper filler metals. If PH alloys are brazed in the hardened condition, residual stresses are often high enough to initiate cracking.

Cleanliness, as in all metallurgical joining operations, is important when brazing nickel and nickel-base alloys. Cleanliness of base metal, filler metal, flux (when used for torch or induction brazing), and purity of atmosphere should be as high as practical to achieve the required joint integrity. Elements that cause surface contamination or interfere with braze wetting or flow should be avoided in prebraze processing. All forms of surface contamination such as oils, chemical residues, scale, or other oxide products should be removed by using suitable cleaning procedures. The use of nickel-base filler metals can offer some cost effectiveness in this regard because certain nickel-base brazing filler metals containing boron and/or silicon are known to be self-fluxing and thus more forgiving to slight imperfections in cleanliness.

Attempting to braze over the refractory oxides of titanium and aluminum that may be present on PH nickel-base alloys must be avoided. Procedures to prevent or inhibit the formation of these oxides before and/or during brazing include special treatments of the surfaces to be joined or brazing in a highly controlled atmosphere. Surface treatments include electrolytic nickel plating and reducing the oxides to metallic form. As stated earlier in this section, a typical practice is to nickel plate the joint surface of any alloy that contains aluminum and/or titanium. For vacuum brazing of alloys containing aluminum and titanium in trace amounts, use of 0.0025 to 0.0075 mm (0.0001 to 0.0003 in.) thick plate is considered optimal. Alloys with up to 4% Al and/or titanium require 0.010 to 0.015 mm (0.0004 to 0.0006 in.) thick plate, and alloys with aluminum and/or titanium contents greater than 4% require 0.020 to 0.030 mm (0.0008 to 0.0012 in.) thick plate. When brazing in a pure dry hydrogen atmosphere, thicker plating (0.025 to 0.038 mm, or 0.001 to 0.0015 in.) is desirable for alloys with high (>4%) aluminum and/or titanium contents.

Atmospheres. Dry, oxygen-free atmospheres that are frequently used include inert gases, reducing gases, and vacuum. The brazing atmosphere, whether gaseous or vacuum, should be free from harmful constituents such as sulfur, oxygen, and water vapor. When brazing in a gaseous atmosphere, monitoring of the water vapor content of the atmosphere (that is, the dew point) is the common practice. A dew point of –50 °C (–60 °F) results in average brazeability; –60 °C (–80 °F) or below produces a better quality braze.

Stresses. During brazing, residual or applied tensile stress should be eliminated or minimized as much as possible. Also, inherent stresses present in the PH alloys may lead to SCC. Therefore, stress relieving or annealing prior to brazing is also recommended for all furnace, induction, or torch brazing operations. Brazing filler metals that melt below the annealing temperature are likely to cause SCC of the base metal.

Thermal Cycles. Consideration must be given to the effect of the brazing thermal cycle on the base metal. Filler metals that are suitable for brazing nickel-base alloys may require relatively high temperatures. This is particularly true for the filler-metal alloy systems most frequently used in brazing of nickel-base alloys—the nickel-chromium-silicon or nickel-chromium-boron systems.

Solid-solution-strengthened nickel-base alloys such as Inconel 600 may not be adversely affected by brazing temperatures of 1010 to 1230 °C (1850 to 2250 °F). Precipitation-strengthened alloys such as Inconel 718 may, however, display adverse property effects when exposed to brazing cycles with maximum temperatures that are higher than their normal solution heat treatment temperatures. Inconel 718, for example, is solution heat treated at 955 °C (1750 °F) for optimum stress-rupture life and ductility. Braze temperatures of 1010 °C (1850 °F) or above result in grain growth and a corresponding decrease in stress-rupture properties, which cannot be recovered by subsequent heat treatment.

Consideration of base-metal property requirements for service enables selection of an appropriate braze alloy. Lower melting temperature (below 1040 °C, or 1900 °F) braze filler metals are available within the nickel-base alloy family and within other brazing filler-metal systems (see Table 22).

Inconel 718 is often used in the fabrication of air diffusers for aerospace turbine engines. One manufacturer found that vacuum brazing

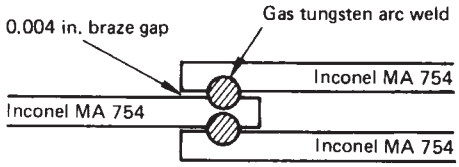


Fig. 28 Brazing specimen assembly used to evaluate stress-rupture properties of brazed Inconel MA 754

of diffuser components at 10^{-4} torr in a cold-walled vacuum furnace provided the best results. Prior to brazing, all joint surfaces were nickel plated to 0.005 to 0.015 mm (0.0002 to 0.0006 in.) thicknesses. Plating was done in accordance with specification AMS 2424 or equivalent. Prior to assembly, application of BNi-2 braze filler metal tape (approximately 0.11 mm, or 0.0045 in., thick) was preplaced between all joint surfaces. After assembly, an additional braze slurry of BNi-2 filler metal was applied to all joints to ensure joint soundness.

Brazing of Oxide Dispersion-Strengthened (ODS) Alloys

Oxide dispersion-strengthened alloys are P/M alloys that contain stable oxides evenly distributed throughout the matrix. The oxide does not go into solution in the alloy even at the liquidus temperature of the matrix. However, the oxide is usually rejected from the matrix on melting of the matrix, which occurs during fusion welding, and cannot be redistributed in the matrix on solidification; therefore, these alloys are usually joined by brazing.

Inconel MA 754, dispersion-strengthened nickel alloys, and dispersion-strengthened nickel-chromium alloys are the easiest to braze of the family of ODS alloys. Vacuum, hydrogen, or inert atmospheres can be used for brazing. Prebraze cleaning consists of grinding or machining the faying surfaces and washing with a solvent that evaporates without leaving a residue. Generally, brazing temperatures should not exceed 1315 °C (2400 °F) unless demanded by a specific application that has been well examined and tested. The brazing filler metals for use with these ODS alloys usually are not classified by AWS. In most cases, the brazing filler metals used with these alloys have brazing temperatures in excess of 1230 °C (2250 °F). These include proprietary alloys that are based on nickel, cobalt, gold, or palladium.

Brazements made of ODS alloys to be used at elevated temperature must be tested at elevated temperature to prove fitness-for-purpose. In the case of stress-rupture testing, AWS specification C3.2 may be used as a guide because it gives the actual joint configuration. The configuration shown in Fig. 28 is preferred by some as a test model, although any test configuration without stress raisers is adequate. The elevated-temperature brazement properties for Inconel alloy MA 754 should meet the following requirements:

Shear stress		Temperature		Service
MPa	ksi	°C	°F	life, h
26	3.8	980	1800	>1000
9.0	1.3	1095	2000	>1000

Inconel MA 6000 is a nickel-base ODS alloy that is also γ' strengthened. The amount of alloying elements in the base metal matrix plus the γ' precipitations cause an interesting problem in the brazing of this alloy. Inconel MA 6000 has a solidus temperature of 1300 °C (2372 °F); therefore, the brazing temperature should be no higher than 1250 °C (2282 °F). Additionally, because 1230 °C (2250 °F) is the γ' solution treatment temperature, it becomes important to carefully select the brazing filler metal and to heat treat the assembly after brazing. The AWS-specified BNi and BCo filler metals, as well as specially formulated filler metals, have been used for this alloy.

Inconel MA 6000 is used for its high-temperature strength and corrosion resistance; unfortunately, the passive oxide scale that provides good corrosion resistance also prevents wetting and flow of brazing filler metal. Therefore, correct cleaning procedures are very important. Surfaces to be brazed should be mechanically cleaned with a water-cooled, low-speed belt or wheel of approximately 320-grit and stored in a solvent, such as methanol, until immediately before the beginning of the brazing cycle.

ACKNOWLEDGMENTS

Portions of this article were adapted from the following:

- E.B. Hinshaw, Welding of Nickel Alloys, *Welding, Brazing, and Soldering,* Vol 6, *ASM Handbook,* ASM International, 1993, p 740–751
- D. Manente, Brazing of Heat-Resistant Alloys, Low-Alloy Steels, and Tool Steels, *Welding, Brazing, and Soldering,* Vol 6, *ASM Handbook,* ASM International, 1993, p 924–930
- S.J. Matthews, Selection of Nickel-Base Corrosion-Resistant Alloys Containing Molybdenum, *Welding, Brazing, and Soldering,* Vol 6, *ASM Handbook,* ASM International, 1993, p 592–597
- D.J. Tillack, Selection of Nickel, Nickel-Copper, Nickel-Chromium, and Nickel-Chromium-Iron Alloys, *Welding, Brazing, and Soldering,* Vol 6, *ASM Handbook,* ASM International, 1993, p 586–592

REFERENCES

1. J.M. Sarver, J.R. Crum, and W.L. Mankins, "Carbide Precipitation and the Effect on Thermal Treatments on the Stress Corrosion Cracking Behaviour of Inconel Alloy 690," paper presented at Corrosion '87, NACE, 1987
2. B.B. Weiss, G.E. Rotke, and R. Stickler, Physical Metallurgy of Hot Ductility Testing, *Weld. J.*, Oct 1970, p 471s–422s
3. W.F. Savage and J.J. Pepe, Effects of Constitutional Liquation in 18-Ni Maraging Steel Weldments, *Weld. J.*, Sept 1967, p 411s–422s
4. D.A. Canonico, W.F. Savage, W.J. Werner, and G. M. Goodwin, Effects of Minor Additions on Weldability of Incoloy 800, *Proc. Welding Research Council Symposium on Effects of Minor Elements on the Weldability of High-Nickel Alloys,* Welding Research Council, Oct 1967
5. "Welding Technical Bulletin," Inco Alloys International, July 1991, p 29
6. W.F. Savage, Weldments, Physical Metallurgy and Failure Phenomena, *Proc. Fifth Bolton Landing Conf.*, Aug 1978, p 16
7. "Welding Technical Bulletin," Inco Alloys International, July 1991, p 23
8. M.A. Streicher, The Relationship of Heat Treatment and Microstructure to Corrosion Resistance in Wrought Ni-Cr-Mo Alloys, *Corrosion,* Vol 19, 1963, p 272t–284t
9. M.A. Streicher, The Effect of Composition and Structure on Crevice, Intergranular, and Stress Corrosion of Some Wrought Ni-Cr-Mo Alloys, *Corrosion,* Vol 32, 1976, p 79–93
10. A.I. Asphahani and F.G. Hodge, Nickel-Base Molybdenum-Containing Alloys for the Chemical Process Industry, *Alloys for the Eighties,* R.Q. Barr, Ed., Climax Molybdenum Co., 1980
11. S.J. Matthews, Simulated Heat-Affected Zone Studies of Hastelloy Alloy B-2, *Weld. J. Res. Suppl.*, March 1979
12. A.I. Asphahani and S.J. Matthews, "High Molybdenum Nickel-Base Alloy," U.S. Patent 4,846,885, 11 July 1989
13. E.M. Horn, P. Mattern, H. Schlecke, J. Korkhaus, A.I. Asphahani, and S.J. Matthews, Hastelloy Alloy B-42 Weld Overlay Welding, *Werkst. Korros.*, Vol 43, 1992, p 396–401
14. M.J. Cieslak, T.J. Headley, and J. Romig, The Welding Metallurgy of Hastelloy Alloys C-4, C-22, and C-276, *Metall. Trans. A,* Vol 17, Nov 1986, p 2035–2047
15. S. Kou, Precipitation-Hardening Materials, II: Nickel-Base Alloys, *Welding Metallurgy,* John Wiley & Sons, 1987, p 297–316
16. M. Prager and C.S. Shira, Welding of Precipitation-Hardening Nickel-Base Alloys, *Weld. Res. Counc. Bull.*, No 128, 1968
17. R.M. Wilson, Jr. and L.W.G. Burchfield, *Weld J.*, Vol 35, 1956, p 32s
18. W. Yeniscavitch, Joining, *Superalloys II,* C.T. Sims, N.S. Stoloff, and W.C. Hagel, Ed., John Wiley & Sons, 1987, p 495–516
19. T.F. Berry and W.P. Hughes, *Weld J.*, Vol 46, 1969, p 505s

ASM Specialty Handbook: Nickel, Cobalt, and Their Alloys
J.R. Davis, editor, p 273-280
DOI:10.1361/ncta2000p273

Copyright © 2000 ASM International®
All rights reserved.
www.asminternational.org

Cleaning and Finishing of Nickel Alloys

CLEANING AND FINISHING procedures for both corrosion resistant and heat resistant nickel-base alloys are described in this article; a brief description of applicable coating processes is also provided. Additional information on coatings can be found in the article "High-Temperature Coatings for Superalloys" in this Handbook

Cleaning and Finishing of Corrosion Resistant Nickel Alloys

Nickel alloys do not require special techniques or precautions for the removal of shop soils such as soap, drawing compound, oil, grease, cutting fluid, and polishing compound. Oxide, scale, tarnish, or discoloration can be removed from nickel and nickel alloys by mechanical methods such as grinding or abrasive blasting or by chemical methods such as pickling. Conventional methods of cleaning with alkaline compounds, emulsions, or solvents or vapor degreasing may be employed. These processes are described in *Surface Engineering,* Volume 5 of *ASM Handbook.*

Pickling

Pickling is a standard method for producing bright, clean surfaces on nickel alloys, either as an intermediate step during fabrication or as a last step on finished parts. Procedures used for pickling nickel alloys are governed by both material composition and prior thermal treatment. The necessity of pickling can be avoided by using bright-heating practices, that is, the use of a protective inert and/or vacuum furnace atmosphere to prevent oxidation. Pickling should not be used to overhaul material by dissolving away appreciable amounts of metal. This practice can cause severe, irreversible damage such as pitting and intergranular attack. Significant material dimensional loss can readily occur if process parameters (e.g., continued maintenance of bath chemistry, temperatures, and immersion time) are ignored. Caution should be observed when pickling bimetallic items, weldments, and components with platings or coated surfaces, because selective, localized attack may occur, depending on system dynamics.

Oxidizing furnace atmospheres, high-sulfur-content fuels, and air leakage in furnaces during high-temperature operations can cause heavy scale to form on unprotected nickel alloys. Securely oxidized nickel alloys have a dull, spongy appearance. Hairline cracks are sometimes present, and patches of scale may break away from the surface. In such cases, the rough underlying metal will not allow an attractive finish to be attained by any pickling method. Table 1 provides selected formulas for pickling nickel alloys, and the table below will aid in preparing these formulas:

Acid	°Bé(a)	Specific gravity	Concentration,wt%
HNO_3	42	1.41	67
H_2SO_4	66	1.84	93
HCl	20	1.16	32
HF	30	1.26	70

(a) Baumé hydrometer reading, in degrees

The best methods for removing heavy scale are mechanical removal techniques such as abrasive blasting or grinding, usually with aluminum oxide or silicon carbide, followed by flash pickling. Abrasive blasting requires a relatively low capital investment compared to pickling, considering the extensive equipment needed for pickling and the cost of complying with environmental regulations. Abrasive blasting also eliminates the need to use and dispose of acids and the need to treat the rinse water. However, the removed scale and spent media may be considered a solid waste for disposal purposes. An alternative method is to soak the oxidized material in hydrochloric acid pickle (Formula 11, Table 1), followed by flash pickling if brightening is required.

Precautions must be taken in handling pickling solutions, because noxious and sometimes toxic fumes are liberated. Positive ventilation, either the use of a ventilating hood over the bath or provision of a controlled draft, is required to remove the fumes. Pickling acids must be handled with care, particularly hydrofluoric acid. Protective clothing, face shields, and rubber gloves must be used at all times. When solutions are prepared, acid should always be added to the water. This is especially important when sulfuric acid is diluted. In preparing the solutions shown in Table 1, the ingredients should be added to the water in the order listed.

Bath Life. Pickling baths should be analyzed regularly to determine acidity. Only total acidity can be determined in baths composed of more than one acid; it is impossible to distinguish acidity contributed by one acid source from that contributed by another. However, when the acidity of a bath is being maintained, the ingredients should be added in the proportions used for the original solution. Bath analysis should be performed by a qualified individual, by either wet chemistry or another acceptable means, on an established schedule. Subsequent additions should be made to maintain the bath at the initial acidity level.

With the exception of flash pickling solutions, bath solution should be disposed of when the total metallic content reaches 150 g/L (20 oz/gal). If the bath is used for only one type of alloy, only one element needs to be determined in the analysis. The remaining metallic elements can be determined from the percentage of each in the composition of the alloy. For example, in analyzing baths used for pickling nickel-chromium alloys, the nickel content determines whether the total metallic content is within the 150 g/L limitation.

Flash pickling solutions continue to perform satisfactorily even when nearly saturated with metal salts. Fresh solution should be made up only when salts begin to crystallize on the side of the bath container.

Alloy Groups

For the purpose of discussing pickling procedures, the nickel alloys can be divided into four groups:

- *High-nickel alloys* such as Nickel 200, Nickel 201, Nickel 270, and Duranickel alloy 301
- *Nickel-copper alloys* such as Monel alloys 400 and K-500
- *Nickel-chromium alloys* such as Inconel alloys 600, 625, 718, and X-750
- *Nickel-iron-chromium (Ni-Fe-Cr) alloys* such as Incoloy alloys 800 and 825

All alloys within any one group have virtually the same pickling characteristics. However, the pickling procedures for alloys within a group must be varied to suit the surface condition of the metal.

Table 1 Formulas for pickling nickel alloys

Formula No.	Reagents	Weight, %	Amount		Temperature	
			mL	oz	°C	°F
1	Nitric acid (HNO_3) 1.41 sp gr	20	300	10	70	160
	Water		1000	34		
2(a)	Nitric acid (HNO_3) 1.41 sp gr	10	133	4	75	170
	Sodium chloride (NaCl)	5	63 g	2		
	Water		1000	34		
3	Nitric acid (HNO_3) 1.41 sp gr	20	315	11	50	125
	Hydrofluoric acid (HF) 1.26 sp gr	2	34	1		
	Water		1000	34		
4	Sulfuric acid (H_2SO_4) 1.84 sp gr	25	200	8	80	180
	Water		1000	34		
5	Sulfuric acid (H_2SO_4) 1.84 sp gr	15	111	4	80	180
	Sodium chloride (NaCl)	5	63	2		
	Water		1000	34		
6	Sulfuric acid (H_2SO_4) 1.84 sp gr	15	119	4	20–40	70–100
	Sodium dichromate ($Na_2Cr_2O_7$)	10	135 g	5		
	Water		1000	34		
7	Sulfuric acid (H_2SO_4) 1.84 sp gr	12	82	3	Ambient	Ambient
	Sodium fluoride (NaF)	2	23 g	1		
	Water		1000	34		
8	Sulfuric acid (H_2SO_4) 1.84 sp gr	20	171	6	80	180
	Sodium chloride (NaCl)	5	73 g	3		
	Sodium nitrate ($NaNO_3$)	5	73 g	3		
	Water		1000	34		
9	Sulfuric acid (H_2SO_4) 1.84 sp gr	35	1200	41	20–40	70–100
	Nitric acid (HNO_3) 1.41 sp gr	30	1860	63		
	Sodium chloride (NaCl)	0.5	30 g	1		
	Water		1000	34		
10	Hydrochloric acid (HCl) 1.16 sp gr	6	200	7	60	140
	Water		1000	34		
11	Hydrochloric acid (HCl) 1.16 sp gr	12	535	18	80	180
	Cupric chloride ($CuCl_2$)	2	33 g	1		
	Water		1000	34		
12	Hydrochloric acid (HCl) 1.16 sp gr	1	30	1	Ambient	Ambient
	Ferric chloride ($FeCl_3$)	1	11 g	0.3		
	Water		1000	34		
13	Sodium hydroxide (NaOH)	15	188 g	7	80	180
	Potassium permanganate ($KMnO_4$)	5	63 g	2		
	Water		1000	34		
14	Ammonium hydroxide (NH_4OH)	2(b)	20	0.5	Ambient	Ambient
	Water		1000	34		
15	Alkaline cleaner		60–75 g/L	7–9 oz/gal	80	180
	Water		1000	34		
16	Agar-agar	1	10 g	0.3	20–65	70–150
	Potassium ferricyanide ($K_3Fe(CN)_6$)	0.1	1 g	0.03		
	Sodium chloride (NaCl)	0.1	1 g	0.03		
	Water		1000	34		

(a) An addition of at least 40 g of nickel per liter to Formula 2 will prevent overpickling of chromium-bearing alloys. (b) Volume %

Surface Conditions

Alloys within each composition group that have similar surface conditions are pickled in the same solutions using the same procedures. Three different surface conditions are generally encountered, primarily depending on the method of prior heating:

- *Bright annealed white surface* requiring removal of tarnish by flash pickling
- *Bright annealed oxidized surface* requiring removal of a layer of reduced oxide, sometimes followed by a flash pickle to brighten
- *Black or dark-colored surface* requiring removal of adherent oxide film or scale

Tarnish and dullness from bright annealed metal can be removed by flash pickling or bright dipping. Bright annealed white surfaces are generally found on drawn and spun shapes, cold-headed rivets, cold-drawn wire, and other cold-worked products. The white surface is a result of annealing in a reducing, sulfur-free atmosphere and cooling either out of contact with oxygen or by quenching in a 2 vol% alcohol solution.

Flash pickling solutions act rapidly, and care must be exercised to prevent overpickling and etching. These solutions are used at room temperature. If the bath is cold, it should be warmed slightly to prevent unduly slow action. Best results with flash pickling are obtained by warming the parts by dipping them in hot water, placing them in the acid for a few seconds, and rinsing them again with hot water. A second dip in acid may be used if necessary. Badly tarnished metal may require a total of 3 min in acid, but the material should be withdrawn frequently from the bath and inspected to prevent overpickling.

Reduced-oxide surfaces occur when hot-worked products, such as forged and hot-rolled material, are heated after hot working in a reducing, sulfur-free atmosphere and are cooled out of contact with air or quenched in an alcohol solution. On such products, pickling produces a clean surface for further processing by cold forming, or it produces the finished surface necessary for items such as rivets.

At annealing temperatures in reducing atmospheres, oxides formed on the high-nickel alloys, except those containing chromium, are readily converted to a spongy, tightly adherent layer. On nickel alloys, the layer consists of metallic nickel. On Monel alloys the layer is a mixture of metallic nickel and copper. The oxide film formed on nickel-chromium alloys and NI-Fe-Cr alloys does not undergo complete reduction in reducing atmospheres, which makes pickling more difficult. The oxide on these alloys is selectively reduced to a mixture of metallic nickel and chromic oxide. The surface color ranges from the characteristic chrome green of chromic oxide to dark brown.

Oxidized or scaled surfaces are present on all hot-worked products and heat treated material cooled in air. This type of surface also occurs on the nickel-chromium and Ni-Fe-Cr alloys in all conditions except bright heated. The oxide film forms on properly heated nickel and nickel-copper alloys during contact with air after the work is withdrawn from the furnace. The nickel-chromium and Ni-Fe-Cr alloys form oxide films even when heated and cooled in atmospheres that keep other alloys bright. Thus, the usual pickling procedure for Inconel and Incoloy alloys is designed to remove oxide and scale.

Nickel-Copper Alloys

Depending on the methods of prior heating and cooling, nickel-copper alloys can have any of the surface conditions discussed previously. Accordingly, the appropriate pickling procedure depends on the surface condition of the material.

Tarnish is best removed from bright annealed nickel-copper alloys by pickling in two solutions in sequence. First, the metal should be pickled thoroughly in Formula 2 (Table 1) in brief exposures and rinsed in water at 80 °C (180 °F). After rinsing, the metal should be dipped in Formula 1. The second dip should be followed by rapid rinsing of the workpiece and neutralization in a 1 to 2 vol% solution of ammonia (Formula 14). To dry, small workpieces should be dipped in boiling water and rubbed in sawdust or with a clean, dry cloth.

Reduced-Oxide Surfaces. Formula 8 is recommended for reduced-oxide surfaces on nickel-copper alloys if pickling is done on a large scale. This acid mixture is more destructive to tanks and racks than solutions used for steel or copper. Steel tanks lined with 4.8 mm ($\frac{3}{16}$ in.) thick natural rubber and a double layer of yellow acid bricks have proven to be the best and most economical containers for this corrosive solution. After pickling in Formula 8, the metal should be rinsed in hot water and neutral-

ized in a 1 to 2 vol% ammonia solution. The Formula 8 pickling solution works best after a short period of use. Therefore, when new solutions are prepared, about 2 vol% of spent solution should be added to the fresh mixture to improve its action.

When a pickling room is not regularly operated, the time required for complete pickling of small lots in Formula 8 is usually a disadvantage. Adequate results in most cases can be obtained by using flash pickling solutions (Formulas 1 and 2). However, Formula 8 may be used for occasional small jobs if ceramic vessels or wooden barrels are used as containers. The solution can be heated and agitated by injecting live steam, either through a rubber hose or through a carbon pipe that has a perforated carbon-block end.

Oxidized or Scaled Surfaces. Oxidized nickel-copper alloys having a thin to moderately thick oxide are pickled by immersion in Formula 11, followed by brightening in Formula 6. After treatment in the first bath, the work should be rinsed in hot water before it is transferred to the brightening dip. The second dip in Formula 6 should be followed by rinsing the work in cold water and neutralizing it in a 1 to 2 vol% ammonia solution (Formula 14).

High-Nickel Alloys

Nickel 200, Nickel 201, Nickel 270, Duranickel alloy 301, and similar alloys can have any of the three types of surface conditions. With the exception of flash pickling, high-nickel alloys are pickled in the same solutions used for Monel alloys. However, maintaining separate baths for the two groups of alloys is usually advisable.

Tarnish. Only one dip, Formula 9, is required to remove tarnish from bright annealed high-nickel alloys. The metal should first be dipped in hot water to warm it. Immersion in the acid bath for 5 to 20 s is usually sufficient to produce bright, clean surfaces. After the metal is removed from the pickling solution, it should be rinsed in hot or cold water and neutralized in a dilute ammonia solution.

The pickling action of Formula 9 can be retarded, if necessary, by decreasing the amount of acid to as little as one-third the volume that is added to the standard formula (e.g., as low as 400 mL, or 13.5 oz, of sulfuric acid or 620 mL, or 21 oz, of nitric acid). Normally, however, the formula gives the best results in the proportions given in Table 1.

Reduced-Oxide Surface. The solution used to pickle reduced-oxide surfaces on nickel-copper alloys, Formula 8, is also used for high-nickel alloys. The procedure is the same as the procedure for reduced-oxide surfaces, described earlier for nickel-copper alloys. If both groups of alloys are being pickled, separate baths should be maintained. Formula 8 may be used for occasional small lots, but suitable results can usually be obtained in less time by flash pickling in Formula 9.

Oxidized or scaled surfaces on high-nickel alloys can be pickled with the hydrochloric acid/cupric chloride solution (Formula 11) used for nickel-copper alloys. A longer time is required, however. Immersion from 1 to 2 h is necessary to obtain a good pickle on high-nickel alloys. After removal from the pickling bath, the work should be rinsed with hot water and dipped for a few seconds in Formula 9, if brightening is required. The brightening dip should be followed with a cold-water rinse and neutralization in a dilute ammonia solution.

Nickel-Chromium and Ni-Fe-Cr Alloys

Tarnished or reduced-oxide surfaces are usually not encountered on nickel-chromium or Ni-Fe-Cr alloys. These alloys can only be bright annealed in very dry hydrogen or in a vacuum. Oxides formed on their surfaces in other atmospheres do not undergo complete reduction. Oxide or scale is the usual surface pickled on nickel-chromium and Ni-Fe-Cr alloys.

Pretreating in a fused-salt bath is strongly recommended to facilitate pickling of oxidized or scaled surfaces. However, if the metal has been properly heated and cooled, it will usually have a surface suitable for direct pickling in Formula 3. If a fused-salt bath is used for pretreating, the following procedure should be used for pickling nickel-chromium and Ni-Fe-Cr alloys:

- Treat in fused-salt bath.
- Quench in and spray with water.
- Immerse in Formula 4.
- Withdraw from bath and rinse with water.
- Immerse in Formula 1.
- Withdraw from bath and rinse with water.
- Pickle in Formula 3 as required.

As with the nickel-copper alloys and high-nickel alloys, an alternative procedure employing a salt bath and Formula 8, with 10 g/L (1 oz/gal) of ferric chloride added to the formula, effectively removes oxide from hot-rolled or annealed Inconel alloys 601 and 671 and from Incoloy alloys 804 and 903.

If the oxide film cannot be readily removed by pickling directly in Formula 3, or if a fused-salt bath is not available, Formula 13 is a useful pretreatment. The work should be soaked for 1 to 2 h in Formula 13, removed, rinsed to remove all of the caustic solution, and pickled in Formula 3. On highly refractory oxides, it is sometimes necessary to repeat the cycle. Adding 7 to 10 g/L (0.9–1 oz/gal) of iron to Formula 3 decreases the danger of overpickling. This can be done conveniently by adding the proper weight of scrap iron to the bath when it is prepared.

The nitric acid/hydrofluoric acid bath (Formula 3) must be used with care. Nickel-chromium and Ni-Fe-Cr alloys are subject to intergranular attack in this solution if they have been sensitized by heating in, or slowly cooling through, the 540 to 760 °C (1000–1400 °F) temperature range. Time in the bath should be kept to a minimum, and bath temperature must not exceed 50 °C (125 °F). Stress-relieved and age-hardened material can also be sensitive to intergranular attack if the heat treatment involved exposure to sensitizing temperatures.

Salt Baths

Pretreatment baths of fused salts aid in the pickling of many alloys. They are particularly effective in pickling nickel-chromium and Ni-Fe-Cr alloys. Several proprietary baths are commercially available; information on their use can be obtained from manufacturers.

Precautions must be taken in handling salt baths. Protective clothing, face shields, and suitable gloves should be used. Room-temperature solution, or powder residue, may cause severe chemical burns. Extreme temperatures of working salt baths exacerbate the need for constant vigilance. Operators should avoid mixing salt bath constituents with those of pickling baths. Typically, rinse water should be used after salt bath processing and prior to pickling. Tank carryout should be minimized by sufficient draining. *Caution: Operators should not dispose of salt bath and pickling bath materials in the same container without approval from qualified personnel.*

Bath Life. Salt baths are basically alkaline and not acid in constitution. Bath maintenance should be in accordance with the supplier's instructions. Bath monitoring and control will be similar to that described earlier for pickling.

Salt baths are of three types: reducing, oxidizing, and electrolytic. Oxidizing baths are usually the least expensive to operate and the easiest to control, whereas reducing baths are no longer in common use. Electrolytic baths, although more expensive to install and operate, are quite effective for nickel alloys.

Oxidizing salt baths have a base of either sodium hydroxide or potassium hydroxide. Other salts, such as sodium nitrate and sodium chloride, are added to provide controlled oxidizing properties. The sodium hydroxide bath is operated at temperatures of 425 to 540 °C (800–1000 °F); a temperature of 480 °C (900 °F) is preferred for descaling nickel alloys. The potassium hydroxide bath operates at lower temperatures, usually 200 to 260 °C (400–500 °F). Treatment time in oxidizing baths is usually 5 to 20 min. In the operation of continuous strand pickling lines, the time may be as short as 15 to 60 s.

The salt bath oxidizes the lower oxides on the surface of the work to form soluble salts and water. Quenching after treatment removes part of the scale and loosens the remainder so that it is easily removed by appropriate acid dips. Oxidizing salt baths are also effective cleaners. They remove oil, grease, organic materials, and some inorganic substances from metal surfaces.

Electrolytic salt baths have a sodium hydroxide base and contain other salts, such as sodium chloride and sodium carbonate, that form

reducing agents at the cathode and oxidizing agents at the anode when electrically activated. Baths are usually operated at about 480 °C (900 °F), and although electrolytic salt baths can be used as a batch process, they are more suitable for continuous operations such as descaling of strip. Two tanks are normally used for continuous processes. The work is made anodic in the first tank and cathodic in the second.

Specialized Pickling Operations

Although pickling is most often used to remove the oxide or scale formed during heating, it is also used to remove foreign metals and other substances. Several procedures specifically designed for such purposes are applicable to nickel alloys.

Removal of Lead and Zinc. Lead and zinc embrittle high-nickel alloys at elevated temperatures. Consequently, when the alloys are formed in dies made of materials containing lead and zinc, all traces of the die material picked up during forming should be removed. When parts will be given intermediate anneals for processing, or when they will be exposed to high temperatures during service, removal of lead and zinc becomes especially important.

Formula 10 is used to remove lead and zinc from nickel and nickel-copper alloys. For nickel-chromium and Ni-Fe-Cr alloys, a bath of nitric acid similar to Formula 1 (but with the concentration of nitric acid increased to 30%) is used. After being immersed in the appropriate bath for 15 min, the work is removed, rinsed in water, and dried.

Detection and Removal of Embedded Iron. During mechanical operations such as rolling to shape or hot pressing, small particles of iron may become so firmly embedded in the surfaces of nickel alloys that they cannot be removed by the cleaning methods normally used for dissolving grease or cutting compounds. Under certain corrosive conditions, such iron particles can initiate local attack. For that reason, it is often necessary to test for iron traces and remove them.

For large-scale testing, a solution of about 1% sodium chloride is effective. A chemically pure grade of salt should be used to prevent false results from iron that might be present in less pure grades. When compressed air is available, it is usually less expensive to keep the tank full of salt spray with an atomizer than to fill it with the solution. After 12 to 24 h in the dilute salt solution, any iron particles in the nickel alloy will appear as rust deposits.

The ferroxyl test works well for small-scale testing. A potassium ferricyanide solution, made up in approximately the proportions shown in Formula 16, is applied to the surface of the material. The ingredients are mixed in earthenware, glass, or ceramic vessels and then boiled until all of the agar-agar is dissolved and a clear liquor is formed. Chemically pure sodium chloride should be used to prevent iron contamination of the test solution. The warm solution is applied to the surface to be tested and allowed to remain for at least 1 h. The solution gels as it cools, and the presence of iron on the metal surface is indicated by blue spots in the gel.

The ferroxyl test is sensitive enough that minute particles of iron that collect on the surface in the form of shop dust will appear as small blue spots in the gel. Because the iron dust will be washed off with the gel, the small spots should be distinguished from the larger ones caused by embedded iron. If spots of relatively major proportions develop, large iron particles are probably present.

A solution of hydrochloric acid and ferric chloride, Formula 12, is used to remove embedded iron. This solution should be used cold and should remain in contact with the metal for only the minimum time required for iron removal, not exceeding 1 h. After the work is removed from the solution, it should be rinsed thoroughly in cold water, then rinsed again in warm water. The detection tests should be repeated to verify the removal of the iron.

Prevention and Removal of Copper Flash. Copper flash sometimes forms on the surface of nickel alloys during pickling. For copper deposits to form, copper ions in the solution must be in the cuprous state, or they must pass from the cupric to the cuprous state during the cementing process. Consequently, any agents in the pickling bath that tend to maintain the cupric state will help prevent coppering.

Oxidizing agents such as nitric acid and sodium nitrate promote the action of pickling solutions, but become depleted with use. As the pickling bath ages, the concentration of copper ions increases while the concentration of oxidizing agents decreases. Thus, aging the bath facilitates coppering on areas where the reducing effect of the metal exceeds the oxidizing power of the bath.

When coppering occurs on Monel alloy 400 and other high-nickel alloys containing an appreciable amount of copper, the bath can be restored by adding small amounts of nitric acid or sodium nitrate. Nickel has greater reducing capacity than Monel alloy 400 and requires a greater concentration of oxidizing agents to prevent coppering in solutions containing copper salts. For this reason, Nickel 200 and similar alloys must not be pickled in solutions that have been used for nickel-copper alloys.

Patches of copper will plate out on nickel-copper alloys if steel contacts the alloys while they are wet with acid. Steel tongs or other devices used to handle the work are the usual sources of coppered areas. Coppering is prevented by using handling devices made of Nickel 200 or Monel alloy 400.

Copper flash is readily removed by immersing the alloy in an aerated, 4 to 5% ammonia solution at room temperature. The solution composition should be approximately 125 mL of ammonia to 1 L of water, or 1 pint of commercial aqua ammonia to 1 gal of water. The work should be immersed for about 1 min only, then rinsed in water.

Electrolytic Pickling. Light oxide films on any of the nickel alloys can be removed by electrolytic pickling in Formula 7. The work should be made anodic by using a current density of 5.4 to 10.75 A/dm^2 (50–100 A/ft^2). Electrolytic pickling is also useful for etching ground material to obtain a surface suitable for inspection.

Electropolishing of high-nickel alloys smooths the surface by removing metal through a controlled electrochemical process that is similar to, but essentially the reverse of, electroplating. When the alloy is immersed into an electrolyte and maintained anodic, metal is electrochemically removed ion by ion. This simultaneously deburrs the alloy, maximizes tarnish protection, and reduces surface fouling while producing a uniformly bright and smooth surface luster. Properly electropolished surfaces are microscopically featureless, noncontaminating, nonparticulating, and effectively stress relieved. Such high-performance and high-purity metal surface finish properties are unattainable by more traditional mechanical finishing techniques.

High-quality electropolishing of the high-nickel alloys produces brilliant lustered reflectivity. Best results are obtained from metals with fine grain boundaries that are free of nonmetallic inclusions and seams. Electropolished surfaces should not exhibit frosting, shadows, streaks, stains, pitted areas, or an “orange peel” or pebbly appearance.

Important factors in final finish quality are proper electrolyte selection, bath temperature, and bath maintenance (specific gravity, acid concentration, and metals content) and direct current from a ripple-free source applied at optimal voltage and current density. More complex configurations require adequate cathode design for effective polishing in inaccessible areas, inside corners, and in other areas of low current density. Agitation of either the electrolyte or the metal may be necessary to prevent gas entrapment, gassing streaks, flow marks, or similar undesirable markings.

Cleaning for Welding. Before maintenance welding is done on high-nickel alloys that have been in service, products of corrosion and other foreign materials must be removed from the area to be welded. Clean, bright base metal should extend 50 to 75 mm (2–3 in.) from the joint on both sides of the material to prevent the corrosion products from embrittling at welding temperatures.

Cleaning can be done mechanically (by grinding with a fine wheel or disk) or chemically (by pickling). Mechanical cleaning methods usually use an abrasive medium containing either aluminum oxide or silicon carbide grit. Care must be taken to avoid embedding abrasive grit into the weldment surface. Sometimes wire brushing with an austenitic stainless steel brush and/or local macroetching with a Schantz etch, or similar flash pickling, is an appropriate procedure immediately prior to welding.

Flash pickling solutions are effective in cleaning before welding. The solutions can be applied

by swabbing, brushing, or dipping, if the parts are easily handled. A single dip in Formula 2 is adequate for the nickel-copper alloys. Formula 1 is used for nickel alloys, and Formula 3 is useful for nickel-chromium and Ni-Fe-Cr alloys.

Finishing

Nickel alloys can be ground, polished, buffed, or brushed by all methods commonly used for other metals. For high-nickel alloys, a series of operations is required to produce a satisfactory finish. The number and type of operations required depend on the initial finish of the material, the desired final finish, and the type of equipment used. The pressures and speeds of the finishing equipment must be closely controlled. The high-nickel alloys, particularly nickel-chromium and Ni-Fe-Cr alloys, do not conduct heat away as rapidly as copper and aluminum. Excessive heat will destroy the true color of the metal and may warp flat, thin articles.

Some general recommendations for finishing operations are given in Table 2. Table 3 lists spindle speeds and corresponding surface speeds for various wheel diameters.

Grinding, often the first operation in a finishing sequence, is used to remove large surface imperfections and to rough-down welds prior to polishing and buffing. Rubber-bond grinding wheels are used for nickel and Monel nickel--copper alloys for their cutting effectiveness and for their relative softness, which reduces the heat generated. Rubber-bond wheels should be operated at a surface speed of 40 to 45 m/s (8000–9000 sfm). Vitrified-bond wheels are preferred for grinding harder alloys such as the Inconel and Incoloy alloys. These wheels should be operated at a surface speed of 25 to 30 m/s (5000–6000 sfm). Light welds can be ground efficiently with a No. 36 grit wheel, whereas a No. 24 grit is more practical for heavy welds.

Polishing. The first polishing operation should be done with very fine grit to remove all surface defects and give a base upon which to build the final finish. Wheels of No. 60 to 80 grit are usually required to remove heavy oxide or deep defects.

The first operation should be done dry. After the initial roughing, tallow should be used on all roll-head wheels of No. 150 grit or finer. Tallow clogs the wheel, giving a smoother finish and reducing the amount of heat generated.

When flat work is polished, each subsequent operation should be done with a grit 30 to 40 numbers finer than the previous one, until the surface is ready for the brushing or bobbing operations needed to prepare for buffing.

When possible, the scratches produced by the abrasive should cross the scratches left by the preceding operation. When polishing is done in only one direction, the finer abrasive will follow in the grooves made by the coarser abrasive, and the efficiency of the polishing wheels will be impaired.

Wheels for roughing and dry finishing should be made of tightly woven, unbleached cotton fabric. To prevent chattering, the wheels should be perfectly balanced and should have a soft or cushioned face. Fine grit wheels require more cushions than coarse wheels.

A more resilient and flexible wheel should be used for greasing operations. Greasing wheels should be made of 64- to 68-count unbleached sheeting and should have more cushion than the wheels used for coarser polishing. Grease coloring may be done on a full-disk, quilted sheepskin wheel or on a spirally sewn wheel made of fine-count (88-88) heavy sheeting. Compounds of artificial abrasives are preferred for roughing and dry finishing. Turkish emery is usually used for greasing and grease coloring.

Bobbing done with emery grout is more like burnishing than polishing, and if it is performed in one operation, it is best done with leather wheels. If it is done in two operations, the second should be done with a medium-density felt wheel, because felt wheels require less pressure. The best results are obtained from emery roll-head wheels at surface speeds of 33 to 38 m/s (6500–7500 sfm). The metal drags at slower speeds, and at excessive speeds, the wheel tends to pull up the surface of the metal.

Buffing. For good results in buffing, a high-quality wheel of the proper construction and material is essential. Wheels should be of sturdy, closely woven, high-count sheeting. The close weave gives good cutting, and the heavy threads provide good coloring.

Buffing is usually done in two operations. The first, the cutting-down operation, is done with a sewn buffing wheel operating at a surface speed of 40 to 45 m/s (8000–9000 sfm). The second, the coloring operation, is done with a loose-disk wheel operating at a surface speed of approximately 50 m/s (10,000 sfm). A loose disk, Canton-flannel wheel is best for buffing to a mirror finish. The high speeds used in buffing create a high heat. Consequently, less pressure is necessary than for polishing.

The cutting-down operation is normally performed with tripoli compound, which leaves

Table 2 Recommended finishing procedures

Operation	Wheel	Grit No.	Compound	Speed	
				m/s	sfm
Grinding	Rubber bond	24 or 36	None	40–45	8,000–9,000
	Vitrified bond	24 or 36	None	25–30	5,000–6,000
Roughing	Cotton fabric, sewn sections	60 or 80	None	30–40	6,000–7,500
Dry fining	Cotton fabric, sewn sections	100 or 120	None	30–40	6,000–7,500
Greasing	64-68 unbleached sheeting, spirally sewn sections	150 or 180	Polishing tallow or No. 180 emery grease cake	30–40	6,000–7,500
Grease coloring	88-88 unbleached sheeting, spirally sewn or loose disk; or quilted sheepskin	200 or 220	Polishing tallow or "F" emery grease cake	30–40	6,000–7,500
Bobbing and sanding	Leather wheel for two bobbing operations, second with medium-density felt wheel	…	Grout	25	5,000
Cutting down	88 unbleached sheeting, loose spirally sewn sections or loose-disk wheel	…	Tripoli	40–45	8,000–9,000
Coloring bright finish	88-88 unbleached sheeting, loose spirally sewn sections or loose-disk wheel	…	White aluminum oxide	50	10,000
Coloring mirror finish	Loose-disk, 88-88 unbleached sheeting or Canton flannel	…	Green chromium oxide	50	10,000
Brushing	Tampico	…	"F" emery grease cake or grout	5–15	1,200–3,000

Table 3 Spindle speeds for various surface speeds and wheel diameters

Surface speed		Spindle speed, rev/min for indicated wheel diameter						
m/s	sfm	150 mm (6 in.)	200 mm (8 in.)	250 mm m (10 in.)	300 mm (12 in.)	360 mm (14 in.)	410 mm (16 in.)	460 mm (18 in.)
15	3,000	1,930	1,450	1,150	950	820	710	640
20	4,000	2,550	1,900	1,500	1,300	1,100	950	850
25	5,000	3,200	2,400	1,900	1,600	1,375	1,200	1,050
28	5,500	3,500	2,600	2,100	1,750	1,500	1,300	1,175
30	6,000	3,800	2,850	2,300	1,900	1,650	1,425	1,275
38	7,500	4,800	3,550	2,850	2,400	2,100	1,800	1,600
40	8,000	5,100	3,800	3,100	2,550	2,200	1,900	1,700
45	9,000	5,750	4,300	3,450	2,850	2,450	2,150	1,900
50	10,000	6,400	4,750	3,800	3,200	2,750	2,400	2,100

a haze on high-nickel alloys. Buffing compound with less grease should be used to promote deep color. White aluminum oxide and green chromium oxide compounds can be used for the final coloring. Chromium oxide compounds produce less friction and give a truer color.

Brushing. A tampico or wire wheel produces a brushed finish on the high-nickel alloys. Tampico wheels usually produce a better finish and higher luster, and because of their flexibility, they are better for irregular shapes. A tampico wheel is used with emery paste or grout to produce a satin finish, or with pumice and water or pumice and oil to produce a better finish. For wet brushing, tampico wheels should have wooden hubs.

Wire brushes can be used to produce a satin finish on sheet metal articles. Brushes should have a wire diameter of 0.10 to 0.20 mm (0.004–0.008 in.). They should not be made of steel or brass wire, because small particles from the brush are always embedded in the metal during the process. Steel particles rust, and brass particles discolor the nickel alloys.

Brushing is done at slower speeds than those used for polishing. Brushing speeds are normally 5 to 15 m/s (1200 to 3000 sfm), depending on the final finish desired. Higher speeds, 20 to 30 m/s (4000–6000 sfm), are required to produce a bright wire brush finish. Wire brushes operated at too slow a speed produce coarse, undesirable scratches.

Blasting. Abrasive media blasting has the ability to produce a cosmetically appealing, uniform, matte gray appearance that varies from dull to a high-sheen luster. The appearance depends on the medium chosen (aluminum oxide, silicon carbide, glass bead, steel shot, crushed plastic, etc.), particle size (No. 24 grit for rough finishes versus No. 220 for smooth finishes) and particle shape (angular grit or cut shot for a dull appearance versus crushed plastic, round glass beads, or cast steel shot for luster and sheen).

Nondestructive Inspection

Care must be taken in finishing high-nickel alloys when subsequent inspection will be performed with an ultrahigh-sensitivity, fluorescent penetrant nondestructive method. Under certain conditions, finishing operations using plastics, such as plastic blasting media, plastic brushes, or buffing pads with embedded grit, leave a residue of thin, smeared plastic on the surface that introduces high background fluorescence during fluorescent penetrant inspection. Similarly, coarse abrasive blasting may hamper the detection of surface flaws by penetrant methods. On the other hand, fine grit blasting (No. 60 or finer) has been successfully used to enhance detection of surface flaws, such as investment casting defects.

Cleaning and Finishing of Heat Resistant Nickel Alloys

Cleaning is required to remove contaminants from the surfaces of parts made from heat resistant alloys. Shop soils such as oil, grease, and cutting fluids can be removed by conventional solvents or soaps. Metallic contaminants, tarnish, and scale resulting from hot working or heat treating operations must also be removed.

Metallic Contaminant Removal

Parts made from heat resistant alloys can accumulate traces of other metals on their surfaces after contacting cutting tools, forming dies, and heat treating fixtures. Although metal contamination is not always harmful, its presence can be highly deleterious in certain cases. For example, Inconel X-750 may be unaffected by traces of zinc from drawing dies, but even the smallest particle of aluminum will readily alloy with the Inconel at elevated temperatures and degrade the corrosion resistance and mechanical integrity of the affected areas. Copper is another example of a metal that may affect some nickel-base alloys when they are subsequently exposed to high temperatures. Therefore, all surface contaminants should be removed from heat resistant alloys before they are heat treated or subjected to service at elevated temperatures.

In operations such as cutting and forming, the use of lubricants can either prevent or sharply reduce metal contamination. This is the preferred practice, because lubricants can be removed easily and inexpensively, if they have not been baked or fired.

When contamination is unavoidable, testing is recommended to determine the seriousness of the contamination. After heat treating operations, metallographic examination can be conducted to detect alloy diffusion, and bend or hardness tests can be conducted to detect embrittlement. For example, lead can be detected by the yellow precipitate that forms when a test solution of chromic acid (10 wt%), sodium chlorate (1.5 wt%), and water (88.5 wt%) is applied to the suspected surface at temperatures ranging from 21 to 60 °C (70–140 °F).

Mechanical removal methods used for metallic contaminants include dry or wet abrasive blasting with metal-free abrasives, polishing with ceramic materials, and wet tumbling. The shape of a part, the required surface finish, the allowable loss of gage, and residual stress considerations will determine the suitability of these mechanical methods.

Chemical removal methods, however, are used more often than mechanical methods to remove metallic contaminants. A typical procedure for chemically removing iron, zinc, and thin films of lead is to first perform vapor degreasing or alkaline cleaning, and then immerse the parts in a 1-to-1 solution (by volume) of nitric acid (1.41 sp gr) and water for 15 to 30 min at approximately 35 °C (95 °F). Water rinsing, followed by drying, completes the process.

Another procedure that had been successful in removing brass, lead, zinc, bismuth, and tin from nickel-base alloys involves vapor degreasing or alkaline cleaning, followed by soaking at room temperature in a solution of nitric acid (54 g/L, or 7.22 oz/gal), acetic acid (150–375 g/L, or 20–50 oz/gal), and hydrogen peroxide (19–64 g/L, or 2.5–8.5 oz/gal). Depending on the severity of the contamination, the soaking time can vary from 20 min to 4 h, as determined by visual observation of the reaction. After this treatment, parts must be rinsed thoroughly in water and dried. When possible, a test specimen should be immersed for the maximum time anticipated and then examined for chemical attack before the first load of parts is processed.

Nickel-base alloys should be acid etched to prepare for subsequent nondestructive inspection. The etching process removes smeared metal that may be present as a thin surface layer after machining and/or blast cleaning. The parts can be etched by immersing them in a bath containing hydrochloric acid (80%), hydrofluoric acid (13%), and nitric acid (7%) to remove the disturbed or smeared layer. This bath may leave smut that must be removed by a second bath containing iron chloride (22%), hydrochloric acid (75%), nitric acid (2%), and water. After being rinsed and dried, the parts can undergo visual and penetrant inspections. The extent of etching depends on the depth or thickness of the smeared layer. All of this layer should be removed. However, overetched parts will retain excessive amounts of penetrant.

Tarnish Removal

Tarnish, which is a thin oxide film, does not always have a harmful effect on the end use of parts made from heat resistant alloys. In fact, it can even be useful, such as when it functions as a bond for paint, a barrier to prevent diffusion from another alloy, or a retardant to further oxidation. However, other functional requirements can necessitate the removal of tarnish from parts. Tarnish should always be removed before welding or brazing.

Abrasive cleaning methods, such as those used to remove metallic contaminants, are also used to remove tarnish. The applicability of these methods is determined by part shape, required surface finish, and allowable loss of gage or dimension.

However, abrasive cleaning can remove some metal and degrade surface finishes. Therefore, flash pickling is used more often than abrasive cleaning to remove tarnish. A typical flash-pickling formula uses nitric acid (1.41 sp gr; 23 vol%), hydrofluoric acid (1.26 sp gr; 4 vol%), and water (73 vol%). Parts are immersed in this solution for 1 to 5 min at approximately 52 °C (125 °F). Warming the parts in hot water before

flash pickling speeds tarnish removal. Water rinsing and drying must follow pickling.

Reduced Oxide and Scale Removal

The most widely used methods for removing oxides or scale from heat resistant alloys, in order of decreasing preference based on economic considerations, are acid pickling, abrasive cleaning by tumbling or blasting, and descaling in molten salt. Alkaline scale conditioning is helpful in modifying the scale to facilitate its removal by these methods. When extremely heavy oxide layers must be removed, grinding is an appropriate preliminary operation. Combinations of two or more methods are often used. Before these removal methods are discussed, the characteristics of the various products that need to be removed are described.

Reduced oxide films will form on parts that are heated in reducing atmospheres, out of contact with air. Sometimes, these oxides can be removed by immersing the parts for 5 to 15 min in a tarnish-removing, flash-pickling bath, such as that with the formulation given above. However, most heat resistant alloys form a tenacious coating in the presence of carbon monoxide or water because of their high content of oxide-forming metals, such as nickel, cobalt, and chromium. The resulting oxides vary widely with alloy composition and furnace atmosphere. Usually, pickling is required for their removal. Scale conditioners are useful.

Scale develops on hot-forged, hot-formed, or heat treated parts that are processed in air. Usually, scale is tenacious and occurs in all gradations, including thick layers that result from heating in an oxidizing furnace using high-sulfur fuels. The scale that forms under such conditions had a dull, spongy appearance. Fine cracks may be present, and patches of scale may break from the surface. The underlying metal is rough and cannot be corrected by pickling. In these extreme conditions, grinding or abrasive blasting to sound metal, followed by flash pickling, is recommended.

Scale conditioning is used to soften, modify, or reduce scale to promote easier and more uniform acid pickling, but is seldom required to remove discolorations or thin interference coatings. A scale-conditioning bath consists of a highly alkaline aqueous solution, sometimes containing complexing and chelating compounds. The main purpose of these agents is to solubilize the scale as much as possible. The performance of a particular chelating agent depends on the affinity of the compound for the metal ions present, the pH of the scale-conditioning solution, and the physical and chemical composition of the scale. Typical multicycle descaling operations, including scale conditioning, are defined in Tables 4 and 5.

Minimal scale removal occurs during treatment in the alkaline scale-conditioning bath. Further treatment in highly alkaline solutions containing a strong oxidizing material, such as potassium permanganate, is often necessary. The scale on heat resistant alloys sometimes contains carbon and incompletely burned and polymerized residues, as well as metallic oxides. These organic components react with the oxygen that is released by the alkaline oxidizing bath.

Acid Pickling. After the scale is conditioned, it is subjected to acid pickling, during which most of the high-temperature scale either breaks away from or becomes so loosely attached to the parts that pressure rinsing with water completes the descaling. The acid pickle is usually a dilute nitric acid or a hydrofluoric-nitric acid solution. In addition to removing scale, pickling solutions that contain nitric acid will remove many surface contaminants through oxidation. However, because the acid solution attacks the base metal, it is necessary to limit the pickling time to prevent excessive metal loss or metal surface roughening.

Parts made from alloys that are high in aluminum and titanium, such as M252 and René 41, must undergo a special procedure before welding or brazing. When parts are in the solution-treated condition and descaling is required, they are treated in a scale-conditioning solution, as previously described, after which they are immersed in a solution of nitric acid (30 wt%) and hydrofluoric acid (3 wt%) for 5 to 10 min. Alloys in the aged condition are descaled anodically in an acid solution. A solution made for this procedure should contain sulfuric acid (75 wt%) and hydrofluoric acid (3 wt%). It should be operated using a current density of 215 to 430 A/mm^2 (20–40 A/ft^2) and graphite cathodes. The material should be immersed in the electrolytic cleaning bath for 3 to 12 min, and the operation will be complete when the amperage drops to nearly zero. Sodium sulfite (1.6 wt%) is used to reactivate the solution after a period of operation.

Weld areas typically differ, in terms of composition and structure, from the base metal and react differently to conditioning and pickling cycles. Weld areas or heat-affected zones are often susceptible to selective attack during pickling. Although inhibitors can eliminate or reduce this elective attack, it is preferable to use abrasive or other mechanical descaling methods, rather than acid pickling, to remove scale from welded parts, unless a safe pickling procedure has been found for a given application.

Hydrogen embrittlement does not occur in nickel-base alloys as a result of aqueous descaling.

Abrasive blasting with dry aluminum oxide can be used to remove oxide and scale from all types of worught and cast heat resistant alloys. Silicon carbide is more expensive than aluminum oxide and is seldom used. Silica (silicon dioxide, or sand) has a limited application because of its lack of cutting ability. It is sometimes used to clean refractory metal forgings prior to pickling. Grit sizes as coarse as No. 30 (0.59 mm, or 0.023 in.) are recommended for

Table 4 Procedure for removing scale from heat resistant alloys

Operation	Time, min	Temperature °C	Temperature °F	Solution	Concentration
Precleaning cycle					
Vapor degreasing	5–10	87–88	185–190	Stabilized trichloroethylene	…
Emulsion cleaning	10–20	54–66	130–150	Emulsion cleaner	20 vol%
Scale-conditioning cycle					
Alkaline chelating	15–30	125–135	260–275	Caustic solution containing alkanol amines and aliphatic hydroxy acids	…
Alkaline oxidizing	60–120	95–105	205–220	Potassium permanganate	5 wt%
				Sodium hydroxide	20 wt%
				Water	Remainder
Pickling cycle					
Acid pickling	5–30	49–60	120–140	Hydrofluoric acid	4 wt%

Table 5 Procedure for removing scale from Inconel alloys

Operation	Time	Temperature °C	Temperature °F	Solution(a)	Concentration(a)
Alkaline conditioning	1–2 h	96–105	205–220	Sodium hydroxide	20 wt%
				Potassium permanganate	5 wt%
Rinse	15–30 s	Not heated	Not heated	Water quench and water spray	…
Acid pickling	5–10 min	60–71	140–160	Sulfuric acid (1.83 sp gr)	7.5 vol%
				Hydrochloric acid (1.16 sp gr)	12 vol%
Rinse	15–30 s	Not heated	Not heated	Water	…
Acid pickling	10–20 min	60–71	140–160	Nitric acid (1.41 sp gr)	20 vol%
Rinse	15–30 s	Not heated	Not heated	Water	…
Acid pickling	5–60 min(b)	49–54	120–130	Hydrofluoric acid (1.26 sp gr)	3.7 vol%
				Nitric acid (1.41 sp gr)	22 vol%
Rinse	15–30 s	Not heated	Not heated	Water	…

(a) Undefined remainder is water. (b) Type of oxide will determine immersion time required; until immersion time is established, inspect frequently to avoid overpickling.

cleaning forgings and castings. Finer grits, such as No. 90 and 100 (0.17 and 0.15 mm, or 0.0065 and 0.0059 in., respectively), are used for general blasting.

Metallic shot and grit should not be used to descale heat resistant alloys unless their use is followed by pickling to remove metal contamination. For parts that must be welded or brazed, or that have highly tenacious scales produced by furnace atmospheres, pickling after dry abrasive cleaning is recommended, regardless of the abrasive used.

Wet abrasive blasting, also referred to as vapor honing, is also used to clean heat resistant alloys. This process uses No. 200 to 1250 silica abrasive particles (0.074–0.010 mm, or 0.0029–0.0004 in.) mixed with water to produce a slurry that removes loose scale, discoloration, and soils. Metal loss is not excessive when normal pressures and exposure times are used.

When spherical beads made of high-quality optical crown glass are used as the abrasive, stock loss is minimized. Bead sizes of 0.038 to 0.074 mm (0.0015–0.0029 in.) are generally used, and blasting pressures are kept below 410 kPa (60 psi) to prevent the beds from fracturing.

Surfaces that have been wet blasted are usually suitable for welding, brazing, electroplating, and final inspection processes. Further cleaning is seldom necessary. Exceptions are alloys with a high titanium and aluminum content, which require the special procedure discussed earlier under "Acid Pickling."

Most of the general advantages and limitations associated with the abrasive cleaning of steel will also apply to heat resistant alloys. However, there is a risk of contamination from either metallic abrasives or abrasives that have been used to clean parts made from metals of widely different compositions. For example, heat resistant alloys should not be blasted with abrasive material that has been used to clean low-alloy steel, aluminum, copper, or magnesium. However, abrasives used to clean titanium and corrosion resistant steels have been used to clean heat resistant alloys without serious contamination. The flash pickling of these alloys after abrasive cleaning provides additional assurance that no harmful surface contamination remains.

Wet tumbling by the barrel or vibratory method can be used to descale heat resistant alloys if the shape and size of the parts are suitable. The removal of burrs and sharp edges is accomplished in the same operation. Shop soils are also removed, thus eliminating the need for preliminary degreasing.

Parts are tumbled or vibrated in a mixture of acid descaling compound and metal-free abrasives and then subjected to a neutralizing cycle. Precautions regarding metal contamination are similar to those noted previously for abrasive blasting.

Pickling is required after tumbling and before resistance welding to remove residual smut, which can cause poor-quality weldments. There is less need for pickling prior to fusion welding, unless an inspection of the weldments reveals porosity or inclusions that are a result of pickup from the tumbling process.

Wire brushing is sometimes used to remove very light scale or surface discoloration. All brushes used on heat resistant alloys must have stainless steel bristles.

Salt-bath descaling is an effective first step in removing scale from heat resistant alloys. The process is generally more expensive than acid pickling, particularly if production is intermittent, because of the cost of maintaining the bath during idle time. The electrolytic salt bath used to descale heat resistant alloys contains fused caustic soda, rather than sodium hydride. The parts and the tank are alternately negative and positive poles of a direct current circuit.

This fused caustic soda bath, which contains oxidizing salts such as sodium nitrate, is operated at 425 to 540 °C (800–1000 °F). It is slightly more effective than the sodium hydride bath on high-chromium alloys. Processing steps are similar. Parts are immersed in the oxidizing bath for 5 to 15 min, quenched in water, soaked in a solution of 5 to 10% sulfuric acid at 70 °C (160 °F) for 1 to 5 min, and then dipped in a solution of 15 to 20% nitric acid and 2 to 4% hydrofluoric acid at 54 to 60 °C (130–140 °F) for 2 to 15 min.

Applicable Finishing and Coating Processes

Many finishing operations that are commonly used for steel and other metals are not required for the heat resistant alloys for several reasons. First, these alloys are inherently resistant to corrosion in a wide range of environments. Second, the applications of parts made from these alloys do not typically require a polished finish.

The oxide coating that is obtained during processing is frequently of value to heat resistant alloys that are subjected to elevated temperatures in service. Consequently, the dense, tenacious oxide that develops on formed or machined finished parts during final heat treatment is allowed to remain as protection against further oxidation.

Polishing of heat resistant alloys is sometimes used to obtain a desired surface finish, as well as to remove light scale or oxide from parts that are to be welded or brazed. Silicon carbide in various grit sizes is commonly used to prepare surfaces for brazing.

Surfaces are usually prepared for welding by polishing with No. 90 grit aluminum oxide, set up with sodium silicate on a cloth wheel. Discoloration can be removed by polishing with No. 120 grit aluminum oxide, used with a greaseless compound and a cloth wheel. Buffing is seldom required for the finishing of heat resistant alloys.

Electroplating. Chromium, copper, nickel, and silver are sometimes electroplated on heat resistant alloys in order to:

- Prepare for brazing
- Provide antigalling characteristics
- Repair expensive parts or correct dimensional discrepancies

Conventional nickel plating processes are often used to assist in brazing (see the article "Welding and Brazing of Nickel Alloys" in this Handbook). Deposits can vary in thickness from 2.5 to 25 μm (0.1–1 mil). Alloys that contain titanium or aluminum will require the thicker deposits.

Electrodeposited silver or nickel is used in special applications for antigalling purposes. Either nickel or chromium can be used to repair worn parts or build up dimensions.

Ceramic coatings are frequently applied to heat resistant alloys to increase the oxidation resistance of parts exposed to extremely high temperatures, such as gas turbine and missile components. Several types of ceramics are currently used, and some serve as thermal barriers, as well. Thermal barrier coatings are described in the article "High-Temperature Coatings for Superalloys" in this Handbook.

Diffusion coatings of aluminum, chromium, silicon, or combinations thereof, also are used to protect heat resistant alloy parts from high-temperature corrosion and to prolong part life. The coating of engine exhaust valves with aluminum is a common example. Diffusion coatings are also described in the article "High-Temperature Coatings for Superalloys."

Shot peening is currently used to improve the mechanical properties of compressor blades, turbine-blade dovetails, and latter-stage turbine-blade airfoils by introducing favorable patterns of residual stress. Although all turbine-blade dovetails are peened with steel shot, glass beads are sometimes favored over metallic shot in other shot-peening applications. The advantages of glass beads are that they:

- Pose no risk of metal contamination
- Remove virtually no metal
- Are available in smaller sizes than metallic shot and can therefore be used to peen areas that are difficult to reach when using metallic shot

However, glass beads are not equivalent to metal shot for improving mechanical properties.

ACKNOWLEDGEMENTS

This article was adapted from:

- F.S. Pettit, Surface Engineering of Heat-Resistant Alloys, *Surface Engineering*, Vol 5, *ASM Handbook*, ASM International, 1994, p 779–783
- R.C. Buckley, Surface Engineering of Nickel and Nickel Alloys, *Surface Engineering*, Vol 5, *ASM Handbook*, ASM International, 1994, p 864–869

ASM Specialty Handbook: Nickel, Cobalt, and Their Alloys
J.R. Davis, editor, p 281-290
DOI:10.1361/ncta2000p281

Copyright © 2000 ASM International®
All rights reserved.
www.asminternational.org

High-Temperature Coatings for Superalloys

DEMANDING OPERATING CONDITIONS for gas turbine engines have led to a variety of coatings designed to protect superalloy turbine components from corrosion caused by the combined effect of atmospheric contaminants, fuel impurities, and elevated temperature. To achieve the high-temperature mechanical properties required by modern gas turbine technology, superalloys have had to sacrifice the oxidation and hot corrosion resistance that was inherent in previously used heat resistant alloys with higher chromium contents. Consequently, coatings are relied on to protect superalloy components such as turbine blades and vanes from environmental attack. The development and application of high-temperature coatings have led to improved performance and fuel economy in aircraft, marine, and land-based industrial turbines.

Coating Requirements

The exclusive purpose of a coating on a superalloy is to prevent environmental attack of the substrate for the maximum possible time with the maximum degree of reliability. General categories of environmentally induced degradation that affect turbine components include oxidation and hot corrosion. Each degradation mechanism will tend to predominate in a specific temperature regime, and each involves interactions between the alloy and environment. These interactions have been reviewed extensively (Ref 1, 2).

Superalloys generally react with oxygen, which is the primary environmental condition that affects service life. At moderate temperatures of about 870 °C (1600 °F), and lower, general uniform oxidation is not a major problem. At higher temperatures, commercial nickel- and cobalt-base superalloys are attacked by oxygen. The level of oxidation resistance at temperatures below 980 °C (1800 °F) is a function of chromium content; chromia (Cr_2O_3) forms a protective oxide scale. At temperatures above 980 °C (1800 °F), aluminum content becomes more important in oxidation resistance; alumina (Al_2O_3) forms a protective oxide scale. Chromium and aluminum can contribute to oxidation protection in an interactive manner: as the chromium level increases, less aluminum may be required to form a highly protective Al_2O_3 layer. However, the aluminum contents of some superalloys are insufficient to provide long-term Al_2O_3 protection. The complex interactions between chromium and aluminum additions, as well as other alloying elements, for optimal oxidation performance are reviewed in Ref 3.

In lower-temperature operating conditions, such as ≤870 °C (≤1600 °F), accelerated oxidation can occur in superalloys through the operation of selective fluxing agents. One of the most well-known accelerated oxidation processes is hot corrosion (sometimes known as sulfidation). The hot corrosion process is separated into two regimes: low temperature and high temperature. High-temperature attack (type I) occurs at temperatures between 900 and 1050 °C (1650 and 1920 °F), and low-temperature attack (type II) occurs at temperatures between 680 and 750 °C (1255 and 1380 °F). Hot corrosion is triggered by the presence of sulfur in fuel and impurities, particularly salt, in the environment.

Both hot corrosion and oxidation involve rapid attack and consumption of hardware, and coatings are designed to resist the specific attack expected for particular turbine applications. Marine propulsion turbines, for example, are susceptible to both forms of hot corrosion, whereas aircraft gas turbines are more subject to oxidation, and sometimes to high-temperature hot corrosion, if the aircraft operates consistently in a coastal or marine environment. The problem of hot corrosion first became evident in large industrial and power-generated gas turbines that used low-quality fuels containing sulfur and sodium contaminants and other impurities, or that were located in areas where harmful species were ingested through air intakes, such as in marine and desert environments.

In addition to corrosion resistance, coatings for superalloys are required to resist both thermal cycling, often at rapid rates, and mechanical forces acting on hardware, without cracking. The protective oxide film (alumina), on which coatings for superalloys rely for protection, does not readily span even small gaps. Cracking of protective coatings is soon followed by a breakdown in protection, and localized substrate attack follows shortly. The thermal expansion match between coating and substrate is important, and coatings with a modicum of ductility are desirable from a corrosion standpoint. The coatings also must withstand combustion char and solid particulates ingested during turbine operations that result in erosive action.

Coatings must be reasonably compatible with the substrates to which they are applied. Components of the coating and the method of coating application should be selected to avoid undesirable reaction phases between coating and substrate and rapid penetration of the substrate by coating elements. The presence of' such phases and/or interdiffusion leads to void formation, or cracking at the interface, and coating spall. These imperfections compromise the mechanical performance capability of the system and the protection it provides.

Types of Coatings

As a result of many years of development and use in government and industry, two basic types of corrosion resistant coatings for superalloys have emerged. These are diffusion coatings and overlay coatings. Both depend on the sacrificial oxidation of aluminum in the coating to provide a spall-resistant, protective Al_2O_3 coating to protect or strongly inhibit further attack.

In recent years, ceramic thermal barrier coatings (TBCs) have been developed. These coatings, which are commonly used in conjunction with corrosion resistant coatings, enable a large improvement in turbine durability or performance by reducing the operating temperature on the superalloy surface or by allowing hotter gas temperatures. Thermal barrier coatings are described later in a separate section.

Diffusion Coatings. In the diffusion coating application process, aluminum is made to react at the surface of the substrate, forming a layer

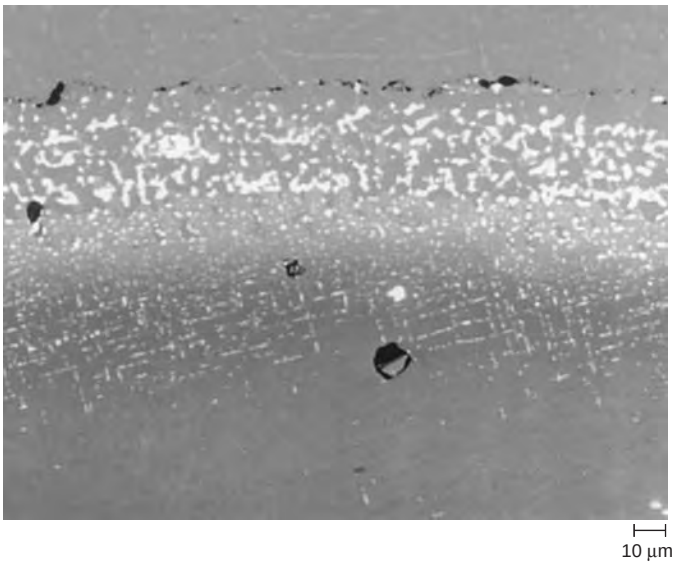


Fig. 1 Microstructure of a platinum-modified aluminide diffusion coating on a single-crystal nickel-base superalloy after engine exposure. The outer layer is depleted NiAl, with particles of Ni_3Al forming at grain boundaries. The inner layer is an interdiffusion zone, enriched in alloying elements due to nickel dilution in forming the outer layer. A modified substrate structure is formed beneath this, with topologically closed-packed chromium-rich phases.

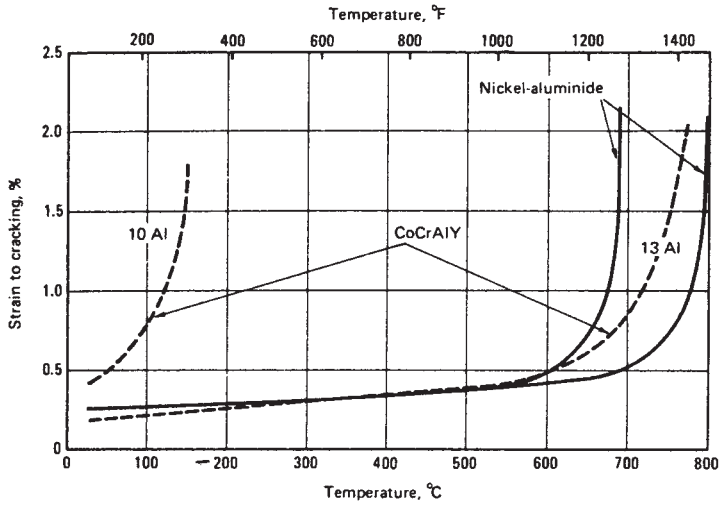


Fig. 2 Ductility of CoCrAlY overlay and diffusion aluminide coatings. CoCrAlY overlay coatings show significant ductility (1–3%) at lower temperature ranges (ambient temperature to 650 °C, or 1200 °F), with ductility continuously increasing as the volume fraction of CoAl is decreased.

of monoaluminide (known generically as MAl). For coatings applied over nickel-base superalloys, nickel aluminide (NiAl) is the resulting species, and over cobalt, it is cobalt aluminide (CoAl). This type of coating is modified to some extent by the elements contained in the substrate as the diffusion reaction proceeds, and usually is further modified by other metallic elements intentionally added during the coating process to improve coating and/or system performance for specific expected service conditions.

The most widespread aluminum modification is platinum. For example, a 20 μm layer of platinum is first electroplated onto the superalloy surface and then aluminized to form a $PtAl_2$-(Ni,Pt)Al two-phase mixture or layered structure. Platinum serves several purposes: it stabilizes an aluminum-rich surface phase for continued Al_2O_3 formation; it improves Al_2O_3 scale adhesion; and it improves the hot corrosion resistance of NiAl. An example of a platinum-aluminide coating on a single-crystal nickel-base superalloy is shown in Fig. 1.

Silicon is especially beneficial in coatings exposed to high concentrations of sulfur in marine environments. Silicon-modified aluminides are resistant to both high-temperature and low-temperature hot corrosion on both nickel and cobalt alloys in marine service. They are also a less expensive alternative to platinum-aluminide coatings.

In addition to the aluminide and modified aluminide diffusion coatings described above, chromide coatings are also used. Chromized coatings provide protection against scale-fluxing attack (hot corrosion) that occurs under a molten sulfate deposit. Such coatings are used on components in the latter stages of the turbine (low-pressure turbine) where the temperatures are reduced to below 900 °C (1650 °F).

Overlay coatings differ from diffusion coatings in that interdiffusion of the coating with the substrate is not required to generate the desired coating structure/composition. Overlay coatings do not rely on reaction with the substrate for their formation. Instead, a prealloyed material applied over the substrate determines the coating composition and microstructure, and adhesion of the coating to the substrate is effected by some elemental interdiffusion.

Coatings of this type in current use are generally called MCrAlY overlay coatings, where M represents Ni, Co, Fe, or some combination of these metals. These coatings essentially comprise a monoaluminide (MAl) component contained in a more ductile matrix of solid solution (γ), in the case of CoCrAlY coatings, or a mixture of γ and γ′Ni_3Al, phase in the case of NiCrAlY coatings. NiCoCrAlY and FeCrAlY modifications are also available.

The matrix is nickel- or cobalt-base and contains a rather large amount of chromium and an intermediate amount of aluminum. Aluminum provides the primary protection against oxidation through the formation of a slow-growing Al_2O_3 scale. The supply of aluminum for formation of protective Al_2O_3 scales comes largely from the dispersed MAl phase during the useful life of such coatings. The contained chromium is important in combatting hot corrosion and also increases the effective aluminum chemical activity. The solid-solution matrix provides ductility in this coating class that is generally not possible with diffusion coatings (Fig. 2), and it imparts much improved resistance to thermal fatigue cracking (Fig. 3). A small amount of yttrium is usually included in overlay coatings to improve the adherence of the oxidation product.

CoCrAlY coatings are recognized as being superior in hot corrosion resistance, whereas NiCrAlY coatings possess the better oxidation resistance. The range of NiCoCrAlY coatings may be tailored for a desired compromise between oxidation and hot corrosion resistance.

The composition of overlay coatings, as well as that of the substrate, affects the extent of coating-substrate interdiffusion during service. Coating composition may also be adjusted to achieve a good thermal expansion fit with a given superalloy substrate. MCrAlY coatings

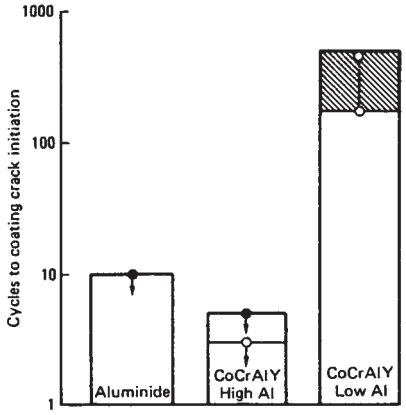


Fig. 3 Thermal mechanical fatigue behavior of brittle (high-aluminum) and ductile (low-aluminum) overlay coatings, compared with aluminide diffusion coating. When thermal strain reaches its maximum value of relatively low temperatures, substantial improvement in thermal fatigue behavior can be achieved with a ductile MCrAlY coating. All specimens were cycled between 425 and 925 °C (800 and 1700 °F). Open circles, ±3% strain; closed circles, ±0.25% strain

may contain 15 to 25% Cr, 10 to 15% Al, and 0.2 to 0.5% Y.

The general features of a MCrAlY coating are an oxide scale on the outer surface, material immediately beneath the scale that has a modified composition depleted in aluminum, a layer of the coating alloy, and an interdiffusion zone in contact with the substrate. The composition and microstructure of the coating alloy depend on post-deposition treatment and service exposure. The interdiffusion zone functions as a bonding layer between coating and underlying alloy substrate. Figure 4 shows the microstructure of a CoCrAlY overlay coating.

Methods of Applying Diffusion Coatings

Diffusion coatings can be applied via pack cementation, out-of-contact chemical vapor deposition (CVD), and slurry-fusion. Electrophoretic techniques have also been used. Of these diffuse coating processes, the pack cementation process is the most commonly employed.

Pack Cementation

A flow path for a typical production-scale pack cementation process is shown in Fig. 5. Practical manufacturing aspects of the various steps of the process are described below.

Inspection. Visual and flow inspection of cooled airfoils before coating affords the last opportunity to determine if all surfaces are suitable for the intended use. Oxidized surfaces and the remains of investment casting core and shell materials can interfere with coating deposition and compromise useful service lives.

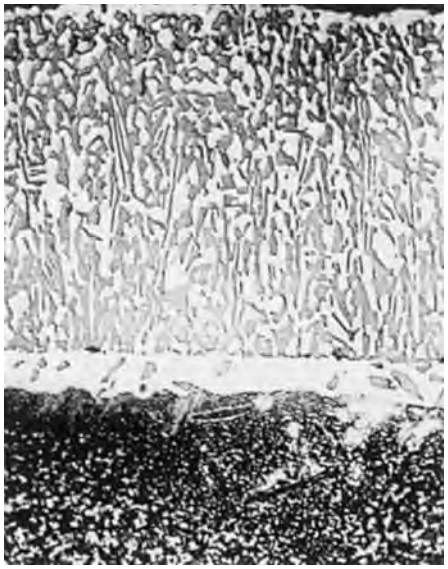


Fig. 4 Microstructure of a two-phase CoCrAlY overlay coating

Surface Preparation. Surface preparation to remove superficial oxides is usually accomplished by grit blasting with intermediate-sized alumina grit. Grit blasting with silicon carbide is avoided because any entrapped grit forms low-melting eutectic phases with superalloys. Vibratory finishing is used where a surface finish is specified to achieve aerodynamic design intent. Removal of oily residues from machining by vapor degreasing or low-temperature burnout may be required.

Masking to prevent coating on critical mechanical contact surfaces, such as blade roots, may be required. This can be accomplished with mechanical, oxide barrier, or chemically reactive masks. Complete exclusion of coating by mechanical masks is difficult for processes with high throwing power, a property common to those run at higher temperatures, for example, >870 °C (>1600 °F). Chemically reactive masks containing elemental or alloy powders that react with the coating species to prevent coating deposition on the surface are more effective at higher processing temperatures. Coating before machining, to obviate expensive masking requirements, is strongly recommended.

Pack Mix (Source) Preparation. Preparation of pack mixes requires the use of large-scale powder handling equipment designed for effective mixing, storage, and dispensing. Examples of mix (source) compositions are given in Table 1. Closed handling systems are now required for health and safety reasons. The possibility of explosive burning of metal powders must be excluded. In general, various chemical engineering technologies are applicable.

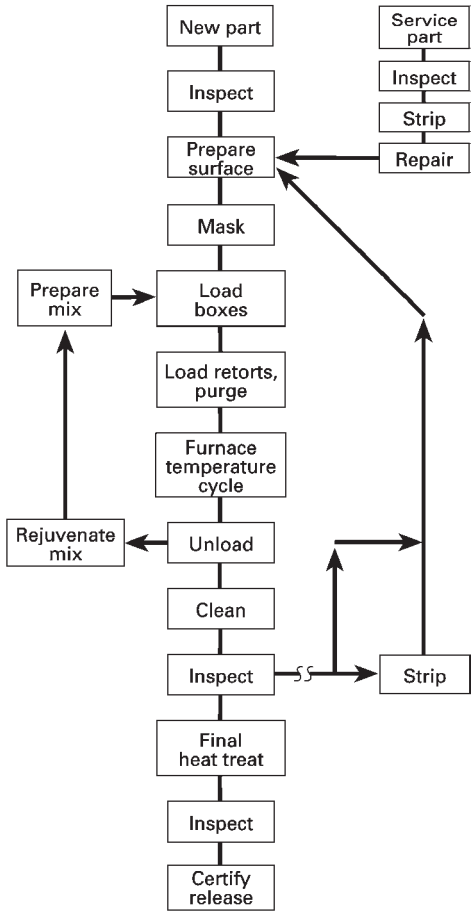


Fig. 5 Flow diagram for typical pack cementation processes

Loading Boxes and Retorts. Loading of parts, which consists of embedding parts in coating powder mixtures in controlled positions in coating boxes ("boats"), is labor intensive and environmentally unfriendly. Automation with robotics is theoretically possible, but no such systems are known to be in use.

Furnace Temperature Cycle and Heat Treatments. Furnaces with specified temperature capability and uniformity and associated inert gas delivery systems are the most costly components of coating plants. For most processes, coating boxes are loaded into retorts constructed of high-temperature alloys, for example, Inconel 600 or 601, and are capable of being sealed (sand, glass, or water-cooled seals) to exclude air. Retorts for gas-fired or electrically fired pit furnaces can be as large as 1.2 m (4.0 ft) in diameter and 2.4 m (8.0 ft) tall. A supply of inert gas, argon, or hydrogen is required to purge retorts free of air and moisture and to maintain an inert environment during the coating cycle.

A coating cycle includes bringing the retort and contents to temperature, holding at temperature for several hours, and then cooling to ambient temperature while maintaining the inert gas environment. Coating temperatures range from 650 °C (1200 °F) for low-temperature inward diffusion aluminizing to as high as 1150 °C (2100 °F) for outward-diffusion aluminizing of nickel superalloys. Processing times range from 4 to 24 h, respectively. Some examples of time-temperature cycles are given in Table 1. Temperature uniformity within the retort load during the holding period is usually required to be within 14 °C (25 °F) of nominal. Off-gases from the process, carried by the inert gas flow, contain environmentally harmful chemicals such as aluminum chloride, hydrogen chloride, aluminum fluoride, hydrogen fluoride, and chromium chloride. These must be captured by scrubbing and filtering before the inert gas is vented to the atmosphere and then disposed of in accord with applicable environmental regulations.

Unloading the retorts and boxes, separating the parts from powders and masking devices, and cleaning the parts, including thorough water washing, are currently labor intensive. Blades and vanes may require further heat treatment to cause proper development of the coating and/or to obtain optimal mechanical properties of the substrate alloy. Such treatments require inert or vacuum environments with the same rigid temperature controls as the coating thermal cycle.

Source Rejuvenation. It is common practice to rejuvenate powder mixes by additions of coating elements and alloys and activators.

Chemical analysis of the used mixes facilitates control of critical constituents. For simple systems historical data can sometimes be applied empirically for these purposes. Disposal of used mixes is quite costly under current environmental regulations. Recovery and recycling of expensive metals is being practiced with increasing frequency.

Quality Control. The most widely accepted quality control practice requires coating of representative samples with each processing cycle and destructively evaluating these to determine accordance with user specifications for thickness (in the range of 25–100 μm, or 1–4 mils for most applications) and microstructure. Quantitative analysis by x-ray fluorescence or electron microprobe for elemental composition, for example, aluminum, chromium, and platinum content, may also be required. Complete coating coverage can be confirmed by contact thermocouple measurement or by heat tinting aluminized nickel alloys in air at 621 °C (1150 °F) for one hour—coated areas exhibit a gold color and uncoated areas a dark blue color. Procedures for nondestructive coating thickness measurements are available, but are not widely used for control of new coating production. There is increasing interest in measuring coating thickness and aluminum content to judge the remaining life of coatings on used parts.

If inspection reveals faulty coatings, parts may be overcoated using appropriate time-temperature cycles. In extreme cases the coatings are stripped in acid solutions, for example, nitric or hydrochloric acid for aluminide coatings, and subjected to another full coating cycle. This is to be avoided because aluminide coatings are formed by consumption of the nickel component of the alloy and removal of the coating can result in significant reduction in critical part dimensions. Increasingly, statistical process control is being used to avoid these problems.

Repair. It is frequently possible to repair blades and vanes that have been in service for some time. To accomplish this, the first coating, now depleted during service, is removed by acid stripping. Parts are then repaired as appropriate, by welding, and/or brazing and remachining. Suitable coatings are then reapplied as shown in Fig 5.

Out-of-Contact Processes and Slurry Aluminization

Out-of-Contact Processes. When aluminizing and/or chromizing are to be accomplished by out-of-contact CVD processes, all preparation steps are as described previously. For simple static aluminizing or chromizing, parts may be surrounded by suitable source material in the form of granules contained in baskets in a variety of coating box designs. A typical example is shown schematically in Fig. 6. Activator chemicals are simply sprinkled into the boxes, which are then covered, placed in retorts, purged with inert gas, and subjected to the usual time-temperature cycles. If coating of blade and vane cooling passages is required, a flow of the inert gas is used to carry the coating species through the passages. Alternatively, pressure can be lowered or cycled to accomplish internal passage coating. For so-called CVD processes, the coating species may be generated by passing reactive gases, based on hydrogen chloride or hydrogen fluoride in a carrier gas over the source material in a separate reactor with the gas stream directed into the main coating chamber to coat external or internal surfaces or both. In any case, all other items shown in Fig. 5 still apply.

Slurry Aluminization. An alternative to the CVD processes described previously is the slurry aluminization coating process. The slurry consists of an aluminum powder in an acidic water-base solution of chromates and phosphates. The slurry is applied by brush or conventional spray methods. Melting and subsequent diffusion of the aluminum slurry onto the substrate surface to form an aluminide coating occurs at temperatures above 870 °C (1600 °F).

Another slurry aluminization method utilizes a modified aluminum-silicon slurry. This slurry has been used for more than 30 years to repair imperfections and touch up parts coated with pack aluminides and MCrAlY coatings. The application and diffusion cycles for the aluminum-silicon slurry are similar to those used for the slurry containing aluminum only. Since the aluminization proceeds from a liquid state, transport of silicon to the surface of the part occurs simultaneously with the aluminization process. The slurry, which contains about 12% Si, produces a 50 to 75 μm thick diffused aluminide coating that contains about 10% Si. Pack cementation alloy powder mixes containing an equal amount of silicon produce a NiAl layer containing less than 1% Si. As mentioned previously, silicon-modified aluminide coatings are highly resistant to high- and low-temperature hot corrosion (Ref 4, 5).

Properties of Diffusion Coatings

Coating Formation Mechanisms. Diffusion aluminide coatings on superalloys are classified by microstructure as being of the "inward diffusion" or "outward diffusion" type. The classification of diffusion coatings is derived from the work of Goward and Boone (Ref 6), who studied aluminide coating formation on Udimet 700 (a typical nickel-base superalloy having a nominal chemical composition of Ni-15Cr-17Co-5Mo-4Al-3.5Ti). They observed that for pack mixes containing aluminum (unit or "high" activity), coatings were formed by predominant inward diffusion of aluminum through Ni_2Al_3, and deeper in the coating, through aluminum-rich NiAl (for pure nickel, by inward diffusion through Ni_2Al_3 only). The diffusion rates are abnormally high: practical coating thicknesses could be achieved in a few hours at 760 °C (1400 °F).

A typical as-coated microstructure is shown in Fig. 7(a). Upon further heat treatment at, for example, 1080 °C (1975 °F) for 4 h, the microstructure shown in Fig. 7(b) is formed. The coating matrix is now NiAl. The single-phase region in the center of the coating is nickel-rich NiAl, grown by predominant outward diffusion of nickel from the substrate alloy to react with aluminum from the top layer. The inner layer, or so-called interdiffusion

Table 1 Examples of pack mixes/sources and processing parameters for various coatings on nickel and cobalt superalloys

Coating type	Source composition	Processing parameters
Pack aluminizing, inward diffusion in Ni_2Al_3 in nickel alloys	5–20% Al (Al-10Si), 0.5–3% NH_4Cl, balance Al_2O_3 powder	1–4 h at 650–680 °C (1200–1255 °F) in air, argon, H_2; heat treat 4–6 h at 1095 °C (2000 °F) in argon
Pack aluminizing, inward diffusion in NiAl in nickel alloys	44% Al, 56% $CrNH_4Cl$, balance Al_2O_3 powder	5–10 h at 1040 °C (1900 °F) in vacuum (argon, H_2)
Pack aluminizing, outward diffusion in NiAl in nickel alloys	2–3% Al, 20% Cr, 0.25% NH_4HF_2, balance Al_2O_3 powder	25 h at 1040 °C (1900 °F) in argon
Pack aluminizing of cobalt alloys	8% Al, 22% Cr, 1% NH_4F, balance Al_2O_3 powder	4–20 h at 980–1150 °C (1800–2100 °F) in argon
Gas-phase aluminizing, outward diffusion in NiAl in nickel alloys	10% Co_2Al_5, 2.5% NaCl, 2.5% $AlCl_3$, balance Al_2O_3 powder	3 h at 1095 °C (2000 °F) in argon
Gas-phase aluminizing, outward diffusion in NiAl in nickel alloys	30% Al-70% Cr alloy granules, NH_4F	4 h at 1150 °C (2100 °F) in argon
Pack or gas-phase chromizing of nickel alloys	15% Cr, 4% Ni, 1% Al, 10.25% NH_4Br or NH_4Cl, balance Al_2O_3 powder	3 h at 1040 °C (1900 °F) in argon

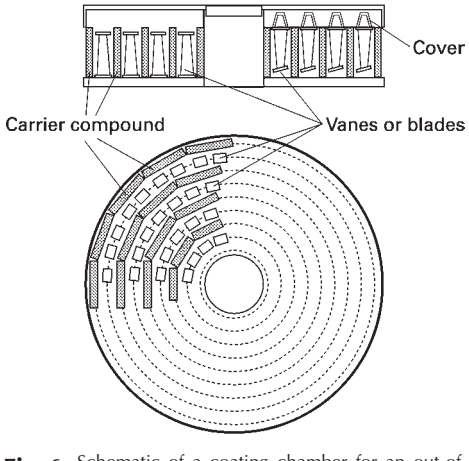


Fig. 6 Schematic of a coating chamber for an out-of-contact CVD aluminizing process

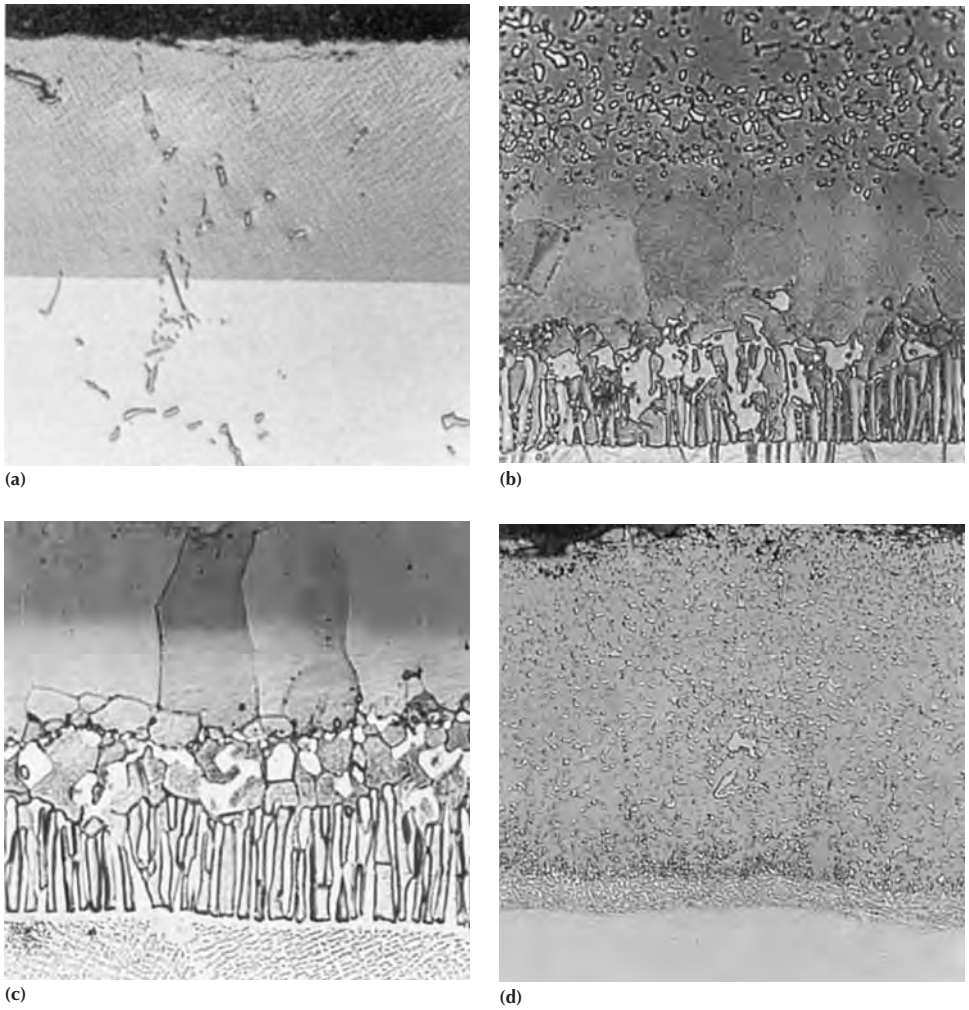


Fig. 7 Typical microstructures of aluminide coatings on a nickel-base superalloy. (a) Inward diffusion based on Ni_2Al_3 (and aluminum-rich NiAl). (b) Same as (a) but heat treated at 1080 °C (1975 °F). (c) Outward diffusion of nickel in nickel-rich NiAl. (d) Inward diffusion of aluminum in aluminum-rich NiAl

zone, consists of refractory metal (tungsten, molybdenum, tantalum, etc.) carbides, and/or complex intermetallic phases in a NiAl and/or Ni_3Al matrix, formed by the removal of nickel from the underlying alloy, thereby converting its Ni-Ni_3Al structure to those phases.

Conversely, if the activity of aluminum in the source is reduced by alloying with, for example, nickel or chromium, to a level where nickel-rich NiAl is formed at the surface, the coating grows by predominant outward diffusion of nickel from the substrate to form NiAl by reaction with aluminum from the source (Fig. 7c). The lower layer of this coating is formed as previously described. Diffusion rates are relatively low, so the coating process must be carried out at higher temperatures, usually greater than 1000 °C (1830 °F). At the high-aluminum limit of NiAl, diffusion is by predominant motion of aluminum. Figure 7(d) shows a coating with a matrix of NiAl formed by this diffusion mechanism. Upon further heat treatment, this coating will stabilize with a structure similar to that shown in Fig. 7(b).

The above coating formation mechanisms apply equally to those coatings formed by out-of-contact CVD processes, slurry fusion, or electrophoresis. Coatings applies by spraying or electrophoretically deposited (e.g., silicon-modified aluminides), and then heat treated, form by dissolution of the superalloy into the melt until the melt solidifies, followed by diffusion of aluminum similar to that described previously.

Figure 8 illustrates diffusion chromide coatings formed on a nickel superalloy by pack cementation and out-of-contact processes. The coating deposited by pack cementation is overlaid with a thin layer of α-chromium, as shown in Fig. 8(a). Users generally require that this phase be absent. It must then be removed chemically, or alternatively, the coating must be applied by an out-of-contact process to produce the structure shown in Fig. 8(b). These coatings usually then contain 20 to 25% Cr at the outer surface. Coating formation, from chromium-alumina-activator packs (usually ammonium chloride) or from out-of-contact sources (powders or chromium granules), involves approximately equal rates of interdiffusion of chromium and nickel. Significant depletion of titanium and aluminum from the alloy surface occurs because the sources do not contain these elements. The desired coatings are thus solid solutions of chromium in the remaining nickel-base alloy. Internal oxides of aluminum and titanium can form because the oxygen potential of the sources is normally sufficient to cause internal oxidation. This can be avoided by adding aluminum to the sources in amounts just below that which would cause aluminizing rather than chromizing.

Coating Protection and Degradation. Simple aluminide coatings resist high-temperature oxidation by the formation of protective layers of alumina and can be used up to about 1150 °C (2100 °F). The coatings degrade by loss of aluminum due to spalling of oxides under thermal cycling conditions. Incorporation of reactive elements, such as yttrium and hafnium, by codeposition during aluminizing can significantly improve adherence of the protective alumina scales and therefore extend coating life. At temperatures above about 1000 °C (1830 °F) interdiffusion of the coatings with substrates contribute significantly to degrada-

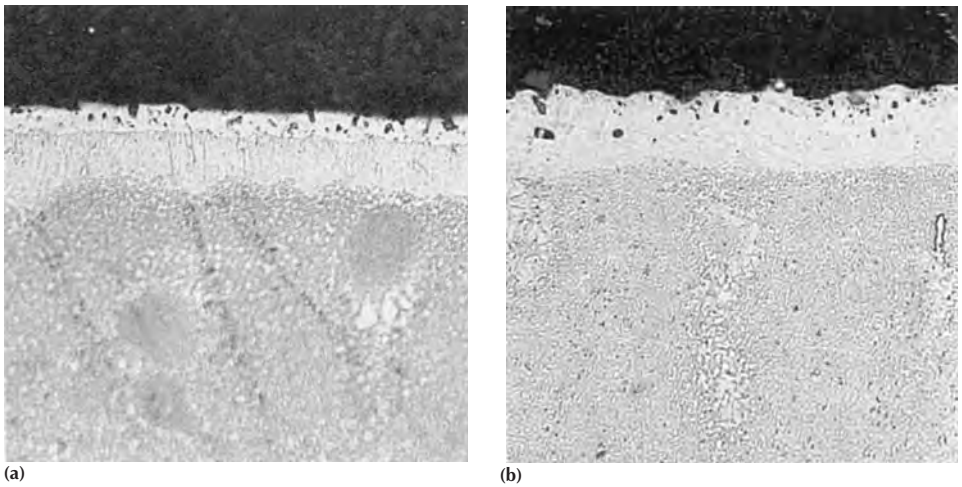


Fig. 8 Chromium diffusion coatings on a nickel superalloy by (a) pack cementation and (b) out-of-contact gas-phase processing. Both at 500×

tion. Practical coating service lives are limited to operating temperatures of 870 to 980 °C (1600–1800 °F) with only short excursions at the highest temperatures.

Chromium modifications, made by diffusion chromizing prior to aluminizing or by codeposition of aluminum and chromium have enhanced resistance to various forms of molten-salt hot corrosion. Electroplating with a thin layer of platinum followed by aluminizing forms a coating with substantially improved resistance to both oxidation and high-temperature (type I) molten-salt corrosion. Additions of up to about 12% Si improve both oxidation and hot corrosion resistance.

The oxidation and hot corrosion resistance of these coatings are more or less influenced by the composition of substrate alloys. Tantalum and hafnium improve cyclic oxidation and hot corrosion resistance, the latter element by improving the adherence of the protective layer of alumina. Molybdenum and tungsten compromise hot corrosion resistance.

Because of the brittle fracture behavior of NiAl up to temperatures of 650 to 775 °C (1200–1400 °F), all aluminide coatings exhibit such fracture below these temperatures, while above these limits ductile behavior occurs. This behavior can either compromise or enhance thermal fatigue resistance of substrate alloys depending on such complex factors as the exact nature of the thermal cycle and the structure—equiaxed, directionally solidified, or single crystal—of the alloys. If these effects are limiting, designers may require use of more expensive overlay coatings and/or thermal barrier (zirconia) types.

Practical Applications of Diffusion Coatings

For aircraft gas turbine blades fabricated from moderately corrosion resistant nickel alloys (those containing 12–15% Cr), simple aluminide coatings of the inward and outward diffusion types provide adequate protection for many contemporary engines. Figure 9 shows the protection afforded a 12% Cr superalloy via a NiAl diffusion coating. When alloys are more corrosion prone (those containing 7–10% Cr), current practice is to modify aluminide coatings by chromizing prior to aluminizing. Aluminizing should be by inward diffusion of aluminum to locate the higher chromium concentration in the outer layer of the coating. For more severe type I hot corrosion resulting from exposure of engines to salt spray from marine environments, modification of aluminide coatings with silicon (or better, by platinum) can prove to be more cost effective.

If more expensive structural modifications of nickel superalloys, such as single crystals, are used to full strength-temperature capabilities to enhance fuel efficiency, contemporary diffusion coatings may not meet design objectives for oxidation and/or thermal fatigue service lives of the turbine. For these conditions use of the more expensive MCrAlY overlay and/or ceramic (zirconia-based) thermal barrier coatings may be in order.

Ground-Based and Marine Gas Turbines. Achieving cost-effective hot corrosion protection for ground- or marine-based gas turbines is a more complex problem because of wide variations in local environments with respect to air contaminants (salts, sulfur oxides, and other industrial pollutants) and fuel constituents (salts, sulfur, vanadium, etc.). Chromizing is effective in ground-based engines subjected to severe type II hot corrosion at the metal temperature of about 740 °C (1365 °F)—this in comparison to silicide, platinum-aluminide, and some MCrAlY type coatings. Chromide coatings are, however, not satisfactory above 800 °C (1470 °F). Platinum aluminides provide moderate protection at somewhat higher temperatures but may not be sufficiently resistant to lower-temperature type II hot corrosion. Similar considerations appear to apply for marine environments.

The trend for most ground-based gas turbines is toward the use of various modifications of MCrAlY type coatings, particularly those

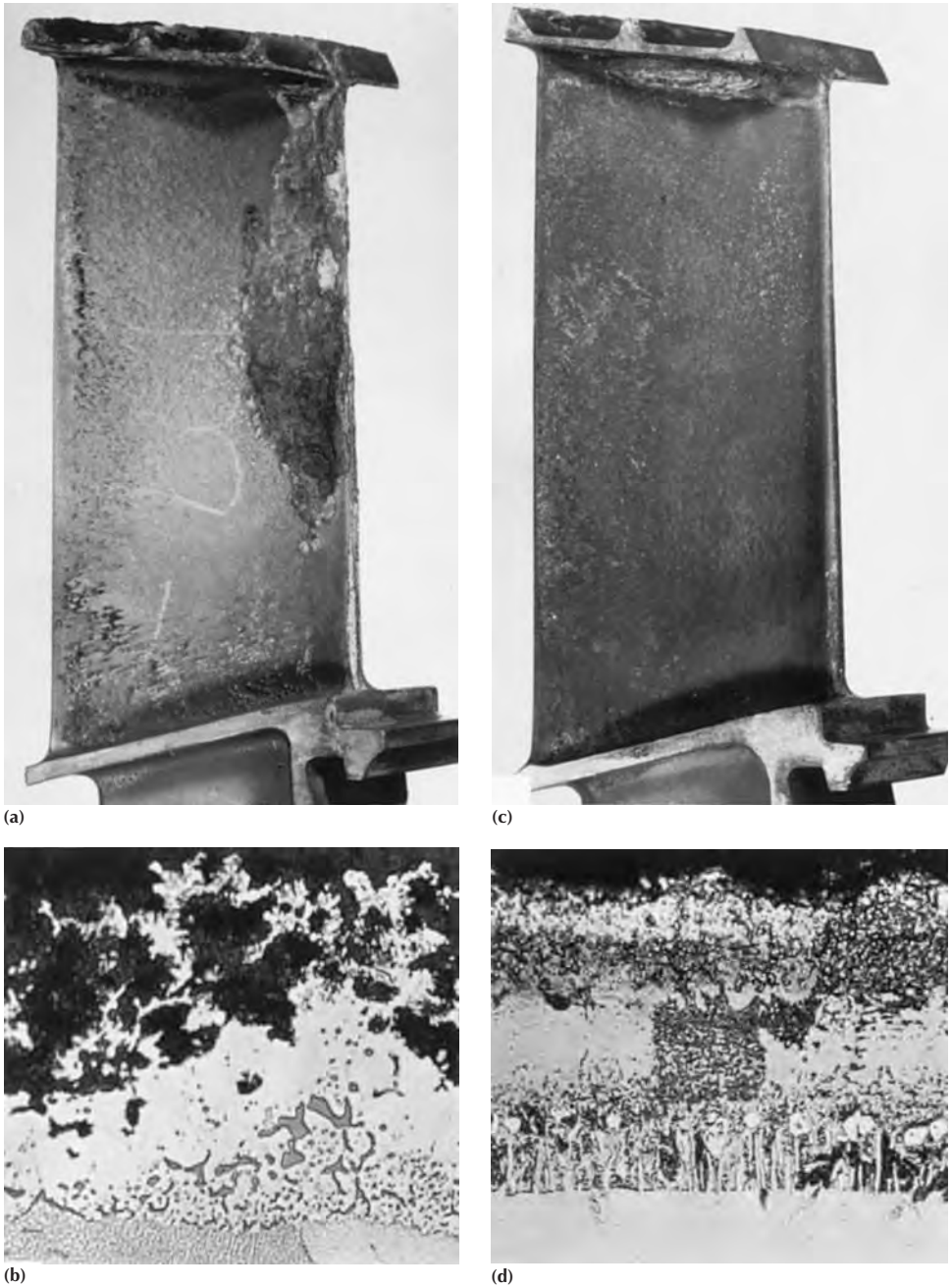


Fig. 9 Effect of an aluminide-type (nickel-aluminum) coating on the hot corrosion resistance of an IN-713 turbine blade compared with that of an uncoated blade. (a) Uncoated turbine blade after 118 programmed cycles. 1.8×. (b) Severe degradation of the uncoated blade by hot corrosion. Etched with ferric chloride. 450×. (c) Aluminide-coated blade after accelerated hot corrosion testing in an engine. 1.8×. (d) Slight degradation of the aluminide coating. Etched with ferric chloride. 450×

with higher chromium and perhaps silicon additions. For the very latest machines operating at the higher temperatures for improved fuel efficiency, these coatings may be overaluminized and internal cooling passages simultaneously aluminized to resist increasingly severe oxidation conditions.

Methods of Applying Overlay Coatings

Overlay coating processes of primary importance today are electron-beam physical vapor deposition (EB-PVD) and plasma spraying. While CVD can be used, it is not practical from a cost standpoint because of very low deposition rates and the difficulty in controlling complex coating compositions. The EB-PVD technique generally produces higher-quality coatings, while plasma spraying has an equipment-cost advantage.

Electron-beam physical vapor deposition emerged in the 1960s as the primary overlay coating production method. The process allows the deposition of metals via vapor transport in a vacuum without the need for a chemical reaction. The vapor source can be produced by several methods, but EB evaporation is the most commonly used technique for coating turbine components.

A cloud of metal atoms impinges on the preheated part surface and condenses out into equilibrium or metastable phases. Carrying out the process at elevated temperatures promotes the formation of a dense coating and coating adhesion.

The process results in an as-deposited coating structure that is typically oriented perpendicular to the substrate surface (columnar structure). This is caused by fast-growing grains of the coating alloy that propagate through the coating thickness. Separations between adjacent grains of the deposited coating, known as "leader defects," or columnar voids, often are present, especially on convex surfaces. Shot peening and laser glazing can be used to close these defects to prevent premature corrosive attack and thermal fatigue cracking. The microstructure of an EB-PVD coating can be altered by varying the substrate temperature and by bombarding the substrate with energetic particles, such as plasma or ion beam, that can break up the columnar structure and improve coating density.

The composition and microstructure of the deposited film are the two major factors that determine its corrosion resistance. The typical composition of a MCrAlY film is 20% Cr, 10% Al, and 0.3% Y, with the balance M (Fe, Co, or Co-Ni). Acceptable composition tolerances depend on the specified nominal composition. The compositions of films obtained in practice usually fall within acceptable tolerance ranges. For example, the chromium, aluminum, and yttrium contents of a NiCoCrAlY deposit typically are 80%, 60%, and 60%, respectively, of the acceptable tolerance ranges. Similarly, the cobalt, chromium, aluminum, and yttrium contents of a CoCrAlY deposit are 60%, 45%, 60%, and 60%, respectively. Stated another way, if the chromium range specified for a NiCoCrAlY deposit is 16 to 22%, the range for a production coating will be approximately 16.5 to 21.5%.

Plasma sprayed coatings are produced by injecting a prealloyed powder into a high-temperature plasma gas stream (via a plasma spray gun) and depositing the melted particles on the substrate surface. The molten particles solidity on contact, forming the coating. The process generally is carried out in a low-pressure vacuum chamber (hence the term low-pressure plasma spraying, LPPS), which minimizes the formation of oxide defects within the as-deposited coating.

The high velocity at which the molten metal particles are directed at the substrate causes the molten droplets to "splat" against the substrate and spread out in a direction parallel to the surface. A typical as-coated microstructure contains splat interfaces parallel to the surface. A diffusion heat treatment eliminates the individual splat layers, and the resulting structure assumes a two-phase nature similar to that of an EB-PVD coating.

The surface finish of a plasma sprayed coating generally is rougher than that of an EB-PVD coating. A finishing operation, such as abrasive slurry or controlled vapor blasting, can be used to achieve the required smooth surface.

Thermal Barrier Coatings

The hot corrosion (and oxidation) resistance of coated blades can be further improved by applying a layer of thermal insulation. This TBC must be sufficiently thick, have a low thermal conductivity and high thermal shock resistance, and have a high concentration of internal voids to further reduce thermal conductivity to a value well below that of the bulk material. The temperature difference between the outer surface of a TBC and the outer surface of the underlying corrosion resistant film can be as high as 150 °C (270 °F). In addition to reducing the temperature at the surface of the superalloy, these coatings also reduce thermal shock loads on the blades: rapid changes in ambient temperature are moderated and attenuated before they reach the substrate.

A TBC system consists of an insulating ceramic outer layer (top coat) and a metallic inner layer (bond coat) between the ceramic and the substrate. Both the top coat and bond coat can be applied by plasma spraying (air and low pressure) and EB-PVD. A schematic of a typical system is shown in Fig. 10. Current state-of-the-art TBCs are zirconium oxide (ZrO_2), or zirconia, with 6 to 8% (by weight) of yttrium oxide (Y_2O_3), or yttria, to partially stabilize the tetragonal phase for good strength, fracture toughness, and resistance to thermal cycling. The coatings are relatively inert, have a high melting point, and have low thermal conductivity.

Air plasma sprayed coatings contain porosity and microcracks that help to redistribute thermal stresses but also provide corrosion paths through the coating. Low-pressure plasma spray coatings provide high coating purity and essentially eliminate oxides and porosity. EB-PVD coatings have a columnar grain morphology (Fig. 11, 12) in which individual grains are strongly bonded at their base, but have a weak bond between grains. The major advantage of this columnar outer structure lies in the fact that it reduces stress buildup within the body of the coating. Strain within the coating is accommodated by free expansion (or contraction) of the columns into the gaps, which results in negligible stress buildup. The columnar structure of EB-PVD zirconia TBCs has the disadvantage, however, of increasing heat conductivity by a factor of about 2 as compared to plasma sprayed TBCs.

Figure 11 also shows that a thin, dense ZrO_2 layer occurs between the bond coat surface and the upper columnar zirconia structure. This phase grows under oxygen-deficient conditions just at the beginning of zirconia deposition, and its thickness is controlled by how quickly the oxygen bleed is activated in the vacuum chamber of the EB-PVD apparatus after zirconia coating commences. This dense, interfacial ZrO_2 film is critical to the life of the EB-PVD coating in that it provides for chemical bonding between the columnar zirconia and the oxidation resistant bond coat. If, however, this interfacial film becomes too thick (>2 μm), it may sustain and transmit compressive stresses sufficient to cause cracking within the outer zirconia coating.

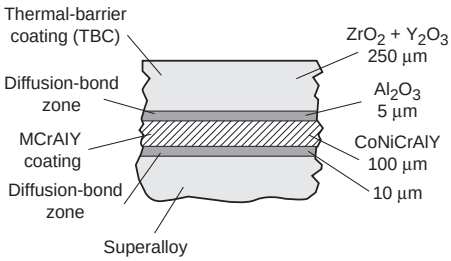


Fig. 10 Schematic of a multilayer TBC system produced using a combination of EB-PVD and plasma spray techniques

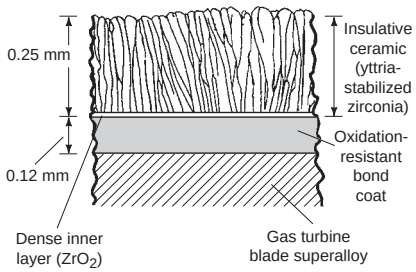


Fig. 11 Cross section illustrating the strain-tolerant columnar ZrO_2 microstructure of EB-PVD zirconia TBCs. Source: Ref 7

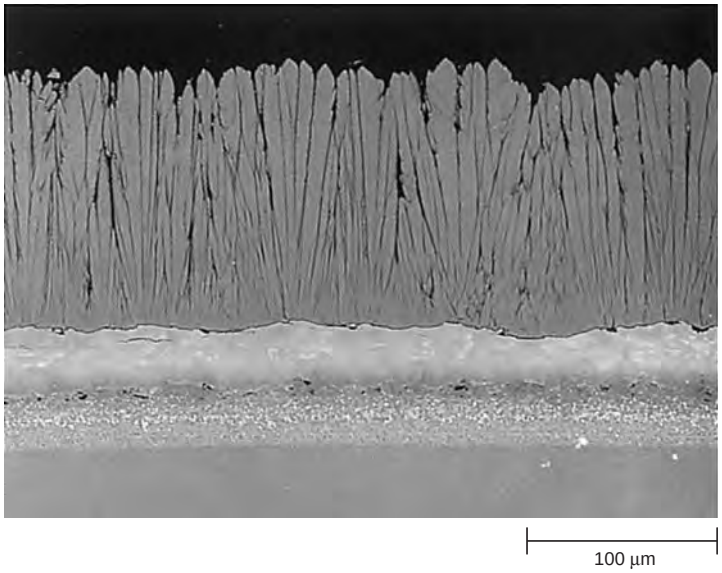


Fig. 12 Columnar structure of an EB-PVD 7% yttria-zirconia TBC on a platinum-aluminide-coated single-crystal superalloy. 250×

The metallic (MCrAlY) bond coat aids in the adhesion of the ceramic topcoat, protects the substrate from hot corrosion and oxidation, and helps in handling expansion mismatch between the ceramic and superalloy. For best adhesion of EB-PVD TBCs, the bond coat surface should be smooth, or preferably polished, in contrast to plasma sprayed TBCs, which require a rough bond coat.

High-pressure/high-velocity oxygen fuel (HP/HVOF) spraying also is being evaluated to produce MCrAlY coatings, which could be used as bond coats for TBCs in aircraft turbine applications.

Coating Performance

The ability of a coating to provide satisfactory performance in high-temperature applications is measured by whether it can remain intact, resist oxidation and corrosion, and avoid cracking. Generally, diffusion aluminide coatings are limited by their oxidation behavior, overlay coatings are limited by their susceptibility to thermal fatigue cracking in cyclic conditions, and TBCs are limited by the thermal expansion mismatch between the ceramic and metallic layers and by environmental attack of the bond coat.

Coating Ductility

Coatings must be capable of tolerating strain due to thermal expansion mismatch and mechanical loads in order to retain coating-substrate integrity. The ductile-to-brittle transition temperature (DBTT) is used to describe the ability of a coating to tolerate strain. Above the DBTT, the coating behaves in a ductile manner; below the DBTT the coating is brittle. The DBTT is affected by several factors, including coating composition, coating application process, coating thickness, surface finish, and strain rate. The DBTT should be as low as possible so that cracking in the coating does not occur in service, since the cracks may then propagate into the substrate.

MCrAlY overlay coatings generally have a lower DBTT than diffusion coatings because their chemical composition can be controlled. The DBTT of aluminide diffusion coatings is a function of aluminum content, increasing with increasing aluminum. Platinum additions also raise the DBTT of aluminide coatings. Figure 13 shows the DBTT of aluminide and overlay coatings.

For overlay coatings, NiCrAlY coatings have a higher DBTT than CoCrAlY coatings (due to a lower DBTT of NiAl). The DBTT of both coatings is increased with increasing chromium and/or aluminum content. NiCoCrAlY coatings containing 20 to 26% Co are significantly more ductile than either NiCrAlY or CoCrAlY coatings.

Ductility of aluminide diffusion coatings can sometimes be enhanced by laser remelting of the coating. A thin surface layer of the coating is melted and rapidly quenched by the cold bulk solid substrate, which refines the grain size.

Oxidation

Aluminide coatings degrade in service through cyclic oxidation, hot corrosion, erosion, interdiffusion, and thermomechanical fatigue cracking. Aluminum in the coating combines with oxygen at the substrate surface, forming a protective Al_2O_3 scale. When the scale cracks and spalls from thermal cycling, additional aluminum from the coating diffuses to the surface to reform the scale. Aluminum from the coating also diffuses into the substrate, and as aluminum is depleted in the coating, βNiAl converts to $\gamma' Ni_3Al$ and then to γNi solid solution. When the aluminum content in the coating drops to about 4 to 5 wt%, the Al_2O_3 scale can no longer form and rapid oxidation occurs. The rate of aluminum diffusion is influenced by substrate composition.

If the coating undergoes thermal fatigue cracking, refractory elements in the diffusion zone may be exposed to the oxidizing environment and oxidize rapidly. This effect must be considered when selecting a coating for use in cyclic conditions.

Incipient melting in the diffusion zone also can result in rapid oxidation penetration. Such melting can occur at temperatures as low as 1120 °C (2050 °F), well below the melting point of NiAl (1590 °C, or 2900 °F).

It is well established that platinum in diffusion aluminides extends the lives of such coatings in oxidizing environments (Fig. 14, 15). The mechanism by which platinum affects coating service lives is not completely understood. It may improve Al_2O_3 adherence, causing an Al_2O_3 scale to develop with slower transport properties due to higher purity, and it may inhibit interdiffusion between the coating and the substrate (Ref 10). Other precious elements such as rhodium produce similar effects, and more recent results show that palladium may also produce beneficial effects (Ref 10).

Enhanced oxidation resistance may also be possible through the use of ion implantation. The addition of yttrium or hafnium by this technique improves coating adherence and reduces scale growth rate.

Overlay Coatings. The oxidation pattern of MCrAlY overlay coatings is similar to that of diffusion aluminide coatings. Elements such as chromium and yttrium improve the resistance of the Al_2O_3 scale to spallation. The most widely used overlay coating for oxidation resistance is the NiCoCrAlY type. Figure 15 compares the oxidation resistance of a single-crys-

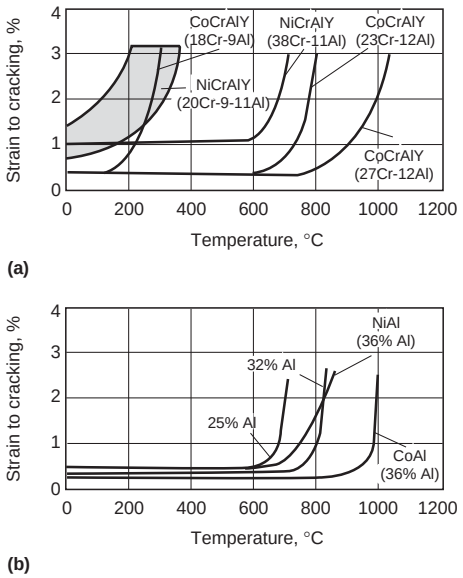


Fig. 13 Ductility/temperature characteristics of (a) MCrAlY coatings and (b) aluminide diffusion coatings

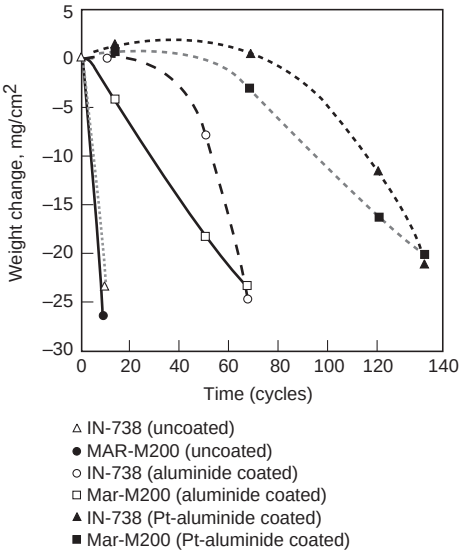


Fig. 14 Cyclic oxidation data at 1200 °C (2190 °F) for uncoated superalloys and for superalloy-diffusion coated with aluminides and aluminides containing platinum (Pt). Source: Ref 8

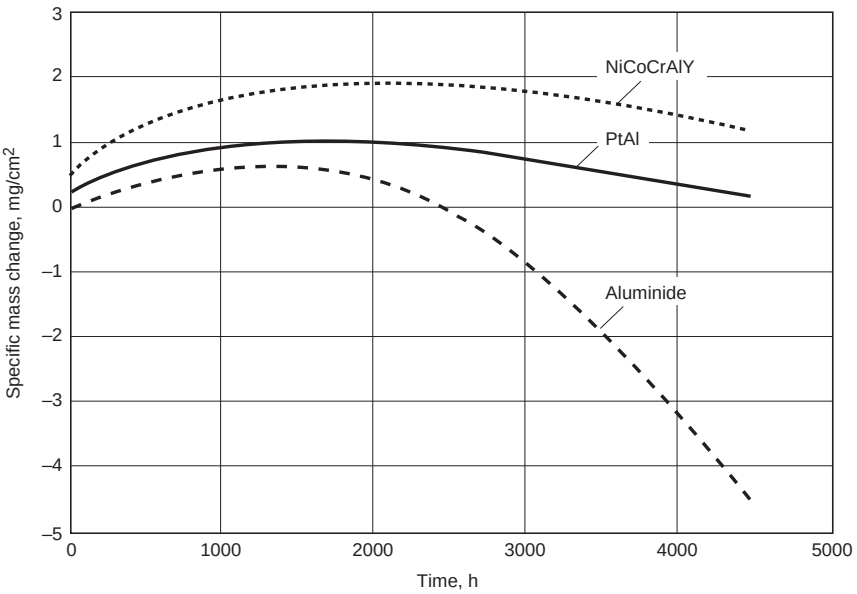


Fig. 15 Dynamic cyclic oxidation, 1040 °C (1900 °F), test results of coated CMSX-4. Source: Ref 9

tal nickel-base superalloy coated by NiAl, PtAl, and NiCoCrAlY.

In the oxidation process, grains of aluminum-rich β phase convert to islands of γ′, eventually leaving only the less oxidation resistant γ matrix phase. Substrate composition can influence oxidation resistance.

MCrAlY overlay coatings have a higher melting point than diffusion coatings, so melting does not occur in the interdiffusion zone at temperatures lower than the melting point of the bulk coating. Coatings have survived exposure temperatures as high as 1290 °C (2350 °F) without melting.

The addition of elements such as silicon, tantalum, and hafnium can improve oxidation resistance at the expense of some ductility. Compositional flexibility offers the opportunity to tailor coatings for optimum performance. Figure 16 shows how silicon and hafnium can improve coating performance.

High-Temperature Hot Corrosion

High-temperature hot corrosion resistance is required more in marine and industrial turbine applications than in aircraft applications. Coatings are used to prevent catastrophic failure of components in conditions involving dirty fuels or contaminants in the atmosphere. Figure 17 compares the resistance to high-temperature hot corrosion of diffusion and overlay coatings.

Diffusion Coatings. Conventional coatings have unsatisfactory performance in high-temperature hot corrosion applications. Platinum-aluminide coatings offer improved hot corrosion resistance by increasing aluminum activity at the surface and by enhancing scale adherence and the rate of scale formation (Fig. 17). Degradation of platinum coatings results when the aluminum is depleted to a point where a protective scale cannot form. Molten alkali metal salts speed up the destruction of the scale, which accelerates aluminum consumption.

As aluminum is consumed, the βNiAl matrix phase is transformed to γ′, which ends effective corrosion protection. In the advanced stages of attack, chromium-rich internal sulfides form in the substrate and in the substrate/coating interdiffusion zone.

Overlay coatings have very good resistance to high-temperature hot corrosion. The best in this regard are cobalt-base coatings having high chromium-aluminum ratios. As indicated in Fig. 17, NiCoCrAlY coatings also offer superior resistance to hot corrosion. Nickel- and iron-base coatings offer good oxidation resistance and

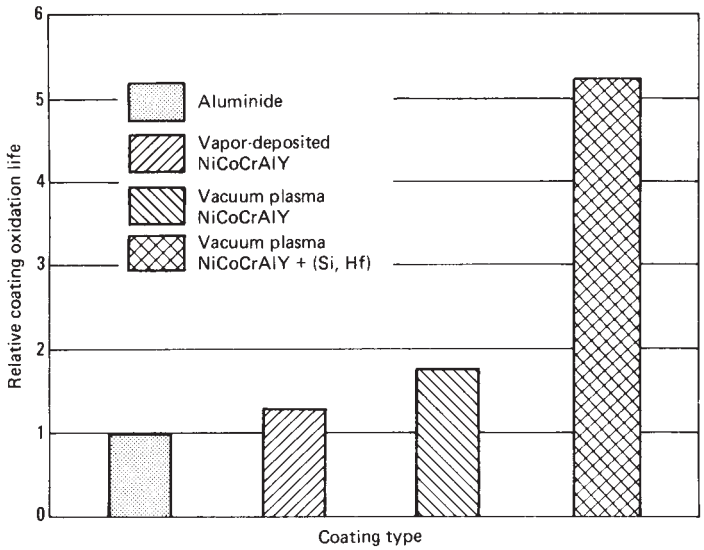


Fig. 16 Coating performance of PWA 1480 at 1149 °C (2100 °F). Burner rig oxidation test. Source: Ref 10

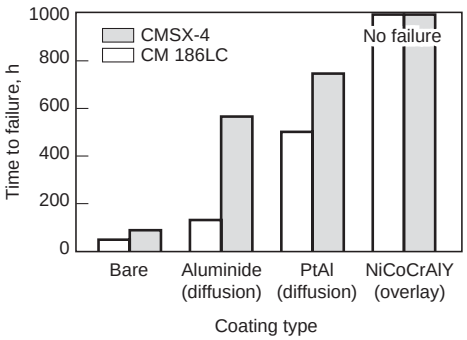


Fig. 17 Hot corrosion resistance of uncoated and coated CMSX-4 (nickel-base single-crystal superalloy) and CM186LC (nickel-base directionally solidified superalloy) test specimens. The accelerated hot corrosion tests were carried out at 900 °C (1650 °F) in fuel containing 1% S and 10 ppm salt. The diffusion coatings were applied by a proprietary electrophoresis process. The NiCoCrAlY coating was applied by EB-PVD. Source: Ref 11

good resistance to mild hot corrosion environments. Increasing the Cr-Al ratio in cobalt-base coatings increases hot corrosion resistance at the expense of some oxidation resistance.

MCrAlY coating degradation is characterized by the presence of sulfides and oxides in the coating; chromium-rich sulfides precede oxides. However, coating failure occurs due to aluminum and chromium depletion, which are needed to form the protective scale. Thicker coatings can provide the required protection in applications where thermal cycling is not severe.

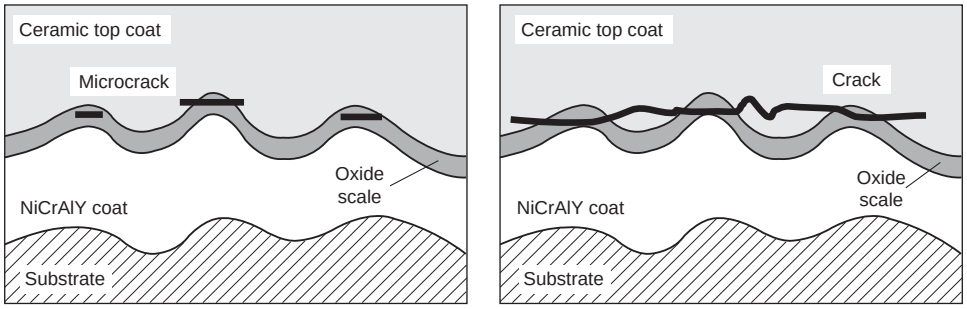


Fig. 18 Failure mechanism in a TBC. Microcracks develop in the aluminum oxide scale on the bond coat (a) and propagate along the lamellar interfaces, leading to spalling of the ceramic TBC or complete delamination (b).

Low-Temperature Hot Corrosion

Coatings developed to resist oxidation and high-temperature hot corrosion generally are ineffective against low-temperature hot corrosion (i.e., 680–750 °C, or 1255–1380 °F). Instead, Cr_2O_3 and silica (SiO_2) scales offer the best protection.

Diffusion Coatings. Chromide diffusion coatings rapidly form a continuous, adherent Cr_2O_3 scale for protection. Because interdiffusion is small in lower-temperature environments, chromide coatings are relatively thin (0.04–0.05 mm, or 1.5–2.0 mils). The thinner coating is more favorable with respect to mechanical properties because chromium compositions are prone to cracking due to lower ductility.

Overlay Coatings. High CrCo-, nickel-, and iron-base coatings are effective against low-temperature hot corrosion. Cobalt-base coatings with high chromium content are preferred because the operating temperature range in many turbine air-foil applications necessitates protection against both oxidation and corrosion.

Performance of Thermal Barrier Coatings

As discussed previously, TBCs generally consist of a metallic bond coating (typically MCrAlY applied by vacuum plasma spraying or PVD) and a thick ceramic top coat (typically stabilized ZrO_2 deposited by low-pressure plasma spray or EB evaporation). Despite their columnar microstructure, thin PVD coatings can be dense and serve as a diffusion gas barrier at high temperatures, and the columnar structure guarantees an improved strain and stress tolerance. Thermal stress within the coatings occurs due to a mismatch between the thermal expansion coefficients of the metallic substrate and the coating, and due to transient thermal gradients during rapid thermal cycling. Depending on deposition conditions, the PVD technique may also induce some stress within the coating. This intrinsic compressive stress of the sputtered bond coating may act as a "prestress" that diminishes coating failure due to tensile thermal stresses at elevated temperatures.

The plasma spraying process also induces some residual stress, due to substrate heating and deposition of a stress-free coating at the deposition temperature. Thermal residual stress develops during cooling to room temperature.

Failure of TBCs in service generally is attributed to stress that develops during cooling after high-temperature exposure and to transient thermal stress that develops during rapid thermal cycling. Failure occurs primarily due to thermal expansion mismatch between the ceramic and metallic layers and environmental attack of the bond coat.

The stress state in the ceramic layer is biaxial compressive in the plane of the coating. Strains induced by these stresses increase during repeated thermal cycling, which results in crack initiation and eventual spalling of the coating, as shown in Fig. 18. The use of Y_2O_3 to stabilize the ceramic coat, together with an MCrAlY-type bond coat, significantly improves the thermal fatigue resistance of TBCs.

ACKNOWLEDGMENT

This article was adapted from:

- Protective Coatings for Superalloys, *ASM Specialty Handbook: Heat-Resistant Materials*, J.R. Davis, Ed., ASM International, 1997, p 335–344
- G.W. Goward and L.L. Seigle, Diffusion Coatings for Gas Turbine Engine Hot Section Parts, *Surface Engineering*, Vol 5, *ASM Handbook*, ASM International, 1994, p 611–617

REFERENCES

1. F.S. Pettit and C.S. Giggins, *Superalloys II*, C.T. Sims, N.S. Stoloff, and W.C. Hagel, Ed., John Wiley & Sons, 1987, p 327
2. K.T. Chiang, F.S. Pettit, and G.H. Meier, *High Temperature Corrosion*, R.A. Rapp, Ed., NACE International, 1983, p 519
3. J.L. Smialek, C.A. Barrett, and J.C. Schaeffer, Design for Oxidation Resistance, *Materials Selection and Design*, Vol 20, *ASM Handbook*, ASM International, 1997, p 589–602
4. T.A. Kircher, B.G. McMordie, and A. McCarter, Performance of a Silicon-Modified Aluminide Coating in High Temperature Hot Corrosion Test Conditions, *Surface and Coatings Technology*, Elsevier Science S.A., Vol 68/69, 1994, p 32–37
5. D. Berry, M.C. Meelu, B.G. McMordie, and T.A. Kircher, Enhancing Performance of Silicon-Modified Slurry Aluminides on Turbine Components Operating in Marine Environments, presented at the *International Gas Turbine and Aeroengine Congress and Exposition* (Houston, TX), American Society of Mechanical Engineers, 5–8 June 1995
6. G.W. Goward and D.H. Boone, *Oxid. Met.*, Vol 3, 1971, p 475–495
7. R.L. Jones, Thermal Barrier Coatings, *Metallurgical and Ceramic Protective Coatings*, K.H. Stern, Ed., Chapman & Hall, 1996, p 194–235
8. N. Birks, G.H. Meier, and F.S. Pettit, Degradation of Coatings by High Temperature Atmospheric Corrosion and Molten Salt Deposits, *Metallurgical and Ceramic Protective Coatings*, K.H. Stern, Ed., Chapman & Hall, 1996, p 290–305
9. P.S. Burkholder et al., "Allison Engine Testing CMSX-4 Single Crystal Turbine Blades and Vanes," presented at Third International Charles Parsons Turbine Conf. Materials Engineering in Turbines and Compressors (Newcastle-upon-Tyne, U.K.), 25–27 April 1995
10. M. Gell, D.N. Duhl, D.K. Gupta, and K.D. Sheffler, Advanced Superalloy Airfoils, *J. Met.*, July 1987, p 11–15
11. P.S. Korinko, M.J. Barber, and M. Thomas, "Coating Characterization and Evaluation of Directionally Solidified CM 186 LC and Single Crystal CMSX-4," presented at ASME Turbo Expo '96 (Birmingham, U.K.), 10–13 June 1996

SELECTED REFERENCES

- N.B. Dahotre, J.M. Hampikian, and J.J. Stiglich, Ed., *Elevated Temperature Coatings*, TMS-AIME, 1995
- A.K. Koul, V.R. Parameswaran, J.P. Immarigeon, and W. Wallace, Ed., *Advances in High Temperature Structural Materials and Protective Coatings*, National Research Council of Canada, 1994

ASM Specialty Handbook: Nickel, Cobalt, and Their Alloys
J.R. Davis, editor, p 293-297
DOI:10.1361/ncta2000p293

Copyright © 2000 ASM International®
All rights reserved.
www.asminternational.org

Metallography and Microstructures of Nickel, Nickel-Copper, and Nickel-Iron Alloys

THE PRIMARY OBJECTIVE of metallographic examination is to reveal, by means of the microscope, the constituents and structure of metals and their alloys. Successful microstructural interpretation is dependent on proper selection and preparation of the metallographic specimen. In terms of specimen selection, the primary requirement is that the specimen be representative of the material being studied, but the actual selection of a specimen depends on the size and shape of the material, the portion or section of the material that is of interest, and the purpose for which the study is being made. For more detailed discussion of this subject, see ASTM E 3, "Standard Methods of Preparation of Metallographic Specimens." The remainder of this article deals with preparation of nickel, nickel-copper, and nickel-iron specimens. A companion article that covers metallographic preparation of more highly alloyed solid-solution-strengthened and precipitation-hardenable alloys follows immediately (see "Metallography and Microstructures of Heat Resistant Alloys" in this Handbook).

Metallography and Microstructures of Nickel and Nickel-Copper Alloys

The preparation of metallographic specimens and the microstructures of alloys containing 96% or more nickel (high-nickel alloys) and nickel-copper alloys containing 30% Cu are considered in this section. Table 1 lists the nominal compositions of these alloys. Micrographs of these alloys are shown in Fig. 1 to 15.

The procedures and materials for sectioning, mounting, grinding, and polishing specimens are essentially the same for all nickel alloys regardless of specimen size or sophistication of laboratory facilities. In preparing specimens for metallographic examination, it is important to prevent working of the surface.

Preparation for Microscopic Examination

The specimen to be examined is cut to a convenient size with a silicon carbide water-cooled cutoff wheel, then mounted in a hard phenolic thermosetting resin or a hard epoxy resin. Next, the mounted specimen is ground flat on a belt grinder using 120-grit abrasive and water coolant. In general, it is preferable that the exposed area of the specimen not exceed about 1.6 cm^2 (0.25 $in.^2$).

Grinding may be performed manually or on power-driven wheels using silicon carbide paper disks, starting with 220-grit and following with 320-grit, 400-grit, and 600-grit. The specimen is then washed thoroughly and cleaned ultrasonically to remove any abrasive particles remaining on the surface.

Polishing. All scratches from grinding are removed by polishing on a nylon cloth charged with 6 μm diamond paste and lubricated with lapping oil. An alternate method is to polish on a broadcloth-covered wheel using 5 μm levigated alumina (Al_2O_3) powder suspended in water.

Final polishing may be performed in one or two stages with a polishing wheel or vibratory polisher. If a polishing wheel is used, Microcloth and γ-Al_2O_3 powder (<0.1 μm particle size) suspended in water are recommended. An alternative requires semifinal and final polishing using a vibratory polisher. Semifinal polishing employs a nylon polishing cloth and a slurry of 0.3 μm Al_2O_3 and distilled water. A 350 g weight is placed on the specimen throughout the polishing cycle. At the conclusion of each polishing cycle, the specimen is cleaned ultrasonically. Final polishing employs a short-nap microcloth and a slurry of 0.05 μm Al_2O_3 and distilled water. Polishing continues until the surface is free of scratches.

Electropolishing. Nickel and nickel-copper alloys can be electropolished satisfactorily, although best results are generally obtained with specimens that first have been polished mechanically through 600-grit. Recommended electrolytes and current densities for electropolishing these alloys are given in Table 2. A platinum cathode is suggested and the electrolyte should be water cooled and continuously stirred.

Etching. The solutions and conditions for etching nickel alloys for microscopic examination are described in Table 3. The acids used should be concentrated; when water is indicated, use distilled water only.

Table 1 Nominal compositions of nickel and nickel-copper alloys described in this article

UNS No.	Alloy	Composition
N02200	Nickel 200	99.5Ni-0.08C-0.18Mn-0.20Fe
N02270	Nickel 270	99.98Ni-0.01C
N03300	Permanickel 300	98.5Ni-0.02C-0.25Mn-0.30Fe-0.35Mg-0.40Ti
N03301	Duranickel 301	96.5Ni-0.15C-0.25Mn-0.30Fe-0.63Ti-4.38Al
N04400	Monel 400	66.5Ni-31.5Cu-0.15C-1.0Mn-1.25Fe
N04405	Monel R-405	66.5Ni-31.5Cu-0.15C-1.0Mn-1.25Fe-0.043S
N05500	Monel K-500	66.5Ni-29.5Cu-0.13C-0.75Mn-1.0Fe-0.60Ti-2.73Al

Preparation for Macroscopic Examination

Surfaces to be etched for macroscopic examination may be prepared by surface grinding to a fine finish with 180-grit and 240-grit silicon carbide paper. Finer grinding, although unnecessary, yields a finer surface before etching, which requires less severe macroetching to reveal the metal structure.

Etching of nickel alloys for macroscopic examination is performed by immersing or swabbing the ground specimen for 5 to 20 s in an etchant composed of equal parts (by volume) of concentrated nitric acid (HNO_3) and glacial acetic acid.

Macroetching of nickel-copper alloys is done by immersing or swabbing the ground speci-

Table 2 Electrolytes and current densities for electropolishing of nickel and nickel-copper alloys

Electrolyte composition	Applicable alloys	Current density	
		A/cm^2	A/$in.^2$
37 mL H_3PO_4 (conc), 56 mL glycerol, 7 mL H_2O	Nickel 200 Nickel 270 Duranickel 301 Monel 400	1.4–1.5 1.5–1.8 1.25–1.5 0.9–1	9–10 10–12 8–10 6–7
33 mL HNO_3 (conc), 66 mL methanol	Monel 400, R-405, K-500	1.5–2.3	10–15

conc, concentrated

Table 3 Etchants for microscopic examination of nickel and nickel-copper alloys for grain boundaries and general structure

Composition of etchant	Conditions for use
Etchants for Nickel 200 and 270; Permanickel; Duranickel 301; and Monel 400, R-450, and K-500	
1 part 10% aqueous solution of NaCN (sodium cyanide), 1 part 10% aqueous solution of $(NH_4)_2S_2O_8$ (ammonium persulfate). Mix solutions when ready to use.	Immerse or swab specimen for 5–90 s(a)
1 part HNO_3 (conc), 1 part acetic acid (glacial). Use fresh solution.	For revealing grain boundaries. Immerse or swab specimen for 5–20 s
7.5 mL HF, 2.5 mL HNO_3, 200 mL methanol	Immerse sample 2–4 min
5 g $FeCl_3$, 50 mL HCl, 100 mL H_2O	Immerse or swab specimen up to a few minutes
Alternate etchant for Monel K-500	
Glyceregia: 10 mL HNO_3 (conc), 20 mL HCl (conc), 30–40 mL glycerol	Etch by immersing or swabbing the specimen for 30 s to 5 min

(a) This cyanide-containing etchant is very hazardous in its preparation and use. Cyanide, even in small quantities, as dust, solution, or fumes may be fatal when taken into the body. A fume hood should be utilized.

men in concentrated HNO_3. Colorless acid should be used to avoid staining. Depending on the purpose of examination, etching time should be 3 to 5 min. Within this range, shorter etching times will reveal sulfur embrittlement and details of welds in Monel; longer times will reveal general structure, including surface and subsurface cracks, porosity, and forging flow lines. Macroetching can be hastened by warming the specimen in hot water prior to etching.

Microstructures of Nickel and Nickel-Copper Alloys

High-Nickel Alloys. The microstructure of Nickel 200 typically contains some nonmetallic inclusions (principally oxide). Prolonged exposure to temperatures from 425 to 650 °C (800 to 1200 °F) results in the precipitation of graphite from the nickel solid solution.

Although Nickel 270 (99.98% Ni) is less likely than Nickel 200 to contain nonmetallic inclusions, their structures are similar, assuming that mechanical working and thermal treatments are similar (compare Fig. 1 and 2 to Fig. 3 and 4).

Permanickel 300 is an age-hardening alloy that, in the solution-annealed condition, shows randomly dispersed particles of titanium nitride (TiN) and graphite when observed through an optical microscope. When subsequently age hardened, the alloy has a similar appearance (Fig. 5), but it also contains a fine granular precipitate. This phase is not resolvable by optical microscopy in material aged at a normal aging temperature (480 °C, or 900 °F) but is visible in overaged material. The phase or phases responsible for the age hardening of this alloy have not been positively identified. The mechanism appears to be complex; carbon, magnesium, and titanium are required for full hardness. Precipitation of a compound such as $Ni_3(Mg, Ti)C_x$ seems likely during age hardening.

Duranickel 301, an age-hardening alloy, combines the corrosion resistance of unalloyed nickel with increased strength and hardness. After solution annealing, this alloy is age hardened by holding in the temperature range of 425 to 705 °C (800 to 1300 °F), which precipitates the phase $Ni_3(Al,Ti)$ throughout the structure. In the solution-annealed and properly aged condition (see Fig. 6), the precipitated phase is not resolved by an optical microscope. Some particles of graphite, however, are usually visible.

Nickel-Copper Alloys. Monel 400 is a stable solid solution of nickel and copper. Nonmetallic inclusions often appear in the microstructure (see Fig. 7).

Monel R-405 is a free-machining grade of Monel 400. The microstructures of these two alloys are similar for the same mechanical and thermal treatment, except for the sulfide particles in Monel R-405, which improve machinability (Fig. 8).

Monel K-500 is produced by adding aluminum and titanium to the basic nickel-copper composition. Solution annealing and aging produce a γ' precipitate throughout the matrix. In material aged at the normal temperature of 595 °C (1100 °F), this precipitate is not resolvable by an optical microscope (Fig. 12 and 13). However, in material that is overaged—by holding at 705 °C (1300 °F), for example—the precipitate is visible by optical microscopy (Fig. 14 and 15). In addition to the precipitate, particles of TiN are usually present in the microstructure.

Metallography and Microstructures of Nickel-Iron Alloys

The nickel-iron alloys described in this section are soft magnetic materials containing from 36 to about 80% Ni. Additional information on these alloys may be found in the article "Special-Purpose Nickel Alloys" in this Handbook.

Metallographic Preparation

Nickel-iron alloys require preparation procedures similar to those described for nickel and nickel-copper alloys. Because they are rather soft, care must be taken during preparation to prevent distortion and smearing. Elimination of fine polishing scratches is most difficult; vibratory final polishing is very useful, as is electropolishing.

Macroetching of nickel-iron alloys is commonly performed by thermal etching. Cold-rolled strip specimens are annealed several hours in dry hydrogen at 1175 °C (2150 °F), followed by furnace cooling. Thermal etching will reveal grain structures, and subsequent etching with Marble's reagent or other solutions will enhance grain contrast. Larger specimens are macroetched during manufacturing using standard hot-acid etching procedures associated with plain carbon steels.

Sectioning and mounting of nickel-iron strip is performed in the same manner as that for most metals. Strip specimens may be bent into self-supporting shapes for mounting, or plastic clamps may be used to support the specimens. Most mounting resins can be used, but thin sheets may fold over during compression mounting. Cold-setting resins can be used to avoid this problem. For edge protection, plating the surface prior to mounting may be beneficial.

Grinding and polishing procedures are basically the same as those for low-carbon steel specimens. Wet grinding is recommended to minimize heating problems and abrasive embedment. Silicon carbide of 120, 240, 320, 400, and 600 grit is used with 45 to 90° rotation of the specimen between grinding steps. Rough polishing is performed using 6 μm or 3 μm diamond abrasive (paste, spray, or slurry) on a napless or low-nap cloth. Selection of the cloth is often a matter of personal preference. Rough polishing may be followed by a 1 μm diamond polish on a medium-nap cloth. Final polishing may involve one or two grades of alumina (Al_2O_3), for example, 0.3 and 0.05 μm Al_2O_3 on a medium-nap cloth. These procedures may be executed manually using a rotating polishing wheel or by automated devices. Final polishing using a vibratory polisher may be preferred for scratch removal.

Electropolishing is an alternative for obtaining high-quality surface finishes on these soft alloys and is especially useful for annealed vacuum-melted alloys. The specimen is usually ground to a 600-grit finish before electropolishing. Through-thickness specimens are difficult to handle; planar surfaces are easier to handle. Table 4 lists commonly used electrolytes and polishing conditions.

Etchants for nickel-iron and iron-cobalt alloys are usually more aggressive than those for

Table 4 Electropolishing solutions for nickel-iron metallographic specimens

No.	Solution	Comments
1.	135 mL glacial acetic acid, 25 g CrO_3, 7 mL H_2O	Use at 80 V dc, 0.8–1.6 A/cm^2 (5–10 A/in.^{2}), 7 °C (45 °F) max. Grind samples to 600-grit surface finish.
2.	185 mL H_3PO_4, 765 mL acetic anyhdride, 50 mL H_2O	Age solution 24 h before use; use at 50 V dc (external), <30 °C (85 °F) , 0.1 A/cm^2 (0.6 A/in.^{2}), 4–5 min; use large iron or aluminum cathode
3.	10 mL $HClO_4$ and 100 mL glacial acetic acid	Use at 45 V dc, 0.2 A/cm^2 (1.3 A/in.^{2}), 24 °C (75 °F), 3–4 min

dc, direct current

electrical steels, although nital may be satisfactory for some specimens. Choice of etchants (Table 5) is often a matter of personal preference. Complete delineation of all the grains in nickel-iron alloys can be difficult.

Microstructures of Nickel-Iron Alloys

The nickel-iron soft magnetic alloys are the most ductile and most versatile soft magnetic alloys currently in use. Compared to silicon-iron electrical steels, they exhibit much higher permeabilities and lower core losses. Their exceptional ductility permits production of thin foil or wire shapes. Additionally, a large number of elements can enter into solid solution, permitting tailoring of their magnetic and physical properties. Three ranges of nickel content are used as soft magnetic alloys: 36% Ni for maximum resistivity, 50% Ni for maximum saturation magnetization, and 80% Ni for optimum initial and maximum permeabilities. Of these alloys, the 50 and 80% Ni alloys are the most widely used. Microstructures of these alloys are shown in Fig. 16 to 22.

Many of these alloys are modified using additions of molybdenum, silicon, manganese, copper, or chromium to produce specific magnetic properties. Alloys in the range of 50 to 65% Ni can be annealed in a magnetic field to produce an easy axis of magnetization and a substantial increase in permeability. Grain-oriented (001) [100] cube-texture 50Ni-50Fe alloys are also produced for applications requiring a square hysteresis loop. As with the silicon-iron electrical steels, high-temperature annealing in dry hydrogen is performed to reduce the carbon, sulfur, and oxygen contents, which greatly improves magnetic properties, especially permeability.

The nickel-iron alloys with 36% or more Ni are austenitic single-phase alloys and exhibit numerous annealing twins due to low stacking-fault energies. Their microstructures are similar to those of austenitic stainless steels.

Table 5 Etchants for microscopic examination of nickel-iron alloys

No.	Etchant composition	Procedure for use
1.	5 g $FeCl_3$, 15 mL HCl, 60 mL alcohol	Immerse or swab 5–10 s; good for replica work
2.	50 mL HCl, 2 mL 30% H_2O_2, 50 mL H_2O	Immerse 10–30 s; do not store
3.	60 mL HCl, 20 mL HNO_3, 40-60 mL glycerol	Glyceregia; orientation sensitive etch; use fresh under a hood; do not store; swab up to 1 min; discard when solution turns dark yellow
4.	Saturated aqueous $(NH_4)_2S_2O_8$ (ammonium persulfate)	For 50Ni-50Fe alloy; immerse 20–30 s
5.	100 mL HCl, 2 g $CuCl_2$ (cupric chloride), 7 g $FeCl_3$, 200 mL methanol, 100 mL H_2O	Immerse or swab 10–15 s; general purpose etch
6.	3 parts HCl and 1 part HNO_3; saturate with $CuCl_2$	For high nickel alloys, e.g., Moly Permalloy; swab 2–3 s
7.	50 mL HCl, 10 g $CuSO_4$ (copper sulfate), 50 mL H_2O	Marble's reagent; good for grain structure

ACKNOWLEDGMENTS

This article was adapted from the following:

- W.L. Mankins, Nickel and Nickel-Cooper Alloys, *Metallography and Microstructures*, Vol 9, *ASM Handbook*, ASM International, 1985, p 435–438
- G.F. Vander Voort, Magnetic and Electrical Materials, *Metallography and Microstructures*, Vol 9, *ASM Handbook*, ASM International, 1985, p 531–549



Fig. 1 Nickel 200, cold drawn and annealed in a continuous process at 830 °C (1525 °F). Structure: nickel solid solution. See also Fig. 2. NaCN, $(NH_4)_2S_2O_8$. 100×

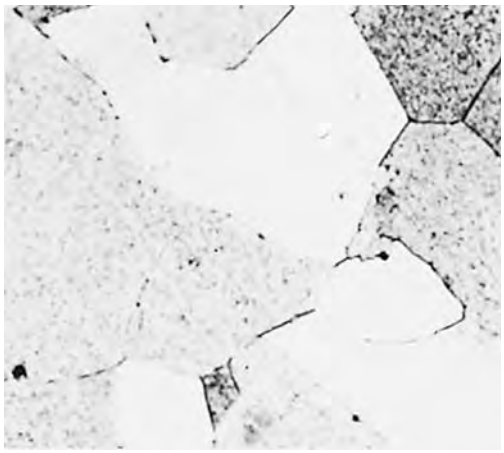


Fig. 2 Same as Fig. 1 but at higher magnification. Variation in shade of grains is caused by variation in grain orientation. NaCN, $(NH_4)_2S_2O_8$. 500×

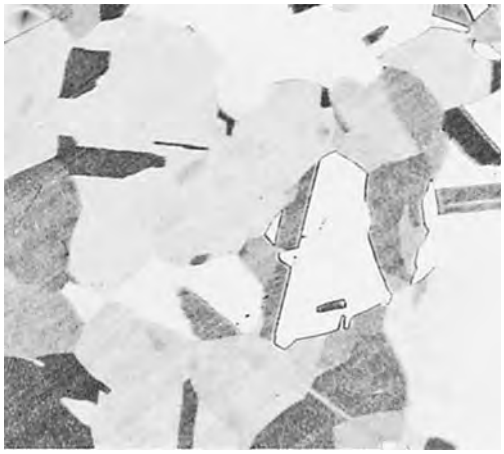


Fig. 3 Nickel 270, hot rolled and annealed in a continuous process at 830 °C (1525 °F). Structure: nickel solid solution. See also Fig. 4. NaCN, $(NH_4)_2S_2O_8$. 100×



Fig. 4 Same alloy and same processing as in Fig. 3 but shown at a higher magnification. The variation in shade of the grains (dark, gray, and white) is the result of variation in grain orientation. NaCN, $(NH_4)_2S_2O_8$. 500×

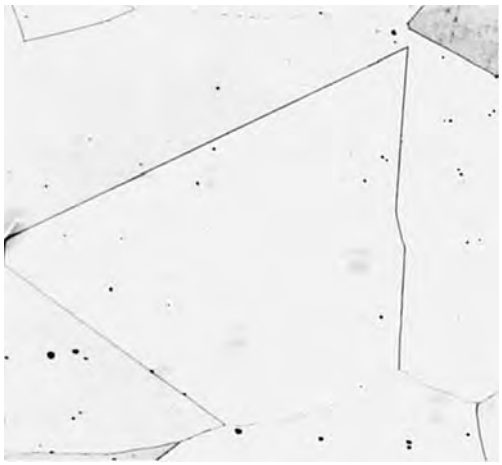


Fig. 5 Permanickel 300, solution annealed 1 h at 1205 °C (2200 °F) and water quenched, aged 10 h at 480 °C (900 °F) and water quenched. Dispersed particles of TiN and graphite (black dots) in nickel solid solution. NaCN, $(NH_4)_2S_2O_8$. 100×

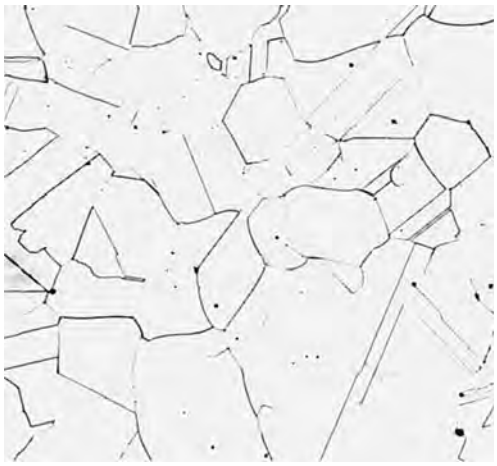


Fig. 6 Duranickel 301, solution annealed for 30 min at 980 °C (1800 °F) and water quenched, aged for 20 h at 480 °C (900 °F) and water quenched. Microstructure: nickel solid solution; graphite particles (black dots). NaCN, $(NH_4)_2S_2O_8$. 50×



Fig. 7 Monel 400, cold drawn and annealed in a continuous process at 830 °C (1525 °F). Nickel-copper solid solution with a few unidentified nonmetallic inclusions (black). NaCN, $(NH_4)_2S_2O_8$. 100×

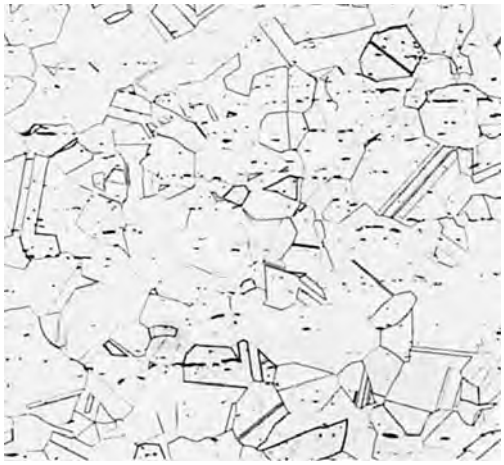


Fig. 8 Monel R-405, cold drawn, and annealed in a continuous process at 830 °C (1525 °F). Microstructure: nickel-copper solid solution with sulfide stringers (black constituent). NaCN, $(NH_4)_2S_2O_8$. 100×



Fig. 9 Monel K-500 in the hot rolled condition. Structure: nickel-copper solid solution. Variation in shade of grains is the result of variation in grain orientation. Glyceregia. 100×



Fig. 10 Monel K-500, solution annealed for 1 h at 1205 °C (2200 °F) and quenched in water. Nickel-copper solid-solution matrix. See also Fig. 11 to 15. NaCN, $(NH_4)_2S_2O_8$. 100×

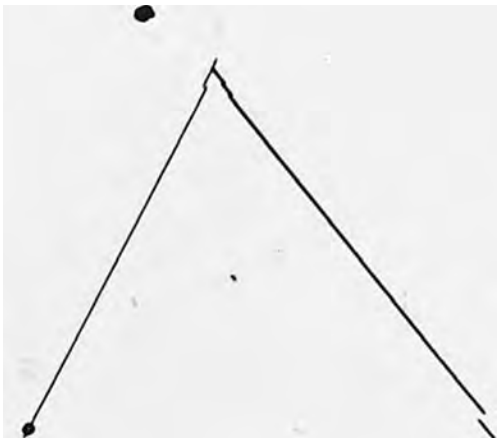


Fig. 11 Same as Fig. 10, but at higher magnification. Portions of only three grains are visible. The black dots are nitride particles. See also Fig. 10 and 12 to 15. NaCN, $(NH_4)_2S_2O_8$. 1000×



Fig. 12 Monel K-500, held 1 h at 1205 °C (2200 °F), transferred to a furnace at 595 °C (1100 °F) and aged 4 h, water quenched. Solid-solution matrix; nitride particles. See also Fig. 10, 11, and 13 to 15. NaCN, $(NH_4)_2S_2O_8$. 100×

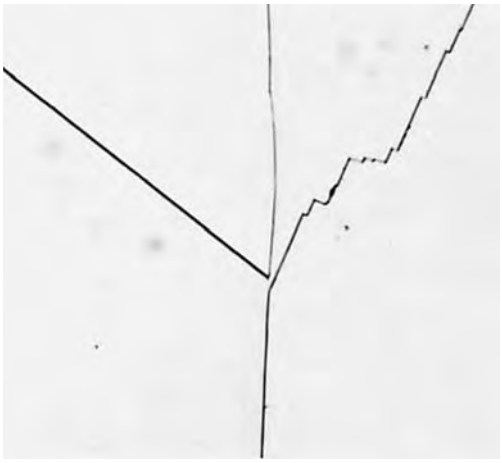


Fig. 13 Same as Fig. 12, but at higher magnification. Structure contains precipitated $Ni_3(Al,Ti)$, resolvable only by electron microscopy unless aging temperature is higher than 595 °C (1100 °F). See also Fig. 10 to 12 and 14, 15. NaCN, $(NH_4)_2S_2O_8$. 1000×

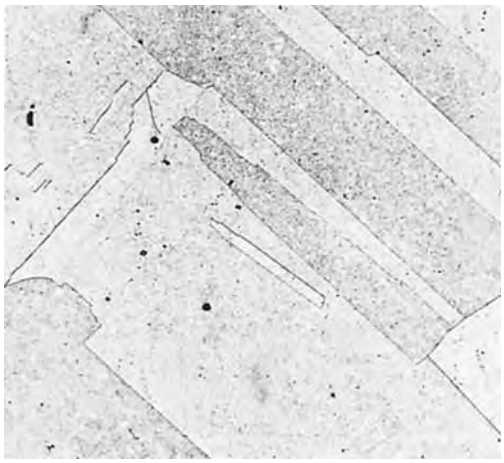


Fig. 14 Monel K-500, held 1 h at 1205 °C (2200 °F), transferred to a furnace at 705 °C (1300 °F) and aged 4 h, water quenched. Precipitated $Ni_3(Al,Ti)$ appears as tiny particles dispersed in the matrix solid solution. See also Fig. 10 to 13 and 15. NaCN, $(NH_4)_2S_2O_8$. 100×

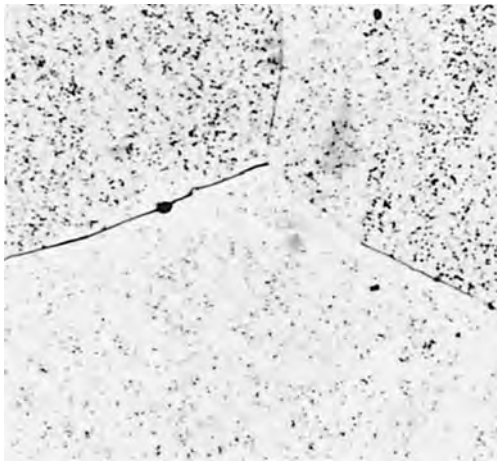


Fig. 15 Same as Fig. 14 except at a higher magnification. The $Ni_3(Al,Ti)$ precipitate is better resolved. When this precipitate is resolvable by optical microscopy, averaging is indicated. See also Fig. 10 to 14. NaCN, $(NH_4)_2S_2O_8$. 1000×

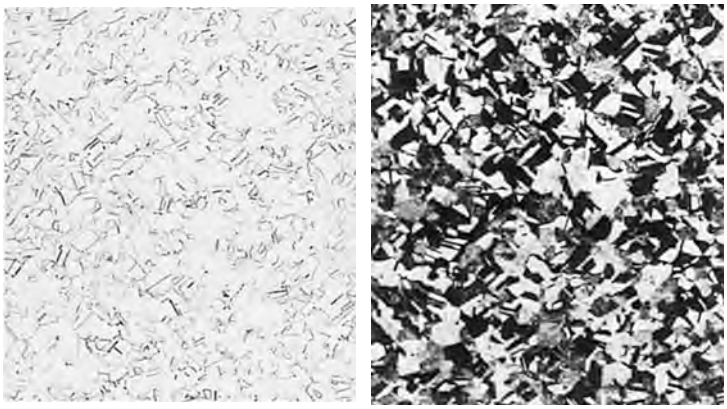


Fig. 16, 17 Austenitic Fe-50.5Ni soft magnetic alloy, showing the effects of different etchants. Fig. 16: etched using a flat etchant, glyceregia. Fig. 17: etched using a grain contrast etchant, Marble's reagent. Both 100×. See Fig. 18 to 20 for the effects of deformation (cold rolling) and heat treatment on the structure of a similar Fe-50Ni alloy.



Fig. 18 Fe-50Ni cold-rolled 0.15 mm strip, annealed 2 h in H_2 at 900 °C and furnace cooled. Structure: primary recrystallized grains of austenite. 60 mL ethanol, 15 mL HCl, and 5 g anhydrous $FeCl_3$. 100×

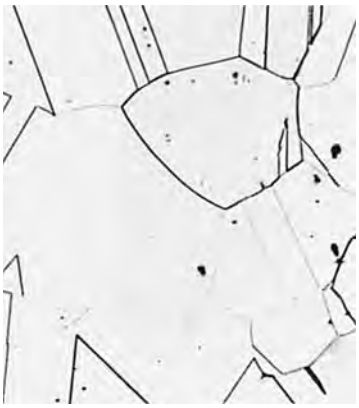


Fig. 19 Fe-50Ni cold-rolled 0.03 mm strip, annealed 4 h at 1175 °C (2150 °F) in dry H_2 and furnace cooled. Structure is nonoriented primary recrystallized grains. See also Fig. 20. Saturated $(NH_4)_2S_2O_8$. 100×

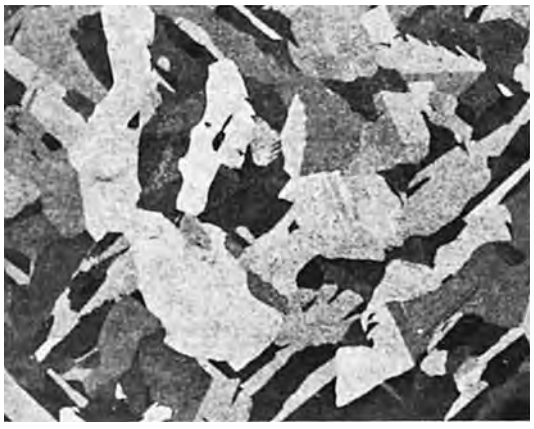


Fig. 20 Fe-50Ni cold-rolled strip, 0.03 mm (0.014 in.) thick, annealed same as Fig. 19. The structure is comprised of nonoriented secondary recrystallized grains. Thermal etch in hydrogen at 1175 °C (2150 °F). 3×

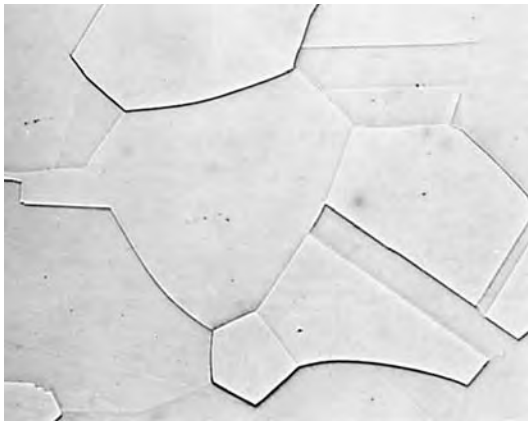


Fig. 21 4-79 Moly Permalloy (4Mo-79Ni-17Fe), cold-rolled strip 0.03 mm (0.014 in.) thick, annealed 4 h in dry hydrogen at 1175 °C (2150 °F) and cooled at 320 °C (575 °F) per hour to room temperature. The structure is coarse-grained austenite. HCl, $CuCl_2$, $FeCl_3$, HNO_3, methanol, and H_2O. 100×

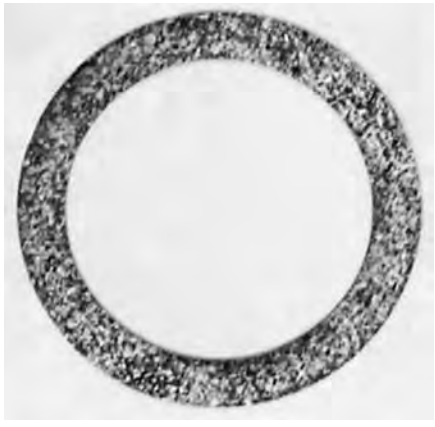


Fig. 22 4-79 Moly Permalloy magnetic test-ring specimen taken from 0.3 mm (0.014 in.) thick cold-rolled strip, annealed 4.5 h at 1120 °C (2050 °F) in dry hydrogen. The structure is austenite grains. Marble's reagent. 0.875×

ASM Specialty Handbook: Nickel, Cobalt, and Their Alloys
J.R. Davis, editor, p 298-330
DOI:10.1361/ncta2000p298

Copyright © 2000 ASM International®
All rights reserved.
www.asminternational.org

Metallography and Microstructures of Heat Resistant Alloys

HEAT RESISTANT ALLOYS cover a wide range of chemical compositions, microstructural constituents, and mechanical properties. This article summarizes metallographic techniques and microstructural constituents of three types of heat resistant alloys: iron-base, nickel-base, and cobalt-base. Aspects particularly significant to the preparation and microstructural examination of wrought alloys are emphasized. It should be noted, however, that the metallographic methods discussed are suitable for preparing equivalent cast heat resistant alloys; microstructural constituents are quite similar except for obvious differences in homogeneity and porosity.

Table 1 lists the nominal compositions of the alloys illustrated in this article. As indicated in this table, wrought iron-base and iron-nickel-base alloy microstructures are shown in Fig. 1 to 60; wrought nickel-base alloys are shown in Fig. 61 to 119. Wrought cobalt-base alloys are shown in Fig. 120 to 152; cast nickel-base alloys are shown in Fig. 153 to 211. Cast cobalt-base alloys are shown in Fig. 212 to 235.

Specimen Preparation

The procedures used to prepare metallographic specimens of wrought heat resistant grades are quite similar to those for iron-base alloys, particularly wrought austenitic stainless steels. Information on metallographic practices for wrought stainless steels can be found in the *ASM Specialty Handbook: Stainless Steels* (see pages 439 to 444) and in *Metallography and Microstructures*, Volume 9 of the *ASM Handbook* (see the article "Wrought Stainless Steels" on pages 279 to 296).

Macroetching. Wrought heat resistant alloys are examined for macrostructure in the same manner as tool steels and stainless steels. Disks are cut (usually from billet samples) at representative locations, such as the top and bottom of ingots or remelted stock, and are ground before macroetching. Macroetchants for wrought nickel-base and cobalt-base heat resistant alloys are given in Table 2. Macroetchants for iron-base heat resistant alloys are the same as those recommended for stainless steels.

Macroetched features in consumable-electrode remelted superalloys are different from those observed in ingot cast steels. Unique macroetch features observed in these remelted alloys include freckles, radial segregation, and ring patterns (Ref 1–7). Freckles are dark-etching spots due to localized segregation or to enrichment of carbides or Laves phase. They are detrimental to material quality. Radial segregation appears as dark-etching elongated spots in a radial or spiral pattern. Ring patterns are concentric rings that etch lighter (usually) or darker than the matrix. They are revealed only by macroetching. The nature of ring patterns remains obscure. Examination has revealed little difference between ring and matrix areas and no measurable influence on mechanical properties.

Sectioning. Various sectioning devices have been used with superalloys. The usual precautions regarding excessive heating should be followed. For austenitic grades, which are sensitive to deformation, the more vigorous sectioning techniques, such as band sawing or power hacksawing, may introduce excessive distortion or work hardening, depending on the alloy and heat treatment condition. Such methods are suitable for initial sectioning of large pieces, but final cutting of specimens is best performed using abrasive cutoff machines. Heavy deformation introduced by sawing may be difficult to remove by subsequent grindings and polishings. Abrasive cutoff wheels used are usually the consumable type. Abundant coolant should be used; submerged cutting is preferred.

Mounting. Many bulk specimens can be ground and polished without mounting. Some automatic grinding and polishing devices require a mounted specimen, which is usually 25, 32, or 38 mm (1, 1¼, or 1½ in.) in diameter; others do not. Mounting facilitates polishing of small or irregularly shaped specimens.

It may sometimes be necessary to view the microstructure at the extreme edge of a specimen. Optimum results are obtained when the edge of interest is plated with electroless or electrolytic nickel before mounting. Good results can be obtained without plating if the specimen is mounted using a compression-molded epoxy resin, particularly if automatic polishing is used.

When edge retention is not a primary requirement, specimens can be mounted using any of the popular compression-mounting materials or castable resins. Most produce acceptable results; each resin has advantages and disadvantages. The selection of a particular resin is often based on familiarity.

Grinding of specimens takes place by hand or by use of automatic devices. Grinding is performed using water-cooled silicon carbide paper at 150 to 600 rpm. The usual grit-size sequence is 120, 240, 320, 400, and 600 grit; finer grits are occasionally used. Grit sizes finer than 600 can be useful for preparing nickel-base superalloys. This eliminates coarse diamond paste polishing and may improve retention of carbides and intermetallic phases and reduce relief.

Moderately heavy pressure is used for hand grinding. The specimen must be held flat against the paper. After each grinding, the specimen is rinsed, wiped clean, and rotated 45 to 90° before grinding with the next paper. Grinding should proceed for approximately twice as long as needed to remove all the scratches from the previous step; 1 to 2 min per step is usually adequate. Automatic grinding produces omnidirectional scratch patterns. Wrought superalloys are not susceptible to embedding of silicon carbide from the grinding paper, but if the specimen contains cracks or pores, it should be cleaned ultrasonically. For most specimens, a simple wash under running water will remove any loose abrasive or grinding debris. Specimens should be washed in alcohol (preferably ethanol) and dried in hot air.

Rough polishing often begins using 6 μm or 3 μm diamond abrasive, generally as a paste, although aerosols or slurries are also used. The use of 5 μm alumina (Al_2O_3) for rough polishing has been largely replaced by the more efficient diamond abrasives.

Although a wide range of cloths is available, low-nap or napless cloths are generally used for rough polishing. Canvas, which is quite popular, provides economical durability. Synthetic napless chemotextile cloths are also used.

Billiard cloth and red felt are sometimes preferred. A lubricant/extender fluid should always be added to reduce friction and drag and to promote more efficient cutting. Wheel speeds are 150 to 300 rpm. Moderate pressure is applied.

During hand polishing, the specimen should be rotated counter to wheel rotation while it is moved slowly from center to edge. Again, the specimen must be held firmly against the wheel to avoid rocking. Polishing should continue until grinding scratches are removed; 1 to 2 min is usually adequate.

A second diamond polishing step generally using 1 μm diamond is often performed. A synthetic suede medium-nap cloth is commonly used, but other cloths may also yield good results. This step is carried out in the same manner as the initial diamond polishing. After each diamond polishing, the specimen should be carefully cleaned to remove abrasive, extender oil, and polishing debris. Ultrasonic cleaning produces excellent results but is not always required.

Table 1 Nominal compositions of the heat resistant alloys for which microstructures are shown in this article

Alloy	Fig. No.	Composition, %							
		C	Fe	Ni	Co	Cr	Ti	Mo	Others
Wrought iron-nickel-base alloys									
A-286	1–14	0.05	bal	26.0	…	15.0	2.15	1.25	0.3V, 0.2Al, 0.003B
Discaloy	15–23	0.04 max	bal	25.0	…	13.5	1.75	3.0	0.1Al
Incoloy 800	24	0.05	bal	32.5	…	21.0	0.38	…	0.38Al
Incoloy 901	25–27	0.05	bal	42.7	…	13.5	2.5	6.2	0.25Al
N-155 (Multimet)	28–29	0.15	bal	20.0	20.0	21.0	…	3.0	2.5W, 1.0Nb + Ta, 0.15N
16-25-6	30–32	0.08 max	bal	25.0	…	16.0	…	6.0	0.15N
Hastelloy X	33–36	0.10 max	18.5	bal	1.5	22.0	…	9.0	0.6W
Pyromet 31	37–42	0.04	bal	55.5	…	22.7	2.5	2.0	1.5Al, 1.1Nb, 0.005B
Alloy 718	43–60	0.04	18.5	bal	…	19.0	0.9	3.05	5.13Nb + Ta, 0.5Al
Wrought nickel-base alloys									
Astroloy	61–68	0.06	…	bal	17.0	15.0	3.5	5.25	4.0Al, 0.03B
Alloy 600	69	0.1 max	8.0	bal	…	15.5	…	…	…
Alloy 625	70	0.1 max	5.0 max	bal	1.0 max	21.5	0.4 max	9.0	3.65 Nb + Ta, 0.4 Al max
Alloy X-750	71–78	0.04	7.0	bal	…	15.5	2.5	…	0.95 Nb + Ta, 0.7Al
Nimonic 80	79–82	0.10 max	5.0 max	bal	2.0 max	19.5	2.25	…	1.13Al
René 41	83–86	0.09	…	bal	11.0	19.0	3.1	10.0	1.5Al, 0.010 B max
René 95	87–89	0.15	…	bal	8.0	14.0	2.5	3.5	3.5Al, 3.5W, 3.5Nb
TD-Nickel	90–91	…	…	bal	…	…	…	…	$2ThO_2$
U-700	92–99	0.15 max	1.0 max	bal	18.5	15.0	3.5	5.2	4.25Al, 0.05B
U-710	100–102	0.07	…	bal	15.0	18.0	5.0	3.0	2.5Al, 1.5W, 0.02B
50Cr-50Ni	103–106	0.06	…	bal	…	50.0	1.0	…	…
Waspaloy	107–119	0.07	…	bal	13.5	19.5	3.0	4.3	1.4Al, 0.07Zr, 0.006B
Wrought cobalt-base alloys									
Elgiloy	120–121	0.15	15.0	15.0	bal	20.0	…	7.0	2.0Mn
S-816	122–128	0.38	4.0	20.0	bal	20.0	…	4.0	4.0W, 4.0Nb
Haynes 25 (L-605)	129–138	0.10	…	10.0	bal	20.0	…	…	15.0W, 1.5Mn, 0.55Si
Haynes 188	139–143	0.10	1.5	22.0	bal	22.0	…	…	14.0W, 0.08La
Stellite 6B	144–146	1.1	3.0 max	3.0 max	bal	30.0	…	…	4.5W
MP35N	147–152	0.025 max	1.0 max	35.0	bal	20.0	1.0 max	10.0	0.010 B max
Cast nickel-base alloys									
B-1900	153–159	0.10	0.35	bal	10.0	8.0	1.0	6.0	6.0Al, 4.3Ta, 0.1Nb max, 0.015B, 0.08Zr
Hastelloy B	160–161	0.10	5.0	bal	2.5	0.6	…	28.0	0.30V
Hastelloy C	162–163	0.07	5.0	bal	2.5	16.0	…	17.0	4.0W
IN-100	164–178	0.15	…	bal	15.0	10.0	4.7	3.0	5.5Al, 1.0V, 0.06Zr, 0.015B
Alloy 713C	179–190	0.12	2.5	bal	…	12.5	0.80	4.2	6.1Al, 0.10Zr, 0.012B
Alloy 718	191–192	0.04	18.5	bal	…	19.0	0.9	3.05	5.13Nb + Ta, 0.5Al
IN 738	193–196	0.17	0.50	bal	8.5	16.0	3.4	1.75	3.4Al, 0.9Nb, 2.6W, 1.75Ta, 0.10Zr, 0.01B
MAR-M246	197–205	0.15	…	bal	10.0	9.0	1.5	2.5	5.5Al, 10.0W, 1.5Ta, 0.05Zr, 0.015B
TRW-NASA V1A	206–207	0.13	…	bal	7.5	6.1	1.0	2.0	5.4Al, 5.5W, 9.0Ta, 0.5Nb, 0.43Hf, 0.2Re, 0.13Zr, 0.02B
U-700	208–211	0.15 max	1.0 max	bal	18.5	15.0	3.5	5.2	4.25Al, 0.05B
Cast cobalt-base alloys									
Haynes 21	212-217	0.25	1.0	3.0	bal	27.0	…	5.0	…
Haynes 31	218–220	0.50	2.0	10.5	bal	25.5	…	…	7.5W, 0.01B
Haynes 151	221–223	0.50	…	…	bal	20.0	…	…	12.7W
98 M2 Stellite	224–229	1.7–2.2	…	2.0–2.5	bal	28.0–32.0	…	…	17.0–20.0W, 3.7–4.7V, 0.7–1.5B
WI-52	230	0.45	2.0	1.0	bal	21.0	…	…	11.0W, 2.0Nb
MAR-M 302	231–232	0.85	…	…	bal	21.5	…	…	10.0W, 9.0Ta, 0.20B, 0.005Zr
MAR-M 509	233–235	0.60	…	10.0	bal	24.0	0.20	…	7.0W, 3.5Ta, 0.50Zr

Final polishing may involve one or more steps, depending on the need to remove all scratches. For routine inspection, polishing to a 1 μm diamond finish may be adequate. When photomicroscopy is anticipated, additional steps are usually required. A wide range of final polishing abrasives may be used. Alumina slurries are quite common, using 0.3 μm and/or 0.05 μm Al_2O_3. Colloidal silica (SiO_2) (Ref 1) produces exceptional results with these alloys.

Final polishing is generally performed using synthetic suede medium-nap cloths at approximately 150 rpm. During hand polishing, the specimen should be rotated counter to wheel rotation while it is moved from center to edge. The slurry is occasionally added to the cloth during polishing. Moderate pressure is used, and care must be taken to avoid rocking the specimen. A polishing time of 1 to 2 min is usually adequate. After polishing, the specimen should be carefully cleaned and dried to avoid staining. When hand polishing, the operator's hands must be cleaned after each rough and final polishing to prevent contamination.

Automatic polishing machines are quite useful for final polishing. A wide variety of devices is available. The time required using these units ranges from a few minutes to approximately 30 min for vibratory polishing.

Mechanical polishing is sometimes followed with a brief electropolish to remove any smeared or flowed metal without introducing preferential attack of the second phase constituents. Extended electropolishing should be avoided. Table 3 lists appropriate electropolishing solutions for wrought nickel-base and cobalt-base heat resistant alloys. Electropolishing solutions for wrought iron-nickel-cobalt austenitic alloys are the same as those used for wrought austenitic stainless steels.

Etching. Some minor phases in superalloys can be observed easily in the as-polished condition. Minimal relief can be introduced during final polishing to accentuate these particles. They can be observed in bright-field illumination by color contrast, which is useful for phase identification. The nitrides, carbonitrides, borides, and metal carbides are readily observed without etching.

The wrought iron-nickel-base heat resistant alloys are basically austenitic stainless steels. Therefore, the techniques for etching and identifying phases in wrought austenitic stainless steels apply to these alloys.

Glyceregia is one of the most prevalent reagents for revealing the general structure of iron-nickel and nickel-base heat resistant alloys. It should always be mixed fresh and discarded when it turns orange. Glyceregia will etch all the heat resistant grades, except some of the high cobalt content superalloys. For etching solution-annealed nickel-base alloys, glyc-

erol content is often decreased, and nitric acid (HNO_3) content is often increased. The standard composition is ideal for solution-annealed and aged specimens, which are easier to etch. The mixture of hydrochloric acid, sulfuric acid, and nitric acid (HCl-H_2SO_4-HNO_3) (95-5-3) is also quite popular for these alloys and is used similarly. For grain size examination in aged specimens, etching with waterless Kalling's or Marble's reagents is quite common. Several electrolytic reagents are also commonly used. Color etchants, though not widely used for these alloys, produce very good results.

Table 4 lists some of the more commonly used reagents for etching iron-nickel-base, nickel-base, and cobalt-base heat resistant alloys. Additional information regarding the etching of wrought heat resistant alloys can be found in Ref 1 and 8 to 15.

Some electropolishing procedures are useful for microstructural examination using scanning electron microscopy (SEM) or transmission electron microscopy (TEM) (replicas). The electropolish sometimes produces attack of the γ' phase, and subsequent etching is unnecessary. For replica examination, it is often helpful to use a reagent or an electropolish that attacks γ' so that this phase is readily distinguished from other phases (Ref 16–18). In such cases the γ' is recessed, but other second phases are in relief.

Selective etchants and heat tinting have been commonly used to differentiate various carbide types and to identify σ phase. Borides, which are similar in appearance to metal carbides, can be discriminated by selective etching. Metal carbides are selectively colored; borides are unaffected (Ref 19).

Table 2 Macroetchants for wrought nickel-base and cobalt-base heat resistant alloys

Composition	Comments
1. 1 part 30% H_2O_2, 2 parts HCl, 2 or 3 parts H_2O	Recommended for nickel-chromium alloys; use fresh solution. Reveals grain structure; if the surface is stained, remove with 50% aqueous HNO_3. Etch approximately 2 min.
2. (a) 15 g $(NH_4)_2S_2O_8$ (ammonium persulfate) and 75 mL H_2O; (b) 250 g $FeCl_3$ and 100 mL HCl; (c) 30 mL HNO_3	Lepito's macroetch for general macrostructure and weldments. Mix a and b; add c. Immerse 30–120 s at room temperature.
3. 200 g $FeCl_3$, 200 mL HCl, H_2O to 1000 mL	For nickel-base superalloys. Etch to 90 min at 100 °C (212 °F).
4. HCl saturated with $FeCl_3$	For cobalt-base superalloys. Add 5% HNO_3 before use at room temperature. Clean surface by dipping in 50% aqueous HCl.
5. (a) 21 mL H_2SO_4, 15 mL HCl, 21 mL HNO_3, 21 mL HF, 22 mL H_2O; (b) 40 mL 20% aqueous $CuCl_2$ (copper chloride), 40 mL HCl, 20 mL HF	For cobalt-base superalloys. Etch 5 min in (a), then 5 min in (b).
6. 50 mL saturated aqueous $CuSO_4$ (copper sulfate) and 50 mL HCl	For iron-nickel-base and nickel-base alloys. Swab or immerse at room temperature.

Whenever water is specified, use distilled water.

Table 3 Electropolishing techniques for wrought nickel-base and cobalt-base heat resistant alloys

Electrolyte composition	Comments
1. 37 mL H_3PO_4, 56 mL glycerol, 7 mL H_2O	For Inconel 625, use 1.2–1.6 A/cm^2 (8–10 A/in.^{2}); for Incoloy 800, use 3.1 A/cm^2 (20 A/in.^{2}); platinum cathode
2. 25 mL H_3PO_4, 25 mL HNO_3, 50 mL H_2O	For Inconel 600 and X-750, use 17.8 A/cm^2 (115 A/in.^{2}), 5–10 s; platinum cathode
3. 144 mL ethanol, 10 g $AlCl_3$ (anhydrous aluminum chloride), 45 g $ZnCl_2$ (anhydrous zinc chloride), 16 mL N-butyl alcohol, 32 mL H_2O	For cobalt-base superalloys; use 23–25 V dc at room temperature with successive 1 min periods
4. 40 mL $HClO_4$ (perchloric acid), 450 mL acetic acid, 15 mL H_2O	For Nimonic alloys; use 15 V dc, 0.1 A/cm^2 (0.65 A/in.^{2}) below 25 °C (77 °F)
5. 10 mL $HClO_4$ and 90 mL acetic acid	For nickel-base alloys, use at 0.5–0.9 A/cm^2 (3–6 A/in.^{2}), 30 s for aged specimens, longer for solution-annealed ones; keep cool (10–15 °C, or 50–60 °F); best results by polishing in 5 s intervals
6. 70 mL methanol and 10 mL H_2SO_4	For nickel-base superalloys, use at 20–25 V dc, 0.3–0.8 A/cm^2 (2–5 A/in.^{2}), room temperature; 10–15 s after a 600-grit finish or 5 s after a 0.3 μm Al_2O_3 finish; γ' slightly etched, carbides in relief
7. 60 mL methanol, 10 mL H_2SO_4, 5 mL HCl	Use same as No. 6; produces more etching of γ' phase; if HNO_3 is substituted for HCl, the surface will be smooth without relief or attack
8. 7 mL ethanol, 20 mL $HClO_4$, 10 mL glycerol	Use same as No. 6; mix carefully, keep cool; produces smooth surfaces
9. 15 mL HCl and 85 mL methanol	For nickel-base superalloys, use at 30–40 V dc, 0.3–1.2 A/cm^2 (2–8 A/in.^{2}), at room temperature for 5–10 s after a 600-grit silicon carbide finish or 2–5 s after a 0.3 μm Al_2O_3 finish; produces strong carbide relief, etches γ'; very good for SEM examination

Microexamination

Transmission Electron Microscopy. Because some of the important constituents in wrought heat-resistant alloys, such as γ' phase, are generally too small to observe using the optical microscope, considerable use has been made of TEM. Besides affording greater resolution and higher magnification, TEM provides means for phase identification by electron diffraction and, when equipped with x-ray detectors, can provide chemical analysis data. Such analytical procedures are necessary to understand the strengthening mechanisms for heat resistant alloys.

Several types of specimens can be prepared for TEM examination; each type has advantages and disadvantages. The replica method, which had been prevalent, is being replaced by use of the scanning electron microscope (Ref 17, 18). A well-polished and properly etched specimen can be examined by SEM at magnifications of 50,000× or more. Therefore, much of the structural examination role of TEM replicas can be accomplished without replica preparation and the complication of replica interpretation or artifact control.

In addition, the contrast mechanisms operable in the scanning electron microscope are valuable for structural examination. Because chemical analysis using SEM is limited to features larger than a few microns, TEM examination and analysis of extracted constituents remains an important procedure. Procedures for preparing structural and extraction replicas are discussed in the article "Transmission Electron Microscopy" in *Metallography and Microstructures,* Volume 9 of the *ASM Handbook,* and in Ref 20 to 28. Direct examination of the fine structure of wrought heat resistant alloys is also performed by TEM examination of thin foils. As with extraction replicas, electron diffraction and chemical analysis can be performed.

Because the beam size in a transmission electron microscope or a scanning transmission microscope is much smaller than in a scanning electron microscope, much finer particles can be analyzed using thin foils without interference from the surrounding matrix. Extremely small particles are difficult to analyze, even with a scanning transmission electron microscope. Extraction replicas are useful, because matrix effects can be eliminated. In addition, using a scanning transmission electron microscope, microdiffraction patterns are obtainable from individual particles rather than many particles. The microdiffraction pattern is of great value in basic structural studies of the constituents.

Thin foils are prepared by the window method or the disk method described in Ref 20 to 22 and 28 to 31. These methods involve careful sectioning to obtain a relatively thin slice of the material free of artifacts, followed by mechanical, chemical, or electrolytic thinning until a small area is thin enough for electron transmission. Table 5 lists several popular electropolishing procedures for preparing thin foils of wrought heat resistant alloys.

Bulk Extractions. X-ray diffraction studies of phases extracted electrolytically is a widely practiced, important tool for phase identification in wrought heat resistant alloys (Ref 32–40). Because of the complex nature of these alloys, such techniques must be carefully controlled to ensure good results. Qualitative identification of the phases by this method is considerably easier than quantitative evaluations. The extraction method must be designed to permit separation of the carbides, nitrides, γ', and topologically close-packed (tcp) phases. Once separated, the phases can be analyzed using

x-ray diffraction, chemical analysis (elemental), and optical and electron microscopy procedures.

Considerable research has been conducted to establish reliable procedures for bulk extraction in wrought heat resistant alloys (Ref 32–40). Anodic dissolution using 10% HCl in methanol, which dissolves γ′ and the austenitic matrix, is implemented to extract carbides, borides, nitrides, and tcp phases. If the alloy to be digested contains substantial amounts of tungsten, tantalum, or niobium, 1% tartaric acid is added to prevent contamination of the residue.

To extract γ′ from nickel-base alloys, two electrolytes have been used: (a) 20% aqueous phosphoric acid (H_3PO_4) or (b) an aqueous solution containing 1% ammonium sulfate [$(NH_4)_2SO_4$1 and 1% citric acid or tartaric acid. The latter electrolyte produces better recovery of γ′. When the ammonium sulfate/citric or tartaric acid electrolyte is used, the residue will also contain carbides, nitrides, and borides (if present in the alloy). All the γ′ morphologies are extracted using this electrolyte. Details concerning the use of these electrolytes, and others given in Table 6, are provided in Ref 32 to 40.

Table 4 Microetchants for wrought heat resistant alloys

Composition	Comments
1. 3 parts glycerol, 2–3 parts HCl, 1 part HNO_3	Glyceregia; mix fresh, do not store; discard when solution is orange; use by immersion or swabbing 5–60 s; very popular general etch for structure of iron-base and nickel-base superalloys; γ′ in relief
2. 5 mL HF, 10 mL glycerol, 85 mL ethanol	Electrolytic etch at 0.04–0.15 A/cm^2 (0.25–1.0 A/in.^{2}), 6–12 V dc; for nickel-base alloys, γ′ in relief; stop etch when edges are brownish; excellent etch for TEM replica work
3. 12 mL H_3PO_4, 47 mL H_2SO_4, 41 mL HNO_3	Electrolytic etch, 6 V dc, 0.12–0.15 A/cm^2 (0.75–1.0 A/in.^{2}), a few seconds; add to 100 mL H_2O to slow etch; for nickel-base alloys; use under hood; mix H_3PO_4 and HNO_3, then add H_2SO_4; stains matrix when γ′ is present; good for revealing segregation and for examining γ′ with TEM replicas; attacks Bakelite; stop etch when edge of specimen is brownish
4. 30 mL lactic acid, 20 mL HCl, 10 mL HNO_3	For nickel-base superalloys
5. 5 g $CuCl_2$, 100 mL HCl, 100 mL ethanol	Waterless Kalling's reagent; immerse or swab to a few minutes; for iron-base and nickel-base superalloys
6. 10 g $CuSO_4$, 50 mL HCl, 50 mL H_2O(a)	Marble's reagent for iron-nickel and cobalt-base superalloys; immerse or swab 5–60 s; a few drops of H_2SO_4 will increase etch activity; reveals grain boundaries and second-phase particles
7. 5 mL H_2SO_4, 3 mL HNO_3, 92 mL HCl	For iron-base and nickel-base alloys; add H_2SO_4 to HCl, stir, allow to cool, add HNO_3; discard when orange; swab 10–30 s; use under hood; do not store
8. 20 mL HNO_3 and 60 mL HCl	Aqua regia; for iron-base and nickel-base superalloys; use under hood, do not store; immerse or swab 5–60 s; attacks σ phase, outlines carbides, reveals grain boundaries
9. 50 mL HCl and 1–2 mL 30% H_2O_2	For nickel-base alloys; attacks γ′-phase; immerse 10–15 s
10. 5 mL H_2SO_4, 8 g CrO_3, 85 mL H_3PO_4	Electrolytic etch at 10 V dc, 0.2 A/cm^2 (1.3 A/in.^{2}), 5–30 s; reveals inhomogeneities in nickel-base alloys
11. 10 mL HNO_3, 10 mL acetic acid, 15 mL HCl, 2–5 drops glycerol	Use fresh, same precautions as glyceregia; used for hard to etch solution-treated nickel-base alloys
12. (a) 33 mL HCl and 67 mL H_2O (b) 50 mL HCl and 50 mL H_2O	Beraha's tint etch for nickel-base alloys; add 0.6–1 g $K_2S_2O_5$ (potassium metabisulfite) to 100 mL stock solution (a); immerse (never swab) 60–150 s, slowly agitate; if colors are not developed, add 1–1.5 g $FeCl_3$ or 2–10 g $NH_4F{\cdot}HF$ (ammonium bifluoride) to 100 mL stock solution (b); immerse 60–150 s, agitate gently; colors matrix
13. 10 g $K_3Fe(CN)_6$ (potassium ferricyanide), 10 g KOH, 100 mL H_2O	Murakami's reagent; for iron-base and nickel-base superalloys; use hot (75 °C, or 170 °F) to darken σ phase; use at room temperature to darken carbides; better results may be obtained if the specimen is first etched in 50% aqueous HNO_3 at 8 V dc; use under a hood
14. 10 g CrO_3 and 100 mL H_2O	Electrolytic etch, 6 V dc, 10–30 s; for iron-base and nickel-base superalloys; σ attacked, carbides outlined or attacked
15. 80 mL H_3PO_4 and 10 mL H_2O	Electrolytic etch for nickel-base superalloys at 3 V dc (closed-circuit), 0.11–0.12 A/cm^2 (0.7-0.8 A/in.^{2}), 7–9 s; if the surface is stained, swab with the electrolyte; use fresh solution; used to determine the degree of carbide continuity at the grain boundaries
16. 25 g CrO_3, 130 mL acetic acid, 7 mL H_2O	Electrolytic etch for nickel-base superalloys at 10 V dc (closed circuit) for 2 min; the current density will drop during the first 20 s; use fresh; used to reveal prior grain boundaries
17. 30 mL HCl, 7 mL H_2O, 3 mL 30% H_2O_2	Popular etch for cobalt-base superalloys
18. 100 mL HCl and 5 mL 30% H_2O_2	Popular etch for cobalt-base superalloys; up to 20% H_2O_2 has been used; mix fresh; immerse 1–10 s
19. 5–10 mL HCl and 95–90 mL H_2O	Electrolytic etch for cobalt-base superalloys; use at 3 V dc, 1–5 s, carbon cathode
20. 2 mL H_2SO_4 and 98 mL H_2O	Etch first with glyceregia to dissolve matrix uniformly; then etch electrolytically at 6–12 V dc, 0.12–0.15 A/cm^2 (0.75-1.0 A/in.^{2}) until edge of specimen is brownish; good for TEM replica studies
21. 5 mL HF, 10 mL glycerol, 10–50 mL ethanol, H_2O to 100 mL total volume	Etch first with glyceregia to dissolve matrix uniformly; then etch with solution at left to dissolve γ′; use at 6–12 V dc, 0.12–0.15 A/cm^2 (0.75–1.0 A/in.^{2}) for less than 1 s; good for TEM replica work or SEM examination

dc, direct current. (a) When water is specified, use distilled water.

Table 5 Electropolishing solutions for TEM thin foils of wrought heat resistant alloys

Composition	Comments
1. 950 mL acetic acid and 50 mL $HClO_4$	Popular electropolish for wrought superalloys for perforation; use at 70–80 V dc, 100–120 mA, 15 °C (60 °F)
2. 133 mL acetic acid, 25 g CrO_3, 7 mL H_2O	Best for window method; opacity makes jet thinning difficult; use at 10–12 V dc, 20 °C (70 °F)
3. 77 mL acetic acid and 23 mL $HClO_4$	For cobalt-base superalloys; keep temperature below 30 °C (85 °F), stainless steel cathode; used with the window method; use at 22 V dc, 0.08 A/cm^2 (0.5 A/in.^{2})
4. 600 mL methanol, 250 mL butanol, 60 mL $HClO_4$	Two step procedure: (a) 0.13 mm (0.005 in.) disk, polished 15–30 min at 30 V; (b) final thinning at 16–24 V; use at –60 to –70 °C (–75 to –95 °F)

Microstructures of Wrought Heat Resistant Alloys

Wrought heat resistant alloys are designed for use above approximately 540 °C (1000 °F). In general, they have an austenitic (γ-phase) matrix and contain a wide variety of secondary phases. The most common second phases are metal carbides (MC, $M_{23}C_6$, M_6C, and M_7C_3) and γ′, the ordered face-centered cubic (fcc) strengthening phase $Ni_3(Al,Ti)$ found in iron-nickel-base and nickel-base superalloys. In alloys containing niobium or niobium and tantalum, the primary strengthening phase is γ″, a body-centered tetragonal (bct) phase. Other phases, generally undesirable, may be observed due to variations in composition or processing or due to high-temperature exposure. Included in this group are orthorhombic δ-phase (Ni_3Nb), σ-phase, Laves, and the hexagonal close-packed (hcp) η-phase (Ni_3Ti). Nitrides are also commonly observed, and borides may be present in some alloys.

The physical metallurgy of these systems is extremely complex, perhaps more challenging than that of any other alloy system. In addition, as demonstrated in Table 1, the compositions of these alloys are complex as well. In general, the iron-nickel-base alloys tend toward formation of tcp phases, such as σ, μ, Laves, and χ phase. The nickel-base alloys are prone to precipitation of ordered geometrically close-packed (gcp) phases, such as γ′ and η. Such phases are not common in cobalt-base alloys, because γ′ is not a suitable strengthening agent. The cobalt-base alloys contain various carbides, nitrides, σ, and μ, depending on composition, processing, and exposure conditions.

References 41 to 52 provide basic review articles on the physical metallurgy of nickel-base, iron-base, and cobalt-base heat resistant superalloys. Similar information can also be found in the article "Superalloys" in this Handbook.

Iron-Nickel-Base Alloys. Several types of iron-nickel-base alloys have been developed.

Table 6 Techniques for bulk electrolytic extractions

Solution	Comments
1. 10% HCl in methanol	For extraction of carbides, borides, topologically close-packed phases, and geometrically close-packed phases from nickel-base and iron-nickel-base alloys; solution may dissolve Ni_3Ti; maintain bath at 0–30 °C (32–85 °F); for alloys containing tungsten, niobium, tantalum, or hafnium, add 1% tartaric acid; use 0.05–0.1 A/cm^2 (0.33–0.65 A/in.^{2}) for 4 h or longer (additional details in ASTM E 963)
2. 0.5–2% citric acid and $(NH_4)_2SO_4$ in H_2O (1% of each is most common)	Used to extract γ′ phase in nickel-base Udimet 700; use at 0.03 A/cm^2 (0.2 A/in.^{2}) for 3 h at room temperature; minor amounts of carbides and borides will also be extracted (additional details in Ref 35–38)
3. 10 or 20% H_3PO_4 in H_2O	Used to extract γ′ in nickel-base alloys; may etch the γ′ phase, although results have been contradictory
4. 50 mL HNO_3, 20 mL $HClO_4$, 1000 mL H_2O	For extraction of γ′ and η in nickel-base superalloys; use at 0.1 A/cm^2 (0.65 A/in.^{2}), 25 °C (75 °F)
5. 300 g KCl (potassium chloride), 30 g citric acid, 50 mL HCl, 1000 mL H_2O	For extraction of carbides from nickel-base superalloys; use at 0.1 A/cm^2 (0.65 A/in.^{2}), 25 °C (75 °F)

These alloys contain at least 10% Fe, but generally 18 to approximately 55%. The most important iron-nickel-base alloys are those with an austenitic matrix that are strengthened by γ′, such as A-286. Some of these alloys are quite similar to wrought austenitic stainless steels with the addition of the γ′ strengthening agent; therefore, metallographic procedures for these alloys are identical to those for wrought austenitic stainless steels. Other iron-nickel-base alloys, such as Inconel 718, contain less iron plus additions of niobium and tantalum to obtain strengthening from γ″. Another group of iron-nickel-base alloys contains rather high carbon contents and is strengthened by carbides, nitrides, carbonitrides, and solid-solution strengthening. Other iron-nickel-base alloys, such as Hastelloy X, derive most of their strength from solid-solution alloying, with a minor influence from carbide precipitation.

Nickel-Base Alloys. Nickel-base high-temperature alloys are basically of two types: solid solution and precipitation hardenable (PH). The solid-solution alloys contain little or no aluminum, titanium, or niobium; the PH alloys contain several percent aluminum and titanium. A few PH alloys contain substantial niobium.

The age-hardenable alloys are strengthened by γ′ precipitation by the addition of aluminum and titanium, by carbide, and by solid-solution alloying. The nature of the γ′ is of primary importance in obtaining optimum high-temperature properties. Compositionally, the aluminum and titanium content and the aluminum/titanium ratio are very important, as is heat treatment. Increasing the aluminum/titanium ratio improves high-temperature properties. The volume fraction, size, and spacing of γ′ are important parameters to control. Alloys with low amounts of γ′ require greater attention to γ′ spacing than alloys with high amounts. Other factors, such as coherency strain due to the lattice mismatch between γ and γ′, appear to be important in certain alloys, such as Waspaloy.

Grain size is an important microstructural parameter. Fine grain sizes normally provide superior room-temperature properties, such as toughness, strength, and fatigue resistance. Coarse grain sizes generally yield better creep resistance at elevated temperatures, although properties under other types of loading may suffer. Duplex grain structures generally are undesirable. Grain size also affects carbide precipitation at the grain boundaries. Coarse grain sizes have less grain-boundary surface area; therefore, carbide precipitation will be more continuous and thicker, thus impairing properties. Due to these problems, a uniform, intermediate grain size is generally preferred.

Cobalt-Base Alloys. Cobalt-base superalloys are strengthened by solid-solution alloying and carbide precipitation. The grain-boundary carbides inhibit grain-boundary sliding. Unlike the iron-nickel-base and nickel-base alloys, no intermetallic phase has been found that will strengthen cobalt-base alloys to the same degree that γ′ or γ″ strengthens the other superalloys. Gamma is not stable at high temperatures in cobalt-base alloys. The carbides in cobalt-base superalloys are the same as those in the other systems.

Phases in Wrought Heat Resistant Alloys

The microconstituents observed in iron-nickel and nickel-base wrought heat resistant superalloys are identical, with a few exceptions. The cobalt-base alloys are not strengthened by precipitated intermetallics but share many common features. All the alloys have an austenitic (γ phase) matrix that is strengthened by solid-solution alloying and by carbide precipitation. Most of the phases discussed subsequently have some degree of solubility for other elements; therefore, their true compositions will vary from alloy to alloy and may be altered by heat treatment and thermal exposure. Not all phases permit substitution, however. Eta phase (Ni_3Ti) has no significant solubility for other elements. Table 7 summarizes data on the commonly encountered constituents in these alloys.

Gamma prime, a gcp phase, has an ordered fcc $L1_2$ crystal structure and is Ni_3Al or Ni_3(Al,Ti), although considerable elemental substitution occurs. For example, cobalt and chromium will replace some of the nickel, and titanium will replace part of the aluminum. Iron can replace nickel or aluminum. The lattice parameters of γ and γ′ are similar, resulting in coherency, which accounts for the value of γ′ as the principal strengthening agent in iron-nickel-base and nickel-base superalloys.

Gamma prime is spherical in iron-nickel-base and in some of the older nickel-base alloys, such as Nimonic 80A and Waspaloy. In the more recently developed nickel-base alloys, γ′ is generally cuboidal. Experiments have shown that variations in molybdenum content and in the aluminum/titanium ratio can change the morphology of γ. With increasing γ/γ′ mismatch, the shape changes in the following order: spherical, globular, block, and cuboidal (Ref 53). When the γ/γ′ lattice mismatch is high, extended exposure above 700 °C (1290 °F) causes undesirable η (Ni_3Ti) or δ (Ni_3Nb) phases to form.

The volume fraction, size, and distribution of γ′ are important parameters for control of properties. The volume fraction of γ′ increases with the addition of aluminum and titanium, but the amounts of each must be carefully controlled. Gamma prime contents above approximately 45% render the alloy difficult to deform by hot or cold working. In the iron-nickel-base alloys, the volume fraction of γ′ phase is less than 0.2%, and it is usually spherical. Optimum strength results when the γ′ is in the size range of 0.01 to 0.05 μm, much too small to be seen using the optical microscope. If the aluminum/titanium ratio is equal to or greater than 1, extended high-temperature exposure results in replacement of γ′ by Ni_2AlTi, NiAl, or Ni(Al,Ti). These phases overage rapidly at moderately high temperatures, forming massive platelike precipitates.

Alloys with γ′ contents below 20%, such as Nimonic 80A, are heat treated using a simple two-step process of solution annealing and aging. The solution anneal recrystallizes the austenite matrix and dissolves any γ′ and $M_{23}C_6$ carbides present. Aging precipitates γ′ uniformly throughout the matrix and precipitates $M_{23}C_6$ carbides at grain and twin boundaries. Alloys with γ′ contents of approximately 30%, such as Waspaloy or Udimet 500, are solution treated, then given two aging treatments. Alloys with 40 to 45% γ′, such as Udimet 700, are solution treated, then given three aging treatments.

Positive identification of γ′ is usually performed by x-ray diffraction of the residue of bulk extractions or by electron diffraction using extraction replicas. Some of the electrolytes that selectively attack γ′ can be quite useful, because the γ′ will be recessed below the matrix, and the other second phases will be in relief or plane with the surface depending on the preparation procedure.

Gamma double prime has an ordered bct $D0_{22}$ crystal structure with an Ni_3Nb composition and is found in iron-nickel-base alloys containing niobium. It gained prominence as the strengthening phase with the introduction of Inconel 718 (Ref 54). Early studies of the strengthening mechanism produced conflicting results until the precise details of γ″-phase for-

Table 7 Constituents observed in wrought heat resistant alloys

Phase	Crystal structure	Lattice parameter, nm	Formula	Comments
γ′	fcc (ordered $L1_2$)	0.3561 for pure Ni_3Al to 0.3568 for $Ni_3(Al_{0.5}Ti_{0.5})$	Ni_3Al; Ni_3(Al, Ti)	Principal strengthening phase in many nickel-base and nickel-iron-base superalloys; crystal lattice varies slightly in size (0 to 0.5%) from that of austenite matrix; shape varies from spherical to cubic; size varies with exposure time and temperature
η	hcp ($D0_{24}$)	a_0 = 0.5093; c_0 = 0.8276	Ni_3Ti (no solubility for other elements)	Found in iron-, cobalt-, and nickel-base superalloys with high titanium/aluminum ratios after extended exposure; may form intergranularly in a cellular form or intragranularly as acicular platelets in a Widmanstätten pattern
γ″	bct (ordered $D0_{22}$)	a_0 = 0.3624; c_0 = 0.7406	Ni_3Nb	Principal strengthening phase in Inconel 718; γ″ precipitates are coherent disk-shaped particles that form on the {100} planes (avg diam approximately 600 Å, thickness approximately 50 to 90 Å); metastable phase
Ni_3Nb (δ)	Orthorhombic (ordered Cu_3Ti)	a_0 = 0.5106–0.511; b_0 = 0.421–0.4251; c_0 = 0.452–0.4556	Ni_3Nb	Observed in overaged Inconel 718; has an acicular shape when formed between 815 and 980 °C (1500 and 1800 °F); forms by cellular reaction at low aging temperatures and by intragranular precipitation at high aging temperatures
MC	Cubic	a_0 = 0.430–0.470	TiC; NbC; HfC	Titanium carbide has some solubility for nitrogen, zirconium, and molybdenum; composition is variable; appears as globular, irregularly shaped particles that are gray to lavender; "M" elements can be titanium, tantalum, niobium, hafnium, thorium, or zirconium
$M_{23}C_6$	fcc	a_0 = 1.050–1.070 (varies with composition)	$Cr_{23}C_6$; $(Cr,Fe,W,Mo)_{23}C_6$	Form of precipitation is important; it can precipitate as films, globules, platelets, lamellae, and cells; usually forms at grain boundaries; "M" element is usually chromium, but nickel-cobalt, iron, molybdenum, and tungsten can substitute
M_6C	fcc	a_0 = 1.085–1.175	Fe_3Mo_3C; Fe_3W_3C-Fe_4W_2C; Fe_3Nb_3C; Nb_3Co_3C; Ta_3Co_3C	Randomly distributed carbide; may appear pinkish; "M" elements are generally molybdenum or tungsten; there is some solubility for chromium, nickel-niobium, tantalum, and cobalt
M_7C_3	Hexagonal	a_0 = 1.398; c_0 = 0.4523	Cr_7C_3	Generally observed as a blocky intergranular shape; observed only in alloys such as Nimonic 80A after exposure above 1000 °C (1830 °F), and in some cobalt-base alloys
M_3B_2	Tetragonal	a_0 = 0.560–0.620; c_0 = 0.300–0.330	Ta_3B_2; V_3B_2; Nb_3B_2; $(Mo,Ti,Cr,Ni,Fe)_3B_2$; Mo_2FeB_2	Observed in iron-nickel-base and nickel-base alloys with about 0.03% B or greater; borides appear similar to carbides, but are not attacked by preferential carbide etchants; "M" elements can be molybdenum, tantalum, niobium, nickel, iron, or vanadium
MN	Cubic	a_0 = 0.4240	TiN; (Ti,Nb,Zr)N; (Ti,Nb, Zr) (C,N); ZrN; NbN	Nitrides are observed in alloys containing titanium, niobium, or zirconium; they are insoluble at temperatures below the melting point; easily recognized as-polished, having square to rectangular shapes and ranging from yellow to orange
μ	Rhombohedral	a_0 = 0.475; c_0 = 2.577	Co_7W_6; $(Fe, Co)_7(Mo, W)_6$	Generally observed in alloys with high levels of molybdenum or tungsten; appears as coarse, irregular Widmanstätten platelets; forms at high temperatures
Laves	Hexagonal	a_0 = 0.475–0.495; c_0 = 0.770–0.815	Fe_2Nb; Fe_2Ti; Fe_2Mo; Co_2Ta; Co_2Ti	Most common in iron-base and cobalt-base superalloys; usually appears as irregularly shaped globules, often elongated, or as platelets after extended high-temperature exposure
σ	Tetragonal	a_0 = 0.880–0.910; c_0 = 0.450–0.480	FeCr; FeCrMo; CrFeMoNi; CrCo; CrNiMo	Most often observed in iron-base and cobalt-base superalloys, less commonly in nickel-base alloys; appears as irregularly shaped globules, often elongated; forms after extended exposure between 540 and 980 °C (1005 and 1795 °F)

mation, composition, crystallography, and stability were determined (Ref 55–60).

Gamma double prime has a disk-shaped morphology and precipitates with a well-defined relationship to the austenite matrix:

$$[001]_{\gamma''} \parallel \langle 001\rangle_{\gamma} \text{ and } \{100\}_{\gamma''} \parallel \{100\}_{\gamma}$$

Strengthening is due to the coherency strains produced by the low degree of γ′/γ′ lattice mismatch. Although γ″ and γ′ are present in Inconel 718 after aging, the amount of γ′ is much less, and γ″ is the primary strengthening agent. Other alloys strengthened by γ″ include Inconel 706 and Udimet 630.

Because γ″ is not a stable phase, application of alloys such as Inconel 718 is restricted to below 700 °C (1290 °F). Above this temperature, extended exposure produces a loss of strength due to rapid coarsening of γ″, solutioning of γ″ and γ′, and formation of the stable orthorhombic form of Ni_3Nb, which has an acicular, platelike shape.

Positive identification of bct γ″ is more difficult than γ′, because x-ray diffraction of bulk extraction residues will not detect γ″. The failure to detect bct γ″ is attributed to line broadening due to the very fine particle size that obscures the peaks of interest (Ref 57). Electron diffraction will, however, detect the superlattice lines of bct γ″. Bright-field TEM examination is unsatisfactory for resolving γ″ due to the high density of the precipitates and the strong contrast from the coherency strain field around the precipitates. However, dark-field TEM examination provides excellent imaging of the γ″ by selective imaging of precipitates that produce specific superlattice reflections (Ref 57). In addition, γ″ can be separated from γ′ using the dark-field mode, because the γ″ dark-field image is substantially brighter than that of γ′ (Ref 57).

Eta phase has a hexagonal $D0_{24}$ crystal structure with a Ni_3Ti composition. Eta can form in iron-nickel-base, nickel-base, and cobalt-base superalloys, especially in grades with high titanium/aluminum ratios that have had extended high-temperature exposure. Eta phase has no solubility for other elements and will grow more rapidly and form larger particles than γ′, although it precipitates slowly. Coarse η can be observed using the optical microscope.

Two forms of η may be encountered. The first develops at grain boundaries as a cellular constituent similar to pearlite, with alternate lamellae of γ and η; the second, intragranularly as platelets with a Widmanstätten pattern (Ref 61–63). The cellular form is detrimental to notched stress-rupture strength and creep ductility, and the Widmanstätten pattern impairs stress-rupture strength but not ductility. Eta phase is relatively easy to identify due to its characteristic appearance. Most of the general-purpose reagents will reveal η, as will x-ray diffraction of bulk-extracted residues.

Carbides, which are important constituents, are present in all the wrought heat resistant superalloys. Four basic types are encountered: MC, $M_{23}C_6$, M_6C, and M_7C_3 (where M represents one or more metallic elements). Carbides in these alloys serve three principal functions. First, grain-boundary carbides, when properly formed, strengthen the grain boundary, prevent or retard grain-boundary sliding, and permit stress relaxation. Second, if fine carbides are precipitated in the matrix, strengthening results. This is important in cobalt-base alloys that cannot be strengthened by γ′. Third, carbides can tie up certain elements that would otherwise promote phase instability during service. Carbide precipitation in nickel-base alloys has a stronger tendency to form at grain boundaries than in iron-nickel-base or cobalt-base alloys. Although grain-boundary carbides, depending on their morphology, can degrade properties, reducing carbon content to low levels substantially reduces creep life and ductility in nickel-base alloys.

Aging of iron-nickel-base and nickel-base superalloys causes $M_{23}C_6$ to form at the grain boundaries. The optimum situation is a chain of discrete globular $M_{23}C_6$ particles at the grain boundaries. This form benefits creep-rupture life. However, if the carbides precipitate as a

continuous grain-boundary film, properties will be seriously degraded. It is not uncommon to observe zones around the grain boundaries that are devoid of γ'. Such precipitate-free zones can significantly influence stress-rupture life, depending on the width of the zones (Ref 64).

In these alloys, MC-type carbide is most frequently titanium carbide; other types, such as niobium carbide, tantalum carbide, or hafnium carbide, are less common. Titanium carbide has some solubility for other elements, such as nitrogen, zirconium, and molybdenum. They are large, globular particles observable on the as-polished surface, particularly if some relief is introduced during final polishing. Metal carbides usually are irregular in shape or cubic. They can be preferentially colored by certain etchants.

The most important carbide in superalloys is $M_{23}C_6$, because it forms at the grain boundaries during aging and, when properly formed, increases the strength of the grain boundaries to balance the matrix strength. Although chromium is the primary "M" element, other metallic elements, such as nickel, cobalt, iron, molybdenum, and tungsten, can substitute for it. The discrete globular form is the most desirable morphology; films, platelets, lamellae, and cells have also been observed.

The M_6C carbide is generally rich in molybdenum or tungsten, but other elements such as chromium, nickel, or cobalt, may substitute for it to some degree. It is the most commonly observed carbide in the cobalt-base superalloys and in nickel-base alloys with high molybdenum and/or tungsten contents. In these alloys, M_6C is often observed in the as-cast condition randomly distributed throughout the matrix. In wrought alloys, it will usually be dissolved during heating before hot working. It may precipitate at the grain boundaries in a blocky form or intragranularly in a Widmanstätten pattern and can be preferentially stained by certain etchants.

Although M_7C_3 is not widely observed in superalloys, it is present in some cobalt-base alloys and in Nimonic 80A, a nickel-chromium-titanium-aluminum superalloy, when heated above 1000 °C (1830 °F). Additions of such elements as cobalt, molybdenum, tungsten, or niobium to nickel-base alloys prevents formation of M_7C_3. Massive Cr_7C_3 is formed in Nimonic 80A in the grain boundaries after heating to 1080 °C (1975 °F). Subsequent aging at 700 °C (1290 °F) to precipitate γ' impedes precipitation of $M_{23}C_6$ due to the previously formed Cr_7C_3, which generally exhibits a blocky shape when present at grain boundaries.

Borides. Boron is added in small amounts to many superalloys to improve stress-rupture and creep properties or to retard formation of η phase, which would impair creep strength. Boron retards formation of the cellular grain boundary form of η, but has no influence on the intragranular Widmanstätten η. Consequently, boron influences grain-boundary structures. Boron also reduces the solubility of carbon in austenite, which increases precipitation of finer-sized MC and $M_{23}C_6$ carbides. If the boron addition is sufficiently high, detrimental borides will form. Borides are hard and brittle and precipitate at the grain boundaries. Borides are generally of M_3B_2 composition with a tetragonal structure (Ref 65). Molybdenum, tantalum, niobium, nickel, iron, or vanadium can be "M" elements. The identification of borides in Udimet 700 has been documented (Ref 65).

Laves phase, a tcp phase, has a $MgZn_2$ hexagonal crystal structure with a composition of the AB_2 type. Typical examples include Fe_2Ti, Fe_2Nb, and Fe_2Mo, but a more general formula is $(Fe,Cr,Mn,Si)_2(Mo,Ti,Nb)$. They are most commonly observed in the iron-nickel-base alloys as coarse intergranular particles; intragranular precipitation may also occur. Silicon and niobium promote formation of Laves phase in Inconel 718. Excessive amounts will impair room-temperature tensile ductility; creep properties are not significantly affected. Laves phases have been observed in certain cobalt-base alloys and have been identified as Co_2W, Co_2Ti, or Co_2Ta.

Sigma phase is a tetragonal intermetallic tcp phase that forms with a wide range of compositions. Various morphologies may be encountered, some of which are quite detrimental to properties. However, the presence of σ in superalloys is not necessarily damaging to properties. Sigma in the form of platelets or as a grain-boundary film is detrimental, but globular intragranular precipitation can improve creep properties.

Considerable effort has been devoted to determining how composition influences σ-phase formation, particularly in nickel-base superalloys. References 66 to 70 present examples of the many studies that have been conducted. This work has substantially influenced alloy development.

Sigma can be preferentially attacked or stained by a number of reagents. However, because of the wide range of alloy compositions that may contain σ and the variable nature of its composition, positive identification by etching is not always possible. X-ray diffraction of bulk extraction residues is a more reliable technique. Etching procedures are best applied when they can be tested for response on specimens of the alloy known to contain σ-phase.

Mu phase is a rhombohedral (triagonal) intermetallic tcp phase with a W_6Fe_7 structure (Ref 71). In general, it has little influence on properties. Mu precipitates as coarse, irregularly shaped platelets in a Widmanstätten pattern. A general formula for μ is $(Fe,Co)_7(Mo,W)_6$. Nickel can substitute for part of the iron or the cobalt.

Nitrides are commonly observed in superalloys containing titanium or niobium as titanium nitride (most common) or niobium nitride. Nitrides are not influenced by heat treatment and are insoluble to the melting point. Nitrides are easily identified in the as-polished condition or after etching due to their regular, angular shapes and distinct yellow-to-orange color. Nitrides are quite hard and will appear in relief after polishing. They have some solubility for carbon and may be referred to as Ti(C,N),Nb(C,N), and so on. They should not be confused with carbonitrides, which are much richer in carbon and lower in nitrogen. Nitrides, often duplex, include an embedded phase or a surrounding film; this second phase is generally a darker colored nitride containing considerable carbon. The usual amounts present in superalloys generally have little influence on properties.

Other Phases. A few other phases are less frequently observed in wrought heat resistant alloys. For example, a few cobalt-base alloys have been developed that attain some degree of strengthening by precipitation of intermetallic phases, such as CoAl, Co_3Mo, or Co_3Ti. In alloys similar to A-286, G phase (Ni_{18}-Ti_8Si_6) has been observed (Ref 72, 73). This phase has a globular shape and precipitates in grain boundaries. It is detrimental to stress-rupture life. A chromium-iron niobide, Z phase, has been observed in an Fe-18Cr-12Ni-1Nb alloy after creep testing at 850 °C (1560 °F) (Ref 74). Inclusions, some of which are similar to those found in steels, can also be found in these alloys. However, in the nickel-base alloys, titanium sulfides may be observed. Oxides, such as Al_2O_3 or magnesia, may also be present. Oxides and sulfides may be observed at the surface of components due to environmental effects. Coatings are also used on some alloys, and their microstructures may be of interest (Ref 75, 76). Coatings are described in the article "High-Temperature Coatings for Superalloys" in this Handbook.

ACKNOWLEDGMENTS

This article was adapted from the following:

- Heat-Resistant Casting Alloys, Wrought Heat-Resistant Alloys, *Metallography and Microstructures*, Vol 9, *ASM Handbook*, ASM International, 1985, p 330–350
- G.F. Vander Voort and H.M. James, Wrought Heat-Resistant Alloys, *Metallography and Microstructures*, Vol 9, *ASM Handbook*, ASM International, 1985, p 305–329

REFERENCES

1. G.F. Vander Voort, *Metallography: Principles and Practice*, McGraw-Hill, 1984
2. C.E. Smeltzer, Solve Steel "Freckle" Mystery, *Iron Age*, Vol 184, 10 Sept 1959, p l88–189
3. G.C. Gould, Freckle Segregation in Vacuum Consumable-Electrode Ingots, *Trans. AIME*, Vol 233, July 1965, p 1345–1351
4. J. Preston, Segregation in Vacuum-Arc-Melted Alloy Steel Ingots, *International Trans. Vacuum Metallurgy Conf. 1967*, American Vacuum Society, New York, 1968, p 569–588

5. R.C. Buehl and J.K. McCauley, Processing Improvement in Vacuum-Arc Remelting of Ingots, *International Trans. Vacuum Metallurgy Conf. 1967*, American Vacuum Society, New York, 1968, p 695–709
6. A.F. Giamei and B.H. Kear, On the Nature of Freckles in Nickel Base Superalloys, *Metall. Trans.*, Vol 1, Aug 1970, p 2185–2192
7. R. Schlatter, Electrical and Magnetic Interactions in Vacuum-Arc Remelting and Their Effect on the Metallurgical Quality of Specialty Steels, *J. Vac. Sci. Technol.*, Vol 11, Nov/Dec 1974, p 1047–1054
8. R.L. Anderson, "Revealing Microstructures in Metals," Westinghouse Research Laboratory Scientific Paper 425-C000-P2, 22 Dec 1961
9. G. Petzow, *Metallographic Etching*, American Society for Metals, 1978
10. C.H. Lund and H.J. Wagner, "Identification of Microconstituents in Superalloys," DMIC Memorandum 160, Battelle Memorial Institute, Columbus, OH, 15 Nov 1962
11. H.J. Beattie and F.L. Ver Snyder, Microconstituents in High Temperature Alloys, *Trans. ASM*, Vol 45, 1953 p 397–428
12. J.W. Weeton and R.A. Signorelli, Effect of Heat Treatment Upon Microstructures, Microconstituents, and Hardness of Wrought Cobalt Base Alloy, *Trans. ASM*, Vol 47, 1955, p 815–852
13. H. Meisel et al., Metallographic Development of the Structure of Nickel Based Alloys, *Pract. Metallog.*, Vol 17, 1980, p 261–272
14. F.R. Morral, Metallography of Cobalt-Base and Cobalt-Containing Alloys, *Pract. Metallog.*, Vol 10, 1973, p 398–413
15. E. Kohlhaas and A. Fischer, The Metallography of Superalloys, *Pract. Metallog.*, Vol 8, Jan 1971, p 3–25
16. W.C. Bigelow et al., Electron Microscopic Identification of the γ′ Phase of Nickel-Base Alloys, *Proc. ASTM*, Vol 56, 1956, p 945–953
17. L. Bartosiewicz, Preferential Electrolytic Etching Technique to Reveal the γ′ Phase in Nickel Base Alloys, *Pract. Metallog.*, Vol 10, 1973, p 450–461
18. P.K. Footner and B.P. Richards, A Rapid Method for Measurement of γ′ Size Distribution in Nickel-Base Superalloys, *Pract. Metallog.*, Vol 17, 1980, p 489–496
19. C.P. Sullivan, The Metallographic Identification of Borides in Udimet 700, *Trans. ASM*, Vol 58, 1965, p 702–705
20. G.N. Maniar and A. Szirmae, Ed., *Manual on Electron Metallography Techniques*, STP 547, ASTM, Philadelphia, 1973
21. I.S. Brammar and M.A.P. Dewey, *Specimen Preparation for Electron Metallography*, Blackwell Scientific, 1966
22. G. Thomas, *Transmission Electron Microscopy of Metals*, John Wiley & Sons, 1964
23. J.R. Mihalisin, The Selective Identification of Constituents in Nimonic 80 by Extraction-Replica Technique, *Trans. AIME*, Vol 212, June 1958, p 349–350
24. E. Kohlhaas and A. Fischer, The Use of the Carbon-Extraction Technique in Investigations of Superalloys, *Pract. Metallog.*, Vol 6, 1969, p 291–298
25. R.J. Seher and G.N. Maniar, Analytical-Preshadowed Extraction Replica Technique, *Metallography*, Vol 5, 1972, p 409–414
26. W.L. Mankins, Chromic Acid as an Electrolytic Etchant and Electrolyte for the Extraction of γ′ in Nickel-Base Superalloys, *Metallography*, Vol 9, 1976, p 227–232
27. A.J. Portner and B. Ralph, A Technique for the Replication of γ′ in Nickel-Base Superalloys, *Pract. Metallog.*, Vol 16, 1979, p 592–601
28. K.C. Thompson-Russell and J.W. Edington, *Electron Microscope Specimen Preparation Techniques in Materials Science*, Part 5, *Practical Electron Microscopy in Materials Science*, Philips Electronic Instruments, Eindhoven, Holland, 1977
29. L. Bartosiewicz, Improved Techniques of Thin Foil Preparation of Ni Base Alloys for Electron Microscopy, *Pract. Metallog.*, Vol 9, 1972, p 525–534
30. C. Hays and D.A. Nail, Transmission Electron Microscopy of Incoloy Alloy 901, *Metallography*, Vol 7, 1974, p 59–68
31. R.E. Schafrik and M. Henry, Transmission Electron Microscopy Foil Preparation and Results for Incoloy 901, *Metallography*, Vol 13, 1980, p 157–165
32. T.P. Hoar and K.W.J. Bowen, The Electrolytic Separation and Some Properties of Austenite and Sigma in 18-8-3-1 Chromium-Nickel-Molybdenum-Titanium Steel, *Trans. ASM*, Vol 45, 1953, p 443–474
33. J.F. Brown et al., The Extraction of Minor Phases from Austenitic Steel, *Metallurgia*, Vol 56, Nov 1957, p 215–223
34. K.W. Andrews and H. Hughes, *The Isolation, Separation, and Identification of Microconstituents in Steels*, STP 393, ASTM, Philadelphia, 1966, p 3–21
35. O.H. Kriege and C.P. Sullivan, The Separation of Gamma Prime from Udimet 700, *Trans. ASM*, Vol 61, 1968, p 278–282
36. O.H. Kriege and J.M. Baris, The Chemical Partitioning of Elements in Gamma Prime Separated from Precipitation-Hardened, High-Temperature Nickel-Base Alloys, *Trans. ASM*, Vol 62, 1969, p 195–200
37. M.J. Donachie and O.H. Kriege, Phase Extraction and Analysis in Superalloys—Summary of Investigations by ASTM Committee E-4 Task Group 1, *J. Mater.*, Vol 7, Sept 1972, p 269–278
38. O.H. Kriege, *Phase Separation as a Technique for the Characterization of Superalloys*, STP 557, ASTM, Philadelphia, 1974, p 220–234
39. E. Kny, On the Methodology of Phase Extraction in Ni-Base Superalloys, *Pract. Metallog.*, Vol 13, Nov 1976, p 549–564
40. "Practice for Electrolytic Extraction of Phases from Ni and Ni-Fe Base Superalloys Using a Hydrochloric-Methanol Electrolyte, E 963, *Annual Book of ASTM Standards*, ASTM, Philadelphia, 1984
41. C. Razim, Metallography of Heat Resistant and High Temperature Alloys, *Pract. Metallog.*, Vol 5, May 1968, p 225–241; June 1968, p 299–309
42. G.P. Sabol and R. Stickler, Microstructure of Nickel-Base Superalloys, *Phys. Status Solidi*, Vol 35 (No. 1), 1968, p 11–52
43. P.S. Kotval, The Microstructure of Superalloys, *Metallography*, Vol 1, 1969, p 251–285
44. F.R. Morral et al., Microstructure of Cobalt-Base High-Temperature Alloys, *ASM Met. Eng. Q.*, Vol 9, May 1969, p 1–16
45. J.F. Radavich and W.H. Couts, Metallography of the Superalloys, *Rev. High-Temp. Mater.*, Vol 1, Aug 1971, p 55–96
46. C.P. Sullivan and M.J. Donachie, Some Effects of Microstructure on the Mechanical Properties of Nickel-Base Superalloys, *ASM Met. Eng. Q.*, Vol 7, Feb 1967, p 36–45
47. R.F. Decker, Strengthening Mechanisms in Nickel-Base Superalloys, *Symposium: Steel-Strengthening Mechanisms*, 5-6 May 1969, Zurich, 1970, p 147–170
48. C.T. Sims and W.C. Hagel, Ed., *The Superalloys*, John Wiley & Sons, 1972
49. C.P. Sullivan et al., Relationship of Properties to Microstructure in Cobalt-Base Superalloys, *ASM Met. Eng. Q.*, Vol 9, May 1969, p 16–29
50. C.P. Sullivan and M.J. Donachie, Microstructures and Mechanical Properties of Iron-Base (-Containing) Superalloys, *ASM Met. Eng. Q.*, Vol 11, Nov 1971, p l–11
51. D.R. Muzyka, Controlling Microstructure and Properties of Superalloys Via Use of Precipitated Phases, *ASM Met. Eng. Q.*, Vol 11, Nov 1971, p 12–20
52. D.R. Muzyka and G.N. Maniar, *Microstructure Approach to Property Optimization in Wrought Superalloys*, STP 557, ASTM, Philadelphia, 1974, p 198–219
53. W.T. Loomis et al., The Influence of Molybdenum on the γ′ Phase in Experimental Nickel-Base Superalloys, *Metall. Trans.*, Vol 3, April 1972, p 989–1000
54. J.F. Barker, A Superalloy for Medium Temperatures, *Met. Prog.*, Vol 81, May 1962, p 72–76
55. I. Kirman and D.H. Warrington, Identification of the Strengthening Phase in Fe-Ni-Cr-Nb Alloys, *J. Iron Steel Inst.*, Vol 205, Dec 1967, p 1264–1265
56. P.S. Kotval, Identification of the Strengthening Phase in "Inconel" Alloy 718, *Trans. AIME*, Vol 242, Aug 1968, p 1764–1765
57. D.F. Paulonis et al., Precipitation in Nickel-Base Alloy 718, *Trans. ASM*, Vol 62, 1969, p 611–622
58. W.J. Boesch and H.B. Canada, Precipitation Reactions and Stability of Ni_3Cb in Inconel Alloy 718, *J. Met.*, Vol 21, Oct 1969, p 34–38

59. I. Kirman and D.H. Warrington, The Precipitation of Ni_3Nb Phases in a Ni-Fe-Cr-Nb Alloy, *Metall. Trans.*, Vol 1, Oct 1970, p 2667–2675
60. R. Cozar and A. Pineau, Morphology of γ′ and γ″ Precipitates and Thermal Stability of Inconel 718 Type Alloys, *Metall. Trans.*, Vol 4, Jan 1973, p 47–59
61. J.R. Mihalisin and R.F. Decker, Phase Transformations in Nickel-Rich Nickel-Titanium-Aluminum Alloys, *Trans. AIME*, Vol 218, June 1960, p 507–515
62. B.R. Clark and F.B. Pickering, Precipitation Effects in Austenitic Stainless Steels Containing Titanium and Aluminum Additions, *J. Iron Steel Inst.*, Vol 205, Jan 1967, p 70–84
63. L.K. Singhal and J.W. Martin, Precipitation Processes in an Austenitic Stainless Steel Containing Titanium, *J. Iron Steel Inst.*, Vol 205, Sept 1967, p 947–952
64. E.L. Raymond, Effect of Grain Boundary Denudation of Gamma Prime on Notch-Rupture Ductility of Inconel Nickel-Chromium Alloys X-750 and 718, *Trans. AIME*, Vol 239, Sept 1967, p 1415–1422
65. H.J. Beattie, The Crystal Structure of a M_3B_2-Type Double Boride, *Acta Crystallogr.*, Vol 11, 1958, p 607–609
66. L.R. Woodyatt et al., Prediction of Sigma-Type Phase Occurrence from Compositions in Austenitic Superalloys, *Trans. AIME*, Vol 236, 1966, p 519–527
67. E.O. Hall and S.H. Algie, The Sigma Phase, *Met. Rev.*, Vol 11, 1966, p 61–88
68. J.R. Mihalisin et al., Sigma—Its Occurrence, Effect, and Control in Nickel-Base Superalloys, *Trans. AIME*, Vol 242, Dec 1968, p 2399–2414
69. R.G. Barrows and J.B. Newkirk, A Modified System for Predicting σ Formation, *Metall. Trans.*, Vol 3, Nov 1972, p 2889–2893
70. E.S. Machlin and J. Shao, SIGMA-SAFE: A Phase Diagram Approach to the Sigma Phase Problem in Ni Base Superalloys, *Metall. Trans. A*, Vol 9, April 1978, p 561–568
71. A. Raman, The μ Phases, *Z. Metallkd.*, Vol 57, April 1966, p 301–305
72. H.J. Beattie and F.L. Ver Snyder, A New Complex Phase in a High-Temperature (Iron-Nickel-Chromium-Molybdenum) Alloy, *Nature*, Vol 178 (No. 4526), 1956, p 208–209
73. H.J. Beattie and W.C. Hagel, Intermetallic Compounds in Titanium-Hardened Alloys, *Trans. AIME*, Vol 209, July 1957, p 911–917
74. K.W. Andrews and H. Hughes, Discussion of Aging Reactions in Certain Superalloys, *Trans. ASM*, Vol 49, 1957, p 999
75. G.F. Slattery, Microstructural Aspects of Aluminized Coatings on Nickel-Base Alloys, *Met. Technol.*, Vol 10, Feb 1983, p 41–51
76. G.W. Goward et al., Formation and Degradation Mechanisms of Aluminide Coatings on Nickel-Base Superalloys, *Trans. ASM*, Vol 60, 1967, p 228–241

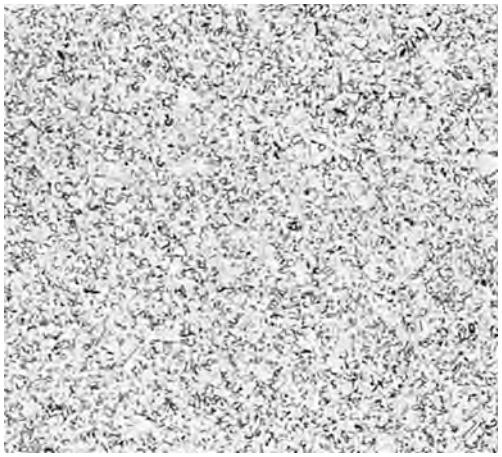


Fig. 1 Alloy A-286 (AISI 660, 195 HV), solution annealed 2 h at 900 °C (1650 °F) and oil quenched. Specimen has a very fine austenite grain size. Glyceregia. 100×



Fig. 2 Same alloy and processing as Fig. 1, but showing an area near the surface of the specimen with a duplex grain structure. Tint etch: 20 mL HCl, 100 mL H_2O, 2.4 g $NH_4F{\cdot}HF$, and 0.8 g $K_2S_2O_5$. 100×

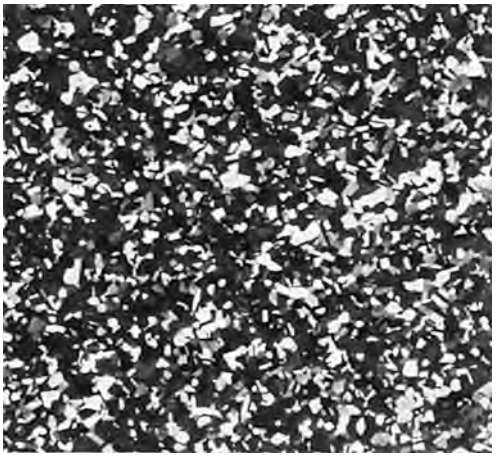


Fig. 3 Same alloy and processing as Fig. 1, showing the very fine austenite matrix grains. Tint etch: 20 mL HCl, 100 mL H_2O, 1 g $NH_4F{\cdot}HF$, 0.5 g $K_2S_2O_5$. 200×

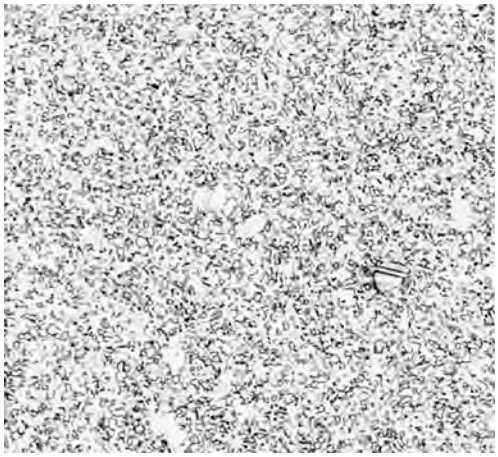


Fig. 4 Alloy A-286 (AISI 660, 357 HV), solution annealed 2 h at 900 °C (1650 °F), oil quenched, and held 16 h at 720 °C (1325 °F). A very fine-grained structure similar to that shown in Fig. 1. Glyceregia. 100×

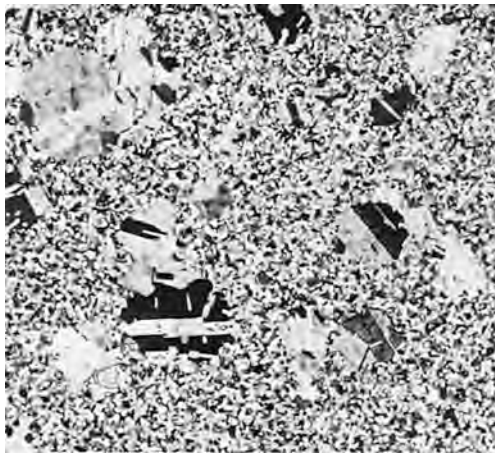


Fig. 5 Same alloy and processing as Fig. 4 but showing a region near the surface of the specimen with a fine grain structure. Tint etched same as Fig. 2. 100×

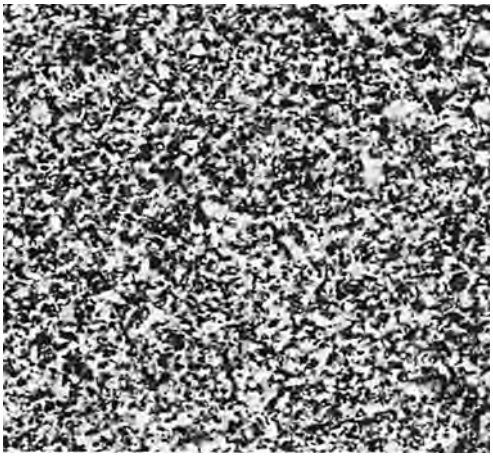


Fig. 6 Same alloy and processing as Fig. 4, showing the very fine matrix grain structure. Tint etched same as Fig. 2. 100×



Fig. 7 Alloy A-286 (AISI 660, 150 HV), solution annealed 1 h at 980 °C (1800 °F) and oil quenched, showing a coarser grain structure than that shown in Fig. 1 to 6 due to the higher solutionizing temperature. Glyceregia. 100×

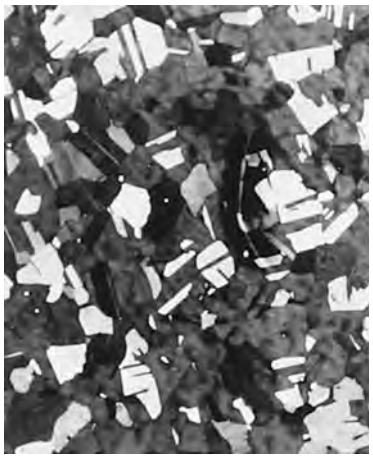


Fig. 8 Same alloy and processing as Fig. 7 but tint etched using 20 mL HCl, 100 mL H_2O, 1 g $NH_4F{\cdot}HF$, and 0.5 g $K_2S_2O_5$. 100×

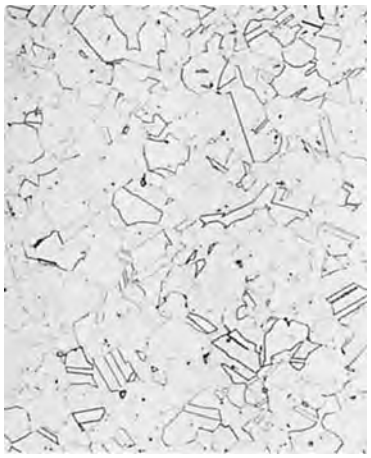


Fig. 9 Alloy A-286 (AISI 660, 318 HV), solution annealed 1 h at 980 °C (1800 °F), oil quenched, aged 16 h at 720 °C (1325 °F), and air cooled. Glyceregia. 100×



Fig. 10 Same alloy and processing as Fig. 9 but tint etched. Only the matrix phase has been colored. 20 mL HCl, 100 mL H_2O, 1 g $NH_4F{\cdot}HF$, and 0.5 g $K_2S_2O_5$. 100×

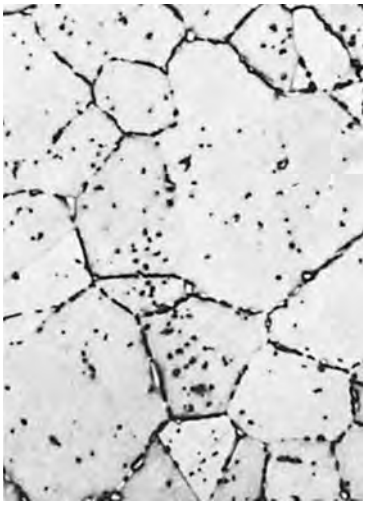


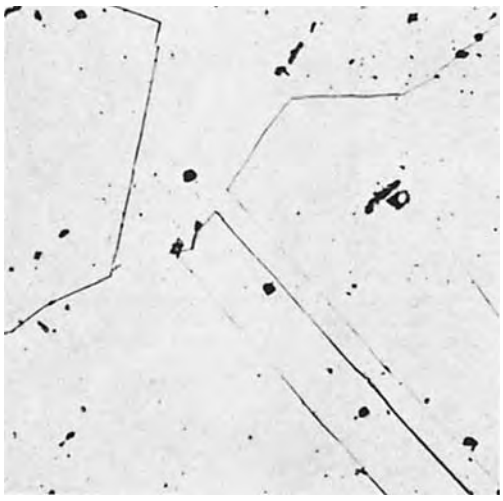


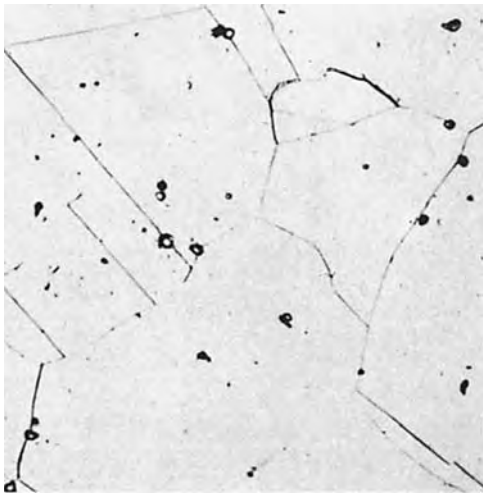


Fig. 11, 12, 13 A-286 (AISI 660), solution annealed 1 h at 980 ° C (1800 ° F) and aged 16 h at 720 ° C (1325 ° F), then air cooled and creep tested to rupture. Fig. 11: tested 7131 h at 650 °C (1200 °F). Matrix and grain-boundary precipitates have coalesced. 31.5 HRC. Fig. 12: tested 1232 h at 730 °C (1350 °F). Grain-boundary precipitates have coalesced; the matrix is darkened by γ′ precipitation. HRC 25.5. Fig. 13: tested 546 h at 815 °C (1500 °F). Grain-boundary precipitates have coalesced, and the averaged matrix contains needlelike η phase (Ni_3Ti). HRB 88.5. 15 mL HCl, 10 mL HNO_3, and 10 mL acetic acid. 1000×



Fig. 14 A-286 (AISI 660), showing lamellar or cellular precipitation of η phase (Ni_3Ti) caused by overaging or by insufficient boron. Cold working accelerates the response to aging. 15 mL HCl, 10 mL HNO_3, and 10 mL acetic acid. 1000×





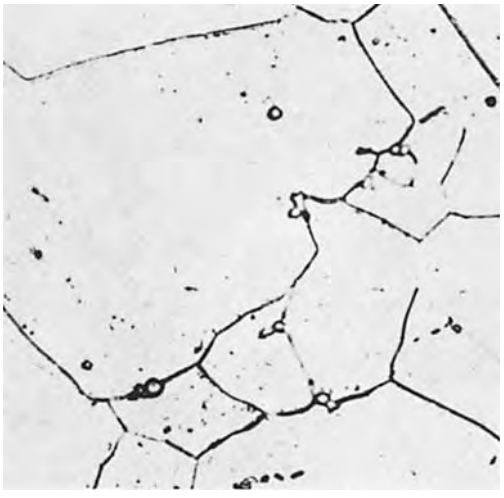


Fig. 15, 16, 17 Discaloy iron-nickel-base alloy (AISI 662), solution annealed 1 h at 1065 °C (1950 °F), showing the effects of different aging processes. Fig. 15: oil quenched; 139 HV. Fig. 16: aged 64 h at 650 °C (1200 °F); 249 HV. Fig. 17: aged 512 h at 650 °C (1200 °F); 315 HV. Glyceregia. 500×. (R.L. Anderson)

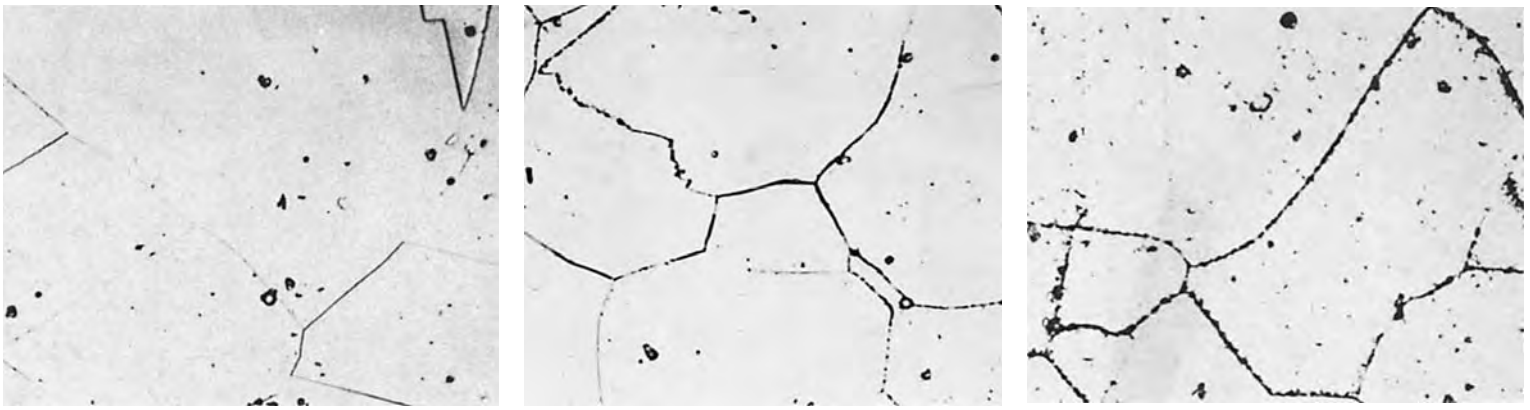


Fig. 18, 19, 20 Same material and solution annealing treatment as Fig. 15 to 17. Fig. 18: aged 2 h at 705 °C (1300 °F); 223 HV. Fig. 19: aged 64 h at 705 °C (1300 °F); 292 HV. Fig. 20: aged 272 h at 705 °C (1300 °F); 295 HV. Glyceregia. 500×. (R.L. Anderson)

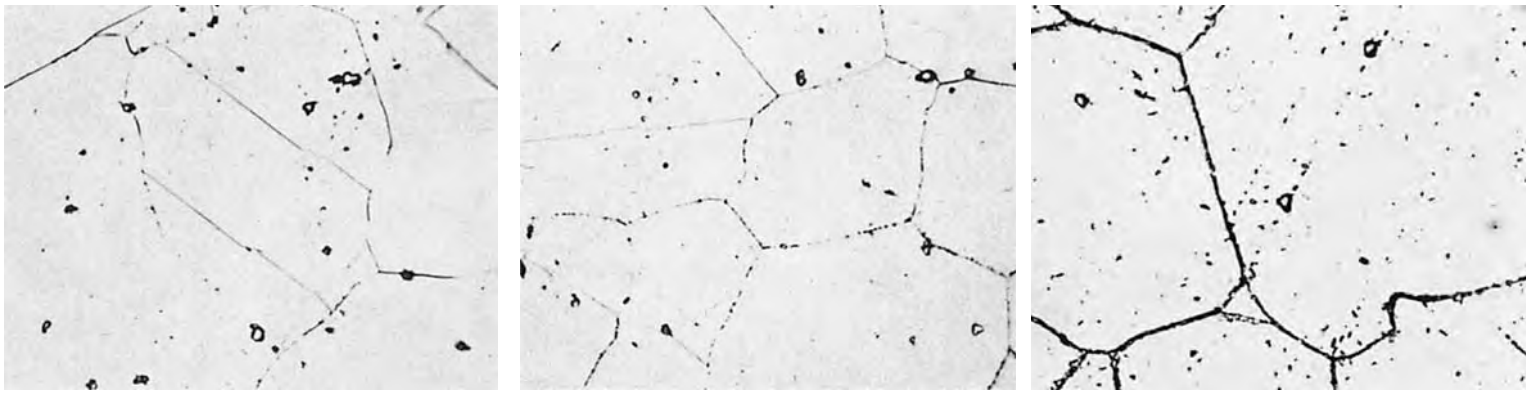


Fig. 21, 22, 23 Same material and solution annealing as Fig. 15 to 17. Fig. 21: aged 1 h at 760 °C (1400 °F); 248 HV. Fig. 22: aged 8 h at 760 °C (1400 °F);258 HV. Fig. 23: aged 128 h at 760 °C (1400 °F); 253 HV. Glyceregia. 500×. (R.L. Anderson)

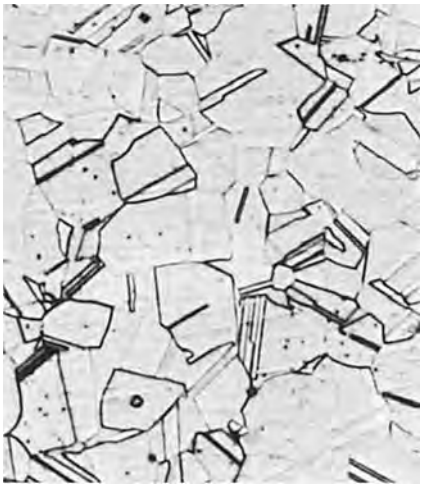


Fig. 24 Incoloy 800 strip in the mill-annealed condition. The microstructure consists of a solid-solution matrix in which some grains are delineated by precipitated carbide particles at the boundaries and by twinning lines. Glyceregia. 250×

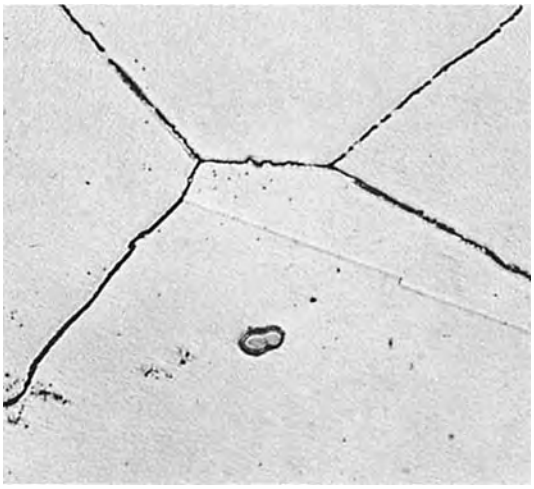


Fig. 25 Incoloy 901, solution annealed 2 h at 1065 °C (1950 °F), water quenched, aged 2 h at 800 °C (1475 °F), air cooled, aged 24 h at 730 °C (1350 °F), and air cooled. Structure is grain-boundary envelope and MC carbide (large particle) in a γ matrix. See also Fig. 26. 1:1 HCl and H_2O. 1000×

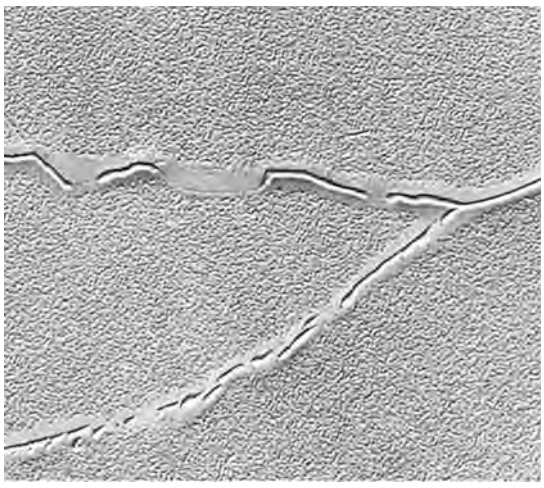


Fig. 26 Replica electron micrograph of the specimen in Fig. 25. The grain-boundary constituents (MC, M_3B_2, or both) contributed to low ductility. Note the grain-boundary depleted zone. The γ matrix contains γ′ precipitate. Electrolytic: H_2SO_4, H_3PO_4, and HNO_3. 10,000×

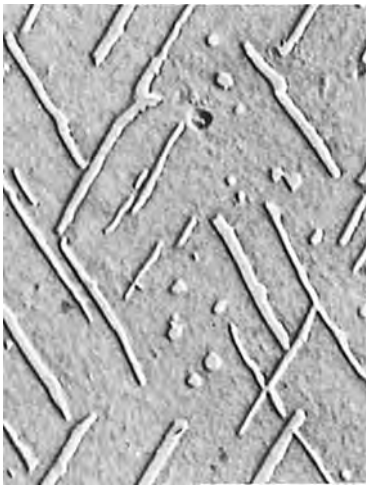


Fig. 27 Negative replica electron micrograph of Incoloy 901, creep tested to rupture at 138 MPa (20 ksi) for 7380 h at 730 °C (1350 °F). The needlelike constituent is η phase (Ni_3Ti); the remainder of the structure is γ′ in a γ matrix. Glyceregia. 15,000×



Fig. 28 N-155 (AISI 661), solution annealed 1 h at 1150 °C (2100 °F) and water quenched. Primary carbide particles are mostly dispersed within grains; some are at grain boundaries. 1:1 HCl and H_2O. 500×



Fig. 29 N-155 (AISI 661), solution annealed same as Fig. 28, then aged 5 h at 760 °C (1400 °F) and air cooled. Precipitated secondary carbide (M_6C or $M_{23}C_6$) at grain boundaries and within grains. 20% HCl, methanol, and 1% H_2O_2, 5 s. 500×



Fig. 30 16-25-6 (AISI 650) alloy, after forging between 650 and 705 °C (1200 and 1300 °F) and stress relieving. The solid-solution matrix exhibits bonding because of carbide segregation. See also Fig. 31 and 32. Marble's reagent. 100×

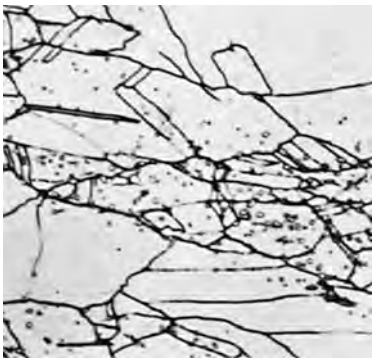


Fig. 31 Same alloy, forging temperature, and stress relief treatment as Fig. 30 but at a higher magnification to reveal the carbide segregation in banding. The matrix is austenitic solid solution. Marble's reagent. 500×

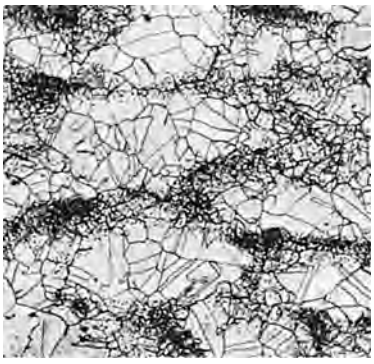


Fig. 32 Same alloy and processing as Fig. 30. Here the carbide segregation is dispersed, not banded, in the solid-solution matrix. Compare with Fig. 30. Marble's reagent. 100×

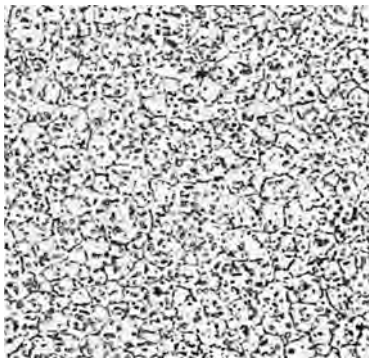


Fig. 33 Hastelloy X (AISI 680), solution annealed at 1065 °C (1950 °F) and aged 100 h at 760 °C (1400 °F). The structure is mixed carbide particles in a γ matrix. Electrolytic: oxalic acid. 500×

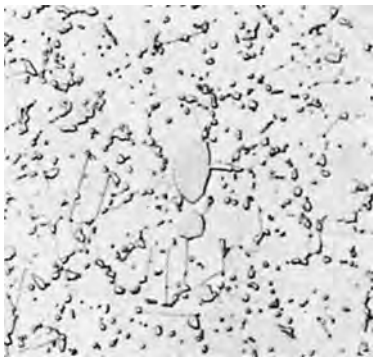


Fig. 34 Same alloy and processing as Fig. 33, shown at twice the magnification to reveal more clearly the carbide particles in the γ matrix. Electrolytic: oxalic acid. 1000×

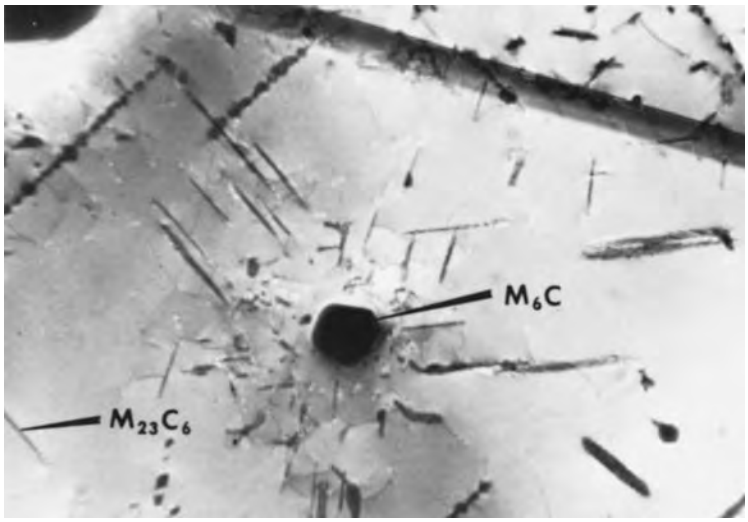


Fig. 35 Thin-foil transmission electron micrograph of Hastelloy X, solution annealed 1 h at 1175 ° C (2150 °F), water quenched, and aged 500 h at 705 °C (1300 °F). The structure is primarily M_6C and needlelike $M_{23}C_6$ carbides that have precipitated at dislocations generated around primary carbide. The matrix is γ solid solution. Not polished, not etched. 11,000×

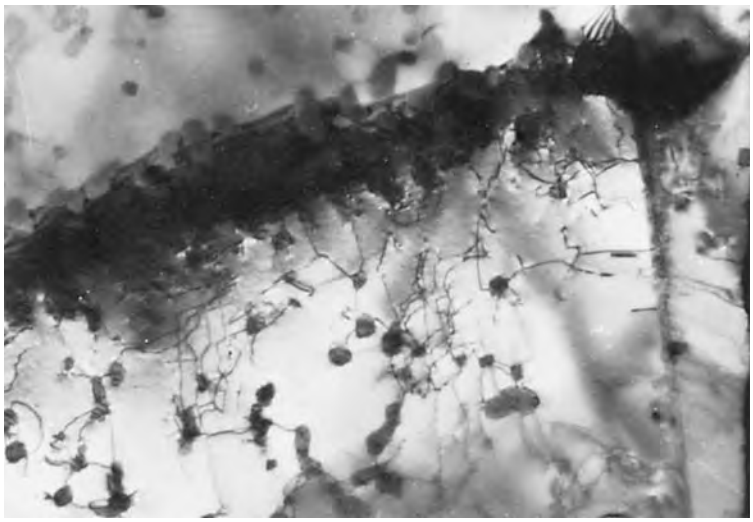


Fig. 36 Thin-foil transmission electron micrograph of Hastelloy X, solution annealed 1 h at 1175 °C (2150 °F), water quenched, deformed 2% by reduction at room temperature, and aged 144 h at 705 °C (1300 °F). Structure is a band of high dislocation density and precipitated $M_{23}C_6$ carbide at sites of high dislocation density and adjacent locations. Not polished, not etched. 40,000×

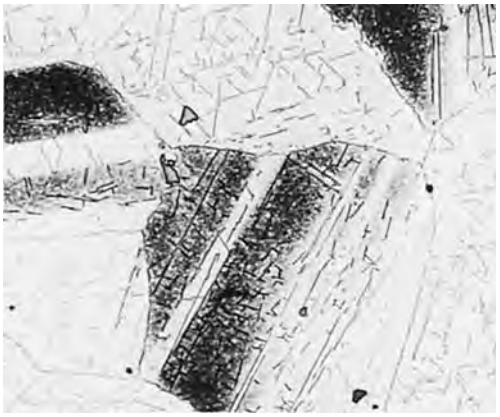


Fig. 37 Pyromet 31 alloy (325 HV), heat treated 1500 h at 815 °C (1500 °F) to form coarse needles of η (Ni_3Ti) phase. See also Fig. 38. Glyceregia. 400×

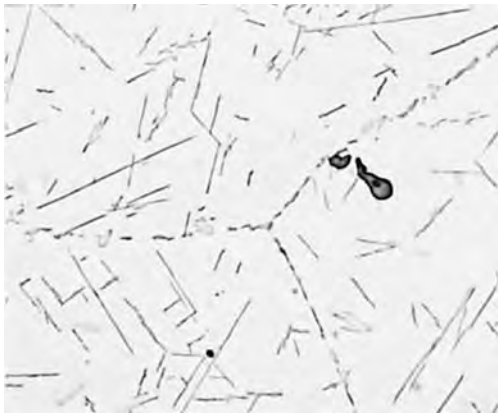


Fig. 38 Same as Fig. 37 but at a higher magnification. Parts of only a few grains are visible. Glyceregia. 1000×



Fig. 39 Pyromet 31 (260 HV), heat treated 4 h at 955 °C (1750 °F) to form needles of η (Ni_3Ti) phase. See also Fig. 37, 38, and 40. Glyceregia. 1000×

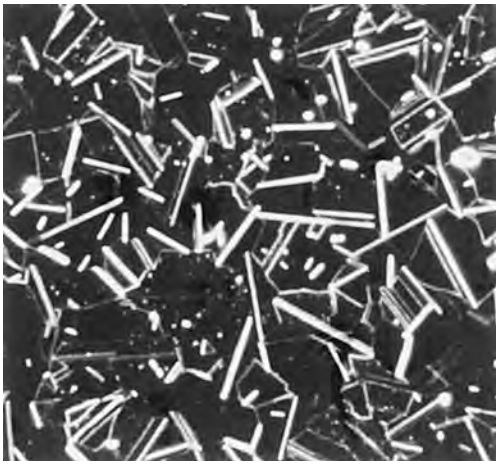


Fig. 40 Same alloy and processing as Fig. 39, but shown with dark-field illumination. See also Fig. 37 and 38. Glyceregia. 1000×

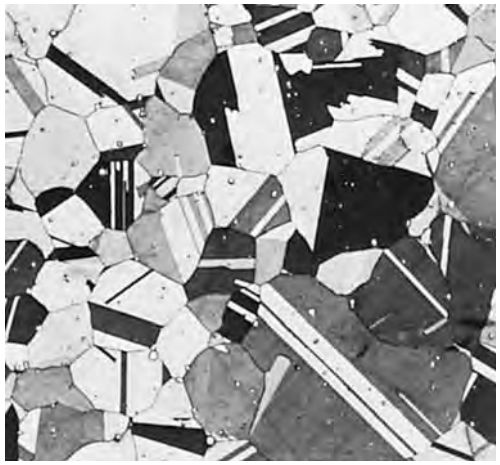


Fig. 41 Pyromet (40 HRC), solution annealed and aged. The specimen was tint etched with 66 mL HCl, 33 mL H_2O, and 1 g $K_2S_2O_5$. See also Fig. 42. 100×

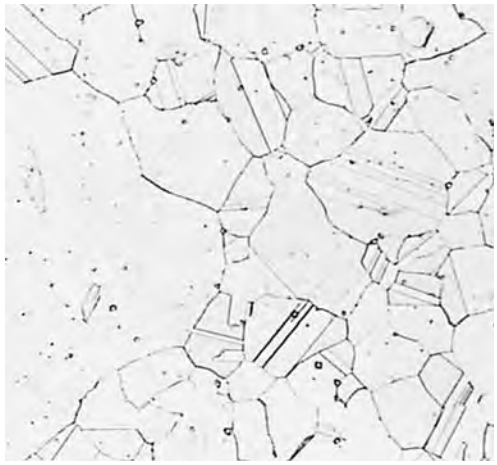


Fig. 42 Same material and processing as Fig. 41 but etched using Kalling's reagent 2 ("waterless" Kalling's). See also Fig. 41. 100×

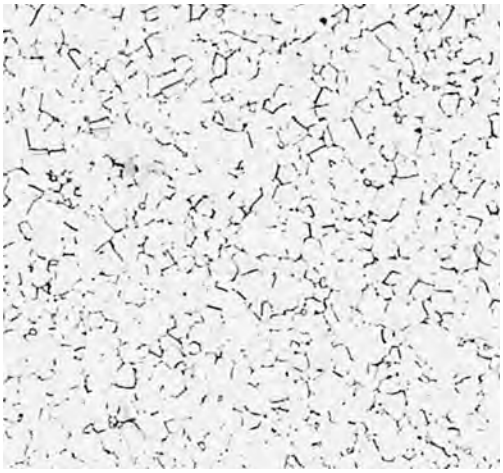


Fig. 43 Alloy 718 (89 HRB), solution annealed 1 h at 955 °C (1750 °F) and air cooled. Large particles are MC carbides (see also Fig. 44). Glyceregia. 100×

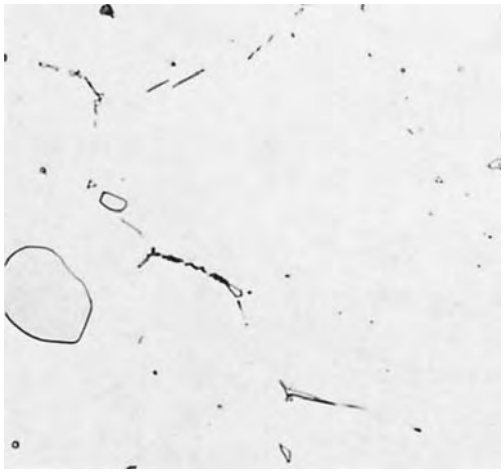


Fig. 44 Same alloy and processing as Fig. 43 but at a higher magnification, showing large MC carbides and fine δ phase (Ni_3Nb) at the austenite grain boundaries. Glyceregia. 1000×



Fig. 45 Alloy 718 (37 HRC), solution annealed 1 h at 955 °C (1750 °F), air cooled, aged 8 h at 720 °C (1325 °F), and air cooled. Structure is MC carbides in an austenite matrix. Glyceregia. 100×

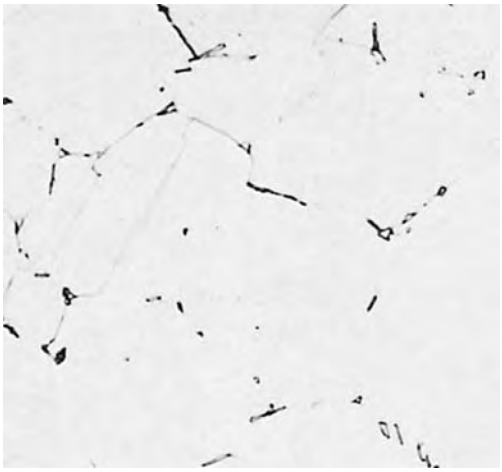


Fig. 46 Same alloy and processing as Fig. 45 but at a higher magnification, showing a cube-shaped nitride, large MC carbides, and fine δ phase at the austenite grain boundaries. Glyceregia. 1000×

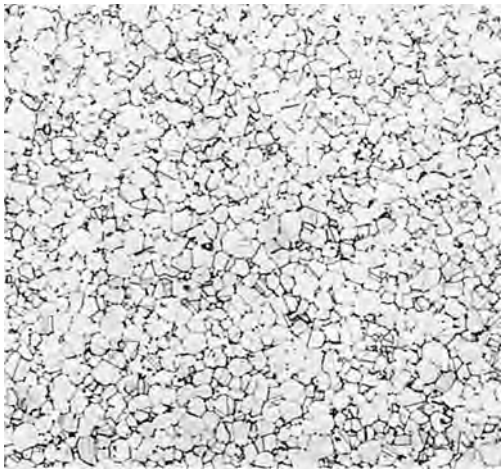


Fig. 47 Alloy 718 (40 HRC), solution annealed 1 h at 955 ° C (1750 °F), air cooled, aged 8 h at 720 °C (1325 °F), cooled 55 °C (100 °F) per hour to 620 °C (1150 °F), held 8 h, and air cooled. Structure is carbides in an austenite matrix. Glyceregia. 100×

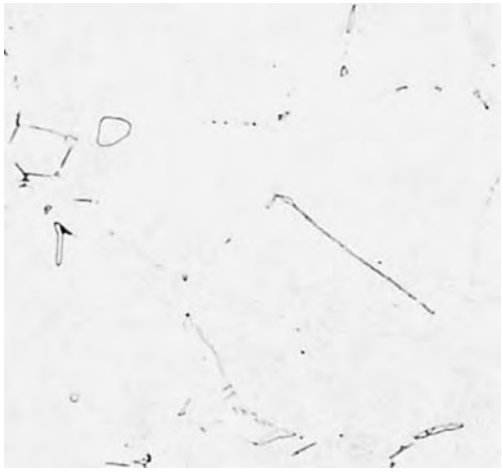


Fig. 48 Same alloy and processing as Fig. 47 but at higher magnification to show MC carbides and fine δ phase at the austenite grain boundaries. Glyceregia. 1000×

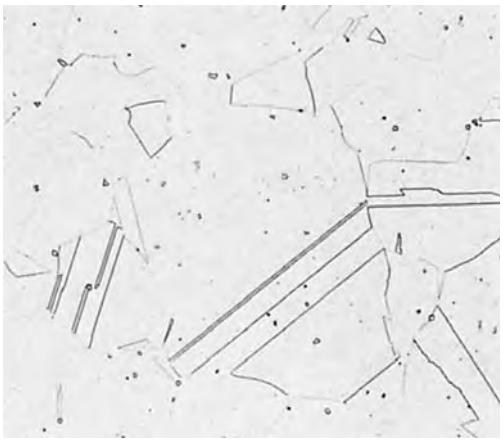


Fig. 49 Alloy 718 (80 HRB), solution annealed 2 h at 1065 °C (1950 °F) and air cooled. Nitrides and MC carbides are visible. Compare grain size to that in Fig. 43. Glyceregia. 100×

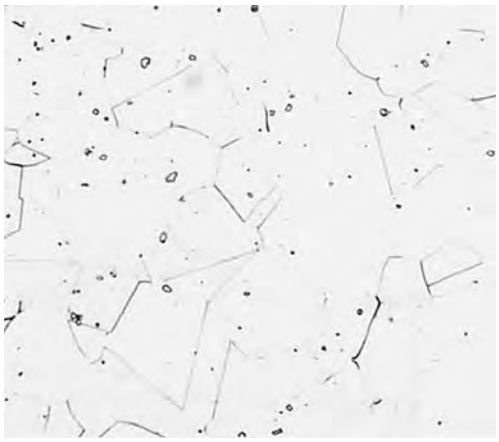


Fig. 50 Alloy 718 (29 HRC), solution annealed 2 h at 1065 °C (1950 °F), air cooled, aged 8 h at 720 °C (1325 °F), and air cooled. Compare with Fig. 51. Glyceregia. 100×



Fig. 51 Same alloy (37 HRC) and annealing treatment as Fig. 50 but aged 8 h at 720 °C (1325 °F), cooled 55 °C (100 °F) per hour to 620 °C (1150 °F), held 8 h, and air cooled. Glyceregia. 100×

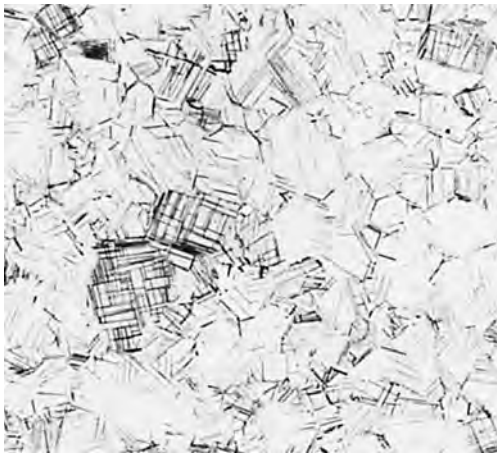


Fig. 52 Alloy 718, solution annealed 1 h at 955 °C (1750 °F), air cooled, and aged 100 h at 870 °C (1600 °F) to form coarse δ (Ni_3Nb) needles. See also Fig. 53. Glyceregia. 200×

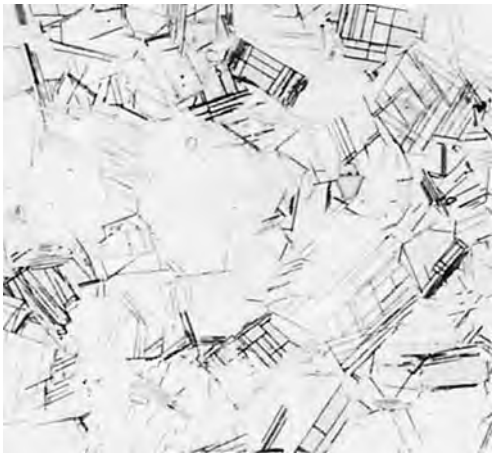


Fig. 53 Same alloy and processing as Fig. 52 but at a higher magnification. See also Fig. 54. Glyceregia. 400×

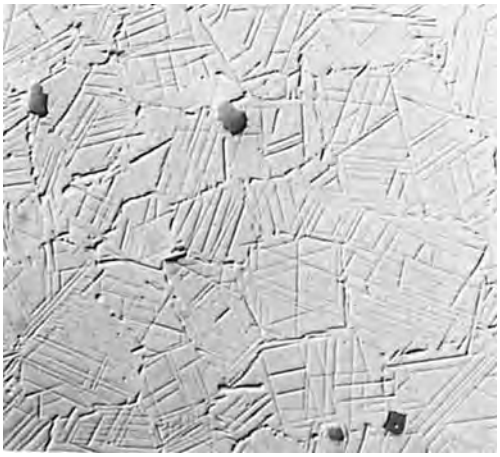


Fig. 54 Same alloy and processing as Fig. 52, but shown using differential interference contrast. Delta needles are recessed, MC carbides stand in relief, and nitrides (lower right) are flush with the matrix. As-polished. 400×

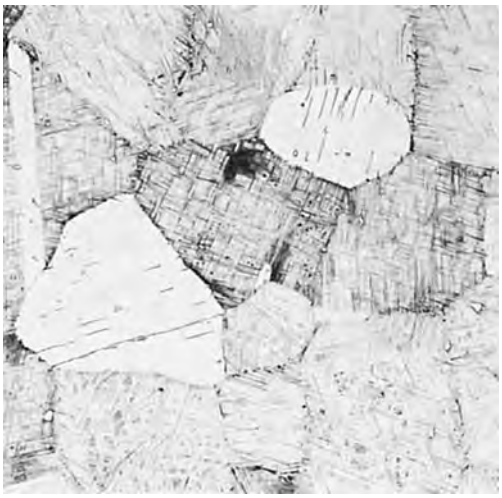


Fig. 55 Alloy 718 (21.5 HRC), solution annealed 1 h at 1150 °C (2100 °F),air cooled, and aged 100 h at 870 °C (1600 °F) to form coarse needles of δ phase (Ni_3Nb). See also Fig. 54. Glyceregia. 100×



Fig. 56 Same alloy and processing as Fig. 55, but using differential interference contrast illumination to show δ phase in four austenite grains. Hard MC carbide is in relief. As-polished. 400×

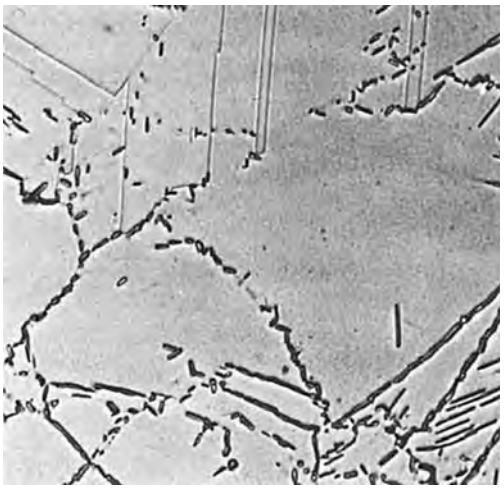


Fig. 57 Alloy 718, solution annealed 1 h at 955 °C (1750 °F), air cooled, aged 8 h at 720 °C (1325 °F), and furnace cooled in 10 h to 620 °C (1150 °F). Structure is δ phase (Ni_3Nb) in a γ matrix. See also Fig. 59. Electrolytic: H_2SO_4, H_3PO_4, and H_2CrO_4. 1000×

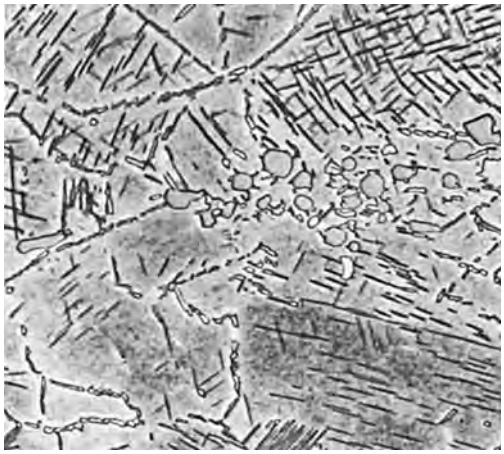


Fig. 58 Alloy 718, solution annealed 1 h at 955 °C (1750 °F), air cooled, and aged 10 h at 760 °C (1400 °F) and at 650 °C (1200 °F). Structure is Laves phase (light gray particles), MC carbide (dark), and needlelike δ. The matrix is γ phase. See also Fig. 60. Electrolytic: H_2SO_4, H_3PO_4, and H_2CrO_4. 1000×

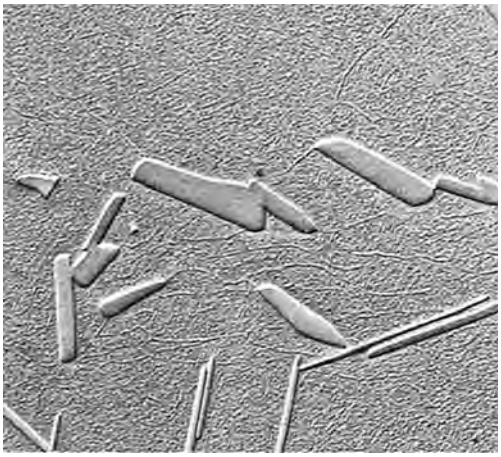


Fig. 59 Replica electron micrograph of same alloy and processing as Fig. 57, showing details of δ-phase crystals. γ′ precipitate is visible in the γ matrix. Electrolytic: H_2SO_4, H_3PO_4, and HNO_3. 10,000×

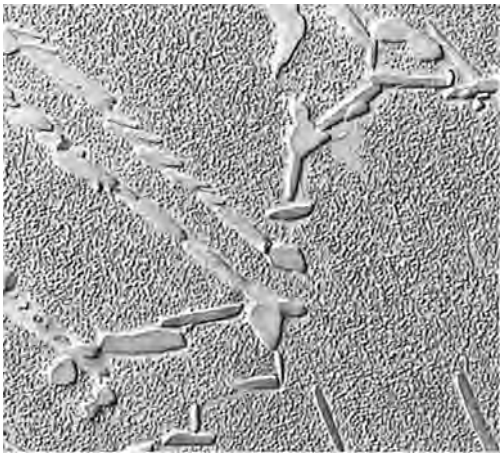


Fig. 60 Replica electron micrograph of same alloy and processing as Fig. 58, showing precipitated carbide and needlelike Ni_3Nb as well as γ′ in the γ matrix. Electrolytic: H_2SO_4, H_3PO_4, and HNO_3. 10,000×

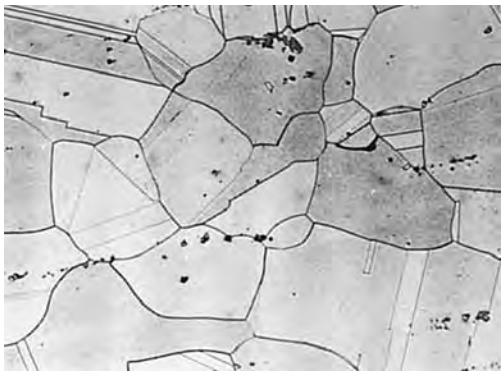


Fig. 61 Astroloy forging, solution annealed 1 h at 1150 °C (2100 °F) and air cooled, showing grain boundaries and fine MC carbides in a γ-phase matrix. See also Fig. 62. Kalling's reagent 2. 100×

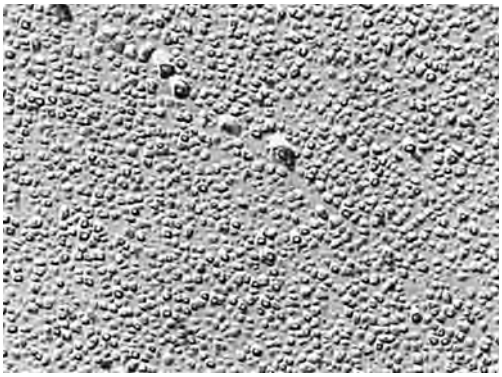


Fig. 62 Replica electron micrograph of same alloy and processing as Fig. 61, showing a clean grain boundary (diagonal). γ′ precipitate is visible in the γ matrix. Electrolytic: H_2SO_4, H_3PO_4, and HNO_3. 10,000×



Fig. 63 Astroloy forging, solution annealed 4 h at 1150 °C (2100 °F), air cooled, aged 4 h at 1080 °C (1975 °F), oil quenched, aged 4 h at 845 °C (1550 °F), air cooled, aged 16 h at 760 °C (1400 °F), and air cooled. See Fig. 64 for identification of constituents. Kalling's reagent 2. 100×

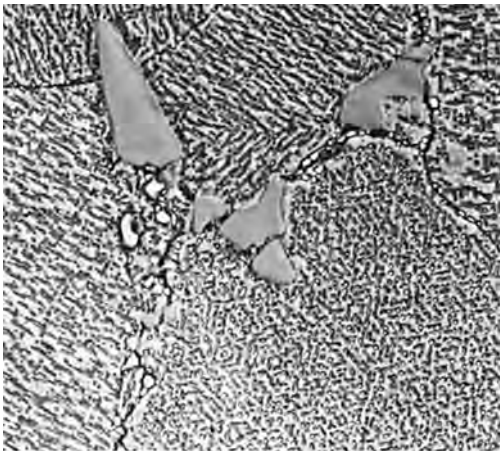


Fig. 64 Same alloy and processing as Fig. 63 but at a higher magnification. MC carbides are precipitated at grain boundaries; the solid-solution matrix contains γ' particles. See also Fig. 65. Kalling's reagent 2. 1000×

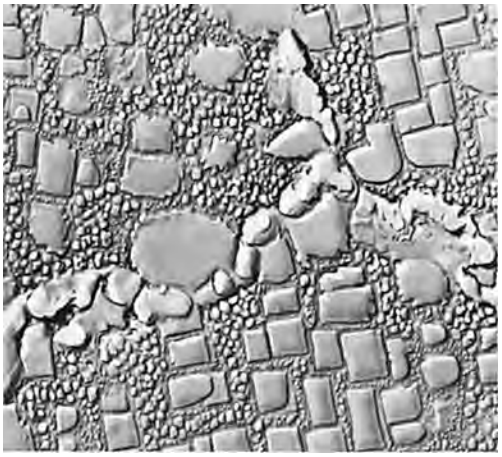


Fig. 65 Replica electron micrograph of same alloy and processing as Fig. 63, showing intergranular γ' precipitated at 1080 °C (1975 °F) as well as fine γ' precipitated at 845 °C (1550 °F) and 760 °C (1400 °F). Carbide particles are visible at grain boundaries. Electrolytic: H_2SO_4, H_3PO_4, and HNO_3. 10,000×

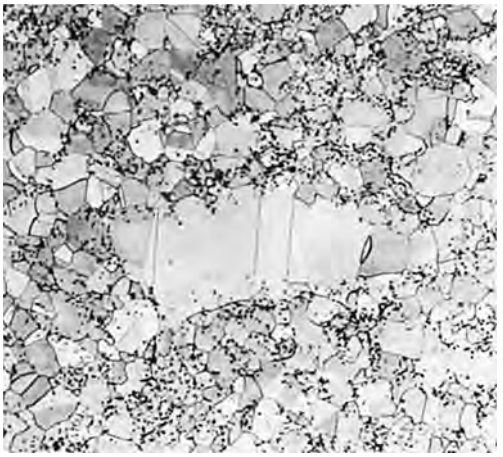


Fig. 66 Astroloy forging, solution annealed 4 h at 1115 °C (2040 °F), air cooled, aged 8 h at 870 °C (1600 °F), air cooled, aged 4 h at 980 °C (1800 °F), air cooled, aged 8 h at 650 °C (1200 °F), air cooled, aged 8 h at 760 °C (1400 °F), and air cooled. The γ matrix contains some undissolved γ'. See also Fig. 67 and 68. Kalling's reagent 2. 100×



Fig. 67 Same alloy and processing as Fig. 66 but at a higher magnification to delineate MC carbides (large, white particles) and undissolved γ' (small, white particles). Kalling's reagent 2. 1000×

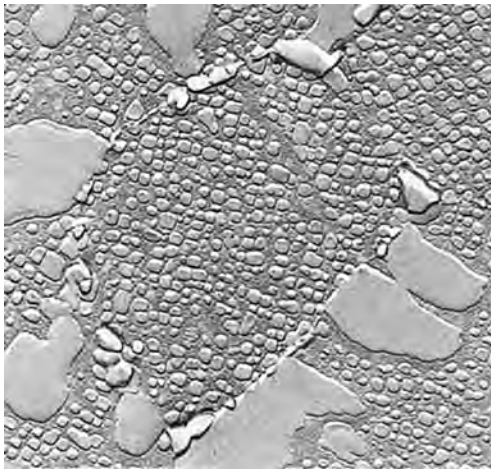


Fig. 68 Replica electron micrograph of same alloy and processing as Fig. 66, showing $M_{23}C_6$ carbides (white, irregular) and γ' precipitates. Electrolytic: H_2SO_4, H_3PO_4, and HNO_3. 10,000×

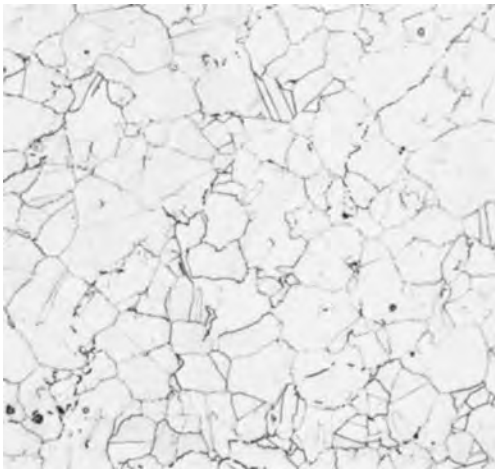


Fig. 69 Alloy 600 (202 HV), as-forged. Specimen is from the center of a 305 mm (12 in.) diameter bar. Glyceregia. 100×



Fig. 70 Alloy 625 (190 HV), solution annealed 30 min at 980 °C (1800 °F) and air cooled. Specimen is a longitudinal section from the mid-radius of a 140 mm (5.5 in.) diameter bar. 15 mL HCl, 10 mL acetic acid, 5 mL HNO_3, and 2 drops glycerol. 100×

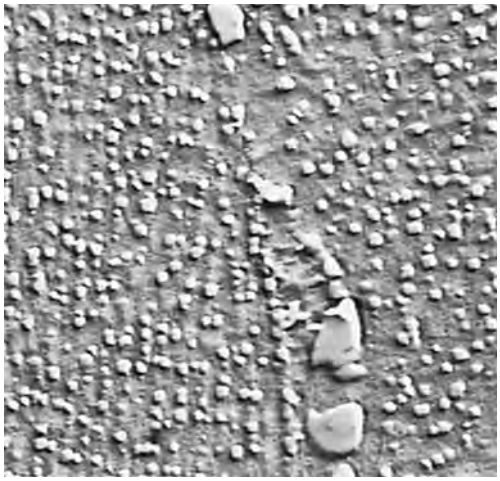


Fig. 71 Replica electron micrograph of Inconel X-750, solution annealed 2 h at 1150 °C (2100 °F) and air cooled, then aged 24 h at 815 °C (1500 °F). Structure is small, uniformly dispersed γ' precipitate and large, discontinuous $M_{23}C_6$ carbide at the grain boundary. Glyceregia. 15,000×

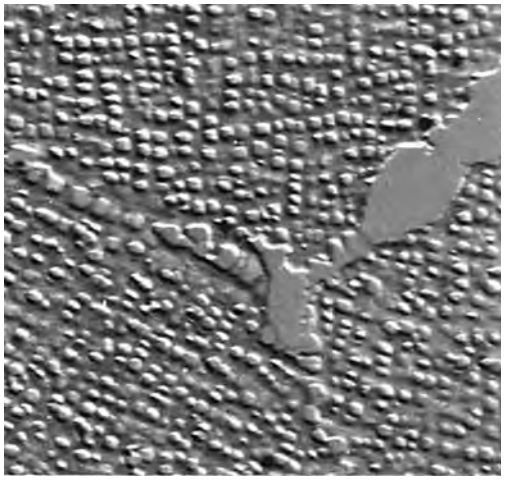


Fig. 72 Replica electron micrograph of same alloy and annealing treatment as Fig. 71, but aged 24 h at 845 °C (1550 °F) and then 24 h at 705 °C (1300 °F). Grain-boundary $M_{23}C_6$ carbide is stabilized, and precipitation of fine γ' particles has increased. Glyceregia. 15,000×

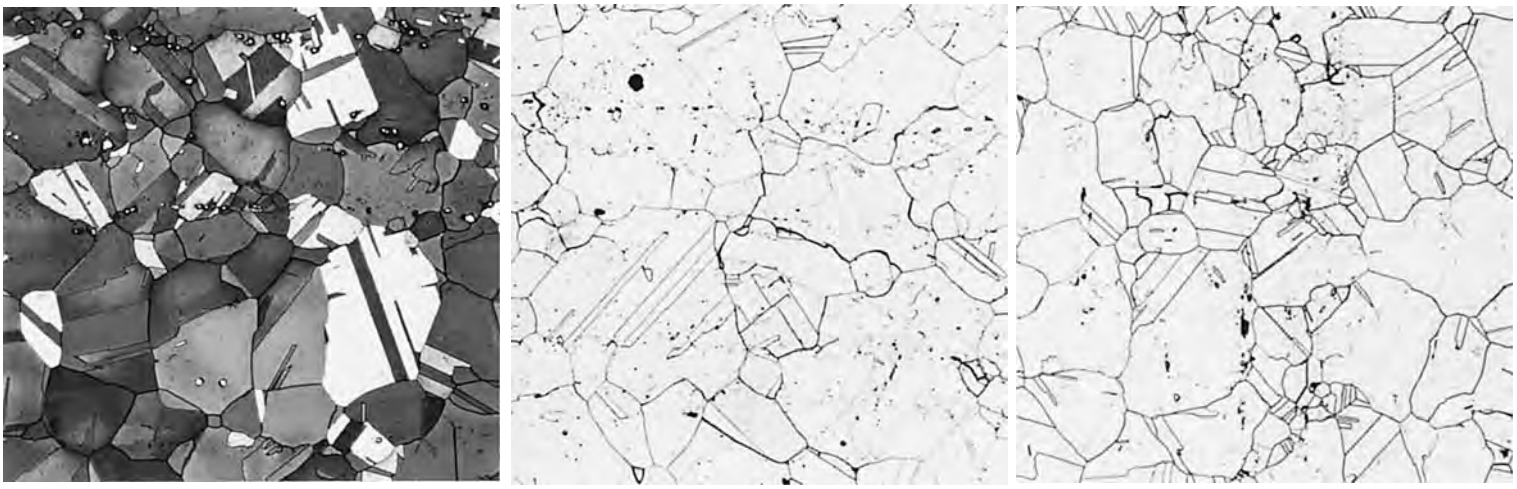


Fig. 73, 74, 75 The effects of different etchants on solution-annealed and aged alloy X-750. Fig. 73: tint etched in 50 mL HCl, 50 mL H_2O, and 1 g $K_2S_2O_5$. Fig. 74: etched using Kalling's reagent 2. Fig. 75: etched using glyceregia. (see also Fig. 76 to 78). All 100×



Fig. 76, 77, 78 Different etchants used to delineate the structure of solution-annealed and aged alloy X-750. Fig. 76: etched using Marble's reagent. Fig. 77: etched using aqua regia. Fig. 78: etched using HCl + 1% Na_2O_2. All 100×

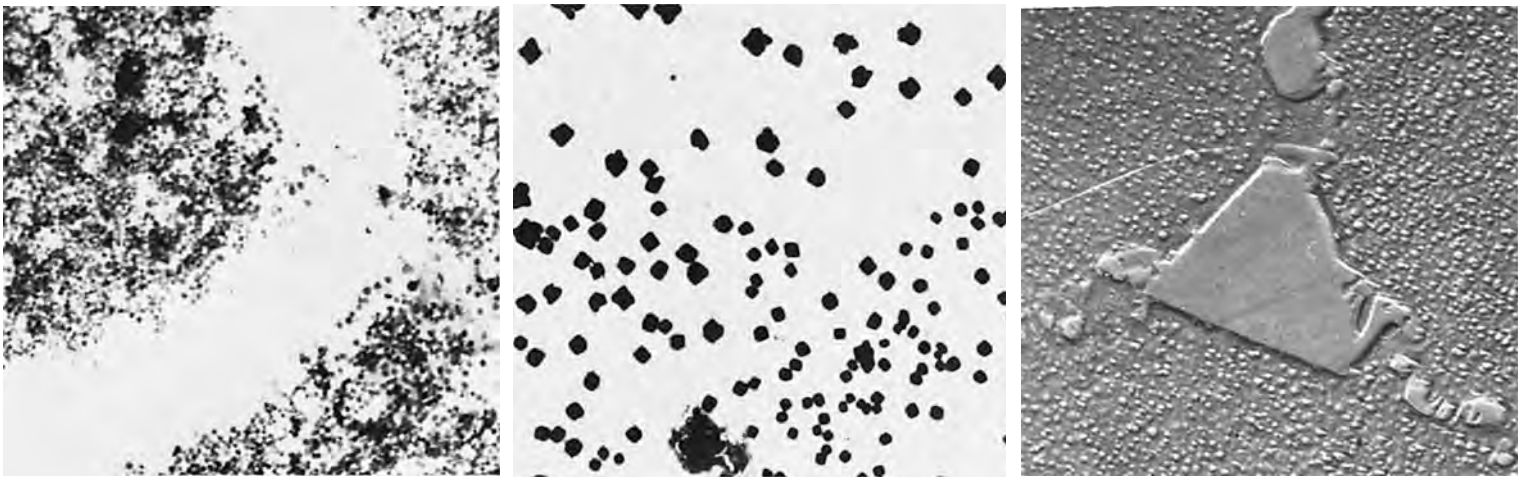


Fig. 79 Extraction replica electron micrograph of Nimonic 80, solution annealed 8 h at 1075 °C (1965 °F) and aged 16 h at 705 °C (1300 °F). The structure is extracted γ′ phase. Electrolytic: 2% H_2SO_4 and H_2O. 15,000×

Fig. 80 Extraction replica electron micrograph of Nimonic 80, solution annealed 1 h at 1205 °C (2200 °F) and aged 16 h at 900 °C (1650 °F). Structure is extracted cubes of γ′ phase. Electrolytic: 10% H_2SO_4 and H_2O. 15,000×

Fig. 81 Negative replica electron micrograph of Nimonic 80, solution annealed 8 h at 1075 °C (1965 °F) and aged 16 h at 705 °C (1300 °F). Structure is grain-boundary carbide ($M_{23}C_6$) and uniformly dispersed γ′ in a matrix of γ solid solution. Glyceregia, then electrolytic: 2% H_2SO_4 and H_2O. 15,000×

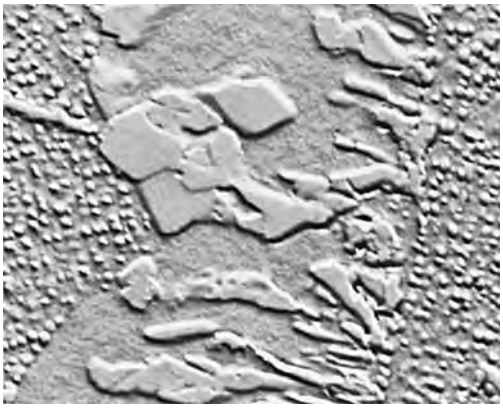


Fig. 82 Negative replica electron micrograph of Nimonic 80, solution annealed same as Fig. 80, furnace cooled to 980 °C (1800 °F) and held 8 h, water quenched, and aged 168 h at 750 °C (1380 °F). Discontinuous precipitation of $M_{23}C_6$ carbide at grain boundaries and γ′ in the matrix. Glyceregia, then electrolytic: 1% H_2SO_4 and H_2O. 15,000×



Fig. 83 René 41, solution annealed 4 h at 1065 °C (1950 °F) and air cooled. Structure consists of stringers of carbide in a γ solid-solution matrix. See also Fig. 84 for a higher magnification of this structure. Kalling's reagent 2. 100×

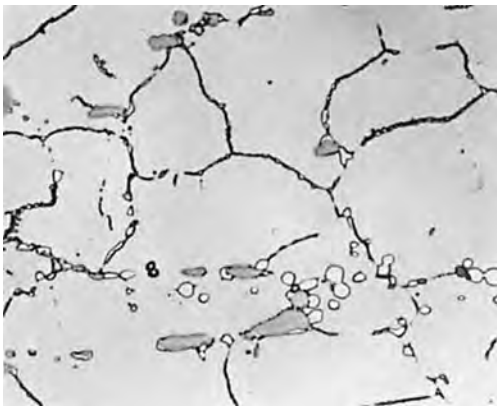


Fig. 84 Same alloy and processing as Fig. 83 but at a higher magnification. Light, globular particles are M_6C; gray particles are MC carbide; grain-boundary envelopes are M_6C or $M_{23}C_6$. See also Fig. 85 and 86. Kalling's reagent 2. 500×

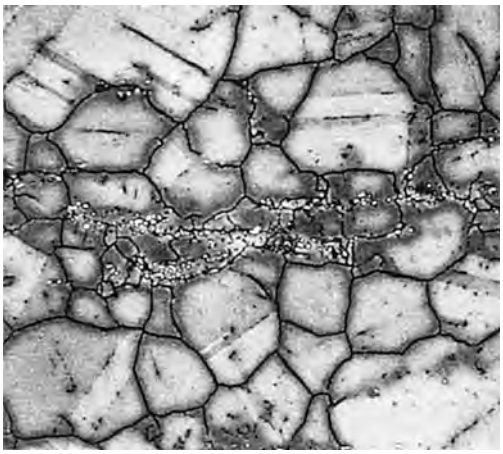


Fig. 85 René 41, solution annealed 4 h at 1065 °C (1950 °F), air cooled, aged 16 h at 760 °C (1400 °F), and air cooled. Particles of mixed carbides are present in the γ solid-solution matrix, which was darkened by the formation of γ′ at 760 °C (1400 °F). See also Fig. 86. Kalling's reagent 2. 110×

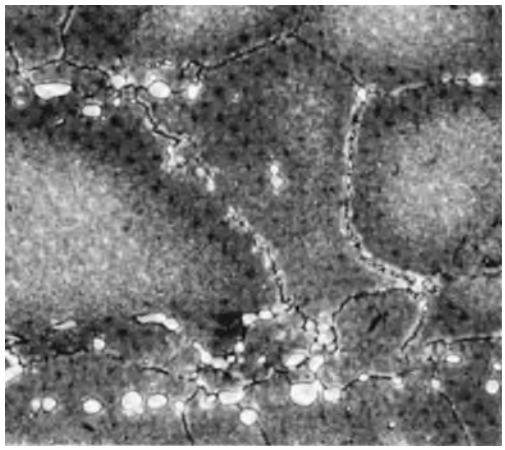


Fig. 86 Same as Fig. 85 but at a higher magnification, showing particles of M_6C (white), MC (gray), and $M_{23}C_6$ (at grain boundaries). Grain-boundary borders are darkened by γ′. Kalling's reagent 2.

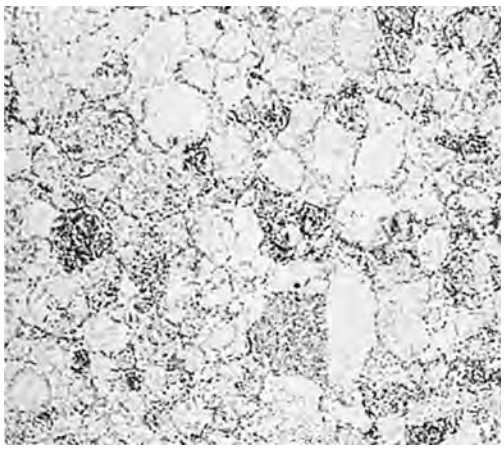
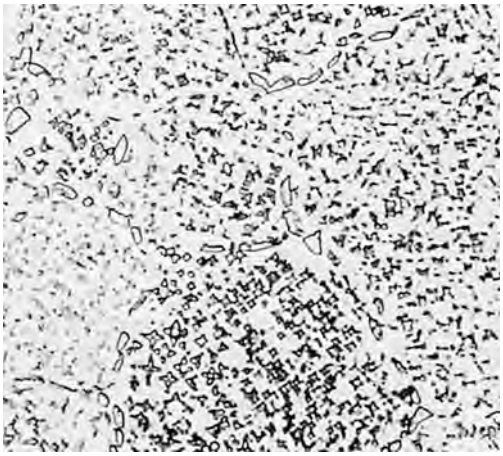


Fig. 87 Powder-made René 95, hot isostatically pressed. Structure includes large, coarse γ′. Prior particle boundaries are also visible (see also Fig. 88 and 89). Glyceregia. 200×



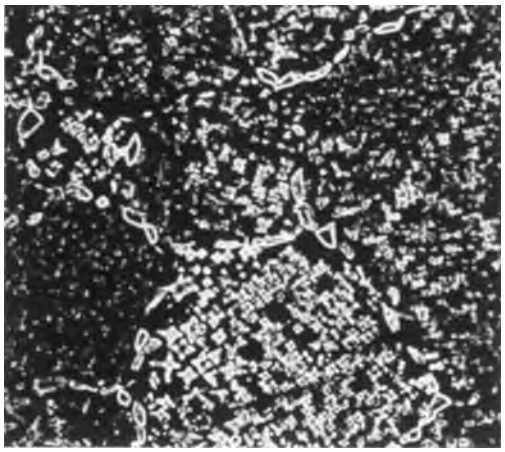


Fig. 88, 89 The use of different illumination modes to delineate the structure of the same alloy and processing as Fig. 87. Fig. 88: bright-field illumination. Fig. 89: dark-field illumination. Some carbide networks are visible at this magnification. Glyceregia. 1000×

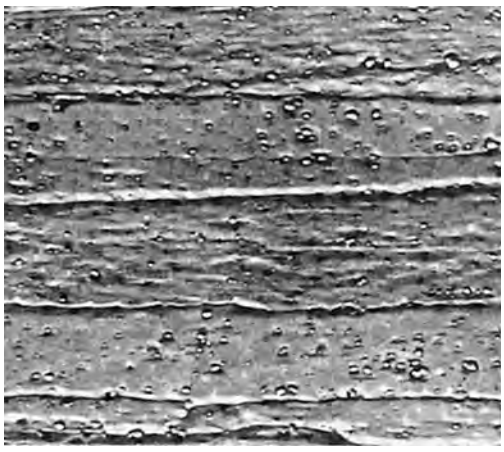


Fig. 90 Replica electron micrograph of a longitudinal section of rolled TDNi (thoriated nickel), annealed 1 h at 1315 °C (2400 °F), showing grain structure and dispersion of ThO_2. Electrolytic: H_2SO_4 and methanol. 7560×

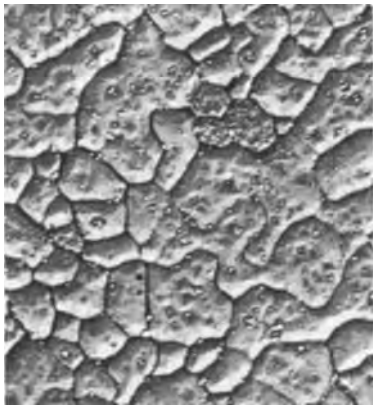


Fig. 91 Same as Fig. 90, but this replica electron micrograph shows the grain structure and the dispersion of ThO_2 in a transverse section of the rolled, annealed alloy. Electrolytic: H_2SO_4 and methanol. 7000×

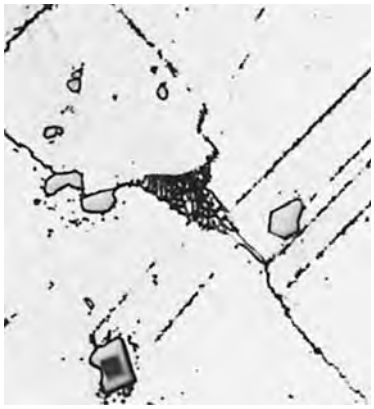


Fig. 92 U-700, as forged. Structure is nickel-rich solid-solution matrix, eutectic with M_3B_2 formed by fusion at 1205 °C (2200 °F), large crystals of MC carbide, and $M_{23}C_6$ carbide at grain and twin boundaries. Kalling's reagent. 500×

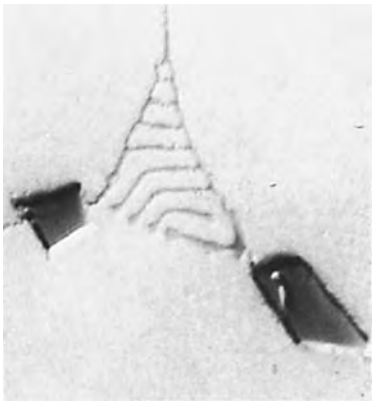


Fig. 93 Same alloy and condition as Fig. 92 but at a higher magnification. The lamellar constituent is a boride (M_3B_2) formed by incipient fusion. The two large crystals are MC carbide. As-polished. 1500×

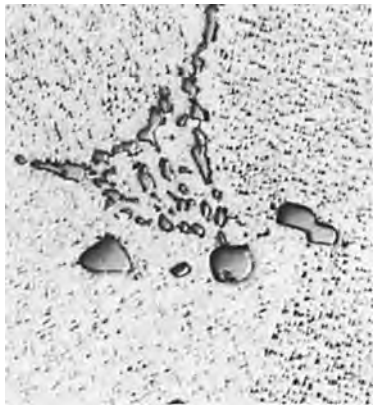


Fig. 94 U-700, solution annealed 4 h at 1175 °C (2150 °F) and aged 4 h at 1080 °C (1975 °F). $M_{23}C_6$ has dissolved, and borides have been spheroidized. Large crystals are MC carbide; the oriented precipitate is γ′. Kalling's reagent. 1000×

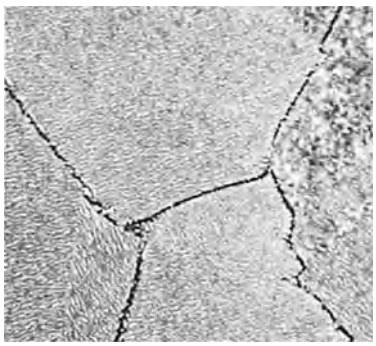


Fig. 95 U-700, solution annealed 4 h at 1175 °C (2150 °F), aged 4 h at 1080 °C (1975 °F), aged 24 h at 845 °C (1550 °F), and aged 16 h at 760 °C (1400 °F). Carbides and boride particles are present at grain boundaries; remaining structure is MC carbide and γ′ in a γ matrix. Kalling's reagent 2. 500×

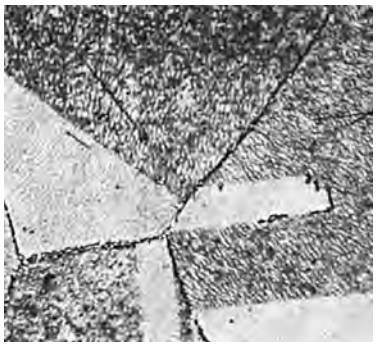


Fig. 96 U-700, processed the same as Fig. 95, then held 500 h at 870 °C (1600 °F). Light, acicular σ phase has formed in the γ-γ′ matrix; some σ is also visible at boundaries of the platelets. Kalling's reagent 2. 500×



Fig. 97 U-700, heat treated same as Fig. 95, then held 1500 h at 870 °C (1600 °F). Needles of σ phase are longer and better resolved than in Fig. 96. Sigma foundation adversely affects high-temperature tensile properties. Kalling's reagent 2. 500×

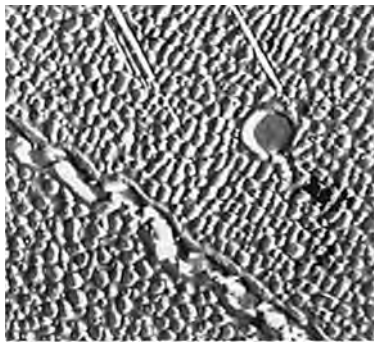


Fig. 98 Replica electron micrograph of U-700, solution annealed same as Fig. 97 and aged 1500 h at 815 °C (1500 °F). Structure is acicular σ phase, $M_{23}C_6$ carbide at grain boundary, and γ′ within the γ matrix grains. HCl, ethanol, and H_2O_2. 4500×

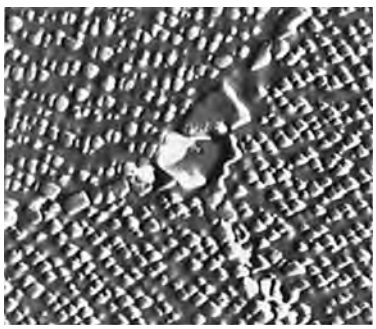


Fig. 99 Replica electron micrograph of U-700, solution annealed same as Fig. 97 and aged 24 h at 980 °C (1800 °F). Precipitated carbide at grain boundaries and γ′ within grains of the γ solid-solution matrix. HCl, ethanol, $CuCl_2$, and H_2O_2. 4500×

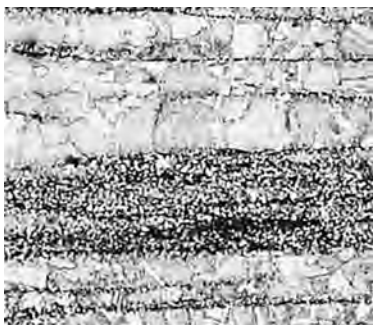


Fig. 100 U-710 bar, solution annealed 2 h at 1120 °C (2050 °F), aged 1.5 h at 1040 °C (1900 °F), and air cooled. Longitudinal section shows recrystallized bands (light) and bands containing residual primary γ′. Kalling's reagent. 100×



Fig. 101 U-710 bar, solution annealed 4 h at 1175 °C (2150 °F) and air cooled. Structure is dispersed primary MC carbide and M_3B_2 boride in a γ matrix. γ′ is in solution. Kalling's reagent. 100×

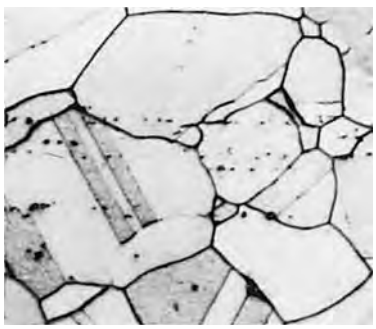


Fig. 102 U-710 bar, solution annealed same as Fig. 101, aged 24 h at 845 °C (1550 °F), air cooled, aged 16 h at 760 °C (1400 °F), and air cooled. $M_{23}C_6$ precipitate along grain and twin boundaries. Kalling's reagent. 100×



Fig. 103 50Cr-50Ni sheet, 3.2 mm (0.125 in.) thick, annealed at 980 °C (1800 °F) for 1 h. Structure contains particles of chromium-rich phase (dark) and nickel-rich phase (light). Electrolytic: 1% H_2CrO_4. 500×



Fig. 104 Same alloy as Fig. 103, annealed at 980 °C (1800 °F) for 120 h. Structure has same constituents as Fig. 103 but shows effects of long-time annealing on phase distribution. Electrolytic: 1% H_2CrO_4. 500×

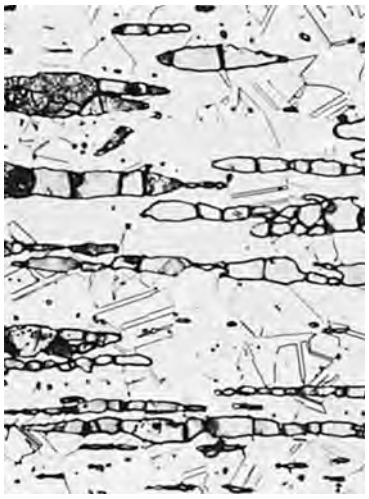
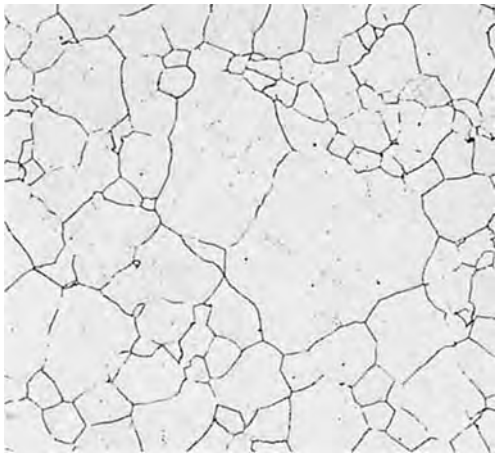
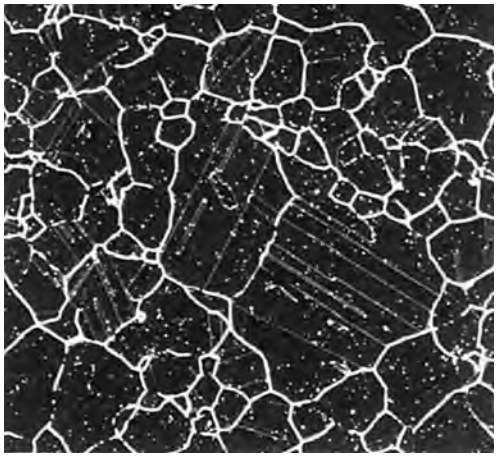


Fig. 105 50Cr-50Ni, hot rolled, annealed at 1205 °C (2200 °F), and water quenched. Chromium-rich phase (dark) is elongated in the rolling direction. The light matrix is a nickel-rich phase. Electrolytic: 1% H_2CrO_4. 200×



Fig. 106 Same material as Fig. 105, hot rolled and annealed at 1315 °C (2400 °F), then water quenched. High annealing temperature caused agglomeration of chromium-rich phase (dark). Nickel-rich phase is light. Electrolytic: 1% H_2CrO_4. 200×





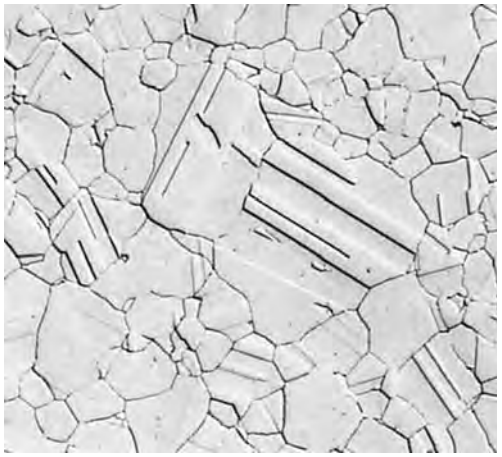


Fig. 107, 108, 109 Waspaloy (37 HRC), solution annealed 4 h at 1035 °C (1900 °F), water quenched, aged 4 h at 845 °C (1550 °F), air cooled, aged 16 h at 760 °C (1400 °F), and air cooled. Fig. 107: bright-field illumination. Fig. 108: dark-field illumination. Fig. 109: differential interference contrast. Glyceregia. 100×

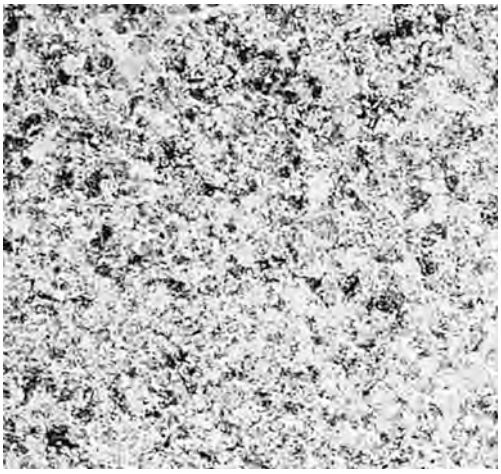


Fig. 110 Waspaloy (265 HV), solution annealed 4 h at 1010 °C (1850 °F) and water quenched. Compare with Fig. 111 and 112. Glyceregia. 200×

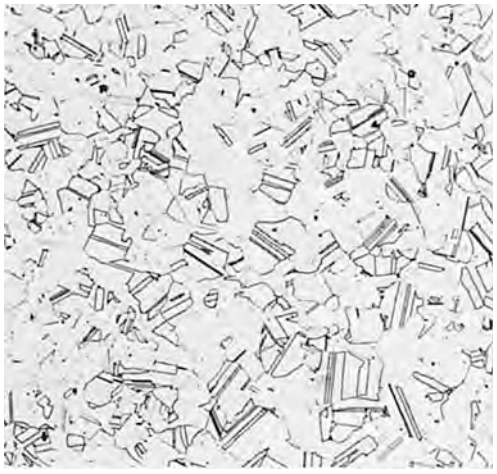


Fig. 111 Same material as Fig. 110, solution annealed 4 h at 1035 °C (1900 °F) and water quenched. 223 HV. Compare with Fig. 112. Glyceregia. 100×

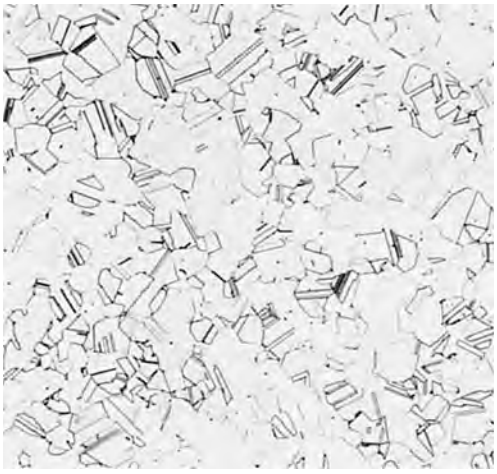


Fig. 112 Waspaloy, solution annealed 4 h at 1065 °C (1950 °F) and water quenched. Higher temperatures caused increased grain size, complete solutioning, and decreased hardness. Compare with Fig. 110 and 111. Glyceregia. 100×

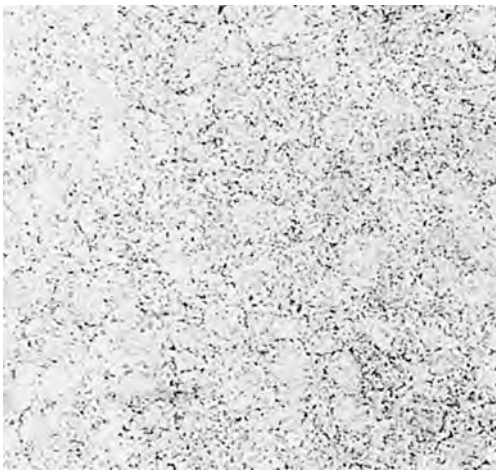


Fig. 113 Waspaloy (42 HRC), solution annealed 4 h at 1010 °C (1850 °F), water quenched, aged 4 h at 845 °C (1550 °F), air cooled, aged 16 h at 760 °C (1400 °F), and air cooled. Glyceregia. 200×

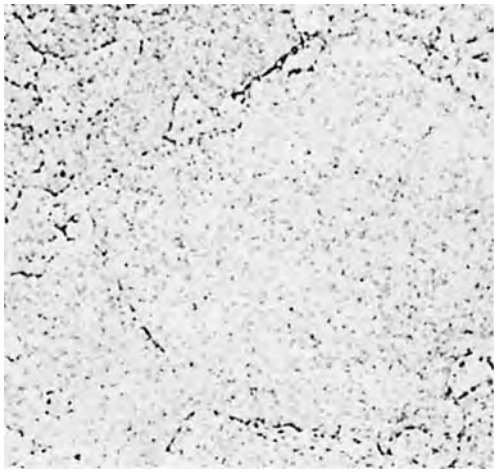


Fig. 114 Same alloy and processing as Fig. 113, but at a higher magnification showing residual γ' from hot working that was not dissolved. Glyceregia. 1000×

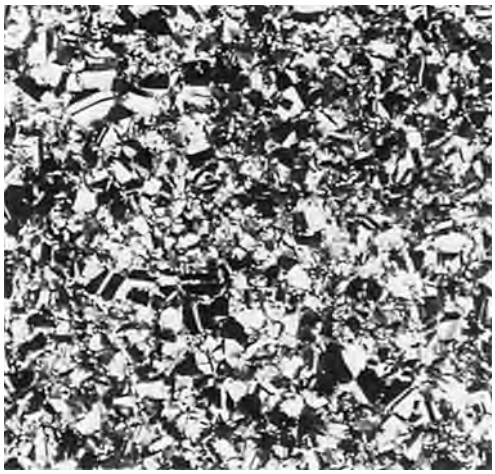


Fig. 115 Same material and processing as Fig. 113, but tint etched to color matrix phase. See also Fig. 114. 50 mL HCl, 50 mL H_2O, and 1 g $K_2S_2O_5$. 100×

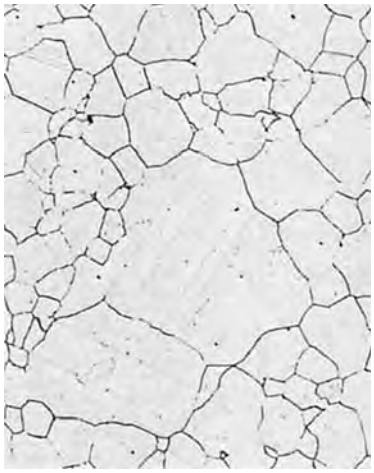




Fig. 116, 117 Waspaloy (37 HRC), solution annealed 4 h at 1035 °C (1900 °F), water quenched, aged 4 h at 845 °C (1550 °F), air cooled, aged 16 h at 760 °C (1400 °F), and air cooled. Fig. 116: etched in glyceregia. Fig. 117: tint etched in 50 mL HCl, 50 mL H_2O, and 1 g $K_2S_2O_5$. Both 100×

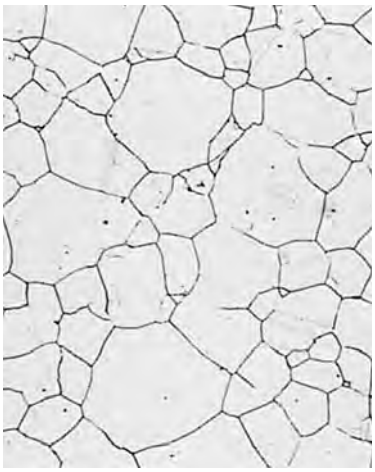




Fig. 118, 119 Waspaloy (35 to 36 HRC), solution annealed 4 h at 1065 °C (1950 °F), water quenched, aged 4 h at 845 °C (1550 °F), air cooled, aged 16 h at 760 °C (1400 °F), and air cooled. Fig. 118: etched in glyceregia. Fig. 119: tint etched using 50 mL HCl, 50 mL H_2O, 3 g $NH_4F{\cdot}HF$, and 1.5 g $K_2S_2O_5$. Both 100×



Fig. 120 Elgiloy, cold drawn to 50 to 55% reduction, showing grains and dispersed stringers of carbide elongated in the rolling direction. Compare with Fig. 121. HCl, HNO_3, and $FeCl_3$. 250×

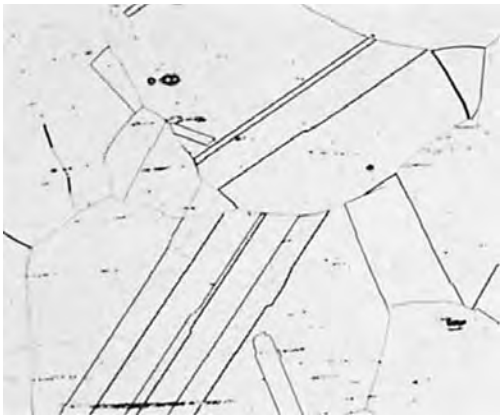


Fig. 121 Same material and drawing process as Fig. 120, soluion annealed 1 h at 1230 °C (2250 °F) and air cooled. The cold-worked grains have been fully recrystallized. HCl, HNO_3, and $FeCl_3$. 250×

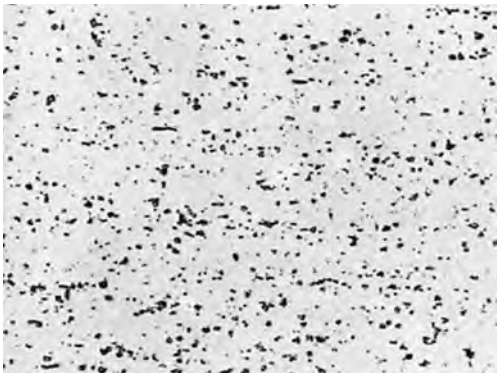


Fig. 122 S-816 alloy as-forged bar. The randomly dispersed carbide particles in the solid-solution matrix are primarily NbC. The high hardness of the carbides has caused them to show in relief. See also Fig. 123 to 125. As-polished. 100×

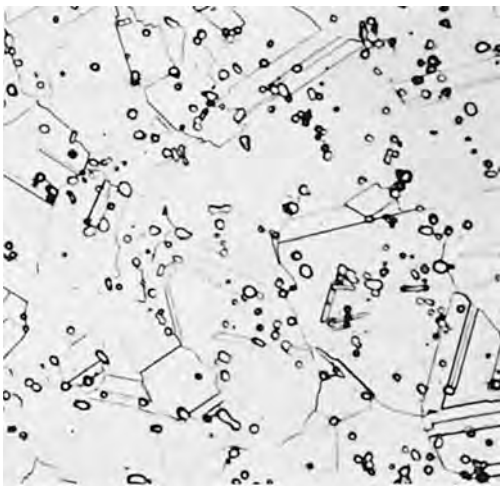


Fig. 123 S-816 (20 HRC), solution annealed 1 h at 1175 °C (2150 °F) and water quenched. Particles of NbC are dispersed in the fcc matrix. There is no grain-boundary precipitate. 92 mL HCl, 5 mL H_2SO_4, and 3 mL HNO_3. 500×

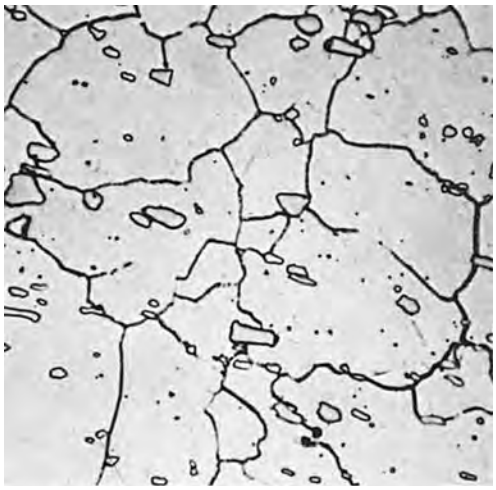


Fig. 124 Same material and annealing treatment as Fig. 123, but aged 16 h at 760 °C (1400 °F) and air cooled. Grain-boundary precipitate (primarily $Cr_{23}C_6$) and dispersed NbC particles in the fcc matrix. 30 HRC. 92 mL HCl, 5 mL H_2SO_4, and 3 mL HNO_3. 500×

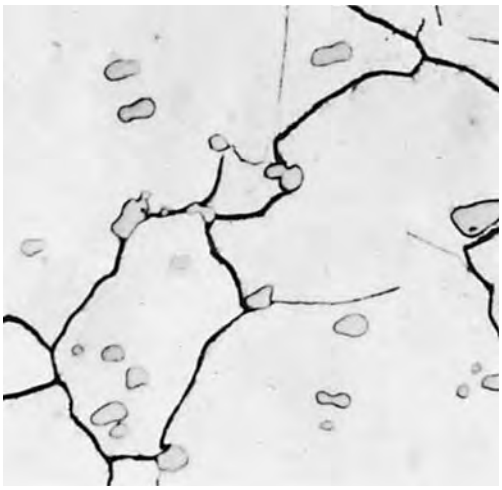


Fig. 125 S-816 (35 HRC), solution annealed 1 h at 1290 °C (2350 °F), water quenched, aged 16 h at 760 °C (1400 °F), and air cooled. Structure is dispersed NbC particles and grain-boundary $Cr_{23}C_6$ in the fcc matrix. See also Fig. 126 to 128. 92 mL HCl, 5 mL H_2SO_4, and 3 mL HNO_3. 1000×



Fig. 126 Same alloy and condition as Fig. 125, creep-rupture tested at 650 °C (1200 °F) for 3992 h at 276 MPa (40 ksi). Precipitation of $M_{23}C_6$ at grain boundaries and within grains has increased. The dispersed large particles are NbC. 39 HRC. 92 mL HCl, 5 mL H_2SO_4, and 3 mL HNO_3. 1000×

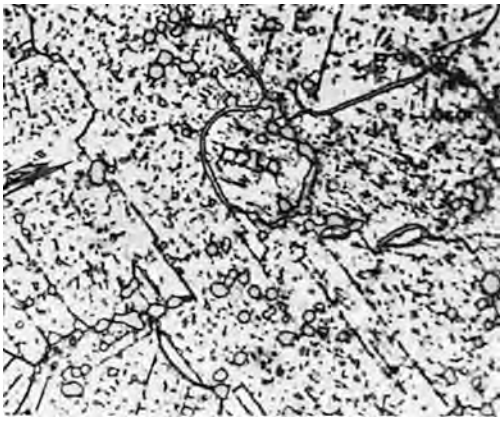


Fig. 127 Same alloy and condition as Fig. 125, creep-rupture tested 25,500 h at 730 °C (1350 °F) and 172 MPa (25 ksi). Particles of $M_{23}C_6$ at grain boundaries and within grains have coalesced. Dispersed large particles are NbC. 38.5 HRC. 92 mL HCl, 5 mL H_2SO_4, and 3 mL HNO_3. 1000×



Fig. 128 Same alloy and condition as Fig. 125, creep-rupture tested 19,650 h at 815 °C (1500 °F) and 86 MPa (12,500 psi). Coalescence of $M_{23}C_6$ at grain boundaries and within grains has increased. Large particles are NbC. 34 HRC. 92 mL HCl, 5 mL H_2SO_4, and 3 mL HNO_3. 1000×

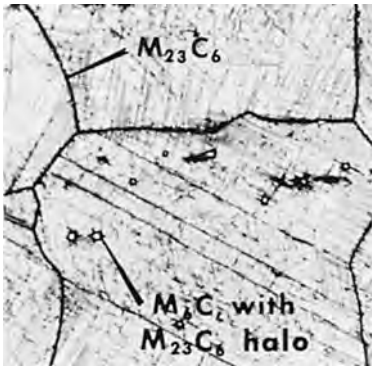


Fig. 129 Haynes 25 (L-605), solution annealed at 1205 °C (2200 °F) and aged 3400 h at 650 °C (1200 °F). Structure is M_6C and $M_{23}C_6$ carbides in a mixed fcc and hcp matrix. Electrolytic: HCl and H_2O_2. 500×

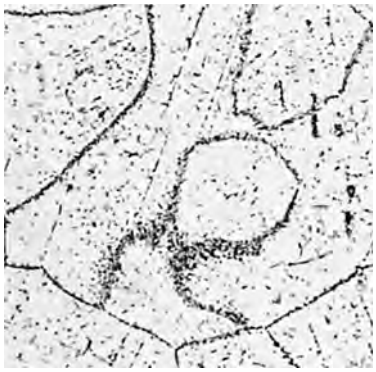


Fig. 130 Haynes 25 (L-605), solution annealed same as Fig. 129 and aged 3400 h at 815 °C (1500 °F). Structure is precipitates of M_6C and "Co_2W" intermetallic in a fcc matrix. Electrolytic: HCl and H_2O_2. 500×

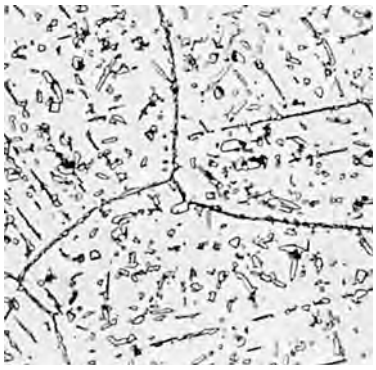


Fig. 131 Haynes 25 (L-605), solution annealed same as Fig. 129 and aged 3400 h at 870 °C (1600 °F). Structure is the same as Fig. 130. Electrolytic: HCl and H_2O_2. 500×

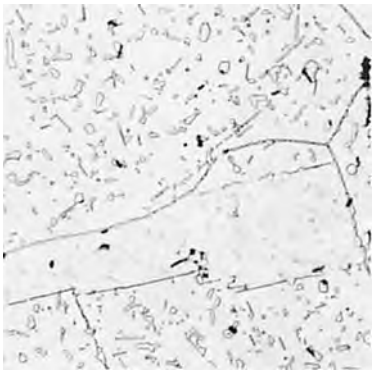


Fig. 132 Haynes 25 (L-605), solution annealed same as Fig. 129 and aged 3400 h at 925 °C (1700 °F). Structure consists of M_6C (primary) and "Co_2W" intermetallic (secondary) in a fcc matrix. Electrolytic: HCl and H_2O_2. 500×

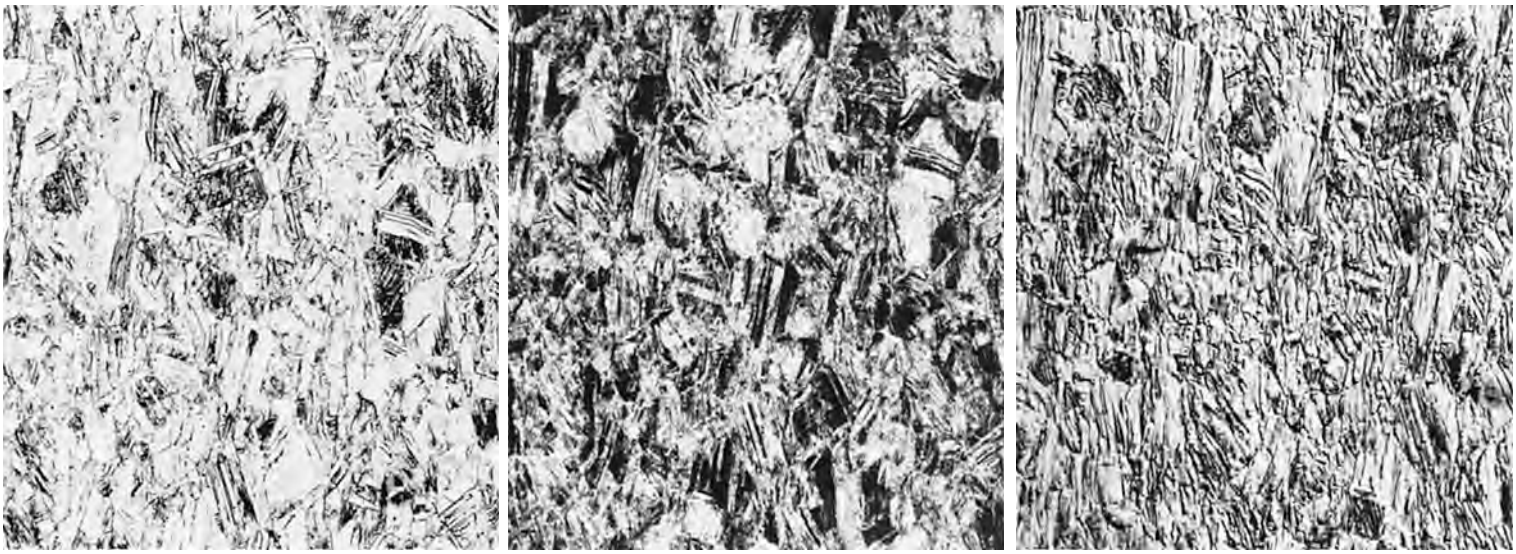


Fig. 133, 134, 135 Haynes 25 (L-605, 486 HV), solution annealed and cold worked to 35% reduction. Longitudinal section. Fig. 133: bright-field illumination. Fig. 134: dark-field illumination. Fig. 135: differential interference contrast. All etched with 15 mL HCl, 10 mL acetic acid, 5 mL HNO_3, and 2 drops glycerol. 100×

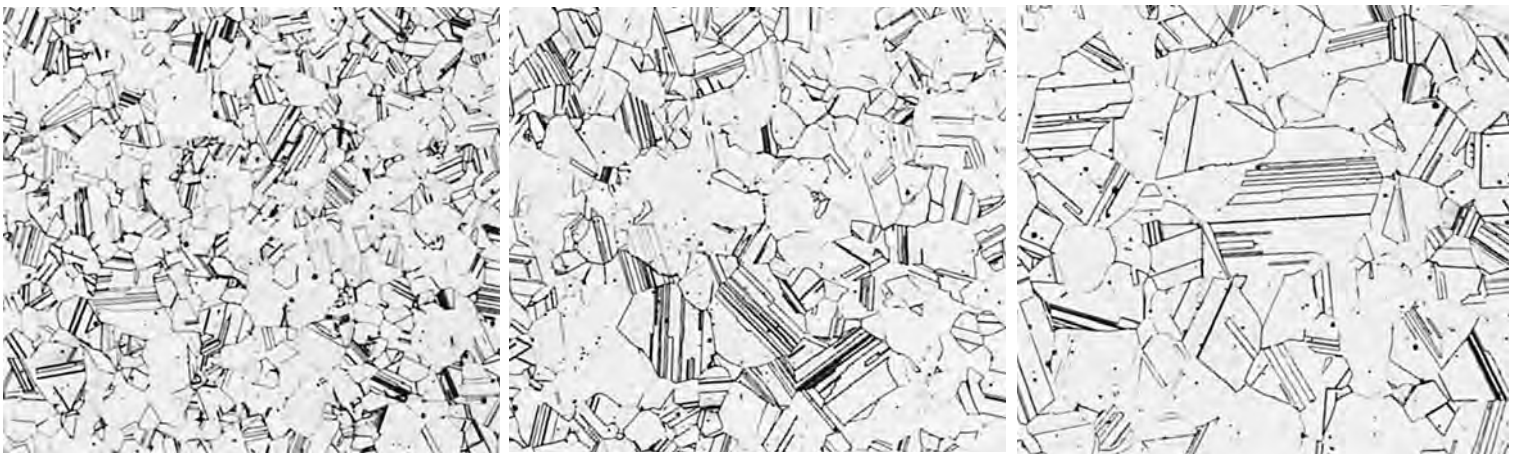


Fig. 136, 137, 138 Haynes 25 (L-605), cold worked same as Fig.133 to 135 and given different solution-annealing treatments. Grain size increases with increasing annealing temperature and time. Fig. 136: solution annealed 2.5 min at 1150 °C (2100 °F); 261 HV. Fig. 137: solution annealed 4.25 min at 1150 °C (2100 °F); 254 HV. Fig. 138: solution annealed 2.5 min at 1205 °C (2200 °F); 246 HV. 15 mL HCl, 10 mL acetic acid, 5 mL HNO_3, and 2 drops glycerol. 100×



Fig. 139 Haynes 188, cold rolled 50%, heated to 815 °C (1500 °F) for 1 h and water quenched. The partly recrystallized structure contains M_6C and $M_{23}C_6$ carbides in a fcc matrix. Electrolytic: HCl and H_2O_2. 1000×



Fig. 140 Haynes 188, cold rolled 20% and solution annealed at 1175 °C (2150 °F) for 10 min, then water quenched. The fully annealed structure consists of M_6C particles in a fcc matrix. Electrolytic: HCl and H_2O_2. 500×

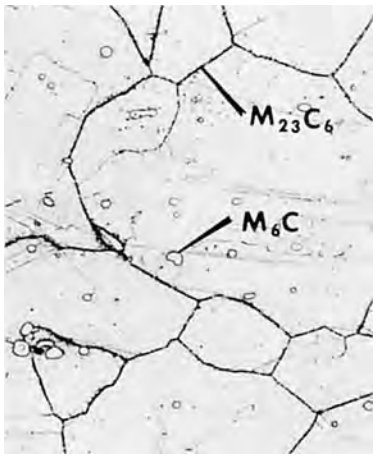


Fig. 141 Haynes 188, solution annealed at 1175 °C (2150 °F) and aged 3400 h at 650 °C (1200 °F). Structure is M_6C and $M_{23}C_6$ particles in a fcc matrix. Electrolytic: HCl and H_2O_2. 500×

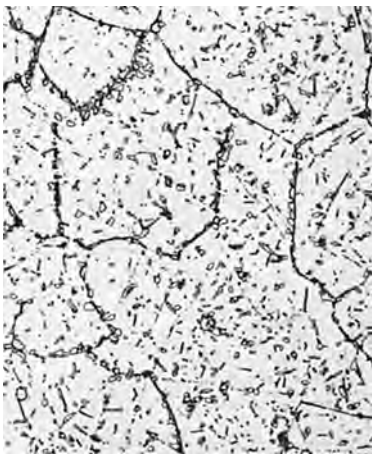


Fig. 142 Haynes 188, solution annealed at 1175 °C (2150 °F) and aged 6244 h at 870 °C (1600 °F). Structure is $M_{23}C_6$, Laves phase, and probably M_6C in a fcc matrix. Electrolytic: HCl and H_2O_2. 500×



Fig. 143 Haynes 188, solution annealed at 1175 °C (2150 °F), aged 6244 h at 980 °C (1800 °F). Structure consists of M_6C and $M_{23}C_6$, and probably Laves phase, in a fcc matrix. Electrolytic: HCl and H_2O_2. 500×

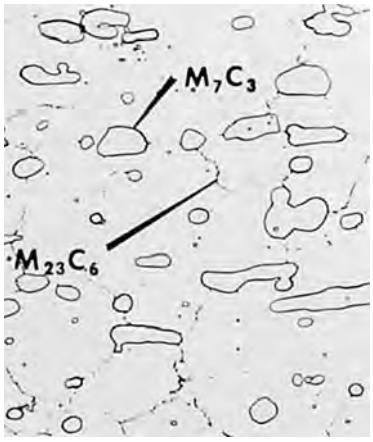


Fig. 144 Stellite 6B, solution annealed at 1230 °C (2250 °F) and aged 8 h at 900 °C (1650 °F). Structure is M_7C_3 and $M_{23}C_6$ carbides in a fcc matrix. Electrolytic: HCl and H_2O_2. 500×



Fig. 145 Stellite 6B, solution annealed at 1230 °C (2250 °F) and aged 8 h at 900 °C (1650 °F). M_7C_3 and $M_{23}C_6$ carbides in a predominantly fcc matrix with some hcp crystals. Electrolytic: HCl and H_2O_2. 500×

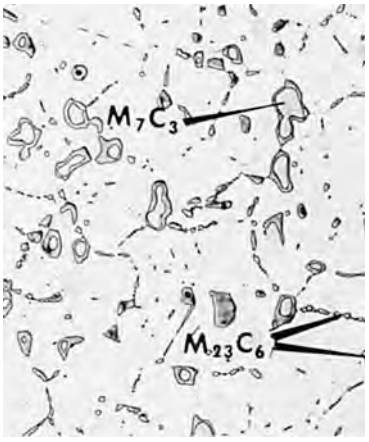


Fig. 146 Stellite 6B, solution annealed at 1230 °C (2250 °F) and aged 8 h at 1150 °C (2100 °F). Dark areas around primary M_7C_3 show it changing to $M_{23}C_6$. Matrix is fcc. Electrolytic: 2% H_2CrO_4; $KMnO_4$ stain. 500×

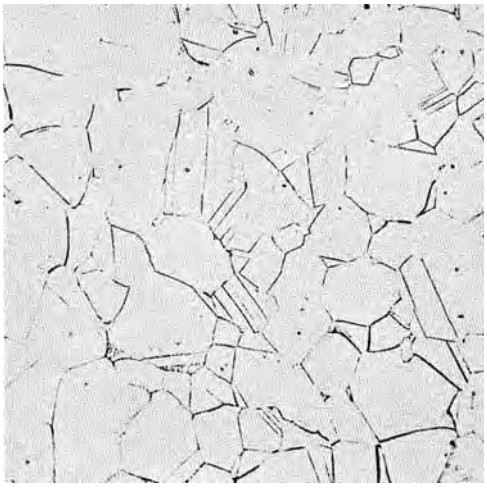


Fig. 147 Annealed

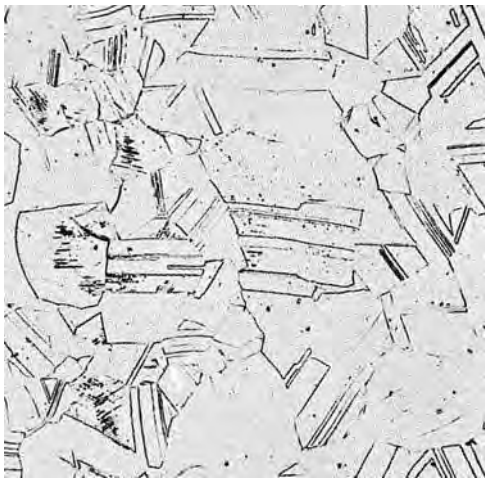


Fig. 148 15% cold drawn

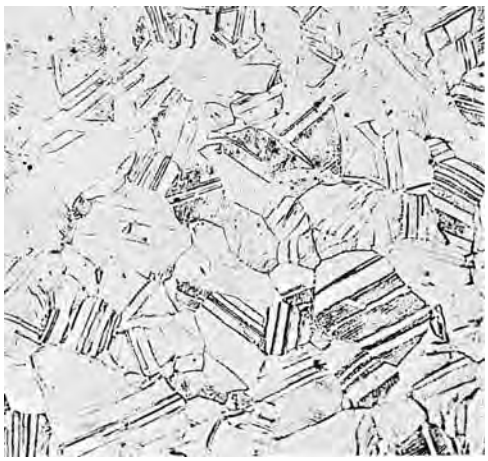


Fig. 149 24.5% cold drawn



Fig. 150 36.5% cold drawn



Fig. 151 44.0% cold drawn



Fig. 152 51.2% cold drawn

Fig. 147 to 152 Effect of cold work on the microstructure of MP35N that was solution annealed 1 h at 1065 °C (1950 °F), then air cooled to room temperature. The as-annealed structure in Fig.147 is typical of most cobalt-base or nickel-base alloys with a fcc matrix. In the annealed condition, the hardness is less than HRC 10. Work-hardening levels of 45 to 50% can produce hardness levels of about 45 HRC. 50 mL HCl, 5 g $CuCl_2$, 25 mL alcohol, and 45 mL H_2O. All at 250×

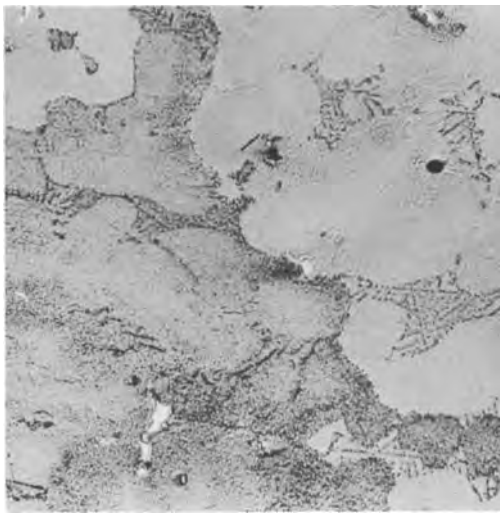


Fig. 153 B-1900 nickel-base alloy, as-cast. Structure consists of nickel-rich γ solid-solution matrix containing a few light-etching carbide particles and dispersed γ′ (see also Fig. 154 and 155 for details of the structure). Kalling's reagent. 100×

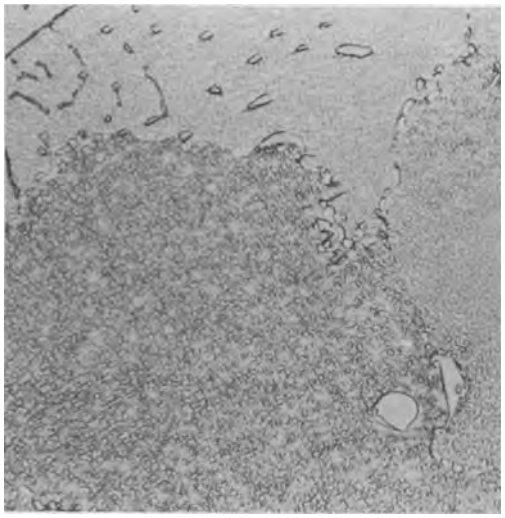


Fig. 154 Same alloy and condition as Fig. 153 but at a higher magnification. The light-etching carbide particles are dispersed and at grain boundaries. The fine constituent within grains is γ′ (see also Fig. 155). Kalling's reagent 2. 500×

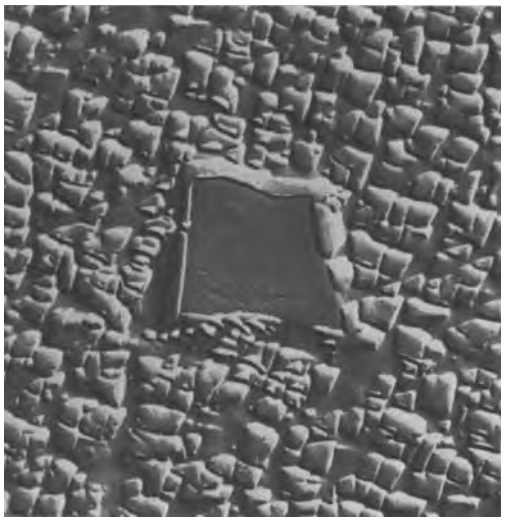


Fig. 155 Same alloy and condition as Fig. 153, but at a higher magnification and a replica electron micrograph showing details of a large MC carbide particle and particles of γ′ in the γ matrix. HCl, ethanol, $CuCl_2$, and H_2O_2. 7500×

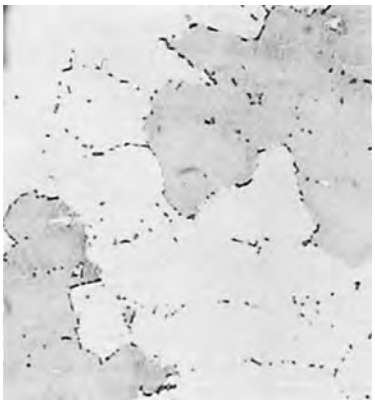


Fig. 156 B-1900 shell mold casting, as-cast. The structure consists of nickel-rich solid-solution matrix containing dispersed and grain-boundary (Ta,Mo)C and γ′ (barely visible). See also Fig. 157. Kalling's reagent. 100×



Fig. 157 Same alloy and condition as Fig. 156, but at a higher magnification. Precipitated primary (Ta,Mo)C is at grain boundaries and within grains; precipitated γ′ Ni_3(Al,Ti) is within grains. Kalling's reagent. 600×



Fig. 158 B-1900 shell mold casting, solution annealed 4 h at 1080 °C (1975 °F), aged 10 h at 900 °C (1650 °F). Grain-boundary carbide and boride and precipitated γ′ in γ matrix. Black spots are voids. See also Fig. 159. Kalling's reagent. 100×

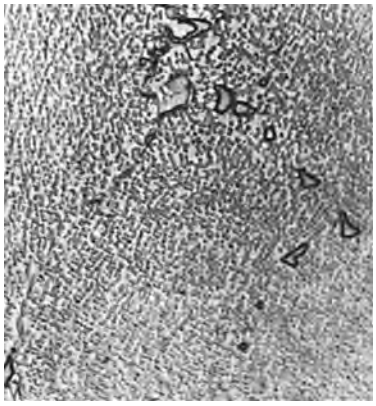


Fig. 159 Same alloy and heat treatment as Fig. 158 but at a higher magnification, which reveals details of particles of MC and M_3B_2 at grain boundary and primary precipitated γ′ Ni_3(Al,Ti) in the matrix. Kalling's reagent. 600×



Fig. 160 Hastelloy B, as-cast. Structure consists of M_6C at grain boundaries and as islands in the γ matrix. Electrolytic etch: HCl and CrO_3. 300×

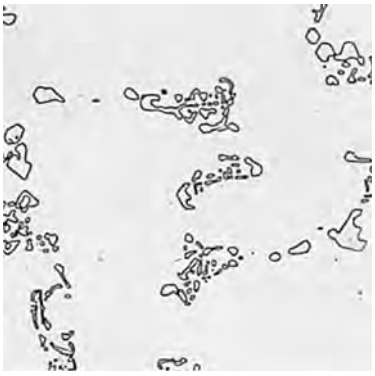


Fig. 161 Hastelloy B casting, annealed at 1175 °C (2150 °F) for 2 h and water quenched. M_6C islands in the matrix. Electrolytic etch: HCl and CrO_3. 300×



Fig. 162 Hastelloy C, as-cast. Structure consists of M_6C at grain boundaries and as islands in the γ matrix. Electrolytic etch: CrO_3. 300×

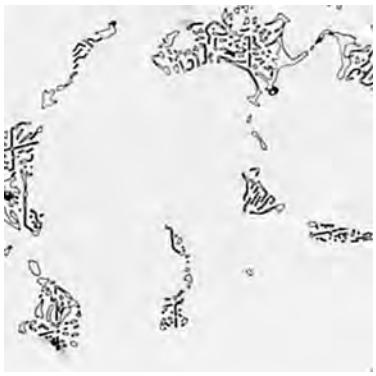


Fig. 163 Hastelloy C casting, annealed at 1230 °C (2250 °F) for 2 h and water quenched. M_6C in γ matrix. Electrolytic etch: CrO_3. 300×

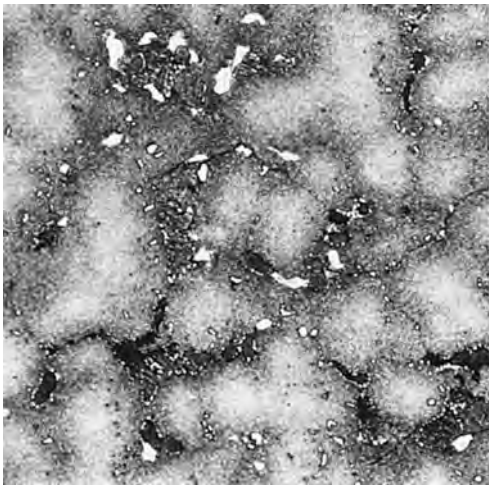


Fig. 164 IN-100, as-cast. Small, white islands are primary (eutectic) γ′; peppery gray constituent is precipitated γ′; black constituent is probably perovskite, a complex carbide. $Ni_3(Al,Ti)C$; matrix is nickel-rich γ. See also Fig. 165 and 166. Marble's reagent. 100×

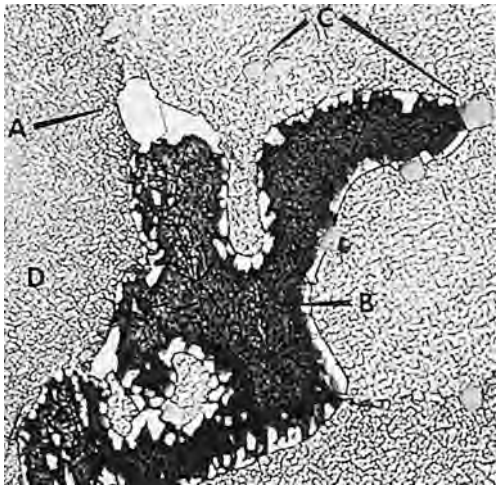


Fig. 165 Same as Fig. 164 but at a higher magnification. Light constituent (A) is primary (eutectic) γ′; dark (B), probably perovskite, $Ni_3(Al,Ti)C$. Dispersed carbide particles are shown at C. Gamma matrix contains precipitated (D). See also Fig. 166. Marble's reagent. 500×

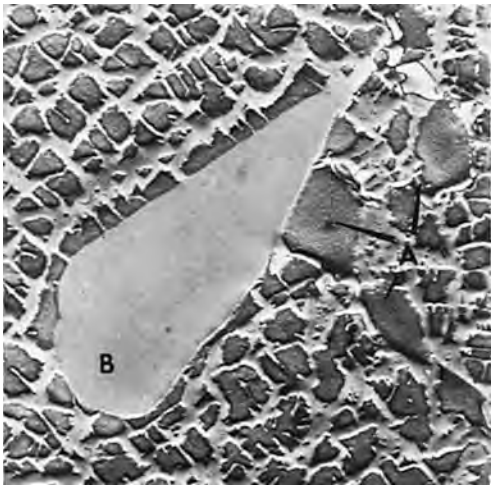


Fig. 166 Same casting as for Fig. 164 and 165 but at a higher magnification and a replica electron micrograph showing islands of primary carbide γ′ (A), a large particle of primary carbide (B), and dispersed particles of precipitated γ′ in γ matrix. Marble's reagent. 5000×

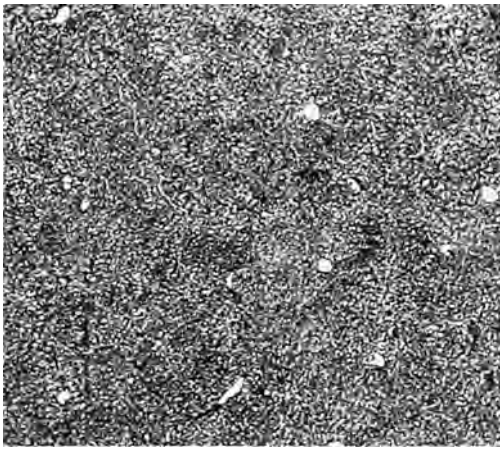


Fig. 167 IN-100, as-cast. The white islands are primary, or eutectic, γ′. Precipitated γ′ is barely visible in the γ matrix. See also Fig. 168. Marble's reagent. 100×

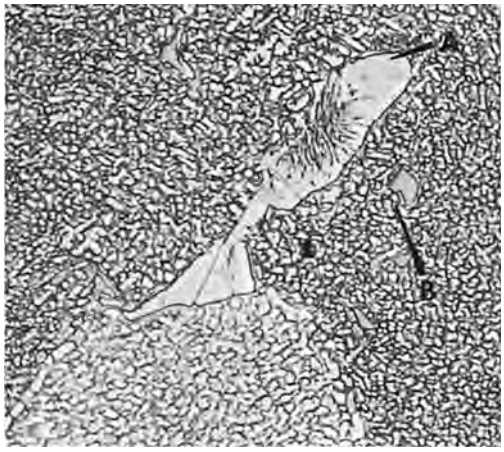


Fig. 168 Same as Fig. 167 but at a higher magnification. Island of primary (eutectic) γ′ (A), dispersed carbide (B), and precipitated γ′ in γ matrix. Marble's reagent. 500×

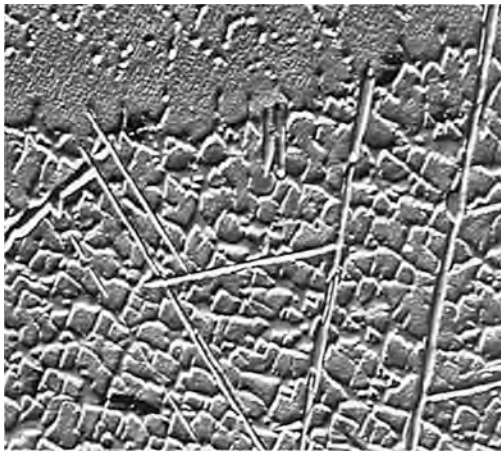


Fig. 169 IN-100 casting, held at 760 °C (1400 °F) for 5000 h. Replica electron micrograph. Platelets of σ and primary and precipitated γ′ in γ matrix. HCl, ethanol, and H_2O_2. 4500×

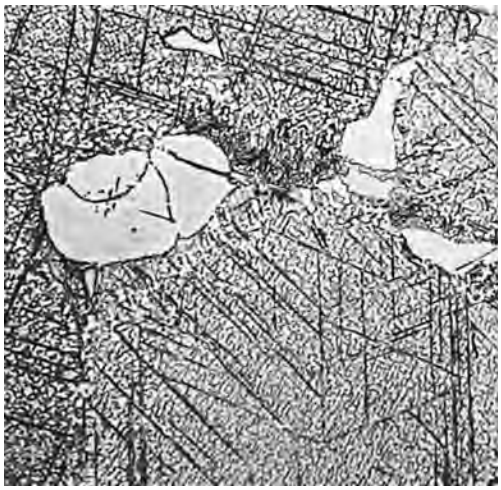


Fig. 170 IN-100 casting, held at 815 °C (1500 °F) for 5000 h. Structure consists of massive MC particles, platelets of σ phase, and primary and precipitated γ′ in the γ matrix. See also Fig. 171. HCl, ethanol, and H_2O_2. 500×

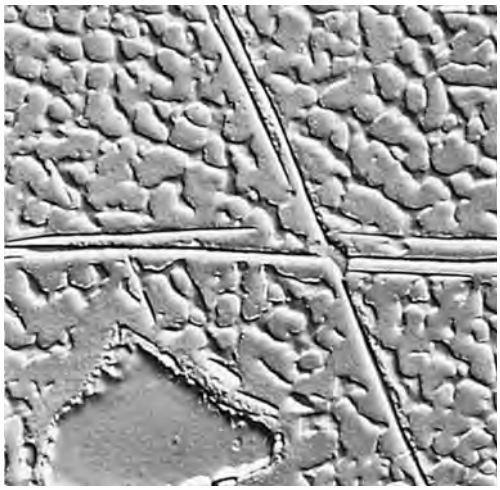


Fig. 171 IN-100 casting, held at 815 °C (1500 °F) for 5000 h. Replica electron shows a massive particle of MC, Widmanstätten platelets of σ phase, and γ′ in the γ matrix. HCl, ethanol, and H_2O_2. 4500×



Fig. 172 IN-100 casting held at 925 °C (1700 °F) for 36 h. Replica electron micrograph. No σ formed at this temperature. The structure is grain-boundary carbide and γ′ in the γ matrix. HCl, ethanol, $CuCl_2$, and H_2O_2. 4500×

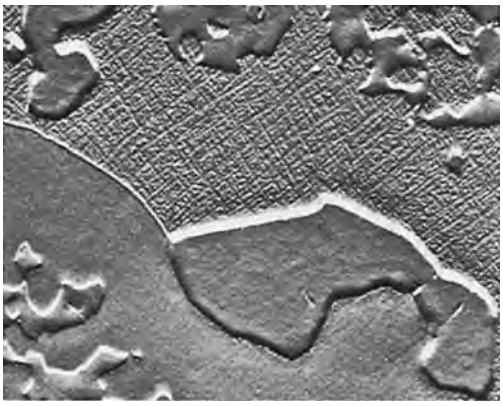


Fig. 173 IN-100 casting, held at 925 °C (1700 °F) for 5000 h. Replica electron micrograph. No σ formed at this temperature. The structure is grain-boundary $M_{23}C_6$ and γ′ in the γ matrix. HCI, ethanol, and H_2O_2. 4500×

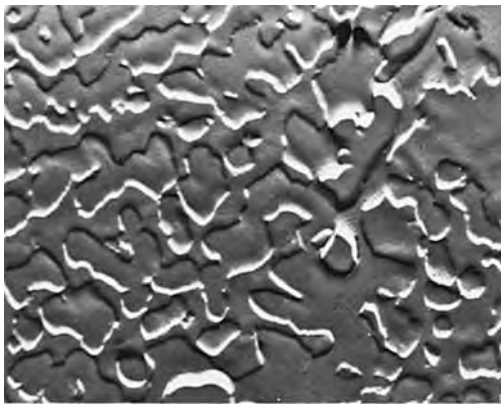


Fig. 174 IN-100 casting, held at 1040 °C (1900 °F) for 16 h. A replica transmission electron micrograph. Note the absence of σ phase in this structure and the presence of coarsened γ′ in the γ matrix. HCI, ethanol, $CuCl_2$, and H_2O_2. 4500×

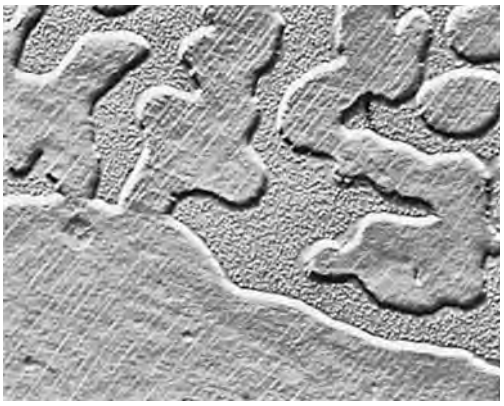


Fig. 175 IN-100 casting, held at 1040 °C (1900 °F) for 5000 h. A replica transmission electron micrograph. Structure consists of blocky γ′ and fine precipitated γ′ in a matrix of γ solid solution. HCI, ethanol, and H_2O_2. 4500×

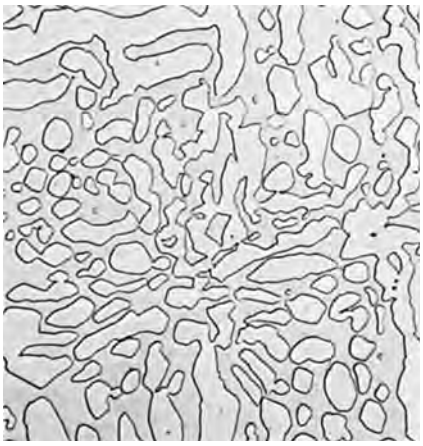


Fig. 176 IN-100 casting, held at 1095 °C (2000 °F) for 5000 h. Optical micrograph shows random dispersion of large and small islands of γ′ in the γ matrix. HCI, ethanol, and H_2O_2. 500×

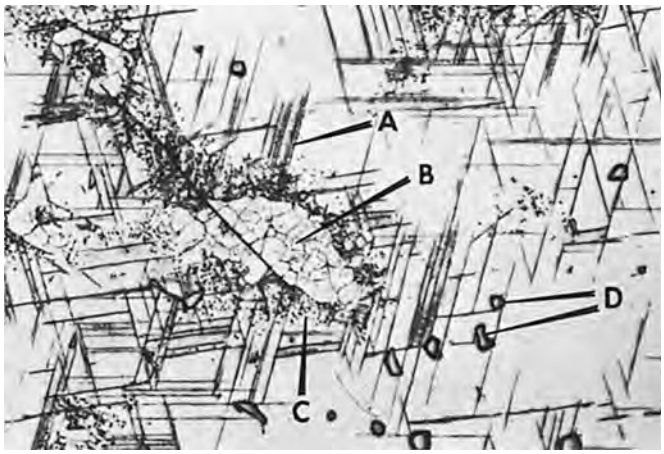


Fig. 177 IN-100 casting, creep-rupture tested at 815 °C (1500 °F) for 1113.6 h at 276 MPa (40 ksi). The structure consists of Widmanstätten σ phase (A), primary (eutectic) γ′ (B), precipitated γ′ (C), and particles of carbide (D), in the γ matrix. Glyceregia. 500×

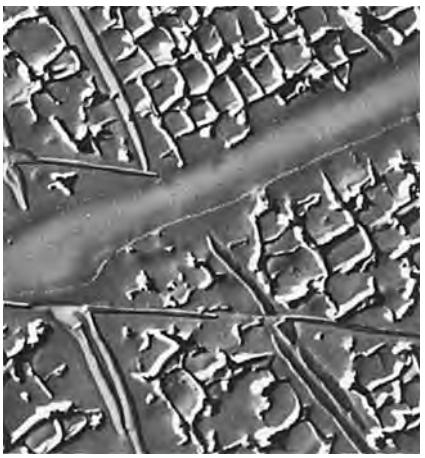


Fig. 178 Same as Fig. 177 but at a higher magnification and a replica electron micrograph showing platelets of σ emerging from carbide and precipitated γ′ in the γ matrix. Electrolytic etch: H_2SO_4 and methanol. 10,000×



Fig. 179 Alloy 713C ingot, 250 mm (10 in.) diameter, as-cast. Structure is a matrix of γ solid solution containing "script" MC carbide in a characteristic dendritic arrangement. HCI, methanol, and $CuCl_2$. 100×



Fig. 180 Alloy 713C, as-cast. The MC arrangement is in a "script" pattern (see Fig. 181 for a random pattern of carbide particles). The matrix is γ solid solution. As-polished. 100×

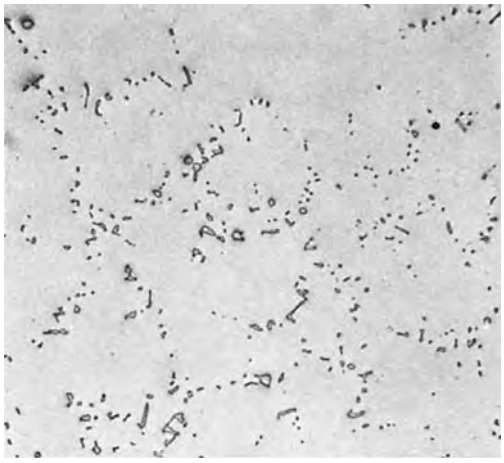


Fig. 181 Alloy 713C, as-cast. A random pattern of MC particles appears in this structure (see Fig. 180 for a "script" pattern of carbide). The matrix is γ solid solution. As-polished. 100×



Fig. 182 Alloy 713C, as-cast. Note the dendritic pattern. The dark areas contain carbide particles and some primary γ′ (white plates). Matrix is γ solid solution. Marble's reagent. 500×

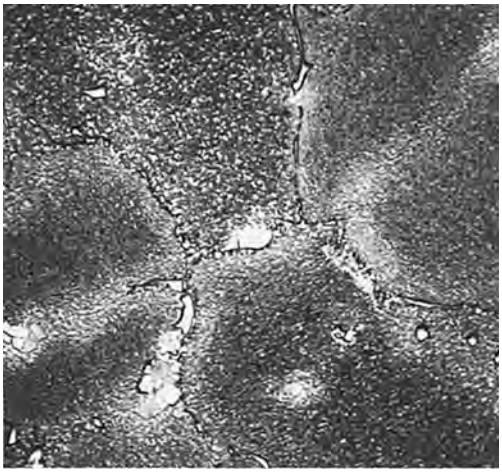


Fig. 183 Alloy 713C, as-cast. The massive white particles are primary γ′; the grain-boundary film is MC particles. Gamma matrix contains γ′. Glyceregia.

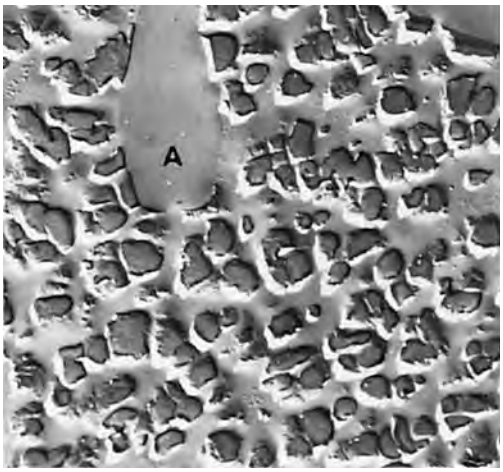


Fig. 184 Alloy 713C, as-cast. Replica electron micrograph. Structure shown consists of large particles of carbide (A) and γ′ in the matrix of γ solid solution. Marble's reagent. 5000×

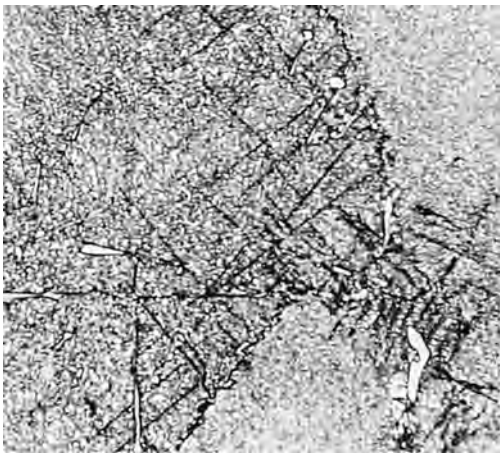


Fig. 185 Alloy 713C casting held 5000 h at 760 °C (1400 °F). Widmanstätten σ phase, grain-boundary carbide, and precipitated γ′ in the γ matrix. See also Fig. 186. HCl, ethanol, and H_2O_2. 500×

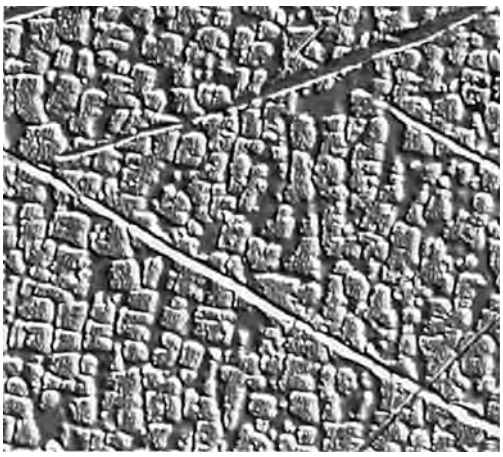


Fig. 186 Same as Fig. 185 but at a higher magnification and a replica electron micrograph showing Widmanstätten pattern of σ platelets and γ′ in the γ matrix. HCl, ethanol, and H_2O_2. 4500×

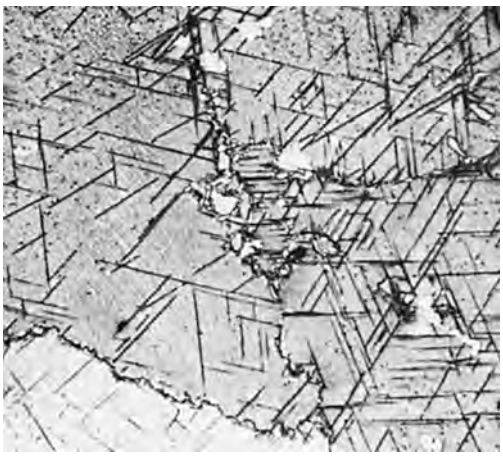


Fig. 187 Alloy 713C casting, held at 845 °C (1550 °F) for 1000 h, air cooled. Note Widmanstätten pattern of phase and grain-boundary carbide (white) in γ matrix. Marble's reagent. 500×

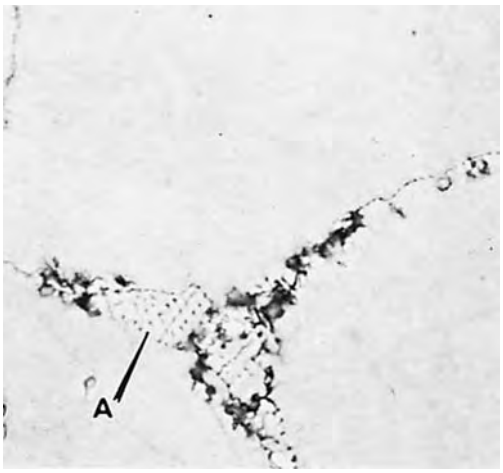


Fig. 188 Alloy 713C casting, heated to 1260 °C (2300 °F). The grain-boundary eutectic structure (A) indicates incipient melting. Matrix is γ (see also Fig. 189). Marble's reagent. 500×

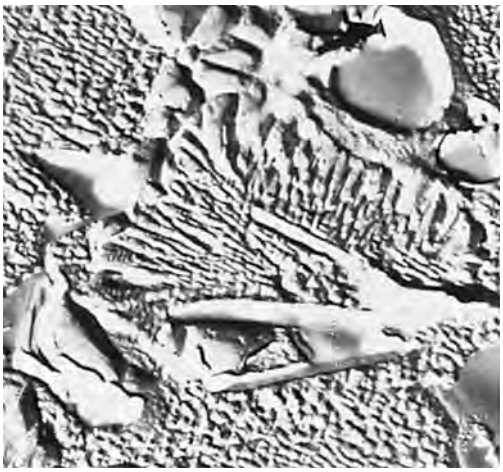


Fig. 189 Same as Fig. 188 but at a higher magnification and a replica electron micrograph showing eutectic structure at area of incipient melting and γ′ in γ matrix. Marble's reagent. 5000×

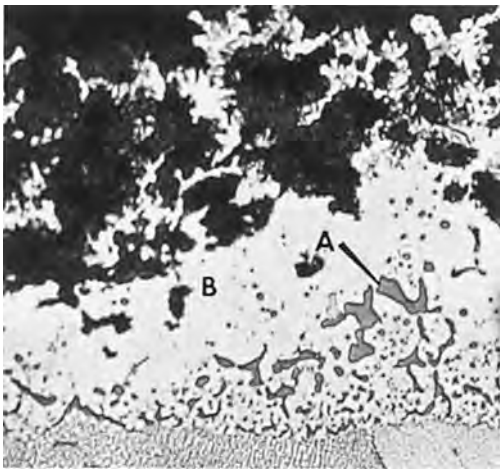


Fig. 190 Alloy 713C, exposed to sulfidation at elevated temperature. Sulfur-rich surface layer (dark, at top), chromium sulfide particles (A), and alloy-depleted zone (B). HCl, methanol, and $FeCl_3$. 500×

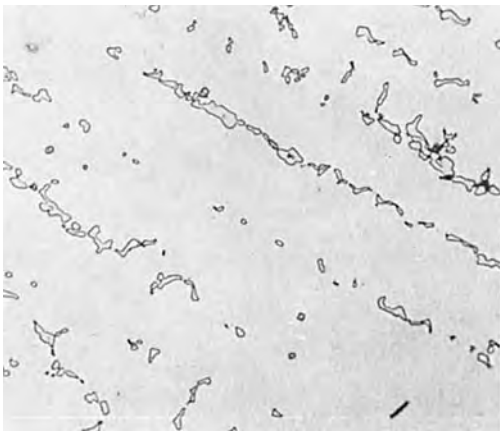


Fig. 191 Alloy 718, vacuum cast, solution annealed 2 h at 1095 °C (2000 °F), air cooled, reannealed 1 h at 980 °C (1800 °F), air cooled, aged 16 h at 720 °C (1325 °F), air cooled. Structure: chainlike precipitate of M_2(Nb,Ti) Laves phase in the γ matrix. Compare with Fig. 192. HCl, methanol, and $FeCl_3$. 250×

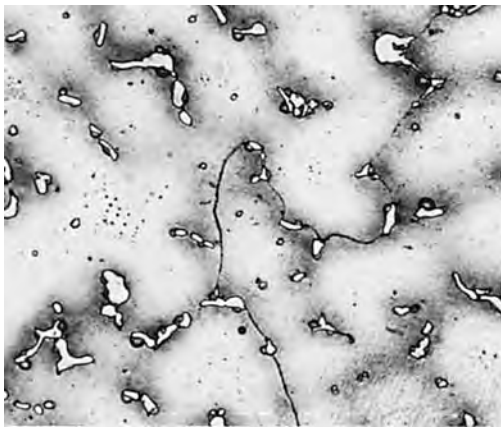


Fig. 192 Alloy 718, vacuum cast and heat treated as for Fig. 191, except solution annealing at 1095 °C (2000 °F) was for only 1 h and all furnace heating was done under a protective atmosphere of argon. Laves phase (white islands) has precipitated at dendrites in the γ matrix. HCl, methanol, and $FeCl_3$. 250×

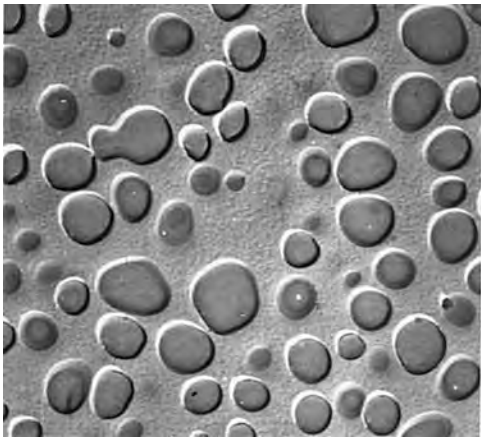


Fig. 193 IN-738 casting, after holding at 815 °C (1500 °F) for 1000 h. A replica electron micrograph. Structure consists of rounded γ′ particles in γ matrix. Compare with Fig. 196. Electrolytic etch: H_2SO_4 and methanol. 20,000×

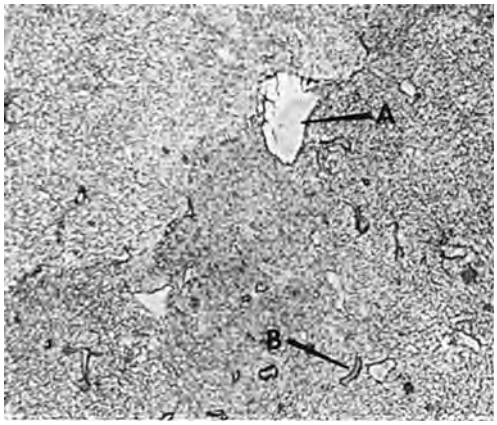


Fig. 194 IN-738, as-cast. The structure consists of primary , of eutectic, γ′ islands (shown at A), dispersed carbide particles (shown at B), and precipitated γ′ in the matrix of γ solid solution. See also Fig. 195. Marble's reagent. 500×

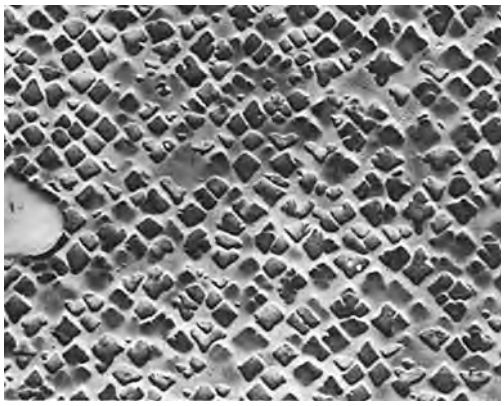


Fig. 195 Same as Fig. 194, except at higher magnification and a replica electron micrograph showing randomly distributed precipitated γ′, Ni_3(Al, Ti) and a carbide particle (at right edge) in matrix of γ solid solution. Marble's reagent. 5000×

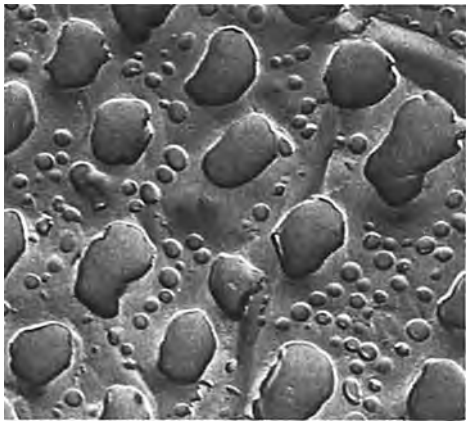


Fig. 196 IN-738 solution annealed 2 h at 1120 °C (2050 °F), held 24 h at 845 °C (1550 °F), replica electron micrograph. Gamma-prime particles in γ; the smaller particles formed in cooling. Electrolytic etch: H_2SO_4 and methanol. 25,000×

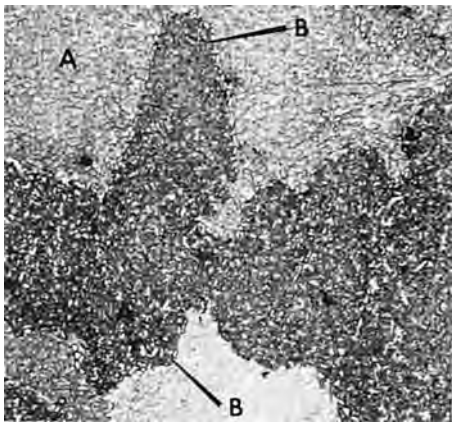


Fig. 197 MAR-M 246, as-cast. Structure consists of precipitated γ′ in the γ matrix (A) and fine particles of carbide or primary γ′ at grain boundaries (B). See also Fig. 198. Marble's reagent. 500×

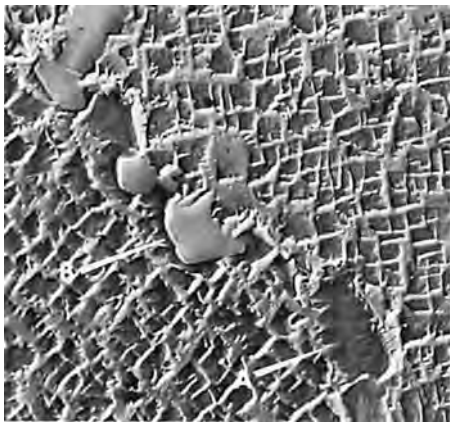


Fig. 198 Same as Fig. 197 but at a higher magnification and a replica electron micrograph showing primary γ′ (A) and carbide (B) at a grain boundary and randomly dispersed γ′ in the γ matrix. Marble's reagent. 5000×

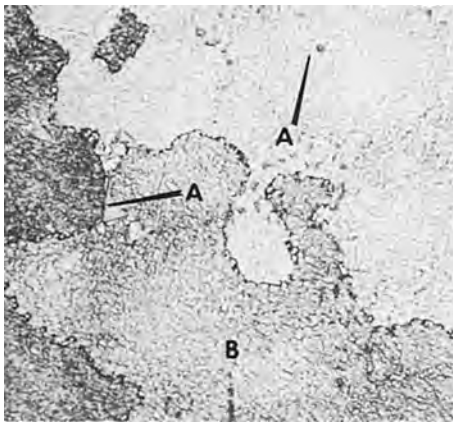


Fig. 199 MAR-M 246 casting held 50 h at 845 °C (1550 °F), air cooled. Grain-boundary and matrix carbide (A) and dispersed γ′ in γ matrix (B). Compare with Fig. 200, a casting cooled more slowly from liquidus. Marble's reagent. 500×

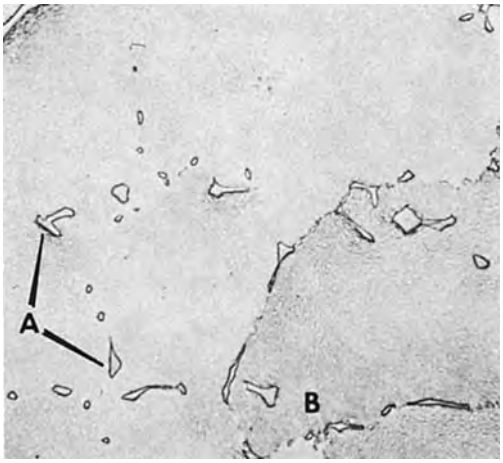


Fig. 200 MAR-M 246 casting cooled more slowly from liquidus than that in Fig. 199, then given some heat treatment. Grain-boundary and matrix carbide (A) and a dispersion of fine γ′ in the γ matrix (B). Marble's reagent. 500×

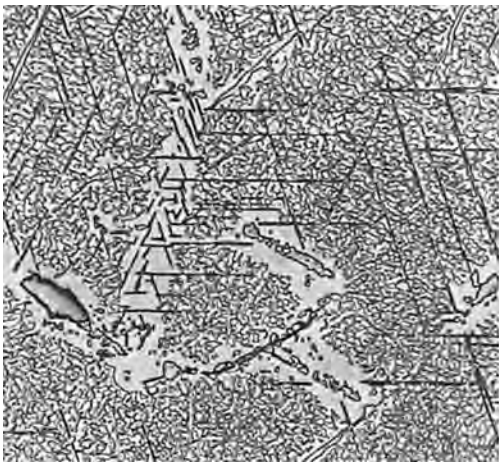


Fig. 201 MAR-M 246 casting, held at 980 °C (1800 °F) for 5000 h. The structure consists of needlelike particles of M_6C and γ′ in the γ matrix. See Fig. 202 for better resolution of constituents. HCl, ethanol, and H_2O_2. 500×

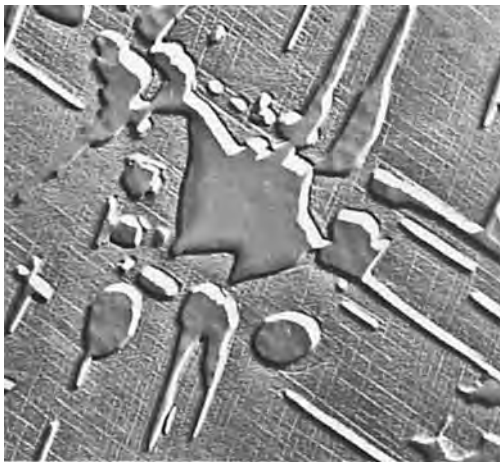


Fig. 202 Same alloy and treatment as Fig. 201 but at a higher magnification. A replica transmission electron micrograph. Structure consists of needlelike particles of M_6C and γ′ in the γ matrix. HCl, ethanol, and H_2O_2. 4500×



Fig. 203 MAR-M 246 casting, exposed to temperatures above 980 °C (1800 °F). Chainlike $M_{23}C_6$ particles at grain boundaries and needlelike M_6C within grains. Matrix is γ. Marble's reagent. 500×

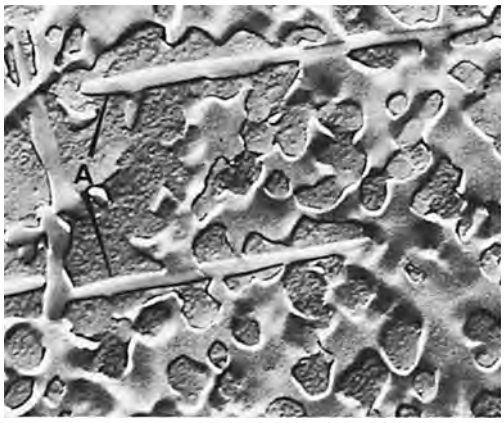




Fig. 204, 205 Same as Fig. 203 but at a higher magnification and replica electron micrographs. Fig. 204: needles of M_6C (A), $M_{23}C_6$ at grain boundaries, and γ′ $Ni_3(Al,Ti)$. Fig. 205: a large particle of $M_{23}C_6$ and a connecting carbide (B), and a γ′ envelope (C). The matrix is γ. Marble's reagent. 5000×



Fig. 206 TRW-NASA VIA, as-cast. Blocky, light constituent is primary γ′; the black spots are carbide particles; the mottled gray areas are precipitated γ′ in a matrix of γ solid solution (see also Fig. 207). Electrolytic etch: H_2SO_4 and methanol. 250×



Fig. 207 Same alloy and condition as Fig. 206 but at a higher magnification. Replica electron micrograph. Large particles are MC carbide; primary (eutectic) γ′ is at lower right; remainder is γ′ in γ matrix. Electrolytic etch: H_2SO_4 and methanol. 3000×

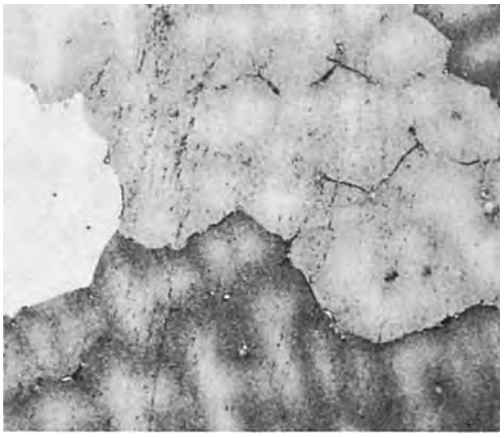


Fig. 208 U-700 as-cast. Small, white crystals are carbide particles; darkened areas include primary (eutectic) γ′; matrix is γ solid solution. Kalling's reagent. 100×



Fig. 209 U-700 casting, solution annealed and furnace cooled to 1080 °C (1975 °F), then aged at 760 °C (1400 °F) for 16 h and air cooled. Small, white crystals are carbide; mottled gray areas include γ′. See also Fig. 210. Kalling's reagent. 100×

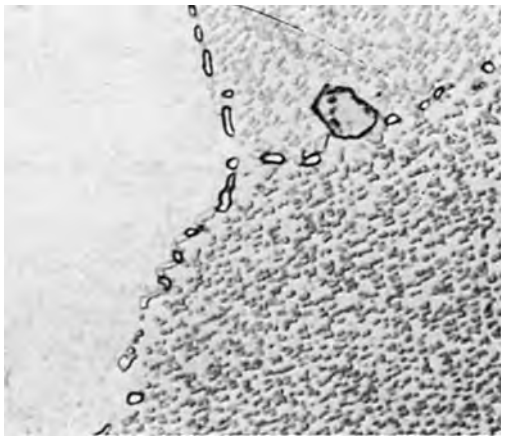


Fig. 210 Same alloy and heat treatment as Fig. 209 but at a higher magnification. $M_{23}C_6$ has precipitated along grain boundaries. Large carbide particles dispersed within grains. Remainder is γ′ in γ matrix. Kalling's reagent. 1000×

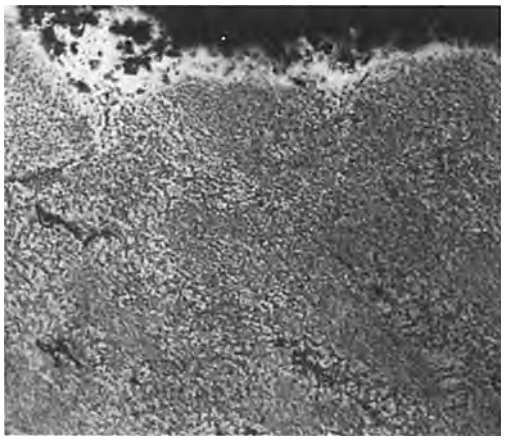


Fig. 211 U-700 cast blade after 190 h cyclic sulfidation-erosion testing using turbine fuel and 3.5 ppm synthetic sea salt. Note erosive attack and sulfur-rich corrosion products at surface (top). Kalling's reagent. 250×

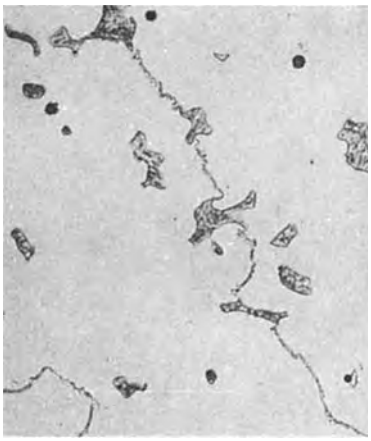


Fig. 212 Haynes 21 cobalt-base alloy, as-cast. Structure consists of primary M_7C_3 particles in an α (fcc) matrix. See Fig. 213 to 214 for effects of heat treatment. Electrolytic etch: HCl. 200×

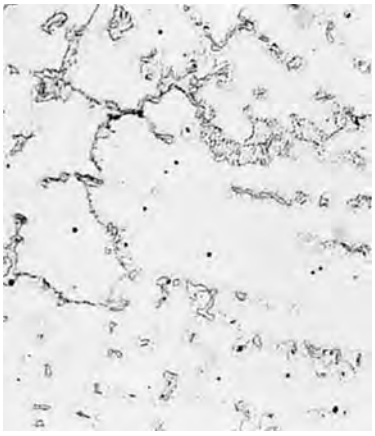


Fig. 213 Haynes 21 casting aged 24 h at 760 °C (1400 °F). M_7C_3 (large particles) and precipitated $M_{23}C_6$ at grain boundaries and in grains of fcc matrix. See also Fig. 214. Electrolytic etch: HCl. 500×



Fig. 214 Same as Fig. 213 but at a higher magnification; replica electron micrograph. M_7C_3 particles, and $M_{23}C_6$ at grain boundaries and within grains of matrix. See also Fig. 215. Electrolytic etch: HCl. 3000×



Fig. 215 Same as Fig. 214 but showing a massive particle of primary M_7C_3 and secondary $M_{23}C_6$ in the fcc matrix. Carbides were determined by diffraction analysis. Electrolytic etch: HCl. 3000×

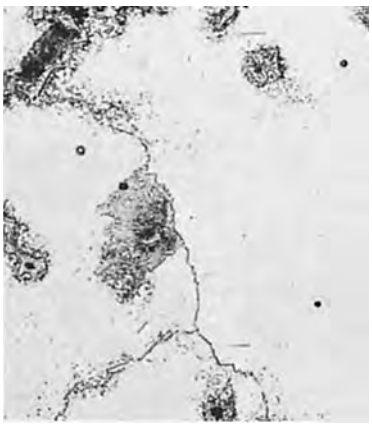


Fig. 216 Haynes 21 casting aged 24 h at 870 °C (1600 °F). M_7C_3 particles and precipitated $M_{23}C_6$ at grain boundaries and in grains of fcc matrix. See also Fig. 217. Electrolytic etch: HCl. 500×

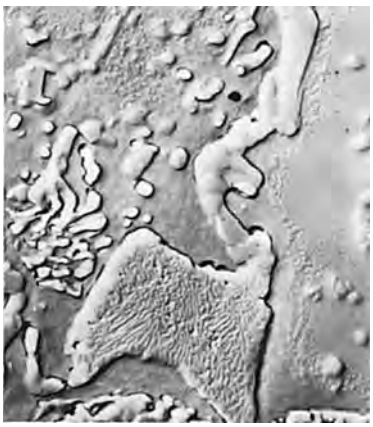


Fig. 217 Replica electron micrograph of Fig. 216. Massive primary M_7C_3 particle and secondary precipitate of $M_{23}C_6$ at grain boundaries and within grains. Electrolytic etch: HCl. 3000×



Fig. 218 Haynes 31, as-cast. Structure consists of large, primary M_7C_3 particles and grain-boundary $M_{23}C_6$ in an α (fcc) matrix. See also Fig. 219 and 220. Electrolytic etch: 2% CrO_3. 400×

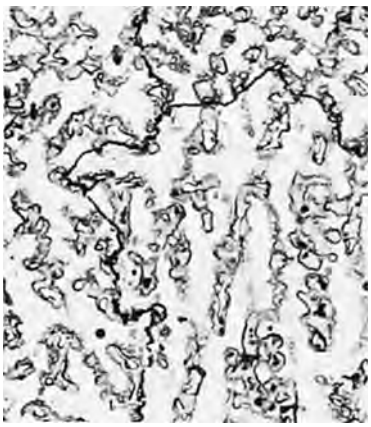


Fig. 219 Haynes 31, as-cast thin section, aged 22 h at 730 °C (1350 °F). Precipitated $M_{23}C_6$ at grain boundaries and adjacent to primary carbide (M_7C_3) particles. Electrolytic etch: 2% CrO_3. 400×



Fig. 220 Haynes 31, as-cast thick section, aged 22 h at 730 °C (1350 °F). Large particles are M_7C_3; grain-boundary and mottled dispersions are $M_{23}C_6$; fcc matrix. Electrolytic etch: 2% CrO_3. 500×

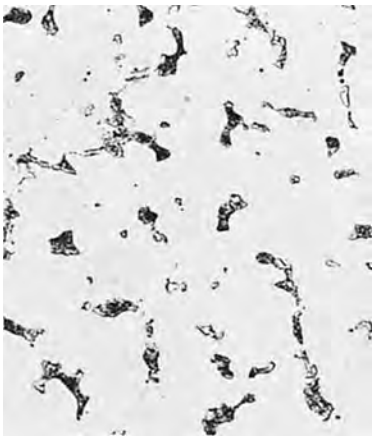


Fig. 221 Haynes 151, as-cast. Structure consists of dispersed islands of large primary carbide (M_6C) in the α (fcc) matrix. See also Fig. 222. Electrolytic etch: HCl and CrO_3. 200×

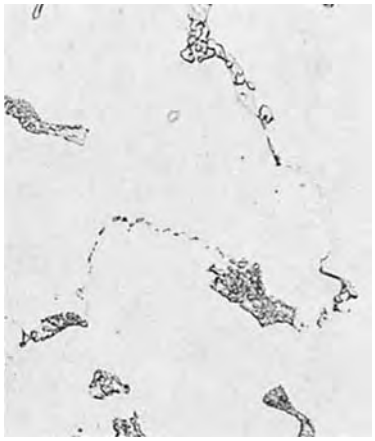


Fig. 222 Same as Fig. 221 but at a higher magnification, which reveals details of the M_6C (note the lamellar form) in the α (fcc) matrix. Electrolytic etch: HCl and CrO_3. 500×



Fig. 223 Haynes 151 casting aged 16 h at 760 °C (1400 °F) M_6C particles and precipitated $M_{23}C_6$ at grain boundaries and next to M_6C particles in the fcc matrix. Electrolytic etch: HCl and CrO_3. 500×

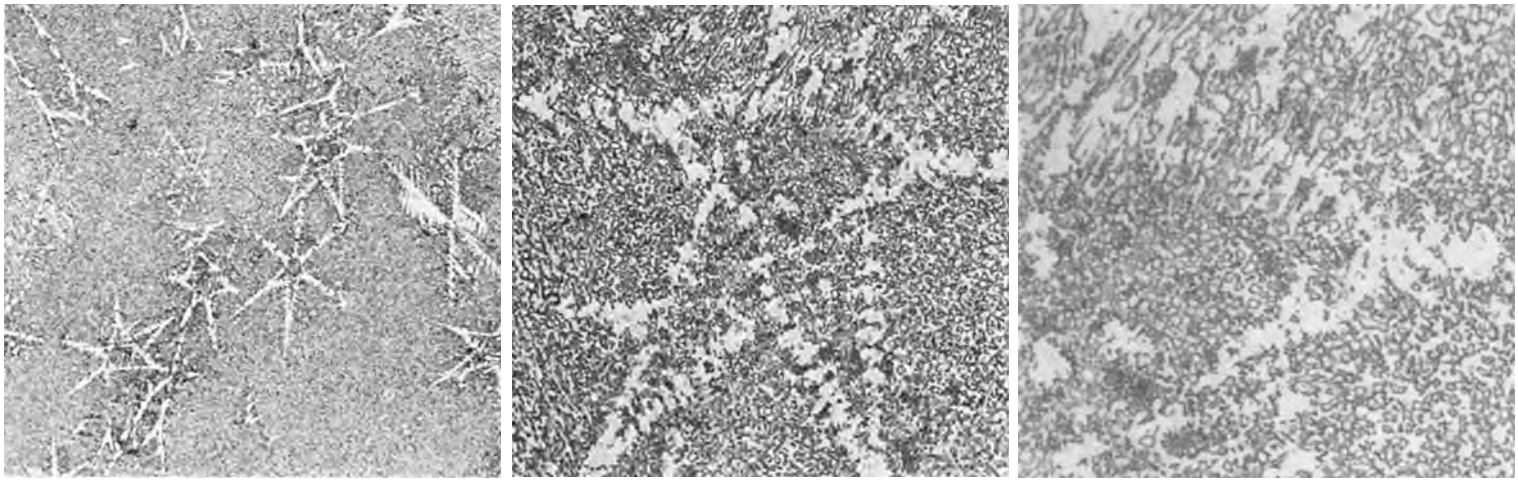


Fig. 224, 225, 226 98M2 Stellite, as-investment-cast ring. Microstructure consists of large primary carbides in a matrix of secondary carbides and cobalt-chromium-tungsten solid solution. Some primary carbides have solidified in a star-like array. Electrolytic etch: 50% HNO_3. Fig. 224: 100×; Fig. 225: 500×; Fig. 226: 1000×. (S.E. Wall and R.L. Snyder)

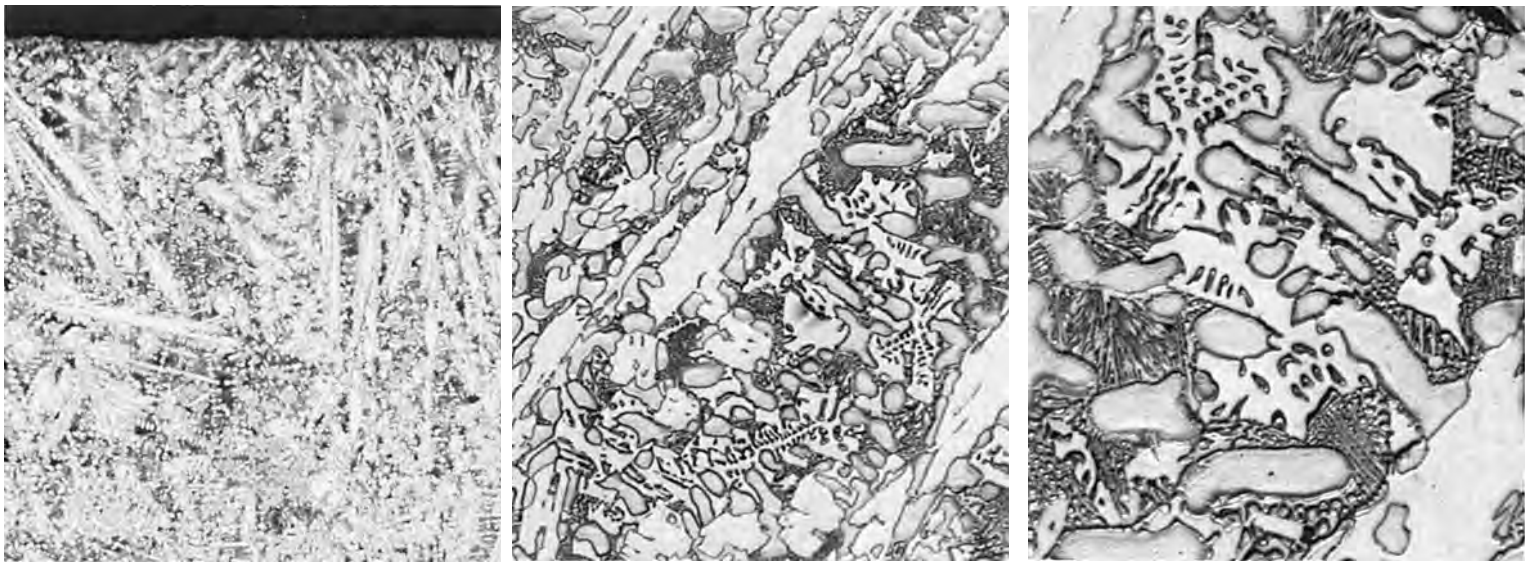


Fig. 227, 228, 229 98M2 Stellite, as-investment-cast bar. Very large primary carbides in a matrix of smaller secondary carbides and cobalt-chromium-tungsten solid solution. Electrolytic etch: 50% HNO_3. Fig. 227: 100×; Fig. 228: 500×; Fig. 229: 1000×. (S.E. Wall and R.L. Snyder)



Fig. 230 WI-52, as-cast. The solid gray islands are complex chromium-tungsten carbide; particulated islands are niobium carbide. The dark dots are silicate inclusions in the matrix of cobalt-chromium solid solution. Electrolytic etch: 5% H_3PO_4. 500×

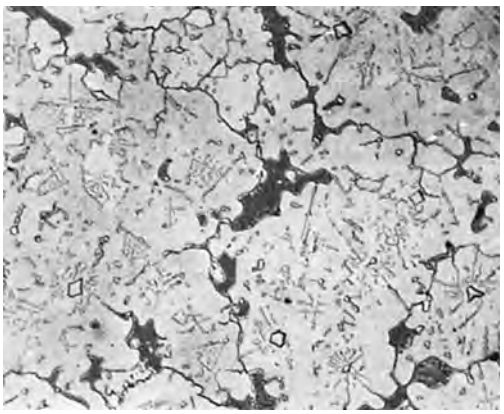


Fig. 231 MAR-M 302, as-cast. Structure consists of primary, or eutectic, M_6C particles (dark gray) and MC particles (small white crystals) in the matrix of cobalt-chromium-tungsten solid solution. See Fig. 232 for better resolution of constituents. Kalling's reagent. 100×

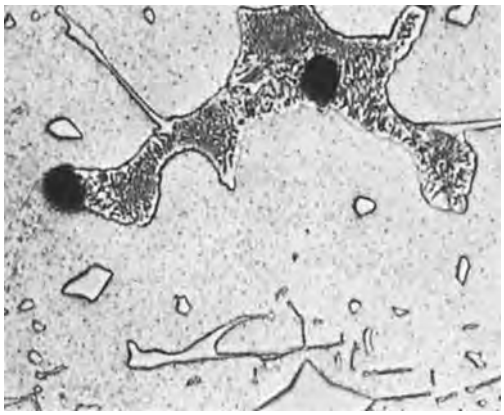


Fig. 232 MAR-M 302, as-cast, at a higher magnification than Fig. 231. The mottled gray islands are primary eutectic carbide; the light crystals are MC particles. The peppery constituent within grains of the matrix is $M_{23}C_6$. Kalling's reagent. 500×

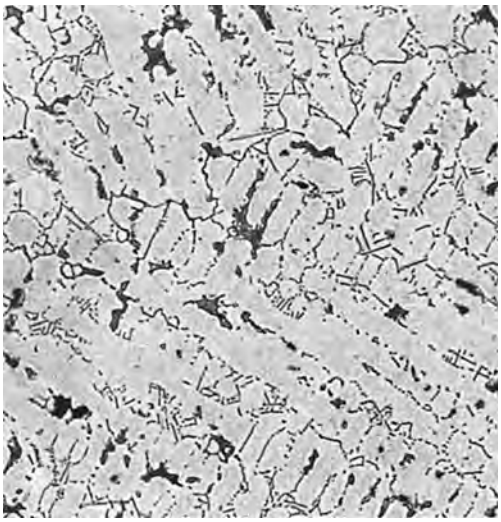


Fig. 233 MAR-M 509, as-cast. The structure consists of MC particles in script form and $M_{23}C_6$ particles in eutectic form (gray areas) and precipitate form in the dendritic α solid-solution matrix (fcc). Kalling's reagent. 100×

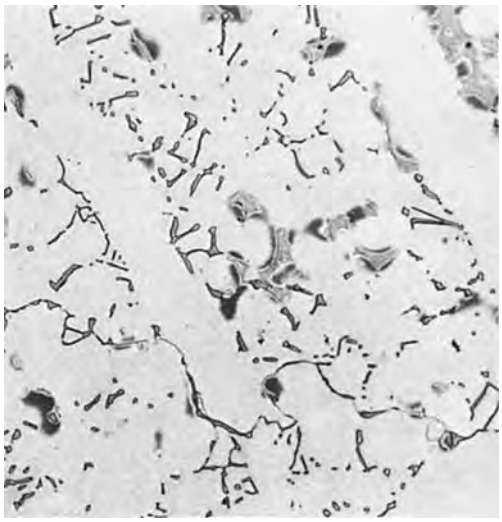


Fig. 234 Same as Fig. 233 but at a higher magnification to reveal morphology of MC script particles, primary eutectic particles ($M_{23}C_6$), and precipitated $M_{23}C_6$ (shadowy constituent) in the α (fcc) matrix. Electrolytic etch: 5% H_3PO_4. 500×



Fig. 235 MAR-M 509, aged at 705 °C (1300 °F). Thin-foil electron micrograph. Top left to bottom right: precipitated $M_{23}C_6$; α (fcc) matrix; blocky $M_{23}C_6$ with cobalt; cobalt with internal precipitate; lamellar $M_{23}C_6$ in matrix. As-polished. 10,000×

ASM Specialty Handbook: Nickel, Cobalt, and Their Alloys
J.R. Davis, editor, p 331-341
DOI:10.1361/ncta2000p331

Copyright © 2000 ASM International®
All rights reserved.
www.asminternational.org

Phase Diagrams of Binary and Ternary Nickel Systems

PHASE DIAGRAMS covering many of the commercially important nickel alloy systems are presented in this article. Crystallographic data in tabular form accompany some of the diagrams. The binary alloy diagrams included here (Fig. 1–13, Tables 1–13) are the result of critical assessment by experts in the field under the coordination of the International Programme for Alloy Phase Diagrams. The ternary alloy diagrams (Fig. 14–44) were selected from the comprehensive collection of ternary diagrams, the multivolume *Handbook of Ternary Alloy Phase Diagrams*, P. Villars, A. Prince, and H. Okamoto, Ed., published by ASM International in 1994. All of the binary and ternary phase diagrams presented herein were also published in *Alloy Phase Diagrams*, Volume 3, of the *ASM Handbook.* This volume should be consulted for original bibliographic citations relating to specific phase diagrams.

Nickel Alloy Systems. Nickel is used industrially in the nominally pure form and as a constituent of many different alloys. Nickel-base alloys range from simple two-component (binary) alloy systems to highly complex alloys containing as many as 12 alloying elements. The primary elements nickel is associated with in commercial alloys include iron, chromium, copper, molybdenum, and cobalt, but as inferred above, many other elements are included in certain alloys to impart the particular characteristics required—strength, ductility, corrosion resistance, and so forth. For example, aluminum added to nickel alloys introduces precipitation hardening via formation of the Ni_3Al, or γ', phase (Fig. 1). Hardening precipitates and/or intermetallics are also produced by titanium and niobium additions. Even nonmetallic materials are sometimes added to nickel alloys. For example, some powder metallurgy alloys are strengthened by dispersion of inert particles such as yttria, coupled in some cases with γ' precipitation.

This article reviews the constitution of simple binary and ternary systems on which the more complex commercial alloys are based. The binary systems examined include Ni-Al, Ni-B, Ni-C, Ni-Co, Ni-Cr, Ni-Cu, Ni-Fe, Ni-Mo, Ni-Nb, Ni-P, Ni-Si, Ni-Ti, and Ni-W. Ternary systems illustrated include Ni-Al-Cr, Ni-Cr-Fe, Ni-Cr-Mo, Ni-Cr-Nb, Ni-Cr-Ti, Ni-Cr-W, Ni-Fe-Mo, Ni-Fe-W, Ni-Co-Cr, Ni-Co-Fe, and Ni-Al-Cu. The ternary diagrams are all isothermal sections at various temperatures. Solidus and liquidus projections for some of these ternary systems can be found in Volume 3 of the *ASM Handbook.* Additional information may be found in Ref 1 and 2.

REFERENCES

1. W. Betteridge, Constitution of Nickel Alloy Systems, *Nickel and Its Alloys*, Ellis Horwood Ltd., 1984, p 38–62
2. H. Baker, Introduction to Phase Diagrams, *Alloy Phase Diagrams*, Vol 3, *ASM Handbook*, ASM International, 1992, p 1-1 to 1-29

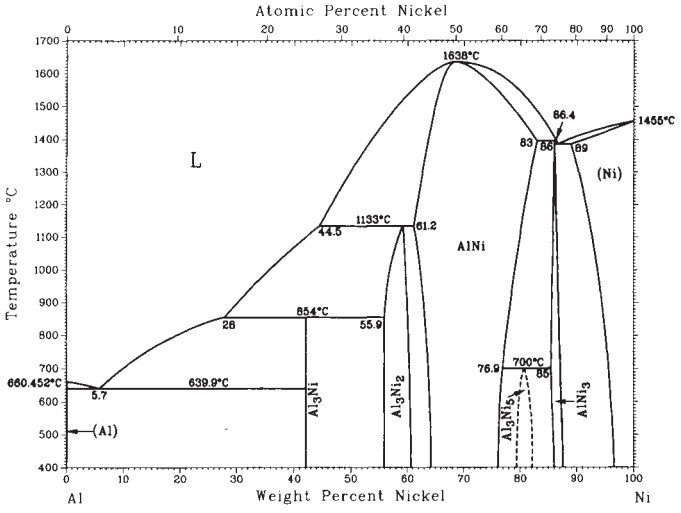


Fig. 1 The nickel-aluminum (Ni-Al) binary phase diagram

Table 1 Ni-Al crystal structure data

Phase	Composition, wt% Ni	Pearson symbol	Space group
(Al)	0–0.24	*cF*4	$Fm\bar{3}m$
Al_3Ni	42	*oP*16	*Pnma*
Al_3Ni_2	55.9–60.7	*hP*5	$P\bar{3}m1$
AlNi	61–83.0	*cP*2	$Pm\bar{3}m$
Al_3Ni_5	79–~82	…	*Cmmm*
$AlNi_3$	85–87	*cP*4	$Pm\bar{3}m$
(Ni)	89.0–100	*cF*4	$Fm\bar{3}m$

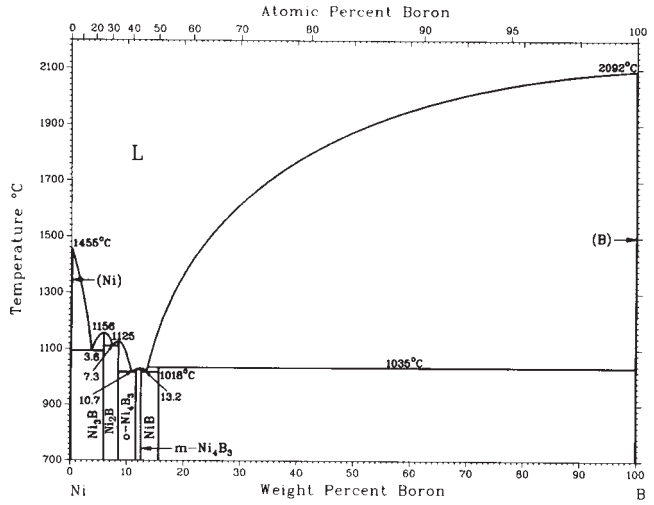


Fig. 2 The nickel-boron (Ni-B) binary phase diagram

Table 2 Ni-B crystal structure data

Phase	Composition, wt% B	Pearson symbol	Space group
(Ni)	0	*cF*4	$Fm\bar{3}m$
Ni_3B	6	*oP*6	*Pnma*
Ni_2B	8.4	*tI*12	*I*4/*mcm*
Ni_4B_3	11.5	(a)	*Pnma*
Ni_4B_3	12.5	(b)	*C*2/*c*
NiB	16	*oC*8	*Cmcm*
NiB_2(c)	26.9	(d)	…
NiB_{12}(c)	68.8	(d)	…
(βB)	100	*hR*108	$R\bar{3}m$

(a) Orthorhombic. (b) Monoclinic. (c) Existence of these compounds has been reported, but is highly unlikely. (d) Cubic

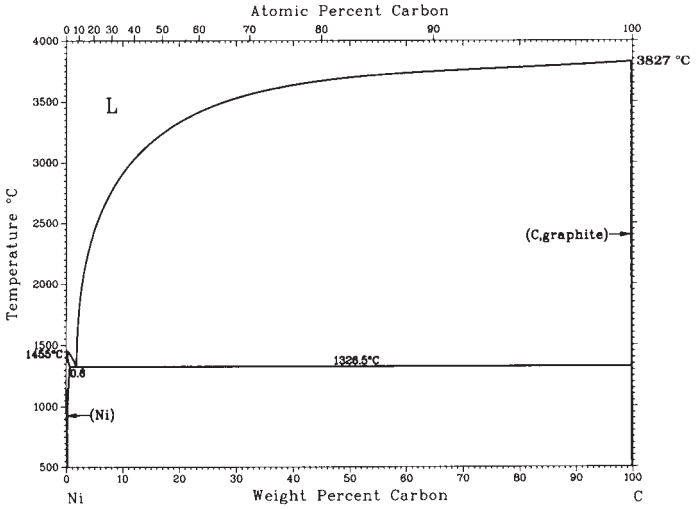


Fig. 3 The nickel-carbon (Ni-C) binary phase diagram

Table 3 Ni-C crystal structure data

Phase	Composition, wt% C	Pearson symbol	Space group
(Ni)	0–0.6(a)	*cF*4	$Fm\bar{3}m$
(C, graphite)	~100	*hP*4	$P6_3/mmc$
Metastable phase			
Ni_3C	...	*oP*16	*Pnma*

(a) Can be extended to 1.6 wt% C at 1314 °C

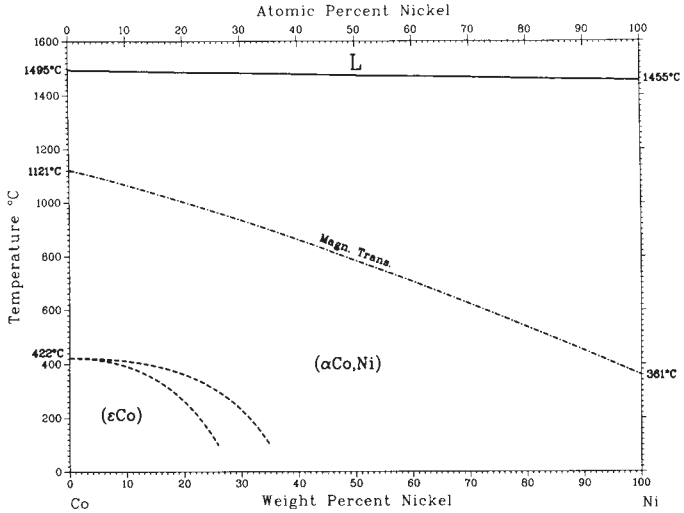


Fig. 4 The nickel-cobalt (Ni-Co) binary phase diagram

Table 4 Ni-Co crystal structure data

Phase	Composition, wt% Ni	Pearson symbol	Space group
(αCo,Ni)	0–100	*cF*4	$Fm\bar{3}m$
(εCo)	0–35	*hP*2	$P6_3/mmc$

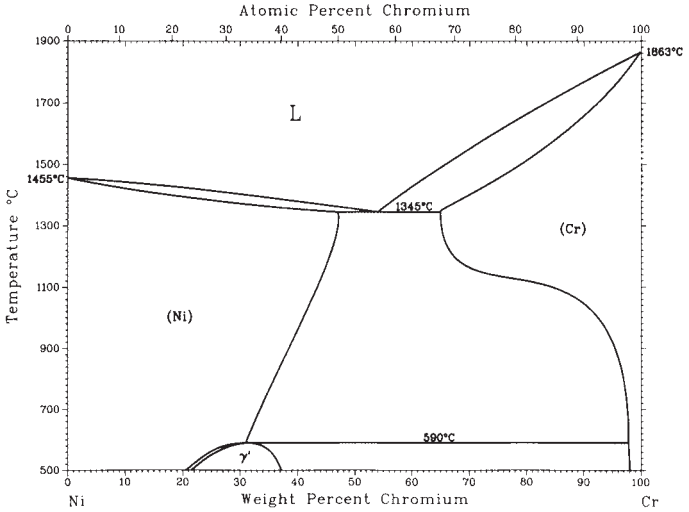


Fig. 5 The nickel-chromium (Ni-Cr) binary phase diagram

Table 5 Ni-Cr crystal structure data

Phase	Composition, wt% Cr	Pearson symbol	Space group
(Ni)	0–47.0	*cF*4	$Fm\bar{3}m$
Ni_2Cr or γ′	21–37	*oI*6	*Immm*
(Cr)	65–100	*cI*2	$Im\bar{3}m$
Metastable phases			
σ	~28	*tP*30	$P4_2/mnm$
δ	100	*cP*8	$Pm\bar{3}m$

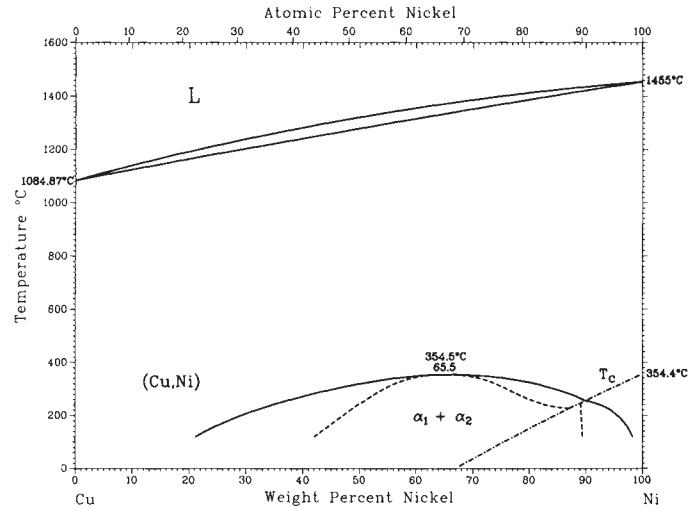


Fig. 6 The nickel-copper (Ni-Cu) binary phase diagram

Table 6 Ni-Cu crystal structure data

Phase	Composition, wt% Ni	Pearson symbol	Space group
(Cu,Ni)	0–100(a)	*cF*4	$Fm\bar{3}m$

(a) Above 354.5 °C

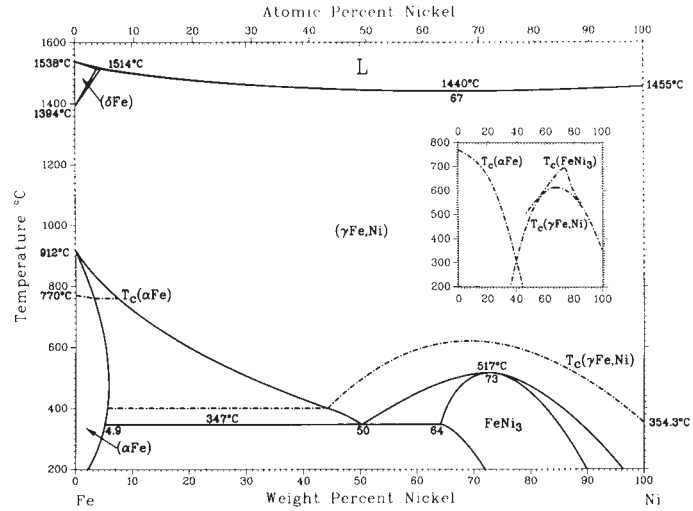


Fig. 7 The nickel-iron (Ni-Fe) binary phase diagram

Table 7 Ni-Fe crystal structure data

Phase	Composition, wt% Ni	Pearson symbol	Space group
(δFe)	0–3.7	*cI*2	$Im\bar{3}m$
(γFe,Ni)	0–100	*cF*4	$Fm\bar{3}m$
(αFe)	0–5.8	*cI*2	$Im\bar{3}m$
Fe_3Ni(a)	26	*cP*4	$Pm\bar{3}m$
FeNi(a)	51	*tP*2	*P4/mmm*
$FeNi_3$	64–~90	*cP*4	$Pm\bar{3}m$

(a) Metastable

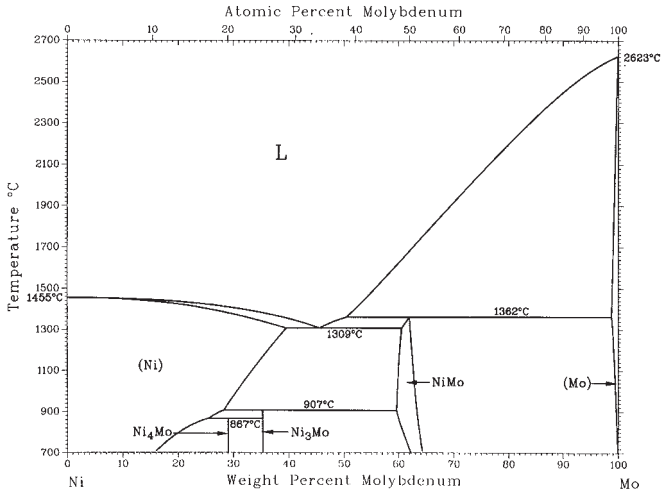


Fig. 8 The nickel-molybdenum (Ni-Mo) binary phase diagram

Table 8 Ni-Mo crystal structure data

Phase	Composition, wt% Mo	Pearson symbol	Space group
(Ni)	0–38(a)	*cF*4	$Fm\bar{3}m$
Ni_4Mo	29.0	*tI*10	*I*4/*m*
Ni_3Mo	35.3	*oP*8	*Pmnn*
NiMo	63.9–65.7	*oP*112	$P2_12_12_1$
(Mo)	98.9–100(b)	*cI*2	$Im\bar{3}m$
Metastable phases			
Ni_2Mo	…	*oI*6	…
Ni_3Mo	…	*tI*8	*I*4/*mmm*
Ni_4Mo	…	*tI*10, *cF*4	…
$Ni_{17}Mo_5$	…	…	…

(a) At 1317 °C. (b) At 1362 °C

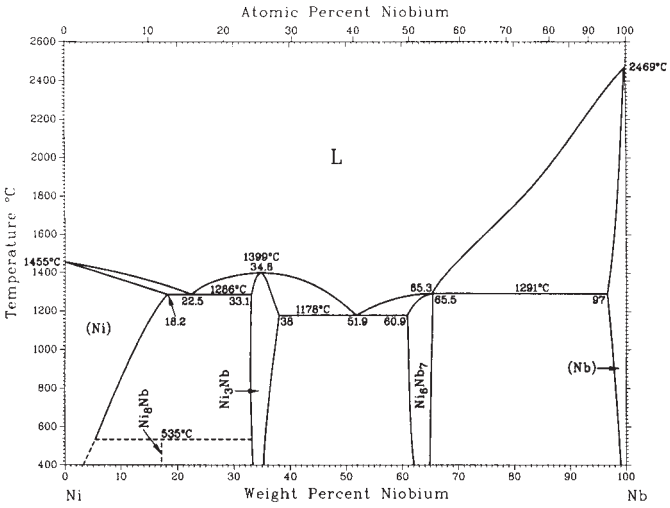


Fig. 9 The nickel-niobium (Ni-Nb) binary phase diagram

Table 9 Ni-Nb crystal structure data

Phase	Composition, wt% Nb	Pearson symbol	Space group
(Ni)	0–18.2	*cF*4	$Fm\bar{3}m$
Ni_8Nb	16.5	*tI*36	…
Ni_3Nb	33.1–38.0	*oP*8	*Pmmn*
Ni_6Nb_7	60.9–65.5	*hR*13	$R\bar{3}m$
(Nb)	97–100	*cI*2	$Im\bar{3}m$

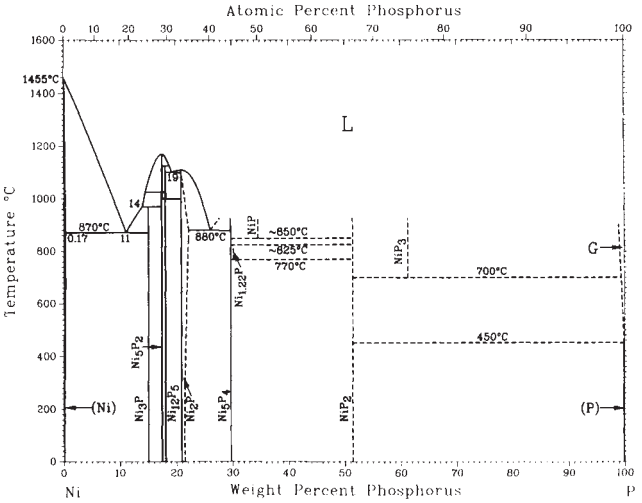


Fig. 10 The nickel-phosphorus (Ni-P) binary phase diagram

Table 10 Ni-P crystal structure data

Phase	Composition, wt% P	Pearson symbol	Space group
(Ni)	0–0.17	*cF*4	$Fm\bar{3}m$
Ni_3P	15	*tI*32	$I\bar{4}$
βNi_5P_2	17.5	…	…
αNi_5P_2	17.5	*hP*168(a)	$P\bar{3}$
$\delta Ni_{12}P_5$	18.0	…	…
$\gamma Ni_{12}P_5$	18.0	*tI*34	*I*4/*m*
Ni_2P	20.9–?	*hP*9	$P\bar{6}2m$
			$P3_21$
Ni_5P_4	29.6	*hP*36	$P6_3mc$
$Ni_{1.22}P$	30.2	…	…
NiP	34.5	*oP*16	*Pcba*
NiP_2	51.4	*mC*12	*C*2/*c*
NiP_3	61	*cI*32	$Im\bar{3}$
P (red)	100	…	…
High-pressure phase			
NiP_2	51.4	*cP*12	$Pa\bar{3}$
Metastable phases			
"Ni_5P_2"	11–18	*h***	…
α	8–15	*c***	…
α_1	8–15	*h***	…
α_2	8–15	*h***	…
α_3	8–15	*h***	…
"αNi_3P"	15	*t***	…
"βNi_3P"	15	*h***	…
"γNi_3P"	15	*c***	…
α (amorphous)	~15	(b)	…
β (amorphous)	~15	(c)	…

(a) Might be *hP*336. (b) Liquidlike. (c) Molecular cluster

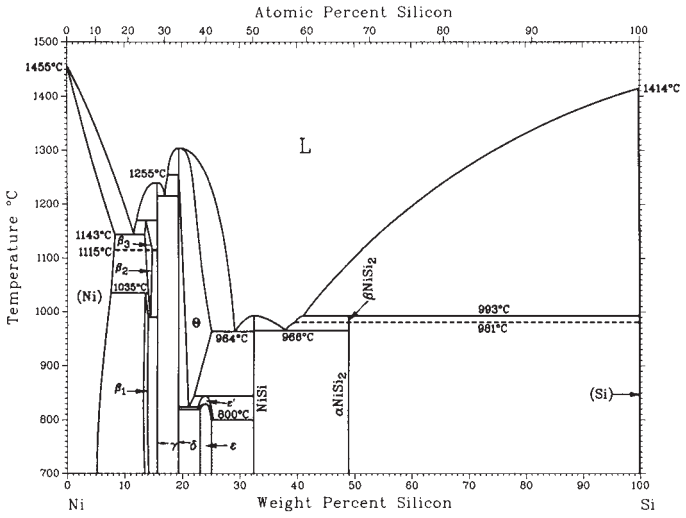


Fig. 11 The nickel-silicon (Ni-Si) binary phase diagram

Table 11 Ni-Si crystal structure data

Phase	Composition, wt% Si	Pearson symbol	Space group
(Ni)	0–8.2	*cF*4	$Fm\bar{3}m$
β_1 (Ni_4Si)	12.4–13.4	*cP*4	$Pm\bar{3}m$
β_3 (Ni_3Si)	~13.4–14.1	*mC*16	…
β_2 (Ni_3Si)	~13.4–14.1	*mC*16	…
$\gamma(Ni_{31}Si_{12})$	15.6	*hP*14	…
θ (Ni_2Si)	19.4–25	*hP*6	…
δ (Ni_2Si)	19.3	*oP*12	…
ε (Ni_3Si_2)	23–25	*oP*80	…
NiSi	32.4	*oP*8	*Pnma*
$\beta NiSi_2$	48.9	?	…
$\alpha NiSi_2$	48.9	*cF*12	$Fm\bar{3}m$
(Si)	~100	*cF*8	$Fd\bar{3}m$

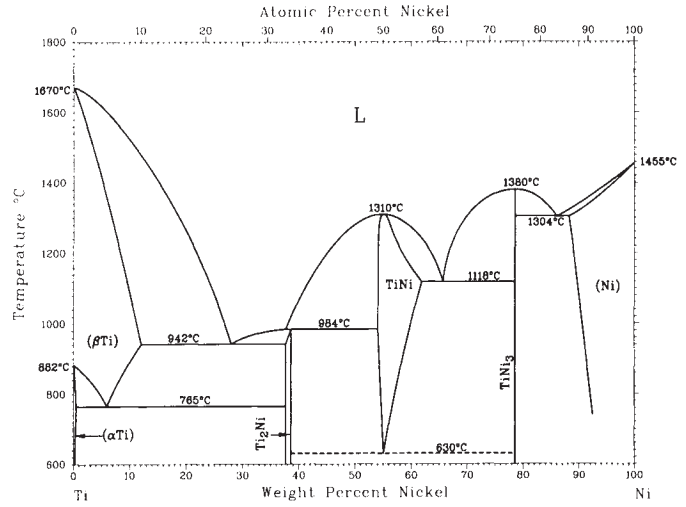


Fig. 12 The nickel-titanium (Ni-Ti) binary phase diagram

Table 12 Ni-Ti crystal structure data

Phase	Composition, wt% Ni	Pearson symbol	Space group
(βTi)	0–12	*cI*2	$Im\bar{3}m$
(αTi)	0–0.3	*hP*2	$P6_3/mmc$
ω(a)	~10	*hP*3	*P*6/*mmm* or $P\bar{3}m1$
Ti_2Ni	38.0	*cF*96	$Fd\bar{3}m$
TiNi′(a)	~54–58	*mP*4	$P2_1/m$
TiNi	54.6–62	*cP*2	$Pm\bar{3}m$
γ″ $TiNi_3$(a)	~77	*hR*21	$R\bar{3}m$
$TiNi_3$	79	*hP*16	$P6_3/mmc$
γ′ $TiNi_3$(a)	~86–90	*cP*4	$Pm\bar{3}m$
(Ni)	88.4–100	*cF*4	$Fm\bar{3}m$

(a) Metastable

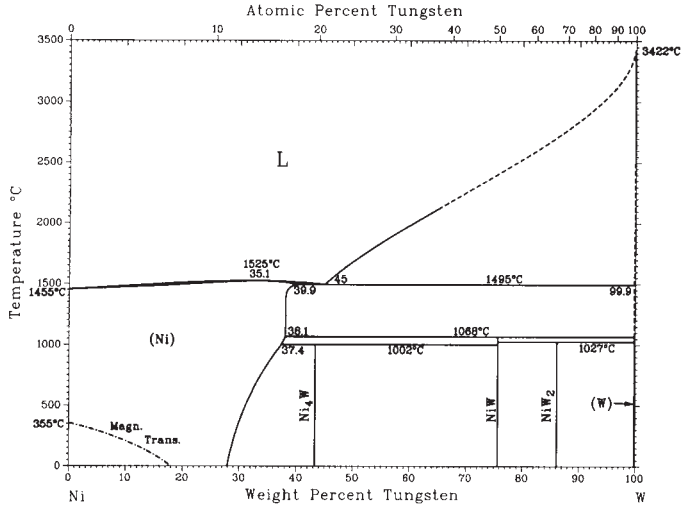


Fig. 13 The nickel-tungsten (Ni-W) binary phase diagram

Table 13 Ni-W crystal structure data

Phase	Composition, wt% W	Pearson symbol	Space group
(Ni)	0–39.9	*cF*4	$Fm\bar{3}m$
Ni_4W	~44	*tI*10	*I*4/*m*
NiW	~75.8	*o***	…
NiW_2	86.3	*tI*96	$I\bar{4}$
(W)	99.9–100	*cI*2	$Im\bar{3}m$

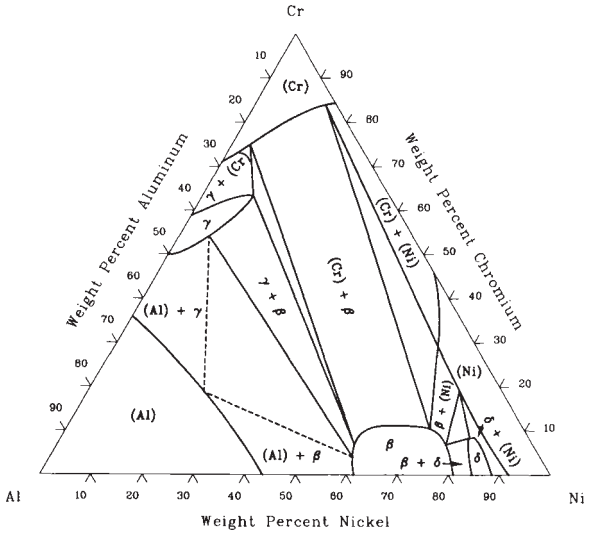
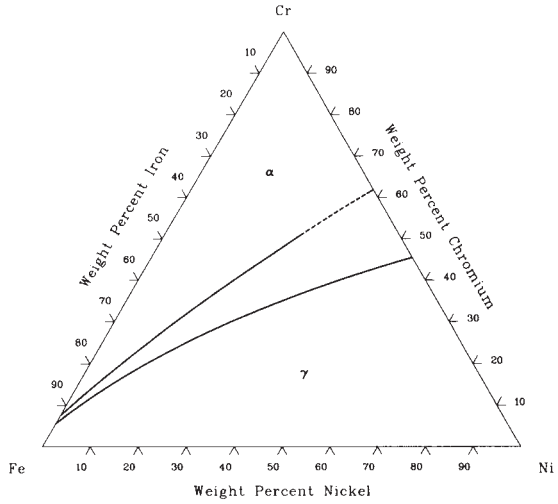
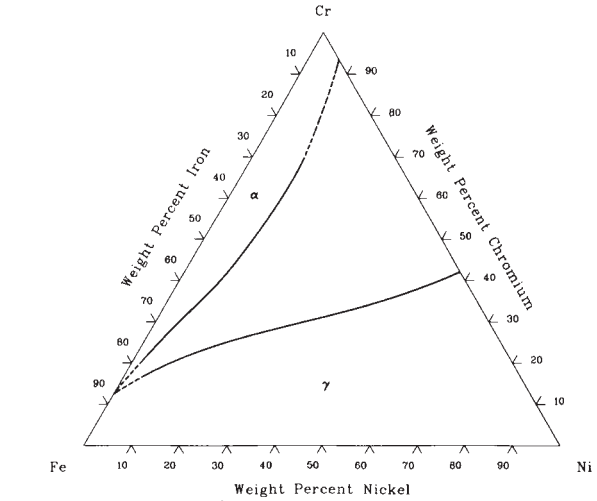


Fig. 14 Ni-Al-Cr isothermal section at 1150 °C (2100 °F)



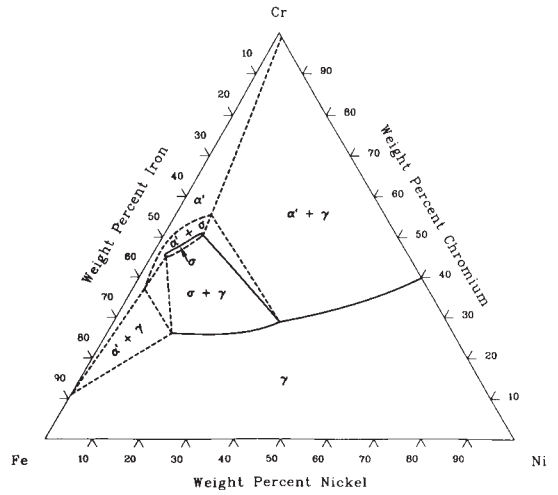
Note: α = (αFe,Cr); γ = (γFe,Ni)

Fig. 15 Ni-Cr-Fe isothermal section at 1300 °C (2370 °F)



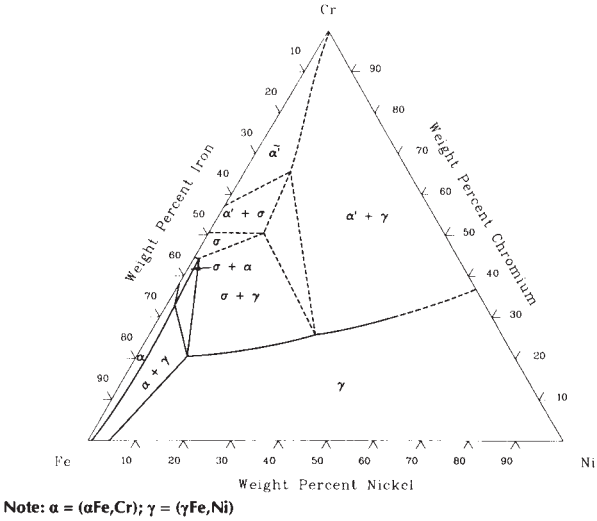
Note: α = (αFe,Cr); γ = (γFe,Ni)

Fig. 16 Ni-Cr-Fe isothermal section at 1000 °C (1830 °F)



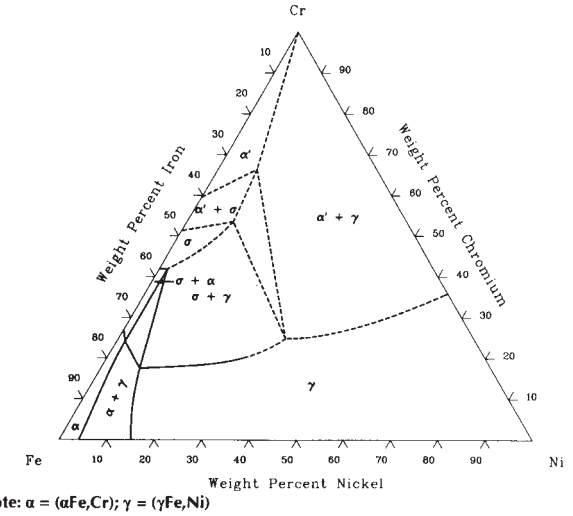
Note: α = (αFe,Cr); γ = (γFe,Ni)

Fig. 17 Ni-Cr-Fe isothermal section at 900 °C (1650 °F)



Note: α = (αFe,Cr); γ = (γFe,Ni)

Fig. 18 Ni-Cr-Fe isothermal section at 800 °C (1470 °F)



Note: α = (αFe,Cr); γ = (γFe,Ni)

Fig. 19 Ni-Cr-Fe isothermal section at 650 °C (1200 °F)

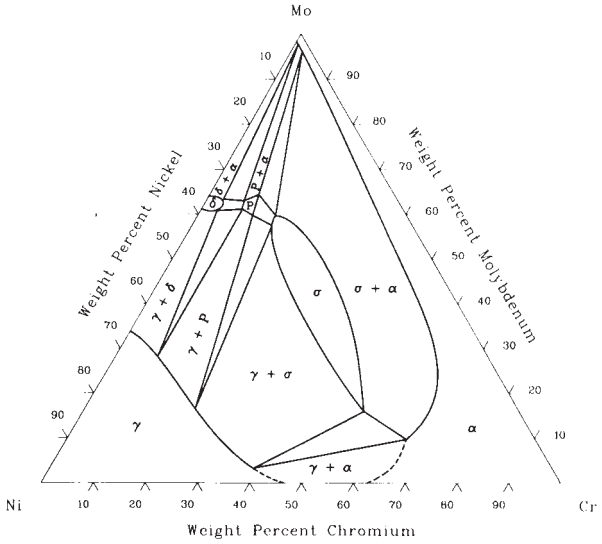


Fig. 20 Ni-Cr-Mo isothermal section at 1250 °C (2280 °F)

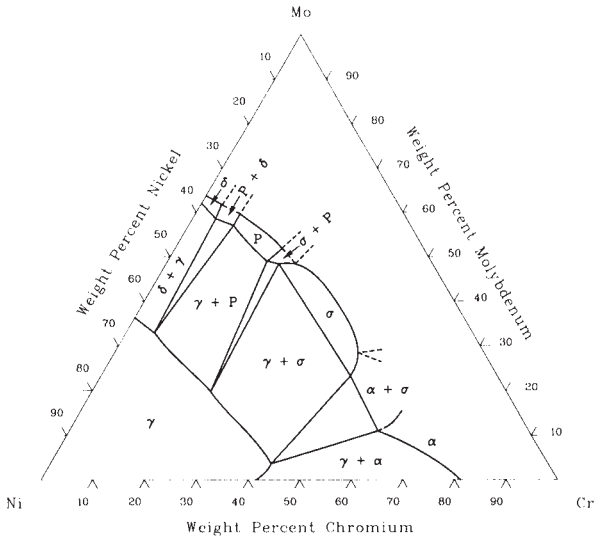


Fig. 21 Ni-Cr-Mo isothermal section at 1200 °C (2190 °F)

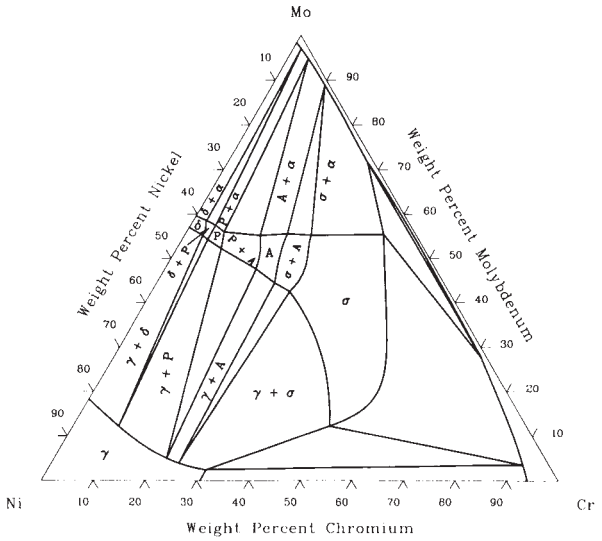


Fig. 22 Ni-Cr-Mo isothermal section at 600 °C (1110 °F)

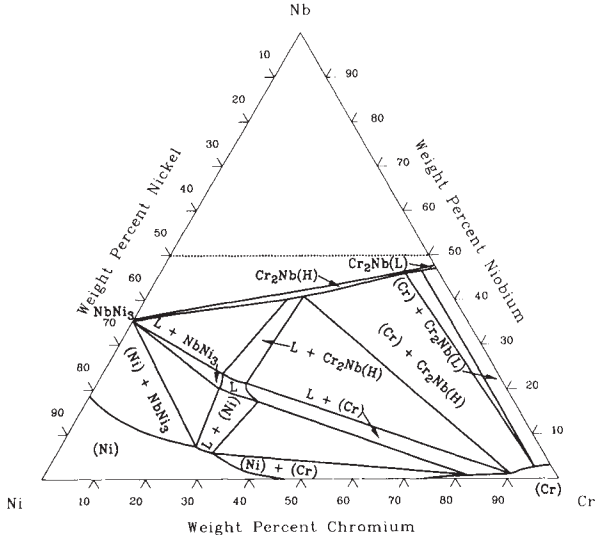


Fig. 23 Ni-Cr-Nb isothermal section at 1200 °C (2190 °F)

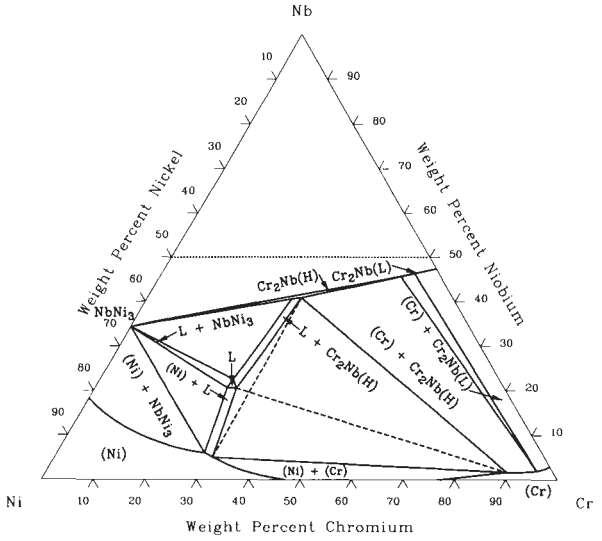


Fig. 24 Ni-Cr-Nb isothermal section at 1175 °C (2145 °F)

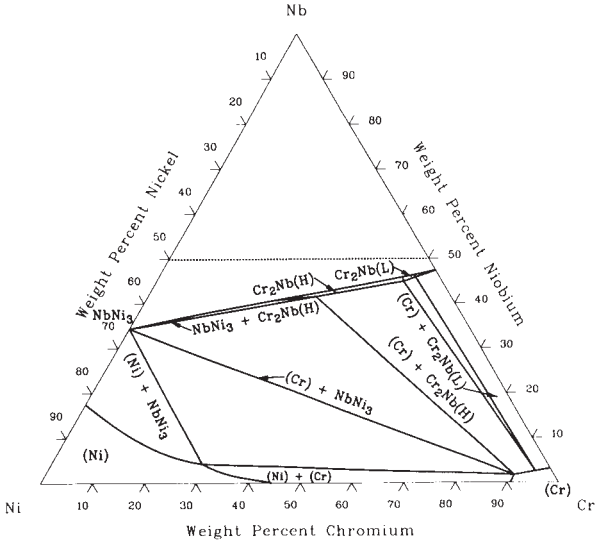


Fig. 25 Ni-Cr-Nb isothermal section at 1100 °C (2010 °F)

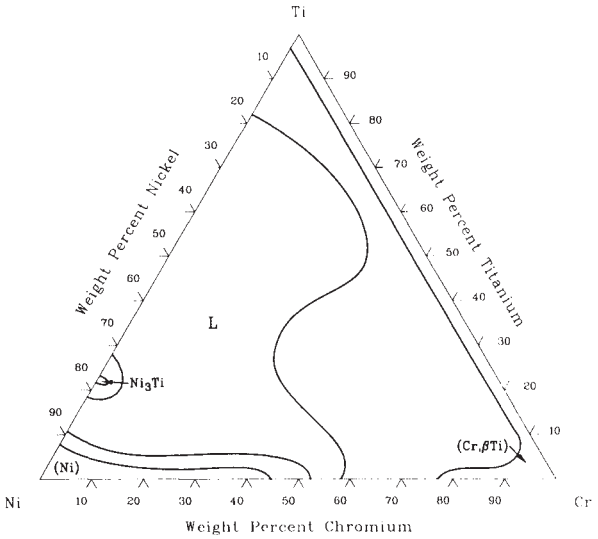


Fig. 26 Ni-Cr-Ti isothermal section at 1352 °C (2465 °F)

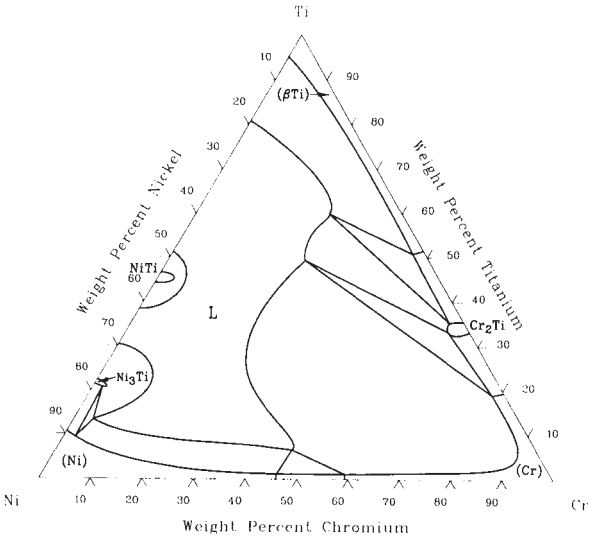


Fig. 27 Ni-Cr-Ti isothermal section at 1277 °C (2330 °F)

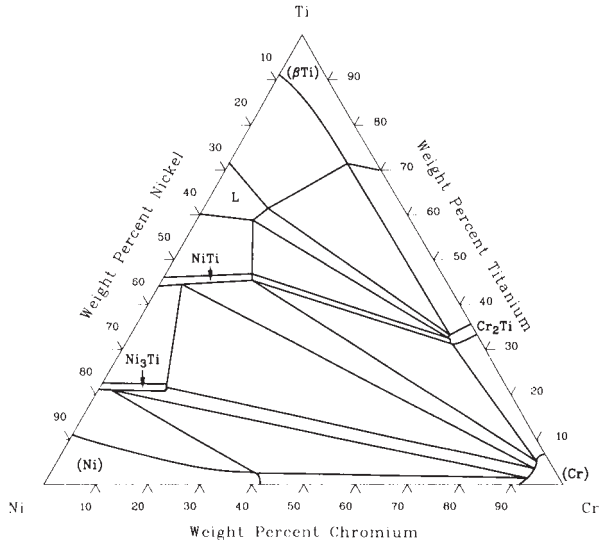


Fig. 28 Ni-Cr-Ti isothermal section at 1027 °C (1880 °F)

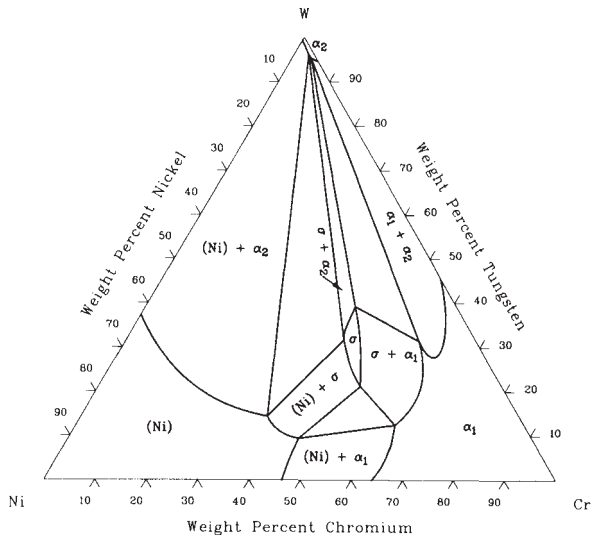


Fig. 29 Ni-Cr-W isothermal section at 1250 °C (2280 °F)

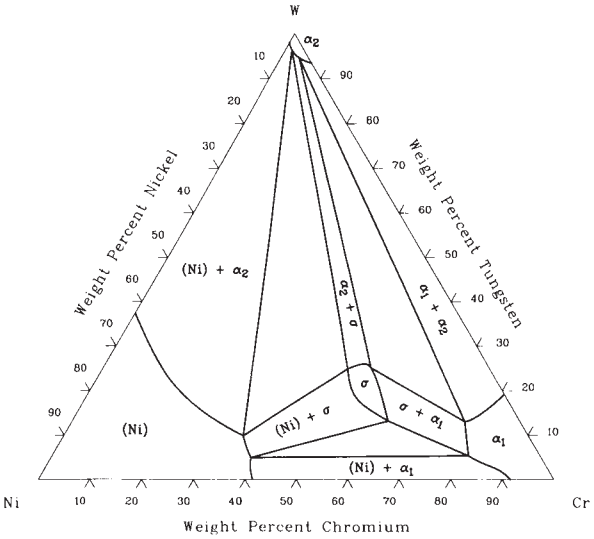


Fig. 30 Ni-Cr-W isothermal section at 1000 °C (1830 °F)

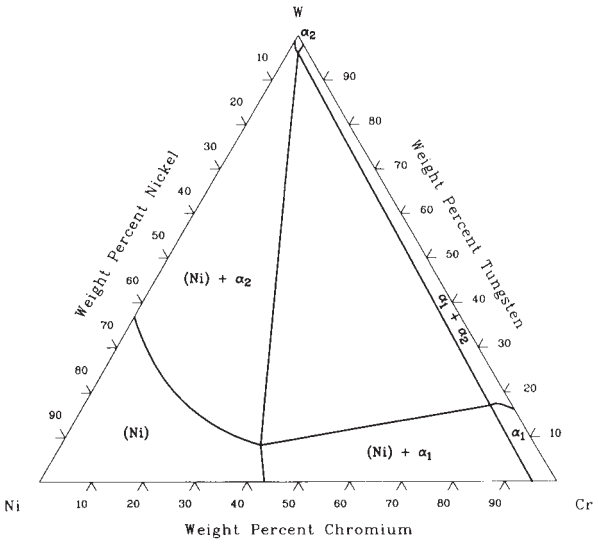


Fig. 31 Ni-Cr-W isothermal section at 900 °C (1650 °F)

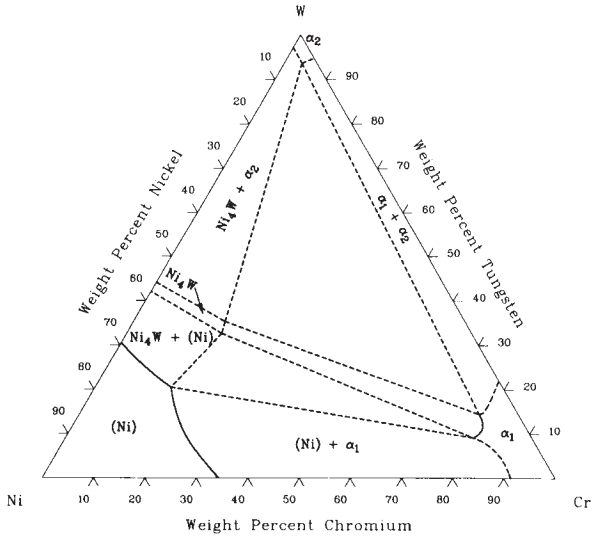


Fig. 32 Ni-Cr-W isothermal section at 800 °C (1470 °F)

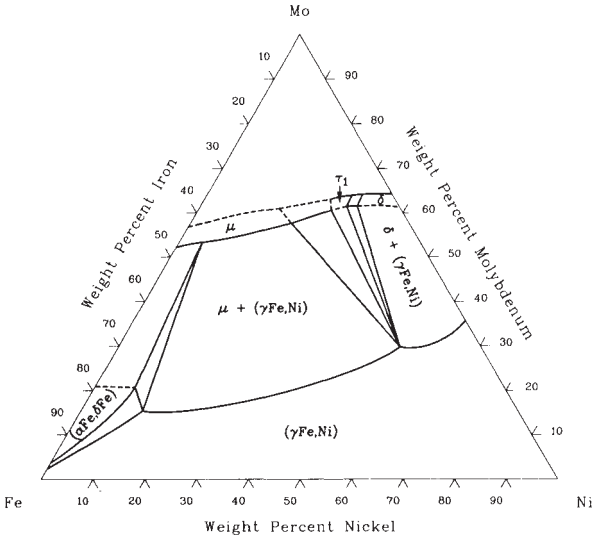


Fig. 33 Ni-Fe-Mo isothermal section at 1200 °C (2190 °F)

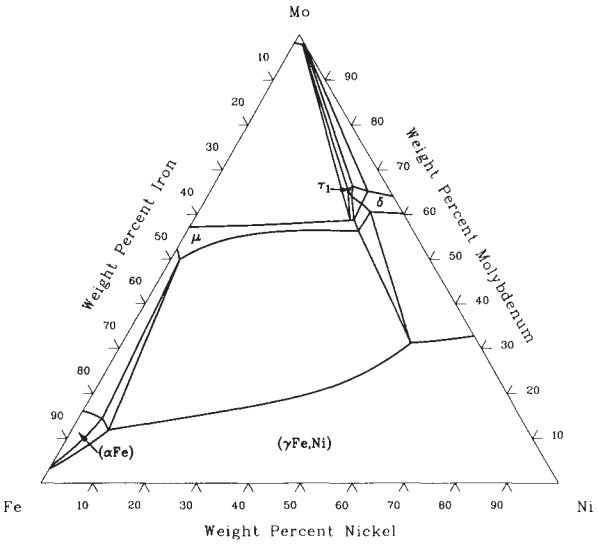


Fig. 34 Ni-Fe-Mo isothermal section at 1100 °C (2010 °F)

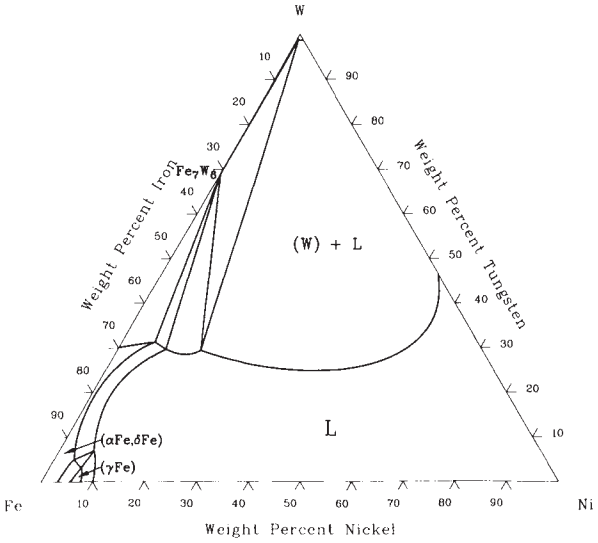


Fig. 35 Ni-Fe-W isothermal section at 1500 °C (2730 °F)

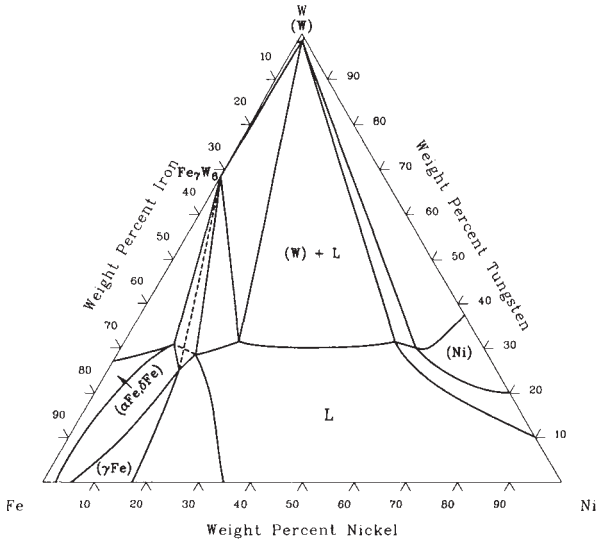


Fig. 36 Ni-Fe-W isothermal section at 1465 °C (2670 °F)

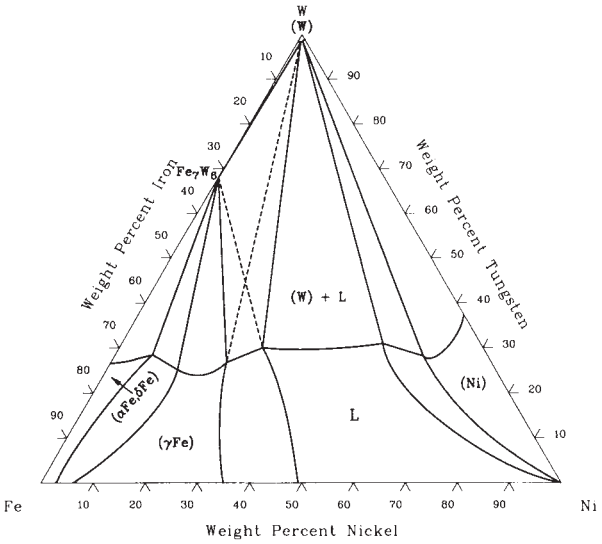


Fig. 37 Ni-Fe-W isothermal section at 1455 °C (2650 °F)

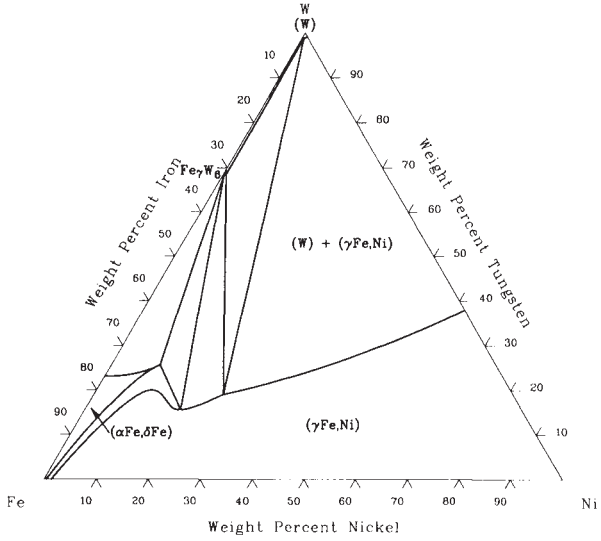


Fig. 38 Ni-Fe-W isothermal section at 1400 °C (2550 °F)

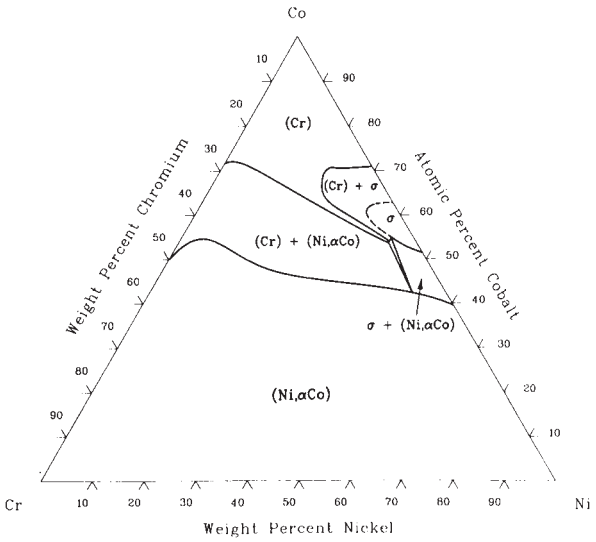


Fig. 39 Ni-Co-Cr isothermal section at 1200 °C (2190 °F)

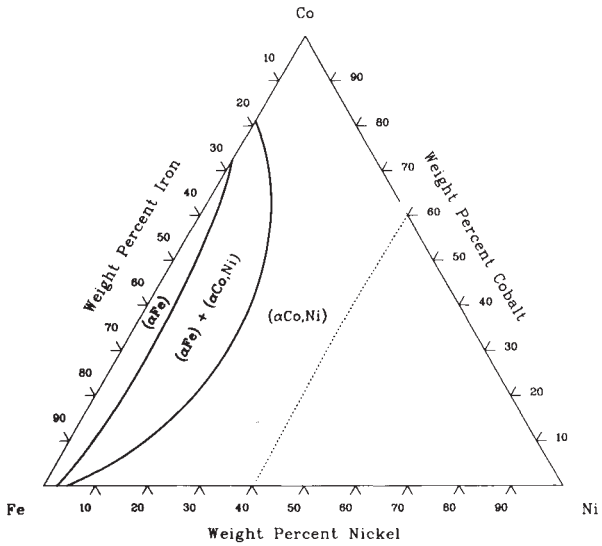


Fig. 40 Ni-Co-Fe isothermal section at 800 °C (1470 °F)

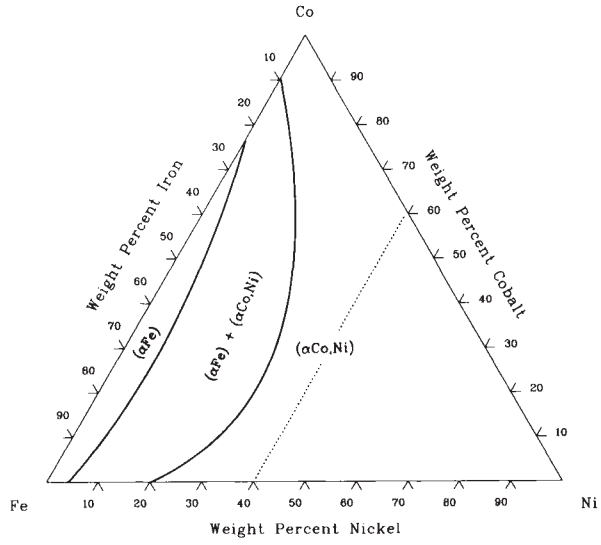


Fig. 41 Ni-Co-Fe isothermal section at 600 °C (1110 °F)

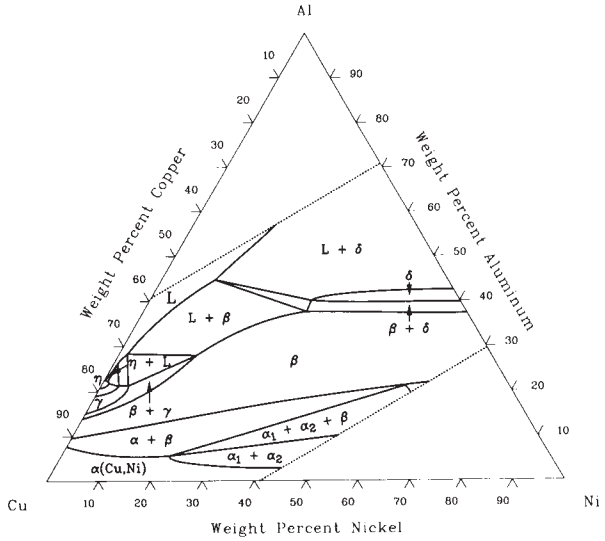


Fig. 42 Ni-Al-Cu isothermal section at 900 °C (1650 °F)

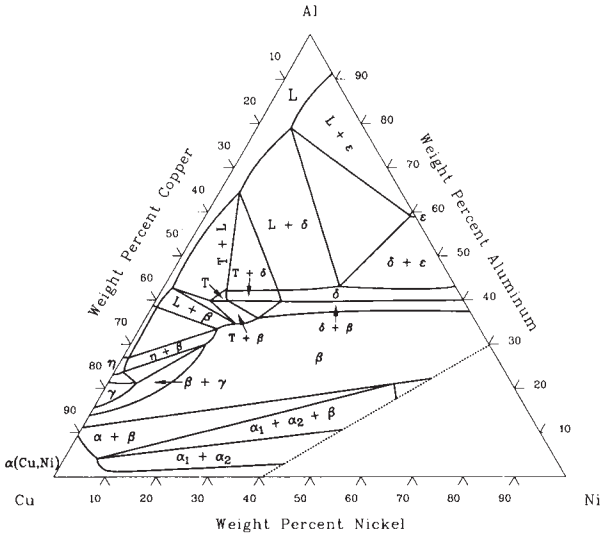


Fig. 43 Ni-Al-Cu isothermal section at 700 °C (1290 °F)

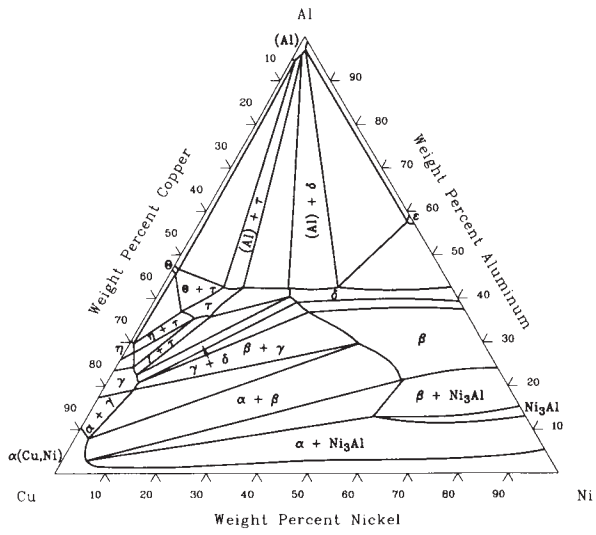


Fig. 44 Ni-Al-Cu isothermal section at 500 °C (930 °F)

ASM Specialty Handbook: Nickel, Cobalt, and Their Alloys
J.R. Davis, editor, p 345-348
DOI:10.1361/ncta2000p345

Copyright © 2000 ASM International®
All rights reserved.
www.asminternational.org

The Cobalt Industry: Occurrence, Recovery, and Consumption

COBALT is classified as a strategic and critical metal because of its applications in defense-related industries and the dependence of industrialized nations on cobalt imports. Cobalt is used to make heat resistant superalloys, corrosion resistant and wear resistant alloys, magnets, high-speed tool steels, and cemented carbides. Some cobalt alloys are also biocompatible, which has prompted their use as orthopedic implants. Cobalt compounds are also important for nonmetallurgical applications, such as catalysts for the petroleum and chemical industries; drying agents for paints, varnishes, and inks; ground coats for porcelain enamels; pigments; batteries; and magnetic recording media.

Elemental Cobalt

Physical Properties. With an atomic number of 27, cobalt (symbol Co) falls between iron and nickel on the periodic table. The density of cobalt is 8.85 g/cm^3, which is similar to that of nickel (8.902). Cobalt is ferromagnetic, exhibiting a room-temperature initial permeability of 68, a maximum permeability of 245, and a Curie temperature of 1121 °C (2050 °F), which is considerably higher than that of iron (770 °C, or 1418 °F) or nickel (358 °C, or 676 °F). Other important physical properties include:

- *Melting point:* 1493 °C (2719 °F)
- *Boiling point:* 3100 °C (5612 °F)
- *Coefficient of thermal expansion:* 13.8 μm/m · K at room temperature
- *Specific heat:* 0.414 kJ/kg · K at room temperature
- *Thermal conductivity:* 69.04 W/m · K at room temperature
- *Electrical conductivity:* 27.6% IACS at 20 °C (68 °F)
- *Electrical resistivity:* 52.5 nΩ · m at 20 °C (68 °F)
- *Coercive force:* 8.9 Oe (708 A/m)
- *Saturation magnetization:* 1.87 T (18.7 kG)
- *Residual magnetization:* 0.49 T (4900 G)

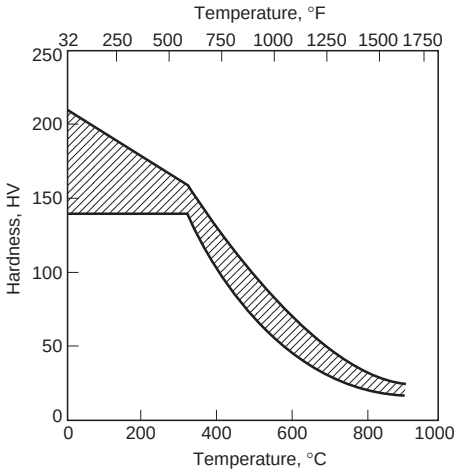


Fig. 1 Hardness of cobalt as a function of temperature. Source: Ref 1

Crystal Structure. At temperatures below 417 °C (783 °F), cobalt exhibits a hexagonal close-packed (hcp) structure (ε-cobalt). Between 417 °C (783 °F) and its melting point of 1493 °C (2719 °F), cobalt has a face-centered cubic (fcc) structure (α-cobalt).

Mechanical Properties. The hardness at room temperature of various samples of cobalt has been reported as falling between 140 and 250 HV (Ref 1). For well-annealed samples of high-purity metal, the values fall between 140 and 160 HV. The variation of hardness with temperature is shown in Fig. 1.

The elastic moduli of cobalt are 211 GPa (30.6 × 10^6 psi) for Young's modulus, 82 GPa (11.9 × 10^6 psi) for shear modulus, and 183 GPa (26.5 × 10^6 psi) for compressive modulus.

For high-purity (99.5%) vacuum-melted cobalt that has been hot worked followed by annealing at temperatures ranging from 800 to 1000 °C (1470–1830 °F), the tensile properties obtained fall with the following ranges (Ref 1):

- *0.2% yield strength:* 305 to 345 MPa (44–50 ksi)
- *Tensile strength:* 800 to 875 MPa (116–127 ksi)
- *Elongation:* 15 to 30%

Air-melted materials are much less ductile.

Occurrence and Supply

Cobalt occurs in nature in a fairly widespread but dispersed form, being detectable in trace quantities in many rocks, coals, soils, plant life, and manganese-rich marine nodules. The currently exploited sources of cobalt, however, are mainly those where it originates as a byproduct of other more abundant or more valuable metals, particularly copper and nickel, but also zinc, lead, and platinum-group metals. As shown in Table 1, cobalt-containing ores include various copper and nickel sulfides, oxides, and arsenides. Tables 2 and 3 list mining and refining statistical data for cobalt. As these data indicate, the so-called "Copper Belt" in Africa, which includes the Democratic Republic of Congo (formerly Zaire) and Zambia, is the largest supplier of cobalt. Other countries where the mining or refining of cobalt is significant include Canada, Russia, Australia, Finland, and Norway.

Extraction and Refining

Because cobalt production is usually subsidiary to that of copper or nickel, extraction procedures vary according to which of these metals is associated with the cobalt. The extraction process varies from ore to ore and also depends on the extractor. Hydrometallurgical, pyrometallurgical, vapormetallurgical, and electrolytic processes, or combinations of these pro-

Table 1 The principal cobalt-containing ores

Ore	Composition	Locations
Skutterudite	$(Co,Ni)As_3$	Bou-Azzer, Morocco; Cobalt, Ontario, Canada
Carrolite	$CuCo_2S_4$ or $CuSCo_2S_3$	Congo; Zambia
Linnaeite	Co_3S_4 (+Ni,Cu,Fe)	Congo; U.S. (Mississippi Valley); Zambia
Cattierite	CoS_2	Congo
Nickel cattierite	$(Co,Ni)S_2$	Congo
Cobaltite	CoAsS	U.S. (Idaho); Cobalt, Ontario, Canada
Heterogenite	$2Co_2O_3CuO{\cdot}6H_2O$	Congo
Asbolite	Mixed manganese-iron oxides + Co	Congo; Zambia; New Caledonia
Pyrrhotite	Ni,Cu,(Co) sulfides	Sudbury, Ontario, Canada
Laterites	Weathered igneous rock containing silicates, magnesium oxide, limonite, and 2–3% Ni+Co	Moa Bay, Cuba; various locations in the U.S., Australia, Brazil, and Russia

cesses, are used to extract and refine cobalt. Several examples are described below. Additional information on recovery of cobalt from nickel-bearing ores can be found in the article "The Nickel Industry: Occurrence, Recovery, and Consumption" in this Handbook.

Recovery from Copper-Cobalt Sulfide Concentrates (Ref 2). The copper-cobalt sulfide ores of central Africa (Congo and Zambia) are treated by a sulfatizing roast in a fluidized-bed furnace to convert copper and cobalt sulfides into soluble oxides and iron into insoluble hematite. The calcine is subseqently leached with sulfuric acid from the spent copper recovery electrolyte. Oxide concentrates are introduced at this leaching step to maintain the acid balance in the circuit. Iron and aluminum are removed from the leach solution, and copper is electrowon on copper cathodes. A part of the spent electrolyte enters the cobalt recovery circuit and is purified by removal of iron, copper, nickel, and zinc prior to precipitation of cobalt as its hydroxide. In the final stages, this cobalt hydroxide is redissolved and the metal is refined by electrolysis. Figure 2 shows the flow diagram for this process as used at the Générale des Carrières et des Mines (Gécamines) in the Congo.

Recovery from Nickel-Cobalt Sulfide Concentrates. Nickel sulfide concentrates can be treated by either roasting or flash smelting to produce a matte from which nickel and cobalt can be recovered hydrometallurgically, or they may be treated by an ammonia solution pressure leach. In the Sherritt Gordon process used at Fort Saskatchewan in Alberta, Canada, a feed of matte and sulfide concentrate containing approximately 0.4% cobalt and 30% sulfur is pressure leached at elevated temperature and pressure in an ammoniacal solution to produce a solution containing nickel, copper, and cobalt. Copper is precipitated as sulfide, and the solution is then reduced with hydrogen, again at high temperature and pressure, to precipitate nickel powder. The remaining solution contains approximately equal proportions of nickel and cobalt, and these are separated by further selective reduction processes carried out under controlled conditions of pH, temperature, and pressure, yielding cobalt powder with a purity of approximately 99.6%. The flow diagram of this process is shown in Fig. 3. A more detailed description of the Sherritt process for producing cobalt powders can be found in *Powder Metal Technologies and Applications*, Volume 7 of the *ASM Handbook* (Ref 3).

Cobalt-containing mattes and sulfide concentrates have also been treated by pressure leaching and by leaching in chloride media. Details of these processes can be found in Ref 2.

Recovery from Copper-Cobalt Oxide Concentrates. The heterogenite mineral from the Congo (see Table 1) is obtained from open-pit mines, and the crude ore is crushed and milled before concentration of the metal-bearing fraction by froth flotation. In this process, the milled ore is suspended in an aqueous medium through which air is blown and to which specific frothing and surface-active agents are added. These selectively carry the valuable mineral from the unwanted gangue. The cobalt-rich oxides, with roughly equal copper and cobalt contents, are then sintered to pellets and fed to electric smelting furnaces along with selected high-grade ores that are suitable for smelting without prior concentration. The cobalt-bearing concentrate is then mixed with lime and coal and melted in a reducing atmosphere to produce cobalt-copper (+Fe) alloys. Two types are obtained: a heavy red alloy containing approximately 5% cobalt that is processed for copper, and a lighter white alloy containing approximately 40% cobalt that is further refined by hydrometallurgical processing to produce cobalt of 99% purity.

Cobalt is also recovered from copper oxide ores containing much smaller proportions of cobalt, on the order of 1 part cobalt to 25 to 30 parts copper. These minerals undergo a combination of hydrometallurgical and electrolytic processing (Ref 1).

Recovery from Laterite Ores. Laterites consist of a mantle of completely weathered igneous rocks forming a soil, from approximately 1 m (3 ft) to more than 30 m (100 ft) thick, found mainly in tropical or subtropical climates. Cobalt-bearing silicate laterites contain hydrated iron oxides, magnesium oxide, 2 to

Table 2 World mine production of cobalt

	Metric tonnes(a)(b)	
Country	1997	1998
Australia	3,000	3,300
Botswana	334	335
Brazil	400	400
Canada	5,709	6,039
China	200	210
Congo (formerly Zaire)	3,500	1,500
Cuba	2,082	2,200
Kazakhstan	300	300
Morocco	714	287
New Caledonia	1,000	1,000
Russia	3,300	3,200
South Africa	450	450
Zambia	6,043	7,000
Zimbabwe	100	90
Total	**27,100**	**26,300**

(a) Data are rounded to three digits; may not add up to totals shown. (b) Includes estimates. Source: U.S. Geological Survey

Table 3 Worldwide cobalt refinery capacity in 1998

Country	Metric tonnes(a)(b)
Australia	2,000
Belgium	1,200
Brazil	500
Canada	4,700
China	1,500
Congo (formerly Zaire)	17,000
Finland	10,600
France	300
Japan	480
Morocco	300
Norway	4,500
Russia	8,000
South Africa	1,500
United States	900
Zambia	5,000
Total	**58,500**

(a) Data are rounded to three digits; may not add up to totals shown. (b) Includes estimates. Source: U.S. Geological Survey

3% nickel, and a cobalt content 1/15th to 1/50th that of nickel. Nickel-cobalt laterite ores can be treated by either hydrometallurgical processes or pyrometallurgical processes, such as matte or ferronickel smelting, which require the entire ore to be melted and the metal values to be separated from the residual components of the ore. The hydrometallurgical processes for laterite ore can use sulfuric acid or ammonia leach solutions.

Recovery from Arsenide Ores. Arsenic-containing concentrates are roasted in a fluidized bed to remove 60 to 70% of the arsenic present as arsenic oxide (Ref 2). The roasted ores can be treated with hydrochloric acid and chlorine or with sulfuric acid to give a leach solution that can be purified by hydrometallurgical methods and from which cobalt can be recovered by electrolysis or by carbonate precipitation.

End Uses of Cobalt

According to the Cobalt Development Institute, worldwide consumption of cobalt can be broken into the following market segments:

Market	Percentage	Form
Superalloys (Ni-base/Co-base/Fe-base)	24.3	Metal
Hardfacing and other alloys	6.9	Powder, metal
Magnets	8.5	Metal, powder
Cemented carbides and diamond tooling	15.2	Powder
Catalysts	8.0	Salts (carbonate, sulfate, nitrate, acetate), metal
Colorizers(a)	11.6	Oxide plus some sulfate, hydroxide, and carbonate
Feedstuff, anodizing, magnetic recording, electrolysis, and copper electrowinning	5.0	Mainly sulfate, but some carbonate and hydroxide
Batteries	9.5	Hydroxide, powder, $LiCoO_2$
Tire adhesives, soaps, and driers (for paint and/or ink)	11.0	Soaps and complexes made from metal starting point
Total	**100**	

(a) For coloring glass, enamels, plastics, ceramics, and fabrics

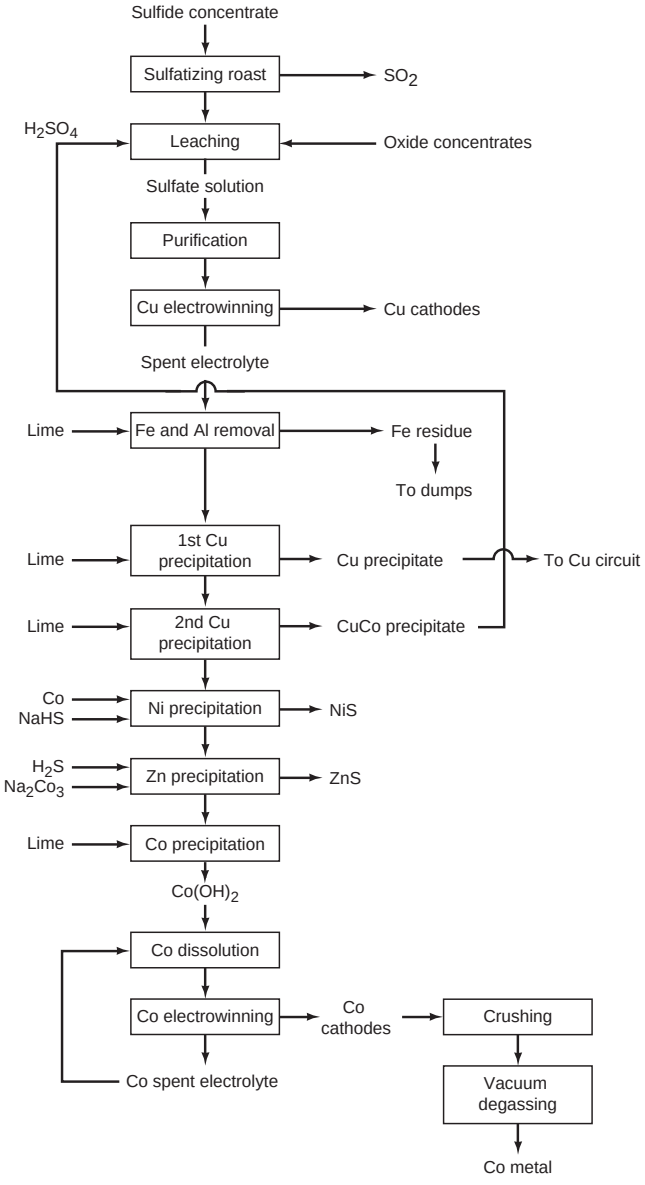


Fig. 2 Flow diagram for recovery of cobalt from copper sulfide concentrates. Source: Ref 2

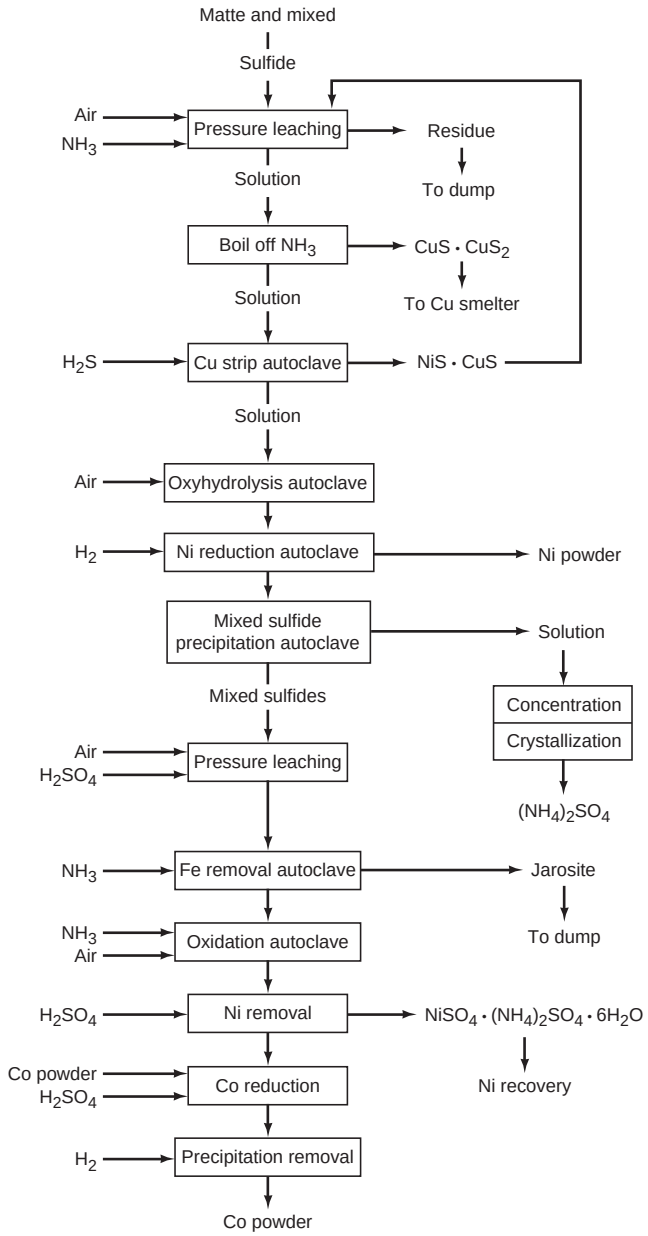


Fig. 3 Flow sheet for recovery of cobalt from nickel sulfide concentrates via hydrometallurgical processing. Source: Ref 2

Table 4 Consumption of cobalt in the United States by end use

	Metric tonnes(a)(b)(c)	
End use	**1997**	**1998**
Steel		
Stainless and heat resisting	38	38
Tool	112	96
Superalloys	4,170	4,110
Alloys (excludes steels and superalloys)		
Magnetic alloys	879	771
Other alloys(d)	342	421
Cemented carbides(e)	789	844
Chemical and ceramic uses		
Catalysts	734	W
Driers in paints or related usage	556	W
Ground coat frit	490	W
Pigments	201	W
Miscellaneous and unspecified(f)	602	2,900
Total	**8,910**	**9,180**

(a) Data are rounded to three significant digits; may not add to totals shown. (b) Includes estimates. (c) W, withheld to avoid disclosing company proprietary data; included with "Miscellaneous and unspecified." (d) Includes nonferrous alloys, welding materials, and wear-resistant alloys. (e) Includes diamond bit matrices, cemented and sintered carbides, and cast carbide dies or parts. (f) Includes feed or nutritive additive, alloy steel, glass decolorizer, and mill products made from metal powder. Source: U.S. Geological Survey

Consumption statistics in the U.S. differ considerably with superalloys making up approximately 47% of all cobalt consumed versus approximately 24% worldwide. Metallurgical uses account for more than 70% of the cobalt consumed in the U.S. In some countries, most notably Japan, nonmetallurgical uses (i.e., cobalt compounds) account for more than 50% of the cobalt consumed. Table 4 lists cobalt consumption by end use in the U.S.

One of the fastest growing markets is the use of cobalt in rechargeable batteries used for portable electronic devices, such as mobile phones, camcorders, and computers. In 1995, worldwide cobalt consumption was estimated to total approximately 700 metric tonnes per year. Current estimates suggest that cobalt consumption in rechargeable batteries—primarily the lithium ion types—could exceed 5000 metric tonnes per year. The increasing use of cobalt in rechargeable batteries for electric vehicle applications is expected to increase this even further.

REFERENCES

1. W. Betteridge, *Cobalt and its Alloys*, Ellis Horwood Limited, 1982
2. *Cobalt in Chemicals*, Cobalt Development Institute, 1986
3. G. Freeman, Production of Cobalt-Base Powders, *Powder Metal Technologies and Applications*, Vol 7, *ASM Handbook*, 1998, p 179–181

SELECTED REFERENCE

- *Cobalt Facts*, Cobalt Development Institute, 2000

ASM Specialty Handbook: Nickel, Cobalt, and Their Alloys
J.R. Davis, editor, p 349-355
DOI:10.1361/ncta2000p349

Copyright © 2000 ASM International®
All rights reserved.
www.asminternational.org

Uses of Cobalt

USES OF COBALT can be broadly classified as metallurgical and nonmetallurgical. Metallurgical uses include the wear resistant, corrosion resistant, and heat resistant cobalt-base alloys, the use of cobalt in nickel-base superalloys (the largest end-use sector for cobalt), iron-base superalloys, cemented carbides, magnetic materials, low-expansion alloys, steels, and, to a lesser extent, nonferrous alloys and cobalt coatings. Nonmetallurgical uses include the use of cobalt compounds in chemicals (for example, pigments, catalysts, driers, and adhesives) and electronic applications (for example, cobalt-containing magnetic recording media and batteries).

Metallurgical Uses of Cobalt

Cobalt-Base Alloys

As a group, the cobalt-base alloys can be generally described as wear resistant, corrosion resistant, and heat resistant (strong even at high temperatures). The single largest use for cobalt-base alloys is in the area of wear resistant components and/or applications. In heat resistant applications, cobalt is more widely used as an alloying element in nickel-base alloys with cobalt tonnages in excess of those used in cobalt-base heat resistant alloys.

Many of the properties of the alloys arise from the crystallographic nature of cobalt (in particular, its response to stress); the solid-solution strengthening effects of chromium, tungsten, and molybdenum; the formation of metal carbides; and the corrosion resistance imparted by chromium. Generally, the softer and tougher compositions are used for high-temperature applications, such as gas turbine vanes and buckets. The harder grades are used for resistance to wear. More detailed information can be found in the article "Cobalt-Base Alloys" in this Handbook.

Cobalt in Superalloys

Cobalt in Nickel-Base Superalloys. In nickel-base superalloys, cobalt (which is present typically in the range of 10–15%) provides solid-solution strengthening and decreases the solubility of aluminum and titanium, thereby increasing the volume fraction of gamma prime, γ', (Ni_3Al), which is the phase required for high-temperature strength and creep resistance. Cobalt in nickel-base superalloys also reduces the tendency for grain boundary carbide precipitation, thus reducing chromium depletion at the grain boundaries.

A number of studies have been conducted to determine the role of cobalt in nickel-base superalloys. The goal of these studies was to determine the effects of the reduction and/or replacement of cobalt on the properties or microstructural characteristics of various superalloys. The NASA program for the conservation of strategic aerospace materials (COSAM) supports these studies (Ref 1).

Waspaloy, which contains 13% Co, is used in turbine disks. Because of the size and weight of the turbine disk, a major portion of the cobalt used in gas turbine engine components is used in this application. The effects of reducing cobalt in Waspaloy are reported in Ref 2. Highlights of that study are shown in Fig. 1. Tensile strength decreased only slightly as the amount of cobalt in the alloy decreased. However, rupture life decreased substantially with decreasing amounts of cobalt. Table 1 summarizes the major findings of this study. In addition to the slight decrease in the amount of γ', the major effects that removing cobalt had on mechanical properties were attributed to a possible higher stacking fault energy of the matrix and to changes in carbide partitioning in grain boundaries. Similar studies have been carried out on Udimet 700 (17% Co) and MAR-M 247 (10% Co). Summaries of these studies can be found in Ref 3.

Cobalt in Iron-Base Superalloys. Cobalt is also an important alloying element in some iron-base superalloys. For example, Haynes 556 (UNS R30556) is a solid-solution-strengthened Fe-Ni-Cr-Co alloy used extensively is sulfur-bearing environments. The resistance of the alloy to sulfidation is due to its comparatively low nickel content (20%) coupled with the addition of cobalt (18%) and a high chromium level (22%). Table 2 compares the sulfidation resistance of alloy 556 with other heat resistant alloys.

Another solid-solution-strengthened iron-base superalloy containing cobalt is Multimet (UNS R30155), which is the predecessor of alloy 556.

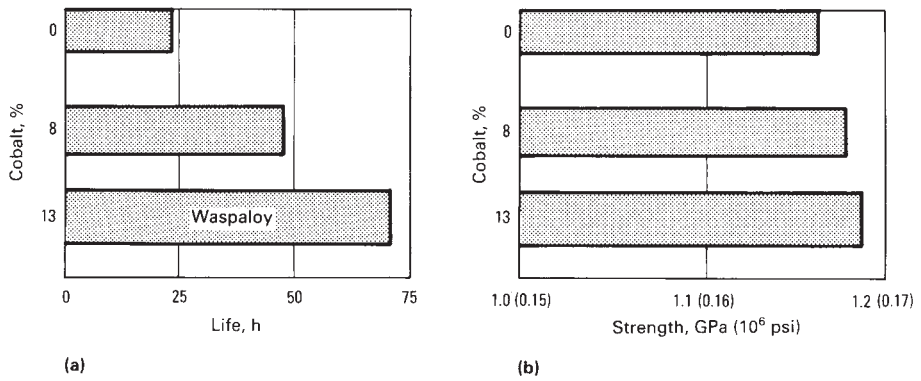


Fig. 1 Effect of cobalt content in Waspaloy on (a) rupture life at 730 °C (1345 °F) and 550 MPa (80 ksi) and (b) tensile strength at 535 °C (995 °F)

Table 1 Effects of removing cobalt from Waspaloy

Property or characteristic	Result
Hot workability	
Heating	No change
Cooling	Decrease
Tensile strength	Slight reduction
Tensile ductility	No change
Stress-rupture life	Major decrease
Creep rate	Six-fold increase
γ' solvus temperature	No change
γ' volume fraction	Slight decrease (18–16%)
γ' chemistry	Decrease of Cr and Ti and increase of Al
Carbides	
Chemistry	More metal carbide as rolled; more $M_{23}C_6$ 843 °C (1550 °F) aging
Morphology	Coarser

This cobalt-containing alloy (20% Co) is used extensively in older aircraft gas turbines.

Some high-strength, precipitation-hardenable iron-base superalloys exhibiting low coefficients of thermal expansion also contain from 13 to 16% Co. Low-expansion alloys are further described later in this article.

Cobalt in Cemented Carbides

The role of cobalt in cemented carbides, or "hard metals," is to provide a ductile metallic binder for hard carbide particles. Cobalt is used as a matrix for carbide particles because its wetting or capillary action during liquid phase sintering allows the achievement of high densities.

Machining Grades. Approximately 50% of all cemented carbide production is used for machining applications, and a wide variety of compositions are available. "Straight" grades, which consist of tungsten carbide bonded with cobalt (WC-Co), generally contain 3 to 12% Co, and carbide grain sizes range from 0.5 to more than 5 μm. Alloy grades, or steel-cutting grades, contain titanium carbide (TiC), titanium carbonitride (TiCN), titanium nitride (TiN), tantalum carbide (TaC) and/or niobium carbide (NbC). Improved wear resistance of cemented carbide tools is achieved by multilayer hard coating of TiC, TiCN, TiN, alumina (Al_2O_3) and occasionally hafnium carbide (HfC). These coatings are normally applied by vapor deposition techniques.

Nonmachining Grades. Cemented carbides are also being used increasingly for nonmachining applications, such as mining, construction, oil and gas drilling, metal forming, structural components, and wear parts. Straight WC-Co grades are used for the majority of these applications. In general, cobalt contents range from 5 to 20% and WC grain sizes from less than 1 to 8 μm and sometimes up to 30 μm.

Influence of Cobalt on Properties. Specific properties of individual grades of cemented carbides depend not only on the composition of the carbide but also on its grain size and on the amount of cobalt binder. For straight grades of comparable WC grain size, increasing cobalt content increases transverse strength and toughness but decreases hardness, compressive strength, elastic modulus, and abrasion resistance (Fig. 2). Table 3 also lists properties of various straight grades with varying cobalt contents.

For complex alloyed grades, comparisons similar to those drawn for the straight grades are not as readily made. Variations in carbide type, as well as binder content, affect properties, which in turn influence suitability for specific types of service. The two complex grades listed in Table 3 contain about the same amount of WC, but one contains about twice as much cobalt binder. The lower-cobalt grade is used for lighter-duty cutting. The alloyed grade high in TiC is relatively low in transverse strength and high in resistance to abrasion and cratering. It is used extensively for high-speed, light-duty finishing. The alloyed grade highest in cobalt content and in TaC is preferred for hot-work tools, in both cutting and shaping of metals.

Cobalt in Magnetic Materials

Magnetic materials can be classified as either soft magnet materials or permanent magnet materials. A soft magnetic material is a ferromagnetic alloy that becomes magnetized readily upon the application of a magnetic field and that returns to practically a nonmagnetic condition when the field is removed. Such alloys exhibit high magnetic permeability, low coercive force, and low magnetic hysteresis loss. A permanent magnet material is a ferromagnetic alloy capable of being magnetized permanently because of its ability to retain induced magnetization and magnetic poles after removal of externally applied fields. Such alloys exhibit a high coercive force. Cobalt, which is naturally ferromagnetic, provides resistance to demagnetization in several groups of magnetic materials.

Soft Magnetic Alloys. For soft magnetic materials, cobalt is alloyed with iron (49Co-49Fe-2V and Fe-27Co-0.6Cr). The iron-cobalt alloys exhibit a high positive magnetostrictive coefficient and high magnetic saturation making them useful in laminations for motors and generators, transformer laminations and tape torroids, magnetic pole caps, and in extremely accurate positioning devices.

Amorphous cobalt-base alloys containing various amounts of metalloids are also available as soft magnetic materials. A typical composition is $Co_{72}Fe_3P_{16}B_6Al_3$. These materials, which are characterized by low hysteresis loss and low coercive force, are used as a core material for power-distribution transformers.

Permanent Magnetic Alloys. In permanent magnets, cobalt increases the Curie temperature and saturation magnetism. On a tonnage basis, cobalt is used to a greater extent in permanent magnets than in soft magnets.

The first cobalt-containing permanent magnets were steels containing 36% Co

Table 2 Sulfidation resistance of various alloys at elevated temperatures

Note the improved performance of the cobalt-containing alloys HR-160 (29% Co) and 556 (18% Co).

	760 °C (1400 °F)(a)				871 °C (1600 °F)(a)			
	Metal loss		Average metal affected(b)		Metal loss		Average metal affected(b)	
Material	μm	mils	μm	mils	μm	mils	μm	mils
HR-160 alloy	5	0.2	30	1.1	3	0.1	95	3.8
556 alloy	65	2.5	95	3.8	130	5.2	295	11.7
Type 310	155	6.2	230	9.1	240	9.5	345	13.5
Alloy 800H	180	7.1	285	11.2	295	11.7	490	19.2
X alloy	>750	>29.5	Perforated		>550	>21.7	Consumed	
Alloy 600	>560	>21.7	Perforated		>550	>21.7	Consumed	
Alloy 601	>750	>29.5	Perforated		>550	>21.7	Perforated	

(a) 215 h exposure in Ar + 5% H_2 + 5% CO + 1% CO_2 + 0.15% H_2S + 0.10% H_2O. (b) Metal loss + average internal penetration

Table 3 Properties of representative cobalt-bonded cemented carbides

Nominal composition	Grain size	Hardness, HRA	Density		Transverse strength		Compressive strength		Modulus of elasticity		Relative abrasion resistance(a)	Coefficient of thermal expansion, μm/m · K		Thermal conductivity, W/m · K
			g/cm³	oz/in.³	MPa	ksi	MPa	ksi	GPa	10⁶ psi		at 200 °C (390 °F)	at 1000 °C (1830 °F)	
97WC-3Co	Medium	92.5–93.2	15.3	8.85	1590	230	5860	850	641	93	100	4.0	…	121
94WC-6Co	Fine	92.5–93.1	15.0	8.67	1790	260	5930	860	614	89	100	4.3	5.9	…
	Medium	91.7–92.2	15.0	8.67	2000	290	5450	790	648	94	58	4.3	5.4	100
	Coarse	90.5–91.5	15.0	8.67	2210	320	5170	750	641	93	25	4.3	5.6	121
90WC-10Co	Fine	90.7–91.3	14.6	8.44	3100	450	5170	750	620	90	22	…	…	…
	Coarse	87.4–88.2	14.5	8.38	2760	400	4000	580	552	80	7	5.2	…	112
84WC-16Co	Fine	89	13.9	8.04	3380	490	4070	590	524	76	5	…	…	…
	Coarse	86.0–87.5	13.9	8.04	2900	420	3860	560	524	76	5	5.8	7.0	88
75WC-25Co	Medium	83–85	13.0	7.52	2550	370	3100	450	483	70	3	6.3	…	71
71WC-12.5TiC-12TaC-4.5Co	Medium	92.1–92.8	12.0	6.94	1380	200	5790	840	565	82	11	5.2	6.5	35
72WC-8TiC-11.5TaC-8.5Co	Medium	90.7–91.5	12.6	7.29	1720	250	5170	750	558	81	13	5.8	6.8	50

(a) Based on a value of 100 for the most abrasion-resistant material

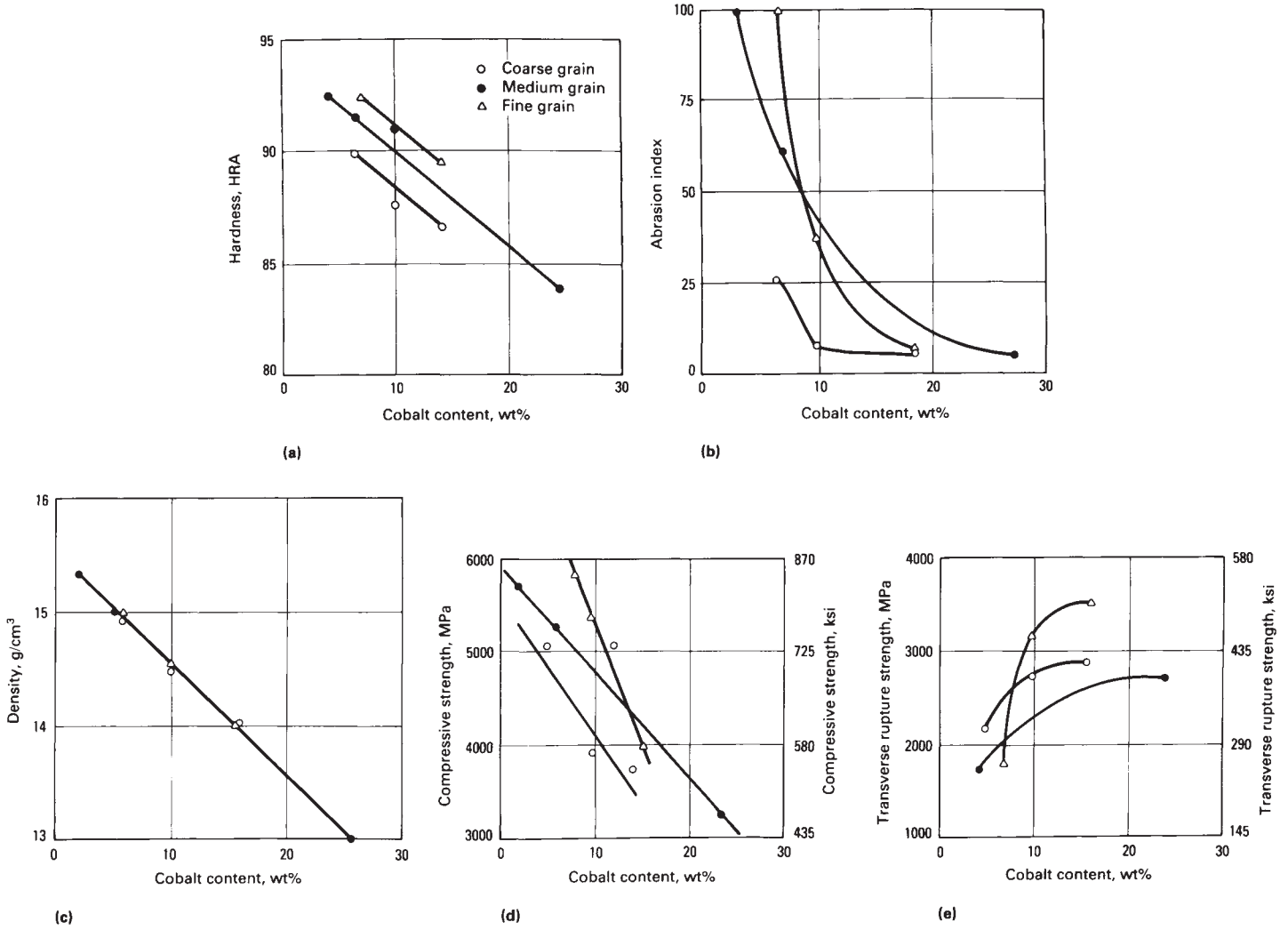


Fig. 2 Variation in properties with cobalt content and grain size for straight WC-Co alloys. (a) Variation in hardness. (b) Variation in abrasion resistance. (c) Variation in density. (d) Variation in compressive strength. (e) Variation in transverse rupture strength

having a coercive force as high as 20 kA · m^{-1} (250 Oe). These materials, which were developed in Japan in 1917, are now considered obsolete.

Alnico alloys (Al-Ni-Co-Fe) constitute a group of industrial permanent magnet materials developed in the 1940s and 1950s that are still widely used. Both cast (with equiaxed or columnar grain structures) and sintered forms of Alnico magnets are available. Cobalt contents in the most commercially important grades range from 5 to 35%. Generally, Alnico alloys are superior to other permanent magnet materials in resisting temperature effects on magnetic performance. Table 4 lists various properties of the six most important cast Alnico alloys.

Platinum-cobalt (23% Co) permanent magnets are isotropic, ductile, easily machined, resistant to corrosion and high temperatures, and have magnetic properties superior to the Alnico alloys. Due to their high cost, however, they

Table 4 Magnetic, mechanical, and physical properties of major cast Alnico alloys

The value $(BH)_{max}$ is the most important because it represents the maximum magnetic energy that a unit volume of the material can produce in an air gap.

								Nominal magnetic properties(c)				Mechanical and physical properties(d)							
	Nominal composition(b), wt%					B_r		H_c		$(BH)_{max}$			Tensile strength		Transverse modulus of rupture		Hardness,	Curie temperature	
Cast alloy(a)	Al	Ni	Co	Cu	Ti	T	kG	A · m^{-1} × 10^4	Oe	J · m^{-3} × 10^4	Mg · Oe	Density, g/cm^3	MPa	ksi	MPa	ksi	HRC	°C	°F
Alnico 2	10	19	13	3	…	0.75	7.5	4.46	560	1.4	1.7	7.1	21	3.0	48	7.0	45	810	1490
Alnico 5	8	14	24	3	…	1.28	12.8	5.09	640	4.4	5.5	7.3	37	5.4	72	10.5	50	860	1580
Alnico 5-7	8	14	24	3	…	1.35	13.5	5.88	740	6.0	7.5	7.3	34	5.0	55	8.0	50	860	1580
Alnico 6	8	16	24	3	1	1.05	10.5	6.21	780	3.1	3.9	7.3	160	23	310	45	50	860	1580
Alnico 8	7	15	35	4	5	0.82	8.2	13.1	1650	4.2	5.3	7.3	70	10	210	30	55	860	1580
Alnico 9	7	15	35	4	5	1.06	10.6	11.9	1500	7.2	9.0	7.3	48	7.0	55	8.0	55	860	1580

(a) Alnico 2 is isotropic. Alnico 5, 5-7, 6, 8, and 9 are aniosotropic. Alnico 5-7 and Alnico 9 are also directional grain (columnar crystals). (b) The composition balance for all alloys is iron. Small percentages of silicon, zirconium, niobium, and sulfur may also be present in certain alloys. (c) B_r, remanent magnetization; H_c, normal coercive force; $(BH)_{max}$, maximum magnetic energy = magnetic induction × magnetic field strength. (d) Measurement of properties, such as hardness plus tensile and rupture strength, can be determined only under laboratory conditions and only for comparison purposes.

Table 5 Compositions, thermal expansion coefficients, and room-temperature tensile properties of high-strength controlled-expansion alloys

Alloy designation	UNS No.	Composition, %	Coefficient of thermal expansion, from room temperature to: 260 °C (500 °F) ppm/°C	ppm/°F	370 °C (700 °F) ppm/°C	ppm/°F	415 °C (780 °F) ppm/°C	ppm/°F	Inflection temperature °C	°F	Ultimate tensile strength MPa	ksi	0.2% yield strength MPa	ksi	Elongation, %	Reduction in area, %
Incoloy 903 and Pyromet CTX-1	N19903	0.03 C, 0.20 Si, 37.7 Ni, 16.0 Co, 1.75 Ti, 3.0 (Nb + Ta), 1.0 Al, 0.0075 B, bal Fe	7.51	4.17	7.47	4.15	7.45	4.14	440	820	1480	215	1310	190	15	45
Incoloy 907 and Pyromet CTX-3	N19907	0.06 C max, 0.5 Si, 38.0 Ni, 13.0 Co, 1.5 Ti, 4.8 (Nb + Ta), 0.35 Al max, 0.012 B max, bal Fe	7.65	4.25	7.50	4.15	7.55	4.20	415	780	1170	170	825	120	15	25
Incoloy 909 and Pyromet CTX-909	N19909	0.06 C max, 0.40 Si, 38.0 Ni, 14.0 Co, 1.6 Ti, 4.9 (Nb + Ta), 0.15 Al max, 0.012 B max, bal Fe	7.75	4.30	7.55	4.20	7.75	4.30	415	780	1310	190	1070	155	10	20

have been replaced by rare earth-cobalt alloys except in very specialized applications.

Rare earth permanent magnets using cobalt additions include the samarium-cobalt compounds $SmCo_5$ and Sm_2Co_{17}. Developed around 1970, these were the materials of choice for most small, high-performance devices operating between 175 and 350 °C (345–660 °F) until the subsequent development of the less expensive, more powerful neodymium-iron-boron alloys in 1983. For more corrosion resistant applications, small amounts of cobalt are added to NdFeB alloys.

Cobalt in Low-Expansion Alloys

Low-expansion or controlled-expansion alloys are materials with dimensions that do not change appreciably with temperature. Although iron-nickel alloys such as Invar (UNS K93603), a 64%Fe-36%Ni alloy, are the best known of the low-expansion alloys, ternary alloys of Fe-Ni-Co, Fe-Co-Cr, and high-strength controlled-expansion alloys containing cobalt are also of commercial and technical importance.

Fe-Ni-Co Alloys. Replacement of some of the nickel by cobalt in an alloy of the Invar composition lowers the thermal expansion coefficient and makes the expansion characteristics of the alloy less susceptible to variations in heat treatment. One such alloy is the Super Invar with a nominal 32% Ni and 4 to 5% Co. Its expansion coefficient is lower than that of Invar, but over a narrower temperature range.

Kovar (UNS K94610) is a nominal 29% Ni-17%Co-54%Fe alloy that is a well-known glass-sealing alloy suitable for sealing to hard (borosilicate) glasses. Kovar has a nominal expansion coefficient of approximately 5 ppm/°C and inflection temperature of approximately 450 °C (840 °F).

Fe-Co-Cr Alloys. An alloy containing 36.5 to 37% Fe, 53 to 54.5% Co, and 9 to 10% Cr has an exceedingly low, and at times, negative (over the range from 0 to 100 °C, or 32 to 212 °F) coefficient of expansion. This alloy has a good corrosion resistance compared with low-expansion alloys without chromium. Consequently, it has been referred to as "Stainless Invar."

High-Strength, Controlled-Expansion Alloys. There is a family of Fe-Ni-Co alloys strengthened by the addition of niobium and titanium that show the strength of precipitation-hardened superalloys while maintaining low coefficients of thermal expansion typical of certain alloys from the Fe-Ni-Co system. Table 5 shows compositions and properties of these alloys. The combination of exceptional strength and low coefficient of expansion makes this family useful for applications requiring close operating tolerances over a range of temperatures. Several components for gas turbine engines are produced from these alloys.

Cobalt in Steels

Cobalt is not one of the common elements added to low-alloy steels, because its direct effect on properties is generally less than that obtained from other more economical elements, such as nickel or molybdenum. Cobalt does, however, influence the behavior of some specialty steels.

High-Speed Tool Steels. The main effect of cobalt in high-speed tools steels is to increase the hot hardness (Fig. 3) and thus increase the cutting efficiency when high tool temperatures are attained during the cutting operation. Cobalt is used in both molybdenum high-speed steels and tungsten high-speed steels in contents ranging from about 5 to 12% (Table 6).

Cobalt is also used in some hot- and cold-work tool steels. For example, H19, a chromium hot-work steel contains 4 to 4.50% Co; D5, a high-chromium cold-work steel contains 2.50 to 3.50% Co.

Maraging steels comprise a special class of ultrahigh-strength steels that differ from conventional steels (e.g., medium-carbon content 4340 low-alloy steel) in that they are hardened by a metallurgical reaction that does not involve carbon. Instead, these steels are strengthened by the precipitation of intermetallic compounds (Ni_3Mo, Fe_2Mo, and Ni_3Ti) at temperatures of approximately 480 °C (900 °F). The term maraging is derived from martensite age hardening and denotes the age hardening of the low-carbon, iron-nickel lathe martensite matrix.

Commercial maraging steels are designed to provide specific levels of yield strength from 1380 to 2415 MPa (200–350 ksi). These steels typically have very high nickel, cobalt, and molybdenum contents and very low carbon contents. Carbon, in fact, is considered an impurity in these steels.

As indicated in Table 7, cobalt contents in standard maraging steels range from 8.5 to 12.5%. The main contribution of cobalt is to lower the solubility of molybdenum in the martensitic matrix and thus increase the amount of Ni_3Mo precipitate formed during age hardening. Some hardening also results from a short-range ordering reaction in the matrix that involves cobalt.

High-fracture toughness steels are structural steels capable of yield strengths of 1380 MPa (200 ksi) and fracture toughness (K_{Ic}) values of 100 MPa (90 ksi) or more. Examples include HP-9-4-30 (4.50% Co), AF1410 (14.0% Co), and AerMet 100 (13.4% Co). Compositions for these steels are listed in Table 8. Cobalt enhances the precipitation of the $(Mo,Cr)_2C$ phase, thereby increasing strength. It also raises the martensite transition temperature, counteracting the effects of the high nickel

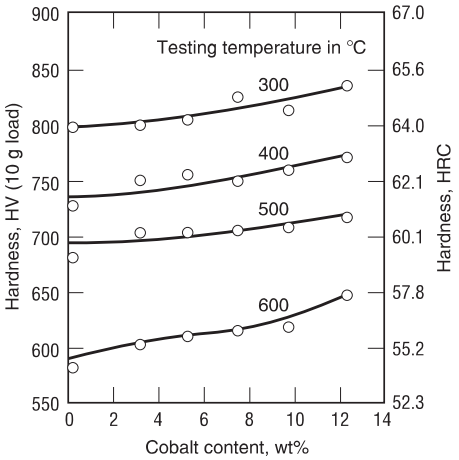


Fig. 3 Effect of cobalt content on the hot hardness of T1 high-speed steel. Initial hardness of 66 HRC at different testing temperatures

Table 6 Nominal compositions of high-speed tool steels

AISI type	UNS designation	Composition, % C	Si	Cr	V	W	Mo	Co
Molybdenum high-speed tool steels								
M1	T11301	0.83	0.35	3.75	1.18	1.75	8.70	…
M2								
Regular C	T11302	0.83	0.33	4.13	1.98	6.13	5.00	…
High C	…	1.00	0.33	4.13	1.98	6.13	5.00	…
M3								
Class 1	T11313	1.05	0.33	4.13	2.50	5.88	5.63	…
Class 2	T11323	1.20	0.33	4.13	3.00	5.88	5.63	…
M4	T11304	1.33	0.33	4.25	4.13	5.88	4.88	…
M6	T11306	0.80	0.33	4.13	1.50	4.25	5.00	12.00
M7	T11307	1.01	0.38	3.75	2.00	1.75	8.70	…
M10								
Regular C	T11310	0.89	0.33	4.13	2.00	…	8.13	…
High C	…	1.00	0.33	4.13	2.00	…	8.13	…
M15	T11315	1.50	0.33	4.00	5.00	6.50	3.50	5.00
M30	T11330	0.80	0.33	4.00	1.25	2.00	8.00	5.00
M33	T11333	0.89	0.33	3.75	1.18	1.70	9.50	8.25
M34	T11334	0.89	0.33	3.75	2.10	1.75	8.48	8.25
M35	T11335	0.80	0.33	4.00	2.00	6.00	5.00	5.00
M36	T11336	0.85	0.33	4.13	2.00	6.00	5.00	8.25
M41	T11341	1.10	0.33	4.13	2.00	6.63	3.75	8.25
M42	T11342	1.10	0.40	3.88	1.15	1.50	9.50	8.25
M46	T11346	1.26	0.53	3.95	3.15	2.05	8.25	8.30
M48	T11348	1.50	0.33	3.88	3.00	10.00	5.13	9.00
M50 (a)	T11350	0.80	0.40	4.13	1.00	…	4.25	…
M52 (a)	T11352	0.90	0.40	4.00	1.93	1.25	4.45	…
M62	T11362	1.30	0.28	3.88	2.00	6.25	10.50	…
Tungsten high-speed tool steels								
T1	T12001	0.73	0.30	4.13	1.10	18.00	…	…
T4	T12004	0.75	0.30	4.13	1.00	18.25	0.70	5.00
T5	T12005	0.80	0.30	4.38	2.10	18.25	0.88	8.25
T6	T12006	0.80	0.30	4.38	1.80	19.75	0.70	12.00
T8	T12008	0.80	0.30	4.13	2.10	14.00	0.70	5.00
T15	T12015	1.55	0.28	4.38	4.88	12.38	1.00	5.00

(a) Intermediate high-speed tool steel

content. Applications for high-fracture toughness steels include landing gear components, arresting hooks, catapult hooks, fasteners, structural members, armor, actuators, ordnance, ballistic-tolerant components, jet engine shafts, drive shafts, helicopter masts, and containment rings.

High Strength-to-Density Ratio Steels. A companion to AerMet 100, AerMet 310, which contains 15% Co (Table 8), has a strength-to-density ratio greater than that of Ti-6Al-4V (Table 9). Although AerMet 310 has a lower fracture toughness than its predecessor alloy AerMet 100, its higher yield and ultimate tensile strengths make it a candidate for landing gear and other critical aircraft components where high strength is required in combination with smaller size and/or lighter weight.

Stainless Steels. Some high-performance carburizing martensitic stainless steels for bearing and gear applications also contain cobalt. Examples include Pyrowear 675 (5.40% Co) and CSS-42L (12.5% Co). Compositions for these steels are listed in Table 8. Cobalt contributes to the high fracture toughness, hot hardness, metal-to-metal wear resistance, and corrosion resistance. Figure 4 compares the hot hardness of these cobalt-containing steels with comparative alloys.

Stainless steel hardfacing alloys containing cobalt have also been developed. Cobalt-containing (9% Co) austenitic stainless steel hardfacing alloys are used for repair of the cavitation erosion damage of hydraulic turbines in electric power plants. Cobalt-containing (2.5% Co) martensitic stainless steel hardfacing alloys are used as weld overlays on continuous caster rolls. The cobalt contributes to wear resistance and enhances resistance to thermal fatigue cracking. Compositions of cobalt-containing stainless steel hardfacing alloys are listed in Table 8.

Table 7 Nominal compositions of cobalt-containing maraging steels

Grade	Composition(a), % Ni	Mo	Co	Ti	Al
18Ni(200)	18	3.3	8.5	0.2	0.1
18Ni(250)	18	5.0	8.5	0.4	0.1
18Ni(300)	18	5.0	9.0	0.7	0.1
18Ni(350)	18	4.2(b)	12.5	1.6	0.1
18Ni(cast)	17	4.6	10.0	0.3	0.1
12-5-3(180) (c)	12	3	…	0.2	0.3

(a) All grades contain no more than 0.3% C. (b) Some producers use a combination of 4.8% Mo and 1.4% Ti, nominal. (c) Contains 5% Cr

Table 8 Nominal compositions of cobalt-containing steels

Alloy	Composition, % C	Cr	Ni	Mo	Co	Others
High-fracture toughness steels						
AF1410	0.15	2.0	10.0	1.0	14.0	…
HP-9-4-30	0.31	1.0	7.5	1.0	4.5	0.09V
AerMet 100	0.23	3.0	11.5	1.2	13.4	…
High strength-to-density ratio steel						
AerMet 310	0.25	2.4	11.0	1.4	15.0	…
Stainless steels						
CSS-42L	0.12	14.0	2.0	4.75	12.5	0.6V; 0.02Nb
Pyrowear 675	0.07	13.0	2.6	1.8	5.4	0.06V; 0.4Si
IRECA	0.2	17.0	…	…	9.0	9.5 Mn; 0.2N
Thermaclad 423	0.12	13.5	2.5	1.2	2.5	1.2 Mn; 0.4 Si; 0.18V; 0.18Nb

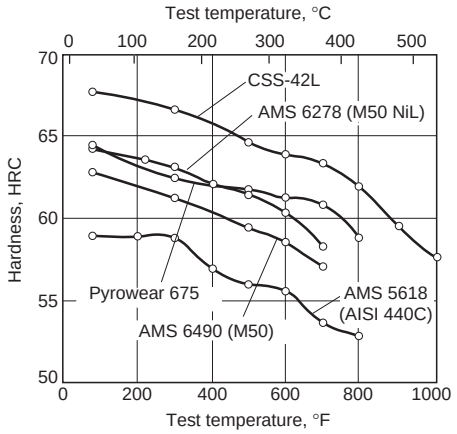


Fig. 4 Hot hardness of case-carburized cobalt-containing stainless steel (CSS-42L and Pyrowear 675) and comparative alloys

Cobalt in Nonferrous Alloys

Beryllium copper alloys are high-copper alloys containing 0.2 to 2.85% Be. They are used for a variety of electronic components and electrical equipment. The beryllium additions promote strengthening through precipitation hardening. The addition of cobalt (and/or nickel) to the binary Cu-Be system restricts grain growth during annealing by establishing a dispersion of beryllide, (Cu,Co)Be, particles in the matrix. Cobalt additions (from a minimum of 0.20% up to 2.7% Co) also enhance the magnitude of the age-hardening response and retards the tendency to overage or soften at extended aging times and higher aging temperatures.

High-Strength Aluminum Alloys. Rapid solidification processing is used to produce

Table 9 Strength-to-density ratios for various alloys

Alloy	Ratio km	in. × 10^6
AerMet 310	27.9	1.10
AerMet 100	25.7	1.01
Ti-6Al-4V	25.4	1.00
Marage 300	25.4	1.00
Custom 465	23.4	0.92

Source: Ref 2

Al-Zn-Mg-Cu alloys 7090 and 7091, which are similar in composition to conventional wrought (ingot metallurgy) alloy 7175, but contain 1.5 and 0.4% Co, respectively. Cobalt forms Co_2Al_9 or $(Co,Fe)_2Al_9$ particles, which are homogeneously dispersed. These dispersoids refine the grain size for improved high strength and ductility and enhance resistance to stress-corrosion cracking.

Cobalt in Coatings

Hardfacing. The most common application of cobalt-base coatings is that of wear-resistant hardfacing alloys deposited by welding or thermal spraying (plasma arc spray or high-velocity oxyfuel powder spray). Examples include the well-known Stellite alloys, which are cobalt-chromium alloys containing varying amounts of tungsten, molybdenum, and/or nickel and Co-Mo-W-Si (Tribaloy) alloys. These materials are described in the articles "Cobalt-Base Alloys" and "Wear Behavior of Cobalt Alloys" in this Handbook.

Overlay coatings are deposited on superalloys to increase their resistance to high-temperature corrosion. Either electron-beam physical vapor deposition or plasma spraying can produce such coatings, which are generally referred to as MCrAlY overlay coatings, where M represents Co, Ni, Fe, or some combination of these metals. More detailed information on CoCrAlY coatings can be found in the article "High-Temperature Coatings for Superalloys" in this Handbook.

Electroplating. Although cobalt is readily electrodeposited from a number of electrolytes (Table 10), nominally pure cobalt electrodeposits are not of commercial or technical importance. Cobalt does, however, play an important role as a constituent in a number of alloy electrodeposits. For example, cobalt additions to nickel plating solutions increase the hardness and strength of nickel plating, especially in electroforming. Most of the published data about nickel-cobalt plating were determined using a 600 g/L (8 oz/gal) nickel sulfamate solution (Ref 4). As shown in Fig. 5, a peak hardness of 520 HV is attained with 6 g/L (0.8 oz/gal) Co in the solution, which gives an alloy containing about 34% Co. Other cobalt-containing electrodeposits include cobalt-tungsten, cobalt-molybdenum, and zinc-cobalt. Additional information on these coatings can be found in *Surface Engineering*, Volume 5 of the *ASM Handbook*, and Ref 5.

Electroless Cobalt Alloy Plating. Nonelectrolytically produced cobalt alloy coatings have been used in a limited number of magnetic and wear applications. Examples include Co-P, Co-W-P, Co-B, and Co-W-B. Table 11 lists property and application information on these cobalt alloy coatings.

Conversion Coating. Cobalt/molybdenum-base conversion coatings are being developed as possible replacements for chromate conversion coatings, which pose health and safety risks and which are under increasing regulatory scrutiny. Laboratory tests have shown that the cobalt/molybdenum process, which uses cobalt and molybdates rather than chromates, is capable of imparting corrosion protection and paint adhesion required by the aerospace industry (particularly for aluminum alloys).

Nonmetallurgical Uses of Cobalt

Chemical and Ceramic Uses

Catalysts. Cobalt has marked catalytic activity and is widely used in the petrochemical and plastic industries. The most widely used cobalt catalyst consists of cobalt and molybdenum oxides supported on alumina. This is used for the hydrogen desulfurization of petroleum feedstocks; desulfurization enables high-sulfur crude oils to be used, reduces atmospheric pollution, and prevents poisoning of platinum catalysts used on later stages of the reforming process.

The second major use of cobalt is in the mixed cobalt acetate/manganese sodium bromide catalyst for production of terephthalic acid and di-methylterephthalate. These materials are used to manufacture resin for plastic bottles and also to make the strong plastics used in recording tapes.

Driers. Cobalt salts of the higher carboxylic acids (cobalt soaps) are used to accelerate drying in oil-base paints, varnishes, and inks.

Pigments for Ceramics and Glasses. Complex cobalt oxides are used for coloring and decorating ceramics and glasses. The colors obtained by cobalt-containing pigments are generally blue to green and are largely based on co-

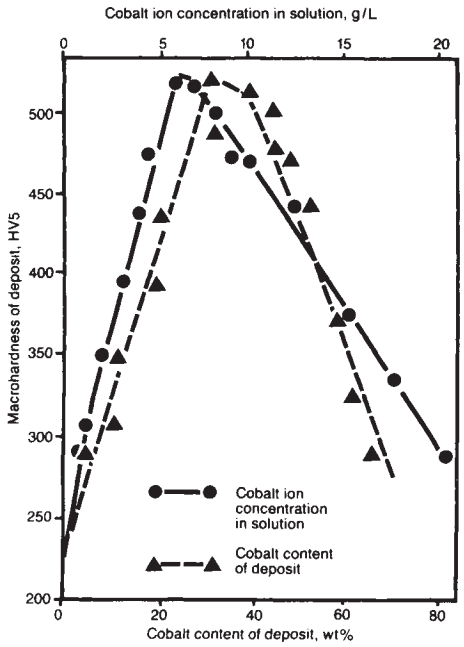


Fig. 5 Relationship between deposit hardness and cobalt concentration in the sulfamate solution and in the deposit. Source: Ref 4

Table 10 Electrolytes and operating conditions for cobalt electroplating

Electrolyte	Concentration	pH	Temperature, °C	Temperature, °F	Current density, A/dm^2
(1) Cobalt sulfate ($CoSO_4 \cdot 7H_2O$),	332 g/L	1–4	20–50	68–122	0.5–5
boric acid (H_3BO_3)	30 g/L	1–4	20–50	68–122	0.5–5
(2) Cobalt chloride ($CoCl_2 \cdot 6H_2O$),	300 g/L	1–4	20–50	68–122	0.5–5
boric acid (H_3BO_3)	30 g/L	1–4	20–50	68–122	0.5–5
(3) Cobalt ammonium sulfate	200 g/L	5.2	25	77	1–3
$(Co(NH_4)_2(SO_4)_2 \cdot 6H_2O)$	25 g/L	5.2	25	77	1–3
boric acid (H_3BO_3)					
(4) Cobalt sulfamate ($Co(SO_3NH_2)_2 \cdot 4H_2O$),	450 g/L	…	20–50	68–122	1–5
formamide ($HCONH_2$)	30 ml/L	…	20–50	68–122	1–5
(5) Cobalt fluoborate,	116–154 g/L	3.5	50	122	5.6
boric acid (H_3BO_3)	15 g/L	3.5	50	122	5.6

Source: Cobalt Development Institute

Table 11 Electroless cobalt alloy plating systems

Alloy	Hardness, HK_{100}	Environments in which plating has demonstrated corrosion resistance	Significant properties and applications	Availability
Hypophosphite-reduced cobalt-phosphorus (3–6% P, bal Co)	550–650	Alkali, brine solutions	Magnetic and medical applications	Production
Hypophosphite-reduced cobalt-tungsten-phosphorus (4–8% P, 1–5%W, bal Co)	570–640	…	High-temperature wear resistance	Production
Boron-reduced cobalt-boron (3–4% B, bal Co)	350–500(a)	…	Wear resistance in high-temperature applications	Laboratory; limited application
Boron-reduced cobalt-tungsten-boron (3–5% B, 1–5%W, bal Co)	750–850	…	Wear applications requiring resistance to galling can be used at higher temperatures than phosphorus systems	Laboratory

(a) As plated; 800–1000 HK_{100} after 30 min at 400 °C (750 °F)

Table 12 Cobalt-containing pigments for coloring ceramics

Pigment system	Chemical formula
Green	
Cobalt-chromite blue-green spinel	$Co(Al_2Cr)_2O_4$
Cobalt-chromite green spinel	$CoCr_2O_4$
Cobalt-titanate green spinel	Co_2TiO_4
Blue	
Cobalt-aluminate blue spinel	$CoAl_2O_4$
Cobalt-zinc-aluminate blue spinel	$(Co,Zn)Al_2O_4$
Cobalt-silicate blue olivine	Co_2SiO_4
Cobalt-zinc-silicate blue phenacite	$(Co,Zn)_2SiO_4$
Cobalt-tin blue-gray spinel	Co_2SnO_2
Cobalt-tin-alumina blue spinel	$CoAl_2O_4/Co_2SnO_4$
Black	
Iron-cobalt black spinel	$(Fe,Co)Fe_2O_4$
Iron-cobalt-chromite black spinel	$(Co,Fe)(Fe,Cr)_2O_4$
Gray	
Cobalt-nickel gray periclase	(Co,Ni)O

balt spinel or cobalt silicate. Various cobalt oxides used for coloring ceramics are listed in Table 12.

Pigments for Paints. Cobalt salts and oxides play a prominent role in the manufacture of paint pigments and, in combination with other oxides or acid radicals, yield a wide range of colors. Table 13 shows the pigments used in paints and the final colors produced.

Enamel Frits. Cobalt oxide (Co_3O_4) is a constituent in ground coat frits used in porcelain enameling of steel sheet. Cobalt oxide contents range from 0.65 to 1.27%.

Adhesives. Cobalt complex salts are incorporated into the rubber stock used in radial tire manufacturing. They improve the bond between the rubber and the brass-coated steel cords.

Table 13 Cobalt compounds in paint pigments

Color	Compounds
Purple-blue	$CoO/SiO_2/K_2O$
Blue	CoO/Al_2O_3
Violet	CoO/P_2O_5
Green	CoO/ZnO
Light blue	$CoO/SnO_2/SiO_2$
Turquoise	$CoO/Cr_2O_3/Al_2O_3$
Pink	CoO/MgO
Brown	CoO/FeO
Yellow	$K_3Co(NO_2)_6$

Electronic Uses

Batteries. One of the fastest growth areas for cobalt is its use in rechargeable batteries used in power tools, toys, electric vehicles, computers, cellular phones, camcorders, and similar electronic devices. In nickel-cadmium and nickel-metal hydride batteries, fine powders of cobalt oxide or hydroxide are added to improve battery performance. In lithium-ion batteries, $LiCoO_2$ accounts for 50% of the weight of the cathode (the electrode through which electrons enter a cell).

Magnetic Recording Media. Cobalt-modified iron oxide (Fe_2O_3) particles are the predominant material used in video tapes. Cobalt thin films (CoNi, CoP, CoCr) with high coercivities are also deposited on video and audio tapes and discs using evaporation and sputtering techniques.

Other electronic uses for cobalt include semiconductors, integrated circuits, solar collectors, gas sensors, piezoelectric transducers, zinc oxide varistors, and negative temperature coefficient thermistors. More detailed information on these applications can be found in Ref 6.

REFERENCES

1. F.E. Sczerenie and G.E. Maurer, "COSAM (Conservation of Strategic Aerospace Materials) Program Overview," NASA TM-83006, National Aeronautic and Space Administration, 1982
2. J.M. Dahl and P.M. Novotny, Airframe and Landing Gear Alloy, *Adv. Mater. Process.*, March 1999, p 23–25
3. Strategic Materials Availability and Supply, *Properties and Selection: Iron, Steels, and High-Performance Alloys*, Vol 1, *ASM Handbook*, ASM International, 1990, p 1009–1022
4. S.A. Watson, Nickel Alloy Plating, *Surface Engineering*, Vol 5, *ASM Handbook*, ASM International, 1994, p 266–269
5. J.D. Donaldson, S.J. Clark, and S.M. Grimes, Cobalt Chemicals in Electro- and Electroless-Plating, in *Cobalt in Chemicals*, Cobalt Development Institute, 1986
6. J.D. Donaldson, S.J. Clark, and S.M. Grimes, *Cobalt in Electronic Technology*, Cobalt Development Institute, 1988

SELECTED REFERENCES

- W. Bettridge, *Cobalt and Its Alloys*, Ellis Horwood Ltd., 1982
- *Cobalt Facts*, Cobalt Development Institute, 2000

ASM Specialty Handbook: Nickel, Cobalt, and Their Alloys
J.R. Davis, editor, p 356-361
DOI:10.1361/ncta2000p356

Copyright © 2000 ASM International®
All rights reserved.
www.asminternational.org

Phase Diagrams of Binary and Ternary Cobalt Systems

PHASE DIAGRAMS covering many of the commercially important cobalt alloy systems are presented in this article. Crystallographic data in tabular form accompany some of the diagrams. The binary alloy diagrams included here (Fig. 1–6, Tables 1–6) are the result of critical assessment by experts in the field under the coordination of the International Programme for Alloy Phase Diagrams. The ternary alloy diagrams (Fig. 7–25) were selected from the comprehensive collection of ternary diagrams, the multivolume *Handbook of Ternary Alloy Phase Diagrams*, edited by P. Villars, A. Prince, and H. Okamoto, and published by ASM International in 1994. All of the binary and ternary phase diagrams presented herein were also published in *Alloy Phase Diagrams*, Vol 3 of the *ASM Handbook*. This Volume should be consulted for original bibliographic citations relating to specific phase diagrams.

A full understanding of the constitution and structure of cobalt-containing alloys important in industry must be based on a study of the simpler binary and ternary systems from which more complex alloys have been developed. The allotropic transformation of cobalt—that is, the transformation from a stable hexagonal close-packed (hcp) structure (ε-cobalt) to a stable face-centered cubic (fcc) structure (α-cobalt)—makes even the simplest binary system a little more complex than the equivalent nickel alloy system. The transformation temperature of pure cobalt is 417 °C (783 °F). Alloying elements such as nickel, iron, and carbon (within the soluble range) are known as fcc stabilizers, and they suppress the transformation temperature. Chromium, tungsten, and molybdenum, on the other hand, are hcp stabilizers and have the opposite effect. In reality, the transformation is extremely sluggish, and most cobalt-base alloys exhibit a metastable fcc structure at room temperature, even if their transformation temperatures are considerably higher.

Because of the sluggishness of the transformation in alloys, very few published phase diagrams indicate the presence of a two-phase α + ε field, as is required for compliance with the phase rule (Ref 1, 2). Although pure cobalt transforms from one structure to the other at a fixed temperature (as described above), alloys transform gradually over a temperature range with both phases present in the intervening field. To a first approximation, the quoted temperatures for the ε → α and α → ε transformations in the binary phase diagrams may be taken as indicating the completion of the transformations and, hence, as representing the equilibrium boundaries of the two-phase field (Ref 1).

The binary systems included in this article include C-Co, Co-Cr, Co-Fe, Co-Mo, Co-Ni, and Co-W. Ternary systems illustrated include Co-Cr-Fe, Co-Cr-Ni, Co-Cr-W, Co-Fe-Mo, Co-Fe-Ni, Co-Fe-W, and Co-Mo-Ni. The ternary diagrams are all isothermal sections at various temperatures. Solidus and liquidus projections for some of these ternary systems can be found in Volume 3 of the *ASM Handbook*.

REFERENCES

1. W. Betteridge, Constitution and Metallography of Cobalt Alloys, *Cobalt and its Alloys*, Ellis Horwood Ltd., 1982, p 41–59
2. H. Baker, Introduction to Phase Diagrams, *Alloy Phase Diagrams*, Vol 3, *ASM Handbook*, ASM International, 1992, p 1-1 to 1-29

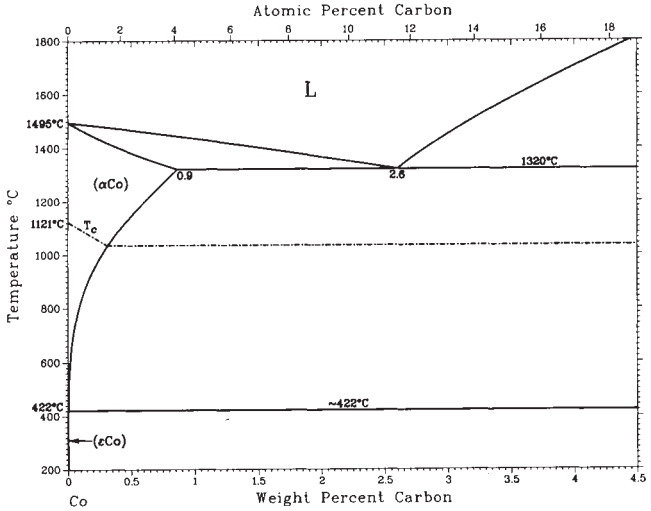


Fig. 1 Cobalt-carbon (Co-C) binary phase diagram

Table 1 Co-C crystal structure data

Phase	Composition, wt% C	Pearson symbol	Space group
(αCo)	0 to 0.9	*cF*4	$Fm\bar{3}m$
(εCo)	~0	*hP*2	$P6_3/mmc$
C	~100	*hP*4	$P6_3/mmc$
Metastable phases			
(ε′Co)	~0.3 to ~0.4	(a)	…
Co_3C	6	*oP*6	*Pnma*
Co_2C	9	*oP*6	*Pnnm*

(a) Hexagonal

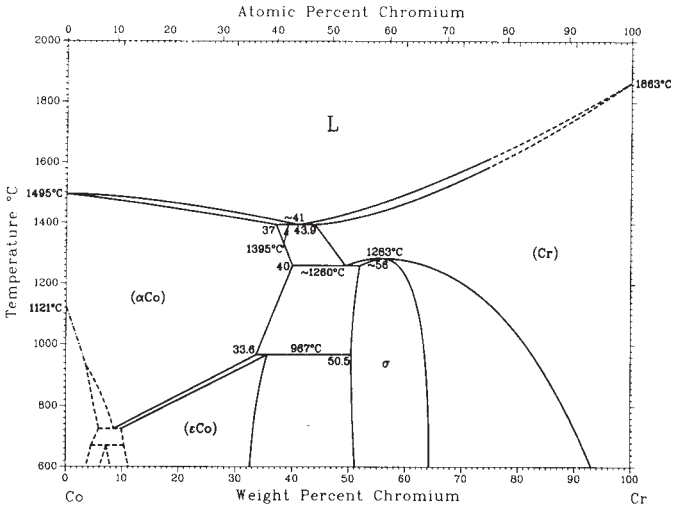


Fig. 2 The cobalt-chromium (Co-Cr) binary phase diagram

Table 2 Co-Cr crystal structure data

Phase	Composition, wt% Cr	Pearson symbol	Space group
(αCo)	0–40	*cF*4	$Fm\bar{3}m$
(εCo)	0–36	*hP*2	$P6_3/mmc$
(αCr)	43.9–100	*cI*2	$Im\bar{3}m$
σ	50.5–63	*tP*30	$P4_2/mnm$
Metastable phases			
(αCr)	~16	*cI*2	$Im\bar{3}m$
(αCo)	40–62.9	*cF*4	$Fm\bar{3}m$
(δCr)	54–100	*cP*8	$Pm\bar{3}n$
Co_3Cr	23	*hP*8	$P6_3/mmc$

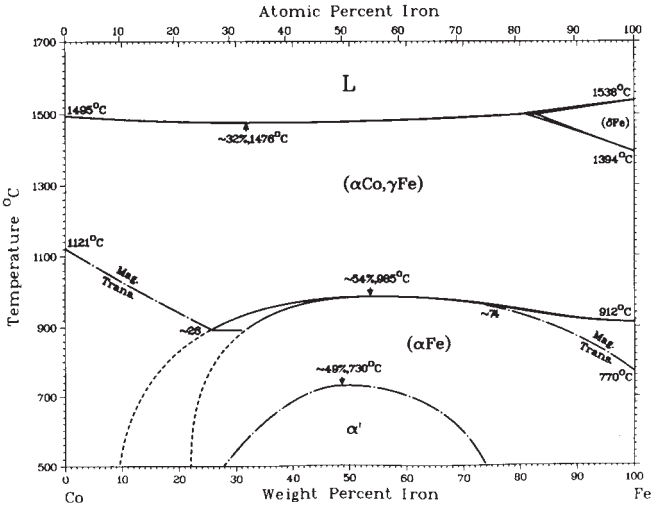


Fig. 3 The cobalt-iron (Co-Fe) binary phase diagram

Table 3 Co-Fe crystal structure data

Phase	Composition, wt% Fe	Pearson symbol	Space group
(αCo, γFe)	0–100	*cF*4	$Fm\bar{3}m$
α′	~28 to ~74	*cP*2	$Pm\bar{3}m$
(αFe)	~22–100	*cI*2	$Im\bar{3}m$
(δFe)	82–100	*cI*2	$Im\bar{3}m$
Metastable phase			
η	0.5–5.7	*hP*4	$P6_3/mmc$

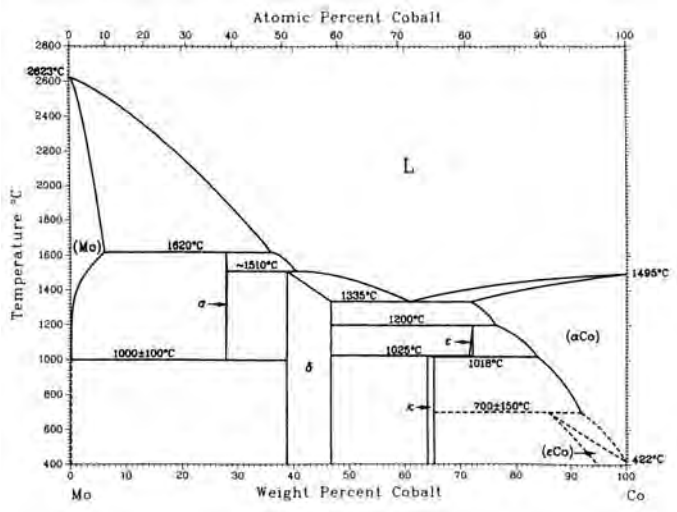


Fig. 4 The cobalt-molybdenum (Co-Mo) binary phase diagram

Table 4 Co-Mo crystal structure data

Phase	Composition, wt% Co	Pearson symbol	Space group
(Mo)	0 to ~6	*cI*2	$Im\bar{3}m$
σ	~27.8–28	*tP*30	$P4_2/mnm$
ε	~38.8 to ~46.7	*hR*13	$R\bar{3}m$
K	~64.2 to ~65.4	*hP*8	$P6_3mmc$
cph	~72	*hP*2	$P6_3/mmc$
(αCo)	~72–100	*cF*4	$Fm\bar{3}m$
(εCo)	~86–100	*hP*2	$P6_3/mmc$

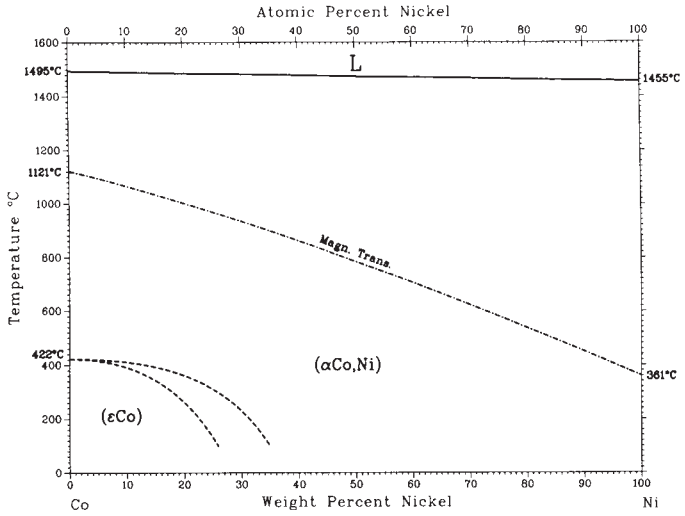


Fig. 5 The cobalt-nickel (Co-Ni) binary phase diagram

Table 5 Co-Ni crystal structure data

Phase	Composition, wt% Ni	Pearson symbol	Space group
(αCo,Ni)	0–100	*cF*4	$Fm\bar{3}m$
(εCo)	0–35	*hP*2	$P6_3/mmc$

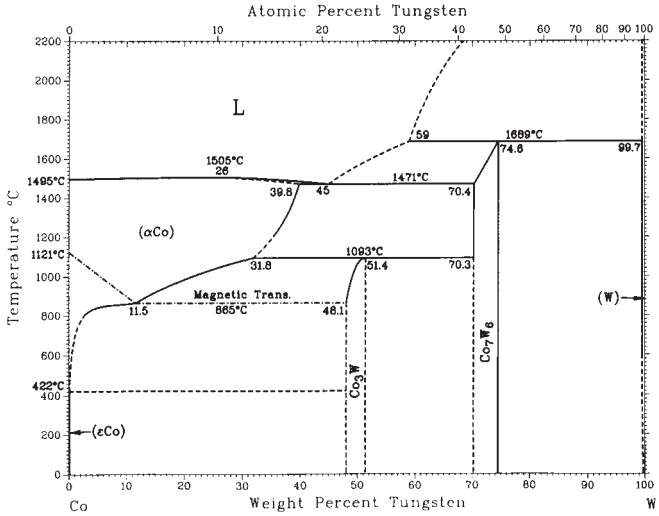


Fig. 6 The cobalt-tungsten (Co-W) binary phase diagram

Table 6 Co-W crystal structure data

Phase	Composition, wt% W	Pearson symbol	Space group
(αCo)	0–39.8	*cF*4	$Fm\bar{3}m$
(εCo)	0	*hP*2	$P6_3/mmc$
Co_3W	48.1–51.4	*hP*8	$P6_3/mmc$
Co_7W_6	70.3–74.6	*hR*13	$R\bar{3}m$
(W)	99.7–100	*cI*2	$Im\bar{3}m$

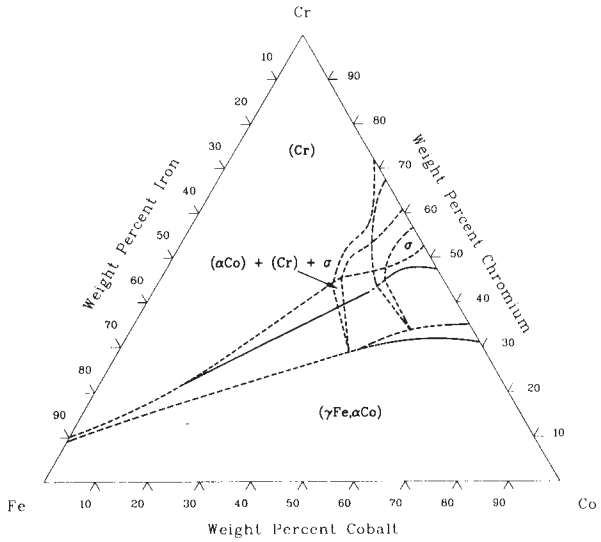


Fig. 7 Co-Cr-Fe isothermal section at 1200 °C (2190 °F)

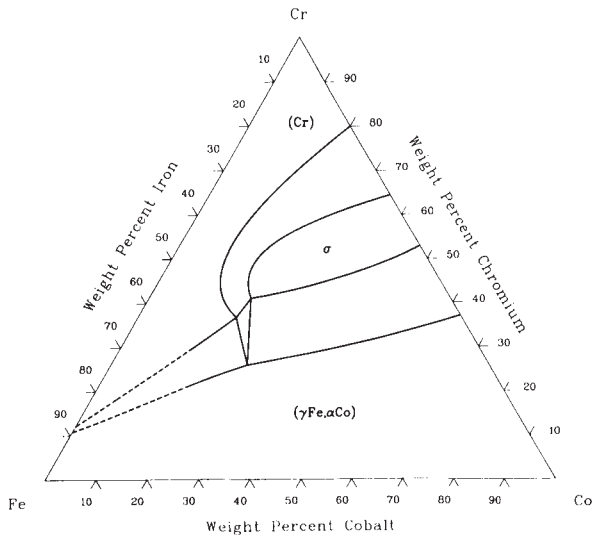


Fig. 8 Co-Cr-Fe isothermal section at 1000 °C (1830 °F)

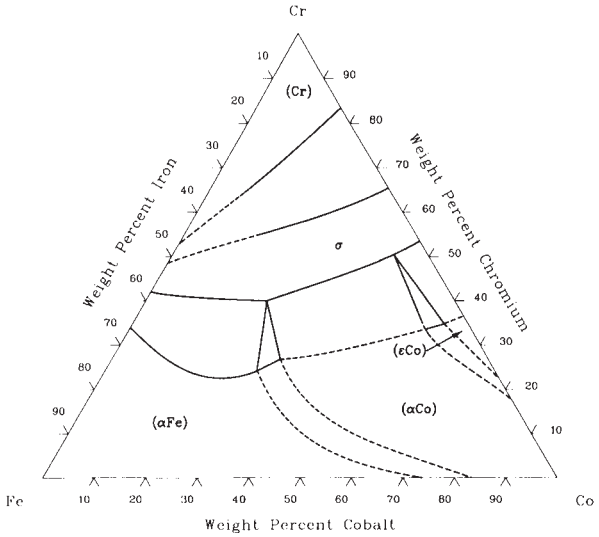


Fig. 9 Co-Cr-Fe isothermal section at 800 °C (1470 °F)

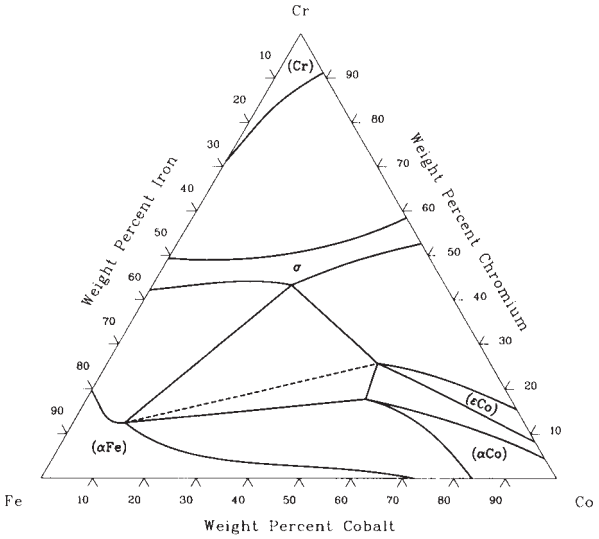


Fig. 10 Co-Cr-Fe isothermal section at 600 °C (1110 °F)

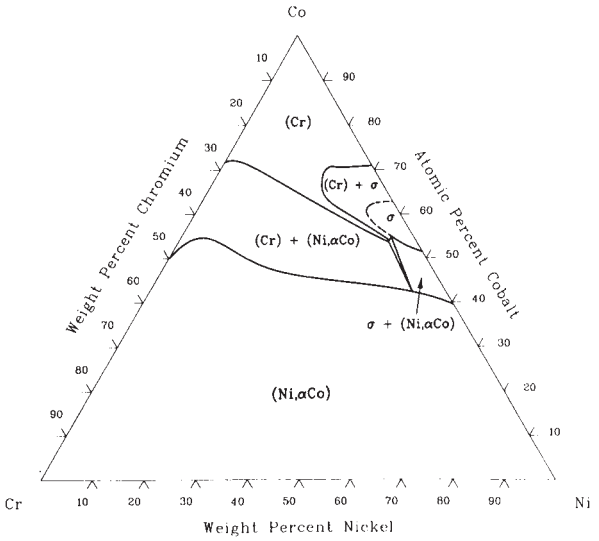


Fig. 11 Co-Cr-Ni isothermal section at 1200 °C (2190 °F)

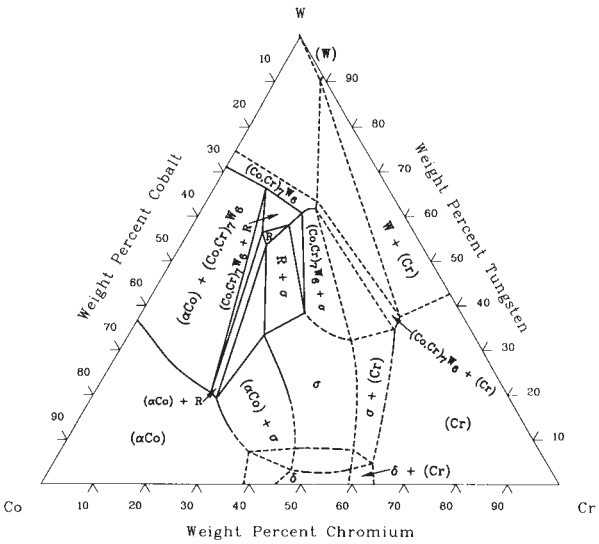


Fig. 12 Co-Cr-W isothermal section at 1350 °C (2460 °F)

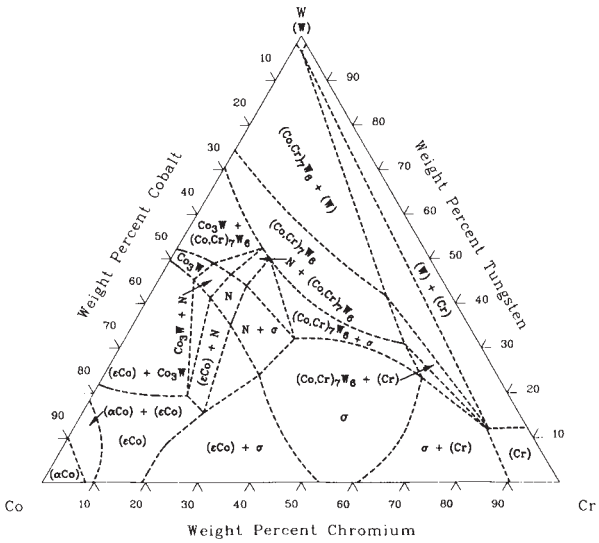


Fig. 13 Co-Cr-W isothermal section at 700 °C (1290 °F)

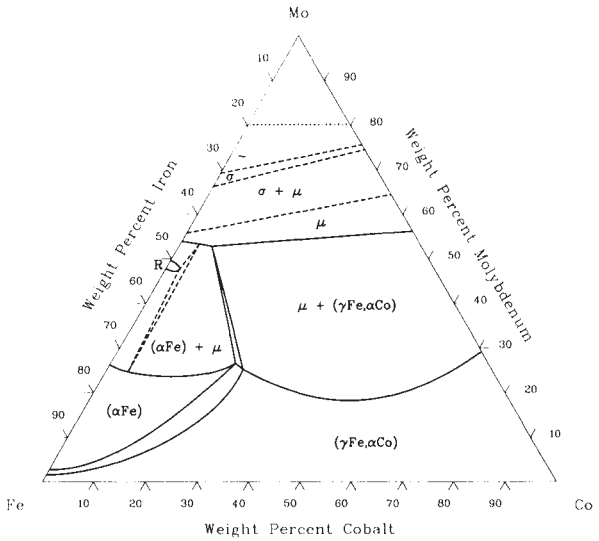


Fig. 14 Co-Fe-Mo isothermal section at 1300 °C (2370 °F)

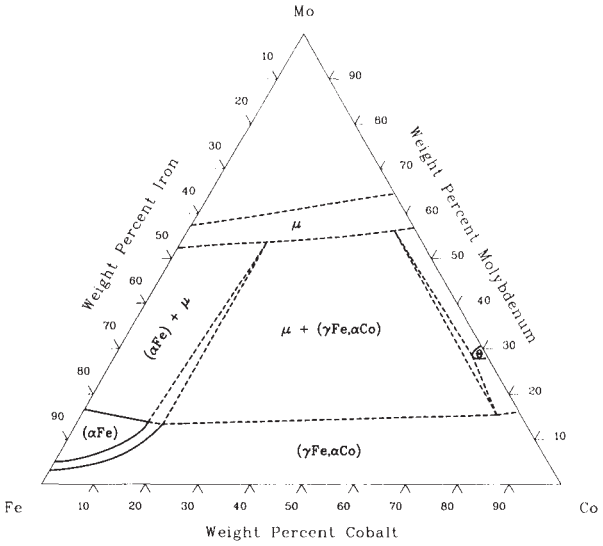


Fig. 15 Co-Fe-Mo isothermal section at 1093 °C (2000 °F)

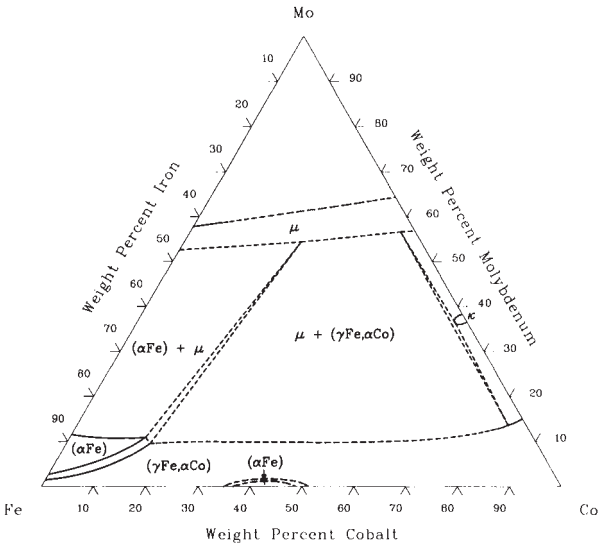


Fig. 16 Co-Fe-Mo isothermal section at 982 °C (1800 °F)

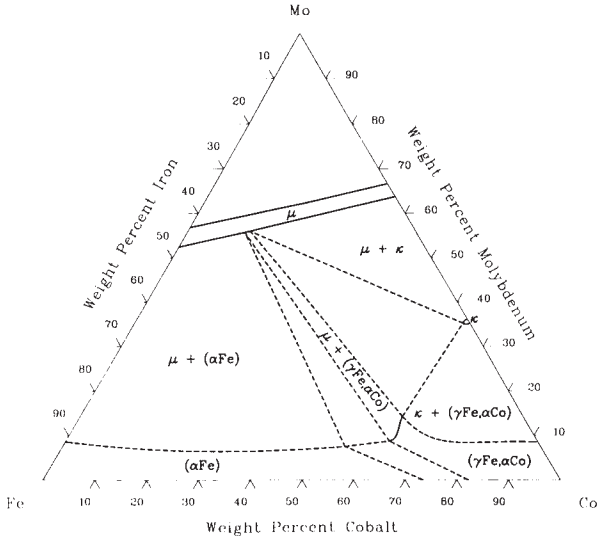


Fig. 17 Co-Fe-Mo isothermal section at 800 °C (1470 °F)

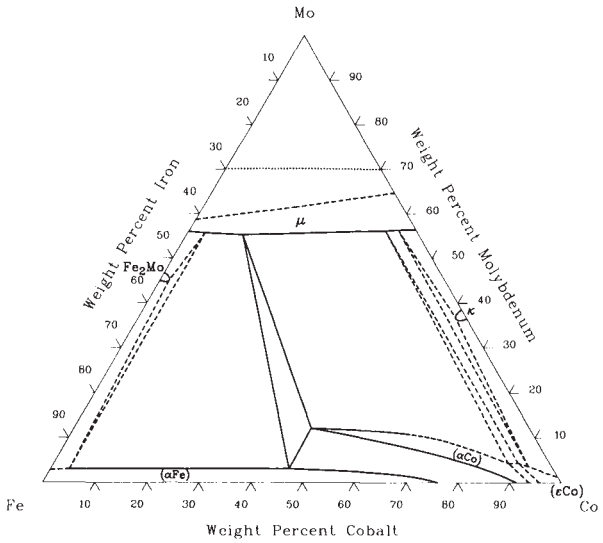


Fig. 18 Co-Fe-Mo isothermal section at 20 °C (70 °F)

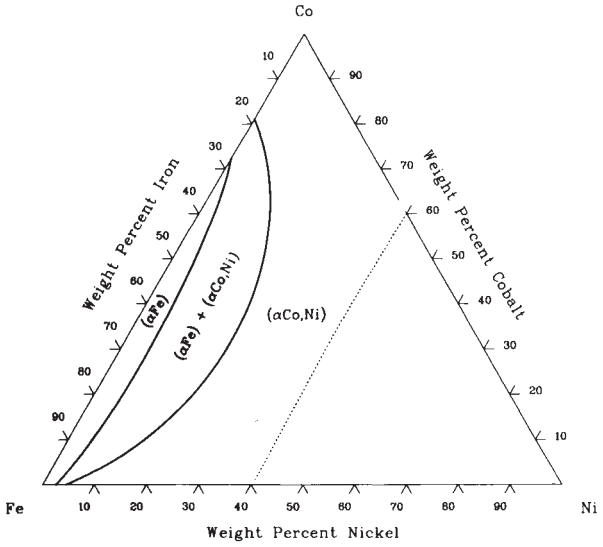


Fig. 19 Co-Fe-Ni isothermal section at 800 °C (1470 °F)

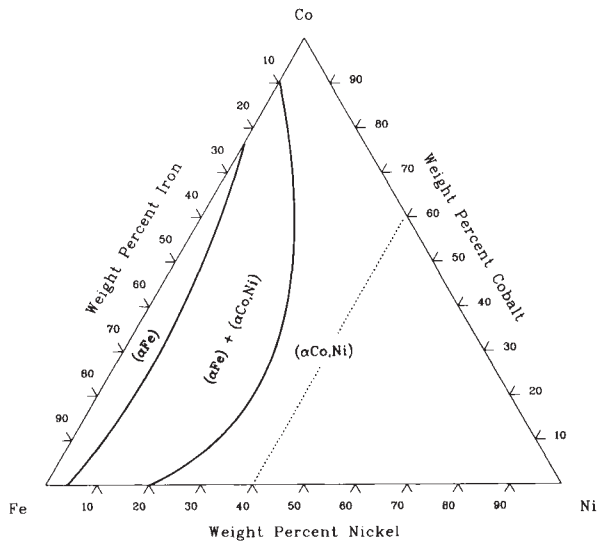


Fig. 20 Co-Fe-Ni isothermal section at 600 °C (1110 °F)

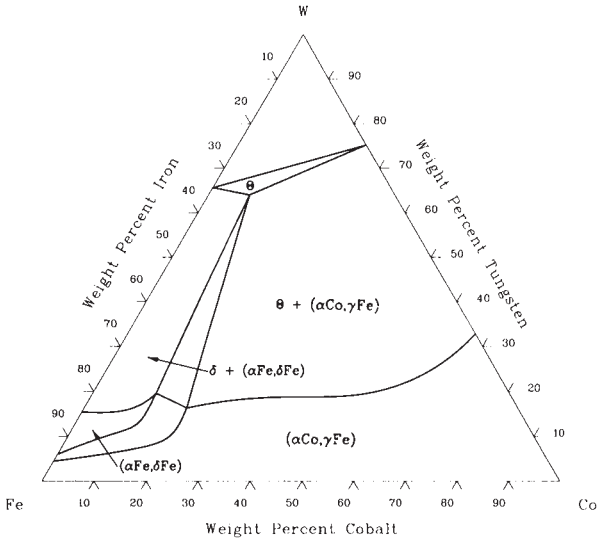


Fig. 21 Co-Fe-W isothermal section at 1200 °C (2190 °F)

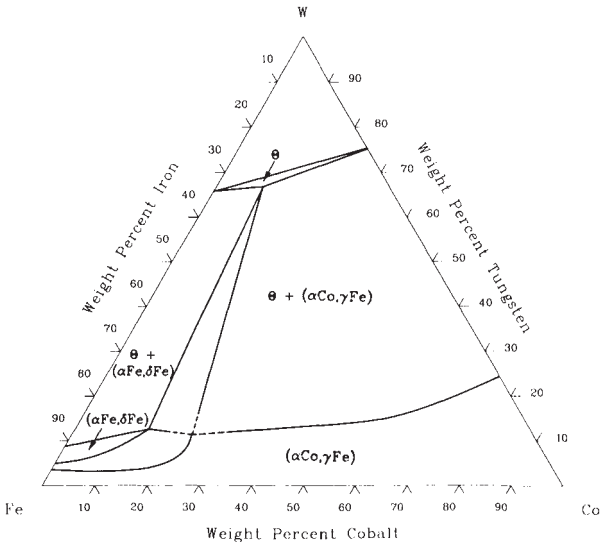


Fig. 22 Co-Fe-W isothermal section at 1000 °C (1830 °F)

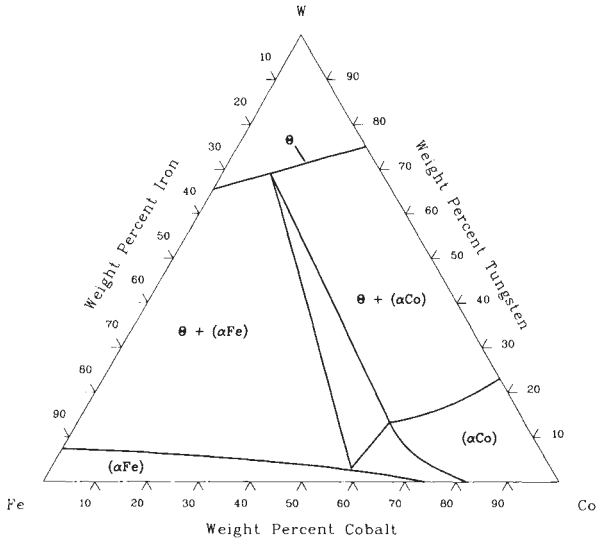


Fig. 23 Co-Fe-W isothermal section at 800 °C (1470 °F)

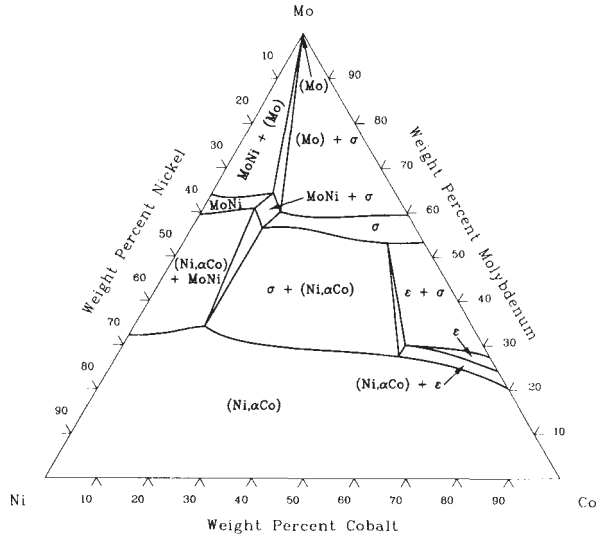


Fig. 24 Co-Mo-Ni isothermal section at 1100 °C (2010 °F)

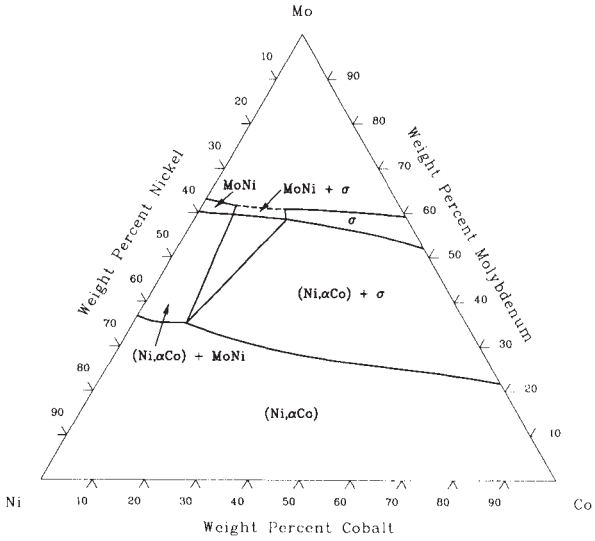


Fig. 25 Co-Mo-Ni isothermal section at 1200 °C (2190 °F)

ASM Specialty Handbook: Nickel, Cobalt, and Their Alloys
J.R. Davis, editor, p 362-370
DOI:10.1361/ncta2000p362

Copyright © 2000 ASM International®
All rights reserved.
www.asminternational.org

Cobalt-Base Alloys

COBALT-BASE ALLOYS can conveniently be categorized as follows:

- High-carbon alloys designed for wear service
- Low-carbon alloys designed for high-temperature service
- Low-carbon alloys designed to combat corrosion or simultaneous corrosion and wear

Table 1 lists typical compositions of present-day cobalt-base alloys in these three application areas. Many of the properties of the alloys arise from the crystallographic nature of cobalt, Co (in particular its response to stress), the solid-solution-strengthening effects of chromium, Cr, tungsten, W, and molybdenum, Mo, the formation of metal carbides, and the corrosion resistance imparted by chromium. Generally, the softer and tougher compositions are used for high-temperature applications, such as gas-turbine vanes and buckets. The harder grades are used for resistance to wear.

Historically, many of the commercial cobalt-base alloys are derived from the Co-Cr-W and Co-Cr-Mo ternaries first investigated by Elwood Haynes at the turn of the century. He discovered the high strength and stainless nature of the binary cobalt-chromium alloy, and he later identified tungsten and molybdenum as powerful strengthening agents within the cobalt-chromium system. When he discovered these alloys, Haynes named them the Stellite alloys after the Latin, *stella*, for star because of their star-like luster. Having discovered their high strength at elevated temperatures, Haynes also promoted the use of Stellite alloys as cutting tool materials.

Following the success of cobalt-base tool materials during World War I, they were then used from about 1922 in weld overlay form to protect surfaces from wear. These early cobalt-base "hardfacing" alloys were used on plowshares, oil well drilling bits, dredging cutters, hot trimming dies, and internal combustion engine valves and valve seats.

Later in the 1930s and early 1940s, cobalt-base alloys for corrosion and high-temperature applications were developed in a series of related events involving the Austenal Laboratories and the Haynes Stellite Division of Union Carbide. Of the corrosion resistant alloys, a Co-Cr-Mo alloy with a moderately low carbon content was developed to satisfy the need for a suitable investment-cast dental material. This biocompatible material, which has the tradename Vitallium, is in use today for surgical implants. In the 1940s this same alloy also underwent investment casting trials for World War II aircraft turbocharger blades, and, with modifications to enhance structural stability, was used successfully for many years in this and other elevated-temperature applications. This early high-temperature material, Stellite alloy 21, is still in use today, but predominantly as an alloy for wear resistance.

Table 1 Compositions of various cobalt-base alloys

Alloy tradename	UNS No.	Nominal composition, wt%									
		Co	Cr	W	Mo	C	Fe	Ni	Si	Mn	Others
Cast, P/M, and weld overlay wear resistant alloys											
Stellite 1	R30001	bal	30	13	0.5	2.5	3	1.5	1.3	0.5	…
Stellite 3 (P/M)	R30103	bal	30.5	12.5	…	2.4	5 (max)	3.5 (max)	2 (max)	2 (max)	1 B (max)
Stellite 4	R30404	bal	30	14	1 (max)	0.57	3 (max)	3 (max)	2 (max)	1 (max)	…
Stellite 6	R30006	bal	29	4.5	1.5 (max)	1.2	3 (max)	3 (max)	1.5 (max)	1 (max)	…
Stellite 6 (P/M)	R30106	bal	28.5	4.5	1.5 (max)	1	5 (max)	3 (max)	2 (max)	2 (max)	1 B (max)
Stellite 12	R30012	bal	30	8.3	…	1.4	3 (min)	1.5	0.7	2.5	…
Stellite 21	R30021	bal	27	…	5.5	0.25	3 (max)	2.75	1 (max)	1 (max)	0.007 B(max)
Stellite 98M2 (P/M)	…	bal	30	18.5	0.8 (max)	2	5 (max)	3.5	1 (max)	1 (max)	4.2 V, 1 B (max)
Stellite 703	…	bal	32	…	12	2.4	3 (max)	3 (max)	1.5 (max)	1.5 (max)	…
Stellite 706	…	bal	29	…	5	1.2	3 (max)	3 (max)	1.5 (max)	1.5 (max)	…
Stellite 712	…	bal	29	…	8.5	2	3 (max)	3 (max)	1.5 (max)	1.5 (max)	…
Stellite 720	…	bal	33	…	18	2.5	3 (max)	3 (max)	1.5 (max)	1.5 (max)	0.3 B
Stellite F	R30002	bal	25	12.3	1 (max)	1.75	3 (max)	22	2 (max)	1 (max)	…
Stellite Star J (P/M)	R30102	bal	32.5	17.5	…	2.5	3 (max)	2.5 (max)	2 (max)	2 (max)	1 B (max)
Stellite Star J	R31001	bal	32.5	17.5	…	2.5	3 (max)	2.5 (max)	2 (max)	2 (max)	…
Tantung G	…	bal	29.5	16.5	…	3	3.5	7 (max)	…	2 (max)	4.5 Ta/Nb
Tantung 144	…	bal	27.5	18.5	…	3	3.5	7 (max)	…	2 (max)	5.5 Ta/Nb
Laves-phase wear resistant alloys											
Tribaloy T-400	R30400	bal	9	…	29	…	…	…	2.5	…	…
Tribaloy T-800	…	bal	18	…	29	…	…	…	3.5	…	…
Wrought wear resistant alloys											
Stellite 6B	R30016	bal	30	4	1.5 max	1	3 (max)	2.5	0.7	1.4	…
Stellite 6K	…	bal	30	4.5	1.5 max	1.6	3 (max)	3 (max)	2 (max)	2 (max)	…
Wrought heat resistant alloys (see Table 4 for cast alloy compositions)											
Haynes 25 (L605)	R30605	bal	20	15	…	0.1	3 (max)	10	0.4 (max)	1.5	…
Haynes 188	R30188	bal	22	14	…	0.1	3 (max)	22	0.35	1.25	0.03 La
Inconel 783	R30783	bal	3	…	…	0.03 (max)	25.5	28	0.5 (max)	0.5 (max)	5.5 Al, 3 Nb, 3.4 Ti (max)
UMCo-50	…	bal	28	…	…	0.02 (max)	21	…	0.75	0.75	…
S-816	R30816	40 (min)	20	4	4	0.37	5 (max)	20	1 (max)	1.5	4 Nb
Corrosion resistant alloys											
Ultimet (1233)	R31233	bal	26	2	5	0.06	3	9	0.3	0.8	0.08 N
MP159	R30159	bal	19	…	7	…	9	25.5	…	…	3 Ti, 0.6 Nb, 0.2 Al
MP35N	R30035	35	20	…	10	…	…	35	…	…	…
Duratherm 600	R30600	41.5	12	3.9	4	0.05 (max)	8.7	bal	0.4	0.75	2 Ti, 0.7 Al, 0.05 Be
Elgiloy	R30003	40	20	…	7	0.15 (max)	bal	15.5	…	2	1 Be (max)
Havar	R30004	42.5	20	2.8	2.4	0.2	bal	13	…	1.6	0.06 Be (max)

P/M, powder metallurgy; bal, balance

Cobalt-Base Wear Resistant Alloys

The cobalt-base wear alloys of today are little changed from the early alloys of Elwood Haynes. The most important differences relate to the control of carbon and silicon (which were impurities in the early alloys). Indeed, the main differences in the current Stellite alloy grades are carbon and tungsten contents (hence the amount and type of carbide formation in the microstructure during solidification).

Physical Metallurgy

Carbides. As can be deduced from Table 1, the chief difference among the individual Stellite wear resistant alloys is carbon content and, thus, carbide volume fraction in the material. For example, at a carbon level of 2.4 wt% (Stellite 3), the carbides constitute about 30 wt% of the material. These are of the M_7C_3 (chromium-rich primary) and M_6C (tungsten-rich eutectic) types, where M represents the metal component (e.g., M_7C_3 corresponds to Cr_7C_3). At 1 wt% carbon (Stellite 6B), the carbides constitute approximately 13 wt% of the material, these being predominantly chromium-rich eutectic carbides of the M_7C_3 type.

The size and shape of the carbide particles within the Stellite alloys are strongly influenced by cooling rate and subtle chemistry changes. This is illustrated in Fig. 1 and 2, which show typical overlay (hardfacing) microstructures as applied by different welding processes. Such changes markedly affect abrasion resistance because there is a distinct relation-

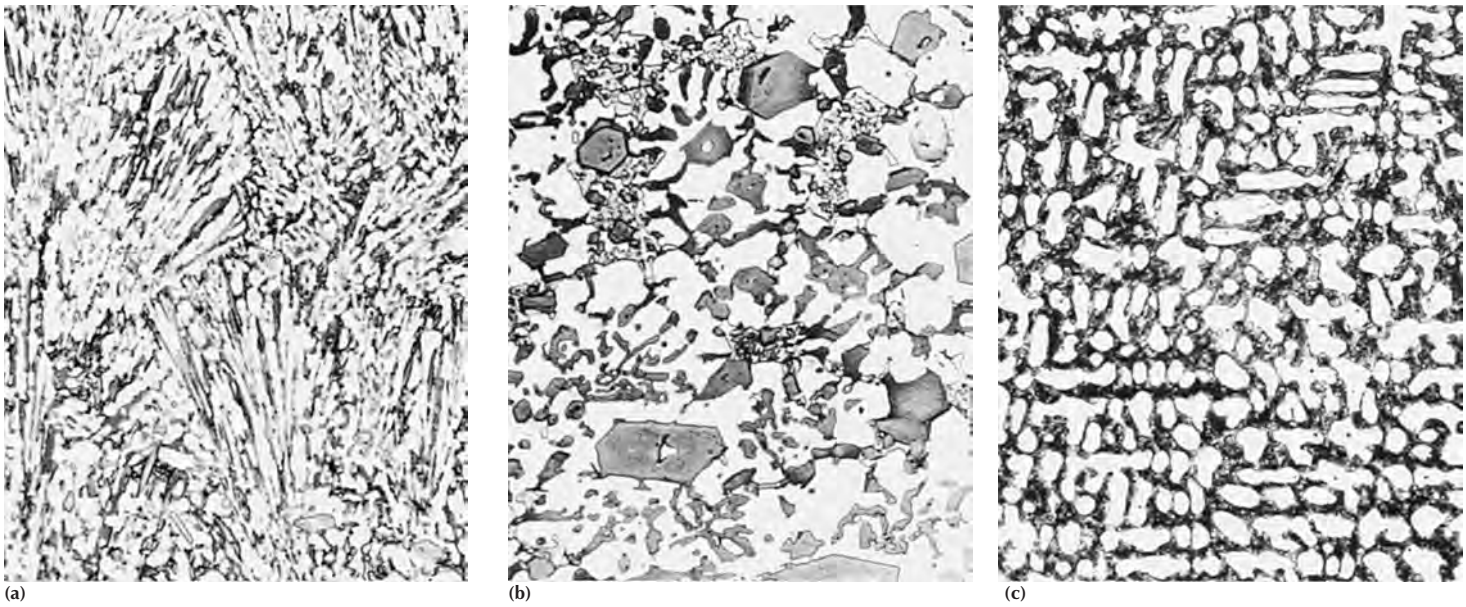


Fig. 1 Typical overlay microstructures of Stellite 1 alloy applied by different weld processes. (a) Three-layer gas tungsten arc. (b) Three-layer oxyacetylene. (c) Three-layer shielded metal arc. See also Fig. 2. All 500×

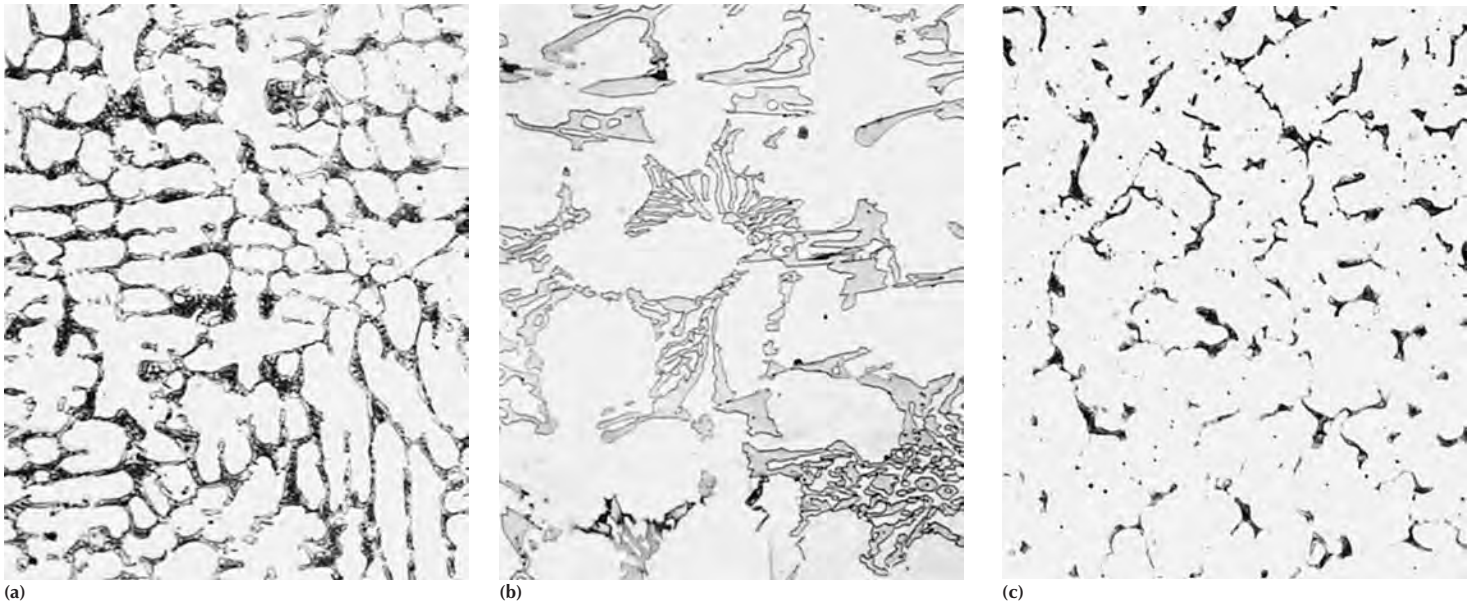


Fig. 2 Typical overlay microstructures of Stellite 6 alloy applied by different weld processes. (a) Three-layer gas tungsten arc. (b) Three-layer oxyacetylene. (c) Three-layer shielded metal arc. See also Fig. 1. All 500×

ship among the size of abrading species, the size of the structural hard particles, and the rate of abrasive wear.

Chromium has a dual function in the Stellite alloys. It is both the predominant carbide former (i.e., most of the carbides are chromium rich) and the most important alloying element in the matrix, where it provides added strength (as a solute) and resistance to corrosion and oxidation. The most common carbide in the Stellite alloys is a chromium-rich M_7C_3 type, although chromium-rich $M_{23}C_6$ carbides are abundant in low-carbon alloys such as Stellite alloy 21.

Tungsten and molybdenum in the Stellite alloys serve to provide additional strength to the matrix. They do so by virtue of their large atomic size (i.e., they impede dislocation flow when present as solute atoms). When present in large quantities (e.g., in Stellite alloy 1), they participate in the formation of carbides during alloy solidification and promote the precipitation of M_6C. They also improve general corrosion resistance of the alloys. Although these alloying elements are critical to the performance of the Stellite alloys in service, the main reason for the commercial success of the Stellite alloys is the cobalt.

Cobalt imparts to its alloys an unstable, face-centered cubic (fcc) crystal structure with a very low stacking fault energy. The instability arises from the fact that elemental cobalt, if cooled extremely slowly, transforms from an fcc to a hexagonal close-packed (hcp) crystal structure at 417 °C (782.6 °F). In most cobalt alloys, the transformation temperature is somewhat higher.

Because of the sluggish nature of the transformation, the fcc structure in cobalt and its alloys is usually retained to room temperature, and hcp formation is triggered only by mechanical stress or time at elevated temperature. The unstable fcc structure and its associated low stacking fault energy are believed to result in:

- High yield strengths
- High work-hardening rates (due to the interaction between stacking faults)
- Limited fatigue damage under cyclic stresses (due to the lack of cell walls within plastically deformed material)
- The ability to absorb stresses (through transformation of the structure to hcp)

The first three of these attributes are believed to be important in preventing metallic damage during sliding wear. The last two are believed to be responsible for the outstanding resistance to cavitation and erosion-corrosion of the cobalt alloys.

Alloy Compositions and Product Forms

The chemical compositions of various cobalt-base wear resistant alloys are given in Table 1. The type of wear encountered (e.g., abrasive wear, sliding wear, or erosive wear) in a particular application is an important factor that influences the selection of these alloys. More detailed information on the selection of cobalt-base alloys for wear resistant applications can be found in the article "Wear Behavior of Cobalt Alloys" in this Handbook.

The Stellite alloys listed in Table 1 are generally used in the form of castings or weld overlays (hardfacing alloys). Some alloys (e.g., Stellite alloys 1, 6, and 12) are derivatives of the original Co-Cr-W alloys developed by Haynes. These alloys are characterized by their carbon and tungsten contents, with Stellite alloy 1 being the hardest, most abrasion resistant, and least ductile (Table 2). The carbides in the Co-Cr-W-base Stellites are generally of the chromium-rich M_7C_3 type, although in high-tungsten alloys (such as Stellite alloy 1) tungsten-rich M_6C carbides usually are present also.

Stellite alloy 21 differs from the three alloys mentioned above in that it employs molybdenum, rather than tungsten, to strengthen the solid solution. Stellite alloy 21 also contains considerably less carbon. By virtue of the high molybdenum content, and the fact that most of the chromium is in solution (rather than in Cr_7C_3 carbides), the alloy is more resistant to corrosion than Stellite alloys 1, 6, and 12.

The most recently developed alloys in the Stellite family are those in the 700 series (alloys 703, 706, 712, and 720 in Table 1). As with Stellite alloy 21, the tungsten in these alloys has been replaced by molybdenum (molybdenum contents range from 5 to 18%). The 700 series alloys possess excellent corrosion resistance in reducing environments. Molybdenum also partitions in the carbides formed in these alloys to enhance the wear resistance.

Powder metallurgy (P/M) versions of several Stellite alloys (typically containing low levels of boron—1.0% max as listed in Table 1—to enhance sintering) are available for applications where the P/M process is cost effective (e.g., high-volume production of small simple shapes). Powder metallurgy components have outstanding wear resistance and mechanical properties and provide exceptional reliability needed for anything from aerospace bearings to industrial saw teeth. The microstructure of P/M Stellite alloys contains complex combinations of M_7C_3, M_6C, and $M_{23}C_6$ carbides embedded in a Co-Cr-W matrix. Figure 3 shows a range of structures that can be tailored to give a desired combination of wear, corrosion, and mechanical properties.

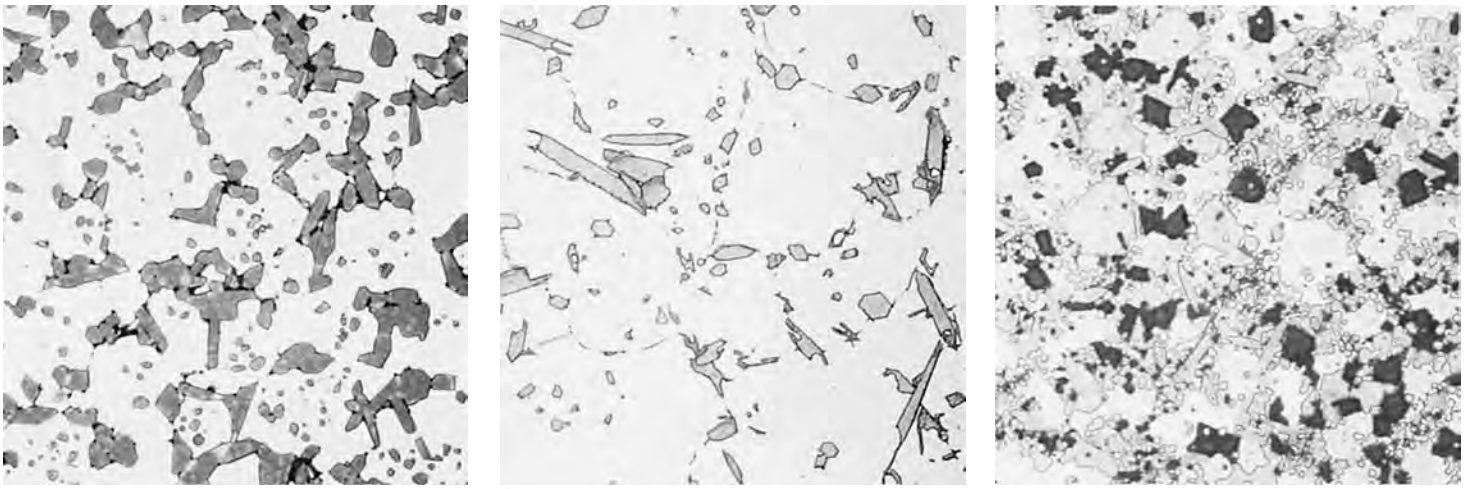
Cast cobalt-base cutting tools have been widely used for machining steel, gray iron, malleable iron, cast steel, brass, bronze, aluminum, and most other machinable materials. These alloys, which include Tantung G, Tantung 144, and Stellite 100 described in Table 1, were developed to bridge the gap between high-speed tool steels and cemented carbides.

Although comparable in room-temperature hardness to high-speed steel tools, cast cobalt alloy tools retain their hardness to a much higher temperature and can be used at higher (~20%) cutting speeds than high-speed steel tools. Unlike the high-speed steels that can be heat treated to obtain the desired hardness, cast cobalt alloys are hard in the as-cast condition and cannot be softened or hardened by heat treatment. Figure 4 shows the typical microstructure of permanent graphite mold-cast Tantung G. Additional information on cast cobalt alloys for machining applications can be found in the *ASM Specialty Handbook: Tool Materials* (see pages 32–35).

Table 2 Properties of selected cobalt-base hardfacing alloys

Property	Stellite 21	Stellite 6	Stellite 12	Stellite 1	Tribaloy T-800
Density, g/cm^3 (lb/in.^{3})	8.3 (0.30)	8.3 (0.30)	8.6 (0.31)	8.6 (0.31)	8.6 (0.31)
Ultimate compressive strength, MPa (ksi)	1295 (188)	1515 (220)	1765 (256)	1930 (280)	1780 (258)
Ultimate tensile strength, MPa (ksi)	710 (103)	834 (121)	827 (120)	620 (90)	690 (100)
Elongation, %	8	1.2	1	1	<1
Coefficient of thermal expansion, °C^{-1} (°F^{-1})	14.8×10^{-6} (8.2×10^{-6})	15.7×10^{-6} (8.7×10^{-6})	14×10^{-6} (7.8×10^{-6})	13.1×10^{-6} (7.3×10^{-6})	12.3×10^{-6} (6.8×10^{-6})
Hot hardness, HV, at:					
445 °C (800 °F)	150	300	345	510	659
540 °C (1000 °F)	145	275	325	465	622
650 °C (1200 °F)	135	260	285	390	490
760 °C (1400 °F)	115	185	245	230	308
Unlubricated sliding wear (a), mm^3 (in.$^3 \times 10^{-3}$) at:					
670 N (150 lbf)	5.2 (0.32)	2.6 (0.16)	2.4 (0.15)	0.6 (0.04)	1.7 (0.11)
1330 N (300 lbf)	14.5 (0.90)	18.8 (1.17)	18.4 (1.14)	0.8 (0.05)	2.1 (0.13)
Abrasive wear(b), mm^3 (in.$^3 \times 10^{-3}$)					
OAW	…	29 (1.80)	12 (0.75)	8 (0.50)	…
GTAW	86 (5.33)	64 (3.97)	57 (3.53)	52 (3.22)	24 (1.49)
Unnotched Charpy impact strength, J (ft · lbf)	37 (27)	23 (17)	5 (4)	5 (4)	1.4 (1)
Corrosion resistance(c):					
65% nitric acid at 65 °C (150 °F)	U	U	U	U	S
5% sulfuric acid at 65 °C (150 °F)	E	E	E	E	…
50% phosphoric acid at 400 °C (750 °F)	E	E	E	E	E

(a) Wear measured from tests conducted on Dow-Corning LFW-1 against 4620 steel ring at 80 rev/min for 2000 rev varying the applied load. (b) Wear measured from dry sand rubber wheel abrasion tests. Tested for 2000 rev at a load of 135 N (30 lbf) using a 230 mm (9 in.) diam rubber wheel and American Foundrymen's Society test sand. OAW, oxyacetylene welding; GTAW, gas-tungsten arc welding. (c) E, less than 0.05 mm/yr (2 mils/year); S, 0.5 to less than 1.25 mm/yr (over 20 to less than 50 mils/year); U, more than 1.25 mm/year (50 mils/year)



(a) (b) (c)

Fig. 3 Microstructure of Stellite powder metallurgy materials. Chromium and tungsten alloy carbides are supported by a cobalt-base matrix. Carbide level varies from 5 to 60 vol%. (a) Stellite 12. (b) Stellite 31. (c) Stellite 98M2. All 500×

Laves-phase alloys include the Tribaloy family of wear resistant materials. Two cobalt-base Laves-type alloy compositions (T-400 and T-800) are listed in Table 1. In these materials, molybdenum and silicon are added at levels in excess of their solubility limit with the objective of inducing the precipitation of the hard (and corrosion resistant) Laves phase (CoMoSi or Co_3Mo_2Si). Carbon is held as low as possible in these alloys to discourage carbide formation.

Because the Laves intermetallic phase is so abundant in these alloys (35–70 vol%), its presence governs all the material properties. Accordingly, the effects of the matrix composition in these alloys are less pronounced than in the case for the cobalt-base carbide-type alloys (Stellite), for example. The Laves phase is specifically responsible for outstanding abrasion resistance, but it severely limits the material ductility and the impact strength. In fact, it is difficult to attain crack-free overlays on all but the smallest components given adequate preheat. For this reason, these alloys have been more successful as thermal (plasma) spray coatings.

Properties of alloy T-800 are summarized in Table 2. A typical microstructure of a T-800 weld overlay is shown in Fig. 5.

Wrought Alloys. The high-carbon alloys, such as Stellite alloys 6B and 6K in Table 1, are essentially wrought versions of the hardfacing (Stellite) alloys described above. Wrought processing improves chemical homogeneity (important in a corrosion sense), markedly increases ductility, and modifies substantially the geometry of the carbide precipitates within the alloys (blocky carbides within the microstructure enhance abrasion resistance). In terms of composition, the alloys are essentially Co-Cr-W-C quaternaries with chromium providing strength and corrosion resistance to the solid solution in addition to functioning as the chief carbide former (during alloy solidification). Tungsten provides additional solid-solution strength. Alloy 6B (Fig. 6a) contains approximately 12.5 wt% carbides of the M_7C_3 and $M_{23}C_6$ types in the ratio 9 to 1. Alloy 6K (Fig. 6b) exhibits an even greater carbide volume fraction, again with the M_7C_3 as the predominant type. Additional information pertaining to alloys 6B and 6K can be found in the articles "Properties of Cobalt Alloys" and "Wear Behavior of Cobalt Alloys" which immediately follow in this Handbook.

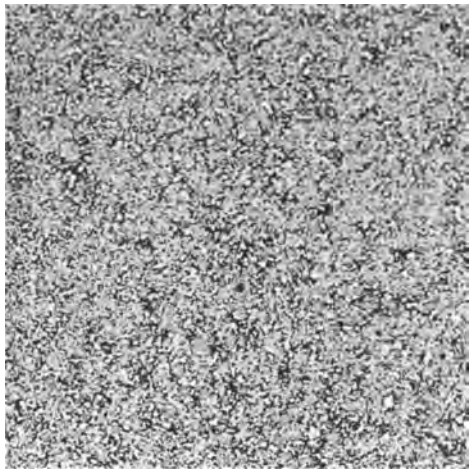


Fig. 4 Microstructure of permanent graphite mold-cast Tantung G alloy. The typical as-cast hardness for this material and similar alloys ranges from 60 to 65 HRC. Etched with Murakami's reagent. 400×

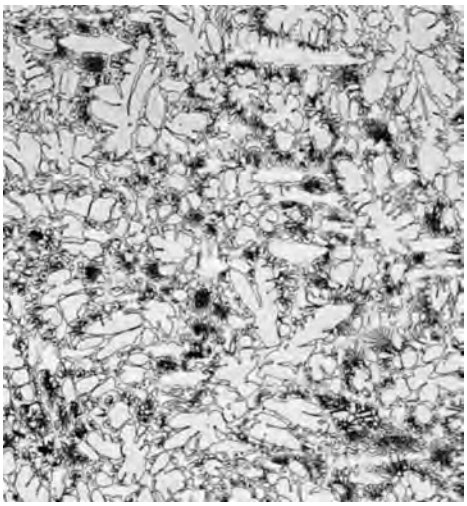


Fig. 5 Microstructure of Laves-phase alloy T-800 (two-layer plasma transferred arc deposit). 200×

Cobalt-Base Heat Resistant Alloys

For many years, the predominant user of heat resistant alloys was the gas turbine industry. In the case of aircraft gas turbine power plants, the chief material requirements were elevated-temperature strength, resistance to thermal fatigue, and oxidation resistance. For land-base gas turbines, which typically burn lower grade fuels and operate at lower temperatures, sulfidation resistance was the major concern. Today, the use of heat resistant alloys is more diversified, as more efficiency is sought from the burning of fossil fuels and waste, and as new chemical processing techniques are developed.

Although cobalt-base alloys are not as widely used as nickel and nickel-iron alloys in high-temperature applications, cobalt-base heat resistant alloys nevertheless play an important role, by virtue of their excellent resistance to sulfidation, hot corrosion, and their strength at temperatures exceeding those at which the gamma-prime and gamma-double-prime precipitates in the nickel and nickel-iron alloys dissolve.

As previously noted, Stellite 21 was an early type of cobalt-base heat resistant alloy that is used now primarily for wear resistance. Since the early use of Stellite 21, cobalt-base heat resistant materials have gone through various stages of development to increase their high-temperature capability. The use of tungsten (or

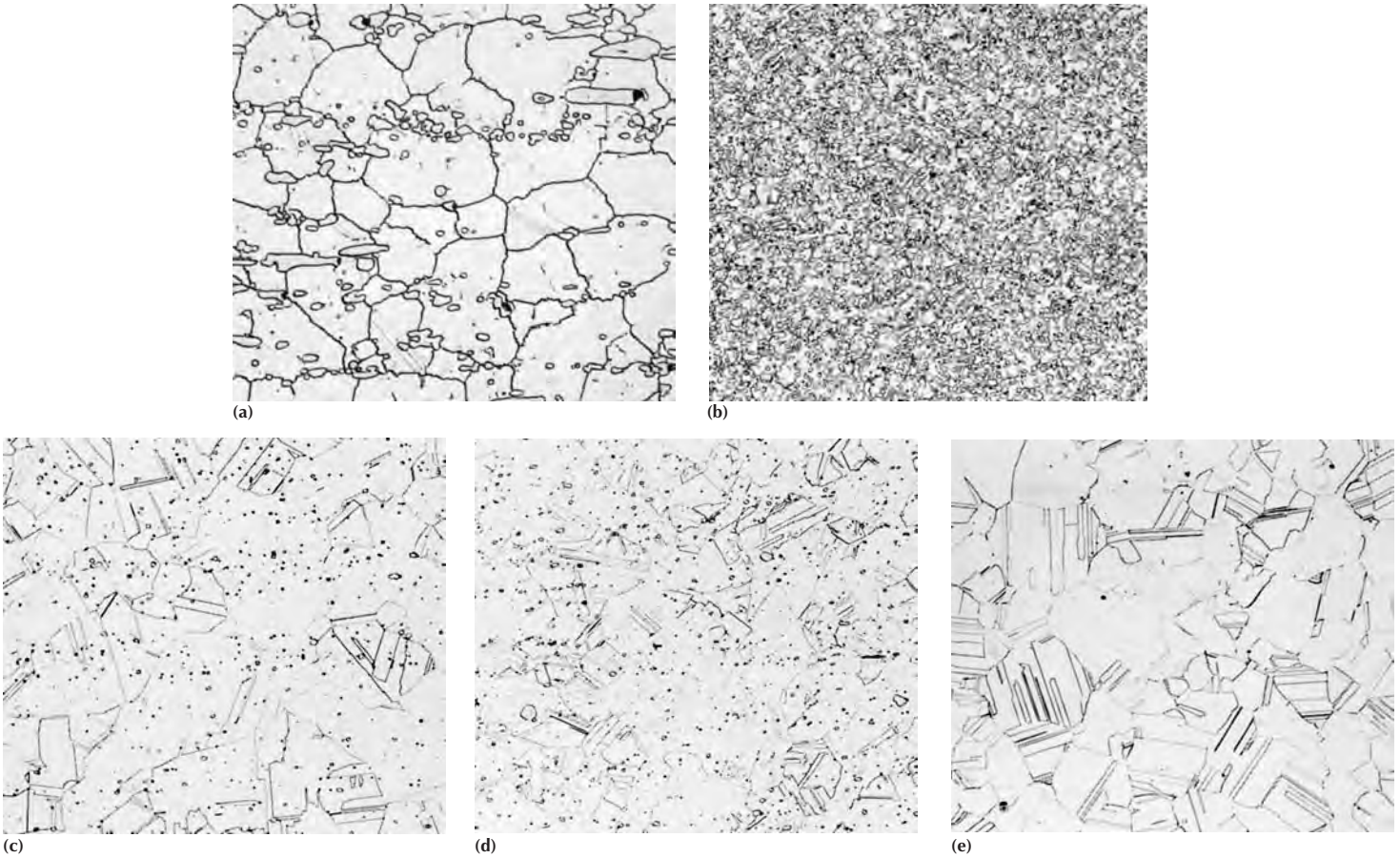


Fig. 6 Microstructure of wrought cobalt-base alloys etched with hydrochloric acid/oxalic acid solution. (a) Alloy 6B. (b) Alloy 6K. (c) Alloy 25. (d) Alloy 188. (e) Ultimet alloy. All 200×

tantalum) rather than molybdenum, moderate nickel and chromium contents, lower carbon contents, and rare-earth additions typify cobalt-base high-temperature alloys of today. Table 3 summarizes some of the effects various alloying elements can produce in cobalt-base heat resistant alloys.

Alloy Compositions and Product Forms

Wrought Heat Resistant Alloys. Table 1 lists typical wrought compositions developed for high-temperature use. Alloys 25 (Fig. 6c) and 188 (Fig. 6d) are considerably more ductile, oxidation resistant, and microstructurally stable than the wear resistant wrought cobalt alloys. Both alloys contain approximately 0.1 wt% C (about one-tenth of that in alloy 6B), which is sufficient to provide carbide strengthening, yet low enough to maintain ductility. Carbide precipitation, which is predominately of the M_6C type, is important to the high-temperature properties of these materials, partially because it restricts grain growth during heat treatment and service. Structural stability is enhanced in these alloys by nickel, which decreases the fcc/hcp transformation temperature in cobalt-base alloys.

Alloys 25 (also known as L605) and 188, which are the most frequently employed cobalt-base heat resistant alloys, are available in the form of sheets, plates, bars, pipes, and tubes (together with a range of matching welding products for joining purposes). Haynes 25 has been widely used for hot sections of gas turbines, components of nuclear reactors, devices for surgical implants, and, in the cold-worked condition, for fasteners and wear pads. Haynes 188 is an alloy that was specially designed for sheet-metal components, such as combustors and transition ducts, in gas turbines. The basic composition, provided that lanthanum, silicon, aluminum, and manganese contents are judiciously controlled, provides excellent qualities, such as oxidation resistance at temperatures up to 1100 °C (2000 °F), hot corrosion resistance, creep resistance, room-temperature formability, and ductility after long-term aging at service temperatures. Additional information on alloys 25 and 188 can be found in the articles "Properties of Cobalt Alloys" and "Corrosion Behavior of Cobalt Alloys" in this Handbook.

Inconel 783 has a low coefficient of thermal expansion (approximately 20% less than the nickel-iron alloy Inconel 718), good oxidation resistance up to and beyond 705 °C (1300 °F), and better impact resistance and metallurgical stability than the low-expansion Fe-Ni-Co alloy Incoloy 909 up to 715 °C (1300 °F). It also has a lower density (7.78 g/cm^3, or 0.281 lb/in.^{3}) than competing alloys 718 and 909, which contributes to an important improvement in

Table 3 Effects of alloying elements in cobalt-base heat resistant alloys

Element	Effect(a)
Chromium	Oxidation and sulfidation resistance, carbide former (M_7C_3 and $M_{23}C_6$)
Molybdenum, tungsten	Solid-solution strengtheners, carbide former (M_6C), intermetallic compound (Co_3M)
Tantalum, niobium	Solid-solution strengtheners, carbide former (MC) and (M_6C), intermetallic compound (Co_3M)
Aluminum	Oxidation resistance, intermetallic compound (CoAl)
Titanium	Carbide former (MC), intermetallic compound (Co_3Ti and with sufficient nickel Ni_3Ti)
Nickel	Stabilize fcc form of matrix, intermetallic compound (Ni_3Ti) facilitates working
Boron, zirconium	Increase stress-rupture strength
Carbon	Formation of carbides (MC, M_7C_3, M_6C, $M_{23}C_6$)
Yttrium, lanthanum	Oxidation resistance

(a) Not all these effects necessarily occur in a given alloy.

Table 4 Nominal compositions of cast cobalt-base heat resistant alloys

Alloy designation	Nominal composition, %											
	C	Ni	Cr	Co	Mo	Fe	Al	B	Ti	Ta	W	Zr	Other
AiResist 13	0.45	…	21	62	…	…	3.4	…	…	2	11	…	0.1 Y
AiResist 213	0.20	0.5	20	64	…	0.5	3.5	…	…	6.5	4.5	0.1	0.1 Y
AiResist 215	0.35	0.5	19	63	…	0.5	4.3	…	…	7.5	4.5	0.1	0.1 Y
FSX-414	0.25	10	29	52.5	…	1	…	0.010	…	…	7.5	…	…
Haynes 25 (L-605)	0.1	10	20	54	…	1	…	…	…	…	15	…	…
J-1650	0.20	27	19	36	…	…	…	0.02	3.8	2	12	…	…
MAR-M 302	0.85	…	21.5	58	…	0.5	…	0.005	…	9	10	0.2	…
MAR-M 322	1.0	…	21.5	60.5	…	0.5	…	…	0.75	4.5	9	2	…
MAR-M 509	0.6	10	23.5	54.5	…	…	…	…	0.2	3.5	7	0.5	…
NASA Co-W-Re	0.40	…	3	67.5	…	…	…	…	1	…	25	1	2 Re
S-816	0.4	20	20	42	…	4	…	…	…	…	4	…	4 Mo, 4 Nb, 1.2 Mn, 0.4 Si
V-36	0.27	20	25	42	…	3	…	…	…	…	2	…	4 Mo, 2 Nb, 1 Mn, 0.4 Si
WI-52	0.45	…	21	63.5	…	2	…	…	…	…	11	…	2 Nb + Ta
Stellite 23	0.40	2	24	65.5	…	1	…	…	…	…	5	…	0.3 Mn, 0.6 Si
Stellite 27	0.40	32	25	35	5.5	1	…	…	…	…	…	…	0.3 Mn, 0.6 Si
Stellite 30	0.45	15	26	50.5	6	1	…	…	…	…	…	…	0.6 Mn, 0.6 Si
Stellite 31 (X-40)	0.50	10	22	57.5	…	1.5	…	…	…	…	7.5	…	0.5 Mn, 0.5 Si

strength-to-weight ratios. Inconel 783 is used for gas turbine casings, rings, and seals.

UMCo-50, which contains approximately 21% iron, is not as strong as Haynes 25 or 188. It is not used extensively in the United States, and especially not in gas turbine applications. In Europe, on the other hand, it is used extensively for furnace parts and fixtures. Additional information on UMCo-50 can be found in the article "Properties of Cobalt Alloys" in this Handbook.

Alloy S-816 originally was used extensively in turbochargers, as well as gas turbine wheels, blades, and vanes, but has been largely replaced by higher-strength, lower-density nickel-base alloys with improved resistance to adverse environments.

Cast heat resistant alloys, such as alloys MAR-509, FSX-414, and the others listed in Table 4, are designed around a cobalt-chromium matrix with chromium contents ranging from approximately 18 to 30%. The high chromium content contributes to oxidation resistance, hot corrosion resistance (Fig. 7), and sulfidation resistance, but also participates in carbide formation (Cr_7C_3 and $M_{23}C_6$) and solid-solution strengthening. Carbon content generally ranges from 0.25 to 1.0%, with nitrogen occasionally substituting for carbon.

These alloys also contain significant levels of both nickel and tungsten. The addition of nickel helps to stabilize the desired fcc matrix, while tungsten provides solid-solution strengthening and promotes carbide formation. Other alloying elements contributing to the solid-solution and/or carbide formation are tantalum, niobium, zirconium, vanadium, and titanium. Yttria is also added to some alloys for improved oxidation resistance.

Investment-cast cobalt alloys are generally used for complex shapes such as first- and second-stage vanes/nozzles in gas turbine engines. Stress-rupture properties of commonly used cobalt-base casting alloys are shown in Fig. 8. Additional information can be found in the article "Properties of Cobalt Alloys" in this Handbook.

Cobalt-Base Corrosion Resistant Alloys

Although the cobalt-base wear resistant alloys possess some resistance to aqueous corrosion, they are limited by grain boundary carbide precipitation, the lack of vital alloying elements in the matrix (after formation of the carbides or Laves precipitates), and, in the case of the cast and hardfacing materials, by chemical segregation in the microstructure.

By virtue of their homogeneous microstructures and lower carbon contents, the wrought cobalt-base high-temperature alloys (which typically contain tungsten rather than molybdenum) are even more resistant to aqueous corrosion, but still fall well short of the Ni-Cr-Mo alloys in corrosion performance.

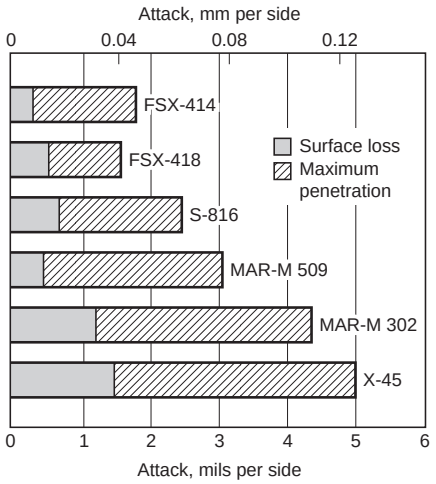


Fig. 7 Relative hot corrosion resistance of cobalt-base alloys obtained from burner rig tests using 3% S residual oil and 325 ppm NaCl in fuel (equivalent to 5 ppm NaCl in air) at 870 °C (1600 °F) for 600 h

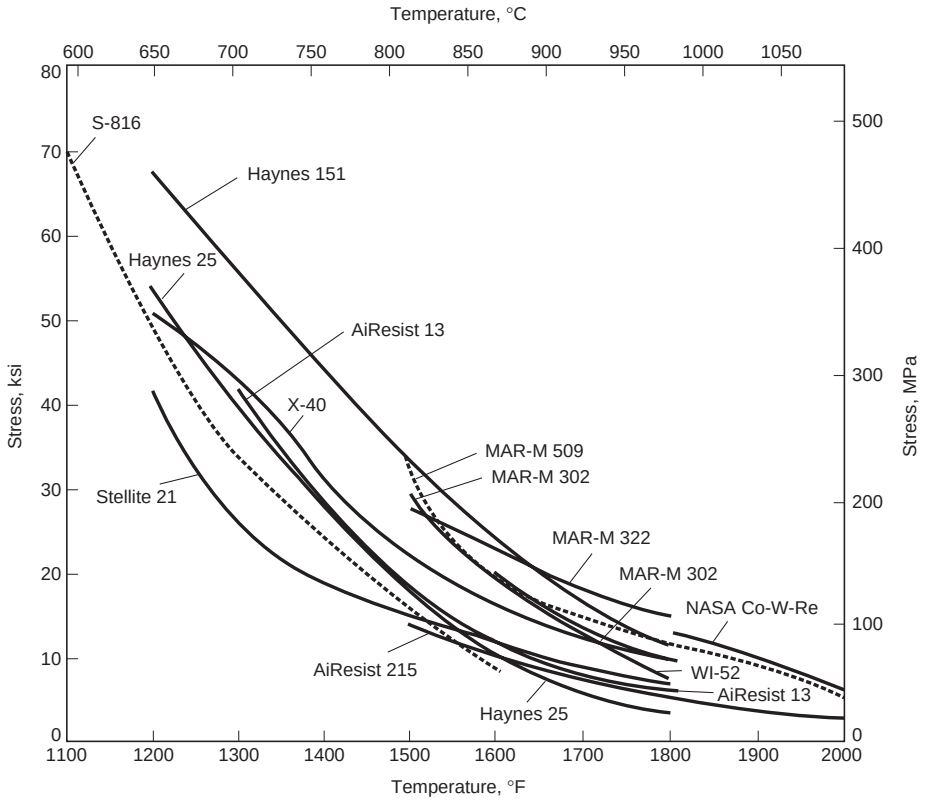


Fig. 8 Stress-rupture curves for 1000 h life of cast cobalt-base superalloys

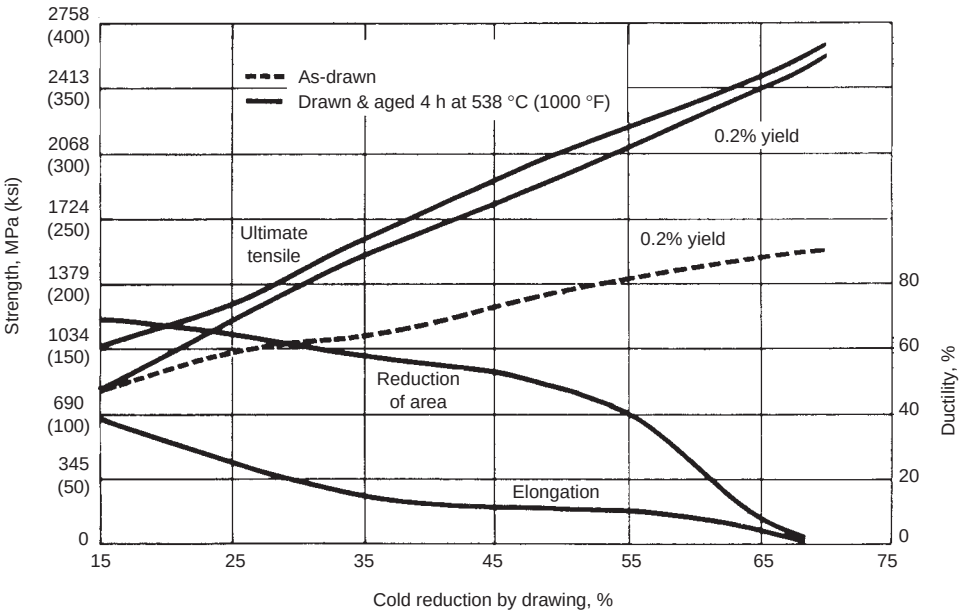


Fig. 9 Tensile properties of cold-drawn and aged MP35N alloy



Fig. 10 Microstructure of cold-worked and aged MP35N. Electrolytic etch: 80 mL $HC_2H_3O_2$ and 20 mL HCl at 6 V for 5–60 s

To satisfy the industrial need for alloys that exhibit outstanding resistance to aqueous corrosion, yet share the attributes of cobalt as an alloy base (resistance to various forms of wear and high strength over a wide range of temperatures), several low-carbon, wrought Co-Ni-Cr-Mo alloys are produced. Molybdenum additions in these alloys (in preference to tungsten) impart a greater degree of resistance to a variety of wet corrosive media. In addition, carbon contents in these alloys are held within the soluble range to improve resistance to heat-affected-zone sensitization during welding.

Alloy Compositions and Product Forms

Ultimet alloy (Fig. 6e) is typical of the low-carbon corrosion resistant alloys in that it exhibits no intragranular or grain boundary carbide precipitation, although a sparse dispersion of nitrides is evident in the structure. Available in a variety of wrought forms, castings, and weld overlays, this alloy was designed to solve some of the chronic problems related to premature materials degradation due to the combined effects of corrosion and wear. Ultimet is resistant to localized corrosion (pitting and crevice corrosion), offers resistance to many aggressive environments, and exhibits excellent wear properties, particularly with regard to slurry erosion, cavitation erosion, and galling. Comparative wear and corrosion data on Ultimet and other high-performance alloys can be found in the articles "Wear Behavior of Cobalt Alloys" and "Corrosion Behavior of Cobalt Alloys" in this Handbook. Properties (including resistance to specific corrosive media), specifications, and applications related to Ultimet alloy are described in the article "Properties of Cobalt Alloys."

Multiphase (MP) Alloys. Alloys MP35N and MP159 are high-performance aerospace fastener alloys that combine ultrahigh strength, high ductility, and corrosion resistance, including resistance to stress-corrosion cracking in the high-strength condition. The prime strengthening mechanism in these alloys is the solid-state phase transformation of part of the matrix from an fcc crystal structure to an hcp structure by cold working. This transformation occurs because of the high cobalt content in the

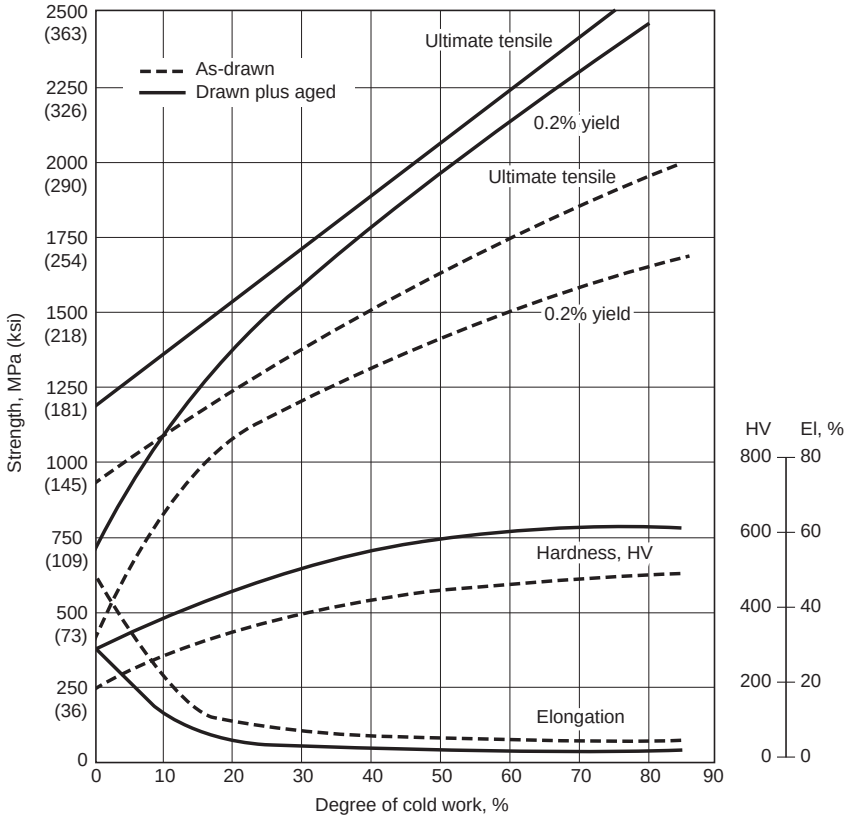


Fig. 11 Tensile properties of cold-drawn and aged Duratherm 600 alloy

Table 5 Compositions of cobalt-base surgical implant alloys

ASTM specification	Composition, wt%								
	Co	Cr	Ni	Mo	Fe	C	Mn	Si	Other
F75	bal	27.0–30.0	1.0	5.0–7.0	0.75	0.35	1.0	1.0	…
F90	bal	19.0–21.0	9.0–11.0	…	3 (max)	0.05–0.15	1.0–2.0	0.4	14.0–16.0 W
F562	bal	19.0–21.0	33.0–37.0	9.0–10.5	1 (max)	0.025 (max)	0.15 (max)	0.15 (max)	1.0 Ti (max)

Table 6 Mechanical properties of cobalt-base surgical implant alloys

ASTM specification	Alloy system	Condition	Yield strength		Tensile strength		Elongation, %	Elastic modulus	
			MPa	ksi	MPa	ksi		GPa	10^6 psi
F75	Co-Cr-Mo	Cast	450	65	655	95	8	248	36
F799	Co-Cr-Mo	Thermomechanically processed	827	120	1172	170	12	…	…
F90	Co-Cr-W-Ni	Wrought	379	55	896	130	…	242	35
F562	Co-Ni-Cr-Mo	Annealed	241–448	35–65	793–1000	115–145	50	228	33
		Cold-worked and aged	1586	230	1793	260	8	…	…

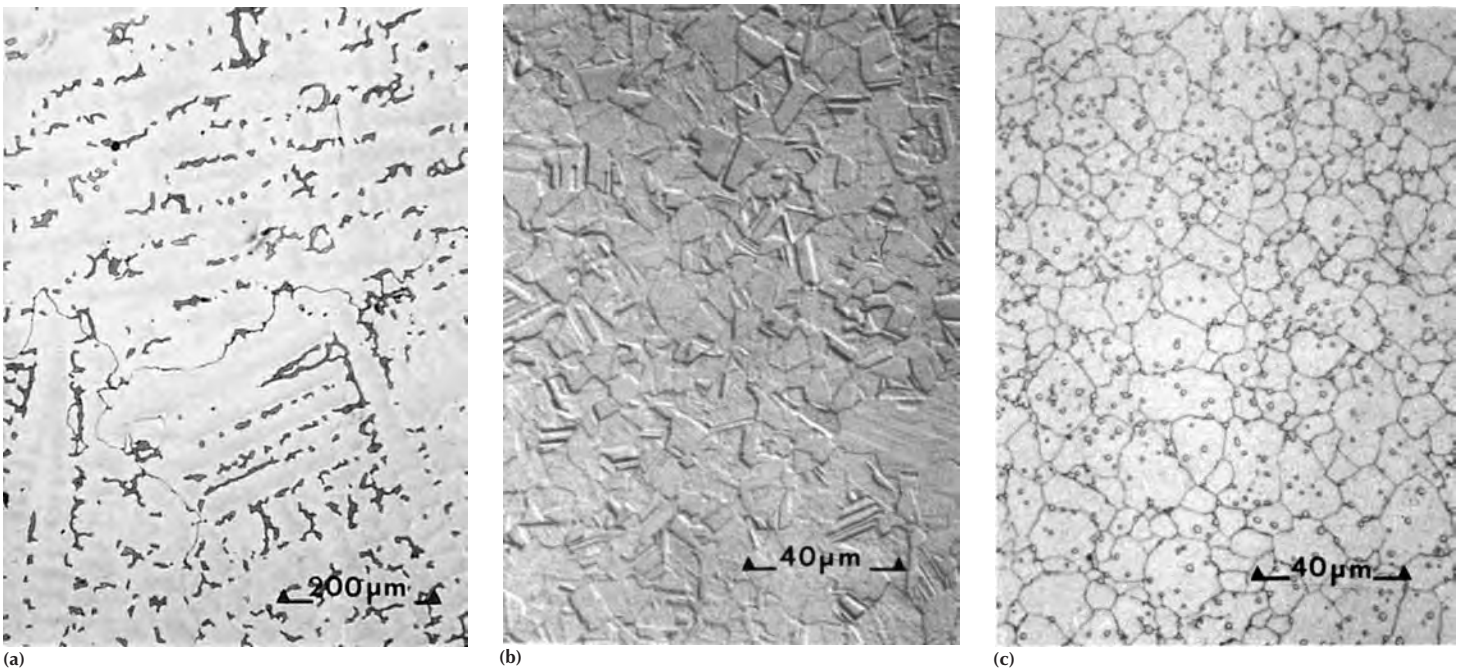
alloys, and has been termed the "multiphase reaction." The presence of two distinct crystal structures poses a barrier to the motion of dislocations and leads to pronounced strengthening. Subsequent age hardening acts to stabilize these two phases through the process of solute partitioning, which contributes to further strengthening. Both MP35N and MP159 are produced by vacuum induction melting followed by vacuum arc remelting (VIM/VAR) to provide optimum control of chemistry and preferred ingot solidification. Table 1 lists the compositions of both alloys, which are available in a variety of wrought product forms.

MP35N is work strengthened and aged for 4 h in the 425 to 650 °C (800–1200 °F) range to obtain strength levels of 1795 to 2070 MPa (260–300 ksi). Figure 9 shows the effects of cold work and cold work plus aging on the tensile properties of the alloy. The microstructure of MP35N in the hardened (by cold working) and aged condition is shown in Fig. 10. The maximum operating temperature for MP35N is 400 °C (750 °F). Since its development, MP35N has been used successfully in applications outside the aerospace industry. For example, it is the highest strength material approved for structural components in aggressive, sour well environments (NACE specification MR0175, "Sulfide Stress Cracking Resistant Materials for Oil Equipment"). Additional information on MP35N can be found in the articles "Properties of Cobalt Alloys" and "Corrosion Behavior of Cobalt Alloys" in this Handbook.

MP159 was developed in response to the need for a fastener alloy that could perform under the higher operating temperatures developed by turbine engines. The maximum operating temperature for MP159 is 595 °C (1100 °F). This alloy is work strengthened and aged for 4 h at approximately 660 °C (1225 °F) to obtain strength levels in excess of 1825 MPa (265 ksi). In addition to undergoing the multiphase reaction, MP159 also benefits from a second strengthening mechanism. Titanium, aluminum, and niobium have also been added to the composition to cause precipitation of the gamma prime phase during age hardening. Additional information on MP159 can be found in the article "Properties of Cobalt Alloys" in this Handbook.

Other age-hardenable cobalt alloys that offer high strength combined with good corrosion resistance include the spring alloys Duratherm 600, Elgiloy, and Havar (see Table 1). Through various combinations of cold work and aging, these alloys obtain hardness levels ranging from 45 to 60 HRC (500–600 HV), tensile strengths ranging from approximately 1700 to 2400 MPa (250–350 ksi), and yield strengths ranging from approximately 1400 to 2100 MPa (200–300 ksi). Figure 11 shows the effects of cold work and aging on the tensile properties of Duratherm 600. Additional information on Duratherm 600 and Elgiloy can be found in the article "Properties of Cobalt Alloys" in this Handbook.

Cobalt Alloys for Surgical Implants. Cobalt-base alloys are widely used for the fabrication of various devices that are surgically implanted in the body. Applications include hip replacements, knee replacements, and implants that fix



(a) (b) (c)

Fig. 12 Effect of processing on the microstructure of Co-Cr-Mo surgical implant alloys. (a) Investment-cast, carbide-strengthened Co-Cr-Mo alloy. Note that the grains in this microstructure are quite coarse (ASTM macrograin size 7.5), and the carbides are large. (b) Higher-strength, fine-grained Co-Cr-Mo alloy made by forging of nitrogen-strengthened bar stock. (c) Higher-strength fine-grained Co-Cr-Mo alloy made by hot isostatic pressing of carbide-strengthened powders

bone fractures (bone screws, staples, and plates). The support structures for heart valves are often fabricated from cobalt alloys. A variety of dental implants have also been produced from cobalt alloys.

Most of the cobalt-base alloys currently in use as implants meet the requirements of ASTM F 75, F 799, F 90, and F 562. Standards F 75 and F 799 describe requirements for cast and thermomechanically processed Co-Cr-Mo, respectively, F 90 describes wrought Co-Cr-W-Ni, and F 562 describes wrought Co-Ni-Cr-Mo. Compositions of these alloys are given in Table 5. The properties of interest for orthopedic implants include biocompatibility, corrosion resistance, wear resistance, and such mechanical properties as strength, ductility, and high-cycle fatigue behavior. As shown in Table 6, the properties of cobalt-base implant alloys are highly sensitive to processing history. Figure 12 shows the influence of processing on the microstructures of both cast and wrought Co-Cr-Mo alloys.

SELECTED REFERENCES

- W. Betteridge, *Cobalt and Its Alloys*, Ellis Horwood Ltd., 1982
- J.D. Donaldson and S.J. Clark, *Cobalt in Superalloys*, Cobalt Development Institute, 1985
- R.B. Herchenroeder and W.T. Ebihara, In-Process Metallurgy of Wrought Cobalt-Base Alloys, *Met. Eng. Q.*, May, 1969, p 313–324
- *Multiphase Alloys*, Timkin Latrobe Steel, Latrobe, PA, 1994
- C.P. Sullivan, J.D. Varin, and M.J. Donachie, Jr., Relationship of Properties to Microstructure in Cobalt-Base Superalloys, *Met. Eng. Q.*, May, 1969, p 299–312
- H.J. Wagner and A.M. Hall, "The Physical Metallurgy of Cobalt-Base Superalloys," DMIC Report 171, 6 July 1962

ASM Specialty Handbook: Nickel, Cobalt, and Their Alloys
J.R. Davis, editor, p 373-386
DOI:10.1361/ncta2000p373

Copyright © 2000 ASM International®
All rights reserved.
www.asminternational.org

Properties of Cobalt Alloys

THE 18 DATA SHEETS included in this article describe the specifications, applications, and properties of the following alloys in alphabetical order.

AiResist 13 (AR-13)

Chemical Composition

Typical composition. 58 Co; 21 Cr; 11.0 W; 3.5 Al; 2.5 Fe; 2.0 Ta; 1.0 Ni; 0.50 Mn; 0.45 C; 0.1 Y

Mechanical Properties

Tensile properties. See Table 1.

Physical Properties

Density. 8.43 g/cm^3 (0.305 lb/in.^{3}) at 20 °C (68 °F)

Table 1 Typical mechanical properties of AR-13

Temperature		Tensile strength		Yield strength		Elongation,
°C	°F	MPa	ksi	MPa	ksi	%
21	70	600	87	530	77	1.5
650	1200	475	69	385	56	4.5
760	1400	420	61	330	48	4.5
870	1600	290	42	275	40	21.0

AiResist 213 (AR-213)

Chemical Composition

Typical composition. 66.0 Co; 19.0 Cr; 6.5 Ta; 4.7 W; 3.5 Al; 0.18 C; 0.15 Zr; 0.1 Y

Applications

Typical uses. For gas turbine components

Mechanical Properties

Tensile properties. See Table 2.
Hardness. Age-hardened: 47 HRC

Physical Properties

Density. 8.51 g/cm^3 (0.307 lb/in.^{3}) at 20 °C (68 °F)

Chemical Properties

Resistance to specific corroding agents. Sulfidation and oxidation resistant

Table 2 Typical mechanical properties of AR-213

Temperature		Tensile strength		Yield strength		Elongation,
°C	°F	MPa	ksi	MPa	ksi	%
21	70	1120	162	625	91	14
650	1200	960	139	455	66	28
760	1400	485	70	385	56	47
870	1600	315	46	220	32	55

AiResist 215 (AR-215)

Chemical Composition

Typical composition. 64.0 Co; 19.0 Cr; 7.5 Ta; 4.5 W; 4.3 Al; 0.35 C; 0.13 Zr; 0.17 Y

Mechanical Properties

Tensile properties. See Table 3.

Physical Properties

Density. 8.47 g/cm^3 (0.306 lb/in.^{3}) at 20 °C (68 °F)

Table 3 Typical mechanical properties of AR-215

Temperature		Tensile strength		Yield strength		Elongation,
°C	°F	MPa	ksi	MPa	ksi	%
21	70	690	100	485	70	4
650	1200	570	83	315	46	12
870	1600	275	40	215	31	59

Duratherm 600

Specifications

UNS number. R30600

Chemical Composition

Nominal composition. 41.5 Co; 12 Cr; 4 Mo; 3.9 W; 8.7 Fe; 2 Ti; 0.7 Al; bal Ni

Applications

Typical uses. Springs in electric irons, deep fryers, and hot plates; corrosion resistant membranes in pressure gages; spring elements exposed to cyclic stress; temperature-resistant and corrosion resistant plate springs for the chemical industry; nonmagnetic wear-resistant magnetic head distance foils with low eddy current losses (low electrical conductivity)

Mechanical Properties

Tensile properties. See Tables 4 and 5.
Hardness. See Tables 4 and 5.
Elastic modulus (tension). Hard, 205 GPa (29.7 × 10^6 psi); hard + age hardened, 225 GPa (32.6 × 10^6 psi)
Shear modulus. Hard, 85 GPa (12.3 × 10^6 psi); hard + age hardened, 93 GPa (13.5 × 10^6 psi)

Physical Properties

Density. Hard, 8.45 g/cm^3 (0.305 lb/in.^{3}) at 20 °C (68 °F); hard + age hardened, 8.50 g/cm^3 (0.307 lb/in.^{3}) at 20 ° C (68 °F)
Liquidus temperature. 1350 °C (2462 °F)
Coefficient of linear thermal expansion. 13.5 μm/m · K (7.5 μin./in./°F)
Thermal conductivity. 10 W/m · K (5.78 Btu/ft · h · °F)
Curie temperature. Hard, –30 °C (–22 °F); hard + age hardened, –40 °C (–40 °F)
Magnetic permeability. 1.015 at 300 A/cm in the age-hardened condition

Chemical Properties

Resistance to specific corroding agents. Resistant to both freshwater and salt water and a number of aggressive environments (see Table 6)

Table 4 Typical mechanical properties of Duratherm 600 prior to age hardening

Product form/condition	Degree of cold work, %	Tensile strength MPa	Tensile strength ksi	Yield strength, offset 0.2% MPa	Yield strength, offset 0.2% ksi	Elongation(a), %	Hardness, HV	Bending fatigue strength(b) MPa	Bending fatigue strength(b) ksi
Strip/soft	0	850 ± 100	123 ± 14.5	380 ± 100	55 ± 14.5	>35	210 ± 30	330	48
Wire/soft	0	940 ± 100	136 ± 14.5	420 ± 100	61 ± 14.5	>35	220 ± 30	…	…
Strip/½ hard	20	1100 ± 200	160 ± 29	970 ± 200	141 ± 29	>5	350 ± 40	470	68
Wire/½ hard	20	1250 ± 200	181 ± 29	1140 ± 200	165 ± 29	>4	380 ± 40	…	…
Strip/hard	60	1550 ± 150	225 ± 22	1450 ± 150	210 ± 22	>1	460 ± 30	580	84
Wire/hard	60	1750 ± 200	254 ± 29	1500 ± 250	218 ± 36	>1	470±30	…	…

(a) Gage length: 50 mm (2 in.) for strip; 100 mm (4 in.) for wire. (b) 10^7 stress cycles, values refer to specimens 0.15 mm (0.006 in.) thick with a fracture probability of 1%

Table 5 Typical mechanical properties for Duratherm 600 after age hardening

Product form/condition	Age hardening cycle	Tensile strength MPa	Tensile strength ksi	Yield strength, +0.2% offset MPa	Yield strength, +0.2% offset ksi	Elongation(a), %	Hardness, HV	Bending fatigue strength(b) MPa	Bending fatigue strength(b) ksi
Strip/soft	4 h 750 °C (1380 °F)	1100 ± 150	160 ± 22	650 ± 150	94 ± 22	>20	310 ± 40	380	55
Wire/soft	4 h 750 °C (1380 °F)	1200 ± 150	174 ± 22	700 ± 150	102 ± 22	>20	320 ± 40	…	…
Strip/½ hard	4 h 650 °C (1200 °F)	1350 ± 200	196 ± 29	1150 ± 200	167 ± 29	>3	420 ± 50	520	75
Wire/½ hard	4 h 650 °C (1200 °F)	1500 ± 200	218 ± 29	1400 ± 250	203 ± 36	>3	460 ± 50	…	…
Strip/hard	2 h 650 °C (1200 °F)	1880 ± 200	273 ± 29	1850 ± 200	268 ± 29	>1	580 ± 40	680	99
Wire/hard	2 h 650 °C (1200 °F)	2200 ± 200	319 ± 29	2150 ± 200	312 ± 29	>1	600 ± 40	…	…

(a) Gage length: 50 mm (2 in.) for strip; 100 mm (4 in.) for wire. (b) 10^7 stress cycles, values refer to specimens 0.15 mm (0.006 in.) thick with a fracture probability of 1%

Table 6 Corrosion rates of Duratherm 600 and type 316L in various corrosive media

Medium	Temperature °C	Temperature °F	Duratherm 600, μm/yr	Type 316L stainless steel, μm/yr
Acetic acid, 10%	RT	RT	0.1	0.1
	80	175	0.1	0.2
Hydrochloric acid, 10%	Boiling	Boiling	40,000	375,000
Nitric acid, 10%	RT	RT	0.3	0.1
	80	175	16	0.1
Nitric acid, 65%	RT	RT	0.6	0.3
	80	175	70	13
Sulfuric acid, 10%	RT	RT	0.7	0.1
	80	175	80	120
Sulfuric acid, 20%	RT	RT	2	0.1
	80	175	170	14,000
Lactic acid, 10%	80	175	2.6	0.01
Ferric chloride, 10%	RT	RT	0.1	4
	80	175	1,500(a)	10,000(a)
Streicher test, 50% H_2SO_4 + 42 g/L $Fe_2(SO_4)_3$	Boiling	Boiling	770	106

RT, room temperature. (a) Pitting resulted

Elgiloy

Specifications

AMS. 5833, 5834, 5875, 5876
ASTM. F 1058
ASME. SFA5.21 (ERCoCr-F)
AWS. A.521 (ERCoCr-F)
NACE International. MR0175-94
UNS number. R30003

Chemical Composition

Composition limits. 39.0 to 41.0 Co; 19.0 to 21.0 Cr; 14.0 to 16.0 Ni; 6.0 to 8.0 Mo; 1.5 to 2.5 Mn; 0.15 max C; 0.10 max Be; bal iron

Applications

Typical uses. Main springs, power springs, coil springs, torsion bars, ball bearings, textile thread guides, valve parts, textile cutting wire, pivot points, high-temperature aircraft cable, oceanographic cable, artificial heart springs, helical springs, corrosion resistant springs, and pressure transducers and diaphragms

Mechanical Properties

Tensile properties. See Tables 7 and 8.
Hardness. 45 to 60 HRC
Elastic modulus. See Table 9.
Modulus of rigidity. See Table 9.
Poisson's ratio. See Table 9.
Fatigue strength. See Table 10.

Physical Properties

Density. 8.30 g/cm^3 (0.30 lb/in.^{3})
Melting temperature. 1427 °C (2600 °F)
Coefficient of linear thermal expansion. 12.7 μm/m · K (7.05 μin./in. · °F)

Table 8 Tensile properties of heat treated Elgiloy wire

Cold reduction,%	Tensile strength		Yield strength, 0.2% offset	
	MPa	ksi	MPa	ksi
0	1020	148	690	100
20	1379	200	1241	180
40	2000	290	1862	270
60	2551	370	2241	325

Note: Heat treated at 525 °C (980 °F) for 5 h

Table 9 Effect of temperature on modulus of elasticity of Elgiloy

Temperature		Modulus of elasticity,	Modulus of rigidity,	Poisson's ratio,
°C	°F	*E* GPa (10^6 psi)	*G* GPa (10^6 psi)	μ=(*E*/2*G*)–1
24	75	190 (27.500)	77 (11.219)	0.226
–18	0	194 (28.125)	79 (11.415)	0.232
–73	–100	198 (28.750)	80 (11.669)	0.232
–129	–200	203 (29.375)	82 (11.900)	0.234
–184	–300	206 (29.844)	83 (12.106)	0.233

Table 10 Fatigue strength of heat treated Elgiloy strip and wire

Form	Type of test	Fatigue strength, MPa (ksi), in: 10^5 cycles	10^6 cycles
Strip(a)	Reverse bending	1241 (180)	862 (125)
Wire(b)	Torsion	724 (105)	483 (70)

(a) 85% cold reduced, heat treated. (b) 45–48% cold reduced, heat treated

Thermal conductivity. 12.5 W/m · K (7.23 Btu/ft · h · °F)
Magnetic permeability. 1.0004 at room temperature

Chemical Properties

Resistance to specific corroding agents. Resistant to attack by the atmosphere, salt spray, most organic acids, sodium chloride, sodium sulfate, sodium cyanide, ammonium chloride, ammonium sulfate, and many other salts. See Table 11 for a comparison of Elgiloy with Hastelloy C-276 and type 316 stainless steel.

Table 7 Tensile properties of heat-treated Elgiloy strip

Strip thickness		Cold reduction, %	Tensile strength		Yield strength, 0.2% offset		Elongation, 50 mm (2 in.),
mm	in.		MPa	ksi	MPa	ksi	%
0.51	0.020	85	2344	340	1965	285	1.0
0.63	0.025	69	2255	327	1917	278	1.0
1.20	0.047	62	2082	302	1862	270	1.0
1.91	0.075	40	1682	244	1517	220	3.0
2.54	0.100	20	1165	169	965	140	10.0

Note: Heat treated at 525 °C (980 °F) for 5 h

Table 11 Performance of Elgiloy in various corrosive media

Corrosive media	Concentration,%	Temperature °C	Temperature °F	Elgiloy	Hastelloy C-276	Type 316 stainless steel
Acetic acid	50%	106	223	E	G	S
Acetic acid	10%	99–104	210–220	E	…	E
Ammonium chloride	50%	113	235	E	S	…
Ammonium chloride	10%–15%	104	220	E	E	E
Ammonium sulfate	10%	99–104	210–220	E	E	…
Calcium chloride	10%	103	218	E	E	E
Chromic acid	10%	107	224	U	U	…
Citric acid	10%	106	222	E	E	E
Cupric chloride	10%	102	215	U	…	U
Deionized water	…	27	80	E	E	…
Ferric chloride	10%	102	216	U	…	U
Ferric chloride	10%	24	75	E	E	E
Ferric sulfate acid	50%	Boiling temperature		S	S	…
Hydrochloric acid	Concentrated	24	75	F	…	…
Hydrochloric acid	50%	24	75	G	…	…
Hydrochloric acid	10%	24	75	G	G	U
Hydrochloric acid	Concentrated	66	150	U	…	…
Hydrochloric acid	50%	66	150	U	…	…
Hydrochloric acid	10%	66	150	U	…	U
Hydrochloric acid	Concentrated	110	230	U	…	U
Hydrochloric acid	50%	110	230	U	…	U
Hydrochloric acid	10%	102	216	U	U	U
Lactic acid	10%	104	219	E	G	…
Mercuric acid	10%	101	214	E	…	U
Nitric acid	Concentrated	110	230	F	…	S
Nitric acid	50%	110	230	G	…	G
Nitric acid	10%	102	216	E	G	…
Oxalic acid	10%	102	216	G	G	U
Phenol	10%	104	219	E	…	E
Phosphoric acid	Concentrated	166	330	U	…	U
Phosphoric acid	50%–55%	116–121	240–250	S	G	U
Phosphoric acid	10%	107	225	E	…	G
Seawater	…	RT–BP	RT–BP	E	E	…
Sodium chloride	10%	103	218	E	E	E
Sodium cynanide	10%	103	218	E	…	E
Sodium hydroxide	Any concentration	RT–BP	RT–BP	E	F	…
Sodium sulfide	10%	104	220	E	…	E
Sodium sulfite	10%	104	220	E	…	E
Stannous chloride	10%	102	216	E	…	E
Sulfuric acid	Concentrated	259	498	U	…	U
Sulfuric acid	50%	150	302	U	…	U
Sulfuric acid	10%	105	221	U	S	U
Tartanic acid	10%	104	219	E	…	E
Zinc chloride	10%	103	217	E	E	E

RT, room temperature; BP, boiling point. E, excellent (<0.05 mm/yr, or 2 mils/yr); G, good (0.05–0.25 mm/yr, or 2–10 mils/yr); S, satisfactory (0.25–0.51 mm/yr, or 10–20 mils/yr); F, fair (0.51–1.27 mm/yr, or 20–50 mils/yr); U, unsatisfactory (>1.27 mm/yr, or 50 mils/yr)

FSX-414

Chemical Composition

Typical composition. 52 Co; 29 Cr; 10 Ni; 7.5 W; 1.0 Fe; 0.25 C; 0.010 B

Applications

Typical uses. Gas turbine vanes

Mechanical Properties

Tensile properties. See Table 12.

Stress-rupture characteristics (*typical*):

Temperature		Rupture strength	
°C	°F	MPa	ksi
At 100 h			
815	1500	160	23
870	1600	110	16
925	1700	83	12
980	1800	55	8
1040	1900	34	5
1090	2000	24	3.5
At 1000 h			
760	1400	165	24
815	1500	115	16.5
870	1600	83	12
925	1700	55	8
980	1800	34	5
1040	1900	21	3

Physical Properties

Density. 8.30 g/cm^3 (0.300 lb/in.^{3}) at 20 °C (68 °F)

Table 12 Typical mechanical properties of FSX-414

Temperature		Tensile strength		Yield strength		Elongation,
°C	°F	MPa	ksi	MPa	ksi	%
21	70	740	107	440	64	11
540	1000	540	78	240	35	15
650	1200	485	70	215	31	15
760	1400	400	58	195	28	18
870	1600	310	45	165	24	23

Haynes 25 (L-605)

Specifications

AMS. 5537 (sheet, strip, and plate), 5759 (bar, rings, and forgings), 5796 (welding wire), 5797 (coated welding electrodes)
UNS number. R30605

Chemical Composition

Composition limits. 19.00 to 21.00 Cr; 14.00 to 16.00 W; 9.00 to 11.00 Ni; 3.00 max Fe; 1.00 to 2.00 Mn; 0.4 max Si; 0.05 to 0.15 C; 0.030 P; 0.030 max S; bal Co

Applications

Typical uses. Suitable for a number of component applications in the aerospace industry, including parts in established military and commercial gas turbines. In modern engines, Haynes 25 has largely been replaced by Haynes 188, described in the next data sheet, and by nickel-base heat resistant alloys. Alloy 25 is also used as a bearing material, both for balls and races.

Mechanical Properties

Tensile properties. See Tables 13 and 14.

Hardness. HRC 22 for solution-treated sheet up to 48 HRC for 25% cold-worked sheet at 20 °C (70 °F)
Elastic modulus (average in tension for solution heat treated sheet):

Temperature		Elastic modulus	
°C	°F	GPa	10^6 psi
25	77	225	32.6
100	212	222	32.2
200	392	214	31.0
300	572	204	29.6
400	752	197	28.6
500	932	188	27.3
600	1112	181	26.3
700	1292	174	25.2
800	1472	163	23.7
900	1652	154	22.4
1000	1832	146	21.2

Creep-rupture characteristics. See Table 15.
Impact strength. Typical Charpy V-notch for solution heat treated plate

Temperature		Mean Charpy,	V-notch strength,
°C	°F	J	ft · lbf
–195	–321	148	109
–138	–216	182	134
–78	–108	212	156
–29	–20	243	179
20	68	262	193
260	500	297	219
540	1000	273	201
650	1200	230	170
760	1400	194	143
870	1600	163	120
980	1800	144	106

Fatigue strength. Solution heat treated sheet. At 816 °C (1500 °F): 275 MPa (40 ksi) at 10^7 cycles; 215 MPa (31 ksi) at 10^8 cycles. At 980 °C (1800 °F): 145 MPa (21 ksi) at 10^6 cycles; 105 MPa (15 ksi) at 10^7 cycles; 90 MPa (13 ksi) at 10^8 cycles

Physical Properties

Density. 9.130 g/cm^3 (0.330 lb/in.^{3}) at 22 °C (72 °F)
Liquidus temperature. 1410 °C (2570 °F)
Solidus temperature. 1329 °C (2425 °F)
Coefficient of thermal expansion (linear):

Temperature		Average coefficient	
°C	°F	μm/m · K	μin./in. · °F
21–935	70–200	12.3	6.8
21–205	70–400	12.9	7.2
21–315	70–600	13.5	7.6
21–425	70–800	13.9	7.8
21–540	70–1000	14.4	8.0
21–650	70–1200	14.8	8.2
21–760	70–1400	15.4	8.6
21–870	70–1600	16.2	9.1
21–980	70–1800	16.9	9.4
21–1090	70–2000	17.7(a)	9.8(a)

(a) Extrapolated data

Specific heat. 384 J/kg · K (0.092 Btu/lb · °F) at 28 to 100 °C (80 to 212 °F)

Table 13 Typical tensile properties of cold-rolled and solution-annealed Haynes 25 sheet

Test temperature		Ultimate tensile strength		0.2% yield strength		Elongation in 50 mm
°C	°F	MPa	ksi	MPa	ksi	(2 in.), %
Room	Room	1005	146	475	69	51
540	1000	770	112	330	48	60
650	1200	745	108	330	48	60
760	1400	640	93	285	41	42
870	1600	415	60	250	36	45
980	1800	235	34	125	18	36
1095	2000	160	23	76	11	48

Thermal conductivity:

Temperature		Conductivity	
°C	°F	W/m · K	Btu/ft · h · °F
20	70	9.8(a)	5.6(a)
100	100	11.2(a)	6.5(a)
200	300	13.0	7.5
300	500	14.7	8.5
400	700	16.6	9.6
500	900	18.5	10.7
600	1100	20.4	11.8
700	1300	22.4	12.9
800	1500	24.4	14.1
900	1700	26.5	15.3

(a) Extrapolated data

Electrical resistivity:

Temperature		Resistivity,
°C	°F	nΩ · m
24	75	890
240	460	970
450	840	990
650	1200	1060
740	1360	1070
815	1500	1080
950	1740	970
1000	1830	950
1080	1980	1000

Magnetic permeability. <1.0 at 9 kA/m (116 oersteds)

Chemical Properties

Resistance to specific corroding agents. Haynes alloy 25 was not designed for resistance to corrosive aqueous media. It does, however, exhibit good resistance to oxidizing environments up to 980 °C (1800 °F) for prolonged exposures and excellent resistance to sulfidation.

Table 14 Effect of cold working on the tensile properties of 1.3 mm (0.050 in.) thick Haynes 25 sheet

Cold reduction, %	Test temperature		Ultimate tensile strength		0.2% yield strength		Elongation
	°C	°F	MPa	ksi	MPa	ksi	in 50 mm (2 in.), %
10	20	70	1070	155	725	105	41
	540	1000	785	114	540	78	48
	650	1200	795	115	550	80	37
	760	1400	600	87	460	67	8
	870	1600	425	62	325	47	13
	980	1800	270	39	185	27	15
15	20	70	1145	166	855	124	30
	540	1000	925	134	740	107	29
	650	1200	890	129	765	111	15
	760	1400	715	104	595	86	5
	870	1600	485	70	360	52	9
	980	1800	275	40	205	30	5
20	20	70	1260	183	970	141	19
	540	1000	1075	156	915	133	18
	650	1200	945	137	825	120	2
	760	1400	740	107	660	96	3
	980	1800	285	41	205	30	4

Table 15 Typical creep and stress-rupture properties of cold-rolled and solution-annealed Haynes 25 sheet

Test temperature			Approximate initial stress in MPa (ksi) to produce specified creep in:					
			10 h		100 h		1000 h	
°C	°F	Creep, %	MPa	ksi	MPa	ksi	MPa	ksi
650	1200	0.5	425	62.0	330	47.5	230	33.5
		1.0	490	71.0	370	54.0	270	39.0
		Rupture	565	82.0	475	69.0	395	57.0
705	1300	0.5	295	43.0	205	30.0	145	21.0
		1.0	340	49.5	210	35.0	160	23.2
		Rupture	440	64.0	345	50.0	260	38.0
760	1400	0.5	195	28.0	135	19.5	100	14.8
		1.0	220	32.0	150	21.5	110	16.2
		Rupture	325	47.0	250	36.0	180	26.0
815	1500	0.5	130	18.5	97	14.0	70	10.2
		1.0	140	20.2	105	15.5	85	12.3
		Rupture	235	34.0	170	24.7	125	18.1
870	1600	0.5	94	13.7	68	9.9	48	6.9
		1.0	105	15.2	83	12.0	61	8.9
		Rupture	165	24.0	120	17.5	83	12.0
925	1700	0.5	67	9.7	47	6.8	31	4.5
		1.0	83	12.0	61	8.8	39	5.6
		Rupture	120	17.3	81	11.8	50	7.2
980	1800	0.5	47	6.8	31	4.5	18	2.6
		1.0	61	8.8	39	5.6	21	3.0
		Rupture	81	11.8	50	7.2	28	4.0

Haynes 188

Specifications

AMS. 5608 (sheet, strip, and plate), 5772 (bar, rings, and forgings), 5801 (welding wire)
UNS number. R30188

Chemical Composition

Composition limits. 20.0 to 24.0 Ni; 21.0 to 23.0 Cr; 13.0 to 15.0 W; 3.0 max Fe; 1.25 max Mn; 0.20 to 0.50 Si; 0.05 to 0.15 C; 0.02 to 0.12 La; 0.015 max B; bal Co

Applications

Typical uses. Widely used in established military and commercial gas turbine engines for combustion cans, transition ducts, and afterburner components

Mechanical Properties

Tensile properties. See Table 16.
Hardness:

Temperature		Average hardness, HRA, after indicated time at temperature	
°C	°F	200 h	500 h
980	1800	62	61
925	1700	63	63
870	1600	63	64
815	1500	64	63
760	1400	64	63
705	1300	64	64
650	1200	62	62
590	1100	62	61
540	1000	61	61
480	900	62	61

Creep-rupture characteristics. See Table 17.

Physical Properties

Density. 8.98 g/cm^3 (0.324 lb/in.^{3}) at 20 °C (70 °F)
Melting range. 1315 to 1410 °C (2400 to 2570 °F)
Coefficient of thermal expansion (linear):

Temperature		Average coefficient	
°C	°F	μm/m · K	μin./in. · °F
25–100	70–200	11.9	6.6
25–200	70–400	12.6	7.0
25–300	70–600	13.2	7.4
25–400	70–800	13.8	7.8
25–500	70–1000	14.5	8.2
25–600	70–1200	15.2	8.6
25–700	70–1400	15.8	9.0
25–800	70–1600	16.5	9.4
25–900	70–1800	17.1	9.9
25–1000	70–2000	17.9	10.3

Specific heat:

Temperature		Specific heat	
°C	°F	J/kg · K	Btu/lb · °F
Room	Room	403	0.096
100	200	423	0.101
200	400	444	0.106
300	600	465	0.112
400	800	486	0.117
500	1000	502	0.122
600	1200	523	0.127
700	1400	540	0.131
800	1600	557	0.136
900	1800	573	0.140
1000	2000	590	0.145

Thermal conductivity:

Temperature		Conductivity	
°C	°F	W/m · K	Btu · in./ft^2 · h · °F
Room	Room	10.4	72
100	200	12.2	84
200	400	14.3	100
300	600	15.9	112
400	800	17.5	125
500	1000	19.3	138
600	1200	21.1	152
700	1400	23.0	167
800	1600	24.8	174
900	1800	25.5	189
1000	2000	27.6	204

Electrical resistivity:

Temperature		Restitivity	
°C	°F	μΩ · cm	μΩ · in.
Room	Room	101.0	39.6
100	200	103.0	40.3
200	400	105.0	41.5
300	600	107.7	42.7
400	800	110.5	43.8
500	1000	112.7	44.7
600	1200	114.8	45.6
700	1400	116.4	46.1
800	1600	117.5	46.5
900	1800	118.3	46.7
1000	2000	119.1	46.8

Magnetic permeability. 1.01 at 16 kA/m (200 oersteds) and 20 °C (68 °F)

Chemical Properties

Resistance to specific corroding agents. Haynes alloy 188 was not designed for resistance to corrosive aqueous media. It does, however, combine excellent high-temperature strength with very good resistance to oxidizing environments up to 1095 °C (2000 °F) for prolonged exposures and excellent resistance to sulfate deposit hot corrosion. It is also highly resistant to molten chloride salts and has good resistance to gaseous sulfidation.

Table 16 Typical tensile properties for cold-rolled and solution-annealed Haynes 188 sheet and plate

Test temperature		Ultimate tensile strength		0.2% yield strength		Elongation in 50 mm
°C	°F	MPa	ksi	MPa	ksi	(2 in.), %
Sheet						
RT	RT	945	137.2	465	67.3	53
540	1000	750	108.5	290	42.0	61
650	1200	710	103.3	275	39.7	59
760	1400	620	89.9	270	38.9	63
870	1600	415	60.0	250	35.9	64
980	1800	245	35.2	130	19.0	59
1095	2000	130	18.7	64	9.3	32
Plate						
RT	RT	985	142.6	470	68.5	56
540	1000	775	112.6	275	39.9	69
650	1200	755	109.8	265	38.3	73
760	1400	650	94.0	270	38.9	70
870	1600	450	65.3	250	36.1	77
980	1800	265	38.7	185	27.1	84
1095	2000	145	21.0	88	12.8	89
1150	2100	96	13.9	48	6.9	60
1205	2200	83	12.0	28	4.0	71

RT, room temperature

Table 17 Typical creep and stress-rupture properties of cold-rolled and solution-annealed Haynes 188 sheet

Test temperature		Creep,	Approximate initial stress in MPa (ksi) to produce specified creep in:					
			10 h		100 h		1000 h	
°C	°F	%	MPa	ksi	MPa	ksi	MPa	ksi
760	1400	0.5	155	22.5	115	16.4	81	11.7
		1.0	175	25.5	130	18.5	92	13.3
		Rupture	295	43.0	220	32.0	160	23.0
815	1500	0.5	105	15.5	77	11.1	54	7.8
		1.0	120	17.6	87	12.6	61	8.8
		Rupture	215	31.0	150	21.7	105	15.0
870	1600	0.5	74	10.7	52	7.5	34	5.0
		1.0	84	12.2	58	8.4	39	5.7
		Rupture	145	21.0	99	14.4	65	9.4
925	1700	0.5	50	7.3	34	4.9	21	3.1
		1.0	57	8.2	39	5.6	25	3.6
		Rupture	99	14.3	63	9.1	38	5.5
980	1800	0.5	34	4.9	21	3.1	12	1.8
		1.0	39	5.6	25	3.6	14	2.1
		Rupture	63	9.1	37	5.4	17	2.4

MAR-M 302

Specifications

AMS. 5384 (investment castings)

Chemical Composition

Composition limits. Typical. 58.0 Co; 21.5 Cr; 10.0 W; 9.0 Ta; 0.85 C; 0.005 B; 0.20 Zr. Range. 20 to 23 Cr; 9 to 11 W; 8 to 10 Ta; 0.78 to 0.93 C; 0.75 to 1.5 Fe; 0.10 to 0.40 Si; 0.10 to 0.30 Zr; 0.10 max Mn; 0.010 max B; bal Co

Applications

Typical uses. For turbine vanes, nozzle guide vanes, and buckets in gas turbines. For service to 1150 °C (2100 °F)

Mechanical Properties

Tensile properties. See Table 18.

Stress-rupture characteristics (typical at 100 h):

Temperature		Rupture strength	
°C	°F	MPa	ksi
815	1500	250	36
870	1600	185	27
925	1700	140	20
980	1800	97	14
1040	1900	69	10
1090	2000	41	6

Table 18 Typical mechanical properties of MAR-M 302

Temperature		Tensile strength		Yield strength		Elongation,
°C	°F	MPa	ksi	MPa	ksi	%
21	70	930	135	690	100	2
540	1000	795	115	505	73	…
650	1200	785	114	450	65	…
760	1400	705	102	385	56	8
870	1600	450	65	310	45	11
980	1800	275	40	215	31	15
1090	2000	150	22	150	22	21

Physical Properties

Density. 9.21 g/cm^3 (0.333 lb/in.^{3}) at 20 °C (68 °F)

Coefficient of thermal expansion (linear):

Temperature		Mean coefficient	
°C	°F	μm/m · K	μin./in. · °F
205	400	12.4	6.9
315	600	13.0	7.2
425	800	13.3	7.4
540	1000	13.7	7.6
650	1200	14.0	7.8
760	1400	14.4	8.0
870	1600	14.9	8.3
980	1800	15.7	8.7
1090	2000	16.6	9.2

Thermal conductivity:

Temperature		Conductivity	
°C	°F	W/m · K	Btu/ft · h · °F
21	70	18.7	10.8
93	200	19.2	11.1
205	400	20.2	11.7
315	600	21.2	12.2
425	800	21.7	12.5
540	1000	22.2	12.8
650	1200	22.3	12.9
760	1400	22.6	13.1
870	1600	23.2	13.4
980	1800	24.2	14.0

MAR-M 322

Chemical Composition

Composition limits. Typical. 61.0 Co; 21.5 Cr; 9.0 W; 4.5 Ta; 0.75 Ti; 1.0 C; 2.25 Zr. Range. 20 to 23 Cr; 8 to 10 W; 4 to 5 Ta; 2 to 2.5 Zr; 0.90 to 1.1 C; 0.65 to 0.85 Ti; 1.5 max Fe; 0.20 max Mn; 0.20 max Si; bal Co

Applications

Typical uses. For turbine vanes and blades, jet engine components

Mechanical Properties

Tensile properties. See Table 19.

Physical Properties

Density. 8.91 g/cm^3 (0.322 lb/in.^{3}) at 20 °C (68 °F)

Chemical Properties

General corrosion behavior. Oxidation resistant to 1090 °C (2000 °F)

Table 19 Typical mechanical properties of MAR-M 322

Temperature		Tensile strength		Yield strength		Elongation,
°C	°F	MPa	ksi	MPa	ksi	%
21	70	825	120	625	91	3.2
540	1000	655	95	415	60	6
650	1200	655	95	415	60	6
760	1400	625	91	380	55	6.5
870	1600	550	80	345	50	12

MAR-M 509

Chemical Composition

Composition limits. Typical. 55.0 Co; 23.5 Cr; 10.0 Ni; 7.0 W; 3.5 Ta; 0.20 Ti; 0.60 C; 0.50 Zr. Range. 21.0 to 24.0 Cr; 9.0 to 11.0 Ni; 6.5 to 7.5 W; 3.0 to 4.0 Ta; 0.55 to 0.65 C; 0.4 to 0.6 Zr; 0.15 to 0.25 Ti; 1.50 max Fe; 0.4 max Si; 0.1 max Mn; 0.01 max B; 0.015 max S; bal Co

Applications

Typical uses. For aircraft and industrial turbines

Mechanical Properties

Tensile properties. See Table 20.
Hardness. 24 to 34 HRC
Elastic modulus:

Temperature		Modulus of elasticity	
°C	°F	GPa	10^6 psi
21	70	225	32.7
205	400	215	30.9
425	800	195	28.4
650	1200	180	25.8
760	1400	165	23.9
870	1600	155	22.5
980	1800	135	19.8

Stress-rupture characteristics (*typical*):

Temperature		Rupture strength	
°C	°F	MPa	ksi
At 100 h			
760	1400	345	50
815	1500	250	36.5
870	1600	180	26
925	1700	135	19.5
980	1800	105	15
1040	1900	79	11.5
1090	2000	52	7.5
At 1000 h			
760	1400	260	38
815	1500	195	28
870	1600	140	20
925	1700	105	15
980	1800	79	11.5
1040	1900	55	8
1090	2000	34	5

Physical Properties

Density. 8.85 g/cm^3 (0.320 lb/in.^{3}) at 20 °C (68 °F)
Incipient melting temperature. 1290 °C (2350 °F)
Liquidus temperature. 1400 °C (2550 °F)
Softening temperature. 1340 °C (2450 °F)
Coefficient of thermal expansion (linear):

Temperature		Mean coefficient	
°C	°F	μm/m · K	μin./in. · °F
315	600	14.6	8.1
425	800	15.3	8.5
540	1000	15.9	8.85
650	1200	16.2	9.0
760	1400	16.7	9.3
870	1600	17.2	9.55
980	1800	17.6	9.8
1090	2000	18.2	10.1

Thermal conductivity:

Temperature		Conductivity	
°C	°F	W/m · K	Btu/ft · h · °F
425	800	25.2	14.6
540	1000	27.9	16.1
650	1200	31.1	18.0
760	1400	34.3	19.8
870	1600	37.6	21.7
980	1800	41.2	23.8
1090	2000	44.6	25.8

Table 20 Typical mechanical properties of MAR-M 509

Temperature		Tensile strength		Yield strength		Elongation,
°C	°F	MPa	ksi	MPa	ksi	%
21	70	785	114	570	83	4
540	1000	570	83	400	58	6
650	1200	560	81	370	54	7
760	1400	570	83	365	53	10
870	1600	350	51	290	42	20
980	1800	215	31	180	26	26

MP35N

Specifications

ASTM. F 562 (surgical implants)
AMS. 5758 (centerless ground bars), 5844 (cold drawn bars), 5845 (cold drawn and aged bars), 7468 (bolts and screws)
NACE International. MR0175-94
UNS number. R30035

Chemical Composition

Composition limits. 35.0 Co; 35.0 Ni; 20.0 Cr; 9.75 Mo; 1.0 max Fe; 1.0 max Ti; 0.025 max C; 0.15 max Mn; 0.15 max Si

Applications

Typical uses. Because of its combination of ultrahigh tensile strength (up to 2070 MPa, or 300 ksi), good ductility and toughness, and excellent corrosion resistance, MP35N has been used in a wide variety of applications. Examples include fasteners used for aerospace, marine, medical, and petroleum industry applications, drive shafts for down hole oil pumps, surgical implants, springs, nonmagnetic electrical components, and oil industry tubular goods.

Mechanical Properties

Tensile properties. See Table 21.
Hardness. See Table 21.
Elastic modulus. See Table 22.
Shear modulus. See Table 23.
Stress-rupture properties. See Table 24.
Impact strength. See Table 25.
Fatigue strength. See Table 26.

Physical Properties

Density. 8.43 g/cm^3 (0.304 lb/in.^{3})
Melting range. 1315 to 1440 °C (2400 to 2625 °F)

Mean coefficient of thermal expansion (linear):

Temperature range		Average coefficient	
°C	°F	μm/m · K	μin./in. · °F
21–93	70–200	12.8	7.1
21–204	70–400	13.7	7.6
21–316	70–600	14.8	8.2
21–427	70–800	14.9	8.3
21–538	70–1000	15.7	8.7

Thermal conductivity:

Temperature			
°C	°F	W/m · K	Btu · in./ft^2 · h · °F
–184	–300	6.5	45
–73	–100	9.1	63
21	70	11.2	78
93	200	12.7	88
204	400	15.0	104
316	600	17.0	118
427	800	19.2	133
538	1000	21.3	148
649	1200	23.4	162

Electrical resistivity:

Temperature		Resistivity	
°C	°F	μΩ/mm	μΩ/in.
–184	–300	986	38.82
–73	–100	1011	39.79
21	70	1033	40.67
93	200	1051	41.37
204	400	1078	42.43
316	600	1104	43.45
427	800	1129	44.45
538	1000	1154	45.44
649	1200	1179	46.43

Magnetic permeability. 1.0009 at 25 °C (77 °F)

Chemical Properties

Resistance to specific corroding agents. MP35N possesses excellent resistance to most mineral acids (including nitric, hydrochloric, and sulfuric acids), hydrogen sulfide, seawater, and salt spray environments. It features exceptional resistance to stress-corrosion cracking (SCC) and hydrogen embrittlement at very high strength levels under severe environmental conditions that can crack most conventional corrosion resistant alloys. It is also highly resistant to other forms of localized attack, such as pitting and crevice corrosion. In seawater, MP35N is virtually immune to general, crevice, and stress corrosion, regardless of strength level or process condition.

Table 21 Typical room-temperature tensile properties of MP35N

Cold reduction,%	Ultimate tensile strength MPa	Ultimate tensile strength ksi	0.2% yield strength MPa	0.2% yield strength ksi	Elongation, %	Reduction of area, %	Hardness, HRC
Work strengthened							
0	931	135	414	60	70	70	8
15	1069	155	814	118	41	70	29
25	1172	170	1034	150	28	65	34
35	1336	194	1062	154	22	67	42
45	1572	228	1303	189	17	62	47
55	1827	265	1413	205	12	50	47
65	1931	280	1620	235	11	49	50
Work strengthened + aged 538 °C (1000 °F) 4 h, air cooled							
0	931	135	414	60	68	77	7
15	1089	158	862	125	39	70	33
25	1282	186	1207	175	24	65	39
35	1400	203	1344	195	21	62	43
45	1772	257	1731	251	12	52	46
53	2068	300	1999	290	10	48	50

Table 22 Elastic modulus of MP35N at various temperatures

Temperature		Annealed		Cold worked and aged	
°C	°F	GPa	10^6 psi	GPa	10^6 psi
26	78	232.8	33.76	234.8	34.05
232	450	216.0	31.33	219.0	31.76
482	900	201.0	29.15	201.3	29.19

Table 23 Shear modulus of MP35N at various temperatures

Temperature		Annealed		Cold worked and aged	
°C	°F	GPa	10^6 psi	GPa	10^6 psi
26	78	83.36	12.09	80.95	11.74
232	450	77.84	11.29	74.74	10.84
482	900	70.60	10.24	67.78	9.83

Table 24 Stress-rupture properties of MP35N

Condition	Test temperature °C	Test temperature °F	Stress for rupture in: 10 h MPa	10 h ksi	200 h MPa	200 h ksi	1000 h MPa	1000 h ksi
1517 MPa (220 ksi) strength level	538	1000	1288	187	1151	167	951	138
	593	1100	1137	165	916	133	661	96
	649	1200	916	133	641	93	…	…
1827 MPa (265 ksi) strength level	538	1000	1440	209	1233	179	985	143
	593	1100	1219	177	951	138	661	96
	649	1200	944	137	641	93	…	…

Table 25 Charpy V-notch impact strength of MP35N at a strength level of 1930 MPa (280 ksi)

Condition	Test temperature °C	Test temperature °F	Impact strength J	Impact strength ft · lbf
Cold drawn 49% and aged 1200 °F (649 °C) 4 h; air cool	24	75	25.6	18.9
	–73	–100	23.2	17.1
	–129	–200	20.7	15.3
	–196	–320	21.8	16.1
	–253	–423	18.3	13.5

Table 26 Room-temperature R.R. Moore bending fatigue strength of MP35N

Condition	Stress for cycles to failure: 10^6 MPa	10^6 ksi	10^7 MPa	10^7 ksi	10^8 MPa	10^8 ksi
Cold drawn and aged to 1517 MPa (220 ksi) strength level	689	100	620	90	606	88
Cold drawn and aged to 1827 MPa (265 ksi) strength level	744	108	682	99	668	97

MP159

Specifications

AMS. 5842 (bars), 7475 (bolts)
UNS number. R30159

Chemical Composition

Nominal composition. 35.7 Co; 25.5 Ni; 19.0 Cr; 9.0 Fe; 7.0 Mo; 3.0 Ti; 0.6 Nb; 0.2 Al

Applications

Typical uses. Fasteners used in gas turbine engines, airframes, the Space Shuttle propulsion system, aircraft landing gear, chemical processing apparatus, petrochemical refineries, pulp and paper processing plants, and power generation equipment

Mechanical Properties

Tensile properties. See Table 27.
Elastic modulus. See Table 28.
Shear modulus. See Table 29.

Physical Properties

Density. 8.37 g/cm^3 (0.302 lb/in.^{3})

Table 27 Typical room-temperature tensile properties of MP159

Condition	Tensile strength MPa	Tensile strength ksi	Yield strength (0.2% Offset) MPa	Yield strength (0.2% Offset) ksi	Elongation,%	Reduction of area,%
Annealed(a)	850	123	400	58	60	69
Cold worked 48%	1585	230	1415	205	12	46
Cold worked 48% + aged(b)	1895	275	1825	265	8	35

(a) Annealed at 1050 °C (1925 °F) for 4 h, water quenched. (b) Aged at 660 °C (1225 °F) for 4 h, air cooled

Melting range. 1260 to 1385 °C (2300 to 2525 °F)
Mean coefficient of thermal expansion:

Temperature range °C	Temperature range °F	Average coefficient μm/m · K	Average coefficient μin./in. · °F
25–100	77–212	14.3	7.95
25–200	77–392	14.2	7.90
25–300	77–572	14.2	7.88
25–400	77–752	14.6	8.09
25–500	77–932	14.9	8.29
25–600	77–1112	15.1	8.39
25–700	77–1292	16.0	8.90
25–800	77–1472	18.2	10.13

Table 28 Elastic modulus of MP159 at various temperatures

Temperature °C	Temperature °F	Annealed GPa	Annealed 10^6 psi	Cold worked and aged GPa	Cold worked and aged 10^6 psi
26	78	222	32.2	243	35.3
232	450	211	30.2	226	32.8
482	900	187	27.1	206	29.9

Chemical Properties

General corrosion behavior. Although not as corrosion resistant as MP35N, alloy MP159 is extremely resistant to SCC and hydrogen embrittlement at high strength levels. It is also resistant to crevice and pitting corrosion in chloride-containing environments (e.g., 10% ferric chloride test solutions). Cold worked and aged MP159 exhibits no cracking or evidence of corrosion on U-bend specimens after 30 days exposure in 0.5% acetic acid + 0.5 *M* NaCl saturated with H_2S.

Table 29 Shear modulus of MP159 at various temperatures

Temperature °C	Temperature °F	Annealed GPa	Annealed 10^6 psi	Cold worked and aged GPa	Cold worked and aged 10^6 psi
26	78	81	11.7	78	11.3
232	450	76	11.0	72	10.5
482	900	68	9.9	65	9.4

Stellite 6B (Haynes 6B)

Specifications

AMS. 5894 (all product forms)
UNS number. R30016

Chemical Composition

Composition limits. 28.00 to 32.00 Cr; 3.50 to 5.50 W; 3.00 max Fe; 3.00 max Ni; 2.00 max Si; 1.50 max Mo; 0.90 to 1.40 C; bal Co

Applications

Typical uses. Wear plates and bars, bushings, and sleeves for shafts operating in hot or possibly corrosive atmospheres where lubrication is difficult or impossible

Mechanical Properties

Tensile properties. See Table 30.
Compressive properties. Compressive strength, 2399 MPa (348 ksi)
Hardness. 2 mm (0.063 in.) sheet, 39 HRC; 13 mm (0.5 in.) plate, 38 HRC

Hot hardness:

Temperature °C	Temperature °F	Hardness(a) HB
540	1000	226
650	1200	203
760	1400	167
870	1600	102

(a) Mutual indentation method

Impact strength (Charpy):

Temperature °C	Temperature °F	Type of test	Longitudinal J	Longitudinal ft · lbf
3 mm (1/2 in.) plate(a)				
RT	RT	Unnotched	97.6	72
		Notched	8.1	6
540	1000	Unnotched	110	81
		Notched	20.3	15
675	1250	Unnotched	160	116
		Notched	20.3	15
815	1500	Unnotched	170	126
		Notched	20.3	15

(a) Solution heat treated at 1230 °C (2250 °F), rapid air cooled

Creep and stress-rupture properties. See Table 31.

Physical Properties

Density. 8.380 g/cm^3 (0.303 lb/in.^{3}) at 22 °C (72 °F)
Liquidus temperature. 1355 °C (2470 °F)
Solidus temperature. 1265 °C (2310 °F)
Coefficient of thermal expansion (linear):

Temperature °C	Temperature °F	Mean coefficient μm/m · K	Mean coefficient μin./in. · °F
0–100	32–212	13.9	7.7
0–200	32–392	14.1	7.8
0–300	32–572	14.5	8.0
0–400	32–752	14.7	8.2
0–500	32–932	15.0	8.3
0–600	32–1112	15.3	8.5
0–700	32–1292	15.8	8.8
0–800	32–1472	16.3	9.1
0–900	32–1652	16.9	9.4
0–1000	32–1832	17.4	9.7

Specific heat. 421 J/kg · K (0.101 Btu/lb · °F)

Thermal conductivity. 14.7 W/m · K (8.5 Btu/ft · h · °F) at 22 °C (72 °F)
Electrical resistivity. 910 nΩ · m at 22 °C (72 °F)
Magnetic permeability. <1.2 at 16 kA/m (200 oersteds) at 22 °C (72 °F)

Chemical Properties

General corrosion behavior. Highly resistant to atmospheric oxidation at ordinary temperatures with good resistance to oxidation at elevated temperatures. Also has good resistance to a variety of aqueous corrosive media. Combination of wear and corrosion resistance makes Stellite 6B useful in such applications as food handling machinery and chemical equipment.
Resistance to specific corroding agents. See Table 32.

Table 30 Typical tensile properties for Stellite 6B

Temperature		Tensile strength		Yield strength		Elongation,
°C	°F	MPa	ksi	MPa	ksi	%
1.6 mm (0.063 in.) sheet						
20	68	1010	146	635	92	11
815	1500	510	74	310	45	17
870	1600	385	56	270	39	18
980	1800	230	33	140	20	36
1090	2000	140	20	76	11	44
1150	2100	90	13	55	8	22
13 mm (½ in.) plate						
20	68	1020	148	605	88	7
540	1000	915	133	405	59	9
675	1250	795	115	420	61	9
16 mm (⅝ in.) bar						
20	68	1060	154	640	93	17(a)
315	600	1020	148	515	75	30(a)
540	1000	890	129	460	67	28(a)
815	1500	515	75	325	47	38(a)
870	1600	400	58	260	38	34(a)

Note: All specimens solution heat treated at 1232 °C (2250 °F) and rapid air cooled; limited number of tests. (a) Elongation in 25 mm or 1 in.

Table 31 Typical creep-rupture characteristics for Stellite 6B

	Stress		Initial elongation,		Time (h) for total elongation of:			Elongation of rupture,
Temperature, °C	MPa	ksi	%	Life, h	0.5%	1.0%	2.0%	%
1.6 mm (0.063 in.) sheet								
540	415	60	0.70	192.8(a)	…	…	…	0.8
650	345	50	0.45	361.4	0.5	113.8	…	3.0
760	240	35	0.35	59.3	0.4	3.8	16.3	5.1
815	170	25	0.35	70.6	0.2	4.3	16.9	4.7
870	130	19	0.10	57.9	0.5	2.2	11.1	4.3
925	83	12	0.19	104.0	1.8	20.9	89.9	2.6
980	55	8	0.05	113.4	5.1	22.7	57.6	5.5
1090	18	2.6	0.004	116.7	5.4	…	…	13.3
16 mm (⅝ in.) bar								
540	310	45	0.79	330.8(a)	…	…	…	0.83
	450	65	1.03	329.9	…	…	…	…
650	275	40	0.06	164.6(a)	…	…	…	0.44
	310	45	0.70	367.1	…	15.9	117.5	11.6
	345	50	0.54	282.3(a)	…	163.6	…	1.73
730	240	35	0.37	137.7(a)	1.57	11.3	55.7	3.22
	275	40	0.17	13.6	…	…	…	16.0
	310	45	0.27	62.7	1.03	4.75	9.8	16.9
870	105	15	0.40	130.9	0.03	1.77	7.6	13.3
	125	18	0.42	52.7	0.05	0.68	2.9	11.0
	130	19	0.22	55.9	0.20	0.70	2.4	20.0

Note: Specimens solution heat treated 1232 °C (2250 °F), rapid air cooled prior to testing. (a) Test discontinued before rupture

Table 32 Average corrosion data for Stellite 6B

Media	Concentration, wt%	Test temperature		Average penetration rate(a)(b)	
		°C	°F	mm/yr	mils/yr
Acetic acid	10	BP		0.002	0.08
Acetic acid	30	BP		0.001	0.04
Acetic acid	50	BP		<0.001	0.02
Acetic acid	70	BP		<0.002	0.06
Acetic acid	99	BP		<0.001	0.03
Chromic acid	10	66	150	2.41	95
Formic acid	10	BP		0.51	20
Formic acid	30	BP		0.66	26
Formic acid	50	BP		1.19	47
Formic acid	70	BP		1.27	50
Formic acid	88	BP		0.58	23
Hydrochloric acid	2	RT		<0.003	0.1
Hydrochloric acid	5	RT		1.60	63
Hydrochloric acid	10	RT		2.74	108
Hydrochloric acid	20	RT		2.36	93
Hydrochloric acid	2	66	150	<0.003	0.1
Hydrochloric acid	5	66	150	>25.4	>1000
Hydrochloric acid	10	66	150	>25.4	>1000
Hydrochloric acid	20	66	150	>25.4	>1000
Nitric acid	10	BP		<0.004	0.15
Nitric acid	30	BP		0.15	6
Nitric acid	50	BP		>25.4	>1000
Nitric acid	70	BP		>25.4	>1000
Phosphoric acid	10	BP		Nil	Nil
Phosphoric acid	30	BP		0.05	2
Phosphoric acid	50	BP		0.48	19
Phosphoric acid	70	BP		0.58	23
Phosphoric acid	85	BP		15.5	611
Sodium hydroxide	30	BP		0.33	13
Sulfuric acid	10	RT		<0.001	0.02
Sulfuric acid	30	RT		Nil	Nil
Sulfuric acid	50	RT		0.01	0.4
Sulfuric acid	77	RT		0.02	0.7
Sulfuric acid	10	66	150	<0.001	0.02
Sulfuric acid	30	66	150	<0.003	0.09
Sulfuric acid	50	66	150	>25.4	>1000
Sulfuric acid	77	66	150	4.5	176
Sulfuric acid	2	BP		0.79	31
Sulfuric acid	5	BP		2.31	91
Sulfuric acid	10	BP		3.99	157
Sulfuric acid	20	BP		9.14	360
Sulfuric acid	50	BP		>25.4	>1000
Sulfuric acid	30	BP		>25.4	>1000
Sulfuric acid	77	BP		>25.4	>1000
Ferric chloride (10 days without crevice)	10	RT		0.33(c)	13
Ferric chloride (10 days with crevice bolt)	10	RT		0.23(c)	9(b)
5% ferric chloride + 10% sodium chloride (10 days)	…	RT		0.46(c)	18
2% potassium permanganate + 2% sodium chloride (120 h)	…	90	194	0.20	8

BP, boiling point; RT, room temperature. (a) Determined in laboratory tests. It is recommended that samples be tested under actual plant conditions. (b) Corrosion rates for all duplicate samples based on an average of 4-24 hour test periods. (c) Samples pitted during test

Stellite 6K

Chemical Composition

Composition limits. 28.00 to 32.00 Cr; 3.50 to 5.50 W; 3.00 max Fe; 3.00 max Ni; 2.00 max Si; 2.00 max Mn; 1.40 to 1.90 C; 1.50 max Mo; bal Co

Applications

Typical uses. Machine knives for cutting rubber, plastics, wood, leather, food products, synthetic fibers, and paper

Mechanical Properties

Tensile properties. See Table 33.
Compressive properties. Compressive strength, sheet: 2240 MPa (325 ksi)
Hardness. 2 mm (0.063 in.) sheet, 46 HRC; 13 mm (0.5 in.) and 23 mm ($^7/_8$ in.) plate 45 HRC

Physical Properties

Density. 8.38 g/cm^3 (0.303 lb/in.^{3}) at 22 °C (72 °F)

Table 33 Typical tensile properties for Stellite 6K

Temperature		Tensile strength		Yield strength		Elongation,
°C	°F	MPa	ksi	MPa	ksi	%
1.6 mm (0.063 in.) sheet						
20	68	1220	177	710	103	4
650	1200	1010	146	…	…	8
815	1500	485	70	310	45	17
980	1800	235	34	130	19	28
1090	2000	115	17	59	8.6	53
13 mm ($^1/_2$ in.) and 23 mm ($^7/_8$ in.) plate						
20	68	1010	146	745	108	1
316	600	785	114	560	81	2
540	1000	730	106	515	75	3

Note: All specimens solution heat treated at 1232 °C (2250 °F) and rapid air cooled; limited number of tests

Liquidus temperature. 1317 °C (2403 °F)
Solidus temperature. 1257 °C (2295 °F)
Coefficient of thermal expansion (linear):

Temperature		Mean coefficient	
°C	°F	μm/m · K	μin./in. · °F
0–100	32–212	13.8	7.7
0–200	32–392	13.8	7.7
0–300	32–572	13.8	7.7
0–400	32–752	13.8	7.7
0–500	32–932	13.8	7.7
0–600	32–1112	14.0	7.8
0–700	32–1292	14.2	7.9
0–800	32–1472	14.5	8.1
0–900	32–1652	14.9	8.3
0–1000	32–1832	15.5	8.6

Magnetic permeability. <1.2 at 16 kA/m (200 oersteds) at 22 °C (72 °F)

Ultimet

Specifications

ASTM. B 815 (rod) and B 818 (sheet, strip, plate)
ASME. Section VIII, Division 1, Code Case 2121
NACE International. MR0175-94
DIN specification. CoCr26Ni9Mo5W, No. 2.4681
UNS number. R31233

Chemical Composition

Nominal composition. 54 Co; 26 Cr; 9 Ni; 5 Mo; 3 Fe; 2 W; 0.3 Si; 0.08 N; 0.06% C

Applications

Typical uses. Agitators, blenders, bolts, dies, extruders, fan blades, filters, glass plungers, nozzles, pumps, rolls, screw conveyors, and valve parts requiring a combination of high wear resistance, corrosion resistance, and high tensile strength

Mechanical Properties

Tensile properties. See Table 34.

Hardness:

Condition	Form	Hardness
Mill annealed	Sheet	HRC 30
10% cold worked	Sheet	HRC 40
20% cold worked	Sheet	HRC 43
40% cold worked	Sheet	HRC 49
As-cast	Investment	HB 96

Elastic modulus. See Table 35.
Impact strength. See Table 36.

Physical Properties

Density. 8.47 g/cm^3 (0.306 lb/in.^{3})
Melting range. 1332 to 1354 °C (2430 to 2470 °F)
Mean coefficient of thermal expansion:

Temperature range		Average coefficient	
°C	°F	μm/m · K	μin./in. · °F
26–93	78–200	13.0	7.2
26–204	78–400	13.5	7.5
26–316	78–600	14.0	7.8
26–427	78–800	14.5	8.0
26–538	78–1000	14.8	8.2
26–649	78–1200	15.1	8.4
26–760	78–1400	15.9	8.8
26–871	78–1600	16.4	9.1
26–982	78–1800	16.9	9.4

Thermal conductivity:

Temperature		Conductivity	
°C	°F	W/m · K	Btu · in./h · ft^2 · °F
23	73	12.3	85
100	212	13.8	96
200	392	15.6	108
300	572	17.5	121
400	752	19.4	134
500	932	21.5	149
600	1112	23.9	166

Electrical resistivity:

Temperature		Resitivity	
°C	°F	μΩ/m	μΩ/in.
23	75	0.87	34.2
100	212	0.89	35.4
200	392	0.93	36.6
300	572	0.96	38.1
400	752	1.00	39.3
500	932	1.03	40.5
600	1112	1.05	41.3

Chemical Properties

General corrosion behavior. Ultimet is considered a "corrosion-wear" resistant alloy that of-

Table 34 Typical tensile properties for solution heat treated Ultimet

Form	Test temperature °C	Test temperature °F	Ultimate tensile strength MPa	Ultimate tensile strength ksi	Yield strength at 0.2% offset MPa	Yield strength at 0.2% offset ksi	Elongation in 50 mm (2 in.), %
Sheet 1.6 mm (0.063 in.)	RT		952	138	496	72	42
	93	200	931	135	400	58	50
	204	400	924	134	310	45	62
	316	600	896	130	296	43	75
	427	800	827	120	283	41	76
Plate 6.3–38.1 mm (¼–1½ in.)	RT		1020	148	545	79	36
	93	200	986	143	483	70	40
	204	400	986	143	379	55	61
	316	600	952	138	331	48	70
	427	800	917	133	310	45	70
	538	1000	862	125	262	38	70
	649	1200	683	99	255	37	66
	760	1400	524	76	269	39	70
	871	1600	352	51	193	28	77
	982	1800	214	31	110	16	100
Bar 12.7–50.8 mm (½–2 in.)	RT		1014	147	524	76	38
	93	200	965	140	483	70	49
	204	400	965	140	359	52	66
	316	600	910	132	303	44	77
	427	800	903	131	296	43	84
	538	1000	793	115	276	40	79

RT, room temperature

fers corrosion resistance to many aggressive environments comparable to that of the molybdenum-bearing Hastelloy alloys (particularly with regard to oxidizing acids and to localized corrosion), while exhibiting wear resistance comparable to that of Stellite alloys (particularly with regard to cavitation-erosion, slurry-erosion, and galling). It is also resistant to high-temperature forms of corrosive attack, for example, oxidation, molten zinc, and sulfidation.

Resistance to specific corroding agents. See Table 37.

Table 35 Typical dynamic modulus of elasticity for Ultimet

Form	Condition	Test temperature °C	Test temperature °F	Average dynamic modulus of elasticity GPa	Average dynamic modulus of elasticity 10^6 psi
Plate	Heat-treated at	204	400	215	31.2
	1120 °C	316	600	206	29.9
	(2050 °F),	427	800	197	28.6
	water quenched	538	1000	189	27.4
		649	1200	180	26.1

Table 36 Typical room-temperature impact strength for Ultimet plate

Aging temperature °C	Aging temperature °F	Aging time, h	V-notch strength J	V-notch strength ft · lbf
Mill annealed		…	176	130
204	400	100	191	141
		1000	203	150
316	600	100	203	150
		1000	217	160
538	1000	100	217	160
		1000	206	152
649	1200	100	159	117
		1000	26	19
761	1400	100	26	19
		1000	9	7
871	1600	100	31	23
		1000	23	17
982	1800	100	76	56
		1000	60	44

Table 37 Comparative corrosion data for Ultimet and other alloys

	Concentration, wt%	Test temperature °C	Test temperature °F	Average corrosion rate, mm/yr (mils/yr) Ultimet alloy	6B alloy	C-276 alloy	Alloy 20Cb-3
Hydrochloric acid	1	BP		0.0075 (0.3)	4.25 (170)	0.33 (13)	2.03 (81)
Nitric acid	65	BP		0.15 (6)	135.8 (5434)	21.2 (848)	0.2 (8)
P_2O_5 (commercial grade)	54	116	240	0.2 (8)	0.38 (15)	0.7 (28)	0.9 (36)
Sulfuric acid	10	BP		2.48 (99)	5.8 (232)	0.45 (18)	0.55 (22)
Sulfuric acid + 1.2% HCl + 1% $FeCl_3$ + 1% $CuCl_2$ (ASTM G 28B)	11.5	BP		0.05 (2)	72.2 (2888)	1.38 (55)	68.0 (2720)
Sulfuric acid + 42 g/L $Fe_2(SO_4)_3$ (ASTM G 28A)	50	BP		0.2 (8)	0.35 (14)	6.25 (250)	0.25 (10)

UMCo-50 (Haynes 150)

Chemical Composition

Composition limits. 48 to 52 Co; 27 to 29 Cr; 0.5 to 1.0 Mn; 0.5 to 1.0 Si; 0.05 to 0.12 C; 0.02 max P; 0.02 max S; bal Fe

Applications

Typical uses. Furnace grates, trays, and rolls; skids and rails in heat treating furnaces; slag-notch rings and tundishes

Mechanical Properties

Tensile properties. See Table 38.
Hardness. See Table 38.
Elastic modulus. Tension, 215 GPa (31.5 × 10^6 psi)
Impact strength. Charpy, 95 J (70 ft · lb) at 20 °C (68 °F)
Creep-rupture characteristics. See Table 39.

Physical Properties

Density. 8.050 g/cm^3 (0.29 lb/$in.^3$)
Liquidus temperature. 1395 °C (2540 °F)
Solidus temperature. 1380 °C (2515 °F)
Coefficient of thermal expansion. Linear, 16.8 µm/m · K (9.33 µin./in. · °F) at 20 to 1000 °C (68 to 1830 °F)
Thermal conductivity. 8.9 W/m · K (5.1 Btu/ft · h · °F) at 20 °C (68 °F)
Electrical resistivity. 825 nΩ · m at 25 °C (77 °F)

Chemical Properties

General corrosion behavior. Resistant to attack by dilute sulfuric acid and by boiling nitric acid; rapidly attacked by hydrochloric acid.

High degree of oxidation resistance, for example, comparable to 25Cr-20Ni steel in air up to 1200 °C (2190 °F). High degree of hot corrosion resistance to oxidizing-sulfidizing environments as well as in combustion products from sulfur-bearing fuel oils. Resistant to molten copper but rapidly attacked by molten aluminum.

Table 38 Typical tensile properties and hardness for UMCo-50 alloy

Temperature		Tensile strength		0.2% offset yield strength		Elongation,	Hardness,
°C	°F	MPa	ksi	MPa	ksi	%	HV
UMCo-50, as-cast							
25	70	550	80.0	315	45.6	8	250
700	1290	195	28.6	150	21.4	19	163
900	1650	130	18.6	110	15.7	9	72
1000	1830	79	11.4	69	10.0	18	…
UMCo-50, wrought							
25	70	925	134	610	88.5	10	350
500	930	885	128	570	83.0	23	…
700	1290	325	47	225	32.8	21	210
900	1650	155	22.8	150	21.4	12	…
1000	1830	79	11.4	59	8.6	18	…

Table 39 Typical creep resistance of wrought UMCo-50

Temperature		Stress to cause creep elongation of: 1%		0.5%	
°C	°F	MPa	ksi	MPa	ksi
In 10 h					
850	1560	61	8.9	55	8.0
900	1650	35	5.1	30	4.3
950	1740	23	3.3	19	2.7
1000	1830	16	2.3	14	2.0
In 100 h					
800	1470	61	8.9	53	7.7
850	1560	34	5.0	30	4.3
900	1650	21	3.1	18	2.6
950	1740	14	2.1	12	1.8
In 1000 h					
750	1380	64	9.3	58	8.4
800	1470	34	5.0	30	4.3
850	1560	21	3.1	18	2.6
900	1650	14	2.1	12	1.7
In 10,000 h					
700	1290	72	10.4	63	9.2
750	1380	37	5.3	32	4.6
800	1470	21	3.1	19	2.7
850	1560	14	2.1	12	1.8

X-40/X-45

Specifications

AMS. 5382 (investment castings)

Chemical Composition

Typical composition. 54.0 Co; 25.5 Cr; 10.5 Ni; 7.5 W; 0.75 Mn; 0.75 Si; 0.50 C; 0.25 C for X-45

Mechanical Properties

Tensile properties. See Table 40.

Stress-rupture characteristics (typical):

Temperature		Rupture strength	
°C	°F	MPa	ksi
At 100 h			
650	1200	385	56
760	1400	260	38
870	1600	140	20
980	1800	76	11
At 1000 h			
650	1200	350	51
760	1400	230	33
870	1600	110	16
980	1800	68	9.8

Physical Properties

Density. 8.60 g/cm^3 (0.311 lb/in.^{3}) at 20 °C (68 °F)

Coefficient of thermal expansion (linear):

Temperature		Coefficient	
°C	°F	μm/m · K	μin./in. · °F
315	600	14.0	7.8
425	800	14.6	8.1
540	1000	15.1	8.4
650	1200	15.8	8.75
760	1400	16.6	9.2

Thermal conductivity:

Temperature		Conductivity	
°C	°F	W/m · K	Btu/ft · h · °F
21	70	11.8(a)	6.8(a)
93	200	13.5	7.8
205	400	15.1	8.7
315	600	17.9	10.3
425	800	19.1	11.0
540	1000	21.6	12.5
650	1200	22.8(a)	13.2(a)

(a) Extrapolated values

Table 40 Typical mechanical properties of X-40

Temperature		Tensile strength		Yield strength		Elongation,
°C	°F	MPa	ksi	MPa	ksi	%
21	70	745	108	525	76	9
540	1000	550	80	275	40	17
650	1200	515	75	260	38	12
760	1400	485	70	…	…	10
870	1600	325	47	…	…	16
980	1800	200	29	…	…	31

ASM Specialty Handbook: Nickel, Cobalt, and Their Alloys
J.R. Davis, editor, p 387-394
DOI:10.1361/ncta2000p387

Copyright © 2000 ASM International®
All rights reserved.
www.asminternational.org

Wear Behavior of Cobalt Alloys

THE SINGLE LARGEST APPLICATION for cobalt alloys is for wear resistance. As shown in Table 1, weld overlay (hardfacing) alloys, wrought alloy 6B (UNS R30016) and its higher carbon version 6K, and Ultimet (R31233) are the alloys most frequently employed for wear resistant applications. It should be noted, however, that some cobalt alloys developed for heat resistant applications (e.g., alloy 25) or corrosion resistant applications (e.g., MP35N) also exhibit very good wear resistance when compared to other ferrous or nonferrous alloys.

In this article, emphasis has been placed on wear data generated on wrought and hardfacing alloys. Chemical composition, mechanical and physical properties, and the metallurgy associated with these alloys can be found in the article "Cobalt-Base Alloys" in this Volume. In addition, that article also describes some cobalt alloys processed by powder metallurgy methods that are used for wear components.

Types of Wear

There are several distinct types of wear, which generally fall into three main categories:

- Abrasive wear
- Sliding wear
- Erosive wear

The type of wear encountered in a particular application is an important factor that influences the selection of a wear resistant material.

Abrasive Wear

Mechanisms. Abrasive wear is encountered when hard particles, or hard projections (on a counterface) are forced against, and moved relative to, a surface. The terms *high-stress* and *low-stress abrasion* relate to the condition of the abrasive medium (be it hard particles or projections) after interaction with the surface. If the abrasive medium is crushed, then the high-stress condition is said to prevail. If the abrasive medium remains intact, the process is described as *low-stress abrasion.* Typically, high-stress abrasion results from the entrapment of hard particles between metallic surfaces (in relative motion), while low-stress abrasion is encountered when moving surfaces come into contact with packed abrasives, such as soil and sand.

Materials Performance. In alloys such as the cobalt-base wear alloys, which contain a hard phase, the abrasion resistance generally increases as the volume fraction of the hard phase increases. Abrasion resistance is, however, strongly influenced by the size and shape of the hard phase precipitates within the microstructure, and the size and shape of the abrading species.

Sliding Wear

Of the three major types of wear, sliding is perhaps the most complex, not in concept, but in the way different materials respond to sliding conditions. Sliding wear is a possibility whenever two surfaces are forced together and moved relative to one another. The chances of damage are increased markedly if the two surfaces are metallic in nature, and if there is little or no lubrication present.

Mechanisms. Sliding wear generally occurs by one or more of three mechanisms. In the first mechanism, oxide control of the sliding wear process, along with low wear rates, are experienced when surface temperatures are high, by virtue of either a high ambient temperature or frictional heating. This is because oxide growth rates increase dramatically with temperature. In some cases, so-called "oxide glazes" are formed on the surfaces. These "oxide glazes" are very smooth, highly reflective regions, caused by the shearing of oxide asperities (peaks) and redistribution of the oxide debris in the surface valleys. There are times when the oxide debris, if trapped as discrete particles or flakes between the sliding surfaces, can become abrasive. This is an important consideration when the surfaces oscillate with respect to one another over small amplitudes. The combined sliding-abrasive wear mechanism set up under these conditions is known as fretting.

Table 1 Typical applications of various cobalt-base wear resistant alloys

Applications	Alloy	Forms	Mode of degradation
Automotive industry			
Engine valve seating surfaces	6, F	Weld overlay	Solid-particle erosion, hot corrosion
Power industry			
Control valve seating surfaces	6, 21	Weld overlay	Sliding wear, cavitation erosion
Steam turbine erosion shields	Alloy 6B	Wrought sheet	Liquid-droplet erosion, particulate erosion
Marine industry			
Rudder bearings	306	Weld overlay	Sliding wear
Steel industry			
Hot shear edges	6	Weld overlay	Sliding wear, impact, abrasion
Bar mill guide rolls	12	Weld overlay	Sliding wear, impact, abrasion
Electrogalvanizing rolls	Ultimet	Wrought sheet	Erosion-corrosion
Chemical processing industry			
Control valve seating surfaces	6	Weld overlay	Sliding wear, cavitation erosion
Plastic extrusion screw flights	1, 6, 12	Weld overlay	Sliding wear, abrasion
Pump seal rings	6, 12	Weld overlay	Sliding wear
Dry battery molds	4	Casting	Abrasion
Pulp and paper industry			
Chain saw guide bars	6, alloy 6B	Weld overlay, wrought sheet	Sliding wear, abrasion
Textile industry			
Carpet knives	6K, 12	Wrought sheet, weld overlay	Abrasion
Oil and gas industry			
Rotary drill bearings	190	Weld overlay	Abrasion, sliding wear

The second mechanism of sliding wear is normally associated with high contact stresses and assumes breakdown of the oxide films to the point where true metal-to-metal contact is established. Under these conditions, there is an opportunity for cold welding of the surfaces to occur, and for subsequent movement to result in fracture of small pieces away from the original interface (normally in the weaker of the two mating materials). Damage caused by this mechanism is termed galling. Substantial metal transfer from one surface to the other and gross deformation of surface materials are typical of this condition.

The third mechanism of sliding wear, which can also produce substantial metallic damage, is one of subsurface fatigue. This mechanism is associated with cyclic stress conditions caused by materials periodically pressing on one another. Material is lost through fatigue crack nucleation and growth at a specific depth.

Materials Performance. The metallic materials that perform well under sliding conditions do so either by virtue of their oxidation behavior or their ability to resist deformation and fracture. Little is known of the influence of metal-to-metal bond strength during cold welding. For materials such as the cobalt-base wear alloys with a hard phase dispersed throughout a softer matrix, the sliding-wear properties are controlled predominantly by the matrix. Indeed, within the cobalt alloy family, resistance to galling is generally independent of hard-particle volume fraction and overall hardness.

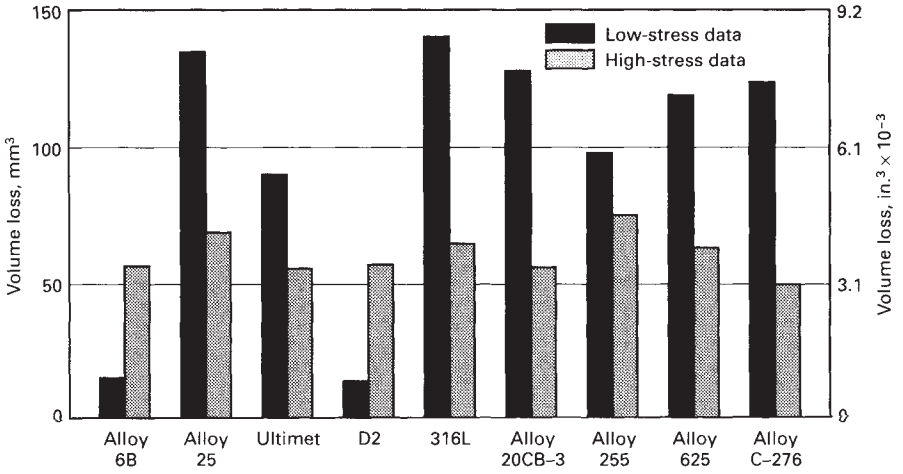


Fig. 1 Room-temperature abrasion test results of wrought cobalt-base alloys compared with other alloys. (a) Low-stress data per ASTM G 65 dry sand and rubber wheel test (procedure B). (b) High-stress data per ASTM B 611 slurry and steel wheel test. See Fig. 2 for the test apparatus and test parameters.

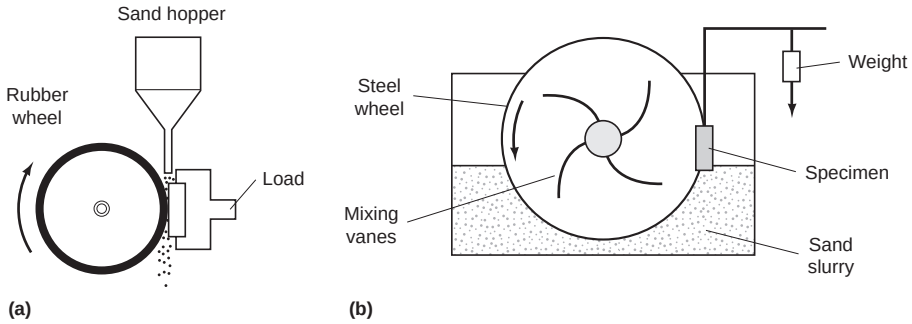


Fig. 2 Standard tests used to obtain abrasive-wear data. (a) ASTM G 65 dry sand and rubber wheel test (procedure B) for obtaining low-stress abrasion data. Test parameters: load, 13.6 kg (30 lb); flow rate, 390 g/min (0.86 lb/min); wheel speed, 200 rev/min; test revolutions, 2000. (b) ASTM B 611 slurry and steel wheel test for obtaining high-stress abrasion data. Test parameters: load, 22.7 kg (50 lb); slurry, 1500 g (3.3 lb) sand plus 940 g (2.1 lb) water; wheel speed, 240 rev/min; test revolutions, 250. Both tests use quartz sand of 212 –300 μm diam as abrasive.

Erosive Wear

Four distinct forms of erosive wear have been identified:

- Solid-particle erosion
- Liquid-droplet erosion
- Cavitation erosion
- Slurry erosion

Solid-particle erosion is caused by the impingement of small, solid particles against a surface. The solid particles themselves are typically airborne or entrained in some other gaseous environment. Particle sizes typically range from 5 to 500 μm. Typical velocities associated with solid-particle erosion range from 2 m/s (6 ft/s) in fluid bed combustors to 500 m/s (1650 ft/s). The rate of solid-particle erosion depends on the velocity of the particles, their impingement angle (the angle dependency generally is different for ductile materials than it is for brittle materials), and the nature of the erodent (shape, size, strength).

Slurry erosion, or liquid-solid particle erosion, is similar to solid-particle erosion, except that there are differences in the viscosity of the carrier fluid (gas in solid-particle erosion, liquid carrier in slurry erosion). Slurry erosion occurs at the surfaces impinged by the solid particles in the liquid stream. The similarity to abrasion arises from the fact that the particles are hydrodynamically forced against the surface.

Liquid-Droplet and Cavitation Erosion. Although quite different mechanistically, liquid-droplet erosion and cavitation erosion have a similar effect on a surface. They both result in a succession of shock (or stress) waves into the surface. For this reason, those materials that resist liquid-droplet erosion also perform well under cavitation conditions and vice versa.

Liquid-droplet erosion is easily envisaged, whereas cavitation erosion is a more complex phenomenon. For cavitation erosion to occur, the surface must be in contact with a liquid undergoing pressure changes. Surface damage results from the collapse of near-surface bubbles in the liquid, or, more precisely, from the action of liquid jets that arise during bubble implosion. The bubbles themselves are created when the pressure in the liquid falls below its vapor pressure. Collapse is induced by subsequent pressure increases.

Materials Performance. The abrasion resistance of cobalt-base alloys, like other wear resistant alloys, generally depends on the hardness of the carbide phases and/or the metal matrix. With the complex mechanisms of solid-particle and slurry erosion, however, such generalizations may not be warranted. In solid-particle erosion, for example, ductility can also be a factor (see the discussion on solid-particle impingement erosion in the following section of this article "Wrought Alloy Wear Data").

As for liquid-droplet or cavitation erosion, the performance of a material largely depends on its ability to absorb the shock (stress) waves without, essentially, microscopic fracture. In cobalt-base wear alloys, it has been found that carbide volume fraction (hence, bulk hardness) has very little effect on resistance to liquid-droplet and cavitation erosion (Ref 1). Much more important are the properties of the matrix.

Wrought Alloy Wear Data

Abrasive Wear Data

The low-stress and high-stress abrasive wear characteristics for three wrought cobalt alloys, relative to other common alloys, are shown in Fig. 1. The test apparatus and/or parameters used to obtain these data are shown in Fig. 2.

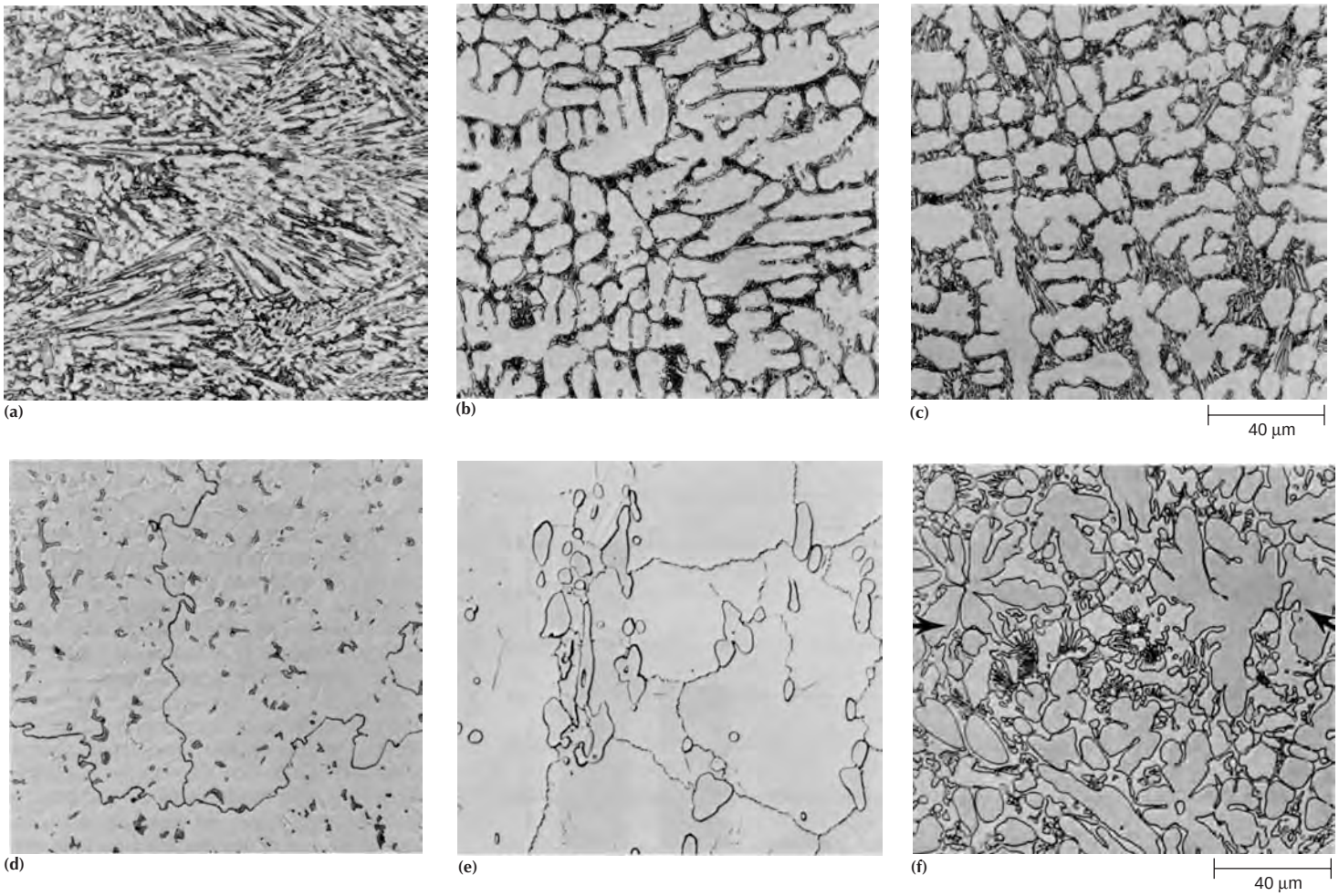


Fig. 3 Microstructures of various cobalt-base wear resistant alloys. (a) Stellite 1, two-layer GTA deposit. (b) Stellite 6, two-layer GTA deposit. (c) Stellite 12, two-layer GTA deposit. (d) Stellite 21, two-layer GTA deposit. (e) Haynes alloy 6B, 13 mm (0.5 in.) plate. (f) Tribaloy alloy (T-800) showing the Laves precipitates (the largest continuous precipitates, some of which are indicated with arrows). All 500×

Review of these room-temperature data reveals:

- The importance of hard phases (carbides) within the microstructure, under conditions conducive to low-stress abrasion
- Their lack of importance under high-stress conditions. (The performance of the carbide-containing alloy 6B is similar to that of the carbide-free Ultimet alloy.)

Low-Stress Abrasive Wear. The importance of the carbide precipitates, in particular their size and shape, under low-stress conditions can be appreciated by comparing the microstructures and volume losses for alloy 6B and alloy 6 in Fig. 3 and 4, respectively. Large blocky carbides have been found to be of most benefit under such conditions (Ref 2). Table 2 compares the low-stress volume losses of various alloys, including Ultimet, alloy 6B, and hardfacing alloys Stellite 1, 6 and 21.

The low-stress abrasion results for alloy 25, Ultimet, stainless steels, and the high-nickel alloys correlate well with the annealed hardnesses of the samples (Table 3) with the exception of alloy 25.

High-Stress Abrasive Wear. For the high-stress test, no relationship between room-temperature hardness and performance is evident (Table 2). In fact, all the alloys, including alloy 6B and D2 tool steel, fall within a narrow performance band, suggesting that resistance to fracture is at least as important as resistance to deformation under such conditions. It is note worthy that the duplex (austenitic-ferritic) microstructure of alloy 255 is beneficial under low-stress conditions, but detrimental in the high-stress case.

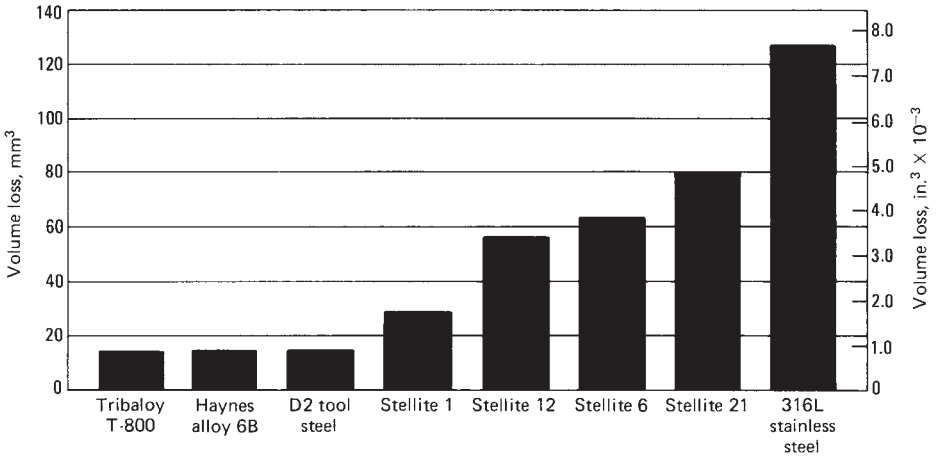


Fig. 4 Low-stress abrasion data for various cobalt-base alloys tested per ASTM G 65 (procedure B). The benefits of wrought processing (refer to alloy 6B) and the effectiveness of the Laves phase are evident.

Table 2 Comparative resistance to abrasion for various alloys

Material	Volume loss, mm^3 ($in.^3 \times 10^{-3}$)	
	Low stress (a)	High stress (b)
Ultimet alloy	90.4 (5.5)	56.1 (3.4)
Haynes 6B alloy	15.3 (0.9)	57.0 (3.5)
Haynes 625 alloy	119.3 (7.3)	63.4 (3.9)
Hastelloy C-22 alloy	114.0 (7.0)	64.9 (4.0)
Hastelloy C-276 alloy	123.5 (7.5)	49.8 (3.0)
Ferralium alloy 255	97.5 (5.9)	75.0 (4.6)
Type 316L stainless steel	140.4 (8.6)	64.8 (3.9)
Type D-2 tool steel (HRC 60)	15.2 (0.9)	56.9 (3.5)
Carpenter 20Cb-3 alloy	127.9 (7.8)	56.4 (3.4)
Nitronic 60	145.8 (8.9)	…
Type 1020 carbon steel	130.0 (7.9)	…
Stellite 1 (c)	29.4 (1.8)	…
Stellite 6 (c)	63.8 (3.9)	…
Stellite 21 (c)	80.3 (4.9)	…

(a) Data per ASTM G 65. (b) Data per ASTM B 611 (c) Two-layer gas-tungsten arc weld deposit. Source: Haynes International data sheet on Ultimet alloy

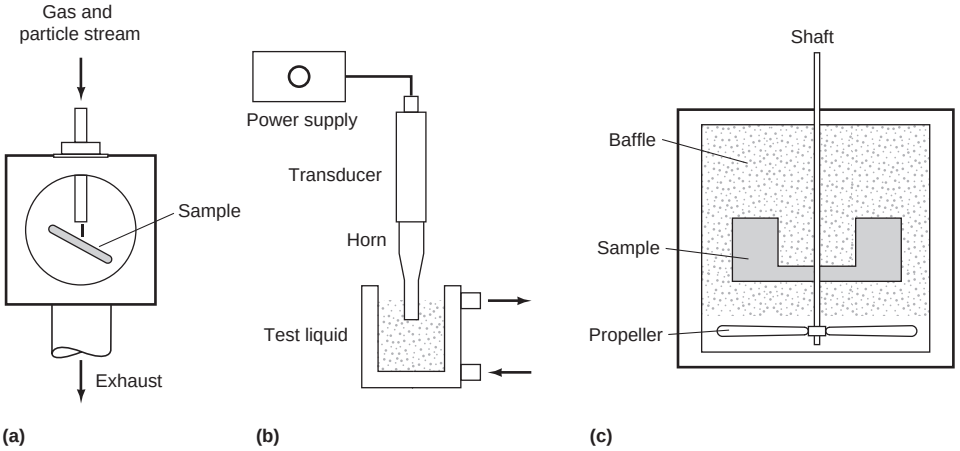


Fig. 5 Tests used to obtain erosive wear data. (a) ASTM G 76 solid-particle test. See Fig. 6–9 for test parameters. (b) ASTM G 32 cavitation test. Test parameters: frequency, 20 kHz; amplitude, 0.05 mm (0.002 in.); test liquid, distilled water; test duration, 24 h; test temperature, 16 °C (61 °F). (c) Slurry test. Test parameters: medium, 80 μm alumina in tap water; velocity, 5 m/s (16.4 ft/s); particle loading, 0.12 kg/L; test duration, 40 h; test temperature, 20 °C (70 °F)

Table 3 Annealed hardnesses of low-stress abrasion samples of wrought cobalt-base alloys relative to other alloys

Alloy	Hardness, HRC
Alloy 6B	38.1
Alloy 25	24.7
Ultimet	35.6
D2 tool steel	59.5
316L stainless steel	81.6(a)
Alloy 20Cb-3	86.8(a)
Alloy 255	27.2
Alloy 625	20.2
Alloy C-276	89.8(a)

(a) HRB

Erosive Wear Data

Solid-Particle Impingement Erosion. To define the behavior of the cobalt-base wrought alloys under solid-particle impingement erosion conditions, the results of two independent studies (using the ASTM G 76 test apparatus shown in Fig. 5a) are presented in graphical form in Fig. 6 to 9. In the first study by Ninham (Ref 3), alloy 6B and alloy 188 were compared with alloy C-276, alloy 255, and alloy 718 at three impact angles (30, 60, and 90°) and for two types of erodent (silicon carbide particles of 250 to 300 μm, or 0.010 to 0.012 in., diameter and angular quartz particles of 70 to 200 μm, or 0.003 to 0.008 in., diameter). To assess the influence of alloy condition, alloy 188 and alloy C-276 were tested in both the solution-annealed and 30% cold-worked conditions, and alloy 718 was tested in both the solution-annealed and aged (precipitation-hardened) condition. Alloy 6B was tested in the solution-annealed condition, and alloy 255 was cold worked by 30% prior to being tested.

Review of the data from Ref 3 (Fig. 6 and 7), which were generated at room temperature, reveals the following:

- For a given erodent and impact angle, there is little to differentiate the alloys tested.
- Neither cold working nor precipitation hardening has a strong effect on solid-particle erosion resistance.
- For silicon carbide, erosion rate decreases as impact angle increases, in the range 30 to 90°; this is consistent with other erosion studies of ductile materials (Ref 4).
- For quartz, this relationship does not apply because the materials tested have exhibited a maximum erosion rate at an impact angle of 60°; alloy 6B is one of the two exceptions in this regard, having exhibited a maximum erosion rate at 90°.

In the second solid-particle erosion study involving the cobalt-base wrought alloys, alloy 6B, alloy 25, and Ultimet alloy were compared with alloy C-276, type 316L stainless steel, alloy 625, and 20Cb-3 alloy at both room temperature and elevated temperature. In this case, all samples were in the solution-annealed condition, and the tests were run at a particle velocity of 20 m/s (70 ft/s), as opposed to 60 m/s (200 ft/s) for the previous work. The

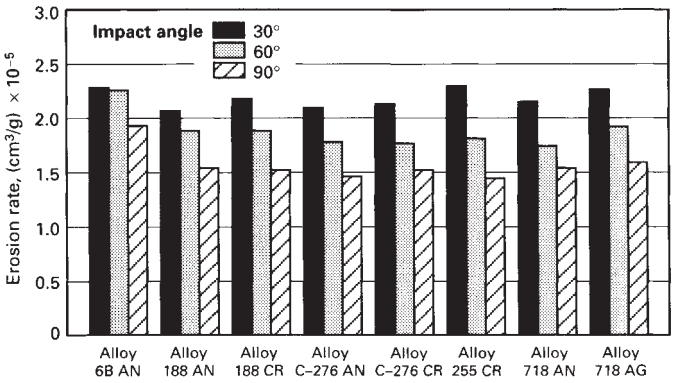


Fig. 6 Solid-particle impingement erosion test (ASTM G 76) results to compare cobalt-base alloys with selected alloys using a 250–300 μm (0.010–0.012 in.) diam silicon carbide erodent at impact angles of 30, 60, and 90°. Tests conducted at room temperature with 60 m/s (200 ft/s) particle velocity. AN, annealed; CR, cold reduced; AG, aged. Source: Ref 3

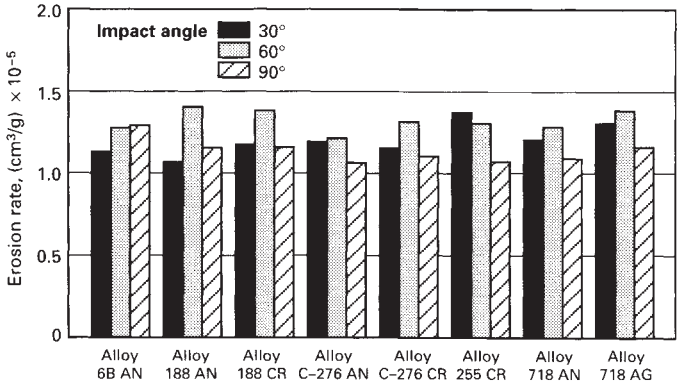


Fig. 7 Solid-particle impingement erosion test (ASTM G 76) results to compare cobalt-base alloys with selected alloys using a 75 to 200 μm (0.003 to 0.008 in.) diam quartz erodent at impact angles of 30, 60 and 90°. Tests conducted at room temperature with 60 m/s (200 ft/s) particle velocity. AN, annealed; CR, cold reduced; AG, aged. Source: Ref 3

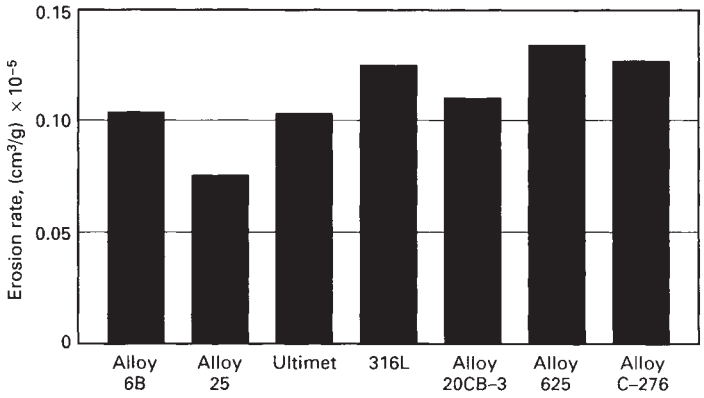


Fig. 8 Solid-particle impingement erosion test (ASTM G 76) results to compare cobalt-base alloys with selected alloys using a 400 μm (0.016 in.) mean diam silicon carbide erodent at an impact angle of 60°. Test parameters: test temperature, 20 °C (70 °F); particle velocity, 20 m/s (65 ft/s); particle feed rate, 0.02 g/s (4 × 10^{-5} lb/s)

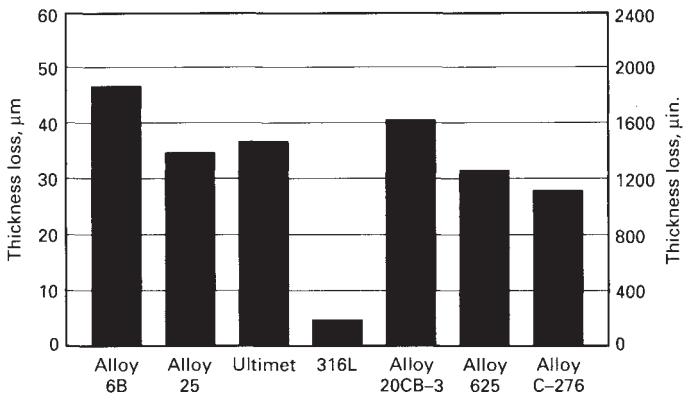


Fig. 9 Solid-particle impingement erosion test (ASTM G 76) results to compare cobalt-base alloys with selected alloys using an 80 μm (0.003 in.) mean diam alumina erodent at an impact angle of 30°. Test parameters: test temperature, 850 °C (1560 °F); particle velocity, 20 m/s (65 ft/s); particle feed rate, 0.02 g/s (4 × 10^{-5} lb/s)

room-temperature tests (the results of which are shown in Fig. 8) were performed with silicon carbide particles of 400 μm (0.016 in.) diameter, at an impact angle of 60°. The elevated-temperature (850 °C, or 1560 °F) tests were run with 80 μm (0.003 in.) diameter alumina particles at an impact angle of 30°; the results are shown in Fig. 9.

Under the conditions of the room-temperature test, the three cobalt-base alloys exhibited the lowest erosion rates. Alloy 25, in particular, was significantly more resistant to erosion than the other test alloys. At elevated temperature, however, 316L was by far the most erosion-resistant material, presumably due to the characteristics of the oxide scale during impingement.

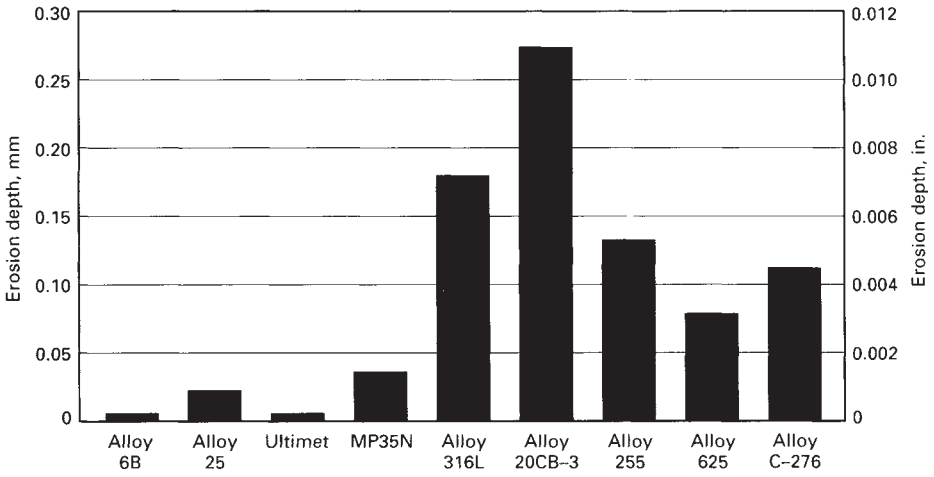


Fig. 10 Vibratory cavitation erosion test (ASTM G 32) results to relate cobalt-base wrought alloys with comparable alloys. All samples were solution annealed with the exception of MP35N alloy, which was tested in the work-hardened condition. See Fig. 5(b) for test parameters.

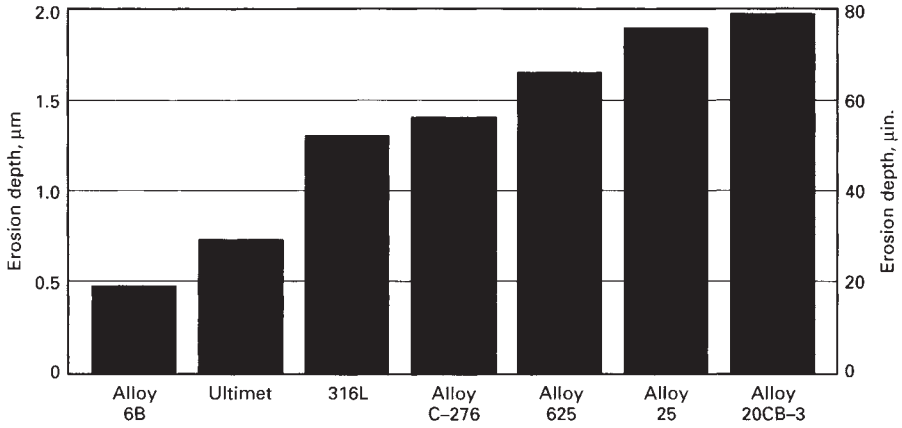


Fig. 11 Slurry erosion pot test data to relate cobalt-base wrought alloys with comparable alloys. See Fig. 5(c) for test parameters

Cavitation Erosion. Comparison of the cavitation erosion resistance of several cobalt-, nickel-, and iron-base alloys (Fig. 10) using the ASTM G 32 test apparatus shown in Fig. 5(b) indicates that cobalt is extremely beneficial in this type of wear. In Ref 5, the outstanding cavitation properties of the cobalt-base alloys are attributed to the low stacking fault energies of their face-centered cubic (fcc) structures. These energies, it is believed, lead to planar slip, which in turn delays crack nucleation (assuming the cavitation process is similar to high-cycle fatigue on a fine scale). References 1 and 6, on the other hand, suggest that the fcc to hexagonal close-packed (hcp) transformation is important (in the latter case because it enhances fatigue life by reducing internal strain).

The effect of carbon content (hence carbide volume fraction, and, indirectly, hardness) on cavitation erosion resistance was studied in Ref 1. In the range studied (0.12–1.35 wt%), carbon content was found to have little effect above about 0.3 wt%. Below this level, cavitation erosion resistance was found to decrease with decreasing carbon content, although these experiments addressed neither the issue of solubility limit nor the effect of carbon within the soluble range. It is interesting to note that the cavitation erosion resistance of Ultimet alloy (the carbon content of which is within the soluble range) is similar to that of alloy 6B (at 1.0 wt% C).

Slurry Erosion. The slurry erosion properties of alloy 6B, alloy 25, and Ultimet alloy are presented in Fig. 11, together with data for commonly used stainless steels and nickel-base alloys. From these data, it is evident that cobalt as an alloy base can be beneficial, although the performance of alloy 25 in this test (the details of which are described in Ref 7) was poor relative to most of the other alloys tested. It is also

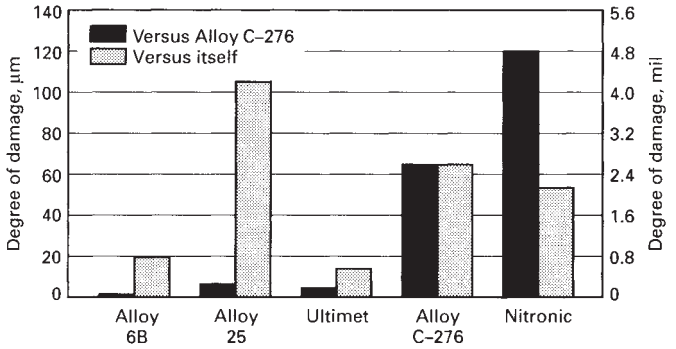


Fig. 12 Comparison of galling test data for cobalt-base wrought alloys with other selected alloys. Pin-on-block test parameters: test temperature, 20 °C (70 °F); number of strokes, 10 strokes through 120° arc; load, 2722 kg (6000 lb)

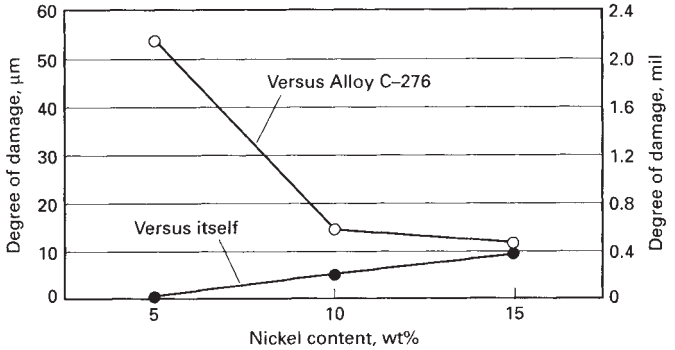


Fig. 13 Effect of nickel content on the antigalling properties of Ultimet alloy. Pin-on-block test parameters: test temperature, 20 °C (70 °F); number of strokes, 10 strokes through 120° arc; load, 2722 kg (6000 lb)

evident that carbide precipitates within the microstructure can be beneficial (comparing the erosion depths for alloy 6B and Ultimet alloy).

These results are somewhat consistent with previous slurry erosion test data (Ref 8) on cobalt-base hardfacing alloys, albeit in a sand-water slurry, as opposed to the alumina-water medium used to generate the values in Fig. 11. In the previous work, a wide spectrum of engineering materials was tested, and, of these, alloy 6 (the cast counterpart of alloy 6B) was among the most resistant, wearing at only 5.5% of the rate of carbon steel. The results in Ref 8 indicated that the cast cobalt-base alloys of higher carbon content (and higher hardness) were much less resistant to slurry erosion, suggesting that the relationship between carbide volume fraction and slurry erosion resistance is far from linear for the cobalt-base alloys.

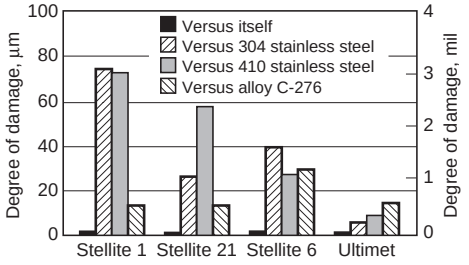


Fig. 14 Comparison of galling test data for wrought Multimet alloy with cobalt-base hardfacing deposits (two-layer gas-tungsten arc deposits). See Fig. 12 and 13 for test parameters.

Sliding Wear Data

Galling. The outstanding resistance of the cobalt-base wrought alloys to galling, under self-mated conditions, is apparent from the pin-on-block test data presented in Fig. 12. Unfortunately, the test conditions (ten strokes through an arc of 120°) were too severe for the standard (austenitic and ferritic-austenitic) stainless steels. Even Nitronic 60, a type 200 stainless steel known for its resistance to galling, exhibited considerable damage (change in surface roughness) at the test load employed.

As may be deduced from Fig. 12, the coupling of dissimilar materials in a sliding system complicates the issue of wear performance, possibly because the interfacial bonding characteristics are difficult to predict. Nickel in Ultimet alloy, for example, is detrimental under self-mated conditions, but beneficial when sliding against alloy C-276 (Fig. 13). Additional galling data on Ultimet, as well as cobalt-base hardfacing alloys, are provided in Fig. 14.

Oxide Control. Although elevated-temperature sliding-wear data for the cobalt-base wrought alloys are not available, work with cobalt-base castings and weld overlays (Ref 9, 10) indicates that maximum wear rates occur at approximately 250 °C (480 °F) under a variety of sliding conditions and that above this temperature, oxide control of the sliding-wear process is prevalent. Both Ref 9 and 10 discuss the advantages of cobalt as an alloy base over nickel (relative to sliding wear at low temperatures).

The unlubricated dynamic coefficient of friction was found to vary with time in both of these studies. In Ref 9, the coefficient was found to vary between 0.4 and 1.4 for alloy 31 (self-mated) at room temperature (the value increasing with test time). At high temperatures, friction coefficient values appear to be more stable, after a short, running-in period. At 800 °C (1470 °F), for example, alloy 31 (self-mated) exhibited a value of between 0.3 and 0.4 after 15 min, up to completion of the test at 67 h.

Hot Hardness Values for Wrought Alloys

Because they may be of some relevance to low-stress hot abrasion resistance, hot hardness values are presented in Table 4 for wear resistant alloy 6B, heat resistant alloys 25 and 188, and corrosion resistant Ultimet alloy. It is significant that despite the considerable spread in their room-temperature hardness values, these alloys possess nearly equal resistance to deformation at 871 and 982 °C (1600 and 1800 °F).

Table 4 Hot hardnesses of cobalt-base wrought alloys

Temperature		Hardness for indicated alloy, DPH(a)			
°C	°F	Alloy 6B	Alloy 25	Alloy 188	Ultimet
RT(b)	RT(b)	374	285	248	296
427	800	269	171	170	173
538	1000	247	160	159	162
649	1200	225	150	147	158
760	1400	153	134	129	134
871	1600	91	93	89	89
982	1800	55	52	49	50

(a) DPH, diamond pyramid hardness. (b) RT, room temperature. Source: Haynes International

Table 5 Chemical compositions of cobalt-base hardfacing alloys

UNS No.	Alloy tradename	AWS designation	Composition(a), wt% C	Cr	Fe	Mn	Mo	Ni	Si	W	Others
Carbide-containing alloys											
R30006	Stellite No. 6	ERCoCr-A	0.9–1.4	27.0–31.0	3.0 max	1.0 max	1.5 max	3.0 max	1.5 max	2.60–3.00	…
R30012	Stellite No. 12	ERCoCr-B	1.4 nom	30.0 nom	3.0 max	2.5 nom	…	1.5 nom	0.7 nom	8.3 nom	…
R30001	Stellite No. 1	ERCoCr-C	2.5 nom	30.0 nom	3.0 min	0.5 nom	0.5 nom	1.5 nom	1.3 nom	13.0 nom	…
R30021	Stellite No. 21	ERCoCr-E	0.20–0.30	25.0–29.0	3.0 max	1.0 max	5.0–6.0	1.75–3.75	1.0 max	…	0.07 max B
R30002	Stellite F	ERCoCr-F	1.5–2.0	23.0–27.0	6.0 max	1.0 nom	1.0 max	20.5–23.5	0.8–1.5	10.5–13.5	…
Laves-phase alloys											
R30400	Tribaloy T-400	…	0.8 max	7.5–8.5	…	…	27.0–29.0	…	2.2–2.6	…	Fe + Ni 3.0 max
…	Tribaloy T-800	…	…	18.0 nom	…	…	29.0 nom	…	3.5 nom	…	…

(a) Max, maximum; nom, nominal; min, minimum

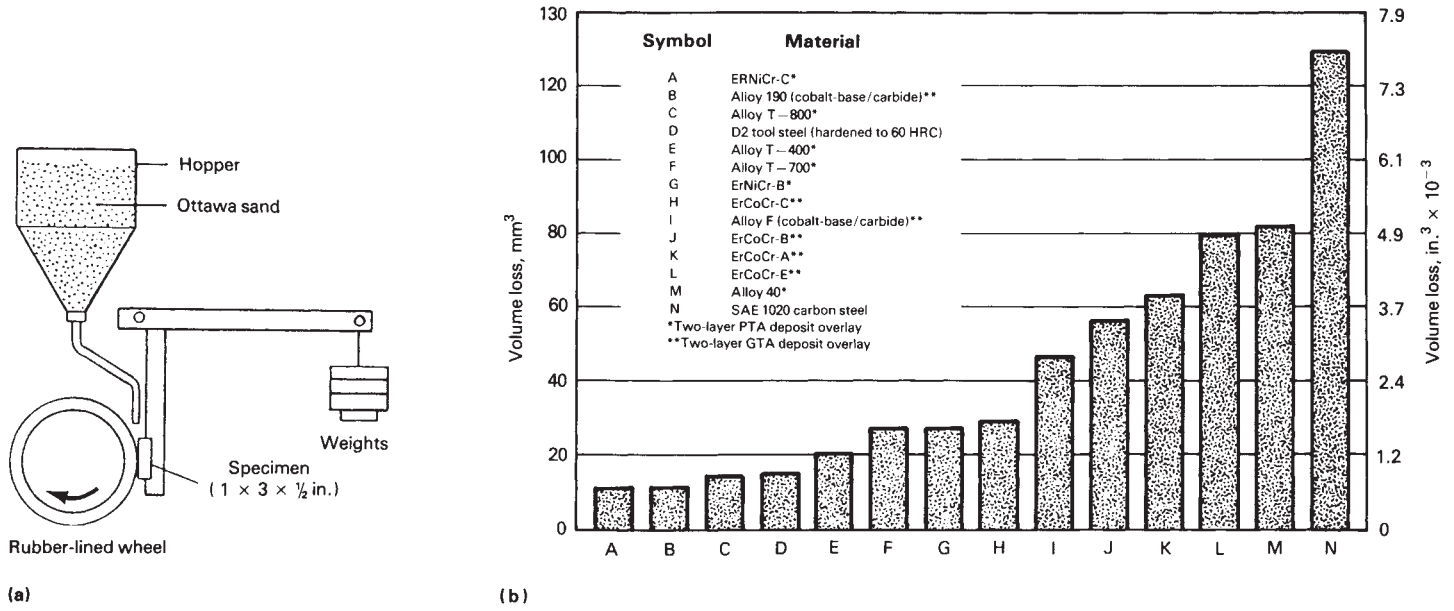


Fig. 15 Comparison of hardfaced cobalt- and nickel-base alloys to tool steel and carbon steel reference materials using ASTM G 65 low-stress abrasion test. (a) Schematic of G 65 dry sand and rubber wheel test apparatus. (b) Low-stress abrasion test data. G 65 test parameters: procedure B; room temperature; 13.6 kg (30 lb) load; quartz grain sand diameter of 212 to 300 μm (8.48 to 12 mil); 2000 rev at 200 rev/min; 390 g/min (0.86 lb/min) feed rate

Wear-Related Applications for Wrought Alloys

As may be deduced from the wear data presented in this article, the cobalt-base alloys provide high resistance to sliding wear, slurry erosion, and cavitation erosion (relative to the stainless steels, nickel-base superalloys, and high-nickel corrosion alloys). Alloy 6B and alloy 6K also possess outstanding resistance to low-stress abrasion. Industrial applications of the alloys tend to reflect these general properties and their resistance to corrosion and high-temperature strength.

The alloys are used for sliding-wear applications such as valves, both in the chemical processing industries and in the power industries (largely for steam control). Furthermore, alloy 25 is used as a bearing material, and alloy 6B is widely used to protect the nose sections of industrial chain saws. Ultimet alloy has been used for electrogalvanizing rolls, where both corrosion and sliding-wear resistance are required.

The erosion properties of the cobalt-base alloys have led to their use in nozzles, valves (subjected to cavitation damage or slurries), pumps, and mixing blades. Alloy 6B is also used to protect steam turbine blades from liquid-droplet erosion (it appears that the advantages of cobalt as an alloy base extend to this form of erosion also).

From an abrasion standpoint, notable applications of alloy 6B and alloy 6K include scraper knives and blades (for the chemical and food processing industries) and knives for the textile industries.

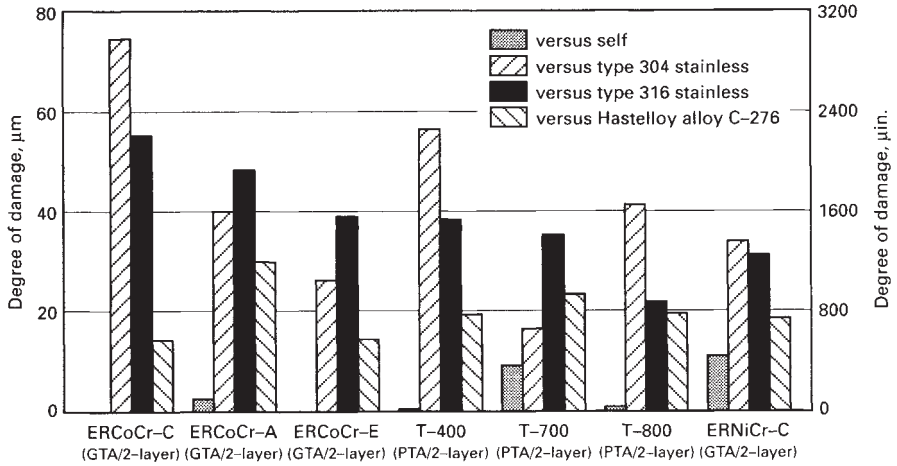


Fig. 16 Galling property evaluation of cobalt- and nickel-base hardfacing alloys versus selected alloys (itself, stainless steels, and a Ni-Mo-Cr alloy). Data obtained using pin-on-block test with following parameters: 2722 kg (6000 lb) load; 10 strokes through 120° arc. GTA, gas tungsten arc

Wear Behavior of Cobalt-Base Hardfacing Alloys

The two types of commercially available cobalt-base hardfacing alloys are carbide-containing alloys and alloys containing Laves phase. Compositions of these alloys are given in Table 5.

Carbide-containing cobalt-base alloys have been widely used since the early 1900s, when a cobalt-base alloy with the nominal composition of Co-28Cr-4W-1.1C (alloy 6) was first developed. The chief difference between the various carbide-containing cobalt-base alloys is in carbon content (hence, carbide volume fraction, room-temperature hardness, and level of abrasion resistance). Chromium-rich M_7C_3 is the predominant carbide in these alloys, although tungsten-rich M_6C is evident in those alloys having a high tungsten content, and chromium-rich $M_{23}C_6$ is common in the low-carbon alloys.

Low-stress abrasion, galling, and cavitation erosion data are presented for cobalt and nickel-base hardfacing alloys in Fig. 15 to 17. Figure 15 relates the carbon content and the resistance to low-stress abrasion for the carbide-containing cobalt-base alloys (ERCoCr-A, -B, -C, and -E). From Fig. 16 and 17, it is evident that the cobalt-base matrix (solid solution) is responsible for the excellent self-mated sliding properties and cavitation erosion resistance of these alloys.

Figure 4 shows that within the Stellite family (Table 5), the abrasion resistance is a func-

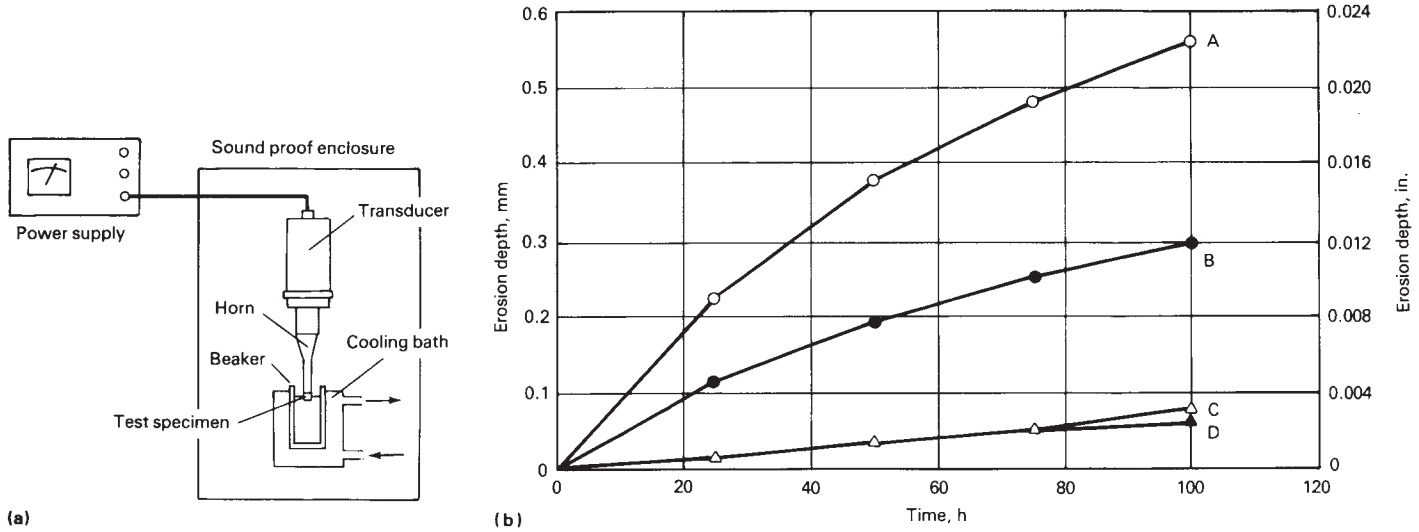


Fig. 17 Comparison of two cobalt-base hardfacing alloys to a stainless steel and a Ni-Mo-Cr alloy using ASTM G 32 vibratory cavitation test. (a) Schematic showing G 32 test apparatus. (b) Cavitation erosion test data. G 32 test parameters: medium, distilled water; test temperature, 16 °C (61 °F); vibration, 20 kHz frequency at 0.05 mm (0.002 in.) amplitude. A, type 410 stainless steel (hardness, 23 HRC); B, Hastelloy alloy C-276; C, ERCoCr-E (two-layer GTA deposit); D, ERCoCr-A (two-layer GTA deposit)

tion of carbon and tungsten content. As the carbon content increases in Co-Cr-W Stellite alloys, so does the tungsten content. This results in an increase in carbide content and, thus, hardness.

Photomicrographs of gas-tungsten arc two-layer deposits are shown in Fig. 3. The differences in carbide volume fractions and geometry are evident from these micrographs.

Laves-Type Alloy Compositions. Two cobalt-base Laves-type alloy compositions are presented in Table 5. In these materials, molybdenum and silicon are added at levels in excess of their solubility limit with the objective of inducing the precipitation of the hard (and corrosion resistant) Laves phase (an intermetallic compound). Carbon is held as low as possible in these alloys to discourage carbide formation. The microstructure of an alloy T-800 hardfacing deposit is shown in Fig. 3(f).

Because the Laves intermetallic phase is so abundant in these alloys, its presence governs all the material properties. Accordingly, the effects of the matrix composition in these alloys are less pronounced than is the case for the carbide-containing cobalt alloys. The Laves phase is specifically responsible for outstanding abrasion resistance (Fig. 4), but it severely limit the material ductility (< 1% elongation) and the impact strength. In fact, it is difficult to attain crack-free overlays on all but the smallest components given adequate preheat. For this reason, these alloys have been more successful as thermal spray materials.

Applications. A list of typical applications of cobalt-base hardfacing alloys is given in Table 1. Generally, these alloys are used in moderately corrosive and/or elevated-temperature environments.

ACKNOWLEDGMENTS

This article was adapted from:

- P. Crook, Cobalt and Cobalt Alloys, *Properties and Selection: Irons, Steels, and High-Performance Alloys*, Vol 1, *ASM Handbook*, 1990, p 446–454
- P. Crook, Friction and Wear of Cobalt-Base Wrought Alloys, *Friction, Lubrication, and Wear Technology*, Vol 18, *ASM Handbook*, 1992, p 766–771
- P. Crook and H.N. Farmer, Friction and Wear of Hardfacing Alloys, *Friction, Lubrication, and Wear Technology*, Vol 18, *ASM Handbook*, 1992, p 758–765

REFERENCES

1. K.C. Antony and W.L. Silence, The Effect of Composition and Microstructure on Cavitation Erosion Resistance, *Proc. of the 5th Int. Conf. on Erosion by Solid and Liquid Impact*, Cambridge University Press, 1979, p 671
2. W.L. Silence, Effect of Structure on Wear Resistance of Co-, Fe-, and Ni-Base Alloys, *Wear of Materials*, American Society of Mechanical Engineers, 1977, p 77
3. A. Ninham, The Effect of Mechanical Properties on Erosion, *Wear*, Vol 121, 1987, p 307
4. I.M. Hutchings, *The Erosion of Materials by Solid Particle Impact*, No. 10, Materials Technology Institute of the Chemical Processing Industry, 1983
5. D.A. Woodford, Cavitation-Erosion-Induced Phase Transformation in Alloys, *Metall. Trans. A*, Vol 3, 1972, p 1137
6. C.J. Heathcock, B.E. Protheroe, and A. Ball, The Influence of External Variables and Microstructure on the Cavitation Erosion of Materials, *Proc. of the 5th Int. Conf. on Erosion by Solid and Liquid Impact*, Cambridge University Press, 1979, p 631
7. A.V. Levy and S. MacAdam, "Erosion-Corrosion of Materials in Coal-Water Slurries," Report AP-5628, Electric Power Research Institute, 1988
8. W.A. Stauffer, Wear of Metals by Sand Erosion, *Met. Prog.*, Jan 1956, p 102
9. F.H. Stott, C.W. Stevenson, and G.C. Wood, Friction and Wear Properties of Stellite 31 at Temperatures from 293 to 1073 K, *Met. Technol. Q.*, Feb 1977, p 66
10. P. Crook and C.C. Li, The Elevated Temperature Metal-to-Metal Wear Behavior of Selected Hardfacing Alloys, *Wear of Materials*, American Society of Mechanical Engineers, 1983, p 272

ASM Specialty Handbook: Nickel, Cobalt, and Their Alloys
J.R. Davis, editor, p 395-400
DOI:10.1361/ncta2000p395

Copyright © 2000 ASM International®
All rights reserved.
www.asminternational.org

Corrosion Behavior of Cobalt Alloys

FROM A CORROSION STANDPOINT, cobalt alloys can be broadly classified into two categories. Alloys in the first category contain low levels of carbon (0.025–0.15%) and are intended for use in severely corrosive environments, at high temperatures, or where ductility is an important consideration (Ref 1). Alloys in the second category have high carbon contents (1 to >3%), exhibit high hardnesses, and provide resistance to low-stress abrasion (in addition to other forms of wear), but they exhibit low ductilities.

Although the higher-carbon content cobalt-base wear resistant alloys possess some resistance to aqueous corrosion, they are limited by grain boundary carbide precipitation, the lack of vital alloying elements in the matrix (after formation of carbides or Laves precipitates), and in the case of cast and weld overlay (hardfacing) materials, by chemical segregation in the microstructure. Examples of wear resistant alloys include the Stellite family of alloys (e.g., alloys No., 1, 6, 12, and 21) and wrought alloy 6B (UNS R30016).

By virtue of their homogenous microstructures and lower carbon contents, the wrought cobalt high-temperature alloys (which typically contain tungsten rather than molybdenum) are even more resistant to aqueous corrosion, but still fall quite short of the Ni-Cr-Mo alloys in corrosion performance. Example of wrought heat resistant cobalt alloys include alloys 25/L-605 (R30605) and 188 (R30188).

To satisfy the industrial need for alloys that exhibit outstanding resistance to aqueous corrosion, yet share the attributes of cobalt as an alloy base (resistance to various forms of wear and high strength over a wide range of temperatures), several low-carbon, wrought Co-Ni-Cr-Mo alloys are produced. These include the "multiphase" alloys MP35N (R30035) and MP159 (R30159), which possess the unique combination of ultrahigh strength, toughness, ductility, and corrosion resistance, and Ultimet (R31233), which combines excellent corrosion resistance to pitting (especially in oxidizing acids) with very high wear resistance (cavitation erosion, galling, and abrasion).

The Effect of Alloying Elements

The roles of various alloying elements in the cobalt-base alloys parallel those seen in the nickel-base alloys (Ref 1). Chromium, molybdenum, and tungsten, for example, are highly soluble in both the face-centered cubic (fcc) and hexagonal close-packed (hcp) atomic forms of cobalt. Chromium is added to most of the commercially important alloys and provides passivity over a wide range of potentials and resistance to oxidation. Molybdenum and tungsten enhance resistance to corrosion within the active regime. Nickel serves to stabilize the fcc structure with a view toward improved ductility during service. Nickel also improves resistance to mineral acids and stress-corrosion cracking (SCC). The quaternary alloy MP35N (35Co-35Ni-20Cr-10Mo) resists corrosion in hydrogen sulfide, salt water, and other chloride solutions, as well as the mineral acids (nitric, hydrochloric, and sulfuric). In addition, it has exceptional resistance to crevice corrosion and SCC.

Table 1 Compositions of the corrosion resistant wrought cobalt alloys described in this article

Alloy	UNS designation	Composition, %								
		C	Co	Cr	Fe	Mo	Ni	Si	W	Other
Elgiloy	R30003	0.15(a)	40	20	16	7	15.5	…	…	…
Havar	R30004	0.20	42.5	20	19	2.5	13.0	…	3	…
Alloy 6B	R30016	1.2	57	30	3(a)	1.5(a)	3	1.5(a)	4.5	…
Alloy 21	R30021	0.25	60	27	3(a)	5.5	3	1.0(a)	…	…
MP35N	R30035	0.025(a)	35	20	1(a)	10	35	0.15(a)	…	…
Ultimet	R31233	0.06	54	26	3	5	9	0.3	2	0.08N
Alloy 188	R30188	0.15(a)	39	22	3(a)	…	22	0.5(a)	14	0.15La(a)
Alloy 25	R30605	0.1	42	20	3	…	10	…	15	…
Alloy 556	R30556	0.1	19	22	29	3.5	21	0.8(a)	3	1.25Ta(a), 0.2N

(a) Maximum

Behavior of Cobalt Alloys in Corrosive Aqueous Environments

A variety of cobalt-containing alloys, ranging in cobalt content from 19 to 60%, will be discussed in this section (see Table 1). Because the corrosion properties of these alloys have thus far not been examined systematically with respect to such variables as alloying elements, the aim in this discussion is to describe the corrosion resistance of commercially available cobalt-base alloys in various environments. Emphasis has been placed on wrought alloys. Additional corrosion data can be found in the article "Properties of Cobalt Alloys" in this Handbook.

General Corrosion. The corrosion behavior of pure cobalt has not been documented as extensively as that of nickel. The behavior of cobalt is similar to that of nickel, although cobalt possesses lower overall corrosion resistance (Ref 2). For example, the passive behavior of cobalt in 1 *N* sulfuric acid (H_2SO_4) has been shown to be similar to that of nickel, but the critical current density necessary to achieve passivity is 14 times higher for nickel (Ref 3). Several investigations have been carried out on binary cobalt-chromium alloys. In cobalt-base alloys, it has been found that as little as 10% Cr is sufficient to reduce the anodic current density necessary for passivation from 500 to 1 mA/cm^2 (3225 to 6.5 mA/in.^{2}) (Ref 3). For nickel, approximately 14% Cr is needed to reduce the passivating anodic current density to the same level. The corrosion rates of a variety of cobalt-chromium alloys in several oxidizing and reducing media are shown in Table 2. In another study, researchers measured the open-circuit potentials in a dilute salt solution (Ringers solution) of a number of cast binary cobalt-chromium alloys having 10 to 40% Cr (Ref 5). They found that the behavior of the alloy was controlled not only by chromium

Table 2 Corrosion of cobalt- and nickel-base alloys in aqueous solutions

Alloy	Solution and temperature	Corrosion rate		Ref
		mm/yr	mils/yr	
Cobalt	1 *N* HNO_3, 25 °C (75 °F)	223	8,900	3
Nickel	1 *N* HNO_3, 25 °C (75 °F)	19	770	3
Ni-20Cr	11% HNO_3, hot	Nil	Nil	4
Co-20Cr	11% HNO_3, boiling	Nil	Nil	4
Co-20Cr	11% H_2SO_4, boiling	110	4,400	4
Co-20Cr	10% HCl, boiling	250	10,000	4

Table 3 Effect of alloying additions on the corrosion of cobalt-base alloys in acid media

Alloy composition	Weight loss, mg/cm^2	
	10% H_2SO_4	28% P_2O_5 + 13% H_2SO_4 + 2% HF
Co-2.1C-31Cr-12W	0.03	0.09
Co-2.1C-32Cr-12.5W-19.5Ni	0.02	0.03
Co-2.2C-32Cr-18.8Ni-14W	0.04	0.06
Co-2.3C-32Cr-14W-9.4Mo	0.06	0.06
Co-2.1C-32Cr-17.6Ni-13W	Nil	Nil
Co-2.2C-31Cr-18Ni-15W-9Mo-4Cu	1.8	1.0
Co-2.1C-32Cr-13.6W-4.2Cu	Not determined	Not determined

Data obtained in 192 h tests at 25 °C (75 °F). Source: Ref 6

Table 4 Corrosion of various wrought cobalt-base alloys in H_2SO_4 solutions

Alloy	Corrosion rate											
	2% boiling		10% 66 °C (150 °F)		10% boiling		20% 66 °C (150 °F)		20% boiling		80% boiling	
	mm/yr	mils/yr	mm/yr	mils/yr	mm/yr	mils/yr	mm/yr	mils/yr	mm/yr	mils/yr	mm/yr	mils/yr
Alloy 6B	0.8	31	0.0005	0.02	3.99	157	…	…	9.2	361	250	10,000
Alloy 25	0.86	34	0.2	8	4.4	174	0.5	20	10	395	>250	10,000
Alloy 188	0.89	35	Nil	Nil	3.02	119	0.25	10(a)	5.6	220	…	…
Alloy 556	0.76	30	Nil	Nil	3.45	136	0.33	13	8	316	…	…
Alloy 21	…	…	…	…	1.83	72	…	…	…	…	…	…
Havar	…	…	…	…	3	120	…	…	…	…	…	…
MP35N	…	…	…	…	1.3	51	…	…	…	…	…	…

Tests were conducted in four 24 h periods. (a) Corrosion rate varied within test period.

content but also by microstructural changes produced by the addition of chromium to cobalt. Addition of up to 25% Cr made the alloys more noble. However, above 25% Cr, precipitation of chromium-rich σ-phase made the alloys more active because of local chromium depletion around the σ-phase precipitates. Unfortunately, they did not measure corrosion rates of these alloys.

Another study examined the effect of alloying elements in cobalt-base alloys in H_2SO_4 and phosphoric acid (H_3PO_4) (Ref 6). These alloys contained 2% C for abrasive wear resistance. The data are given in Table 3. It can be seen that addition of nickel and copper lowered the corrosion rates significantly. Addition of molybdenum or nickel plus molybdenum did not have a great effect, possibly because of intermetallic precipitation. These researchers also conducted tests in an H_3PO_4 solution under abrasive conditions and found molybdenum, nickel, and copper to be highly beneficial (Ref 6).

The corrosion resistance of a number of commercial cobalt-base alloys in H_2SO_4 and hydrochloric acid (HCl) is given in Tables 4 and 5. It should be noted that all of these alloys, regardless of their chromium and molybdenum contents, exhibit similar corrosion resistance in dilute H_2SO_4 (Table 4). Thus, the high-chromium alloys 6B and 21 show approximately the same corrosion rates as the lower-chromium alloys 188 and 556. Similar behavior has been observed in the Ni-Fe-Cr-Mo alloys (Ref 7). In H_2SO_4 and HCl, the nickel and cobalt contents govern the behavior of the alloy as long as minimum amounts of chromium and molybdenum or tungsten are present. The corrosion resistance of wrought cobalt-base alloys in HCl solutions is given in Table 5. Again, as with the Ni-Fe-Cr-Mo alloys, the corrosion resistance of cobalt-base alloys is not good except in very dilute HCl.

Table 5 Corrosion of various wrought cobalt-base alloys in HCl solutions

Alloy	Corrosion rate							
	1% boiling		2.5% boiling		5% boiling		10% room temperature	
	mm/yr	mils/yr	mm/yr	mils/yr	mm/yr	mils/yr	mm/yr	mils/yr
Alloy 6B	…	…	96.5	3800	>250	10,000	…	…
Alloy 25	0.56	22	57.4	2260	188	7,400	Nil	Nil
Alloy 188	Nil(a)	Nil(a)	61	2400	140	5,500	0.008–0.8	0.3–31(b)
Alloy 556	Nil(a)	Nil(a)	63.5	2500	167.6	6,600	0.6	23

Tests were conducted in four 24 h periods except for the 5% HCl test, which was for one 24 h period. (a) Corrosion decreased from a high value. (b) Corrosion rate oscillated during the test period.

Because many of the commercial alloys contain appreciable amounts of chromium, their corrosion resistance to dilute nitric acid (HNO_3) is quite good (Table 6). However, in concentrated HNO_3, alloy 6B exhibited high corrosion rates, while alloys 188 and 25, which have lower chromium, showed lower corrosion rates. This could have been a consequence of the high carbon content of alloy 6B. High carbon and chromium are present intentionally in this alloy to provide chromium carbides for abrasion resistance. However, concentrated HNO_3 is known to attack high-chromium phases such as σ-phase and chromium-rich carbides.

Table 6 Corrosion resistance of various wrought cobalt-base alloys in HNO_3 solutions

Alloy	Average corrosion rate					
	10% boiling		65% boiling		70% boiling	
	mm/yr	mils/yr	mm/yr	mils/yr	mm/yr	mils/yr
Alloy 188	0.02	0.8(a)	0.56	22(b)	…	…
Alloy 25	0.02	0.8(a)	0.99	39(b)	0.94	37(b)
Alloy 6B	0.023	0.9(a)	…	…	96.5	3800(a)
Alloy 21	0.025	1.0(a)	…	…	…	…
Alloy 556	…	…	0.28	11(b)	…	…
Havar	0.066	2.6	…	…	…	…
MP35N	0.056	2.2	…	…	…	…

(a) One 24 h test period. (b) Five 24 h test periods

The corrosion resistance of some cobalt-base alloys in a variety of reducing and oxidizing environments is given in Table 7. In highly oxidizing chromic acid (H_2CrO_4), the chromium-containing alloys, whether cobalt- or nickel-base, do not show good resistance because the passive chromium oxide film is unstable in this acid. However, high amounts of tungsten seem to decrease the corrosion rates of alloys 188 and 25. In H_3PO_4, the corrosion rates of the cobalt-base alloys are very high. Although there are no compositionally equivalent nickel-base alloys, the corrosion rates of many of the commercial Ni-Cr-Mo-Fe alloys in H_3PO_4 are lower (Ref 8). In acetic acid, the corrosion rates of all of the alloys are quite low. Nickel is widely used in caustic service. The Ni-Cr-Mo alloys offer lower corrosion resistance than nickel. In comparison, the cobalt-base alloys do not offer very high resistance to corrosion in caustic environments. Indeed, the data in Table

Table 7 Corrosion of cobalt-base alloys in a variety of environments at boiling temperature

Alloy	Corrosion rate									
	99% acetic acid		85% phosphoric acid		60% formic acid		10% chromic acid		50% sodium hydroxide	
	mm/yr	mils/yr	mm/yr	mils/yr	mm/yr	mils/yr	mm/yr	mils/yr	mm/yr	mils/yr
Alloy 6B	0.0008	0.03	15.5	610	1.22	48	…	…	2.74	108
Alloy 21	0.017	0.67	17.3	680	…	…	…	…	…	…
Alloy 25	0.0056	0.22	19.2	754	0.61	24	1.0	40	0.53	21
Alloy 188	0.005	0.20	13.5	530	…	…	1.37	54	0.43	17
Alloy 556	0.005	0.20	0.84	33	…	…	2.8	110	…	…
MP35N	0.015	0.6	12.7	500	…	…	…	…	…	…
Havar	0.078	3.1	>100	4000	…	…	…	…	…	…

Table 8 Corrosion of cobalt-base alloys in a boiling oxidizing mixture of 50% H_2SO_4 and 2.5% $Fe_2(SO_4)_3$

Alloy	Corrosion rate	
	mm/yr	mils/yr
Havar	0.72	28.5
MP35N	0.41	16.2
Alloy 21	0.36	14.0
Alloy 25	0.66	26.0
Alloy 188	0.43	17.0
Alloy 556	0.36	14.0
Ultimet	0.20	8.0
Alloy 6B	0.36	14.0

7 seem to indicate that the corrosion rates of the three cobalt-base alloys tested in caustic decreased with increasing nickel content (alloy 6B < 25 < 188).

Addition of oxidizing agents to H_2SO_4 results in lower corrosion rates for the Co-Cr-Mo-W alloys, just as in the case of the nickel-base alloys. This is shown in Table 8 for the 50% H_2SO_4 + 2.5% ferric sulfate [$Fe_2(SO_4)_3$] mixture recommended by ASTM as an intergranular corrosion test solution.

Comparative isocorrosion curves for Ultimet and nickel-base alloy C-22 (UNS N06022), which has a nominal composition of Ni-21.5Cr-13.5Mo-4Fe-2.5 max Co, are shown in Fig. 1. These curves represent the concentrations and temperatures at which corrosion rates of 0.13 mm/yr (5 mils/yr) and 0.51 mm/yr (20 mils/yr) were encountered in various mineral acids. Given the chromium (26%) and molybdenum (5%) levels that exist in Ultimet, these curves suggest that the two elements are at least as effective in cobalt as they are in the iron- and nickel-base alloys, provided they remain in solution (i.e., do not partition to primary or secondary carbides) (Ref 1).

The general corrosion properties of Ultimet, relative to a number of well known nickel-base and iron-base corrosion resistant alloys, are summarized in Table 9. Tables 10 and 11 compare the corrosion resistance of MP35N with other high-nickel alloys. As shown in Table 10, higher strength levels developed by work hardening or work hardening plus aging do not appreciably increase corrosion rates in various mineral acids.

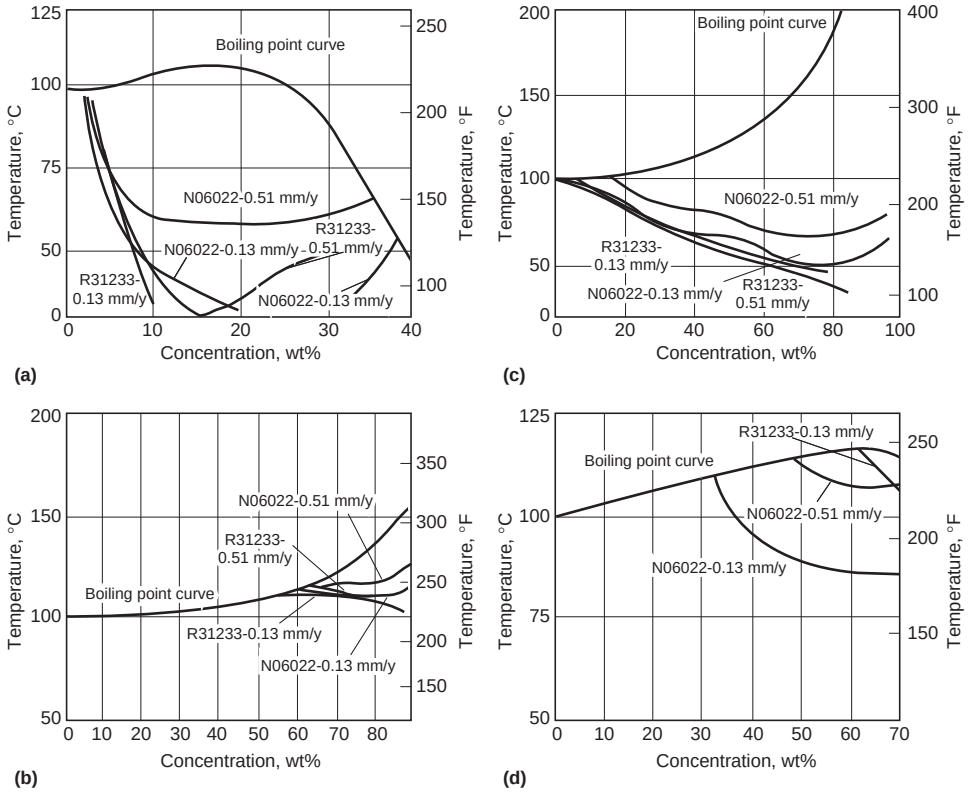


Fig. 1 Isocorrosion curves for Ultimet (UNS R31233) and alloy C-22 (UNS N06022). (a) Hydrochloric acid. (b) Phosphoric acid. (c) Sulfuric acid. (d) Nitric acid. Source: Ref 1

Localized Corrosion. The resistance to localized corrosion (pitting and crevice corrosion) of the cobalt-base alloys is generally determined by the chromium, molybdenum, and tungsten contents. Generally, localized corrosion resistance is measured by immersion tests in oxidizing chloride solutions or by electrochemical tests in chloride solutions. Crevice corrosion resistance is usually measured by attaching blocks to the sample in order to create a crevice between the sample and the block. The test methods are outlined in Ref 8 to 11.

An example of the localized corrosion resistance of several cobalt-base alloys in an oxidizing chloride-containing test solution is given in Table 12. This is an extremely acidic chloride solution containing ferric and cupric salts to increase the oxidizing potential of the solution. As the results indicate, there is a wide variation in alloy performance. Havar alloy and alloy 556 start to corrode at a rapid rate at

Table 9 Comparison of corrosion rates for selected cobalt-base, iron-base, and nickel-base alloys in various solutions

Alloy	Corrosion rate, mm/year							
	Boiling 99% acetic acid	Boiling 65% nitric acid	Boiling 1% hydrochloric acid	Boiling 2% hydrochloric acid	54% P_2O_5 at 116 °C (240 °F)	Boiling 10% sulfuric acid	Boiling ASTM G28A solution	Boiling ASTM G28B solution
Ultimet	<0.01	0.15	0.01	13.49	0.19	2.52	0.20	0.02
C-276	<0.01	21.51	0.52	1.90	0.58	0.51	8.05	0.86
625	0.01	0.51	0.03	14.15	0.30	0.64	0.43	71.08
20Cb-3	0.11	0.19	1.80	5.77	0.92	0.40	0.25	69.08
316L	0.19	0.24	13.31	25.15	5.11	47.46	0.94	80.51

Table 10 Comparison of corrosion rates of MP35N (various conditions) and nickel-base alloy C-276 in various solutions

Alloy	Condition	Corrosion rate							
		Boiling 10% nitric acid		10% hydrochloric acid at 65 °C (150 °F)		Boiling 10% sulfuric acid		Boiling 16.4% sulfuric acid	
		mm/yr	mils/yr	mm/yr	mils/yr	mm/yr	mils/yr	mm/yr	mils/yr
MP35N	Annealed	0.0325	1.3	1.19	47.5	0.573	22.9	3.87	154.7
	Work-hardenened 50%	0.018	0.7	1.11	44.2	0.553	22.1	4.14	165.7
	Work-hardened 50% plus aged 4 h at 565 °C (1050 °F)	0.01	0.4	1.46	58.4	0.85	34.0	4.24	169.7
C-276	Annealed	0.243	9.7	0.665	26.6	4.24	169.7	0.45	18.0

Tests were conducted in five 24 h periods.

Table 11 Comparison of corrosion rates of MP35N and various nickel- and iron-base alloys in sulfuric acid solutions

Alloy	Corrosion rate			
	10% sulfuric acid at 80 °C (175 °F)		30% sulfuric acid at 80 °C (175 °F)	
	mm/yr	mils/yr	mm/yr	mils/yr
MP35N	0.193	7.7	1.65	65.9
C-276	0.083	3.3	0.08	3.2
625	0.018	0.7	0.773	30.9
20Cb-3	0.323	12.9	0.455	18.2

All specimens were tested in the annealed condition. Tests were conducted in five 24 h periods.

Table 12 Results of pitting corrosion tests in an aqueous mixture of 11.5% H_2SO_4 + 1.2% HCl + 1% $CuCl_2$ + 1% $FeCl_3$ at various temperatures

Alloy	Corrosion rate, mm/yr (mils/yr)		
	Room	70 °C (160 °F)	Boiling
Havar	Nil	15 (600)	56 (2200)
MP35N	Nil	Nil–0.015 (0.6)	0.076–50 (3–2000)
Alloy 21	Nil	Nil	0.76 (30)
Alloy 188	Nil–0.01 (0.4)	0.005–0.2 (0.2–8)	2.5–24.1 (100–950)
Alloy 25	0.0076–0.025 (0.3–1.0)	Nil–0.01 (0.4)	Nil–0.05 (2)
Alloy 556	0.0025–0.023 (0.1–0.9)	1.3–19.3 (50–760)	14.2–53 (560–2100)
Multimet	…	…	Nil–0.05 (2)
Alloy 6B	…	…	73.4 (2888)

Test duration: 24 h

approximately 70 °C (160 °F). Alloys MP35N, 188, and 21 begin to corrode rapidly near the boiling point of the solution. Alloy 25 exhibits the highest resistance of these cobalt-base alloys. Alloy 6B is not listed in Table 12 because it exhibits a high corrosion rate even in less severe solutions, such as 10% ferric chloride ($FeCl_3$). The corrosion rates of the alloys tested are given in Table 12. In the 20 to 22% Cr alloys, the alloys containing the lowest amounts of molybdenum and tungsten (alloys Havar and 556) show the highest corrosion rates. The alloy with the intermediate molybdenum level (alloy MP35N) shows lower corrosion rates, while the alloys with high levels of tungsten (alloy 25) and high chromium plus molybdenum (alloy 21) show even lower rates. The exception to this case is alloy 188, which shows higher corrosion rates than alloy 25 in spite of similar composition. Unfortunately, no data are available at intermediate temperatures, so a more accurate comparison of alloys cannot be made.

Results of corrosion tests conducted in a milder localized test environment of $FeCl_3$ are given in Table 13. Again, the trend is similar to that shown in Table 12 in that alloys 188 and 25 are superior in pitting resistance to alloy 556. In summary, it is believed that the effects of alloying elements (chromium, molybdenum, and tungsten) on pitting resistance are qualitatively similar in cobalt-base alloys to those observed in nickel-base alloys. Their effects in cobalt-base alloys cannot be predicted precisely, however, because of the lack of extensive data.

The outstanding resistance to pitting and crevice corrosion of low-carbon cobalt-base alloys is presented in Tables 14 and 15, respectively. Even the higher-carbon wear resistant alloy 6B has improved localized corrosion resistance when compared with conventional austenitic stainless steels like type 316L.

Table 13 Corrosion of cobalt-base alloys in 3.8% $FeCl_3$ solutions

Alloy	Corrosion rate, mm/yr (mils/yr)		
	Room	70 °C (160 °F)	Boiling
Alloy 188	Nil	Nil	Nil
Alloy 25	0.013 (0.5)	Nil	Nil
Alloy 556	0.033 (1.3)	14 (550)	36 (1419)

24 h test; all alloys in the mill-annealed condition

Environmental Embrittlement of Cobalt Alloys

Hydrogen Embrittlement

Cobalt-base alloys can be used to combat hydrogen embrittlement where steels have failed by this mechanism. The literature on the hydrogen embrittlement of cobalt-base alloys is not very extensive. Most of the experimental work has been performed on alloys 188, 25, and MP35N. The performance of these alloys is in many ways similar to that of many nickel-base alloys (Ref 12, 13).

Effects of Strength Level. The cobalt-base alloys can be processed to achieve much higher yield and/or tensile strengths than most of the nickel-base alloys. Susceptibility to hydrogen embrittlement is closely related to yield strength; therefore, the potential for hydrogen embrittlement in cobalt-base alloys may be higher than in nickel-base alloys, not because of a higher inherent susceptibility to embrittlement, but because of the higher strength levels achievable in cobalt-base alloys.

Annealed cobalt-base alloys do not show significant susceptibility to hydrogen embrittlement, even in the most severe hydrogen-charging conditions. When cold worked to levels exceeding 1380 MPa (200 ksi) yield strength, the cobalt-base alloys may not exhibit embrittlement (Ref 14). Two factors—impressed hydrogen charging and low-temperature aging (as is the case for nickel-base alloys)—are often required to produce hydrogen embrittlement.

External Hydrogen Charging. Because of the high corrosion resistance of many cobalt-base alloys, the alloys may not corrode at a sufficient rate even in acid systems to charge hydrogen into the alloys. Hydrogen charging will often be achieved through the cathodic protection systems used to protect other components in a system or through the galvanic coupling of cobalt-base alloys to more actively corroding metals. Hydrogen entry can be enhanced by the presence of hydrogen recombination poisons, such as sulfides, cyanides, or other substances commonly found to be effective hydrogen recombination poisons on steels. Under such conditions, cobalt-base alloys with yield strengths over 1380 MPa (200 ksi), and especially greater than 1724 MPa (250 ksi), can exhibit hydrogen embrittlement. The time to failure (usually by an intergranular mode) is strongly dependent on the charging current (Ref 15).

Effect of Thermal Treatments. The aging of cobalt alloys has two opposite effects on hydrogen embrittlement, depending on the temperature range. At temperatures ranging from 205 to approximately 650 °C (400–1200 °F), aging is highly detrimental to hydrogen embrittlement resistance (Ref 16, 17). Aging above approximately 760 °C (1400 °F) is highly beneficial (Ref 18). The most susceptible microstructures are produced by a combination of cold work and aging near 540 to 650 °C (1000–1200 °F). Aging at temperatures above 790 °C (1450 °F) produces microstructures that are extremely resistant to embrittlement.

Long-term aging treatments that take place for periods of years at temperatures as low as 205 °C (400 °F) can have a noticeable detrimental effect (Ref 19, 20). Very high strength levels and hydrogen charging are both required to produce this effect.

Effect of Other Factors. Anisotropy in mechanical properties can play an important role in hydrogen embrittlement (Ref 17). Crack path sensitivity is greater in directions transverse to the direction of mechanical working. Other factors, such as stress level, environmental temperature, and environment corrosivity, have effects similar to those seen in steels and nickel-base alloys.

Stress-Corrosion Cracking

Only a limited number of environments have been reported to cause SCC of cobalt-base alloys. These include two general classes of environments: acid chlorides and strong alkalies. Both of these environments produce SCC only at temperatures exceeding approximately 150 to 175 °C (300–350 °F) (Ref 21), although useful lives can be expected even above 205 °C (400 °F) (Ref 22). The fracture mode in sodium hydroxide (NaOH) was intergranular on alloy

Table 14 Comparative critical pitting temperatures of various cobalt-, nickel-, and iron-base alloys tested in 11.5% H_2SO_4 + 1.2% HCl + 1% $FeCl_3$ + 1% $CuCl_2$ for 24 h

Alloy	Critical pitting temperature	
	°C	°F
C-22	120	248
Ultimet	120	248
C-276	110	230
625	75	167
6B	45	113
Type 316L stainless steel	25	77

Table 15 Comparative critical crevice corrosion temperatures of various cobalt-, nickel-, and iron-base alloys tested in oxidizing 6% $FeCl_3$ solution for 72 h

Alloy	Critical crevice corrosion temperature	
	°C	°F
C-22	70	158
Ultimet	65	149
C-276	65	149
625	30	86
6B	25	77
Type 316L stainless steel	<0	<32

Table 16 Results of stress-corrosion cracking tests carried out on MP35N and several iron-base alloys

Alloy	Condition	Results in boiling 42% $MgCl_2$, 192 h(a)
MP35N	Solution annealed + 60% cold work	No cracks
Type 316 stainless steel	Annealed	Stress-corrosion cracks within 4 h
20Cb-3	Annealed	Etched and pitted, no cracks
Alloy 800	Annealed	Etched and pitted, no cracks
Alloy 825	Annealed	Etched and pitted, no cracks

(a) Per ASTM G 36, "Practice for Performing Stress-Corrosion Cracking Tests in a Boiling Magnesium Chloride Solution"

Table 17 Stress-corrosion cracking tests carried out on MP35N in NACE solution 5% NaCl + 0.5% acetic acid saturated in H_2S at room temperature

Source	Material test condition(a)	Results
INCO	Cold-drawn bar aged to 0.2% YS of 1937–1972 MPa (281–286 ksi). Tested at 1931 MPa (280 ksi)	No visible corrosion after 30 days exposure
Cameron Iron Works	As cold worked to 1372 MPa (199 ksi) 0.2% YS and cold worked + aged to 1937 MPa (281 ksi) 0.2% YS. Tested at 100% of 0.2% YS	No failure in 30 days
The Timken Company	Cold-drawn bar aged to 0.2% YS levels of 1510 MPa (219 ksi) and 1786 MPa (259 ksi). Tested at 107–137% of the 0.2% YS	No cracking or corrosion observed for entire duration of test, 1 month
Exxon Production Research	Sheet and bar cold worked and aged to 1896–2006 MPa (275–291 ksi) 0.2% YS. Tested at 1965 MPa (285 ksi)	No cracking or corrosion in the 30 day duration of test
Otis Engineering	Helical compression spring compressed to the torsional elastic limit, 703 MPa (102 ksi) at a deflection of 71.1 mm (2.80 in.)	No failure in 28 day duration of test
The Timken Company	Cold-drawn bar aged to 0.2% YS level of 1903–2117 MPa (276–307 ksi). Tested at 95–127% of 0.2% YS. Material contains up to 5% Fe and 0.045% C.	No failure in 40 day duration of test

All of the tests were conducted on longitudinal samples taken from MP35N bar. YS, yield strength. (a) All aging treatments, 593 °C (1100 °F) for 4 h. Air cooled

6B (Ref 23). In acid chlorides containing hydrogen sulfide (H_2S), the SCC of alloy 188 was intergranular; cracking of alloy MP35N was reported to be transgranular (Ref 21).

Minor surface SCC has been reported for MP35N in hypersaline geothermal brine at 200 to 230 °C (390–445 °F) (Ref 24). In some conditions, cobalt-base alloys have been shown to be susceptible to SCC in boiling magnesium chloride ($MgCl_2$) at 155 °C (310 °F) (Ref 25), although other alloys are resistant at this temperature (Ref 26). Table 16 compares the resistance of MP35N to boiling 42% $MgCl_2$ with other iron-base alloys.

Alloy MP35N is also very resistant to SCC in hydrogen sulfide environments and is being used increasingly for sour gas oil field equipment (e.g., tubing and springs). Table 17 lists the results from six companies that tested MP35N in the NACE International solution (5% NaCl + 0.5% acetic acid saturated in H_2S). The NACE standard MR-01-75 approves the use of MP35N in sour gas environments.

High-Temperature Corrosion of Cobalt Alloys

Cobalt alloys exhibit excellent resistance to various forms of high-temperature corrosive attack including oxidation, sulfidation, and carburization. This section briefly reviews several studies on the high-temperature corrosion behavior of cobalt-base alloys. Additional information can be found in the article "High-Temperature Corrosion Behavior of Nickel Alloys" in this Handbook and in the *ASM Specialty Handbook: Heat-Resistant Materials.*

Oxidation Resistance. Dynamic oxidation data for alloys 25 and 188 relative to the nickel-base alloys X and 601 are presented in Fig. 2. The values represent the total depth of metal affected (that is, the depth of metal turned to oxide plus the depth subjected to internal oxidation). The 100 h test involved cooling the samples every half hour to 540 °C (1000 °F). The test atmosphere contained the combustion products of A-640 aviation kerosene, using an air-to-fuel ratio of 40 to 1. The test gas velocity was approximately 390 km/h (355 ft/s). The improved performance of alloy 188 in this test is attributable to effects of lanthanum on oxide scale adherence.

Sulfidation Resistance. Cobalt-base alloys as well as cobalt-containing alloys (e.g., Fe-Ni-Co-Cr) generally have better sulfidation resistance than nickel-base alloys and Fe-Cr-Ni alloys. Sulfidation test results at 980 °C (1800 °F) for alloys 25 and 188, relative to the nickel-base alloys—X, 601, and Waspaloy alloy—are presented in Fig. 3. These results, which were generated in an environment with a sulfur partial pressure of 0.4 Pa (4×10^{-6} atm) and an oxygen partial pressure of 3×10^{-12} Pa (3×10^{-17} atm), show the outstanding sulfidation resistance of the cobalt-base high-temperature alloys relative to both γ′-strengthened and solid-solution-strengthened high-temperature nickel alloys. Of the alloys tested under these conditions, only alloy 6B and alloy HR-160 (a high-silicon, cobalt-containing alloy) exhibit superior properties.

Carburization Resistance. Lai (Ref 27) studied the carburization resistance of more than 20 commercial wrought alloys, ranging from stainless steels to iron-, nickel-, and cobalt-base alloys. The relative performance rankings for alloys tested at 870, 930, and 980 °C (1600, 1700, and 1899 °F) are shown in Fig. 4. Although some nickel alloys, most notably alloy 214, generally outperformed the cobalt alloys, alloys 6B, 25, and 188 exhibited very good to excellent carburization resistance (particularly at 930 °C, or 1700 °F, for 215 h).

ACKNOWLEDGMENTS

This article was adapted from:

- A.I. Asphahani et al., Corrosion of Cobalt-Base Alloys, *Corrosion,* Vol 13, *ASM Handbook,* 1987, p 658–668

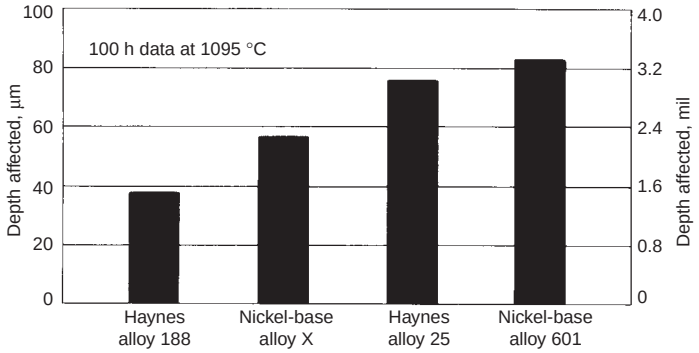


Fig. 2 Dynamic oxidation data for selected high-temperature cobalt alloys and nickel-base alloys at 1095 °C (2000 °F)

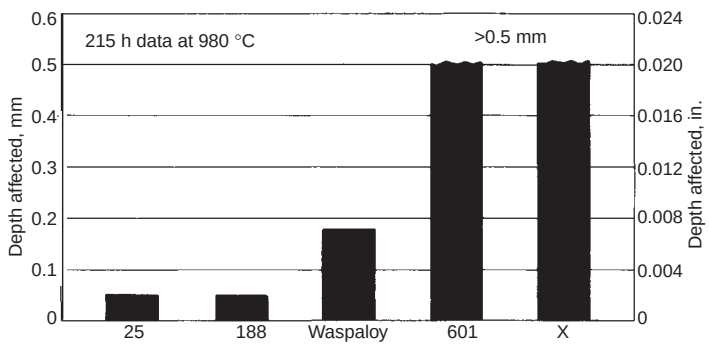


Fig. 3 Sulfidation data of Haynes alloys 25 and 188 relative to selected nickel-base alloys at 980 °C (1800 °F)

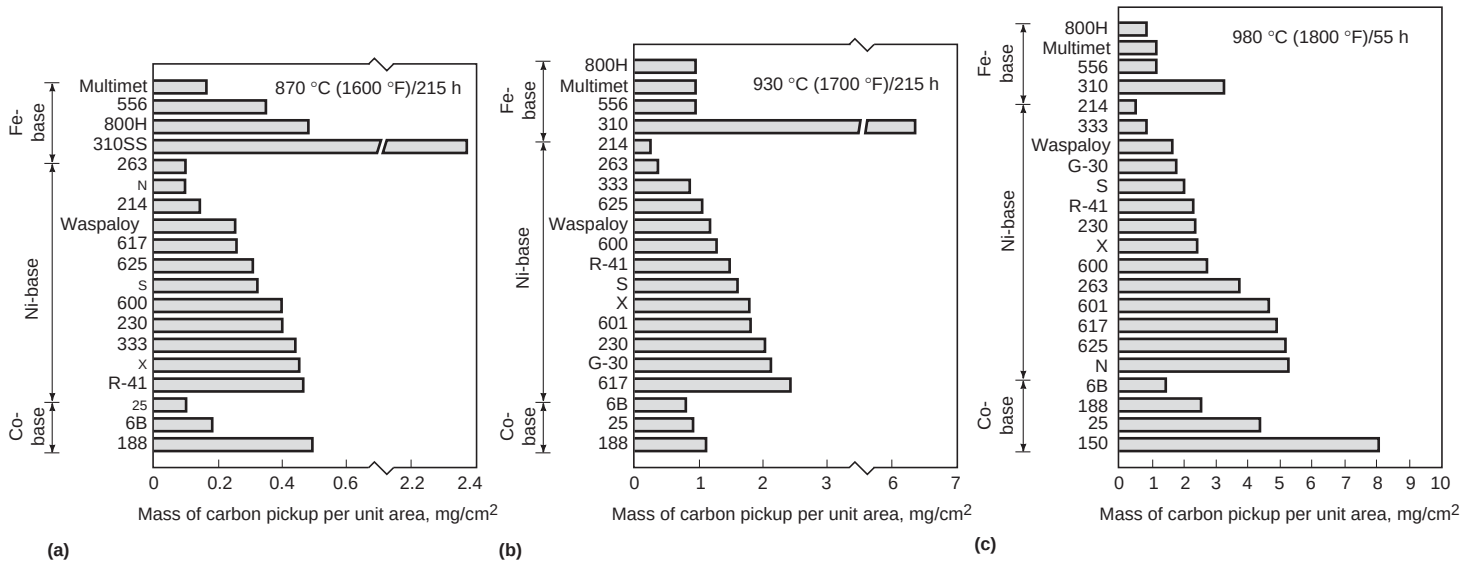


Fig. 4 Carburization resistance of various iron-, nickel-, and cobalt-base alloys tested in Ar-5H_2-5CO-5CH_4 at (a) 870 °C (1600 °F)/215 h, (b) 930 °C (1700 °F)/215 h, and (c) 980 °C (1800 °F)/55 h. Source: Ref 27

- P. Crook, Cobalt and Cobalt Alloys, *Properties and Selection: Nonferrous Alloys and Special-Purpose Materials*, Vol 2, *ASM Handbook*, 1990, p 446–454

REFERENCES

1. P. Crook, Cobalt-Base Alloys, *Corrosion Tests and Standards: Application and Interpretation*, R. Baboian, Ed., ASTM, 1995, p 486–492
2. H.H. Uhlig and A.I. Asphahani, *Mater. Perform.*, Vol 18 (No. 11), 1979, p 9
3. A.P. Bond and H.H. Uhlig, *J. Electrochem. Soc.*, Vol 107, 1960, p 488
4. F. Wever and V. Hashimoto, *Die Korros. Metall. Werkst.*, Vol 2, 1938, p 745
5. A. Acharya, E. Freise, and E.H. Greener, *Cobalt*, Vol 47, June 1970, p 75
6. A. Davin and D. Coutsouradis, *Cobalt*, Vol 52, Sept 1971, p 160
7. N. Sridhar, Paper 19, presented at *Corrosion/87*, San Francisco, CA, National Association of Corrosion Engineers, March 1987
8. "Standard Recommended Practice for Laboratory Immersion Corrosion Testing of Metals," G 31, *Annual Book of ASTM Standards*, ASTM
9. "Standard Test Methods for Pitting and Crevice Corrosion Resistance of Stainless Steels and Related Alloys by the Use of Ferric Chloride Solution," G 48, *Annual Book of ASTM Standards*, ASTM
10. "Standard Practice for Conducting Cyclic Potentiodynamic Polarization Measurements for Localized Corrosion," G 61, *Annual Book of ASTM Standards*, ASTM
11. "Standard Test Method for Pitting at Crevice Corrosion of Metallic Surgical Implant Materials," F 746, *Annual Book of ASTM Standards*, ASTM
12. E.P. Whelan, *Hydrogen Effect in Metals*, I.M. Bernstein and A.W. Thompson, Ed., The Metallurgical Society, 1981, p 979
13. A.I. Asphahani, paper presented at the *Second International Congress on Hydrogen in Metals*, Paris, 1977
14. J.P. Stroup, A.H. Bauman, and A. Simkovich, *Mater. Perform.*, Vol 15, June 1976, p 43
15. R.D. Kane, *Corrosion*, Vol 34 (No. 12), 1978, p 442
16. R.D. Kane and B.J. Berkowitz, *Corrosion*, Vol 36 (No. 1), 1980, p 29
17. R.D. Kane, M. Watkins, N.F. Jacobs, and G.L. Hancock, *Corrosion*, Vol 33 (No. 9), 1977, p 309
18. J. Kolts, Paper 407, presented at *Corrosion/86*, National Association of Corrosion Engineers, 1986
19. R.D. Kane and J.B. Greer, Paper SPE 6798, presented at Society of Petroleum Engineers, 1977
20. K. Kolts, Paper 323, presented at *Corrosion/86*, National Association of Corrosion Engineers, 1986
21. R.D. Kane et al., Paper 174, presented at *Corrosion/79*, National Association of Corrosion Engineers, 1979
22. G.A. Vaughn and H.-E. Chaung, Paper 182, presented at *Corrosion/81*, National Association of Corrosion Engineers, 1981
23. A.I. Asphahani, in *Stress Corrosion Cracking: The Slow Strain Rate Technique*, STP 665, American Society for Testing and Materials, 1979, p 279
24. A. Goldberg and R.P. Kershaw, "Evaluation of Materials Exposed to Scale Control/Nozzle-Exhaust Experiments at the Salton Sea Geothermal Field," Report UCRL 52664, Lawrence Livermore Laboratory, Feb 1979
25. A.I. Asphahani, Paper 42, presented at *Corrosion/78*, National Association of Corrosion Engineers, 1978
26. E. Taylor, *Mater. Prot.*, March 1970, p 29
27. G.Y. Lai, *High Temperature Corrosion in Energy Systems*, Proc. TMS-AIME Symposium, M.F. Rothman, Ed., The Metallurgical Society of AIME, 1985, p 551

ASM Specialty Handbook: Nickel, Cobalt, and Their Alloys
J.R. Davis, editor, p 401-406
DOI:10.1361/ncta2000p401

Copyright © 2000 ASM International®
All rights reserved.
www.asminternational.org

Fabrication and Metallography of Cobalt Alloys

THE FABRICATION CHARACTERISTICS of cobalt alloys vary widely due to their carbon contents, carbide volume fractions, and work-hardening properties. In general, the high-carbon wear resistant alloys, such as Stellite 6B, exhibit the poorest fabrication characteristics while the high-nickel corrosion resistant grades, such as MP35N, are much more readily formed and machined.

Heat Treatment

Wear resistant alloys 6B and 6K are supplied in the solution heat-treated condition unless otherwise specified. The standard heat treatment is at 1230 °C (2250 °F) followed by air cooling.

Heat resistant alloys 25 and 188 are normally solution heat treated at 1175 ± 14 °C (2150 ± 25 °F) and rapidly cooled or water quenched for optimal properties.

MP35N alloy should be annealed at 1040 to 1095 °C (1900–2000 °F) for 1 to 4 h, followed by air cooling. After work hardening, MP35N can be aged in the temperature range of 425 to 650 (800–1200 °F) for increased strength. The alloy will respond to aging only if first work hardened. No increase in strength will result from aging annealed material. For optimum mechanical properties, cold-worked MP35N alloy should be aged at 540 to 595 °C (1000–1100 °F) for 4 h, then air cooled. Relevant specification requirements should be consulted prior to any heat-treating operation. See the article "Properties of Cobalt Alloys" in this Handbook for the combined effects of cold work and aging on properties.

MP159 Alloy. The atmosphere for heat treating MP159 should be neutral or oxidizing and low in sulfur. A typical heat-treating/cold-working treatment involves solution annealing at 1050 °C (1925 °F) for 4 h, water quenching, work strengthening, and aging at 665 °C (1225 °F) for 4 h, followed by air cooling. A nominal cold reduction of 48% results in a tensile strength of approximately 1585 MPa (230 ksi). Aging increases the strength to approximately 1895 MPa (275 ksi) by a γ′ precipitation mechanism.

Age-Hardening Alloys Elgiloy, Duratherm 600, and Havar. The mechanical properties of these alloys are derived from a combination of cold work and subsequent heat treatment. Variations in either or both of these can be made to meet the requirements for specific applications or properties, for example, strength, fatigue, and hardness. Heat treatment cycles for these alloys are:

- *Elgiloy wire/spring:* cold work 45 to 48% (the normal coil spring range), heat treat at 525 ± 5.5 °C (980 ± 10 °F) for 5 h, air cool.
- *Elgiloy flat strip:* cold work to desired property level (85% cold work is the maximum hardness), heat treat at 480 ± 5.5 °C (900 ± 10 °F) for 5 h, air cool.
- *Duratherm 600 soft strip/wire:* cold work to desired property level, heat treat at 750 °C (1380 °F) for 4 h, air cool.
- *Duratherm 600 ½ hard strip/wire:* cold work to desired property level, heat treat at 650 °C (1200 °F) for 4 h, air cool.
- *Duratherm 600 full hard strip/wire:* cold work to desired property level, heat treat at 650 °C (1200 °F) for 2 h, air cool.
- *Havar strip:* cold roll, heat treat in vacuum between 455 and 540 °C (850–1000 °F) for 3 to 5 h, air cool. When heated in air the strip must be pickled in a solution of 4% hydrofluoric acid and 12% nitric acid (balance water) to remove oxide surface layer.

Workability

Wear Resistant Alloys

The hot workability of alloys 6B and 6K is somewhat limited because of the high carbon/carbide contents and high strengths. In general these alloys cannot be successfully forged, although special forming operations can be performed at temperatures above 980 °C (1800 °F). The alloy producer should be consulted for forming recommendations.

Heat Resistant Alloys

Forging. Both alloys 25 and 188 are forgeable. Forging temperatures for these alloys are:

- *Alloy 25:* upset and breakdown temperature, 1230 °C (2250 °F); finish forging temperature, 1230 °C (2250 °F)
- *Alloy 188:* upset and breakdown temperature, 1205 °C (2200 °F); finish forging temperature, 1175 °C (2150 °F)

The strength of these alloys at elevated temperatures, including the temperatures at which they are forged, is considerably higher than that for iron-base alloys; consequently, the pressures required in forging them are several times greater than those for the iron-base alloys.

Even when forged at its maximum forging temperature, alloy 25 work hardens; therefore, forging pressure must he increased with greater reductions. Accordingly, this alloy generally requires frequent reheating during forging to promote recrystallization and to lower the forging pressure for subsequent steps.

Forging conditions (temperature and reduction) have a significant effect on the grain size of cobalt-base alloys. Because low ductility, notch brittleness, and low fatigue strength are associated with coarse grains, close control of forging and of final heat treatment is important.

Cobalt-base alloys are susceptible to grain growth when heated above approximately 1175 °C (2150 °F). They heat slowly and require a long soaking time for temperature uniformity. Forging temperatures and reductions, therefore, depend on the forging operation and the part design.

The alloys are usually forged with small reductions in initial breakdown operations. The reductions are selected to impart sufficient strain to the metal so that recrystallization (and usually grain refinement) will occur during subsequent reheating. Because the cross section of a partly forged section has been reduced, less time is required to reach temperature uniformity in reheating. Consequently, because reheating time is shorter, the reheating temperature may sometimes be increased 30 to 85 °C

(50–150 °F) above the initial forging temperature without harmful effects. However, if the part receives only small reductions in subsequent forging steps, forging should be continued at the lower temperatures. These small reductions, in turn, must be in excess of about 5 to 15% to avoid abnormal grain growth during subsequent annealing.

Cold working for heat resistant alloys should be carried out on solution-treated material. Because these alloys work harden very rapidly, frequent intermediate annealing treatments are needed for complex forming operations. Bending, spinning, and deep drawing are typical of the cold-working operations carried out on alloys 25 and 188.

MP35N

Hot Working. MP35N Alloy forges and rolls much like an age-hardening nickel-chromium steel like A-286 and is slightly more resistant to deformation than the 300 series of stainless steels. The maximum furnace temperature for forging or rolling is 1150 °C (2100 °F). For the breakdown of cast structure, deformation should not be continued below approximately 870 °C (1600 °F) to prevent surface tearing. Wrought structure may be deformed at any temperature up to 1150 °C (2100 °F) within the limits of the processing equipment.

Cold Working. Practically any form of cold deformation can be applied to MP35N Alloy that can be used with the 300 series stainless steels. The excellent ductility of the alloy makes possible large reductions without annealing. Work-hardening rate is similar to 304 stainless steel and less than that of 301 stainless steel. Drawing, swaging, rolling, and shear forming are all excellent ways of deforming for work strengthening.

Forming. Operations such as brake-press bending, cup drawing, punching, and spinning can be done easily in the annealed condition. Extra attention should be given to ensure that adequate power is available to form the alloy in the higher-strength condition and that the forming tools are harder than MP35N Alloy after it has been formed.

Lubricants are helpful for all forming operations and necessary for some. Standard copper plating, molybdenum disulfide (MoS_2) solid lubricant, and soap lubricants are used for drawing. High-sulfur oils or grease are recommended for swaging and spinning at room temperature, and graphite-grease lubricants for warm operations.

Age-Hardening Alloys Elgiloy, Duratherm 600, and Havar

Elgiloy. Forming should be carried out prior to heat treatment because the heat-treating process strengthens the material and makes it more difficult to form. For strip, bending should take place perpendicular to the direction of rolling so that it will be across the elongated grain structure rather than parallel to it. In forming a 90° bend, the radius should be at least 5 times the thickness; in a 360° bend, a diameter of 18 to 25 times the thickness is usually acceptable. Wire should not be formed beyond a mean diameter of 4 times the wire size.

Duratherm 600. The forming characteristics of Duratherm are similar to Elgiloy described above.

Havar. Even after rolling and subsequent work hardening, Havar can be sheared, coiled, or formed into simple shapes. In the annealed state, the alloy is remarkably ductile (40% elongation in 50 mm, or 2 in.) and offers excellent workability when worked either hot or cold. It can also be formed to a limited extent after aging.

Joinability

Wear Resistant Alloys

Welding. In decreasing order of preference, alloys 6B and 6K can be welded by gas-tungsten arc welding (GTAW) with an argon flow of 12 L/min (25 ft^3/h), gas-metal arc welding (GMAW), shielded-metal arc welding (SMAW) with coated electrodes, and oxyacetylene welding (OAW). The OAW method should be used with caution in that these alloys will "boil" during welding, which may cause porosity. A 3× reducing flame is recommended to reduce oxidation, penetration, and interalloying.

Both alloys 6B and 6K should be preheated and maintained at 540 °C (1000 °F) to prevent cracking during welding and then still air cooled. Fixturing, which could chill the weld rapidly, should not be used. Standard weld joints are recommended.

Recommended filler metals for joining alloy 6B to softer materials, such as carbon steel or stainless steel, include Inconel filler metals 82 (AWS ERNiCr-3), 92 (AWS ERNiCrFe-6), and 625 (AWS ERNiCrMo-3). Harder cobalt-base filler metals, such as Stellite 6 and 21, are recommended for joining 6B to itself, especially if wear resistance is needed in the weld area. For wear-resistance welds, filler metals 82, 92, and 625 can be used for the root passes and then be weld overlayed with the harder cobalt alloy. Gas shielding of the root side of the gas-tungsten arc (GTA) weldments is recommended in order to improve weld penetration.

Brazing. Alloys 6B and 6K are readily joined to other materials by brazing. All forms of surface contamination, such as paint, ink, oil, and chemical residues, must be removed from the mating parts by pickling, solvent degreasing, or other means. In addition, fluxing will be required during torch brazing operations when using silver (BAg) brazing filler metal to help clean the joint and allow the filler metal to flow more freely over the mating surfaces. Joint areas should be brushed generously with brazing flux prior to heating. When torch or induction brazing, as soon as the brazing filler metal melts, the source of the heat should be removed and the parts positioned. The assembly should then be pressed together to squeeze out the excess flux and still air cooled. The parts should not be quenched.

In addition to silver brazing filler metals, gold, palladium, and nickel-base alloys are also satisfactory for joining 6B and 6K. Brazing filler metal selection depends on the service conditions expected. Producers of brazing filler metals should be consulted.

A close fit of the mating surfaces is recommended. The finished joints will have greater strength if the filler metal is very thin, generally about 0.03 to 0. 13 mm (0.001–0.005 in.) thick.

Brazing with high-temperature filler metals is generally performed in a furnace. Induction, resistance, and dip brazing have limited application. Vacuum furnaces or controlled-atmosphere furnaces, having adequate moisture control at brazing temperature (less than –60 °F, or –50 °C, dew point), produce the most satisfactory results. Furnace atmospheres, such as hydrogen or dissociated ammonia, are suitable for brazing wear resistant alloys.

Heat Resistant Alloys

Welding. The welding characteristics of alloys 25 and 188 are quite similar. They can be joined by GTAW, GMAW, SMAW, electron beam welding, and resistance welding. Submerged arc welding is not recommended because this process is characterized by high heat input to the base metal and slow cooling of the weld. These factors can increase weld restraint and promote cracking.

The joint surface and adjacent area should be thoroughly cleaned before welding. All grease, oil, crayon marks, sulfur compounds, and other foreign matter should be removed. Contact with copper or copper-bearing materials in the joint area should be avoided. It is preferable, but not necessary, that the alloy be in the solution-annealed condition when welded.

Matching composition filler metal is recommended for joining alloy 188. For joining section thicknesses greater than 9.5 mm ($\frac{3}{8}$ in.), 230-W filler wire is suggested. For SMAW, Haynes alloy 25 electrodes (AMS 5796) are suggested. For dissimilar metal joining of alloy 188 to nickel-, cobalt-, or iron-base materials, alloy 188 itself, 230-W filler wire, 556 alloy, Hastelloy alloy S (AMS 5838), or Hastelloy alloy W (AMS 5786, 5787) welding products are suggested, depending on the particular case. Filler metal selection recommendations for alloy 25 are nearly identical.

Brazing. The brazing of both wrought and cast heat resistant cobalt alloys is readily accomplished with the same techniques used for nickel-base heat resistant alloys (see the article "Welding and Brazing of Nickel Alloys" in this Handbook). Because most heat resistant cobalt alloys do not contain substantial amounts of

aluminum or titanium found in precipitation-hardenable nickel alloys, brazing atmosphere requirements are less stringent. Cobalt alloys can be brazed in either a hydrogen atmosphere or a vacuum. Filler metals are usually nickel-base or cobalt-base alloys or gold-palladium compositions. Silver-base or copper-base filler metals may not have sufficient strength and oxidation resistance in many high-temperature applications. An electroplate or flash of nickel is often used to promote better wetting of the brazing filler metal.

Nickel-base brazing alloys, such as AWS BNi-3, have been used successfully on alloy 25 for honeycomb structures. After brazing, a diffusion cycle was reportedly used to raise the braze joint remelt temperature to 1260 to 1315 °C (2300–2400 °F). Table 1 presents the effects of a high-temperature braze (1225 °C, or 2240 °F, for 15 min) on the mechanical properties of alloy 25. One cobalt-base brazing filler metal (AWS BCo-1, see Table 2) appears to offer a good combination of strength, oxidation resistance, and remelt temperature for use on alloy 25 foil.

Cobalt-base alloys, much like nickel-base alloys, can be subject to liquid metal embrittlement or stress-corrosion cracking when brazed under residual or dynamic stresses. This frequently is observed when using silver- or silver-copper-base (BAg) filler metals. Liquid metal embrittlement of cobalt-base alloys by copper-base (BCu) filler metals occurs with or without the application of stress; therefore, BCu filler metals should be avoided when brazing cobalt-base alloys.

MP35N and MP159

In general, the welding of both MP35N and MP159 is similar to that of type 304 austenitic stainless steel and the same preparations and precautions used to weld 304 should be employed. Weld parameters for MP35N have been developed using the GTAW method. The work was carried out on 1.5 mm (0.060 in.) thick sheet and 6.4 mm (1.250 in.) thick plate. The following GTAW parameters are recommended:

- *Argon gas flow rate:* 9.4 to 11.8 L/min (20–25 ft^3/h)
- *Weld speed:* 140 mm/min (5.5 in./min)
- *Voltage:* 10 V
- *MP35N filler wire feed:* 355 to 560 mm/min (14–22 in./min)

Welding current should be adjusted to ensure that the heat input per pass is low, that is, ½ to ⅔ of the heat input used to weld maraging steel or type 304 stainless steel. For the weld parameters used in this example, currents of 50 to 60 A were used for the sheet. Total heat input was 2165 to 3740 J/cm (5500–9500 J/in.). For plate, the current ranged from 100 to 160 A and heat inputs were 4330 to 7480 J/cm (11,000–19,000 J/in.).

Age-Hardening Alloys Elgiloy, Duratherm 600, and Havar

Elgiloy. Whenever possible, it is best to use some mechanical fastening method to join Elgiloy to itself or any other material. If mechanical fastening procedures cannot be used, spot welding, laser beam welding, or electron beam welding should be employed. Elgiloy can also be joined by soldering or brazing if a very active flux is used, and the temperature is kept below 595 to 760 °C (1100–1400 °F). Because of the latter requirement, furnace brazing is recommended.

Duratherm 600 can be welded by spot welding, electron beam welding, or laser welding. Welding should be carried out prior to aging, and short welding times are recommended.

Soldering is always carried out after aging. Flux selection is critical and soldering experts should be consulted. Where necessary, complex joints should be precoated with tin first.

Silver brazes with a low melting point are recommended for brazing, which can also be performed on age-hardened parts without affecting the mechanical behavior. Suitable joints are only achieved on clean, oxide-free surfaces and with suitable fluxes. An electroplate of nickel plating is sometimes used to improve filler metal wetting of the joint.

Havar can be welded by GMAW and resistance welding. It is also possible to solder and braze. The alloy producer should be consulted for specific joining parameters.

Machinability

Wear Resistant Alloys. Although the high-carbon alloys 6B and 6K are more difficult to machine than the lower-carbon heat and corrosion resistant cobalt alloys, they can be machined using tungsten carbide tools. Carbide inserts are used with a 5° negative tool holder and a 30° or 45° lead angle. Tools for facing or boring are essentially the same except for greater clearances where needed. For best results in drilling, the drill web should be kept thin. Screw-machine length, carbide-tipped drills should be used. High-speed taps are not recommended for 6B and 6K, but threads can be produced by electrical-discharge machining. For better surface finish, these alloys should be ground. Table 3 gives some general information that can be used as a guide for machining 6B and 6K.

Stellite hardfacing alloys can be machined using polycrystalline cubic boron nitride (PCBN) tools. Cutting speeds in the range of 200 to 250 mm/min (650–820 sfm) are generally recommended. Because of the work-hardening nature of these alloys, feed rates should not be less than 0.2 mm/rev (0.008 in./rev). Round, chamfered PCBN inserts should be

Table 1 Effect of brazing on mechanical properties of alloy 25

Condition	Test temperature(a) °C	Test temperature(a) °F	Ultimate strength MPa	Ultimate strength ksi	0.2% offset yield strength MPa	0.2% offset yield strength ksi	Elongation, %
Tensile testing							
Mill anneal	RT	RT	1020	147.9	477	69.2	56
After braze cycle	RT	RT	747	108.3	477	69.2	12
Mill anneal	815	1500	396	57.4	210	30.5	17
After braze cycle	815	1500	393	57.0	229	33.2	24
Mill anneal	980	1800	145	21.0	125	18.1	35
After braze cycle	980	1800	148	21.5	130	18.8	35

Condition	Test temperature °C	Test temperature °F	Stress MPa	Stress ksi	Time to rupture, h
Stress-rupture testing					
Mill anneal	815	1500	169	24.5	82
After braze cycle	815	1500	169	24.5	72.3
Mill anneal	900	1650	103	15.0	56
After braze cycle	900	1650	103	15.0	36
Mill anneal	980	1800	45	6.5	110
After braze cycle	980	1800	45	6.5	120

(a) RT, room temperature

Table 2 AWS cobalt-base brazing alloy for elevated-temperature service

AWS classification	Composition, wt% Cr	Ni	Si	W	Fe	B	C	P	S	Al	Ti	Zr	Co	Other elements total	Solidus °C	Solidus °F	Liquidus °C	Liquidus °F	Brazing range °C	Brazing range °F
BCo-1	18.0–20.0	16.0–18.0	7.5–8.5	3.5–4.5	1.0	0.7–0.9	0.35–0.45	0.02	0.02	0.05	0.05	0.05	bal	0.50	1120	2050	1150	2100	1150–1230	2100–2250

Source: AWS 5.8

Table 3 Recommended guidelines for machining alloys 6B and 6K

			Roughing				Finishing			
	Speed		Feed/rev		Depth of cut		Feed/rev		Depth of cut	
Operation	m/s	sfm	mm	in.	mm	in.	mm	in.	mm	in.
Turning(a)	0.25–0.35	50–70	0.20–0.28	0.008–0.012	1.27–5.08	0.050–0.200	0.05–0.13	0.002–0.005	0.63–0.18	0.025–0.007
Facing(a)	0.25–0.35	50–70	0.20–0.28	0.008–0.012	1.27–2.54	0.050–0.100	0.15–0.25	0.006–0.010	0.63 or less	0.025 or less
Boring(a)	0.25–0.30	50–60	0.13–0.20	0.005–0.008	0.63–2.54	0.025–0.100	0.13–0.08	0.005–0.003	0.63–0.18	0.025–0.007
			Depends on bar and size of tool							
Drilling(b)	0.15–0.18	30–35	…	…	…	…	0.03–0.13	0.001–0.005	…	…
								Depends on size of drills		
Reaming(c)	0.20–0.25	40–50	0.03–0.13 per tooth	0.001–0.005 per tooth	0.38–0.76	0.015–0.030	0.03–0.10 per tooth	0.001–0.004 per tooth	0.18–0.63 (Based on dia.)	0.007–0.025 (Based on dia.)
Threading	Use single point C-3 tungsten carbide tools. 0.05–0.13 m/s (10–25 sfm) based on number of threads per mm (in.)									

(a) Use C-3 tungsten carbide tools. Coolant—water base fluid diluted 15 parts water to one part fluid. Tools for facing and boring are basically the same as turning tools except for greater clearances where needed. (b) C-2 tungsten carbide twist drills with drill web kept as thin as possible. Coolant—same as (a) above. (c) C-2 tungsten carbide tools. Reamers should have a 45° (0.79 radius) side cutting edge angle. Coolant—same as (a) above.

used whenever possible, and the depth of cut should be sufficient to enable the tool to penetrate the solid underlying material, thereby avoiding the interruptions and damaging abrasiveness of the weld-deposited alloy skin.

Whenever close tolerances are required, grinding is recommended for finishing alloys 6B and 6K. Honing can be used to finish inside diameters. Grinding speeds should be kept between 14 and 31 m/s (2800 and 600 sfm). Alloys being ground should not be quenched because this can cause surface checking.

Heat resistant alloys are more difficult to machine than austenitic stainless steels and lower feeds, speeds, and depth of cut are recommended. For drilling use 4.5 m/min (15 sfm) and 0. 025 to 0.1 mm/rev (0.001–0.004 in./rev) feed. For turning use 6 m/min (20 sfm) and 0.05 mm/rev (0.002 in./rev) feed. Cobalt grades of high-speed steels or tungsten carbide tools should be used with rigid setups. Tools should be maintained sharp. Tool geometries should be similar to those used for nickel-base high-temperature alloys. The high work-hardening rate and high shear strength of heat resistant alloys complicate their machining. Sulfochlorinated cutting oil should be used for all machining. More detailed information on machining and grinding both wrought and cast heat resistant cobalt alloys can be found in *Machining*, Volume 16, of the *ASM Handbook* (see the article "Machining of Heat-Resistant Alloys").

MP35N and MP159. The machinability of these alloys is similar to that of the Ni-Co-Cr alloy Waspaloy. Both MP35N and MP159 can be machined in the work-hardened and aged condition. For drilling use 7.6 m/min (25 sfm) and 0.10 mm/rev (0.005 in./rev) feed. For turning use 9.1 m/min (30 sfm) and 0.254 mm/rev (0.010 in./rev) feed. Both high-speed steels and carbide tools can be used. Soluble oil (1:20), sulfurized oil, or chlorinated oil are recommended cutting fluids. Alloy producers should also be consulted when machining these alloys.

Age-Hardening Alloys Elgiloy, Duratherm, and Havar. These alloys are difficult to machine because they work harden rapidly in front of the cutting tool. Machining is normally carried out prior to heat treatment. The tooling and setup of the workpiece should be very rigid with the machine tool in good condition, with minimum backlash and ample power and rigidity to maintain a positive feed (except in drilling). Because of the rapidity with which these alloys work harden, the power required for machining is greater than for steels of the same hardness. To minimize work hardening, cutting edges should be ground as sharp as possible. A copious flow of cutting fluid must be used with high-speed steels and will help greatly improve tool life and surface finish with carbide tools. Sulfurized oil or sulfochlorinated cutting fluids are recommended. Alloy producers will provide information on parameters such as speeds, feeds, and cutting angles.

Table 4 Electrolytic polishing solutions for cobalt and cobalt alloys

	Conditions				
Electrolyte composition	Current density	Voltage, dc	Temperature, °C (°F)	Time, min	Comments
1. 50 mL HCl 50 mL ethanol	2.5 A/cm^2	8–9	20 (68)	30–90 s	Use stainless steel cathode. Bluish-green anode film dissolves in water. Slight etching
2. 5 g $ZnCl_2$ 15 g $AlCl_3 \cdot 6H_2O$ 200 mL methanol 30 mL H_2SO_4	1–2 A	…	RT	2	Use 10 by 10 mm sample size. Grind to 600 grit. Use platinum for cathode and anode lead wires. Agitate cathode. Dissolve salts in methanol, add H_2SO_4 slowly.
3. 100 mL perchloric acid 142 mL water 758 mL methanol	9 A/cm^2	48	RT	3 s	For Vitallium. Used 1 cm^2 area, ground to 600 grit. Stainless steel or Vitallium cathode, vertical, 25 mm spacing. Agitate and cool solution during use.
4. H_3PO_4, concentrated	1–2 A/dm^2	1–1.5	20 (68)	5–10	Produces slight etching. Solid black anode film can be wiped off with cotton. Produces a rise in current density to 12–16 A/dm^2
5. 14 mL water 75 mL ethanol 6 mL perchloric acid	10–12 A/in.^{2} (1.55–1.85 A/cm^2)	6–10	25–55 (78–131)	10–20 s	For Co-Cr-Fe-Ni alloys

Source: Ref 2

Metallography

This section describes polishing and etching techniques specific to wear, heat, and corrosion resistant cobalt alloys. Additional information on procedures to prepare metallographic specimens of cobalt alloys can be found in the article "Metallography and Microstructures of Heat Resistant Alloys" in this Handbook. A review of the metallography of cobalt and cobalt alloys is presented in Ref 1.

Grinding and Polishing. Grinding with silicon carbide papers is suitable for cobalt-base alloys. Polishing is generally accomplished using diamond abrasive, generally as a paste. Electrolytic polishing is frequently used for cobalt alloys, and a number of electrolytes have been developed for this purpose. Table 4 provides a list of those recommended for cobalt alloys, with some indications of the conditions under which they can be operated. The current density and voltage are interdependent and related to the temperature and to the electrode spacing, so that conditions must be adjusted by trial and error until satisfactory polishing is achieved. Chemical polishing solutions can also be employed when only a limited number of samples are being prepared. These include a solution containing 40 mL lactic acid, 30 mL hydrochloric acid, and 5 mL nitric acid, and also a solution consisting of 1 part acetic acid and 1 part nitric acid.

Etching. Because cobalt-rich alloys are corrosion resistant to many mild reagents, vigorous

etching reagents are necessary to develop their structures. For macroetching, strong mineral acids are generally called for, and two procedures used for cobalt alloys are given in Table 5.

As indicated in Table 6, there are a number of microetching reagents for cobalt alloys. For pure cobalt and cobalt-base alloys, the standard solution for immersion etching is the mixture of hydrochloric, nitric, and acetic acids shown as etchant composition No. 2 in Table 6. Young (Ref 3) has described etching methods for delineating oxide and sulfide phases in cobalt (see etchant No. 12 in Table 6). Weeton and Signorelli (Ref 4) have described different procedures for identifying sigma phase and carbides in wrought Stellite 21. These procedures are listed in Table 7. Beraha (Ref 5) has developed a tint etch for cobalt alloys (see etchant No. 18 in Table 6). Electrolytic etching is often more controlled than immersion or swab etching. As shown in Table 6, both heat resistant and hardfacing alloy specimens are prepared using electrolytic etchants. The structures of various cobalt alloys revealed by the use of the etchants described above are shown in the article "Metallography and Microstructures of Heat Resistant Alloys" in this Handbook (see Fig. 120 to 150 for wrought structures and Fig. 210 to 233 for cast structures).

Table 5 Macroetchants for cobalt and cobalt alloys

Etchant composition	Comments
1. Solution A Saturated solution of $FeCl_3$ in HCl Solution B Add 5% HNO_3 to solution A prior to use.	Use at room temperature. After etching dip sample in 1:1 solution of HCl and H_2O.
2. Solution A 21 mL H_2SO_4 15 mL HCl 21 mL HNO_3 21 mL HF 22 mL H_2O Solution B 40 mL of a solution of 1 g $CuCl_2 \cdot 2H_2O$ and 5 mL H_2O 40 mL HCl 20 mL HF	Etch sample 5 min in solution A and then 5 min in solution B.

Table 6 Etchants for cobalt and alloys

Etchant composition	Comments
Immersion or swab etchants	
1. 90 mL methanol 10 mL HNO_3	For Co and Co-Fe alloys. Immerse sample for up to 30 s (1–50% nital has been used). Do not store.
2. 15 mL HNO_3 15 mL acetic acid 60 mL HCl 15 mL water	For Co and alloys. Age 1 h before use. Immerse sample for up to 30 s. Standard etchant.
3. 7.5 mL HF 2.5 mL HNO_3 200 mL methanol	General etch for Co and alloys. Immerse sample 2–4 min.
4. 100 mL HCl 5 mL H_2O_2 (30%)	For Co hardfacing alloys and high-temperature alloys. Use under a hood. Use fresh. Immerse sample a few seconds.
5. 5 mL HNO_3 200 mL HCl 65 g $FeCl_3$	For Co high-temperature alloys. Immerse sample a few seconds. Use under a hood.
6. 50 mL water 50 mL HCl 10 g $CuSO_4$	Marbles reagent. For Co high-temperature alloys. Immerse or swab sample for up to 1 min. Can add a few drops of H_2SO_4 to increase activity.
7. 100 mL water 100 mL HCl 200 mL methanol 5 mL HNO_3 7 g $FeCl_3$ 2 g cupric chloride	For Co-Fe magnetic alloys. Immerse or swab sample for 10–15 s.
8. 100 mL water 1 mL acetic acid 1 mL HNO_3	For Co-Sm alloys. Immerse sample a few seconds.
9. 100 mL water 2 mL HF 5 mL H_2O_2 (30%)	For Co-Ti alloys
10. 3 parts HNO_3 1 part HCl	For Co-Pt alloys (48–54 atomic % Co)
11. 95 mL water 1 g KOH 4 g $KMnO_4$	For Co-40.7Cr-2.4C alloy. Colors M_7C_3 gray and $M_{23}C_6$ black
12. Solution A 1 g mercuric chloride 99 mL water Solution B 35 g sodium bisulfite 100 mL water	Etch with solution A for 30 s or with solution B for 2 min to distinguish between Co metal, cobalt oxide, and sulfides. Both stain the Co matrix brown, oxide remains dark gray, cobalt sulfide remains yellowish and MnS remains bluish gray.
13. 30 mL water 40 mL HCl 5 g $CuCl_2$ 25 mL alcohol	Fry's reagent. For MP35N alloy. Swab sample for 30 s up to 2 min. Reveals hexagonal close-packed (hcp) platelets on face-centered cubic (fcc) matrix.
Immersion or swab etchants (continued)	
14. 45 mL water 50 mL HCl 5 g $CuCl_2$ 25 mL alcohol	Modified Fry's reagent. For MP35N alloy. Swab sample for 30 s up to 2 min. Reveals hcp platelets on fcc matrix.
15. 25 mL water 50 mL HCl 15 g $FeCl_3$ 3 g cuprous ammonium chloride	For Co and Co-Al alloys
16. 25 mL water 25 mL acetic acid 50 mL HNO_3	For Co alloys
17. 80 mL lactic acid 10 mL H_2O_2 (30%) 10 mL HNO_3	For Co alloys
Tint etch	
18. Solution A: HCl and water (1:1) (stock solution) Ingredient b: 0.6–1 g potassium metabisulfite Ingredient c: 1–1.5 g $FeCl_3$	Beraha's tint etch for Co-base alloys. Add ingredient b to 100 mL of stock solution A, then add ingredient c. Immerse sample at 20 °C (68 °F) for 60–150 s, agitate sample. Matrix is colored; carbides and nitrides are unaffected.
Electrolytic etchants	
19. 100 mL water 5–10 mL HCl	For Co and Co high-temperature alloys. Use at 3 V dc, 2–10 s, graphite cathode. Pitting sometimes occurs.
20. 100 mL water 2–10 g CrO_3	For Co hardfacing alloys. Use at 3 V dc for 2–10 s.
21. 100 mL water 5 mL HCl 10 g $FeCl_3$	For Co and Co-Al alloys. Use at 6 V dc, few seconds, stainless steel cathode.
22. Solution A 100 mL water 2 g CrO_3 Solution B 85 mL water 4 g NaOH 10 g $KMnO_4$	For Co hardfacing alloys and Co high-temperature alloys. Use solution A at 3 V dc for 2 s. Rinse in water and immerse sample in solution B for 5–10 s. Use solution B fresh.
23. 140 mL HCl 1 g CrO_3	For Co high-temperature alloys. Use at 3 V dc for 2–10 s.
24. 100 mL HCl 0.5 mL H_2O_2 (30%)	For Co high-temperature alloys. Use at 4 V dc for 3–5 s.
25. 940 mL water 45 mL HNO_3 15 mL HCl	For Co. Use stainless steel cathode, 3.5 V dc, 0.75 A/cm^2, 15 s, 20 °C (68 °F).

Source: Ref 2

Table 7 Staining and heat-tinting procedures for identification of sigma phase and carbides in wrought Stellite 21

Coloring process	Method	Purpose	First etchant		Staining method		Colors of minor phases obtained by previous investigators
			Solution	Method	Solution	Method	
1	Etch	To stain sigma phase	8% oxalic acid; 92% water	Electrolytic etch; 8–10 s; 6V; room temperature	5 g $KMnO_4$; 5 g NaOH; 90 mL water	Immerse 10–20 s; room temperature	Sigma: bright green or red to purple
2	Etch	To differentiate between carbides and sigma phase	10% NaCN; 90% water	Electrolytic etch; 10–20 s; 1.5 V	Murakami's 10 g $K_3Fe(CN)_6$; 10 g KOH; 100 mLwater	Immerse 2–4 s; room temperature	Carbides: straw to yellow-brown or buff Gamma (sigma): grey to blue or greenish grey
3	Etch	To identify carbides	2% chromic acid; 98% water	Light electrolytic etch	1 part (20% $KMnO_4$, 80% water); 1 part (8% NaOH, 92% water)	Immerse 7 s; room temperature	$Cr_{23}C_6$: brown Cr_7C_3: pale yellow to light tan M_6C: red, green, yellow, blue (also reticulation)
4	Heat tint	To identify carbides and sigma phase	5% HCl; 95% water	Light electrolytic etch; 1 s; 5 V	…	Heat polished specimen to dull red Held at temperature until surface becomes colored Air cooled or Hg-quenched	Sigma: dark medium brown $Cr_{23}C_6$: white M_6C: dark Note: M_6C and sigma cannot be differentiated in same structure

Source: Ref 4

REFERENCES

1. F.R. Morral, Metallography of Cobalt-Base and Cobalt-Containing Alloys, *Prakt. Metallogr.*, Vol 10, 1973, p 398–413
2. G.F. Vander Voort, *Metallography: Principles and Practice*, McGraw-Hill Inc. (now published by ASM International), 1984, p 514, 569, 620–621
3. R.S. Young, Metallographic Differentiation of Cobalt Metal, Oxide, and Sulphide, *Metallurgia*, Vol 59, April 1959, p 210
4. J.W. Weeton and R.A. Signorelli, Effect of Heat Treatment upon Microstructures, Microconstituents, and Hardness of a Wrought Cobalt Base Alloy, *Trans. Am. Soc. Met.*, Vol 47, 1955, p 815–852
5. E. Beraha, Two New Metallographic Reagents for Stainless Steels and Heat-Resisting Alloys, *J. Iron Steel Inst.*, Vol 204, 1966, p 248–251

© 2000 ASM International. All Rights Reserved.
ASM Specialty Handbook: Nickel, Cobalt, and Their Alloys (#06178G)

Subject Index

A

Abrasion
high-stress . . . . . 387, 389, 390(T)
low-stress . . . . . 387, 389(F), 390(T)
Abrasive blasting 273, 278
heat-resistant nickel alloys 279–280
Abrasive flow machining, of nickel alloys. 244
Abrasive wear. *See* Wear, abrasive.
Acetic acid
corrosion of cobalt-base alloys . . . 396(T), 397(F,T)
corrosion of iron-base alloys . . . . . 397(T)
corrosion of nickel-base alloys . . . . . 397(T)
corrosion rate of CW-12MW . . . . . 58(T)
corrosion rate of Hastelloy D . . . . . 59(T)
corrosion rate of N-12MV . . . . . 58(T)
Acetic acid, glacial, corrosion rate of electroless nickel coatings . . . . . 118(T)
Acetic acid corrosion . . . . . 133, 134(T)
Acetone, corrosion rate of electroless nickel coatings . . . . . 118(T)
Acid media corrosion, of cobalt alloys . . . . . 396(T), 397(F,T)
Acrylic acid corrosion 134
Age hardening. *See* Heat treating of nickel alloys.
Air-hardening cold-work tool steels 8
Air plasma sprayed coatings 287
Alkali corrosion . . . . . 135–136(F)
Alkali metal sulfates 62
Alkaline fuel cells, functional, service, and structural requirements . . . . . 211(T)
All-chloride nickel plating solution . . . . . 112(T), 113
cathode current density . . . . . 112(T)
composition . . . . . 112(T)
mechanical properties . . . . . 112(T)
pH value . . . . . 112(T)
temperature range . . . . . 112(T)
Allied Signal, production of dual-alloy turbine disk/wheels . . . . . 224(F)
Alloy phase diagrams. *See* Phase diagrams.
Alloy steels, nickel consumption, % 6
All-sulfate nickel plating solution . . . . . 112(T), 113
cathode current density . . . . . 112(T)
composition . . . . . 112(T)
mechanical properties . . . . . 112(T)
pH value . . . . . 112(T)
temperature range . . . . . 112(T)
Alnico alloys . . . . . 10, 351(T)
mechanical properties . . . . . 351(T)
physical properties . . . . . 351(T)
Aluminide (diffusion) coatings, for superalloys. . 87–88
Aluminized Cr-Mo steel, corrosion rates in molten drawsalt . . . . . 185(T)
Aluminum
alloying element effect in cobalt-base heat-resistant alloys 366
alloying element effect on nickel-and iron-base superalloys . . . . . 167(T)
alloying element effects on corrosion resistance . . . . . 17(T)
alloying element effects on nickel alloy corrosion resistance . . . . . 129–130(F)
alloying element range in superalloys. . . . . 69(T)
cold work effect on hardness . . . . . 191(F)
content effect on nickel alloy weldability 248
corrosion rates in molten drawsalt. . . . . 185(T)
effect on oxidation resistance of superalloys 85, 89(F)
as gamma prime former 15
molten, corrosion by . . . . . 186(T)
as solid-solution strengthener in nickel. . . . . 14(F)
Aluminum sulfate, corrosion rate of electroless nickel coatings . . . . . 118(T)
American Iron and Steel Institute 6
Ammonia, corrosion rate of electroless nickel coatings . . . . . 118(T)
Ammoniacal leaching of sulfides, equation 208
Ammonia nitrate, corrosion rate of electroless nickel coatings . . . . . 118(T)
Ammonium sulfate, saturated, corrosion rate of electroless nickel coatings . . . . . 118(T)
Annealing. *See* Heat treating of nickel alloys.
Annulus 74
Anode efficiency in nickel plating 107
Anodizing, market segment percentage and form of cobalt consumption 347
Aqueous environment corrosion, of cobalt alloys . . . . . 395–398(F,T)
Argon-oxygen decarburization (AOD) process 75, 251
Asbolite
composition . . . . . 346(T)
mining locations. . . . . 346(T)
Ash/salt deposit corrosion 183
ASTM G 28 solutions
corrosion of cobalt-base alloys . . . . . 397(T)
corrosion of iron-base alloys . . . . . 397(T)
corrosion of nickel-base alloys . . . . . 397(T)
Atmospheric corrosion . . . . . 130(T)
Atmospheric-pressure carbonyl process 4
Atomization . . . . . 210–211(F)
Austempered ductile irons, nickel content effect 9
Austempering 137
Austenitic manganese steels
mechanical properties 8
nickel content effects . . . . . 8(T)
physical properties. . . . . 252(T)
Auxiliary brighteners 108–109

B

Band sawing, of nickel alloys. . . . . 243–244(T)
Barren solution 210
Batteries, market segment percentage and form of cobalt consumption 347
Belt grinding, of nickel alloys. 244
Bending
compression 195
draw 195
hot 195–196
of plate, sheet, and strip. . . . . 196(T)
press 195
rod and bar 196
roll 195
tube and pipe . . . . . 195–196(T)
Bending fatigue strength, of cobalt alloys, individual alloy values . . . . . 374(T), 381(T)
Benzene, corrosion rate of electroless nickel coatings . . . . . 118(T)
Benzotrichloride
corrosion rate of electroless nickel-phosphorus coatings. . . . . 118(T)
corrosion rate of mild steel . . . . . 118(T)
corrosion rate of nickel 200 . . . . . 118(T)
corrosion rate of stainless steel (Type 316) . . 118(T)
Benzoyl chloride
corrosion rate of electroless nickel-phosphorus coatings. . . . . 118(T)
corrosion rate of mild steel . . . . . 118(T)
corrosion rate of nickel 200 . . . . . 118(T)
corrosion rate of stainless steel (Type 316) . . 118(T)
Beryllium-copper alloys, cobalt content effect . . . 353
Bessemer matte 4
Binary phase diagrams
cobalt-carbon . . . . . 356(T)
cobalt-nickel . . . . . 358(F)
cobalt-tungsten . . . . . 358(F)
nickel-aluminum . . . . . 331(F)
nickel-boron . . . . . 332(F)
nickel-carbon . . . . . 332(F)
nickel-chromium . . . . . 333(F), 357(F)
nickel-cobalt . . . . . 332(F)
nickel-copper . . . . . 333(F)
nickel-iron . . . . . 333(F), 357(F)
nickel-molybdenum. . . . . 334(F)
nickel-niobium . . . . . 334(F)
nickel-phosphorus . . . . . 334(F)
nickel-silicon . . . . . 335(F)
nickel-titanium . . . . . 335(F)
nickel-tungsten . . . . . 335(F)
Biomedical applications, nickel-titanium shape memory alloys. 102
Black nickel (chloride bath) plating solution . . . . . 112(T), 113
cathode current density . . . . . 112(T)
composition . . . . . 112(T)
mechanical properties . . . . . 112(T)
pH value . . . . . 112(T)
temperature range . . . . . 112(T)
Black nickel (sulfate bath) plating solution . . . . . 112(T), 113
cathode current density . . . . . 112(T)
composition . . . . . 112(T)
mechanical properties . . . . . 112(T)
pH value . . . . . 112(T)
temperature range . . . . . 112(T)
Blanking 193
Blasting, as finishing operation. 278

© 2000 ASM International. All Rights Reserved.
ASM Specialty Handbook: Nickel, Cobalt, and Their Alloys (#06178G)

Bobbing and sanding, wheel, compound and speed used . . . . . 277(T)
Body-centered tetragonal phase (γ'') 15
Boiling point, of cobalt. 345
Boride-containing nickel-base alloys 121–122(F,T)
Borides 304
Boring, of nickel alloys . . . . . 237–240(T)
Boron
alloying element effect in cobalt-base heat-resistant alloys 366
content effect on boride-containing nickel-base alloys. . . . . 121–122(F,T)
content effect on nickel alloy weldability 248
content effect on superalloy microstructure. 80
effect on superalloy mechanical properties 84
Boron-reduced cobalt-boron, electroless cobalt alloy plating systems . . . . . 354(T)
Boron-reduced cobalt-tungsten-boron, electroless cobalt alloy plating systems . . . 354(T)
Brazing 79
cobalt-base heat-resistant alloys . . . . . 402–403(T)
of heat-resistant nickel-base alloys . . . 267–272(F,T)
Brazing of nickel alloys. . . . . 267–272(F,T)
atmosphere control 270–271
cleanliness. 271
filler metal compositions . . . . . 267–268(T)
filler metal product forms 268–269
fixturing 270
oxide dispersion-strengthened (ODS) alloys . . 272(F)
precipitation-hardening alloys. 271
stress elimination or relieving 271
surface cleaning and preparation . . . . . 269–270(F)
temperatures and thermal cycles 271
Brighteners 108–109
Brine, 3.5% salt, CO_2 saturated, corrosion rate of electroless nickel coatings . . . . . 118(T)
Brine, 3.5% salt, H_2S saturated, corrosion rate of electroless nickel coatings . . . . . 118(T)
Briquetting . . . . . 5, 6(F), 210(F)
Broaching, of nickel alloys . . . . . 242, 243(T)
Bromides, causing stress-corrosion cracking . . . . . 145–146(T)
Brunauer-Emmett-Teller (BET) method 206
Brushing
as finishing operation 278
wheel, compound and speed used . . . . . 277(T)
Brush plating. 106
Buffing, as finishing operation 277–278
Bulk electrolytic extractions . . . . . 300–301, 302(T)

C

Calcium chloride, corrosion rate of electroless nickel coatings . . . . . 118(T)
Carbide films . . . . . 76(F)
Carbides 15, 301, 303–304
chromium-rich 142
effect on nickel alloy corrosion resistance 130
effect on stress-corrosion cracking . . . . . 141–143(F)
for tooling . . . . . 237–240(F,T)
in cobalt-base wear resistant alloys . . . . 363–364(F)
in nickel alloy microstructures . . . . . 308(F), 309(F), 310(F), 313(F), 314(F), 315(F), 322(F), 324(F), 327(F)
in superalloys . . . . . 80(F), 83–84(F)
Carbide strengthening, of nickel alloys 15
Carbon
alloying element effect in cobalt-base heat-resistant alloys 366
alloying element effect on nickel-and iron-base superalloys . . . . . 167(T)
alloying element effects on corrosion resistance . . . . . 17(T)
content effect on cavitation erosion of cobalt alloys 391
content effect on nickel alloy weldability 248
welding products for dissimilar-metal joints with nickel-base alloys . . . . . 250(T)
Carbonates, molten, corrosion by . . . . . 185–186(T)
Carbon steel
corrosion in chlorine-bearing environments 179(T)
corrosion in molten aluminum, static immersion tests . . . . . 186(T)
corrosion rates in molten drawsalt. . . . . 185(T)
physical properties. . . . . 252(T)
Carbon tetrachloride, corrosion rate of electroless nickel coatings . . . . . 118(T)
Carbonyl clusters 204
Carbonyl vapormetallurgy . . . . . 203–206(F)
Carburization . . . . . 172–173(F,T)
of cobalt alloys. . . . . 399, 400(F)
Carriers 108–109
Carrolite
composition . . . . . 346(T)
mining locations. . . . . 346(T)
CASS testing . . . . . 111(T)
Cast cobalt-base heat resistant alloys
alloying elements effects 367
chemical properties . . . . . 367(F)
compositions. . . . . 367(T)
mechanical properties . . . . . 367(F)
physical properties. 367
Cast corrosion-resistant nickel alloys . . . 55–61(F,T)
alloy classifications. . . . . 55–57(T)
applications. 55
composition. . . . . 55(T)
mechanical properties . . . . . 55, 56(T)
standard grades . . . . . 55–57(T)
Cast heat resistant nickel alloys . . . . . 62–67(F,T)
applications. 62
chemical properties 62
compositions . . . . . 62, 63(T), 65(T), 67(T)
elevated temperature mechanical properties. . . . . 62, 66(T)
mechanical properties . . . . . 66(T), 67(T)
Cast heat resistant nickel-chromium alloys
applications 62, 63
chemical properties . . . . . 62, 63(T)
development 62
Castings
chromium-nickel alloy standard specification (ASTM A 560) 63
nickel alloy, welding of 250
nickel and nickel alloy, standard specifications (ASTM A 494) 55
Cast irons
corrosion in chlorine-bearing environments . 179(T)
nickel consumption in U.S. by end use . . . . . 6(T)
nickel content effect . . . . . 8–9(T)
Cast nickel alloys
applications. 56
compositions . . . . . 55(T), 56
corrosion rates 56
mechanical properties 56
weldability 56, 260
Cast nickel-base proprietary alloys . . . . . 57–61(F,T)
compositions . . . . . 57, 58(T)
mechanical properties . . . . . 57, 58(T)
Cast nickel-chromium alloys, chemical properties. 62
Cast nickel-chromium-iron alloys
applications 56, 57, 67
composition . . . . . 55(T), 56, 66, 67(T)
elevated-temperature mechanical properties . . 57(T)
mechanical properties . . . . . 56(T), 57(T), 66(T), 67(T)
weldability 57
Cast nickel-chromium-iron-cobalt-copper-silicon alloys . . . . . 61(F)
applications. 61
chemical properties . . . . . 61(F)
sulfuric acid corrosion . . . . . 61(F)
Cast nickel-chromium-iron-molybdenum-cobalt-copper-silicon alloys
applications. 61
corrosion resistance. . . . . 60–61(F)
Cast nickel-chromium-molybdenum alloys
applications. 57
chemical properties . . . . . 57, 58(T)
compositions . . . . . 55(T), 57
corrosion rates . . . . . 57, 58(T)
heat treatment 57
mechanical properties . . . . . 56(T), 57
oxidation resistance 57
weldability 57
Cast nickel-chromium-molybdenum-copper-iron alloys, chemical properties . . . . . 59–60(F)
Cast nickel-copper alloys . . . . . 55(T), 56
applications. 56
compositions. . . . . 55(T)
galling resistance 56
heat treatment 56
mechanical properties . . . . . 56(T)
weldability 56
Cast nickel-iron-chromium alloys
compositions . . . . . 63, 65(T)
elevated-temperature mechanical properties . . . . 64, 66(T)
mechanical properties . . . . . 64, 66(T), 67(F)
Cast nickel-molybdenum alloys . . . . . 57–59(F,T)
compositions . . . . . 55(T), 57, 58(T)
corrosion resistance. . . . . 57, 58(T)
heat treatment 57
mechanical properties . . . . . 56(T), 57
weldability 57
Cast nickel-molybdenum-chromium alloys . . . . . 57–59(F,T)
compositions . . . . . 57, 58(T)
corrosion resistance. . . . . 57–59(F)
sulfuric acid corrosion. . . . . 57–59(F)
Cast nickel-silicon-copper alloys 59
corrosion rates . . . . . 59(T)
Catalysts
market segment percentage and form of cobalt consumption 347
nickel-base 7
Catastrophic carburization 172–173
Cathode efficiency, in nickel plating 107
Cattierite
composition . . . . . 346(T)
mining locations. . . . . 346(T)
Caustic environments, and stress-corrosion cracking . . . . . 154–157(F)
Caustic soda corrosion, of nickel 200 . . . . . 20(T)
Cavitation erosion, of cobalt alloys. . . . . 388, 391(F)
Cemented carbides
cobalt content effect . . . . . 350(T), 351(F)
market segment percentage and form of cobalt consumption 347
nickel content effect. . . . . 12, 13(F)
nickel effect on corrosion resistance . . . . . 12, 13(F)
Centerless grinding, of nickel alloys. 244
Centrifugal atomization . . . . . 210, 211(F), 215
Ceramics, for tooling . . . . . 237–240(F,T)
CGDS alloys. *See* Columnar-grain directionally solidified alloys.
Chalcopyrite 4
Chamfering . . . . . 240(F)
Chemical milling, of nickel alloys. 243, 244
Chemicals, nickel consumption in U.S. by end use . . . . . 6(T)
Chemical vapor deposition (CVD). 106
Chemical waste incinerator, temperature range and contaminants encountered . . . . . 183(T)
Chip breakers 242

© 2000 ASM International. All Rights Reserved.
ASM Specialty Handbook: Nickel, Cobalt, and Their Alloys (#06178G)

Chlorides
causing stress-corrosion cracking . . . . 144–145(F,T)
molten, corrosion by . . . . . 184(F,T)
Chlorine, wet
corrosion rate of CW-12MW . . . . . 58(T)
corrosion rate of Hastelloy D . . . . . 59(T)
corrosion rate of N-12MV . . . . . 58(T)
Chlorine-bearing environments, and corrosion . . . . . 177–181(F,T)
Chromia scale 167, 169
Chromic acid
corrosion of cobalt alloys . . . . . 396(T)
corrosion of cobalt-base alloys at boiling temperature . . . . . 396(T)
corrosion rate of CW-12MW . . . . . 58(T)
corrosion rate of Hastelloy D . . . . . 59(T)
corrosion rate of N-12MV . . . . . 58(T)
Chromium
alloying element effect in cobalt-base heat resistant alloys 366
alloying element effect on nickel- and iron-base superalloys . . . . . 167(T)
alloying element effect on corrosion resistance . . . . . 17(T)
alloying element effect on nickel alloy corrosion resistance . . . . . 129(F)
alloying element range in superalloys . . . . . 69(T)
content effect in cobalt-base alloys 364
content effect on corrosion resistance of superalloys 87
content effect on nickel alloy weldability 248
effect on oxidation resistance of superalloys . . . . . 85, 89(F)
as solid-solution strengthener in nickel . . . . . 14(F)
Chromium-carbon ($Cr_2_3C_6$) precipitate, in cobalt alloy microstructures . . . . . 319(F)
Chromizing 286
Citric acid, saturated, corrosion rate of electroless nickel coatings . . . . . 118(T)
Classification number, for electrodeposited coatings 111
Clydach, Wales, refinery 205
Coatings 10
ceramic, for heat resistant nickel alloys 280
cobalt content effects . . . . . 354(F,T)
conversion cobalt content effect 354
diffusion, for heat resistant nickel alloys 280
for heat resistant nickel alloys 280
for superalloys 87–89
high-temperature, for superalloys . . . . 281–290(F,T)
nickel containing . . . . . 106–123(F,T)
overlay, cobalt content effect 354
Coatings, high-temperature, for superalloys . . . . . 281–290(F,T)
alloying element effects on hot corrosion resistance and oxidation resistance 286
aluminide, oxidation of . . . . . 288, 289(F)
application methods for overlay coatings . . . . 287(F)
chromide 286–287
chromium diffusion coatings . . . . . 285(F)
coating formation mechanisms . . . . . 284–285(F)
cobalt aluminide . . . . . 282(F)
CVD aluminizing process . . . . . 284(F), 285(F)
diffusion . . . . . 281–283(F)
applications . . . . . 286–287(F)
high-temperature hot corrosion . . . . . 289(F)
low-temperature hot corrosion 290
diffusion coating application methods . . 283–284(F)
ductility . . . . . 288(F)
electron-beam physical vapor deposition method . . . . . 287–288(F)
high-temperature hot corrosion resistance . . . . . 289–290(F)
low-temperature hot corrosion 290
MCrAlY overlay coatings 288–289
monoaluminide . . . . . 281–282(F)
nickel aluminide . . . . . 282(F)
out-of-contact CVD processes . . . . . 284(F)
overlay 282
high-temperature hot corrosion . . . . . 289–290(F)
low-temperature hot corrosion 290
oxidation . . . . . 281, 288–289(F)
pack cementation process . . . . . 283–284(F,T)
performance . . . . . 288–290(F)
plasma sprayed . . . . . 287(F)
platinum aluminides 286
precious metals in 288
protection and degradation of 285–286
requirements 281
slurry aluminization 284
thermal barrier coatings (TBCs) . . . . . 281, 286, 287–288(F), 290(F)
types . . . . . 281–283(F)
Cobalt
alloying element effect on nickel- and iron-base superalloys . . . . . 167(T)
alloying element effects on corrosion resistance . . . . . 17(T)
alloying element effects on nickel alloy corrosion resistance . . . . . 129(F)
alloying element range in superalloys . . . . . 69(T)
applications 349
electronic 355
nonmetallurgical . . . . . 354–355(T)
consumption by end use in U.S. (1997, 1998) 348(T)
content effect in cobalt-base alloys 364
end uses, market segments 347
extraction and refining 345–346
for electroplating . . . . . 354(F,T)
in beryllium-copper alloys 353
in cemented carbides . . . . . 350(T), 351(F)
in cobalt-base alloys 349
in conversion coatings 354
in electroless cobalt alloy plating . . . . . 354(T)
in hardfacing alloy coatings 354
in high-fracture toughness steels . . . . . 352–353(T)
in high-speed tool steels . . . . . 352(F), 353(T)
in high-strength aluminum alloys 353–354
in high strength-to-density ratio steels . . . . . 353(T)
in magnetic materials . . . . . 350–352(F,T)
in maraging steels . . . . . 352, 353(T)
in nickel-base superalloys, properties given by 349
in nickel low-expansion alloys . . . . . 352(T)
in overlay coatings 354
in paint pigment compounds . . . . . 355(T)
in pigments for coloring ceramics . . . . . 355(T)
in stainless steels . . . . . 353(F,T)
in steels . . . . . 352–353(F,T)
mechanical properties . . . . . 345(F)
metallographic examination . . . . . 404–406(T)
metallurgical uses . . . . . 349–354(F,T)
microstructure 345
nonmetallurgical uses . . . . . 354–355(T)
physical properties 345
production . . . . . 345, 346(T)
recovery from arsenide ores 347
recovery from copper-cobalt oxide concentrates . . . . . 346(T)
recovery from copper-cobalt sulfide concentrates . . . . . 346, 347(F)
recovery from laterite ores 346–347
recovery from nickel-cobalt sulfide concentrates . . . . . 346, 347(F)
refinery capacity, worldwide (1998) . . . . . 346(T)
as solid-solution strengthener in nickel . . . . . 14(F)
sources, ores . . . . . 345–346(T)
uses of . . . . . 349–355(F,T)
Cobalt alloys
alloying element effects on corrosion resistance 395
applications 345
biocompatibility 345
corrosion . . . . . 395–400(F,T)
heat treatment 401
metallographic examination . . . . . 404–406(T)
wear . . . . . 387–394(F,T)
workability 401–402
Cobalt ammonium sulfate + boric acid, operating conditions for cobalt electroplating . . . . . 354(T)
Cobalt-base alloys
applications, high-temperature 362
biocompatible compositions 362
compositions . . . . . 362(T), 364
as cutting tools 364
microstructures . . . . . 302, 318–321(F), 328–330(F)
Cobalt-base corrosion-resistant alloys 367–368
chemical properties 368
compositions 368
Cobalt-base hardfacing alloys
abrasive wear . . . . . 389(F), 394
applications . . . . . 387(T), 394
carbide-containing wear behavior . . . . . 393–394(F)
compositions . . . . . 392(T)
market segment percentage and form of cobalt consumption 347
mechanical properties . . . . . 364(T)
microstructure . . . . . 389(F), 394
physical properties . . . . . 364(T)
Cobalt-base heat resistant alloys . . . . . 365–367(F,T)
alloying elements effects . . . . . 366–367(T)
brazing . . . . . 402–403(T)
cold working 402
forging 401–402
machining 404
mechanical properties 365
physical properties 365
welding 402, 403
workability 401–402
Cobalt-base superalloys. *See also* Superalloys.
alloying element effects . . . . . 69(T)
carbide precipitation . . . . . 83–84(F)
cast
compositions . . . . . 72(T)
microstructure . . . . . 70(F)
compositions . . . . . 71(T)
joining 78
market segment percentage and form of cobalt consumption 347
melting of 75–76
microstructure 72–73
welding 78
Cobalt-base surgical implant alloys
applications 370
compositions . . . . . 369(T)
mechanical properties . . . . . 369(T)
microstructure . . . . . 369(F)
Cobalt-base wear resistant alloys . . . . 363–365(F,T)
applications . . . . . 387(T), 393
hot hardness . . . . . 392(T)
machinability . . . . . 403–404(T)
microstructure . . . . . 389(F)
welding 402
workability 401
Cobalt-carbon binary phase diagram, crystal structure data . . . . . 356(T)
Cobalt chloride + boric acid, operating conditions for cobalt electroplating . . . . . 354(T)
Cobalt-chromium binary phase diagram, crystal structure data . . . . . 357(T)
Cobalt-chromium-iron isothermal section
at 600 °C . . . . . 359(F)
at 800 °C . . . . . 359(F)
at 1000 °C . . . . . 358(F)
at 1200 °C . . . . . 358(F)

© 2000 ASM International. All Rights Reserved.
ASM Specialty Handbook: Nickel, Cobalt, and Their Alloys (#06178G)

Cobalt-chromium-nickel isothermal section at 1200 °C . . . . . 359(F)
Cobalt-chromium-tungsten isothermal section
at 700 °C . . . . . 359(F)
at 1350 °C . . . . . 359(F)
Cobalt Development Institute 347
Cobalt fluoborate, operating conditions for cobalt electroplating . . . . . 354(T)
Cobalt-iron binary phase diagram, crystal structure data . . . . . 357(T)
Cobalt-iron-molybdenum isothermal section
at 20 °C . . . . . 360(F)
at 800 °C . . . . . 360(F)
at 982 °C . . . . . 360(F)
at 1093 °C . . . . . 360(F)
at 1300 °C . . . . . 359(F)
Cobalt-iron-nickel isothermal section
at 600 °C . . . . . 360(F)
at 800 °C . . . . . 360(F)
Cobalt-iron-tungsten isothermal section at 1200 °C . . . . . 361(F)
Cobaltite
composition . . . . . 346(T)
mining locations . . . . . 346(T)
Cobalt-molybdenum binary phase diagram, crystal structure data . . . . . 357(T)
Cobalt-molybdenum-nickel isothermal section
at 1100 °C . . . . . 361(F)
at 1200 °C . . . . . 361(F)
Cobalt-nickel binary phase diagram, crystal structure data . . . . . 358(T)
Cobalt sulfamate + boric acid, operating conditions for cobalt electroplating . . . . . 354(T)
Cobalt sulfate + boric acid, operating conditions for cobalt electroplating . . . . . 354(T)
Cobalt-tungsten binary phase diagram, crystal structure data . . . . . 358(T)
Coercive force
of cobalt 345
of nickel 3
Coercivity, of powder-rolled nickel strip . . . . . 214(T)
Coiling, rod and bar 196–197
Coinage alloys 10
Cold heading 197
Cold-working capacity, of powder-rolled nickel strip . . . . . 214(T)
Coloring bright finish, wheel, compound and speed used . . . . . 277(T)
Coloring mirror finish, wheel, compound and speed used . . . . . 277(T)
Colorizers, market segment percentage and form of cobalt consumption 347
Columnar-grain directionally solidified (CGDS) alloys
microstructure . . . . . 84, 84(F)
structures . . . . . 73(T), 77
Columnar voids 287
Commercially pure nickels 15–16
applications 16, 92
compositions . . . . . 15(T)
corrosion resistance . . . . . 127(T)
heat treatment 16
mechanical properties 16, 92
physical properties 92
temperature range 16
Compressive strength, of cobalt alloys, individual alloy values 382, 384
Compressive yield strength, of nickel and nickel alloys, individual alloy values . . . 19–54(T)
Computer-aided design (CAD) 78
Computer-aided design (CAD) model, laser-assisted rapid prototyping and manufacturing 225
Conservation of strategic aerospace materials (COSAM), NASA program 349
Constantan (55Cu-45Ni), electrical properties 10
Constant-deflection tests 160
Constant-load tests 160
Constrained recovery devices 102
Copper
alloying element effects on corrosion resistance . . . . . 17(T)
alloying element effects on nickel alloy corrosion resistance . . . . . 129(F)
cold work effect on hardness . . . . . 191(F)
content effect on nickel alloy weldability 248
corrosion rate, in propionic acid, boiling . . . . 135(F)
welding products for dissimilar-metal joints with nickel-base alloys . . . . . 250(T)
Copper-accelerated acetic acid salt spray (fog) testing (CASS test) (ASTM B 368) . . 111(T)
Copper-base alloys, nickel consumption, % 6
Copper Cliff Nickel Refinery 205–206
Copper electrowinning, market segment percentage and form of cobalt consumption . . 347
Copper flash 276
Copper-nickel alloys. *See* Cupronickels.
Corrosion of cobalt alloys . . . . . 395–400(F,T)
by acetic acid . . . . . 396(T), 397(T)
by acid media . . . . . 395–396(T), 397(F,T)
by acid media at boiling temperature . . . . . 396(T), 397(F,T)
by aqueous environments . . . . . 395–398(F,T)
by chromic acid . . . . . 396(T)
by ferric sulfate mixture . . . . . 397(T)
by formic acid . . . . . 396(T)
by hydrochloric acid . . . . . 396(T), 397(F,T)
by iron chloride solutions . . . . . 398(T)
by nitric acid . . . . . 396(T), 397(F,T)
by phosphoric acid . . . . . 396(T), 397(F)
by sodium hydroxide . . . . . 396(T)
by sulfuric acid . . . . . 396(T), 397(F,T)
carburization resistance . . . . . 399, 400(F)
high-temperature . . . . . 399(F), 400(F)
hydrogen embrittlement 398
oxidation resistance . . . . . 399(F)
stress-corrosion cracking . . . . . 398–399(T)
sulfidation resistance . . . . . 399(F)
Conventional P/M superalloy processing . . . . . 215–220(F,T)
centrifugal atomization process 215
compositions of superalloys . . . . . 216–220(F,T)
consolidation of powder 215–216
heat treatments 216
mechanical properties of superalloys 216–220(F,T)
postconsolidation processing 216
production by gas atomization . . . . . 211(F), 215
production by plasma rotating electrode process (PREP) 215
production by vacuum atomization . . 211(F), 215(F)
screening, cleanliness evaluation, and outgassing 215
steps in process 215
superalloys in commercial production 216
superalloys in early stages of development 216
Corrosion of nickel and nickel alloys . . 127–140(F,T)
atmospheric . . . . . 130(T)
by acetic acid . . . . . 133, 134(T)
by acrylic acid 134
by alkalis . . . . . 135–136(F)
by distilled water 130
by formic acid . . . . . 133–134(F,T)
by freshwater 130
by hydrochloric acid . . . . . 131(F), 132(F,T)
by hydrofluoric acid . . . . . 133(T)
by lauric acid 134
by nitric acid . . . . . 132(F)
by organic acids . . . . . 133–134(F,T), 135(F,T)
by phosphoric acid . . . . . 132–133(T)
by propionic acid . . . . . 134, 135(F,T)
by seawater . . . . . 130–131(T)
by steam/hot water systems 130
by stearic acid 134
by sulfuric acid . . . . . 131(F)
in acid mixtures . . . . . 134–135(F), 136(F)
in flue gas desulfurization environments 137
in fused salts 137
in petrochemical and refining environments . . . 137, 138(F)
in pulp and paper mill environments 136–137
in sour gas environments 137
individual alloy values . . . . . 19–54(F,T)
of superalloys 87, 89–90
of weldments, nickel and high-nickel alloys . . . . . 137–139(F)
Corrosion rates
in chlorine-bearing environments . . . . 177–181(F,T)
in fluorine-bearing environments 181–182
Corrosion resistance
alloy characteristics . . . . . 127–129(T)
alloying element effects . . . . . 129–130(F)
of cobalt alloys, individual alloy values 373, 374(T), 375(T), 377, 378, 381
of electroless nickel coatings . . . 118(T), 119(T), 120
of superalloys 68
Creep strength
of cobalt alloys, individual alloy values . . . . 377(T), 378(T), 383(T), 385, 386(T)
of nickel and nickel alloys, individual alloy values . . . . . 21–54(F)
C-ring tests 147, 160
Crown 74
Cupric chloride, corrosion rate of electroless nickel coatings . . . . . 118(T)
Cupronickels . . . . . 10, 12(T)
alloying additions effects on corrosion resistance . . . . . 129(F)
composition . . . . . 12(T)
mechanical properties . . . . . 12(T)
nickel consumption in U.S. by end use . . . . . 6(T)
product forms . . . . . 12(T)
weldable grades, welding . . . . . 268(T)
Curie temperature
of cobalt 345
of Duratherm 600 374
of nickel 3
of nickel and nickel alloys, individual alloy values 19–54
of powder-rolled nickel strip . . . . . 214(T)
Cutting down, wheel, compound and speed used . . . . . 277(T)
Cyaniding 137

D

Deep drawing . . . . . 191(F), 193–194
Deep-hole drilling, of nickel alloys . . 240–241, 242(T)
Deformation mode . . . . . 159–160(F)
Delta phase 301
in nickel alloy microstructures . . . . . 310(F), 311(F), 312(F)
in nickel-base superalloys 76–77
in superalloys 69
Dendritic white spots 74
Densification 208
Density
of cobalt 345
of cobalt alloys, individual alloy values . . . 373–386
of nickel 3
of nickel and nickel alloys, individual alloy values 19–54
of powder-rolled nickel strip . . . . . 214(T)
of superalloys 68
Depth-of-cut (DOC) notch effect . . . . . 239–240(F)

© 2000 ASM International. All Rights Reserved.
ASM Specialty Handbook: Nickel, Cobalt, and Their Alloys (#06178G)

Diamond tooling, market segment percentage and form of cobalt consumption 347
Diffusion bonding 79
Dilute aqueous solutions, stress-corrosion cracking . . . . . 152–154(F)
Directed light fabrication (DLF) . . . . . 225, 226(F)
Directional solidification 78
Direct metal deposition . . . . . 225, 226(F)
Discrete white spots 74
Disk method for preparing thin foils 300
Driers (for paint and/or ink), market segment percentage and form of cobalt consumption 347
Drilling, of nickel alloys . . . . . 240–241, 242(T)
Drip short 75
Drip short frequency (DSF) 75
Drop-in defect 74
Dry fining, wheel, compound and speed used . . 277(T)
Dry sand and rubber wheel abrasion test (procedure B) (ASTM G 65) . . . . 388(F), 389(F)
Dual-alloy turbine disk/wheels . . . . . 224–225(F)
mechanical properties . . . . . 224–225(F)
physical properties 224–225
processing scenarios 225
Ductile cast irons, compositions . . . . . 9(T)
Ductile-to-brittle transition temperature, of coatings, and strain tolerance . . . . . 288(F)

E

Elastic modulus
of cobalt alloys, individual alloy values 374, 375(T), 380, 381(T), 382(T), 385(T)
of nickel 4
of nickel and nickel alloys, individual alloy values 19–54
Electrical conductivity
of cobalt 345
of nickel 3
of nickel and nickel alloys, individual alloy values 19–54
of nickel-beryllium alloys . . . . . 104(T)
Electrical contact materials, nickel content effect 12–13
Electrical discharge machining, of nickel alloys 241, 243
Electrical resistance alloys 10
Electrical resistivity
of cobalt 345
of cobalt alloys, individual alloy values . . . 377, 378, 381, 383, 384, 385
of nickel 3
of nickel and nickel alloys, individual alloy values . . . . . 20–54(T)
Electric uses, nickel consumption in U.S. by end use . . . . . 6(T)
Electrochemical machining, of nickel alloys 243
Electrocrystallization process 106
Electrodeposited coatings, classification number 111
Electrodeposited coatings of copper plus nickel plus chromium and nickel plus chromium, standard specification (ASTM B 456) 111
Electroforming . . . . . 3, 107, 114–115(T)
advantages 114
applications 114
definition 114
disadvantages 114
nickel-cobalt plating 114
nickel solutions for 115
process 115
Electroless cobalt alloy plating . . . . . 354(T)
Electroless nickel-boron coatings, corrosion rates in various chemical process environments . . . . . 118(T)
Electroless nickel coatings 10
Electroless nickel (hardened), Taber abraser resistance . . . . . 118(T)
Electroless nickel-phosphorus coatings
corrosion rate in caustic solutions (NAOH + NaCl) or (NaOH) . . . . . 119(T)
corrosion rates in various chemical process environments . . . . . 118(T)
Electroless nickel plating . . . . . 115–120(F,T)
accelerators 116
advantages 115
aminoborane-reduced electroless nickel plating solutions . . . . . 116(T)
applications 115
both composition and characteristics . . . 115–116(T)
borohydride-reduced electroless nickel plating solutions . . . . . 116(T)
complexing agents 116
corrosion of coatings in various environments . . . . . 118(T), 119(T), 120
energy content 116
hypophosphite-reduced electroless nickel plating solutions . . . . . 116(T)
inhibitors 116
limitations 115
mechanical properties . . . . . 117(T), 118
microstructure of coatings 116
nickel-boron coatings . . . . . 118–119(T)
nickel composite coatings . . . . . 119–120(F,T)
nickel-phosphorus coatings . . 116–118(F,T), 119(T)
physical properties . . . . . 117(T), 118(T), 119(T)
process 115
reducing agents 115–116
ternary nickel alloy coatings . . . . . 119(F,T)
Electroless plating 106
Electrolysis, market segment percentage and form of cobalt consumption 347
Electrolytic polishing, of cobalt and cobalt alloys . . . . . 404(T)
Electron-beam machining, of nickel alloys 241
Electron-beam physical vapor deposition method . . . . . 287–288(F)
Electron-beam remelting/refining (EBR) 75
Electron vacancy number 143
Electroplating. *See also* Nickel plating. 106–114(F,T)
of cobalt . . . . . 354(F,T)
heat resistant nickel alloys 280
nickel consumption in U.S. by end use . . . . . 6(T)
with platinum before aluminizing 286
Electroplating solutions, copper and nickel, for electroforming (ASTM B 503) 115
Electropolishing . . . . . 299, 300(T), 301(T)
of high-nickel alloys . . . . . 276, 293(T)
nickel-copper alloys . . . . . 293(T)
nickel-iron alloys . . . . . 294(T)
Electroslag remelting (ESR) process . . . . . 74(F), 75
Elevated temperatures, forming cold-formed parts 197
Elongation
of cobalt 345
of cobalt alloys, individual alloy values 373–386(T)
of nickel 3
of nickel and nickel alloys, individual alloy values . . . . . 19–54(F,T)
EPR test for sensitization to intergranular corrosion 151
Erosive wear. *See* Wear, erosive.
ESR-VAR remelting process 74, 75
Eta-carbides 143
Eta (η) phase 15, 301, 303
crystal structure, lattice parameter, formula, and comments . . . . . 303(T)
in nickel alloy microstructures . . . . . 307(F), 309(F), 310(F)
in superalloys 69, 80, 83
Etchants
for cobalt and cobalt alloys . . . . . 404–406(T)
for high-nickel alloys . . . . . 294(T)
for nickel-copper alloys . . . . . 294(T)
for nickel-iron alloys . . . . . 295(T)
Etching . . . . . 299–300, 301(T)
cobalt and cobalt alloys . . . . . 404–406(T)
of high-nickel alloys . . . . . 293, 294(T)
nickel-copper alloys . . . . . 293, 294(T)
nickel-iron alloys . . . . . 295(T)
Ethylene glycol, corrosion rate of electroless nickel coatings . . . . . 118(T)
Expanding 196
Extrusion
cold 197
of superalloy powders 216
to consolidate powders 77

F

Faraday's law for nickel 107
Fatigue strength
of cobalt alloys, individual alloy values . . . . . 375(T)
of nickel and nickel alloys, individual alloy values . . . . . 20–54(T)
Feedstuff, market segment percentage and form of cobalt consumption 347
Ferric chloride, corrosion rate of electroless nickel coatings . . . . . 118(T)
Ferric sulfate mixture corrosion, of cobalt alloys . . . . . 397(T)
Ferronickel . . . . . 5–6(F)
Ferronickel smelting 347
Ferroxyl test 276
Filter elements, functional, service, and structural requirements . . . . . 211(T)
Finishing, of nickel alloys . . . . . 277–278(T)
Flash pickling 273, 274, 275, 276–277
of heat resistant nickel alloys 280
Flue gas desulfurization (FGD) systems . . . 251, 264
as corroding agents 137
Fluoborate nickel plating solution . . . . . 112–113(T)
cathode current density . . . . . 112(T)
composition . . . . . 112(T)
mechanical properties . . . . . 112(T)
pH value . . . . . 112(T)
temperature range . . . . . 112(T)
Fluorides
causing stress-corrosion cracking . . . . . 146–147(F)
molten, corrosion by 185
Fluorine-bearing environments, and corrosion 181–182
Forging. *See also* Thermomechanical processing.
of consumably remelted superalloys 76
cooling after 199
die materials for 198
heating for . . . . . 198–199(F)
hot-forming pressures . . . . . 198(T)
isothermal 202
lubricants 198
of nickel alloys . . . . . 198–202(F,T)
specific alloys, practice for . . . . . 199–201(F)
thermal-mechanical processing . . . . . 201–202(T)
Formic acid
corrosion of cobalt alloys . . . . . 396(T)
corrosion of cobalt-base alloys at boiling temperature . . . . . 396(T)
corrosion rate of electroless nickel coatings . . . . . 118(T)

© 2000 ASM International. All Rights Reserved.
ASM Specialty Handbook: Nickel, Cobalt, and Their Alloys (#06178G)

Formic acid corrosion. . . . . 133–134(F,T)
Forming
alloy condition effect on formability 192
annealing treatments for precipitation-hardenable alloys 192
bending, of tube and pipe . . . . . 195–196(T)
blanking 193
cobalt alloys. 401–402
cold extrusion. 197
cold-formed parts for high-temperature service . . 197
cold heading 197
cold vs. hot 192
composition effect on formability 191–192
deep drawing 193–194
die materials. 192–193
equipment operation 193
expanding 196
galling effect on formability 191
lubricants for 192, 193, 194, 197
of nickel alloys. . . . . 191–197(F,T)
piercing 193
plate, sheet, and strip . . . . . 196(T)
of rod and bar. 196–197
rolling direction effect. . . . . 192(F)
shearing. 193
solution annealing effect. 192
spinning. . . . . 194–195(F,T)
straightening. 197
strain hardening effect on formability. . . . . 191(F)
temper effect on formability 191
tool design. 193
tube and pipe . . . . . 195–196(T)
Foundry products, nickel consumption, % 6
Freckles. 74, 75, 78, 298
Friction sawing, of nickel alloys . . . . . 243–244(T)
Froth flotation method 346
Fuel oil ash corrosion . . . . . 62–63(T)
Fuel oils, residual, constituent amounts from various crudes . . . . . 62(T)
Fused salts, as corroding agents 137

G

Galling, of cobalt alloys . . . . . 388, 392(F)
Gamma double prime phase. 302–303
in superalloys. 69, 82–83
Gamma double prime precipitate-free zone (PFZ) 83
Gamma phase, crystal structure, lattice parameter, formula, and comments. . . . . 303(T)
Gamma-prime phase (gcp phase) 302
crystal structure, lattice parameter, formula, and comments . . . . . 303(T)
in cobalt alloy microstructures. . . . . 318(F), 328(F)
and electropolishing 300
in nickel alloy microstructures . . . . . 309(F), 312(F), 313(F), 314(F), 315(F), 316(F), 322(F), 323(F), 324(F), 325(F), 326(F), 327(F)
in nickel and nickel alloys 15
in nickel-base alloys 302
in superalloys . . . . . 69, 80(F)
Garnierite. 4
Gas atomization . . . . . 211(F), 215
Gas-metal arc welding (GMAW) . . . 259(F), 261(T), 262–263(T)
joint configurations for applications . . . . . 259(F)
Gas-tungsten arc welding (GTAW) . . . . . 259(F), 260–262(F,T)
joint configurations for applications . . . . . 259(F)
General Electric, production of dual-alloy turbine disk/wheels . . . . . 224–225(F)
General Electric's clean metal spray forming 227(F)
Glyceregia 299–300
G phase 304
Grain size 302
Graphite
maximum furnace operating temperature in air . . . . . 93(T)
mechanical properties . . . . . 93(T)
physical properties. . . . . 93(T)
Gray cast irons, compositions. . . . . 9(T)
Grease coloring, wheel, compound and speed used . . . . . 277(T)
Greasing, wheel, compound and speed used. . . 277(T)
Grinding 273, 298
cobalt and cobalt alloys. 404
as finishing operation 277
high-nickel alloys 293
of nickel alloys. 244
nickel-copper alloys 293
nickel-iron alloys. 294
wheel, compound and speed used . . . . . 277(T)
Grooving, of nickel alloys 237–240

H

Hafnium, effect on superalloy mechanical properties. 84
Halide environments, stress-corrosion cracking. . . . . 143–147(F,T)
Halogenation. . . . . 177–182(F,T)
Hard chromium, corrosion rates in various chemical process environments. . . . . 118(T)
Hardenable low-expansion/constant-modulus alloys . . . . . 100–101(T)
heat treatment. 101
mechanical properties . . . . . 101(T)
physical properties. . . . . 101(T)
Hardness
of cobalt alloys, individual alloy values . . . . . 373, 374(T), 375, 378, 380, 381(T), 382, 384, 386(T)
of nickel. 3–4
of nickel and nickel alloys, individual alloy values . . . . . 19–54(T)
Hard nickel plating solution . . . . . 112(T), 113
cathode current density . . . . . 112(T)
composition . . . . . 112(T)
mechanical properties . . . . . 112(T)
pH value . . . . . 112(T)
temperature range . . . . . 112(T)
Hastelloy alloys. *See also* Alloy Index for individual alloys.
castings, welding of 254–255
dissimilar metal welding . . . . . 252(T), 254
fusion zone, welding considerations . . . 252–254(F)
heat-affected zone, welding considerations. . . . . 252, 253(F)
postweld heat treatment . . . . . 254(T)
repair welding 255
welding . . . . . 251–255(F,T)
for weld cladding. 122
Heat-resistant nickel alloys
abrasive blasting. 278, 279–280
acid pickling. 279
brazing. . . . . 267–272(F,T)
chemical removal methods for metal contaminants. 278
cleaning and finishing . . . . . 278–280(T)
coatings. 280
compositions. . . . . 299(T)
electroplating 280
fusion zone, welding considerations. 255
heat-affected zone, welding considerations . . 255(F)
metal contaminant removal 278
microstructures . . . . . 306–330(F)
phases in wrought alloys . . . . . 302–303(T)
polishing. 278, 280
postweld heat-treatment (strain-age) cracking. . . . . 255–257(F,T)
reduced oxide film removal 279
salt-bath descaling. 280
scale conditioning . . . . . 279(T)
scale removal procedures . . . . . 279(T)
shot peening 280
tarnish removal 278–279
temperature range for use. 301
welding of. . . . . 255–257(F,T)
wet tumbling 278, 280
wire brushing 280
Heat tinting 300
Heat treating of cobalt alloys. 401
age hardening of cobalt alloys, individual alloy values . . . . . 374(T)
and hydrogen embrittlement of cobalt alloys . . . 398
Heat treating of nickel alloys. . . . . 230–234(F,T)
age hardening . . . . . 230, 233–234(T)
aging, and carbide precipitation 303–304
annealing . . . . . 230(F), 231–233(F,T)
annealing process control factors . . . . . 232–233(T)
annealing temperature, of powder-rolled nickel strip. . . . . 214(T)
batch annealing 231
bright annealing. . . . . 232–233(T)
continuous annealing. . . . . 231(T)
and corrosion infused salts. 137
dead-soft annealing. 232
effect on stress-corrosion cracking. . . 151, 154, 155, 156(F), 160
precipitation hardening . . . . . 230, 233–234(T)
solution annealing. . . . . 230, 234(T)
solution treating. 230
specialty annealing. 231–232
stress equalizing . . . . . 230(F), 231(T), 233
stress relieving. . . . . 230(F), 231(T), 233
sulfur exposure minimized. 230
of superalloy powders. 216
thermomechanical processing. 234
torch annealing. 232
types of treatment. . . . . 230(F)
and welding of nickel alloys 257–258
Heat treating, of superalloys. . . . . 80, 81(T), 82, 83(F), 84, 85
Heterocarbonyls. 204
Heterogenite
composition . . . . . 346(T)
mining locations. . . . . 346(T)
High-cycle fatigue (HCF), in superalloys. 84
High-fracture toughness steels, cobalt content effect . . . . . 352–353(T)
High-nickel alloys
electropolishing 276
metallographic examination. . . . . 293–294(T), 295–297(F)
microstructures . . . . . 294, 295(F), 296(F)
pickling. 273, 275
High-pressure/high-velocity oxygen fuel (HP/HVOF) spraying 288
High-speed tool steels, cobalt content effect . . 352(F), 353(T)
High-strength aluminum alloys, cobalt content effect. 353–354
High-strength controlled-expansion superalloys. 101
composition . . . . . 101(T)
physical properties. . . . . 101(T)
High-strength-to-density ratio steels, cobalt content effect. . . . . 353(T)
High sulfate nickel plating solution. . . . . 112(T), 113
cathode current density . . . . . 112(T)
composition . . . . . 112(T)

© 2000 ASM International. All Rights Reserved.
ASM Specialty Handbook: Nickel, Cobalt, and Their Alloys (#06178G)

mechanical properties . . . . . 112(T)
pH value . . . . . 112(T)
High-temperature coatings for superalloys . . . . . 281–290(F,T)
High-temperature water, stress-corrosion cracking . . . . . 152–154(F)
Homogenization 76
of cast nickel-copper alloys 56
Honing, of nickel alloys 244
Hospital waste incinerator, temperature range and contaminants encountered . . . . . 183(T)
Hot corrosion . . . . . 182–183(F,T)
and coatings 281, 286
of superalloys 87
Hot cracking . . . . . 78, 79(F)
Hot-forming capacity, of powder-rolled nickel strip . . . . . 214(T)
Hot isostatic pressing, of superalloy powders 77, 215–216
Hot-work temperature, of powder-rolled nickel strip . . . . . 214(T)
Howmet process 227
Hydrochloric acid
corrosion rate of
cobalt-base alloys . . . . . 396(T), 397(F,T)
CW-12MW . . . . . 58(T)
electroless nickel coatings . . . . . 118(T)
Hastelloy D . . . . . 59(T)
iron-base alloys . . . . . 397(T)
N-12MV . . . . . 58(T)
nickel-base alloys . . . . . 397(T)
Hydrochloric acid corrosion . . . . . 131(F), 132(F,T), 181, 182(F,T)
Hydrofluoric acid
corrosion rate of
CW-12MW . . . . . 58(T)
Hastelloy D . . . . . 59(T)
N-12MV . . . . . 58(T)
Hydrofluoric acid corrosion . . . . . 133(T)
Hydrogen embrittlement . . . . . 157–160(F,T)
of cobalt alloys 398
not resulting from aqueous descaling of nickel-base alloys 279
of superalloys 89–90
Hydrogen fluoride cleaning . . . . . 270(F)
Hydrogen reduction process 208
Hydrogen sulfide, causing stress-corrosion cracking 147–148
Hypophosphite-reduced cobalt-phosphorus, electroless cobalt alloy plating systems . . . 354(T)
Hypophosphite-reduced cobalt-tungsten-phosphorus, electroless cobalt alloy plating systems . . . . . 354(T)
Hysteresis loss, of nickel 3

I

Impact strength
of cobalt alloys, individual alloy values . . 381(T), 382 385(T)
of nickel and nickel alloys, individual alloy values . . . . . 19–54(T)
Incinerators, and corrosion encountered . . . . . 183–184(T)
Inconel alloys. *See also* Alloy Index for individual alloys.
for weld cladding 122
scale removal procedures, finishing and cleaning . . . . . 279(T)
Inco pressure carbonyl process 205
Industrial waste incinerator, temperature range and contaminants encountered . . . . . 183(T)
Ingot slag skin . . . . . 74(F), 75
Initial permeability, of powder-rolled nickel strip . . . . . 214(T)
Insert drilling, of nickel alloys . . . . . 240, 242(T)
Interdiffusion zone 284–285
Intermetallic phases
effect on nickel alloy corrosion resistance 130
effect on stress-corrosion cracking 143
Investment casting, of superalloys . . . . . 77–78(F)
Iodides, causing stress-corrosion cracking . . . . 146(T)
Iron
alloying element effects on corrosion resistance . . . . . 17(T)
alloying element effects on nickel alloy corrosion resistance . . . . . 129(F)
content effect on nickel alloy weldability 248
as solid-solution strengthener in nickel . . . . . 14(F)
Iron-nickel alloys. *See* Low-expansion alloys.
Iron chloride corrosion, of cobalt alloys . . . . . 398(T)
Iron-nickel-base superalloys. *See also* Superalloys.
alloying element effects . . . . . 69(T)
cobalt content effect . . . . . 349–350(T)
compositions . . . . . 71(T)
joining . . . . . 78–79(F)
market segment percentage and form of cobalt consumption 347
microstructures . . . . . 69, 70(F), 301–302
welding . . . . . 78–79(F)
Iron-nickel-chromium alloys 18
applications 18, 100
composition . . . . . 16(T), 100
physical properties 100
stress-corrosion cracking . . . . . 144(F)
Iron-nickel-cobalt alloys
applications 100
physical properties 100
Isothermal forging 202

J

Joining. *See also* Brazing; Diffusion bonding; Welding.
cobalt-base superalloys 78
iron-nickel-base superalloys . . . . . 78–79(F)
nickel-base superalloys . . . . . 78–79(F)
superalloys . . . . . 78–79(F)

K

Knife-line attack . . . . . 138(F)
Kobe Steel, production of dual-alloy turbine disk/wheels . . . . . 224(F)

L

Lactic acid, corrosion rate of electroless nickel coatings . . . . . 118(T)
Lanthanum
alloying element effect in cobalt-base heat-resistant alloys 366
alloying element effects on corrosion resistance . . . . . 17(T)
Laser-aided direct metal deposition (LADMD) 225
Laser-assisted rapid prototyping and manufacturing . . . . . 225(F)
alloys under development . . . . . 225–226(T)
direct metal deposition . . . . . 225, 226(F)
selective laser sintering . . . . . 225(F)
Laser-engineered net shaping (LENS) 225
Laser glazing 287
Laser machining, of nickel alloys 241
Laterites (laterite ores) 4
composition . . . . . 346(T)
mining locations . . . . . 346(T)
recovery of nickel from . . . . . 5–6(F)
Lauric acid corrosion 134
Laves phase . . . . . 304, 365(F)
crystal structure, lattice parameter, formula, and comments . . . . . 303(T)
in cobalt alloy microstructures . . . . . 320(F), 321(F)
in cobalt alloys 394
in nickel alloy microstructures . . . . . 326(F)
in superalloys 85
macroetching 298
and stress-corrosion cracking 143
Laves phase alloys . . . . . 122(T), 365(F)
Leaching 207–208
Lead
content effect on nickel alloy weldability 249
molten, corrosion by 186
Lead acetate, corrosion rate of electroless nickel coatings . . . . . 118(T)
Leader defects 287
Light-etching defect 74
Limonitic-type ore 4
Linnaeite
composition . . . . . 346(T)
mining locations . . . . . 346(T)
Liquid-droplet erosion, of cobalt alloys 388
Liquid-metal embrittlement 157
Liquidus temperature
of cobalt alloys, individual alloy values . . . 374, 380, 382, 384, 385
of nickel and nickel alloys, individual alloy values 19–54
Lithium, molten, corrosion by 186
Low-alloy nickels 16–17
compositions . . . . . 15(T)
Low-alloy steels
compositions . . . . . 8(T)
for cryogenic service 8
mechanical properties 8
nickel content effects . . . . . 8(F,T)
welding products for dissimilar-metal joints with nickel-base alloys . . . . . 250(T)
Low-angle boundaries (LAB) 78
Low-carbon mold steels 8
Low-cycle fatigue (LCF), in superalloys 84
Low-expansion alloys. *See* Nickel low-expansion alloys.
Low-level radioactive waste incinerator, temperature range and contaminants encountered . . . . . 183(T)
Low-nickel alloys . . . . . 96(F)
Low-pressure plasma spraying (LPPS) . . . . . 287(F), 290
for applying coatings to superalloys 89
Low-stress abrasion test procedure (ASTM G 65) . . . . . 393(F)
Lubricants
for forging 198
for forming 192, 193, 194, 197

M

Machinability, categories of . . . . . 235(F), 236(T)
Machining of nickel alloys . . . . . 235–244(F,T)
boring . . . . . 237–240(T)
broaching . . . . . 242, 243(T)
categories of machinability . . . . . 235, 236(F,T)
coolants 237, 240

© 2000 ASM International. All Rights Reserved.
ASM Specialty Handbook: Nickel, Cobalt, and Their Alloys (#06178G)

Machining of nickel alloys (continued)
cutting tool selection . . . 237, 238(T)
drilling . . . 240–241, 242(T)
grinding . . . 244
grooving . . . 237–240
lubricants . . . 237
milling . . . 242–243, 244(T)
operation at 50% of machine capacity . . . 237
planing . . . 242, 243(T)
reaming . . . 241
sawing . . . 243–244(T)
shaping . . . 242, 243(T)
surface finishing . . . 244
tapping . . . 241–242(T)
threading . . . 242(T)
tooling inserts . . . 239–240(F)
turning . . . 237–240(F,T)
work hardening avoidance . . . 236–237
Macroetchants . . . 298, 300(T)
Macroetching . . . 298, 300(T)
nickel-iron alloys . . . 294
Magnesium, content effect on nickel alloy weldability . . . 248
Magnetic permeability
of cobalt alloys, individual alloy values . . . 374, 375, 377, 378, 381, 383, 384
of nickel . . . 3
of nickel and nickel alloys, individual alloy values, alloys . . . 19, 21, 22, 27, 28, 30, 31, 35, 36, 38, 39, 54
Magnetic properties, of nickel and nickel alloys . . . 22–23, 24–25
Magnetic recording, market segment percentage and form of cobalt consumption . . 347
Magnetostriction (soft) 1590 A/m, of powder-rolled nickel strip . . . 214(T)
Magnets
market segment percentage and form of cobalt consumption . . . 347
nickel consumption in U.S. by end use . . . 6(T)
Manganese
alloying element effect on nickel- and iron-base superalloys . . . 167(T)
content effect on nickel alloy weldability . . . 248
Manganins . . . 10
Manual spinning . . . 194(T)
Maraging steels
cobalt content effect . . . 352, 353(T)
compositions . . . 8(T)
heat treatments . . . 8(T)
mechanical properties . . . 8(T)
nickel content effect . . . 8(T)
Martempering . . . 137
Matte smelting . . . 347
Maximum permeability, of powder-rolled nickel strip . . . 214(T)
M_eB_2 phase
crystal structure, lattice parameter, formula, and comments . . . 303(T)
in nickel alloy microstructures . . . 308(F), 322(F)
MC carbides . . . 15, 301, 303–304
crystal structure, lattice parameter, formula, and comments . . . 303(T)
in cobalt alloy microstructures . . . 329(F), 330(F)
in nickel alloy microstructures . . . 308(F), 310(F), 311(F), 312(F), 313(F), 315(F), 316(F), 322(F), 323(F), 324(F), 325(F), 327(F)
in superalloys . . . 80, 83, 85
and stress-corrosion cracking . . . 141, 142, 143
and thermal-mechanical processing . . . 201
M_6C carbides . . . 15, 301, 303–304
in cobalt alloy microstructures . . . 319(F), 320(F), 321(F), 329(F), 330(F)
in cobalt-base alloys . . . 363, 364, 366
in cobalt alloys, and wear resistance . . . 393
crystal structure, lattice parameter, formula, and comments . . . 303(T)
in nickel alloy microstructures . . . 315(F), 322(F), 327(F)
in superalloys . . . 80, 83, 85
and stress-corrosion cracking . . . 141, 142, 143
and thermal-mechanical processing . . . 201
M_7C_3 carbides . . . 15, 301, 303–304
crystal structure, lattice parameter, formula, and comments . . . 303(T)
in cobalt-base alloys . . . 363, 364, 365
in cobalt alloy microstructures . . . 321(F), 328(F), 329(F)
in cobalt alloys, and wear resistance . . . 393
in superalloys . . . 80
$M_{23}C_6$ carbides . . . 301, 303–304
crystal structure, lattice parameter, formula, and comments . . . 303(T)
in cobalt alloy microstructures . . . 319(F), 320(F), 321(F), 328(F), 329(F), 330(F)
in cobalt alloys, and wear resistance . . . 393
in cobalt-base alloys . . . 364, 365, 367
in nickel alloy microstructures . . . 302, 309(F), 313(F), 314(F), 315(F), 316(F), 324(F), 327(F)
in nickel-chromium-molybdenum alloys . . . 139
in superalloys . . . 80, 83, 85
and stress-corrosion cracking . . . 142(F), 143, 150
and thermal-mechanical processing . . . 201
MCrAl coatings . . . 88
MCrAlY coatings . . . 88, 288
ductility . . . 288(F)
overlay . . . 282–283(F), 284, 286–287
performance . . . 288–290(F)
Mechanical alloying . . . 77, 220–224(F,T)
applications of superalloy powders . . . 223–224(F)
commercial alloys . . . 222–223(F,T)
compositions of nickel-base superalloys . . . 222(T)
definition . . . 221
equipment . . . 221–222
mechanical properties of nickel-base superalloys . . . 223(T)
of nickel powders . . . 211
powder characteristics . . . 222, 223(F)
processing bath . . . 221, 222(F)
production of oxide-dispersion-strengthened (ODS) superalloy powders . . . 222
Melting point
of cobalt . . . 345
of nickel and nickel alloys, individual alloy values . . . 22, 29, 31, 34, 36, 42, 44, 48, 54
Melting temperature, of cobalt alloys, individual alloy values . . . 375, 378, 380, 382, 384
Metal air cells, functional, service, and structural requirements . . . 211(T)
Metal carbonyls . . . 203–206(F)
Metal dusting . . . 172–173
Metallographic examination . . . 298–304(T)
of cobalt and cobalt alloys . . . 404–406(T)
of high-nickel alloys . . . 293–294(T), 295–297(F)
of nickel-copper alloys . . . 293–294(T), 295–297(F)
of nickel-iron alloys . . . 294–295(T), 297(F)
objective . . . 293
specimen preparation . . . 298–300(T)
Metallographic specimen preparation methods
Microcast-X method . . . 77
Microcracking, of nickel platings . . . 110
Microdiffraction patterns . . . 300
Microetchants . . . 299–300, 301(T)
Microexamination . . . 300–301(T)
Microfissuring . . . 79
Mild steel, corrosion rate in various solutions . . . 118(T), 119(F)
Mill-annealed and sensitized (MAS) alloy, stress-corrosion cracking . . . 151
Milling, of nickel alloys . . . 243, 244(T)
MN phase, crystal structure, lattice parameter, formula, and comments . . . 303(T)
Moa Bay hydrometallurgical process . . . 207, 208(F)
Moa sulfides, composition . . . 207
Modulus of rigidity, of cobalt alloys, individual alloy values . . . 375(T)
Molten carbonates, corrosion by . . . 185–186(T)
Molten chlorides, corrosion by . . . 184(F,T)
Molten fluorides, corrosion by . . . 185
Molten metal corrosion . . . 186(F,T)
Molten nitrates, corrosion by . . . 184–185(F,T)
Molten nitrites, corrosion by . . . 184–185(F,T)
Molten salt corrosion . . . 184–186(F,T)
Molybdenum
alloying element effect in cobalt-base heat resistant alloys . . . 366
alloying element effect on nickel- and iron-base superalloys . . . 167(T)
alloying element effects on corrosion resistance . . . 17(T)
alloying element effects on nickel alloy corrosion resistance . . . 129(F)
alloying element range in superalloys . . . 69(T)
content effect in cobalt-base alloys . . . 364
maximum furnace operating temperature in air . . . 93(T)
mechanical properties . . . 93(T)
physical properties . . . 93(T)
as solid-solution strengthener in nickel . . . 14(F)
Mo_2C carbides . . . 143
$Mo_{12}C$ carbides . . . 142, 143
Molybdenum disilicide
maximum furnace operating temperature in air . . . 93(T)
mechanical properties . . . 93(T)
physical properties . . . 93(T)
$MoSi_2$ + 10% ceramic additives
maximum furnace operating temperature in air . . . 93(T)
mechanical properties . . . 93(T)
physical properties . . . 93(T)
MolyPermalloys . . . 95
Mond-Langer process . . . 205
Monels. *See also* Alloy Index for individual alloys.
for weld cladding . . . 122
Mounting . . . 298
nickel-iron alloys . . . 294
Multiphase (MP) alloys . . . 368–369
MuMetals . . . 95
Municipal waste incinerators, temperature range and contaminants encountered . . . 183(T)
Mu phase . . . 304
crystal structure, lattice parameter, formula, and comments . . . 303(T)
and stress-corrosion cracking . . . 143

N

NACE TM-01-77 tensile test . . . 160
NACE specification MR-01-75, alloys which passed initial corrosion screening tests . . . 137
Near-net shape processing . . . 12
Nickel
alloying element effect in cobalt-base heat resistant alloys . . . 366
alloying element effect on nickel- and iron-base superalloys . . . 167(T)

© 2000 ASM International. All Rights Reserved.
ASM Specialty Handbook: Nickel, Cobalt, and Their Alloys (#06178G)

alloying element effects on corrosion resistance . . . 17(T)
alloying element effects on stainless steels . . . 7
alloying element range in superalloys . . . 69(T)
applications . . . 6(T), 7–13(F,T), 9–10, 11(T)
atomic weight . . . 3
characteristics . . . 9
chemical properties . . . 4
consumption in U.S. by end use . . . 6(T)
corrosion in chlorine-bearing environments 179(T)
corrosion in molten eutectic sodium-potassium carbonate . . . 185(T)
corrosion rates in molten drawsalt . . . 185(T)
corrosion resistance . . . 4
corrosion-resistant wrought, compositions . . . 15(T)
electrical properties . . . 3
end uses . . . 6(T)
extraction and refining . . . 4–6(F)
in austenitic manganese steels . . . 8(T)
in cast irons . . . 8–9(T)
in cemented carbides . . . 12, 13(F)
in cobalt-base alloys . . . 10
in electrical contact materials . . . 12–13
in low-alloy steels . . . 8(F,T)
in maraging steels . . . 8(T)
in P/M nickel steels . . . 10–13(F)
in stainless steels . . . 7–8(F,T)
in tool steels . . . 8
magnetic properties . . . 3(F)
market segments of worldwide consumption . . . 6
mechanical properties . . . 3–4, 17(T), 19–22(F,T)
microstructure . . . 3, 9
nickel consumption in U.S. by end use . . . 6(T)
occurrence (resources) . . . 4
physical properties . . . 3, 19–22(F,T)
thermal properties . . . 3

Nickel alloy powders, atomized, for coating material . . . 10

Nickel alloys
alloy composition effect on corrosion behavior 141
alloying element effects on corrosion resistance . . . 17(T)
applications . . . 6(T), 7–13(F,T)
cast corrosion-resistant . . . 55–61(F,T)
cast heat resistant . . . 62–67(F,T)
characteristics . . . 9
corrosion . . . 127–140(F,T)
corrosion-resistant wrought, composition . . . 15(T)
heat treating . . . 230–234(F,T)
intermetallic phases . . . 9
mechanical properties . . . 17(T), 22–54(F,T)
microstructure . . . 9
nickel consumption in U.S. by end use . . . 6(T)
physical properties . . . 22–54(F,T)
powder metallurgy processing . . . 203–228(F,T)
solution hardening . . . 9
welding . . . 245–267(F,T)

Nickel aluminide alloys . . . 104–105(F,T)
applications . . . 105
as coatings, applications . . . 286–287(F)
as coatings for superalloys . . . 282(F), 284–285(F)
compositions . . . 104(T)
corrosion resistance . . . 104–105(F)
mechanical properties . . . 104, 105(F)
microstructure . . . 104

Nickel-aluminum binary phase diagram, crystal structure data . . . 331(T)

Nickel-aluminum-chromium isothermal section, at 1150 °C . . . 336(F)

Nickel-aluminum-copper isothermal section
at 500 °C . . . 341(F)
at 700 °C . . . 341(F)
at 900 °C . . . 341(F)

Nickel and nickel alloys, physical metallurgy . . . 14–15(F)

Nickel-base alloys
cast . . . 55(T), 56
microstructure . . . 302
nickel consumption, % . . . 6

Nickel-base/boride alloys . . . 10

Nickel-base corrosion-resistant alloys 245–250(F,T)
alloying elements effects on weldability 248–249(F)
composition . . . 245(T)
dissimilar welding of plate-to-plate specimens . . . 249, 250(T)
fusion zone, welding considerations . . . 247(F)
heat-affected zone welding considerations . . 247(F)
mechanical properties . . . 245(T)
nickel-clad steel welding . . . 249–250(F)
physical properties . . . 245–246(T)
postweld heat treatment . . . 249(T)
repair welding . . . 250
unmixed zone, welding considerations . . . 247–248
welding of . . . 245–250(F,T)
welding of castings . . . 250
weld overlay cladding . . . 250

Nickel-base directionally solidified castings, compositions . . . 73(T)

Nickel-base hardfacing alloys . . . 10
boride-containing nickel-base alloys . 121–122(F,T)
compositions . . . 121(T), 122(T)
Laves phase alloys . . . 122(T)
mechanical properties . . . 122(T)
physical properties . . . 122(T)
as weld-overlay coatings . . . 121–122(F,T)

Nickel-base/Laves phase alloys . . . 10

Nickel-base single crystal castings, compositions . . . 73(T)

Nickel-base superalloys. *See also* Superalloys.
alloying additions effects on corrosion resistance . . . 129(F)
alloying element effects . . . 69(T)
cast
compositions . . . 72(T)
microstructure . . . 70(F)
cobalt content effect . . . 349(F,T)
compositions . . . 71(T), 72(T)
joining . . . 78–79(F)
market segment percentage and form of cobalt consumption . . . 347
microstructure . . . 70, 70(F), 80(F)
vacuum induction melting . . . 73–74(F)
welding . . . 78–79(F)

Nickel-beryllium alloys . . . 102–104(F,T)
applications . . . 102–103
castability . . . 102
compositions . . . 102(T), 103
electrical properties . . . 104(T)
heat treatment . . . 103(T)
mechanical properties . . . 102, 103(T), 104(F)
microstructure . . . 103(F)
physical properties . . . 102, 103(T), 104(T)
product forms . . . 102

Nickel-boron binary phase diagram, crystal structure data . . . 332(T)

Nickel-boron castings . . . 10

Nickel-cadmium alkaline rechargeable batteries, functional, service and structural requirements . . . 211(T)

Nickel carbonate
formula . . . 106
nickel content . . . 106

Nickel-carbon binary phase diagram, crystal structure data . . . 332(T)

Nickel cattierite
composition . . . 346(T)
mining locations . . . 346(T)

Nickel chloride
formula . . . 106
nickel content (%) . . . 106

Nickel-chromium alloys
alloy content (%) of nickel-bearing steels . . . 8(T)
cast heat resistant . . . 62, 63(T)
pickling . . . 273, 275–276
pretreatment . . . 275

Nickel-chromium binary phase diagram, crystal structure data . . . 333(T)

Nickel-chromium boride . . . 10

Nickel-chromium carbide . . . 10

Nickel-chromium-iron alloys . . . 17–18
cast . . . 55(T), 56(T), 57(T), 66(T), 67(T)
compositions . . . 16(T), 17, 55(T)
corrosion resistance . . . 17, 127(T), 128
temperature range . . . 17–18

Nickel-chromium-iron isothermal section
at 650 °C . . . 336(F)
at 800 °C . . . 336(F)
at 900 °C . . . 336(F)
at 1000 °C . . . 336(F)
at 1300 °C . . . 336(F)

Nickel-chromium-iron-molybdenum alloys . . . 18
compositions . . . 16(T), 18
corrosion resistance . . . 128–129(T)

Nickel-chromium-molybdenum alloys . . . 18, 127–128(T)
alloy content (%) of nickel-bearing steels . . . 8(T)
applications . . . 18
cast . . . 55(T), 56(T), 57, 58(T)
compositions . . . 16(T), 55(T)
corrosion in weldments . . . 138–139(F)
stress-corrosion cracking . . . 147

Nickel-chromium-molybdenum isothermal section
at 600 °C . . . 337(F)
at 1200 °C . . . 337(F)
at 1250 °C . . . 337(F)

Nickel-chromium-niobium isothermal section
at 1100 °C . . . 337(F)
at 1175 °C . . . 337(F)
at 1200 °C . . . 337(F)

Nickel-chromium-titanium isothermal section
at 1027 °C . . . 338(F)
at 1277 °C . . . 338(F)
at 1352 °C . . . 338(F)

Nickel-chromium-tungsten alloys . . . 16(T), 18

Nickel-chromium-tungsten isothermal section
at 800 °C . . . 339(F)
at 900 °C . . . 339(F)
at 1000 °C . . . 338(F)
at 1250 °C . . . 338(F)

Nickel coatings. *See also* Coatings . . . 10, 106–123(F,T)
solid state nickel cladding . . . 122–123
thermal spray coatings . . . 120(F), 121(T)

Nickel-cobalt binary phase diagram, crystal structure data . . . 332(T)

Nickel-cobalt-chromium isothermal section, at 1200 °C . . . 340(F)

Nickel-cobalt-chromium-silicon alloys, compositions . . . 16(T)

Nickel-cobalt-iron isothermal section
at 600 °C . . . 340(F)
at 800 °C . . . 340(F)

Nickel-cobalt-phosphorus alloys, as electroless plating systems . . . 119(T)

Nickel-cobalt-phosphorus electroless plating system
availability . . . 119(T)
environments where corrosion resistant . . . 119(T)
physical properties . . . 119(T)

Nickel composite coatings . . . 10

Nickel-copper alloys . . . 17
applications . . . 17
cast . . . 55(T), 56
compositions . . . 15(T), 55(T)
corrosion resistance . . . 127–128(T)

© 2000 ASM International. All Rights Reserved.
ASM Specialty Handbook: Nickel, Cobalt, and Their Alloys (#06178G)

Nickel-copper alloys (continued)
metallographic examination . . . . . 293–294(T), 295–297(F)
microstructures . . . . . 294, 296(F), 297(F)
nickel consumption in U.S. by end use . . . . . 6(T)
pickling 273, 274–275
welding products for dissimilar-metal joints with nickel-base alloys . . . . . 250(T)
Nickel-copper binary phase diagram, crystal structure data . . . . . 333(T)
Nickel-copper-phosphorus alloys, as electroless plating systems . . . . . 119(T)
Nickel-copper-phosphorus electroless plating system
availability . . . . . 119(T)
environments where corrosion resistant . . . . . 119(T)
physical properties . . . . . 119(T)
Nickel dermatitis 10
Nickel Development Institute 6
Nickel electroforming 107
Nickel flashing 270
Nickel hydridocarbonyl 203
Nickel-iron alkaline rechargeable batteries, functional, service, and structural requirements . . . . . 211(T)
Nickel-iron alloys
metallographic examination . . . 294–295(T), 297(F)
microstructures . . . . . 295, 297(F)
Nickel-iron binary phase diagram, crystal structure data . . . . . 333(T)
Nickel-iron-chromium alloys
compositions . . . . . 16(T), 18
pickling 273, 275–276
pretreatment 275
Nickel-iron-chromium-molybdenum alloys, stress-corrosion cracking . . . . . 148(F)
Nickel-iron-molybdenum isothermal section
at 1100 °C . . . . . 339(F)
at 1200 °C . . . . . 339(F)
Nickel-iron NILO alloys, forming 191
Nickel-iron phosphorus alloys, as electroless plating systems . . . . . 119(T)
Nickel-iron-phosphorus electroless plating systems
availability . . . . . 119(T)
environments where corrosion resistant . . . . . 119(T)
physical properties . . . . . 119(T)
Nickel-iron soft magnetic alloys . . . . . 94–96(F,T), 97(T), 98(T)
applications . . . . . 94–95(T)
heat treatment 95
mechanical properties 94
microstructure 95
physical properties . . . . . 94–96(F,T), 97(T), 98(T)
Nickel-iron-tungsten isothermal section
at 1400 °C . . . . . 340(F)
at 1455 °C . . . . . 340(F)
at 1465 °C . . . . . 339(F)
at 1500 °C . . . . . 339(F)
Nickel low-expansion alloys . . . . . 96–101(F,T)
applications 96–97
cobalt content effect . . . . . 352(T)
composition . . . . . 100(F)
heat treatment effect . . . . . 99(T)
magnetic properties 98
mechanical properties . . . . . 99(T)
nickel consumption in U.S. by end use . . . . . 6(T)
nickel effect on thermal expansion of iron . . 97, 99(F)
physical properties . . . . . 98–100(F,T)
Nickel-molybdenum alloys 17
alloy content (%) of nickel-bearing steels . . . . . 8(T)
cast . . . . . 57–59(F,T)
compositions . . . . . 16(T), 55(T)
corrosion in weldments . . . . . 138(F), 139(F)
corrosion resistance . . . . . 127(T), 128
Nickel-molybdenum binary phase diagram, crystal structure data . . . . . 334(T)
Nickel-niobium alloys, microstructure 82
Nickel-niobium binary phase diagram, crystal structure data . . . . . 334(T)
Ni_3Nb (δ) phase, crystal structure, lattice parameter, formula, and comments . . . . . 303(T)
Ni_3Nb orthorhombic phase, in superalloys 80
Nickel phosphorus plating section . . . . . 112(T), 113
cathode current density . . . . . 112(T)
coatings 10
composition . . . . . 112(T)
mechanical properties . . . . . 112(T)
pH value . . . . . 112(T)
temperature range . . . . . 112(T)
Nickel-phosphorus binary phase diagram . . . 334(T)
crystal structure data . . . . . 334(T)
Nickel-phosphorus-molybdenum alloys, as electroless plating systems . . . . . 119(T)
Nickel-phosphorus-molybdenum electroless plating system
availability . . . . . 119(T)
environments where corrosion-resistant . . . . 119(T)
physical properties . . . . . 119(T)
Nickel plating . . . . . 10, 106–114(F,T)
alloys to be thermal sprayed 120
average coating thickness estimation . . . . . 107(T)
consumption worldwide for decorative applications 106
corrosion resistance of decorative coatings . . . . . 110–111(T)
coumarin process 110
decorative applications 106
decorative bright nickel . . . . . 108–109(T)
decorative nickel-iron alloy plating 111
decorative plating 106
development history . . . . . 106(F)
electroless nickel plating . . . . . 115–120(F,T)
engineering applications 106
fluoborate solution . . . . . 112–113(T)
microcracked chromium 110
microdiscontinuous chromium 110
microporous chromium 110
multilayer decorative . . . . . 109–110(T)
nickel-chromium plating 114
nickel-cobalt plating 113–114
nickel-iron plating . . . . . 113, 114(T)
nickel-manganese plating 114
nickel-molybdenum plating 114
noncoumarin process 110
process 107
solution for . . . . . 108(T)
tin-nickel plating 114
Watts and nickel sulfamate solutions for engineering applications . . . . . 108(T), 111–112, 113
Watts solution . . . . . 107–108(F,T), 109(F)
effect on mechanical properties . . . . . 108, 109(F)
effect on physical properties . . . . . 108, 109(F)
weld overlay coatings . . . . . 120–122(F,T)
zinc-nickel plating 114
Nickel powders . . . . . 10–13(F)
applications 12–13
Nickel-rhenium phosphorus alloys, as electroless plating systems . . . . . 119(T)
Nickel-rhenium phosphorus electroless plating system
availability . . . . . 119(T)
environments where corrosion resistant . . . . . 119(T)
physical properties . . . . . 119(T)
Nickel-silicon binary phase diagram, crystal structure data . . . . . 335(T)
Nickel-silvers . . . . . 10, 12(T)
composition . . . . . 12(T)
mechanical properties . . . . . 12(T)
product forms . . . . . 12(T)
Nickel steels, alloy content (%) of nickel-bearing steels . . . . . 8(T)
Nickel sulfamate . . . . . 108(T), 112
formula 106
mechanical properties . . . . . 108(T)
nickel content 106
formula 106
nickel content 106
Nickel sulfide matte technique 5
Nickel tetracarbonyl . . . . . 203, 204–205(F)
decomposition 205
formation reaction 205
industrial application 205
physical properties 205
safety precautions 205
Nickel-thallium-boron alloys, as electroless plating systems . . . . . 119(T)
Nickel-thallium-boron electroless plating system
availability . . . . . 119(T)
environments where corrosion resistant . . . . . 119(T)
physical properties . . . . . 119(T)
Nickel-tin-boron alloys, as electroless plating systems . . . . . 119(T)
Nickel-tin-boron electroless plating system
availability . . . . . 119(T)
environments where corrosion resistant . . . . . 119(T)
physical properties . . . . . 119(T)
Nickel-titanium binary phase diagram
crystal structure data . . . . . 335(T)
Ni_3Ti orthorhombic phase 13
Nickel-titanium shape memory alloys . . 101–102(T)
applications 102
composition 101–102
heat treating 102
mechanical properties . . . . . 101, 102(T)
physical properties . . . . . 102(T)
processing 102
Nickel-tungsten binary phase diagram, crystal structure data . . . . . 335(T)
Nickel-tungsten carbide 10
Nickel-tungsten phosphorus alloys
as electroless plating systems . . . . . 119(T)
availability . . . . . 119(T)
Nickel-tungsten-phosphorus electroless plating system
environments where corrosion resistant . . . . . 119(T)
physical properties . . . . . 119(T)
Nickel-zinc alkaline rechargeable batteries, functional, service, and structural requirements . . . . . 211(T)
Ni-Hard white irons
compositions . . . . . 9(T)
microstructure 9
Niobium
alloying element effect
in cobalt-base heat-resistant alloys 366
on nickel- and iron-base superalloys . . . . . 167(T)
on corrosion resistance . . . . . 17(T)
on nickel alloy corrosion resistance . . . . . 129(F)
alloying element range in superalloys . . . . . 69(T)
as gamma prime former 15
Ni-Resist irons, compositions . . . . . 9(T)
physical properties 9
Nitrates, molten, corrosion by . . . . . 184–185(F,T)
Nitric acid
corrosion of cobalt-base alloys . . . 396(T), 397(F,T)
corrosion of iron-base alloys . . . . . 397(T)
corrosion of nickel-base alloys . . . . . 397(T)
corrosion rate of
cobalt-base alloys . . . . . 397(T)
CW-12MW . . . . . 58(T)
electroless nickel coatings . . . . . 118(T)
nickel-base alloys . . . . . 397(T)
N-12MV . . . . . 58(T)
as corroding agent . . . . . 135(F), 136(F)

© 2000 ASM International. All Rights Reserved.
ASM Specialty Handbook: Nickel, Cobalt, and Their Alloys (#06178G)

Nitric acid + hydrofluoric acid, as corroding agent . . . . . 135, 136(F)
Nitric acid corrosion . . . . . 132(F)
Nitridation . . . . . 173–176(F,T)
Nitrides 304
Nitrites, molten, corrosion by . . . . . 184–185(F,T)
Nitrogen, alloying element effects on corrosion resistance . . . . . 17(T)
Nomograms, for machining tool speed and feed balance . . . . . 239(F)
Nondestructive inspection
acid etching of nickel-base alloys before 278
and finishing operations 278
Notch stress rupture (NSR), of superalloys. 84

O

Oil ash corrosion . . . . . 62–63(T)
Oil refinery heaters, oil ash corrosion. . . . . 63, 64(F)
Ordered intermetallic alloys of Ni_3Al 104–105(F,T)
Organic acid corrosion . . . . . 133–134(F,T), 135(F,T)
Orthochlorobenzyl chloride
corrosion rate of
electroless nickel-phosphorus coatings . . . 118(T)
mild steel. . . . . 118(T)
nickel 200 . . . . . 118(T)
Orthochlorobenzyl chloride (crude)
corrosion rate of
electroless nickel-phosphorus coatings . . . 118(T)
mild steel. . . . . 118(T)
nickel 200 . . . . . 118(T)
Osprey Metals, spray forming process 77, 227
Overlay coatings, for superalloys 87, 88
Oxalic acid, corrosion rate of electroless nickel coatings . . . . . 118(T)
Oxidation . . . . . 167–172(F,T), 281, 286
alloying element effects 167
of cobalt alloys . . . . . 399(F)
Oxide-dispersion-strengthened (ODS) alloys 70, 77
Oxide-dispersion-strengthened (ODS) superalloy powders. 220, 222
Oxide glazes. 387
Oxide intrusions (pegs) 167–168
Oxide/nitride stringers 74
Oxides 304
Oxidized or scaled surfaces 274
on high-nickel alloys. 275
on nickel-copper alloys. 275
Oxydrolysis 208

P

Pack cementation process . . . . . 283–284(F,T)
Packer fluids, causing stress-corrosion cracking . . . . . 145–146(T)
Partially melted zone. 267
Partially stabilized zirconia (PSZ) thermal barrier coatings 88
Pentlandite 4
Permanent magnetic alloys 10
cobalt content effect . . . . . 350–352(T)
Perovskite, in nickel alloy microstructures . . . . 323(F)
Petrochemical and refining environments, as corroding agents . . . 137, 138(F
PHACOMP 143
Phase control electron vacancy number. 85
Phase diagrams
of binary cobalt systems . . . . . 356–358(F,T)
of binary nickel systems . . . . . 331–335(F,T)
of ternary cobalt systems . . . . . 358–361(F)
of ternary nickel systems . . . . . 336–341(F)
Phenol, corrosion rate of electroless nickel coatings . . . . . 118(T)
Phosphoric acid
corrosion. . . . . 132–133(T)
of cobalt alloys. . . . . 396(T), 397(F)
of cobalt-base alloys at boiling temperature . . . . . 396(T)
corrosion rate of
CW-12MW. . . . . 58(T)
electroless nickel coatings . . . . . 118(T)
electroless nickel-phosphorus coatings . . . 118(T)
Hastelloy D. . . . . 59(T)
mild steel. . . . . 118(T)
nickel 200 . . . . . 118(T)
N-12MV . . . . . 58(T)
Phosphorus, content effect on nickel alloy weldability 249
Phosphorus oxychloride
corrosion rate of
electroless nickel-phosphorus coatings . . . 118(T)
mild steel. . . . . 118(T)
nickel 200 . . . . . 118(T)
Physical vapor deposition
for applying overlay coatings to superalloys 89
for coatings, performance of 290
Pickling. 273
after wet tumbling 280
alloy groupings for procedures 273
bath analysis 273
as cleaning for welding 276–277
copper flash prevention and removal 276
electrolytic 276
electrolytic salt baths 275–276
electropolishing 276
embedded iron detection and removal 276
formulas of reagents for pickling nickel alloys 274(T)
heat-resistant nickel alloys. 279
high-nickel alloys 273, 275
lead removal. 276
nickel-chromium alloys 273, 275–276
nickel-copper alloys. 273, 274–275
nickel-iron-chromium alloys 273, 275–276
oxidizing salt baths 275
safety precautions for workers. 275
salt baths. 275–276
surface conditions 274
zinc removal. 276
Piercing. 193
Pin-on-block test, for cobalt alloys. . . . . 392(F)
Pixie process 110
Planar deformation 159
Planar slip 391
Planing, of nickel alloys. . . . . 242, 243(T)
Plasma arc welding (PAW). 263–264
Plasma rotating electrode process (PREP) 215
Plating, nickel consumption, %. 6
Platinum
maximum furnace operating temperature in air . . . . . 93(T)
mechanical properties . . . . . 93(T)
physical properties. . . . . 93(T)
Poisson's ratio
of Elgiloy. . . . . 375(T)
of nickel. 4
of nickel and nickel alloys, individual alloy values. 19–54
Polishing
cobalt and cobalt alloys. . . . . 404(T)
final 299
as finishing operation 277
heat-resistant nickel alloys. 280
high-nickel alloys 293
nickel-copper alloys 293
nickel-iron alloys. 294
rough. 298–299
Polythionic acid cracking 150–151
Positive back-rake angles. 238
Potassium hydroxide, corrosion rate of electroless nickel coatings . . . . . 118(T)
Powder injection molding (PIM) . . . . . 226(T)
Powder metallurgy nickel alloy strip, roll compacted and sintered nickel, pore size distribution . . . . . 212(F)
Powder metallurgy nickel alloy strip, roll compacted strip, physical properties. . . . . 212(T)
Powder metallurgy nickel-base superalloys 12
applications. 12
Powder metallurgy (P/M) processing of nickel alloys. . . . . 203–228(F,T)
ammonium sulfate recovery. 210
applications. 210
atomization. . . . . 210–211(F)
briquetting. . . . . 210(F)
carbonyl vapormetallurgy . . . . . 203–206(F)
conventional superalloy . . . . . 215–220(F,T)
mechanical alloying 211
powder applications . . . . . 206, 207(F)
powder properties. . . . . 206(F)
production of nickel powders . . . . . 203–211(F,T)
production of powder by hydrometallurgical processing . . . . . 206–210(F,T)
roll compacting . . . . . 214–215(F,T)
Sherritt ammonia pressure leach process. . . . . 206–210(F,T)
Sherritt's standard grade nickel powder, properties. . . . . 209(T)
sintering . . . . . 211–213(F,T)
specialized superalloy. . . . . 220–228(F,T)
sulfide precipitation. 210
techniques. 203
Powder metallurgy superalloys, microstructure . . 84
Powder processing, of superalloys 77
Powder-rolled nickel strip . . . . . 214–215(F,T)
advantages 214
applications. . . . . 214(F)
mechanical properties . . . . . 214(T)
physical properties. . . . . 214(T)
powders used 214
production. 214
Power spinning. . . . . 194–195(F)
Power station boiler components, oil ash corrosion. . . . . 63, 65(F)
Precipitation hardening. *See* Heat treating of nickel alloys.
Precipitation-hardening alloys
brazing. 271
chemical properties 18
compositions . . . . . 16(T), 18
welding of. 260
Precracked samples, for stress-corrosion cracking 160–161
Processing maps 76
Propionic acid corrosion . . . . . 134, 135(F,T)
Pulp and paper mill environmental corrosion 136–137
Pulsed-current plating 106
Pyrrhotite 4
composition . . . . . 346(T)
mining locations. . . . . 346(T)

R

Radial segregation 298
Radio alloys 10
Rake angle 242
Ramping . . . . . 240(F)

© 2000 ASM International. All Rights Reserved.
ASM Specialty Handbook: Nickel, Cobalt, and Their Alloys (#06178G)

Rapid prototyping 78
Rapid solidification 12
Rapid-solidification-rate (RSR) technology 77
Rare earths, alloying element effect on nickel- and iron-base superalloys . . . . . 167(T)
Reaming, of nickel alloys 241
Recrystallization, and thermal mechanical processing 201
Recrystallization temperature
of nickel 3
of nickel and nickel alloys . . . . . 22(F)
Reduced-oxide surfaces 274
on high-nickel alloys 275
on nickel-copper alloys 274–275
Reducing agents, for electroless nickel plating 115–116
Reduction of area, of cobalt alloys, individual alloy values . . . . . 381(T), 382(T)
Reduction smelting 4
Relief angles 238
Remanance, of powder-rolled nickel strip . . . . 214(T)
Residual induction, of nickel 3
Residual magnetization, of cobalt 345
Resistance heating alloys . . . . . 92–94(F,T)
applications . . . . . 92–93(T), 94(F)
mechanical properties . . . . . 92–93(T)
physical properties . . . . . 92–93(T), 94(F)
Rhenium
alloying element effect on superalloys 80
alloying element range in superalloys . . . . . 69(T)
Richardson free-energy chart . . . . . 212, 213(F)
Ring patterns 298
Roll compacting of nickel and nickel alloys . . . . . 214–215(F,T)
Roughing, wheel, compound and speed used . . 277(T)

S

Salt-bath descaling, heat-resistant nickel alloys 280
Salt fluxing model, hot corrosion 182
Saturation induction, of powder-rolled nickel strip . . . . . 214(T)
Saturation magnetization
of cobalt 345
of nickel 3
Sawing, of nickel alloys . . . . . 243–244(T)
Secondary reaction zone (SRZ), of superalloys . . . 84
Sectioning 298
nickel-iron alloys 294
Selective etchants 300
Selective laser sintering . . . . . 78, 225(F)
Selective plating 106
Sensitization . . . . . 139(F), 142(F), 143, 145(T)
and stress-corrosion cracking 151
Shape memory actuation devices 102
Shape memory alloys, nickel-titanium . . 101–102(T)
applications 102
composition 101–102
heat treating 102
mechanical properties . . . . . 101, 102(T)
physical properties . . . . . 102(T)
processing 102
Shaping, of nickel alloys . . . . . 242, 243(T)
Shearing 193
Shear modulus
of cobalt alloys, individual alloy values . . . . . 374, 381(T), 382(T)
of nickel 4
of nickel and nickel alloys 36
Shelf 74
Sherritt ammonia pressure leach process . . . . . 206–210(F,T)
Sherritt process . . . . . 5(F)
Shielded metal arc welding (SMAW) . . . . . 259(F), 263(T), 264–265(F,T)
joining configurations for applications . . . . . 259(F)
Shot peening 287
heat-resistant nickel alloys 280
Sigma (σ) phase 301, 304
crystal structure, lattice parameter, formula, and comments . . . . . 303(T)
in nickel alloy microstructures . . . . . 316(F), 323(F), 324(F), 325(F)
in superalloys . . . . . 85(F)
and stress-corrosion cracking 143
SIGMA-SAFE 143
Silicate-type ore 4
Silicon
alloying element effect on
nickel- and iron-base superalloys . . . . . 167(T)
corrosion resistance . . . . . 17(T)
nickel alloy corrosion resistance . . . . . 129(F)
content effect on nickel alloy weldability 248
Silicon carbide
maximum furnace operating temperature in air . . . . . 93(T)
mechanical properties . . . . . 93(T)
physical properties . . . . . 93(T)
Silver-nickel P/M composites 12–13
Simultaneous thickness and electrochemical potential (STEP) (ASTM B 764) 110
Single-crystal (SC) alloys, microstructure 83, 84
Single-crystal (SC) processing . . . . . 73(T), 78(F)
Sintering of nickel and nickel alloys . . 211–213(F,T)
dense products 212
porous products . . . . . 207(F), 211–212(F,T)
Richardson free-energy chart . . . . . 212, 213(F)
selective laser . . . . . 225(F)
Skutterudite
composition . . . . . 346(T)
mining locations . . . . . 346(T)
Slag charge 75
Slag pool depth 75
Slivers 78
Slow-strain-rate tests . . . . . 160(T), 161
Slurry erosion, of cobalt alloys . . . . . 388, 391–392(F)
Soaps, market segment percentage and form of cobalt consumption 347
Sodium, molten, corrosion by . . . . . 186(F)
Sodium carbonate, saturated, corrosion rate of electroless nickel coatings . . . . . 118(T)
Sodium hydroxide
corrosion of cobalt alloys . . . . . 396(T)
corrosion of cobalt-base alloys at boiling temperature . . . . . 396(T)
corrosion rate of
CW-12MW . . . . . 58(T)
electroless nickel coatings . . . . . 118(T)
Hastelloy D . . . . . 59(T)
N-12MV . . . . . 58(T)
Sodium sulfate, corrosion rate of electroless nickel coatings . . . . . 118(T)
Softening temperature, of cobalt alloys, individual alloy values 380
Soft magnetic alloys
cobalt content effect 350
microstructures . . . . . 295, 297(F)
Solidification white spots 74
Solid-particle impingement erosion, of cobalt alloys . . . . . 388, 390–391(F)
Solid-particle impingement test procedure (ASTM G 76) . . . . . 390(F), 391(F)
Solid-solution nickel alloys 18
Solid-solution strengtheners 14–15
Solid-state cladding techniques 106
Solid-state nickel cladding 122–123
Solidus temperature
of cobalt alloys, individual alloy values 382, 384, 385
of nickel and nickel alloys, individual alloy values 19–54
Soluble gas atomization . . . . . 210, 211(F)
Solution-annealed and sensitized (SAS) alloy, stress-corrosion cracking 151
Solution treating. *See* Heat treating of nickel alloys.
Solvay process 203
Sour gas environment NACE International Standard (MR-01-75) 399
Sour gas environments, as corroding agents 137
Spalling, of coatings 285
Specialized powder metallurgy superalloy processing, ... 220–228(F,T)
dual-alloy turbine disk/wheels . . . . . 224–225(F)
laser-assisted rapid prototyping and manufacturing . . . . . 225(F)
mechanical alloying . . . . . 220–224(F,T)
powder injection molding . . . . . 226(T)
spray forming . . . . . 226–228(F)
Specific heat
of cobalt 345
of cobalt alloys, individual alloy values . . . 378, 382
of nickel 3
of nickel and nickel alloys, individual alloy values 19–54
Spindle speeds . . . . . 227(T)
Spinning . . . . . 194–195(F,T)
s phase 80
Spraycast-X process . . . . . 227(F)
Spray-and-fuse process 120
Spray forming of nickel alloys . . . . . 226–228(F)
advantages 226
alloys under development 227–228
disadvantages 226–227
Spurious grains 78
Stacking-fault energy 159
Stainless steels
alloying additions effects on corrosion resistance . . . . . 129(F)
austenitic, composites . . . . . 7(T)
cobalt content effect . . . . . 353(F)
nickel consumption, % 6
nickel consumption in U.S. by end use . . . . . 6(T)
welding products for dissimilar-metal joints with nickel-base alloys . . . . . 250(T)
Stearic acid corrosion 134
Steels
cobalt content effect . . . . . 352–353(F,T)
cold work effect on hardness . . . . . 191(F)
heat resistant, nickel consumption in U.S. by end use . . . . . 6(T)
nickel consumption in U.S. by end use . . . . . 6(T)
Stellite alloys. *See also* Alloy Index for individual alloys.
compositions . . . . . 362(T), 364
corrosion resistance 364
molybdenum content effects 364
powder metallurgy versions 364
Stereolithography 78
Straightening 197
Stress-corrosion cracking
alloy composition effect . . . . . 149(F), 152, 153(F), 155–156(F)
alloy composition effect in nickel alloys 141
alloy strength effect 149
by fluorides . . . . . 146–147(F)
by iodides . . . . . 146(T)
carbide precipitation effect . . . . . 141–143(F)
chloride, with elemental sulfur 149
of cobalt alloys . . . . . 398–399(T)
electrode potential effect . . . . . 149(F), 156(F)
environmental variables effect . . . . . 151–152, 153, 155–156(F), 157–158(F)

© 2000 ASM International. All Rights Reserved.
ASM Specialty Handbook: Nickel, Cobalt, and Their Alloys (#06178G)

environments causing, evolution of ..... 141(T)
heat treatment effect ..... 151, 154, 155, 156(F), 160
in bromides ..... 145–146(T)
in caustic environments ..... 154–157(F)
in chlorides ..... 144–145(F,T)
in dilute aqueous solutions ..... 152–154(F)
in environments containing sulfur species ..... 147–152(F,T)
in halide environments ..... 143–147(F,T)
inhibitors of ..... 148–149(T)
in high-temperature water ..... 152–154(F)
in polythionic acid solutions 150–151
intermetallic phases effects 143
in tetrathionate-containing solutions 151–152
in thiosulfate-containing solutions 151–152
liquid-metal embrittlement 157
metallurgical variables effect ..... 158–160(F,T)
microstructure as factor 152–153
nickel addition effect in stainless steels ..... 7(F)
pH effect 149
precipitation effect ..... 150(F,T)
precipitation hardening effect ..... 145(T)
sensitization effect ..... 145(T)
slow-strain-rate tests vs. constant-deflection tests 147
of superalloys 89–90
testing methods ..... 160–161(T)
Stress equalizing. *See* Heat treating of nickel alloys.
Stress relieving. *See* Heat treating of nickel alloys.
Stress-rupture strength
of cobalt alloys, individual alloy values ..... 376, 377(T), 378(T), 379, 380, 381(T), 383(T), 385, 386(T)
of nickel and nickel alloys, individual alloy values ..... 19–54(F,T)
Stringers 74
Submerged arc welding (SAW) ..... 261(T), 265–266(T)
Subsolvus solution treatment 216
Sulfate chloride nickel plating solution ..... 112(T), 113
cathode current density ..... 112(T)
composition ..... 112(T)
mechanical properties ..... 112(T)
pH value ..... 112(T)
temperature range ..... 112(T)
Sulfidation ..... 176–177(F,T), 178(F), 179(F), 281
of cobalt alloys ..... 399(F)
resistance in cobalt-containing alloys ..... 350(T)
Sulfide ores 4
recovery of nickel from ..... 4–5(F)
Sulfide precipitation reaction 210
Sulfide stress cracking resistant materials for oil equipment (MR0175) NACE specification 369
Sulfides 304
Sulfur
alloying element effects on corrosion resistance 17(T)
causing stress-corrosion cracking ..... 148–149(F,T)
content effect on nickel alloy weldability ..... 248–249(F)
Sulfur embrittlement, of nickel 270 22
Sulfuric acid
corrosion of
cobalt-base alloys ..... 396(T), 397,(F,T)
iron-base alloys ..... 397(T)
nickel-base alloys ..... 397(T)
corrosion rate of
cobalt-base alloys ..... 397(T)
CW-12MW ..... 58(T)
electroless nickel coatings ..... 118(T)
Hastelloy D ..... 59(T)
iron-base alloys ..... 397(T)
nickel-base alloys ..... 397(T)
N-12MV ..... 58(T)
Sulfuric acid + hydrochloric acid (or chloride), as corroding agent ..... 135(F)
Sulfuric acid+ nitric acid, as corroding agent ..... 134–135(F)
Sulfuric acid corrosion ..... 131(F)
Superalloys. *See also* Cobalt-base superalloys; Iron-nickel-base superalloys; Nickel-base superalloys ..... 12, 68–90(F, T)
alloying element
amounts ..... 69(F)
effects ..... 69(T)
ranges ..... 69(T)
effects on microstructure ..... 79–80(F)
applications 73, 79
carbide precipitation ..... 83–84(F)
coatings for 87–89
chemical properties ..... 68, 85–90(F)
corrosion resistance 87, 88–90
environmental effects ..... 85–90(F)
forgeability ratings ..... 76(T)
formability 68, 69
gamma double prime precipitation 82–83
gamma prime precipitation ..... 81–82(F)
heat treatment ..... 80, 81(T), 82, 83(F), 84, 85
high-temperature coatings ..... 281–290 (F,T)
inert environment effects on mechanical properties 90
investment casting ..... 77–78(F)
joining ..... 78–79(F)
market segment percentage and form of cobalt consumption 347
mechanical properties ..... 68(F), 69, 79–85(F,T), 86(T), 87(T), 88(T), 89(T)
melting temperatures and melting ranges 68
microstructure ..... 68, 69(F,T), 70(F), 79–85(F,T)
nickel consumption in U.S. by end use ..... 6(T)
oxidation resistance ..... 80, 86–87, 89(F)
physical properties 68–69
powder processing 77
processing ..... 73–79(F,T)
temperature range 68
tramp element effects 80
transition-element phase formation 85
weldability 68
Superelastic devices 102
Supersolvus solution treatment 216
Surface finishing, of nickel alloys 244
Surface grinding, of nickel alloys 244

T

Taber Abraser Index values,
for nickel coatings ..... 117–118(T), 119, 120(T)
for silicon carbide composite coatings ..... 120(T)
Tampico wheels 278
Tantalum
alloying element effect in cobalt-base heat resistant alloys 366
alloying element effects on nickel alloy corrosion resistance ..... 129(F)
alloying element range in superalloys ..... 69(T)
as gamma prime former 15
maximum furnace operating temperature in air ..... 93(T)
mechanical properties ..... 93(T)
physical properties ..... 93(T)
Tapping, of nickel alloys ..... 241–242(T)
Tarnish 130, 274, 275
on high-nickel alloys 275
on nickel-copper alloys 274
Tempering 137
Tensile strength
of cobalt 345
of cobalt alloys, individual alloy values ..... 373–386(T)
of nickel 3
of nickel and nickel alloys ..... 19–54(F, T)
Ternary phase diagrams
Co-Cr-Fe
at 600°C ..... 359(F)
at 800°C ..... 359(F)
at 1000°C ..... 358(F)
at 1200°C ..... 358(F)
Co-Cr-Ni at 1200°C ..... 359(F)
Co-Cr-W
at 700°C ..... 359(F)
at 1350°C ..... 359(F)
Co-Fe-Mo
at 20°C ..... 360(F)
at 800°C ..... 360(F)
at 982°C ..... 360(F)
at 1093°C ..... 360(F)
at 1300°C ..... 359(F)
Co-Fe-Ni
at 600°C ..... 360(F)
at 800°C ..... 360(F)
Co-Fe-W at 1200°C ..... 361(F)
Co-Mo-Ni
at 1100°C ..... 361(F)
at 1200°C ..... 361(F)
Ni-Al-Cr at 1150°C ..... 336(F)
Ni-Al-Cu
at 500°C ..... 341(F)
at 700°C ..... 341(F)
at 900°C ..... 341(F)
Ni-Cr-Fe
at 650°C ..... 336(F)
at 800°C ..... 336(F)
at 900°C ..... 336(F)
at 1000°C ..... 336(F)
at 1300°C ..... 336(F)
Ni-Cr-Mo
at 600°C ..... 337(F)
at 1200°C ..... 337(F)
at 1250°C ..... 337(F)
Ni-Cr-Nb
at 1100°C ..... 337(F)
at 1175°C ..... 337(F)
at 1200°C ..... 337(F)
Ni-Cr-Ti
at 1027°C ..... 338(F)
at 1277°C ..... 338(F)
at 1352°C ..... 338(F)
Ni-Cr-W
at 800°C ..... 339(F)
at 900°C ..... 339(F)
at 1000°C ..... 338(F)
at 1250°C ..... 338(F)
Ni-Co-Cr at 1200°C ..... 340(F)
Ni-Co-Fe
at 600°C ..... 340(F)
at 800°C ..... 340(F)
Ni-Fe-Mo
at 1100°C ..... 339(F)
at 1200°C ..... 339(F)
Ni-Fe-W
at 1400°C ..... 340(F)
at 1455°C ..... 340(F)
at 1465°C ..... 339(F)
at 1500°C ..... 339(F)
Tetrathionate-containing solutions, and stress-corrosion cracking 151–152
Tetrathionic acid, and stress-corrosion cracking 150
Thermal barrier coatings (TBCs), for superalloys 87, 88
Thermal conductivity
of cobalt 345

© 2000 ASM International. All Rights Reserved.
ASM Specialty Handbook: Nickel, Cobalt, and Their Alloys (#06178G)

Thermal conductivity (continued)
of cobalt alloys, individual alloy values . . . 374, 375, 377, 378, 379, 380, 383, 384, 385, 386
of nickel . . . 3
of nickel and nickel alloys, individual alloy values . . . 20–54(T)
of powder-rolled nickel strip . . . 214(T)
Thermal diffusivity, of nickel and nickel alloys . . . 42, 43, 52
Thermal expansion coefficient
of cobalt . . . 345
of nickel and nickel alloys, individual alloy values . . . 20–54(F,T)
of powder-rolled nickel strip . . . 214(T)
Thermal expansion coefficient (linear)
of cobalt alloys, individual alloy values . . . 374, 375, 378, 379, 380, 382, 384, 385, 386
of nickel . . . 3
Thermal expansion coefficients (CTES), and dissimilar metal welding . . . 267
Thermal shock . . . 239, 240, 287
Thermal spray coatings . . . 10, 120(F), 121(T)
Thermal spraying . . . 106
Thermocouple alloys . . . 10, 94(T)
Thermocouple thermometers . . . 94
Thermomechanical fatigue (TMF), in superalloys . . . 84
Thermomechanical processing (TMP) . . . 201–202(T), 234
Thermomechanical working, of superalloys . . . 84
Thionyl chloride
corrosion rate of
electroless nickel-phosphorus coatings . . . 118(T)
mild steel . . . 118(T)
nickel . . . 118(T), 200
stainless steel (Type 316) . . . 118(T)
Thiosulfate-containing solutions, and stress-corrosion cracking . . . 151–152
Thoria-dispersed nickel . . . 222–223
Thoriated nickel, microstructure . . . 315(F), 316(F)
Threading, of nickel alloys . . . 242(T)
Throwing power . . . 112
Tin-containing nickel castings . . . 61
applications . . . 61
chemical properties . . . 61
Tire adhesives, market segment percentage and form of cobalt consumption . . . 347
Titanium
alloying element effect
in cobalt-base heat resistant alloys . . . 366
on corrosion resistance . . . 17(T)
on nickel alloy corrosion resistance . . . 129–130(F)
on nickel- and iron-base superalloys . . . 167(T)
alloying element range in superalloys . . . 69(T)
content effect on nickel alloy weldability . . . 248
corrosion in molten aluminum, static immersion tests . . . 186(T)
corrosion rates in molten drawsalt . . . 185(T)
as gamma prime former . . . 15
as solid-solution strengthener in nickel . . . 14(F)
Tool steels, nickel content effects . . . 8
Tramp elements, content effect in superalloys . . . 80
Transient liquid phase (TLP) bonding . . . 79
Tungsten
alloying element effect
in cobalt-base heat resistant alloys . . . 366
on nickel- and iron-base superalloys . . . 167(T)
on corrosion resistance . . . 17(T)
on nickel alloy corrosion resistance . . . 129(F)
alloying element range in superalloys . . . 69(T)
content effect in cobalt-base alloys . . . 364
maximum furnace operating temperature in air . . . 93(T)
mechanical properties . . . 93(T)
physical properties . . . 93(T)
as solid-solution strengthener in nickel . . . 14(F)
Turning, of nickel alloys . . . 237–240(F,T)
Two-fluid atomization . . . 210, 211(F)
Twin bands . . . 15
Twin ends . . . 15
Twist drilling, of nickel alloys . . . 240, 241(T)
Typical semibright bath, mechanical properties . . . 108(T)

U

Ultimate tensile strength, of cobalt alloys, individual alloy values . . . 377(T), 378(T), 381(T), 385(T)
Ultrahigh strength steels . . . 8
Ultrasonic atomization . . . 210, 211(F)
Unmixed zone . . . 267

V

Vacuum arc remelting (VAR) process . . . 74–75(F)
Vacuum atomization . . . 210, 211(F), 215
Vacuum induction melting . . . 73–74(F)
of nickel-iron soft magnetic alloys . . . 95
Vacuum plasma sprayed coatings . . . 290
Vanadium, as solid-solution strengthener in nickel . . . 14(F)
Vanadium pentoxide, and hot slag corrosion of nickel alloys . . . 62
Vapor honing, of heat resistant nickel alloys . . . 280
Vibratory cavitation test procedure (ASTM G 32) . . . 390(F), 391(F), 394(F)
VIM-ESR-VAR (triple melt) . . . 75
Vitallium . . . 362
Volt swing . . . 75

W

Wackenroder's solution . . . 150
Waste incineration environments, corrosion in . . . 183–184(T)
Water, corrosion rate of electroless nickel coatings . . . 118(T)
Water atomization, schematic of process . . . 211(F)
Watts nickel
corrosion rates in various chemical process environments . . . 118(T)
electrolyte composition . . . 108(T)
mechanical properties . . . 108(T)
operating conditions . . . 108(T)
Wear of cobalt alloys . . . 387–394(F,T)
abrasive . . . 387, 388–389(F)
high-stress . . . 387, 389, 390(T)
low-stress . . . 387, 389(F), 390(T)
carbide-containing . . . 393–394(F)
erosive . . . 388, 390–392(F)
cavitation . . . 391(F), 394(F)
slurry . . . 391–392(F)
solid-particle impingement . . . 390–391(F)
galling . . . 392(F), 393(F)
Laves-type alloy compositions . . . 394
sliding . . . 387–388, 392(F)
sliding, oxide control . . . 392
types . . . 387
Weldability, and galling . . . 191
Weld cladding alloys . . . 10, 122
Welding of cobalt alloys
cobalt-base heat resistant alloys . . . 402, 403
cobalt-base superalloys . . . 78
cobalt-base wear resistant alloys . . . 402
Welding of nickel alloys . . . 245–267(F,T), 268(T)
cast nickel alloys . . . 260
cleaning of workpieces . . . 258
consumables selection for joining applications . . . 268(T)
corrosion-resistant alloys . . . 245–250(F,T)
corrosion-resistant alloys containing molybdenum . . . 251–255(F,T)
defects of welds, minimizing . . . 265(F), 266–267
dissimilar metals . . . 267
gas-metal arc welding . . . 259(F), 261(T), 262–263(T)
gas-tungsten arc welding . . . 259(F), 260–262(F,T)
Hastelloy alloys . . . 251–255(F,T)
heat-resistant alloys . . . 255–257(F,T)
heat treatment . . . 257–258
iron-nickel-base superalloys . . . 78–79(F)
joint configurations and dimensions . . . 258–260(F)
nickel-base superalloys . . . 78–79(F)
plasma arc welding . . . 263–264
precipitation-hardenable (PH) alloys . . . 260
processes used . . . 252
shielded metal arc welding . . . 259(F), 263(T), 264–265(F,T)
submerged arc welding . . . 261(T), 265–266(T)
weldability . . . 245
weld cladding alloys . . . 122
weld-overlay coatings . . . 120–122(F,T)
Weldments
corrosion in specific environments . . . 137–139(F)
defect minimization . . . 265(F), 266–267
stress-corrosion cracking . . . 157
Weld-overlay coatings . . . 10
weld cladding alloys . . . 122
Weld surfacing . . . 106
Western Mining Corporation refinery . . . 207
Wet abrasive blasting, of heat-resistant nickel alloys . . . 280
Wet tumbling, of heat-resistant nickel alloys . . . 280
Widmanstatten structures
in nickel-base superalloy after deformation processing . . . 76
in superalloys . . . 84, 85
and phases and carbides . . . 303–304
with carbide precipitation in superalloys . . . 83
Window method, for preparing thin foils . . . 300
Wire brushing, of heat-resistant nickel alloys . . . 280
Work hardening, avoidance in machining . . . 236–237

Y

Yield strength
of cobalt . . . 345
of cobalt alloys, individual alloy values . . . 373–386(T)
of nickel . . . 3
of nickel and nickel alloys, individual alloy values . . . 19–54(F,T)
Yttria, as thermal barrier coating . . . 287, 290
Yttria-zirconia, as thermal barrier coating . . . 288(F)
Yttrium
alloying element effect in cobalt-base heat-resistant alloys . . . 366
alloying element effect on nickel- and iron-base superalloys . . . 167(T)
alloying element effects on corrosion resistance . . . 17(T)
Yttrium oxide
alloying element effects on corrosion resistance . . . 17(T)
as thermal barrier coating . . . 287, 290

© 2000 ASM International. All Rights Reserved.
ASM Specialty Handbook: Nickel, Cobalt, and Their Alloys (#06178G)

Z

Zero Emission Batterie Research Activity (ZEBRA) 6
Zinc, molten, corrosion by . . . . . 186(T)
Zirconia, as thermal barrier coating. 287, 290
Zirconium
alloying element effect in cobalt-base heat-resistant alloys 366
content effect on nickel alloy weldability 248
effect on superalloy mechanical properties 84
Zirconium oxide, as thermal barrier coating 287, 290
Z phase 304

ASM International is the society for materials engineers and scientists, a worldwide network dedicated to advancing industry, technology, and applications of metals and materials.

ASM International, Materials Park, Ohio, USA
www.asminternational.org

This publication is copyright © ASM International®. All rights reserved.

Publication title	Product code
ASM Specialty Handbook: Nickel, Cobalt, and Their Alloys	#06178G

To order products from ASM International:

Online Visit www.asminternational.org/bookstore

Telephone 1-800-336-5152 (US) or 1-440-338-5151 (Outside US)

Fax 1-440-338-4634

Mail Customer Service, ASM International
9639 Kinsman Rd, Materials Park, Ohio 44073-0002, USA

Email CustomerService@asminternational.org

In Europe American Technical Publishers Ltd.
27-29 Knowl Piece, Wilbury Way, Hitchin Hertfordshire SG4 0SX, United Kingdom
Telephone: 01462 437933 (account holders), 01462 431525 (credit card)
www.ameritech.co.uk

In Japan Neutrino Inc.
Takahashi Bldg., 44-3 Fuda 1-chome, Chofu-Shi, Tokyo 182 Japan
Telephone: 81 (0) 424 84 5550

Terms of Use. This publication is being made available in PDF format as a benefit to members and customers of ASM International. You may download and print a copy of this publication for your personal use only. Other use and distribution is prohibited without the express written permission of ASM International.

No warranties, express or implied, including, without limitation, warranties of merchantability or fitness for a particular purpose, are given in connection with this publication. Although this information is believed to be accurate by ASM, ASM cannot guarantee that favorable results will be obtained from the use of this publication alone. This publication is intended for use by persons having technical skill, at their sole discretion and risk. Since the conditions of product or material use are outside of ASM's control, ASM assumes no liability or obligation in connection with any use of this information. As with any material, evaluation of the material under end-use conditions prior to specification is essential. Therefore, specific testing under actual conditions is recommended.

Nothing contained in this publication shall be construed as a grant of any right of manufacture, sale, use, or reproduction, in connection with any method, process, apparatus, product, composition, or system, whether or not covered by letters patent, copyright, or trademark, and nothing contained in this publication shall be construed as a defense against any alleged infringement of letters patent, copyright, or trademark, or as a defense against liability for such infringement.